CONTENTS

No. 1, February 1992

BEHAVIOR

DEVELOPMENT AND REPRODUCTION

ECOLOGY AND EVOLUTION

GENERAL BIOLOGY

PHYSIOLOGY

RESEARCH NOTES

CONTENTS

No. 2, April 1992

No. 3, June 1992

PHYSIOLOGY

VIEWS AND DISCUSSION

Volume 182 Number 1

THE BIOLOGICAL BULLETIN

FEBRUARY, 1992

Published by the Marine Biological Laboratory

THE BIOLOGICAL BULLETIN

PUBLISHED BY
THE MARINE BIOLOGICAL LABORATORY

FEBRUARY, 1992

Printed and Issued by
LANCASTER PRESS, Inc.
PRINCE & LEMON STS.
LANCASTER, PA

THE BIOLOGICAL BULLETIN

THE BIOLOGICAL BULLETIN is published six times a year by the Marine Biological Laboratory, MBL Street, Woods Hole, Massachusetts 02543.

Subscriptions and similar matter should be addressed to Subscription Manager, THE BIOLOGICAL BULLETIN, Marine Biological Laboratory, Woods Hole, Massachusetts 02543. Single numbers, $30.00. Subscription per volume (three issues), $77.50 ($155.00 per year for six issues).

Communications relative to manuscripts should be sent to Michael J. Greenberg, Editor-in-Chief, or Pamela L. Clapp, Managing Editor, at the Marine Biological Laboratory, Woods Hole, Massachusetts 02543. Telephone: (508) 548-3705, ext. 428. FAX: 508-540-6902. E-mail: pamcl@hoh.mbl.edu.

POSTMASTER: Send address changes to THE BIOLOGICAL BULLETIN, Marine Biological Laboratory, Woods Hole, MA 02543.

Second-class postage paid at Woods Hole, MA, and additional mailing offices.
ISSN 0006-3185

INSTRUCTIONS TO AUTHORS

The Biological Bulletin accepts outstanding original research reports of general interest to biologists throughout the world. Papers are usually of intermediate length (10–40 manuscript pages). A limited number of solicited review papers may be accepted after formal review. A paper will usually appear within four months after its acceptance.

Very short, especially topical papers (less than 9 manuscript pages including tables, figures, and bibliography) will be published in a separate section entitled "Research Notes." A Research Note in *The Biological Bulletin* follows the format of similar notes in *Nature*. It should open with a summary paragraph of 150 to 200 words comprising the introduction and the conclusions. The rest of the text should continue on without subheadings, and there should be no more than 30 references. References should be referred to in the text by number, and listed in the Literature Cited section in the order that they appear in the text. Unlike references in *Nature*, references in the Research Notes section should conform in punctuation and arrangement to the style of recent issues of *The Biological Bulletin*. Materials and Methods should be incorporated into appropriate figure legends. See the article by Lohmann *et al.* (October 1990, Vol. **179**: 214–218) for sample style. A Research Note will usually appear within two months after its acceptance.

The Editorial Board requests that regular manuscripts conform to the requirements set below; those manuscripts that do not conform will be returned to authors for correction before review.

1. ***Manuscripts.*** Manuscripts, including figures, should be submitted in triplicate. (Xerox copies of photographs are not acceptable for review purposes.) The original manuscript must be typed in no smaller than 12 pitch, using double spacing (*including* figure legends, footnotes, bibliography, etc.) on one side of 16- or 20-lb. bond paper, 8½ by 11 inches. Please, no right justification. Manuscripts should be proofread carefully and errors corrected legibly in black ink. Pages should be numbered consecutively. Margins on all sides should be at least 1 inch (2.5 cm). Manuscripts should conform to the *Council of Biology Editors Style Manual*, 5th Edition (Council of Biology Editors, 1983) and to American spelling. Unusual abbreviations should be kept to a minimum and should be spelled out on first reference as well as defined in a footnote on the title page. Manuscripts should be divided into the following components: Title page, Abstract (of no more than 200 words), Introduction, Materials and Methods, Results, Discussion, Acknowledgments, Literature Cited, Tables, and Figure Legends. In addition, authors should supply a list of words and phrases under which the article should be indexed.

2. ***Title page.*** The title page consists of: a condensed title or running head of no more than 35 letters and spaces, the manuscript title, authors' names and appropriate addresses, and footnotes listing present addresses, acknowledgments or contribution numbers, and explanation of unusual abbreviations.

3. ***Figures.*** The dimensions of the printed page, 7 by 9 inches, should be kept in mind in preparing figures for publication. We recommend that figures be about 1½ times the linear dimensions of the final printing desired, and that the ratio of the largest to the smallest letter or number and of the thickest to the thinnest line not exceed 1:1.5. Explanatory matter generally should be included in legends, although axes should always be identified on the illustration itself. Figures should be prepared for reproduction as either line cuts or halftones. Figures to be reproduced as line cuts should be unmounted glossy photographic reproductions or drawn in black ink on white paper, good-quality tracing cloth or plastic, or blue-lined coordinate paper. Those to be reproduced as halftones should be mounted on board, with both designating numbers or letters and scale bars affixed directly to the figures. All figures should be numbered in consecutive order, with no distinction between text and plate figures. The author's name and an arrow indicating orientation should appear on the reverse side of all figures.

4. ***Tables, footnotes, figure legends, etc.*** Authors should follow the style in a recent issue of *The Biological Bulletin* in preparing table headings, figure legends, and the like. Because of the high cost of setting tabular material in type, authors are asked to limit such material as much as possible. Tables, with their headings and footnotes, should be typed on separate sheets, numbered with consecutive Roman numerals, and placed after

the Literature Cited. Figure legends should contain enough information to make the figure intelligible separate from the text. Legends should be typed double spaced, with consecutive Arabic numbers, on a separate sheet at the end of the paper. Footnotes should be limited to authors' current addresses, acknowledgments or contribution numbers, and explanation of unusual abbreviations. All such footnotes should appear on the title page. Footnotes are not normally permitted in the body of the text.

5. ***Literature cited.*** In the text, literature should be cited by the Harvard system, with papers by more than two authors cited as Jones *et al.*, 1980. Personal communications and material in preparation or in press should be cited in the text only, with author's initials and institutions, unless the material has been formally accepted and a volume number can be supplied. The list of references following the text should be headed Literature Cited, and must be typed double spaced on separate pages, conforming in punctuation and arrangement to the style of recent issues of *The Biological Bulletin*. Citations should include complete titles and inclusive pagination. Journal abbreviations should normally follow those of the U. S. A. Standards Institute (USASI), as adopted by BIOLOGICAL ABSTRACTS and CHEMICAL ABSTRACTS, with the minor differences set out below. The most generally useful list of biological journal titles is that published each year by BIOLOGICAL ABSTRACTS (BIOSIS List of Serials; the most recent issue). Foreign authors, and others who are accustomed to using THE WORLD LIST OF SCIENTIFIC PERIODICALS, may find a booklet published by the Biological Council of the U.K. (obtainable from the Institute of Biology, 41 Queen's Gate, London, S.W.7, England, U.K.) useful, since it sets out the WORLD LIST abbreviations for most biological journals with notes of the USASI abbreviations where these differ. CHEMICAL ABSTRACTS publishes quarterly supplements of additional abbreviations. The following points of reference style for THE BIOLOGICAL BULLETIN differ from USASI (or modified WORLD LIST) usage:

A. Journal abbreviations, and book titles, all underlined (for *italics*)

B. All components of abbreviations with initial capitals (not as European usage in WORLD LIST *e.g., J. Cell. Comp. Physiol.* NOT *J. cell. comp. Physiol.*)

C. *All* abbreviated components must be followed by a period, whole word components *must not* (*i.e., J. Cancer Res.*)

D. Space between all components (*e.g., J. Cell. Comp. Physiol.*, not *J.Cell.Comp.Physiol.*)

E. Unusual words in journal titles should be spelled out in full, rather than employing new abbreviations invented by the author. For example, use *Rit Vísindafjélags Islendinga* without abbreviation.

F. All single word journal titles in full (*e.g., Veliger, Ecology, Brain*).

G. The order of abbreviated components should be the same as the word order of the complete title (*i.e., Proc.* and *Trans.* placed where they appear, not transposed as in some BIOLOGICAL ABSTRACTS listings).

H. A few well-known international journals in their preferred forms rather than WORLD LIST or USASI usage (*e.g., Nature, Science, Evolution* NOT *Nature, Lond., Science, N.Y.; Evolution, Lancaster, Pa.*)

6. ***Reprints, page proofs, and charges.*** Authors receive their first 100 reprints (without covers) free of charge. Additional reprints may be ordered at time of publication and normally will be delivered about two to three months after the issue date. Authors (or delegates for foreign authors) will receive page proofs of articles shortly before publication. They will be charged the current cost of printers' time for corrections to these (other than corrections of printers' or editors' errors). Other than these charges for authors' alterations, *The Biological Bulletin* does not have page charges.

ERRATUM

The Biological Bulletin, Volume **180,** Number 2, page 314

The following correction should be made in the article by Anthony Pires and Michael G. Hadfield titled, "Oxidative breakdown products of catecholamines and hydrogen peroxide induce partial metamorphosis in the nudibranch *Phestilla sibogae* Bergh (Gastropoda: Opisthobranchia)" (*Biol. Bull.* **180:** 310–317).

On page 314, the second sentence of the second paragraph in the left hand column, which reads "Concentration threshold for velar loss after 7-h exposure to fresh DA. . ." should read, "Concentration threshold for velar loss after 7-h exposure to *aged* DA. . ." The word "aged" replaces the word "fresh."

Reference: *Biol. Bull.* **182:** 1–7. (February, 1992)

Fast-Strike Feeding Behavior in a Pteropod Mollusk, *Clione limacina* Phipps

COLIN O. HERMANS[1] AND RICHARD A. SATTERLIE

Department of Zoology, Arizona State University, Tempe, Arizona 85287
and Friday Harbor Laboratories, Friday Harbor, Washington 98250

Abstract. High speed cinematography and video recordings were used to evaluate the fast-strike feeding response by which *Clione limacina* captures its prey, *Limacina helicina*. The acquisition phase of feeding involves rapid mouth opening and extrusion of three pairs of buccal cones. Mouth opening occurs in 10 to 20 ms, while hydrostatic inflation of the buccal cones takes 50 to 70 ms. Buccal cones are immediately retracted if prey are not contacted. Buccal cones surround the prey and release a viscous material that may be used as an adhesive attachment to the prey shell. Surface ultrastructure of the buccal cones reveals that they are studded with clusters of capitulate papillae, which appear to be the source of the viscous secretory material.

Introduction

The pteropod mollusk *Clione limacina* feeds exclusively on shelled pteropods (Lalli and Gilmer, 1989). Due to the extremely limited dietary breadth of *Clione*, as well as the active swimming characteristics of both predator and prey (*Limacina helicina* in Friday Harbor, Washington), it is not surprising to find rapidly activated and highly specialized feeding structures in *Clione*. For prey acquisition, *Clione* rapidly extrudes three pairs of oral appendages, called buccal cones, which surround and adhere to the prey (see Lalli, 1970). Each buccal cone is cone shaped when retracted, but becomes more cylindrical when extruded. Extrusion of buccal cones is primarily due to hydraulic inflation (Lalli and Gilmer, 1989). The acquisition phase of feeding is followed by a manipulative phase, during which the prey is turned so that the shell opening is over the mouth of *Clione*. Manipulation is performed by the buccal cones and is followed by the consumptive phase, during which the prey is extricated from its shell. Extrication involves the use of two specialized hook sacs that form part of the buccal apparatus (Lalli, 1970). Each hook sac contains tufts of recurved chitinous hooks, which are protracted into the shell opening to grasp and pull the prey from its shell. Soft tissues of the prey are dislodged by alternate protractions and retractions of the hook sacs. Swallowing is aided by protraction and retraction movements of the radula, which is also part of the buccal apparatus. The soft tissues of the prey are swallowed whole (Wagner, 1885; Litvinova and Orlovsky, 1985; for other references see Lalli and Gilmer, 1989).

Two distinct forms of feeding behavior are observed. In the first, referred to here as the fast-strike response, *Clione* enters the acquisition phase of feeding from an unexcited, slow swimming activity state. During acquisition, swimming changes from slow to fast, and continues fast throughout the consummatory phase. During fast swimming, bending of the tail leads to frequent turning and looping movements of the entire body. If a fast-strike fails, and prey is not acquired, the buccal cones are immediately withdrawn, and fast swimming is terminated. The fast-strike response, which is initiated by prey contact, thus represents a sudden change to feeding behavior; if unsuccessful, the response is terminated by an equally sudden return to pre-strike swimming activity.

The second type of feeding behavior is initiated without direct physical contact with the prey. This activity involves fast swimming with loops and turns, as well as buccal cone extrusion and is referred to as "hunting behavior" (Litvinova and Orlovsky, 1985). Hunting behavior can be induced by placing an animal in seawater containing prey homogenates, by placing non-feeding *Clione* individuals close to feeding individuals, or by injecting sero-

Received 5 June 1991; accepted 25 November 1991.

[1] Present address: Department of Biology, Sonoma State University, Rohnert Park, California 94928.

tonin into the hemocoel (Litvinova and Orlovsky, 1985; Kabotyanski and Sakharov, 1988). Hunting behavior is similar to fast-strike feeding behavior in that the mouth is held open with the buccal cones protruding, and swimming is fast with frequent changes in direction. The behaviors differ in two important ways. First, hunting behavior does not require direct contact with an intact prey. Second, buccal cone extension and fast swimming are maintained in hunting behavior, whereas both are terminated immediately in the fast-strike if a prey item is not acquired. Note that the prey acquisition responses of *Clione* form a continuum, with fast-strike feeding at one extreme and indefinite hunting behavior at the other.

In this paper, we describe behavioral and morphological aspects of the acquisition phase of fast-strike feeding; a cine analysis of mouth and buccal cone movements and a description of the surface morphology of the buccal cones are included. This work provides the background for an ongoing electrophysiological investigation into the acquisition phase of feeding behavior and the role of putative modulators on the motivational states underlying feeding behavior. It also extends the cinematic analysis of *Clione* feeding behavior by Litvinova and Orlovsky (1985).

Materials and Methods

Both *Limacina* and *Clione* were collected from the breakwater at Friday Harbor Laboratories, Friday Harbor, Washington, and held in one-gallon glass jars in a seawater table. Individual animals were filmed in a small glass chamber filled with seawater at room temperature (16–18°C). Fast-strike sequences were filmed, within five days of animal collection, at 100 frames/s with a Redlake Locam high speed 16 mm camera containing Kodak Plus-X negative film. Additional feeding sequences were "filmed" with a Sony CCD video camera HVM-200, equipped with a Nikon Micro-Nikkor lens, at the equivalent of 60 frames/s and were recorded on a Canon VR-30 4-head portable video recorder. Feeding sequences were obtained by touching the prey, *Limacina helicina,* to swimming individuals of *Clione. Limacina* were attached with "Super Glue" to a human head hair or held in fine forceps.

A hair was attached to the *Limacina* shell as follows. A *Limacina* was placed in a shallow container on the stage of a dissecting microscope and the water level in the container was lowered until the shell, which is very hydrophobic, broke through the surface film of the water. The *Limacina* was then turned to achieve the desired orientation. The root of a human hair was quickly dipped in a small droplet of "super glue" and applied to the surface of the shell.

Fast-strike responses were recorded from five different individuals. One complete response (from initiation through acquisition) was recorded from each of these animals, but unsuccessful strikes were often recorded before the complete event. Unsuccessful strikes were also recorded from three other individuals that never produced a complete response. All animals were between 1.4 and 2.2 cm in body length.

Film sequences were analyzed frame-by-frame by making photographic prints of the sequences, and by projecting individual frames onto tracing paper. Tracings were made of body, wing, head, and buccal cone positions. In one case, the images from sequential frames were digitized from tracings with a Jandel Scientific digitizing pad and processed with a computer-assisted three-dimensional reconstruction software program, (PC3D™, Jandel Scientific, Corte Madera, California). Photographic prints were made by projecting 16-mm frames directly onto photographic paper with a standard photographic enlarger. Video sequences, advanced frame-by-frame, were traced directly from a television screen during viewing.

For scanning electron microscopical investigation, specimens that were not adhering to prey were anesthetized by immersion in a 1:1 solution of 0.33 *M* magnesium chloride and seawater. A *Clione* adhering to its prey was prepared as follows. First, a *Limacina,* glued to a hair, was dangled in an aquarium so as to contact swimming individuals of *Clione.* When one of the pteropods struck at and gripped the prey, it was immediately pulled out of the aquarium and dropped directly into the primary fixative solution. The specimen continued to grip its prey as they were both being fixed, and remained attached until CO_2 turbulence, during critical point drying, accidentally separated them, exposing the adherent surfaces. Fixation was completed by immersion in isotonic, cacodylate-buffered 2% glutaraldehyde, pH 7.3, at room temperature for 2 h, and postfixation was in cacodylate-buffered 1% osmium tetroxide for 1 h at room temperature. The specimens were dehydrated in ethanol, critical point dried from carbon dioxide, and sputter coated with gold and palladium before examination with an AMRay 1000 (Figs. 1, 4A) or a JEOL JSM-35 (Fig. 4B) scanning electron microscope.

Results

Acquisition behavior

Fast-strike feeding behavior was initiated by bringing a tethered *Limacina* into contact with the oral region of a freely swimming *Clione.* In our experience, the success rate of inducing fast-strikes was extremely low. With some animals, a day or more would pass without a strike being elicited; *Clione* apparently feeds irregularly. The degree of satiation in individual animals could not, therefore, be determined. The success rate was equally low, however, in animals that had been held in a jar for more than a

week. With other animals, strikes could be obtained with some dependability. On one occasion, a response was obtained although the prey was not in contact with the oral region of *Clione*. In this case, the *Limacina* began rapid swimming movements when brought near the oral region of *Clione*, triggering an immediate fast-strike response.

In all observed fast-strike responses, the initial response of the acquisition phase was rapid mouth opening. When closed, the mouth forms a dorsoventral slit on the anterior margin of the head (Fig. 1A). Lip retraction pulls the lips laterally, causing mouth gaping and protrusion of the buccal cones (Fig. 1B). The degree of mouth opening can be judged from the position of the anterior tentacles, as recorded on film and video prior to and during fast-strike responses (Figs. 2, 3). The mouth of *Clione* is flanked by a pair of anterior tentacles that project from the anterolateral margins of the head (Fig. 1A). When *Clione* is hovering or slowly swimming forward (upward), the anterior tentacles are normally inflated and project forward (Figs. 1A, 2A). During mouth opening, lip retraction, and protrusion of the buccal cones, the anterior tentacles rotate laterally 90°, so that their projection is perpendicular to the longitudinal axis of the animal (Figs. 2D, 3). Mouth opening occurs in the first 20 ms of the fast-strike and is accompanied by full exposure and partial protraction of the buccal cones (Fig. 3). This can be demonstrated by pulling open the mouth of an anesthetized animal, which exposes the buccal cones and causes them to bulge slightly out of the mouth (similar to that seen in Fig. 1B). Three buccal cones lie on either side of the buccal mass (a muscular organ containing the radula and a pair or hook sacs), in a line parallel to the lips. The retracted cones are not inverted, but rather are collapsed and retracted into small cavities, or cheek pouches, adjacent to the buccal mass. Buccal cones protract when they are inflated with hemolymph (Lalli and Gilmer, 1989). This is supported by our physiological experiments in which induced activity in buccal cone protraction motor neurons causes mouth opening, contraction of head musculature, but only partial extension of buccal cones (Norekian and Satterlie, in prep.). In these preparations, full expansion of the buccal cones is impossible because the head hemocoel is compromised to allow electrophysiological recordings. In intact animals, expanded cones can extend approximately one-half body length from the mouth. Expansion is accompanied by a decrease in the diameter of the head and the appearance of a distinct circular constriction in the neck region (Figs. 2D, 3). In two recorded sequences in which the head and neck outlines were clearly shown, the reduction in head diameter averaged 22.7% while the reduction in neck diameter averaged 20.2%. Full expansion of the buccal cones, including the initial mouth opening, takes from 50 to 70 ms (Fig. 3). If the prey is not contacted during buccal cone expansion, the cones are immediately retracted, the mouth is closed, and the animal returns to slow swimming. Retraction of buccal cones is not a passive deflation, because the cones can be fully retracted in 70 to 90 ms (based on three unsuccessful strikes). On two occasions, strikes were aborted when the buccal cones were inflated to only 10 to 20% of the body length. In these cases, the cones were immediately retracted as in unsuccessful strikes.

Inflation of the buccal cones occurs from the base outward; the tips of the cones do not inflate until late in cone expansion. The uninflated tips are more opaque than the inflated parts of the buccal cones (Fig. 2D). As the cones

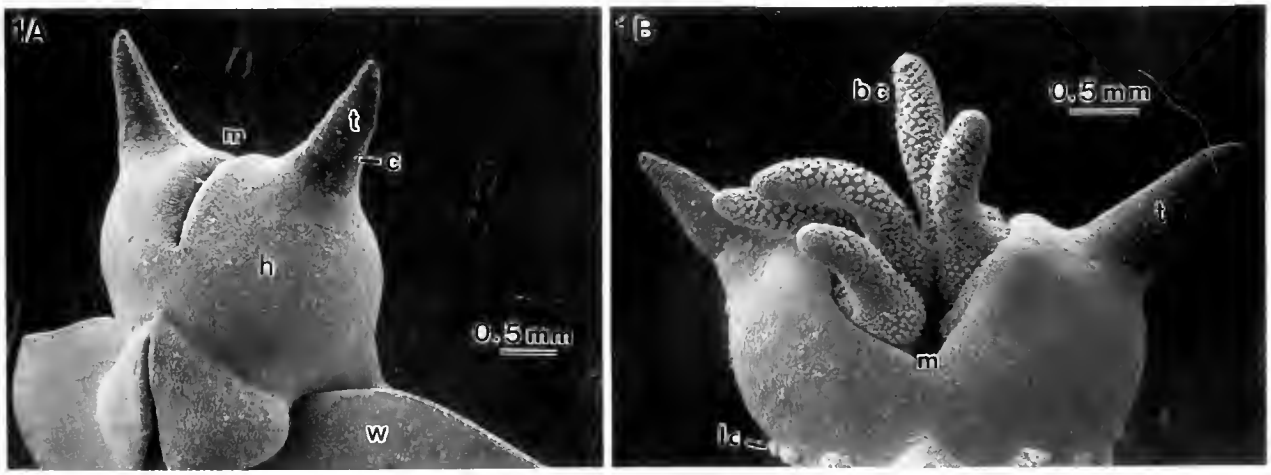

Figure 1. Scanning electron micrographs showing ventral views of heads of *Clione* in normal swimming posture (1A) and with mouth (m) open and five of six buccal cones (bc) partially protruded (1B). Note the pair of anterior tentacles (t) that bear ciliary tufts (c). The head (h) is covered with a coat of motile cilia. w—wings, lc—tufts of large neck cilia.

Figure 2. Representative frames from cinematographic series taken at 100 frames/s showing a tethered *Limacina* being offered to a *Clione*. cw—wings of *Clione*, wl—wings of *Limacina*, bc—buccal cones, t—anterior tentacles of *Clione*. (A) Predator and prey 200 ms (20 frames) before first sign of response to contact. (B) First sign of response to contact. Note the slight bulge on head of *Clione* (arrow). (C) Next frame (10 ms) after (B), showing buccal cones exploding from cheek pouches and forming grasping tentacles. (D) 4 frames (40 ms) after (C), showing buccal cones near full extension and beginning to grip the *Limacina*. Note the decreased diameter of the head, and the prominent neck constriction.

are extruded, they project outward at approximately 45° with a slight concave curvature with respect to the mouth. As the cones reach full expansion, they bend around the prey and adhere to its shell (Fig. 3).

Limacina shells pulled from the grasp of *Clione* buccal cones were coated with a viscous residue in the regions contacted by buccal cones. Clear viscous material produced by the buccal cones could be gripped with fine forceps and lifted in fine strands from the surface of the seawater containing the *Clione*. During hunting behavior, the protracted buccal cones frequently adhered to the wall of the container following contact with it. Removal of an adhering animal revealed residue on the glass, apparently adhesive.

Surface ultrastructure of the buccal cones

The surface of each buccal cone is studded with clusters or rosettes of capitulate papillae (Fig. 4). The number of papillae in each cluster varies from two or three to about a dozen. The clusters near the bases of the buccal cones contain the fewest papillae per rosette, those toward the tips contain more. Each papilla is about 15 μm high and somewhat less than 10 μm in diameter. The tip of each papilla is slightly inflated, forming a lumpy capitulum about 10 μm in diameter. Each rosette has a common stalk, about 20 μm in diameter and 20 μm in height. Long cilia protrude from the sides of the papillae and project from the surface of the buccal cone between the papillae. Tight clusters of cilia protrude from the centers of some of the papillary rosettes. Isolated clusters of cilia, were also observed, but they were not common (Fig. 4A).

When the buccal cones are retracted, the epidermis between the clusters of papillae is deeply folded, and the capitula and cilia form a tightly packed feltwork or welter on the surface of each cone. When the buccal cones are extended, the rosettes of papillae stand up above a smooth, simple squamous epithelium that stretches tightly over the tentacular surface between the rosettes of papillae (Fig. 4A).

The surface of the shell of *Limacina*, to which the buccal cones adhere, is very smooth, transparent, and very hydrophobic; it appears smooth when viewed with a scanning electron microscope. The shells of dead *Limacina* lose their hydrophobic properties rapidly. Where the shell of a *Limacina* is contacted by the buccal cones of a fast-striking *Clione* are fine threads, observable by SEM, that correspond to those that appear on the surfaces of the buccal cones where they contact the *Limacina* shell (Fig. 4B). These threads appear to originate from the tips of the capitulate papillae, but this possibility is difficult to establish with certainty.

Discussion

The fast-strike response of *Clione* consists of a rapid opening of the mouth and a hydraulic inflation of the six buccal cones, the entire response occurring in 50 to 70 ms. In aborted or unsuccessful strikes, withdrawal of buc-

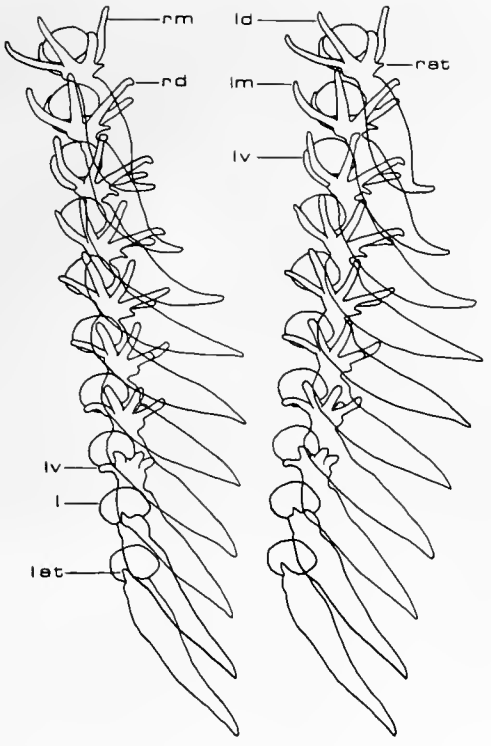

Figure 3. Tracings of *Clione* and *Limacina* from cine series with time intervals of 10 ms between frames and covering the 100 ms interval from one frame (10 ms) prior to the first sign of response to the prey through the initial grasping of the shell. The sequence has been plotted twice with a 7° shift in the y-axis. When viewed with a stereoscopic viewer or with crossed eyes, the sequence will appear in 3-dimensions with time represented in the z-plane. Buccal cone labels: (ld)—left dorsal, (lm)—left median, (lv)—left ventral, (rd)—right dorsal, (rm)—right medial. Right (rat) and left (lat) anterior tentacles are also labelled.

cal cones is nearly as rapid. This would suggest that both expansion and withdrawal are active responses. Fast-strike prey acquisition is thus distinct from the hunting behavior described by Litvinova and Orlovsky (1985) in which *Clione* rapidly swim with the buccal cones held in an expanded state. The initial phase of hunting behavior presumably involves similar mouth opening and buccal cone inflation.

The low success rate in triggering a fast-strike under laboratory conditions suggests that the fast-strike response has a high threshold for activation. Lowering of this threshold could result in behavior that is more disposed toward feeding, such as hunting behavior. In this case, the difference between responses to prey during normal swimming and those during hunting behavior might be one of motivational state. This difference can best be illustrated by comparing buccal cone responses during hunting and during an unsuccessful fast-strike response. In the former, the buccal cones are held in an expanded position despite the lack of mechanical contact with the prey. In the latter case, lack of prey contact results in a rapid withdrawal of the buccal cones and a return to normal swimming behavior. In hunting behavior, therefore, buccal cone withdrawal must be suppressed, even in the absence of direct mechanical contact with prey.

The nature of the trigger underlying the change in behavioral state, from hunting to fast-strike, is not known. It may, however, involve serotonergic input to the feeding system, because bath application or hemocoel injection of serotonin can trigger behavioral responses similar to those of hunting behavior; *i.e.,* the responses can be evoked although the animal has not been exposed to prey or prey extracts (Kabotyanski and Sakharov, 1988). The external stimulus for a switch to hunting behavior presumably involves chemosensory input because *Limacina* extracts, or proximity to feeding *Clione,* can initiate hunting behavior (Litvinova and Orlovsky, 1985).

Inflation of the buccal cones is remarkable for its great speed. Expansion is associated with a decrease in head and neck diameter, suggesting that increased hemocoelic pressure is associated with buccal cone inflation. Arshavsky *et al.* (1990) have shown that heart rate in *Clione* increases during hunting behavior, further supporting the idea that feeding responses are associated with increases in hemocoelic pressure. Pressure changes can be localized in the head as a muscular diaphragm separates head and body hemocoels. The diaphragm surrounds the anterior aorta and may act as a physiological valve further regulating blood flow to the hemocoel in the head (Lalli, 1967).

With buccal cones protruded, the *Clione* appear much like small squid. This led Wagner (1885) and Pelseneer (1885) to consider the possibility of homology between *Clione* buccal cones and squid tentacles. However, embryonic origins and innervation patterns demonstrate that they are not homologous (see Lalli and Gilmer, 1989, for a discussion of pteropod systematics and affinities). The mechanisms by which the two types of tentacles move to grasp their prey are quite distinct. Kier demonstrated that cephalopod tentacles are muscular hydrostats (Kier, 1982, 1987, 1988; Smith and Kier, 1989). Muscular hydrostats are readily distinguishable from hydrostatic skeletons that use a hydraulic mechanism in that their volumes are made up almost entirely of muscular tissue. Therefore, although they can undergo extensive changes in shape, muscular hydrostats do not substantially change volume. Hydraulic hydrostatic skeletons, in contrast, are fluid-filled cavities surrounded by muscular or fibrous tissues that resist the hydrostatic pressure within (Smith and Kier, 1989).

No clear differences are found when the speed of tentacle protractions in muscular hydrostats is compared with that of the hydraulic system of *Clione,* because the range of protraction speeds found in muscular hydrostat systems is very wide. For example, each of the 19 pairs of digital tentacles of *Nautilus* consists of an extensible, muscular,

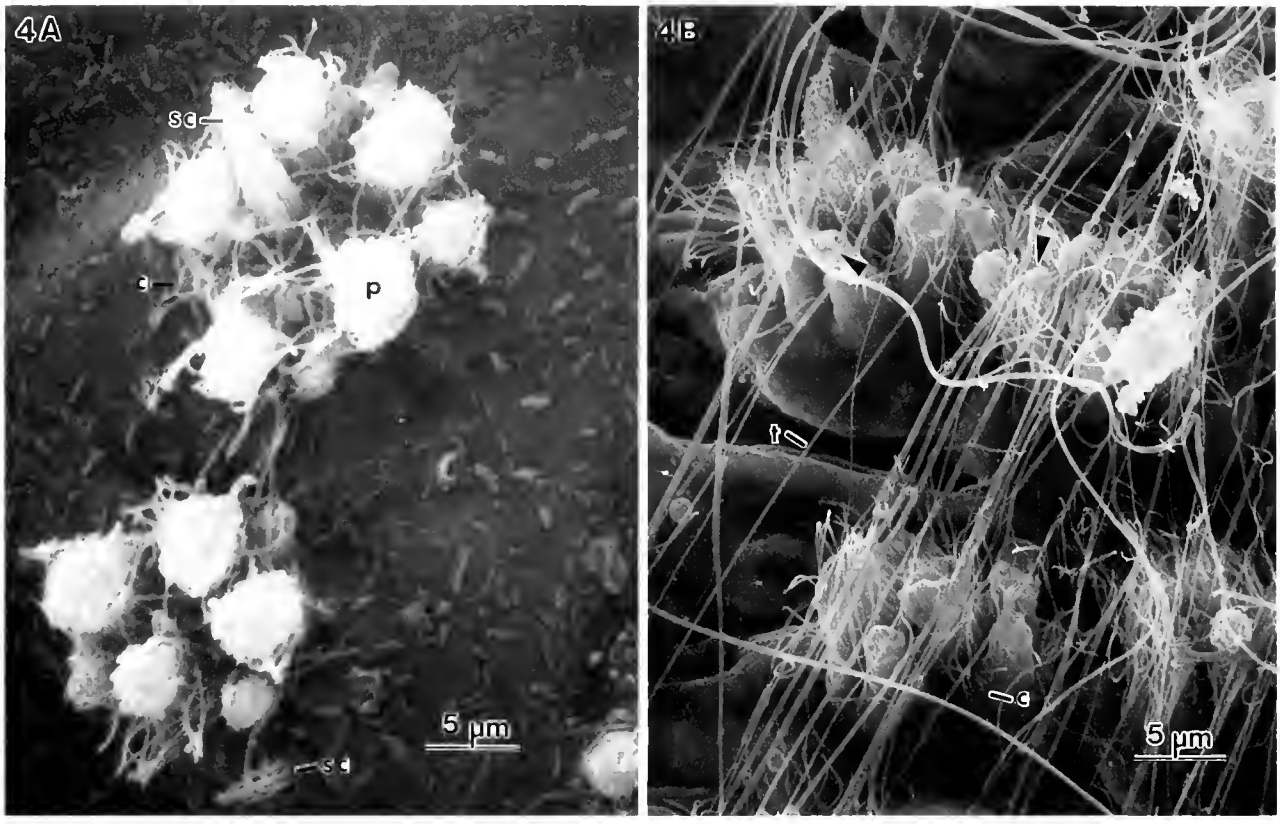

Figure 4. (A) Enlarged view of a part of one of the partially protruded buccal cones shown in Figure 1B. The head of each papilla (p) in the rosettes is studded with bumps. Motile cilia (c) project from the shaft of each papilla, whereas tufts of cilia (sc) project from the centers of rosettes, or less commonly are isolated from the rosettes. (B) Similar view of a region on a buccal cone of a different specimen, which was allowed to adhere to a *Limacina* shell and was fixed while grasping the prey. Dense mats of thread-like structures (t) can be seen on the adherent surfaces of buccal cones. Some appear to originate from the tips of capitulate papillae (arrows).

adhesive cirrus enclosed in a protective sheath. Protrusion of the cirrus from the tip of its sheath, which is necessary for it to grasp prey, requires 5–10 s or longer (Kier, 1987). At the opposite extreme, the tentacles of squid elongate fully in 15 to 30 ms (Keir, 1982, 1985).

The buccal cones of *Clione* can be protruded in less than 100 ms, and this performance is best appreciated when compared to other fast invertebrate prey capture behaviors that have been subjected to cine analysis. For example, prey seizure in the opisthobranch mollusk *Navanax* occurs in 380 ms; this is a muscular phenomenon involving a pharyngeal lunge followed by lip closure around the prey (Susswein *et al.*, 1984; Susswein and Achituv, 1987). Prey acquisition behaviors involving the movement of body parts that are supported by hard skeletal elements can be much faster; *e.g.*, the strike of the second thoracic appendages of stomatopod crustaceans occurs in 4–8 ms (Burrows, 1969).

Other gastropods can strike rapidly. In particular, the proboscides of toxoglossans, which contain poisonous, dart-like radular teeth, are potentially as rapid as the *Clione* buccal cone system. Predatory strikes have been described and photographed in a turrid, *Ophiodermella inermis* (Shimek and Kohn, 1981), and in *Conus* (Nybakken, 1967). The proboscis of *Conus* is protruded as a hydrostatic skeleton (Greene and Kohn, 1989), but the speed with which these strikes occur has not been analyzed by high speed cine or video.

Whereas some gymnosomatous pteropods do apprehend their prey with suction cups, somewhat like coleoidean cephalopods (Lalli and Gilmer, 1989; Kier and Smith, 1990), the adhesiveness of the buccal cones of *Clione* resembles that of the digital tentacles of *Nautilus*. The digital tentacles grip prey by means of ridges on the cirri that protrude from the tips of the sheaths that form the bases of the tentacles (Fukuda, 1987; Kier, 1987). In both *Nautilus* and *Clione*, the adhesive structures are ensheathed when not in use. In both cases, a question remains: to what degree are the prey simply gripped, and to what extent do the tentacles adhere? Fukuda (1987)

suggested that the ensheathing of the cirri in *Nautilus* might serve to save mucus.

Apprehension of the prey by *Clione* may be partly by chemical adhesion and partly by the physical gripping of the *Limacina* shell by the enclosing buccal tentacles. The capitula of the papillae on the buccal tentacles might be thrust through the boundary layer of water, covering the hydrophobic surface of the *Limacina* shell and providing the means of attachment to, or gripping of the shell, just like the beaded gloves used by soccer goalies and football wide receivers aid in gripping the wetted, hydrophobic surfaces of footballs. In both cases, the bumps aid in adhesion; they penetrate the boundary layer of water, eliminating this weak boundary layer by driving it into the spaces between the bumps (Waite, 1987).

Because the buccal tentacles appear to be chemically adhesive and yet can detach to manipulate the shell of the prey so that the opening is aligned with the *Clione* mouth, the possibility that both adhesive and releasing chemicals are secreted must be considered (Hermans, 1983). Examination of the ultrastructure of the buccal cones and their secretions, as well as analyses of the control of feeding behavior, will help answer this and other questions about prey acquisition in *Clione*.

Acknowledgments

We thank Dr. Tigran Norekian for translating Litvinova and Orlovsky (1985), Ms. Michelle Lagro for preparing specimens of *Clione* for electron microscopy, Prof. A. O. D. Willows of Friday Harbor Laboratories for space and equipment, Prof. R. Strathmann for use of his cine camera and the macro lens and video equipment, Dr. Tom Schroeder for instruction in SEM, also Mr. W. Sharp for instruction in EM and for the use of the Biological Electron Microscope Facility at Arizona State University, Mr. Chaz. Kazelik for help with the PC3D stereoscopic imaging program, Drs. Claudia Milis and Norm McLean for collecting and shipping specimens, and several other friends, colleagues, staff, and family at the Friday Harbor Labs for help in collecting specimens and for many other kindnesses. Thanks also to Sarah Cohen for suggesting the use of "Super Glue." Our perspective on the potential similarities between the strikes of toxoglossans and *Clione* has benefitted from discussions with Drs. Ron Shimek, Matt James, and Ed Smith.

Literature Cited

Arshavsky, Y. I., T. G. Deliagina, I. M. Gelfand, G. N. Orlovsky, V. V. Panchin, G. A. Pavlova, and L. B. Popova. 1990. Neural control of heart beat in the pteropod mollusc *Clione limacina:* coordination of circulatory and locomotor systems. *J. Exp. Biol.* **148:** 461–475.

Burrows, M. 1969. The mechanics and neural control of the prey capture strike in the mantid shrimps *Squilla* and *Hemisquilla. Z. Vergl. Physiol.* **62:** 361–381.

Fukuda, Y. 1987. Histology of the long digital tentacles. Pp. 249–256 in *Nautilus: The Biology and Paleobiology of a Living Fossil,* W. B. Saunders and N. H. Landman, eds. Plenum, New York.

Greene, J. L., and A. J. Kohn. 1989. Functional morphology of the *Conus* proboscis (Mollusca: Gastropoda). *J. Zool., Lond.* **219:** 487–493.

Hermans, C. O. 1983. The duo-gland adhesive system. *Oceanogr. Mar. Biol. Ann. Rev.* **21:** 283–339.

Kabotyanski, E. A., and D. A. Sakharov. 1988. Monoamine-dependent behavioural states in the pteropod mollusc *Clione limacina. Symposia Biologica Hungarica* **36:** 463–477.

Kier, W. M. 1982. Functional morphology of the musculature of squid (Loliginidae) arms and tentacles. *J. Morphol.* **172:** 179–192.

Kier, W. M. 1985. The musculature of squid arms and tentacles: ultrastructural evidence for functional differences. *J. Morphol.* **185:** 223–239.

Kier, W. M. 1987. The functional morphology of the tentacle musculature of *Nautilus pompilius.* Pp. 257–269 in *Nautilus: The Biology and Paleobiology of a Living Fossil,* W. B. Saunders and N. H. Landman, eds. Plenum, New York.

Kier, W. M. 1988. The arrangement and function of molluscan muscle. Pp. 211–252 in *The Mollusca, Form and Function,* Vol. 11, E. R. Trueman and M. R. Clarke, eds. Academic Press, New York.

Kier, W. M., and A. M. Smith. 1990. The morphology and mechanics of octopus suckers. *Biol. Bull.* **178:** 126–136.

Lalli, C. M. 1967. Studies on the structure and biology of two gymnosomatous pteropods, *Clione kincaidi* Agersborg and *Crucibranchaea macrochira* (Meisenheimer). Ph.D. Dissertation, University of Washington. 175 pp.

Lalli, C. M. 1970. Structure and function of the buccal apparatus of *Clione limacina* (Phipps) with a review of feeding in gymnosomatous pteropods. *J. Exp. Mar. Biol. Ecol.* **4:** 101–118.

Lalli, C. M., and R. W. Gilmer. 1989. *Pelagic Snails: The Biology of Holoplanktonic Gastropod Mollusks.* Stanford University Press, Stanford. 259 pp.

Litvinova, N. M., and G. N. Orlovsky. 1985. Feeding behavior of the pteropod mollusc *Clione limacina. Byull. MOIP, Otd. biol.* **90:** 73–77.

Nybakken, J. 1967. Preliminary observations on the feeding behavior of *Conus purpurascens* Broderip, 1833. *Veliger* **10:** 55–57.

Pelseneer, P. 1885. The cephalic appendages of the gymnosomatous pteropoda, and especially of *Clione. Q. J. Microsc. Sci.* **25:** 491–509.

Shimek, R. L., and A. J. Kohn. 1981. Functional morphology and evolution of the toxoglossan radula. *Malacologia* **20:** 423–438.

Smith, K. K., and W. M. Kier. 1989. Trunks, tongues, and tentacles: moving with skeletons of muscle. *Am. Sci.* **77**(1): 28–35.

Susswein, A. J., and Y. Achituv. 1987. Pharyngeal movements during feeding sequences of *Navanax inermis* (Gastropoda: Opisthobranchia) in successive stages of dissection. *J. Exp. Biol.* **128:** 323–333.

Susswein, A. J., Y. Achituv, M. S. Cappell, D. C. Spray, and M. V. L. Bennett. 1984. Pharyngeal movements during feeding sequences in *Navanax inermis:* a cinematographic analysis. *J. Comp. Physiol.* **155:** 209–218.

Wagner, N. 1885. *Die Wirbellosen des Weissen Meeres.* Wilhelm Engelmann, Leipzig. Pp. 1–168.

Waite, J. H. 1987. Nature's underwater adhesive specialist. *Int. J. Adhesion and Adhesives* **7:** 9–14.

Reference: *Biol. Bull.* **182:** 8–14. (February, 1992)

Effects of Photoperiod and Temperature on Egg-Laying Behavior in a Marine Mollusk, *Aplysia californica*

NANCY L. WAYNE AND GENE D. BLOCK

Department of Biology, University of Virginia, Charlottesville, Virginia 22901

Abstract. The primary purpose of these studies was to determine whether photoperiodic signals could influence seasonal egg-laying behavior in the marine mollusk, *Aplysia californica*. Egg-laying behavior was monitored from groups of animals that were collected at four times of year and maintained in different temperature and photoperiodic conditions in the laboratory. Animals that were obtained in autumn and kept in warm water laid eggs more frequently than those in cold water, regardless of photoperiod. Furthermore, animals maintained on short days and warm water laid eggs more frequently than those on long days and warm water. Animals in cold water showed little to no egg laying, and a photoperiodic response was not evident. Animals that were collected in either winter or spring and maintained in warm water showed little or no spontaneous egg laying throughout the study, regardless of photoperiod. As with the autumn animals, *Aplysia* individuals obtained in summer and kept on short days and warm water laid eggs more frequently than those kept on long days and warm water. These results provide the first evidence that the reproductive system of *A. californica* is responsive to photoperiod. Overall, the data suggest that warm water is permissive for egg laying, and that short days can further stimulate this behavior. However, there is a strong inhibition of spontaneous egg laying during the winter and spring, which neither warm water nor short photoperiod can overcome. The role of the eyes in mediating the photoperiodic response was also investigated. A control group of intact animals kept on short days laid eggs more frequently than those on long days, but this photoperiodic response was not evident in eyeless animals. These results suggest that the eyes play a role in mediating the effects of photoperiod on egg laying behavior.

Received 12 August 1991; accepted 31 October 1991.

Introduction

Like many animals living in the temperate zone, the marine mollusk *Aplysia californica* breeds seasonally. Both field and laboratory observations indicate that this species is reproductively competent during the summer and autumn, and reproductively quiescent during the winter and spring (Strumwasser *et al.*, 1969; Audesirk, 1979; Berry, 1982). The onset of the breeding season is indicated by a significant increase in the incidence of copulation and egg laying (Strumwasser *et al.*, 1969; Audesirk, 1979), as well as increased synthesis of the hormone that controls egg laying (egg laying hormone; Berry, 1982).

Earlier work has shown that egg laying hormone, a peptide synthesized and secreted by the neuroendocrine bag cells, is responsible for triggering egg-laying behavior (Strumwasser *et al.*, 1969; Kupfermann, 1970; Arch, 1972; Dudek *et al.*, 1980; Stuart *et al.*, 1980; Chiu and Strumwasser, 1981; Blankenship *et al.*, 1983). Although much is known about the molecular biology of bag-cell peptides (Chiu *et al.*, 1979; Heller *et al.*, 1980; Scheller *et al.*, 1982; Mahon and Scheller, 1983) and about the electrophysiological properties of bag cells (Kupfermann and Kandel, 1970; Kaczmarek *et al.*, 1978, 1982; Kaczmarek and Strumwasser, 1981), the seasonal regulation of bag-cell activity and egg laying remains obscure. The general goal of this and future studies is to gain insight into the mechanisms underlying seasonal fluctuations in egg laying behavior and in reproductive neuroendocrine function.

The occurrence of reproductive activity at a particular time of year suggests the involvement of some environmental timing agent (*e.g.*, ambient temperature, photoperiod, food availability, specific nutritional cue). Previous studies in *Aplysia* have shown that warm water can stimulate egg laying, whereas cold temperatures inhibit this behavior (Berry, 1984; Pinsker and Parsons, 1985). Although the authors interpreted their results to suggest that changes in the rate of egg laying are solely dependent on seasonal cycles of temperature, the studies did not test for effects of other environmental variables, such as photoperiod.

The annual cycle of photoperiod is the most regular and predictable environmental factor, and is therefore used by a wide variety of temperate-zone species to time reproduction to the appropriate season (mammals: Turek and Campbell, 1979; birds: Rowan, 1926; reptiles: Licht, 1967; insects: Lees, 1966; terrestrial slugs: Sokolove *et al.*, 1984). *A. californica* are intertidal organisms, spending much of their time near the water surface (Audesirk, 1979); thus they would be exposed to annual changes in day length. *A. californica* might use photoperiodic information, as well as temperature cues, to synchronize reproduction to a particular time of year. The main goal of this study was to determine whether egg laying behavior can be influenced by photoperiodic signals.

Materials and Methods

General

Specimens of *Aplysia californica* (200–300 g) were captured off the coast of California (approximately 34°N latitude) by Alacrity Marine Supply, Redondo Beach, California. At the collection sites, the annual range in water temperature is from approximately 10 to 20°C (Dan Stark, Alacrity Marine Supply, pers. comm.), and the annual range in photoperiod is from 11 to 15.5 h light/day (includes 1 h civil twilight). Upon arrival in the laboratory, animals were maintained in temperature- and light-controlled seawater tanks (475 liters; light intensity at water surface was 700 lux as measured with a photographic light meter). Water was recirculated through undergravel filters within the tanks. Treatment groups (initially, 12 animals per group; 0–3 animals/group died during the course of the studies) were maintained in separate tanks, and all animals were kept in single, perforated plastic buckets (20 cm in diameter) so that each individual could be monitored throughout the studies.

To document the egg laying capability (*i.e.*, reproductive maturity) of each animal, atrial gland extract was injected into the hemolymph of all animals upon arrival in the laboratory (Nagle *et al.*, 1985). Animals with a mature reproductive system will lay eggs in response to atrial gland extract, while immature animals will not lay eggs. An *Aplysia* that did not lay eggs spontaneously during the course of the studies was again treated with atrial gland extract at the end of each study to assess maturity. Only those animals that were reproductively mature by the end of the studies were included in the analysis. Animals were fed a combination of Romaine lettuce and dried seaweed (Msubi Nori, Japan Food Corp.) daily. Egg masses were recorded daily from individual buckets. Because *Aplysia* lays eggs at a maximal rate of once per day and does not consume its own eggs (unpub. obs.), the presence or absence of an egg mass is an excellent indication of whether an animal exhibited egg laying behavior on any given day.

The effects of photoperiod on egg laying behavior were determined as follows. Specimens of *Aplysia* were collected and shipped to our seawater facilities at four different times of year. Animals that arrived in the early AUTUMN 1988 (Sept. 22) were all reproductively mature at the beginning of the study and were divided into four treatment groups. *Aplysia* individuals were kept either on short days (8 h light/day) or on long days (16 h light/day); animals on these two photoperiods were further divided and maintained either in warm (20°C) or in cold (15°C) water. Thus the combined effects of photoperiod and water temperature on egg laying could be investigated. Animals maintained in cold water rarely, if ever, layed eggs, so we dropped the cold-water group from the remaining studies. *Aplysia* individuals that arrived in the early WINTER 1989 (Jan. 3) and the early SPRING 1989 (Mar. 31) were reproductively immature at the beginning of the studies; but they had all reached maturity by the end of the experiments. In these two studies, all animals were maintained in warm water and kept either on short or on long days. *Aplysia* individuals that arrived in the early SUMMER 1989 (June 23) were reproductively mature at the beginning of the study and were maintained in warm water and kept either on short or on long days.

The role of the eyes in mediating the effects of photoperiod on egg laying was investigated with specimens of *Aplysia* that were brought to the laboratory in the late SUMMER 1990 (Aug. 7) and maintained in warm water and 14.25 h light/day (photoperiod in mid-August at 34°N latitude) for three days. All of these animals were immobilized with $MgCl_2$ (injected into hemolymph); half of them were bilaterally enucleated, and the other half served as intact controls. Following surgery, animals were further divided and kept either on short (8 h light/day) or on long days (16 h light/day), making a total of four treatment groups.

Analysis of data

Differences in egg laying between treatment groups were assessed by Chi-square analysis. Values were significantly different if $P < 0.05$.

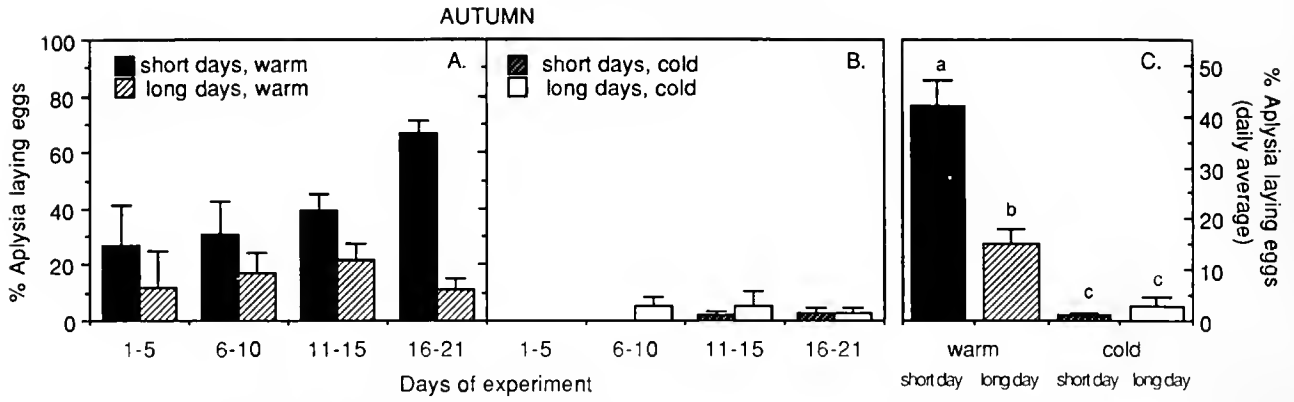

Figure 1. Percent of *Aplysia* individuals laying eggs during the early AUTUMN 1988. Panel A: Animals were kept in warm (20°C) water and either short (8 h light/day) or long (16 h light/day) days. Data were averaged (+sem) into 5-day bins. Panel B: Animals were kept in cold (15°C) water and either short (8 h light/day) or long (16 h light/day) days. Data are presented as in panel A. Panel C: Data from the 4 groups are presented as the percent of animals laying eggs each day, averaged (+sem) over the entire 21-day study. Different letters indicate values are significantly different (at least $P < 0.05$).

Results

Photoperiodic effects on egg laying

Overall, photoperiod and temperature can both affect the frequency of egg laying. In the AUTUMN, *Aplysia* individuals kept in warm water laid eggs more frequently than those kept in cold water (Fig. 1). Furthermore, animals maintained on short days and warm water laid eggs more frequently than those kept on long days and warm water. However, in the WINTER (Fig. 2) and in the SPRING (Fig. 3), egg laying frequency overall was suppressed in all groups (even though animals were reproductively mature by the end of the studies; see Materials and Methods), and there was no apparent effect of photoperiod on egg laying. In the SUMMER (Fig. 4), we once again observed the emergence of a photoperiodic effect: *Aplysia* maintained on short days and warm water laid eggs more frequently than those kept on long days and warm water. This photoperiodic response in the summer was not as robust as that seen during the previous autumn (compare Figs. 1c and 4b).

Photoperiodic effects in intact vs. eyeless animals

The eyes appear to play a role in transducing photoperiodic information to the reproductive axis responsible for regulating egg laying (Fig. 5). Once again, control animals kept in short days and warm water laid eggs more frequently than those kept on long days and warm water.

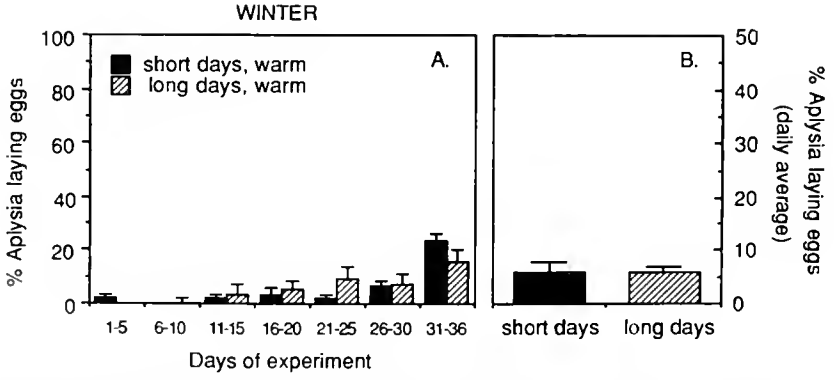

Figure 2. Percent of *Aplysia* individuals laying eggs during the early WINTER 1989. Animals were kept in warm (20°C) water and either short (8 h light/day) or long (16 h light/day) days. Panel A: Data were averaged (+sem) into 5-day bins. Panel B: Data are presented as the percent of animals laying eggs each day, averaged (+sem) over the entire study. There was no significant difference between the values of the two groups.

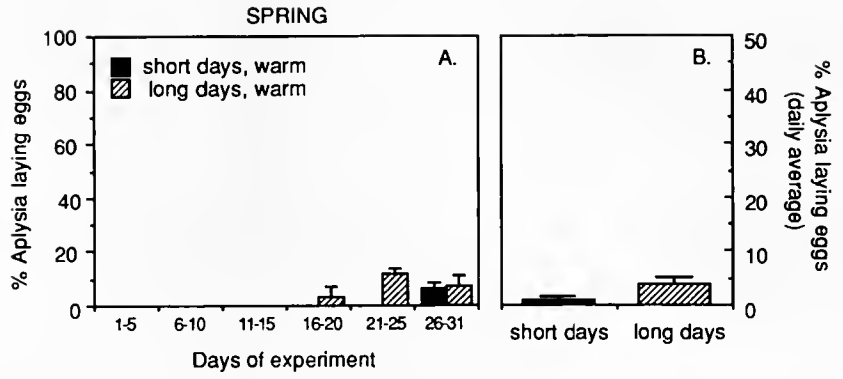

Figure 3. Percent of *Aplysia* individuals laying eggs during the early SPRING 1989. Data are presented as in Figure 2.

On the other hand, there was no significant difference in the frequency of egg laying between the two eyeless groups. Although the photoperiodic response in the intact control group was significant, it was not nearly as robust as that seen in a previous study (see Fig. 1).

Discussion

This study provides the first evidence that the reproductive system of *Aplysia* is responsive to photoperiodic signals. The results suggest that both photoperiod and temperature can influence the seasonal rhythm of egg laying. Specifically, warm temperature is permissive for the expression of the stimulatory effects of short days. Studies in another poikilotherm, the lizard *Anolis carolinensis*, have also documented that the reproductive response to stimulatory day lengths is evident in warm, but not cool, temperatures (Licht, 1967). In addition, recent work in the edible snail *Helix pomatia* has shown that egg-laying behavior is regulated by both photoperiod and temperature cues (Gomot, 1990). In the wild, the reproductive activity of *Aplysia californica* peaks in late summer-autumn (Strumwasser *et al.*, 1969; Audesirk, 1979; Berry, 1982). At this time of year, water temperature is reaching a maximum off the coast of California, and day length is decreasing. Our findings that warm water and short days stimulate egg laying are therefore consistent with the behavior of the animal in its natural environment.

Animals brought to the laboratory in the winter and spring layed eggs infrequently, if at all, regardless of environmental treatment. That is, an average of less than 10% of the winter and spring animals laid eggs on any given day during the course of the two studies—even under stimulatory conditions of short days and warm water. Although these animals were reproductively immature at the onset, towards the end of the studies they had reached maturity and were capable of laying eggs following hormonal stimulation (see Materials and Methods). Therefore, ovotesticular function was most likely not the limiting factor in these studies (however, we do not know when during the studies animals attained reproductive maturity).

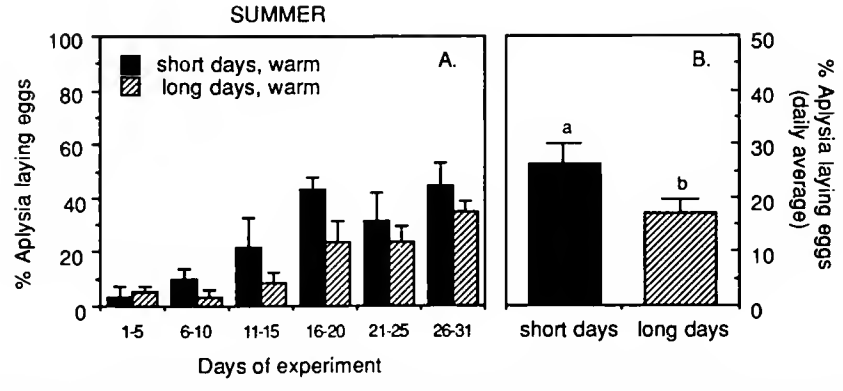

Figure 4. Percent of *Aplysia* individuals laying eggs during the early SUMMER 1989. Data are presented as in Figure 2. In Panel B, different letters indicate values are significantly different ($P < 0.05$).

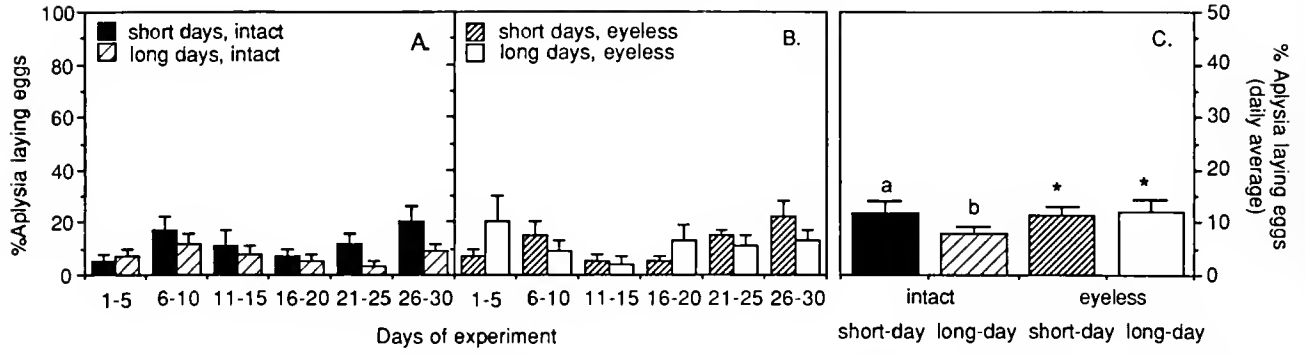

Figure 5. Percent of *Aplysia* individuals laying eggs during the late SUMMER 1990. All animals were maintained in warm (20°C) water. Panel A: Intact, control animals were kept on short (8 h light/day) or long (16 h light/day) days. Data were averaged (+sem) into 5-day bins. Panel B: Bilaterally enucleated animals were kept on short (8 h light/day) or long (16 h light/day) days. Data are represented as in panel A. Panel C: Data from the 4 groups are presented as the percent of animals laying eggs each day, averaged (+sem) over the entire 30-day study. The letters a and b indicate values that are significantly different ($P < 0.05$). *Indicates that values approached significant difference compared to that of the intact, long-day control group ($P < 0.10$).

A common phenomenon among some seasonally breeding vertebrates is a spontaneous shutdown of the reproductive system during the non-breeding season (lizard: Cueller and Cueller, 1977; birds: Hamner, 1967; Robinson and Follett, 1982; mammal: Robinson and Karsch, 1984). During this period of reproductive quiescence, previously inductive photoperiodic cues no longer stimulate reproductive activity. This period of insensitivity to stimulatory photoperiod (commonly labelled 'photorefractoriness') is an endogenous process and can be 'broken' by exposing the animal to a bout of inhibitory photoperiod, followed by a stimulatory day length (Jackson *et al.*, 1988). In *Aplysia*, we have shown that previously stimulatory environmental cues (warm water, short days) did not stimulate spontaneous egg laying during the non-breeding season in winter and spring. *Aplysia* may therefore behave like many other seasonal breeders and become refractory to stimulatory signals. If this is so, then pretreatment with long days and cold temperatures should be able to break refractoriness to stimulatory short days and warm temperatures.

But mechanisms other than an endogenous refractoriness to an environmental signal might equally well underlie the cessation of spontaneous egg laying by *Aplysia* during winter and spring. For instance, one or more key components of the reproductive neural axis may be developmentally immature during the winter and spring (even though the reproductive tract can mature in the laboratory). Alternatively, some environmental cue (*e.g.*, food or other nutritional item necessary for high levels of spontaneous egg laying) may be missing during that time of year.

Further, our results suggest that the eyes play a role in mediating photoperiodic information to the reproductive axis responsible for regulating egg laying behavior. Specifically, photoperiod had no effect on egg laying in those animals that were bilaterally enucleated. The eyes of *Aplysia* contain both photoreceptors and a circadian pacemaker (Jacklet, 1969; Eskin, 1971). The circadian system is involved in the neural pathway mediating photoperiodic responses in most animals investigated (Follett and Sharp, 1969; Elliott, 1976; Almeida and Lincoln, 1982). Furthermore, both ocular and extraocular photoreceptors mediate photoperiodic responses in a variety of species (Reiter, 1969; Follett *et al.*, 1975; Legan and Karsch, 1983; Foster and Follett, 1985). In *Aplysia*, photoreceptors are found not only in the eye, but also in structures as diverse as the abdominal ganglion (Andresen and Brown, 1982), the cerebral ganglion (Block and Smith, 1973), the rhinophores (Jacklet, 1980), the oral veil (Cook *et al.*, 1991), and the siphon (Lukowiak and Jacklet, 1972). Therefore, the relative roles of the ocular photoreceptors and ocular pacemakers in mediating the effects of photoperiod on egg laying are not clear. For instance, both the ocular photoreceptors and ocular pacemakers may be playing a role in photoperiodic time measurement. Alternatively, extraocular photoreceptors may be transmitting light signals to the ocular circadian pacemaker, which then sends its signals to the next step in the photoperiodic response system.

Nevertheless, we must stress that our results are difficult to interpret, because the photoperiodic response in the intact controls in the last experiment was weak compared to that seen in the first experiment (compare Fig. 1 with

Fig. 5). An intriguing mystery arising from these studies is the source of the variability in the photoperiodic response from one year to the next. Because we work with animals captured in the wild, we have no control over the environmental history of the animal. That is, we cannot control for variations in microhabitat (*i.e.*, local and year-to-year variability in water temperature, food availability, sexual experience). Large, year-to-year fluctuations in the availability of the algae that *Aplysia* feed upon were observed during the course of these experiments: algae were abundant in the summer to early autumn of 1988, but scarce in the summer to early autumn of 1989 and 1990 (Dan Stark, Alacrity Marine Supply, pers. comm.); and these fluctuations were associated with similar changes in the robustness of the photoperiodic response. In addition to photoperiodic and temperature signals, there are other environmental variables (*e.g.*, food or nutritional cues) that might affect spontaneous egg laying. All of these environmental cues may act in combination such that one variable alters the effectiveness of the other variables on the frequency of egg laying. For instance, the photoperiodic response during the breeding season may be more robust in those animals with a high level of nutrition; low nutrition may weaken the photoperiodic response. Food availability has pronounced effects on the photoperiodic diapause response in some insect species (Saunders, 1979). Future work investigating the role of food cues may provide some information on its importance in the expression of a robust photoperiodic response in *Aplysia*.

Acknowledgments

This work was supported by NIH grants NS-08725 to NLW and NS-15264 to GDB.

Literature Cited

Andresen, M. C., and A. M. Brown. 1982. Cellular basis of the photoresponse of an extraretinal photoreceptor. *Experientia* **38**: 1001–1006.

Almeida, O. F. X., and G. A. Lincoln. 1982. Photoperiodic regulation of reproductive activity in the ram: evidence for the involvement of circadian rhythms in melatonin and prolactin secretion. *Biol. Reprod.* **27**: 1062–1075.

Arch, S. 1972. Biosynthesis of the egg-laying hormone (ELH) in the bag cell neurons of *Aplysia californica*. *J. Gen. Physiol.* **60**: 102–119.

Audesirk, T. E. 1979. A field study of growth and reproduction in *Aplysia californica*. *Biol. Bull.* **157**: 407–421.

Berry, R. W. 1982. Seasonal modulation of synthesis of the neurosecretory egg-laying hormone of *Aplysia*. *J. Neurobiol.* **13**: 327–335.

Berry, R. W. 1984. Environmental temperature modulates the rate of synthesis of egg-laying hormone in *Aplysia*. *J. Comp. Physiol. B* **154**: 545–548.

Blankenship, J. E., M. K. Rock, L. C. Robbins, C. A. Livingston, and H. K. Lehman. 1983. Aspects of copulatory behavior and peptide control of egg laying in *Aplysia*. *Fed. Proc.* **42**: 96–100.

Block, G. D., and J. T. Smith. 1973. Cerebral photoreceptors in *Aplysia*. *Comp. Biochem. Physiol.* **46a**: 115–121.

Chiu, A. Y., and F. Strumwasser. 1981. An immunohistochemical study of the neuropeptidergic bag cells of *Aplysia*. *J. Neurosci.* **1**: 812–826.

Chiu, A. Y., M. W. Hunkapiller, E. Heller, D. K. Stuart, L. E. Hood, and F. Strumwasser. 1979. Purification and primary structure of the neuropeptide egg-laying hormone of *Aplysia californica*. *Proc. Natl. Acad. Sci.* **76**: 6656–6660.

Cook, D. G., M. Stopfer, and T. J. Carew. 1991. Identification of a reinforcement pathway necessary for operant conditioning of head waving in *Aplysia californica*. *Behav. Neural Biol.* **55**: 313–337.

Cueller, H. S., and O. Cueller. 1977. Refractoriness in female lizard reproduction: a probable circannual clock. *Science* **197**: 495–497.

Dudek, F. E., G. Weir, J. Acosta-Urquidi, and S. S. Tobe. 1980. A secretion from neuroendocrine bag cells evokes egg release *in vitro* from ovotestis of *Aplysia californica*. *Gen. Comp. Endocrinol.* **40**: 241–244.

Elliott, J. A. 1976. Circadian rhythms and photoperiodic time measurement in mammals. *Fed. Proc.* **35**: 2339–2346.

Eskin, A. 1971. Properties of the *Aplysia* visual system: *in vitro* entrainment of the circadian rhythm and centrifugal regulation of the eye. *Z. Vgl. Physiol.* **74**: 353–371.

Follett, B. K., and P. J. Sharp. 1969. Circadian rhythmicity in photoperiodically induced gonadotropin release and gonadal growth in the quail. *Nature* **223**: 968–971.

Follett, B. K., D. T. Davies, and V. Magee. 1975. The rate of testicular development in Japanese quail (*Coturnix coturnix japonica*) following stimulation of the extra-retinal photoreceptor. *Experientia* **31**: 48–49.

Foster, R. G., and B. K. Follett. 1985. The involvement of rhodopsin-like photopigment in the photoperiodic response of the Japanese quail. *J. Comp. Physiol. A* **157**: 519–528.

Gomot, A. 1990. Photoperiod and temperature interaction in the determination of reproduction of the edible snail, *Helix pomatia*. *J. Reprod. Fert.* **90**: 581–585.

Hamner, W. M. 1967. The photorefractory period of the house finch. *Ecology* **49**: 211–227.

Heller, E., L. K. Kaczmarek, M. W. Hunkapiller, L. E. Hood, and F. Strumwasser. 1980. Purification and primary structure of two neuroactive peptides that cause bag cell afterdischarge and egg-laying in *Aplysia*. *Neurobiology* **77**: 2328–2332.

Jacklet, J. W. 1969. Circadian rhythm of optic nerve impulses recorded in darkness from isolated eye of *Aplysia*. *Science* **164**: 562–563.

Jacklet, J. W. 1980. Light sensitivity of the rhinophores and eyes of *Aplysia*. *J. Comp. Physiol.* **136**: 257–262.

Jackson, G. L., M. Gibson, and D. Kuehl. 1988. Photoperiodic disruption of photorefractoriness in the ewe. *Biol. Reprod.* **38**: 127–134.

Kaczmarek, L. K., and F. Strumwasser. 1981. The expression of long lasting afterdischarge by isolated *Aplysia* bag cell neurons. *J. Neurosci.* **1**: 626–634.

Kaczmarek, L. K., K. Jennings, and F. Strumwasser. 1978. Neurotransmitter modulation, phosphodiesterase inhibitor effects, and cyclic AMP correlates of afterdischarge in peptidergic neurites. *Proc. Natl. Acad. Sci.* **75**: 5200–5204.

Kaczmarek, L. K., K. R. Jennings, and F. Strumwasser. 1982. An early sodium and late calcium phase in the afterdischarge of peptide-secreting neurons in *Aplysia*. *Brain Res.* **238**: 105–115.

Kupfermann, I. 1970. Stimulation of egg laying by extracts of neuroendocrine cells (bag cells) of abdominal ganglion of *Aplysia*. *J. Neurophysiol.* **33**: 877–881.

Kupfermann, I., and E. R. Kandel. 1970. Electrophysiological properties and functional interconnections of two symmetrical clusters (bag cells) in abdominal ganglion of *Aplysia*. *J. Neurophysiol.* **33**: 865–876.

Legan, S. J., and F. J. Karsch. 1983. Importance of retinal photoreceptors to the photoperiodic control of seasonal breeding in the ewe. *Biol. Reprod.* **29:** 316–325.

Lees, A. D. 1966. Photoperiodic timing mechanisms in insects. *Nature* **210:** 986–989.

Licht, P. 1967. Environmental control of annual testicular cycles in the lizard *Anolis carolinensis*. I. Interaction of light and temperature in the initiation of testicular recrudescence. *J. Exp. Zool.* **165:** 505–516.

Lukowiak, K., and J. W. Jacklet. 1972. Habituation and dishabituation: interactions between peripheral and central nervous systems in *Aplysia*. *Science* **178:** 1306–1308.

Mahon, A. C., and R. H. Scheller. 1983. The molecular basis of neuroendocrine fixed action pattern: egg laying in *Aplysia*. *Cold Spring Harbor Symp. Quant. Biol.* **48:** 405–412.

Nagle, G. T., S. D. Painter, K. L. Kelner, and J. E. Blankenship. 1985. Atrial gland cells synthesize a family of peptides that can induce egg laying in *Aplysia*. *J. Comp. Physiol. B* **156:** 43–55.

Pinsker, H. M., and D. W. Parsons. 1985. Temperature dependence of egg laying in *Aplysia brasiliana* and *A. californica*. *J. Comp. Physiol. B* **156:** 21–27.

Reiter, R. J. 1969. Pineal function in long term blinded male and female golden hamsters. *Gen. Comp. Endocrinol.* **12:** 460–468.

Robinson, J. E., and B. K. Follett. 1982. Photoperiodism in Japanese quail: the termination of seasonal breeding by photorefractoriness. *Proc. R. Soc. London B* **215:** 95–116.

Robinson, J. E., and F. J. Karsch. 1984. Refractoriness to inductive day lengths terminates the breeding season of the Suffolk ewe. *Biol. Reprod.* **31:** 656–663.

Rowan, W. 1926. On photoperiodism, reproductive periodicity, and the annual migrations of birds and certain fishes. *Proc. Boston Soc. Natl. Hist.* **38:** 147–189.

Saunders, D. S. 1979. *Insect Clocks*. Pergamon Press, New York. Pp. 102–107.

Scheller, R. H., J. F. Jackson, L. B. McAllister, J. H. Schwartz, E. R. Kandel, and R. Axel. 1982. A family of genes that codes for ELH, a neuropeptide eliciting a stereotyped pattern of behavior in *Aplysia*. *Cell* **28:** 707–719.

Sokolove, P. G., E. J. McCrone, J. van Minnen, and W. C. Duncan. 1984. Reproductive endocrinology and photoperiodism in a terrestrial slug. Pp. 189–203 in *Photoperiodic Regulation of Insect and Molluscan Hormones*. Pitman, London.

Strumwasser, F., J. W. Jacklet, and R. B. Alvarez. 1969. A seasonal rhythm in the neural extract induction of behavioral egg-laying in *Aplysia*. *Comp. Biochem. Physiol.* **29:** 197–206.

Stuart, D. K., A. Y. Chiu, and F. Strumwasser. 1980. Neurosecretion of egg-laying hormone and other peptides from electrically active bag cell neurons of *Aplysia*. *J. Neurophysiol.* **43:** 488–498.

Turek, F. W., and C. S. Campbell. 1979. Photoperiodic regulation of neuroendocrine-gonadal activity. *Biol. Reprod.* **20:** 32–50.

Reference: *Biol. Bull.* **182**: 15–30. (February, 1992)

The Development and Larval Form of an Echinothurioid Echinoid, *Asthenosoma ijimai*, Revisited

S. AMEMIYA[1] AND R. B. EMLET[2]*

[1]*Misaki Marine Biological Station, Miura-shi, Kanagawa 238-02, Japan and* [2]*Department of Biological Sciences, University of Southern California, Los Angeles, California 90089-0371*

Abstract. The modified development from cleavage to late larval form of the echinothurioid echinoid, *Asthenosoma ijimai*, was re-examined using light microscopy and scanning electron microscopy of whole and sectioned stages. Although an original study (Amemiya and Tsuchiya, 1979) reported direct development without evidence of a pluteus larva, we found that the unusual development can be interpreted as a topologically reflected, reduced pluteus, with vestigial larval arms and a greatly reduced larval skeleton. This developmental pattern produces the third and most reduced pluteus form known among the six echinoid lineages with modified development that have been studied thus far. Features such as an equal fourth cleavage, extrusion of yolk into the blastocoel, and the presence of large numbers of cells within the blastocoel are convergent with traits reported for other species with modified development. Coelom formation is clearly modified from that of species with feeding larval development, but notably the hydrocoel begins to develop podial buds prior to separation from the archenteron. Echinothurioid sea urchins are considered to be the most primitive living euechinoids, and in *A. ijimai* the timing of mesenchyme cell ingression and the formation of epineural folds were similar to these features in other euechinoids. Indentation of the juvenile oral surface relatively late in larval development raises the possibility that the amniotic invagination (vestibule), common in all other euechinoids, may be a trait incorporated into the development of echinoids at the time of origin of the echinothurioids. The structural comparisons reported here show a need for further detailed morphological studies of developmental modifications in other echinoid species.

Received 31 July 1991; accepted 25 November 1991.

* Order of authorship was determined alphabetically.

Introduction

Most sea urchins species (*ca.* 66%) develop through a feeding larval stage, the echinopluteus, for several to many weeks before metamorphosing into juvenile echinoids (see review by Emlet *et al.*, 1987). At least 14 times among living taxa, however, the feeding larval stage has been lost, and these species undergo a modified and abbreviated development before juvenile sea urchins are formed (Emlet, 1990; see also Strathmann, 1978; Raff, 1987). At present, about ten species from six of the lineages with modified development have been investigated, and some description of their embryonic and larval development is available. Descriptive and analytical research has been conducted on the following: two cidaroids (*Phyllacanthus imperialis*, Olson *et al.*, 1988; *P. parvispinus*, Mortensen, 1921; Parks *et al.*, 1989); two echinothurioids (*Asthenosoma ijimai*, Amemiya and Tsuchiya, 1979; *A. sp.*, Uehara and Amemiya, unpub. obs.); one temnopleuroid (*Holopneustes purpurescens*, V. Morris, Univ. Sydney, unpub.); one echinometrid (*Heliocidaris erythrogramma*, Mortensen, 1921; Williams and Anderson, 1975; Parks *et al.*, 1988); two clypeasteroids (*Peronella japonica*, Mortensen, 1921; Okazaki and Dan, 1954; Okazaki, 1975; *P. rubra*, Amemiya and Emlet, unpub. obs.); and two brooding spatangoids (*Abatus agassizi*, Larrain, 1973; *A. cordatus*, Schatt, 1985, 1988). Many of the other echinoid lineages with modified development occur in deeper seas or antarctic seas and are difficult to collect for study (*e.g.*, lineages of temnopleuroids, holasteroids and other lineages of cidaroids and spatangoids, *c.f.*, Mortensen, 1936; Fell, 1976).

The most recent studies have focused on species with very highly modified development, often referred to as direct development. These studies have examined heterochrony (changes in relative timing) of developmental events, modifications of cleavage patterns, the resultant cell lineages, and cell movements (*e.g.*, Parks *et al.*, 1988, 1989; Wray and Raff, 1989, 1990; Henry and Raff, 1990). Additional immunofluorescence studies have drawn inferences about gene expression from specific markers for gene products [*e.g.*, the monoclonal antibody B2C2 to mesenchyme-derived antigens or antibodies to serotonergic neurons (above citations, Bisgrove and Raff, 1989)]. Due to the extreme degree of developmental modifications, these studies usually emphasize how different the morphogenetic patterns are from those of species that develop through a pluteus larva (*e.g.*, *Heliocidaris erythrogramma*, Wray and Raff, 1990). With the exception of the above mentioned studies on *Abatus cordatus*, *Heliocidaris erythrogramma*, and *Peronella japonica*, either no information or only limited information is available on the internal morphological aspects of development of species with modified development. Both the extreme modification, and a lack of detailed morphological information, limit our understanding of how these developmental modifications may have evolved.

This report—an extension of an earlier one (Amemiya and Tsuchiya, 1979)—describes selected features of morphogenesis in the echinothurioid echinoid *Asthenosoma ijimai*, from cleavage through late larval development. Comparisons are also made with unmodified pluteal development, as well as with the modified developmental patterns occurring in other species. The echinothurioids are a particularly important group to study: first, because all of them seem to have modified development (reviewed in Emlet *et al.*, 1987); and second, because they are considered to be the earliest living branch of the euechinoid lineage, and thus the second oldest lineage of echinoids after the cidaroids (Smith, 1984). Because the cidaroids and euechinoids differ in many developmental features (Emlet, 1988), we should inquire whether the development of the echinothurioids shows greater affinity with other euechinoids, or with the more primitive cidaroids. The observations presented here, together with the comparisons with other species, point up the need for additional morphological studies of developmental modifications in other echinoid species.

Materials and Methods

Adults and larvae

Adults of *Asthenosoma ijimai* Yoshiwara were collected at a depth of 20 m off Misaki Marine Biological Station in Sagami Bay, Japan. Adult specimens were dissected, and fully matured gametes were obtained. Eggs were washed twice in filtered seawater (0.22 μm) and fertilized by mixing with a small amount of undiluted sperm. Fertilized eggs were washed three times in filtered seawater, and cultured in unstirred, one-liter glass beakers at 20°C or at room temperature (25–28°C). The stages and times for sectioned material presented here are from cultures at room temperature. No food was added to the larval cultures. At various times after fertilization, living larvae were photographed under a dissecting microscope, and aliquots were fixed for examination by light or scanning electron microscopy (SEM).

Preparation of sectioned and stained material

Larvae were fixed for 1 h in seawater containing 4% or 10% formalin at room temperature and preserved in 70% EtOH. Preserved specimens were dehydrated through graded ethanol series and embedded in Spurr embedding media (Polysciences, Inc). Sections, 5–8 μm thick, were stained with Richardson's stain (1% Azure II in distilled water combined with 1% methylene blue in 1% sodium borate, Richardson *et al.*, 1960). The serial sections of larvae embedded in epoxy resin were traced with camera lucida and digitized so that 3-D images of the sections could be constructed (PC3D program, Jandel Scientific, Inc.).

Immunofluorescence and H33258 staining

Immunofluorescence staining with skeletogenic mesenchyme specific monoclonal antibody B2C2 was conducted according to the methods of Parks *et al.* (1988). Embryos, larvae, and juveniles were fixed for 50 min in seawater containing 4% formalin, washed in artificial seawater, dehydrated in a graded ethanol series, embedded in polyester wax (BDH, Ltd), and sectioned at a thickness of 5 μm. The rehydrated sections were washed with phosphate-buffered saline containing 0.05% Tween 20 (PBS-TW20) and incubated with culture fluid containing the monoclonal antibody B2C2, diluted 1:20 in PBS-TW20, for 40 min at room temperature in a humidified chamber. The slides were washed in PBS-TW20, incubated with FITC-conjugated, goat anti-mouse, IgG antibodies (diluted 1:200 in PBS-TW20) for 40 min, and rinsed again. For detection of cell nuclei, some sections were incubated with H33258 (Hechst, Inc.) at a concentration of 0.5 μg/ml PBS for 10 min instead of, or after, treatment in primary and secondary antisera. Fluorescence was observed and photographed with a Nikon fluorescence microscope.

Scanning Electron Microscopy (SEM)

Specimens were fixed and preserved as indicated above, or they were fixed for 1 h in a mixture of 2% gluteraldehyde (Taab Lab.) and 1% osmium tetroxide (OsO_4, Taab Lab.)

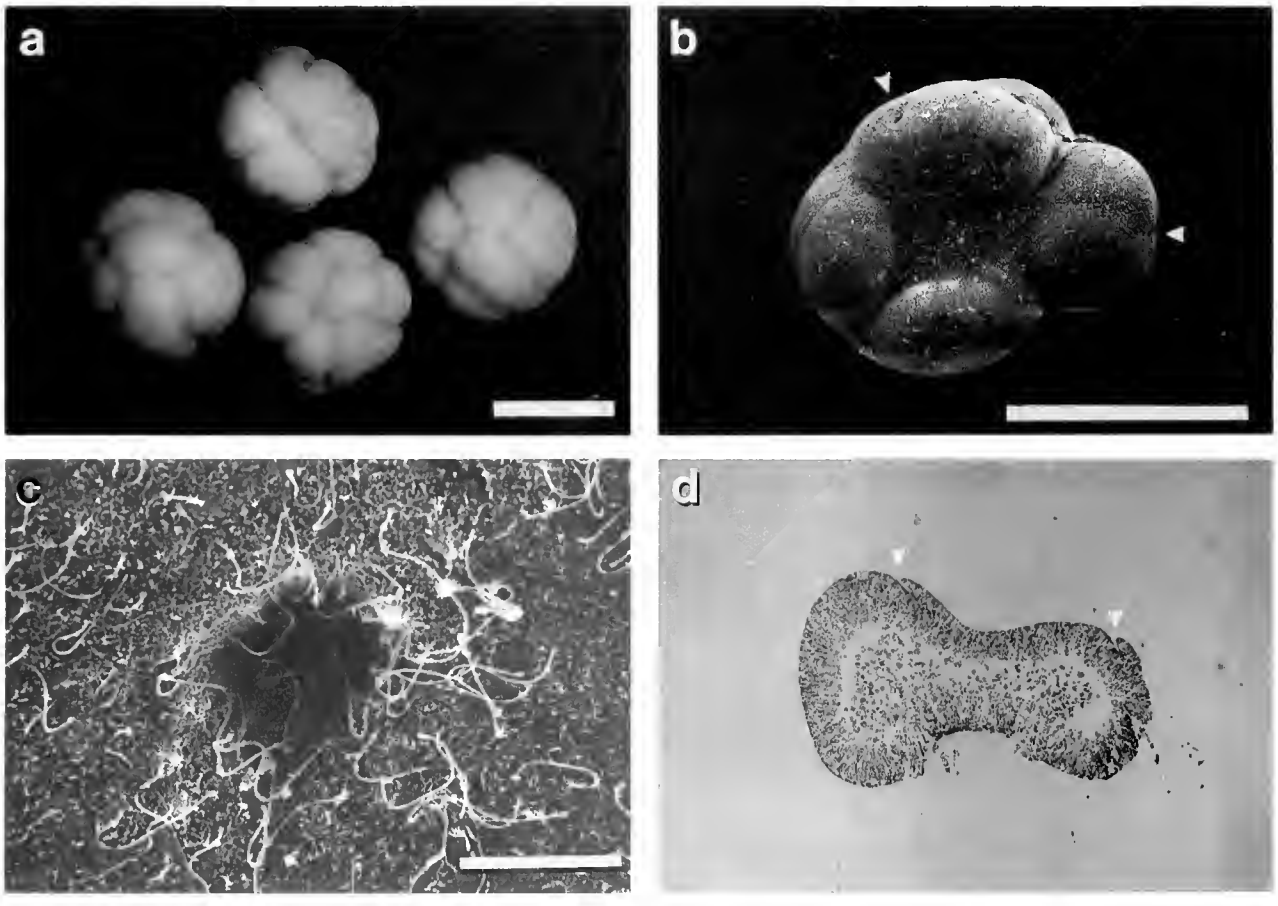

Figure 1. Early embryonic stages of *Asthenosoma ijimai*. a. Sixteen-cell stage embryos randomly oriented, show that all cells are approximately the same diameter after the fourth cleavage. Scale bar, 1 mm. b. SEM of a 21.5-h, lobate blastula. Arrowheads mark pits in ectoderm. Scale bar, 1 mm. c. Close-up SEM of ectodermal pit marked by right arrow in b. Scale bar, 25 μm. d. Section of a 21.5-h blastula shows yolky cytoplasm in the blastocoel and ectodermal pits (arrowheads). Same scale as b.

in 0.45 *M* sodium acetate buffer (pH 6.4) at room temperature (Harris and Shaw, 1984) and preserved in 70% EtOH at 4°C. The preserved specimens were dehydrated through a graded ethanol series, dried at the critical point (Hitachi HCP-1 drier) with liquid CO_2 as a transitional fluid, and sputter-coated with gold (Eiko IB-3 ion coater). Observations were made with a Hitachi HHS-2R SEM. To examine the inside of larvae with SEM, specimens were embedded in polyester wax and sectioned by microtome to expose a particular cross section. These specimens were incubated in absolute ethanol at 40°C for 12 h to remove wax (Armstrong and Parenti, 1973) and then subjected to critical point drying as described above.

Clearing larvae

Live larvae of *Asthenosoma* are opaque orange-yellow (Amemiya and Tsuchiya, 1979), and it was impossible to see internal structures in these or in fixed, preserved specimens. However, larvae could be rendered translucent by clearing with solutions of benzyl benzoate and benzyl alcohol mixed in ratios of 2:1, 1:1, or 1:2, depending on the desired refractive index. Fixed larvae were first dehydrated to 100% EtOH, then transferred into the clearing solution where the remaining EtOH was allowed to evaporate. Upon clearing, larval dimensions remained the same, and no osmotic effects were discerned. To search for calcareous deposits, cleared larvae were observed under crossed-polarized light.

Results

Observations on soft-tissue development

Eggs, cleavage, external aspects of larvae, and metamorphosis have been described by Amemiya and Tsuchiya (1979). The fourth cleavage of embryos of *Asthenosoma ijimai* was almost equal, giving rise to 16 blastomeres of similar size. Figure 1a shows that there was some

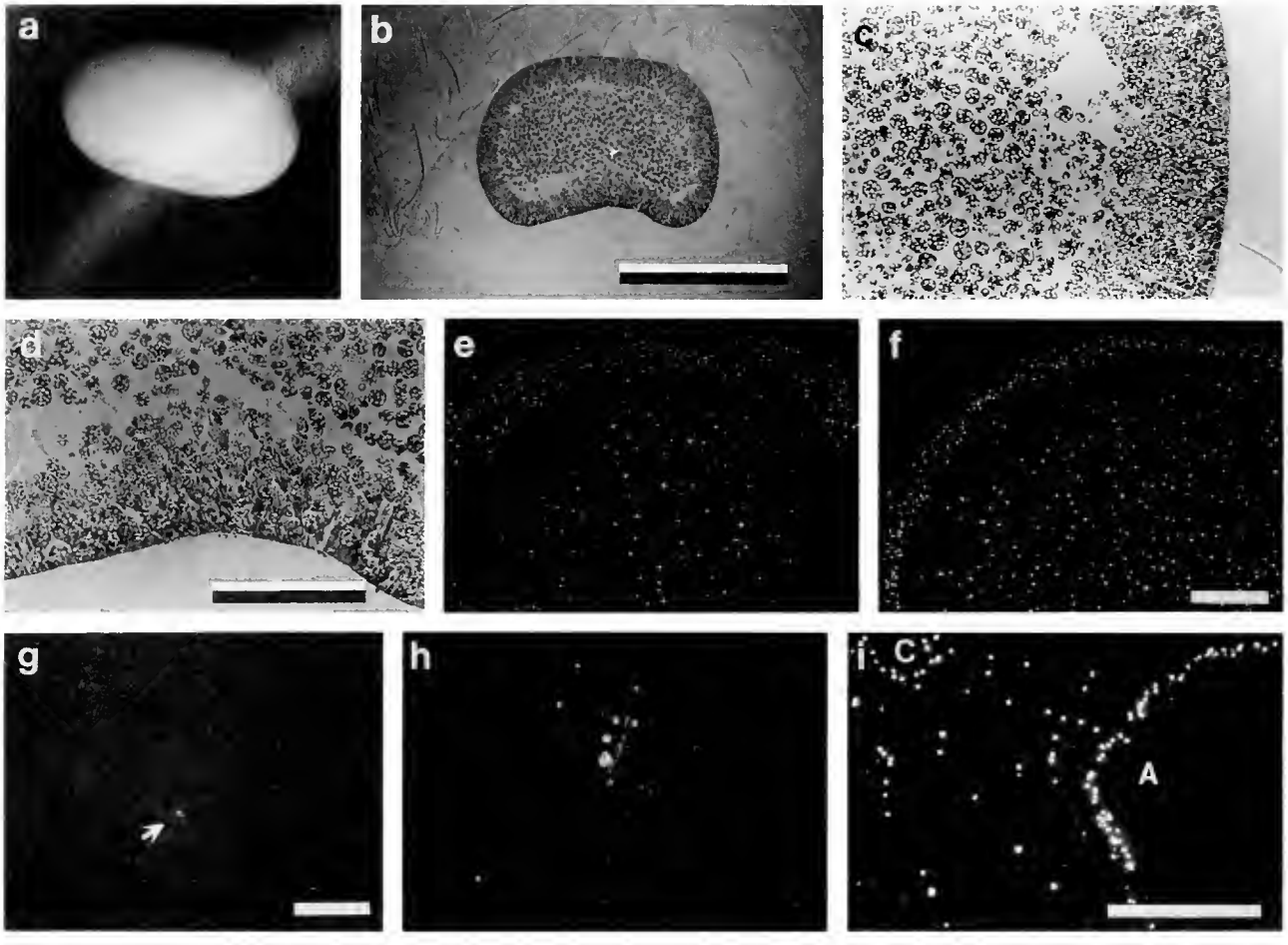

Figure 2. Later embryonic stages of *Asthenosoma ijimai*. All embryos and sections are oriented with the animal pole up. a. Light micrograph of a live, 25.5-h-old, early gastrula. Same scale as b. b. Section through animal-vegetal axis of flattened gastrula (25.5 h), showing blastocoel filled with yolky cytoplasm. Scale bar, 1 mm. c. Lateral wall of gastrula (25.5 h), shows yolky cytoplasm exocytosing from basal ends of ectodermal cells. Same scale as d. d. Vegetal wall of gastrula (25.5 h), showing exocytosis of cytoplasm and ingression of cells. Scale bar, 200 μm. e. Section of a 25.5-h gastrula shows fluorescently staining nuclei (H33258 fluorescent dye) of ectodermal and probable mesenchyme cells. Same scale as f. f. Section of 35-h gastrula, with fluorescently stained nuclei. Scale bar, 200 μm. g. Section of 51.5-h embryo, stained with B2C2 antibody, arrow shows first occurrence of expression of MSP-130 glycoprotein associated with blastocoelic cells. Scale bar, 50 μm. h, i. Section of an 88.5-h larva, doubly stained with B2C2 antibody (h) and H33258 fluorescent dye (i) shows not all blastocoelic cells express MSP-130. The concentrated clusters of nuclei in (i) are epithelia of the archenteron (A) and a coelomic compartment (C). Scale bar, 200 μm.

variation in size of the blastomeres in 16-cell embryos, but there was no evidence of micromeres at the vegetal pole. The absence of an unequal, fourth cleavage parallels the cleavage patterns of other echinoid species large yolky eggs and modified development (Williams and Anderson, 1975; Raff, 1987; Parks *et al.*, 1989).

Like other echinoderm species with yolky eggs, embryos of *Asthenosoma ijimai* formed wrinkled blastulae (Amemiya and Tsuchiya, 1979; Parks *et al.*, 1989). This stage was followed by egression and loss of wrinkles and led to a lobate blastula (Fig. 1b). At this stage, small, cylindrical pits were present on the external surface of the embryo and passed into the ectodermal layer (Fig. 1b, c, d). Serial sections showed that some of these pits terminated blindly within the ectoderm, while others passed through the ectoderm to another external opening. Several of these pits or passages coincided with large indentations in the embryo's surface and, therefore, may have been the remnants of the wrinkled indentations. Parks *et al.* (1989) reported pits in the yolky embryo of the cidaroid *Phyllacanthus parvispinus*, though they did not see any association of pits with egression tracks, where wrinkles diminished. Further work is necessary to determine whether the pits in the two species arise by similar mechanisms.

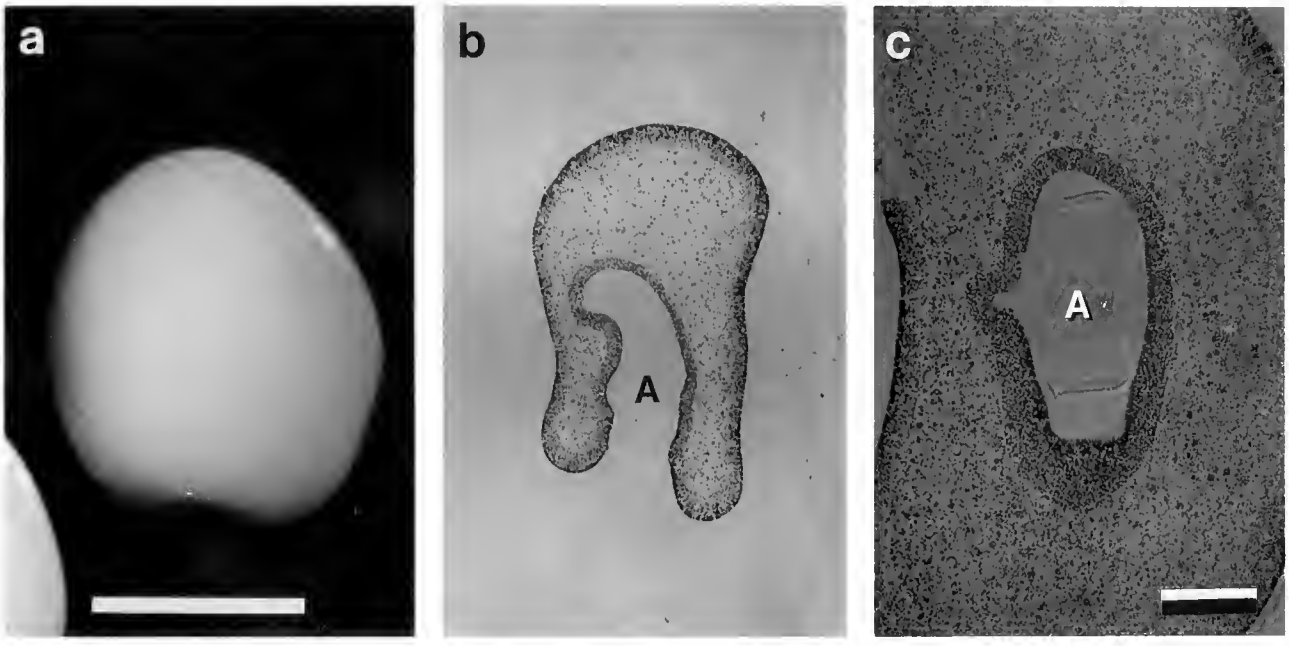

Figure 3. A 51.5-h larvae of *Asthenosoma ijimai*, all with anterior end up. a. Light micrograph of a live larva with dorsal swelling on the right. Scale bar, 1 mm. b. Medial sagittal section through late gastrula. The tip of archenteron (A) has curved toward the ventral surface. Same scale as a. c. Frontal section shows a small outpocketing on the left side of the archenteron (A) that extends dorsally in other sections. Scale bar, 200 μm.

Sections of this 21.5 h stage showed anucleate, yolky cytoplasm being released into the blastocoel from the basal ends of most ectodermal cells (Fig. 1d, see also Fig. 2c, d). Sections also revealed that one indented surface was extruding considerably more material than other surfaces into the blastocoel (Fig. 1d). The fluorescent stain, H33258, revealed considerable numbers of nuclei in the blastocoel, indicating mesenchyme-like cell ingression at the onset of gastrulation.

Gastrulation had begun by 25.5 h after fertilization, and embryos were compressed along the animal-vegetal axis, with a large indentation at the vegetal pole (Fig. 2a). At this stage, the blastocoel was filled with yolky cytoplasm (Fig. 2b, c, d). Counts of fluorescently stained nuclei showed a mean of 98 cells per 5-μm section (n = 3 sections, S.D. = 11) and were scattered among the yolky cytoplasm in the blastocoel (Fig. 2e). The number of staining nuclei, and thus the number of cells, increased to a mean of 375 per section (n = 3 sections, S.D. = 9.6) in the mid-gastrula stage at 35 h (Fig. 2f). The source of these additional blastocoelic cells is either ingression from the vegetal pole (Fig. 2d) or cell division. Fluorescent staining also showed that cell division in the ectoderm was continuing because the number of nuclei in the ectoderm increased between 25.5 and 35 h (Fig. 2e, f).

A positive reaction of B2C2 antibody with blastocoelic cells, indicating expression of MSP-130 glycoprotein, was found first at 51.5 h post fertilization (Fig. 2g). Later observations on mesenchyme cells associated with skeleton in larvae of *Asthenosoma ijimai* showed that these cells reacted with B2C2, suggesting that MSP-130 is expressed by the skeletogenic cells in this species just as in other echinoids. By 88.5 h post fertilization, after skeletogenesis had begun, sections labeled with both nuclear stain (H33258) and B2C2 antibody revealed that only a fraction of blastocoelic cells were skeletogenic (Fig. 2h, i).

In the present paper, the identities of the dorsal and ventral surfaces are reversed from those described in the initial paper on development of *Asthenosoma ijimai* (Amemiya and Tsuchiya, 1979). By 35 h post fertilization, the embryos elongated along the animal-vegetal axis, with the blastopore located off center, toward the ventral surface. At 51.5 h, the late gastrulae had swollen dorsal sides (Fig. 3a). Internally, the archenteron had grown over half the length of the embryo, and the apical (anterior) end curved toward the ventral side of the embryo (Fig. 3b). In addition to the large curved tip of the archenteron, another small outpocketing was forming on the left side of the archenteron and was growing dorsally (Fig. 3c).

Serial sections of stages at 51.5, 56.5, and 63 h post-fertilization showed progressive changes in the development of the archenteron and coelomic pouches (Fig. 4). When the archenteron reached its full length, one or two slender, epithelial projections on the left side and an-

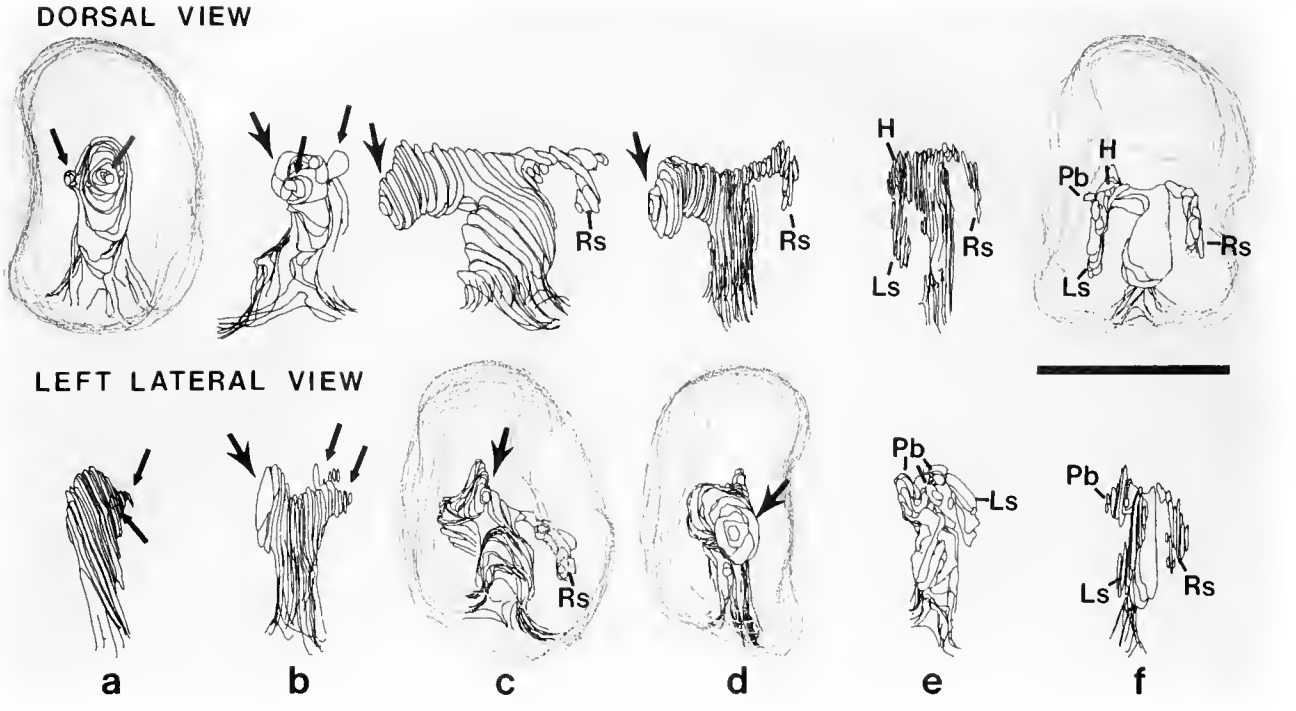

Figure 4. Three-dimensional reconstructions of the archenteron and coelomic pouches from serial sections of 51.5-, 56.5-, and 63-h larvae of *Asthenosoma ijimai*. In each column the same larva is shown in approximate dorsal view and approximate left lateral view. The animal pole, corresponding to the anterior end, is toward the top of the figure; the vegetal pole, corresponding to the posterior end, is toward the bottom of the figure. Line segments are tracings of the inner surface of the archenteron and coelomic pouches (black). The outer surface of the larval ectoderm (gray) is included in a, c, d and f for reference. Small arrows, left lateral and dorsal projections from archenteron; large arrow, tip of archenteron; Rs, right somatocoel; Ls, left somatocoel; H, hydrocoel; Pb, podial bud of hydrocoel. See text for explanation. a., b. 51.5 h. c., d. 56.5 h. e., f. 63 h. Scale bar, 1 mm.

terodorsal surface of the archenteron grew dorsally (small arrows, Fig. 4a, b). Of the three 51.5-h specimens that were serially sectioned, two showed both projections (Fig. 4a, b), and one showed a left lateral projection only (not figured). With further development, the much larger ventral tip of the archenteron bent and extended ventrally without contacting the blastocoel wall (large arrow, Fig. 4b, c). Between 51.5 and 56.5 h, the archenteron underwent torsion, twisting approximately 90° counterclockwise, when viewed from the animal pole. This twist reoriented the tip of the archenteron toward the left side of the larva, and the slender projections toward the right side of the larva (Fig. 4b, c). One of the two slender projections extended laterally and posteriorly (toward the vegetal end) to form the right somatocoel (Fig. 4c–f). Comparisons among serially sectioned larvae suggest that either of the slender projections could form the right somatocoel, and the other slender projection apparently did not continue to grow. Subsequent to 56.5 h, the tip of the archenteron grew a projection dorsally and posteriorly, which formed the left somatocoel (Fig. 4e, f). By 63 h, while still attached to the main body of the archenteron, the tip of the archenteron began to develop into the left hydrocoel with buds that became the coelomic lining of the five, primary podia (Fig. 4e, f; Fig. 5c, d).

Externally, changes between the 56.5 and 63 h stages produced four large and rounded lobes that grew into projections called "para-arms" by Amemiya and Tsuchiya (1979). One pair of these bilaterally symmetrical projections is located dorsally and laterally relative to the blastopore and projects posteriorly, away from the animal pole. The second pair is located on the dorsal surface just anterior to the other pair and also projects dorsally (Fig. 5a). The surfaces of the larvae were uniformly ciliated (Fig. 5b). No developing stages, even in the region of the para-arms, showed cilia collected into discrete rows such as found in the ciliated bands of pluteus larvae. No dorsal hydropore was present despite internal development of somatocoels and the left hydrocoel.

By 75.5 h post-fertilization, the five bulges of the primary podia were externally visible and arranged in a circle on the left lateral surface (Fig. 6a). Sections of this stage

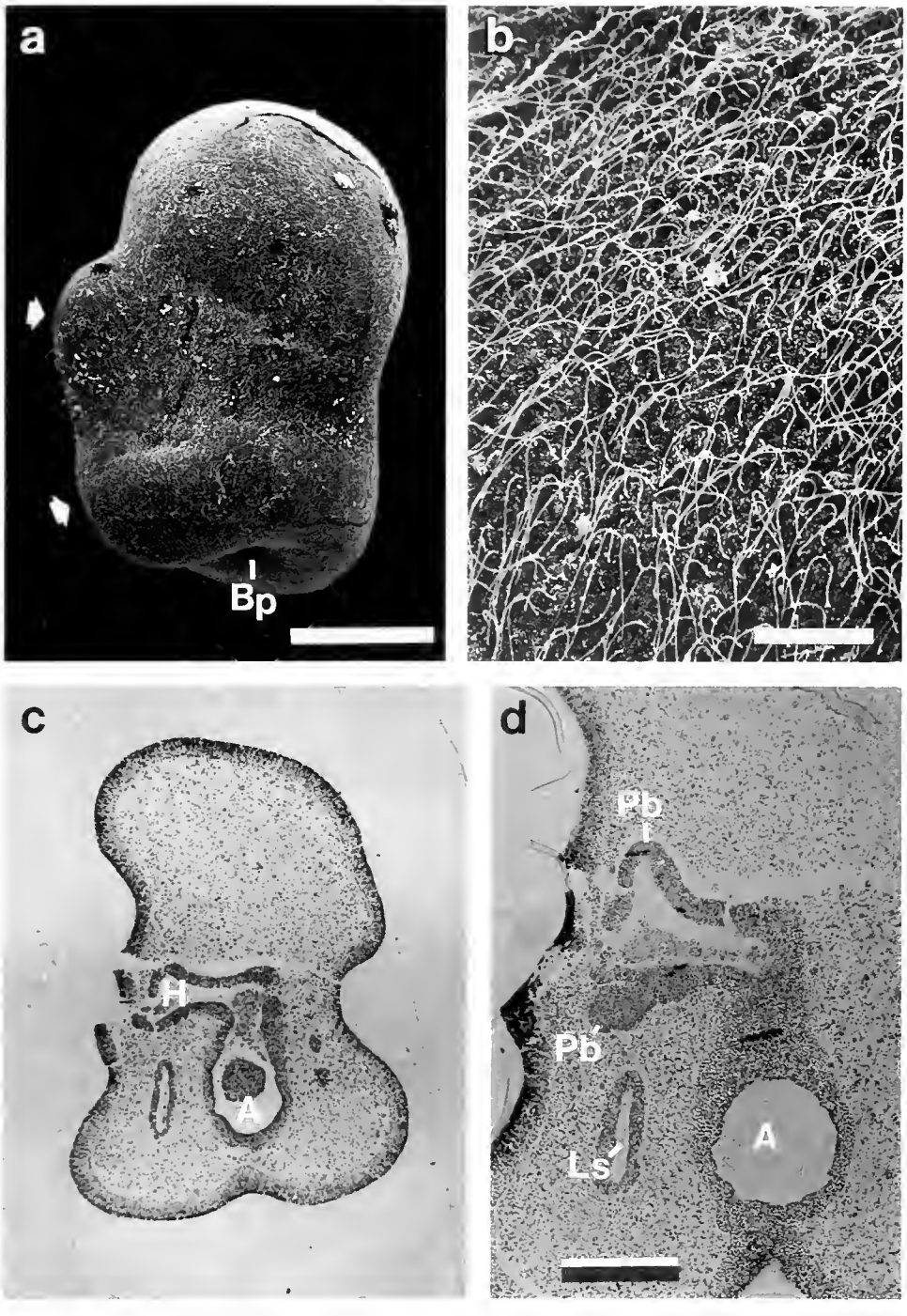

Figure 5. A 63-h larvae of *Asthenosoma ijimai*, all oriented with the anterior end toward the top of the figure. a. SEM of a whole larva, right ventral view (dorsal side is on the left) shows two right para-arms (arrows) and the blastopore (Bp). Scale bar, 0.5 mm b. Close-up of uniformly ciliated epidermis. Scale bar, 25 μm. c. Frontal section shows the leftward oriented archenteron with coelomic components of podia near its tip. The hydrocoel (H) is developing before being separated from the archenteron (A). (This larva was damaged during embedding, but a clear interpretation of sections was still possible.) Same scale as a. d. Higher magnification of a more dorsally located frontal section from same larva as c. Hydrocoelic components of podial buds (Pb) are present. Ls, left somatocoel. Scale bar, 200 μm.

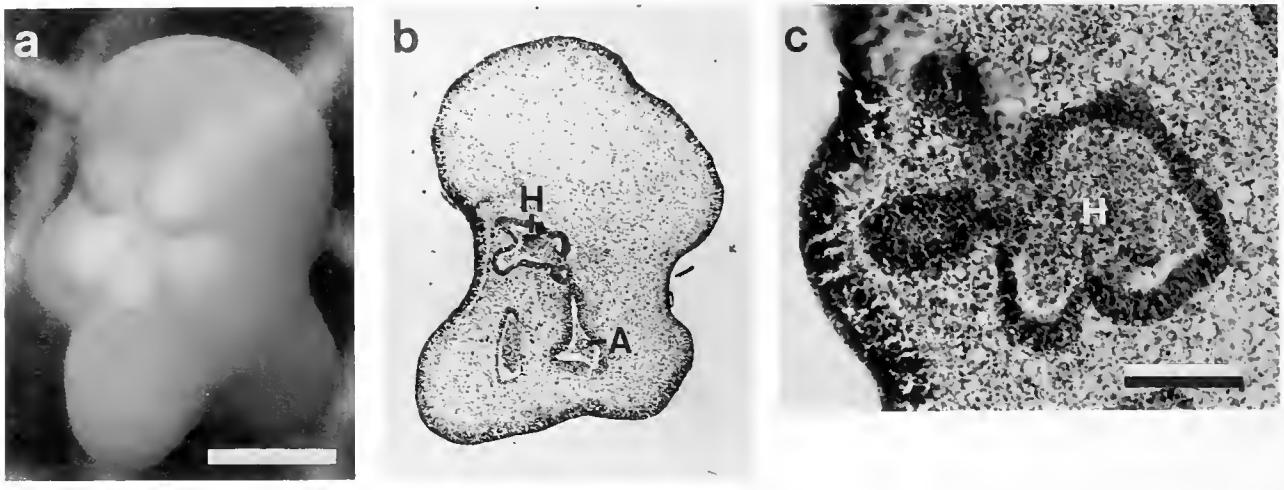

Figure 6. A 75.5-h larvae of *Asthenosoma ijimai*. a. Light micrograph of live specimen shows five primary podia just beginning to form on left side of larva. Scale bar, 0.5 mm. b. Frontal section with continued hydrocoelic (and podial) development. The hydrocoel (H) is almost completely separated from the archenteron (A). Same scale as a. c. Detail of hydrocoel (H) with parts of two podial extensions from a different section of the same larva as b. Scale bar, 100 μm.

showed the hydrocoelic compartments with thickened epithelia beneath the podial swelling of the ectoderm (Fig. 6c). Serial sections revealed that the connection between the hydrocoel and archenteron was greatly reduced in one larva (Fig. 6b) and completely severed in a second larva examined. All coelomic and archenteric cavities contained stained materials that appeared to be yolky cytoplasm and some cells (Fig. 6b, c).

By 101 h post fertilization, primary podia elongated to 0.2 mm length (Fig. 7b, c, d). Sections of the juvenile oral surface showed folds of ectodermal tissue lying between the five primary podia (Fig. 7c, d). These folds were evidently epineural folds that were growing over the juvenile oral surface to form the epineural sinus (von Ubisch, 1913; Hyman, 1955; Emlet, 1988). SEM observations of the external surface of the developing juvenile oral region confirm that these epineural folds were spreading toward the oral center (Fig. 7f–h).

Coincident with the lengthening of the primary podia and development of the epineural folds, the oral surface sank to become indented in the surface of the developing larva. This indentation was notable in live specimens viewed from the side at 101 h (Fig. 7b), as well as in sectioned material (Fig. 7c) and in specimens fixed for SEM (Fig. 7f). Though the developing juvenile oral surface was never deeply enclosed as occurs within the amniotic invagination (or vestibule) of the euechinoids, the oral surface was further sunken in living larvae nine days postfertilization (Fig. 8a). Fourteen days after fertilization, the oral surface was no longer evidently sunken, and the larval para-arms and anterior yolky mass have moved away from the oral surface toward the aboral surface of the juvenile (Fig. 8b, c).

At 101 h post-fertilization, a hydropore was evident on the dorsal surface of the larva (Fig. 7a). The location of this pore was near the median side of the base of right anterior para-arm. Sections of 101-h-old larvae showed that the hydropore was joined to the hydrocoel via a canal lined by a thick epithelium (Fig. 7e). In sections of younger larvae (88.5 h), this hydroporic canal invaginated from the larval surface but was not yet joined to the coelomic cavities. Sections of 14-day larvae showed the hydropore connected to the hydrocoel by a stone canal (Fig. 8c, e). Also by this stage, epineural folds had joined to form an epineural sinus (Fig. 8d, e).

Observations on the calcitic skeleton

Larval stages at 58, 63, 75.5, 88.5, and 101 h after fertilization were cleared to look for calcareous skeletal spicules within developing embryos. No evidence of calcification was seen in 58- and 63-h specimens, even though the latter had begun to form the para-arms (Figs. 4f and 9a). The first evidence of calcification was found in 75.5-h specimens (Fig. 9b). In these, para-arms were well formed, and podial bulges had just begun to form. One calcareous plate-like ossicle was embedded in the base of each para-arm. In the more advanced 75.5-h specimen of the two observed, a fifth calcareous ossicle was present and located centrally between the four para-arms (Fig. 9b). In 88.5-h specimens, the five ossicles had grown into plates, and those in the para-arms had formed fenestrated rods that projected toward the distal ends of the para-

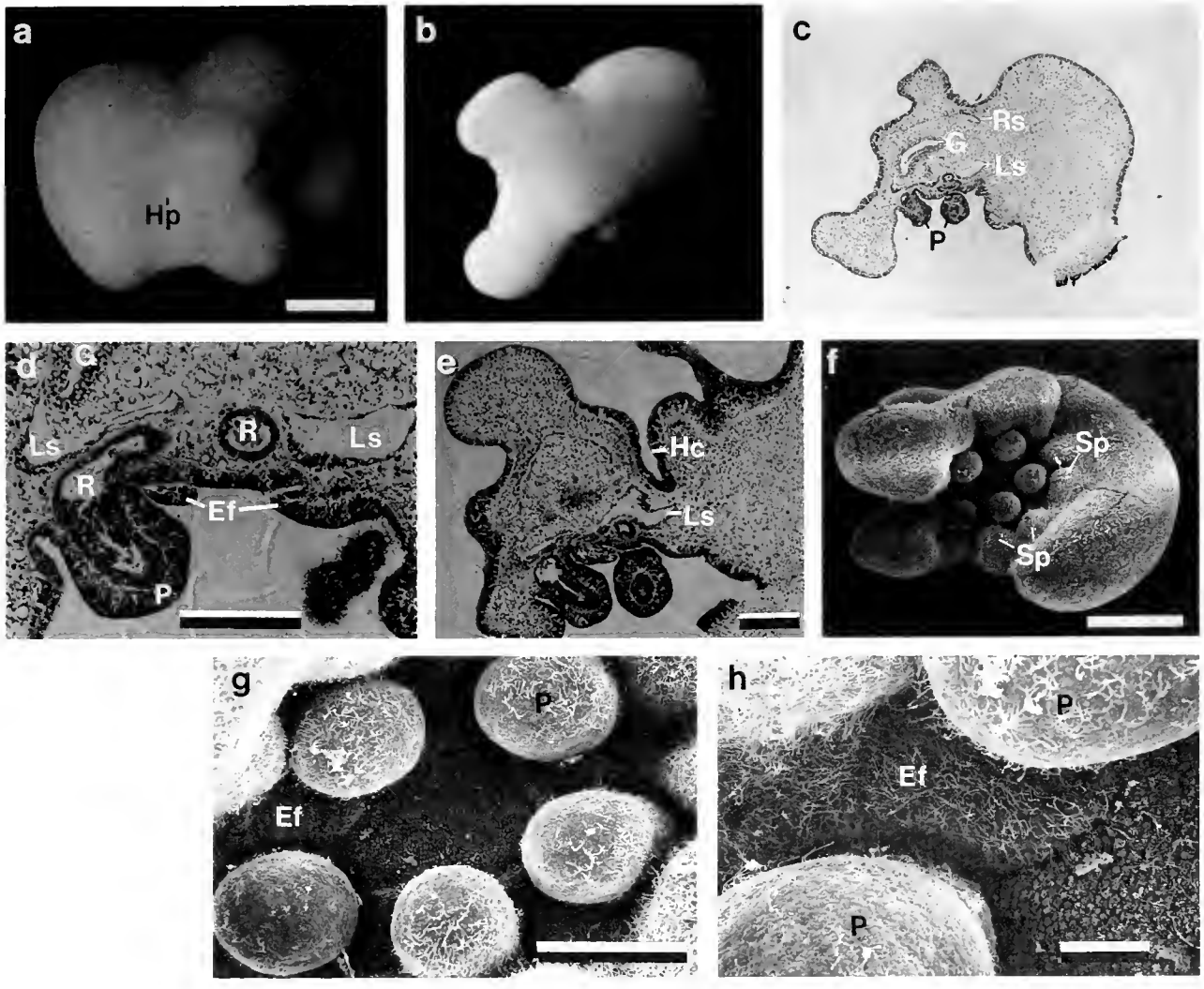

Figure 7. A 101-h larvae of *Asthenosoma ijimai*. a. Light micrograph of dorsal side of live specimen. Note the hydropore (Hp) and four para-arms (to right). The anterior end is to the left of figure. Scale bar, 0.5 mm. b. Light micrograph of ventral side of live specimen. The anterior end is to the right of figure. Same scale as a. c. Medial frontal section through larva shows developing internal structures and juvenile oral region. P, podia; Rs, right somatocoel; Ls, left somatocoel; G, remnant of archenteron and future gut. Same scale as a. d. Close-up of juvenile oral region, with podia (P), epineural folds (Ef), radial canals of water vascular system (R), and left somatocoel (Ls). Scale bar, 200 μm. e. Section at the level of the hydropore shows invaginated canal (Hc). In an adjacent section, the canal joins the hydrocoel. Scale bar, 200 μm. f. SEM of oral region of larva, shows five podia, and bulges for spines (Sp) sunken into the left larval surface. Scale bar, 0.5 mm. g. Close-up SEM of oral region showing inward movement of epineural folds (Ef) between podia (P). The infolding epidermis is strongly ciliated whereas the original floor of the oral region is sparsely ciliated. Scale bar, 200 μm. h. High magnification view of a single epineural fold (Ef) moving between two adjacent podia (P). Scale bar, 50 μm.

arms (Fig. 9c). These rods were particularly well developed in the two right para-arms and had just begun to form in the two left para-arms. The centrally located plate showed no evidence of an attached rod. Each of the calcified skeletal plates, with or without rods attached, behaved optically like a single crystal when rotated through polarized light (Fig. 9d–f). This observation confirmed the structural appearance that plates with attached rods were a single skeletal unit. Also in the 88.5-h larvae, several other calcification centers had formed and ossicles were growing (Fig. 9c).

Calcification in 101-h larvae was even more developed (Fig. 9g). These larvae had well-developed podial buds (Fig. 7b) and, on one specimen, the buds for spines were developing on the circumference of the juvenile oral surface (see Fig. 7f). As with earlier stages, fenestrated rods

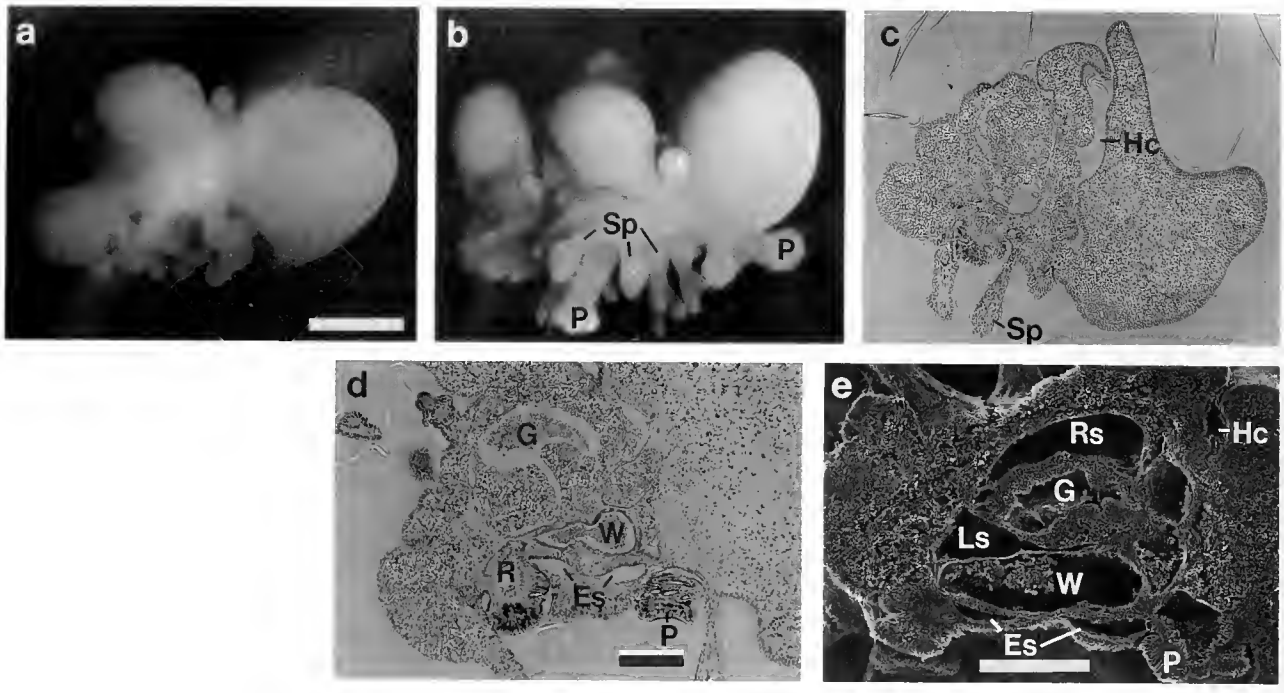

Figure 8. Later stages of larval development of *Asthenosoma ijimai*. For all specimens, the anterior end is to the right of figure. a. Ventral side of live specimen nine days after fertilization. Scale bar, 0.5 mm. b. Ventral side of live specimen 14 days after fertilization. The larval para-arms and anterior yolky mass have been contorted toward the juvenile aboral surface. P, podia; Sp, spines. Same scale as a. c. Fourteen-day post fertilization, approximate frontal section at the level of the hydropore and hydroporic canal (Hc). Same scale as a. d. Close-up of juvenile oral region showing epineural sinuses (Es), gut (G), water vascular system (W), radial canal (R), and podia (P). Compare with e. Scale bar, 200 μm. e. SEM of partially sectioned specimen showing similar structures as seen in d. Hc, hydroporic canal; Rs, right somatocoel (aboral part of body cavity); Ls, left somatocoel (oral part of body cavity). Scale bar, 200 μm.

were associated with plates in the para-arms and not with other ossicles. In one larva, each of the spine buds contained a growing spicule. In this same larva, the two ossicles of the left para-arms and three additional ossicles formed a circle beneath the juvenile oral surface that represented the five ocular plates of the adult skeleton.

Discussion

Larval structure of Asthenosoma ijimai

Our re-examination of the larval development of *Asthenosoma ijimai* has demonstrated several morphological features that were not reported in the initial study of this species. Amemiya and Tsuchiya (1979) reported that the early post-gastrula of *A. ijimai* resembled an early bipinnaria and not a prism larva. That study also reported the appearance of para-arms later in development and distinguished these projections from pluteus larval arms, because the former apparently lacked larval spicules and apparently arose from different regions of the larva. On this basis Amemiya and Tsuchiya concluded that, during development, *A. ijimai* passes from the gastrula stage to metamorphosis without showing any evidence of a pluteus larval form. They also concluded that the development of *A. ijimai* represents a second example of direct development (*sensu* Hyman, 1955) for an echinoid, the first being that of *Heliocidaris erythrogramma* (development originally described by Mortensen, 1921, but also by Williams and Anderson, 1975). Amemiya and Tsuchiya (1979) identified the surface on which para-arms arose in embryos of *Asthenosoma* as the ventral surface because of its resemblance to the ventral (oral) surface of early bipinnaria larvae of asteroids. Amemiya and Tsuchiya (1979) also incorrectly stated that the five primary podia were on the ventral surface, although Amemiya (1980) reported that primary podia arise lateral to the ventral surface. In the present study, the surface on which the para-arms arose has been identified as the dorsal surface based on observations of internal structures and on comparison with the primitive pluteus morphology. In this new orientation, the primary podia form on the left side of the larva.

A number of newly observed structures and their positions lead us to reinterpret the larval development of

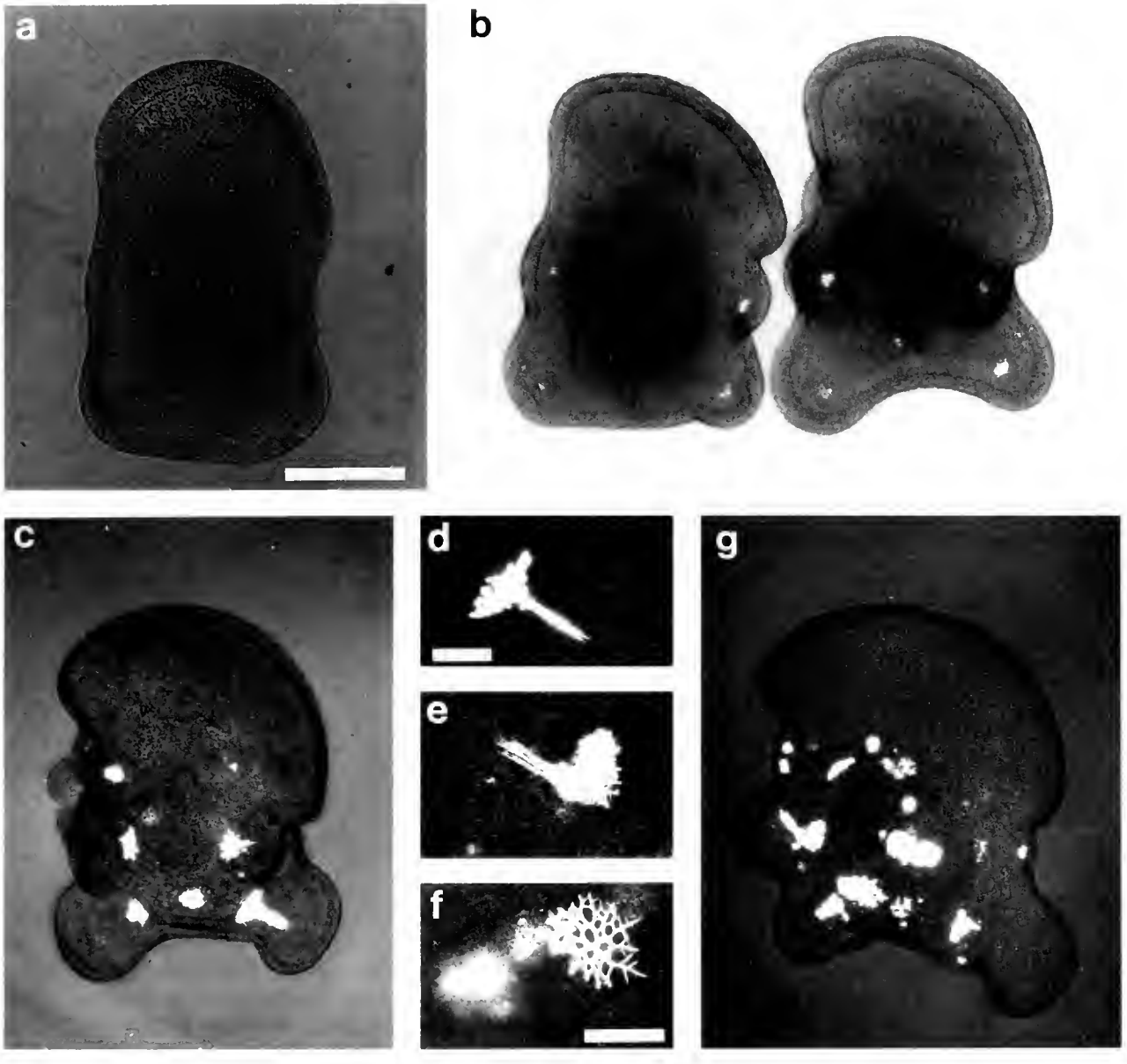

Figure 9. Skeletal development in various, cleared stages of larvae of *Asthenosoma ijimai*. All larvae are viewed from the dorsal side in partially polarized light. a. A 63-h larva shows no evidence of calcareous skeletal elements. Scale bar, 0.5 mm. b. Two 75.5-h specimens show the very first signs of skeletal development. One calcareous element is associated with each para-arm. The specimen on the right was an additional calcareous element centrally located between the para-arms. Same scale as a. c. A 88.5-h larva with continued skeletal development. Each calcareous element associated with a para-arm has formed a plate-like ossicle and shows substantial or initial formation of a rod attached to the plate. Other calcification centers have also begun. Same scale as a. d. Close-up of plate-like ossicle and rod from right posterior para-arm of a 88.5-h larva. Scale bar, 100 μm. e. Another plate-like ossicle and rod from a 101-h larva. Same scale as d. f. Central plate-like ossicle without an associated rod from a 101-h larva. Scale bar, 100 μm. g. A 101-h larva with many calcification sites. Same scale as a.

Asthenosoma ijimai as that of a highly modified pluteus larva. The two pair of bilaterally symmetrical para-arms arising from posterior and dorsal parts of embryo, each one containing a calcareous, fenestrated skeletal element, appear to be vestigial larval arms. We reject an alternative interpretation that the fenestrated rods are juvenile spines, because the spines form in association with plates that are separate elements (Gordon, 1926a, b). Because the skeletal elements are fenestrated, we interpret the para-arms as reduced post-oral and postero-dorsal arms (the

1st and 3rd pairs of arms) of a pluteus. Fenestrated skeletal rods are only known for these arm pairs in pluteus larvae (Mortensen, 1921; Emlet, 1982). In typical plutei, the second pair of arms to form is the anterolateral pair that always contains simple calcareous rods (Mortensen, 1921). Each anterolateral rod is an outgrowth from the pair of spicules that also form the postoral rods and body skeleton. The postoral rods are so reduced in *A. ijimai* that anterolateral rods are absent.

There are also several differences in the early formation of fenestrated spicules in a pluteus and those in *A. ijimai.* (1) In the pluteus, a fenestrated rod grows from a triradiate spicule (Okazaki, 1975) and later elaborates a plate at its proximal base (Emlet, 1985, and unpub. obs.). In contrast, skeletal elements in *A. ijimai* form proximal, reticulate plate-like ossicles that later form reduced, fenestrated rods. (2) In a pluteus, calcareous rods extend and consequently the arms elongate (*e.g.,* Okazaki, 1975); in larvae of *A. ijimai,* para-arms are already present before spicules elongate. In actuality, formation of arm buds in the absence of spicules can still occur in plutei (Yasumasu *et al.,* 1985; Emlet, pers. obs.) indicating that the epidermis of the arm regions is apparently distinct prior to its association with spicules. This last observation is consistent with the formation of arm buds in *A. ijimai.*

Additional support for the identification of the para-arms as homologues of the first and third arm pairs of a pluteus larva comes from the following evaluation of arm position. Rather than being directed anteriorly (in the direction of swimming) as they are for a pluteus larva, arms and their associated skeletal elements are reflected dorsally and posteriorly at the surface of the very large yolky larva (Fig. 10). In echinoids with plutei, the gastrula forms a prism larva when rods of the first pair of larval spicules lengthen into postoral, body, and anterolateral rods and deform the ectoderm (Horstadius, 1939; Okazaki, 1975). The prism's ventral surface (defined by the association of the archenteron tip with that surface) flattens to become the pluteus oral surface; the prism's dorsal surface (opposite the ventral surface) distends to become the aboral surface, terminating at the posterior end of the pluteus. During the prism stage, the ciliated band forms and serves as a landmark dividing oral and aboral ectoderm (*c.f.,* Davidson, 1986). The postoral arms grow anteriorly from the positions lateral to the blastopore. Late in the four-armed stage, a second pair of triradiate spicules appears at dorsolateral edges of aboral surface near the ciliated band (see Fig. 10), and these form the (usually) fenestrated posterodorsal rods (*e.g.,* Mortensen, 1921; Okazaki, 1975). The postoral and posterodorsal arms thus extend the ciliated band anteriorly and are located at the edge of the concave oral and convex aboral ectoderm. If the posterior end of the pluteus were not convex, and if the aboral surface lay in one plane, the positions of the postoral and

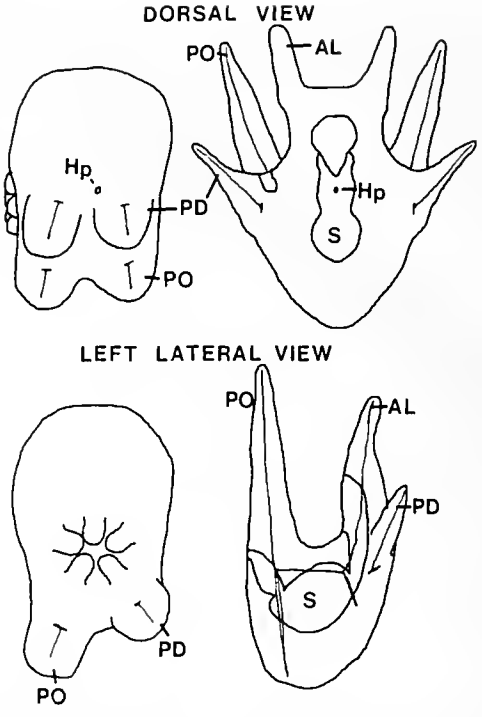

Figure 10. Schematic of a larva of *Asthenosoma ijimai* and a pluteus (*Strongylocentrotus franciscanus*) viewed from dorsal and left lateral orientations. In *A. ijimai* the para-arms are reflected posteriorly and contain reduced skeletal elements. These bilaterally symmetric arms and spicules are in positions that can be considered homologous with the postoral (PO) and posterodorsal arms (PD) of the pluteus. The anterolateral arms and rods (AL) have been lost in *A. ijimai.* Hp, hydropore; S, stomach.

posterodorsal arms of a pluteus would conform with the para-arms of *Asthenosoma ijimai* (see Fig. 10). This description is consistent with the hypothesis of homology between the identified arms and skeletal elements in plutei and larvae of *A. ijimai.*

The position of another newly observed structure, the hydropore, is also consistent with and supports this interpretation of vestiges of pluteus larval development. In both pluteus larvae and those of *Asthenosoma ijimai,* the hydropore opens medially to, and anterior of, the bases of the posterodorsal arms (Figs. 10, 7a). A clear difference is, however, that the hydropore opens just after coelom formation in pluteus development and it opens only after advanced coelomic development in *A. ijimai.*

If the boundary between oral and aboral ectoderm has remained associated with the epidermal regions of the arms, this reinterpretation of the larval form of *Asthenosoma ijimai* implies that the large, rounded, anterior end of the larva is covered by oral ectoderm and that aboral ectoderm may be restricted to that region associated with the para-arms. For *A. ijimai,* there may be a reversal in the relative area (and shape) of the oral ectoderm and aboral ectoderm compared to that in plutei (Fig. 10). It

may be possible to test this hypothesis with cell lineage studies or with immunocytochemical probes to transcripts of the CyIII actin gene or the Spec gene, which are specific to aboral ectoderm in plutei of *Strongylocentrotus purpuratus* (Cox *et al.*, 1986; Davidson, 1986). Enlargement of the oral ectoderm and reduction of aboral ectoderm has been demonstrated in cell lineage studies of *Heliocidaris erythrogramma* (Wray and Raff, 1990). Further work will be required to determine whether this apparent similarity represents a new case of parallelism in echinoid developmental patterns.

Comparisons between pluteus development and modified development

Even though larvae of *Asthenosoma ijimai* retain several reduced pluteus structures, several other features are partially convergent with other echinoid species that have modified development. Developmental comparisons among species that form plutei, *A. ijimai,* and other species with modified development allows inferences about morphogenetic changes that may occur during evolution from pluteus development to highly modified (*e.g.*, direct) development.

An equal fourth cleavage, documented here for *Asthenosoma ijimai,* is a common feature of species with highly modified development and is correlated with the production of a large number of mesenchyme cells (Raff, 1987; Parks *et al.*, 1989). Raff (1987) suggested that the large number of mesenchyme cells is a requirement for acceleration of development of the adult rudiment. For *A. ijimai,* only a fraction of the large number of blastocoelic cells become skeletogenic and only after a delay relative to species with feeding larvae. A large number of mesenchyme cells is also produced from the relatively large micromeres of an unequal fourth cleavage by embryos of *Peronella japonica,* and some of these cells also produce larval skeletal rods (Okazaki and Dan, 1954; Okazaki, 1975). These comparisons suggest that the loss of the expression of larval skeleton is independent of, and follows amplification of, the cell lineage that putatively produces adult skeleton.

The growth and behavior of the archenteron and coeloms of *Asthenosoma ijimai* appears to be intermediate between that of species with pluteus development and that of the other species with modified development. In species with feeding larvae, the archenteron grows into the blastocoel, reaching approximately $^4/_5$ of the distance toward the animal pole prior to bending toward, and attaching to, the blastocoel wall where the larval mouth forms. In most species for which modified development has been described, the archenteron invaginates less than half way into the blastocoel: *Peronella japonica* (Mortensen, 1921; Okazaki, 1975); *Heliocidaris erythrogramma* (Williams and Anderson, 1975; Wray and Raff, 1989); *Phyllacanthus parvispinus* (Parks *et al.*, 1989). In *Asthenosoma ijimai,* the archenteron invaginated as much as $^2/_3$ of the way into the blastocoel. Unlike what has been reported for other species with modified development, in *A. ijimai* the tip of the archenteron curved toward the ventral surface of the blastocoel and subsequently underwent torsion to the left side of the larva.

Enterocoely, where left and right coelomic pouches are budded off completely from the anterior end of the archenteron, is the only means of coelom formation known in pluteus development (*e.g.*, Okazaki, 1975). Both of these pouches divide again to form anterior axocoelic and posterior somatocoelic sacs. The left axocoel subsequently grows a canal to form the dorsal hydropore, and another extension of this sac forms the left hydrocoel (Hyman, 1955). Development of bilateral coelomic pouches followed by posterior growth and formation of somatocoels also occurs in *Asthenosoma ijimai,* yet in a distinctive way: two outpocketings from the archenteron form the left and right somatocoels, and precocious hydrocoelic lobes grow from the tip of the archenteron (Figs. 4; 5c, d). No obvious axocoelic sacs and no hydroporic canal are formed during this sequence. Later, a hydropore does form and joins with the water vascular system. In other species with modified development, the coelomic pouches are usually produced in pairs at the tip of the archenteron, with one sac substantially larger than the other (*e.g.*, Williams and Anderson, 1975; Wray and Raff, 1989). Several species with highly modified development are reported to form additional coelomic sacs by shizocoely from aggregated mesenchyme cells (*e.g.*, Williams and Anderson, 1975; Schatt, 1985). These patterns suggest that a transition from enterocoely to a combination of enterocoely and shizocoely may take place only after considerable modification of development has already occurred. For species with modified development in general, detailed descriptions of how coelomic pouches give rise to different coelomic sacs are currently lacking, and additional studies are needed.

The orientation of the adult oral-aboral axis relative to the plane of bilateral symmetry of the pluteus is conserved in several species with modified development, but is apparently lost in others. Loss of symmetry is not related to the degree of loss of pluteus features. Evidence for retention of pluteus larval symmetry and its relation to juvenile rudiment formation has already been presented for *Asthenosoma ijimai.* In *Phyllacanthus imperialis,* with two pairs of larval arms, a reduced preoral region, and no larval mouth, the juvenile oral surface forms on the left side of the larval body (Olson *et al.*, 1988). A reduced bilateral symmetry is also present in *Heliocidaris erythrogramma,* which has one coelomic pouch (the left one) larger than the other (Williams and Anderson, 1975) and

a bilaterally symmetric (larval) serotonergic ganglion (Bisgrove and Raff, 1989). In *H. erythrogramma,* the coincident arrangement of these two sources of bilaterality provides evidence for conservation of the adult oral-aboral axis (Bisgrove and Raff, 1989). Departures from conservation of relative positions of larval and adult axes occur for three other species. *Peronella japonica* and *P. rubra* (with very similar development) have bilaterally symmetric larvae, but the juvenile rudiment forms centrally, with the juvenile oral surface directed anteriorly and dorsally (Okazaki, 1975; Amemiya and Emlet, unpub. obs.). Loss of the primitive larval-adult arrangement of axes may be related to the retention of one pair of larval arms (postorals) and the loss of the more dorsal pair. Retention of only one well-developed pair of larval arms may force the rudiment to develop on the dorsal side, whereas in the absence or reduction of both pairs (*e.g., H. erythrogramma, A. ijimai*), or retention of both pairs (*P. imperialis*), the juvenile oral surface would not be shifted. This mechanistic hypothesis does not apply to *Phyllacanthus parvispinus* which lacks a larval skeleton and has bilobed, asymmetric coeloms which do not coincide with the orientation of the serotonergic neurons (Park *et al.,* 1989). Further morphological studies of the formation and growth of the archenteron and coeloms of both *P. japonica* and *P. parvispinus* are needed to determine how primitive larval and adult oral aboral axes have been rearranged.

Euechinoid characters in echinothurioid development

Early ingression of cells from the blastular wall in *Asthenosoma ijimai* (Fig. 1d) is comparable to primary mesenchyme ingression, which occurs prior to gastrulation in other euechinoids and is different from the later ingression known among the cidaroids (Schroeder, 1981).

Beginning with the first appearance of podia and continuing until the adult skeleton is well-developed (Fig. 8b, c), the juvenile oral region of *Asthenosoma ijimai* sinks into the surface of the larva (Figs. 7b, c, f; 8a). Within this indentation, both podia and oral spines grow. Though there is no early invagination and enclosure of the juvenile oral surface that could be clearly identified as an amniotic invagination, the strong indentation may be a morphogenetic process equivalent to vestibule formation. Other species with modified development either have or lack an amniotic invagination, consistent with their phylogenetic position as cidaroids or euechinoids (see Parks *et al.,* 1989), and this sunken condition is, therefore, not simply due to the yolkiness of the larva. A comparison of our figures with those of the cidaroid *Phyllacanthus parvispinus,* which lacks an amniotic invagination, shows that the oral surface of *A. ijimai* is considerably more indented than that of the cidaroid (Parks *et al.,* 1989, fig. 3f). Our observations raise the possibility that a partial, possibly primitive, form of an amniotic invagination may be present in echinothurioids.

Parks *et al.* (1989) also examined sectioned material of *A. ijimai* and concluded that an amniotic invagination was absent. These authors hypothesized that an amniotic invagination arose in the euechinoid lineage after the echinothurioid branch. They hypothesized further that, because the two most primitive lineages of echinoids, the cidaroids and echinothurioids, lacked an amniotic invagination, the absence of this character was primitive for echinoids. Our observations suggest that their first phylogenetic hypothesis may not be accurate, but our findings are consistent with the hypothesis that the amniotic invagination is a derived character in euechinoids. Based on comparisons of the fate of larval epidermis among echinoderm classes, Emlet (1988) suggested the same hypothesis that the primitive condition for echinoids is the absence of an amniotic invagination.

The formation of epineural sinuses in *Asthenosoma ijimai* matches very closely the original descriptions of the same process occurring within the amniotic invagination of other euechinoids [compare Fig. 7f–h with original text-figs. e–h of von Ubisch, 1913 (text-figs. f, g reprinted in Hyman, 1955, p. 497)]. By contrast, epineural sinus formation in this echinothurioid differs from that described for the cidaroid, *Eucidaris thouarsi* (Emlet, 1988). In *E. thouarsi,* epineural folds were present, but not clearly evident when observed by SEM. Sections of *E. thouarsi* showed epineural folds closely adhered to the developing juvenile oral surface on the left side of the larva, whereas in euechinoids, the epineural folds were not so closely adhered. Emlet (1988) hypothesized that the pattern in *E. thouarsi* might reflect a different mechanism of epineural fold movement (from that in euechinoids) but might also result from the open condition of the surface upon which this process occurs in *E. thouarsi.* The largely open nature of the oral surface in *A. ijimai,* and the distinctly euechinoid appearance of its epineural folds, suggest that the open condition of the epineural folds in *E. thouarsi* was not a cause for their appearance. This observation dismisses Emlet's (1988) hypothesized explanation for convergence of the epineural folds of *E. thouarsi* and the ophiuroid, *Ophiopholis aculeata* (Olsen, 1942) but leaves standing the hypothesis that cidaroids and ophiuroids have similar means of epineural sinus formation (Emlet, 1988).

Conclusions

In this re-examination of the larval morphogenesis of *Asthenosoma ijimai,* evidence has been presented to show that *A. ijimai* has retained previously unrecognized, reduced pluteus characters. As such, this larval form is the most reduced pluteus yet described, being considerably

more modified than larvae of *Phyllacanthus imperialis* (Olson *et al.*, 1988) and *Peronella japonica*. This contribution brings to three the number of lineages with modified development and with pluteus characters that are retained to varying degrees. In contrast, four lineages (*Phyllacanthus parvispinus, Heliocidaris erythrogramma,* a temnopleuroid, and *Abatus* species) have lost most, if not all, primitive larval characters. (The genus *Phyllacanthus* stands alone as being represented in both groups, but it is not known whether non-feeding development has evolved independently for the two species: *P. imperialis* and *P. parvispinus*.) Comparative experimental and cell lineage information about species with reduced larval features must now be collected if we are to determine 1) whether there is a common, possibly convergent, theme of developmental changes, or 2) whether modifications to cleavage and cell lineage fates are additional changes occurring after the loss of feeding and the reduction of the pluteus form. The detailed description presented here adds to the growing collection of comparative data on modified development; but it also indicates that the basic morphological changes occurring in other species with modified development—including two that are already well studied, *Heliocidaris erythrogramma* and *Peronella japonica*—ought to be re-examined.

Acknowledgments

This research was supported by grants from the Japanese Society for Promotion of Science (to SA and RBE) and the United States National Science Foundation (BSR-9058139 to RBE). We would like to thank E. Arakawa for technical assistance, M. McFall-Ngai for allowing us to use her digitizing software, I. Lagomarsino for digitizing so many serial sections, and R. A. Raff for providing the B2C2 antibody. We are also grateful to S. Smiley for advice on clearing opaque larvae. Comments of V. Morris and two anonymous reviewers helped improve the manuscript.

Literature Cited

Amemiya, S. 1980. Metamorphosis of an echinothurioid sea urchin, *Asthenosoma ijimai*. Pp. 74–78 in *An Outline of Modern Biology Vol. 11B*, I. Yasumasu *et al.*, eds. Kakayama-shoten, Tokyo. (in Japanese)

Amemiya, S., and T. Tsuchiya. 1979. Development of the echinothurid sea urchin *Asthenosoma ijimai*. *Mar. Biol.* **52:** 93–96.

Armstrong, P. B., and D. Parenti. 1973. Scanning electron microscopy of the chick embryo. *Dev. Biol.* **33:** 457–462.

Bisgrove, B. W., and R. A. Raff. 1989. Evolutionary conservation of the larval serotonergic nervous system in a direct developing sea urchin. *Dev. Growth Differ.* **31:** 363–370.

Cox, K. H., L. M. Angerer, J. J. Lee, E. H. Davidson, and R. C. Angerer. 1986. Cell lineage-specific programs of expression of multiple actin genes during sea urchin embryogenesis. *J. Mol. Biol.* **188:** 159–172.

Davidson, E. H. 1986. *Gene Activity in Early Development*, 3rd edition, Academic Press, Orlando, FL.

Emlet, R. B. 1982. Echinoderm calcite: a mechanical analysis from larval spicules. *Biol. Bull.* **163:** 264–275.

Emlet, R. B. 1985. Crystal axes in recent and fossil adult echinoids indicate trophic mode in larval development. *Science* **230:** 937–940.

Emlet, R. B. 1988. Larval form and metamorphosis of a "primitive" sea urchin, *Eucidaris thouarsi* (Echinodermata: Echinoidea: Cidaroida), with implications for developmental and phylogenetic studies. *Biol. Bull.* **174:** 4–19.

Emlet, R. B. 1990. World patterns of developmental mode in echinoid echinoderms. Pp. 329–335 in *Advances in Invertebrate Reproduction, Vol. 5*, M. Hoshi and O. Yamashita, eds. Elsevier Science Publ., Amsterdam.

Emlet, R. B., L. R. McEdward, and R. R. Strathmann. 1987. Echinoderm larval ecology viewed from the egg. Pp. 55–136 in *Echinoderm Studies, Vol. 2*, M. Jangoux and J. M. Lawrence, eds. Balkema Press, Rotterdam.

Fell, F. J. 1976. The Cidaroida (Echinodermata: Echinoidea) of Antarctica and the southern oceans. Unpublished Ph.D. dissertation, University of Maine, Orono, Maine. 293 pp.

Gordon, I. 1926a. The development of the calcareous test of *Echinus miliaris*. *Philos. Trans. R. Soc. B.* **214:** 259–312.

Gordon, I. 1926b. The development of the calcareous test of *Echinocardium cordatum*. *Philos. Trans. R. Soc. B.* **215:** 255–313.

Harris, P., and G. Shaw. 1984. Intermediate filaments, microtubules and microfilaments in epidermis of sea urchin tubefoot. *Cell Tissue Res.* **236:** 27–33.

Henry, J. J., and R. A. Raff. 1990. Evolutionary change in the process of dorsoventral axis determination in the direct developing sea urchin, *Heliocidaris erythrogramma*. *Dev. Biol.* **141:** 55–69.

Horstadius, S. 1939. The mechanics of sea urchin development, studied by operative methods. *Biol. Rev. Camb. Philos. Soc.* **14:** 132–179.

Hyman, L. H. 1955. *The Invertebrates: Echinodermata, Vol. IV*. McGraw-Hill, New York.

Larrain, A. 1973. Los pedicelarios globiferos y el desarrollo de *Abatus agassizi*. *Bol. Soc. Biol. Concepcion* **46:** 53–63.

Mortensen, T. 1921. *Studies of the Development and Larval Forms of Echinoderms*. G.E.C. Gad, Copenhagen.

Mortensen, T. 1936. Echinoidea and Ophiuroidea. *Discovery Rep.* **12:** 199–348.

Okazaki, K. 1975. Normal development to metamorphosis. Pp. 177–232 in *The Sea Urchin Embryo Biochemistry and Morphogenesis*, G. Czihak, ed. Springer-Verlag, Berlin.

Okazaki, K., and K. Dan. 1954. The metamorphosis of partial larvae of *Peronella japonica* Mortensen, a sand dollar. *Biol. Bull.* **106:** 83–99.

Olsen, H. 1942. Development of a brittlestar *Ophiopholis aculeata*, with a short report on the outer hyaline layer. *Bergens Museum Aarbok. Natur.* **6:** 1–107.

Olson, R. R., J. L. Cameron, and C. M. Young. 1988. Larval development of the pencil urchin *Phyllacanthus imperialis*: a lecithotrophic pluteus. P. 807 in *Echinoderm Biology, Proc. 6th Int'l Echinoderm Conf., Victoria*, R. D. Burke, P. V. Mladenov, P. Lambert, R. L. Parsley, eds. Balkema, Rotterdam.

Parks, A. L., B. A. Parr, J.-E. Chin, D. S. Leaf, and R. A. Raff. 1988. Molecular analysis of heterochronic changes in the evolution of direct developing sea urchins. *J. Evol. Biol.* **1:** 27–44.

Parks, A. L., B. W. Bisgrove, G. A. Wray, and R. A. Raff. 1989. Direct development in the sea urchin *Phyllacanthus parvispinus* (Cidaroidea): phylogenetic history and functional modification. *Biol. Bull.* **177:** 96–109.

Raff, R. A. 1987. Constraint, flexibility, and phylogenetic history in the evolution of direct development in sea urchins. *Dev. Biol.* **119:** 6–19.

Raff, R. A., B. Parr, A. Parks, and G. Wray. 1990. Radical evolutionary change in early development. Pp. 71–98 in *Evolutionary Innovations*, M. H. Nitecki, ed. University of Chicago Press, Chicago, IL.

Richardson, K. C., L. Jarrett, and E. H. Finke. 1960. Embedding in epoxy resin for ultrathin sectioning in electron microscopy. *Stain Technol.* **35:** 313–323.

Schatt, Ph. 1985. Developpement et croissance embryonnaire de l'oursin incubant *Abatus cordatus* (Echinoidea: Spatangoida). These de Doctorat de l'Universite Pierre et Marie Curie. 151 pp.

Schatt, Ph. 1988. Embryonic growth of the brooding sea urchin *Abatus cordatus*. Pp. 225–228 in *Echinoderm Biology, Proc. 6th Int'l Echinoderm Conf., Victoria*, R. D. Burke, P. V. Mladenov, P. Lambert, and R. L. Parsley, eds. Balkema, Rotterdam.

Schroeder, T. E. 1981. Development of a "primitive" sea urchin (*Eucidaris tribuloides*): irregularities in the hyaline layer, micromeres, and primary mesenchyme. *Biol. Bull.* **161:** 141–151.

Smith, A. B. 1984. *Echinoid Palaeobiology*. George Allen and Unwin, London.

Strathmann, R. R. 1978. The evolution and loss feeding larval stages of marine invertebrates. *Evolution* **32:** 894–906.

Ubisch, L. von. 1913. Die entwicklung von *Strongylocentrotus lividus*. (*Echinus microtuberculatus, Arbacia pustulosa*). *Z. Wiss. Zool.* **106:** 409–448.

Williams, D. H. C., and D. T. Anderson. 1975. The reproductive system, embryonic development, larval development and metamorphosis of the sea urchin *Heliocidaris erythrogramma* (Val.) (Echinoidea: Echinometridae). *Aust. J. Zool.* **23:** 371–403.

Wray, G. A., and R. A. Raff. 1989. Evolutionary modification of cell lineage in the direct-developing sea urchin *Heliocidaris erythrogramma*. *Dev. Biol.* **132:** 458–470.

Wray, G. A., and R. A. Raff. 1990. Novel origins of lineage founder cells in the direct-developing sea urchin *Heliocidaris erythrogramma*. *Dev. Biol.* **141:** 41–54.

Yasumasu, I., K. Mitsunaga, and Y. Fujino. 1985. Mechanism for electrosilent Ca^{2+} transport to cause calcification of spicules in sea urchin embryos. *Exp. Cell Res.* **159:** 80–90.

Reference: *Biol. Bull.* **182:** 31–40. (February, 1992)

Purification and Biochemical Characterization of the Nuclear Sperm-Specific Proteins of the Bivalve Mollusks *Agriodesma saxicola*[1] and *Mytilimeria nuttalli*

JUAN AUSIÓ

Department of Biochemistry and Microbiology, University of Victoria, Victoria, British Columbia V8W 3P6, Canada

Abstract. The proteins from the nuclei of the sperm from two different species of the subclass Anomalodesmata of the class Bivalvia have been analyzed for the first time. In both instances—*Agriodesma saxicola* (Baird, 1863) and *Mytilimeria nuttalli* (Conrad, 1837)—the compositional pattern is very similar. The sperm chromatin is organized by a major protamine-like PL-I protein. As in all PL-I, this protein has a trypsin-resistant core. In both species analyzed, PL-I contains cysteine residues that account for the presence of the monomer (M) and dimer (D) forms observed in the total nuclear HCl extracts. The molecular mass of these proteins is 21,000 Da in *A. saxicola*, and 25,000 Da in *M. nuttalli*. All of the specimens of *A. saxicola* analyzed were hermaphrodites. As a result, the nuclear sperm-specific proteins from several preparations were readily and extensively degraded by protease activity from the oocytes. Such degradation was always observed when cross contamination between the two gonadal tissues accidentally occurred during protein extraction.

Introduction

The presence of a highly specialized histone H1 (PL-I protein) seems to be a common feature of the nuclear protein composition of the sperm of bivalve mollusks (Jutglar *et al.*, 1991). Despite the structural heterogeneity of the sperm proteins within this taxonomic group (Ausió, 1986; Zalensky and Zalenskaya, 1980), a PL-I protein has been identified in each of the species analyzed in detail so far. Like histone H1, this protein is soluble in diluted perchloric acid, has a globular trypsin-resistant core, is lysine rich, and yet is compositionally related to the protamines (PL = protamine-like) (Subirana *et al.*, 1973). Of all the different nuclear sperm-specific proteins found within a given species, PL-I is the one with the lowest electrophoretic mobility in urea-acetic acid gels (Ausió, 1986). The presence of a protamine-like histone H1-like protein in bivalve mollusks may have important evolutionary implications, not only within the phylum Mollusca (Subirana and Colom, 1987), but also within other taxonomic groups.

As pointed out by Kasinsky (1989), however, only some of the subclasses within the class Bivalvia have been analyzed so far, and only a few species have been thoroughly characterized. Nevertheless, at least one sperm-specific histone H1 (PL-I) protein has been identified: in *Mytilus californianus* (by Jutglar *et al.*, 1991), *Crassostrea gigas* (by Sellos, 1985), and *Glycymeris yesonensis* (by Odintsova *et al.*, 1989) (subclass Pteriomorphia); in *Ensis minor* (by Giancotti *et al.*, 1983), *Spisula solidissima* (by Ausió *et al.*, 1987) and *Macoma nasuta* (Ausió, 1988) (Subclass Heterodonta); and in *Anodonta piscinallis* (by Rozov *et al.*, 1984) (Subclass Palaeoheterodonta). In some of these species, two histone H1-like proteins have been described.

Although the subclass Heterodonta has been widely studied (Ausió, 1986), three subclasses, according to Barnes's (1980) classification of the bivalve mollusks, have never been characterized: Cryptodonta, Palaeotaxodonta, and Anomalodesmata. In the present work, we have analyzed and characterized the sperm-specific proteins of two species within the subclass Anomalodesmata and have shown that each contains a highly specialized histone H1-

Received 18 June 1991; accepted 25 November 1991.

[1] This species is more commonly referred to as *Entodesma saxicola*, but see Bernard, 1983.

like (PL-I) protein that is the major protein component of the nuclei of the sperm of that organism.

Materials and Methods

Living specimens

Specimens of *Agriodesma saxicola* and *Mytilimeria nuttalli* were collected along the west coast of Vancouver Island, British Columbia, Canada, by SCUBA divers from the Biology Department at the University of Victoria.

Nuclei preparation and protein extraction

Isolation of sperm nuclei and HCl crude extraction of the nuclear basic proteins was performed as described elsewhere (Ausió, 1986). Briefly, after carefully opening the shell, a small incision was made in the gonadal tissue, and the spontaneously released sperm were resuspended in NaCl 0.15 *M*, Tris-HCl 20 m*M* pH 7.6, 0.2 m*M* PMSF (Phenylmethylsulphonyl Fluoride) (buffer A). Because *A. saxicola* is hermaphroditic, its sperm would sometimes be contaminated with oocytes released accidentally from the intimately associated ovaries (see below for discussion).

The sperm suspension was centrifuged at 3000 × *g* for 10 min in a SS-34 Sorvall rotor at 4°C. The pellet obtained was homogenized in buffer A containing 0.5% TritonX-100. After standing for 10 min on ice, the suspension was spun down under the same conditions as before. This step is meant to solubilize most of the cytoplasmic membranes, including the sperm flagella and the acrosome. Notice that this step will also expose the sperm nuclei to egg lysates in those samples of *A. saxicola* contaminated with oocytes; such cytoplasmic contamination may be responsible for the protein degradation observed under these circumstances. The detergent-treated pellet was immediately homogenized in 0.4 *N* HCl. Solubilization was continued for 2 h under stirring at 4°C. Finally, the suspension was centrifuged at 12,000 × *g* for 10 min at 4°C, and the acid extract was precipitated with 6 volumes of acetone, overnight, at −20°C.

Gel electrophoresis

Polyacrylamide gel electrophoresis was carried out on urea-acetic acid gels, as described elsewhere (Ausió, 1986).

Protein purification and fractionation

Ionic exchange chromatography was carried out on a 10 × 100 mm Protein-Pak SP 8HR column from Waters-Millipore as described elsewhere (Mogensen *et al.*, 1991).

Gel filtration was carried out on a 10 × 300 mm FPLC Superose 12HR 10/30 column from Pharmacia. The elution buffer was 6 *M* guanidinium chloride (Gdn-HCl; Schwarz/Mann Biotech), 50 m*M* Tris-HCl pH 7.6.

Reverse phase high pressure liquid chromatography (HPCL)

HPLC was carried out on a 5 μ (25 × 0.46 cm) Vydac C_4 column, with 0.1% trifluoroacetic acid (TFA) as eluant with different acetonitrile gradients.

Determination of the molecular mass

The molecular mass of each protein was determined by gel filtration under denaturing conditions on a Superose 12HR column in the presence of 6 *M* Gdn-HCl (see above). Several protamines, protamine-like proteins, and histones of known molecular mass were used as standards: PL-I from *Spisula solidissima* (Mr: 33,500 Da) (Ausió and Subirana, 1982a); Histone H1 from calf thymus (Mr: 22,000 Da) (DeLange, 1976); PL-III (ϕ1) from *Mytilus edulis* (Mr: 9600 Da) (Ausió and Subirana, 1982b); and unfractionated salmine from *Oncorhynchus* sp. (Mr; 4300 Da) (Ando *et al.*, 1973). Histone H1 from calf thymus was purchased from Worthington, and salmine (sulfate form) was obtained from Sigma. The rest of the protamines were prepared in my laboratory. Globular proteins were also used as a molecular mass markers: bovine serum albumin (Mr: 68,000); ovoalbumin (Mr: 46,000); chymotrypsinogen A (Mr: 25,000); and ribonuclease A (Mr: 13,200). These proteins were purchased from Pharmacia; all of them were subjected to performic acid oxidation before being applied to the column (see below). Vitamin B12 (Mr: 1350) was purchased from Sigma. For the estimation of the molecular mass, the column was calibrated with the above standard proteins, and a plot of K_{av} *versus* log Mr was constructed (Mr = molecular mass; K_{av} = distribution coefficient).

$$K_{av} = \frac{V_e - V_o}{V_t - V_o}$$

where V_o and V_t are the void and total volume of the column, and V_e = the elution volume of a given protein. Blue Dextran and dansyl-L-alanine (Sigma) were used to determine V_o and V_t experimentally. The proteins of unknown Mr were mixed with the protein standards and run together through the column. Their molecular masses were estimated by interpolation of their K_{av} values on the best fitting line of the calibration plot.

Amino acid analysis

Amino acid analysis was carried out on an Applied Biosystems model 420A derivatizer-analyzer system. The hydrolysis was carried out in gas-phase 6 *N* HCl and 1% phenol under an argon atmosphere at 165°C, for 1 h, 2

h, and 4 h, the final amino acid composition was obtained by extrapolation of the data to zero time. So that cysteine could be quantified, all protein samples were pyridylethylated before hydrolysis, as described below.

Chemical modification of proteins

Reduction of SH groups. The SH groups of cysteine were reduced as described by Kuehl (1979). Briefly, the proteins, at 1 mg/ml in 6 *M* urea 20 m*M* Tris-HCl pH 7.6, were reduced in the presence of 8% β-mercaptoethanol for 3 h at room temperature.

Oxidation of SH groups. Oxidation was carried out under the same buffer conditions as above, but in the presence of 0.72 m*M* O-phenanthroline and 0.36 m*M* $CuSO_4$.

Performic acid oxydation. Performic acid was prepared according to Hirs (1967). For the oxidation, 1-mg aliquots of protein were dissolved in 0.5 ml of performic acid, which had been previously cooled on ice. The reaction was allowed to proceed for 4 h in an ice bath in capped tubes. The sample was then resuspended in a 25-fold excess of HPLC grade distilled water and lyophilized.

Cysteine pyridylethylation. Proteins were pyridylethylated, providing for a quantitative estimate of cysteine in the amino acid analysis. The procedure used was as follows: proteins (≅1 nanomol) were dissolved in 44 μl of 6.8 *M* urea, 60 m*M* Tris-HCl, 1.25 m*M* EDTA (pH 7.6), and 2.3% β-mercaptoethanol. The solution was incubated for 3 h at room temperature in the dark. Subsequently, 8

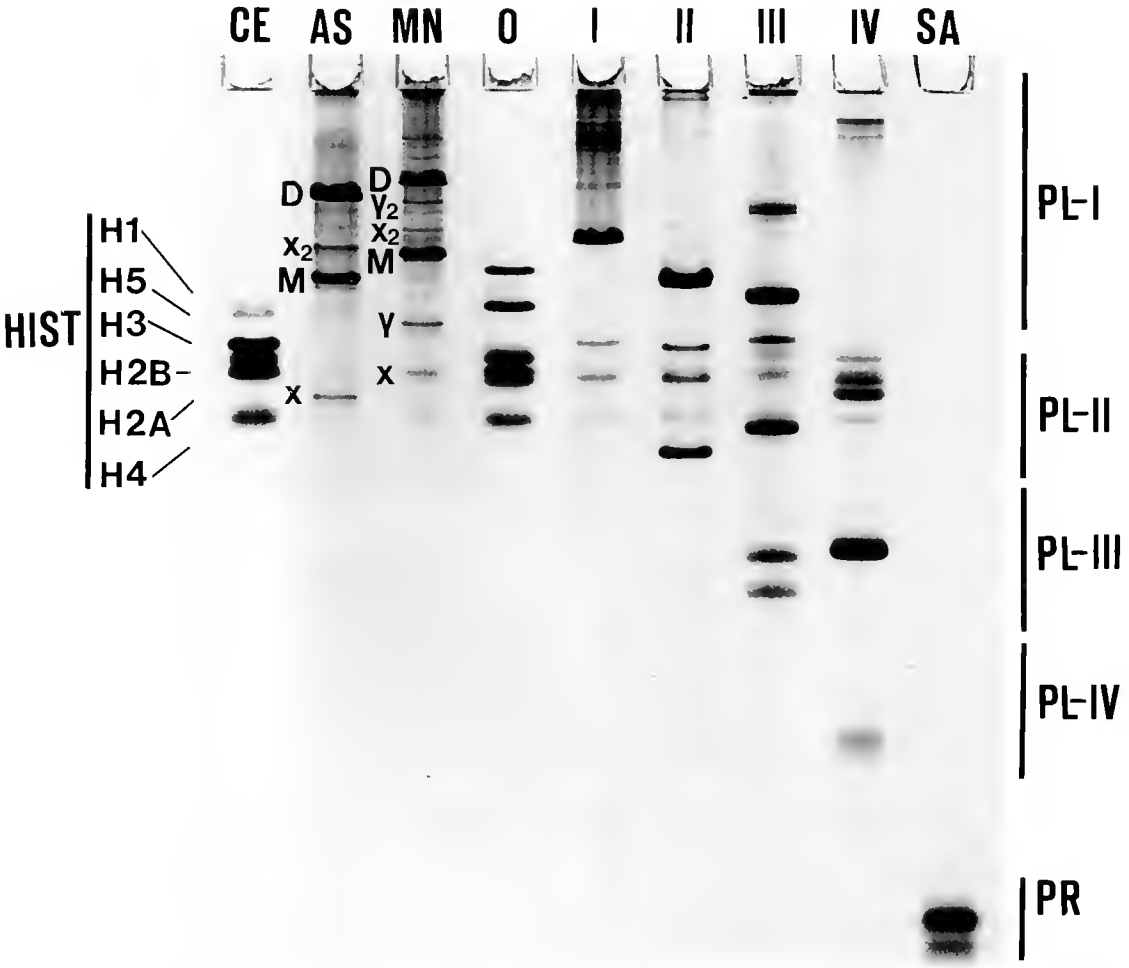

Figure 1. Urea acetic acid PAGE analysis of the nuclear sperm-specific proteins of *Agriodesma saxicola* (AS) and *Mytilimeria nuttalli* (MN) in comparison to a histone standard from chicken erythrocytes (CE) and to a protamine from salmon, salmine (SA). The nuclear sperm-specific proteins of one representative of each of the five groups (O, I, II, III, and IV) of the classification of the bivalve mollusks (Ausió, 1986) are also shown. The representative species chosen for each group were: O: *Pecten maximus;* I: *Spisula solidissima;* II: *Ensis ensis;* III: *Macoma nasuta,* and IV: *Mytilus edulis.* The regions corresponding to the different protamine-like (PL-I, PL-II, PL-III, and PL-IV) proteins defined in Ausió (1986) are also shown. HIST: histone region. PR: protamine. D: dimer form, M: monomer form of the major sperm protein component in each species. X_2, Y_2: possible dimer forms of the minor sperm protein components X, Y.

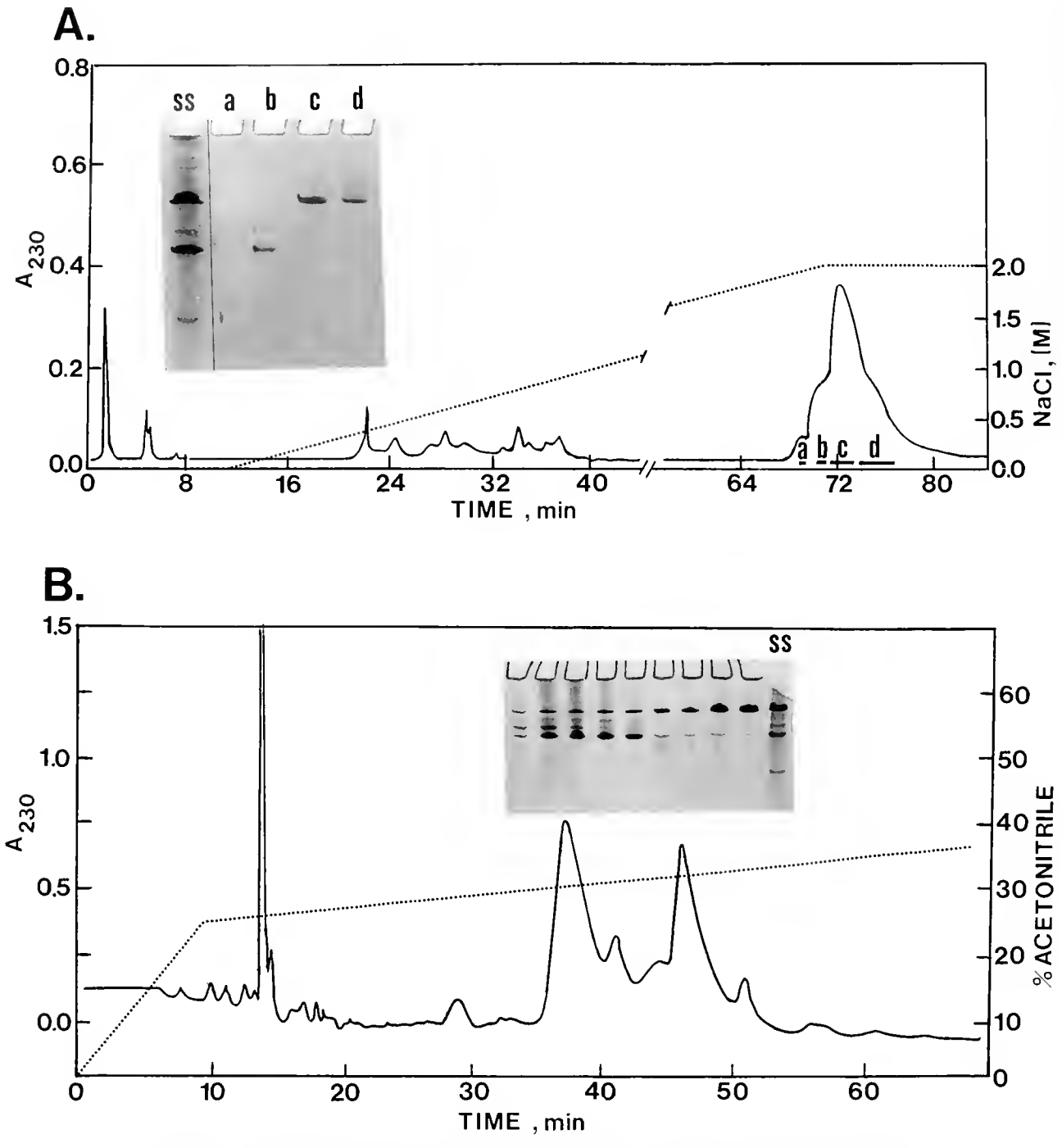

Figure 2. Fractionation of a crude 0.4 *N* HCl extract from the nuclei of the sperm of *Agriodesma saxicola*. (A) Ionic exchange chromatography on a (10 × 100 mm) Protein-Pak SP 8HR column. Proteins were eluted with a linear (0–2 *M*) NaCl gradient in 50 m*M* Na-phosphate buffer (pH 6.8) at a flow rate of 1 ml/min. The inset shows the urea-acetic acid PAGE analysis of the fractions indicated. (B) Reverse-phase HPLC on a Vydac C_4 column. Elution was carried with an acetonitrile gradient in 0.1% trifluoroacetic acid at a flow rate of 1 ml/min. The inset shows the electrophoretic analysis of the fractionation. The lanes shown in the inset, and the chromatogram has been aligned to match the fraction analyzed with its corresponding position in the chromatogram. SS: starting sample.

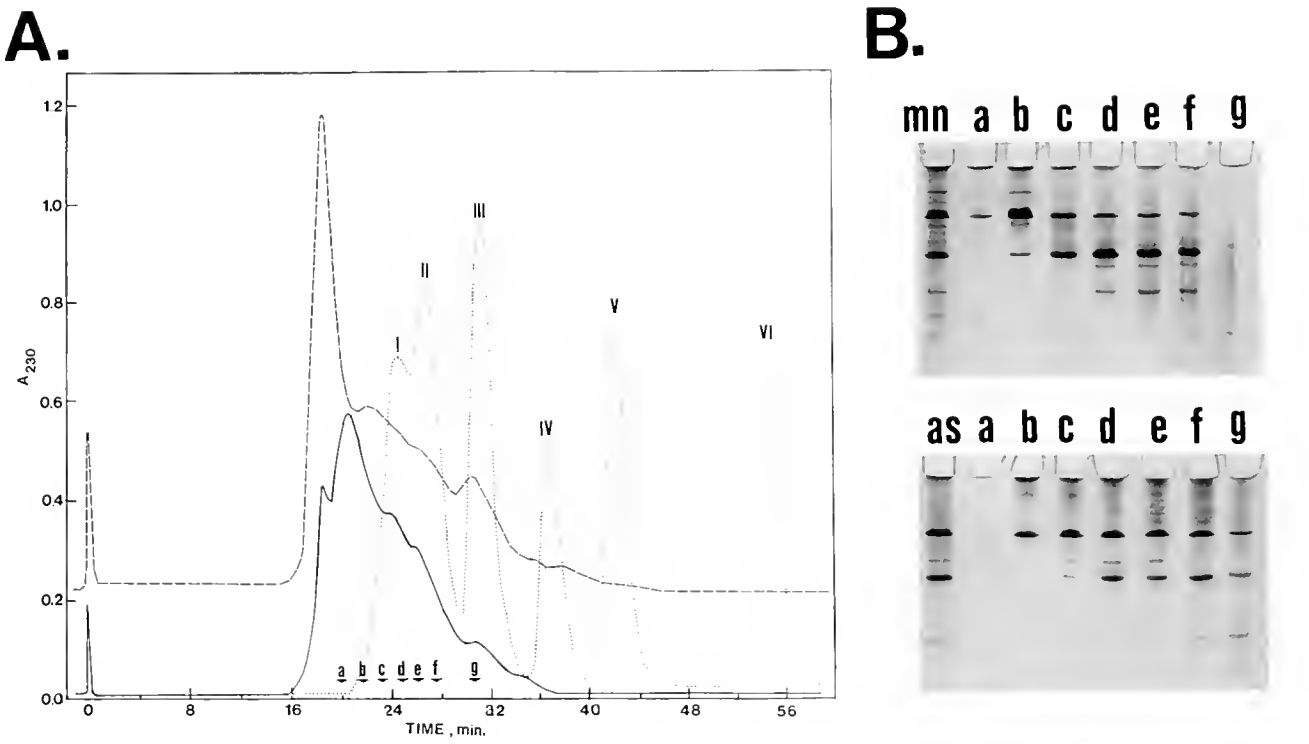

Figure 3. (A) Gel filtration FPLC on a Superose 12 HR 10/30 column. The elution buffer was 6 *M* Gdn-HCl in 50 m*M* Tris-HCl pH 7.6. The flow rate was 0.4 ml/min. The elution profiles of HCl nuclear extracts from the sperm of *Mytilimeria nuttalli* (– – –) and *Agriodesma saxicola* (——) are shown together with the elution profile (· · · ·) of some of the standards used to calibrate this column: I: PL-I from *Spisula solidissima*; II: Histone H1 from calf thymus; III: PL-III from *Mytilus edulis*; IV: protamine salmine; V: vitamin B 12; VI: dansyl-L-alanine. (B) Electrophoretic analysis on urea-acetic acid gels of the fractions a, b, c, d, e, f, g of the elution profiles of *M. nuttalli* and *A. saxicola*. mn: starting sample of *M. nuttalli*. as: starting sample of *A. saxicola*.

μl of 4-vinylpyridine was added, and the reaction was allowed to proceed for 2 h at room temperature. The sample was then immediately desalted in an HPLC reverse phase C_8Vydac column, which was eluted for 5 min with 0.1% TFA (trifluoroacetic acid), and for 20 min with a 0–70% acetonitrile gradient in 0.1% TFA. β-lactoglobulin from Applied Biosystems Inc. was used as a standard for this procedure.

Trypsin digestion. Trypsin digestion of proteins in high salt—2 *M* NaCl, 50 m*M* Na-phosphate buffer (pH 6.8)—was carried out as described elsewhere (Ausió *et al.*, 1987).

Results

Chromatographic analysis and purification of the sperm-specific nuclear proteins from A. saxicola *and* M. nuttalli

Figure 1 shows the 0.4 *N* HCl protein extracts from the nuclei of the sperm of *A. saxicola* and *M. nuttalli*. They are shown in comparison to the five groups previously established for the classification of the nuclear sperm-specific proteins of the bivalve mollusks (Ausió, 1986). In each of the two species analyzed, two major protein bands run in the region of the PL-I proteins (Ausió, 1986). In addition to these proteins, 10–20% of minor protein fractions X and Y, which run in the histone region, are also observed (see Fig. 1-AS and 1-MN). This protein composition was sufficiently novel that the two organisms could not, at first, be assigned to any of the protein groups previously established in my classification of the bivalves (Ausió, 1986). That was not surprising because they belong to a subclass (Anomalodesmata) that had not been analyzed before. I therefore decided to purify and characterize each of the major protein components of these organisms.

The first attempt at fractionation by ionic exchange FPLC under non-denaturing conditions is shown in Figure 2A. Most of the protein components coeluted in a single multiphasic peak at around 2 *M* NaCl, but some protein separation was clearly achieved as is shown in the inset of the same figure.

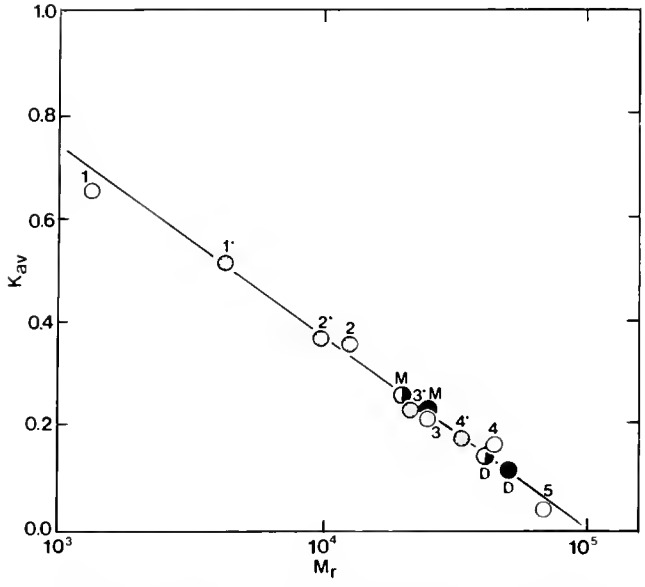

Figure 4. Calibration plot used to determine the molecular mass of the sperm proteins determined on a superose 12 HR 10/30 column under the elution conditions described in Figure 3A. Globular ○ and nonglobular ◍ proteins were used as standards. 1: Vitamin B 12 (Mr: 1,350 Da); 2: ribonuclease A (Mr: 13,200 Da); 3: chymotrypsingen A (Mr: 25,000 Da); 4: ovoalbumin (Mr: 46,000 Da); 5: bovine serum albumin (Mr: 68,000 Da); 1*: protamine salmine (Mr: 4,300 Da); 2*: protein PL-I from *Mytilus edulis* (Mr: 9,600 Da); 3*: histone H1 from calf thymus (Mr: 22,000 Da); 4*: Protein PL-I from *Spisula solidissima* (Mr: 33,000 Da). M = monomer form and D = dimer form of the major sperm protein components of: *Mytillineria nuttalli* ●, and *Agriodesma saxicola* ◑.

To increase the resolution in the separation, the 0.4 *N* HCl protein extracts were fractionated by reverse-phase HPLC; the elution profile is shown in Figure 2B. Although two peaks corresponding to each of the two major components could be clearly separated, both of them exhibited different amounts of what appeared to be overlapping cross-contamination.

Size fractionation of the starting HCl extracts by gel filtration under denaturing conditions in the presence of 6 *M* guanidinium chloride (Gdn-HCl) is shown in Figure 3. Although the peaks could not be completely resolved, the sample was partially fractionated as shown in Figure 3B. Indeed, when some of the eluting fractions from the different regions corresponding to the two major protein components were pooled together and rerun under the same conditions, two distinct peaks could then be clearly resolved. This was used as a basis for estimating the molecular mass of each of these protein components. Nevertheless, when the fraction under each separate peak was analyzed by urea acetic acid PAGE, the same cross-contamination observed in Figure 2B was again observed, although to a lesser extent (results not shown).

Characterization of the sperm-specific nuclear proteins from A. saxicola *and* M. nuttalli

The fractionation problems described in the preceding section began to be elucidated when the molecular mass of these proteins was analyzed. Figure 4 shows the calibration plot used to estimate the molecular mass of proteins from gel filtration analysis. The molecular mass of the two major protein components of the sperm nuclei in *A. saxicola* were: 21,000 Da for the fastest protein component and 43,000 Da for the slowest moving fraction. The values were 25,000 Da and 49,000 Da for *M. nuttalli*. These results suggested a monomer-dimer relationship between the slow and the fast moving protein fractions present in each species. To analyze this relationship, and to examine the nature of the association phenomenon, I incubated the crude HCl extracts in the presence of either β-mercaptoethanol or copper phenanthroline. Figure 5 shows the results of these treatments in the case of *A. saxicola*, and identical results were obtained with *M. nuttalli* (results not shown). The slower moving band completely disappears under reducing conditions for cysteine. Under oxidizing conditions (in the presence of copper phenanthroline) the relative intensity of the faster moving band (see Fig. 5b) slightly decreases, and higher association complexes are formed (see arrow in Fig. 5b). We are therefore dealing with the association of the faster moving protein components. Although the association seems to involve primarily the formation of dimers, the number of cysteines present in the monomer

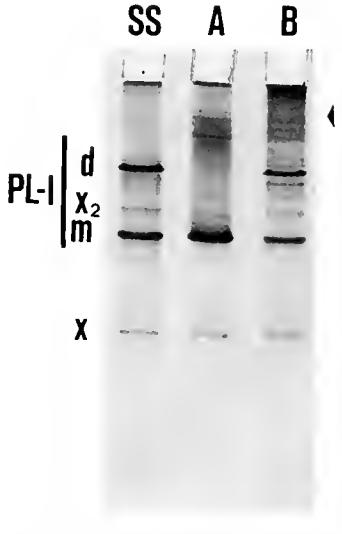

Figure 5. Urea-acetic acid polyacrylamide gel electrophoresis of the nuclear sperm specific proteins from *Agriodesma saxicola* under A: reducing (6% β-mercaptoethanol) or B: oxidizing (copper-phenanthroline) conditions. SS = starting sample. m, d = monomer and dimer of major sperm protein component (PL-I). X, X_2 = monomer and dimer of the minor sperm protein component. The arrowhead indicates the presence of higher association oligomers obtained upon oxidative treatment.

cannot be clearly ascertained from the above experiments. Thus, although the strong tendency toward dimer formation would suggest the presence only of one cysteine per molecule, the lack of complete dimerization observed in Figure 5b, and the presence of association complexes higher than dimers, would strongly suggest the presence of more than one cysteine. The presence of two cysteine residues per molecule, which could easily form an internal disulfide bond, would explain the incomplete polymerization of the monomer, otherwise expected under the oxidizing conditions used here (Fig. 5b).

To determine the number of cysteines, as well as to establish the amino acid composition of the major nuclear protein component of the sperm of *A. saxicola* and *M. nuttalli*, protein fractions such as those shown in the insets of Figure 2A and B were pyridylethylated before amino acid analysis. A β-lactoglobulin sample was simultaneously treated and analyzed to check for the completion of the reaction. The amino acid analyses clearly show (see Table I) that the proteins of both *A. saxicola* and *M. nuttalli* contain two cysteine residues per molecule. Comparison with the amino acid analyses of other PL proteins, reveals the PL-I nature of the major nuclear protein component of the sperm of the two species analyzed. Like other PL-I proteins (Ausió, 1986; Ausió, 1988; Jutglar *et al.*, 1991), these have an internal trypsin resistant core (Fig. 6).

Besides the major protein components M and D, we have also characterized the minor component X of *A. saxicola*. This protein exhibits an amino acid composition that is almost identical to PL-I (see Table I). Although the amino acid analysis was carried out without prior pyridilethylation, trace amounts of cysteine could still be detected. Because of its relative electrophoretic mobility, X_2 (see Fig. 1-AS) most probably represents the dimer form of X. Indeed, X_2 disappears upon β-mercaptoethanol treatment of the starting protein sample (see Fig. 5).

Table I

Amino acid analysis (mol %) of the nuclear sperm-specific PL-I proteins of Agriodesma saxicola *PL-I (AS) and* Mytilimeria nuttalli *PL-I (MN) in comparison to those of* Spisula solidissima *PL-I (SS) (Ausió and Subirana, 1982a) and* Macoma nasuta *PL-I (MC) (Ausió, 1988)*

	P1-I (AS)	PL-I (MN)	PL-I (SS)	PL-I (MC)	X (AS)
Lys	18.7	16.3	24.8	21.8	15.1
His	—	0.4	—	2.3	0.4
Arg	34.8	33.8	23.1	26.9	34.7
Asx	1.5	1.8	0.6	0.8	2.5
Thr	2.0	1.0	4.3	4.0	1.6
Ser	20.8	26.5	21.7	20.2	21.4
Glx	1.1	0.8	0.6	0.8	4.6
Pro	0.5	0.8	2.4	1.8	1.7
Gly	6.0	5.5	3.0	2.2	5.0
Ala	3.3	4.2	14.2	11.3	4.4
1/2 Cys	0.9	0.6	—	0.7	tr.*
Val	3.2	2.4	2.3	2.4	2.8
Met	—	0.2	0.4	0.2	—
Ile	1.2	0.9	0.5	1.4	1.0
Leu	3.6	3.3	1.7	2.1	2.6
Tyr	1.5	1.0	0.3	0.5	1.0
Phe	0.7	0.7	0.3	0.7	1.0
Trp	—	—	0.3	—	

* Determination carried out in the absence of pyridilethylation treatment.

The amino acid analysis of the minor protein component X of *A. saxicola* (AS) is also shown.

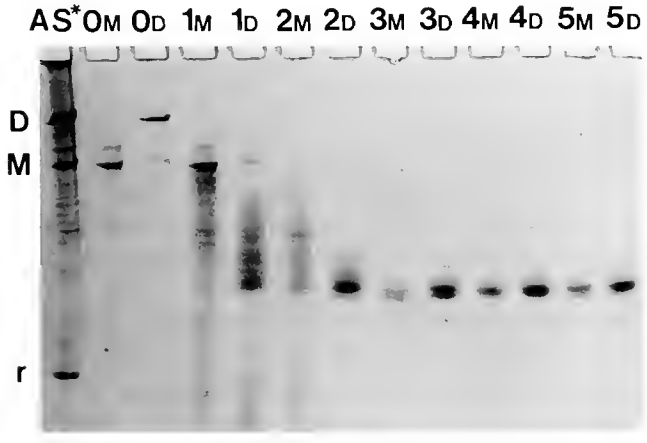

Figure 6. Analysis of the time course of digestion by trypsin of the monomer (M) and dimer (D) of the PL-I protein of *Agriodesma saxicola*. Digestions were carried out in 2 *M* NaCl, 50 m*M* Na phosphate (pH 6.8), at an enzyme:substrate ratio of 1:500. The digestion times were: 0: 0 min; 1: 5 min; 2: 15 min; 3: 30 min; 4: 60 min and 5: 120 min. AS*: nuclear sperm-specific proteins of *A. saxicola* slightly degraded by an egg protease (see legend to Fig. 7). r: peptide resistant to digestion by egg proteases.

Specific degradation of PL-I in A. saxicola

Every specimen of *A. saxicola* analyzed was hermaphroditic. Although the male and female gonads are completely separated, some contamination of the sperm by oocytes sometimes occurred when accidental incisions were made in the ovary as the shells were being opened. The protein composition of the crude HCl nuclear extracts thus obtained showed a complex and highly variable pattern in urea acetic acid gel electrophoresis. Figure 7 shows a light microscope and electrophoretic analysis of several sperm samples with different amounts of contamination by oocytes. In preparations containing pure sperm, the electrophoretic analysis showed two major bands, M and D (Fig. 7a), corresponding to the monomer and dimer of PL-I, as well as a 15–20% of X and X_2. As the extent of contamination by female germinal cells increases (see Fig. 7b, c), the amounts of M and D present in the HCl extracts

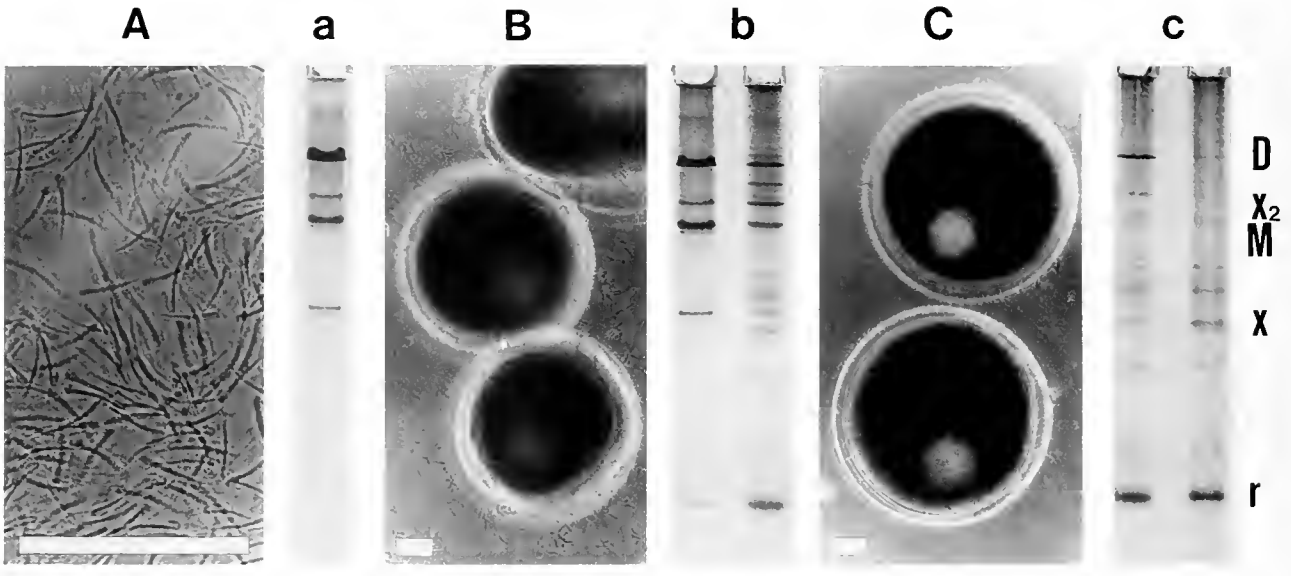

Figure 7. Microscopic analysis with phase contrast of pure sperm (A), and of sperm preparations containing an increasing amount of contamination by eggs (B) and (C). The samples were obtained from different specimens of *Agriodesma saxicola*. a, b, and c: electrophoretic analysis, in urea-acetic acid PAGE, of sperm preparations containing an increasing amount of contamination by eggs. As contamination increases, an extensive degradation of both the monomer (M) and dimer (D) forms of the major nuclear sperm-specific PL-I component is observed. A relatively resistant peptide—r—is generated during this degradation process. The white bar corresponds to 50 μm. X and X_2 are as in Figure 5.

decrease, and the proteins finally disappear completely. This is accompanied by the appearance of a complex pattern of new bands with faster electrophoretic mobility (Fig. 7b, c). Such protein pattern transition is clearly indicative of a degradation process elicited by specific proteases from the contaminating eggs. A similar *in vitro* degradation of sperm histones by the cytoplasm of sea urchin eggs has also been reported (Betzalel and Moav, 1987). A quite resistant degradation peptide, designated r, is produced during this process. Although the composition and nature of peptide r are completely unknown, it is certainly much smaller than the trypsin-resistant peptide obtained under *in vitro* conditions (see Fig. 6). A nuclear HCl protein extract from pure oocytes contained none of the proteins observed in Figure 7 (results not shown).

Discussion

In this work I have analyzed the protein composition of the nuclei of the sperm of two representatives of the subclass Anomalodesmata within the class Bivalvia. In both of the species analyzed—*Agriodesma saxicola* and *Mytilimeria nuttalli*—80–90% of the nuclear sperm-specific proteins consist of a mixture of dimer (D) and monomer (M) forms of a protamine-like (PL-I) protein. The remaining 10–20% includes the minor protein fractions X and Y.

The protamine-like nature of the major proteins is revealed by their amino acid composition (see Table I). They clearly fulfill the compositional definition of protamines (Subirana, 1983): (Lys + Arg) = 45–80%, (Ser + Thr) = 10–25%. Indeed, of all the PL proteins characterized so far, the ones analyzed here exhibit the highest arginine content within the PL classification (Ausió, 1986). The presence of a trypsin-resistant core (see Fig. 6) indicates that these proteins are also related to the proteins of the histone H1 family. Therefore, the PL major components of both *A. saxicola* and *M. nuttalli* should be undoubtedly classified within the PL-I class (Ausió, 1986). The presence of cysteine in these proteins does not seem to be an unusual feature; indeed, two cysteines also occur in the PL-I component of *Macoma nasuta* (Ausió, 1988).

Because the minor protein component X of *A. saxicola* has an amino acid composition indistinguishable from PL-I, these two proteins must be closely related, and X_2 (see Fig. 1-AS) may represent a dimer form of X. The same observations apply to the X and Y components of *M. nuttalli* (results not shown). The structural relationships among PL-I and the X and Y fractions remain obscure, but the similarity of their amino acid analyses to that of the major protein component suggests that X and Y may be proteolytic peptides from PL-I. They could arise from the activity of either a nuclear or an acrosomal sperm protease (Müller-Esterl and Fritz, 1981) during protein extraction. However, they do not seem to be related to any of the protein fragments produced by the protease digestion resulting from oocytic contamination, because

Table II

Classification of the class Bivalvia according to their protamine-like group (Ausió, 1986)

Subclass (a)	Representative species	Protein type (b)	Reference
Cryptodonta	—		—
Palaeotaxodonta			
Palaeoheterodonta	*Anodonta pisciniallis*	I (?)	(c)
Heterodonta	*Spisula solidissima*	I	(d)
	Ensis minor	II	(e)
	Macoma masuta	III	(f)
	Mytilus edulis	IV	(g)
Pteriomorphia	*Crassostrea gigas*	O	(h)
Anomalodesmata	*Agriodesma saxicola*	II	(i)
	Mytilimeria nuttalli	I	(i)

(a) According to Barnes (1980).
(b) According to Ausió (1986).
(c) Rozov *et al.* (1984).
(d) Ausió and Subirana (1982a).
(e) Giancotti *et al.* (1983).
(f) Ausió (1988).
(g) Ausió and Subirana (1982c).
(h) Sellos (1985).
(i) This work.

the presence of X_2 or X does not increase as the level of egg-induced degradation increases (see Fig. 7). Indeed, when whole sperm cells (without any prior preparation of the nuclei) were extracted with HCl for ½ h at 4°C immediately after sperm collection, the overall protein pattern observed was undistinguishable from the pattern of the HCl extracts prepared from nuclei uncontaminated by oocytes. In particular, the X-band was still observed.

The presence of a major PL-I protein in the sperm of the two species analyzed here would allow us to classify them within the protamine-like group I of my earlier classification of the bivalve mollusks (Ausió, 1986; see Table II). Species fulfilling this compositional pattern have also been described in other subclasses, including Palaeoheterodonta and Heterodonta. The presence of a PL-I protein, however, seems to be a common feature to all the species of the class Bivalvia (Jutglar *et al.*, 1991).

All of the PL-I proteins that have been analyzed in detail have structures related to the histone H1 superfamily (Ausió *et al.*, 1987; Ausió, 1988; Jutglar *et al.*, 1991). The structural similarities of PL-I to both histone H1 and the arginine-rich protamines from the vertebrates suggests a close evolutionary relationship between these proteins. In this sense, the increase in arginine and the decrease in lysine and alanine observed in the case of the PL-I proteins analyzed in the present work, when compared to other PL-I proteins, would indicate a further departure from their H1 nature and a closer relationship to the protamines from vertebrates.

Acknowledgments

I am very indebted to Debra Murie, Daryl Parkyn, and Joachim Schnorr von Carosfeld from the Biology Department at the University of Victoria for providing me with the biological specimens used in this work. I am also very grateful to Steve Carlos for his valuable assistance in running the HPLC and FPLC columns and for reading the manuscript. I also would like to thank Mrs. Denise Lunger and Ms. Cheryl Gonnason for typing the manuscript. This work was supported by NSERC Grant OGP 0046399 to Juan Ausió.

Literature Cited

Ando, T., M. Yamasaki, and K. Suzuki. 1973. P. 28 in *Protamines.* Vol. 12 of *Molecular Biology, Biochemistry and Biophysics.* Springer-Verlag, Berlin, Heidelberg, NY.

Ausió, J., and J. A. Subirana. 1982a. A high molecular weight nuclear basic protein from the bivalve molluscs. *J. Biol. Chem.* **257:** 2802–2805.

Ausió, J., and J. A. Subirana. 1982b. Conformational study and determination of the molecular weight of highly charged basic proteins by sedimentation equilibrium and gel electrophoresis. *Biochemistry* **21:** 5910–5918.

Ausió, J., and J. A. Subirana. 1982c. Nuclear proteins and the organization of chromatin in spermatozoa of *Mytilus edulis*. *Exp. Cell. Res.* **141:** 39–45.

Ausió, J. 1986. Structural variability and compositional homology of the protamine-like components of the sperm from the bivalve molluscs. *Comp. Biochem. Physiol.* **85B:** 439–449.

Ausió, J., A. Toumadje, R. McParland, R. R. Becker, W. C. Johnson, Jr., and K. E. van Holde. 1987. Structural characterization of the trypsin resistant core in the nuclear sperm-specific protein from *Spisula solidissima*. *Biochemistry* **26:** 975–982.

Ausió, J. 1988. An unusual cysteine-containing histone H1-like protein and two protamine-like proteins are the major nuclear proteins of the sperm of the bivalve mollusc: *Macoma nasuta*. *J. Biol. Chem.* **263:** 10,141–10,150.

Barnes, R. D. 1980. *Invertebrate Zoology,* 4th ed. Saunders College, Philadelphia.

Bernard, F. R. 1983. Catalogue of the living Bivalvia of the eastern Pacific Ocean: Bering Strait to Cape Horn. *Canadian Special Publication of Fisheries and Aquatic Sciences* **81:** 83.

Betzalel, M., and B. Moav. 1987. Degradation of sperm histones *in vitro* by cytoplasm of the sea urchin egg. *Cell Differ.* **20:** 125–136.

DeLange. 1976. *Handbook of Biochemistry and Molecular Biology.* 3rd ed. (Proteins), G. Fasman, ed. CRC press Boca Raton, FL, vol II, 294 pp.

Giancotti, V., E. Russo, M. Gasparini, D. Serrano, D. Del Piero, A. W. Thorne, P. D. Cary, and C. Crane-Robinson. 1983. Proteins from the sperm of the bivalve mollusc: *Ensis minor*. *Eur. J. Biochem.* **136:** 509–516.

Hirs, C. M. W. 1967. Determination of cysteine as cysteic acid. *Methods Enzymol.* **XI:** 59–62.

Jutglar, L., J. I. Borell, and J. Ausió. 1991. Primary, secondary and tertiary structure of the core of a histone H1-like protein from the sperm of *Mytilus*. *J. Biol. Chem.* **266:** 8184–8191.

Kasinsky, H. E. 1989. Specifity and distribution of Sperm Basic Proteins. Pp. 73–163 in *Histones and Other Basic Nuclear Proteins,* Vol. I, L. S. Hnilica, G. S. Stein, and J. L. Stein, eds. CRC Press, Boca Raton, FL.

Kuehl, J. 1979. Synthesis of high mobility group proteins in regenerating rat liver. *J. Biol. Chem.* **254:** 7276–7281.

Mogensen, C., S. Carlos, and J. Ausió. 1991. Microheterogeneity and interspecific variability of the nuclear sperm proteins from *Mytilus*. *FEBS Lett.* **282:** 273–276.

Müller-Esterl, W., and H. Fritz. 1981. Sperm acrosin. *Methods Enzymol.* **80:** 621–632.

Odintsova, N. A., S. M. Rozov, and I. A. Zalenskaya. 1989. The chromosomal proteins from the sperm of the bivalve molluscs *Swiftopecten swifty* and *Glycymerys yesonensis*. *Comp. Biochem. Physiol.* **93B:** 163–167.

Rozov, S. M., V. A. Bredníkov, F. K. Gorel, M. V. Lavrenteva, and L. P. Solonenko. 1984. Structure of lysine-rich histone from sperm of *Anodonta piscinalis*. *Mol. Biol.* (transl) (USSR) **18:** 1497–1508.

Sellos, D. 1985. The histones isolated from the sperm of the oyster *Crassostrea gigas*. *Cell Differ.* **17:** 183–192.

Subirana, J. A., C. Cozcolluela, J. Palau, and M. Unzeta. 1973. Protamines and other basic proteins from spermatozoa of molluscs. *Biochim. Biophys. Acta* **317:** 364–379.

Subirana, J. A. 1983. *Nuclear Proteins in Spermatozoa and Their Interactions with DNA*, Pp. 197–214 in *The Sperm Cell*, J. André, ed. Martinus Nijhoff B. V., The Hague.

Subirana, J. A., and J. Colom. 1987. Comparison of protamines from freshwater and marine bivalve molluscs: evolutionary implications. *FEBS Lett.* **220:** 193–196.

Zalensky, A. O., and I. A. Zalenskaya. 1980. Basic chromosomal proteins of marine invertebrates II. The proteins from the Bivalvia molluscs. *Comp. Biochem. Physiol.* **66B:** 415–419.

Reference: *Biol. Bull.* **182:** 41–53. (February, 1992)

The Origin of Cortical Vesicles and their Role in Egg Envelope Formation in the "Spiny" Eggs of a Calanoid Copepod, *Centropages velificatus*

PAMELA I. BLADES-ECKELBARGER[1] AND NANCY H. MARCUS[2]

[1]*Darling Marine Center, University of Maine, Walpole, Maine 04573 and* [2]*Department of Oceanography, Florida State University, Tallahassee, Florida 32306*

Abstract. The mature oocytes of the marine calanoid copepod, *Centropages velificatus*, contain two morphologically distinct populations of cortical vesicles that undergo sequential exocytoses at the time of spawning. The contents of the primary cortical vesicles are released first and form the primary egg envelope. This is followed by the exocytosis of the secondary cortical vesicles. These contain numerous intracisternal granules that, upon release into the perivitelline space, transform into a mass of fine fibers. The continual accumulation of fibers constitutes an extracellular matrix between the primary envelope and the egg's plasmalemma. Further amassment of the fibers beneath the primary egg envelope results in the formation of long, spiny projections. The evolution of the cortical vesicles was traced to the early vitellogenic oocytes and appears to be unique. The two populations of cortical vesicles are synthesized together within the same cisternal elements of rough endoplasmic reticulum (RER). The RER originates from membranous blebs off both the nuclear membrane and stacks of annulate lamellae in the early vitellogenic oocytes. Numerous intracisternal granules are present within the RER. Some of these granules fuse, forming a dense, ring-like structure in the extremities of the cisternae. These bud off from the RER to become the primary cortical vesicles. The unfused intracisternal granules remain as discrete bodies within irregular profiles of vesicular ER and comprise the secondary cortical vesicles.

Received 15 July 1991; accepted 2 October 1991.

Contribution Nos.: (PBE) Harbor Branch Oceanographic Institution Contribution No. 892 and Darling Marine Center, University of Maine Contribution No. 244; (NHM) Florida State University Marine Laboratory Contribution No. 1068.

Introduction

The subject of post-embryonic development in free-living copepods has been a favorite research topic for decades. Consequently, the literature abounds with descriptions of naupliar and copepodid developmental stages. However, studies relating to embyronic development, *i.e.*, those stages from spawning to the emergence of the first nauplius, are limited to only a few early publications (Grobben, 1881; Fuchs, 1914; Witschi, 1934; Marshall and Orr, 1954, 1955). In particular, details of the mechanisms of fertilization and egg envelope formation have yet to be elucidated in the Copepoda.

Some marine calanoid species spawn their eggs into ovisacs that remain attached to the female until the emergence of the first or second naupliar stage. The majority of marine calanoids, however, are broadcast spawners, releasing the eggs freely into the surrounding water where they undergo development. Within this latter group, eggs of a variety of shapes and sizes and with different types of surface ornamentation have been observed (Johnson, 1967; Koga, 1968; Kasahara *et al.*, 1974; Uye, 1983; Marcus, 1990). The egg surfaces of most species are smooth, but others may be adorned with flanges or spines of varying shapes and lengths. The production of spiny eggs has been reported for numerous species, *Acartia tonsa* (Zillioux, 1969), *Centropages ponticus* (Sazhina, 1968), *C. hamatus* (Pertzova, 1974), *Pontella mediterranea* (Sazhina, 1968; Grice and Gibson, 1981; Santella and Ionora, 1990), *A. erythraea, C. yamadai, C. abdominalis* (Kasa-

hara *et al.*, 1974), *A. steuri* (Uye, 1983), *C. velificatus* (Marcus, pers. obs.), *Calanus glacialis* (J. Runge and Blades-Eckelbarger, pers. obs.), and *Candacia pachydactyla* (Blades-Eckelbarger, pers. obs.).

Some of the species listed above produce two morphological types of eggs where the spiny form represents a diapause stage (hatching is delayed), and the smooth form typifies a subitaneous stage (no mandatory delay in hatching) *e.g., Centropages hamatus* (Pertzova, 1974) and *C. ponticus* (Sazhina, 1968). *Pontella mediterranea* produces three morphotypes; diapause eggs with long spines, and subitaneous eggs that are either smooth or adorned with short spines (Sazhina, 1968; Grice and Gibson, 1981; Santella and Ionora, 1990). *Acartia tonsa* (Zillioux, 1969) and *A. steuri* (Uye, 1983) have been reported to produce both smooth and spiny eggs, but their physiological classification as diapause or subitaneous is still in question. For the remaining species, only spiny eggs have been observed, and there is no evidence to suggest that they are a diapause stage.

While conducting a morphological survey of copepod eggs found in sea bottom muds, we became intrigued with the spiny modifications of the egg envelopes of some species. Consequently, we initiated a study using light microscopy along with scanning and transmission electron microscopy to investigate the stages of egg envelope development and spine formation in the eggs of *Centropages velificatus.*

Materials and Methods

Adult female *Centropages velificatus* (De Oliveira, 1947) were sorted from plankton tows collected approximately 10 miles due east off the coast of Fort Pierce, Florida. Female's carrying mature, pigmented oocytes were placed in small dishes with filtered seawater that were observed every few minutes for spawned eggs. The eggs were carefully picked up by drawn-out pipettes and placed onto pieces of 35 μm mesh supported by Beem capsules (Flood, 1973). The Beem capsules sat in shallow glass dishes containing 2.5% glutaraldehyde in filtered seawater.

For transmission and scanning electron microscopy (TEM and SEM), eggs in varying stages of development, from polar body extrusion to advanced spine formation, were collected and fixed in this manner. After approximately 100 eggs were placed in a Beem capsule, the capsule was transferred to a 5% Karnovsky's (1965) glutaraldehyde-paraformaldehyde mixture in 0.1 *M* Sorensens phosphate buffer. The capsules were flushed several times with the latter fixative to prevent precipitate caused by seawater mixing with the phosphate buffer. As a matter of convenience, due to the long duration of the complete fixation process, the eggs were held in the Karnovsky's fixative for varying times depending on the time of day collected. Those collected in the morning were held at room temperature for 3 to 6 h. Those collected in the evening were held overnight at 4°C. The lower temperature slows the fixation process. There were no apparent differences in cell or organelle structure among the varying times and temperatures.

Adult females carrying mature oocytes were prepared also for TEM. Initially each individual was placed in a small amount of the Karnovsky's glutaraldehyde mixture for approximately 15 min. The head and urosome were then removed with a sharp razor and the metasomes transferred to a vial containing fresh fixative and held for the same range of times as the eggs.

This primary fixation of both eggs and adult females was followed by 2 or 3 rinses in 0.1 *M* Sorensen's phosphate buffer (pH 7.4) and then held in 2% OsO_4 in 0.1 *M* Sorensen's buffer at room temperature for 1–2.5 h. The samples were rinsed briefly with buffer and dehydrated through an ascending series of alcohols to 70%. At this point, some of the eggs were pipetted onto SEM stubs covered with double-sided sticky tape and allowed to air dry in a desiccator for 2 to 3 days. The air-dried stubs were coated with gold palladium and observed with a Zeiss Novascan 30 SEM.

For TEM examinations, the remaining eggs and female metasomes were dehydrated further to 100% ETOH followed by propylene oxide and infiltrated with three changes of Epon (Luft, 1961). For final embedding, the female metasomes were oriented in flat embedding molds. The eggs were carefully drawn into a wide bore pipette with fresh Epon and dropped into a Beem capsule, which was centrifuged at room temperature for 20 min at setting #6 in a clinical centrifuge. Because the Epon is of a slightly thickened consistency, centrifugation is needed to concentrate the hardened eggs into the tip of the Beem capsule. Extensive sectioning of eggs prepared in this manner revealed no membrane or organelle damage. For light microscopy, 1-μm thick sections were cut with glass knives on a Porter-Blum MT2B ultramicrotome, and stained with Richardson's stain (Richardson *et al.*, 1960). Thin sections for TEM were stained with uranyl acetate followed by lead citrate and examined on a Zeiss EM9-S2 TEM.

It should be noted that the procedures for both SEM and TEM result in minor shrinkage of the eggs. Therefore, all measurements are approximations.

Results

Live observations of spawning and spine formation

Females were observed spawning on several occasions, during which they remained active, swimming in a normal manner around the dish. The oocytes flowed out of one

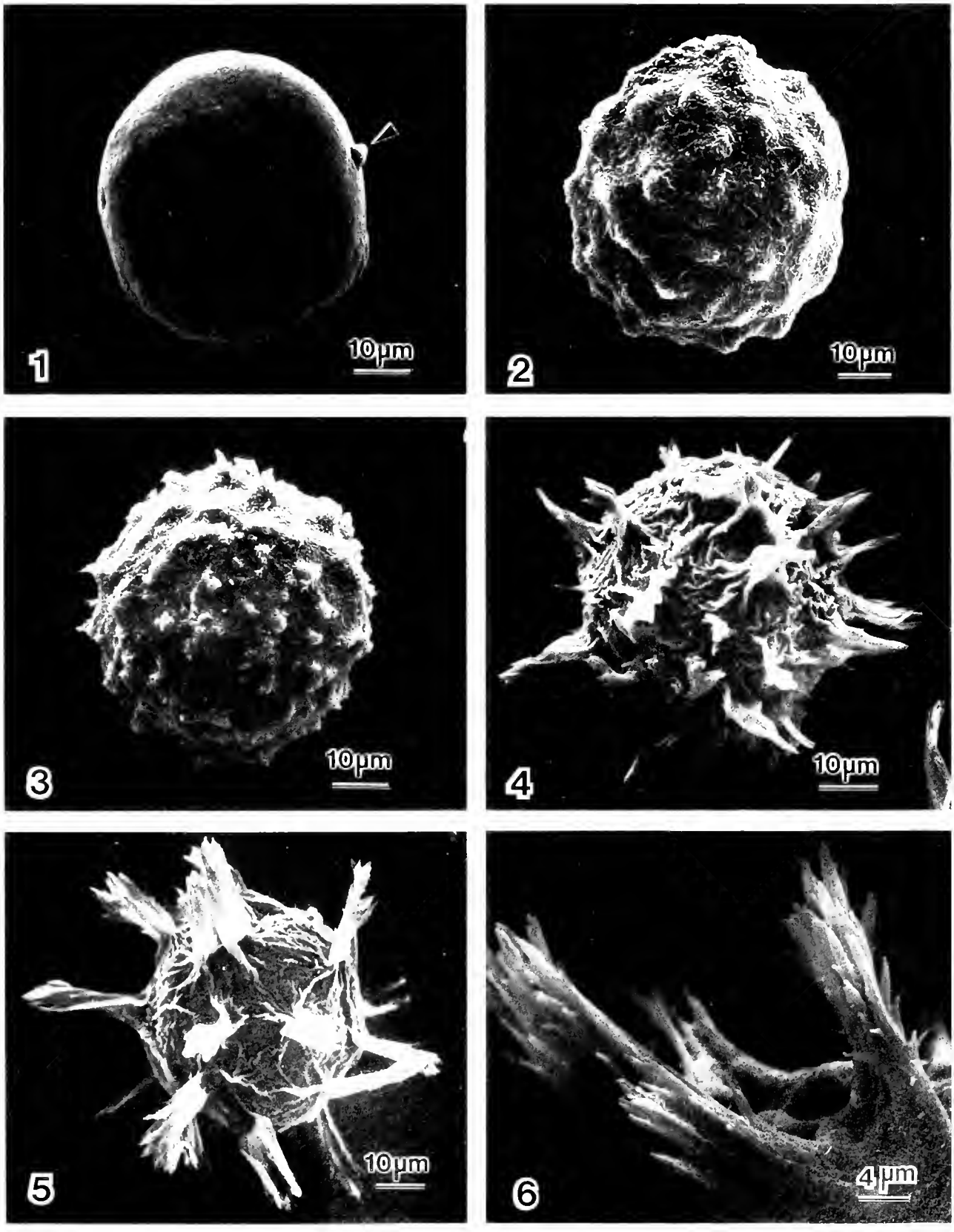

Figures 1–5. SEMs of egg envelope and spine formation from emergence of first polar body (Fig. 1, unlabeled arrow) to 24-h-old embryo (Fig. 5).
Figure 6. SEM. High magnification of spines.

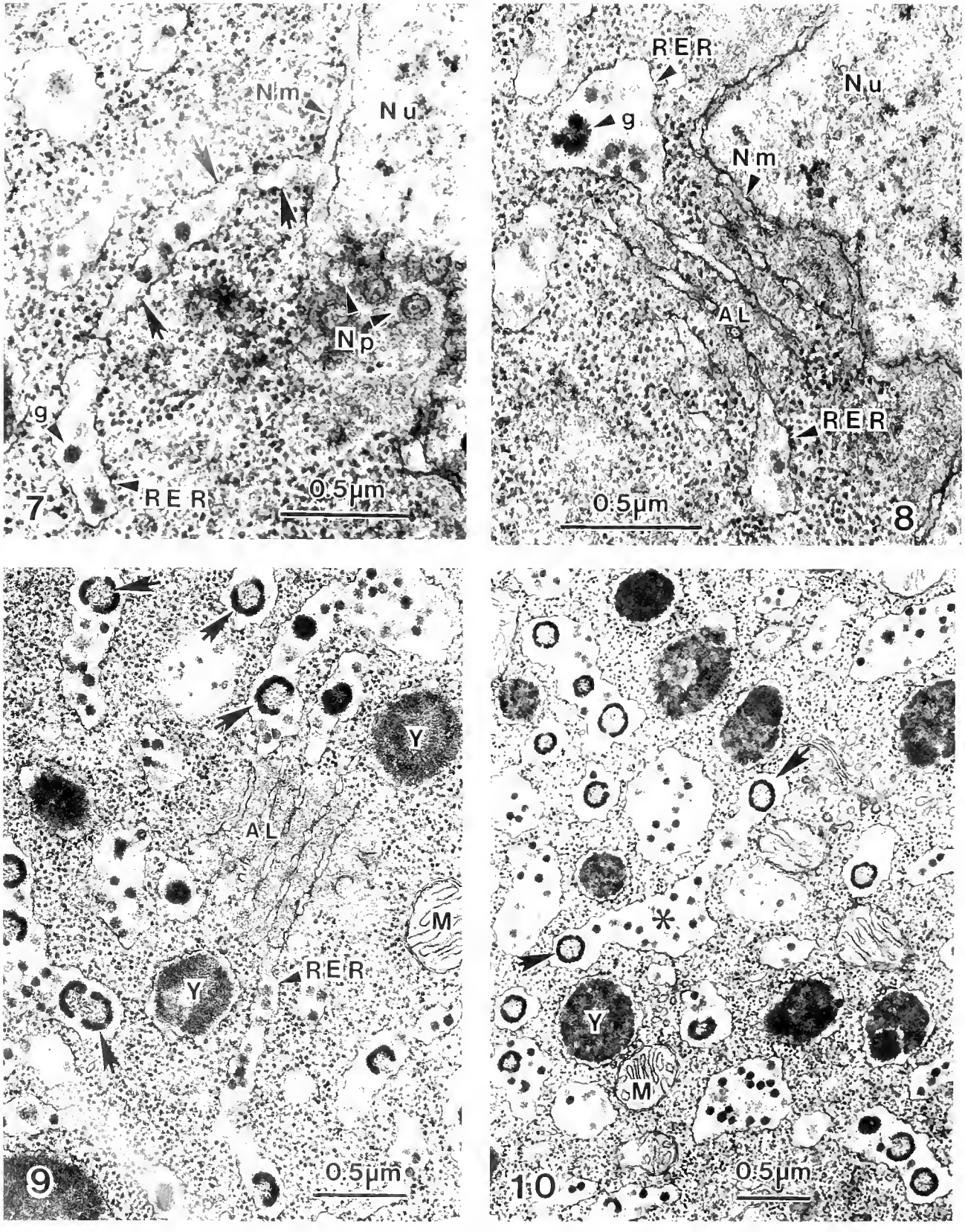

Figure 7. Perinuclear region of vitellogenic oocyte showing nuclear bleb (large arrowheads) extending from nuclear envelope (Nm) in formation of rough endoplasmic reticulum (RER). Note intracisternal granules (g) within nuclear bleb and RER. NP, nuclear pores.

Figure 8. Perinuclear region of vitellogenic oocyte showing annulate lamellae (AL). Note swollen extremities (RER) containing granules (g). Nm, nuclear membrane; Nu, nucleus.

or both oviducts, emerging from the genital pore as a single mass. The female would periodically twitch the urosome, causing the amorphous mass of eggs to break free and fall to the bottom of the dish. Approximately 5–10 s after release from the female, the eggs separated from each other and transformed from an oval to a spherical shape. Release of the first polar body occurred at this time (Figs. 1, 14). The second polar body was not observed. The actual process of sperm and egg fusion in copepods has never been reported, nor was it seen in the present study. Therefore, it could not be ascertained when egg envelope formation began relative to the moment of fertilization.

Figures 1 to 6 present comparative SEM views of the stages of spine formation from emergence of the first polar body (Fig. 1) to a 24-h-old embryo (Fig. 5). Approximately 5 min after spawning, large, rounded bumps appeared on the egg surface (Fig. 2). These bulges became more slender and pointed, forming short jagged spines (Fig. 3). It took approximately 15–20 min for long spines to form. A survey of over 100 eggs that were at least 24 h old revealed individual variations in the morphology, number, and size of the spines.

Cortical vesicle formation in vitellogenic oocytes

Formation of the egg envelope in *Centropages velificatus* involves the exocytosis of two morphologically distinct, membrane-bound inclusions present in the egg's cytoplasm. Prior to spawning, the mature oocytes that reside in the oviducts of the female contain a variety of morphologically distinct granules, vesicles, and inclusions. One type of inclusion, referred to here as the *primary cortical vesicle,* appears as a membrane-bound body containing an electron-dense, granular material that surrounds an electron-lucent core (Figs. 11, 12). Favorable sections through the center of these vesicles present the appearance of a darkly staining ring around a flocculent center (Fig. 12). The *secondary cortical vesicles* appear as irregularly shaped vesicles filled with several moderately dense granules (*ca.* 75–82 nm diameter) (Figs. 11, 12).

Primary and secondary cortical vesicles originate in the very early stages of vitellogenesis, where a blebbing process of the outer lamina of the nuclear membrane is observed (Fig. 7). These nuclear blebs contain numerous moderately dense granules (*ca.* 80 nm diameter) and pinch off to form lamellar and vesicular profiles of rough endoplasmic reticulum (RER). Stacks of annulate lamellae are also observed in the perinuclear region (Fig. 8), as well as in the central cytoplasmic region of mid- and late-vitellogenic stages (Fig. 9). Vesicles containing several dense granules, morphologically identical to the nuclear blebs, also pinch off from the extremities of the annulate lamellae. Fusion of some, but not all, of these intracisternal granules culminates in the formation of the ring-shaped densities that characterize the primary cortical vesicles (Figs. 8–10).

The cytoplasm of mid-vitellogenic oocytes is filled with elongate profiles of RER containing numerous unfused, intracisternal granules residing with one or more ring-shaped densities (Figs. 9, 10). Small Golgi complexes were observed infrequently, but did not appear to contribute to the contents of the RER. In the mature oocytes, the ring-shaped portions bud off from the RER to become the primary cortical vesicles (Figs. 10, 11). They are enclosed by a smooth membrane devoid of ribosomes. The unfused intracisternal granules remain as discrete bodies within irregular profiles of vesicular ER that also have lost the attached ribosomes. These represent the secondary cortical vesicles (Figs. 11, 12).

There is no elaboration of an egg envelope prior to spawning. The oocytes are enclosed by a simple oolemma that is coated with a lightly staining glycocalyx (Fig. 13). The glycocalyx, or vitelline envelope, is deposited over the oolemma by the associated follicle cells during the mid-stages of vitellogenesis (Blades-Eckelbarger and Youngbluth, 1984).

Cortical reaction, egg envelope elaboration, and spine formation

Deposition of the egg envelope results from a cortical vesicle reaction involving two successive stages of exocytosis. Soon after spawning, the majority of yolk bodies and other inclusions accumulate toward the center of the egg, but the primary and secondary cortical vesicles remain in the cortical cytoplasm (Fig. 14). The first cortical reaction is characterized by the exocytosis of the primary cortical vesicles. The bounding membrane of the primary cortical vesicles fuses with the egg's plasmalemma, and the enclosed material is released into the perivitelline space (Figs. 15, 16). This results in the formation of a narrow layer (*ca.* 20 nm thick) of darkly staining material situated slightly above the egg's plasmalemma (Figs. 15, 16, 18, 21). We refer to this first layer as the "primary egg envelope." At this time, the egg surface has a "bumpy" appearance (Figs. 2, 3, 17) where regions of the plasmalemma

Figure 9. Early stage of primary cortical vesicle formation (large arrowheads) in vesicular RER of mid-vitellogenic oocyte. Note annulate lamellae (AL) with swollen extremities (RER). M, mitochondrion; Y, yolk granules.

Figure 10. Mid-vitellogenic oocyte. Ring-shaped densities (large arrowheads) budding off of RER (*) in formation of primary cortical vesicles. M, mitochondrion; Y, yolk granule.

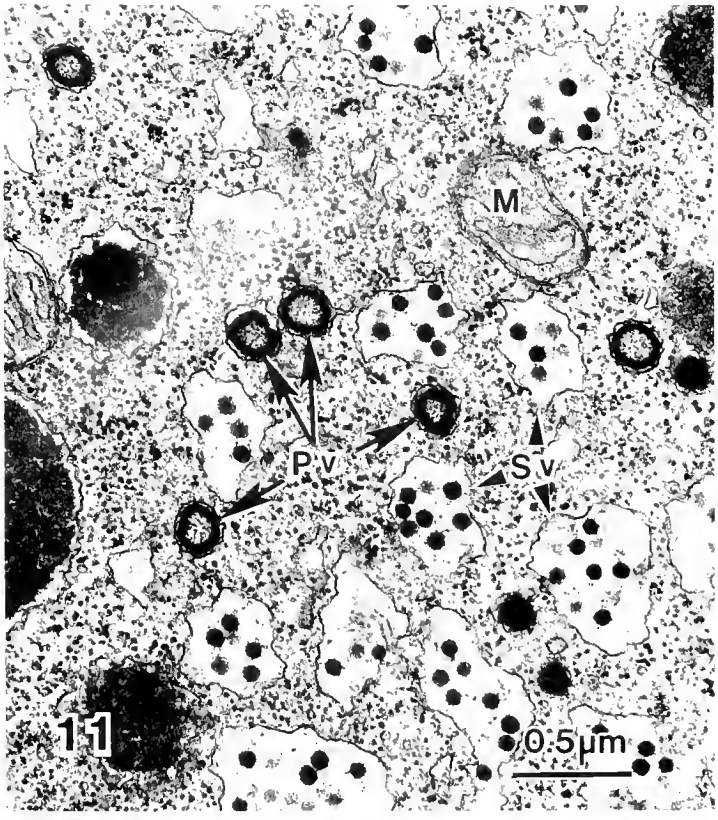

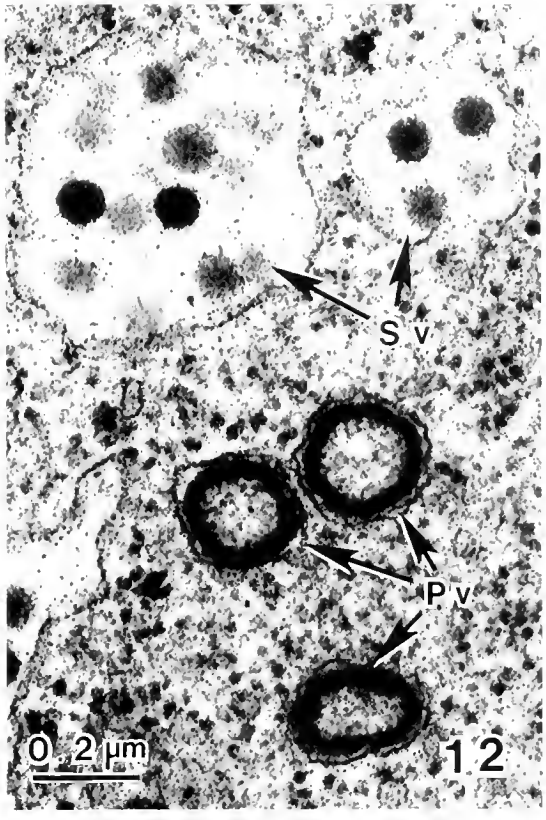

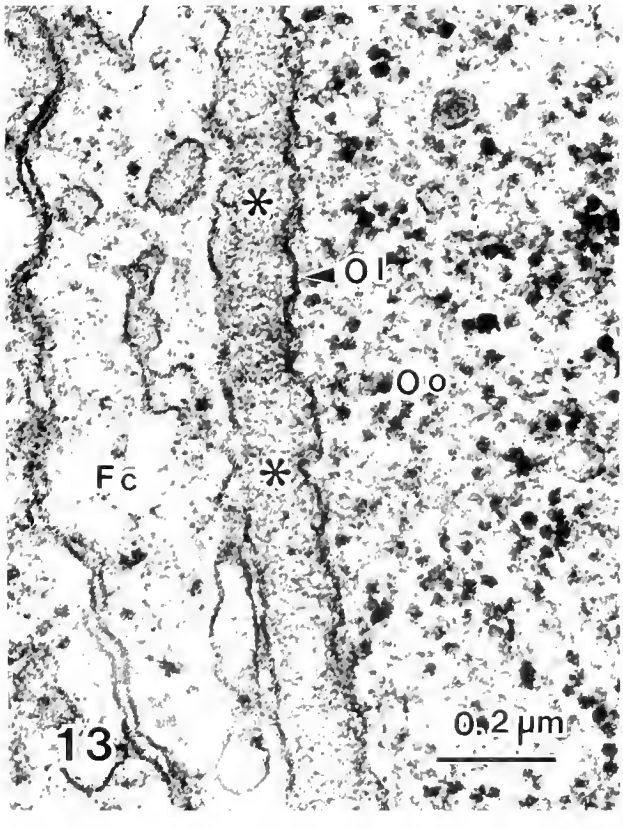

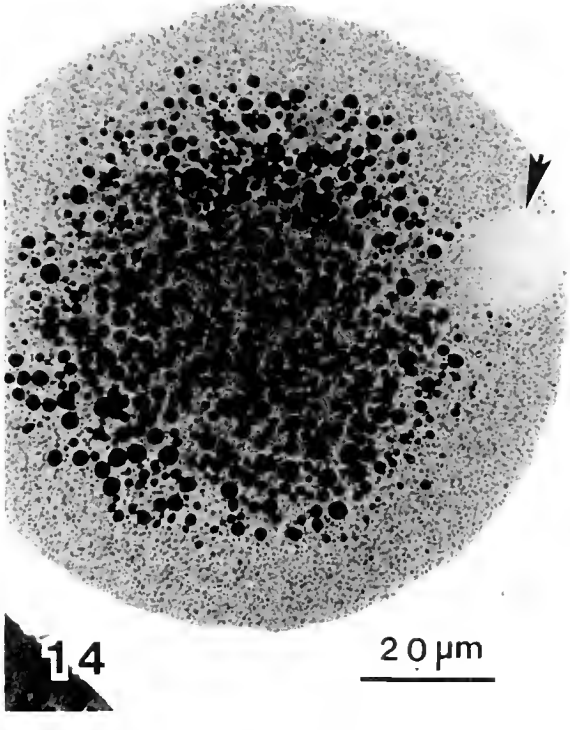

Figure 11. Late vitellogenic oocyte with primary cortical vesicles (Pv) now separate from secondary cortical vesicles (SV). M, mitochondrion.
Figure 12. High magnification showing structure of primary (Pv) and secondary (Sv) cortical vesicles.
Figure 13. Oolemma (Ol) of mature oocyte in oviduct of female covered by vitelline envelope (*). Fc, follicle cell; Oo, ooplasm.
Figure 14. Light micrograph, 1-µm-thick section of newly spawned egg and formation of first polar body (arrowhead). Note centrally located yolk granules with primary and secondary cortical vesicles occupying cortical cytoplasm.

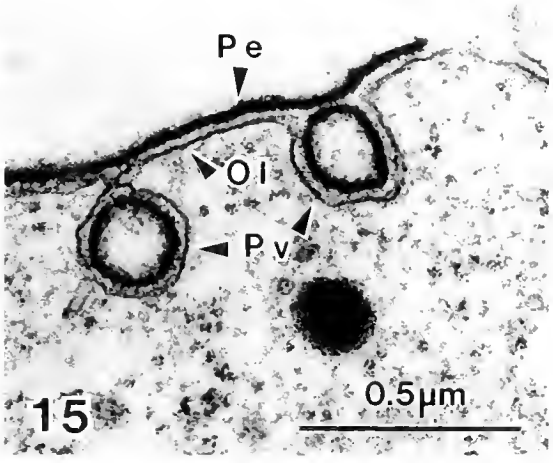

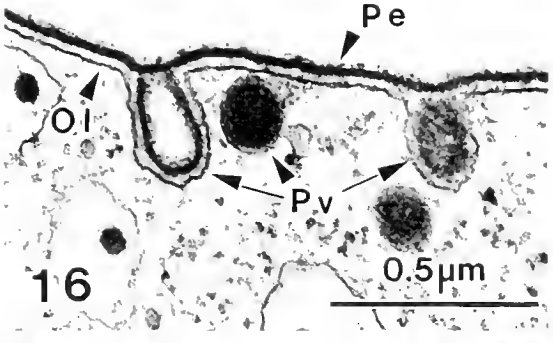

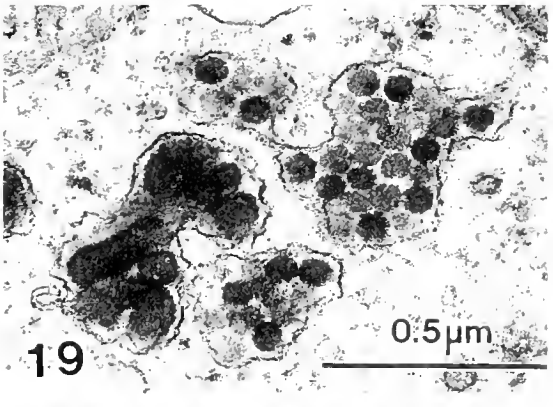

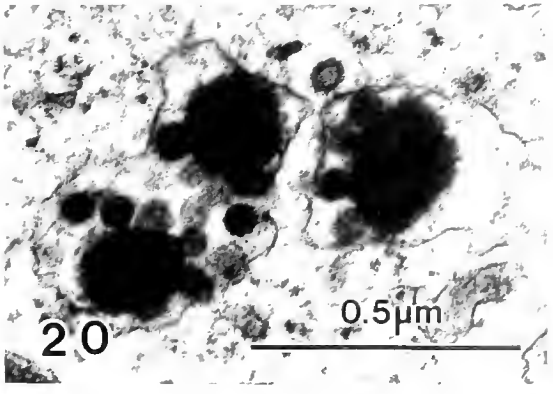

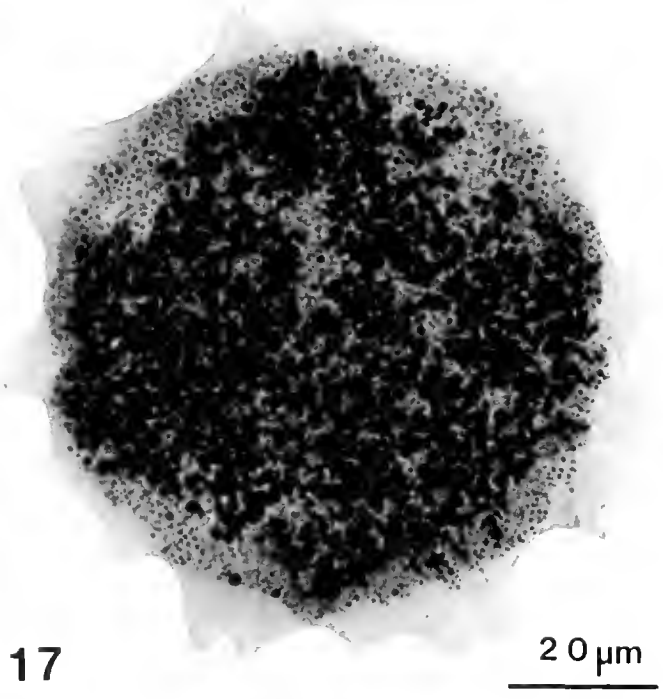

Figures 15 and 16. First cortical reaction. High magnification of egg surface showing fusion of primary cortical vesicles (Pv) with oolemma (Ol) and exocytosis of dense material in formation of primary envelope (Pe).

Figure 17. Light micrograph, 1-μm-thick section of egg during first cortical reaction and exocytosis of primary cortical vesicles. Note that cytoplasm extends into projections of egg surface.

Figure 18. Cortical cytoplasm of egg in late stage of first cortical reaction showing fusion of granules within secondary cortical vesicles (Sv). M, mitochondrion; Ol, oolemma; Pe, primary envelope; Y, yolk granule.

Figures 19 and 20. High magnification of secondary cortical vesicles showing fusion of granules.

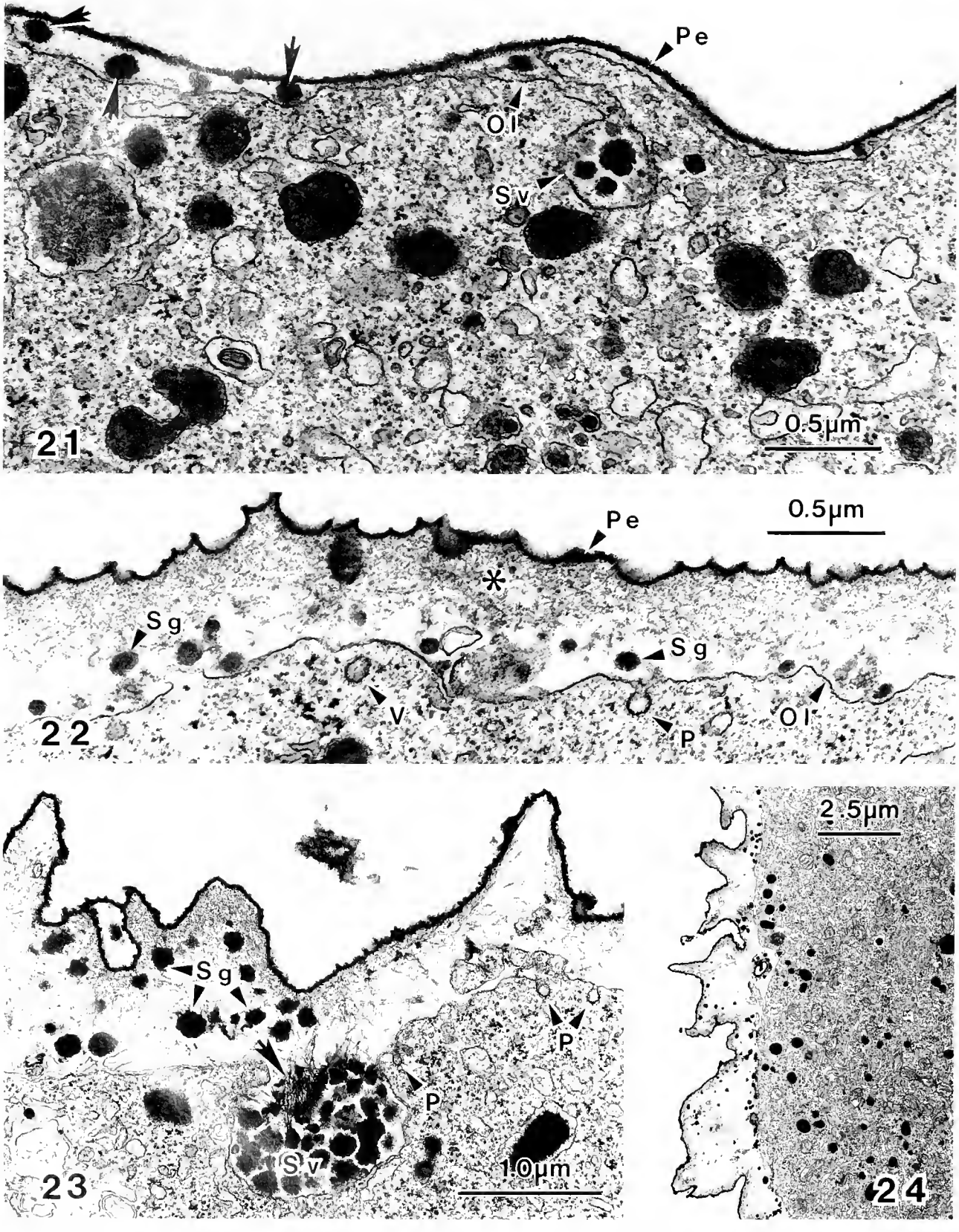

Figure 21. Second cortical reaction showing exocytosis of granules (large arrowheads) from secondary cortical vesicles (Sv). Ol, oolemma; Pe, primary envelope.

bulge out. The egg's cytoplasm projects into these expanded areas (Fig. 17).

A second wave of exocytosis follows soon after the first with the release of the intracisternal granules contained within the secondary cortical vesicles (Figs. 21, 23). Just prior to their release, however, some of the intracisternal granules fuse with each other, forming slightly larger and denser masses (Figs. 18–20). Once in the perivitelline space, the intracisternal granules transform into a meshwork of fibers that adhere to the inner surface of the primary egg envelope (Figs. 22, 23, 25, 27, 28). Concomitant with the second wave of exocytosis is the appearance of numerous endocytotic pits and vesicles along the egg's plasmalemma (Figs. 22, 23).

With the continual accumulation of fibers from the secondary cortical vesicles, the primary envelope lifts higher above the egg's plasmalemma forming an irregular surface sculpturing (Fig. 22), the plasmalemma withdraws from the core of the spines and the egg proper becomes spherical again (Fig. 26). Observations of eggs in multicellular stages (approx. 24 h), during or just after synthesis of the naupliar cuticle, revealed both long and short spines with a crenulated surface (Figs. 27, 28). The space between the cuticle and the egg envelope is composed of a thick mass of fibers (Figs. 27, 28).

Discussion

Based on our observations of the oocytes and eggs of *Centropages velificatus,* we present here the first identification of cortical vesicles, and a description of the cortical reaction and subsequent egg envelope formation in the Copepoda. These processes follow the same general sequence of post-spawning events as reported in other animal species (Schuel, 1985; Longo, 1988). However, where the eggs of some species contain a single, morphologically heterogeneous population of cortical vesicles (or granules), those of *C. velificatus* were found to have two. Consequently, the cortical reaction in the eggs of *C. velificatus,* involves not one, but two exocytotic events.

The presence of structurally different populations of cortical granules has been demonstrated in other crustaceans, the crab *Carcinus maenus* (Goudeau and Becker, 1982) and the decapod shrimp *Sicyonia ingentis* (Pillai and Clark, 1988, 1990). Talbot and Goudeau (1988) reported four distinct cortical vesicles in the oocytes of the lobster *Homarus.* In all cases, the various populations of cortical vesicles exhibited distinctly different morphologies, underwent temporally separated exocytoses, and in *S. ingentis* (Pillai and Clark, 1990) were found to be chemically heterogeneous. Each type of cortical vesicle contributed to different layers of the egg envelope.

During the first cortical reaction in the eggs of *Centropages velificatus,* the contents of the primary cortical vesicles form the outer, or primary, egg envelope. This layer may correspond to the fertilization envelope of other animals, which is formed from the mixing of the vitelline layer with the exocytosed contents of the cortical vesicles (Kay and Shapiro, 1985; Somers and Shapiro, 1989). Exocytosis of the secondary cortical vesicles in the eggs of *C. velificatus* follows soon after the primary egg envelope is complete. The secondary vesicles contain several discrete intracisternal granules that, upon their release into the perivitelline space, transform into a myriad of fibers. The accumulation of these fibers between the egg's plasmalemma and the primary egg envelope forms an extracellular matrix (ECM) that exhibits a similar morphology to ECMs surrounding the eggs and embryos of other marine invertebrates (Spiegel *et al.,* 1989).

The present paper further illustrates the cellular mechanisms by which the two populations of cortical vesicles are synthesized in the vitellogenic oocytes of *Centropages velificatus.* In the oocytes of many animals, the cortical vesicles are derived from the Golgi complex (see Schuel, 1985, and references therein). In the decapod shrimp, *Sicyonia ingentis* (Pillai and Clark, 1988), one population of cortical vesicles is derived from Golgi complexes and the second population from within the cisternae of RER. Cortical vesicle formation in *C. velificatus,* in general, is similar to that of *Carcinus* (Goudeau, 1984) and *Homarus* (Kessel, 1968; Talbot and Goudeau, 1988) in which the vesicles are produced by the ER, and Golgi complexes do not appear to contribute. Other aspects of cortical vesicle formation in *C. velificatus* are unique; (1) both nuclear blebs and annulate lamellae appear to be involved in formation of the vesicular RER that synthesizes the intracisternal granules and, (2) these intracisternal granules appear to be the precursors of both the primary and secondary cortical vesicles. Fusion of some of these granules within the RER cisternae forms the dense, ring-shaped contents of the primary cortical vesicles. The other intracisternal granules do not fuse, but remain distinct and

Figure 22. Second cortical reaction showing lifting of primary envelope (Pe) and filling of perivitelline space with fine fibers (*). Note surface sculpturing of primary envelope as well as coated micropinocytotic pits (p) and vesicles (v) along the oolemma (Ol). Sg, granules from secondary cortical vesicles.

Figure 23. Early spine formation showing massive exocytosis of secondary cortical vesicle (Sv). Large arrowhead denotes transformation of granular material into fine fibers. P, coated micropinocytotic pits; Sg, granules from secondary cortical vesicles in perivitelline space.

Figure 24. Mid-stage of spine formation.

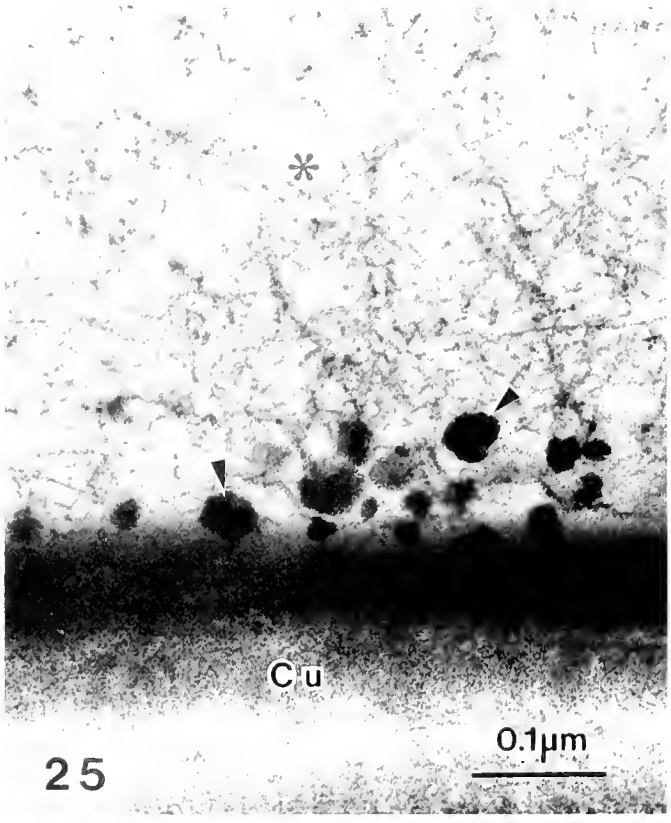

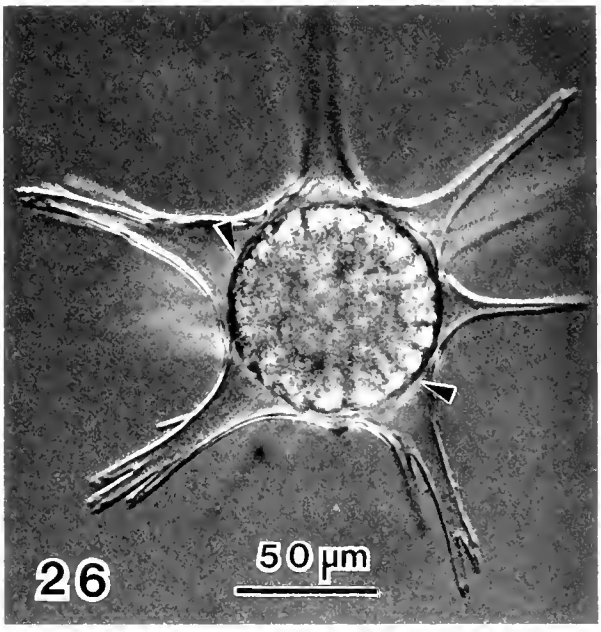

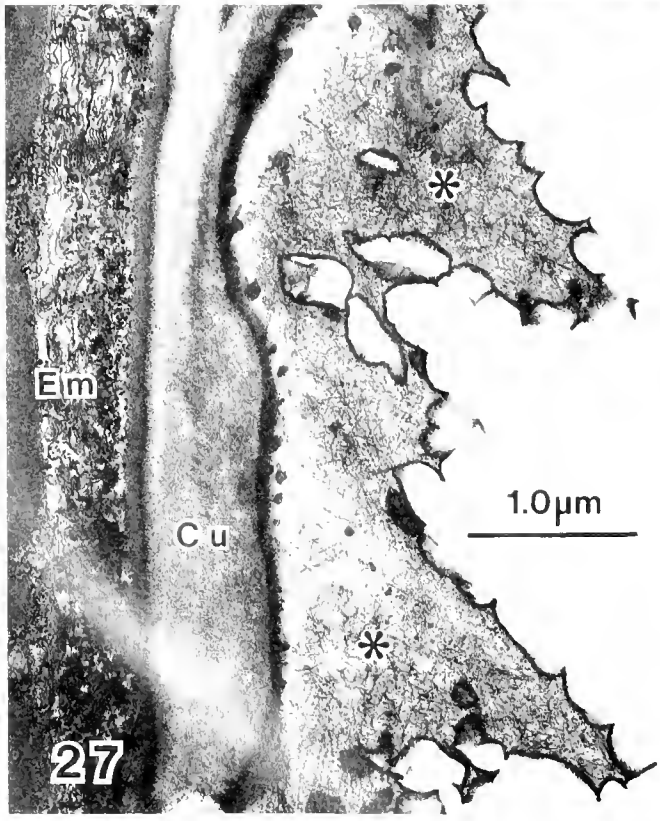

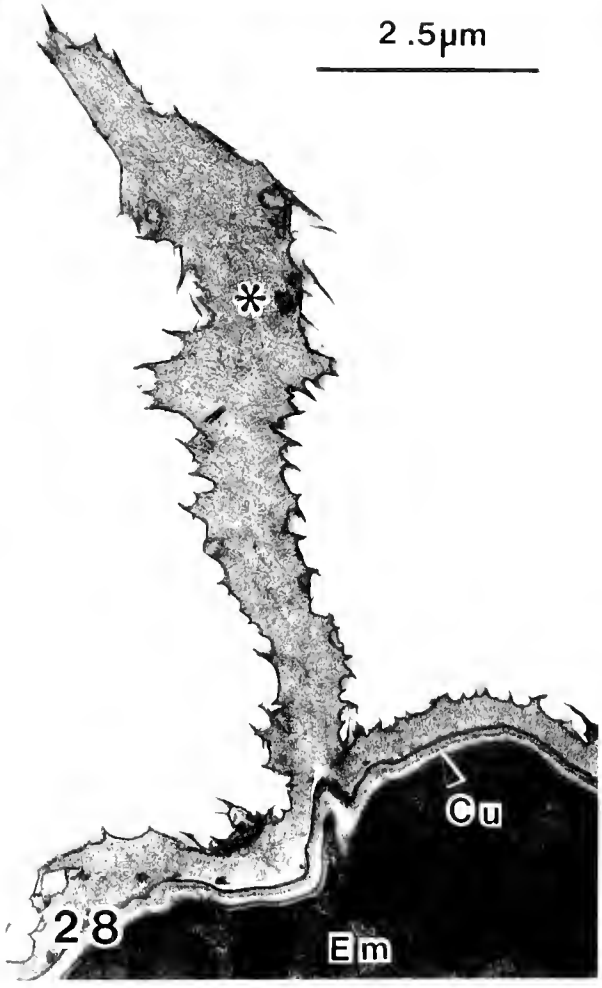

Figure 25. High magnification of perivitelline space in 24-h-old embryo showing transformation of granules (small arrowheads) from secondary cortical vesicles into fine fibers (*). Cu, early cuticle of nauplius.

Figure 26. Light micrograph of live 24-h-old embryo with advanced spine formation. Note that cytoplasm has receded from spines (small arrowheads).

Figures 27 and 28. Advanced spine formation of 24-h-old embryo (Em) showing thick mass of fibers filling spines (*). Cu, cuticle of nauplius.

comprise the secondary cortical vesicles. The primary vesicles separate from the secondary vesicles in the later stages of vitellogenesis.

In the eggs of *Carcinus maenus* (Goudeau and Lachaise, 1980a, b), the cortical vesicles of one type are filled with "ring-shaped" granules that are the precursor of the main layer of the embryonic capsule. The authors emphasized that these ring-shaped granules are homologous to the "disc-shaped granules" or "intracisternal granules" previously considered as endogenous yolk in the vitellogenic oocytes of several decapod crustaceans (Beams and Kessel, 1962, 1963; Kessel, 1968; Ganion and Kessel, 1972). Subsequent studies have confirmed that, instead of possessing nutritive qualities, the ring-shaped granules in these crustacean eggs play a structural role in formation of the egg envelope (Goudeau and Becker, 1982; Goudeau, 1984; Talbot and Goudeau, 1988; Pillai and Clark, 1990).

Within the Calanoida, the secondary cortical vesicles of *Centropages velificatus* appear homologous to the "intracisternal granules representing the endogenous yolk" in the oocytes of *Centropages typicus* (Arnaud *et al.*, 1982) and to the "granular form of type 1 yolk" in the oocytes of *Labidocera aestiva* (Blades-Eckelbarger and Youngbluth, 1984) and *Pontella mediterranea* (Santella and Ianora, 1990). Our present observations parallel those of Goudeau and Lachaise (1980a, b) and Talbot and Goudeau (1988), illustrating that the intracisternal granules previously assumed to represent endogenous yolk in copepod eggs, are actually precursors of the egg envelope. The distinctive morphology of the primary cortical vesicles in *C. velificatus,* however, has no correlate in the eggs of other copepod species studied thus far, even in the oocytes of a congeneric species, *C. typicus* (Arnaud *et al.*, 1982). The fact that the eggs produced by *C. typicus* do not elaborate spines warrants a closer look at morphological differences between the eggs of these congeners.

One consequence of the two exocytotic episodes in the eggs of *Centropages velificatus* is the addition of large quantities of membrane to the egg's plasmalemma. This occurs when the limiting membrane of the cortical vesicles fuses with the plasmalemma of the egg. However, the diameter of the egg does not increase significantly. The presence of numerous endocytotic pits and vesicles observed along the egg's plasmalemma during the second exocytotic event provides a mechanism for the recycling of at least some of the extra surface membrane. This process has been illustrated in the eggs of other animals (see review by Longo, 1988) and conforms with similar observations on mammalian secretory tissues (Mata and Christensen, 1990).

Earlier studies have described two membranes surrounding the copepod egg (see reviews by Davis, 1968, 1981). During hatching, the outer membrane cracks and the inner membrane pushes out. The outer membrane slips off and the nauplius is enclosed within the more delicate inner membrane. The nauplius then breaks open this membrane with its appendages and swims free. The ultrastructural features of the primary egg envelope in *Centropages velificatus* do not exhibit a trilamellar composition indicative of a true membrane. Therefore, we suggest that this layer should be referred to as the hatching envelope, such as described for other crustaceans (Goudeau and Becker, 1982; Pillai and Clark, 1988). The presence and structure of an inner egg membrane around the copepod nauplius has yet to be validated because we did not examine the later embryonic stages.

The morphology of the subitaneous egg envelope of *Centropages velificatus* is very different from that of the envelope encasing diapause eggs as reported for *Hemidiaptomus ingens privinciae* (Champeau, 1970), *Diaptomus sanguineus* (Hairston and Olds, 1984), *Pontella mediterranea* (Santella and Ianora, 1990), and *Anomalocera patersoni* (Ianora and Santella, 1991). The thick, multi-layered envelope surrounding diapause eggs appears as a lamellar arrangement of microfibrils in a helicoidal array and is considered comparable to the typical integument of arthropods (Hairston and Olds, 1984).

The function of the spines that characterize the eggs of *Centropages velificatus* and those of other copepod species remains elusive. During a discussion session of the symposium entitled "Cultivation of Marine Invertebrates" held in Princeton in 1967, it was suggested that spines on copepod eggs might retard sinking (Allen, 1969), enhance gas exchange, and afford protection from predation (Shelbourne, 1969). However, while it seems reasonable that the spines would deter predators, Zillioux (1969) reported that spiny eggs were consumed by adult female *Acartia.* More recently, Santella and Ianora (1990) suggested that the four-layered egg envelope and accompanying spines present on the diapause eggs of *Pontella mediterranea* may supply nutritive material during diapause and provide extra protection from harsh environmental conditions.

Numerous functions have been proposed for the spines that cover the surface of other marine invertebrate eggs. The eggs of some sea urchins, starfish, and sea anemones present a spiny appearance due to the elongation and bundling of cortical microvilli (Schroeder, 1982, 1986). It is suggested that these microvillous "spikes" and "spires" play a role in reinforcing the egg surface (Schroeder, 1982), function to facilitate absorption, and aid in adhesion between dividing cells of the embryo (Schroeder, 1986). Copepod oocytes are not known to possess microvillar modifications of the oolemma (Blades-Eckelbarger and Youngbluth, 1984), nor do the eggs form microvilli after fertilization (present study). Furthermore, the spines of *Centropages velificatus* are not cytoplasmic, but are projections of the outer or primary egg envelope caused by the amassment of an extracellular matrix (ECM) within

the perivitelline space. Recent studies on the ECMs surrounding the embryos of other marine invertebrates may hint to the role of the ECM that coats the eggs of *C. velificatus*. ECMs are believed to provide support and protection to the developing cells, aid in cell movement and cell adhesion, and form a semi-permeable filter for uptake and concentration of substances from the environment needed for growth and differentiation (Spiegel *et al.*, 1989).

Literature Cited

Allen, J. A. 1969. *Marine Biology Vol. V. Proceedings of the Fifth Interdisciplinary Conference on Marine Biology.* J. D. Costlow Jr., ed. Gordon and Breach, Science Publishers, New York, London, and Paris. 606 pp.

Arnaud, J., M. Brunet, and J. Mazza. 1982. Etude de l'ovogenèse chez *Centropages typicus* (Copepoda, Calanoida). *Reprod. Nutr. Dev.* **22:** 537–555.

Beams, J. W., and R. Kessel. 1962. Intracisternal granules of the endoplasmic reticulum in the crayfish oocyte. *J. Cell Biol.* **13:** 158–162.

Beams, J. W., and R. Kessel. 1963. Electron microscope studies on developing crayfish oocytes with special reference to the origin of yolk. *J. Cell Biol.* **18:** 621–649.

Blades-Eckelbarger, P. I., and M. J. Youngbluth. 1984. The ultrastructure of oogenesis and yolk formation in *Labidocera aestiva* (Copepoda: Calanoida). *J. Morphol.* **179:** 33–46.

Champeau, A. 1970. Étude de la vie latent chez les Calanoides (Copépodes). Caractéristiques des eaux temporaires de Basse-Provence. *Ann. Fac. Sci. Marseille* **44:** 155–189.

Davis, C. C. 1968. Mechanisms of hatching in aquatic invertebrate eggs. *Oceanogr. Mar. Biol. Ann. Rev.* **6:** 325–376.

Davis, C. C. 1981. Mechanisms of hatching in aquatic invertebrate eggs. II. *Oceanogr. Mar. Biol. Ann. Rev.* **19:** 95–123.

De Oliveira, L. P. H. 1947. Estudos sôbre o Microplancton capturado durante a viagem do navio hidrografico Lahmeyer nas bâias de Ilha Grande e Sepetiba. *Mem. Inst. Oswaldo Cruz* **44:** 441–488.

Flood, P. R. 1973. A simple technique for the prevention of loss or damage to planktonic specimens during preparation for transmission and scanning electron microscopy. *Sarsia* **54:** 67–74.

Fuchs, K. 1914. Die Keimblätterentwicklung von *Cyclops viridis*. *Zool. Jahrb. Anat.* **38:** 103–56.

Ganion, L. R., and R. G. Kessel. 1972. Intracellular synthesis, transport, and packaging of proteinaceous yolk in oocytes of *Orconectes immunis*. *J. Cell Biol.* **52:** 420–437.

Goudeau, M. 1984. Fertilization in a crab: III. Cytodifferentiation of vesicles enclosing ring-shaped elements involved in the cortical reaction. *Gamete Res.* **9:** 409–424.

Goudeau, M., and J. Becker. 1982. Fertilization in a crab. II. Cytological aspects of the cortical reaction and fertilization envelope elaboration. *Tissue and Cell* **14:** 273–282.

Goudeau, M., and F. Lachaise. 1980a. Fine structure and secretion of the capsule enclosing the embryo in a crab (*Carcinus maenus* (L.)). *Tissue and Cell* **12:** 287–308.

Goudeau, M., and F. Lachaise. 1980b. "Endogenous yolk" as the precursor of a possible fertilization envelope in a crab (*Carcinus maenas*). *Tissue Cell* **12:** 503–512.

Grice, G. D., and V. R. Gibson. 1981. Hatching of eggs of *Pontella mediterranea* Claus (Copepoda: Calanoida). *Vie et Milieu* **31:** 49–51.

Grobben, C. 1881. Die Entwicklungsgeschichte von *Cetochilus septemtrionalis* Goodsir. *Arb. Zool. Inst. Univ. Wien* **3:** 1–40.

Hairston, N. G., and E. J. Olds. 1984. Population differences in the timing of diapause: adaptation in a spatially heterogeneous environment. *Oecologia* **61:** 42–48.

Ianora, A., and L. Santella. 1991. Diapause embryos in the neustonic copepod *Anomalocera patersoni*. *Mar. Biol.* **108:** 387–394.

Johnson, M. W. 1967. Some observations on the hatching of *Tortanus discaudatus* eggs subjected to low temperatures. *Limnol. Oceanogr.* **12:** 405–410.

Karnovsky, M. J. 1965. A formaldehyde-glutaraldehye fixative of high osmolarity for use in electron microscopy. *J. Cell Biol.* **27:** 137A.

Kasahara, S., S. Uye, and T. Onbe. 1974. Calanoid copepod eggs in sea-bottom muds. *Mar. Biol.* **26:** 167–171.

Kay, E. S., and B. M. Shapiro. 1985. The formation of the fertilization membrane of the sea urchin egg. Pp. 45–80 in *Biology of Fertilization*, A. Monroy and C. B. Metz, eds. Academic Press, Inc., New York.

Kessel, R. G. 1968. Mechanisms of protein yolk synthesis and deposition in crustacean oocytes. *Z. Zellforsch.* **89:** 17–38.

Koga, G. 1968. On the pelagic eggs of Copepoda. *J. Oceanogr. Soc. Jpn.* **24:** 16–20.

Longo, F. J. 1988. Reorganization of the egg surface at fertilization. *Int. Rev. Cytol.* **113:** 233–269.

Luft, J. H. 1961. Improvements in epoxy resin embedding methods. *J. Biophys. Biochem. Cytol.* **9:** 409–414.

Marcus, N. H. 1990. Calanoid copepod, cladoceran, and rotifer eggs in sea-bottom sediments of northern California coastal waters: identification, occurrence, and hatching. *Mar. Biol.* **105:** 413–418.

Marshall, S. M., and A. P. Orr. 1954. Hatching in *Calanus finmarchicus* and some other copepods. *J. Mar. Biol. Assoc. U.K.* **33:** 393–401.

Marshall, S. M., and A. P. Orr. 1955. The biology of a marine copepod, *Calanus finmarchicus* (Gunnerus). Oliver & Boyd, Edinburgh and London.

Mata, R. L., and E. I. Christensen. 1990. Redistribution and recycling of internalized membrane in seminal vesicle secretory cells. *Biol. Cell.* **68:** 183–193.

Pertzova, N. M. 1974. Life cycle and ecology of a thermophilous copepod, *Centropages hamatus* in the White Sea. *Z. Zhurnal* **53:** 1013–1022.

Pillai, M. C., and W. H. Clark Jr. 1988. Hatching envelope formation in shrimp (*Sicyonia ingentis*) ova: origin and sequential exocytosis of cortical vesicles. *Tissue Cell* **20:** 941–952.

Pillai, M. C., and W. H. Clark Jr. 1990. Development of cortical vesicles in *Sicyonia ingentis:* their heterogeneity and role in elaboration of the hatching envelope. *Mol. Reprod. Dev.* **26:** 78–89.

Richardson, K. C., L. Jarett, and E. H. Finke. 1960. Embedding in epoxy resins for ultrathin sectioning in electron microscopy. *Stain Technol.* **35:** 313–323.

Santella, L., and A. Ianora. 1990. Subitaneous and diapause eggs in Mediterranean populations of *Pontella mediterranea* (Copepoda: Calanoida): a morphological study. *Mar. Biol.* **105:** 83–90.

Sazhina, L. I. 1968. On hibernating eggs of marine Calanoida. *Zool. Zhurnal* **47:** 1554–1556.

Schroeder, T. E. 1982. Novel surface specialization on a sea anemone egg: "spires" of actin-filled microvilli. *J. Morphol.* **174:** 207–216.

Schroeder, T. E. 1986. The egg cortex in early development of sea urchins and starfish. Pp. 59–100 in *Developmental Biology*, L. W. Browder, ed. Plenum Publishing Corp.

Schuel, H. 1985. Functions of egg cortical granules. Pp. 1–43 in *Biology of Fertilization*. A. Monroy and C. B. Metz, eds. Academic Press, Inc., New York.

Shelbourne, J. C. 1969. In *Marine Biology Vol. V. Proceedings of the Fifth Interdisciplinary Conference on Marine Biology.* J. D. Costlow Jr., ed. Gordon and Breach, Science Publishers, New York, London, and Paris. 606 pp.

Somers, C. E., and B. M. Shapiro. 1989. Insights into the molecular mechanisms involved in sea urchin fertilization envelope assembly. *Dev. Growth Differ.* **31:** 1–7.

Spiegel, E., L. Howard, and M. Spiegel. 1989. Extracellular matrix of sea urchin and other marine invertebrates. *J. Morphol.* **199:** 71–92.

Talbot, P., and M. Goudeau. 1988. A complex cortical reaction leads to formation of the fertilization envelope in the lobster, *Homarus. Gamete Res.* **19:** 1–18.

Uye, S. 1983. Seasonal cycle in abundance of resting eggs of *Acartia steuri* Smirnov (Copepoda, Calanoida) in sea-bottom mud of Onagawa Bay, Japan. *Crustaceana* **44:** 103–105.

Witschi, E. 1934. On determinative cleavage and yolk formation in the harpactid copepod *Tisbe furcata* (Baird). *Biol. Bull.* **68:** 335–340.

Zillioux, E. J. 1969. In *Marine Biology Vol. V, Proceedings of the Fifth Interdisciplinary Conference on Marine Biology,* J. D. Costlow Jr., ed. Gordon and Breach, Science Publishers, New York, London, and Paris. 606 pp.

Reference: *Biol. Bull.* **182:** 54–65. (February, 1992)

The Role of Shell Granules and Accessory Cells in Eggshell Formation in *Convoluta pulchra* (Turbellaria, Acoela)

RESA M. CHANDLER,[1] MARY BETH THOMAS,[1] AND JULIAN P. S. SMITH, III[2]

Department of Biology, The University of North Carolina at Charlotte, Charlotte, North Carolina 28223

Abstract. Most turbellarian embryos are surrounded by a sclerotinized eggshell originating from polyphenol-containing eggshell-forming granules (EFGs). Although embryos of the acoel *Convoluta pulchra* are surrounded by a shell, it is not sclerotinized. Therefore, in the absence of polyphenols as a marker for EFGs, it was not clear which, if any, of the granules of the oocyte function in eggshell synthesis. In this study, electron-opaque, elliptical granules with a characteristic frothy component and a diameter of 480 nm were identified in the oocyte as EFGs by their participation in eggshell formation. In addition, it was shown that accessory cells to the oocyte initiate synthesis of the shell by producing a thin, granular, electron-opaque primary shell, against which the contents of the EFGs are released by exocytosis. Morphological components of the shell and stages of its synthesis are described. A second type of membrane-bound granule and the lipid droplets that occur in the ooplasm were found not to be involved in eggshell formation and are probable sources of nutrients for the developing embryo. Possible implications of the findings for taxonomy and phylogeny are discussed.

Introduction

The zygotes of acoel turbellarians, like those of all platyhelminthes studied to date, are enclosed in a shell following fertilization (see Rieger *et al.*, 1991, for Turbellaria; Fried and Haseeb, 1991, and Coil, 1991, for parasitic platyhelminths). In all cases so far examined, the eggshell appears to arise from eggshell-forming granules (EFGs) exocytosed from one of the cells that ultimately comes to lie within the shell (oocytes in the entolecithal archoophorans, yolk cells in the ectolecithal neoophorans and parasitic platyhelminths). Among archoophoran turbellarians, EFGs have been described by transmission electron microscopy (TEM) from the oocytes of at least one member of most orders (*Polycladida:* Boyer, 1972; Domenici *et al.*, 1975; Gammon, 1979; Ishida *et al.*, 1981; Espinosa, 1986; Ishida and Teshirogi, 1986; *Macrostomida:* Gremigni *et al.*, 1987; Kucera, 1987; *Acoela:* Gremigni, 1988; Smith *et al.*, 1988; *Nemertodermatida:* Smith *et al.*, 1988). Relatively few TEM studies of archoophorans, however, have examined formation of the eggshell (see Ishida, 1989; Falleni and Gremigni, 1989).

Whereas EFGs in most platyhelminths examined to date contain polyphenols, they have not been found in the oocytes of the Acoela (Thomas *et al.*, 1985; Chandler and Thomas, 1986, 1987; Gremigni, 1988; Smith *et al.*, 1988; Falleni and Gremigni, 1989, 1990) or the Nemertodermatida (Thomas *et al.*, 1985; Smith *et al.*, 1988), the presumably primitive turbellarian orders that constitute the Acoelomorpha. In the acoels, the shell is proteinaceous and non-sclerotinized (Falleni and Gremigni, 1989). Because the eggshells of all other non-acoelomorphan platyhelminths studied so far appear to be sclerotinized, the process of eggshell formation in the acoels merits further study. For example, in the absence of the polyphenolic marker, it is difficult to ascertain with certainty which, if any, of the several types of granules in the oocyte give rise to the eggshell. Falleni and Gremigni (1989) have implicated a population of electron-opaque granules with a diameter of 0.4–0.5 μm as EFGs in the oocytes of the acoel "*Convoluta psammophyla*" (? = *Pae-*

Received 24 May 1991; accepted 31 October 1991.

Present addresses: [1]Department of Biology, The University of North Carolina at Charlotte, Charlotte, NC 28223, and [2]Department of Biology, Winthrop College, Rock Hill, SC 29733.

domecynostomum psammophilum Beklemischev, 1957), but have not examined the mechanism by which these granules contribute to the formation of the shell. Although it seems likely that exocytosis of the granules, which occurs during eggshell formation in other turbellarians, is involved in production of the eggshell of the acoels (Falleni and Gremigni, 1990), that is not clear from the published studies.

Also unclear is the question of whether cells other than the oocyte are involved in synthesis of the eggshell in acoels, as they are in other turbellarians (*e.g.*, Giesa, 1966; Bunke, 1982; Ishida, 1989). Mature oocytes in both acoels and nemertodermatids are nearly always surrounded by "follicle" or "accessory" cells, whose function has not been elucidated, although it is usually suggested that they are responsible for heterosynthetic yolk production or that they assist in the production of the eggshell (see Rieger *et al.*, 1991).

The present study examines eggshell formation in the acoel *Convoluta pulchra* with particular attention to the following questions: (1) do any of the granules of the oocyte participate in the formation of the eggshell; (2) if so, what is the mechanism by which they participate; (3) are other cell types involved in eggshell synthesis; and (4) what is the morphology of the shell itself? A preliminary report of these findings has been presented elsewhere (Chandler *et al.*, 1988).

Materials and Methods

Experimental organism

Convoluta pulchra (Family Convolutidae; Smith and Bush, 1991) was extracted according to the methods of Hulings and Gray (1974) from sediment samples collected at mid-tide level at a coastal inlet near Fort Fisher, North Carolina.

Procedures for preliminary observations

To determine the time course of egg-laying in *Convoluta pulchra*, gravid acoels were isolated in pairs in wells of Falcon® 96-well plates. The individual cultures were maintained in Millipore®-filtered seawater (MFSW) at a constant temperature of 20°C and a light:dark cycle of 16:8 h. The worms were monitored closely to determine if the acoels lay their eggs according to a diurnal pattern. Under these conditions, worms began egg-laying within approximately 1 to 1.5 h after exposure to light.

Experimental design

Ten pairs of acoels with large eggs were placed in Falcon® plates. The animals were placed into darkness at 9:30 p.m. and returned to light at 6:30 a.m. Worms were fixed for electron microscopy every half hour, from 7:00 a.m. until 11:30 a.m. Other worms were allowed to lay eggs, which were fixed for electron microscopy.

Procedures for electron microscopy

Adult worms and laid eggs were fixed in 1% glutaraldehyde, 4% paraformaldehyde, 0.1 *M* HEPES buffer (pH 7.4), 1 m*M* $CaCl_2$, and 10% sucrose [modified from McDowell and Trump (1976)], rinsed in buffer, post-fixed in HEPES-buffered 1% OsO_4, and embedded in Spurr's low viscosity epoxy resin (Spurr, 1969). Ultrathin sections were stained with uranyl acetate (Watson, 1958) and lead citrate (Reynolds, 1963), and examined with a Philips 201C transmission electron microscope.

Procedures for morphometric analysis

The Feret diameters (see Weibel, 1979) of the three types of granules were measured with a Zeiss ZIDAS digitizer. The Feret diameter of each granule profile was measured between two lines parallel to the long axis of the photographic print. The most mature stage of development in which all types of granules were present (Primary Shell Synthesis Stage, described below) was chosen for measurement. To avoid measuring the same granule more than once, 1.8 μm separated the thin sections measured and non-overlapping micrographs were taken from each thin section examined. Approximately 200 granules from electron micrographs magnified 28,000× were measured and the size-frequency distribution of Feret diameters for granule Types A and B were plotted. For the Type A granules, the distribution was corrected for profiles overlooked in the smallest categories as described in Weibel (1979). The actual diameter of Type A granules (D) was estimated from the average Feret diameter (d) using the relationship $D \cong \frac{4}{\pi} \cdot d$ (Weibel, 1979).

Oocytes at different stages of shell maturation were analyzed to determine the volume densities (V_v; % of oocyte volume occupied by granules) of Types A and B granules and lipid droplets. Non-overlapping micrographs along two right-angled transects were taken from the germinal vesicle to the oolemma. Volume densities were determined by point-count analysis, using the oocyte as the reference space (Weibel, 1979). To determine whether these volume densities changed in the oocyte as development of the shell proceeded, the volume densities were arcsin-square root transformed and subjected to ANOVA Planned Comparison.

The embryos contained within laid eggs fixed for electron microscopy were observed to be separated from the inner edge of their shells. This could occur if the shell swells and lifts away from the embryo or if the embryo

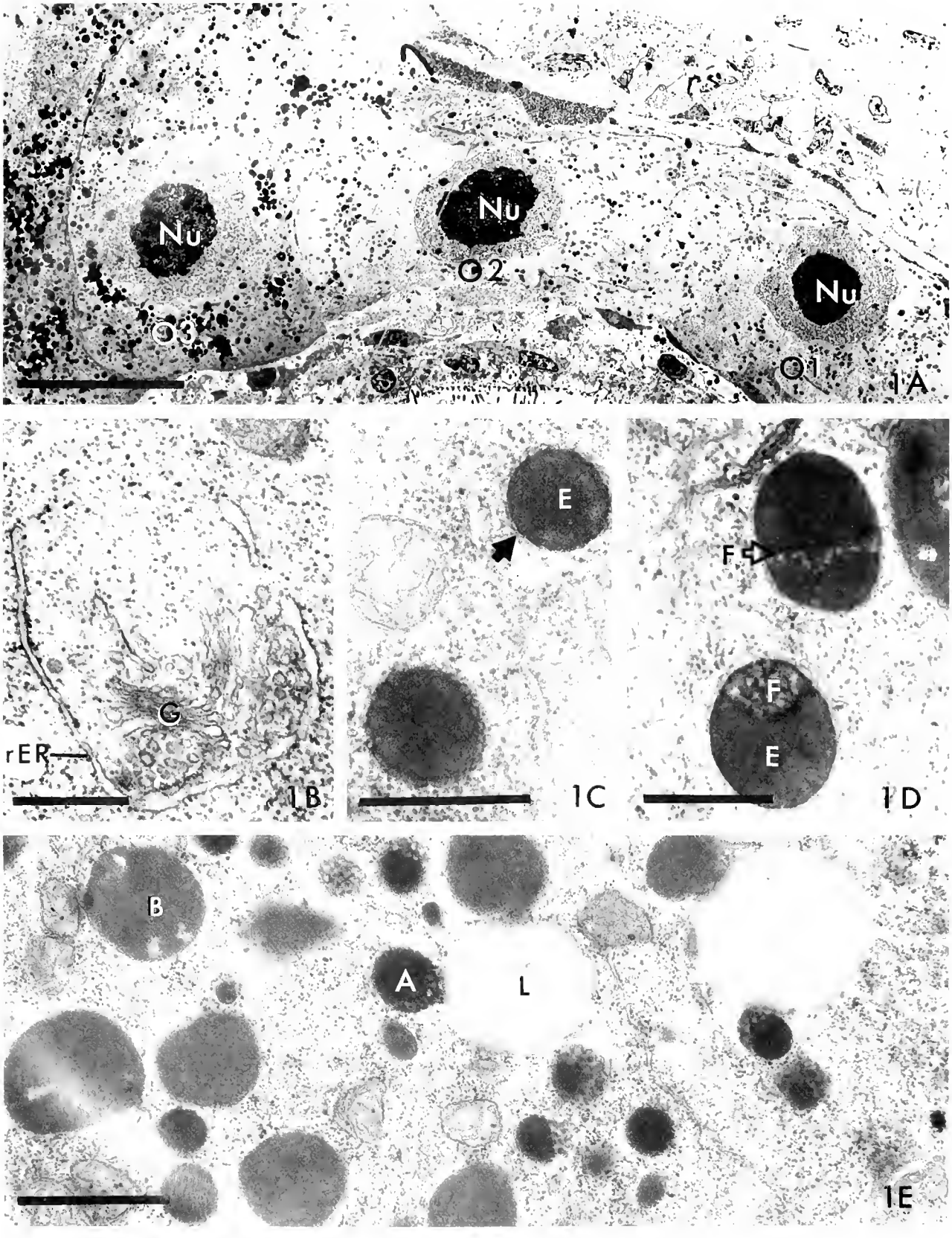

Figure 1. (A) Overview of a column of maturing oocytes showing the nuclei (germinal vesicles) with large nucleoli (Nu) and the increase in the number of granules in the ooplasm with development. O1 = oocyte synthesizing Type A granules only; O2 = oocyte synthesizing Types A and B granules; O3 = oocyte containing Type A and B granules and lipid droplets. Bar = 15.0 μm. (B) Cisternae of rough endoplasmic

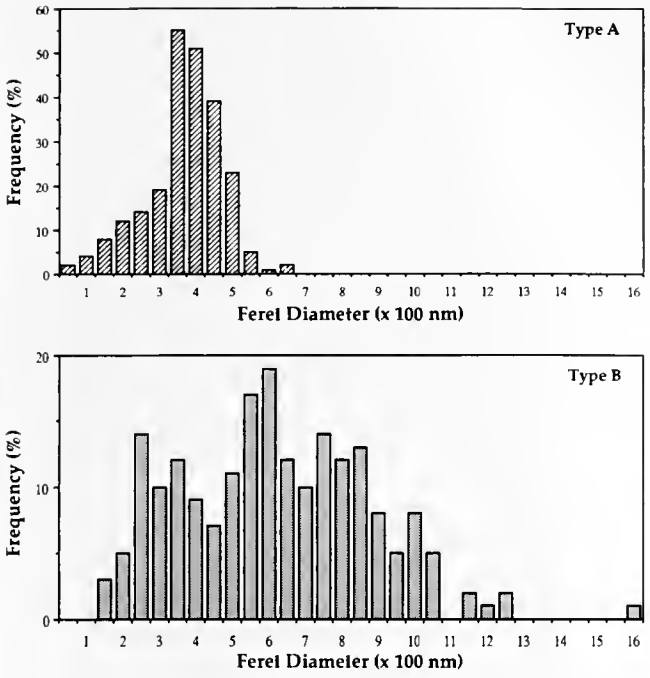

Figure 2. Feret diameter distribution of granule Types A and B. Each number on the abscissa represents the stated value ±0.5; n = 200.

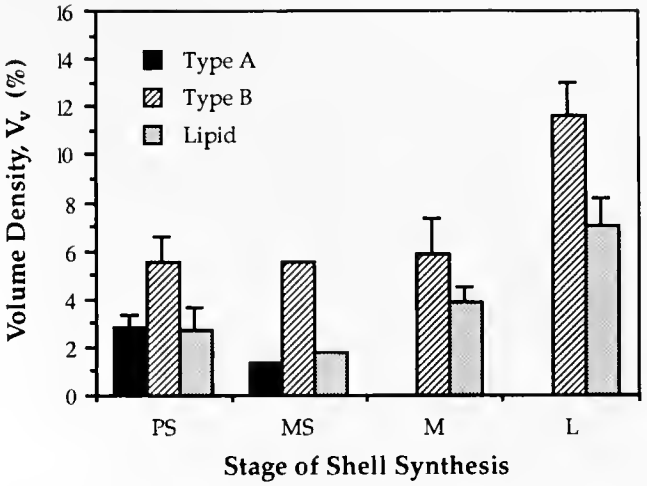

Figure 3. Volume densities of granular inclusions. PS = stage of Primary Shell synthesis; MS = stage of Mature Shell synthesis; M = stage of Mature Shell; L = stage of Laid Shell.

loses some of its volume, shrinking away from the shell. Since the two possibilities affect the interpretation of the changes in volume densities of the granules, the absolute volumes of eggs prior to egg-laying and of embryos after egg-laying were determined. Serial 2 μm-thick sections were viewed with a Zeiss Axioskop light microscope equipped with a Sony DXC-3000A color video camera and a Sony PVM-1343MD Trinitron color monitor. Each section of egg or embryo was traced from the monitor screen onto transparent plastic. The ZIDAS was used to calculate the area of each drawn section; the area, in turn, was multiplied by the thickness of the sections and these numbers summed for all sections to determine the volume of each egg or embryo. Four eggs with mature shells and four laid eggs were analyzed. ANOVA was used to compare the mean volume of eggs with mature shells to that of embryos within the laid eggs.

Results

Stages of shell formation

Based on the ultrastructural features described in detail below, development of the eggshell in *Convoluta pulchra* was divided into four sequential stages: Primary Shell Synthesis, Mature Shell Synthesis, Mature Shell, and Laid Shell. The germinal vesicle persists into the Mature Shell stage, during which it breaks down. Because the time of fertilization is not known for the species, the Mature Shell stage may be an oocyte or a zygote, and will therefore be referred to as the "egg" (unfertilized or fertilized). At the Laid Shell stage, embryos are developing.

Description of granules and lipid droplets

Granules we have termed Type A granules were the first to appear in developing oocytes (Fig. 1A, egg 1). Oocytes at this stage had a large germinal vesicle containing euchromatin and a single prominent nucleolus. Long strands of rER occurred in the cytoplasm. Additional rER and Golgi were often found close to one another, usually with the rER almost encircling the Golgi in a horseshoe configuration (Fig. 1B). Mitochondria were abundant. The forming Type A granules were spherical to ellipsoidal and electron-opaque with slightly lucent internal areas (Fig. 1C); profiles of the granules did not exceed 330 nm in early oocytes.

In more mature primary oocytes, the Type A granules were more complex, larger, and more abundant. Mature Type A granules consisted of two components, electron-

reticulum (rER) almost totally encircling the Golgi (G) in an oocyte synthesizing Types A and B granules. Bar = 0.5 μm. (C) An immature Type A granule before the frothy element is evident. Only the electron-opaque component (E) is present. The membrane surrounding the granule is indicated by the arrow. Bar = 0.5 μm. (D) Two mature Type A granules with their typically elliptical profile. Both the electron-opaque component (E) and the frothy element (F) can be distinguished. Bar = 0.5 μm. (E) A field of granules from an oocyte slightly older than oocyte 3 in Figure 1. Type A granules (A), Type B granules (B), and lipid droplets (L) occur in the cytoplasm. Bar = 1.0 μm.

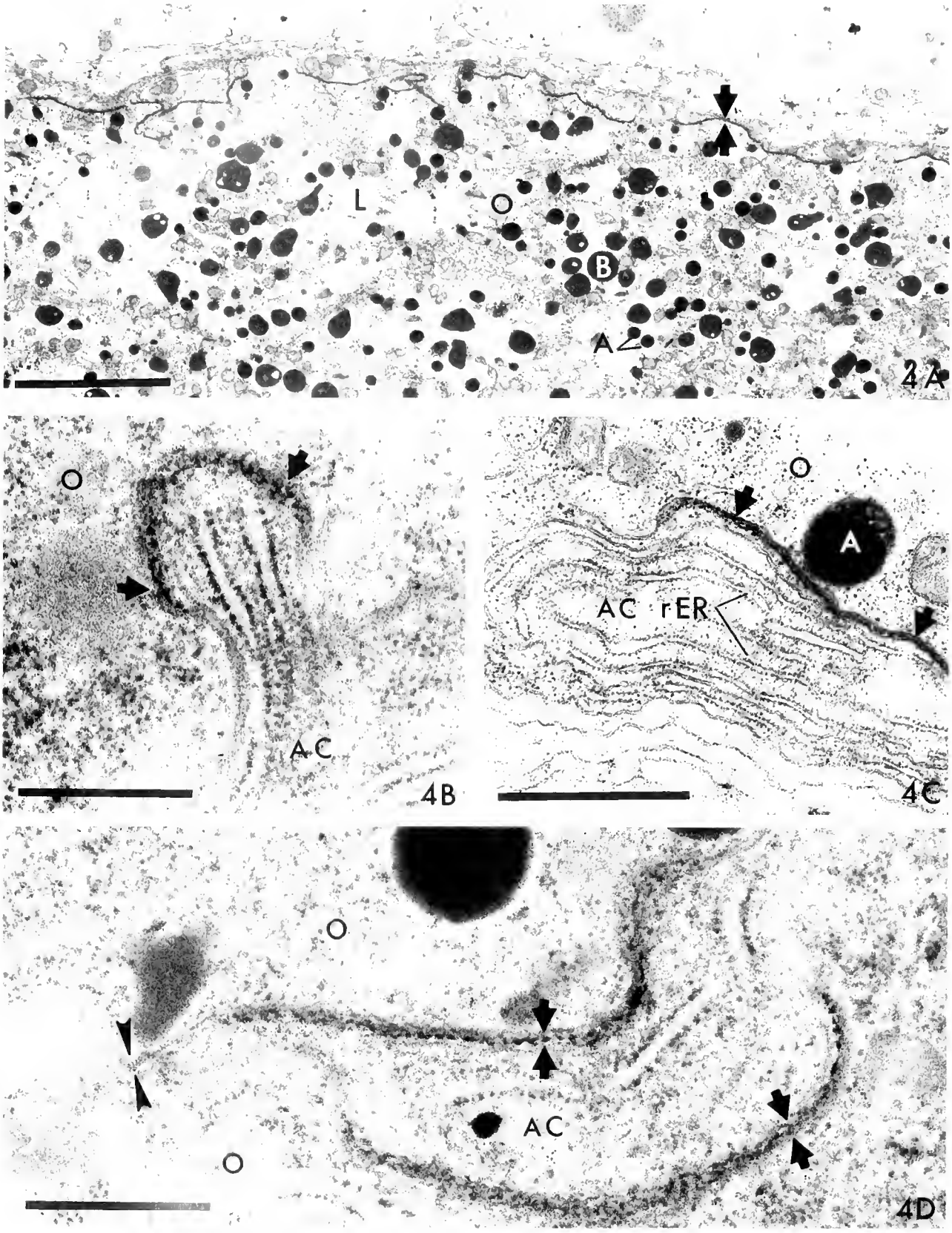

Figure 4. (A) An oocyte (O) with a primary shell (arrows). Type A granules (A), Type B granules (B), and lipid droplets (L) can be identified in the ooplasm. Bar = 5.0 μm. (B) A region of the surface of an oocyte (O) in contact with an accessory cell (AC). In the part of the region of contact indicated by the arrows the granular primary shell has formed. Bar = 1.0 μm. (C) An accessory cell (AC) with an extensive rough

opaque globules and a frothy material that often formed a cap at one pole of the granule (Fig. 1D, 1E). The mature Type A granules from an oocyte in the Primary Shell Synthesis stage exhibited an average Feret diameter of 380 nm (n = 199), giving an estimated average diameter of 480 nm; the largest profile measurement was 640 nm (Fig. 2). Type A granules reached an average volume density of 2.9% in Primary Shell Synthesis stage oocytes (Fig. 3). Although Type A granules were not observed to marginate at the time of eggshell formation, their volume density dropped to 1.4% in the single Mature Shell Synthesis stage oocyte observed, and was zero in both Mature Shell and Laid Shell stages (Fig. 3).

A second type of granule, termed the Type B granule, was first observed in oocytes that still possessed a large germinal vesicle (Fig. 1A, egg 2). More Golgi bodies and rER occurred in these oocytes than in those synthesizing only Type A granules. Mature Type B granules were irregular spheres with a flattened edge (Fig. 1E). The Type B granules were less electron-opaque than the Type A granules and contained internal electron-lucent patches. The mature Type B granules from a Primary Shell Synthesis stage oocyte exhibited an average Feret diameter of 590 nm (Fig. 2); the largest measurement was 1570 nm (n = 200). Calculation of an average diameter from the Feret diameter was not attempted because Type B granules appeared to depart significantly from a spherical shape. The volume density of Type B granules was 5.5% in Primary Shell Synthesis stage oocytes as well as in the single Mature Shell Synthesis stage oocyte, 5.9% in Mature Shell stage oocytes, and 11.6% in Laid Shell stage embryos (Fig. 3). The volume densities of Type B granules were not statistically different during shell deposition (comparing Primary Shell Synthesis stage oocytes to Mature Shell stage oocytes: $F = 0.004$, $df = 1, 10$); however, the increase seen in laid eggs was significant ($F = 11.08$, $df = 1, 10$; $P < .05$).

Lipid droplets (Fig. 1E) appeared in oocytes that had begun synthesis of Type B granules, but were still in the germinal vesicle stage (Fig. 1A, egg 3). Lipid droplets appeared to have no membrane. The volume density of lipid droplets was 2.7% in Primary Shell Synthesis stage oocytes, 1.8% in the single Mature Shell Synthesis stage oocyte, 3.9% in Mature Shell stage oocytes, and 7.0% in laid eggs (Fig. 3). As was the case for the Type B granules, the volume density of lipid droplets was statistically constant during shell synthesis ($F = 0.22$, $df = 1, 10$), but increased significantly in laid eggs ($F = 9.13$, $df = 1, 10$; $P < .05$).

Morphology of eggshell deposition

Primary Shell Synthesis stage. Synthesis of the shell began before the germinal vesicle had broken down. At this stage, both Type A and Type B granules were dispersed throughout the ooplasm, and the oocyte was surrounded wholly or in part by an accessory cell. Electron-opaque material of finely granular composition appeared outside the oocyte, along the irregular contours of the oolemma (Figs. 4A, 4B). This layer was discontinuous in the youngest oocytes of this stage examined, and was only observed where the accessory follicle cell, laden with rER (Figs. 4C, 4D), was in contact with the oolemma. In slightly later stages, this thin primary shell covered the entire oocyte as a layer approximately 50 nm thick.

Mature Shell Synthesis stage. In the single oocyte of this stage encountered, numerous examples of exocytosis of Type A granules were observed (Fig. 5A). Both the homogeneous electron-opaque and the frothy components appeared to be extruded from the cell. Fused granules often produced elongated channels or sacs, the membranes of which were continuous with the plasmalemma (Fig. 5A).

Mature Shell stage. Released Type A granules apparently produced a homogeneous, electron-opaque layer 100–525 nm thick immediately underneath the granular, exogenously originated primary shell, as well as an inner fibrillar network with a thickness of 10–315 nm (Fig. 5B). Clear peripheral vesicles, presumably the remnants of the Type A granules, were visible shortly after exocytosis (Fig. 5B). During the process of exocytosis of the Type A granules, small membrane-bounded fragments of cortical cytoplasm appeared to have been lost from the oocyte (Figs. 5A, 5B).

In somewhat older eggs, a new layer of the shell was observed (Fig. 5C). This thin layer was sandwiched between the granular primary shell and the homogeneous layer produced by the Type A granules and appeared as a stripe that was more electron-opaque than the homogeneous layer. The fibrillar layer was still present just outside the plasmalemma. At this stage, no Type A granules were apparent in the cytoplasm (Fig. 5D).

Laid Shell stage. Laid eggs were encapsulated in a clear, flexible, yet sturdy shell (Fig. 6A). In the laid eggshell, the

endoplasmic reticulum (rER) in contact with an oocyte (O). Arrows indicate the primary shell that has formed along part of the region of contact between the accessory cell and the oocyte. A Type A granule (A) lies close to the region of formation of the thin shell, but exocytosis has not begun at this stage. Bar = 0.5 μm. (D) A region of the plasmalemma of an oocyte (O) with (arrows) and without (darts) an adjacent accessory cell (AC). Note that the primary shell (arrows) is present only where there is an accessory cell. Bar = 0.5 μm.

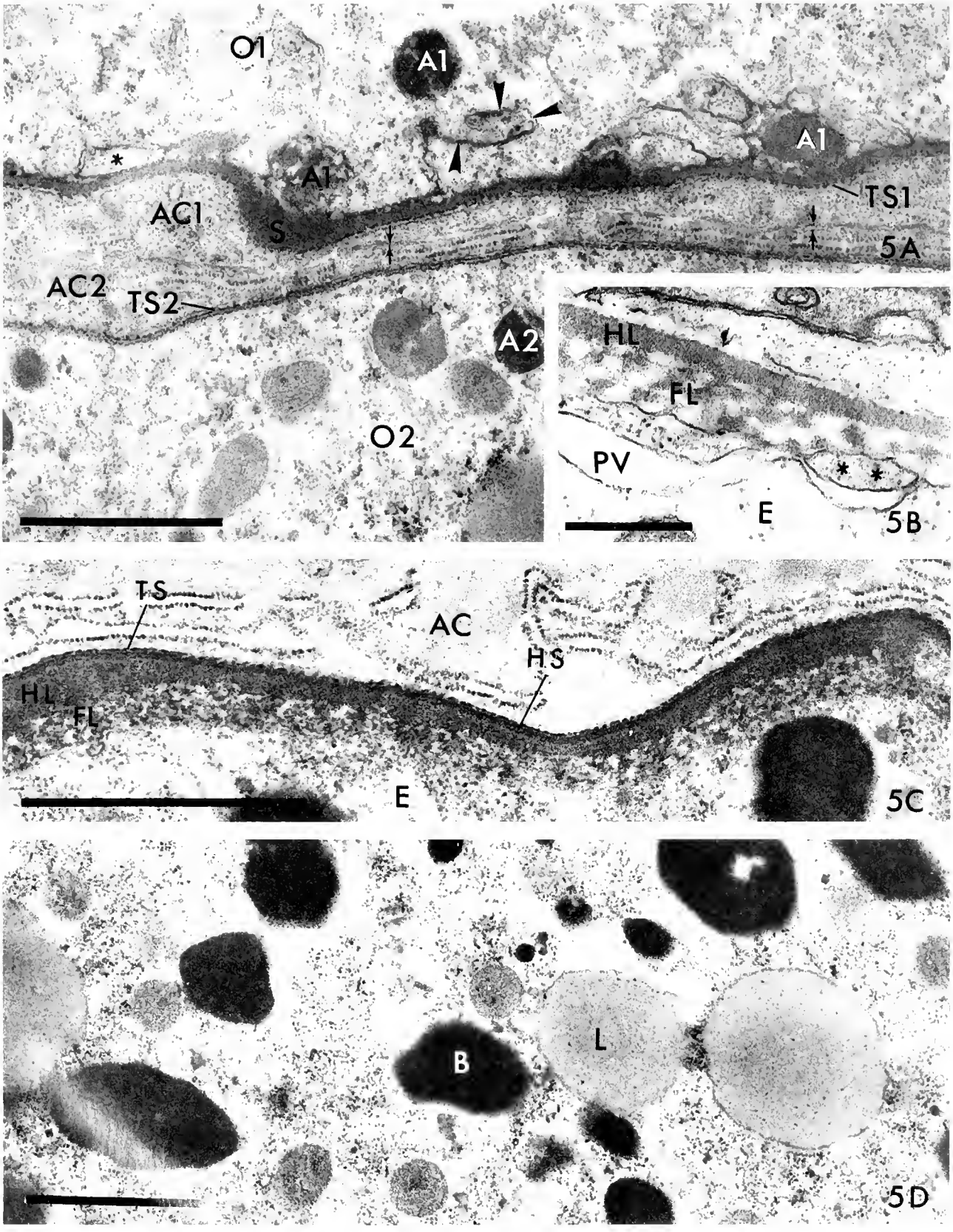

Figure 5. (A) Exocytosis of Type A granules. The contents of Type A granules (A1) are released from the more mature oocyte (O1) to form the layers of its mature shell (S) interior to the thin primary shell (TS1). Darts indicate the long, often tortuous profiles of the membranes of the Type A granules during exocytosis. The asterisk marks a small membrane-bounded fragment of cytoplasm that may no longer be

fibrillar layer could be distinguished, but the granular primary shell, the homogeneous layer, and the stripe could no longer be differentiated; instead, a single, thick, electron-opaque layer occurred peripheral to the fibrillar layer (Fig. 6B). The thickness of the shell was far more homogeneous than that of the forming shell (Fig. 6B). There was a space between the embryo and the shell (Fig. 6A–C). The juvenile worm hatched one day after egg-laying. Before hatching, the worm moved vigorously until the shell gave way.

The mean volume of a Mature Shell stage egg was 325×10^3 μm^3 (n = 4), whereas the mean volume of an embryo after deposition was 180×10^3 μm^3 (n = 4). The volume of the embryo was therefore significantly smaller than that of the unlaid egg ($F = 33.6$, $df = 1, 6$; $P < 0.005$).

Discussion

Eggshell synthesis

Our study demonstrates that the first element of the eggshell in *Convoluta pulchra* is deposited by accessory cells before the Type A granules undergo exocytosis. Accessory cells, laden with rER, appear to envelop an oocyte at the time of primary shell synthesis. This is evidenced by the observation that the thin, granular, primary shell layer appears outside the oolemma in areas of the oocyte surface abutting an accessory cell, whereas regions that do not abut an accessory cell are not covered by primary shell. A role in production of the shell was previously hypothesized for the accessory cell, but not demonstrated (Falleni and Gremigni, 1990). The mechanism by which the material that composes the thin shell is released from the accessory cell is not known. Exocytotic vesicles have not been identified. It is possible that vesicles simply have not been detected, perhaps because they are small, present in low numbers, or do not accumulate in the cytoplasm of the accessory cell. Alternatively, the primary shell may be a product of a reaction between substances located on the surface of the surrounding accessory cell and on the surface of the oocyte. Clearly, the material appears only where the two cells are in contact.

Functionally, the Type A granules of *C. pulchra* are comparable to EFGs of other turbellarians. They undergo exocytosis at the Mature Shell Synthesis stage and are absent from the egg at the end of the Mature Shell stage, indicating that they participate in eggshell deposition.

After the formation of the primary shell, the contents of the Type A granules released by exocytosis become packed against the thin shell made earlier, eventually forming a homogenous layer beneath the primary shell layer. This homogeneous layer probably comes from the electron-opaque portion of the Type A granules. The mature shell enclosing the unlaid egg is characterized by a fibrillar network that forms the innermost layer. The flocculent portion of the Type A granules most likely produces this fibrillar network. These conclusions are based on morphological observations; the detailed cytochemistry of Type A granules is unknown. Also characteristic of the mature shell is an electron-opaque stripe between the primary shell layer and the homogeneous layer. This could represent a zone of reaction between the granular primary shell layer formed by the accessory cell and the homogeneous layer formed from the Type A granule, perhaps associated with some as yet unidentified hardening process. This is suggested by the observation that in the shell of the laid egg, the three outermost layers are no longer discrete. This would be predicted if a reaction between the primary shell and the homogeneous layer produced the stripe and that reaction proceeded until, in the laid eggshell, the stripe replaced the two original layers.

Although the wide variation in the thickness of the components of the shell during early stages of synthesis may be related in part to plane of section, it more likely reflects the number of Type A granules released in a given area. Because the contents of the Type A granules do not maintain their integrity at exocytosis, the contents must be fluid; it is therefore hypothesized that the components

continuous with the egg surface. Two accessory cells (AC1 and AC2), the plasma membranes of which are indicated by arrows, separate the more mature oocyte from a less mature one (O2), which has a thin primary shell (TS2) but has not begun exocytosis of Type A granules (A2). Bar = 1.0 μm. (B) The cortex of the egg after shell formation. Clear peripheral vesicles (PV) occur at the surface of the egg (E) after the homogeneous layer (HL) and fibrillar layer (FL) of the shell have formed around it. The vesicles communicate with extracellular space. Asterisks mark fragments of cortical cytoplasm that may have been cut off from the cytoplasm of the egg. Bar = 0.5 μm. (C) The mature shell of a prelaid egg. The egg (E) is surrounded by its accessory cell (AC) and the thin primary shell (TS). Beneath the primary shell the homogeneous layer (HL) and fibrillar layer (FL) of the mature shell encompass the egg. A homogeneous stripe (HS) can be seen between the primary shell and the homogeneous layer. Although the plasmalemma of the egg is not clearly seen here, adjacent micrographs show that it lies just interior to the fibrillar layer of the shell. Bar = 1.0 μm. (D) A representative section of the ooplasm of the egg after shell formation but before egg-laying. Type B granules (B) and lipid droplets (L) are present, but Type A granules cannot be detected. Compare Figure 5D with Figure 1E, an area of similar size at a stage before formation of the mature shell. Bar = 1.0 μm.

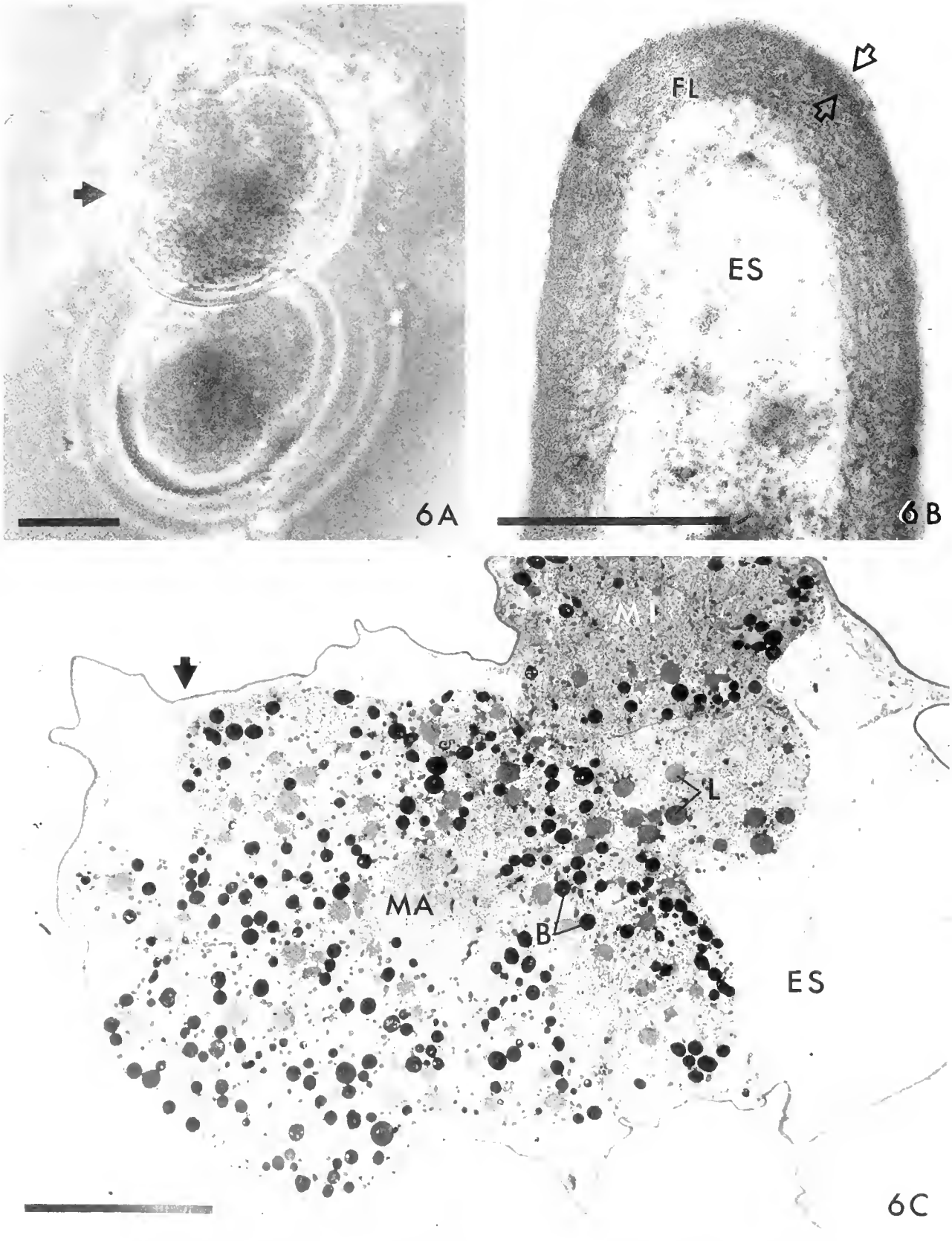

Figure 6. (A) Photomicrograph of two cleaving embryos surrounded by a still flexible, clear eggshell (arrow). Bar = 10.0 μm. (B) A magnified region of the eggshell of a laid embryo. Arrows indicate the layer of the laid shell that probably corresponds to the primary shell, homogeneous stripe, and homogeneous layer; these are no longer discrete. The fibrillar layer (FL) can still be discerned. The thickness of the shell

flow to fill evenly the space between the primary shell and the oolemma before hardening. The shell surrounding the laid embryo shows little variation in thickness.

Because Type A granules are released by exocytosis and profiles in which the membrane of the Type A granule is continuous with the plasmalemma are common, it is likely that the plasma membrane of the egg following shell formation is a mosaic of the original oocyte membrane and the membrane of the Type A granules. The occasional fusion of Type A granules with one another rather than with the plasmalemma could explain what appear to be membrane-bounded fragments of cytoplasm that can sometimes be found between the plasma membrane of the egg and the newly synthesized shell. Because serial sections were not taken, however, it is possible that the apparent fragments are connected to the ooplasm in some plane. The membranes of the clear peripheral vesicles associated with the plasmalemma soon after exocytosis of the Type A granules are hypothesized to be the membranes of the empty Type A granules.

The Type B granules were not observed to participate in eggshell formation. Type B granules are hypothesized to be the yolk granules, as yolk granules occur in the oocytes of all archoophoran platyhelminths.

The observed increase in volume densities of the Type B granules and the lipid droplets in the laid, cleaving embryo when compared to the unlaid egg was initially perplexing. There is no indication of new synthesis of granules. A decrease in volume of the embryo following egg laying was hypothesized. Morphometric measurements of unlaid eggs and laid, developing embryos of *C. pulchra* demonstrated that the volume of the laid embryo is significantly less than that of the unlaid egg. This change in volume, which may well be a fixation artifact, probably accounts for the apparent two-fold increase in volume densities of Type B granules and lipid droplets.

To our knowledge, the only turbellarians for which the origin of eggshells has been examined ultrastructurally are the rhabdocoels *Microdalyellia fairchildi* (Bunke, 1982) and *Mesostoma ehrenbergii* (Domenici and Gremigni, 1977) and the polyclads *Pseudostylochus* sp. and *Planocera multitentaculata* (Ishida and Teshirogi, 1986; Ishida, 1989). In the rhabdocoel *Microdalyellia fairchildi*, some regions of the uterine epithelium release a vesicular secretion against which EFGs from the yolk cells are secreted, although the exact role of this secretion in eggshell formation is not clear (Bunke, 1982). Ishida and Teshirogi (1986) describe a dual origin for the eggshells of the polyclads in which an eggshell envelope is synthesized by the shell glands in the female reproductive system, and the remainder of the shell is formed following release of the EFGs from the oocyte. Ishida (1989) has demonstrated experimentally that the envelope is required for formation of the eggshell. In *C. pulchra* the accessory cells to the oocyte form a thin shell or envelope against which the contents of the Type A granules are released. Thus it appears that an exogenous layer may be required to delineate the parts of the shell formed from EFGs. The origin of the external layer varies among the three groups of turbellarians studied to date. Within the polyclads, however, the origin of the external envelope is constant in the two species examined. Only with additional studies will it be possible to know if the origin of the external layer is a useful taxonomic character.

EFGs in acoelomorphans

The EFGs of *C. pulchra* are similar to the EFGs of other turbellarians in three ways: (1) they contribute to the formation of the eggshell, (2) they have a complex morphology, and (3) the synthesis of EFGs begins prior to the synthesis of yolk granules, as in other turbellarians in which yolk granules are a product of the Golgi. The EFGs of all acoelomorphans (Acoela and Nemertodermatida) studied to date differ from the EFGs of other turbellarians in that the former lack polyphenols (see Gremigni, 1988; Smith *et al.*, 1988; Falleni and Gremigni, 1990). Another apparent difference is that the EFGs found in oocytes of acoelomorphans are smaller than those in oocytes and vitellocytes of other turbellarians. EFGs of most turbellarians are 1–2 μm in diameter, whereas the average diameter of the EFGs of *C. pulchra* is only one-quarter to one-half as large, or 0.48 μm. The EFGs of other acoelomorphans appear like those of *C. pulchra*, with diameters of approximately 0.5 μm (see Gremigni, 1988; Smith *et al.*, 1988). Falleni and Gremigni (1990) have recently suggested that the EFGs of "*Convoluta psammophyla*" fuse as they migrate centripetally to form granules 1–1.2 μm in diameter.

The species of acoels that have been examined for eggshell formation belong to two different families, assuming that the "*Convoluta psammophyla*" examined by Falleni and Gremigni (Gremigni, 1988; Falleni and Gre-

of the laid embryo is much more constant than that of the shell of the unlaid egg. Extra-embryonic space (ES) separates the shell from the developing embryo. Bar = 1.0 μm. (C) The shell (arrow) of the embryo after the first two cleavages. Micromeres (MI) and macromeres (MA) can be distinguished, and Type B granules (B) and lipid droplets (L) occur in both types of blastomeres. The extensive extra-embryonic space (ES) is shown. Bar = 10.0 μm.

migni, 1989, 1990) is, in fact, *Paedomecynostomum psammophilum* (Family Mecynostomidae; see Beklemischev, 1957; Dörjes, 1968). Differences in our results and those of Falleni and Gremigni make a morphological characterization of an EFG within the Acoela difficult at this point. The electron-dense granules similar in size to the Type A granules that form the eggshell in "*Convoluta psammophila*" (Falleni and Gremigni, 1989, 1990) appear to differ from those in *C. pulchra* in at least two ways. First, the shell-forming granules of "*C. psammophila*" occur in clusters in the ooplasm, whereas they appear to be randomly located in the oocytes of *C. pulchra*. Second, in "*C. psammophila*" the granules marginate and fuse with one another to form granules with a diameter 1–1.2 μm. The granules of *C. pulchra* were not observed to fuse with one another except occasionally at the time of exocytosis. Certainly additional studies of eggshell formation in acoelomorphans are required.

Phylogenetic implications

Smith *et al.* (1986) suggested that the Turbellaria may be polyphyletic with three distinct lineages: (1) the Catenulida, (2) the Nemertodermatida-Acoela [=Acoelomorpha (Ehlers, 1984)], and (3) the Haplopharyngida-Macrostomida-Polycladida-Neoophora and all higher parasitic platyhelminths [=Rhabditophora (Ehlers, 1984)].

The discovery that acoels' EFGs lack polyphenols prompted examination of the composition of the EFGs in the sister group to the acoels, the Nemertodermatida (Thomas *et al.*, 1985). The oocytes of the nemertodermatid *Nemertinoides elongatus* were negative for polyphenols (Smith *et al.*, 1988). The absence of polyphenols from EFGs of the Acoelomorpha stands in sharp contrast to the presence of polyphenols in EFGs in the Rhabditophora and provides further evidence supporting phyletic distance between the Acoelomorpha and the Rhabditophora. Yet to be discovered are characters that clearly link the Acoelomorpha to the other groups (Smith *et al.*, 1982). Studies of eggshell formation in the catenulids may provide this link. There are several examples of homology linking the Catenulida and the Rhabditophora, including the ciliary rootlet system in their epidermal cells and the origin of replacement cells for the epidermis in the parenchyma (Ehlers, 1984; Smith *et al.*, 1986). Oocytes of catenulids, which have an eggshell that arises from granules within the oocyte (Borkott, 1970), have never been examined by electron microscopy. It will be interesting to examine the morphology of catenulid EFGs and to find out if they contain polyphenols. If the Catenulida do have polyphenolic EFGs, this fact would further separate the Catenulida and Rhaditophora from the Acoelomorpha. Although one should consider the possibility that the lack of polyphenols in EFGs is derived, if the catenulids have a non-polyphenolic EFGs with the same morphology as the EFGs of *C. pulchra*, the morphology of the EFG could provide a link between the Acoelomorpha and the Catenulida. A non-polyphenolic EFG could then represent a plesiomorphy for the Platyhelminthes as suggested by Falleni and Gremigni (1989, 1990).

Acknowledgments

The authors thank Dr. Lawrence S. Barden and Dr. Larry Leamy for help with statistical analyses and Ms. Sandra F. Zane for assistance in electron microscopy. Laboratory space was kindly provided by the North Carolina Aquarium at Fort Fisher, NC. The work was supported in part by a Sigma Xi Grant-in-Aid (to RMC) and in part by a UNCC Faculty Research Grant (to MBT).

Literature Cited

Beklemischev, V. N. 1957. *Convoluta psammophila* sp. nov. and the tendency toward juvenile oligomerisation of cellular elements in Turbellaria Acoela. *Tr. Leningr. Ova. Estestvoispyt.* **73:** 5–13. [In Russian].

Borkott, H. 1970. Geschlectliche Organisation, Fortpflanzungsverhalten und Ursachen der sexuellen Vermehrung von Stenostomum sthenum nov. spec. (Turbellaria, Catenulida). *Z. Morphol. Tiere* **67:** 183–262.

Boyer, B. C. 1972. Ultrastructural studies of differentiation in the oocyte of the polyclad turbellarian, *Prosthecceraeus floridanus*. *J. Morphol.* **136:** 273–296.

Bunke, D. 1982. Ultrastruktur-untersuchungen zur Eischalenbildung bei Microdalyellia fairchildi (Turbellaria). *Zoomorphology* **101:** 61–70.

Chandler, R. M., and M. B. Thomas. 1986. The ultrastructure of the oocyte of *Convoluta* sp. *J. Elisha Mitchell Sci. Soc.* **102:** 179–180 (abstr.).

Chandler, R. M., and M. B. Thomas. 1987. An ultrastructural examination of late oogenesis and of the laid egg of *Convoluta* sp. *Am. Zool.* **27:** 121A (abstr.).

Chandler, R. M., J. P. Smith, and M. B. Thomas. 1988. A morphometric analysis of egg shell formation in *Convoluta* sp. *J. Elisha Mitchell Sci. Soc.* **104:** 190 (abstr.).

Coil, W. H. 1991. Platyhelminthes: Cestoidea. Pp. 211–283 in *Microscopic Anatomy of Invertebrates*, vol. 3: *Platyhelminthes and Nemertinea*, F. W. Harrison and B. J. Bogitsh, eds. Wiley-Liss, New York.

Dörjes, J. 1968. Die Acoela (Turbellaria) der Deutschen Nordseeküste und ein neues System der Ordnung. *Z. Zool. Syst. Evolutionsforsch.* **6:** 56–452.

Domenici, L., and V. Gremigni. 1977. Fine structure and functional role of the coverings of the eggs in *Mesostoma ehrenbergii* (Focke) (Turbellaria, Neorhabdocoela). *Zoomorphologie* **88:** 247–257.

Domenici, L., L. Galleni, and V. Gremigni. 1975. Electron microscopical study of egg-shell globules in *Notoplana alcinoi*. *J. Submicrosc. Cytol.* **7:** 239–274.

Ehlers, U. 1984. *Das Phylogenetische System der Plathelminthes.* Gustav Fischer Verlag, Stuttgart. 317 pp.

Espinosa, P. L. 1986. Histochemical and ultrastructural studies of oogenesis in the marine polyclad turbellarian *Gnesioceros floridana*. M.S. Thesis, The University of North Carolina at Charlotte, Charlotte, NC.

Falleni, A., and V. Gremigni. 1989. Egg covering formation in the acoel *Convoluta psammophyla* (Platyhelminthes, Turbellaria): an ultra-

structural and cytochemical investigation. *Acta. Embryol. Morphol. Exper. N.S.* **10:** 105–112.

Falleni, A., and V. Gremigni. 1990. Ultrastructural study of oogenesis in the acoel turbellarian *Convoluta. Tissue & Cell* **22:** 301–310.

Fried, B., and M. A. Haseeb. 1991. Platyhelminthes: Aspidogastrea, Monogenea, and Digenea. Pp. 141–209 in *Microscopic Anatomy of Invertebrates,* vol. 3: *Platyhelminthes and Nemertinea,* F. W. Harrison and B. J. Bogitsh, eds. Wiley-Liss, New York.

Gammon, C. 1979. Histochemical and ultrastructural studies of oogenesis in the marine polyclad turbellarian *Stylochus zebra* Verrill. M.S. Thesis, Wake Forest University, Winston-Salem, NC.

Giesa, S. 1966. Die Embryonalentwicklung von *Monocelis fusca* Oersted (Turbellaria, Proseriata). *Z. Morphol. Oekol. Tiere* **57:** 137–230.

Gremigni, V. 1988. A comparative ultrastructural study of homocellular and heterocellular female gonads in free-living Platyhelminthes-Turbellaria. *Fortschr. Zool.* **36:** 245–261.

Gremigni, V., A. Falleni, and P. Lucchesi. 1987. An ultrastructural study of oogenesis in the turbellarian *Macrostomum. Acta Embryol Morphol. Exper. N.S.* **8:** 257–262.

Hulings, N. C., and J. S. Gray. 1974. A manual for the study of meiofauna. *Smithson. Contr. Zool.* **78:** 1–83.

Ishida, S. T. 1989. Further studies on the shell-forming granules and eggshell formation in polyclads (Turbellaria, Platyhelminthes). *Sci. Rep. Hirosaki Univ.* **36:** 55–72.

Ishida, S. T., and W. Teshirogi. 1986. Eggshell formation in polyclads (Turbellaria). *Hydrobiologia* **132:** 127–135.

Ishida, S. T., T. Gotoh, and W. Teshirogi. 1981. Oogenesis and eggshell formation in polyclads. *Rep. Fukaura Mar. Biol. Lab., Hirosaki Univ.* **9:** 32–48. [translated from Japanese].

Kucera, F. P. 1987. An ultrastructural and cytochemical analysis of eggshell-forming granules in *Macrostomum beaufortensis* and *Macrostomum hystricinum marinum* (Turbellaria, Macrostomida). M.S. Thesis, The University of North Carolina, Charlotte, NC.

McDowell, E. M., and B. F. Trump. 1976. Histological fixative suitable for diagnostic light and electron microscopy. *Arch. Pathol. Lab. Med.* **100:** 405.

Reynolds, E. S. 1963. The use of lead citrate at high pH as an electron opaque stain in electron microscopy. *J. Cell Biol.* **17:** 208.

Rieger, R. M., S. Tyler, J. P. S. Smith, and G. E. Rieger. 1991. Platyhelminthes: Turbellaria. Pp. 7–140 in *Microscopic Anatomy of Invertebrates,* vol. 3: *Platyhelminthes and Nemertinea,* F. W. Harrison and B. J. Bogitsh, eds. Wiley-Liss, New York.

Smith, J. P. S., and L. Bush. 1991. *Convoluta pulchra* n.sp. (Turbellaria: Acoela) from the East Coast of North America. *Trans. Am. Microsc. Soc.* **110:** 12–26.

Smith, J. P. S., S. Tyler, M. B. Thomas, and R. M. Rieger. 1982. The morphology of turbellarian rhabdites: phylogenetic implications. *Trans. Am. Microsc. Soc.* **101**(3): 209–228.

Smith, J. P. S., S. Tyler, and R. M. Rieger. 1986. Is the Turbellaria polyphyletic? *Hydrobiologia* **132:** 13–21.

Smith, J. P. S., M. B. Thomas, R. M. Chandler, and S. F. Zane. 1988. Granular inclusions in the oocytes of *Convoluta* sp., *Nemertoderma* sp., and *Nemertinoides elongatus* (Turbellaria, Acoelomorpha). *Fortschr. Zool.* **36:** 263–269.

Spurr, A. R. 1969. A low-viscosity epoxy resin embedding medium for electron microscopy. *J. Ultrastruct. Res.* **26:** 31–43.

Thomas, M. B., J. P. S. Smith, R. M. Chandler, and A. Barker. 1985. Eggshell granules in some primitive Turbellaria: more evidence for polyphyly? *Am. Zool.* **25:** 91A.

Watson, M. L. 1958. Staining of tissue sections for electron microscopy with heavy metals. *J. Biophys. Biochem. Cytol.* **4:** 475–479.

Weibel, E. R. 1979. *Stereological Methods,* vol. 1. Academic Press, Inc., London. 415 pp.

Reference: *Biol. Bull.* **182**: 66–76. (February, 1992)

Isolation of Neurons of a Nudibranch Veliger

FU-SHIANG CHIA, RON KOSS, SHAUNA STEVENS, AND JEFF I. GOLDBERG

Department of Zoology, University of Alberta, Edmonton, Alberta, Canada T6G 2E9

Abstract. A technique was developed to dissociate and culture identified sensory neurons and interneurons from the anterolateral propodial ganglia of metamorphically competent veligers of the nudibranch, *Onchidoris bilamellata*. Receptor cells have been represented as receiving an environmental cue that initiates the settlement response. The ganglionic cells, along with other cell-types from the propodial region housing the ganglia, were excised with a large-bore micropipette, and dissociated by mild trypsin incubation and trituration. Cells and tissues were plated in poly-L-lysine-coated plastic culture dishes containing modified *Aplysia* medium and survived for up to four days. The different cell-types possess diagnostic features, so they can be recognized under culture conditions. Sensory cells were bipolar in profile, with one end of the cell being thickened, representing the receptor apparatus. Interneurons are unipolar or bipolar in shape, and bear thin neurites. Other cell-types, including myocytes, ciliated epidermal cells, nonciliated epidermal cells, and gland cells were identified. Identifications of living cells were corroborated through electron microscopical analysis.

Introduction

The propodium of the advanced veliger larva of the nudibranch *Onchidoris bilamellata* contains a unique set of morphologically identifiable structures called the anterolateral ganglia (Chia and Koss, 1989). These structures are thought to be involved in perception of the environmental cues that induce settlement and metamorphosis (Chia and Koss, 1988). Recently, it has been shown that sensory receptor cells within the anterolateral ganglia respond to a known settlement cue (barnacle-conditioned seawater) by producing slow, low-amplitude depolarizations that can be detected by the application of conventional intracellular recording methods (Arkett *et al.*, 1989). However, the activity of the sensory cells is variable in terms of duration and amplitude. Such variability may be due to the changeable concentration of crude stimulus being administered, the developmental status of the receptors, or the degree of damage caused by the electrode upon entry into the cell. Also unclear is the depth within the ganglion that the electrode was placed, and whether the epidermal tissues overlying these subepidermal structures altered the response of receptor cells.

In this paper we report a technique for excising, dissociating, and culturing the lateral propodial region of the veliger foot of *O. bilamellata*. This work was undertaken with a view to studying the responses of the isolated cells to settlement or metamorphic cues, thereby overcoming many of the limitations presented by the intact preparation.

Received 10 September 1990; accepted 25 November 1991.

Materials and Methods

Egg ribbons from *Onchidoris bilamellata* (Linnaeus, 1767) were collected at Bamfield Marine Station, Bamfield, British Columbia, Canada, and transported to the University of Alberta. Veliger larvae were then raised according to the method of Chia and Koss (1988). The veligers used in these experiments were from the same cohort, and random samples from the cohort were checked for metamorphic competency according to Chia and Koss (1988).

Veligers were pipetted into a Sylgard (Dow Corning)-lined dish containing 2.5 ml of a high Mg^{++}, low Ca^{++} seawater mixture (12–15°C) consisting of natural seawater, isotonic (0.33 *M*) $MgCl_2$, and Co^{++}-seawater in a ratio of 2:1:4.5 (v/v/v). Co^{++}-seawater consisted of 430 m*M* NaCl, 10 m*M* $CoCl_2$, 10 m*M* KCl, 30 m*M* $MgCl_2$, 20 m*M* $MgSO_4$, 10 m*M* TES pH 7.8 (Arkett *et al.*, 1987, 1989). Veligers were tethered with a cactus spine, which was inserted through the base of the velum. A second

spine was placed through the tip of the foot, and a third spine was used to orient the veliger such that one side of the propodium and receptor field faced upward (Figs. 1, 2).

Larvae were subsequently incubated for 5 min in 0.2% trypsin (Sigma) in an *Aplysia* defined medium [mADM: 50% Liebowitz L-15 (Gibco special order); 0.26 *M* NaCl; 9.7 m*M* $CaCl_2$; 4.6 m*M* KCl; 26 m*M* $MgSO_4$; 26 m*M* $MgCl_2$; 2 m*M* $NaHCO_3$; 33 m*M* Dextrose; 10 m*M* Hepes; 0.015% L-glutamine; 50 μg per ml gentamicin] modified from Schacher and Proshansky (1983). This solution was eventually replaced with mADM.

The anterolateral ganglion, which is visible as an oblong cellular mass, was located using a dissecting microscope, and a silicon-coated (Sigmacoat) micropipette, with a bore diameter of 20–30 μm, was placed directly on it. A micromanipulator was used to place the micropipette. The tissue was excised by first applying mechanical force with the micropipette to this region, and then alternating negative and positive pressure within the micropipette through a microsuction device (Canlab). The excised tissues, including the portions of the anterolateral ganglion and propodial epidermis, were triturated in the micropipette. The dissociated cells were then plated on to high molecular weight poly-L-lysine (Sigma) coated plastic 35 mm tissue culture plates (Falcon) in cold mADM. The cultures were maintained at 4°C for 24 to 72 h.

Cell cultures were viewed and photographed live with a Nikon TMD inverted photomicroscope equipped with phase-contrast optics. Cultures to be fixed for transmission electron microscopy (TEM) were stained with Richardson's stain (Richardson *et al.*, 1960) to locate the cells in the culture dish. For TEM, cells were fixed for 1 h in 2.5% glutaraldehyde in 0.2 *M* phosphate buffer (pH 7.6), followed by a 1 h post-fixation in 2% OsO_4 in 1.25% sodium bicarbonate (pH 7.2, Wood and Luft, 1965). They were then dehydrated through an ethanol series, and directly embedded in Medcast (Ted Pella Inc.). After a polymerization period of 72 h, the Medcast was peeled from the culture dish, mounted on Medcast blanks with Krazy Glue, and sectioned with a diamond knife. Sections were stained with uranyl acetate and lead citrate (10 min each). Sections were examined with a Philips E. M. 201 electron microscope.

For scanning electron microscopy (SEM), larvae were relaxed in the Co^{++}-seawater mixture described above, and processed according to the technique of McEuen (1985). Specimens were then examined with a Cambridge Stereoscan 250 SEM.

Results

The foot of the advanced veliger of *O. bilamellata* is a large structure consisting of a metapodium and propodium (Figs. 1, 2). In veligers that have been immobilized in the high Mg^{++}, low Ca^{++} seawater, the location of each anterolateral ganglion is evident as an oblong, cilia-free region on the foremost sides of the propodium (Fig. 2). The sensory fields overlying the anterolateral ganglia are composed of a mosaic of cell-types including the dendrites of sensory cells, epidermal cells, multicellular metapodial glands, and muscle cells (Figs. 3–5). Some untargeted tissues and cells were inevitably excised along with the target tissues, and will be characterized because they are present in cultures of dissociated cells.

The pair of anterolateral propodial ganglia are located below the level of the epidermis (Figs. 3, 5). They are oblong structures, consisting of an outer cortex of cell bodies and an inner neuropil of fibers (Chia and Koss, 1989). The cell-types constituting the cortex include sensory cells, neurons, and sheath cells; neurons occupy the inner layer adjacent to the neuropil, while sensory cells are more numerous and distributed around the outer, lateral perimeter of each ganglion. Bundles of dendritic processes originating from sensory cells traverse the epidermis to form the external sensory fields mentioned above (Figs. 1, 2, 5). Sheath cells encapsulate the ganglia. The anterolateral ganglia are connected to the central nervous system, *i.e.*, cerebral ganglia, by short commissures.

After excision of a ganglion, the dissociated cells settled within 24 h of plating. Cells settled in clusters or as individuals and attached to the substratum. Several cell-types were identifiable at the level of the light microscope on the basis of their size and morphology. These included: epidermal cells (both ciliated and nonciliated), gland cells, muscle cells, neurons, and sensory neurons (Figs. 7, 10, 13, 16, 19, 22, 25, 29). The appearance of these cells was constant in several separate dissociations and was comparable to those identified by *in situ* study. Most importantly, the fine structure of the different cell-types *in situ* was conserved under *in vitro* conditions, thus corroborating the identification of cell-types according to light microscopy.

Epidermal cells

In its natural state, the epidermis covering the anterolateral ganglion is composed primarily of multiciliated cells and cells with long branched microvilli projecting from their apices (Figs. 5, 6, 9). Both cell-types are cuboidal in profile and attach to the basal lamina through a hemidesmosome complex involving numerous microfilaments. Those cells that bear microvilli contain numerous mitochondria within the apical portion of the cell; electron-dense granules of about 0.2 μm in diameter are found immediately below these organelles (Fig. 6). Multiciliated cells also possess numerous distal mitochondria, which

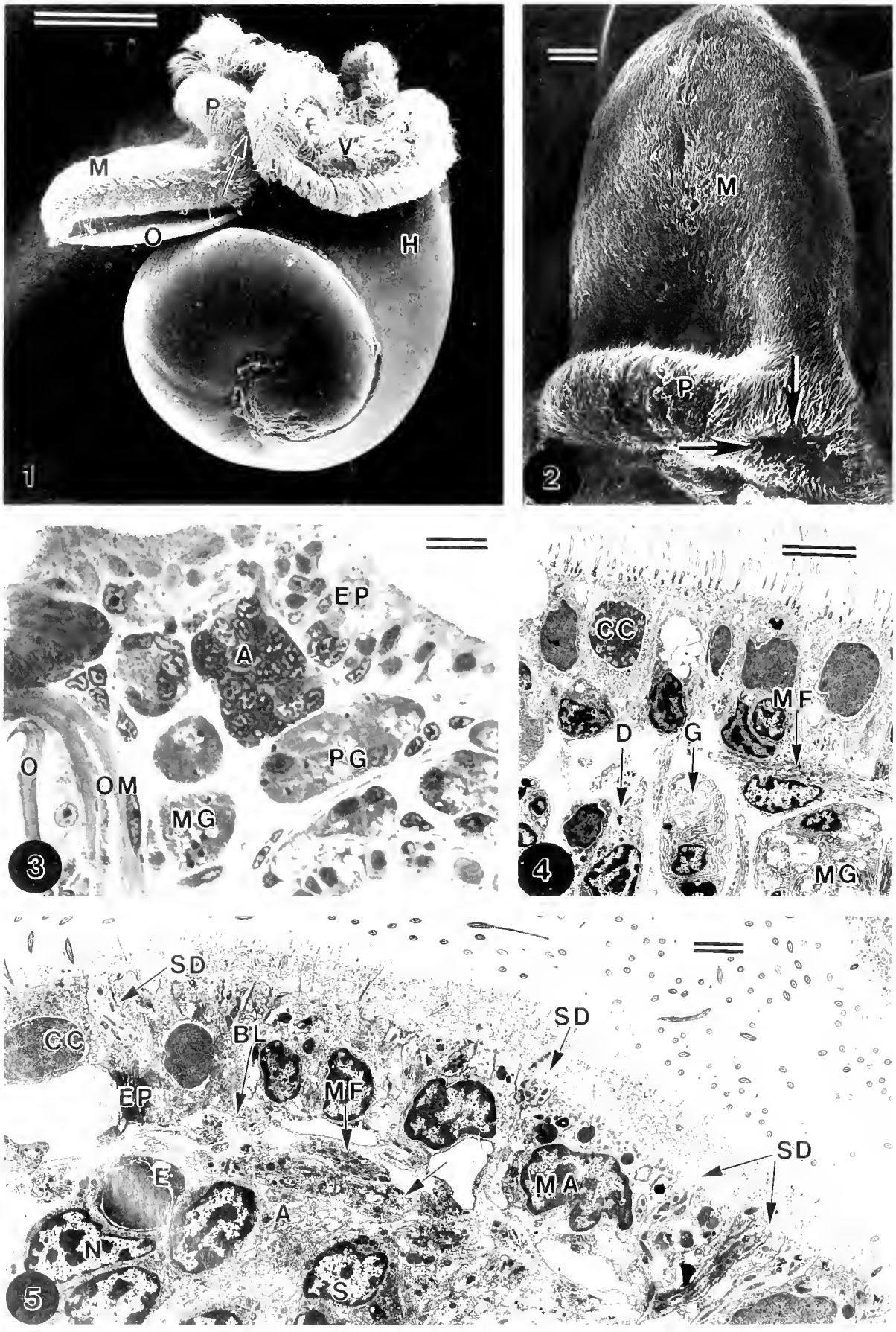
P
V
M
O
H
1
M
P
2
EP
A
PG
O
OM
MG
3
CC
MF
D
G
4
MG
SD
CC
BL
SD
EP
MF
SD
E
MA
A
N
S
5

are distributed among the ciliary rootlets. Nuclei occupy the basal regions of both cell-types. However, the cytoplasm and the nuclei of microvillar cells stain less densely than ciliated cells, while the latter possess unique vacuoles with electron-translucent contents.

Immediately after dissociation of a ganglion, cultures are dominated by ciliated and non-ciliated epidermal cells, many of which fail to attach to the poly-L-lysine substratum. Ciliated and nonciliated epidermal cells were readily recognizable at the light microscopy level because both types of cell were round (Figs. 7, 10). In ciliated cells, the cilia were readily identifiable (Fig. 10). After trituration, both of these types of cell generally remained aggregated. The structural characteristics of the *in situ* and *in vitro* ciliated and nonciliated epidermal cells are similar; those cells found in culture are round to cuboidal and contain microfilaments, numerous mitochondria, and microvilli or cilia (Figs. 5, 6, 8, 9, 11). The substructure of the cilium includes a ciliary rootlet. Within a day, cilia appear to be reabsorbed into the cell. In contrast, nonciliated epidermal cells contain characteristic electron-opaque granules of about 0.5 μm in diameter, and the nucleus stains lightly.

Muscle cells

Muscle cells are numerous throughout the propodium and lie adjacent or attach to the basal lamina. They are filamentous in profile and their contents are dominated by myofilaments (Figs. 3, 4, 12). Mitochondria are scattered around a centrally positioned elliptical nucleus, which is displaced away from the main stream of myofilaments (Fig. 12). Individual muscle cells found under culture conditions are identical in shape and structure. They are large and filamentous in appearance and their nucleus protrudes from one side of the cell (Figs. 13, 14). The cytoplasm contains bundles of myofilaments which extend the length of the cell, and mitochondria which are scattered around the nucleus (Fig. 14).

Secretory cells

The metapodial glands of intact ganglia are flask-shaped structures and are located below the level of the epidermis (Figs. 3–5). They contain two types of gland cells (Figs. 4, 15, 18). The first, or type A secretory cell, contains inclusions that are composed of flocculent material; free ribosomes and rough endoplasmic reticulum are dominant organelles and surround an oblong nucleus (Fig. 15). The second, or type B secretory cell has a densely staining nucleus, and its cytoplasm is filled with small electron-dense granules averaging 0.1 μm in diameter (Fig. 18). Isolated metapodial gland secretory cells had the same overall morphology; they were large and bulbous, with the nucleus occupying the rounded end of the cell (Figs. 15, 17, 18, 20). In certain instances, large secretory vacuoles in type A cells gave the interior of the cell a convoluted appearance when observed by light microscopy. Isolated type A secretory cells contained the vacuoles and extensive rough endoplasmic reticulum observed *in situ* (Fig. 17). Cultured type B cells contained the electron-dense granules present *in situ* and could often be distinguished from type A cells by their smaller cytoplasmic protrusions (Fig. 20).

Ganglionic cells

Anterolateral ganglia are composed of sheath cells, neurons (Figs. 21, 24), and sensory receptor cells (Figs. 27, 28) whose configuration, distribution, and fine structure have been described in detail by Chia and Koss (1989). Sheath cells stain densely and encapsulate the anterolateral ganglia through long, slender processes. How-

Figure 1. Scanning electron micrograph (SEM) of an advanced veliger showing location of one of the pair of settlement receptor fields (arrow), propodium (P), metapodium (M), shell (H), velum (V), and operculum (O). Bar = 100 μm.

Figure 2. Higher magnification SEM showing a receptor field (arrows) and the foot with propodium (P) and metapodium (M). Bar = 20 μm.

Figure 3. Section (1 μm thickness) through the propodium identifying the position of the anterolateral ganglia (A), covering epidermis (EP), operculum (O), and opercular muscle (OM). The multilobular propodial glands (PG) and the smaller metapodial glands (MG) are also shown. Bar = 10 μm.

Figure 4. Transmission electron micrograph of section through a ciliated region of the propodium showing the epidermis composed of ciliated cells (CC), overlying metapodial glands (MG), and muscle cells and fibers (MF). Note that the secretory cells within the metapodial glands are of two types; one type has large electron-translucent inclusions (G) and the other type has darkly staining nuclei and small electron-dense granules (D). Bar = 5 μm.

Figure 5. Cross section through the lateral propodial region showing that the anterolateral ganglion (A) is composed of sensory cells (S) with radiating ciliated dendritic endings (SD), interneurons (N), and sheath cells (E). The epidermis (EP) contains ciliated cells (CC), microvillar cells (MA) with elongate microvilli, and the ramifications of sensory cell terminals. Also note the basal lamina (BL), muscle cell (MF) and metapodial gland cell processes (arrow). Bar = 2.5 μm.

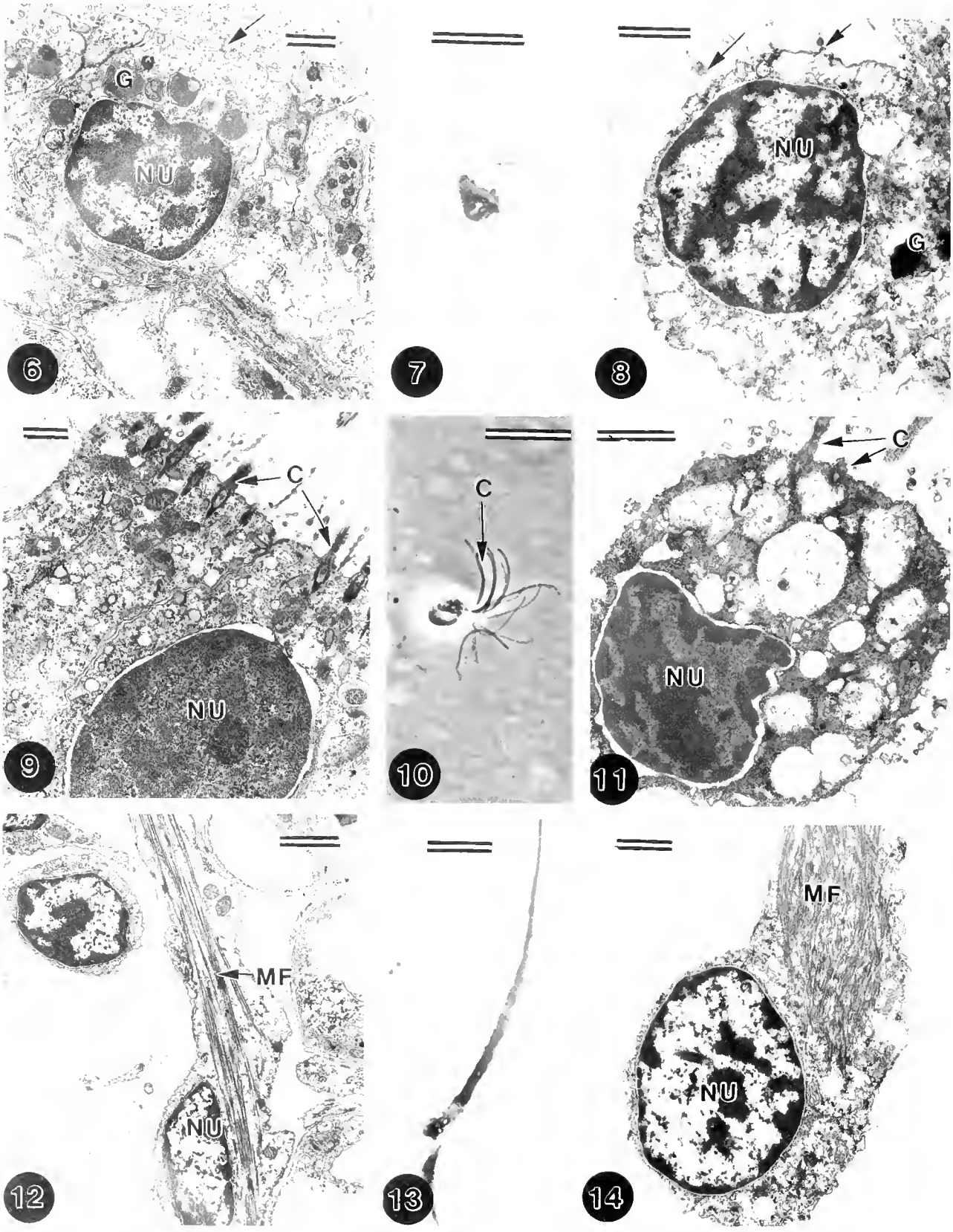

Figure 6. Section through an *in situ* microvillus cell located in the epidermis overlying the anterolateral ganglion. Note the nucleus (NU), electron-dense granules (G) and microvilli (arrow). Bar = 1 μm.

Figure 7. Phase-contrast photomicrograph of a cultured microvillus cell isolated from the lateral propodial region of a competent *Onchidoris* veliger. Bar = 10 μm.

ever, isolated sheath cells were never found in cultures of dissociated cells, although they were rarely observed attached to undissociated clusters of neurons and sensory cells.

Neurons are located deep within an intact ganglion. Their cell bodies contain a relatively clear cytoplasm, a lightly staining nucleus, free ribosomes, and a small number of vesicles (Figs. 21, 24). They possess one or two thin neurites, which, depending upon the location of that neuron within the ganglion, projected from the cell body (Fig. 24) into the neuropil or the commissure that connects to the cerebral ganglion. *In situ* neurites are visualized as thin processes that contain a few vesicles, microtubules, and the occasional mitochondrion (Fig. 24); neurons do not communicate with the external environment and do not possess cilia.

Neurons plated from the anterolateral ganglion were identified by the presence of long thin, sometimes branched processes that extended from a teardrop-shaped unipolar or bipolar cell body (Figs. 22, 25, 29). They were usually found in loose aggregates along with sensory cells, with unipolar or flask-shaped interneurons being the most numerous (Fig. 25). The soma of interneurons ranged from 3–5 μm in diameter, which is the size range of the neuronal soma identified *in situ*. In sectional profile, both *in situ* and isolated neurons possessed long slender neurites that emerge from a bulbous base containing the nucleus (Figs. 21, 24, 26). The nucleus was spherical to cuboidal in form and embedded, along with a few mitochondria, in a finely granular cytoplasm (Figs. 22–25). Neurites contained microtubules and a small number of vesicles ranging from 50 to 80 nm in diameter (Figs. 24, 26). All the above features are identical to those of neurons *in situ* in the anterolateral ganglia of the veliger (Chia and Koss, 1989). No synaptic profiles were observed within the ganglion, although synapses were observed in the connectives that connect to the cerebral ganglion. Similarly, synapses were never observed in dissociated cells, and it was not possible to classify them as motoneurons or interneurons.

The cell bodies of sensory cells *in situ* are located within the ganglion along the lateral margin that borders the epidermis (Figs. 5, 27). They are spindle-shaped, and consist of a lightly staining nucleus, free ribosomes, microtubules, and numerous vesicles, all of which are embedded in a relatively clear cytoplasm (Fig. 27). Axonal processes, which project to the neuropil, contain microtubules, vesicles, and the occasional mitochondrion. The characteristic features of sensory neurons include: (1) dendritic processes that are thicker than axons, (2) dendrites that extend from the cell body through the epidermis to terminate externally as a single cilium. The cilium was observed to possess a basal body but no rootlet, (3) large (0.5 μm) electron-dense granules, and (4) numerous vesicles in the cell body. Their dendrites also contain mitochondria and microtubules. The overall appearance (Chia and Koss, 1989) of these cells is retained following dissociation and plating in the culture dishes (Figs. 27, 29, 30). Isolated sensory neurons were recognizable at the level of light microscopy by their characteristic spindle to cigar shape: one of the two processes that radiated out from the soma was thicker, and often shorter, and presumably represented the dendrite (Fig. 29). The nucleus occupied a central location within the cell (Fig. 29). At the fine structural level, the integrity of the sensory cells also remained unchanged. These cells are characterized by a relatively clear, lightly staining cytoplasm that contains free ribosomes and an elliptical to spherical nucleus (Figs. 27, 28, 30). The nucleus is relatively lightly staining, and the axon and dendritic processes can be recognized. The dendrite possesses a single cilium and mitochondria, is generally wider than the axon, and characteristically contains vesicles and electron-dense granules averaging 0.5 μm in diameter (Figs. 27, 28, 30). The cilium lacks a ciliary rootlet as compared to cilia of general ciliated epidermal cells which have rootlets (Fig. 30). However, the cilium could not always be found in all cells suspected of being sensory cells, possibly because this organelle may sometimes have been reabsorbed or truncated after the dissociation. The axons contain microtubules and vesicles and are similar in appearance to the neurites of interneurons described above.

The diagnostic features of the different cell-types found in intact ganglia and in cultures of dissociated ganglia are summarized in Table I.

Figure 8. Section through an isolated microvillus cell, under *in vitro* conditions, showing microvilli (arrows) electron-dense granules (G) and nucleus (NU). Bar = 1 μm.

Figure 9. *In situ* ciliated epidermal cell showing multiple cilia (C) and a densely staining nucleus (NU). Bar = 1 μm.

Figure 10. Phase-contrast photomicrograph of a cultured ciliated epidermal cell showing multiple cilia (C). Bar = 10 μm.

Figure 11. *In vitro* ciliated cell showing multiple cilia (C) and nucleus (NU). Bar = 1 μm.

Figure 12. *In situ* muscle cell showing nucleus (NU) and myofilaments (MF). Bar = 1 μm.

Figure 13. Phase-contrast photomicrograph of an isolated, cultured muscle cell. Bar = 5 μm.

Figure 14. *In vitro* muscle cell showing myofilaments (MF) and nucleus (NU). Bar = 1 μm.

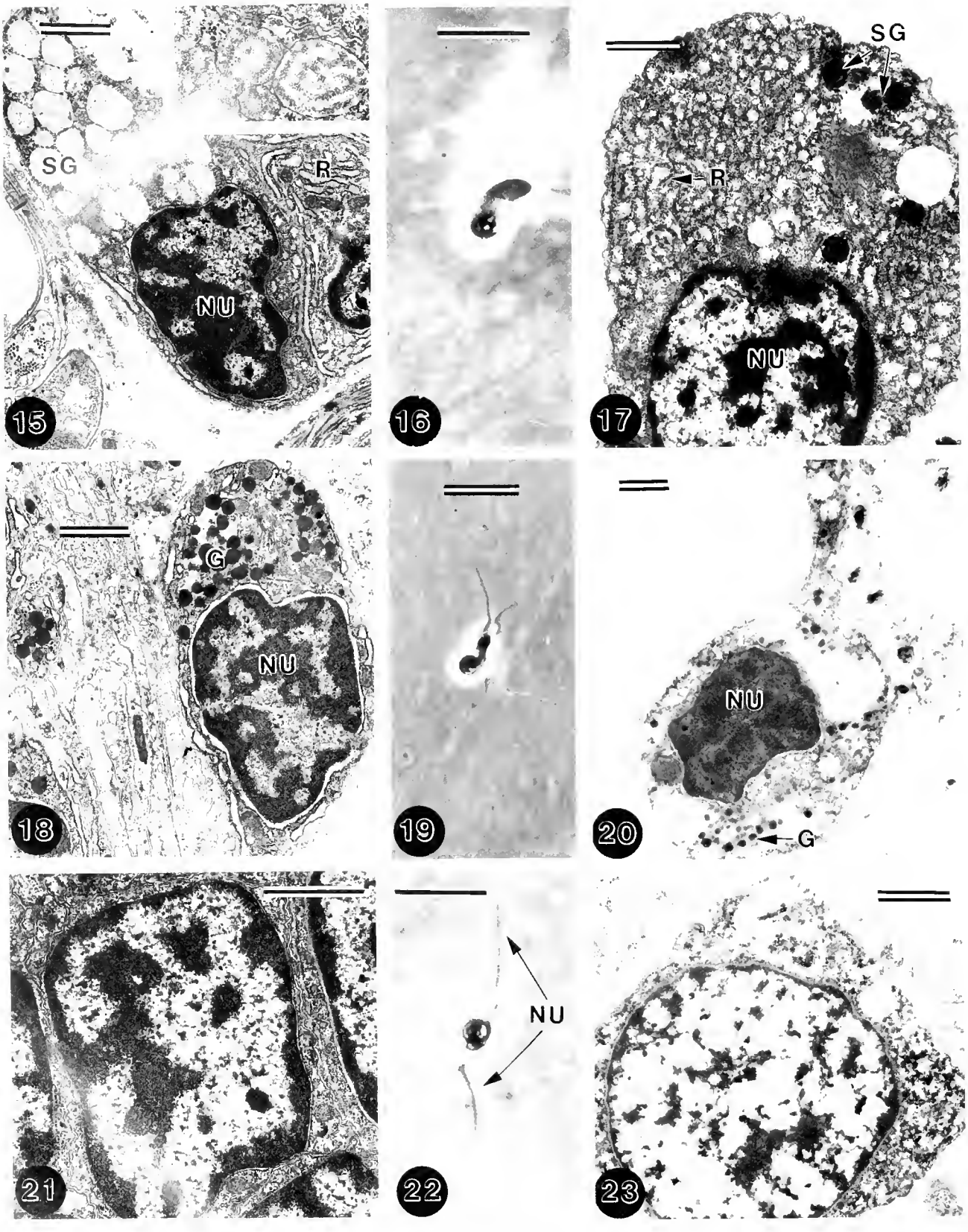

Figure 15. Type A gland cells of an *in situ* metapodial gland showing secretory granules (SG) filled with flocculent material, rough endoplasmic reticulum (R), and a nucleus. Bar = 1 μm. Inset: higher magnification of secretory granules.

Figure 16. Phase-contrast photomicrograph of an isolated, cultured gland cell. Bar = 10 μm.

Table I

Identifying characteristics of cell-types from the anterolateral ganglionic region of Onchidoris bilamellata

Cell-type	Form (*LM and TEM profile)	Staining properties	Size (largest dimension)	Characteristic inclusions and organelles
Metapodial gland cell A	club	lightly granular	10–15 μm	large granules containing flocculent material; rough endoplasmic reticulum
Metapodial gland cell B	flask	densely granular	15 μm	electron-dense granules (0.1 μm diameter)
Muscle cell	thread	densely granular	20–50 μm	myofilaments
Epidermal ciliated cell	cube	densely granular	5–10 μm	multiple cilia; numerous mitochondria
Epidermal microvillus cell	cube	lightly granular	5–10 μm	microvilli; opaque granules (0.2 μm diameter)
Sensory neuron	spindle; one end thicker and often shorter	lightly granular	7–10 μm	single cilium; microtubules; clustered vesicles (0.05–0.08 μm diameter); opaque granules 0.5 μm diameter
Neuron	oval bipolar or unipolar; long slender neurites	lightly granular	10–15 μm	microtubules; few vesicles (0.05–0.08 μm diameter)

* LM = light microscopy; TEM = transmission electron microscopy.
Listed features are shared between identical cell-types found under *in situ* and *in vitro* conditions.

Discussion

Assays that measure whole-organism responses are useful in identifying substances that induce larval settlement and metamorphosis. However, they provide little information about the cellular mechanisms that they activate, or the location (*i.e.,* the structural site) at which they are detected (reviewed by Pawlik, 1990). Therefore, techniques must be developed which enable the study of the precise actions of settlement and metamorphic inducers.

There is considerable evidence suggesting that the induction of settlement and metamorphosis of larval mollusks is mediated by the nervous system (Hadfield, 1978); at the primary level, the process of perceiving natural or artificial inductive substances is ascribed to an external epidermal sensory cell (Baloun and Morse, 1984; Burke, 1983; Morse and Baxter, 1989; Morse, 1990; Trapido-Rosenthal and Morse, 1986; Yool *et al.,* 1986). Receptor cells for these responses in different species of veligers have been localized to the cephalic sensory organ (Bonar, 1978; Morse *et al.,* 1980; Chia and Koss, 1984), rhinophores (Chia and Koss, 1982), and the anterior portion of the foot or propodium (Chia and Koss, 1989). Although the receptive capacities of most of these organs have been inferred from morphological characteristics and relationships, there is little evidence to suggest that all these structures are predisposed to perceive settlement or metamorphic cues. To date, the *Onchidoris* larval foot, or specifically the anterolateral propodial ganglia, represents the only system where morphologically identified chemosensory receptor cells have been shown electrophysiologically to respond to a known settlement cue (Arkett *et al.,* 1989).

In this study we have developed a method for dissociating, isolating, and maintaining the cells that constitute the anterolateral portion of the *Onchidoris* foot, including the sensory neurons and interneurons of the anterolateral ganglia. This technique produces cultures of individual cells, permitting future studies of the cellular mechanisms involved in the detection and transduction of settlement cues; previous studies have been restricted by *in situ* preparations.

This *in vitro* system is unique among preparations for studying veliger settlement because it can be used to study

Figure 17. *In vitro* gland cell showing secretory granules (SG), rough endoplasmic reticulum (R), and nucleus (N). Bar = 1 μm.

Figure 18. Type B secretory cell showing a densely staining nucleus (N) and small electron-dense granules (G). Bar = 1 μm.

Figure 19. Phase-contrast photomicrograph of an isolated, cultured type B gland cell. Bar = 10 μm.

Figure 20. *In vitro* type B gland cell showing small electron-dense granules and a densely staining nucleus. Bar = 1 μm.

Figure 21. Interneuron located in anterolateral ganglion. Bar = 1 μm.

Figure 22. Phase-contrast photomicrograph of a interneuron isolated from the anterolateral ganglion. Note the bipolar shape with neurites (NU) radiating out from the cell body. Bar = 5 μm.

Figure 23. Section through an interneuron under *in vitro* conditions. Bar = 1 μm.

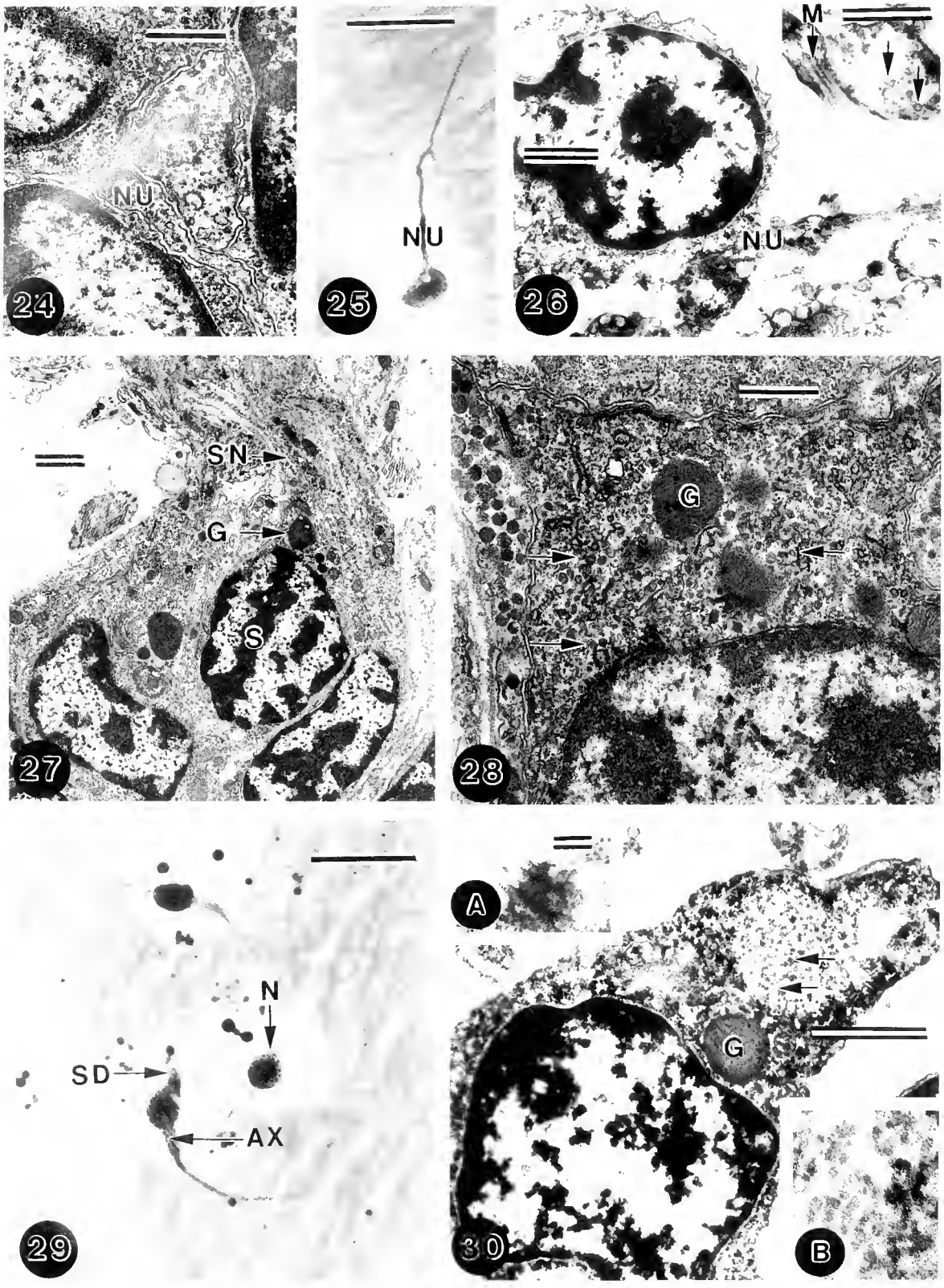

Figure 24. Neurite (NU) of interneuron in an anterolateral ganglion showing vesicles and microtubules. Bar = 1 μm.

Figure 25. Phase-contrast photomicrograph of an isolated interneuron showing a unipolar shape with a single neurite (NU) radiating from the cell body. Bar = 5 μm.

Figure 26. Section through an isolated and cultured interneuron showing a neurite (NU) extending out from the cell body. Inset: neurite with vesicles (arrows) and microtubules. Bars = 0.5 μm.

the immunocytological properties of different cell types, their passive and active electrical properties, and their responses to bioactive substances such as neurotransmitters and neuromodulators. A similar approach has been successfully employed to study the same parameters in neurons dissociated from embryos of the pulmonate, *Helisoma trivolvis* (Goldberg *et al.*, 1988; Goldberg and Price, 1991; Goldberg *et al.*, 1991).

For the most part, the isolated cells retained their basic *in situ* appearance, and could thus be classified according to cell-type by light microscopy. Such classifications were usually confirmed by electron microscopy. There were instances, however, where the appearances of different cell-types overlapped sufficiently to preclude their classification. For instance, the apical ends of many putative sensory cells apparently became rounded following isolation, making them indistinguishable from gland cells. Nevertheless, future studies that combine electrophysiological techniques with those employed here, will ensure accurate diagnosis of each cell-type.

Arkett *et al.* (1989) have demonstrated that settlement receptor cells in *Onchidoris* depolarize in response to a known settlement cue. It is our intention to use the culture system developed in the present study to cultivate the sensory cells and neurons of the anterolateral ganglion for the purpose of voltage- and current-clamping experiments. The electrophysiological effects of settlement inducing-ligands and neurotransmitters can then be directly and precisely monitored on single identified cells. The possible roles of second messengers in mediating settlement and metamorphic responses can then be accurately elucidated.

Acknowledgments

The collection of egg masses, by Dr. A. Martel and M. Sewell, was greatly appreciated. We also wish to thank Dr. D. A. Craig and G. D. Braybrooke for providing Scanning Electron Microscope Facilities, and Dr. S. K. Malhotra for providing Transmission Electron Microscope Facilities. F.-S. C. was supported by NSERC grant #6083 and J.I.G. was supported by NSERC grant #U0553 and the Alberta Heritage Foundation for Medical Research.

Literature Cited

Arkett, S. A., G. O. Mackie, and C. L. Singla. 1987. Neuronal control of ciliary locomotion in a gastropod veliger (*Calliostoma*). *Biol. Bull.* **173:** 513–526.

Arkett, S. A., F.-S. Chia, J. I. Goldberg, and R. Koss. 1989. Identified settlement receptor cells in a nudibranch veliger respond to specific cue. *Biol. Bull.* **176:** 155–160.

Baloun, A. J., and D. E. Morse. 1984. Ionic control of metamorphosis in larval *Haliotis rufescens* (Gastropoda). *Biol. Bull.* **167:** 124–138.

Bonar, D. B. 1978. Ultrastructure of a cephalic sensory organ in larvae of the gastropod *Phestilla sibogae* (Aoelidacea, Nudibranchia). *Tissue Cell* **10:** 153–165.

Burke, R. B. 1983. The induction of metamorphosis of marine invertebrate larvae: stimulus and response. *Can. J. Zool.* **16:** 1701–1719.

Chia, F.-S., and R. Koss. 1982. Fine structure of the larval rhinophores of the nudibranch, *Rostanga pulchra*, with emphasis on the sensory receptor cells. *Cell Tiss. Res.* **225:** 235–248.

Chia, F.-S., and R. Koss. 1984. Fine structure of the cephalic sensory organ in the larva of the nudibranch *Rostanga pulchra* (Mollusca, Opisthobranchia, Nudibranchia). *Zoomorphology* **104:** 131–139.

Chia, F.-S., and R. Koss. 1988. Induction of settlement and metamorphosis of the veliger larva of the nudibranch, *Onchidoris bilamellata*. *Int. J. Invert. Reprod.* **14:** 53–70.

Chia, F.-S., and R. Koss. 1989. The fine structure of the newly discovered propodial ganglia of the veliger larva of the nudibranch, *Onchidoris bilamellata*. *Cell Tiss. Res.* **256:** 17–26.

Goldberg, J. I., D. P. McCobb, P. B. Guthrie, R. A. Lawton, R. E. Lee, and S. B. Kater. 1988. Characterization of cultured embryonic neurons from the snail *Helisoma*. Pp. 85–108 in *Cell Culture Approaches to Invertebrate Neuroscience*. D. J. Beadle, G. Lees, and S. B. Kater, eds. Academic Press, London.

Goldberg, J. I., and C. J. Price. 1991. Voltage-gated ionic currents in neurons isolated from *Helisoma trivolvis* embryos. In *Molluscan Neurobiology*, K. S. Kits, H. H. Boer, and J. Josse, eds. North Holland Publishing Co., Amsterdam (in press).

Goldberg, J. I., L. R. Mills, and S. B. Kater. 1991. Novel effects of serotonin on neurite outgrowth in neurons cultured from embryos of *Helisoma trivolvis*. *J. Neurobiol.* **22:** 182–194.

Hadfield, M. G. 1978. Metamorphosis in marine molluscan larvae: an analysis of stimulus and response. Pp. 165–175 in *Settlement and Metamorphosis of Marine Invertebrate Larvae*, F.-S. Chia and M. E. Rice, eds. Elsevier, New York.

McEuen, F. S. 1985. Reproductive patterns in holothuroids. Ph.D Thesis, The University of Alberta, Edmonton, Canada.

Morse, D. E. 1990. Recent progress in larval settlement: closing the gap between molecular biology and ecology. *Bull. Mar. Sci.* **46**(2): 465–483.

Figure 27. Anterolateral ganglion showing sensory neurons (S) with large electron-dense granules (G) and dendrites (SN) projecting into the epidermis. Bar = 1 μm.

Figure 28. Higher magnification of an *in situ* sensory neuron showing characteristic electron-dense granules (G) interspersed with vesicles (arrows). Bar = 0.5 μm.

Figure 29. Phase-contrast photomicrograph showing an interneuron (N) and a sensory neuron with a shortened dendritic portion (SD) and a thinner axonal segment (AX). Note a second unlabelled sensory cell with a thickened dendritic region. Bar = 5 μm.

Figure 30. Section through a sensory neuron under *in vitro* conditions, showing electron-dense granule (G) and region of vesicles (arrows). Insets: A. Cilium from a dendrite of a sensory neuron. B. Higher magnification of region with vesicles. Bars = 0.5 μm.

Morse, D. E., and G. Baxter. 1989. *In vitro* dissection of chemosensory pathways controlling larval metamorphosis. *Am. Zool.* **29:** 30A.

Morse, D. E., H. Duncan, N. Hooker, A. Baloun, and G. Young. 1980. GABA induces behavioral and developmental metamorphosis in planktonic molluscan larvae. *Fed. Proc.* **39:** 3237–3241.

Pawlik, J. R. 1990. Natural and artificial induction of metamorphosis of *Phragmatopoma lapidosa californica* (Polychaeta: Sabellariidae), with a critical look at the effects of bioactive compounds on marine invertebrate larvae. *Bull. Mar. Sci.* **46**(2): 512–536.

Richardson, K. C., L. Jarrett, and E. H. Finke. 1960. Embedding in epoxy resins for ultrathin sectioning in electron microscopy. *Stain Technol.* **35:** 313–323.

Schacher, S., and E. Proshansky. 1983. Neurite regeneration by *Aplysia* neurons in dissociated cell culture: modulation by *Aplysia* hemolymph and the presence of the initial axonal segment. *J. Neurosci.* **10:** 2403–2413.

Trapido-Rosenthal, H. G., and D. E. Morse. 1986. Availability of chemosensory receptors is down-regulated by habituation of larvae to a morphogenetic signal. *Proc. Natl. Acad. Sci. USA* **83:** 7658–7662.

Wood, R. L., and J. H. Luft. 1965. The influence of buffer systems on fixation with osmium tetroxide. *J. Ultrastruct. Res.* **12:** 22–45.

Yool, A. J., S. M. Grau, M. G. Hadfield, R. A. Jensen, D. A. Markell, and D. E. Morse. 1986. Excess potassium induces larval metamorphosis in four marine invertebrate species. *Biol. Bull.* **170:** 255–266.

Reference: *Biol. Bull.* **182**: 77–96. (February, 1992)

Early Development in the Lancelet (=Amphioxus) *Branchiostoma floridae* from Sperm Entry through Pronuclear Fusion: Presence of Vegetal Pole Plasm and Lack of Conspicuous Ooplasmic Segregation

LINDA Z. HOLLAND AND NICHOLAS D. HOLLAND

Marine Biology Research Division, Scripps Institution of Oceanography, University of California San Diego, La Jolla, California 92093-0202

Abstract. Lancelet eggs are described from serial fine sections before fertilization and at frequent intervals thereafter until the male and female pronuclei meet at 16 min after insemination. In the unfertilized egg, although mitochondria, as well as yolk granules, are evenly distributed (both are absent only from the egg cortex and meiotic spindle), the mitochondria in the animal third have a more electron-lucent matrix than those elsewhere. The cortex of the unfertilized egg is occupied chiefly by cortical granules, and the subcortical cytoplasm in the vegetal third includes sheets of dense granules interleaved with cisternae of endoplasmic reticulum. By 45 s after insemination, (1) the fertilizing sperm enters (in the animal hemisphere in three out of three observations), (2) yolk granules become patchily distributed around the newly entered sperm, (3) cortical granule exocytosis occurs, and (4) the sheets of dense granules and associated endoplasmic reticulum aggregate with numerous mitochondria into whorls in a yolk-free zone near the vegetal pole. These whorls are the vegetal pole plasm, which is segregated into a single blastomere at each cleavage and might play a role in germ line determination. By 2 min after insemination, the zone of cytoplasm near the animal pole with patchily distributed yolk has enlarged, and the male pronucleus has migrated to the vicinity of the vegetal pole and formed an aster, at the center of which a few mitochondria are aggregated. In lancelets, unlike ascidians, there is no obvious widespread ooplasmic segregation or translocation of cytoplasm from animal to vegetal pole accompanying the movement of the sperm. Between 6 and 16 min, (1) the zone of cytoplasm with patchily distributed yolk enlarges to occupy about the animal third of the egg, (2) the female pronucleus forms by fusion of chromosome-containing vesicles and migrates vegetally, leaving a track of yolk-poor cytoplasm, and (3) the male pronucleus, surrounded by increasing numbers of mitochondria, migrates to meet the female pronucleus just above the equator. In contrast to current opinion, lancelets differ from ascidians both in having a vegetal pole plasm and in lacking marked ooplasmic segregation.

Received 26 July 1991; accepted 31 October 1991.

Introduction

The importance of lancelets in chordate evolution was first revealed by the embryological studies of Kowalevsky (1865, 1867). His work stimulated many descriptive studies on the development of lancelets aimed at clarifying their phylogenetic relations (*e.g.*, Hatschek, 1882, 1893; Lwoff, 1892; van Wijhe, 1893; Willey, 1894). In the first experimental study of this problem, Wilson (1893) investigated the development of isolated blastomeres and partial embryos. He concluded that the regulative capacity of lancelets is intermediate between that of echinoids and ascidians; that is, blastomere fates become determined in ascidians, lancelets, and echinoids by the second, third, and fourth cleavages, respectively.

Until recently, studies of lancelet embryology could deal only superficially with events before first cleavage because of difficulty in obtaining the earliest stages: artificial fertilization was never achieved, and, therefore, embryos were collected after males and females had spawned together in the field or the laboratory. Thus, descriptions of early events like the cortical reaction, pronuclear move-

ments, and maturation divisions (van der Stricht, 1896; Sobotta, 1895, 1897; Cerfontaine, 1906) were based on relatively incomplete material.

Conklin (1932, 1933) reinvestigated both the descriptive and the experimental studies with special attention to possible similarities between lancelets and ascidians. He had already established his reputation as an authority on protochordate development with two papers (1905a, b) on the embryology of the ascidian *Styela partita*. His descriptive work (1905a) showed that ooplasmic rearrangements between fertilization and pronuclear fusion in *S. partita* segregated the following five areas of cytoplasm destined to be incorporated into specific embryonic tissues: (1) the yolk-poor, dark yellow myoplasm with abundant mitochondria and pigment granules, destined for the larval tail muscles, (2) an adjacent light yellow mesenchyme material (the myoplasm and mesenchyme together comprise the mesodermal crescent), (3) the yolk-poor, clear ectoplasm, the precursor of the ectoderm, (4) the yolk-rich, dark grey endoplasm, that becomes the endoderm, and (5) a light grey cytoplasm destined for the notochord and neural plate. In his experimental work, Conklin (1905b) reported that individual blastomeres and groups of blastomeres separated at or beyond the second cleavage and reared in isolation had the same developmental fate as in the intact embryo. Thus, he concluded that the ooplasmic segregation created a mosaic of organ-forming substances in the ascidian embryo and determined the fate of each region of the uncleaved, fertilized egg.

In 1910, Conklin began to study lancelet development, but had difficulty obtaining embryos. During the next 22 years, he obtained some additional material, but still lacked the earliest stages. Therefore, when Conklin finally published on lancelet embryology, he was forced to rely on van der Stricht (1896), Sobotta (1897), and Cerfontaine (1906) for all events before first cleavage. Nevertheless, Conklin concluded that in regard to pronuclear movements and ooplasmic segregation lancelets were "precisely like ascidians" (1932) and that "the localizations of materials in the Amphioxus egg are like those of ascidians, although not so sharply differentiated" (1933). In other words, the fate maps of ascidians and lancelets were identical. Furthermore, in contrast to Wilson (1893), Conklin (1933) believed that ooplasmic segregation ensured that "all axes and poles of the future larva are irreversibly determined at or before the first cleavage . . . ," and he concluded that "development in Amphioxus, as also in Ascidians, is a mosaic work." This conclusion has been widely accepted by later biologists (*e.g.*, Brien and Dalcq, 1948; Drach, 1948; Wall, 1990).

It has generally been overlooked that Tung *et al.* (1958, 1960a, b, 1962a, b) repeated and extended Conklin's experiments on lancelet embryos. They made some changes in Conklin's fate map, finding in particular that the distribution of mesodermal material is rather different from that of ascidians, being more like that of amphibians. In addition, Tung *et al.* (1958) supported the view of Wilson (1893) that the lancelet egg has a considerable regulative capacity, and they concluded that "the development of the egg of Amphioxus is, therefore, not a mosaic work as suggested by Conklin."

In light of the work of Tung *et al.* (1958), a reinvestigation with transmission electron microscopy (TEM) of Conklin's descriptive work on early embryology of lancelets is especially important. A recent TEM study of lancelet development by Hirakow and Kajita (1990) relied on natural spawnings and thus included only limited observations on fertilized, uncleaved eggs. This obstacle has recently been overcome with the development of methods for spawning and artificially fertilizing lancelet eggs (Holland and Holland, 1989a). In our initial study on the cortical reaction of *Branchiostoma floridae,* we showed conclusively, that unlike ascidian eggs, which lack cortical granules, lancelet eggs have cortical granules that undergo exocytosis at fertilization and contribute to the formation of the fertilization envelope (Holland and Holland, 1989a). In the present work, we extend our fine structural investigations to cover events between sperm entry and pronuclear fusion. We have followed the formation of the pronuclei and pronuclear migrations and have discovered a conspicuous vegetal pole plasm, but we have found no evidence for extensive ooplasmic segregation of the ascidian type.

Materials and Methods

Specimens of *Branchiostoma floridae* were collected in late summer of 1988, 1989, and 1990 in Old Tampa Bay, Florida. Spawning of females was induced by electrical shock, and sperm motility was stimulated by 10 m*M* NH_4Cl as previously described (Holland and Holland, 1989a). Because only a few of the sperm bound to eggs undergo the acrosome reaction, it was necessary to use a concentrated sperm suspension (roughly 1:500 to 1:1000 dilution of dry sperm) to obtain synchronous fertilization. Development was at 24°C; at that temperature, first cleavage occurs about 30 min after insemination, and gastrulation begins at about 5 h.

For TEM, eggs were fixed in 1% $K_2Cr_2O_7$, 3% glutaraldehyde, 0.7 *M* NaCl pH 7.4, and postfixed in the same buffer plus 1% OsO_4 and 0.7 *M* NaCl (Holland, 1988). For low-power TEM, some unfertilized eggs and some at 45 s after insemination were fixed as above with the NaCl lowered to 0.45 *M* to prevent the shrinkage that occurred before completion of the cortical reaction in eggs fixed in higher tonicity. Eggs were dehydrated in an ethanol series and embedded in Spurr's resin. This method, chosen be-

cause of good preservation of organelles, does not preserve some constituents of the chromosomes, which thus have a low electron density. We fixed unfertilized eggs as well as fertilized eggs at 15-s intervals up to 1.5 min after insemination, at 30-s intervals up to 2 min after insemination, at 1-min intervals up to 10 min after insemination, and at 2-min intervals to 32 min after insemination, the time of first cleavage. To determine the timing of pronuclear movements, serial 1–2 μm sections were stained with 1% toluidine blue in sodium borate and examined by light microscopy (LM). In the light of those results, one to five eggs were serially fine-sectioned at each of the following intervals after insemination: 0 s, 45 s, 2 min, 6 min, 10 min, and 16 min.

Results

Unfertilized egg (Figs. 1, 2)

The spawned, unfertilized egg of *Branchiostoma floridae* is about 140 μm in diameter and is arrested in metaphase of the second meiotic division. The animal pole is marked externally by the first polar body and internally by the second meiotic spindle (Figs. 1; 2A, B). Surrounding the egg and overlying the first polar body is a vitelline layer (Figs. 1; 2A, C; 3D). The egg cytoplasm contains a peripheral layer of cortical granules, which are closely apposed to one another except where the meiotic spindle intervenes (Figs. 1; 2B, C). During the first minute after insemination, the cortical granules undergo exocytosis, initiating elevation of a fertilization envelope as previously described (Holland and Holland, 1989a). The first polar body, of both unfertilized and fertilized eggs (Fig. 3D), typically includes some unreacted cortical granules and a cluster of chromosomes; a nucleus is lacking, although there are frequently a few profiles of nuclear envelope (Fig. 4B).

Within the egg cytoplasm, yolk granules, 2–5 μm in diameter, have a relatively even distribution, being excluded only from the cortical cytoplasm and the meiotic spindle (Fig. 2A). In about a 30° arc near the vegetal pole, just interior to the cortical granules, are several sheets of dense granular material stacked 2–4 deep, parallel to the egg plasma membrane (Figs. 1; 2C, D). These sheets are usually, but not always, interleaved with sheets of smooth endoplasmic reticulum (SER) (Fig. 2D), which are rare elsewhere in the cytoplasm. Although the granules comprising the sheets are similar in size to ribosomes, the arrangement of the granules and ER differs from that of rough ER: between two cisternae of SER there is only one sheet of granules, and it is separated from the SER on each side by a space 50 to 75 nm wide. Some mitochondria are usually situated near the sheets, but not in conspicuously greater abundance than elsewhere in the cytoplasm where they are fairly uniformly distributed (approximately 30/100 μm^3).

Although all the mitochondria in the unfertilized egg are about the same size (0.5 × up to 3 μm), those in a zone about 35 μm deep around the meiotic spindle have an electron-lucent matrix (Fig. 2E), while those elsewhere have a much denser matrix (Fig. 2D). This difference does not appear to be a fixation artifact since there is a narrow transition zone where both types of mitochondria co-occur (Fig. 5C). The distribution of the two types was similar in all eggs examined and did not change after fertilization, at least up until formation of the zygote nucleus.

Sperm entry: 30–45 s after insemination (Figs. 1, 3, 4)

Sperm of *Branchiostoma floridae* have a compact nucleus about 1.5 μm in diameter, a midpiece (with two centrioles and one mitochondrion), and a cup-shaped acrosome that can undergo an acrosome reaction producing a short acrosomal tubule (Holland and Holland, 1989b; unpub.). To determine the timing of sperm entry, 1–2 μm sections of eggs fixed at 15-s intervals after insemination were examined by light microscopy (LM). In two eggs fixed at 30 s after insemination, at the beginning of the cortical reaction, a sperm was seen by LM attached to the egg surface in the animal hemisphere via a short fertilization cone (data not shown). However, since condensed sperm nuclei are about the same density and size as yolk granules, no sperm nucleus could subsequently be detected in 1 μm sections until about 4 min after insemination, when it appeared as a clear sphere about 5 μm in diameter in a small yolk-free zone of cytoplasm near the vegetal pole. Fluorescent DNA-binding dyes also failed to reveal the newly entered sperm because its nucleus could not be differentiated from those of non-fertilizing sperm bound to the fertilization envelope. A large excess of sperm is required for synchronous fertilization, and many remain associated with the fertilization envelope, both at the animal pole and elsewhere, even after the cortical reaction (Fig. 3A, B, D). Therefore, to detect the fertilizing sperm just after entry, serial TEM sections were made through an egg at 45 s after insemination.

Two serial fine sections from the same egg at 45 s after insemination are shown in Figure 3A, B. The section in Figure 3A approximately bisects the egg, and the first polar body marks the animal pole at the top of the figure. Figure 3B, which is in the same orientation, but about half-way between the center and the edge of the egg, includes the fertilizing sperm (arrow). The sperm (shown at higher magnification in Fig. 3C) has just entered the egg and is located in the animal hemisphere underneath the egg plasma membrane about 30° from the animal pole. This result, plus the two LM observations of fertilization cones in the animal hemisphere, shows that sperm can fertilize

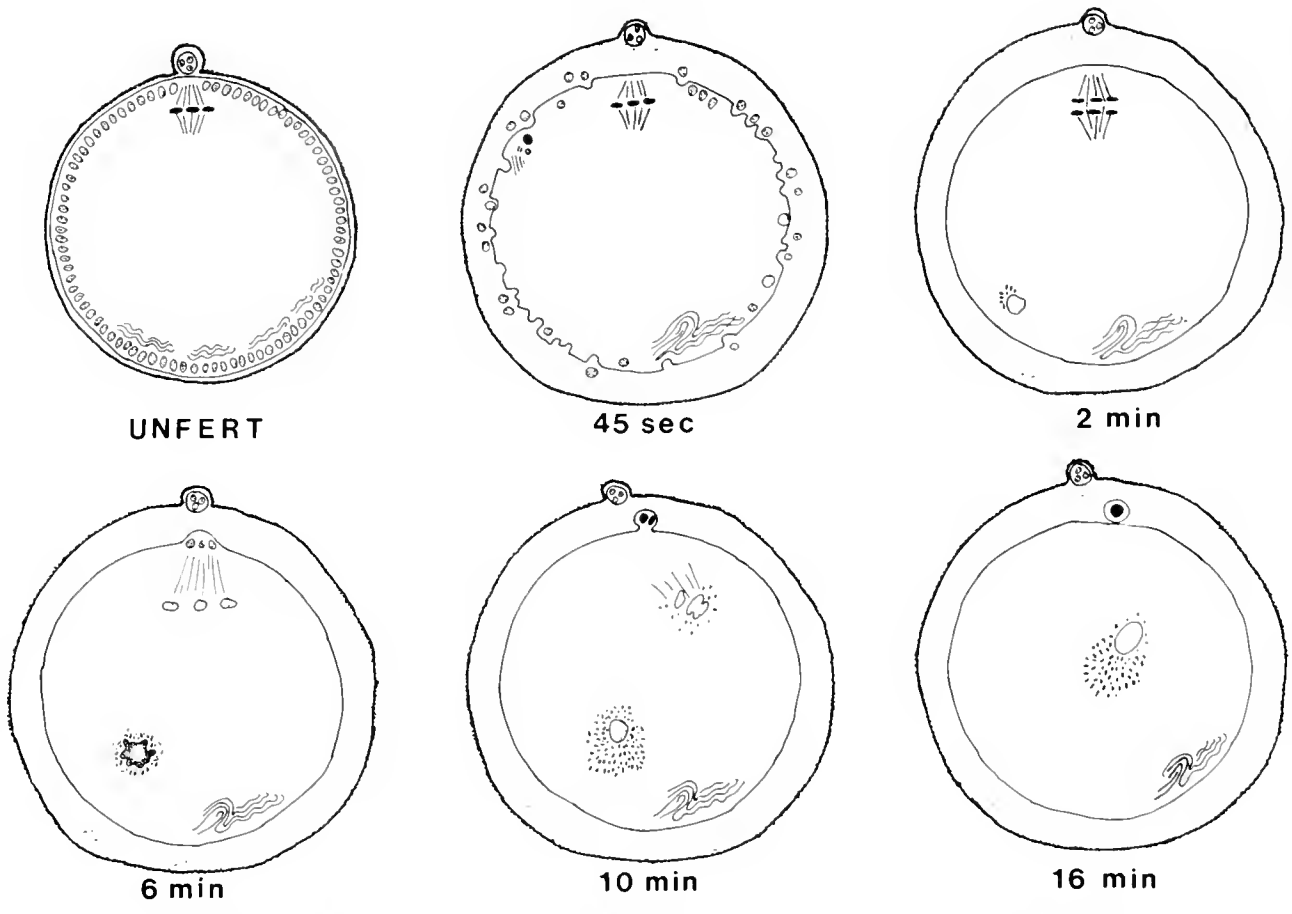

Figure 1. Diagrams of the unfertilized egg and fertilized eggs through 16 min after insemination. The distribution of yolk and the sperm aster are not shown. The unfertilized egg has the first polar body and is in second meiotic metaphase. The egg cortex contains numerous cortical granules, and in the vegetal third of the egg there are sheets of dense granules interleaved with endoplasmic reticulum just beneath the layer of cortical granules. At 45 s, most of the cortical granules have undergone exocytosis, the sperm has entered, the axoneme has largely dispersed, and the sheets of dense granules and endoplasmic reticulum have formed into whorls to constitute the vegetal pole plasm. By 2 min, the egg is in second meiotic anaphase, the cortical reaction is complete, and the sperm nucleus has migrated to the vegetal cytoplasm and formed a small aster, with which a small cluster of mitochondria is associated. By 6 min, the egg is in telophase of the second meiotic division, the sperm nucleus has swollen, and the peripheral chromatin has condensed more than the central chromatin. A cloud of mitochondria surrounds the sperm nucleus. By 10 min, the second polar body has formed. The nuclear envelopes have formed around individual or groups of maternal chromosomes. These chromosome-containing vesicles are fusing to form the maternal pronucleus. The enlarged male pronucleus is surrounded by a larger cloud of mitochondria and has migrated partway towards the female pronucleus. By 16 min, the second polar body has separated from the egg, and the pronuclei have met and are associated with an asymmetric cloud of mitochondria brought by the male pronucleus.

eggs of *Branchiostoma floridae* in the animal hemisphere, although the sample size is far too small to rule out the possibility that sperm can also enter in the vegetal hemisphere.

By 45 s after insemination, the cortical reaction is nearly complete, and only a few unreacted cortical granules remain. The yolk granules are still evenly distributed except in a broad area around the newly entered sperm where they are somewhat sparser (Fig. 3B). At higher magnification, the sperm mitochondrion, one of the two centrioles (the other is out of the plane of section), and microtubules of the axoneme are visible in the egg cytoplasm (Fig. 3C). The nuclear envelope has already disappeared, and the chromatin has decondensed at the nuclear periphery and in patches deeper in the nucleus.

The first polar body adheres to the fertilization envelope as it rises from the egg surface (Fig. 3D). Within the egg, the meiotic spindle, with chromosomes still aligned on the metaphase plate, remains associated with relatively lucent mitochondria and is closely surrounded by yolk

granules (Figs. 3D, 4A). Deeper in the cytoplasm, especially in the animal hemisphere, the mitochondria are frequently aggregated into clusters (Fig. 4D). This arrangement of mitochondria persists at least until first cleavage; there is no apparent movement of mitochondria from the cortical cytoplasm to the vegetal hemisphere to surround the sperm nucleus as occurs in ascidians during ooplasmic segregation. These aggregates of mitochondria and others described below associated with the pole plasm and male pronucleus are very small compared to those in the ascidian myoplasm and are not large enough to be detected in living eggs with fluorescent mitochondrial dyes. Thus both $DioC_3(3)$ and rhodamine 123 seemed to show a uniform distribution of mitochondria for at least 20 min after insemination. Although the subsequent development of eggs in $DioC_3(3)$ was not tested, eggs reared in the dark in rhodamine 123 developed into normal 3-day larvae.

The subcortical sheets of dense granules and associated ER in the vegetal third of the unfertilized egg have come together in a yolk-poor zone of cytoplasm to one side of the vegetal pole; 6 to 10 layers, each composed of a sheet of granules and a cisterna of SER, are roughly spiraled together so that in cross section the pattern resembles that of a fingerprint (Fig. 4C; for higher magnification see appearance at 6 min Fig. 7D). At the periphery of these whorls are numerous mitochondria (Fig. 4C). This reorganization does not appear to be associated with a massive inflow of materials from other regions of the egg. Because of its location, we will call this specialized region of cytoplasm the vegetal pole plasm. From this point in development, the appearance of these whorls remains relatively constant, at least through formation of the zygote nucleus. The pole plasm is visible in toluidine blue-stained, 2 μm sections as reddish-purple strands in a yolk-free zone near the vegetal pole. At each cleavage, at least through the early blastula, it is segregated into a single blastomere (data not shown).

Sperm pronucleus near vegetal pole: 2–6 min after insemination (Figs. 1, 5)

By 2 min after insemination, the male pronucleus, regardless of the point of sperm entry, is located in the egg cortex near the vegetal pole. In TEM sections of an egg at 2 and one at 6 min after insemination (Figs. 5A, 6A), and in LM sections through ten eggs at 3 to 6 min after insemination, the male pronucleus was always near the vegetal pole. These results are consistent with previous LM studies demonstrating that the swollen male pronucleus first becomes visible near the vegetal pole of the egg of *Branchiostoma lanceolatum* (van der Stricht, 1985; Sobotta, 1897; Cerfontaine, 1906). Presumably, as in ascidian eggs (Speksnijder *et al.*, 1989), sperm entering the animal hemisphere of the ascidian egg are rapidly translocated close to the vegetal pole. At 2 min after insemination, the male pronucleus is about 2.5 μm in diameter and is less dense than the cytoplasm (Figs. 5A, B). There is no trace of a nuclear envelope surrounding the male chromatin (Fig. 5B, insert). A sperm aster is present near the male pronucleus (Fig. 5D) (none of our sections went through both the male pronucleus and the aster). We did not see the male centrioles at this time; presumably the sections containing them were lost. The cytoplasm around the male pronucleus is not enriched in mitochondria, as it is in ascidians, although a few mitochondria are aggregated at the convergence of the astral rays (Fig. 5D).

In the cytoplasm, yolk granules are somewhat less numerous in the animal hemisphere than in the vegetal hemisphere (Fig. 5A). This is the opposite of the situation in ascidians where the yolk is concentrated in the animal hemisphere during the first phase of ooplasmic segregation. The meiotic spindle is still present at the animal pole, but the female chromosomes, which are inconspicuous, have begun to migrate to opposite poles of the spindle (data not shown). The pole plasm with its sheets of dense granular material is unchanged from 45 s after insemination (see appearance at 6 min, Figs. 7A, B).

Beginning of pronuclear migration: 6–10 min after insemination (Figs. 1, 6, 7)

By 6 min after insemination, the male pronucleus, which has enlarged to 5 μm in diameter and developed an irregularly lobed outline, has migrated from close to the egg cortex about 30 μm towards the center of the egg (Figs. 1, 6A). The chromatin of the male pronucleus remains decondensed at the center, but has become more condensed in the peripheral lobes and is partly bounded by a nuclear envelope (Fig. 7F, arrow). Numerous mitochondria, apparently recruited from the cytoplasm in the vegetal hemisphere, closely surround the periphery of the male pronucleus (Fig. 7B). Although the sperm aster was not seen at this stage, as in the preceding stage (see Fig. 5D) it is likely that the aggregate of mitochondria also converges upon the sperm aster.

The maternal chromosomes have moved apart on the meiotic spindle. Those destined to form the female pronucleus are rounded, about 6 μm in diameter, and lie in a yolk-poor zone slightly away from, and to one side of, the animal pole (Figs. 6A, C; 7A). A few fragments of nuclear envelope have formed at the periphery of the chromosomes, which are still associated with spindle fibers (Fig. 7A). At the animal pole, there is a bulge in the egg surface, evidently the beginning of the second polar body (Fig. 6D). From previous observations, this polar body forms about 8 min after insemination (Holland and Hol-

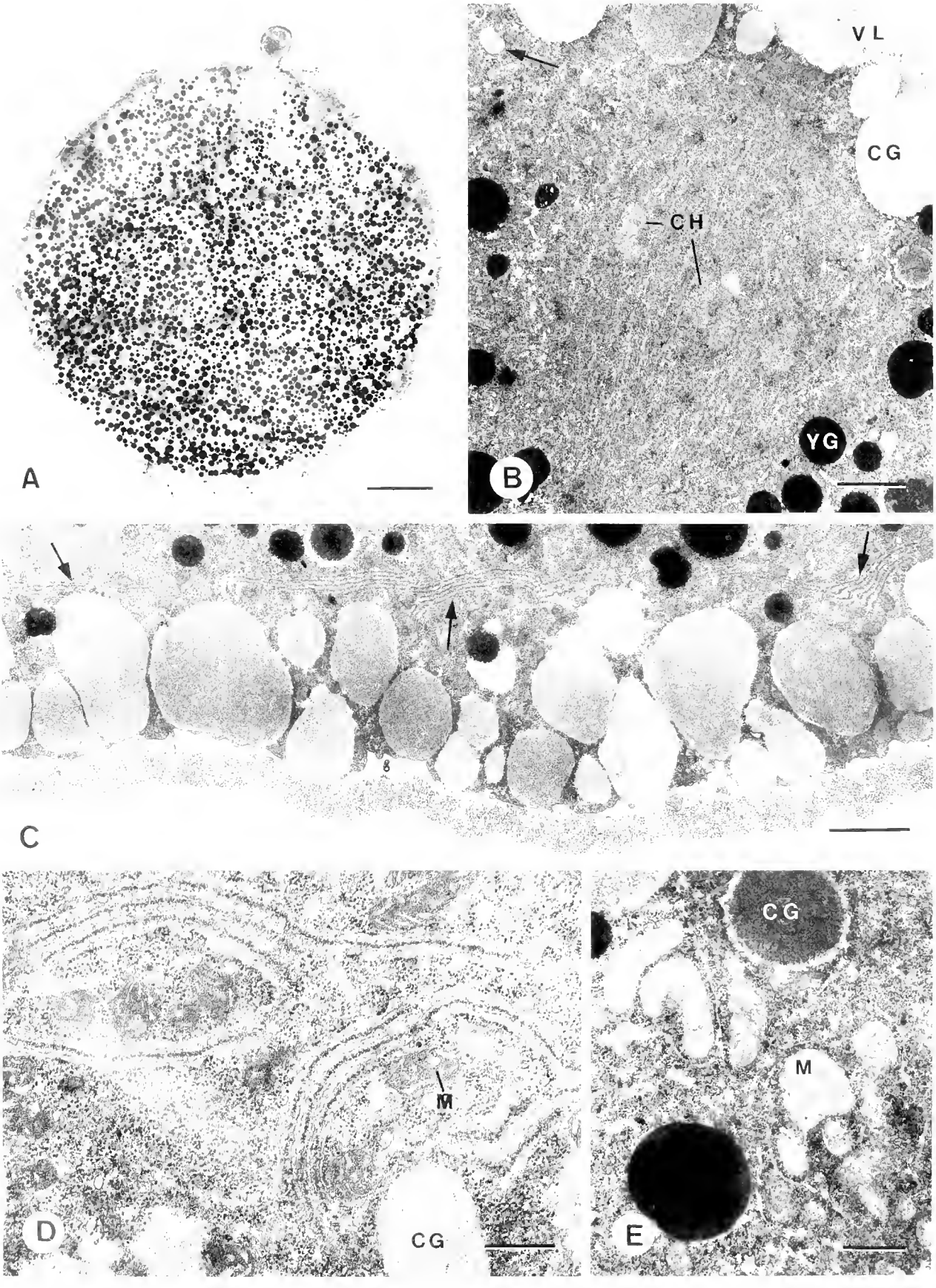
A
B
VL
CG
CH
YG
C
D
M
CG
E
CG
M

land, 1989a). As in the preceding stage, yolk granules are somewhat scarcer in the animal hemisphere (Fig. 6A), and the pole plasm is prominent near the vegetal pole (Figs. 6B; 7C, D).

Formation of the female pronucleus and migration of pronuclei: 10–16 min after insemination (Figs. 1, 8, 9)

By 10 min after fertilization, the male pronucleus has continued its migration towards the female pronucleus and enlarged to about 6 μm in diameter. (Fig. 8B, C). The chromatin is of uniform density, similar to that of the peripheral lobes at 6 min after insemination, and the nucleus is bounded by a nuclear envelope (Fig. 8C). The area of yolk-free cytoplasm around the male pronucleus has enlarged to about 15 μm in diameter and has become rich in mitochondria; there are about four mitochondria per μm^2—approximately ten times the concentration elsewhere in the cytoplasm.

The second polar body has formed, but is still attached to the egg (Figs. 8A, 9D). At the point of attachment, there is a prominent density (Zwischenkörper) through which the spindle microtubules pass (Fig. 9D, insert). In the polar body, there are several chromosome-containing vesicles, each bounded by its own nuclear envelope (Fig. 9D).

Within the egg, individual female chromosomes or groups of chromosomes have become surrounded by nuclear envelopes. Depending on the egg, these chromosome-containing vesicles are either in the process of fusing and are still located close to the animal pole (Fig. 9A–C) or they have completed fusing into a single female pronucleus 5.5 × 8 μm in diameter, which has migrated somewhat off-center to just above the equator (Figs. 1, 8B, D). The female pronucleus does not migrate further. The nuclear matrix is of low electron density but contains small scattered areas of higher density (Figs. 8D; 9B, C). The female pronucleus is in a large, irregular area of yolk-poor cytoplasm, which extends to the yolk-poor cytoplasm near the animal pole (Fig. 8B). Although mitochondria are not uncommon near the female pronucleus, they are four to five times less numerous than those around the male pronucleus (compare Fig. 8D and C).

The pole plasm (Figs. 1; 8A; 9E, F) is little changed from earlier times. However, in some places, the strands of dense material are no longer closely associated with ER and have lost their parallel relation to one another (Fig. 9E, F).

Pronuclear fusion: 16 min after insemination (Figs. 1, 10)

By 16 min after insemination, the male pronucleus has migrated to, and fused with, the female pronucleus (Figs. 1; 10A, E, F). The resulting zygote nucleus, which is about 8 × 12 μm in diameter, lies in a zone relatively free of yolk about 17 μm in diameter in the animal hemisphere just above the equator, about half-way between the edge and the center of the egg. At one side of the nucleus, presumably that deriving from the male pronucleus, is a large aggregate of mitochondria (Fig. 10E). Thus a mitochondria-rich zone of cytoplasm surrounds the newly formed zygote nucleus in both lancelets and ascidians. However, this zone is vastly larger in ascidians, and comes not from the vegetal cytoplasm as the male pronucleus migrates through it, but from the cortical cytoplasm, which collects around the male pronucleus during ooplasmic segregation (Zalokar and Sardet, 1984).

The zygote nucleus contains a few small, dense inclusions like those previously described in the female pronucleus (Fig. 10F) and is bounded everywhere by a nuclear envelope (Fig. 10E, F). Although some microtubules, evidently part of the astral rays, were seen near the nucleus, no centrioles were encountered in our sections.

By 16 min, the second polar body has separated from the egg, but their plasma membranes remain closely apposed (Fig. 10B–D). The second polar body tends to remain at the animal pole during the cleavage stages, although Hirakow and Kajita (1991) sometimes observed it in other locations. Within the polar body, the chromosome-containing vesicles have fused into a single nucleus.

Discussion

Previous work on the early embryology of lancelets has been largely on the European species, *Branchiostoma lanceolatum* (Wilson, 1893; van der Stricht, 1896; Sobotta, 1897; Cerfontaine, 1906; Conklin, 1932, 1933), and to a

Figure 2. TEMs of unfertilized eggs with animal pole uppermost. A. Central section through the first polar body at top adjacent a small yolk-free area including the second meiotic spindle. At this magnification, the spindle fibers and chromosomes cannot be resolved. Scale bar: 20 μm. B. Higher magnification of the second meiotic spindle. The first polar body is not in the plane of section. Mitochondria near the meiotic spindle generally have an electron lucent matrix (arrow). Scale bar: 2 μm. C. The vegetal pole. Parallel sheets of dense granules interleaved with endoplasmic reticulum (arrows) lie just beneath the layer of cortical granules. Scale bar: 2 μm. D. Higher magnification of the sheets of dense granules and associated endoplasmic reticulum at the vegetal pole. Mitochondria (M) have a relatively electron-dense matrix. Scale bar: 0.5 μm. E. Higher magnification of the electron lucent mitochondria (M) near the animal pole. Scale bar: 0.5 μm. Chromosomes (CH), cortical granule (CG), vitelline layer (VL), yolk granule (YG).

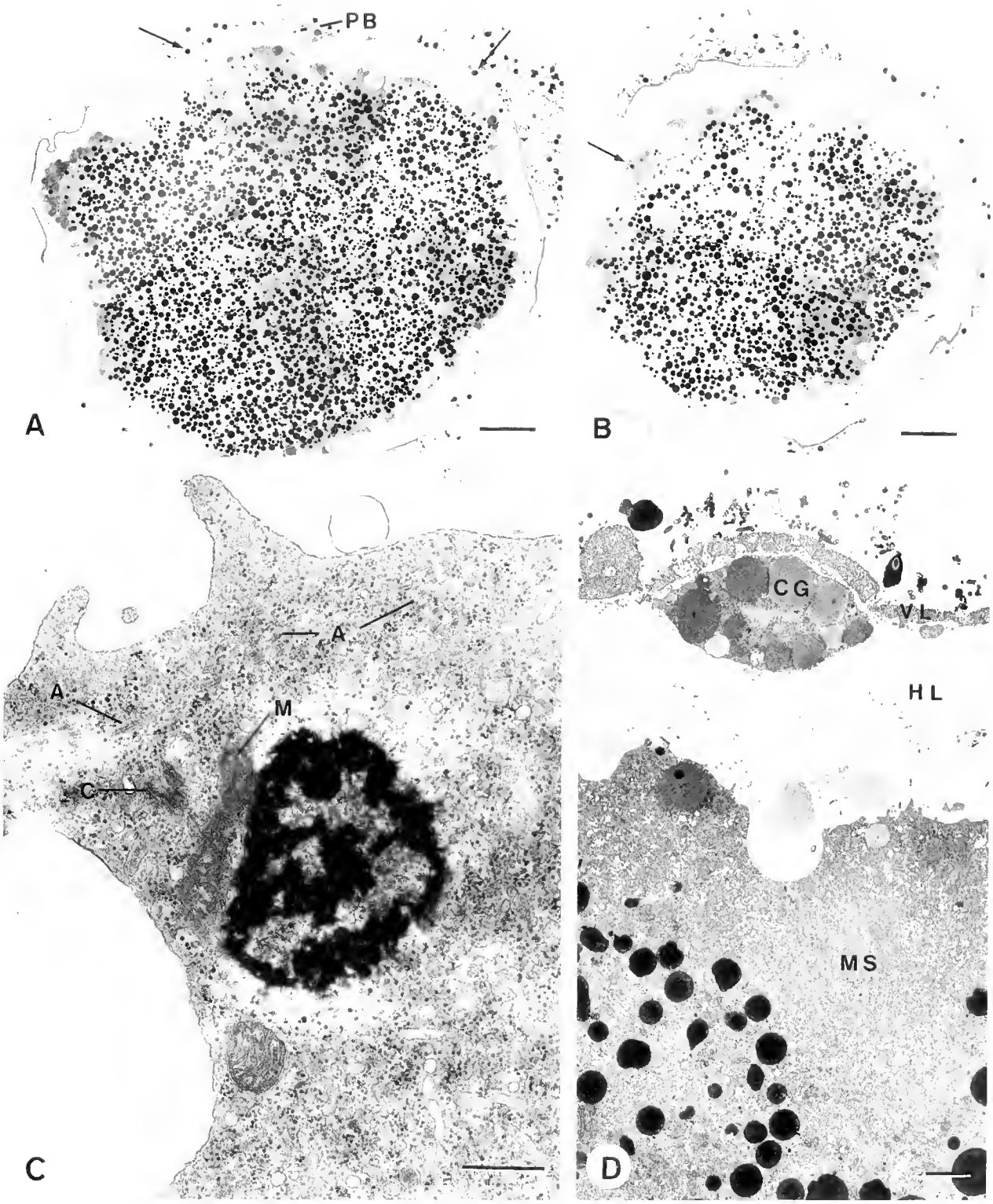

Figure 3. TEMs of eggs at 45 s after insemination. A. Section through the first polar body (PB) at top. The cortical reaction is in progress. Many supernumerary sperm (arrows) are associated with the rising fertilization envelope. The plane of section does not pass through the meiotic spindle. Scale bar: 20 μm. B. Section through the same egg as in (A) in the same orientation about half way between the center of the egg and the periphery. The fertilizing sperm (arrow) has entered into the animal hemisphere, and the yolk is patchy in its neighborhood. Scale bar: 20 μm. C. Higher magnification of the fertilizing sperm in (B). The nucleus is associated with the sperm mitochondrion (M) and centriole (C). The nuclear envelope has disappeared and the chromatin has begun to decondense. The axoneme (A) has largely dispersed. Scale bar: 0.5 μm. D. The first polar body, which contains several unreacted cortical granules (CG), and whorls of nuclear envelope (arrow) is sandwiched between the vitelline layer (VL) and material derived from the cortical granules, the hyaline layer (HL). Yolk granules closely surround the meiotic spindle (MS). Scale bar: 2.0 μm.

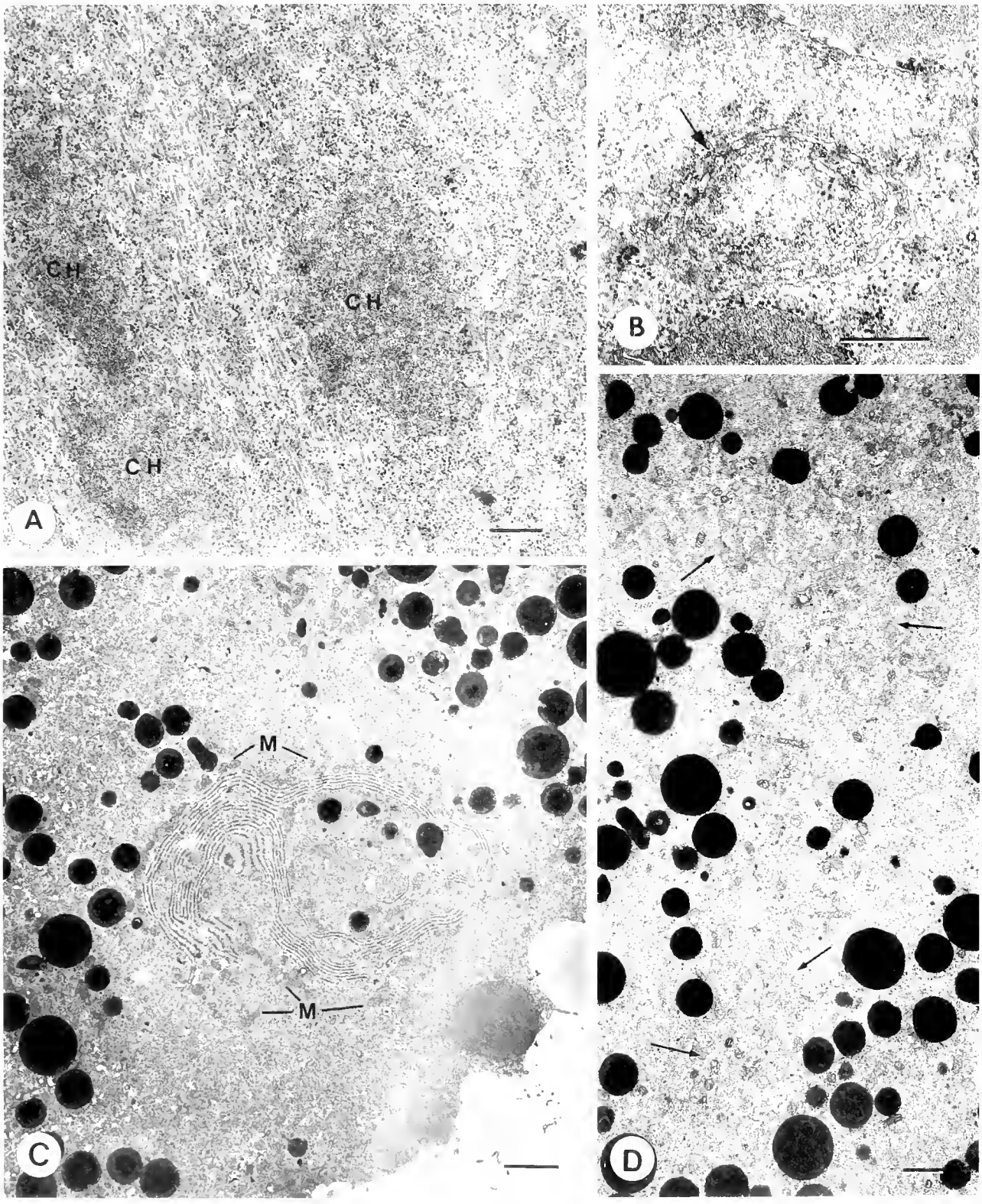

Figure 4. TEMs of eggs at 45 s after insemination. A. Higher magnification of chromosomes (CH) on the meiotic spindle. Scale bar: 0.5 μm. B. Higher magnification of the polar body in 3D showing the whorl of nuclear envelope (arrow). Scale bar: 0.5 μm. C. The sheets of dense granules, endoplasmic reticulum, and mitochondria (M) that constitute the vegetal pole plasm. Scale bar: 2 μm. D. Patchy yolk distribution and aggregated mitochondria (arrows) in the animal hemisphere. Scale bar: 1 μm.

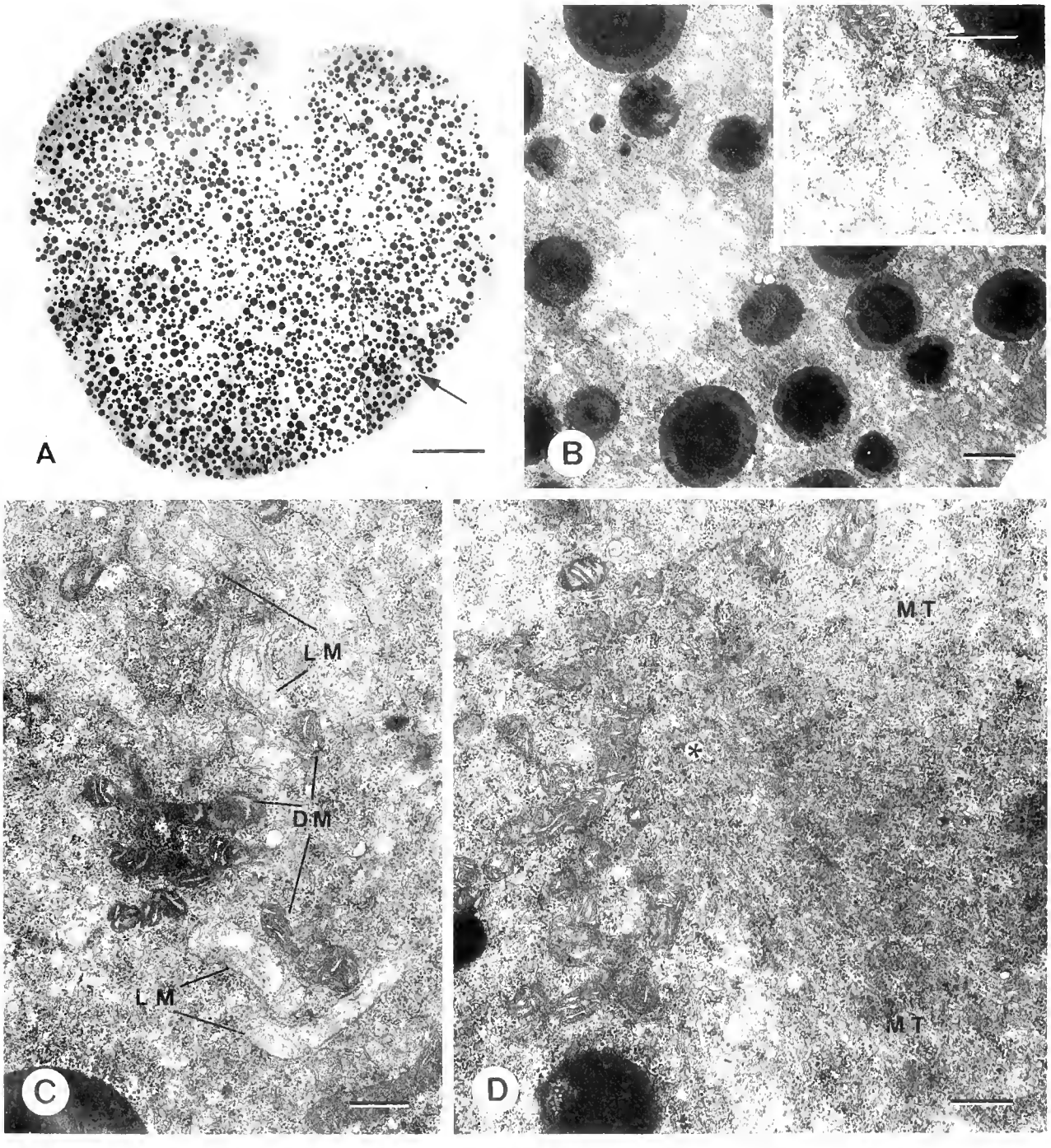

Figure 5. TEMs of eggs at 2 min after insemination. A. Cross section through meiotic spindle (top) and the nucleus of the fertilizing sperm (arrow). The cortical reaction is complete. The indentation in the egg at the animal pole is probably an artifact due to the hypertonicity of the fixative. The polar body and fertilization envelope are not in the figure. Scale bar: 20 μm. B. Higher magnification of the fertilizing sperm nucleus in (A). The aster is out of the plane of section. Scale bar: 1 μm. (B, inset) The edge of the male nucleus at higher magnification. There is no nuclear envelope. Scale bar: 0.5 μm. C. Co-occurrence of mitochondria with dense matrix (DM) and lucent matrix (LM) near the animal pole. Scale bar: 0.5 μm. D. The aster associated with the male nucleus in (D). There is a small cluster of mitochondria where the astral microtubules (MT) converge (asterisk). The male nucleus and centrioles are out of the plane of section. Scale bar: 0.5 μm.

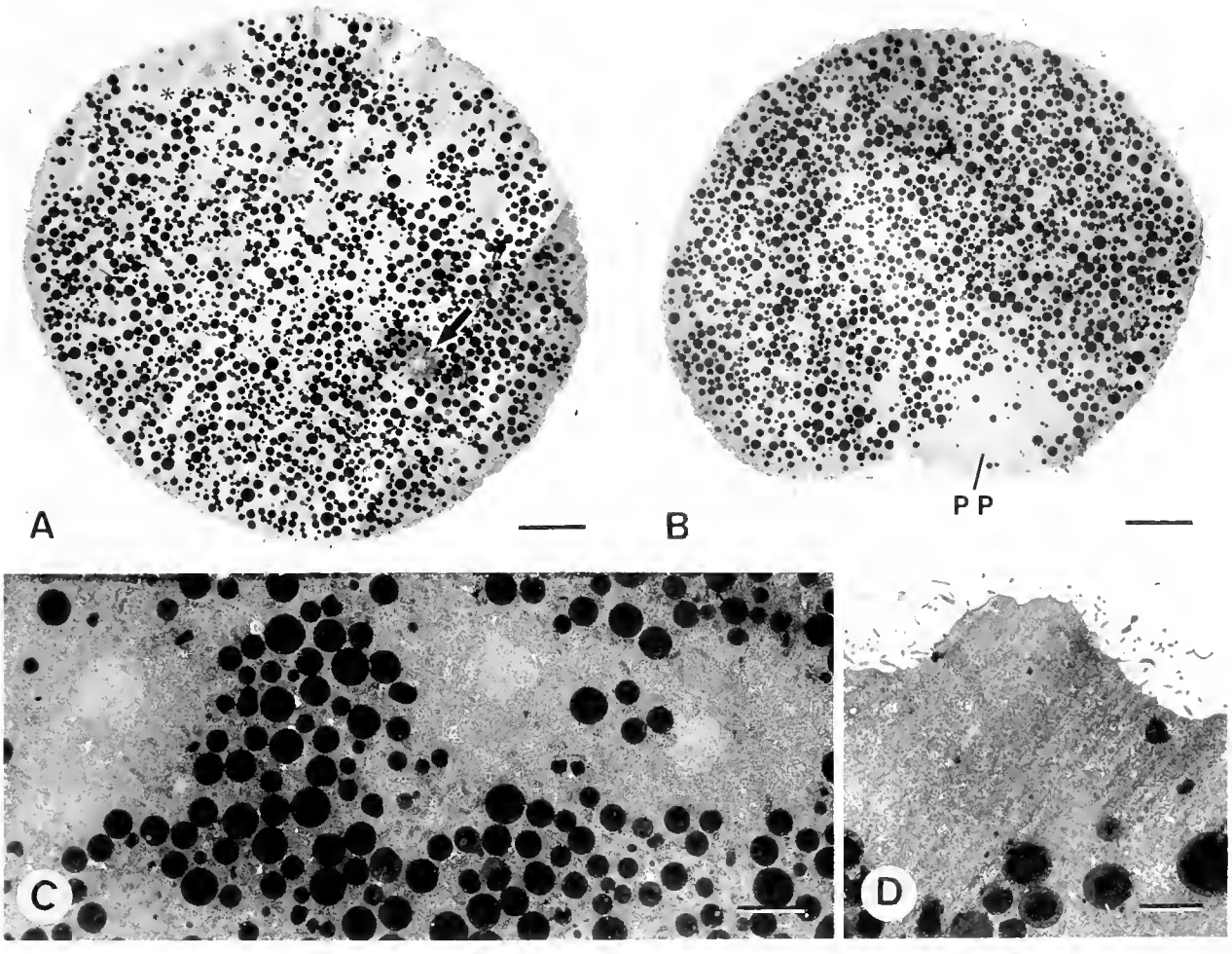

Figure 6. TEMs of eggs fixed at 6 min after insemination. A. Section through the male pronucleus (arrow). Animal hemisphere is uppermost. The section does not pass through the meiotic spindle and polar body. The female chromosomes are located about 11 o'clock near the animal pole (asterisks), but are not visible at this magnification due to their low contrast. Scale bar: 20 μm. B. Section through the same egg as in (A) that passes through the vegetal pole plasm (PP). The indentation at the vegetal pole is probably an artifact due to the high tonicity of the fixative, but marks the site of the future cleavage furrow. Scale bar: 20 μm. C. Three female chromosomes from the same egg as in A and B. Scale bar: 4 μm. D. Bulge at the animal pole at the site of formation of the second polar body. The polar body chromosomes are not in the plane of section. Scale bar: 2 μm.

lesser extent, on the Asian species, *B. belcheri* (Tung *et al.*, 1958, 1960a, b, 1962a, b; Hirakow and Kajita, 1990, 1991). There are no marked differences between these species. Thus, although aside from a few micrographs of Hirakow and Kajita (1990), our work on *B. floridae* is the only TEM study on the earliest embryonic stages, and it is likely that our results also apply to other species of *Branchiostoma;* the largest ovarian oocytes have virtually the same fine structure in *B. floridae, B. lanceolatum,* and *B. belcheri* (reviewed in Holland and Holland, 1991), as do the blastomeres of *B. floridae* and *B. belcheri* (Hirakow and Kajita 1990, 1991; Holland and Holland, unpub.).

Position of sperm entry; formation and migration of the pronuclei

Sobotta (1897) depicted a sperm entering a lancelet egg with its tail extending into the perivitelline space and its nucleus with the same size and staining properties as a yolk granule. He maintained that, although sperm can enter the egg anywhere on the surface, they usually do so near the vegetal pole. He, along with van der Stricht (1896) and Cerfontaine (1906), thought that the fertilizing sperm first developed into a dark-staining irregular mass near the vegetal pole before swelling into a clear, spherical pronucleus. This observation led van der Stricht (1896), Cer-

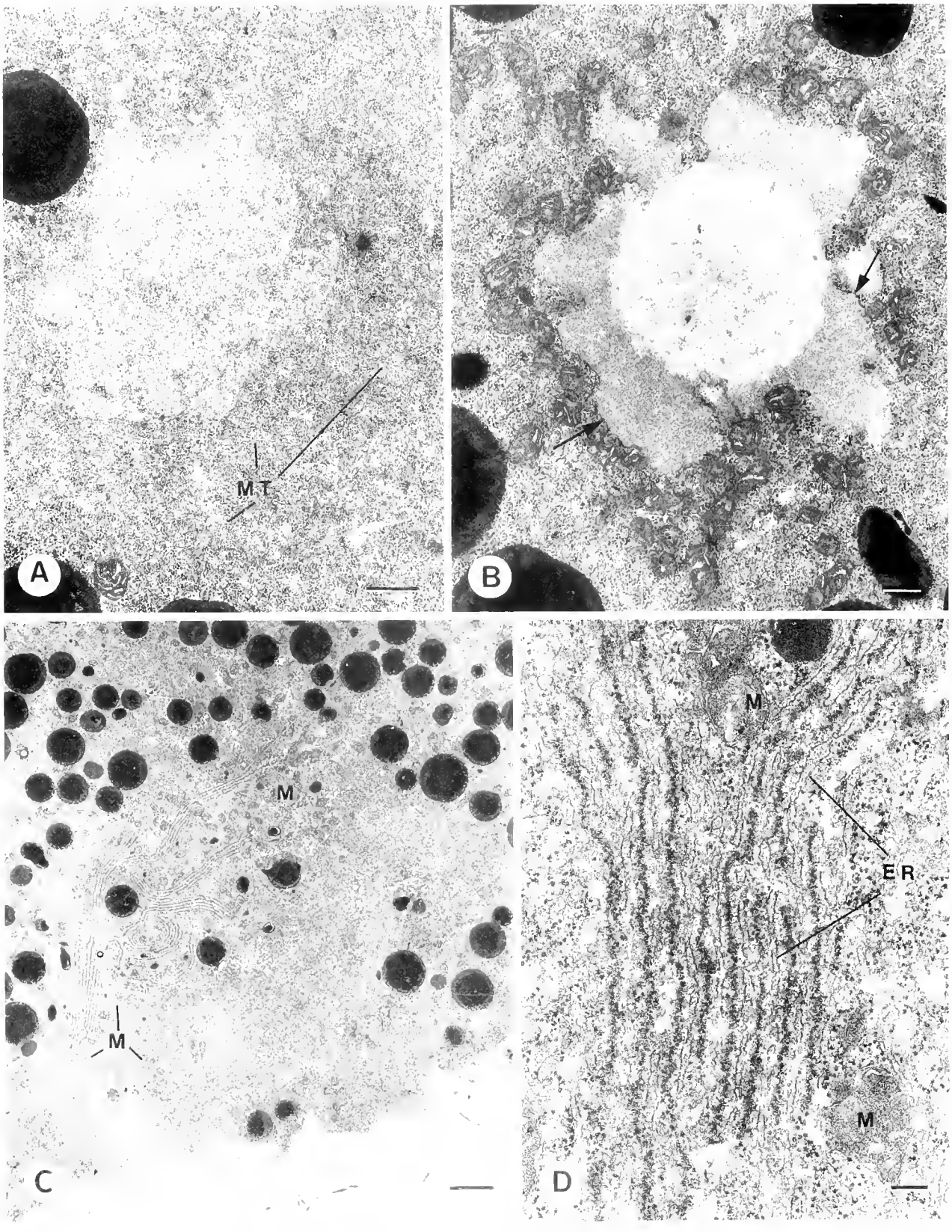

Figure 7. TEMs of eggs at 6 min after insemination. A. Higher magnification of the female chromosome at the far right in Figure 6C. There is no nuclear envelope. The chromosome is still associated with microtubules of the meiotic spindle (MT). Scale bar: 1 μm. B. Higher magnification of the male pronucleus in Figure 6A. It is closely surrounded by mitochondria, and a partial nuclear envelope has formed (arrows). The aster is not in the plane of section. Scale bar: 0.5 μm. C. Higher magnification of the vegetal pole plasm in Figure 6B. Numerous mitochondria (M) are associated with the sheets of dense granules. Scale bar: 2 μm. D. High magnification of the vegetal pole plasm in C. Mitochondria (M) are closely associated with sheets of endoplasmic reticulum (ER) that lie in between the sheets of dense granules. Scale bar: 0.2 μm.

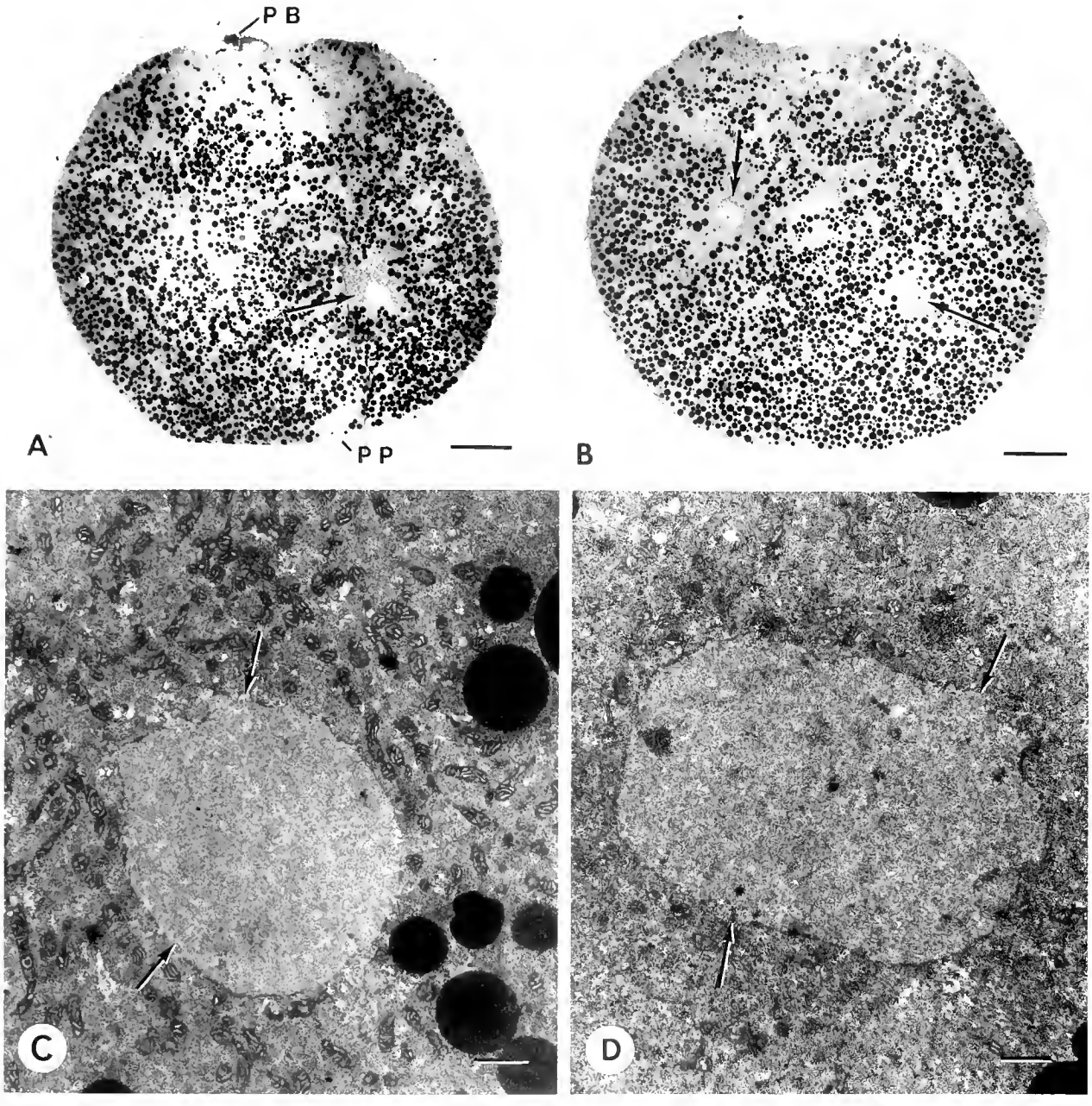

Figure 8. TEMs of eggs at 10 min after insemination. A. Section through the second polar body (PB), male pronucleus (arrow), and vegetal pole plasm (PP). Black dots in the yolk-free zone around the male pronucleus are mitochondria. The yolk is patchily distributed in the animal hemisphere. Scale bar: 20 μm. B. Section through the same egg as in A, about 10 μm deeper, which passes through the female pronucleus (double arrow). The yolk-free patch of cytoplasm underlying the male pronucleus is at lower right (single arrow). Scale bar: 20 μm. C. Higher magnification of the male pronucleus and its cloud of mitochondria in A. The nuclear envelope is complete except in a few spots (arrows). Scale bar: 1 μm. D. Higher magnification of the female pronucleus in B. The nuclear envelope is complete except in a few areas (arrows). The nucleus contains a few dense patches. Scale bar: 1 μm

fontaine (1906), and Conklin (1932) to conclude that the sperm *always* enters near the vegetal pole. In contrast, our results show that the fertilizing sperm can enter the egg near the animal pole (three out of three observations), although more extensive study would be required to show whether they always do so. The axoneme enters with the nucleus, mitochondrion, and centrioles, but rapidly disappears. Then the sperm nucleus undergoes two phases

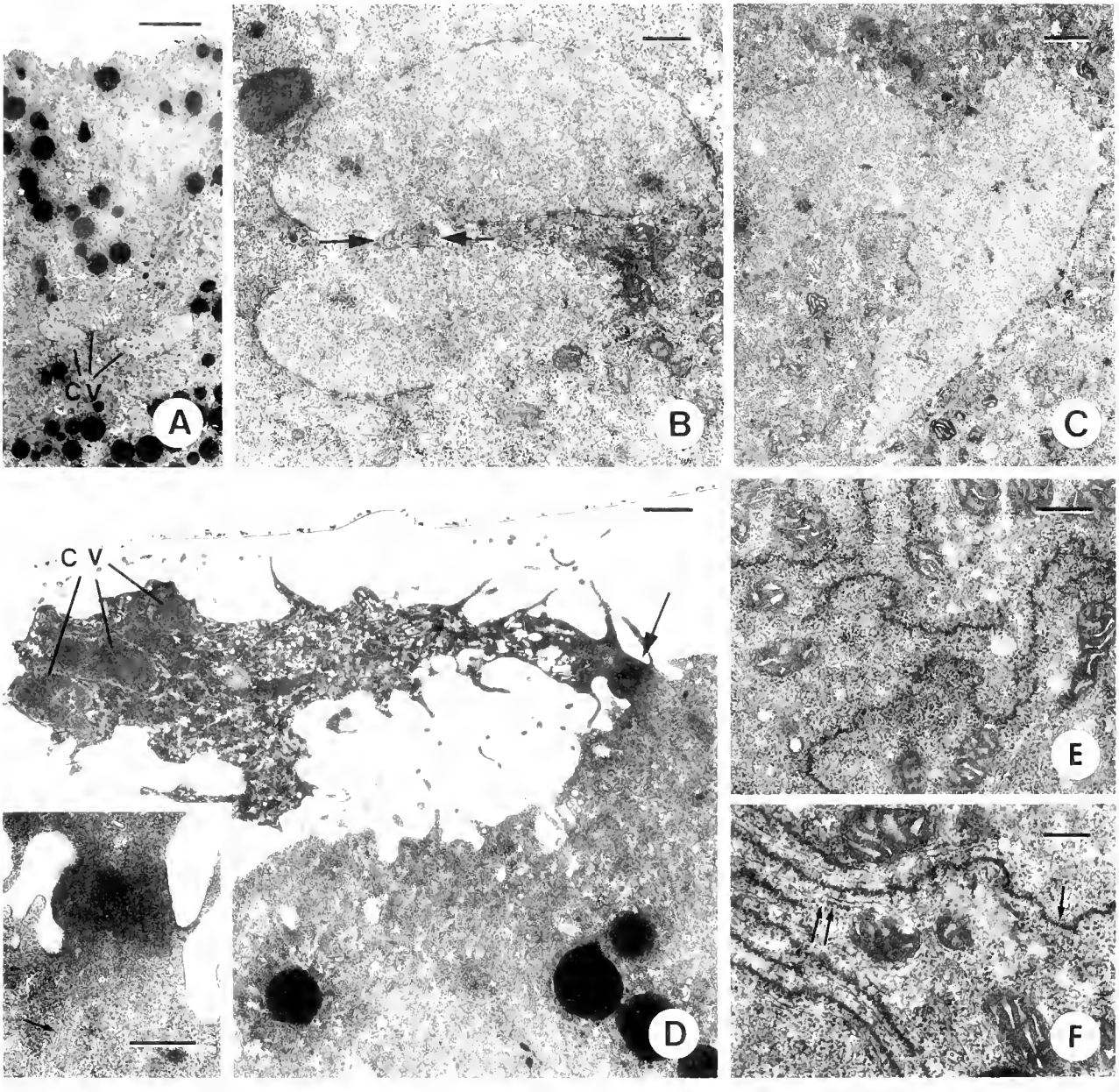

Figure 9. TEMs of eggs at 10 min after insemination. A. Section near the animal pole with three maternal chromosome-containing vesicles (CV). Scale bar: 4.5 μm. B. Higher magnification of two of the maternal chromosome-containing vesicles in A, which have begun to fuse at arrows. Scale bar: 0.5 μm. C. Two maternal chromosome-containing vesicles that have fused and are connected by a broad bridge. Scale bar: 0.5 μm. D. Higher magnification of the second polar body in Figure 8A. Three chromosome-containing vesicles (CV) are visible within it. Where it is connected to the egg there is a dense Zwischenkörper (arrow). Scale bar: 1 μm. (Insert) The Zwischenkörper at higher magnification showing the microtubules (arrow) remaining from the meiotic spindle. Scale bar: 0.5 μm. E. Sheets of dense granules and associated mitochondria in the vegetal pole plasm that are no longer associated with endoplasmic reticulum. Scale bar: 0.5 μm. F. Sheets of dense granules and mitochondria in the vegetal pole plasm in relatively close association with smooth endoplasmic reticulum in some places (twin arrow), but not in others (single arrow). Scale bar: 0.3 μm.

of migration. First, between 45 s and 2 min after insemination, the male pronucleus evidently migrates rapidly to the vicinity of the vegetal pole. Second, between 6 min and 16 min, the male pronucleus migrates slowly back into the animal hemisphere to meet the female pronucleus.

Soon after entering the egg, the sperm nucleus rapidly decondenses, staining less intensely with toluidine blue,

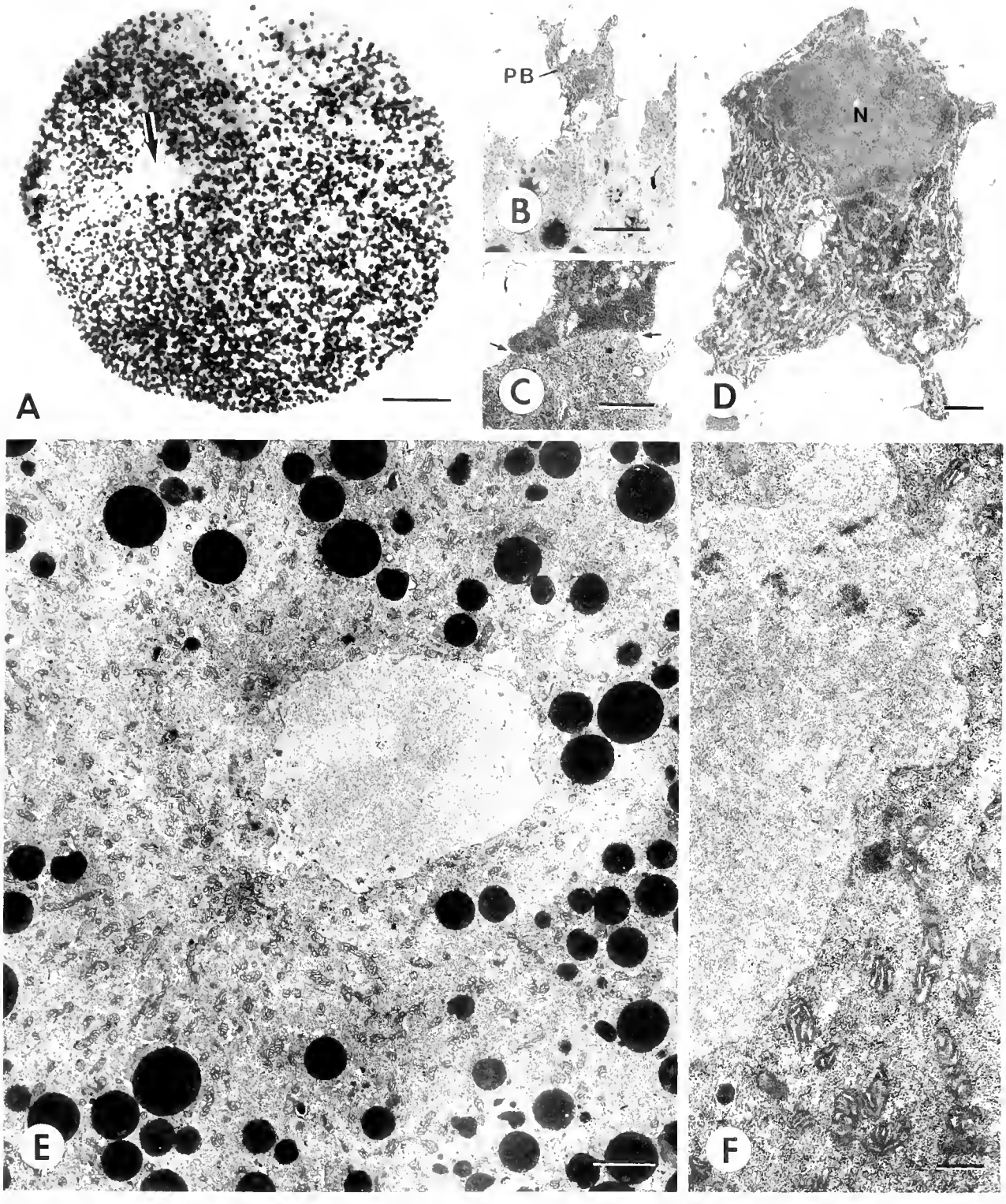

Figure 10. LM (A) and TEMs (B–F) of eggs at 16 min after insemination. A. Section through the animal pole (top) and zygote nucleus (arrow). The yolk remains patchy near the animal pole. Scale bar: 20 μm. B. The proximal part of the second polar body (PB), which has detached from the egg. Scale bar: 5 μm. C. The polar body and egg, although no longer in cytoplasmic continuity, remain very tightly apposed (arrows). Scale bar: 1 μm. D. The distal part of the second polar body. Some of the chromosome-containing vesicles have fused into a nucleus (N). Scale bar: 1 μm. E. The portion of the zygote nucleus probably derived from the male pronucleus has a cloud of mitochondria at one side. Scale bar: 12 μm. F. A portion of the zygote nucleus probably derived from the female pronucleus. There are dense patches within the nucleus and the nuclear envelope is continuous. Scale bar: 0.5 μm.

and cannot be seen by LM until 4–5 min after insemination, when it has swollen considerably. No part of the fertilizing sperm ever becomes the large, dark-staining irregular structure reported by earlier embryologists—this structure is clearly not the sperm at all, but the vegetal pole plasm. The sheets of dense granules belonging to the vegetal pole plasm are certainly responsible for the mistaken view of van der Stricht (1896) and Cerfontaine (1906) that the sperm tail enters along with the head and remains behind near the vegetal pole as a sperm remnant after the male pronucleus swells, develops an aster, and begins its slow migration. Apparently, both Sobotta (1897) and Conklin (1932) overlooked the vegetal pole plasm in eggs with large pronuclei and thus were spared the difficulty of having to explain its presence. The female pronucleus and the swollen male pronucleus are readily visible by LM, and their migrations were correctly described by Sobotta (1895, 1897), van der Stricht (1896), and Cerfontaine (1906).

The second phase of male pronuclear migration begins just before the second polar body forms. The female chromosomes then move to one side of the animal-vegetal axis and join to form a female pronucleus, which migrates to just above the equator to be met by the male pronucleus. Cerfontaine (1906) and Conklin (1932) believed that, as in ascidians, the site where the pronuclei meet is the posterior region of the future embryo. However, in the absence of obvious cytoplasmic markers of either the posterior or anterior poles, it is puzzling how they could make the distinction except by analogy with ascidians, some species of which have yellow pigment granules localized in the egg before cleavage at the posterior pole of eggs and embryos (Conklin, 1905a). Conklin (1932) thought he could distinguish a similar, although less conspicuous, marker of the posterior pole in lancelets; however, as discussed below, the existence of such a marker is most unlikely.

Pronuclear migrations in lancelets and ascidians are similar, although some of the details vary. In ascidians (Conklin, 1905a), as in lancelets, it was formerly believed that the sperm enters near the vegetal pole. However, it has since been shown that ascidian sperm can fuse with all regions of the egg plasma membrane (Ortolani, 1958; Talevi and Dale, 1986), but preferentially enter the animal hemisphere (Speksnijder *et al.,* 1989). In ascidians, as in lancelets, there are two phases of sperm migration. First, the sperm is rapidly transported close to the vegetal pole. Staining with DNA-specific dyes and an anti-tubulin antibody has shown that during this phase, the ascidian sperm nucleus remains condensed and is accompanied by the axoneme (Sawada and Schatten, 1988)—in contrast, as we have demonstrated, soon after entering the egg, the lancelet sperm nucleus decondenses and the axoneme disappears. In both ascidians and lancelets, the male pronucleus, once in the vegetal cytoplasm, swells, develops a large aster, and then, in a second slower phase of migration, moves towards the animal pole. The pronuclei meet just below the equator in ascidians and just above it in lancelets. An aggregation of mitochondria accompanies the male pronucleus in this migration. However, the mitochondria are far more numerous in ascidians than in lancelets and are derived, not by gradual recruitment from the surrounding cytoplasm, but from the mitochondria-rich cortical cytoplasm, which flows along with the male pronucleus from the animal hemisphere to the vegetal pole and then to the posterior pole to form the myoplasmic crescent (Sawada and Schatten, 1988; Speksnijder *et al.,* 1989).

The mechanism for migration of the pronuclei in lancelets is unclear. In ascidians, the first phase of male pronuclear migration occurs concomitantly with a dramatic shape change and segregation of ooplasm (Jeffery, 1984), all of which are inhibited by cytochalasin and are thus probably mediated by the contraction of cortical microfilaments (Sawada, 1988; Sardet *et al.,* 1989). We did not test whether cytochalasin could prevent the first phase of sperm migration in the lancelet; however, lancelet eggs undergo neither a shape change (Holland and Holland, 1989a) nor obvious ooplasmic segregation.

In ascidians, the sperm aster is necessary for the second phase of migration of the male pronucleus and for the movement of the mitochondria-rich myoplasm from the vegetal pole towards the posterior pole; both movements are prevented by agents that disrupt microtubules (Manes and Barbieri, 1977; Sawada and Schatten, 1988). Whether microfilaments are also involved is not known. However, in sea urchins, migration of the male pronucleus, which also depends on microtubules, is independent of microfilaments (Schatten and Schatten, 1981). Thus, in lancelets as well, although microtubule inhibitors have not been tested, the sperm aster is probably necessary for migration of the male pronucleus; the sperm aster is also probably responsible for the aggregation of mitochondria around the male pronucleus. Mitochondria do not aggregate around the female pronucleus, which lacks an aster, or around the male pronucleus before the aster forms. In addition, in somatic cells, mitochondria are frequently seen in close association with microtubules (Heggeness *et al.,* 1978), which have been shown to function as tracks for the movement of organelles, particles, and molecules in somatic cells, eggs, and embryos (Schliwa, 1984; Vale *et al.,* 1985; Hamaguchi *et al.,* 1986; Kobayakawa, 1988; Ressom and Dixon, 1988; Yisraeli *et al.,* 1989).

Vegetal pole plasm

As mentioned above, the vegetal pole plasm was seen with LM in lancelet eggs but misidentified as the fertilizing

sperm (van der Stricht, 1896; Sobotta, 1897; and Cerfontaine, 1906). With TEM, Hirakow and Kajita (1990) illustrated the pole plasm in fertilized, uncleaved eggs in their figure 12, but interpreted it as an "unusual stack of rough endoplasmic reticulum rarely encountered."

The vegetal pole plasm of lancelets has the components typical of pole plasms in other organisms, *i.e.,* numerous mitochondria, conspicuous aggregates of dense fibrogranular material, and profiles of endoplasmic reticulum. The precise configuration of the pole plasm in lancelets, however, has not been described in any other organism. Among the deuterostomes, vegetal pole plasm has been seen only in chaetognaths and anuran amphibians. It does not occur in appendicularian (Holland *et al.,* 1988) or ascidian tunicates, or in echinoderms; its possible presence in hemichordates has not been investigated (Eddy, 1975). In many organisms, the vegetal pole plasm is destined to be included in the primordial germ cells and, thus, is termed "germ plasm." The germ plasm is enriched in RNA, and some mRNAs and proteins specific to it have been identified (Phillips, 1982, 1985; Yamaguchi *et al.,* 1983; Hay *et al.,* 1988; Nakazato and Ikenishi, 1989). Nevertheless, it is not known how the germ plasm acts in germ cell determination for any animal (Davidson, 1986).

The germ cells are typically endodermal derivatives in animals with germ plasm, *e.g.,* chaetognaths and anurans, but are usually mesodermal derivatives in those lacking germ plasm, *e.g.,* urodele amphibians and probably ascidians (Nieuwkoop and Sutasurya, 1976, 1979; Nieuwkoop, 1991). For the lancelet *Branchiostoma belcheri* at the 32 cell-stage, the most vegetal tier of blastomeres, one of which presumably contains the vegetal pole plasm, is destined to form endodermal structures such as the gut; embryos lacking these blastomeres rarely form endodermal structures (Tung *et al.,* 1960a). Thus, the vegetal pole plasm of lancelets may be included in endodermal cells, and the germ cells would thus be expected to be endodermal in origin. In *B. lanceolatum,* Boveri (1892) found primordial germ cells in segmentally arranged outpocketings of the myocoel in relatively late larvae, which suggested to Nieuwkoop and Sutasurya (1979) that the germ cells would be mesodermal, not endodermal, derivatives. However, Boveri lacked earlier larvae and thus could not have determined if the germ cells had arisen in the myocoel or migrated from elsewhere. The possibility that the vegetal pole plasm in lancelets is incorporated into the germ cells merits investigation. The first two blastomeres, when separated, can each give rise to a normal larva (Wilson, 1893; Conklin, 1933; Tung *et al.,* 1958); however, no such embryo has been raised long enough to determine if gonads formed.

The dense granular material in vegetal pole plasm or germ plasm is thought to be related to, and possibly derived from, nuage—dense fibrogranular aggregates containing protein or RNA that frequently occur in association with mitochondria near the nucleus of growing oocytes. Nuage occurs in lancelets (Guraya, 1983; Aizenstadt and Gabaeva, 1987; Holland and Holland, 1991) and in most other organisms that have germ plasm. Nuage is also present in many animals lacking germ plasm, including echinoderms, and among the chordates, ascidians, reptiles, and birds (Eddy, 1975). In the European lancelet *Branchiostoma lanceolatum,* Guraya (1968, 1979) found that nuage contained protein, lipoprotein, and RNA. In mid-oogenesis, the aggregates of nuage break up and are distributed throughout the cytoplasm, becoming localized in the cytoplasm at the vegetal pole in the largest oocytes (Guraya, 1983). At least part of the nuage may be the source of the sheets of dense aggregates present just interior to the cortical granules in *B. floridae,* which coalesce after insemination to form the vegetal pole plasm.

Cytoplasmic specializations at the animal pole

Eggs of *Branchiostoma floridae* have two specializations near the animal pole: first, in both unfertilized and fertilized eggs, animal pole mitochondria are relatively electron-lucent, and second, in fertilized eggs, the yolk becomes patchy in the animal hemisphere. In blastulae of axolotls, there is a similar animal-vegetal difference in mitochondria; those in animal cells are larger and have a much less dense matrix than those of vegetal pole cells (Nelson *et al.,* 1982).

Relatively yolk-poor areas at the animal pole (namely, animal pole plasms) have been described in fertilized eggs of both invertebrates and vertebrates, for example, oligochaetes (Shimizu, 1989), lampreys (Nicander *et al.,* 1968), and amphibians (Wakahara, 1989). Typically, these areas appear either during the meiotic divisions or soon after fertilization. In ascidians, after germinal vesicle breakdown, the material from the germinal vesicle becomes localized at the animal pole. Following fertilization, this yolk-poor cytoplasm follows the myoplasm to the vegetal hemisphere and then migrates with the male pronucleus back towards the animal hemisphere, finally coming to surround the zygote nucleus (Conklin, 1905a, b; Jeffery, 1984). In contrast, in lancelets, the yolk-free patches at the animal hemisphere do not appear to derive from the germinal vesicle. Cerfontaine (1906) mistakenly depicted the remnant of the germinal vesicle persisting to one side of the meiotic spindle; when the germinal vesicle breaks down, however, its substance rapidly blends with the cytoplasm, and the yolk becomes uniformly distributed except immediately around the second meiotic spindle (Conklin, 1933; the present work).

The yolk-free patches that develop after fertilization in the animal hemisphere near the newly entered sperm do not follow it to the vegetal pole. Instead, a yolk-free area

forms *de novo* around the male pronucleus as the second phase of migration begins. The yolk-free patches near the animal pole may form either by one or more of the following: (1) an expansion of the egg volume at the animal pole, or (2) an aggregation and movement of yolk towards the vegetal pole, or (3) a movement of yolk-free cytoplasm to the animal pole. The last explanation is perhaps the most likely because in many eggs (*e.g.*, barnacles, oligochaetes, lampreys, and teleost fish) there is such a flow of cytoplasm to the animal pole from the interior or from the peripheral layers of the egg (reviewed by Wall, 1990).

The animal cytoplasm has been studied much less than the vegetal cytoplasm in regard to its role in embryogenesis. In general, the animal cytoplasm is destined to form ectoderm. In lancelets, the most animal of the four tiers of blastomeres at the 32-cell stage, if isolated, forms only epidermal structures; however, removal of this tier does not affect the normal development of the larva (Tung *et al.*, 1960a). Thus, while destined to form ectoderm, there are no substances unique to this layer that cannot be duplicated by other blastomeres.

Ooplasmic segregation

Since the work of Conklin (1932, 1933), it has been generally believed that ooplasmic segregation occurs in lancelets exactly as in ascidians (*e.g.*, Brien and Dalcq, 1948; Drach, 1948). Conklin maintained that "the localizations of materials in the Amphioxus egg are like those of ascidians, although not so sharply differentiated." Lacking the stages before the pronuclei meet, he found evidence for ooplasmic segregation in lancelets in the figures of Sobotta (1896) and van der Stricht (1897), although they made no such claims. In addition, Conklin (1933) was convinced from his own sections of eggs just before first cleavage that the mesodermal and chorda-neural crescents were distinguishable from endodermal and ectodermal areas; the mesodermal crescent was particularly visible because it consisted of more deeply staining cytoplasm. Curiously, Conklin did not mention the patchiness of yolk at the animal pole, although this was shown by Cerfontaine (1906).

Neither our results, nor those of Hirakow and Kajita (1990), have revealed any evidence for ooplasmic segregation in *Branchiostoma* such as occurs in ascidians. In lancelets, there are some small, localized aggregations of mitochondria in the animal cytoplasm, but no apparent segregation of mitochondria to the vegetal cytoplasm. The mitochondria associated with the zygote nucleus appear to be recruited by the migrating sperm nucleus and do not derive from the peripheral cytoplasm. Nowhere else in the fertilized lancelet egg is there a large concentration of mitochondria, comparable to that in the myoplasm of ascidian eggs. In addition, we found no differences in staining between regions destined to become the mesoderm, notochord, neural plate, or endoderm. As our Figures 8A, B, and 10A show, there is no crescent of more deeply staining cytoplasm anywhere in the egg. In the lancelet egg, the only type of dense granule is the yolk granule. The only regional difference in yolk is that it is scarcer in the animal hemisphere, destined for ectoderm and neural plate, than in the vegetal hemisphere, destined for mesoderm, endoderm, and notochord. It is very unlikely that the discrepancies between Conklin's conclusions and our finding are due to species differences. Although no TEM of fertilized eggs of *B. lanceolatum* has been done, yolk granules in the unfertilized egg are identical to those from *B. floridae* (Holland and Holland, 1991).

Conklin's interpretations of his own sections and the figures of others appear to have been chiefly based on his own preconceptions. In his ascidian paper (1905a), before obtaining any lancelet embryos, Conklin had concluded from van der Stricht (1896) that lancelet eggs must undergo ooplasmic segregation as in ascidians. Subsequently, Conklin interpreted all the evidence to support his ideas. First, he erroneously inferred from Sobotta (1897), who illustrated vesicles in the egg cortex, that the cortex, like that of ascidian eggs, contained not cortical granules, but numerous mitochondria. On the contrary, TEM has demonstrated that the cortex of lancelet eggs is packed with cortical granules and is nearly free of mitochondria (Holland and Holland, 1989a).

Next, Conklin was led further astray by errors of van der Stricht (1896), who thought that cortical granule disappearance resulted from their migration into the interior of the egg where they became the yolk-free patches in the animal cytoplasm. Conklin decided this was wrong in part; on disappearing, the peripheral cytoplasm migrated not into the interior of the egg, but to the vegetal pole and thus was the equivalent of the ascidian myoplasm. In truth, at fertilization, the cortical granules disappear because they undergo exocytosis and contribute to the formation of the fertilization envelope (Sobotta, 1897; Holland and Holland, 1989a). As further evidence of myoplasm, Conklin cited van der Stricht's figure 12, which, in fact, shows the yolk-free cytoplasm surrounding the vegetal pole plasm, which van der Stricht thought was the sperm remnant.

Finally, when interpreting his own sections, Conklin apparently saw things that simply weren't there. Publishing before it was common practice to photograph LM sections, Conklin (1933) drew "actual sections" (his text figure A) of fertilized *Branchiostoma* eggs showing the ectoplasm, the chorda-neural crescent, the endoderm, and the mesodermal crescent with its distinctive granules. This erroneous drawing has been reproduced in modern texts

(*e.g.*, Wickstead, 1975) and is the sole evidence for an ascidian-like ooplasmic segregation in lancelets.

Ooplasmic segregation and chordate phylogeny

Discussions about the phylogenetic origin of the chordates and the arrangements of the chordate subphyla are still highly contentious (*cf.* Ghiselin *et al.*, 1986; Jefferies, 1986; Erwin, 1991). The present study has demonstrated that a conspicuous, ascidian-style ooplasmic segregation does not occur in acraniates. Importantly, we have shown that such segregation is not a synapomorphy of ascidians and acraniates; instead it may be no more than an autapomorphy of ascidian tunicates, because conspicuous cytoplasmic rearrangements apparently do not occur in the fertilized egg in appendicularian tunicates (Holland *et al.*, 1988), which may be closest to the stem tunicate (Remane *et al.*, 1976; Holland, 1991).

Acknowledgments

We are grateful to J. M. Lawrence of the University of South Florida, Tampa, Florida, for the use of his laboratory during the breeding season of *B. floridae*. This work was supported in part by a National Science Foundation grant No. NSF DCB 87-12888 to A. T. C. Carpenter, Biology Department, University of California, San Diego, who generously allowed LZH the use of her electron microscope.

Literature Cited

Aizenstadt, T. B., and N. S. Gavaeva. 1987. The perinuclear bodies (nuage) in the developing germ cells of the lancelet *Branchiostoma lanceolatum*. (In Russian). *Tsitologia* **29:** 137–141.

Boveri, T. 1892. Über die Bildungsstätte der Geschlechtdrüsen und die Entstehung der Genitalkamern beim Amphioxus. *Anat. Anz.* **7:** 170–181.

Brien, P., and A. Dalcq. 1948. Généralités sur les cordés. Pp. 535–543 in *Traité de Zoologie*, Vol. 11, P.-P. Grassé, ed. Masson et Cie, Paris.

Cerfontaine, P. 1906. Recherches sur le développement de l'*Amphioxus*. *Arch. Biol.* **22:** 229–418.

Conklin, E. G. 1905a. Organization and cell-lineage of the ascidian egg. *J. Acad. Nat. Sci. Philadelphia Ser. 2* **13:** 5–119 + plates I–XI.

Conklin, E. G. 1905b. Organ-forming substances in the eggs of ascidians. *Biol. Bull.* **8:** 205–230 + plate XI.

Conklin, E. G. 1932. The embryology of amphioxus. *J. Morphol.* **54:** 69–151.

Conklin, E. G. 1933. The development of isolated and partially separated blastomeres of amphioxus. *J. Exp. Zool.* **64:** 303–375.

Davidson, E. H. 1986. *Gene Activity in Early Development*. Third Edition. Academic Press, Orlando, FL. 670 pp.

Drach, P. 1948. Remarques sur les rapports des Céphalocordés et des vertébrés. Pp. 1031–1037 in *Traité de Zoologie*, Vol. 11, P.-P. Grassé, ed. Masson et Cie, Paris.

Eddy, E. M. 1975. Germ plasm and the differentiation of the germ cell line. *Int. Rev. Cytol.* **43:** 229–280.

Erwin, D. H. 1991. Metazoan phylogeny and the Cambrian radiation. *TREE* **6:** 131–134.

Ghiselin, M. T., K. G. Field, G. J. Olsen, D. J. Lane, R. A. Raff, E. C. Raff, and N. R. Pace. 1986. A phylogenetic tree of chordate subphyla based on 18s ribosomal RNA sequences. *Am. Zool.* **26:** 92A.

Guraya, S. S. 1968. Cytochemistry of yolk elements in the amphioxus egg. *Z. Zellforsch.* **79:** 326–331.

Guraya, S. S. 1979. Recent advances in the morphology, cytochemistry and function of Balbiani's vitelline body in animal oocyte. *Int. Rev. Cytol.* **59:** 24–32.

Guraya, S. S. 1983. Cephalochordata. Pp. 735–752 in *Reproductive Biology of Invertebrates*, Vol. 1, K. G. Adiyodi and R. G. Adiyodi, eds. John Wiley and Sons, Chichester.

Hamaguchi, M. S., Y. Hamaguchi, and Y. Hiramoto. 1986. Microinjected polystyrene beads move along astral rays in sand dollar eggs. *Dev. Growth Differ.* **28:** 461–470.

Hatschek, B. 1882. Studien über Entwicklung des Amphioxus. *Arb. Zool. Inst. Univ. Wien* **4:** 1–88 + plates I–IX.

Hatschek, B. 1893. *The Amphioxus and its Development*, (J. B. Tuckey, translator). Swan, Sonnenschein and Co., London. 181 pp.

Hay, B., L. Ackerman, S. Barbel, L. Y. Jan, and Y. N. Jan. 1988. Identification of a component of *Drosophila* polar granules. *Development* **103:** 625–640.

Heggeness, M. H., M. Simon, and S. J. Singer. 1978. Association of mitochondria with microtubules in cultured cells. *Proc. Natl. Acad. Sci. USA* **75:** 3863–3866.

Hirakow, R., and N. Kajita. 1990. An electron microscopic study of the development of amphioxus, *Branchiostoma belcheri tsingtauense*: cleavage. *J. Morphol.* **203:** 331–344.

Hirakow, R., and N. Kajita. 1991. Electron microscopic study of the development of amphioxus, *Branchiostoma belcheri tsingtauense*: the gastrula. *J. Morphol.* **207:** 37–52.

Holland, L. Z. 1988. Spermatogenesis in the salps *Thalia democratica* and *Cyclosalpa affinis* (Tunicata: Thaliacea): an electron microscopic study. *J. Morphol.* **198:** 189–204.

Holland, L. Z. 1992. The phylogenetic significance of tunicate sperm morphology. *Proc. Sixth Int. Congress Spermatology* (in press).

Holland, L. Z., G. Gorsky, and R. Fenaux. 1988. Fertilization in *Oikopleura dioica* (Tunicata, Appendicularia): acrosome reaction, cortical reaction and sperm-egg fusion. *Zoomorphology* **108:** 229–243.

Holland, N. D., and L. Z. Holland. 1989a. Fine structural study of the cortical reaction and formation of the egg coats in a lancelet (=amphioxus), *Branchiostoma floridae* (Phylum Chordata: Subphylum Cephalochordata = Acrania). *Biol. Bull.* **176:** 111–122.

Holland, N. D., and L. Z. Holland. 1989b. The fine structure of the testis of a lancelet (=amphioxus), *Branchiostoma floridae* (Phylum Chordata: Subphyulum Cephalochordata = Acrania). *Acta Zool. (Stockh.)* **70:** 211–219.

Holland, N. D., and L. Z. Holland. 1991. The fine structure of the growth stage oocytes of a lancelet (=amphioxus), *Branchiostoma lanceolatum*. *Invert. Reprod. Dev.* **19:** 107–122.

Jefferies, R. P. S. 1986. *The Ancestry of the Vertebrates*. British Museum (Natural History), London. 376 pp.

Jeffery, W. R. 1984. Pattern formation by ooplasmic segregation in ascidian eggs. *Biol. Bull.* **166:** 277–298.

Kobayakawa, Y. 1988. Role of mitotic asters in accumulation of pigment granules around nuclei in early amphibian embryos. *J. Exp. Zool.* **248:** 232–237.

Kowalevsky, A. 1865. Istoriya razvitiya *Amphioxus lanceolatus*. (In Russian, not seen by the present authors.) Magister's Thesis, St. Petersburg University, Russia.

Kowalevsky, A. 1867. Entwickelungsgeschichte des *Amphioxus lanceolatus*. *Mém. Acad. Impérial Sci. St. Pétersbourg, Sér. 7* **11:** 1–17 + plates I–III.

Lwoff, B. 1892. Ueber einige wichtige Punkte in der Entwicklung des *Amphioxus*. *Biol. Centralblatt* **12:** 729–744.

Manes, M. E., and F. D. Barbieri. 1977. On the possibility of sperm aster involvement in dorso-ventral polarization and pronuclear migration in the amphibian egg. *J. Embryol. Exp. Morphol.* **40:** 187–197.

Nakazato, S., and K. Ikenishi. 1989. Monoclonal antibody production against a subcellular fraction of vegetal pole cytoplasm containing the germ plasm of *Xenopus* 2-cell eggs. *Cell Differ. Dev.* **27:** 163–174.

Nelson, L., R. Lorentzon, L. Boquist, and S. Lovtrup. 1982. Morphological differentiation of mitochondria in the early amphibian embryo. *Exp. Cell Res.* **137:** 25–29.

Nicander, L., B. A. Afzelius, and I. Sjödèn. 1968. Fine structure and early fertilization changes of the animal pole in eggs of the river lamprey, *Lampetra fluviatilis*. *J. Embryol. Exp. Morphol.* **19:** 319–326.

Nieuwkoop, P. D. 1991. The different origin of the primordial germ cells (PGCs) in various groups of vertebrates. *Proc. K. Ned. Akad. Wet.* **94:** 103–110.

Nieuwkoop, P. D., and L. A. Sutasurya. 1976. Embryological evidence for a possible polyphyletic origin of the recent amphibians. *J. Embryol. Exp. Morphol.* **35:** 159–167.

Nieuwkoop, P. D., and L. A. Sutasurya. 1979. *Primordial Germ Cells in the Chordates. Embryogenesis and Phylogenesis.* Cambridge University Press. Cambridge, London. 187 pp.

Ortolani, G. 1958. Cleavage and development of egg fragments in ascidians. *Acta Embryol. Morphol. Exp.* **1:** 247–272.

Phillips, C. R. 1982. The regional distribution of poly(A) and total RNA concentrations during early *Xenopus* development. *J. Exp. Zool.* **223:** 265–275.

Phillips, C. R. 1985. Spatial changes in poly(A) concentrations during early embryogenesis in *Xenopus laevis:* analysis by *in situ* hybridization. *Dev. Biol.* **109:** 299–310.

Remane, A., V. Storch, and U. Welsch. 1976. *Systematische Zoologie, Stämme des Tierreichs.* Fischer, Stuttgart. 678 pp.

Ressom, R. E., and K. E. Dixon. 1988. Relocation and reorganization of germ plasm in *Xenopus* embryos after fertilization. *Development* **103:** 507–518.

Sardet, C., J. Speksnijder, S. Inoué, and L. Jaffe. 1989. Fertilization and ooplasmic movements in the ascidian egg. *Development* **105:** 237–249.

Sawada, T. 1988. The mechanism of ooplasmic segregation in the ascidian egg. *Zool. Sci.* **5:** 667–675.

Sawada, T., and G. Schatten. 1981. Microtubules in ascidian eggs during meiosis, fertilization, and mitosis. *Cell Motil. Cytoskeleton* **9:** 219–230.

Schatten, G., and H. Schatten. 1988. Effects of motility inhibitors during sea urchin fertilization. *Exp. Cell Res.* **135:** 311–330.

Schliwa, M. 1984. Mechanisms of intracellular organelle transport. Pp. 1–81 in *Cell and Muscle Motility*, Vol. 5, J. W. Shaw, ed. Plenum Publ. Co., New York.

Shimizu, T. 1989. Asymmetric segregation and polarized redistribution of pole plasm during early cleavages in the *Tubifex* embryo: role of actin networks and mitotic apparatus. *Dev. Growth Differ.* **31:** 283–297.

Sobotta, J. 1895. Die Befructung des Eies von *Amphioxus lanceolatus.* Vorläufige Mitteilung. *Anat. Anz.* **11:** 129–137.

Sobotta, J. 1897. Die Reifung und Befruchtung des Eies von *Amphioxus lanceolatus. Arch. Mikr. Anat.* **50:** 15–71 + plates II–V.

Speksnijder, J. E., L. F. Jaffe, and C. Sardet. 1989. Polarity of sperm entry in the ascidian egg. *Dev. Biol.* **133:** 180–184.

Talevi, R., and B. Dale. 1986. Electrical characteristics of ascidian egg fragments. *Exp. Cell Res.* **162:** 539–543.

Tung, T. C., S. C. Wu, and Y. Y. F. Tung. 1958. The development of isolated blastomeres of amphioxus. *Sci. Sin.* **7:** 1280–1320.

Tung, T. C., S. C. Wu, and Y. Y. F. Tung. 1960a. The developmental potencies of the blastomere layers in amphioxus egg at the 32-cell stage. *Sci. Sin.* **9:** 119–141.

Tung, T. C., S. C. Wu, and Y. Y. F. Tung. 1960b. Rotation of the animal blastomere in amphioxus egg at the 8-cell stage. *Sci. Record, N. S.* **4:** 389–394.

Tung, T. C., S. C. Wu, and Y. Y. F. Tung. 1962a. The presumptive areas of the egg of amphioxus. *Sci. Sin.* **11:** 629–645.

Tung, T. C., S. C. Wu, and Y. Y. F. Tung. 1962b. Experimental studies on the neural induction in amphioxus. *Sci. Sin.* **11:** 805–820.

Vale, R. D., B. J. Schnapp, T. S. Reese, and M. P. Sheetz. 1985. Organelle, bead, and microtubule translocations promoted by soluble factors from the squid giant axon. *Cell* **40:** 559–569.

van der Stricht, O. 1896. La maturation et la fécondation de l'oeuf d'*Amphioxus lanceolatus. Arch. Biol.* **14:** 469–495 + plates XX, XXI.

van Wijhe. 1893. Ueber *Amphioxus. Anat. Anz.* **8:** 152–172.

Wakahara, M. 1989. Specification and establishment of dorsal-ventral polarity in eggs and embryos of *Xenopus laevis. Dev. Growth Differ.* **31:** 197–207.

Wall, R. 1990. *This Side Up. Spatial Determination in the Early Development of Animals,* Developmental and Cell Biology Series 24, P. W. Barlow, D. Bray, P. B. Green, J. M. W. Slack, eds. Cambridge University Press, Cambridge. 436 pp.

Wickstead, J. H. 1975. Chordata: Acrania (Cephalochordata). Pp. 283–319 in *Reproduction in Marine Invertebrates,* Vol. 2, A. C. Giese and J. S. Pearse, eds. Academic Press, New York.

Willey, A. 1894. *Amphioxus and the Ancestry of the Vertebrates.* Macmillan and Co., New York. 316 pp.

Wilson, E. B. 1893. *Amphioxus,* and the mosaic theory of development. *J. Morphol.* **8:** 579–639.

Yamaguchi, Y., K. Murakami, M. Furusawa, and J. Miwa. 1983. Germline-specific antigens identified by monoclonal antibodies in the nematode Caenorhabditis elegans. *Dev. Growth Differ.* **25:** 121–131.

Yisraeli, J. K., S. Sokol, and D. A. Melton, 1989. The process of localizing a maternal messenger RNA in *Xenopus* oocytes. *Development* **1989**(suppl.): 31–36.

Zalokar, M., and C. Sardet. 1984. Tracing of cell lineage in embryonic development of *Phallusia mammillata* (Ascidia) by vital staining of mitochondria. *Dev. Biol.* **102:** 195–205.

Reference: *Biol. Bull.* **182**: 97–104. (February, 1992)

The Divergence of Species-Specific Abalone Sperm Lysins is Promoted by Positive Darwinian Selection

YOUN-HO LEE AND VICTOR D. VACQUIER

Marine Biology Research Division 0202, Scripps Institution of Oceanography, University of California, San Diego, La Jolla, California 92093

Abstract. Recognition by sperm lysin of the egg vitelline envelope may be one component in determining the species-specificity of fertilization in abalones. The amino acid sequences of lysin proteins of seven California abalone species were deduced from the cDNA sequences. This is the first extensive comparison of a gamete recognition protein from congeneric species. Each prelysin has a highly conserved signal peptide of 18 amino acids, followed by a mature sequence of 136–138 residues. Of 136 aligned positions, 68 have the same amino acid in all seven sequences. The % identity relative to the red abalone lysin sequence is: white 90%, flat 83%, pinto 82%, pink 78%, black 71%, and green 65%. Hydropathy plots and a distance tree of the seven lysins show that red, white, and flat lysins are more closely related to each other than to the lysins of the other four species. A hypervariable, species-specific, domain exists in all sequences between positions 2–12. Amino acid replacements between any two lysins are mostly nonconservative. Analysis of the cDNA sequences shows the number of nonsynonymous substitutions (amino acid altering) exceeds the number of synonymous substitutions (silent) in 20 of the 21 pairwise comparisons of the seven sequences, indicating that positive Darwinian selection must promote the divergence of lysin sequences.

Introduction

A striking feature of fertilization is the species specificity of sperm-egg interaction in mammals (O'Rand, 1988; Yanagimachi, 1988a, 1988b; Roldan and Yanagimachi, 1989) and invertebrates (Giudice, 1973; Summers and Hylander, 1975, 1976; Osanai and Kyozuka, 1982). Sperm-egg mixtures from the same species usually yield zygotes more efficiently than cross-species mixtures. Although cross-species hybrid zygotes can be obtained in mammals and invertebrates, the general observation is that much higher concentrations of sperm are needed in the insemination mixture to achieve fertilization. Blocks to cross-species fertilization can occur at four points in the process: induction of the sperm acrosome reaction by components of the egg surface, adhesion of sperm to the egg envelope, sperm penetration of the egg envelope, and fusion of sperm and egg cell membranes. In echinoderms, the greatest barrier to cross-species fertilization is the failure of sperm to adhere to the egg vitelline envelope (Summers and Hylander, 1975, 1976); in mammals it is the failure of sperm to adhere to and penetrate the egg zona pellucida (O'Rand, 1988; Yanagimachi, 1988a,b; Roldan and Yanagimachi, 1989).

The divergence of gamete recognition proteins may be important in the establishment of barriers to cross-fertilization between populations. This may be an important factor in the speciation of marine invertebrates using external fertilization. To learn how species-specific gamete recognition proteins have diverged during evolution, we have studied a protein from abalone sperm. Abalones are marine archeogastropods of the genus *Haliotis*. Approximately 70 extant species occur on coastlines of the world, eight of them on the Pacific Coast of North America. Although abalones are members of an ancient group of gastropods, the genus *Haliotis* is relatively recent, most fossils being from the Miocene (5–25 million years; Lindberg, 1991).

The abalone egg is contained within a glycoproteinaceous vitelline envelope (VE) about 0.6 μm in thickness (Lewis *et al.*, 1982). The spermatozoon possesses a relatively enormous acrosome granule (Lewis *et al.*, 1980;

Received 25 July 1991; accepted 11 October 1991.

Abbreviations: Mr, relative molecular mass; VE, vitelline envelopes of abalone eggs.

Shiroya and Sakai, 1983) containing two abundant proteins of about Mr 18,000 and 16,000 (Lewis *et al.*, 1982). During fertilization, the sperm attaches to the egg VE, the acrosome granule opens, and the two proteins are secreted. A hole in the VE, 3 μm in diameter, is created in seconds, and the sperm passes through it to fuse with the egg (Lewis *et al.*, 1982; Sakai *et al.*, 1982). Partial amino acid sequence analysis (41 residues of the NH_2-terminus) shows that the Mr 18,000 protein is not a precursor of the Mr 16,000 protein (Vacquier, unpubl.). When the purified Mr 16,000 acrosomal protein (sperm lysin) is added to eggs, the VE rapidly dissolves by a nonenzymatic mechanism; VE glycoproteins are not degraded and no new NH_2-termini are formed (Haino-Fukushima, 1974; Lewis *et al.*, 1982; Hoshi, 1985). As previously discussed (Lewis *et al.*, 1982; Hong and Vacquier, 1986; Baginski *et al.*, 1990; Vacquier *et al.*, 1990), lysin may act by competing for hydrogen and hydrophobic bonds that hold the glycoproteinaceous fibers of the VE together.

The cDNA for pink and red abalone sperm lysins had been previously cloned and sequenced (Vacquier *et al.*, 1990). To learn about the evolutionary divergence of sperm lysin in California abalones, the polymerase chain reaction was used to generate double stranded cDNA from five additional species. The analysis of the seven deduced amino acid sequences of lysin is the first extensive comparison of a gamete recognition protein in congeneric species. We were surprised to find that the divergence of the lysin sequences is promoted by positive Darwinian selection.

Materials and Methods

The seven species of abalone used in this study were: *Haliotis corrugata* (pink, M34389), *H. cracherodii* (black, M59971), *H. fulgens* (green, M59972), *H. kamtschatkana* (pinto, M59970), *H. rufescens* (red, M34388), *H. sorenseni* (white, M59968), and *H. walallensis* (flat, M59969). The GenBank cDNA sequence accession number follows the common name of each species. The testes of male abalone were removed and poly A+ RNA isolated as described (Chomczynski and Sacchi, 1987; Vacquier *et al.*, 1990). Northern blot analysis with a full length red abalone lysin cDNA as the probe, revealed a single band of hybridization of approximately 660 nucleotides in all seven species (Vacquier *et al.*, 1990; and unpubl.). Oligonucleotide primers were synthesized to the 5′ end of the previously reported red and pink cDNA sequences (primer 6; GAACAGATTACAAG*ATG*AAGCTGT; the italicized ATG being the initiation codon), and to the complementary strand of the 3′ end of the sequence adjoining the poly A tail (primer 7; TAGTAAATCTA*TTTATT*CTGGAAT, the italicized being the complement of the poly A signal sequence; Vacquier *et al.*, 1990).

Two to ten μg of poly A+ RNA were used for first strand synthesis (Frohman, 1990). The RNA was washed twice in 1 ml 80% ethanol, dried, and dissolved in 7 μl water containing 3 μl of primer 7 (30 pMol). The tube was heated to 95°C for 5 min and then placed on ice for 10 min, followed by a 5-s centrifugation (a quick spin). A reaction mixture of 10 μl was added to the tube [the 10 μl contained: 2.5 μl dNTP mix at 2 m*M* of each nucleotide; 2.0 μl 10 × RTC buffer (Frohman, 1990); 1.0 μl human placental RNase inhibitor (Promega, Madison, Wisconsin); 2.0 μl MuLV reverse transcriptase (400 units); and 2.5 μl water]. This mixture of 20 μl was incubated for 1 h at 37°C. An additional 1 μl of MuLV reverse transcriptase was then added (200 units), and the incubation continued 1 h at 45°C. Following incubation, the sample was diluted with 2 ml 0.1 × TE (1 m*M* Tris, 0.1 m*M* EDTA, pH 8.0) and concentrated to 50 μl with a Centricon-30 microconcentrator (Amicon Inc., Beverly, Massachusetts). The redilution in 2 ml 0.1 × TE and concentration to 50–100 μl was done three times. Sixteen μl of this first strand cDNA product was used for the second strand synthesis.

To each tube of 16 μl was added 33 μl of a mixture of 5 μl PCR buffer (Frohman, 1990), 2.5 μl dimethylsulfoxide, 5.0 μl dNTPs at 2 m*M* each nucleotide, 6.0 μl primer 7 in water (30 pMol), 6.0 μl primer 6 (30 pMol), and 8.5 μl water. The 49 μl volume (in a 0.5 ml tube) was heated to 95°C for 5 min and cooled slowly (1 h) to 50°C. After a quick spin, 0.5 μl of Taq polymerase was added (2.5 units, Perkin-Elmer-Cetus, Emeryville, California), the tube vortexed gently, and 50 μl mineral oil added. The tube was incubated for 15 min at 37°C followed by 40 min at 72°C. Amplification of the lysin cDNA was accomplished in a temperature cycler by 40 cycles of 94°C for 1 min, 45°C for 1 min, and 72°C for 2 min. An additional 0.5 μl of the Taq enzyme was added after the first 20 cycles. Following the last cycle, the temperature was held at 72°C for 15 min. The tubes were cooled to 23°C by a quick spin in a microfuge and 1.0 μl of Klenow fragment added, and the incubation continued for 30 min at 23°C. Agarose gel electrophoresis of the 50 μl reaction mixture showed the presence of one product of amplification of approximately 650 nucleotides.

The amplified double stranded cDNA was purified either by three cycles of dilution in 2 ml of 0.1 × TE and concentration to 50–200 μl with a Centricon-30, or by separating the product by electrophoresis in 1% agarose in 0.5 × TAE (0.04 *M* Tris acetate, 0.001 *M* EDTA, pH 8.0). The 650 base pair band was excised from the gel and the cDNA purified with Prep-A-Gene (Biorad Laboratories, Richmond, California). The cDNA was quantitated by spectrophotometry and 1 μg aliquots stored in 100% ethanol at −20°C. For sequencing, 1 μg of DNA was washed twice in 1 ml 80% ethanol and dried. The DNA

```
        -18                                -1 1                                    21
RED   : M K L L V L C I F A M M A T L A M S R - S W H Y V E P K F L N K A F E V A L K V
WHITE : . . . . . . . . . . . . . . . . . . . - R . . . . P . . . . . . . . . . . . . .
FLAT  : . . . . . . . . . . . . . . . . . . . - R . N F . T . R E V . . . . . . . . . .
PINTO : . . . F . . . . . . . . . . . . . . . - . . T . . Q . . . . . . . . . . . . . E
PINK  : . . . . . . . L . . . . . . . . V . . H R F R F I P H . Y I R . E . . . . . . .
BLACK : . . . . . . . V . . . . . . . . V . . - R Y Q F . Q H Q Y I R . . . . . . . . .
GREEN : . . . . . . W V . . . . . . V . . . . - R . T F . R Y H Y I . . . Y . . T M . I

        22                                40                                     61
RED   : Q I I A G F D R G L V K W L R V H G R T L S T V Q K K A L Y F V N R R Y M Q T H
WHITE : . . . . . . . . T . . . . . . T . . G . . . H . . . . . . . . . . . . . . . . .
FLAT  : . . . . . . . . T . . . . . . A . . . S . . H . . . . . . . . . . . . . . . . .
PINTO : E . . V R W . . K . A . . . . . N . G P . . H . . . . . . . . . . . . . . . . .
PINK  : E . . . . . . . T . . . . . . . . . G R . . . . . . . . . . . . . . . . . . . .
BLACK : E . . . . . . . T . . . . . . N . . . G . N E N . R . V . . . . . . . . . . . .
GREEN : . . . S . . . . Q . T A . . . . . . . R . T N N . . . T . F . . . . . . . . . .

        62                                80                                    101
RED   : W A N Y M L W I N K K I D A L G R T P V V G D Y T R L G A E I G R R I D M A Y F
WHITE : . . . . . . . . . . . T . . . . . . . . . . . . . . . . . . . . . . . . . D . .
FLAT  : . . . . . . . V . . . . . . . . . . A . . A . . . . . . . . . . . . . . . D . .
PINTO : . . . . . . . . . . . T . . . . . . . . . . . . R . . . . . . . . . . . . V F .
PINK  : . Q . . . . . . V R . T . . . . . P . . . A . . S . . . . . . . . . . . . . . .
BLACK : . Q . . . . . . V . . T N . . . . P . . . A . . R A . . . . . . . . . . . G . .
GREEN : . Q . . . . . V K R . . K . . . . P A A . . . . . . . . . . . . . . V . . V F .

        102                                120                          136
RED   : Y D F L K D K N M I P K Y L P Y M E E I N R M R P A D V P V K Y M - - G K
WHITE : . N . . . G R . . . . . . . . . . . . . . . . . S . . I . . . . . - - . .
FLAT  : . N . . . G R . . . . . . . . . . . . . . . . . S . . I . I R . R - - . .
PINTO : . K . . S G R . . . . . . M . . . . Q . . . . . A . . I . . . . . - - . .
PINK  : . N . . N G R . . . . . . . . . . . . . . . . . . . . . . . A N R - - . .
BLACK : . N . . . N R V . . . . . . . . . R R L . N . . . E . . . . A N R N P . .
GREEN : . N . . S G R K . . . P . S A . . A K L . A L . . . . . . . . N H - - . .
```

Figure 1. Amino acid sequences of the seven abalone sperm lysins. Dots denote identity to the red lysin sequence, dashes are for alignment, and numbering refers to the red lysin sequence. The signal peptide spans positions −18 to −1. The single letter amino acid code is used.

pellet was dissolved in 10 μl of sequenase buffer (U. S. Biochemicals, Cleveland, Ohio) containing 10 pMol of a sequencing primer. Eight different oligonucleotide primers were used for sequencing, all of them synthesized so as to correspond to the red abalone lysin cDNA sequence (Vacquier *et al.*, 1990). The tube containing the mixture of DNA and primer was heated to 95°C for 5 min and snap frozen 5 min in a dry ice ethanol bath, then placed in an aluminum block precooled to −20°C, which was allowed to warm to 23°C over a 2-h period. Following a quick spin, the Sequenase protocol was performed and the sequences of both strands of cDNA determined a minimum of two times. The cDNA and amino acid sequences were computer aligned and listed in order of similarity using the progressive alignment and tree building program given in Feng and Doolittle (1990). Hydropathy plots with a window of seven amino acids were done by the method of Kyte and Doolittle (1982).

To determine whether amino acid replacement between any two lysin sequences conserved the class of residue, the 20 amino acids were divided into 5 classes following the structural considerations of Dickerson and Geis (1983). Synonymous and nonsynonymous nucleotide substitutions were computed by the methods of Li *et al.* (1985) and Nei and Gojobori (1986).

Results

Deduced amino acid sequences

The deduced amino acid sequences, aligned and listed in order of descending similarity (Feng and Doolittle, 1990), are presented in the single letter code in Figure 1. Assignments of the initiation methionine (M at position −18), the signal sequence of 18 amino acids, the NH_2-terminal residue of the mature lysins being arginine (R at position 1), and the COOH-terminal residue being lysine (K at position 136) have been previously presented (Vacquier *et al.*, 1990). In Figure 1, dots denote identity to the red abalone lysin sequence and dashes are for alignment. The signal sequences (positions −18 to −1) have been highly conserved during evolution and are typical of eukaryotes (von Heijne, 1985). Neither cysteines nor

sites for N-linked glycosylation are found in the mature lysins. The mature pink abalone lysin is 137 residues, black abalone lysin is 138, and the lysins of the five other species are 136 residues in length. Of 136 aligned positions, 68 (50%) have the same amino acid in all seven species. The two longest regions of perfect identity are the eight residues between positions 88–95 and the 11 residues between positions 52–62. There are four occurrences of two contiguous positively charged amino acids in all seven sequences (positions 47–48, 55–56, 71–72, and 94–95). The percent identity in amino acid residues for the 21 pairwise comparisons of the seven lysin sequences (Table I) shows the decrease in similarity progressing from red lysin to green lysin. Green abalone lysin is equally dissimilar from each of the other six lysins, the percent identity varying from 63 to 65%. The region of greatest difference among all seven sequences is the 11 residue segment comprising positions 2–12 (Fig. 1). In this region, no two species have the identical sequence. Considerable difference in charge distribution is seen in this hypervariable segment. For example, the red, flat, and pinto lysins have a net charge of +1, whereas pink abalone lysin has a net charge of +6.

Hydropathy plots and branching order

Hydropathy plots of the seven mature lysin sequences are of value in showing subtle differences throughout the sequences (Fig. 2). The plots of the hypervariable domain of positions 2–12 (shaded) are in most cases species-specific. The upper three plots (red, white, flat) are quite similar, all having a large hydrophobic domain between residues 15–30. The pinto is clearly different from the top three, this large hydrophobic domain being reduced and followed by a hydrophilic domain centered at position 30. The pink lysin has a hydrophilic domain centered at residue 60 that is more similar in shape to the one in the black and green lysins than it is to the other four species. There is a moderately hydrophobic domain at about position 70 in pink lysin shared with only the black species. The pinto and green are the only two lysins having a large hydrophobic peak close to position 100. The plots for the black and green are clearly distinct from the other species in having two large hydrophilic domains centered about positions 45 and 60. However, the plot of the black lysin shows a large hydrophilic domain around position 125 which is not present in the green. The regions of 11 (positions 52–62) and eight (positions 88–95) amino acids that are invariant in all seven sequences are shown as shaded zones (Fig. 2). Both these regions are amphipathic, being hydrophobic in the NH_2-terminal direction and hydrophilic in the COOH-terminal direction.

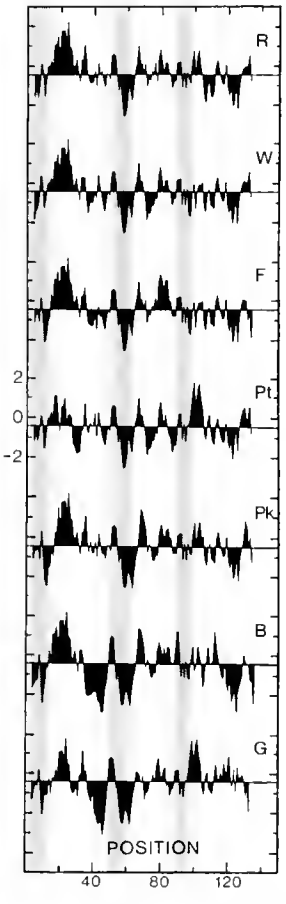

Figure 2. Hydropathy plots of the seven abalone lysin sequences using a window of seven residues. Hydrophobic values are positive and hydrophilic values negative. The hypervariable domain of 2-12, and the two invariant domains of 52-62 and 88-95 are shaded. R, red; W, white; F, flat; Pt, pinto; Pk, pink; B, black; and G, green abalone lysins.

A distance tree depicting the branching order of the seven lysin sequences (Fig. 3) shows red and white lysins to be the most closely related proteins. The black and green lysin sequences are the most divergent; they are far from the other five sequences and also far from each other.

Amino acid replacements and nucleotide substitutions

The 21 possible pairwise comparisons of the 7 lysin sequences were analyzed to determine the fraction of

Table I

Percent identity of amino acid residues in 21 pairwise comparisons in 136 aligned positions of seven lysins

Species	Red	White	Flat	Pinto	Pink	Black
White	90					
Flat	83	88				
Pinto	82	85	76			
Pink	78	80	77	72		
Black	71	72	72	65	78	
Green	65	64	65	63	65	65

Table II

The replacement of amino acids in mature lysins is nonconservative

Species	Red	White	Flat	Pinto	Pink	Black
White	4/13					
Flat	12/23	10/16				
Pinto	5/25	3/21	10/33			
Pink	9/29	9/26	12/30	7/37		
Black	10/40	10/38	11/38	10/47	5/27	
Green	18/48	19/49	21/47	19/51	16/46	15/48

amino acid replacements that were between residues of the same amino acid class (conservative replacement). The data are shown in Table II, where the numerator is the number of replacements between amino acids of the same class, and the denominator is the total number of replacements in each pairwise comparison. In all but two comparisons (flat × red and flat × white), conservative amino acid replacements are far below 50%. In summary, the majority of amino acid replacements between any two lysins involves switching the class of residue.

The number of synonymous (Ds) and nonsynonymous (Dn) nucleotide substitutions per site were computed for the 21 pairwise comparisons of the seven lysin cDNA sequences (Nei and Gojobori, 1986). The data (Table III) show that in all but one comparison (flat × green) Dn is greater than Ds. In 6 of the 21 comparisons, the difference is significant at the 5% level, and in two at the 0.5% level. These data show that positive Darwinian selection is promoting the divergence of lysin sequences. Also, the closely related sequences (Fig. 3) of red, white, flat, and pinto abalone lysins exhibit the positive selection phenomenon more strongly than do the more widely divergent sequences.

Discussion

Amino acid sequences

Homology among the seven mature lysins is readily apparent (Fig. 1). The sequences align perfectly in 952 of 955 amino acids. Lysins are constrained in length, varying from 136 to 138 amino acids. There is conservation of primary structure in that 68 of the 136 aligned positions have the identical amino acid in all seven sequences. With the exception of the hypervariable domain of positions 2–12, these invariant 68 positions are spread throughout the lysin molecule with a slight concentration toward the central portion of the sequence. Of the 68 invariant positions, 14 are occupied by residues that are highly conserved (Graur, 1985; single letter code, W = 3, G = 5, and Y = 6), and 24 by the group of seven amino acids that are replaced most frequently in mammalian proteins (Graur, 1985; T = 1, H = 1, Q = 2, F = 3, I = 4, M = 5,

Table III

Percent synonymous (Ds) and non-synonymous (Dn) nucleotide substitutions per site

Species	Ds	(SE)	Dn	(SE)	$\frac{Dn}{Ds}$	d = Dn − Ds	SE
Red × White	1.62	(1.32)	5.79	(1.40)	3.57	4.17*	1.92
Flat	2.61	(1.69)	10.08	(1.89)	3.86	7.47**	2.54
Pinto	2.76	(1.75)	10.71	(1.95)	3.88	7.95**	2.62
Pink	10.59	(3.53)	14.63	(2.33)	1.38	4.04	4.23
Black	11.08	(3.64)	21.76	(2.95)	1.96	10.68*	4.69
Green	21.27	(5.31)	24.93	(3.22)	1.17	3.66	6.21
White × Flat	4.25	(2.16)	6.36	(1.47)	1.50	2.11	2.61
Pinto	3.30	(1.91)	8.39	(1.70)	2.54	5.09*	2.56
Pink	9.92	(3.40)	13.69	(2.25)	1.38	3.77	4.08
Black	11.42	(3.69)	20.82	(2.87)	1.82	9.40*	4.67
Green	21.12	(5.27)	25.44	(3.26)	1.20	4.32	6.20
Flat × Pinto	5.45	(2.48)	13.59	(2.23)	2.49	8.14*	3.34
Pink	11.67	(3.71)	15.86	(2.45)	1.36	4.19	4.45
Black	13.42	(4.03)	22.70	(3.04)	1.69	9.28	5.05
Green	25.02	(5.84)	23.78	(3.13)	0.95	−1.24	6.63
Pinto × Pink	9.76	(3.39)	18.05	(2.63)	1.85	8.29	4.29
Black	13.71	(4.12)	26.06	(3.31)	1.90	12.35*	5.28
Green	22.66	(5.54)	24.49	(3.18)	1.08	1.83	6.39
Pink × Black	9.31	(3.28)	13.12	(2.19)	1.41	3.81	3.94
Green	16.03	(4.45)	24.02	(3.15)	1.50	7.99	5.45
Black × Green	18.14	(4.80)	27.80	(3.46)	1.53	9.66	5.92

* Significant at 5% level, ** at 0.5% level.

and L = 8). Because the occupancy of these 68 positions is identical in all 7 lysins, we conclude that they are crucial to lysin's role in fertilization in California abalones.

The hypervariable domain (positions 2–12) is strikingly similar to the ligand binding domain of annexin II (Becker *et al.*, 1990), a membrane and lipid binding protein. Annexin II possesses an NH_2-terminal 12 amino acid segment (Ac-STVHEILCKLSL) that binds its ligand (p11). Ligand binding induces the 12 residues to form a positively charged amphipathic α-helix that becomes buried in p11. The important structural features for binding between annexin II and p11 are the hydrophilic residue in position 1 and the hydrophobic side chains at positions 3, 6, 7, and 10. White abalone lysin has residues with hydrophobic side chains at positions 3, 6, 7, and 10, and the same positively charged residues at positions 4 and 9 (His and Lys) as has annexin II. In red, pink, and pinto lysins, 3 out of 4 residues at positions 3, 6, 7, and 10 have hydrophobic side chains. Three of the seven lysins are positively charged at position 4 and six out of seven at position 9. The binding of lysin to its unknown VE ligand may thus be similar to the binding of annexin II to p11 (Becker *et al.*, 1990).

Much has been learned about protein-protein recognition by X-ray crystallographic studies of the binding of proteases with their inhibitor proteins, and the binding of antibody to antigen (Janin and Chothia, 1990). In the protease-inhibitor complexes, 10–15 residues of the inhibitors make contact with 17–29 residues of the proteases. These numbers are consistent with the size of the lysin hypervariable domain. In antibodies, the antigen binding sites are disproportionately rich in residues with aromatic side chains. In the seven lysins, between positions 2–12, 26 residues of a total of 77 (34%) in all 7 sequences have aromatic side chains, whereas by total amino acid composition, only 17% of lysin residues are aromatic. This adds support to the concept that positions 2–12 in lysin may be involved in the binding of its VE ligand. We have not as yet quantitatively determined the ability of lysin to dissolve egg VEs in all 21 pairwise combinations of the 7 species. However, we have demonstrated species specificity in the cross combinations of red and pink abalone lysins and egg VEs proteins (Vacquier *et al.*, 1990).

Positive Darwinian selection in lysin divergence

In most cases, when two orthologous proteins are diverging, the frequency of synonymous (silent) nucleotide substitution (Ds) will be greater than that of nonsynonymous (amino acid altering) substitution (Dn). If positive Darwinian selection is promoting divergence of two proteins, the converse will be true. In positive selection there is adaptive value to alter the amino acid sequence. Positive selection has been proven at the molecular level in the following cases: the class I (Hughes and Nei, 1988; Hughes *et al.*, 1990) and class II (Hughes and Nei, 1989) major histocompatibility complex antigens; the V_H genes of immunoglobulins (Tanaka and Nei, 1989); the circumsporozoite antigen in *Plasmodium* (Hughes, 1991); human influenza A virus (Fitch *et al.*, 1991); and the Adh locus in *Drosophila* (McDonald and Kreitman, 1991). The nonconservative nature of amino acid replacements between lysins (Table II) provided the clue that positive selection might be promoting lysin divergence. Analysis of lysin cDNA sequences by the method of Nei and Gojobori (1986; Table III) shows that Dn exceeds Ds in 20 of 21 pairwise comparisons. Among the closely related sequences of the red, white, flat, and pinto abalone lysins (Fig. 3), Dn shows statistically significant higher values than Ds. Analysis by a similar method (Li *et al.*, 1985) yielded almost the same results. For example, in comparisons of red, white, flat, and pinto lysin sequences, the average nonsynonymous value was 2.4 times greater than the synonymous value. The most extreme comparison was between the red and flat sequences, where the nonsynonymous value was 3.4 times greater than the synonymous value. These data indicate a strong selective advantage in altering the amino acid sequence of lysin. This is the first example of positive selection acting on a gamete recognition protein. With the exception of the Adh locus in *Drosophila*, the common attribute abalone lysins share

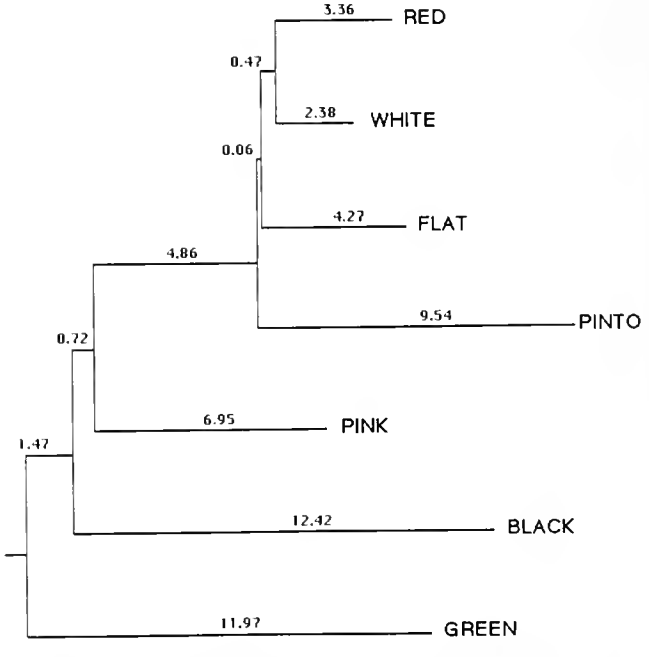

Figure 3. Distance tree showing the branching relationships of the lysin sequences. The root of the tree is placed arbitrarily at the midpoint. The numbers on the branches represent relative evolutionary distances (Feng and Doolittle, 1990).

with the published examples of positive selection is the involvement in extracellular recognition.

We cannot speculate about what could provide the selective pressure acting on lysin divergence. The demonstration of positive selection does not prove that it is a causative factor responsible for speciation in abalones. Experimental evidence exists that abalone embryos tend to settle near their parents (Prince *et al.,* 1987), and that genetic structure can occur within an abalone species in two populations separated by three km (Brown, 1991). Thus, speciation by geographic isolation probably occurs in abalones. Although the demonstration of positive selection in lysin divergence does not indicate how abalone populations split into distinct species, the possibility that it may accompany the speciation process should be considered. The statistically significant data showing positive selection (Table III) are between the closely related abalone species (Fig. 3). This suggests that a high frequency of nonsynonymous substitution (Dn) accompanies initial divergence, but Dn decreases as divergence increases. A similar situation occurs with the class I major histocompatibility genes in which Dn is greater in intralocus as compared to interlocus comparisons (Hughes and Nei, 1988). Thus, the reason that the positive selection data set is so robust for lysin may be due to the relatively recent appearance of these closely related species in the fossil record (20 million years ago; Lindberg, 1991).

One might speculate that positive selection may cause allelic variation in abalone sperm lysins. However, two male pink abalones from San Diego, California and six male red abalones (two from San Nicholas Island, two from Mendocino, California, and two from San Diego) yielded identical species-specific cDNA sequences in both the 462 nucleotide open reading frame and in about 150 nucleotides of the 3′ untranslated region containing the poly A signal sequence (Vacquier *et al.,* 1990). San Diego and Mendocino are separated by roughly 800 km of coastline, and by Point Conception, an important ecological barrier to larval transport. We tentatively conclude from these limited numbers of individuals that there is no major allelic variation in lysin sequences in the red abalone. The species-specific lysin sequences may thus be well fixed in the extant California species. As pointed out by a reviewer, there are currently no models to explain these data; they represent a genuine mystery for future research to solve.

In the class I major histocompatibility antigens, the antigen recognition site exhibits positive selection, but the different alleles share many conserved structural features making their homology obvious over tens of millions of years of evolution (Hughes and Nei, 1988). Abalone sperm lysins are similar in that strong homology exists among all seven lysins, yet 50% of the positions have species-specific amino acid replacements. Knowing the sequences of these seven sperm lysins begs the question as to the nature of sequence variation in the VE ligands that are the lysin "receptors" of the egg surface. We predict that these ligands will show the same pattern of variation; that is, some regions will be conserved in all species, while others will be hypervariable and species-specific.

Acknowledgments

We thank J. W. Swanson, R. McConnaughey, Dr. D. L. Leighton, and Dr. J. R. Pawlik for abalones, Dr. Wen-Hsiung Li for his computer program, Drs. Masatoshi Nei and Tatsuya Ota for their interest and considerable effort in preparing the data presented as Table III. Discussions with Drs. D. W. Smith, D.-F. Feng, R. F. Doolittle, W. M. Fitch, J. E. Minor, R. J. Britten, S. R. Palumbi, D. A. Powers, and F. Azam are gratefully acknowledged. Supported by NIH Grant HD12986 to V.D.V. and by a Korean Government Overseas Scholarship to Y.-H.L. This paper is dedicated to the memory of Professor Alberto Monroy.

Literature Cited

Baginsky, M. L., C. D. Stout, and V. D. Vacquier. 1990. Diffraction quality crystals of lysin from spermatozoa of the red abalone (*Haliotis rufescens*). *J. Biol. Chem.* **265:** 4958–4961.

Becker, T., K. Weber, and N. Johnson. 1990. Protein-protein recognition via short amphiphilic helices; a mutational analysis of the binding site of annexin II for p11. *EMBO J.* **9:** 4207–4213.

Brown, L. D. 1991. Genetic variation and population structure in the blacklip abalone, *Haliotis rubra*. *Aust. J. Mar. Freshwater Res.* **42:** 77–90.

Chomczynski, P., and N. Sacchi. 1987. Single-step method of RNA isolation by acid guanidinium thiocyanate-phenol-chloroform extraction. *Anal. Biochem.* **162:** 156–159.

Dickerson, R. E., and I. Geis. 1983. *Hemoglobin: structure, function, evolution and pathology.* Benjamin/Cummings Inc. Menlo Park, CA.

Feng, D.-F., and R. F. Doolittle. 1990. Progressive alignment and phylogenetic tree construction of protein sequences. *Meth. Enzymol.* **183:** 375–387.

Fitch, W. M., J. M. E. Leiter, X. Li, and P. Palese. 1991. Positive Darwinian evolution in human influenza A viruses. *Proc. Natl. Acad. Sci. USA* **88:** 4270–4274.

Frohman, M. A. 1990. RACE: rapid amplification of cDNA ends. Pp. 28–38 in *PCR Protocols,* M. A. Innis, D. H. Gelfand, J. J. Sninsky and T. J. White, eds. Academic Press, San Diego.

Giudice, G. 1973. Pp. 162–174 in *Developmental Biology of the Sea Urchin Embryo.* Academic Press, San Diego.

Graur, D. 1985. Amino acid composition and the evolutionary rates of protein-coding genes. *J. Mol. Evol* **22:** 53–62.

Haino-Fukushima, K. 1974. Studies on the egg membrane lysin of *Tegula pfeifferi:* the reaction mechanism of the egg membrane lysin. *Biochim. Biophys. Acta* **352:** 179–191.

Hong, K., and V. D. Vacquier 1986. Fusion of liposomes induced by a cationic protein from the acrosome granule of abalone spermatozoa. *Biochemistry* **25:** 543–550.

Hoshi, M. 1985. Sperm lysins. Pp. 431–462 in *Biology of Fertilization,* C. B. Metz and A. Monroy, eds. Academic Press, San Diego.

Hughes, A. L. 1991. Circumsporozoite protein genes of malaria parasites (*Plasmodium* spp.): evidence for positive selection on immunogenic regions. *Genetics* **127:** 345–353.

Hughes, A. L., and M. Nei. 1988. Pattern of nucleotide substitution at major histocompatibility complex loci reveals overdominant selection. *Nature* **335:** 167–170.

Hughes, A. L., and M. Nei. 1989. Nucleotide substitution at major histocompatibility complex class II loci: evidence for overdominant selection. *Proc. Natl. Acad. Sci. USA* **86:** 958–962.

Hughes, A. L., T. Ota, and M. Nei. 1990. Positive Darwinian selection promotes charge profile diversity in the antigen binding cleft of class I MHC molecules. *Mol. Biol. Evol.* **7:** 515–524.

Janin, J., and C. Chothia. 1990. The structure of protein-protein recognition sites. *J. Biol. Chem.* **265:** 16027–16030.

Kyte, J., and R. F. Doolittle. 1982. A simple method for displaying the hydropathic character of a protein. *J. Mol. Biol.* **157:** 105–132.

Lewis, C. A., D. L. Leighton, and V. D. Vacquier. 1980. Morphology of abalone spermatozoa before and after the acrosome reaction. *J. Ultrastruct. Res.* **72:** 39–47.

Lewis, C. A., C. F. Talbot, and V. D. Vacquier. 1982. A protein from abalone sperm dissolves the egg vitelline layer by a nonenzymatic mechanism. *Dev. Biol.* **92:** 227–240.

Li, W.-H., C.-I. Wu, and C.-C. Luo. 1985. A new method for estimating synonymous and nonsynonymous rates of nucleotide substitution considering the relative likelihood of nucleotide and codon changes. *Mol. Biol. Evol.* **2:** 150–174.

Lindberg, D. R. 1991. Evolution, distribution and systematics of Haliotidae. In *Abalone of the World: Biology, Fisheries and Culture,* A. Shepherd, M. J. Tegner, and S. A. Guzman Del Proo, eds. Blackwells Scientific Publishers, London.

McDonald, J. H., and M. Kreitman. 1991. Adaptive protein evolution at the Adh locus in Drosophila. *Nature* **351:** 652–654.

Nei, M., and T. Gojobori. 1986. Simple methods for estimating the numbers of synonymous and nonsynonomous nucleotide substitutions. *Mol. Biol. Evol.* **3:** 418–426.

O'Rand, M. G. 1988. Sperm-egg recognition and barriers to interspecies fertilization. *Gamete Res.* **19:** 315–328.

Osanai, K., and K. Kyozuka. 1982. Cross fertilization between sea urchin eggs and oyster spermatozoa. *Gamete Res.* **5:** 49–60.

Prince, J. D., T. L. Sellers, W. B. Ford, and S. R. Talbot. 1987. Experimental evidence for limited dispersal of haliotid larvae (genus *Haliotis;* Mollusca: Gastropoda). *J. Exp. Mar. Biol. Ecol.* **106:** 243–263.

Roldan, E. R. S., and R. Yanagimachi. 1989. Cross-fertilization between Syrian and Chinese hamsters. *J. Exp. Zool.* **250:** 321–328.

Sakai, Y. T., Y. Shiroya, and K. Haino-Fukushima. 1982. Fine structural changes in the acrosome reaction of the Japanese abalone, *Haliotis discus. Dev. Growth Differ.* **24:** 531–542.

Shiroya, Y., and Y. T. Sakai. 1983. Fine structure of the spermatozoon in the Japanese abalone, *Haliotis discus. J. Wayo Women's Univ.* **24:** 253–267.

Summers, R. G., and B. L. Hylander. 1975. Species-specificity of acrosomal reaction and primary gamete binding in echinoids. *Exp. Cell Res.* **96:** 63–68.

Summers, R. G., and B. L. Hylander. 1976. Primary gamete binding: the species-exclusive event of echinoid fertilization. *Exp. Cell Res.* **100:** 190–194.

Tanaka, T., and M. Nei. 1989. Positive Darwinian selection observed at the variable region genes of immunoglobins. *Mol. Biol. Evol.* **6:** 447–459.

Vacquier, V. D., K. R. Carner, and C. D. Stout. 1990. Species-specific sequences of abalone lysin, the sperm protein that creates a hole in the egg envelope. *Proc. Natl. Acad. Sci. USA* **87:** 5792–5796.

von Heijne, G. 1985. Signal sequences: the limits of variation. *J. Mol. Biol.* **184:** 99–105.

Yanagimachi, R. 1988a. Mammalian fertilization. Pp. 135–185 in *The Physiology of Reproduction,* E. Knobil and J. Neill, eds. Raven Press, New York.

Yanagimachi, R. 1988b. Sperm-egg fusion. *Curr. Top. Membr. Transport* **32:** 3–43.

Reference: *Biol. Bull.* **182:** 105–108. (February, 1992)

Embryos of *Homarus americanus* are Protected by Epibiotic Bacteria

M. SOFIA GIL-TURNES AND WILLIAM FENICAL

Scripps Institution of Oceanography, University of California, San Diego, La Jolla, California 92093-0236

Abstract. Embryos of the American lobster, *Homarus americanus,* are remarkably resistant to infection by the fungus *Lagenidium callinectes,* a pathogen of many crustaceans. The surfaces of healthy lobster embryos are covered almost exclusively by a single, Gram-negative bacterium, which grows in a dense mosaic pattern. In culture, this bacterium produces a compound that completely inhibits the growth of the pathogenic fungus *in vitro* at 10 mcg/ml. Large-scale fermentation, extraction, and subsequent chromatographic purification led to the identification of the antifungal substance as 4-hydroxyphenethyl alcohol (tyrosol), an antibiotic substance known to be produced by terrestrial fungi.

Introduction

Like several other decapod crustaceans, the American lobster *Homarus americanus* incubates its embryos externally, and each female carries a large cluster comprising up to 60,000 embryos. The embryos are attached to specialized abdominal pleopods until hatching some nine months after fertilization (Cobb and Wang, 1985). Throughout this long brooding period, during which the female is said to be "in berry," the embryos are continuously exposed to water-borne microorganisms. It is remarkable that the seemingly unprotected embryos can survive microbial encroachment. The phycomycetous fungus *Lagenidium callinectes* is a pathogen of many crustaceans. Larvae and juveniles of the American lobster, when kept in unnatural conditions, *e.g.,* in aquaria, are extremely vulnerable to infection by this fungus (Fisher *et al.,* 1976; Nilson *et al.,* 1976; Provenzano, 1985). In contrast, *Homarus* embryos, even when detached from the female, appear to be remarkably resistant to fungal attack. This situation is highly analogous to that recently observed for the estuarine shrimp *Palaemon macrodactylus* (Gil-Turnes *et al.,* 1989). Embryos of *P. macrodactylus* were also impervious to attack by *L. callinectes.* In that study, *Palaemon* embryos were found to host an epibiotic bacterium that produced 2,3-indolenedione, a molecule toxic to *L. callinectes.* The intent of this research was to compare *Homarus americanus* with *Palaemon macrodactylus,* and to determine whether lobster embryos are also protected by an association with symbiotic bacteria.

Received 31 July 1991; accepted 7 October 1991.

Materials and Methods

Embryo infection experiment with Lagenidium callinectes

Gravid female *Homarus americanus* were collected in the vicinity of Martha's Vineyard, Massachusetts, air shipped to California, and maintained in aquaria at the Bodega Marine Laboratory in Bodega Bay, California (UC-Davis). The embryos were observed to be at different stages of development. Ten groups of five embryo clusters each were detached from the females. Each cluster was rinsed with three aliquots of sterilized seawater and subsequently suspended from a cotton thread in aerated 125 ml Erlenmeyer flasks containing 75 ml of sterile seawater. A liquid suspension of *Lagenidium callinectes* was prepared by homogenizing a 0.5 cm diameter agar core of fungal hyphae in 10 ml of 2216 Difco Marine Broth medium. The fungus grew for one week, and the culture was then shaken vigorously to break up the hyphae. Aliquots of 1 ml of this thick suspension were added to each experimental flask. Addition of fungal culture was repeated after the fifth day on a daily basis for a period of two weeks.

Isolation and culture of associated bacteria

In a typical experiment, five embryos from each animal were homogenized in an autoclaved tissue grinder with 10 ml of sterile seawater. One drop of the homogenate, and of 1/10 and 1/100 dilutions, were plated on Difco 2216 Marine Agar plates. Colonies were removed and subcultured after 1–3 weeks. Although three or four morphologically variable colonies were generally observed, one distinct bacterium (SGT-76), a salmon-colored, slow-growing (at 21°C), Gram-negative rod, was consistently obtained. In liquid culture, this strain inhibited the growth of *L. callinectes*. Antifungal testing was performed by cutting agar cores, 0.5 cm in diameter, from lawns of the pure bacterium and placing them on agar plates approximately 1 cm from agar cores containing radiating hyphae of *L. callinectes*. Because of the inhibition observed, this bacterium was selected for subsequent chemical studies.

Extraction and purification of the antifungal compound

The Gram-negative, salmon-colored bacterium, SGT-76, was cultured, at 21°C, in a 16-l carboy using a medium composed of 3 g BactoPeptone (Difco) and 5 g yeast extract per liter of seawater. The culture grew, with aeration, for three weeks. The final pH of the medium was 8.8. The entire culture was extracted twice with 4 l ethyl acetate. After evaporation of the combined solvents, the remaining crude extract was fractionated by silica-gel vacuum flash chromatography using variable amounts of ethyl acetate in isooctane. The antifungal activity of each fraction was determined by placing 0.5 mg of each dry fraction onto a 0.5 cm paper disk and placing the disk at the edge of fungal growth. The active compound eluted with 80% ethyl acetate/isooctane. Final purification of the antifungal compound was achieved by size exclusion chromatography on Sephadex LH20 using a mixture of hexane/methylene chloride/methanol (2:5:1). The purified compound was characterized by infrared spectroscopy (IR), by high-resolution mass (HRMS) and by ^1H and ^{13}C nuclear magnetic resonance spectrometry (NMR).

Scanning electron microscopy

Embryos were fixed in 2.5% glutaraldehyde in 3% saline solution for a minimum of 24 h. After three rinses in 3% saline solution (15 min), each specimen was transferred to a solution of 1% osmium tetroxide in 3% saline solution for nine minutes. Specimens were then stored in saline solution overnight and subsequently dehydrated using an acetone/distilled water sequence: 35% for 15 min, 50% for 15 min, 75% for 30 min, 95% for 1 h, and 100% ethanol for 12 h. Critical point drying was done under CO_2 and the gold coating thickness was 300 Å. Electron micrographs were obtained with a Hitachi Model 539 SEM. Pure bacterial films were prepared as follows: a drop of a 3-day liquid culture was deposited on a small millipore filter (0.25 μ pore size) placed on an agar plate. As soon as growth was visible, the specimens were fixed in 3% formaldehyde and 3% glutaraldehyde in 0.2 *M* sodium cacodylate trihydrate buffer (pH 7.4) for 1 h and then washed three times for 5 min in 0.2 *M* cacodylate solution. The specimens were then transferred to 2% osmium tetroxide in 0.2 *M* cacodylate solution for 1 h, and subsequently rinsed six times for 5 min in 0.2 *M* cacodylate solution. After dehydration using a sequence of ethanol/distilled water treatments for 10 min each, the specimens were critical-point dried under CO_2, coated with gold (300 Å), and micrographs obtained with a Hitachi Model S450A SEM.

Results

After 18 days and ten additions of fungal culture, *H. americanus* embryos appeared healthy and free of fungal infection. The visible organ anatomies and heartbeat rates of the treated embryos were identical to those of the controls. Scanning electron micrographs showed that the embryonal surface was covered by an almost monoculture of a rod-shaped bacterial strain (Fig. 1A). Some of the embryos, at different stages of development, were occasionally found to have very sparse coverage by three morphologically different bacteria (Fig. 1B), in addition to the rod-shaped strain. Older embryos, near hatching, were consistently observed to possess dense coverage by an almost monoculture of the rod-shaped bacterium (Fig. 1C).

Replicate inoculations of embryo homogenates on Marine Agar plates resulted in the isolation of a maximum of four, but usually fewer, strains of bacteria. One of the strains (SGT-76), which was consistently isolated, was inhibitory to *L. callinectes*. This bacterium, a Gram-negative rod insensitive to penicillin, was a pale salmon-colored strain, and it was extremely slow growing on agar plates and in liquid medium. For reasons unknown, the pH of the culture medium seemed to rise to 8 or more during fermentation. This rise in pH could provide a possible explanation for the poor growth observed. Scanning electron micrographs of this bacterium, grown on millipore filters, showed that the cells were identical in size and shape, and had an identical growth pattern to those observed on the surface of the natural embryos (Fig. 1D).

An antifungal compound produced by the bacterial strain grown in liquid medium was isolated and identified as tyrosol, 4-hydroxyphenethyl alcohol (Fig. 2). The active compound was isolated as a viscous oil which showed the following spectral characteristics: IR (film): 3400, 3150 cm^{-1}; HRMS requires 138.04 for $C_8H_{10}O_2$, found 136.06; ^1H NMR, 200 MHz (acetone-d_6): 7.0 (d, 2 H, J = 8.6 Hz), 6.6 (d, 2 H, J = 8.6 Hz), 3.7 (t, 2 H), 2.7 (t, 2 H);

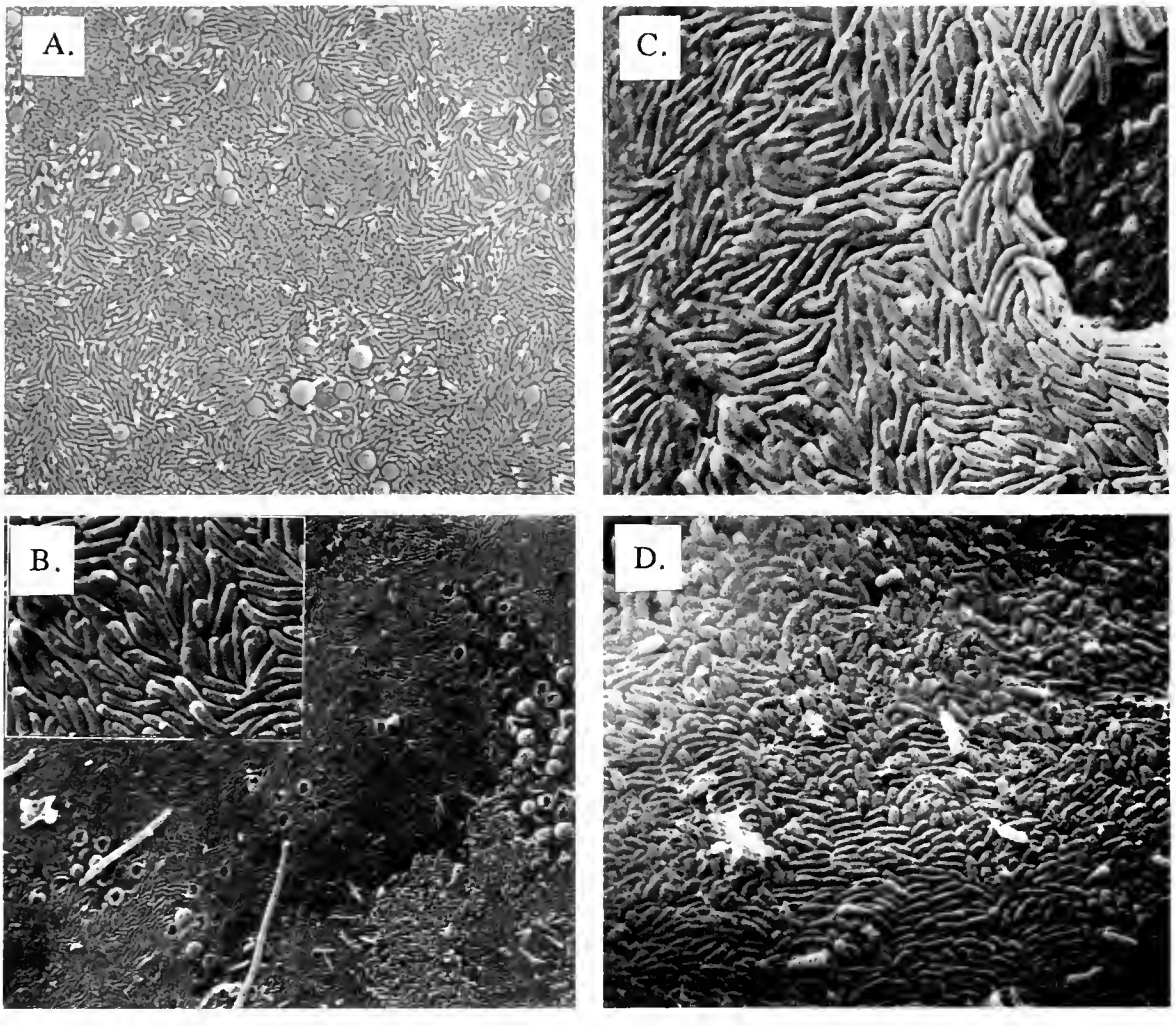

Figure 1. Scanning electron micrographs of healthy embryos of *Homarus americanus* under various conditions. (A) Surface of embryo after exposure to the fungus *Lagenidium callinectes*, illustrating the lack of fungal attachment (1250×). (B) Surface of embryo showing the coverage by the colonial rod morphotype and the other three types occasionally found (1000×). (C) Surface of embryo, at near full gestation, showing extensive and thick coverage by the rod-type bacterium (5000×). (D) Micrograph of the pure bacterium grown on a millipore filter (2000×).

^{13}C NMR, 200 MHz (acetone-d_6): 155.0, 131.0, 130.0, 115.5, 115.4, 63.8, 39.1 (Fig. 2). All chemical and spectral data were identical to those from the commercially-available 4-hydroxyphenethyl alcohol (tyrosol, Aldrich #18,825-5). Tyrosol effectively inhibited growth of *L. callinectes* in liquid culture at a concentration of 10 mcg/ml. In agar plate assays, 100 mcg tyrosol per disk resulted in an 8 mm zone of fungal inhibition.

Discussion

All the embryos observed were covered largely by a single, rod-shaped bacterium, distinguishable from other types by its characteristic dense, mosaic-like growth pattern. The oldest embryos had the thickest coverage by this particular strain, thus health and successful development appear to be related to the degree of bacterial coverage. Harper and Talbot (1984), who investigated embryos of several *Homarus* species to determine if the presence of epibiotic bacterial flora was related to loss of embryos from the pleopods, also observed four bacterial morphotypes. Their bacteria appear to be morphologically identical to those described in this article, including one that they described as a "colonial rod." They found that embryos from wild born and wild spawned *H. americanus* were heavily covered by bacterial rods, and that these embryos were successfully retained by the adult until hatching. Based upon the repetitive isolation of the salmon-colored bacterium (SGT-76) from healthy embryos, and its highly characteristic mosaic growth pattern on natural

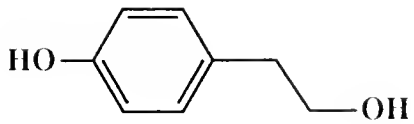

4-hydroxyphenethyl alcohol

"tyrosol"

Figure 2. Chemical structure of the antifungal metabolite 4-hydroxyphenethyl alcohol.

surfaces and on filters, we believe that this bacterium is the natural epibiont of *Homarus* embryos. At the same time, we recognize that this proposal will be difficult to rigorously prove.

The antifungal compound produced by bacterium SGT-76, 4-hydroxyphenethyl alcohol, or tyrosol, has previously been reported as a natural product from two fungal species that are involved in symbiotic associations with plants (Stoessl, 1969; Claydon *et al.*, 1985). In an apparently similar adaptation, those fungi seem to protect their hosts against invasion by pathogenic fungi.

Protection of embryos by epibiotic bacteria has been shown previously (Fisher, 1983; Gil-Turnes *et al.*, 1989) for the caridean shrimp *Palaemon macrodactylus*, also an external brooder. In the present study, the association of *H. americanus* embryos with a Gram-negative, rod-shaped bacterium suggests a similar adaptation in which a vulnerable host is protected against pathogenic microorganisms by symbiotic bacteria. At least one explanation for the resistance of *Homarus* embryos is the bacterial production of the antifungal compound tyrosol in nature. Although tyrosol is only a moderately potent antifungal agent, the dense bacterial coverage observed would easily result in high levels of the compound at the embryo surface. Thus, tyrosol could function effectively to reduce fungal encroachment.

The antifungal agents isolated from crustacean-associated bacteria to date (tyrosol and 2,3-indolinedione from a *Palaemon macrodactylus*-associated bacterium), are simple molecules with only modest potencies. These molecules appear to be unusually effective against *Lagenidium*, however, perhaps suggesting that they are targeted to this and related fungal pathogens.

Studies of the bacterial symbionts of commercially important marine invertebrates could provide important information leading to the control of disease under aquaculture conditions. Indeed, there is a significant need to develop inexpensive and environmentally safe antifungal agents for this specific application. The simple molecules discussed here, which appear to be derived from the common amino acids tyrosine and tryptophane, should be considered in this application.

Acknowledgments

We would like to thank Ashley Yudin, William S. Fisher, Wallis H. Clark, and Prudence Talbot for their assistance in this study. The staff and students at the Bodega Marine Laboratory were extremely helpful and their cooperation is gratefully acknowledged. The work is mainly a result of research sponsored by NOAA, National Sea Grant College Program, Department of Commerce, under grant #NA85AA-D-SG140, project number R/MP-39, through the California Sea Grant Program, and in part by the California State Resources Agency. Portions of this research were also supported by the National Institutes of Health, NCI, under grant CA44848. The U. S. Government is authorized to reproduce and distribute for governmental purposes.

Literature Cited

Claydon, N., J. F. Grove, and M. Pople. 1985. Elm bark beetle boring and feeding deterrents from *Phomopsis oblonga*. *Phytochemistry* **24**(5): 937–943.

Cobb, J. S., and D. Wang. 1985. Fisheries biology of lobsters and crayfishes. Pp. 168–248 in *The Biology of Crustacea*. Vol. 10, Academic Press, New York.

Fisher, W. S. 1983. Eggs of *Palaemon macrodactylus*: II. Association with aquatic bacteria. *Biol. Bull.* **164:** 201–213.

Fisher, W. S., E. H. Nilson, L. F. N. Follett, and R. A. Shleser. 1976. Hatching and rearing lobster larvae (*Homarus americanus*) in a disease situation. *Aquaculture* **7:** 75–80.

Gil-Turnes, M. S., M. E. Hay, and W. Fenical. 1989. Symbiotic marine bacteria chemically defend crustacean embryos from a pathogenic fungus. *Science* **246:** 117–118.

Harper, R. E., and P. Talbot. 1984. Analysis of the epibiotic bacteria of lobster (*Homarus*) eggs and their influence on the loss of eggs from the pleopods. *Aquaculture* **36:** 9–26.

Nilson, E. H., W. S. Fisher, and R. A. Shleser. 1976. A new mycosis of larval lobster (*Homarus americanus*). *J. Invertebr. Pathol.* **27:** 177–183.

Provenzano, A. J., Jr. 1985. Culture of crustaceans: general principals. Pp. 279–280 in *The Biology of Crustacea*, Vol. 10, Economic Aspects: Fisheries Culture. Academic Press, New York.

Stoessl, A. 1969. 8-Hydroxy-6-methoxy-3-methylisocoumarin and other metabolites of *Ceratocystis fimbriata*. *Biochem. Biophys. Res. Comm.* **35**(2): 186–191.

Reference: *Biol. Bull.* **182:** 109–116. (February, 1992)

Are Temperature and Photoperiod Necessary Cues for Encystment in the Marine Benthic Harpacticoid Copepod *Heteropsyllus nunni* Coull?[1]

JUDY WILLIAMS-HOWZE AND BRUCE C. COULL

Department of Biological Sciences and Belle W. Baruch Institute for Marine Biology & Coastal Research, University of South Carolina, Columbia, South Carolina 29208

Abstract. *Heteropsyllus nunni* is a marine copepod that builds a cyst and dwells within it during a period of extended diapause. The field abundance of this copepod has been monitored for 10 years, but nothing is known about the cues that induce and terminate encystment. In the laboratory, different photoperiods and temperatures were tested for their effects on encystment and excystment.

The photoperiod and temperature cues tested neither induced nor inhibited encystment in *H. nunni*. Encystment occurred in all treatments, regardless of temperature or photoperiod, suggesting that internal genetic cues, tied to a specific ontogenetic stage, must be the central causal factor. Copepods in the hot treatments encysted and excysted more rapidly than in the cold. Many copepods in the cold treatment encysted (though later than copepods in the hotter treatments), and most were still within the cyst at the end of the 23-week experiment. There were significantly more males within the full cysts than females. A concurrent field study confirmed the known seasonal patterns in the number of encystments relative to the number of free-living forms; *i.e.*, encystment took place in the summer.

Introduction

A state of dormancy or diapause sometime during development is a common adaptation for a myriad of aquatic, terrestrial, and aerial invertebrates. Many of these invertebrates have developed specialized adaptations that protect against periodic (cyclic or acyclic) harsh environmental conditions, such as dry seasons and extreme high or low temperatures. Diapause and quiescence are two such adaptations. Quiescence is characteristically brief, irregular, and controlled by the effective adverse factors. For example, a cold shock might send an invertebrate into a state of quiescence; *i.e.*, the animal enters and remains in a state of torpor until the temperature rises, causing normal physiological functions to resume. Quiescence is reversible, not fixed to a specific ontogenetic instar, and may be induced repeatedly in the same individual (Andrewartha, 1952; Tauber *et al.*, 1986).

In contrast to quiescence, diapause interrupts the normal metabolic program away from its developmental pathway at a specific ontogenetic stage. Moreover, diapause is not controlled by the direct action of sporadic environmental factors; rather it is cued in advance by some predictable cyclic change in the environment (Andrewartha, 1952; Danks, 1987). Diapause is, by definition, neurohormonally driven (Danks, 1987) and involves a more complicated developmental process that commits the organism to a greater metabolic investment (Tauber *et al.*, 1986). As an alternative to the normal developmental pathway, diapause is favored when the expectation of fitness accruing from active growth and reproduction is less than that from survival in diapause (Cohen, 1970).

Insects are the most extensively studied of the diapausing invertebrates (Tauber and Tauber, 1970; Tauber *et al.*, 1986; Danks, 1987). But copepods also exhibit diverse forms of diapause (Elgmork, 1980; Marcus, 1980; Coull and Grant, 1981; Hairston, 1987), the physical manifestation of the process varying with the order. Of the major free-living orders, the largely planktonic Calanoida produce primarily resting eggs (chitin-covered and desiccant-resistant), although some species of *Calanus* and *Neocalanus* diapause in deep waters as a fifth stage (C-V)

Received 22 July 1991; accepted 31 October 1991.

[1] Contribution No. 892 from the Belle W. Baruch Institute for Marine Biology & Coastal Research.

copepodite (Miller *et al.*, 1991). Diapausing eggs are heavier than the subitaneous (immediately hatching) eggs and will sink to the sediment. They are crucial in the reproductive success of these copepods, as an aid in predator avoidance (Hairston, 1987) and as a mechanism for surviving desiccation during drought (Taylor *et al.*, 1990).

In the Cyclopoida, the individual copepod enters into a state of dormancy at the fourth or fifth copepodite stage (C-IV or V); rarely are resting eggs produced (reported only for *Mesocyclops edax*, Wyngaard, 1988). The diapausing cyclopoids sink to the bottom and remain obscured by mud and detrital coverings (Fryer and Smyly, 1954; Elgmork, 1980; Nilssen, 1980).

Diapausing harpacticoids construct and reside in cysts, typically at the adult stage, but diapause is not common in the Harpacticoida. Most encysting species inhabit fresh water and encyst during summer months (Sarvala, 1979; Coull and Grant, 1981; Nalepa, 1985). Indeed, until the discovery of encysted *Heteropsyllus nunni* Coull (Family Cletotidae) in the marine environment, only freshwater species of the family Canthocamptidae were thought to encyst (Coull and Grant, 1981).

Timing for entering diapause is critical and is integrally linked to reproductive success in copepods (Cohen, 1967, 1970; Taylor, 1980; De Stasio, 1990). This timing is most often cued by photoperiod, temperature, or a combination of both. The production of diapausing eggs by calanoids appears to be controlled by the combined effects of photoperiod (Marcus, 1980, 1982a, b) and temperature (Cooley, 1978; Hairston and Olds, 1984; Marcus, 1987); production may also differ with geography (Hairston and Olds, 1984; Marcus, 1987). In cyclopoids, photoperiod is the cue for induction of diapause (Watson and Smallman, 1971a, b; Elgmork and Nilssen, 1978). The dormant cyclopoid C-IV or C-V stages either overwinter or oversummer, depending on the effect of geography on induction (Elgmork, 1955; George, 1973; Cooley, 1978; Elgmork and Langeland, 1980).

Little is known about the environmental cues that initiate diapause in harpacticoids. Sarvala (1979) determined that a particular combination of photoperiod and temperature were needed to induce encystment and excystment in freshwater *Canthocampus staphylinus*. Changes in this light-temperature regime arrested development of the copepodites, inhibited egg production in mature females, and induced the copepods to produce pre-diapause oil droplets. Exposure to low temperature inhibited encystment in *C. staphylinus*.

Heteropsyllus nunni is a recurring member of the intertidal meiobenthos on South Carolina sandflats (Coull and Grant, 1981). The number of free-living animals, relative to encysted ones, has been monitored for 10 years (Coull, unpub.), but little is known about the biology of this animal related to encystment. The objective of this study was to experimentally investigate the effect of the environmental cues, temperature, and photoperiod, (known to induce diapause in other copepods), on timing, sex ratio, ontogenetic stage specificity, and the number of individuals encysting for the marine harpacticoid copepod *Heteropsyllus nunni*.

Materials and Methods

Laboratory environmental cues experiment

Large numbers of *Heteropsyllus nunni* were collected during January and February, 1990, from an intertidal sand flat at Oyster Landing, North Inlet Estuary, South Carolina, USA (33° 19.0′ N, 79° 11.6′ W). At random sites along the exposed sand flat during low tide, the upper two centimeters of sand containing the copepods were scraped up by hand, placed in a bucket with seawater and transported back to the laboratory in Columbia, South Carolina. Live animals were extracted from the sand using a 3% solution of isotonic magnesium chloride. The magnesium chloride solution was added to small amounts of sand, shaken well, and, within 10 min, all living meiofauna in the sand were anesthetized and then decanted. *H. nunni* were separated from other meiofauna under a stereo dissecting microscope and placed in large petri dishes containing filtered artificial seawater (ASW). All copepods were held in an incubator at 18°C, with 16:8 h day:night cycle until sufficient nauplii had hatched. A sand substrate for culture was prepared as follows. Clean sand (300–500 μm size fractions; obtained from the sand flat at Oyster Landing) in a 500 ml flask, was autoclaved, covered with F/2 medium solution (Guillard, 1972), and autoclaved again for 10 min. The sand and medium were then inoculated with 10 mls of *Phaeodactylum tricornutum*. Within a week, *Phaeodactylum* was growing on the sand grains, providing an adequate grazing substrate for *H. nunni*. The culture dishes could then be prepared as follows. The substrate of sand and algae was removed from the flask with a sterile pipet, washed with filtered seawater to remove the excess culture medium and placed in sterile plastic petri dishes with sterile-filtered ASW (salinity 29–30‰). Nauplii were held in 35 × 10 mm size petri dishes, and all other stages were held in 60 × 20 mm size dishes. All experimental dishes with copepods were established during the same day.

The experiments were conducted in two incubators, one set at the ambient winter temperature (10°C) in North Inlet, South Carolina, and one set at the ambient early summer temperature (20°C). Early summer (May, June) is the time of encystment for *H. nunni* in the field (Coull and Grant, 1981). Within these incubators were black boxes within which a long night:short day (15 h dark:9 h light) regime could be simulated in isolation from the other portion of the incubator which was set for long day:

short night (15 h light:9 h dark). Thus, the four treatment conditions were: cold-short day (Cold-SD), cold-long day (Cold-LD), hot-short day (Hot-SD), and hot-long day (Hot-LD).

The black boxes, each with a hinged lid, were constructed of thick (1.85 cm) styrofoam. A slit was cut in the top, and a time-controlled fluorescent light was placed above the slit. The light and box were completely covered with a double layer of black cloth, and cardboard was taped under the upper black box separating it from the lower open light source. We tested the black box for possible light entrance by placing a 35 mm camera containing 400 ASA film in the box and exposing the film using a delayed automatic timer for 6 exposures. The same camera and film were then taken to a photographic darkroom and another six frames were exposed using the same times and settings. There were no differences between the frames exposed within the black box and those in the darkroom, indicating no significant light leakage into the boxes.

Replicate sets of life-history stages (Table I), chosen to represent a wide range of age classes, were exposed to the environmental conditions constituting each experimental treatment. Each ontogenetic stage was isolated in a separate petri dish so that their growth and encystment could be compared. The number of copepods in each dish was determined by the availability of that life-history stage at the beginning of the experiment.

Nauplii, copepodites, or adults obtained from the field might have been pre-cued by their environments to encyst before the initiation of the experiment. To preclude this, gravid females and females with ovaries full of egg masses were used in each treatment so that hatching nauplii would be exposed only to the temperature and photoperiod regime specified by the experimental protocol.

The photoperiod timers in the incubators were coordinated so that daylight would occur in all treatments from 12 noon to 6 pm daily, allowing all feeding, changing of water, observations, and counts to be made during this "daylight on" time. All copepods were fed concentrated drops of the alga *Isochrysis* sp., or additional sand with *P. tricornutum* (as needed). Water was changed at least once a week, more frequently in the smallest dishes. Excess algal clumps, feces, and detritus were removed by pipet weekly. For each dish, weekly counts were made of mortality, the number of full cysts and empty cysts, the stage of development (of nauplii), the number of females with eggs, females with developing eggs in their ovaries, and mating pairs.

The experiment was initiated on March 15, 1990, and was terminated on August 19, 1990; 23 weeks. At the end of the experiment, all of the dishes were removed from the incubators, and 10% formalin with Rose Bengal was added to each dish to preserve all copepods. Every individual was counted and categorized as to life-history stage (nauplii, copepodite, adult, male, female). Each cyst was noted as being full or empty, and, for all full cysts, the copepod was removed, dissected, and sexed.

Table I

*Number of individuals representing each of five life-history stages of copepods (*Heteropsyllus nunni*) placed within each of four experimental treatments*[a]

Stage	No. in dish	Replicate dishes
Nauplii	20	5
Male	5	3
Females (no eggs; full ovaries)	5	3
Gravid females (with eggs attached)	5	3
Post-gravid females[b]	4	3

[a] The experimental treatments are defined in the legends to Table II and Figure 1.

[b] Females removed from isolated dishes that contained nauplii.

Field population study

A field study was conducted on the same intertidal sand flat at Oyster Landing, North Inlet, South Carolina (USA) from which *H. nunni* had been obtained for the laboratory experiments.

Quantitative collections were made by random hand coring with a 2.54 cm diameter core tube in the upper 10 cm of sediment during low tide. Eight samples were taken monthly for one year (Sept. 1988–Aug. 1989). All samples were immediately preserved with 10% buffered Formalin with Rose Bengal added. In the laboratory, copepods were extracted via elutriation where sand was placed in a separation flask and water was gently bubbled up through the sand. This loosened and released the copepods from the sand grains, allowing them to be captured in the outflowing water. Individuals of *H. nunni* were counted, sexed and life-history stage recorded.

Statistical analysis

Free-living and encysted copepod abundance within the four experimental treatments was analyzed separately by the General Linear Model (GLM) procedure (1-way ANOVA, treatment *vs.* final abundance), and Tukey's multiple comparison procedure of SAS to compare treatment effect (SAS Institute, 1985). Data for all of the life-history stage within a treatment were pooled, because the developmental rates of the representatives of each stage were indistinguishable.

Field data on free-living copepods (males and females) and encysted copepods were $\log_{10}(n + 1)$ transformed to meet the assumptions of normality and homoscedasticity. The seasonal abundance of *H. nunni* in the field, by

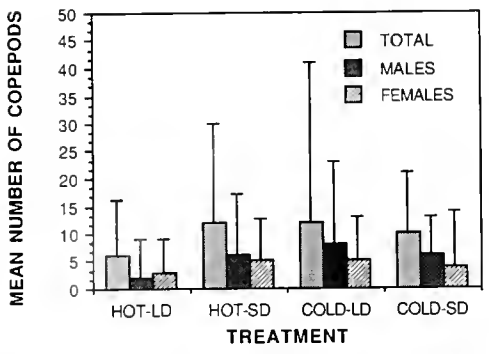

Figure 1. The effect of temperature and photoperiod regimes on the mean number of free-living copepods (*i.e.*, not encysted). The duration of the experiment was 23 weeks. Treatments: Cold, 10°C; Hot, 20°C; LD (long day), 15 h light:9 h dark; SD (short day), 9 h light:15 h dark. Error bars are one standard deviation of mean.

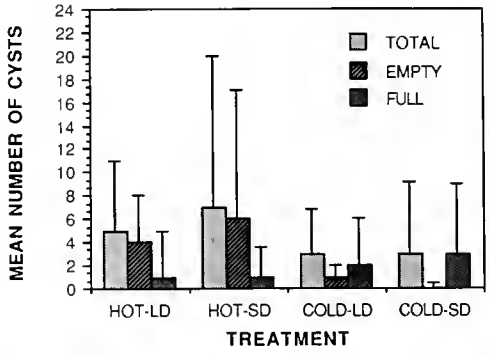

Figure 2. The effect of temperature and photoperiod regimes on the mean number of full and empty cysts. The duration of the experiment was 23 weeks, and treatment conditions are as listed in the legend to Figure 1. Error bars are one standard deviation of mean.

month, as well as the number of females compared to males, were also compared using the GLM procedure (1-way ANOVA, month *vs.* total) and Tukey's multiple comparison procedure. All significance levels were set at alpha < 0.05.

Results

Laboratory environmental cues experiment

A. Free-living Heteropsyllus nunni. The final mean numbers of free-living *H. nunni* in the four experimental treatments were not significantly different ($P = 0.50$; 1-way ANOVA, final number of free-living animals *vs.* treatment). Although the total mean in the Hot-SD treatment was slightly more than double the mean in the Hot-LD (Fig. 1), the great variability within treatment masked any significant difference. There were no significant differences between the number of free-living males compared to free-living females among treatments, again due to high variability within treatment.

B. Encysted H. nunni. Sixteen culture dishes within each treatment represented five different life-history stages. The frequency of encystment events (at least one cyst in a dish) was surprisingly high (69%) in all four treatments. Frequency of encystment events in all dishes (16 total) by treatment was: Hot-SD = 11/16; Hot-LD = 11/16; Cold-SD = 11/16; Cold-LD = 12/16, indicating copepods encysted in most of the five life-history stages originally placed within the dish. The copepods within the cysts were all C-VI, unmated adults that had developed from nauplii in each dish (regardless of the ontogenetic stage placed in the culture dishes). There were no reproductive or post-gravid females, no mated males, and no stages younger than C-VI encysted.

There were significantly more empty cysts compared to full cysts at the end of the experiment ($P = 0.018$) over all four treatments (Fig. 2). Empty cysts in Hot-SD ($\bar{x} = 6.3$), Cold-LD ($\bar{x} = 0.75$), and Cold-SD ($\bar{x} = .37$) conditions were significantly different from each other, but Hot-SD and Hot-LD ($\bar{x} = 3.6$) were not (Tukey's multiple comparison test, $P < 0.05$). There were 48 encystment events in the Cold-LD treatment, 51 in the Cold-SD treatment, 81 in the Hot-LD treatment, and 117 in the Hot-SD treatment, but there was no significant difference ($P = 0.39$) in mean numbers of cysts between treatments (Fig. 2).

The time to first encystment for the Hot treatments was 37 days and 67–77 days for the Cold treatments (Table II); thus, although encystment was delayed in the cold, it was not inhibited. This delay resulted in more cysts with the copepod still inside compared to the Hot treatments, thus, more full cysts than empty cysts at the termination of the experiment (Fig. 2). The number of full cysts among treatments was not significantly different, due, again, to high dish to dish variability.

C. Proportion of males to female H. nunni *in cysts.* There were significantly more ($P = <0.001$) males than

Table II

Time to first encystment for nauplii in four experimental treatments

Treatment*	Begin date	Date 1st encystment observed	Days from nauplii to encystment	No. cysts 1st date observed
Cold-long day	3/15/90	6/1/90	77	3
Cold-short day	3/15/90	5/23/90	67	2
Hot-long day	3/15/90	4/23/90	37	35
Hot-short day	3/15/90	4/23/90	37	9

* Treatment: Cold, 10°C; Hot, 20°C; long day, 15 h light:9 h dark; short day, 9 h light:15 h dark.

Numbers of cysts are totals found on 1st date of encystment. All replicates are combined for each treatment.

females in cysts in all treatments (Fig. 3); mean male/female ratio = 3.5/1.

Field population study

A. Number of free-living H. nunni*/number of cysts over 12 months.* There was a significant difference ($P = <0.001$) between mean copepod abundance by month (Fig. 4). January and February had significantly more free-living *H. nunni* than other months (April–November); March was not significantly different from Jan–Feb or Apr–Nov (Tukey's multiple comparison procedure). Free-living *H. nunni* reached maximum abundance in winter and were low in number, then absent as summer progressed. The mean number of full cysts throughout the year was not significantly different between months, because the number of cysts in the cores was extremely low (Fig. 4). Cysts were most abundant in summer, when free-living *H. nunni* were absent from the core samples (Fig. 4).

B. Free-living males and females over 12-month study. The mean number of males compared to females was significantly different over the one-year sampling period (males and females both with $P = <0.001$) (Fig. 5). The number of males was slightly greater than females in October and November (time of emergence from cysts). The population was dominated by females from December to April, the period of peak egg production (Fig. 5). Free-living males and females disappeared in summer during peak encystment time (May, June, July).

Discussion

In the field, *H. nunni* encysts in early summer (day-length 14 h, temperature 15–18°C). In the laboratory, therefore, we expected *H. nunni* not to encyst under winter (*i.e.*, cold-short day) conditions. Nevertheless, encystment occurred in all treatment conditions and was not inhibited by the dark, cold environment (9 h light at 10°C). Encystment in *H. nunni* must be genetically induced, because sexually immature adults encysted regardless of the surrounding temperature or photoperiod regime. Our results are in direct contrast to those of previous research, which indicate that photoperiod and temperature are necessary mechanisms for inducing copepod diapause, *e.g.*, for calanoids (Marcus, 1980, 1982a, b, 1987; Hairston *et al.*, 1990), cyclopoids (Watson and Smallman, 1971a, b; Elgmork and Nilssen, 1978), and freshwater harpacticoids (Sarvala, 1979). Additionally, no female *H. nunni* dissected from cysts had attached spermatophores, egg sacs, or maturing ova, nor did any males have developing spermatophores. Because mated adults would show at least some of these characteristics, the encysted individuals must not have mated. In *Canthocamptus staphylinus*, however, females with attached spermatophores encyst (Sarvala, 1979), and fertilized, adult females of *Cyclops strenuus* diapause (Naess and Nilssen, 1991).

Although temperature and photoperiod apparently did not specifically cue encystment, they did affect the developmental rates of *H. nunni*. The most significant effect was on nauplii, because naupliar development to adult, and then to encystment, took twice as long in cold treatment (67–77 days) as it did in the hot treatments (37 days) (Table II). In the field, *H. nunni* mate and produce eggs during the winter months. Nauplii hatch from the eggs in late winter or early spring (March, April) when temperatures in the estuary are still quite cool. Therefore, the cold treatments were probably closer to the normal field conditions in temperature and early naupliar devel-

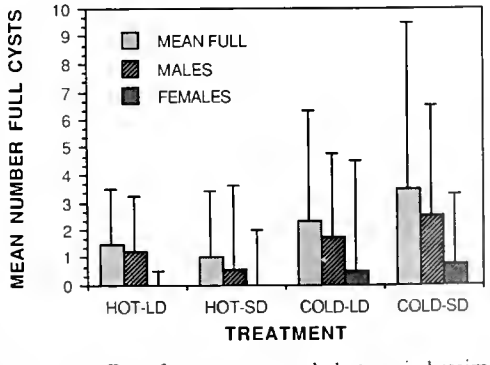

Figure 3. The effect of temperature and photoperiod regimes on the mean number of male compared to female copepods after removal from the full cysts. The duration of the experiment was 23 weeks, and treatment conditions are as listed in the legend to Figure 1. Error bars are one standard deviation of mean.

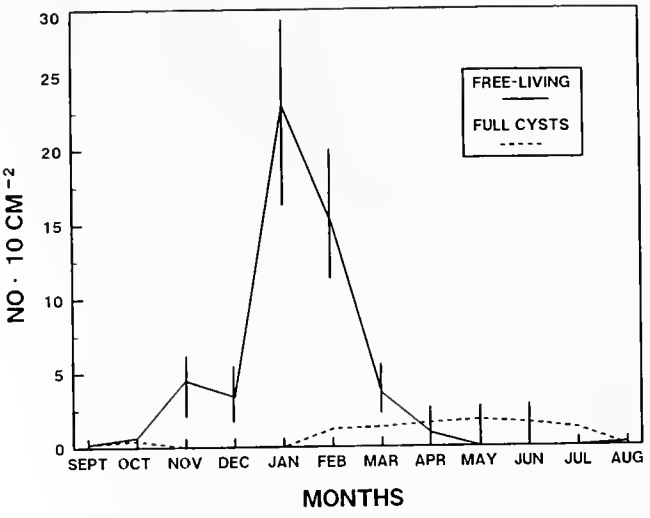

Figure 4. Mean number of encysted and free-living copepods taken from the cores during the field study. Core samples were taken once a month for twelve months. Number per 10 cm^2 is the unit of density for meiobenthos, in contrast to number per m^2 used for macrobenthos. Error bars are one standard deviation of mean.

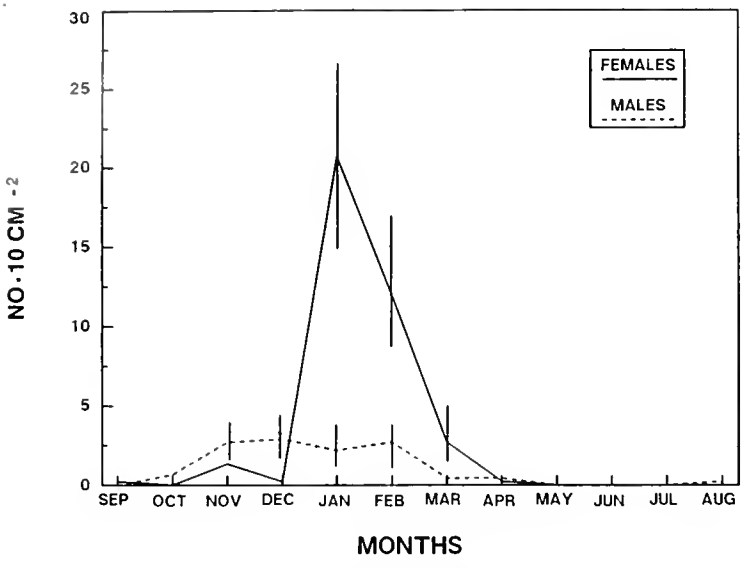

Figure 5. Mean number of free-living male and female copepods taken from the cores during the field study. Core samples were taken once a month for twelve months. Number per 10 cm^2 is the unit of density for meiobenthos, in contrast to number per m^2 used for macrobenthos. Error bars are one standard deviation of mean.

opment than the hot treatment regime. Copepodites normally reach adulthood in early summer (April–May) in the field, and encyst during summer months only (Fig. 4). Greater total number of cysts in the hot treatments (81 Hot-LD, 117 Hot-SD) *versus* the cold treatments (48 Cold-LD, 51 Cold-SD) were probably due to increased rates of development. The high number of encystment events in the hot-short day was unexpected, particularly because longer photoperiod has been implicated as the main cue triggering summer dormancy in other copepods (Watson and Smallman, 1971a, b; Sarvala, 1979).

Not all of the sexually immature adult *H. nunni* encysted. In most treatment dishes there were mating and reproducing free-living copepods throughout the entire 23 weeks, along with encysted individuals; this was unexpected, because no free-living forms have been found in the summer (Coull and Grant, 1981, and Fig. 5). Coull and Grant (1981) hypothesized that the free-living population either moved to another area, or all members encysted. The calanoid copepod *Diaptomus sanguineus* produces diapausing and subitaneous eggs sequentially during the same reproductive period, and Hairston and Munns (1984) suggested that it was using a bet-hedging strategy (*sensu* Stearns, 1976), anticipating that an environmental catastrophe would not occur or would be less severe than expected. Reproductive success could then be insured in either situation. In harpacticoid and cyclopoid copepods, such a bet-hedging strategy is generally not used, because the diapausing stage is not an egg, but an individual (*i.e.*, either copepodite or adult). If the adult is the diapausing organism insuring reproductive success (as opposed to dispersed diapausing eggs), a bet-hedging strategy would not be expected (Hairston, 1987). However, we found free-living harpacticoids along with the encysted ones, as did Cole (1953) and Sarvala (1979). Perhaps these free-living forms are also bet-hedgers, taking the chance that they will not be negatively affected in their non-diapause state. Our inability to find such proposed bet-hedgers in the field (*i.e.*, free-living *H. nunni* in the summer) may be a function of them occurring in very low abundance.

In our laboratory experiment there were consistently more males than females, both in cysts and free-living. These findings are very different from those of Sarvala (1979), who observed that *Canthocamptus staphylinus* males were absent from cysts. However, in the cyclopoid *Cyclops vicinus* and *Thermocyclops crassus*, more males than females emerge from diapause (George, 1973, and Maier, 1989, respectively). The initial data on *H. nunni* (Coull and Grant, 1981) indicated a female to male ratio in the cysts of 2.3:1, but over an 11-year sampling period, the female-to-male ratio for free-living *H. nunni* was 1.6:1 (Coull and Dudley, 1985). Males within cysts outnumbered females by at least 2:1 in the laboratory (Fig. 3). For copepods, a sex ratio other than 1:1 indicates a shift in sexual selection pressure. Male dominance in this experiment may be a laboratory effect, as excessive homozygosity leads to shifting of the sex ratio in favor of males (Hicks and Coull, 1983). An imbalanced ratio could be due to homogeneity of the environment (*i.e.*, small culture dishes), which favors inbreeding, and results in a more homogeneous population. Population density can also

influence sex ratios. Hicks (1984) found that male *Parastenhelia megarostrum* dominated only when the population density was high; in lower densities, females dominated. Another potential influence of gender density is "sexual switching." Hicks and Coull (1983) cite reports of genetic males becoming phenotypic females in response to low population density. In our study, *H. nunni* males dominated over females during Sept–Nov (low density population, 4 per 10 cm^2). In December, the female population increased rapidly from 2 to 23 per 10 cm^2, but the male population remained at previous abundances (Fig. 5). If there were no sex-switching, perhaps this phenomenon was related to developmental differences between males and females.

In certain harpacticoids, males mature much faster than females (Fleeger and Shirley, 1990). Samples taken in early spring had mostly males and copepodites (stages 4–5) and the number of males within the population remained constant; as the copepodites developed, more females appeared, and eventually there were more females than males. Perhaps a similar developmental sequence occurs in *H. nunni,* where males develop, encyst, and excyst earlier than the females, biasing the ratio towards males as the copepods emerge from the cysts. As other individuals mature (females), the ratio then switches to female dominance (Fig. 5).

Biotic factors that induce diapause were not directly tested, but two possibilities exist. Because *H. nunni* cysts are not resistant to desiccation (they collapse around the copepod and dry up when removed from water), perhaps the cyst is used to avoid competition or predation. Where *H. nunni* occurs in South Carolina, the five most abundant copepods (80% of all copepods) have high maximum densities (1056 per 10 cm^2/per) and reproduce from summer through fall (Coull and Dudley, 1985). *Heteropsyllus nunni* reproduces and reaches its maximum population density in winter. In summer months, when other harpacticoids are at their peak, *H. nunni* is within its cyst, dormant. Competition avoidance could possibly be inducing the encystment diapause in *H. nunni.*

Large numbers of juvenile fish that selectively prey on harpacticoid copepods (Ellis and Coull, 1989; Nelson and Coull, 1989) occupy South Carolina estuaries in the spring and summer. A female *H. nunni* carrying eggs is highly visible. The egg sac is large (40+ eggs) and has a bluish tint, and thus *H. nunni* is a susceptible prey item. By reproducing in the winter when there are few juvenile fish, *H. nunni* is less available to predation. As the abundance of juvenile fish increases in the summer, *H. nunni* encysts. *H. nunni* cysts are cryptic (Coull and Grant, 1981) *i.e.,* they are indistinguishable from the surrounding sand. Such camouflage would seem efficient in avoiding visual predators. While there is no field evidence that *H. nunni* is sought as a prey item by young fish, only one fish (*Leiostomus xanthurus*) that consumes mud dwelling harpacticoids has been thoroughly studied from the locale (Feller *et al.,* 1990). Predation avoidance also could be influencing the encystment diapause of *H. nunni.*

We have tested whether temperature and photoperiod (generally important cues for copepod diapause) were significant factors inducing encystment in *H. nunni.* Although cold temperatures slowed development (increasing time to encystment) and hotter temperatures accelerated naupliar development (decreasing time to encystment), photoperiod appeared to have no impact on development or encystment. In the past, perhaps, temperature and photoperiod were important environmental factors cuing these copepods of an impending catastrophe. Now, however, the interactions that induce diapause may be so evolved that the specific catastrophe that favored encystment in the past is obscure. We conclude that for *H. nunni,* the encysted diapause state is a relic adaptive response that has become internalized into a developmental necessity.

Acknowledgments

We gratefully acknowledge Dr. G. T. Chandler for assistance in culturing *H. nunni,* Drs. R. J. Feller, S. E. Stancyk, M. B. Thomas, and N. Watabe, Mrs. B. W. Dudley, and two anonymous reviewers for constructive comments on earlier drafts of this manuscript. This research is part of a dissertation submitted by Judy Williams-Howze as partial fulfillment of the requirements for the Ph.D. degree in Biological Sciences at the University of South Carolina. It was supported by grants in aid from Sigma Xi, the Slocum-Lunz Foundation (JW-H) and the Biological Oceanography section of the National Science Foundation, Grant OCE 89-16255 (BCC).

Literature Cited

Andrewartha, H. G. 1952. Diapause in relation to the ecology of insects. *Biol. Rev.* **27:** 50–107.

Cohen, D. 1967. Optimizing reproduction in a randomly varying environment when a correlation may exist between the condition at the time a choice has to be made and the subsequent outcome. *J. Theor. Biol.* **16:** 1–14.

Cohen, D. 1970. A theorectical model for the optimal timing of diapause. *Am. Nat.* **104:** 389–400.

Cole, G. A. 1953. Notes on copepod encystment. *Ecology* **34:** 208–211.

Cooley, J. M. 1978. The effect of temperature on the development diapausing and subitaneous eggs in several freshwater copepods. *Crustaceana* **35:** 27–34.

Coull, B. C., and J. Grant. 1981. Encystment discovered in a marine copepod. *Science* **212:** 342–344.

Coull, B. C., and B. Dudley. 1985. Dynamics of meiobenthic copepod populations: a long-term study (1973–1983). *Mar. Ecol. Prog. Ser.* **24:** 219–229.

Danks, H. V. 1987. *Insect Dormancy: An Ecological Perspective. Biol. Sur. Can. Mono.* **1:** 439 pp.

DeStasio, B. T. 1990. The role of dormancy and emergence patterns in the dynamics of a freshwater zooplankton community. *Limnol. Oceanog.* **35:** 1079–1090.

Elgmork, K. 1955. A resting stage without encystment in the annual life cycle of the freshwater copepod *Cyclops strenuus strenuus. Ecology* **36:** 739–743.

Elgmork, K., and J. P. Nilssen. 1978. Equivalence of copepod and insect diapause. *Verh. Inter. Verein. Limnol.* **20:** 2511–2517.

Elgmork, K. 1980. Evolutionary aspects of diapause in freshwater copepods. Pp. 411–417 in *Evolution and Ecology of Zooplankton Communities,* C. Kerfoot, ed. University Press, New England.

Elgmork, K., and A. Langeland. 1980. *Cyclops scutifer* Sars—one and two-year cycles with diapause in the meromictic lake Blankvatn. *Arch. Hydrobiol.* **88:** 178–201.

Ellis, M. E., and B. C. Coull. 1989. Fish predation on meiobenthos: field experiments with juvenile spot (*Leiostomus xanthurus*). *J. Exp. Mar. Biol. Ecol.* **130:** 19–32.

Feller, R. J., B. C. Coull, and B. Hentschel. 1990. Meiobenthic copepods: tracers of where juvenile *Leiostomus xanthurus* (Pisces) feed? *Can. J. Fish. Aquat. Sci.* **47:** 1913–1919.

Fleeger, J. W., and T. Shirley. 1990. Meiofaunal responses to sedimentation from an Alaskan spring bloom. II. Harpacticoid population dynamics. *Mar. Ecol. Prog. Ser.* **59:** 239–247.

Fryer, G., and W. J. P. Smyly. 1954. Some remarks on the resting stages of some freshwater cyclopoid and harpacticoid copepods. *Ann. Mag. Nat. Hist.* **7:** 65–72.

George, D. G. 1973. Diapause in *Cyclops vicinus. Oikos* **24:** 136–142.

Guillard, R. L. 1972. Culture of phytoplankton for feeding marine invertebrates. Pp. 20–60 in *Culture of Marine Invertebrate Animals,* W. L. Smith and M. H. Chanley, eds. Plenum Press, New York.

Hairston, N. G., Jr. 1987. Diapause as a predator-avoidance adaptation. Pp. 282–290 in *Predation: Direct and Indirect Impacts on Aquatic Communities,* C. W. Kerfoot and A. Sih, eds. University Press, New England.

Hairston, N. G., Jr., and W. R. Munns Jr. 1984. The timing of copepod diapause as an evolutionary stable strategy. *Am. Nat.* **123:** 733–751.

Hairston, N. G., Jr., and E. J. Olds. 1984. Population differences in the timing of diapause: adaptation in a spatially heterogeneous environment. *Oecologia* **61:** 42–48.

Hairston, N. G., Jr., T. A. Dillon, and B. D. DeStasio. 1990. A field test for the cues of diapause in a freshwater copepod. *Ecology* **71:** 2218–2223.

Hicks, G. R. F., and B. C. Coull. 1983. The ecology of marine meiobenthic harpacticoid copepods. *Oceanogr. Mar. Biol. Ann. Rev.* **21:** 67–175.

Hicks, G. R. F. 1984. Spatio-temporal dynamics of a meiobenthic copepod and the impact of predation-disturbance. *J. Exp. Mar. Biol. Ecol.* **81:** 47–72.

Maier, G. 1989. The seasonal cycle of *Thermocyclops crassus* (Fischer 1853) (Copepoda:Cyclopoida) in a shallow, eutrophic lake. *Hydrobiologia* **178:** 43–58.

Marcus, N. H. 1980. Photoperiodic control of diapause in the marine calanoid copepod *Labidocera aestiva. Biol. Bull.* **159:** 311–318.

Marcus, N. H. 1982a. The reversibility of subitaneous and diapause egg production by individual females of *Labidocera aestiva* (Copepoda: Calanoida). *Biol. Bull.* **162:** 39–44.

Marcus, N. H. 1982b. Photoperiod and temperature regulation of diapause of *Labidocera aestiva* (Copepoda: Calanoida). *Biol. Bull.* **162:** 45–52.

Marcus, N. H. 1987. Differences in the duration of egg diapause of *Labidocera aestiva* (Copepoda: Calanoida) from the Woods Hole, Massachusetts, region. *Biol. Bull.* **173:** 169–177.

Miller, C. B., T. J. Cowles, P. H. Wiebe, N. J. Copley, and H. Grigg. 1991. Phenology in *Calanus finmarchicus;* hypothesis about control mechanisms. *Mar. Prog. Ser.* **72:** 79–91

Naess, T., and J. P. Nilssen. 1991. Diapausing fertilized adults. *Oecologia* **86:** 368–371.

Nalepa, T. F. 1985. Occurrence of a resting stage in cyclopoid and harpacticoid copepods in nearshore Lake Michigan. *J. Great Lakes Res.* **11:** 59–66.

Nelson, A. L., and B. C. Coull. 1989. Selection of meiobenthic prey by juvenile spot (Pisces): an experimental study. *Mar. Ecol. Prog. Ser.* **53:** 51–57.

Nilssen, J. P. 1980. When and how to reproduce: a dilemma for limnetic cyclopoid copepods. Pp. 418–424 in *Evolution and Ecology of Zooplankton Communities,* C. W. Kerfoot, ed. University Press, New England.

Sarvala, J. 1979. A parthenogenetic life cycle in a population of *Canthocamptus staphylinus* (Copepoda, Harpacticoida). *Hydrobiologia* **62:** 113–129.

SAS Institute. 1985. *SAS User's Guide: Statistics,* Version 5th edition. SAS Institute Inc., Cary, North Carolina.

Stearns, S. C. 1976. The evolution of life history traits: a critique of the theory and a review of the data. *Ann. Rev. Ecol. Syst.* **8:** 145–171.

Tauber, M. J., and C. A. Tauber. 1970. Photoperiodic induction and termination of diapause in an insect: response to changing day lengths. *Science* **167:** 170.

Tauber, M. J., C. A. Tauber, and S. Mazaki. 1986. *Seasonal Adaptations of Insects.* Oxford Univ. Press. Pp. 411.

Taylor, F. 1980. Optimal switching to diapause in relation to the onset of winter. *Theor. Pop. Biol.* **18:** 125–133.

Taylor, B. E., G. A. Wyngaard, and D. L. Mahoney. 1990. Hatching of *Diaptomus stagnalis* from a temporary pond after a prolonged dry period. *Arch. Hydrobiol.* **117:** 271–278.

Watson, N., and B. N. Smallman. 1971a. The role of photoperiod and temperature in the induction and termination of an arrested development in two species of freshwater cyclopoid copepods. *Can. J. Zool.* **49:** 855–862.

Watson, N., and B. N. Smallman. 1971b. The physiology of diapause in *Diacyclops navus* Herrick (Crustacea, Copepoda). *Can. J. Zool.* **49:** 1449–1454.

Wyngaard, G. 1988. Variation in dormancy in a copepod: evidence from population crosses. *Hydrobiologia:* **167/168:** 367–374.

Reference: *Biol. Bull.* **182**: 117–128. (February, 1992)

The Nature and Origin of the Epidermal Scales of *Notodactylus handschini*—an Unusual Temnocephalid Turbellarian Ectosymbiotic on Crayfish from Northern Queensland

JOSEPH B. JENNINGS, LESTER R. G. CANNON[1], AND ADRIAN J. HICK

Department of Pure and Applied Biology, Baines Wing, University of Leeds, Leeds LS2 9JT, England and [1]Queensland Museum, PO Box 300, South Brisbane, Queensland 4101, Australia

Abstract. The temnocephalid *Notodactylus handschini*, ectosymbiotic on the crayfish *Cherax quadricarinatus* from northern Queensland, is unique among known turbellarians in having its dorsal epidermis covered by rows of closely adjacent scales. These are borne on epidermal plinths separated by arthrodial gutters and are up to 100 μm tall with rhombic bases 40–55 μm by 15–20 μm. Above the bases, the rhombic cross section gradually becomes oval so that the scales are essentially elongate conoids, the slender tips of which curve inwards towards the worm's mid-line. In mature worms, the more median scales may be reduced distally into squat truncated cones only 40–50 μm tall. The scales consist of glycoprotein; rhabdites discharged from cells in the dorsal parenchyma contribute the protein, whereas the carbohydrate component probably comes from the glycocalyxes of the epidermal microvilli. The latter act as templates around which the glycoprotein mixture coalesces, seemingly by a simple tanning process, into tightly packed tubes 180–200 nm in diameter with walls 40–45 nm thick. The scales lack any limiting wall or membrane other than a loose amorphous layer, 90–150 nm thick, formed by disintegration of the tubes distally and compensated for by continuous growth basally. Each scale is attached to its epidermal plinth by the bases of its constituent tubes ensheathing the microvilli; attachment is reinforced by cross-striated fibrils, probably collagen, embedded in the epidermis and inserted between the microvilli into tube bases near the scales' corners. Scale surfaces bear rich growths of microorganisms. The use of rhabdites to form permanent scales is probably an adaptation to the worm's unusual sedentary habit; it supports, paradoxically, an earlier hypothesis that the primary function of rhabdites in turbellarians other than temnocephalids is to provide a continuously renewable coating compatible with epidermal ciliation.

Received 7 August 1991; accepted 30 September 1991.

Introduction

The epidermis in turbellarian flatworms (comprehensively reviewed by Tyler, 1984) is typically a monolayered ciliated epithelium, with microvilli, made up of distinct cuboidal, squamous, or columnar cells. It can, though, be syncytial or insunk with its nuclei and some cytoplasm lying among or even below the subepidermal musculature. The epidermis is penetrated by the necks of subepidermal glands and the dendrites of sensory structures that pass between or through the epithelial cells when these are present.

These basic patterns are remarkably constant throughout the Turbellaria and persist, for example, in those entoparasitic species that lack normal entodermal alimentary systems and use the epidermis as their sole means of nutrient uptake. In the Fecampiidae, living in the hemocoel of amphipod and isopod crustaceans, the epidermis remains typically turbellarian, and the only apparent structural modification is an increase in the density and length of the microvilli (Jägersten, 1942; Christensen and Kanneworff, 1964; Bresciani and Koie, 1970; Blair and Williams, 1987). The fecampiids take up only soluble nutrients, but even in species where the epidermis actively secretes digestive enzymes and takes up particulate material for completion of digestion intracellularly, as in the

rhabdocoel *Acholades asteris* living in the tube-feet of starfishes, the cells remain columnar, ciliated, and traversed by the necks of subepidermal glands (Jennings, 1989).

The only major departure from the typical turbellarian pattern occurs in the Temnocephalida, which are ectosymbiotes of freshwater decapod crustaceans and a few other hosts. In most temnocephalids, cilia are restricted to small areas of the tentacles or around the excretory pores, locomotion is by muscular looping using the tentacles and simple posterior sucker and not by ciliary gliding, and the syncytial epidermis is bounded distally by a narrow, clear zone of vesicular epitheliosomes (Williams, 1975, 1980, 1986). The epidermal surface still bears microvilli, though, and the syncytium is honeycombed by numerous cell necks through which subepidermal glands discharge their secretions.

The most extreme epidermal modification in the Temnocephalida and, indeed, in the Turbellaria as a whole so far as is presently known, occurs in *Notodactylus handschini*, an ectosymbiote of various crayfishes from Papua New Guinea and northern Australia. In this species, the entire dorsal surface is covered by golden-brown scales that are much taller than the underlying epidermis (Baer, 1945, 1953; Cannon, 1991). These have not yet been described in any detail, and we report here, therefore, on their nature, origin, and mode of formation, as part of a wider study on the general biology of this unusual turbellarian.

Materials and Methods

Adults, juveniles, and hatchlings of *Notodactylus handschini* (Baer 1945) (Turbellaria: Temnocephalida) were collected from the lateral margins of the carapace of the freshwater decapod crustacean *Cherax quadricarinatus* (von Martens 1868), a northern Queensland species held in culture in farm ponds near Gympie, southeast Queensland. Specimens for histological and histochemical studies were fixed in Bouin's fluid, 90% ethanol or 10% formalin buffered to pH 7.0 with 0.1 *M* sodium phosphate and used at 4°C. Paraffin wax serial sections, 4 or 8 μm thick, prepared by standard procedures, were stained by Curtis's Ponceau S method for collagen, Ehrlich's haematoxylin and eosin, Heidenhain's iron haematoxylin and metanil yellow, or Mallory's trichrome stain. Histochemical methods included an alcian blue, periodic acid-Schiff (PAS) and orange G trichrome technique for glycoproteins and mucosubstances, the mercury-bromphenol blue method for proteins, Millon's and Sakaguchi's reactions for tyrosine and arginine, Perls' method for ferrous and ferric iron, and the ammonium hydroxide-alizarin method for calcium (Pearse, 1972).

Polyphenol oxidase activity in the scales was detected by a modification of Johri and Smyth's (1956) method; formalin-fixed whole worms were treated with 0.1% aqueous catechol (1,2 benzenediol) for 1 h, sectioned in paraffin wax at 8 μm and the sections dewaxed, mounted in DPX, and examined using a deep blue filter transmitting at 350–450 nm with peak transmission at 425 nm. Controls were sections of untreated worms and whole mounts of various proseriate and digenean worms showing the vitellaria.

For ultrastructural studies, specimens were fixed for 3 h at 4°C in 3% glutaraldehyde buffered to pH 7.2 with 0.2 *M* phosphate, post-fixed for 1 h in buffered 1% osmium tetroxide, embedded in Spurr's resin, and sectioned. Thin sections, mounted on pioloform films carried on copper slot grids and stained with uranyl acetate and lead citrate, were examined in a JEOL 1200 EX transmission electron microscope. Other sections, 1–2 μm thick, were stained with toluidine blue and studied with the light microscope.

The arrangement and general topography of the scales were studied by light microscopy, using unstained formalin-fixed specimens cleared and mounted in DPX, and by scanning electron microscopy of formalin-fixed worms post-fixed in buffered 2% osmium tetroxide, processed by standard procedures and examined in a Camscan Series 3 SEM.

Results

Notodactylus handschini (Figs. 1, 2) is a broadly oval temnocephalid, 1.0–1.5 mm × 0.75–1.0 mm at maturity, with five anterior tentacles curled ventro-posteriorly when at rest, a pair of eyes anteriorly, and a well-developed sucker posteriorly. The entire dorsal epidermis is covered by golden-brown scales bearing rich growths of epizoic bacteria, cyanobacteria, diatoms, green algae, stalked ciliated protozoans, and sessile rotifers.

The scales lie in close-set rows but do not overlap; they are up to 100 μm tall with rhombic bases 50–55 μm by 15–20 μm, whose long axes lie transversely to the worm's longitudinal axis (Fig. 3). The great majority can be referred to a single basic form in which the rhombic cross-section at the base continues upwards, decreasing in area for some 15–20 μm before gradually becoming oval so that the scales are essentially elongate conoids whose slender tips curve inwards towards the worm's mid-line (Fig. 4).

Scales along the lateral body margins are always of this shape but vary in height according to their position. Those nearest the naked ventral epidermis are the smallest, rarely more than 30–35 μm tall, but the size increases across the dorsal epidermis up to 55–65 μm. In mature worms, the more median scales may be reduced distally into squat truncated conoids no more than 40–50 μm tall (Fig. 6). Their flat or slightly convex tops are covered in epizoic growths of the same variety and abundance as those colonizing other surfaces of the scales, suggesting that loss

of the curved tips is a normal consequence of aging. The smaller, lateral scales bear only light growths, restricted to their lower surfaces, supporting the conclusion that they are younger than their more dorsal counterparts.

Most scales lying along the anterior and posterior body margins are of the curved conoid type, but two or three on each of the antero- and postero-lateral margins are exceptionally tall, stout, and columnar, reaching 90–100 μm in length (Fig. 6). Their cross-sectional shapes and areas do not change along their length, and they remain, in effect, tall rhombic prisms covered on all surfaces by epizoic growths. Their tops, particularly, are prone to colonization by vorticellid ciliates. These columnar scales are especially noticeable in living worms viewed by epi-illumination, when they appear strongly iridescent.

Newly hatched *N. handschini* lack scales and are greyish-white dorsally. Scale rudiments soon appear though (Figs. 19, 20), and recognizable scales of the adult types are present within three days. These are quickly colonized by the characteristic assemblage of epizoites so that juveniles four to five days old are indistinguishable externally from adults, apart from their difference in size.

Retractile papillae, 100–150 μm by 30–40 μm when extended, occur between the rows of scales sub-anteriorly and posteriorly. They are simple outgrowths of the body wall, are devoid of epizoites, and contain muscle fibers continuous with the diagonal muscles of the general body musculature (Fig. 6). They have no connection with the scales and will not be described further here.

Histology and histochemistry of the scales, epidermis, and rhabditogen cells

Scales of all types and ages are strongly acidophilic, staining deeply with eosin, orange G, and the acid fuchsin and picric acid components of Mallory's and Curtis's stains. They also stain strongly with toluidine blue, iron haematoxylin, the mercury-bromphenol blue method for proteins, Sakaguchi's method for arginine and the PAS reaction. They stain only lightly with 1% aqueous alcian blue prior to permanganate oxidation, but more deeply subsequently, very lightly with Millon's reagent for tyrosine, and not at all with the Ponceau S component of Curtis's stain for collagen and Perls' method for inorganic iron. They react positively to the alizarin test for calcium, especially basally; the reaction is strongest in formalin-fixed scales, suggesting that the calcareous component is susceptible to the acidic constituents of Bouin's fixative. This was confirmed by treatment of formalin-fixed sections with 2% hydrochloric acid, which eliminated any subsequent response to alizarin.

Iron haematoxylin staining followed by careful differentiation in iron alum reveals darker staining bands in the basal regions of mature scales, suggestive of growth rings (Fig. 6).

The scales of formalin-fixed worms treated with 0.1% catechol prior to sectioning at 8 μm, showed a significant darkening basally when compared with scales on untreated worms, indicating the presence of polyphenol oxidase or a similar quinone-tanning enzyme system. Because even young scales are golden-brown in color, such darkening is difficult to discern with normal illumination, but using a deep blue filter with peak transmission at 425 nm, the reactive zones showed greater absorption and were clearly seen. Whole mounts and sections of various proseriate and digenean flatworms, showing vitellaria or eggshell-producing glands, acted as positive controls.

The plaque-like growths of epizoites on the scales provided useful controls for all these tests, with at least some of the various organisms showing positive reactions to one or another of them. Positive responses to Perls' test for iron were particularly common.

The combination of reactions shown by the scales indicates that they are glycoproteins tanned into a stable physico-chemical form by a simple quinone-tanning system. Their stability was demonstrated during the application of the Millon's test for tyrosine when they survived immersion in the reagent, containing 10% sulphuric acid, for 5 min at 60°C—a procedure that destroyed all other parts of the sections except the frustules of epizoic diatoms.

The epidermis beneath the scales is syncytial, as is that covering the rest of the body. It is 5.0–5.5 μm deep, with strongly acidophilic cytoplasm, which stains deeply with acid fuchsin, eosin, orange G, and mercury-bromphenol blue. It reacts only weakly to PAS apart from the extreme distal region, which gives a strong positive reaction (Fig. 5); this area appears as a striated border after iron haematoxylin and is obviously the microvillar layer, which is a dominant feature at the ultrastructural level (Figs. 8, 9).

Epidermal nuclei are infrequent but prominent, 6.5–7.5 μm by 4.5–5.0 μm, lying lengthwise in the syncytium and with distinct, deeply staining chromatin. They may cause the epidermis to bulge slightly inwards, but are never insunk.

The epidermis rests on a thick fibrous basement membrane, 7.0–8.0 μm deep, which stains strongly with Curtis's Ponceau S method for collagen but only lightly with PAS.

The epidermis and basement membrane are traversed by the slender necks of rhabdite-secreting gland cells (rhabditogen cells), whose main bodies lie in the parenchyma below the dorsal subepidermal musculature (Figs. 5, 12). The rhabditogen cells occur throughout the dorsal parenchyma but are commonest anteriorly, behind the brain and above the pharynx, and posteriorly in the region of the testes. They are ovoid to spherical, 40–50 μm in diameter, with large nuclei and acidophilic cytoplasm packed with rhabdites. The latter show all the staining reactions given by the scales, including a positive response to the alizarin test for calcium. Significantly, though, they

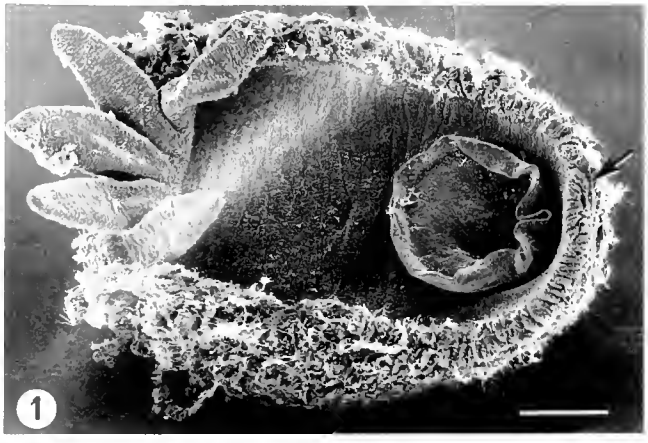

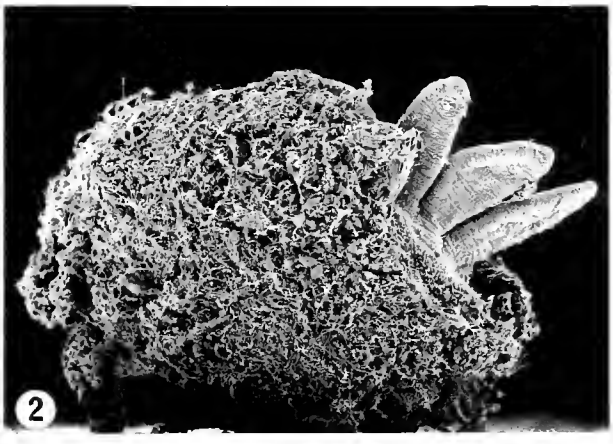

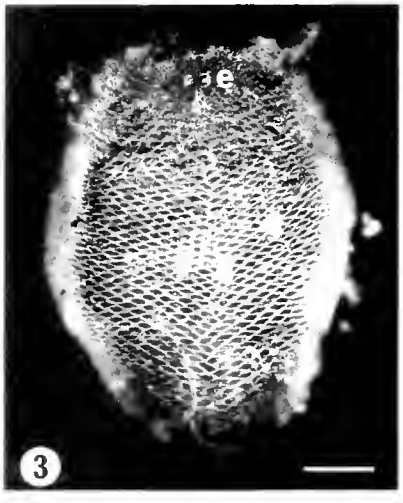

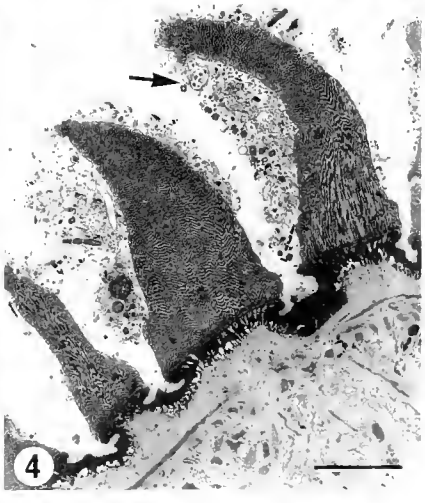

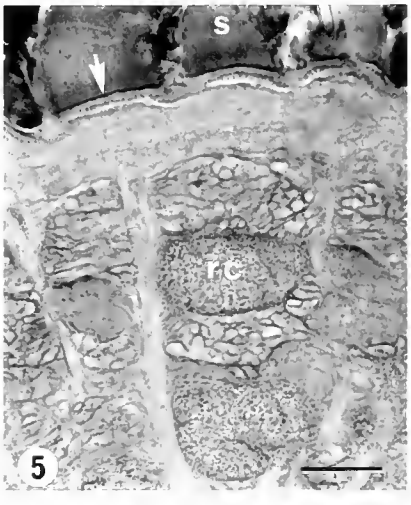

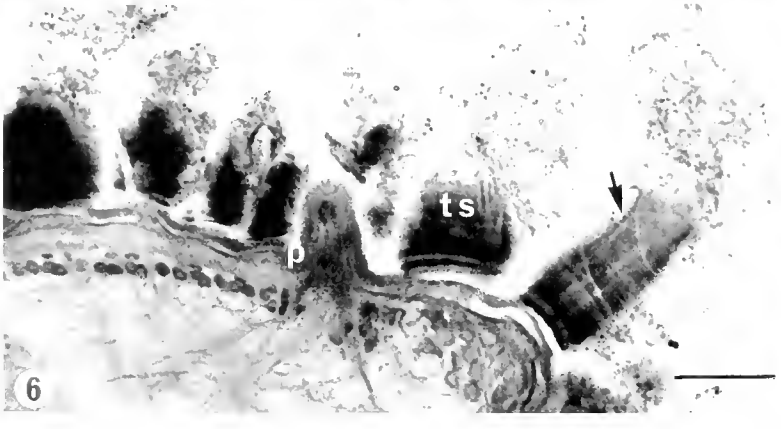

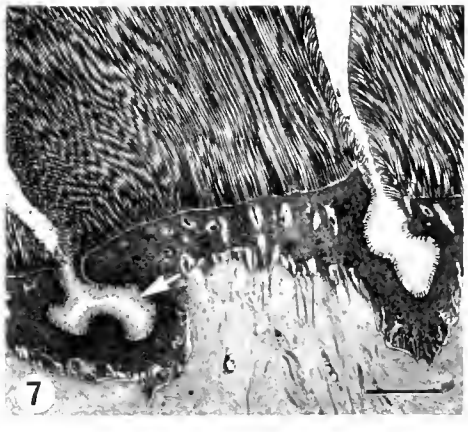

Figure 1. *Notodactylus handschini*, ventro-lateral aspect, showing the five tentacles (left), naked ventral epidermis, posterior sucker, and portions of the latero-dorsal surface covered by epizoic microorganisms growing on the epidermal scales. Some posterior scales (arrowed) bear only few epizoites. Scale bar = 200 μm.

Figure 2. Dorso-lateral aspect, showing the tentacles (right) and heavy growths of epizoites on the dorsal and lateral surfaces. Scale as in Figure 1.

Figure 3. Dorsal view of *N. handschini* photographed by dark-ground illumination after clearing and mounting unstained in DPX. The focal plane is at the level of the rhombic bases of the scales; e, eyes. Scale = 200 μm.

show no reaction to PAS and alcian blue and are extremely susceptible to mineral acids, rapidly disintegrating in the 10% sulphuric acid and 2% hydrochloric acid of Millon's and Perls' reagents. Catechol has no effect on their appearance or staining properties. The rhabdites differ from the scales, therefore, in their lack of carbohydrate and polyphenol oxidase components and solubility in mineral acids.

The cell necks of the rhabditogen cells follow a very sinuous course through the parenchyma and musculature to the epidermis and are almost impossible to trace in their entirety, even in 8 μm sections.

Ultrastructure of the scales

The scales are borne on rhombic epidermal plinths (Fig. 7), which have the same dimensions as the scales' bases. The epidermal syncytium is not noticeably thickened to form the plinths, but the plinth margins are produced into shelf-like overhangs 2.0–2.5 μm wide. These are separated from those of adjacent scales by spaces up to 5 μm wide. The epidermis dips downwards below the overhangs, emphasising the plinth-like effect, but it is turned upwards into a single fold equidistant between their tips. Each plinth is thus surrounded by a shallow gutter, about half as deep as the epidermis and separated from the adjacent gutter by the epidermal fold. The scales do not move relative to each other during the worm's normal movements, using the subepidermal musculature, and maintenance of the scales' positions is presumably due to the hinge-like action of the gutters and compensatory stretching of the epidermal folds. We suggest, therefore, the term 'arthrodial gutters' to describe these structures.

The scales are composed of ranks of uniform, closely packed parallel tubes, 180–200 nm in diameter, and with walls 40–45 nm thick (Figs. 7–11). The tubes run the length of the scales, and the majority have no visible contents; in sections cut obliquely to the scale's long axis, they may have an apparently ordered basket-weave arrangement, but examination of serial sections confirms that this is an effect of the plane of sectioning. The base of each tube encloses a single epidermal microvillus (Figs. 8, 9) but is not closely applied to it; a space 10–12 nm wide remains between the tube- and microvillar walls and is occupied by the glycocalyx. The tube bases, collectively forming the base of the scale, do not rest directly on the epidermal surface but appear to be supported some 80–90 nm above it, presumably by their connection to the microvilli via the glycocalyxes. This space was consistently present, and of the same width, in all wax and resin sections examined and would not seem, therefore, to be a shrinkage artefact. Both it and the tubes' lumina are presumably fluid-filled in life, with the fluid probably contributing significantly to the scales' mechanical stability.

The tube walls are composed of electron-opaque granules, 0.5–1.0 nm in diameter, loosely assembled into straight or slightly curved rod-shaped aggregates 20–30 nm by 8–10 nm (Figs. 9, 13, 15, 16). These tend to be orientated with their long axes at 90° to the walls' long axes. Most tubes lack visible contents, but a smaller number, 10–15% of the total, are twice the diameter of the others and are packed throughout their length with a heterogeneous mixture of granules, similar to those of the walls, and amorphous, less electron-opaque materials (Fig. 9). These larger tubes may each enclose a single microvillus basally, like the narrow tubes, or the microvilli may be lost.

Tubes forming the central bulk of the scales are straight and unbranched throughout their length. Those near the scales' edges, however, curve outwards and often branch dichotomously as they approach the edge (Figs. 10, 11). The branches are always the same diameter as the parent tube.

The scales are bounded by an unstructured layer 90–100 nm thick, which is moderately electron-opaque and formed from the disintegrating ends of the tubes. It is most distinct and uniform along straight edges of the scales near their bases (Fig. 10); it is less uniform on curved

Figure 4. Three conoid scales in vertical section. Two of the scales carry epizoic growths of various microorganisms (arrowed); the middle scale shows the transition basally from rhombic to conoid shape. Scale = 20 μm.

Figure 5. Part of a sagittal section showing the basal regions of three scales (s), the strongly PAS-positive distal border (microvillar layer) of the epidermis (arrowed), subepidermal musculature, and rhabditogen cells (rc) lying between blocks of diagonal muscles. Rhabdites in the cells are PAS-negative; their dark appearance is due to their staining with orange G. Epizoites between the scales have stained deeply with alcian blue and PAS. Section stained with alcian blue, PAS, and orange G. Scale = 20 μm.

Figure 6. Longitudinal section through the anterior region showing a tall columnar scale (arrowed) with bands, a papilla (p) whose muscle fibers extend into the parenchyma, and a truncated conoid scale (ts). Section stained with iron haematoxylin and metanil yellow. Scale = 10 μm.

Figure 7. Basal region of a conoid scale resting on its epidermal plinth, which is separated from adjacent plinths by arthrodial gutters. Microvilli lining the gutters are smaller and less regular than those at the base of the scale but bear long dense glycocalyxes (arrowed). Rhabditogen cell necks containing rhabdites are passing through the epidermal plinth. Scale = 5.0 μm.

edges, but here its origin from the walls is very obvious (Fig. 11). The layers forming the upper surfaces of the truncated scales occurring in the mid-dorsal region are of this latter type, but are usually thicker, reaching 100–150 nm, and with very disorganized lower parts. The underlying tubes, unlike those at the sides of the scales, remain straight and unbranched as they approach the surface, suggesting that the level of the latter is determined by attrition of a pre-existing curved tip.

Ultrastructure of the dorsal epidermis in relation to the scales

Dominant features of the syncytial dorsal epidermis are the tall regular microvilli of the epidermal plinths below the scales, shorter microvilli with long, dense glycocalyxes lining the arthrodial gutters, and the numerous necks of parenchymal rhabditogen and other cells which pass through it to open at the bases of the scales.

The microvilli below the scales are evenly spaced columns 1.25 μm by 0.08 μm, without internal differentiation, and with short rather granular glycocalyxes (Figs. 8, 9). Those lining the arthrodial gutters are smaller (only 0.2–0.25 μm tall), but their glycocalyxes are much larger and denser and appear as a thick fuzzy coat around the microvilli and extending above them for 0.4–0.5 mm (Fig. 7). They gradually become larger and more closely spaced along the overhanging portions of the epidermal plinths and grade into the upper surface types on the shoulder regions where scale tubes begin to form around them.

Most of the cell necks passing through the epidermis are those of rhabditogen cells lying below the subepidermal musculature in the dorsal parenchyma, whose histological and histochemical properties are described above. The cells' ultrastructure and method of rhabdite production (Fig. 12) are the same as in other turbellarians, including temnocephalids (see Smith *et al.*, 1982; Williams and Ingerfeld, 1988), and need not be described further here. Mature rhabdites leaving the cells and migrating out to the epidermis along the cell necks are elongate tapering rods, 1.50–1.75 μm by 0.20–0.25 μm, elecron-opaque, and with a concentric lamellated structure (Fig. 14). They change, however, as they reach the distal epidermis; the internal lamellated structure disappears, the electron-opacity may increase or become much more heterogeneous, and they may become curved (Figs. 13, 16, 17).

The rhabdites may be retained for a time in the distal epidermis, apparently by terminal caps that seal off the cell necks (Fig. 16), but are eventually discharged onto the epidermal surface between the microvilli. On dis-

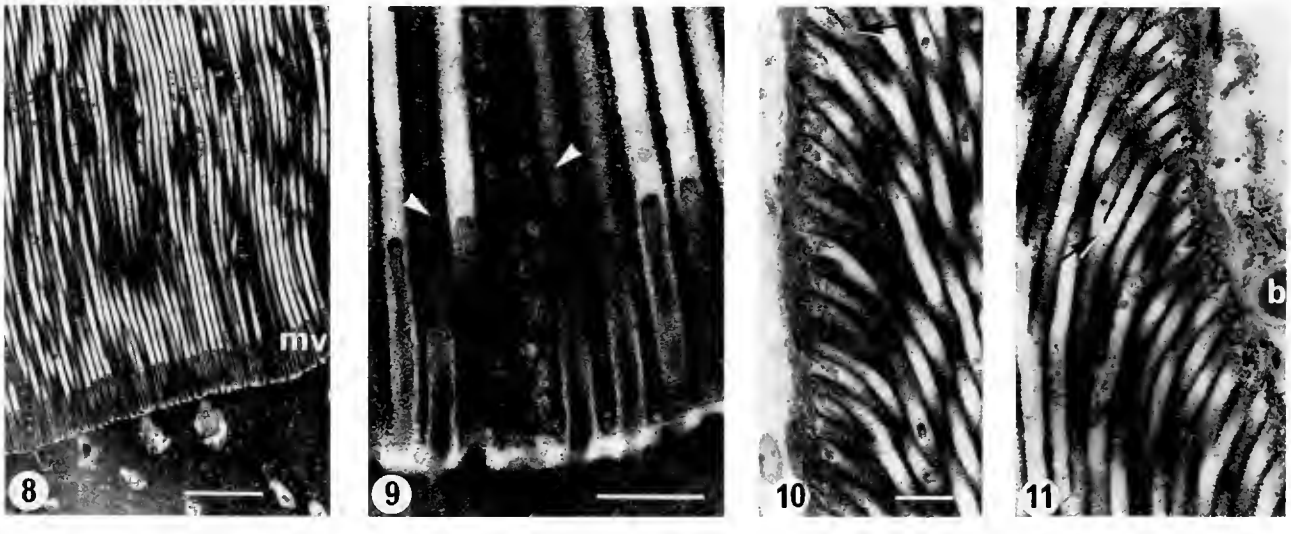

Figure 8. Part of the basal region of a conoid scale. Note the regular microvilli (mv) enclosed by the bases of the scale tubes. Rhabditogen cell necks, some containing rhabdites, are visible in the syncytial epidermis. Scale = 2.0 μm.

Figure 9. Detail from the field seen in Figure 8, showing a large tube (left of centre) whose lumen is packed with tube-wall building material. Grazing sections of walls of the commoner smaller tubes (arrowed) show the rod-shaped aggregates of wall material. Scale = 500 nm.

Figure 10. The uniformly structured layer bounding the basal region of a scale. Note the apparent branching (arrowed) of some of the scale tubes. Scale = 500 nm.

Figure 11. The curved edge of the upper part of the scale. The boundary layer is not as well organized as that shown in Figure 10. The apparent branching of scale tubes, with confluent lumina (arrowed) is clearly seen; b, epizoic bacterium. Scale as in Figure 10.

charge they disintegrate into the electron-opaque granules that form the principal components of the scale tube walls (Fig. 15). The granules are, at first, rather disorganized, but as they pass outwards between the microvilli, they become orientated into the stacked rod-shaped aggregates seen in the tube walls and in the lumina of the larger tubes (Fig. 16). During their passage outward, the aggregates themselves become automatically orientated around the microvilli to form tubes, each of which is separated from its microvillar template by the latter's glycocalyx.

The cell necks of the rhabditogen cells are 400–450 nm in diameter where they open onto the epidermal surface. They are anchored here by inconspicuous zonulae adhaerentes lying immediately above prominent septate desmosomes which encircle the necks to a depth of 450–550 nm (Figs. 13, 15, 16). They are supported internally by microtubules lying just below the cell membrane. Below the desmosomes the necks may be separated from the surrounding syncytium by apparent spaces, but these are so inconsistent in their occurrence, shapes, and sizes that they are probably shrinkage artefacts. Similar spaces occur around the cell necks where they enter the epidermis basally, and around the upward intrusions of the basement membrane into the epidermis.

Cell necks delivering rhabdites to the epidermal surface occur regularly throughout the epidermal plinths. Only occasional ones occur in the portions overhanging the arthrodial gutters, and these are curved as they divert from the main plinth out into the overhangs.

Each scale is anchored to its epidermal plinth by cross-striated fibrils that lie in cell necks opening onto the epidermal surface beneath the corners of the scale's rhombic base but inset from the overhanging portions. Each neck contains a single fibril (Figs. 17, 18); in mature worms, up to four such necks are present per corner, within a roughly circular area 1.5–2.0 μm in diameter. They are not present in hatchlings possessing only rudimentary scales but appear in juveniles, as the scales assume the adult form, within 4–5 days of hatching.

The cell necks are similar to those delivering rhabdites but are consistently larger, with neck diameters in the range 550–600 nm and with the septate desmosomes extending down into the syncytium for 600–700 nm. Unlike those of the rhabditogen cells, though, it was impossible to trace them, with any certainty, beyond the subepidermal musculature and link them with a specific cell type in the parenchyma. This was due to the absence of any identifying structural or histochemical features within the necks below the fibrils and the abundance of gland cell types in the dorsal parenchyma.

The fibrils are cylindrical, 1.5–2.0 μm long and 0.25–0.30 μm in diameter. They are provisionally identified as collagen by virtue of their characteristic appearance, being made up of regularly repeating units of dark and light bands with a periodicity of 62.04 ± 0.36 nm (n = 78, confidence limits 99%). This value was obtained from pooled data gained by direct measurement of prints and from scanning additional TEM negatives in a Fison's 'Vitatron' densitometer, normally used for scanning electrophoresis gels. It was not possible to obtain histochemical confirmation of their nature as the single fibrils could not be located in paraffin wax sections.

Each fibril lies within the cytoplasmic sheath forming the cell neck (Figs. 17, 18). Careful examination of serial sections confirmed this intracellular location; the fibrils do not lie extracellularly between parallel extensions of the cytoplasm as is usual with collagen fibrils in other animals. The cell necks are supported by microtubules, and the cytoplasm generally contains two or three mitochondria closely adjacent to the fibrils (Fig. 17). In contrast, mitochondria were never seen in the cell necks of rhabditogen cells.

The fibrils are inserted distally into the bases of the wider scale tubes that are packed with rhabdite-derived materials throughout their length (Fig. 18). They lose their regular banded structure either just within the cell neck opening or within a few nanometers of entering the scale tube and the fibril ends become frayed and dispersed into the tube contents. Proximally, the fibrils merge with the cytoplasm of the cell necks; fixation and resolution were not adequate for the details of fibril assembly to be seen.

Nothing was found to suggest that the fibrils are ciliary rootlets or the bases of sensory structures. Cilia and ciliary stubs, basal bodies, rootlets, and neuronal connections were found in the groups of sensilla on the ventral surfaces of the tentacles but nothing comparable was seen in association with the fibrils.

The cytoplasm of the syncytium is very electron-opaque and contains scattered mitochondria and profiles of cisternae. Swollen cisternae often occur alongside the cell necks (Fig. 13) but there are no indications of secretory activities into the necks or microvilli, or on to the epidermal surface.

Scale formation in young worms

Rhabditogen cells are dominant elements in the dorsal parenchyma of worms fixed 6 h after hatching, and their necks containing rhabdites are already present in the epidermis and subepidermal tissues (Fig. 12). The epidermis is syncytial and folded in a manner indicative of the future positions of the epidermal plinths. Microvilli are well-developed, especially on the upper surfaces of the folds, and simple scale rudiments may be visible around these, but most of the epidermis is naked.

Epidermal growth and folding continues and at about 12 h after hatching the future plinths and arthrodial gutters

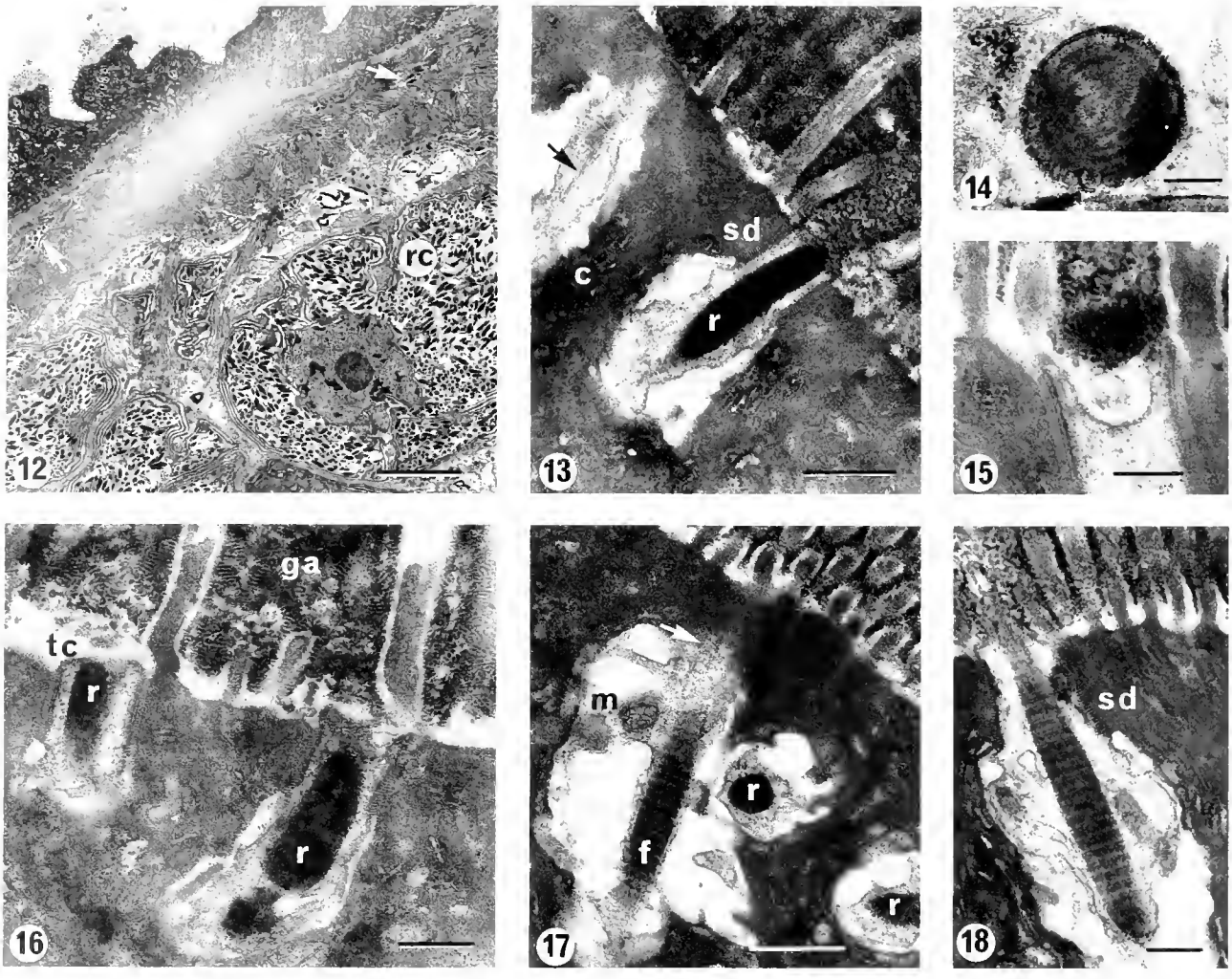

Figure 12. Part of a section from a young *N. handschini* fixed 6 h after hatching. Rhabditogen cells (rc) packed with rhabdites are prominent in the dorsal parenchyma and rhabdites (arrowed) can be seen in transit through subepidermal tissues and the epidermis. The epidermis is folded and microvilli are appearing. Scale = 5.0 μm.

Figure 13. A rhabdite (r) within a rhabditogen cell neck opening onto the epidermal surface between the microvilli. A similar cell neck containing a microtubule (arrowed) but without a rhabdite lies nearby. Note the granular aggregates, derived from discharged rhabdites, around the microvilli; c, swollen cisternae in epidermis; sd, septate desmosome. Scale = 500 nm.

Figure 14. A rhabdite in transverse section within a cell neck, showing its lamellated structure. Scale = 200 nm.

Figure 15. Remains of a discharged rhabdite lying between the bases of two microvilli. Scale = 200 nm.

Figure 16. Rod-shaped granular aggregates adding to tube bases between epidermal microvilli; ga, granular aggregates; r, rhabdites; tc, terminal cap. Scale = 300 nm.

Figure 17. Part of a striated fibril (f) embedded in the cytoplasm of a cell neck. The cytoplasm contains mitochondria (m) and microtubules (arrowed); adjacent cell necks contain rhabdites (r). Scale = 500

Figure 18. A striated fibril in a cell neck with its distal end inserted into the base of a large tube; sd, septate desmosome. Scale = 300 nm.

are recognizable; the microvilli on the presumptive plinths are longer than those in the gutters, scale rudiments are present and many rhabdites are visible, passing through the subepidermal musculature, basement membrane and epidermis (Fig. 19).

Twenty-four hours after hatching, the basic shapes of some epidermal plinths are established, with well-defined gutters and overhangs (Fig. 20). A granular layer, up to 0.5 μm thick, is sometimes present at the level of the microvilli but disappears in older worms; it is probably

rhabdite material poured from the epidermis but not yet organized around the growing microvilli. Scale rudiments at this stage are grey and soft but can be dissected from the epidermis without losing their form, provided they are not put under excessive pressure.

Subsequent development is very rapid, and in juveniles 3–4 days old the epidermis and scales are of the adult type, with the scales' color changing from grey through pale gold to golden brown. It is at this time, significantly, that the basal regions of the scales first show a positive catechol reaction for polyphenol oxidase.

Discussion

The temnocephalid *Notodactylus handschini* is unique among known turbellarians in having its dorsal epidermis covered by precisely formed and arranged permanent scales. The only other reported occurrence of cuticular structures in the Turbellaria is in the polyclad *Enantia spinifera,* which has epidermal spines along the body margins (von Graff, 1889). The spines form as a secretion over an epidermal papilla, but the nature of the secretion and the method of its stabilization are unknown.

Despite the unique nature of the scales in *N. handschini,* their production and maintenance involve only precursors, processes and structures occurring in one form or another throughout the Turbellaria; the scales, therefore, represent exploitation of existing features rather than the evolution of entirely new ones.

The syncytial epidermis upon which the scales rest differs from that described in other temnocephalids (Williams, 1986, and references therein) in its lack of a distal layer of vesicular epitheliosomes, the presence of striated fibrils and its folding into epidermal plinths and arthrodial gutters.

The rhabdites that contribute the bulk of the scale material are of the lamellated type common elsewhere in the temnocephalids (Williams, 1975, 1986; Williams and Ingerfeld, 1988) and other turbellarians (Lentz, 1967; Bowen and Ryder, 1974; Smith *et al.*, 1982). In the temnocephalids, they disintegrate after discharge onto the epidermal surface of the tentacles to form a thin surface film which is stabilized by the microvilli (Williams, 1986). A similar constant discharge, but over the entire body surface, occurs in free-living turbellarians; the rhabdites hydrate and disintegrate to form a semi-fluid film, which is thought to protect the otherwise naked ciliated epidermis while still allowing ciliary activity (Jennings, 1957). The protective film, composed of simple, unconjugated protein, is probably constantly renewed basally as it is eroded or dissolved distally. This interpretation of the primary function of rhabdites explains why they are produced in such vast numbers, in most species, and constantly exported from their formative cells in the parenchyma into and through the epidermis. A secondary function, but still protective, is seen in polyclad turbellarians where both cotyleans and acotyleans use them to form the large gelatinous masses in which the otherwise naked eggs are embedded (Jennings, 1957).

In *Notodactylus handschini,* the protective role of the rhabdites is taken much further by elaborating them into permanent structures—the dorsal scales. Such scales, of course, are incompatible with a ciliated epidermis and ciliary locomotion but *N. handschini,* in common with most other temnocephalids, has lost most of its external ciliation and moves by muscular looping involving the tentacles and posterior sucker.

The rhabdites in *N. handschini* are very similar in histological and histochemical properties to those studied in other turbellarians by Jennings (1957), Pedersen (1959), Skaer (1961), and Bowen and Ryder (1974), and are clearly homologous with these, a view confirmed by further similarities in ultrastructure, method of secretion, and mode of export to the epidermal surface within cytoplasmic strands of the formative cells. Their involvement in scale formation, therefore, has not necessitated any basic changes in these properties. The turbellarian habit of continually discharging rhabdites through the epidermis to maintain the protective surface film lends itself readily to the formation and subsequent growth of structures like the scales of *N. handschini,* provided that the rhabdite-derived material can be stabilized. In *N. handschini,* the stabilizing factor appears to be the combination of the proteinaceous rhabdite material with a carbohydrate moiety and the subsequent tanning of the glycoprotein product by polyphenol oxidase. In view of the histochemical properties of the scales, rhabdites, and epidermis, the only possible source of this carbohydrate would seem to be the glycocalyxes of the microvilli. The polyphenol oxidase appears to be concentrated at the microvillar level, as could be expected, but its source is unknown. Its occurrence, however, is not a novel feature as it is commonly found throughout the Platyhelminthes as a tanning agent in egg capsule production (von Brand, 1973).

The occurrence in the worm's mid-dorsal region of scales that have lost their distal curved tops and become reduced to truncated conoids, shows that, despite their tanning, the scales are susceptible to erosion, perhaps by water currents or the activities of their epizoites. The constant addition of formative materials basally will compensate for this, to some extent, just as the continual discharge and disintegration of rhabdites in other species maintains indefinitely the protective film over their ciliated surfaces.

The factors determining the curved conoid shape of the majority of the scales remain unknown, along with the reasons for the occurrence of the anomalous tall columnar

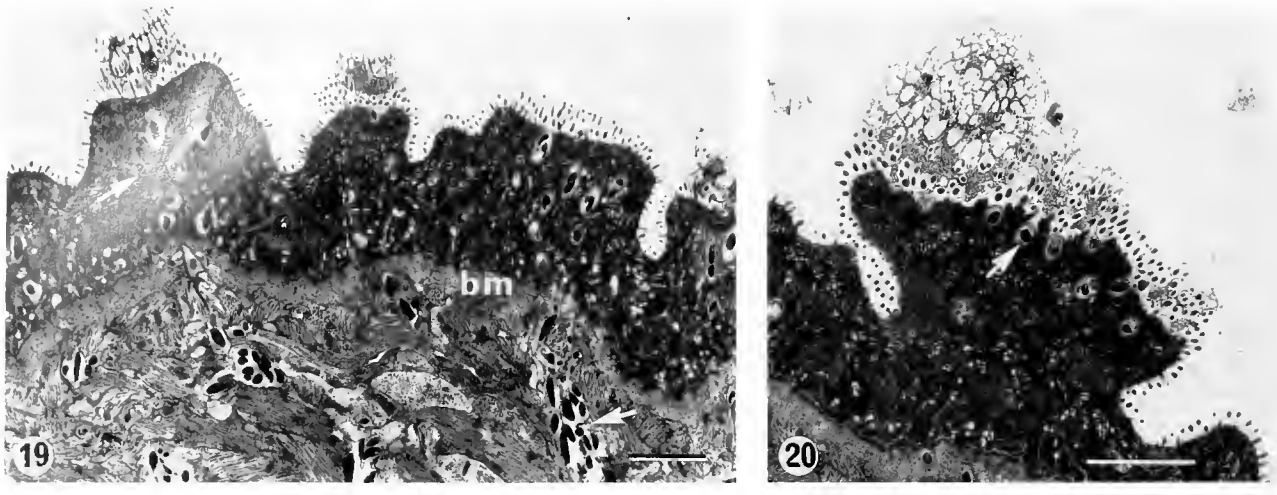

Figure 19. Part of the epidermis and subepidermal tissue of a young *N. handschini* fixed 12 h after hatching. Rhabdites (arrowed) are passing through the subepidermal musculature and folded epidermis, microvilli are well developed and scale rudiments are appearing; bm, basement membrane of epidermis. Scale = 2.0 μm.

Figure 20. An epidermal plinth and well-developed scale rudiment in a worm fixed 24 h after hatching. Rhabdites (arrowed) can be seen below the scale rudiment. Scale = 2.0 μm.

scales on the anterior and posterior body margins. Anomalous, too, is the distal branching of some of the scale tubes below the lateral surfaces of the scales (Figs. 10, 11). The branches are all the same diameter as the other tubes, suggesting, perhaps, that they result from fusion of the distal regions of adjacent tubes rather than from true branching. Alternatively, branching may occur as the tubes form around the microvilli; occasional branched microvilli do occur in young worms. If this is the case, then the distribution of microvilli, including branched ones, on the epidermal plinths is probably the decisive factor in scale morphogenesis.

Microvilli and glycocalyxes are versatile structures put to a variety of uses by animals. Examples are their roles in membrane (contact) digestion in vertebrates (Ugolev, 1965), turbellarian adhesive systems (Tyler, 1976), cuticle formation in oligochaetes and archiannelids (Potswald, 1971; Rieger and Rieger, 1976), cuticle attachment and chaeta formation in annelids (Richards, 1978), and cuticle attachment in pentastomid arthropods (Riley and Banaja, 1975). Their role in stabilizing rhabdite-derived films on the tentacular surfaces of other temnocephalids (Williams, 1986) has already been mentioned; it is not surprising, therefore, to find microvilli intimately involved in the mechanics of scale formation in *N. handschini*, additionally to the probable chemical involvement of their glycocalyxes. Their function as templates, around which the glycoprotein becomes arranged to form the scale tubes, is identical with the role of chaetoblast microvilli in the formation of chaetae from a polymerizing chitin-protein complex in annelids (Richards, 1978). In both instances, the microvilli are long and extremely regular, in accord with the long, regular tubes produced around them.

Attachment of the scales to their epidermal plinths is probably another important function of the microvilli. It is supplemented by the apparent collagen fibrils embedded in the epidermis and inserted into the bases of some of the larger tubes, which are probably strengthening pillars because they are packed with material similar to that of the tube walls.

If the striated fibrils are indeed collagen, then they are the only features associated with the scales that are novel epidermal structures; they have not been reported elsewhere in the Turbellaria. But basement membranes are usually collagenous (Burgeson, 1988), and that of *N. handschini* is probably no exception in view of its fibrous nature and PAS-and Ponceau S-positive reactions. Thus the fibril-secreting cells may well be homologous with those secreting the basement membrane and other components of the extracellular matrix.

Identification of the fibrils as collagen rests mainly upon their size, appearance, and the periodicity of their banding. The periodicity of 62.04 ± 0.36 nm lies well within the range of 55.0–68.0 nm found in examples of collagens taken from all major invertebrate groups from the Porifera to Tunicata (Baccetti, 1985). In particular, it compares with a value for *Fasciola hepatica* of 65.0 nm (Nordwig and Hayduk, 1969), which is the only other one available from the Platyhelminthes. The fibrils' location beneath the scales, their insertion into the bases of the strengthening pillars, their absence from hatchling worms possessing only rudimentary scales, and the absence of as-

sociated basal bodies, recognizable ciliary stumps, and neuronal elements (visible elsewhere in *N. handschini*) all militate against an alternative interpretation of the fibrils as ciliary rootlets. The association of mitochondria with the fibrils (Fig. 17) might be regarded as supporting this latter interpretation because mitochondria do occur alongside the rootlets of monociliated sensory processes in various turbellarians (Ehlers and Ehlers, 1977; Ferrero and Bedini, 1989). In our opinion, though, this single fact does not justify homologizing the fibrils with such rootlets, especially in view of all the other evidence to the contrary.

The fibrils are reminiscient, in position and supposed function if not in shape, of the U-shaped anchoring collagen fibrils occurring in the epidermal-dermal and basal lamina zones of vertebrates (Palade and Farquhar, 1965; Bruns, 1969; Burgeson, 1988). According to Alberts *et al.* (1989), collagen fibrils have the tensile strength of steel so that although the fibrils in *N. handschini* are relatively few in number, per scale, their concentration near the corners of the scales' rhombic bases probably does provide effective reinforcement of the scales' attachment to their epidermal plinths via the microvilli.

The supposed collagen fibrils in *N. handschini* differ in one outstanding respect from those occurring in other animals and that is their indisputably intracellular location over most of their length. There is ample and widely accepted evidence that collagen fibrils, in vertebrates at least, form by self-assembly of their constituent molecules within narrow extracellular compartments formed from parallel but separate cytoplasmic extensions of the parent fibroblasts (Birk and Trelstad, 1985, 1986; Burgeson, 1988). In *N. handschini,* the fibrils remain embedded in the cytoplasmic sheaths forming the cell necks of their formative cells and protrude from these only far enough for insertion into the bases of the larger supporting tubes of the scales. They pass through the distal neck regions, which are encircled by the septate desmosomes locking the necks into the epidermis; below this their accompanying mitochondria confirm their intracellular position.

The occurrence of scales in *N. handschini* is probably correlated with the worm's unusual life style. Other temnocephalids are very active, but this species is remarkably sedentary and remains for many days, perhaps for its entire life span, at the same location on the edge of its host's carapace (Cannon and Jennings, unpub. obs.). Mature worms surround themselves with stockade-like circles of their own egg capsules, some empty, others embryonated or newly laid, and they remain quiescent within these for long periods. They feed on small crustaceans, especially ostracods, which settle on the eggs or nearby, by rapidly extending the body, seizing the prey with their tentacles, and swallowing it intact. This behavior, of course, protects the eggs and can be construed as a form of brooding. The scales' epizoites probably facilitate feeding by concealing the worms from their potential prey; they also conceal them from potential predators while the scales themselves provide a protective shield over the body should an attack occur. *N. handschini* is not known to have any particular predators, but various other temnocepalids occur with it on the same host (Cannon, 1991), and inter-specific predation is common in such communities on other crayfishes (Jennings, 1988).

Acknowledgments

This work was supported by a Royal Society travel grant (SV/Australia 1990) to JBJ and an Australian Biological Resources Survey grant (87/5909) to LRGC.

Literature Cited

Alberts, B., D. Bray, J. Lewis, M. Raff, K. Roberts, and J. D. Watson. 1989. *Molecular Biology of the Cell,* 2nd ed. Garland, New York. 1219 pp.

Baccetti, B. 1985. Collagen and animal phylogeny. Pp. 29–47 in *Biology of Invertebrate and Lower Vertebrate Collagens,* A. Bairati and R. Garrone, eds. Plenum Press, New York.

Baer, J. G. 1945. Un Temnocéphale nouveau, *Temnocephala handschini* n. sp. de la Nouvellie Guinee. *Rev. Suisse Zool.* **52:** 505–512.

Baer, J. G. 1953. Temnocéphales. Zoological results of the Dutch New Guinea Expedition 1939. No. 4. *Zool. Meded. (Leiden)* **32:** 119–139.

Birk, D. E., and R. L. Trelstad. 1985. Fibroblasts create compartments in the extracellular space where collagen polymerizes into fibrils and fibrils associate into bundles. *Ann. N.Y. Acad. Sci.* **460:** 258–266.

Birk, D. E., and R. L. Trelstad. 1986. Extracellular compartments in tendon morphogenesis: collagen fibril, bundle and macroaggregate formation. *J. Cell Biol.* **103:** 231–240.

Blair, D., and J. B. Williams. 1987. A new fecampiid of the genus *Kronborgia* (Platyhelminthes: Turbellaria: Neorhabdocoela) parasitic in the intertidal isopod *Exosphaeroma obtusum* (Dana) from New Zealand. *J. Nat. Hist.* **21:** 1155–1172.

Bowen, I. D., and T. A. Ryder. 1974. The fine structure of the planarian *Polycelis tenuis* (Iijima). III. The epidermis and external features. *Protoplasma* **80:** 381–392.

Brand, T. von. 1973. *Biochemistry of Parasites, 2nd ed.* Academic Press, New York. 499 pp.

Bresciani, J., and M. Køie. 1970. On the ultrastructure of the epidermis of the adult female of *Kronborgia amphipodicola* Christensen and Kanneworff, 1964 (Turbellaria: Neorhabdocoela). *Ophelia* **8:** 209–230.

Bruns, R. R. 1969. A symmetrical extracellular fibril. *J. Cell Biol.* **42:** 418–430.

Burgeson, R. E. 1988. New collagens, new concepts. *Ann. Rev. Cell Biol.* **4:** 551–577.

Cannon, R. G. L. 1991. Temnocephalan symbionts of the freshwater crayfish *Cherax quadricarinatus* from northern Australia. *Hydrobiologia* (in press).

Christensen, A. M., and B. Kanneworff. 1964. *Kronborgia amphipodicola* gen. et sp. nov., a dioecious turbellarian parasitizing ampeliscid amphipods. *Ophelia* **1:** 147–166.

Ehlers, U., and B. Ehlers. 1977. Monociliary receptors in interstitial Proseriata and Neorhabdocoela (Turbellaria, Neophora). *Zoomorphologie* **86:** 197–222.

Ferrero, E. A., and C. Bedini. 1989. Chemoreception in Turbellaria. *Exp. Biol.* **48:** 141–148.

Graff, L. von. 1889. *Enantia spinifera,* der Repräsentant einer neuen Polycladen-Familie. *Naturwiss. Vereines f. Steiermark* **1889:** 1–16.

Jägersten, G. 1942. Zur Kenntnis von *Glanduloderma myzostomatis* n. gen. n. sp., einer eigentumlichen, in Myzostomiden Schmarotzenden Turbellarienform. *Ark. Zool* **33A:** 1–24.

Jennings, J. B. 1957. Studies on feeding, digestion, and food storage in free-living flatworms (Platyhelminthes: Turbellaria). *Biol. Bull.* **112:** 63–80.

Jennings, J. B. 1988. Nutrition and respiration in symbiotic Turbellaria. *Fortschr. Zool.* **36:** 1–13.

Jennings, J. B. 1989. Epidermal uptake of nutrients in an unusual turbellarian parasitic in the starfish *Coscinasterias calamaria* in Tasmanian waters. *Biol. Bull.* **176:** 327–336.

Johri, L. N., and J. D. Smyth. 1956. A histochemical approach to the study of helminth morphology. *Parasitology* **46:** 107–117.

Lentz, T. E. 1967. Rhabdite formation in Planaria: the role of microtubules. *J. Ultrastr. Res.* **17:** 114–126.

Nordwig, A., and U. Hayduk. 1969. Invertebrate collagens: isolation, characterisation and phylogenetic aspects. *J. Mol. Biol.* **44:** 161–172.

Palade, G. E., and M. G. Farquhar. 1965. A special fibril of the dermis. *J. Cell Biol.* **27:** 215–224.

Pearse, A. G. E. 1972. *Histochemistry: Theoretical and Applied, 3rd ed.* Churchill Livingstone, Edinburgh. 1518 pp.

Pedersen, K. J. 1959. Some features of the fine structure and histochemistry of planarian subepidermal gland cells. *Z. Zellforsch.* **50:** 121–142.

Potswald, H. E. 1971. A fine structural analysis of the epidermis and cuticle of the oligochaete *Aeolosoma bengalense* Stephenson. *J. Morphol.* **135:** 185–212.

Richards, K. S. 1978. Epidermis and cuticle. Pp. 33–61 in *Physiology of Annelids,* P. J. Mill, ed. Academic Press, London.

Rieger, R. M., and G. E. Rieger. 1976. Fine structure of the archiannelid cuticle and remarks on the evolution of the cuticle within the Spiralia. *Acta Zool. (Stockholm)* **57:** 53–68.

Riley, J., and A. A. Banaja. 1975. Some ultrastructural observations on the integument of a pentastomid. *Tissue Cell* **7:** 35–50.

Skaer, R. J. 1961. Some aspects of the cytology of *Polycelis nigra*. *Q. J. Microsc. Sci.* **102:** 295–317.

Smith, J., S. Tyler, M. B. Thomas, and R. M. Rieger. 1982. The morphology of turbellarian rhabdites: phylogenetic implications. *Trans. Am. Microsc. Soc.* **101:** 209–228.

Tyler, S. 1976. Comparative ultrastructure of adhesive systems in the Turbellaria. *Zoomorphologie* **84:** 1–76.

Tyler, S. 1984. Turbellarian Platyhelminths. Pp. 112–131 in *Biology of the Integument, Vol. 1 Invertebrates,* J. Bereiter-Hahn, A. G. Matolsky, and K. S. Richards, eds. Springer-Verlag, Berlin.

Ugolev, A. 1965. Membrane (Contact) digestion. *Physiol. Rev.* **45:** 555–595.

Williams, J. B. 1975. Studies on the epidermis of *Temnocephala* I. Ultrastructure of the epidermis of *Temnocephala novae-zealandiae*. *Aust. J. Zool.* **23:** 321–331.

Williams, J. B. 1980. Studies on the epidermis of *Temnocephala* V. Further observations on the ultrastructure of the epidermis of *Temnocephala novae-zealandiae*, including notes on the glycocalyx. *Aust. J. Zool.* **28:** 43–57.

Williams, J. B. 1986. Phylogenetic relationships of the Temnocephaloidea (Platyhelminthes). *Hydrobiologia* **132:** 59–67.

Williams, J. B., and M. Ingerfeld. 1988. Cells in the parenchyma of *Temnocephala*, rhabdite secreting cells of *Temnocephala novae-zealandiae* (Temnocephalidae; Platyhelminthes). *Int. J. Parasitol.* **18:** 651–659.

Reference: *Biol. Bull.* **182:** 129–134. (February, 1992)

Red Blood Cell Oxygen Binding in Capitellid Polychaetes

CHARLOTTE P. MANGUM[1], JAMES M. COLACINO[2], AND JUDITH P. GRASSLE[3,*]

[1]*Department of Biology, College of William and Mary, Williamsburg, Virginia 23185,*
[2]*Department of Biological Sciences, Clemson University, Clemson, South Carolina 29634-3581,*
and [3]*Marine Biological Laboratory, Woods Hole, Massachusetts 02543*

Abstract. The oxygen equilibrium properties of red blood cells that circulate in the coelomic cavities of 10 morphologically similar capitellid polychaetes are generally species specific. Appreciable differences in oxygen affinity distinguish most of the species and, in several instances, cooperativity differs as well. The range of oxygen affinities is far greater than in the other closely related polychaetes examined to date. We suggest that the differences may prove to be adaptations to thermal properties of the environment, body size, or both.

Introduction

The polychaete *Capitella capitata* (Fabricius) is now known to be a number of morphologically similar species that are distinguished by a variety of genetic, developmental and reproductive features (Grassle and Grassle, 1976; Eckelbarger and Grassle, 1987a,b; Grassle *et al.*, 1987). These features clearly indicate that the cryptic species are in fact reproductively isolated from one another. Like other members of the family Capitellidae, these species contain typical annelid red blood cells (RBCs) that circulate in the coelomic cavity.

The respiratory properties of the annelid RBC hemoglobins (Hbs) are known primarily from investigations of the families Glyceridae and Terebellidae (reviewed by Mangum, 1992a). Although no direct comparisons of the Hbs of congeneric or otherwise closely related species have been made, they appear to be fairly similar within each family. These Hbs have high (terebellids) to moderate (glycerids) O_2 affinities, and little or no cooperativity and pH dependence. Although differences between the O_2 binding properties of RBCs and those of purified Hbs have been reported on a few occasions, thorough reinvestigation has indicated that the annelid RBC Hbs are not sensitive to intracellular effectors (Mangum, 1992a). The three additional annelid families with RBCs have received scant attention.

Most members of the genus *Capitella* are very small animals (*e.g.*, as small as 0.28 mg in the present sample), and a broad survey of the O_2 binding properties of their Hbs with the techniques presently in wide use, even those that require only several drops of material would be difficult. The recent development of a microspectrophotometer specifically built for optically heterogeneous preparations (Colacino and Kraus, 1984), however, has made it possible to determine the O_2 binding of a single red blood cell (Mangum *et al.*, 1989). In the present investigation, we have taken advantage of this capability to compare the respiratory properties of the RBCs of six of the species previously regarded as *Capitella capitata*, and four belonging to the closely related genus *Capitomastus*. We have also attempted to relate our findings to O_2 uptake.

Materials and Methods

The animals were obtained from laboratory cultures, either strains that had been maintained continuously for long periods or collected recently and cultured until they produced brood tubes and viable larvae. With one exception, the species designations, collection sites, and culture conditions were described by Grassle *et al.* (1987). *Capitomastus* VOZ was collected in the thermal effluent affected vicinity of a power plant (Millstone) in Connecticut, and cultured at 20°C in 31.8 ‰ seawater.

Received 9 July 1991; accepted 30 September 1991.

* Present address: Department of Marine and Coastal Sciences, Rutgers University, P. O. Box 231, New Brunswick, New Jersey 08903.

O_2 binding

Several individuals of a species were immersed in buffered seawater on the side of a shallow concavity in a depression slide and their body walls slitted, with iridectomy scissors in the case of the larger animals and with fine pins in the case of the smaller ones. On the few occasions when the gut was ruptured, the material was discarded. Otherwise, the RBCs were allowed to gravitate in the central depression free of other body parts and were then transferred to the experimental chamber. This chamber, illustrated by Colacino and Kraus (1984), holds a thin layer of RBCs between two polypropylene membranes (25 μm thickness). A humidified mixture of Research Grade N_2 and O_2, prepared in the present investigation by a gas mixing flowmeter (Cameron Instruments Co.), was passed on either side of the polypropylene sandwich, which was held in a water-cooled brass slide. RBCs were illuminated through glass windows in the brass. In the present investigation, the diode array microspectrophotometer described earlier (Mangum *et al.*, 1989) was used exclusively.

With this apparatus, the entire visible spectrum in the range 380–650 nm is collected. We saw no sign of the spectral changes, denaturation, or precipitation encountered by Wells and Warren (1975) in their investigation of capitellid RBCs, possibly because our RBCs were never exposed to air. Initially, however, several experiments were aborted by cell lysis; the problem was eliminated by first soaking the polypropylene membranes in shaking seawater.

Data analysis

Hill plots of the data were analyzed by each of two procedures. First, each RBC of each species was treated as a unique member of the population. The constants P_{50} (PO_2 at 50% oxygenation, or O_2 affinity) and n_{50} (slope of a Hill plot of O_2 binding at P_{50}, or cooperativity) were obtained from regression lines describing the data for intermediate oxygenation states. The mean values for each species were compared by Student's t test. Second, the RBCs of a particular species were treated as members of a homogeneous population, and a single regression line was constructed for all data in the range 10–90% HbO_2. Ninety-five percent confidence intervals around the regression lines and their slopes are reported below as the error.

O_2 uptake

Oxygen uptake of 2–20 animals, depending on body size (see Results for size range), was determined by recording the decline in PO_2 in a closed container, using a polarographic electrode (Strathkelvin Instrument Co.). The volume of the chamber was 0.4–0.75 ml; stirring was provided from the bottom with a magnetic bar which was isolated from the animals by a disk of stainless steel mesh. Temperature change was controlled to less than 0.1°C.

Results

Like Pals and Pauptit (1979), we noted that *in vivo* the RBCs circulate in clumps. While many kinds of RBCs aggregate *in vitro* when the medium is unstirred, we are unaware of additional reports indicating that the phenomenon is natural. We also noted distinctive and nonoverlapping differences in RBC diameter in several of the species, suggesting that a hematological investigation would be of interest.

RBC O_2 binding

Oxygen affinity of the 10 species examined here ranges from high (2.8 mmHg) to moderately low (11.1 mmHg). Apparent cooperativity ranges from very little (1.6) to pronounced (3.1). While the RBCs of a few of the species clearly showed increases in apparent cooperativity at high oxygenation states (*e.g.*, the increase in slope of the line in Fig. 1), most did not. We did not investigate pH dependence.

When treated as unique entities, the RBCs of a species generally have distinctive O_2 affinities, the mean values of which differ significantly ($P < .05$) from those of most of the other species. Several of the cooperativity values also differ significantly from the others, although less frequently (Tables I, II).

When treated as members of a homogeneous population, the RBCs of a particular species have O_2 affinity

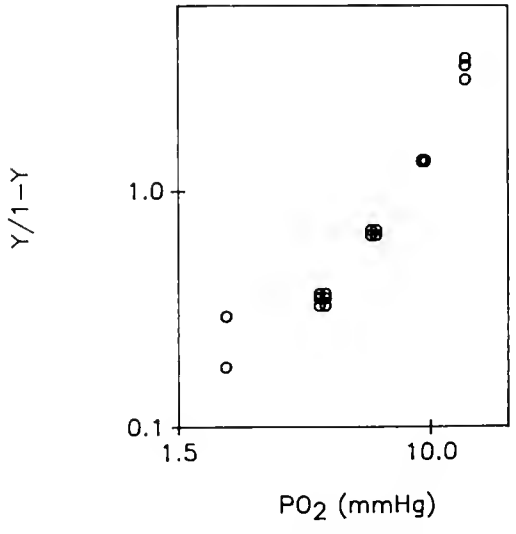

Figure 1. Hill plot (log (y/1 − y) *vs.* log PO_2) of O_2 binding of RBCs from *Capitella* MB/s1, 20°C, pH 7.4.

Table I

O_2 equilibrium constants[a] for RBCs of capitellid polychaetes

Species	P_{50} (mmHg)	n_{50}	n
Capitella			
sp. I	6.88 ± 0.97	2.89 ± 0.82	7
sp. IA	7.99 ± 0.61	2.36 ± 0.38	17
sp. II	5.47 ± 0.43	3.27 ± 0.55	10
sp. IIIA	5.76 ± 1.17	2.61 ± 0.84	6
MB/sl	8.27 ± 0.82	1.68 ± 0.46	6
ORL	11.3 ± 0.9	3.44 ± 0.55	11
Capitomastus			
NCS	9.74 ± 0.93	3.62 ± 0.91	11
TAR	3.85 ± 0.20	2.76 ± 0.33	14
TRIN	3.09 ± 0.79	2.56 ± 1.03	9
VOZ	4.32 ± 0.93	3.03 ± 1.05	6

[a] Mean + S.E., 20°C, pH 7.4.

values that invariably differ significantly from all others (Table III). Again, significant differences in apparent cooperativity are found, but far less frequently (Table III).

O_2 uptake

Oxygen uptake measurements were performed successfully on five of the ten species. Three of the remaining species were unavailable at the time. Individuals of *Capitella* species IIIA and *Capitomastus* NCS, though available, were so small (<1 mg wet wt) and so geonegative that they were able to (and did) crawl out of the chamber through a small groove in the electrode housing that serves as the route of gas escape during sealing.

As expected, the weight-specific rate of O_2 uptake ($\dot{V}O_2$) varies inversely with body size (Fig. 2). $\dot{V}O_2$ was influenced by ambient PO_2 (PiO_2) even less in the present investigation than reported earlier (Mangum and Van Winkle, 1973), in all likelihood due to smaller body size.

Discussion

While the two analytical procedures might seem to yield occasionally contrary results for significant differences in O_2 equilibrium constants, we suggest that they essentially agree from a physiological point of view. Although the analysis reported in Table III requires fewer assumptions, several of the significant differences are trivial. For example, the RBC O_2 affinities of *Capitella* sp. II and IIIA are essentially the same, as are those of *Capitomatsus* VOZ and *Capitomastus* TAR. The difference between *Capitella* sp. I and IA is also small. Of possible relevance, two of these species pairs are known to share the same chromosome numbers. In *Capitella* sp. II and IIIa, 2n = 26;

Table II

Significance of ($P < .05$) differences in mean values of O_2 equilibrium constants in Table I

	Capitella					*Capitomastus*			
	sp. IA	sp. II	sp. IIIA	MB/sl	ORL	NCS	TAR	TRIN	VOZ
A. P_{50}									
Capitella									
sp. I	−	+	−	−	+	+	+	+	+
sp. IA		+	+	−	+	+	+	+	+
sp. II			−	+	+	+	+	+	−
sp. IIIA				+	+	+	+	+	−
MB/sl					+	−	+	+	+
ORL						−	+	+	+
Capitomastus									
NCS							+	+	+
TAR								−	−
TRIN									−
B. n_{50}									
Capitella									
sp. I	−	−	−	+	−	−	−	−	−
sp. IA		−	−	−	+	−	−	−	−
sp. II			−	+	−	−	−	−	−
sp. IIIA				−	−	−	−	−	−
MB/sl					+	−	−	−	−
ORL						−	−	−	−
Capitomastus									
NCS							−	−	−
TAR								−	−
TRIN									−

Table III

Oxygen equilibrium constants and their 95% confidence limits as estimated by regression analysis

Species	P_{50} (mmHg)	L_1	L_2	n_{50}	L_1	L_2
Capitella						
sp. I	7.05	6.65	7.45	2.19	1.27	3.11
sp. IA	7.75	7.68	7.82	2.24	2.05	2.43
sp. II	5.36	5.20	5.48	2.90	2.41	3.39
sp. IIIA	5.79	5.56	5.97	2.77	2.11	3.58
MB/sl	8.35	8.19	8.48	1.66	1.22	2.00
ORL	11.1	10.9	11.3	3.13	2.73	3.47
Capitomastus						
NCS	9.54	9.37	9.71	2.84	2.32	3.36
TAR	3.91	3.86	3.97	2.59	2.28	2.90
TRIN	2.76	2.68	2.84	2.02	1.65	2.39
VOZ	4.18	3.97	4.42	2.98	2.12	3.84

in *Capitella* sp. I and Ia, 2n = 20 (Grassle *et al.*, 1989). The chromosome number in *Capitomastus* VOZ is not known.

More importantly, most of the interspecific differences in O_2 affinity are large and physiologically meaningful. The values can be grouped as follows (1) *Capitomastus* TRIN, (2) *Capitomatsus* VOZ and *Capitomastus* TAR, (3) *Capitella* sp. II and IIIA, (4) *Capitella* sp. I, IA and MB/sl, (5) *Capitomastus* NCS, and (6) *Capitella* ORL.

To emphasize the magnitude of the interspecific differences, the range found in the present investigation is twice as great as that known in four species in the genus *Glycera* (Weber, 1978), which have never been regarded as cryptic. This comparison suffers from the unequal sample sizes. However, if the sample is enlarged and broadened to include all nine annelid and echiuroid RBC Hbs examined in the past two decades at a common temperature of 20°C (Mangum, 1992a), then the range reported here is still somewhat greater, despite the far narrower taxonomic scope. We suggest that the large range of O_2 affinities is due to the similarly large geographic range of our sample (see below). In contrast, the values in the literature do not represent tropical or otherwise warm waters.

We describe the 'cooperativity' of capitellid RBCs as apparent because many RBCs containing only monomeric and, when extracted and purified, non-cooperative Hbs exhibit Hill slopes significantly greater than 1 at high oxygenation states (*e.g.*, Mangum, 1976). This cellular level phenomenon, although very common, is not understood. The only information on the molecular weight of a capitellid Hb other than the anomalously low value of 12 kD for *Heteromastus filiformis* (Pals and Pauptit, 1979) is the figure of 34.5–36.4 kD for *Notomastus latericeus* Hb reported by Svedberg and Eriksson-Quensel (1934), which suggests a dimer. Bivalve dimers exhibit significant cooperativity, although not as much as found in several of the RBCs examined here. The nature of the apparent cooperativity exhibited by capitellid RBCs will remain unclear at least until their Hbs have been investigated in more detail.

Environmental correlates

Because the species in our sample have been recognized as such only recently, their full ecological and geographic ranges are essentially unknown. All of our material was collected from fine sediments in the intertidal or shallow subtidal zones. We know of no factors, behavioral or ecological, that would differentiate them according to ambient PO_2. Their considerable morphological similarity also precludes the likelihood of physiological differences arising from the design of gas exchange and transport systems. We tentatively suggest that at least some of the differences observed here may prove to be related to thermal characteristics of the environment. If the P_{50} values are arranged in series (Table IV), the highest O_2 affinities are found in species living in the warmest waters, and the lowest in species inhabiting colder waters. This relationship is far more clearly characteristic of a variety of other O_2 carriers (Mangum, 1992a,b). It results in more similar O_2 affinities at the natural temperatures than would exist in the absence of the adaptation.

Body size

None of the animals examined here exceeded 1 mm in diameter, and thus O_2 uptake would not be expected to be limited by the diffusion distance until the driving PO_2 gradient reaches quite low levels. The rate of O_2 depletion began to depart from linearity only below 50 mmHg (*e.g.*, Fig. 3) and continued to do so until O_2 uptake ceased.

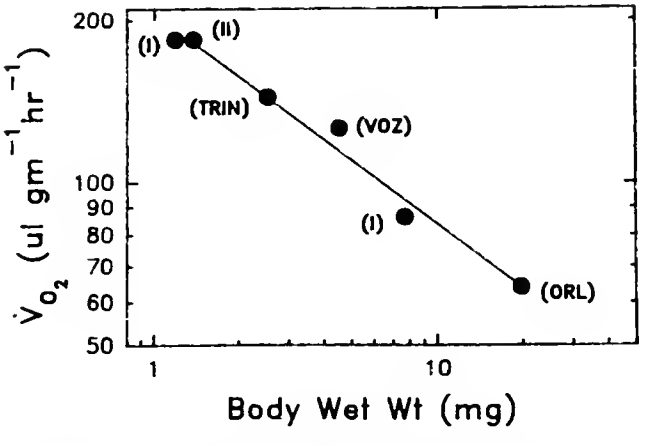

Figure 2. The relationship between O_2 uptake and body size in five capitellids at 20°C. The smallest animals were juveniles of *Capitella* sp. I; the remainder were adults.

Table IV

Oxygen affinity in relation to known geographic distribution

P_{50} (mmHg) at pH 7.4	Species	Distribution
2.76	*Capitomastus* TRIN	Trinidad
3.91	*Capitomastus* TAR	North Carolina
4.18	*Capitomastus* VOZ	Connecticut (thermal effluent)
5.36	*Capitella* sp. II	Marseille, Boston Harbor, and Cape Cod
5.79	*Capitella* sp. IIIA	Boston Harbor and Cape Cod
7.05	*Capitella* sp. I	Temperate zone cosmopolitan
7.75	*Capitella* sp. IA	Boston Harbor to New Bedford
8.35	*Capitella* MBsl	Mission Bay, California
9.54	*Capitomastus* NCS	Uncertain, perhaps Mission Bay, California
11.1	*Capitella* ORL	Cape Cod

The non-linear portion of the records (Fig. 3) represents a combination of (1) Hb deoxygenation and its contribution to the O_2 being consumed and (2) the diffusion-limited component of O_2 uptake. This portion can be bisected to provide a numerical estimate of the ambient PO_2 (PiO_2) at which these two processes occur, best expressed as the half constant [*e.g.*, the intersect of the dashed line and the trace of PO_2 in Fig. 3. The graphical procedure is essentially the same as that detailed by Colman and Longmuir (1963)]. This constant, which would be expected to be strongly influenced by both O_2 affinity and the magnitude of the diffusion limitation, is in fact highly correlated with body size ($r = 0.944$; $P < .05$) and, even more strongly, with P_{50} ($r = 0.977$; $P < .01$) (Fig. 4). The relationship between O_2 affinity, environmental temperature, and body size is actually syllogistic, with larger body size being found at higher latitudes and smaller animals found at lower latitudes. An interrelationship between PO_2, body size, and growth rate has been recently reported in *Capitella* sp. I by Forbes and Lopez (1990).

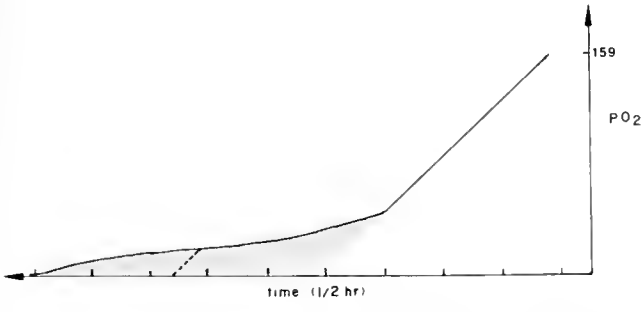

Figure 3. The decline in PO_2 with time due to O_2 uptake by two individuals (mean body wet wt. 39.4 mg) of *Capitella* ORL at 20°C. The shaded area represents the portion of O_2 uptake that is influenced by the release of Hb bound O_2 and by a limiting diffusion distance. The dashed line identifies the PiO_2 of half of the non-linear portion of O_2 uptake.

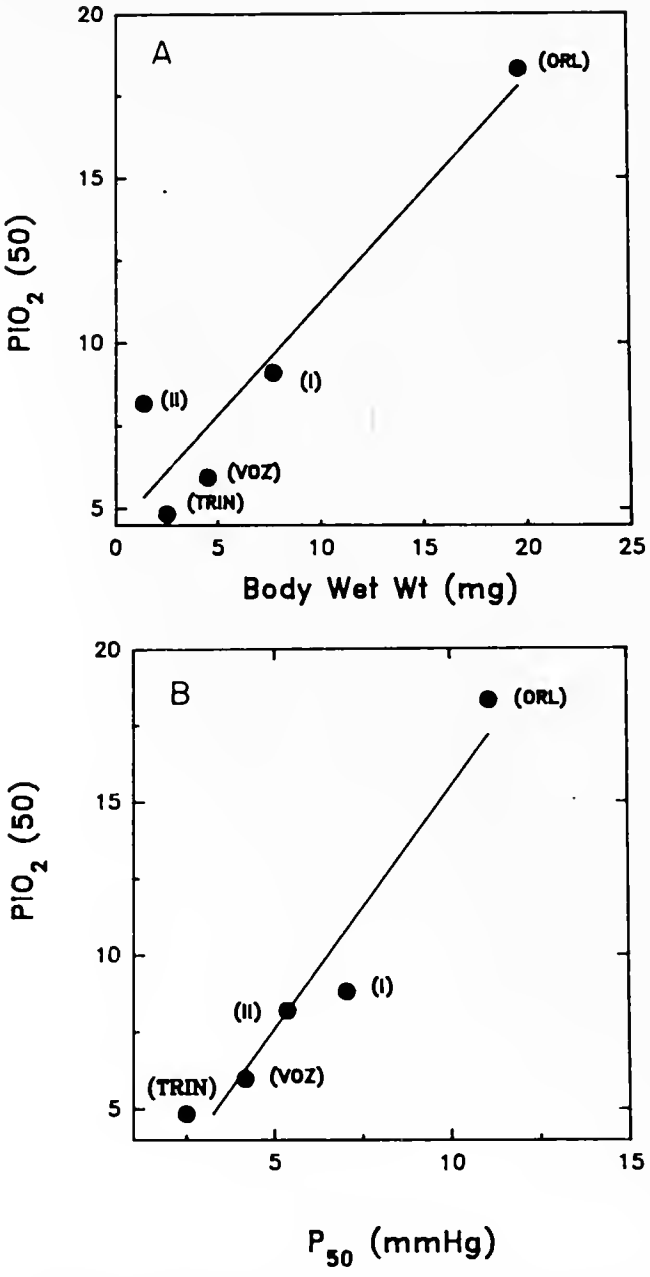

Figure 4. The relationship between the PiO_2 of half of the non-linear component of O_2 uptake (PiO_250) to body size (panel A) and O_2 affinity (panel B).

Most important in the present context, the respiratory properties of the RBCs are distinctive of most of the species examined here, for whatever adaptive reason. In view of the conservatism of the annelid RBC Hbs investigated previously (Weber, 1978; Mangum, 1992a), this was not necessarily an expected finding.

Acknowledgments

Supported by NSF DCB 88-16172 (Physiological Processes) to CPM, DMD 86-00614 (Biological Instrumen-

tation) to JMC, and BSR 86-00648 (Systematic Biology) to JPG.

Literature Cited

Colacino, J. M., and D. W. Kraus. 1984. Hemoglobin-containing cells of Neodasys (Gastrotricha, Chenotida). II. Respiratory significance. *Comp. Biochem. Physiol.* **79A:** 363–370.

Colman, C., and I. S. Longmuir. 1963. A new method for registration of oxy-hemoglobin dissociation curves. *J. Appl. Physiol.* **18:** 420–423.

Eckelbarger, K. J., and J. P. Grassle. 1987a. Spermatogenesis, sperm storage and comparative sperm morphology in nine species of *Capitella, Capitomastus* and *Capitellides* (Polychaeta: Capitellidae). *Mar. Biol.* **95:** 415–429.

Eckelbarger, K. J., and J. P. Grassle. 1987b. Interspecific variation in genital spine, sperm, and larval morphology in six sibling species of *Capitella. Bull. Biol. Soc. Wash.* **7:** 62–76.

Forbes, T. L., and G. R. Lopez. 1990. The effect of food concentration, body size, and environmental oxygen tension on the growth of the deposit feeding polychaete, *Capitella* species 1. *Limnol. Oceanogr.* **35:** 1535–1544.

Grassle, J. P., and J. F. Grassle. 1976. Sibling species in the marine pollution indicator *Capitella* (Polychaeta). *Science* **192:** 567–569.

Grassle, J. P., C. E. Gelfman, and S. W. Mills. 1987. Karyotypes of *Capitella* sibling species and of several species in the related genera *Capitellides* and *Capitomastus* (Polychaeta). *Bull. Biol. Soc. Wash.* **7:** 77–88.

Mangum, C. P. 1976. Primitive respiratory adaptations. Pp. 191–278 in *Adaptation to Environment: Physiology of Marine Animals,* R. C. Newell, ed. Butterworth's & Co., Ltd., London.

Mangum, C. P. 1992a. Respiratory functions of the red blood cell hemoglobins of six animal phyla. In *Blood and Tissue Oxygen Carriers,* C. P. Mangum, ed. Adv. Comp. Env. Physiol., Springer-Verlag, Heidelberg (in press).

Mangum, C. P. 1992b. Respiratory function of the molluscan hemocyanins. In *Blood and Tissue Oxygen Carriers,* C. P. Mangum, ed. Adv. Comp. Env. Physiol., Springer-Verlag, Heidelberg (in press).

Mangum, C. P., and W. Van Winkle. 1973. Responses of aquatic invertebrates to declining oxygen conditions. *Am. Zool.* **13:** 529–541.

Mangum, C. P., J. M. Colacino, and T. L. Vandergon. 1989. Oxygen binding of single red blood cells of the annelid bloodworm *Glycera dibranchiata. J. Exp. Zool.* **249:** 144–149.

Pals, G., and E. Pauptit. 1979. Oxygen binding properties of the coelomic haemoglobin of the polychaete *Heteromastus filiformis* related with some environmental factors. *Neth. J. Sea Res.* **13:** 581–592.

Svedberg, T., and I-B. Eriksson-Quensel. 1934. The molecular weight of erythrocruorin. II. *J. Am. Chem. Soc.* **56:** 1700–1706.

Weber, R. E. 1978. Respiratory pigments. Pp 393–446 in *Physiology of Annelids,* P. J. Mill, ed. Academic Press, London.

Wells, R. M. G., and L. M. Warren. 1975. The function of the cellular haemoglobins in *Capitella capitata* (Fabricius) and *Notomastus latericeus* Sars (Capitellidae: Polychaeta). *Comp. Biochem. Physiol.* **51A:** 737–740.

Reference: *Biol. Bull.* **182:** 135–144. (February, 1992)

Visual Cells and Pigments in a Demersal Fish, the Black Sea Bass (*Centropristis striata*)

K. V. SINGARAJAH* AND F. I. HÁROSI

Laboratory of Sensory Physiology, Marine Biological Laboratory, Woods Hole, Massachusetts 02543, and Department of Physiology, Boston University School of Medicine, Boston, Massachusetts 02118

Abstract. Using a single-beam, wavelength-scanning, dichroic microspectrophotometer, we measured absolute absorbance, bleaching difference absorbance, and linear dichroism spectra from isolated retinal receptors of the black sea bass, *Centropristis striata*. We determined, among other properties, the wavelength of peak α-band absorbance (λ_{max}) of the pigment of the receptor cells. Out of well over 100 recordings, we found only 3 spectral types of visual pigment. The shortest-wavelength-absorbing type (λ_{max} = 463 ± 2 nm) was present only in single cones. Both members of the double cones contained the longest-wavelength-absorbing pigment of the three, with λ_{max} = 527 ± 5 nm. Rods were found to bear a typical rhodopsin, with λ_{max} = 498 ± 2 nm. Thus, the retina of this predatory demersal fish appears to use a set of three closely spaced visual pigments, with λ_{max} clustering about 500 ± 30 nm. This remarkable feature is discussed in relation to photic conditions in the habitat.

Introduction

Because the function of an eye is to detect light from the environment, visual systems must have evolved in harmony with the prevailing photic conditions. An adaptation of certain aspects of eye structure to an animal *habit* was clearly recognized by Schultze (1866, 1867). Being an exceptionally keen observer, he noted a correlation between the preponderance of retinal rods in the eyes of nocturnal animals, and the occurrence of numerous cones in the retinas of diurnal animals. He rightly reasoned that there is no color perception at night, that nocturnal animals are therefore adapted to dim (scotopic), black-and-white conditions, and that their vision is primarily mediated by rods. Diurnal animals, on the other hand, are mainly exposed to bright (photopic) conditions, during which color sensation is most acute, and cones must therefore be the primary mediators of color vision. Thus, Schultze's observations provided the basis for what is now known as the Duplicity Theory, which encompasses some of the most basic features of vertebrate vision.

A second link, between vision and *habitat*, was realized by Clarke (1936). He knew that the peak transmittance of pure water is in the blue part of the spectrum; and the deeper the water column to be penetrated, the more "squeezed" is the daylight spectrum about the blue peak. On the basis of this understanding, he suggested "the possibility of a shift in sensitivity of the eye of a deep water fish toward the blue end of the spectrum." Indeed, not only do fishes of the deep sea have retinas with numerous long rods, but their photosensitive pigments (rhodopsins) also have blue-shifted peak absorbance (λ_{max}) values to match the dominant wavelength of the scarce quanta available to them (Denton and Warren, 1957; Munz, 1958). From these observations stemmed the Sensitivity Hypothesis, which proposes an adaptation to the photic environment by the selection of visual pigments that render the animal's eye most sensitive to the ambient illumination.

To account for the apparent mismatch between the underwater light and the λ_{max} of the visual pigments in a number of animals, other than deep sea fish, the Contrast Hypothesis was proposed (Lythgoe, 1972). The merit of the underlying idea is the recognition that the differential scattering and selective absorption of underwater light may cause an object viewed against its background space-light to be more visible with offset visual pigments than with matched ones. Thus, brightness contrast detection,

Received 3 June 1991; accepted 30 September 1991.

* Permanent address: Laboratory of Marine Biology & Comparative Physiology, DSE–CCEN, Federal University of Paraiba, Joao Pessoa—58059, Pb., Brazil.

in addition to sensitivity, is an important aspect of vision. So is color perception, in which λ_{max} variation of the visual pigment can play a major role. The question, at present, is not so much about the relative importance of these attributes in general, but rather their specific contribution to the evolution of the eye.

Although we still lack a unified theory of visual function, a refinement in the Sensitivity Hypothesis goes a long way toward explaining several vision-related phenomena. This refinement resulted from a series of extensive investigations (Munz and McFarland, 1973; McFarland and Munz, 1975a, b, c) in which not only the visual pigments were determined, but also the spectral radiance of natural light under many different environmental conditions was measured. It was found that the *twilight spectrum* was generally well matched by the scotopic pigments. Thus, the emerging concept was that the spectral location of *scotopic visual pigments* have been selected to enhance photosensitivity at *twilight*, for it is during this period that visual behavior is critical to survival (McFarland and Munz, 1975c).

Investigation of the *photopic visual pigments* has barely begun. Although surveys by Loew and Lythgoe (1978) and Levine and MacNichol (1979) are important contributions, providing correlations between habitat and the photopic pigments (see also Lythgoe, 1984), the development of this area of research is still in its infancy.

For the present study, we chose a day-active predatory fish that inhabits a marine environment with a fairly well delineated photic habitat. By the use of microspectrophotometry, we set out to determine the light absorbing properties of its visual pigments throughout the visible and near ultraviolet spectrum. We also made an attempt to estimate the spectral light available in the fish's environment. We report here our findings concerning the spectroscopic relationship between visual pigments and the ambient irradiance.

Materials and Methods

Experimental animals

Specimens were obtained through the courtesy of the US National Marine Fisheries Service Aquarium at Woods Hole. The fish we used were small specimens that had been trapped in Woods Hole Harbor late in the summer of 1990 (about 6 months prior to their use) and maintained in natural seawater aquaria at about 18°C (65°F). The fish were regularly fed with brine shrimp, clams, and squid, and were kept under artificial illumination (8 h on/16 h off) with some natural light filtering into the building over their tanks.

Preparation

Before use, each fish was dark-adapted for at least 1 h, and anesthetized with aerated seawater containing tricaine methanesulfonate (MS222, Sigma Chemical Company) at a concentration of 0.25 g per liter. Enucleation of the eye was performed under dim red light. The cornea, iris, and lens were removed by a cut with a sharp razor blade, transverse to the anatomical axis, about 1 mm behind the equatorial circumference of the eye, and the entire eyecup was quickly transferred to cold saline solution. With the aid of a modified, low-power dissecting microscope equipped with infrared illumination and an image converter, the retina was eased away from the back of the eye while the eyecup still submerged. From the whole retina, small pieces (about 1 mm^2) were cut, transferred to a No. 1½ coverslip, and teased apart with two pairs of fine forceps in a drop of saline solution. The fragmented retina preparation was covered with a second No. 1½ coverslip of smaller size, blotted gently along its edges, and sealed with a mixture of molten paraffin and Vaseline, as described earlier (Hárosi and MacNichol, 1974a). The saline we used here was a modified marine teleost Ringer solution (Forster and Taggart, 1950), containing 10 m*M* HEPES buffer at pH 7.3.

Spectrophotometer

The spectral measurements were carried out with the help of the dichroic microspectrophotometer (DMSP) described previously (Hárosi and MacNichol, 1974b; Hárosi, 1982, 1987). The DMSP is a computer-controlled, wavelength-scanning, single-beam photometer that records transmitted light fluxes through microscopic samples. The measuring beam is commonly adjusted to about 1 × 3 μm in the plane of the specimen, and its spectral purity (monochromaticity) to about 5 nm. This beam is focused by a quartz field lens onto the back aperture of the condenser through a Glen-Thompson UV polarizer and a CaF_2 photo-elastic modulator. The condenser we routinely used was a 32/0.4 Ultrafluar (Zeiss), whereas the objective was a 100/1.3 UV-F100 (Nikon) microscope objective, both of the glycerine immersion type. Due to limitations imposed by the latter objective, light detection was possible only at wavelengths greater than about 330 nm.

Spectral recording and analysis

Average and modulated light fluxes were detected with a cooled photomultiplier tube (Hamamatsu, Type R375), and photocurrents were recorded into two sets of 75 sequential memory locations as the wavelength was scanned rapidly (500 nm/s) from the short wavelength to the long wavelength end of the spectrum (275–645 nm). Corresponding signals were summed, and the memory locations thus contained numbers signifying transmitted flux amplitudes averaged over 5-nm-wide segments of the spectrum. A typical measurement included 16 background scans from a cell-free area in the preparation (reference measurement), 8–16 prebleach scans (sample measure-

ment), a 2-min exposure to actinic light provided by the measuring beam (the wavelength of which was preset to the vicinity of the expected λ_{max}) if bleaching was desired, and a 16-scan postbleach recording of the sample. The dedicated digital computer of the DMSP subsequently calculated (from the average and modulated transmitted fluxes) the average absolute absorbance (A), the bleaching difference absorbance (BD), and the linear dichroism (LD) spectra. Absorbance (optical density) is defined as $\log(T)^{-1}$, where T is transmittance. Linear dichroism is proportional to sample polarization, defined as $p = (T_{\parallel} - T_{\perp})/(T_{\parallel} + T_{\perp})$. The LD ordinate is calibrated so that a perfect analyzer would yield +1, if crossed, and −1, if parallel to the plane of the polarizer. For details of the measurement technique, the selection of spectra, and data analysis, see Hárosi (1975a, 1987).

Visual pigment characterization

Our spectroscopic description of a pigment is based on A, BD, and LD determinations from optically isolated single or overlapping multiple photoreceptor cells. Empirical evidence suggests that, in general, the three types of measurement yield three λ_{max} values that will "bracket" the "true" λ_{max} of the visual pigment. Occasionally, λ_{max} may be slightly blue-shifted (due to photoproduct absorption and excessive short-wave scattering); BD_{max} is usually red-shifted (because shortwave absorbances, which are subtracted, tend to be exaggerated); whereas LD_{max} should theoretically be close to λ_{max} (provided there is no instrumental delay between the "ac" and "dc" detection channels). Rhodopsins (based on the aldehyde of vitamin A_1, or retinal) and porphyropsins (based on the aldehyde of vitamin A_2, or 3-dehydroretinal) have several distinguishing properties *in situ:* (1) α-band half-bandwidth (HBW) value (*i.e.*, rhodopsins being narrower than porphyropsins); (2) β-band absorbance (*i.e.*, rhodopsins having relatively lower β-band absorbance than porphyropsins); (3) transverse specific density (*i.e.*, rhodopsins have higher molar extinction than porphyropsins); (4) dichroic ratio (*i.e.*, rhodopsin bearing cells show greater optical anisotropy than those with porphyropsin); and (5) absolute λ_{max} value, which is informative only beyond 570 nm (*i.e.*, no purely retinal-based pigment has ever been found with λ_{max} greater than about 570 nm).

Following Fourier smoothing of the "raw" spectra, software algorithms can determine the peak absorbance and half-bandwidth values. The α-band of a typical rhodopsin absorbance spectrum has a HBW of 4000–4100 cm^{-1}, whereas that of a typical porphyropsin is about 4800 cm^{-1}. Moreover, in both classes of visual pigment, the HBW is a function of wavelength, such that with increasing λ_{max}, the HBW progressively narrows, and with decreasing λ_{max}, it progressively broadens. We made use of these properties in our characterization of the sea bass visual pigments.

Quantal absorption of pigments vs. environmental illumination

In search of the correspondence between visual pigments and the photic environment, we analyzed models that are consistent with the premise that photoreceptors are quantum detectors with a response primarily dependent upon the *total number of quanta absorbed per unit time* by their visual pigment (rate of quantum catch), bleaching and regeneration notwithstanding. We further assumed that downward irradiance of solar origin is the primary determinant for the sea bass visual system. We made use of data available in the literature on solar irradiance and on the optical properties of natural bodies of water, and we used our own spectroscopic determinations on the photoreceptors.

We performed the following calculations. (1) Using the standard solar irradiance data of Moon (1940; Table III), by a procedure similar to that adopted by Dartnall (1975), we generated quantal irradiance values expected at sea level in quanta/s × mm^2 × nm, at 1-nm intervals (by linear interpolation). (2) The classification on optical water types and transmittance data of Jerlov (1968; Table XX) permitted the transformation of downward irradiance values to any depth. Following the suggestion of Dartnall (1975), his five oceanic water types were designated JI, JIA, JIB, JII, and JIII, and the five coastal water types as J1, J3, J5, J7, and J9. Downward irradiances were calculated for all 10 water types for depths of 10, 20, 50, 100, 150, and 200 m for 1-nm intervals. (3) The visual pigment absorbance spectra obtained at 5-nm intervals were again interpolated to 1 nm in the available range of 350–650 nm. (4) Rate of quantal absorption (quantum catch) by each visual pigment was determined for the three receptor types at six depths in ten water types. The total absorbed quantum flux density rate Q_t was, in each case, obtained by summing the products of the appropriate quantal irradiance and receptor absorptance at each nanometer of wavelength. Absorptance had the usual definition: $A(\lambda) = 1 - 10^{-D(\lambda)}$, where $D(\lambda) = D_{max} A_{rel}(\lambda)$. The peak absorbance, D_{max}, was obtained as a product $S_{\perp}$ (Table 1) and the axial pathlength through the outer segment of the receptor type containing the pigment. The average lengths observed in our video records for single cone, rod, and double cone outer segments were 9, 20, and 23 μm, respectively. $A_{rel}(\lambda)$ was derived from the normalized absorbance spectra (depicted in Fig. 5).

In an attempt to find criteria by which the correspondence between visual pigment absorptance and environmental light could be judged, we calculated the wavelengths at which 25%, 50%, and 75% of the total quantum catch occurs in each receptor type in a given photic environment. With a symbolic designation of λ_{qc50} for the 50% value, this is analogous to the λP_{50} introduced by Munz and McFarland (1973). Note, however, the differ-

Table I

Spectral data for black sea bass cones

Cone type	No. of determ	λ_{max} [nm]	HBW [cm^{-1}]	A_{max} [OD]	R	d [μm]	$S_{\perp}$ [OD/cm]
Single	6			0.03167 ± 0.0065	1.64 ± 0.19	2.9 ± 0.3	136 ± 22
A	6	463.2 ± 2.2	4638 ± 296				
LD	6	460.3 ± 2.3	4670 ± 625				
BD	3	469 ± 3.5	3737 ± 673				
A + LD	12	461.7 ± 2.7	4654 ± 467				
A + LD + BD	15	463.2 ± 4	4470 ± 616				
Best Estimate		463 ± 4	4500 ± 600				
Double	8			0.04774 ± 0.0160	1.52 ± 0.14	3.0 ± 0.4	161 ± 39
A	8	526.8 ± 5.5	3928 ± 197				
LD	8	527 ± 4.7	3728 ± 237				
BD	5	529.7 ± 4.5	3634 ± 159				
A + LD	16	526.9 ± 5	3828 ± 235				
A + LD + BD	21	527.5 ± 4.9	3782 ± 231				
Best Estimate		527 ± 5	3800 ± 200				

Abbreviations used: HBW, half-bandwidth; A_{max}, peak absorbance; OD, optical density; R, dichroic ratio; d, mean diameter of outer segment; $S_{\perp}$, specific density (transversely polarized); A, α-band of absorbance spectrum; LD, α-band of linear dichroism spectrum; BD, α-band of bleaching difference absorbance spectrum.

ence between the two: while λP_{50} is the wavelength at which 50% of all the quanta occur in the spectrum of 400–700 nm in a given photic setting, λ_{qc50} is a measure of the absorptive interaction between light and pigment throughout their available spectral range.

We also calculated total quantum catch ratios between the receptor types in the retina of this fish. Although each Q_t value is critically dependent on the axial pigment density assumed in the calculation, the Q_t ratios indicate the relative "weight" of the receptor types in the retina. As the spectral distribution of light changes with water type and with depth, the quantum catch by the receptor types vary, and the Q_t ratios may go "out of balance." Although we do not know the range of appropriate quantum catch ratios, we found them to be indicative of the "spectral match" that exists between photoreceptors and environmental light. The second criterion by which to assess the appropriateness of a visual pigment to a given environment is the difference between λ_{qc50} and the λ_{max} of the pigment in question. Again, we do not know how large this difference should be before it becomes unacceptable. Based on the experience gained in this analysis, we tentatively set the limit of acceptability at 30 nm for the difference between λ_{qc50} and λ_{max} of a pigment, and 100% for the change in Q_t ratio of two receptor types.

We made no attempt to account for the retinal distribution of the different pigments, their relative proportions, or the light collecting efficiency of the various cell types. Nor did we consider the light collection efficiency of the eye as a whole, or the losses of light that occur at the ocular media and their interfaces. The modifying effects of these factors we envisage investigating in the future as sufficiently accurate and detailed information becomes available.

Results

Although we measured well over one hundred photoreceptors, permanent records were saved from 17 single cones and 66 outer segments belonging to 39 double cones. Additionally, we recorded from 12 groups of multiple rods. In our fragmented retina preparations, the most frequently occurring cells were rods. While double cones could also be located with relative ease, single cones were less numerous. Photoreceptor morphology is illustrated in Figure 1. With these examples, we wish to make the point that double cones were variable in size and shape: the two members were practically identical in some, but quite different in others. For this reason, we simply refer to them as "double" and refrain from the use of the term "twin," even though the visual pigments in the two members were spectroscopically indistinguishable, as will be shown below.

Single cones

All single cones encountered had one type of shortwave, or blue-absorbing, visual pigment. The outer segments were transversely dichroic, and their pigment content was bleachable. Representative spectra are depicted in Figure 2. Spectral data are summarized in the upper part of Table I; note the several subgroup averages calculated for λ_{max} and HBW. The "best estimate" for each is based on the over-all average.

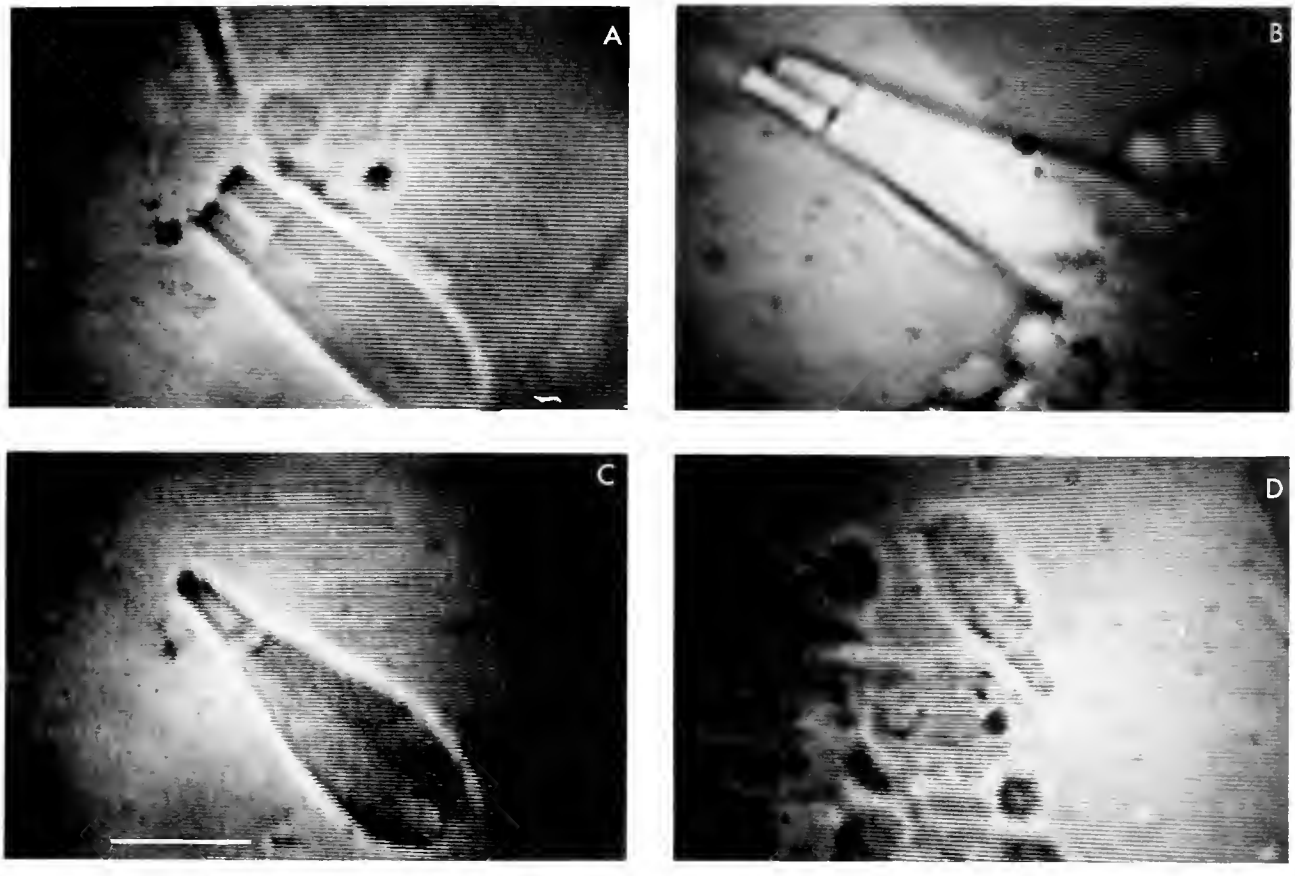

Figure 1. Black sea bass photoreceptors viewed in infrared illumination in the recording microspectrophotometer. The images were captured on video tape and subsequently photographed from a video monitor display. A. Double cone in lateral view, just below a rod outer segment. B. Double cone with unequal outer segments. C. Double cone in a rare orientation, with overlapping outer segments. D. Single cone, proximal to retinal fragments. All four panels have equal magnification and the bar length represents 10 μm.

Double cones

Every outer segment belonging to double cones was transversely dichroic due to the presence of a bleachable pigment. Representative spectra are shown in Figures 3 and 4, and spectral data are presented in the lower part of Table I. The A and BD spectra of Figure 3 were derived from one member of double cones. The spectra of Figure 4 were obtained from overlapping outer segments of double cones (see panel C of Fig. 1). Note the increased spectral absorbance in Figure 4A as compared to that in Figure 3A. The idea we illustrate here is that, when the two outer segments overlap laterally, the transversely scanned absorbance nearly doubles, as it should if the two members are equivalent. However, while the A and BD spectra increase in proportion when measured from two, instead of one member, the λ_{max} and the HBW remain virtually unchanged. This can happen only if the same pigment is contained in both members. There was no evidence for the presence of a second pigment in any of the double cones.

Rods

As is common in teleost retinas, the rods of the black sea bass are numerous; the outer segments are of variable length and slender, with a diameter of 1 μm or less. Recordings from multiple rods yielded A, BD, and LD spectra indicative of a "typical" rhodopsin. Trace B in Figure 5 was derived from such absorbance spectra. The HBW of the α-band of the rod absorbance spectra were within experimental error of the value obtainable from other rhodopsins (such as amphibian or monkey), and this pigment should, therefore, also be based on vitamin A_1. Traces A and C in Figure 5 depict the normalized absorbance spectra of the cone pigments. The two cone pigment spectra flank the rod pigment spectrum on the longwave and shortwave sides by nearly the same distance on the wavelength scale.

Dichroic ratio and transverse specific density

The algebraic relationships necessary to determine cellular dichroic ratios from the A and LD spectral mea-

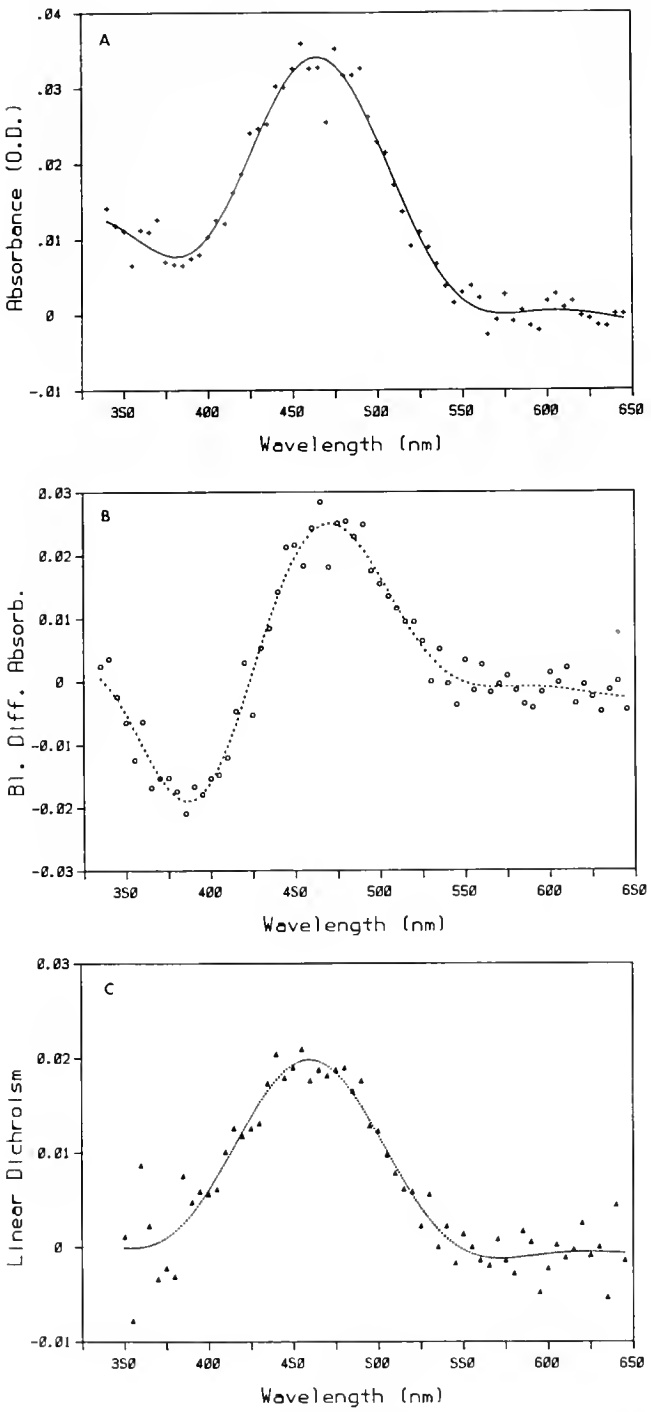

Figure 2. Absorbance, bleaching difference absorbance, and linear dichroism spectra of the visual pigment in single cones of the black sea bass. A. Average absorbance spectrum based on four single-cell recordings (+). The solid curve is the result of Fourier smoothing. Peak absorbance and half-bandwidth are 464 nm and 4430 cm^{-1}, respectively. B. Bleaching difference spectrum from one cell. Data values (○) were derived from prebleach and postbleach measurements consisting of the sum of 16 scans, each. The dashed curve is based on Fourier-smoothed data. The positive band peaks at 471 nm, with HBW = 3140 cm^{-1}; the negative band peaks at 387 nm, with HBW = 3570 cm^{-1}. C. Average linear dichroism from 3 cells (△). The dotted line, again, is the result of Fourier-filtered data with λ_{max} = 460 nm and HBW = 4460 cm^{-1}.

surements have been published previously (Hárosi, 1987). The results for the black sea bass cones are listed in Table I. The last column in Table I shows numerical values for the transverse specific density, $S_\perp$. For this determination, the transversely polarized component of the peak absorbance, $A_\perp$, is needed. The latter is derived from the average (unpolarized) peak absorbance, A, divided by factor f, which in turn depends on the dichroic ratio, R, defined as $R = A_\perp/A_\parallel$. Thus, $f = (1 + R)/2R$ and $A_\perp = A/f$. Finally, $S_\perp = A_\perp/d$, where d is the mean diameter of the compartment (Petry and Hárosi, 1990). Thus, the meaning of $S_\perp$ is peak absorbance for transversely polarized light per unit thickness (measured either in micrometers or centimeters).

Discussion

In our teased preparations obtained from various regions of the retina of the black sea bass, we found rods, double cones, and single cones. The outer segment in each of these cells contained a visual pigment characterized by a typical absorption spectrum, dichroism, and light-sensitive spectral changes (*i.e.*, bleaching). On the basis of half-bandwidth determinations, we identified the chromophore of these pigments as *retinal*. Additional evidence comes from the low β-band absorbances which we commonly observed. The results on specific density ($S_\perp$) also support this, because the cones yielded higher values of this parameter than those obtainable from cells using pigments with 3-dehydroretinal as chromophore, although not quite as high as what has been reported in cases of amphibians and monkeys. This discrepancy may be related to the results on dichroic ratio, which were also below expectation (see below).

The presence of only two cone pigments would make the black sea bass dichromatic in the traditional sense, although we have no evidence which could preclude the rods from chromatic discrimination tasks. Nevertheless, "color vision" can be supported by only two cone mechanisms, as we know from other studies on animals, as well as on humans. The existence of many vertebrates with trichromatic and even tetrachromatic *cone mechanisms* raises the question as to why this species has evolved only two. The simplest answer is, perhaps, that there was no selective pressure to have more. Given the relatively narrow spread of wavelengths at greater depths, there is probably no advantage in having more cone types, even though the eye's spectral resolution could be improved by adding more closely spaced "color channels." While vertebrate eyes would make very poor spectrographs, they nonetheless serve the bearer well. To evaluate just how well an organism is served by its eyes, we would need to know not only the lighting conditions and reflectance properties of all objects, but also the visual tasks that need to be solved in capturing food, avoiding predators, finding

mates, and continuing successful reproduction (Dartnall, 1975; Levine and MacNichol, 1979). Clearly, more knowledge is required before precise answers can be found.

Similar visual pigments have been previously reported for four other species of fish. Also using microspectrophotometry, Loew and Lythgoe (1978) investigated several species of fish from various "environmental groups." In the "moderately deep coastal group" they reported finding two cone pigments with λ_{max} of 460 and 530 nm, respectively, and a 502-nm rod pigment in two species of gurnard (*Trigla lucerna* and *Eutrigla gurnardus*). Two other species of marine fish with similar pigments were found by Levine and MacNichol (1979). These were the sea robin (*Prionotus carolinus*) and the scup (*Stenotomus versicolor*).

Photic habitat of the black sea bass

Although information on habitat is rather scanty, this fish inhabits waters within a depth range of a few meters from the surface, to 165 m. Being demersal, they are caught in large numbers in waters of 50–150 m depth. This species is mainly a bottom feeder, and prefers to be among rocks and reefs. Males have been observed to develop a bright blue color prior to spawning. Spawning involves buoyant eggs in depths ranging between 18–45 m; the larvae tend to move to inshore waters over rocky bottoms (Bigelow and Schroeder, 1953; Perlmutter, 1961; Gordon, 1977).

Relevant spectral data on habitat

There is a general dearth of information, particularly field measurements, on the photic environment of the black sea bass. The specimens we used were caught in Woods Hole Harbor, where the color of the water is green. This agrees with Clarke and Denton (1962), who reported that the maximum transparency of coastal waters can be generally found in the range of 500–600 nm. We think that type 5 of the coastal series of Jerlov (J5) would be appropriate for the optical characterization of this habitat. Because the black sea bass is a widely distributed species, ranging from southern Massachusetts to Florida and from bays and sounds to Georges Bank, it will encounter offshore oceanic waters as well. Based on Jerlov's (1968) regional classification of optical water types, the western North Atlantic is described by type IB of the oceanic series (JIB). Thus, it appears reasonable to assume, as initial conditions, that this fish's visual system needs to cope with photic habitats expected of optical waters from JIB to J5. But these *a priori* assumptions are unnecessary, for similar conclusions can be drawn from the analysis discussed below.

Correlation between downward irradiance and receptor pigments

We calculated the rate of quantum flux density absorption ("quantum catch") by the sea bass visual pigments in the downward solar irradiance (from Moon's data) transformed by the optical water types of Jerlov (see Methods for details). We also determined quantum catch (Q_t) ratios between the receptor types and the wavelength of 50% quantum catch (λ_{qc50}) for each pigment at each depth. Table II depicts some of the results. Overall, the data show good agreement between λ_{qc50} and λ_{max} of the blue pigment in ocean waters and the same for the green pigment in coastal waters. Although the absolute values of Q_t and λ_{qc50} vary for the three receptor types in the depth range of 10–200 m and across the oceanic types JI–JIII, the Q_t ratios show no drastic variations. Nor do the λ_{qc50} and λ_{max} differences. This is not true for the coastal water types. Even at 10 m depth, these parameters undergo significant changes from J1 to the other types, so that in

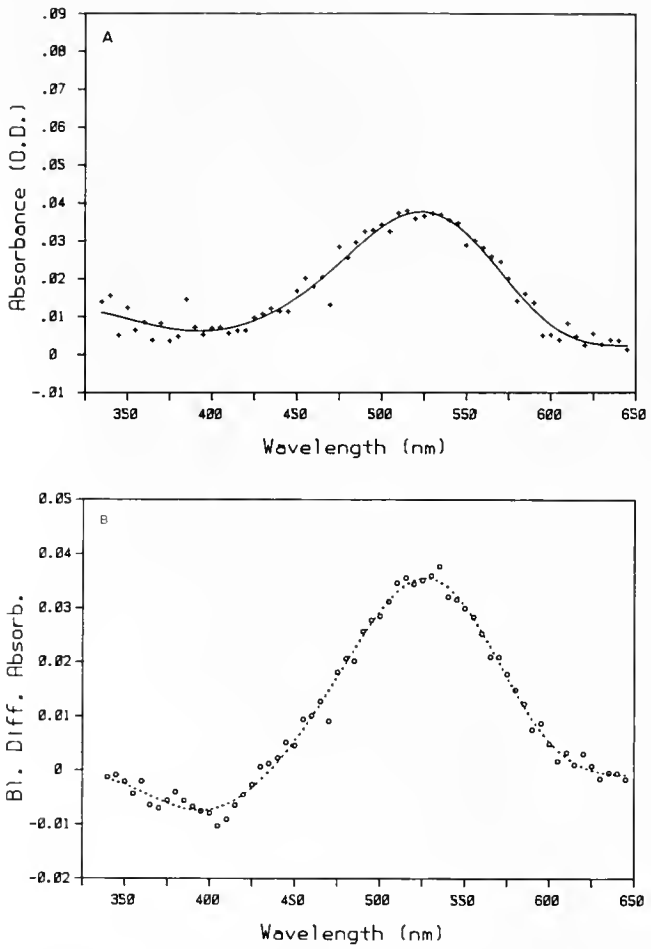

Figure 3. Absorbance and bleaching difference absorbance spectra derived from one of the outer segments of a double cone in the black sea bass. A. Average absorbance obtained in 16 scans (+). The solid curve represents the result of Fourier smoothing; λ_{max} = 524 nm, HBW = 4060 cm^{-1}. B. Average of three bleaching difference spectra, each of which is based on 16 scans (○); the dashed curve is derived from Fourier smoothing. The positive band peaks at 527 nm, with HBW = 3590 cm^{-1}, whereas the negative band peaks at 395 nm, with HBW = 4300 cm^{-1}.

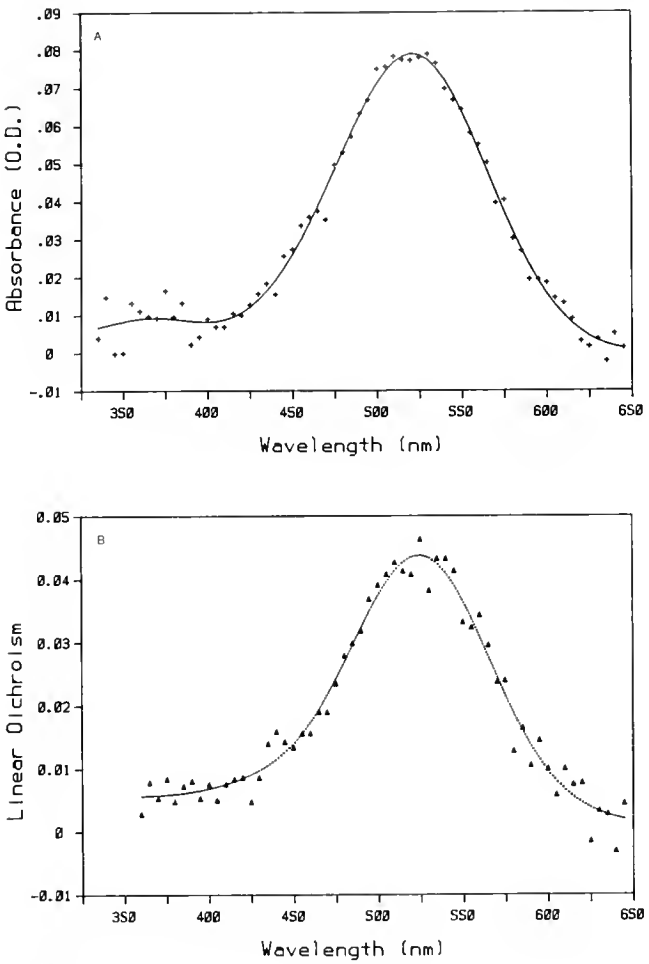

Figure 4. Absorbance and linear dichroism spectra obtained simultaneously from both outer segments (stacked one above the other) of a double cone in the black sea bass. A. Average absorbance, based on 16 scans (+); the solid curve is the product of Fourier smoothing: λ_{max} = 521 nm, HBW = 4010 cm^{-1}. B. Linear dichroism from the corresponding structure, based on 16 scans (△); the dotted curve is the outcome of Fourier filtering. The λ_{max} and the HBW are 525 nm and 3860 cm^{-1}, respectively.

J7, for example, G/B = 10.2, and in J9 it is 26.8. With increasing depth in these types of water, the sea bass visual pigments are clearly out of tune. For the J5 water type, the parameters are probably within acceptable range to depths of 20 m (see Table II). At greater depths, however, the fitness of the pigments become questionable. For instance, in J5 at 50 m depth the λ_{qc50} and λ_{max} differences are 55.6 nm, 27.5 nm, and 2.3 nm for the B, R, and G receptor types, respectively; the absolute Q_t values are down six orders of magnitude with respect to those at 10 m, and the R/B, R/G, and G/B ratios yield 5.3, 0.7, and 7.5, respectively. Although we lack firm criteria by which to interpret these numbers, they probably indicate an intolerable mismatch of the pigments to this photic habitat.

On the magnitude of the dichroic ratio in cones

Ever since the discovery of linear dichroism in laterally viewed rods by Schmidt (1938), the phenomenon has been interpreted in terms of a structural anisotropy in the outer segments of vertebrate photoreceptors. A quantitative measure of this property is the cellular dichroic ratio, R, as was defined in an earlier section. The magnitude of R is an expression of structural "order"; *i.e.*, the larger the R, the more ordered is the disposition of the visual pigment in the cell. Aside the complexities of interpretation, rhodopsin-containing rods yield larger R values than porphyropsin-bearing rods (Hárosi, 1975b). Furthermore, cone dichroic ratios are always smaller than those obtainable from rods, regardless of pigment class. In published accounts, for example, goldfish (Hárosi and MacNichol, 1974a), Japanese dace (Hárosi and Hashimoto, 1983), and carp (Hawryshyn and Hárosi, 1991) yielded mostly values with $R \geq 2$. In comparison, the average values we obtained for the black sea bass were $R_{double} = 1.52 \pm 0.14$ (n = 8) and $R_{single} = 1.64 \pm 0.19$ (n = 6) (see Table I). Although in one instance R = 1.9 was found in a single cone, we conclude that the values are rather smaller than they ought to be. Obviating the trivial interpretation of these results as instrumental artifact, there is the possibility that our experimental specimens were subnormal in their photoreceptors. The notion we entertain here is that these fish, although appearing quite healthy, nonetheless have suffered *subtle structural damage* in their retinal receptors

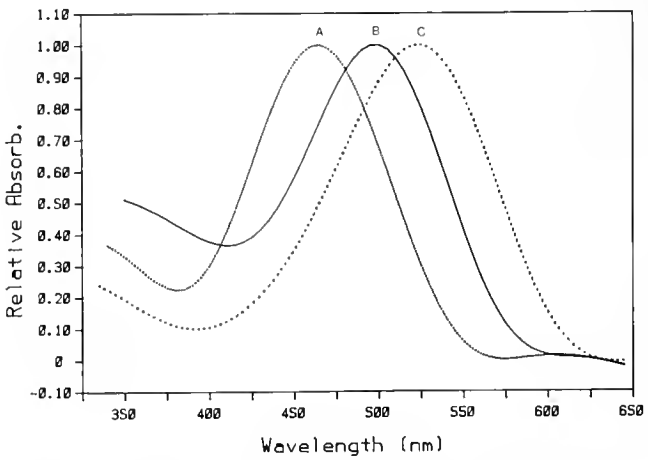

Figure 5. Comparison of relative absorbance spectra determined from the three visual pigments present in the black sea bass. Each curve was obtained from an experimental absorbance spectrum by dividing the data set by its peak value. The dotted curve (A) is based on Figure 1A. The solid curve (B) was derived from two sets of multiple rod absorbance measurements, each consisting of 16 scans. The dashed curve (C) was replotted from the spectrum of Figure 2A. The λ_{max} and the HBW of these spectra are: for single cone, 464 nm, 4430 cm^{-1}; for rod, 498 nm, 4260 cm^{-1}; for double cone, 524 nm, 4060 cm^{-1}, respectively. Note that the two outer segments of double cones contained visual pigments that were spectroscopically indistinguishable from one another.

Table II

Absorbed quantum flux density rates by black sea bass visual pigments, Q_t, in 10^{12} quanta/s × mm² (integrated in 1-nm steps from 350–650 nm) as a function of depth

Depth [m]	Single cone B, λ_{max} = 463 nm		Rod R, λ_{max} = 498 nm		Double cone G, λ_{max} = 527 nm		Quantum catch ratios		
	Q_t	λ_{qc50} [nm]	Q_t	λ_{qc50} [nm]	Q_t	λ_{qc50} [nm]	R/B	R/G	G/B
For oceanic water type JIB:									
10	40.08	472.0	111.49	491.0	122.32	509.2	2.782	.911	3.052
20	27.15	470.0	71.22	486.8	73.18	501.3	2.624	.973	2.696
50	8.762	468.4	20.49	478.8	19.04	487.9	2.338	1.076	2.172
100	1.426	466.1	3.022	472.9	2.630	477.7	2.119	1.149	1.844
150	.2435	465.1	.4901	470.1	.4148	473.5	2.013	1.182	1.704
200	.0427	464.5	.0835	468.6	.0696	471.2	1.953	1.199	1.629
For coastal water type J5:									
10	1.106	499.1	4.429	516.7	6.248	529.1	4.005	.709	5.651
20	.0319	507.9	.1462	521.5	.2088	529.8	4.580	.700	6.541

Notes:

(1) B and G are blue- and green-absorbing visual pigments, while R stands for rhodopsin of the rod.

(2) Absorbed quantum flux density was obtained from absolute *absorptance* of a pigment by the relation $A(\lambda) = 1 - 10^{-D(\lambda)}$, where $D(\lambda)$ is optical density at a given wavelength. $D(\lambda)$ was derived from the relative absorbance values (spectra shown in Fig. 5) multiplied by the peak axial absorbances of the pigments *in situ*. Actual peak absorbances used for the single cone, rod, and double cone pigments were 0.12, 0.32, and 0.37, respectively.

(3) JIB and J5 correspond, respectively, to the optical water types IB and 5 of Jerlov (1968).

(4) λ_{qc50} is the wavelength at which 50% of the "total quantum catch" is attained by a visual pigment in a given photic environment.

due to the artificial illumination (and possibly from nutritional deficiency) while in captivity. In view of a number of recent studies of light damage conducted primarily on mammals, the idea has rational basis and appears worthy of further investigation.

Summary

By determining the visual pigments in the retina of the black sea bass and analyzing the expected quantum catch by the photoreceptor types, we obtained indications for the preferred photic habitat. We used two criteria to assess the fitness of a set of visual pigments to ambient light: (1) ratio of quantum catches by the receptor types; and (2) the deviation of the wavelength at 50% quantum catch from the λ_{max} of each pigment in a given photic environment. Indications were that the black sea bass has a balanced set of three pigments to match the downward irradiance spectrum of clear ocean water to depths of 200 m. However, for coastal waters the fit is limited to the optical types J1, J3, and J5, and the last type to only a depth of about 20 m. Water types J7 and J9 are expected to be unsuitable to the black sea bass at all but the shallowest of depths. *This suggests that the λ_{max} of visual pigments in a multi-pigmented system are selected on the basis of the photic interaction between environmental light and the pigment spectrum to produce a balanced quantum catch in the receptor types.* Whether this is a general rule, or there are other criteria by which one λ_{max} is preferred over another, are questions to be settled by future investigations.

Acknowledgments

We wish to express our appreciation to Fred Nichy and his colleagues of the National Marine Fisheries Service, NOAA, Woods Hole Laboratory for their unfailing support in providing us with the experimental specimens for this work. Financial support was provided by the Federal Government of Brazil—CAPES, Ministry of Education, while one of us was on sabbatical leave (KVS) and grant EY04876 of the USPHS (to FIH).

Literature Cited

Bigelow, H. B., and W. C. Schroeder. 1953. *Fishes of the Gulf of Maine.* Fishery Bulletin of the Fish and Wildlife Service, Vol. 53. U. S. Government Printing Office, Washington, DC. 577 pp.

Clarke, G. L. 1936. On the depth at which fish can see. *Ecology* **17:** 452–456.

Clarke, G. L., and E. J. Denton. 1962. Light and animal life. Pp. 456–468 in *The Sea,* Vol. 1, Physical Oceanography. M. N. Hill, ed. Interscience, New York.

Dartnall, H. J. A. 1975. Assessing the fitness of the pigments for their photic environments. Pp. 543–563 in *Vision in Fishes: New Approaches in Research.* M. A. Ali, ed. Plenum Press, New York.

Denton, E. J., and F. J. Warren. 1957. The photosensitive pigments in the retinae of deep-sea fish. *J. Mar. Biol. Assoc. (U. K.)* **36:** 651–662.

Forster, R. P., and J. V. Taggart. 1950. Use of isolated renal tubules for the examination of metabolic processes associated with active cellular transport. *J. Cell. Comp. Physiol.* **36:** 251–270.

Gordon, B. L. 1977. *The Secret Lives of Fishes.* Grossart & Dunlap Publishers, New York. 305 pp.

Hárosi, F. I. 1975a. Microspectrophotometry: the technique and some of its pitfalls. Pp. 43–54 in *Vision in Fishes: New Approaches in Research,* M. A. Ali, ed. Plenum Press, New York.

Hárosi, F. I. 1975b. Absorption spectra and linear dichroism of some amphibian photoreceptors. *J. Gen. Physiol.* **66:** 357–382.

Hárosi, F. I. 1982. Recent results from single-cell microspectrophotometry: cone pigments in frog, fish and monkey. *Color Res. Applic.* **7** (No. 2, Part 2): 135–141.

Hárosi, F. I. 1987. Cynomologus and rhesus monkey visual pigments: application of Fourier transform smoothing and statistical techniques to the determination of spectral parameters. *J. Gen. Physiol.* **89:** 717–743.

Hárosi, F. I., and Y. Hashimoto. 1983. Ultraviolet visual pigment in a vertebrate: a tetrachromatic cone system in the dace. *Science* **222:** 1021–1023.

Hárosi, F. I., and E. F. MacNichol, Jr. 1974a. Visual pigments of goldfish cones: spectral properties and dichroism. *J. Gen. Physiol.* **63:** 279–304.

Hárosi, F. I., and E. F. MacNichol, Jr. 1974b. Dichroic microspectrophotometer: a computer-assisted, rapid, wavelength-scanning photometer for measuring linear dichroism in single cells. *J. Opt. Soc. Am.* **64:** 903–918.

Hawryshyn, C. W., and F. I. Hárosi. 1991. Ultraviolet photoreception in carp: microspectrophotometry and behaviorally determined action spectra. *Vision Res.* **31:** 567–576.

Jerlov, N. G., 1968. *Optical Oceanography.* Elsevier Publishing Co. Amsterdam, 194 pp.

Levine, J. S., and E. F. MacNichol, Jr. 1979. Visual pigments in teleost fishes: effects of habitat, microhabitat, and behaviour on the visual system evolution. *Sensory Processes* **3:** 95–131.

Loew, E. R., and J. N. Lythgoe. 1978. The ecology of cone pigments in teleost fishes. *Vision Res.* **18:** 715–722.

Lythgoe, J. N. 1972. The adaptations of visual pigments to the photic environment. Pp. 566–603 in *The Handbook of Sensory Physiology.* Vol. VII/1, *Photochemistry of Vision,* H. J. A. Dartnall, ed. Springer, New York.

Lythgoe, J. N. 1984. Visual pigments and environmental light. *Vision Res.* **24:** 1539–1550.

McFarland, W. N., and F. W. Munz. 1975a. Part II: The photic environment of clear tropical seas during the day. *Vision Res.* **15:** 1063–1070.

McFarland, W. N., and F. W. Munz. 1975b. Part III: The evolution of photic visual pigments in fishes. *Vision Res.* **15:** 1071–1080.

McFarland, W. N., and F. W. Munz. 1975c. The visible spectrum during twilight and its implications to vision. Pp. 249–270 in *Light as an Ecological Factor,* G. C. Evans, R. Bainbridge and O. Rackham, eds. Vol. 2. Blackwell, Oxford.

Moon, P. 1940. Proposed standard solar-radiation curves for engineering use. *J. Franklin Inst.* **230:** 583–617.

Munz, F. W. 1958. Photosensitive pigments from the retinae of certain deep sea fishes. *J. Physiol.* **140:** 220–225.

Munz, F. W. 1964. The visual pigments of epipelagic and rocky shore fishes. *Vision Res.* **4:** 441–454.

Munz, F. W., and W. N. McFarland. 1973. The significance of spectral position in the rhodopsins of tropical marine fishes. *Vision Res.* **13:** 1829–1874.

Perlmutter, A. 1961. *Guide to Marine Fishes.* New York University Press. 431 pp.

Petry, H. M., and F. I. Hárosi. 1990. Visual pigments of the tree shrew (*Tupaia belangeri*) and greater galago (*Galago crassicaudatus*): a microspectrophotometric investigation. *Vision Res.* **30:** 839–851.

Schmidt, W. J. 1938. Polarisationsoptische Analyse eines Eiweiß-Lipoid-Systems, erläutert am Außenglied der Sehzellen. *Kolloid-Z.* **85:** 137–148.

Schultze, M. 1866. Zur Anatomie und Physiologie der Retina. *Archiv Mikrosk. Anat.* **2:** 175–286.

Schultze, M. 1867. Ueber Stäbchen und Zapfen der Retina. *Archiv Mikrosk. Anat.* **3:** 215–247.

Reference: *Biol. Bull.* **182**: 145–154. (February, 1992)

Quantitative Analysis of the Structure and Function of the Marsupial Gills of the Freshwater Mussel *Anodonta cataracta*[1]

RICHARD A. TANKERSLEY AND RONALD V. DIMOCK, JR.

Department of Biology, Wake Forest University, Winston-Salem, North Carolina 27109

Abstract. Gravid females of *Anodonta cataracta* incubate shelled larvae (glochidia) in the water tubes of their outer demibranchs which, in turn, undergo extensive morphological changes in becoming marsupia. In this study, the brooding gills of *A. cataracta* were compared to the non-marsupial demibranchs of females and the gills of males. Scanning electron microscopy and video enhanced light microscopy were used, and computer-generated 3D-reconstructions of gill tissue were also prepared from light micrographs of serial histological sections. Marsupial gills possess a tripartite system of water tubes that are not present in non-marsupial gills and include two secondary water channels and one primary water tube (brood chamber) containing glochidia. The lateral dimension (width) of water tubes of the marsupial gills increases nearly 30-fold during brooding, but the anterior-posterior length of the tubes is unaffected. No apparent changes in the morphology of the non-marsupial inner demibranchs were observed. Glochidia are effectively isolated from the surrounding water by secondary septa, positioned between the primary and secondary water tubes. Secondary septa are present during brooding and immediately after larval release, but are not in evidence among females during non-reproductive periods. Quantification by 3D reconstruction revealed that, although secondary water tubes are smaller than the primary water tubes of non-marsupial gills and non-gravid marsupial gills, collectively they provide about the same cross-sectional area as the primary water tubes that are lost to water transport by occlusion with glochidia. However, considering the fluid dynamics of the ciliary gill pump, net water transport through the lumina of marsupial gills is reduced to only about 16% of that in non-gravid marsupial demibranchs.

Received 15 July 1991; accepted 11 October 1991.

[1] Contribution #297 from the Tallahassee, Sopchoppy and Gulf Coast Marine Biological Association.

Abbreviations: ANOVA: analysis of variance; AV, arterial vessel; BC, brood chamber; CE, ciliated water tube epithelial cell; F, gill filament; FT, foot; G, glochidium; ID, inner demibranch; IFC, interfilament water canal; ILS, interlamellar septum; LT, lamellar tissue; MP, melting point; N, nerves; O, ostium; OD, outer demibranch; PWT, primary water tube; SEM, scanning electron microscopy; SS, secondary septa; SWT, secondary water tube; 3D, three dimensional; PC1 & PC2, principal components 1 & 2; PCA, principal components analysis; VM, visceral mass.

Introduction

Unlike their marine counterparts, most freshwater bivalve mollusks, including the Sphaeridae and Unionidae, lack a planktonic larva and bypass the trochophore and veliger stages; rather, they incubate their embryos, larvae, or both in their gills. Moreover, the life cycles of the Unionidae are atypical among bivalves in including both a free-living adult and a short-lived obligatory ecto-parasitic larval (glochidial) phase (Coker *et al.*, 1921; Kat, 1984). Following fertilization in the suprabranchial cavity, embryos develop in the water tubes of the female's gills. During reproduction, both outer (lateral) demibranchs of *Anodonta cataracta* (recently reassigned to the genus *Pygnodon* by Hoeh, 1990) serve entirely as a pair of marsupial chambers and undergo pronounced morphological and architectural changes to accommodate nearly a million developing larvae (Fig. 1). *Anodonta cataracta* is a dioecious long-term (bradytictic) brooder that spawns in the late summer, broods throughout the fall and winter, and releases mature glochidia in the early spring (Tankersley, unpub. data).

General descriptions of the gill structure and anatomy of several unionid species, including *A. cataracta*, and the

Figure 1. Scanning electron micrograph of a frontal cross section of the marsupial gill of *Anodonta cataracta* showing the position of the glochidia larvae (G) in the brood chambers and the location of the secondary water tubes (SWT) and interlamellar septa (ILS). Additional abbreviations: F, gill filament.

role of demibranchs as sites of larval storage during reproduction have been reported previously (Peck, 1877; Lefevre and Curtis, 1910; Ortmann, 1911; Richard *et al.*, 1991). The non-marsupial gills (outer and inner demibranchs of males and inner demibranchs of females) of *A. cataracta* possess continuous interlamellar septa that run dorso-ventrally at right angles to the gill surface and form evenly spaced, uninterrupted water tubes (Fig. 2) (Ridewood, 1903; Heard and Guckert, 1971). The primary water tubes of the marsupial lamellae are more numerous than those in non-marsupial gills and during gravid periods are divided into three separate compartments: a central brood chamber serving as an ovisac, and two temporary secondary water tubes located on both the lateral and medial ends of the brood chamber parallel to the surface of the demibranchs (Fig. 2). These secondary water tubes are formed from extensions of the interlamellar septa prior to larval incubation, and may be associated with the long brooding period of this species; in particular, they are thought to be responsible for maintaining water transport across the gill surface for respiration, filtration, and aeration of developing larvae (Ortmann, 1911; Heard, 1975; Richard *et al.*, 1991).

Investigations of the flow dynamics associated with ciliary suspension feeding in bivalves (see Silvester and Sleigh, 1984; Jørgensen *et al.*, 1988; Silvester, 1988) have prompted several studies of the functional anatomy and ultrastructure of the bivalve gill (Moore, 1971; Owen, 1974; Way *et al.*, 1989). Although the reproductive cycles and glochidial morphology of a variety of unionaceans have been examined (see references in Kat, 1984, and Gordon and Smith, 1990), few studies have documented the changes in gill morphology associated with brooding (Ortmann, 1911; Bloomer, 1934; Heard, 1975; Richard *et al.*, 1991) or examined the functional role of the secondary water tubes as structures necessary for sustaining water transport through the lateral demibranchs. Most contemporary examinations of unionid gill structure and function have focused upon the role of gills as sites for ion transport (Kays *et al.*, 1990), and as storage areas for extracellular calcium phosphate concretions (Silverman *et al.*, 1983, 1989) used during reproduction for embryonic shell development (Silverman *et al.*, 1985, 1987).

The objective of the present study was to use both scanning electron microscopy and video enhanced light microscopy to quantify the seasonal changes in the morphology of the marsupial gills of *A. cataracta* females and to compare these changes with those in the non-marsupial inner demibranchs, and with the inner and outer demibranchs of males. The results indicate that, although the marsupial gills swell to more than thirty times their non-brooding thickness when the primary water tubes are modified as brood chambers and are subsequently obstructed by incubating larvae, the construction of secondary water tubes partially compensates for the loss of passageways available for water transport. In addition, these data are used to make theoretical predictions and estimates of the influence of larval incubation on the fluid dynamics of the gills and on their conventional roles as feeding and respiratory organs.

Materials and Methods

Collection and maintenance of animals

Adult *Anodonta cataracta* were collected from Spea's Pond, Yadkin County, North Carolina, and were maintained at ambient collection temperatures in glass aquaria containing artificial pond water (Dietz and Alvarado, 1970). All mussels were sexually mature (average shell length = 12.8 cm; range: 11.2–14.0 cm), were kept on a 12L:12D photoperiod for up to 10 days prior to use, and their collections were scheduled to coincide with pregravid (early July), gravid (October and December), and post-glochidial release (late February) periods. The sex ratio of mussels in the pond was nearly 1:1, and 100% of the females collected during brooding periods possessed gravid marsupia.

Preparation of gills for light microscopy and computerized analysis of serial sections

Lateral and medial gill tissues (approximately 4 cm^2) for histological examination by video enhanced light microscopy were excised from the central part of their respective demibranchs and fixed in Tissue-Fixx (Lerner Laboratories) for 72 h. Specimens were decalcified in Cal-Ex (Fisher Diagnostics) for 24 h, dissolving larval shell

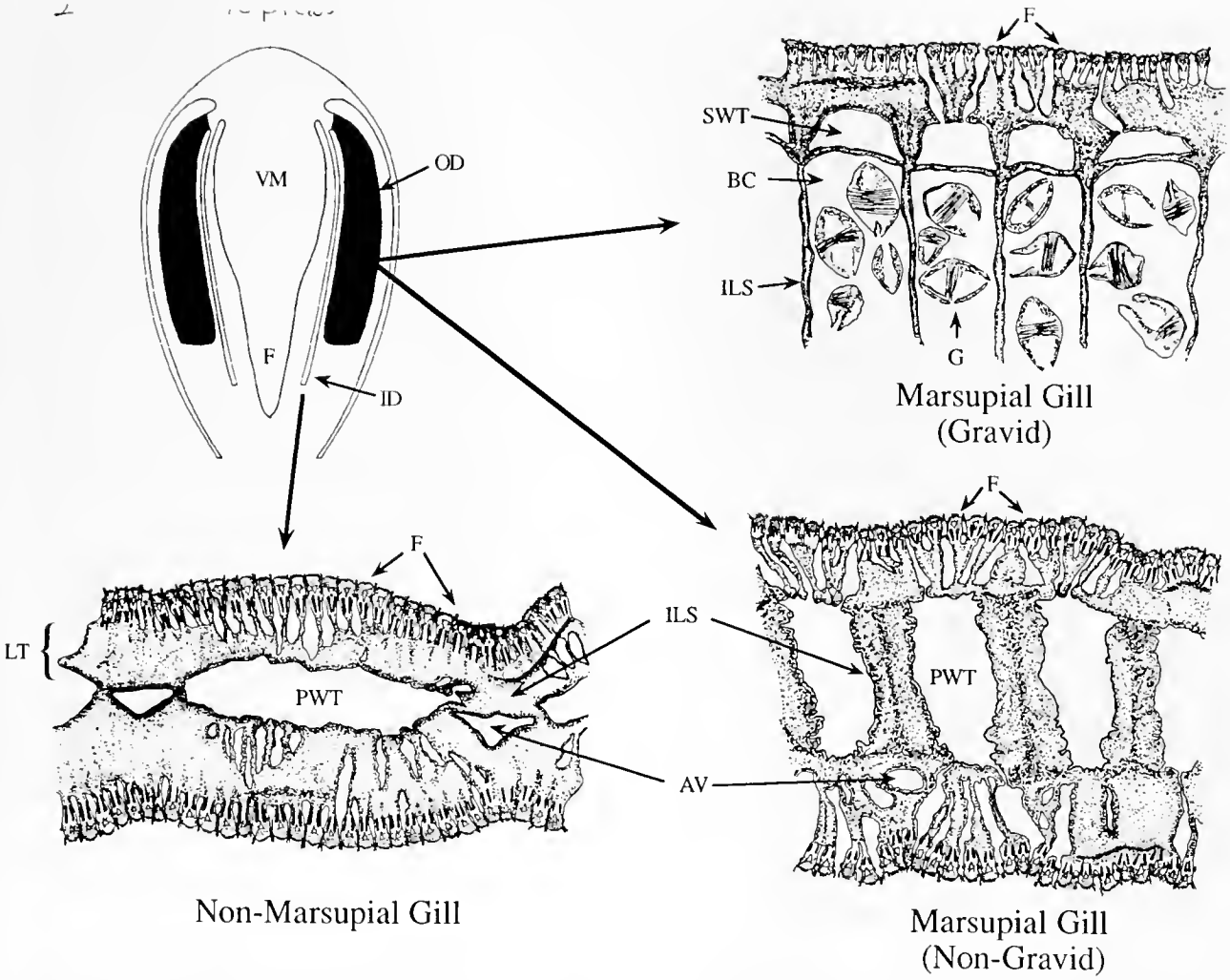

Figure 2. Schematic illustration of a cross section through a gravid female *Anodonta cataracta* showing the position of the lateral and medial demibranchs, and the arrangement of the lamellar tissue (frontal sections) of non-marsupial and marsupial demibranchs during gravid and non-gravid periods. Abbreviations: AV, arterial vessel; BC, brood chamber; F, gill filament; FT, foot; G, glochidium larvae; ID, inner demibranch; ILS, interlamellar septum; LT, lamellar tissue; OD, outer demibranch; PWT; primary water tube; SWT, secondary water tube; VM, visceral mass.

and extracellular calcium concretions that might have interfered with sectioning (Silverman *et al.*, 1985; Richard *et al.*, 1991), and were then dehydrated in ethanol and embedded in paraffin (Paraplast; MP 56°C) by vacuum infiltration (Lipshaw Manufacturing Co.). Serial frontal sections (7–8 μm thick) were mounted on glass slides and stained with hematoxylin and eosin according to the procedures outlined in Humason (1979).

Morphometric measurements (±2.0 μm for linear and 4.0 μm^2 for area measurements) included the area (frontal cross section), length (maximum anterior-posterior axis distance), and width (maximum left-right axis distance) of the primary water tubes (brood chambers in gravid and post-release marsupial gills) and secondary water tubes (gravid and post-release marsupial gills only); the gill thickness (maximum distance between the filaments of opposing lamellae); the thickness of lamellar tissue (maximum distance from the base of filaments to the lumen of the primary or secondary water tubes); and the number of filaments per interlamellar septum (including filaments present on both ascending and descending lamellae). These measurements were made with an Image-1 Video Image Analyzer (Universal Imaging Corp.) and a Hamamatsu C2400 video camera and Javelin color video camera attached to a Zeiss Axiophot microscope and a Nikon SMZ-2T dissection microscope, respectively. Three sets of measurements on every fourth section, for a total of 12 sets per specimen (5–6 specimens/sex/collection pe-

riod), were analyzed to account for any within-individual variation.

We performed a principal components analysis (PCA) (SYSTAT Statistical Software; Wilkinson, 1990) on the original (log transformed) variables to derive a smaller set of uncorrelated variables based on linear combinations of the original gill morphology measurements (Dillon and Goldstein, 1984). The goal of PCA is to extract maximum variance from the original data set with as few orthogonal factors (components) as possible, thereby reducing the variable to sample ratio and precluding statistical problems resulting from multicollinearity. Interpretations of the derived principal components were based upon factor loadings, which represent the correlations of the original variables with the respective components (component-variable correlations). Because loadings with the largest absolute magnitudes have the greatest influence on the components, the subsequent description of each principal component was based upon an appraisal of similarities among those variables with the highest loadings on a given component. We used factor (component) scores (estimates of each sample's value on the derived components based upon weighted combinations of its values on the original variables) in place of the original gill morphology measurements as dependent variables in comparing the morphological features of marsupial and non-marsupial gills throughout the collection period using analysis of variance (ANOVA) (Tabachnick and Fidell, 1989) and Dunn's multiple comparison procedure to establish an experiment-wise error rate of 0.05 (Kirk, 1982).

Preparation of gills for scanning electron microscopy (SEM)

Dissected gill specimens for scanning electron microscopy were fixed in 2% glutaraldehyde in 0.2 *M* Sorenson's sodium phosphate buffer (pH 7.2) at 4°C for 2 h, post-fixed in 2% cacodylate buffered (pH 7.4) osmium tetroxide for an hour, and rinsed with several changes of buffer. A vibratome (Lancer Model 1000) was used to section the gill specimens into 2–8 mm thick segments that were either parallel or perpendicular to the dorsal-ventral axis. This procedure exposed the frontal surface of the gill lamellae and allowed us to examine the arrangement and morphology of the water tubes and the position of the glochidia in the brood chambers. Specimens were later dehydrated through a graded ethanol series, dried in a Pelco CPD-2 critical point drier, mounted on aluminum SEM stubs, and sputter-coated with gold-palladium (Pelco Model SC-4). External gill features, primary and secondary water tubes, brood chambers, and lamellar tissues exposed by sectioning were examined and photographed with a Philips 515 scanning electron microscope operating at 15 kV.

Three-dimensional reconstruction and water tube volume calculation

We used a computerized 3D-reconstruction program (PC3D, Jandel Scientific) to examine and quantify the volumetric changes that take place in the water tubes and brood chambers of marsupial gills as a consequence of brooding. Tissues were prepared for light microscopy as described above, and serial frontal cross sections (10 μm thick) of non-marsupial (inner demibranchs of males or females) and marsupial gills (female pre-brooding and brooding outer demibranchs) were photographed. The water tubes, brood chambers, filaments, and interlamellar tissue of every fifth section were visually aligned (Gaunt and Gaunt, 1978) and digitized using a Summagraphics digitizer (25 digitized sections/sample; 4 samples/gill type) attached to a Zenith Z-386SX computer. We created a three-dimensional image of the gill sample by stacking the sections using the PC3D software; the program's volume calculation subroutines were used to determine the volumes of the primary and secondary water tubes. The final reconstruction represented a slice through the gill approximately 1.25 mm high and perpendicular to the filaments. A Kruskal-Wallis one-way ANOVA (SYSTAT Statistical Software; Wilkinson, 1990) and distribution free multiple comparisons based on rank sums (Hollander and Wolfe, 1973) were used to test for differences between standardized water tube volume measurements.

Results

Description and morphometric analysis of marsupial and non-marsupial gills

The nomenclature and terminology used to describe the gills of *A. cataracta* in the present study are similar to those of previous descriptions of lamellibranch gills by Ridewood (1903) and Ortmann (1911). Compared to non-marsupial demibranchs, the marsupial gills of all female mussels collected throughout the study were subdivided by additional interlamellar septa, resulting in shorter (anterior-posterior axis) water tubes and a lower mean filament/septum ratio (15.2 *vs.* 48.9) (Table I). Water tubes (brood chambers) containing larvae were swollen to more than 30 times their original non-brooding width (medial-lateral axis), producing nearly a 24-fold increase in cross-sectional area and causing the ventral edge of the demibranch to expand into a thin, non-ciliated connection between opposing lamellae. Conversely, brooding had little effect on the spacing and length (anterior-posterior distance) of the water tubes of marsupial gills (Table I). The lamellar tissue of marsupial gills was slightly thinner than in non-marsupial gills, especially during periods of larval incubation, but still possessed well-developed interfilament water canals leading to ostial openings in the la-

Table I

Results (mean ± SE) of morphometric analysis of male and female demibranchs during brooding and non-reproductive periods

Collection period & gill type	Water tube Area (mm^2)	Water tube Width* (mm)	Water tube Length** (mm)	Gill thickness (mm)	Lamellar thickness (mm)	Filaments/ Septum	n
Pre-brooding							
Non-marsupial	0.158 ± 0.021	0.193 ± 0.017	1.028 ± 0.078	0.974 ± 0.034	0.385 ± 0.018	46.5 ± 3.12	15
Marsupial	0.078 ± 0.014	0.135 ± 0.021	0.548 ± 0.041	1.052 ± 0.039	0.273 ± 0.027	16.0 ± 0.89	5
Gravid							
Non-marsupial	0.193 ± 0.022	0.186 ± 0.015	1.153 ± 0.061	0.840 ± 0.033	0.333 ± 0.012	46.2 ± 1.68	32
Marsupial	1.846 ± 0.179	3.938 ± 0.205	0.457 ± 0.032	4.550 ± 0.187	0.186 ± 0.205	13.7 ± 0.77	10
Secondary water tube	0.020 ± 0.005	0.063 ± 0.010	0.370 ± 0.026				
Post-release							
Non-marsupial	0.233 ± 0.032	0.267 ± 0.032	1.077 ± 0.055	1.130 ± 0.076	0.391 ± 0.032	51.1 ± 2.46	15
Marsupial	0.185 ± 0.050	0.768 ± 0.169	0.298 ± 0.097	1.589 ± 0.075	0.240 ± 0.169	16.0 ± 0.86	5
Secondary water tube	0.011 ± 0.002	0.082 ± 0.010	0.215 ± 0.032				

* Medial-Lateral axis.

** Anterior-Posterior axis.

Because there were no significant differences between the respective morphometric characters of all non-marsupial demibranchs, the data for the inner demibranchs of females, and the inner and outer demibranchs of males, for each collection period have been pooled.

mellar walls of the secondary water tubes (Figs. 3, 4, 5). Secondary septa were continuous with the interlamellar septa (Figs. 3, 4) and lacked any apparent openings or ostia leading from the secondary water tubes to the brood chambers, effectively isolating the developing larvae from water flowing through the mantle cavity and the secondary water tubes (Fig. 6). Secondary septa also lacked the ciliated cells present on the lamellar walls of the primary and secondary water tubes (compare Figs. 5, 6).

The interlamellar septa of non-marsupial gills were continuous with the lamellar tissue and contained well-developed arterial vessels (Fig. 7). Comparable vessels were rarer in marsupial gills and were positioned at the base of the septum near the junction with the lamellar tissue.

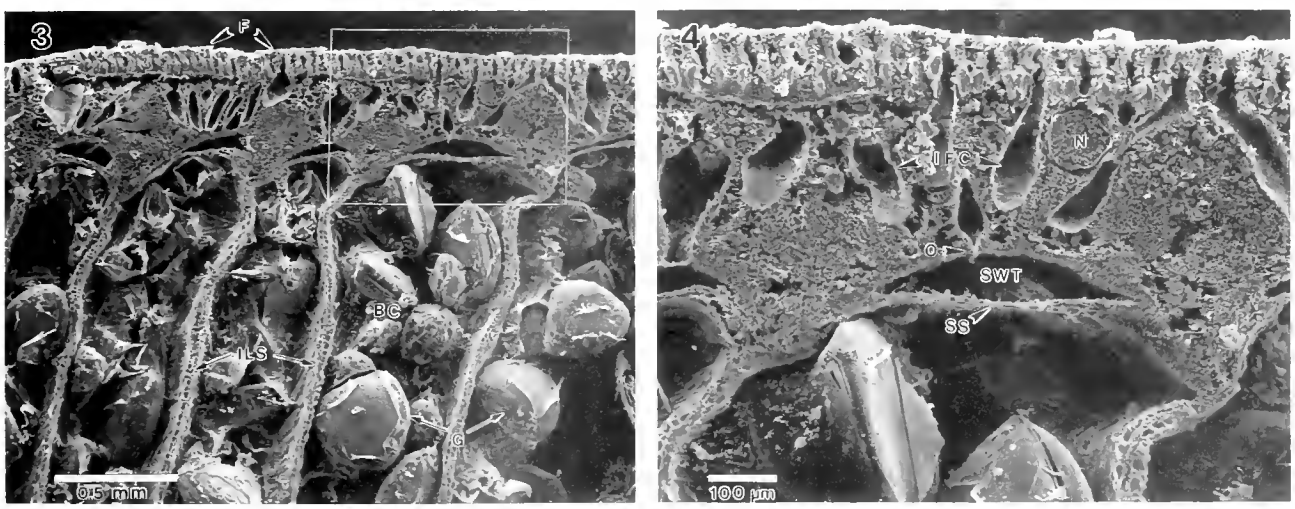

Figures 3 & 4. Frontal section of a marsupial demibranch (only one lamella is shown) containing mature glochidia (G). Brood chambers (BC) are separated by thin interlamellar septa (ILS) which connect the ascending and descending sides of the demibranch. Figure 4 is a higher magnification view of the highlighted area in Figure 3 showing the position of the secondary septa (SS) forming the secondary water tubes (SWT). Well-developed interfilament canals (IFC) are located between adjacent filaments (F) and lead to ostial openings in the lamellar tissue (walls) of the water tubes. Nerves (N) located in the lamellar tissue are also present.

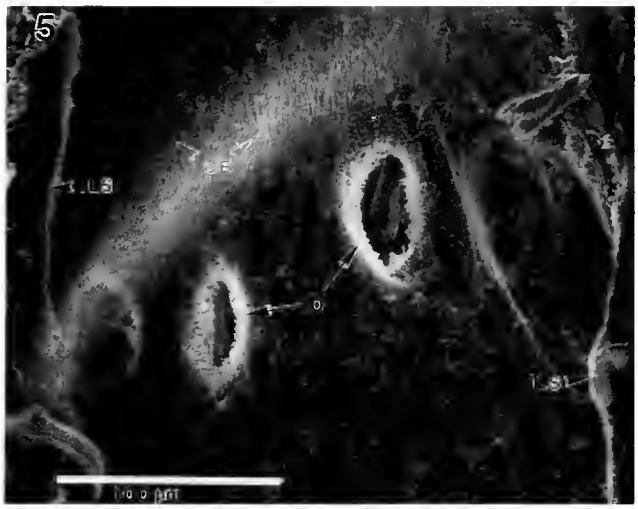

Figure 5. Scanning electron micrograph of the inner lamellar surface of a secondary water tube of a gravid marsupial gill of *Anodonta cataracta*. Water pumped through the interfilament canals by lateral cilia enters the secondary water tubes through well-defined ostia (O). Lamellar walls consisted primarily of ciliated epithelial cells (CE). The edges of the interlamellar septa (ILS) connecting the opposing lamellae and forming the anterior and posterior walls of the secondary water tube are also visible.

Figure 6. Lateral view of the inner surface (brood chamber side) of a secondary septum of a gravid marsupial demibranch (glochidia removed). Note the absence of ciliated epithelial cells and ostia (see Fig. 5) leading from the secondary water tubes. Secondary septa are formed by outgrowths of the interlamellar septa (ILS) prior to larval incubation.

Distended ovisacs and numerous secondary water tubes were still present in the gills of females collected just after glochidial release (Fig. 8), but were not present in gills prior to brooding (Fig. 9). Brooding had no apparent effect on the presence or distribution of frontal cilia or laterofrontal cirri, which were visible on the surface of the gill, and all gills lacked the frontal cirri recently reported found in some other freshwater species (Way *et al.*, 1989). Moreover, there were no seasonal differences between males and females in the morphology of their non-brooding demibranchs.

Principal component analysis on the six gill morphology variables resulted in two components (PC1 & PC2) being retained (eigenvalues > 1) that explained approximately 89% (PC1 = 49%; PC2 = 40%) of the total variance. An orthogonal rotation (varimax) was performed on the extracted factors (components) to improve their interpretability while still maintaining independent factor scores. Water tube area and width and gill thickness all had high loadings on PC1 and represented morphological features associated with the gill's left-right axis dimension (Fig. 10). The remaining three variables, water tube length, filaments/septum ratio, and lamellar tissue thickness, had high loadings on PC2 and characterize features associated with the arrangement, spacing, and number of water tubes. Therefore, PC1 and PC2 were respectively labeled "left-right axis thickness" and "water-tube compactness."

The mean factor scores for both PC1 and PC2 for each type of gill are plotted in Figure 11. There were no significant differences between the inner and outer demibranchs of males (PC1: $F = 5.03$; PC2: $F = 4.58$; d.f. = 1, 20; $P > 0.05$) or between the inner demibranchs of males and females (PC1: $F = 7.63$; PC2: $F = 4.83$; d.f. = 1, 39; $P > 0.05$). Because there were no seasonal differences in the factor scores of any of these non-marsupial gills (PC1: $F = 1.28$; PC2 = 1.36; d.f. = 2, 59, $P > 0.05$), all scores for each type of gill were pooled to simplify the analysis. Marsupial gills containing larvae had higher PC1 factor scores than pre- or post-brooding gills ($F = 81.40$; d.f. = 2, 17; $P < 0.01$). The arrangement of the water tubes (PC2) of marsupial gills differed significantly from that of non-marsupial gills ($F = 70.22$; d.f. = 1, 36; $P < 0.01$) but remained consistent throughout the collection period (*i.e.*, exhibited no significant seasonal variation; $F = 2.57$; d.f. = 2, 17; $P > 0.05$).

3D reconstructions and comparison of primary and secondary water tube volumes

The mean volumes of 1-mm sections of each type of water tube are listed in Table II. Because the total number of tubes present in each demibranch varied with the type of gill (marsupial or non-marsupial) and the mussel's reproductive condition (*i.e.*, marsupial gills had two secondary water tubes/septum during brooding periods), the volume measurements are also expressed as the volume of water tube/100 gill filaments (counted as filaments present on both the ascending and descending lamellae). Although the volume of the primary water tubes of non-marsupial gills, expressed as ml/mm of gill tissue, was significantly larger than that of either the primary or secondary canals of marsupial gills ($H = 9.85$; d.f. = 2; P

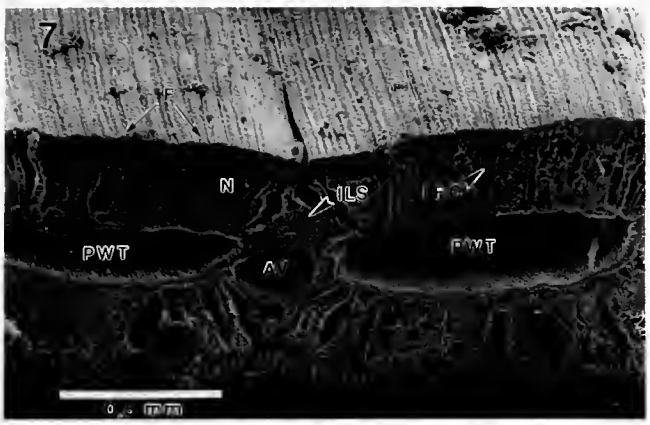

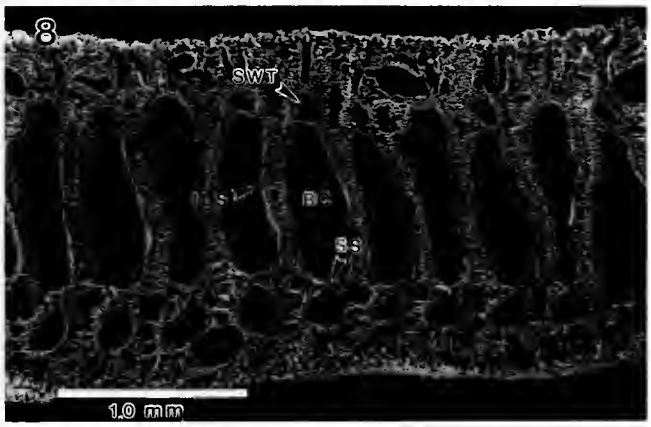

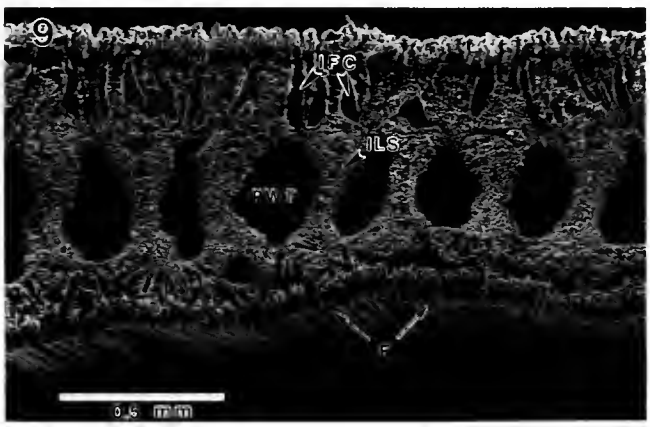

Figure 7. Frontal view of the lamellar surface of a non-marsupial demibranch. Water pumped by lateral cilia present on the gill filaments (F) enters the interfilament canals (IFC), which empty into the primary water tubes (PWT). Arterial vessels (AV) are located between water tubes in the interlamellar septa (ILS). Nerves (N) situated in the lamellar tissue are also visible.

Figure 8. Frontal section of a distended post-brooding marsupial demibranch showing the empty brood chambers (BC) and the stretched interlamellar septa (ILS). Most brood chambers still possessed well-developed secondary septa (SS) forming secondary water tubes on both the lateral and medial sides of the gill, but some secondary septa are lost by this post reproductive stage.

Figure 9. Representative section through a non-gravid marsupial gill showing the crowded organization of the water tubes (PWT). Following larval release, secondary septa and water tubes disappear, the interlamellar septa (ILS) become thickened, and the interfilament water canals (IFC) channel water through ostia located in the walls of the primary water tubes.

< 0.01), differences in water tube volumes standardized by filament number were not significant ($H = 4.88$; d.f. = 2; $P = 0.09$). These data suggest that, although the secondary water tubes of marsupial gills were significantly smaller than the primary water tubes of non-marsupial gills, the tripartite arrangement of the brooding demibranchs partially compensated for the blockage of the brood chambers by developing larvae by supplying approximately the same total volume for irrigation.

Discussion

Ortmann's (1911) early descriptions of the anatomical features of the gills of *Anodonta* emphasized both the tripartite morphology of the marsupia during reproductive periods, and the compact arrangement of their primary water tubes, relative to the inner demibranchs of females and all four demibranchs of males. The permanent differentiation in the architecture of the marsupial gills of *A. cataracta* is represented by the second principal component (PC2) in the current study and remains one of the few sexually dimorphic features of this species. The majority of changes in gill morphology associated with larval incubation occurred within the left-right axis (represented by PC1) but were only transient changes associated specifically with brooding. The unidirectional swelling of the outer gill was accompanied by comparable alterations in the size of the water tube walls and interlamellar septa, but no changes in the spacing or arrangement of the filaments. Furthermore, the presence, in gravid marsupial gills, of well-developed interfilament water canals leading to the secondary water tubes suggests that the marsupial gills continue to transport water and presumably filter particles despite striking changes in their morphology. Brooding caused no corresponding changes in female medial gills, such as an increase in water tube area, that might offset changes in the lateral marsupial demibranchs.

Overall, the morphometric measurements reported in the present study probably represent conservative estimates of gill alterations associated with brooding, because sample preparation, including fixation and dehydration, caused some shrinkage of tissue (Humason, 1979; Gabriel, 1982). Furthermore, water tube measurements may only approximate *in vivo* conditions, because pressure differences maintained by the cilia as they pump water between the mantle cavity and the lumen of the demibranch cause the demibranchs and water tubes to be inflated compared to newly excised tissue (Jørgensen *et al.*, 1986).

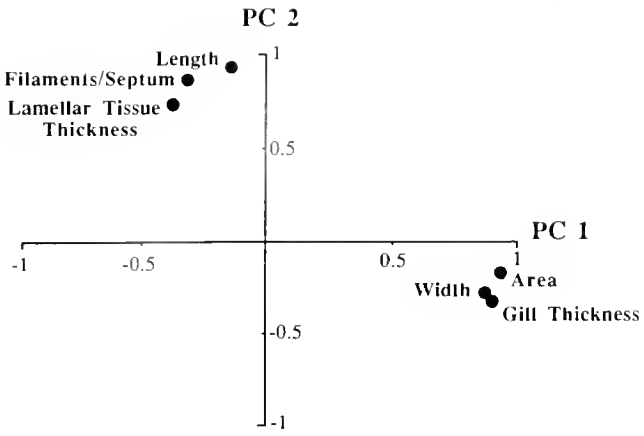

Figure 10. Pairwise plot of the factor loadings (PC1 & PC2) for the six morphometric variables following orthogonal (varimax) rotation.

Many taxonomic schemes established for unionid mussels (for example Ortmann, 1911, and Heard and Guckert, 1971) rely heavily upon reproductive characteristics associated with the marsupial demibranchs, including the number (2 or 4) and location (inner or outer) of the marsupia, the proportion of the demibranch used for brooding, the location of developing larvae within the gills, the arrangement of the brood chambers including the presence of secondary water canals, the magnitude of swelling of the lamellae, and the duration of the incubation period. The bradytictic, ectobranchous, tripartite marsupial arrangement of anodontine mussels, including *A. cataracta*, is considered to be more specialized ("advanced") than that of other mussels, which characteristically have shorter incubation periods, more marsupial demibranchs (tetragenous), and no secondary water tubes (Ortmann, 1911; Heard and Guckert, 1971). The tripartite arrangement of the marsupia of anodontine mussels has long been linked to the lengthy incubation phase of their breeding cycle, because it permits isolation of larvae while providing passageways for the maintenance of water transport. However, the assumption by most researchers, including most recently Richard *et al.* (1991), that secondary water tubes serve as lumina for irrigation during brooding periods has not been confirmed.

Construction of temporary secondary septa and a thin membrane at the dorsal end of the ovisacs of the lateral gills of female *A. cataracta* provides formal barriers to the circulation of water from the mantle cavity through the marsupial gills and effectively isolates and protects the larvae from the surrounding medium. Larval isolation has also been documented in unionids that lack secondary septa, including members of the Lampsilinae, and is thought to be accomplished by the contraction of the ostia that lead from the interfilamentar canals which, in turn, restricts the flow of water into the water tubes (brood chambers) (Richard *et al.*, 1991). Transport of water in these species is probably limited to only the demibranchs or portions of demibranchs not containing glochidia. The mechanism by which tetragenous mussels sustain water transport during brooding is less obvious, because all four demibranchs are used for larval incubation and retain the marsupial morphology. In lampsilines, only a portion of the gill is used for brooding; the remainder possesses water tubes that are similar to those of non-marsupial demibranchs. This may be an alternative mechanism for satisfying the conflicting demands of water transport required for filtration, respiration, and larval incubation, and more specialized than the tripartite arrangement of *A. cataracta* (Heard and Guckert, 1971; Kat, 1984).

In addition to serving as shelters for larval development, brood chambers and the glochidial isolation they provide might also facilitate the transfer of nutrients from the female to the developing larvae. As reported for other unionids (Heard, 1975; Silverman *et al.*, 1987; Richard *et al.*, 1991), the epithelia of the secondary and interlamellar septa of *A. cataracta* lack openings or ostia leading to the secondary water canals and thereby limit direct nutrient or ion exchange with external pond water. Investigations of the maternal investment in larval nutrition and development have been restricted primarily to examinations of the use of maternal calcium reserves for the formation of larval shells (Silverman *et al.*, 1985, 1987). Although the mobilization of calcium concretions in the gills of females and their subsequent incorporation in the shells of brooded embryos is well documented, the mechanism of transfer is still unknown. Wood (1974) re-

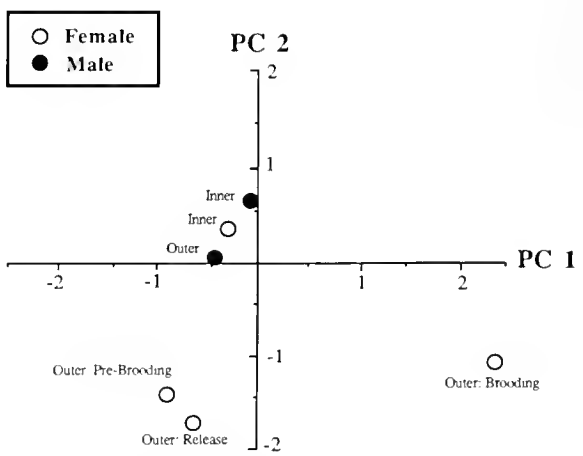

Figure 11. Pairwise plot of the mean factor scores (see Fig. 10: PC1 describes changes in the lateral-medial axis of the demibranchs and brood chambers; PC2 describes the number and arrangement of water tubes and filaments) for male and female inner and outer demibranchs throughout the study. Because there were no significant differences in the factor scores of female inner demibranchs and male inner and outer demibranchs among the collection periods, the scores for each type of gill were pooled to simplify the analysis.

Table II

Water tube volume calculations (mean ± SE; n = 4) based upon 3D reconstructions of non-marsupial and marsupial gills of Anodonta cataracta *during brooding and pre-brooding (non-gravid) periods*

	Non-marsupial gill	Marsupial gill		
		Pre-brooding	Brooding	
	PWT	PWT	BC	SWT
ml/mm of gill ($\times 10^{-5}$)	17.3 ± 2.0	5.3 ± 0.8	161.1 ± 23.6	1.5 ± 0.18
ml/mm/100 filaments ($\times 10^{-5}$)	35.8 ± 4.2	35.6 ± 5.4	1090 ± 158	20.5 ± 2.39*

* Includes two secondary water tubes per brood chamber.

Abbreviations: PWT, primary water tube; BC, brood chamber; SWT, secondary water tube.

ported that gravid *Anodonta cygnea* that were fed ^{14}C-labelled algae incorporated significant concentrations of the label in both the glochidia and interlamellar septa; Wood also suggested that nutrients could have been transferred from the female to the developing larvae via mucus secreted by cells located in the interlamellar septa. Although the lateral swelling of marsupial gills and the packing of the brood chambers with larvae may isolate many of the glochidia from direct contact with the lateral and medial inner surfaces of the gill, the narrow (anterior-posterior dimension) arrangement of the individual brood chambers of *A. cataracta* keeps the larvae in close contact with the interfilamentar septa and may facilitate the transfer of nutrients from the female to developing larvae.

Gill irrigation and suspension feeding in bivalves are dominated by the viscous forces characteristic of low Reynolds numbers (<1), producing a laminar flow of water through the demibranchs (Jørgensen, 1982, 1983). The pump, generated by the beating of lateral cilia present on the gill filaments near the entrance to the interfilament water canals, is influenced by, among other parameters, the velocity of water passing through the interfilament water canals and pressure heads produced by the lateral cilia (Jørgensen *et al.*, 1988). Jørgensen *et al.* (1986) established the following equation for analysis of pump and system characteristics:

$$\Delta H_p = \Delta H_{12} + \Delta H_f + \Delta H_{ex} + \Delta H_{lf}$$

where ΔH_p = pressure difference produced by the pump, ΔH_{12} = back pressure, ΔH_f = frictional resistance of the canal system (including the interfilamentary water canals, the water tubes and exhalent siphon), ΔH_{ex} = exit loss generated by the kinetic energy of the water leaving the exhalent siphon, and ΔH_{lf} = active resistance produced by the beating of the latero-frontal cirri located on the gill filaments. Indirect estimates of the various components of the ciliary pump of the marine mussel *Mytilus edulis* revealed that interfilament canals constituted about 32% of the total resistance in the system (Jørgensen *et al.*, 1986), but the frictional resistance produced by the lumen of the water tubes was assumed to have only a negligible effect on the pump. Although the morphology of the eulamellibranch gill of *A. cataracta* differs markedly from the filibranch gill of *Mytilus*, and detailed comparisons of the properties and energetics of the ciliary pumps of both types of gills are unavailable, larval incubation may have a greater impact on the molluscan pump of brooding eulamellibranchs than is indicated by the current simplified model based on non-brooding, filibranch bivalve characteristics.

Because the flow resistance of a fluid passing through a cylinder is extremely sensitive to reductions in bore size (Vogel, 1981), the use of a series of smaller diameter tubes (secondary water tubes *vs.* primary water tubes) by gravid marsupial gills most likely has a significant impact on the resistance to flow and the cost of pumping. If the primary and secondary water tubes are treated as a series of parallel cylinders, according to Poiseuille's equation, volume flow rate would vary with the fourth power of the tube's radius. Therefore, even if the combined cross-sectional area of the two secondary water tubes were equal to that of a single primary water tube during non-reproductive periods, the overall flow rate in the two smaller tubes would be only one-half that of the larger tube for a given pressure change (Vogel, 1981). Consequently, estimates of flow rates through secondary water tubes based upon the present volume calculations (Table II) would predict that the total flow in marsupial gills during brooding would only be approximately 16% and 4% of that in primary water tubes of non-gravid marsupial and non-marsupial gills, respectively.

Maintenance of flow rates through the secondary water tubes that are comparable to those through unobstructed primary water tubes also would be energetically costly. Because the power required to generate flow through a cylinder is inversely related to the square of its radius, the pressures that would be required to irrigate the smaller diameter secondary water tubes likely exceed the capa-

bility of a ciliary pump (Jørgensen *et al.*, 1986). Thus, the flow rates within brooding marsupial gills are probably much lower than those produced within non-gravid marsupial gills or non-marsupial gills, even though the volume of lumina available for water transport is compensated for by the construction of the secondary water tubes. Changes in total gill volume (swelling during brooding) that modify the flow dynamics within the mantle cavity and additionally restrict water transport, may further reduce the effectiveness of the marsupial gill. It is unclear whether the extensive reorganization of marsupial gill tissue following larval release permits the demibranchs to assume functional characteristics of non-marsupial gills after the brooding season. Investigations are currently underway in our laboratory to assess the impact of larval incubation on the pumping and feeding physiology of *A. cataracta*.

Acknowledgments

The current study was funded in part by a NSF Dissertation Improvement Grant (BSR-9001345) and a Theodore Roosevelt Memorial Grant from the American Museum of Natural History to the senior author. We are grateful to Dr. N. S. Allen for the use of the video microscopy facility and to P. E. Richard *et al.* for allowing us to review a preprint of their manuscript. Special thanks are due to J. Sizemore for sharing her microscopical expertise. J. Fernandez, E. Wetzel, and two anonymous reviewers provided valuable comments on the manuscript.

Literature Cited

Bloomer, H. H. 1934. On the sex, and sex-modification of the gill of *Anodonta cygnea*. *Proc. Malacol. Soc. Lond.* **21:** 21–28.

Coker, R. E., A. F. Shira, H. W. Clarke, and A. D. Howard. 1921. Natural history and propagation of fresh-water mussels. *Bull. U. S. Bur. Fish.* **37:** 75–181.

Dietz, T. H., and R. H. Alvarado. 1970. Ionic regulation in *Lumbricus*. *Biol. Bull.* **141:** 472–484.

Dillon, W. R., and M. Goldstein. 1984. *Multivariate Analysis.* John Wiley & Sons, Inc., New York. 587 pp.

Gabriel, B. L. 1982. *Biological Scanning Electron Microscopy.* Van Nostrand Reinhold Co., New York. 186 pp.

Gaunt, P. N., and W. A. Gaunt. 1978. *Three Dimensional Reconstruction in Biology.* University Park Press, Baltimore. 174 pp.

Gordon, M. E., and D. G. Smith. 1990. Autumnal reproduction in *Cumberlandia monodonta* (Unionoidea: Margaritiferidae). *Trans. Am. Microsc. Soc.* **109:** 407–411.

Heard, W. H. 1975. Sexuality and other aspects of reproduction in *Anodonta* (Pelecypoda: Unionidae). *Malacologia* **15:** 81–103.

Heard, W. H., and R. H. Guckert. 1971. A re-evaluation of the Recent Unionacea (Pelecypoda) of North America. *Malacologia* **10:** 333–355.

Hoeh, W. R. 1990. Phylogenetic relationships among eastern North American *Anodonta* (Bivalvia: Unionidae). *Malacol. Rev.* **23:** 63–82.

Hollander, M., and D. A. Wolfe. 1973. *Nonparametric Statistical Methods* John Wiley & Sons. New York. 503 pp.

Humason, G. L. 1979. *Animal Tissue Techniques.* W. H. Freeman and Co., San Francisco. 661 pp.

Jørgensen, C. B. 1982. Fluid mechanics of the mussel gill: the lateral cilia. *Mar. Biol.* **70:** 275–281.

Jørgensen, C. B. 1983. Fluid mechanical aspects of suspension feeding. *Mar. Ecol. Prog. Ser.* **11:** 89–103.

Jørgensen, C. B., P. S. Larsen, F. Møhlenberg, and H. U. Riisgård. 1988. The mussel pump: properties and modelling. *Mar. Ecol. Prog. Ser.* **45:** 205–216.

Jørgensen, C. B., P. Famme, H. S. Kristensen, P. S. Larsen, F. Møhlenberg, and H. U. Riisgård. 1986. The bivalve pump. *Mar. Ecol. Prog. Ser.* **34:** 69–77.

Kat, P. W. 1984. Parasitism and the Unionacea (Bivalvia). *Biol. Rev.* **59:** 189–207.

Kays, W. T., H. Silverman, and T. H. Dietz. 1990. Water channels and water canals in the gill of the freshwater mussel, *Ligumia subrostrata:* ultrastructure and histochemistry. *J. Exp. Zool.* **254:** 256–269.

Kirk, R. E. 1982. *Experimental Design.* Brooks/Cole Publishing Co., California. 911 pp.

Lefevre, G., and W. C. Curtis. 1910. The marsupium of the Unionidae. *Biol. Bull.* **19:** 31–34.

Moore, H. J. 1971. The structure of the latero-frontal cirri on the gills of certain lamellibranch molluscs and their role in suspension feeding. *Mar. Biol.* **11:** 23–27.

Ortmann, A. E. 1911. A monograph of the najades of Pennsylvania. *Mem. Carnegie Mus.* **4:** 279–347.

Owen, G. 1974. Studies on the gill of *Mytilus edulis:* the eulatero-frontal cirri. *Proc. R. Soc. Lond.* **187:** 83–91.

Peck, R. H. 1877. The minute structure of the gills of the lamellibranch Mollusca. *Q. J. Microsc. Sci.* **17:** 43–66.

Richard, P. E., T. H. Dietz, and H. Silverman. 1991. Structure of the gill during reproduction in the unionids, *Anodonta grandis, Ligumia subrostrata* and *Carunculina parva texasensis*. *Can. J. Zool.* **67:** 1744–1754.

Ridewood, W. G. 1903. On the structure of the gills of Lamellibranchia. *Phil. Trans. Roy. Soc. B* **211:** 147–284.

Silverman, H., W. L. Steffens, and T. H. Dietz. 1983. Calcium concretions in the gills of a freshwater mussel serve as a calcium reservoir during periods of hypoxia. *J. Exp. Zool.* **227:** 177–189.

Silverman, H., W. L. Steffens, and T. H. Dietz. 1985. Calcium from extracellular concretions in the gills of freshwater unionid mussels is mobilized during reproduction. *J. Exp. Zool.* **236:** 137–147.

Silverman, H., W. T. Kays, and T. H. Dietz. 1987. Maternal calcium contribution to glochidial shells in freshwater mussels (Eulamellibranchia: Unionidae). *J. Exp. Zool.* **242:** 137–146.

Silverman, H., P. E. Richard, R. H. Goddard, and T. H. Dietz. 1989. Intracellular formation of calcium concretions by phagocytic cells in freshwater mussels. *Can. J. Zool.* **67:** 198–207.

Silvester, N. R. 1988. Hydrodynamics of flow in *Mytilus* gills. *J. Exp. Mar. Biol. Ecol.* **120:** 171–182.

Silvester, N. R., and M. A. Sleigh. 1984. Hydrodynamic aspects of particle capture by *Mytilus*. *J. Mar. Biol. Assoc. U.K.* **64:** 859–879.

Tabachnick, B. G., and L. S. Fidell. 1989. *Using Multivariate Statistics.* Harper and Row, New York. 746 pp.

Vogel, S. 1981. *Life In Moving Fluids.* Princeton University Press, New Jersey. 352 pp.

Way, C. M., D. J. Hornbach, T. Deneka, and R. A. Whitehead. 1989. A description of the ultrastructure of the gills of freshwater bivalves, including a new structure, the frontal cirrus. *Can. J. Zool.* **67:** 357–362.

Wilkinson, L. 1990. *SYSTAT: The System for Statistics.* SYSTAT, Inc. Evanston, IL. 676 pp.

Wood, E. M. 1974. Development and morphology of the glochidium larva of *Anodonta cygnea* (Mollusca: Bivalvia). *J. Zool.* **173:** 1–13.

Reference: *Biol. Bull.* **182:** 155–158. (February, 1992)

Allorecognition in Colonial Marine Invertebrates: Does Selection Favor Fusion with Kin or Fusion with Self?

MICHAEL FELDGARDEN[1] AND PHILIP O. YUND[2]

[1]*Department of Biology, Yale University, New Haven, Connecticut 06511 and* [2]*Department of Biological Sciences, University of New Orleans, New Orleans, Louisiana 70148*

Previous analyses of the selective forces operating on allorecognition systems in colonial marine invertebrates have suggested that advantages to fusion with kin have selected for the ability to recognize and fuse with related colonies. While this explanation is compatible with the observation of aggregated settlement of fusible larvae in an ascidian species, it is not compatible with two other prominent features of allorecognition systems—the extensive allorecognition allele polymorphism commonly observed in natural populations and the recently reported instability of chimeric colonies. We suggest that selection for fusion with self, rather than fusion with kin, offers a more parsimonious explanation for the two features listed above. Consequently, self fusion may be a major selective force acting on allorecognition systems in colonial invertebrates.

Colonial marine invertebrates typically possess allorecognition systems that control fusion and rejection among conspecific colonies, and such systems are either known or expected to be genetically based (1). The broad distribution of allorecognition in colonial taxa and the parallels between invertebrate allorecognition and the vertebrate immune system have spawned considerable interest in the evolution of allorecognition systems. Previous analyses of the selective forces at work in allorecognition systems have suggested that allorecognition mediates the costs and benefits of fusion with conspecifics (1, 2). Fusion with conspecifics is expected to confer benefits by increasing the size of the resulting chimeric colony (1–3), which in turn decreases the susceptibility of a colony to the impact of ecological processes and increases colony reproductive output (4–7). However, potential costs are incurred in chimeric colonies as well. Because all genotypes in a chimera have access to the production of gametes (4), one genotype can functionally parasitize other members of the chimera by contributing disproportionately to gamete production (somatic cell parasitism) (4, 8). Allorecognition systems are thus thought to function to limit fusion to close relatives, so that the benefits of fusion can be acquired while the potential costs are reduced (2). By restricting fusion to close relatives, allorecognition systems may constrain somatic parasitism to benefit a relative of the victim, hence reducing the negative effect of parasitism on a victim's fitness via a positive effect on inclusive fitness (*i.e.,* kin selection) (2).

Fusion with kin is a well-documented event, and hence kin selection is certainly a potential force acting on allorecognition systems. However, we will argue that there is an additional selective force at work, with the genetic individual as the target of selection, that is more likely to explain two important features of allorecognition systems. Although our argument is applicable to most colonial taxa, we will focus our discussion on botrylloid ascidians and hydractiniid hydroids, the two groups for which the most complete genetic and mechanistic data on allorecognition are currently available.

At the heart of the kin selection argument are the anticipated costs and benefits of fusion. We agree completely with this assessment of costs and benefits, but suggest that allorecognition plays a different role as well—to permit a colony to obtain the benefits of fusion (increased colony size) while completely eliminating the potential costs (somatic cell parasitism). We suggest that rather than simply reducing the potential cost of somatic cell parasitism by limiting fusion to close kin, selection favors colonies that avoid these costs altogether by recognizing and fusing with

Received 28 June 1991; accepted 22 November 1991.

themselves (self fusion). Although fusion between kin occurs, such events may simply represent mistakes in recognition due to the limitations of an imperfect system. If kin fusion events are artifacts of allorecognition, kin selection need not provide the dominant selective force shaping allorecognition systems. Note that selection for both self and kin fusion is generated by the potential for somatic cell parasitism. While fusion with kin will limit this cost, fusion with self will prevent it altogether.

Why would autogeneic fusion (fusion with the same genotype; *i.e.*, self fusion) be selectively favored? Fragmentation is an ubiquitous feature of colonial invertebrates, both through controlled fission and as a result of extrinsic disturbance (9, 11). Surviving colony fragments are likely to re-encounter their own genotype upon subsequent growth and lateral expansion. If no mechanism for self recognition exists, the subdivided colony will compete with itself for space. Hence, autogeneic fusion between colony fragments confers the advantages both of an increase in size, as previously cited, and a release from unnecessary competition.

While fragmentation and subsequent re-contact is likely to be a major source of autogeneic fusion, self fusion is common under other circumstances as well. Many colonial invertebrates (including botrylloid ascidians and hydractiniid hydroids) grow as epibionts on three-dimensional substrata. Consequently, the growing margins of a colony frequently encounter self upon wrapping around the substratum. Even if physiological integration is maintained throughout the intervening regions of the colony, the marginal tissue is confronted with a recognition problem. As in the case of fragmentation, these contacts impose a recognize-or-compete constraint on the colony. In both of these scenarios, autogeneic fusion confers the ecological benefits of fusion without the potential costs of allogeneic fusion (fusion with other genotypes; generally kin fusion).

Early work on the population structure of corals and sponges employed allorecognition as an assay of genetic identity and hence explicitly assumed that fusion only occurred among colonies derived from the same genotype (*i.e.*, that all fusion events were autogeneic) (12–14). These studies were criticized for failing to provide adequate independent verification of genotypic identity (15), and further work suggested that some fusion events were indeed allogeneic (16, 17). The subsequent focus on the existence of allogeneic fusion may have drawn attention from the potential for autogeneic fusion in nature. While the explicit assumption of a correspondence between fusion and genetic identity may not have been valid, the implicit assumption that allorecognition systems served to permit fusion with self may well have been accurate.

To this point, we hope that we have established that the need to recognize and fuse with self theoretically provides a strong selective force on allorecognition systems. In further evaluating the relative impact of selection for kin and self fusion, we will discuss the compatibility of these different selective forces with three documented features of allorecognition systems in botrylloid ascidians and hydractiniid hydroids—the extreme polymorphism of allorecognition alleles, the instability of chimeras formed by the fusion of related colonies, and the aggregated settlement of fusible larvae.

High levels of allotype diversity are a prominent feature of allorecognition systems in most colonial taxa (1). In botrylloid ascidians, where the genetic mechanism of allorecognition is known, allotype diversity is generated by extensive allorecognition allele polymorphism, with the number of alleles detected in natural populations ranging from 40 to 100 (1, 11, 18–20). While the genetics of allorecognition in hydractiniid hydroids has yet to be fully resolved (21, 22), fusion events and chimeric colonies appear to be very rare in natural populations (23), suggesting a similarly high level of allele polymorphism.

Several authors have noted that kin selection does not provide an obvious explanation for high allotype diversity (1, 18, 24, 25). For high levels of polymorphism to occur, alleles must increase in frequency when rare. However, kin selection is likely to lead to the elimination of new alleles, because rare alleles will be involved in few, if any, fusion events (25). Consider the case of an hypothetical new allele arising by mutation. This allele confers no immediate advantage through kin selection, as kin fusion events attributable to this allele are not possible. Selection cannot favor the allele until it has already increased in frequency to the point where kin fusion events are likely to occur. Hence, any new allele is at a selective disadvantage relative to established alleles and is likely to be eliminated. Population models based on the costs and benefits of kin selection (though not explicitly modeling selection at two levels) predict that the initially most frequent allele will quickly increase to fixation in a population (25).

A closely related problem is that in order for the premises of kin selection to be valid, allotype must indicate the degree of relatedness between colonies. However, the possession of a given allorecognition allele is indicative of relatedness only when that allele is rare (25). As an allele increases in frequency, colonies that share this allele are less likely to have inherited it from a recent common ancestor. The sharing of a common allorecognition allele is thus a very poor assay of relatedness. As an allele becomes common, fusion will occur between less related genotypes, leading to the costs of somatic cell parasitism. Due to the failure of alleles to increase when rare and to convey accurate information on relatedness, the observation of high levels of polymorphism at allorecognition loci in natural populations is difficult to reconcile with kin selection.

The assumption of a selective advantage to self fusion rather than kin fusion alters the selective regime on allorecognition alleles to simple frequency-dependent selection. Rare alleles are at a selective advantage due to a greater potential to correctly identify self, while common alleles are at a selective disadvantage due to the propensity to incorrectly identify allogeneic colonies as self. These recognition errors incur for the bearer colony the potential costs of fusion (*i.e.*, somatic cell parasitism). Consider again a new allele arising by mutation. This allele is initially at a selective advantage, as it can be responsible only for autogeneic fusion events and not for accidental allogeneic events. As the allele increases in frequency, the incidence of allogeneic fusion will also increase, and selection on the allele via somatic parasitism will operate in the opposite direction, preventing the allele from reaching fixation in the population.

As a consequence of frequency-dependent selection, high levels of allele polymorphism are expected in populations (26). In addition to preserving new alleles that enter the population by chance, frequency-dependent selection may indirectly increase the rate at which new alleles are generated. Frequency-dependent selection could favor alleles at modifier loci that generate new alleles at the target locus by two different mechanisms. Modifier alleles could increase either mutation rates in the gene coding for allorecognition (27) or recombination rates within this gene sequence (intragenic recombination) (28). Although frequency-dependent selection has previously been recognized as the most likely explanation for high allorecognition allele diversity (1), an ecological scenario that generates frequency-dependent selection has been lacking.

In the colonial ascidian *Botryllus schlosseri*, chimeras formed by the fusion of two colonies of different genotype (allogeneic fusion) eventually terminate in either the absorption of one colony by the other or the separation of the two colonies, often accompanied by the death of one (29–31). Although initially noted in cases where the fusing colonies shared only one allorecognition allele, this result also occurs when both allorecognition alleles are shared (32). This phenomenon is not restricted to ascidians; a high percentage of allogeneic chimeras of the colonial hydroid *Hydractinia symbiolongicarpus* are also unstable (33). The break-up of chimeras in this species is linked to the onset of reproduction, further suggesting that recognition decisions are impacted by the potential for somatic cell parasitism (33).

The observation that most chimeras formed by kin fusion are unstable and temporary is clearly not compatible with a system dominated by kin selection. Few benefits are likely to be received by the participating colonies during a short association, and the ultimate result is generally deleterious to at least one of the participating colonies (29–31). In fact, the negative consequences of kin fusion might be expected to select against the very existence of an allorecognition system. Such a system would only be maintained if selectively favored for other reasons; *i.e.*, the selective advantages to self fusion.

Larvae of *B. schlosseri* settle in proximity to both larvae and adult colonies with which they share an allorecognition allele and hence can fuse upon subsequent growth and contact (34). In contrast, *H. symbiolongicarpus* larvae settle at random with respect to fusible adults and larvae (35). Larval settlement as a function of future fusibility is the sole observation that we are aware of that is consistent with kin selection but not with the selective pressure of self fusion. If fusion with relatives is beneficial and favored by selection, then the ability to exploit this information at the time of settlement will also be favored. Conversely, selection for self fusion will not generate selection for recognition at the larval stage (except perhaps to avoid settlement near fusible larvae and adults).

Hence, allorecognition systems in botrylloid ascidians and hydractiniid hydroids demonstrate features that may have been shaped by the selective pressures of both fusion with kin and fusion with self. Because the aggregation of fusible larvae is absent in hydractiniid hydroids, this family appears to display mainly the effects of selection for self fusion. However, data on botrylloid ascidians provide support for both hypotheses. This is not a surprising result, as these two selective forces are not mutually exclusive and their relative impact may vary among taxa. A more rigorous evaluation of these two hypotheses will require further data on the costs, benefits, and, especially, the relative frequency of self and kin fusion. For the moment, we suggest that current data are at least as consistent with the selective pressures generated by self fusion as they are with kin selection.

The resolution of the issue of the selective forces operating within allorecognition systems has additional implications on our understanding of evolutionary processes. Selection has come to be viewed as a force that operates on many different biological levels, leading some to suggest that the major features of biological organization are established during transitions in levels of selection (8, 36). In this light, kin selection has provided a justification for the suggestion that allorecognition systems function to mediate and control conflict between two different levels of selection, the genotype and the colony (3). If selection is found to occur predominately at the individual level, then allorecognition should be viewed in a very different light, as a system that attempts to restrict selection to a single level by maintaining synonomy between genotype and colony. A logical extension of this perspective suggests that new biological systems may arise not only to accommodate and organize new levels of selection, but also to hinder hierarchical expansion.

Acknowledgments

We thank Leo Buss, John Francis, Steve Gaines, Howie Lasker, Pam O'Neil, and Buki Rinkevich for comments on earlier versions of this manuscript. Financial support was provided by the National Science Foundation (OCE-89-00325 and OCE-91-96014).

Literature Cited

1. **Grosberg, R. K. 1988.** The evolution of allorecognition specificity in clonal invertebrates. *Q. Rev. Biol.* **63:** 377–412.
2. **Buss, L. W., and D. R. Green. 1985.** Histoincompatibility in vertebrates: the relict hypothesis. *Dev. Comp. Immunol.* **9:** 191–201.
3. **Buss, L. W. 1990.** Competition within and between encrusting clonal invertebrates. *Trends Ecol. Evol.* **5:** 352–356.
4. **Buss, L. W. 1982.** Somatic cell parasitism and the evolution of somatic tissue compatibility. *Proc. Natl. Acad. Sci. U.S.A.* **79:** 5337–5341.
5. **Jackson, J. B. C. 1985.** Distribution and ecology of clonal and aclonal benthic invertebrates. Pp. 297–356 in *Population Biology and Evolution of Clonal Organisms,* J. B. C. Jackson, L. W. Buss, and R. E. Cook, eds. Yale University Press, New Haven, CT.
6. **Hughes, T. P., and J. B. C. Jackson. 1985.** Population dynamics and life histories of foliaceous corals. *Ecol. Monogr.* **55:** 141–166.
7. **Wulff, J. L. 1986.** Variation in clone structure of fragmenting coral reef sponges. *Biol. J. Linn. Soc.* **27:** 311–330.
8. **Buss, L. W. 1987.** *The Evolution of Individuality.* Princeton Press, NJ.
9. **McFadden, C. S. 1986.** Colony fission increases particle capture rates of a soft coral: advantages of being a small colony. *J. Exp. Mar. Biol. Ecol.* **103:** 1–20.
10. **Lasker, H. 1990.** Clonal propagation and populations dynamics of a gorgonian coral. *Ecology* **71:** 1578–1589.
11. **Karakashian, S., and R. Milkman. 1967.** Colony fusion compatibility types in *Botryllus schlosseri. Biol. Bull.* **133:** 473.
12. **Hildemann, W. H., I. S. Johnston, and P. L. Jokiel. 1979.** Immunocompetence in the lowest metazoan phylum: transplantation immunity in sponges. *Science* **204:** 420–422.
13. **Jokiel, P. L., W. H. Hildemann, and C. H. Bigger. 1982.** Frequency of intercolony graft acceptance or rejection as a measure of population structure in the sponge *Callyspongia diffusa. Mar. Biol.* **71:** 135–139.
14. **Niegel, J. E., and J. C. Avise. 1983.** Clonal diversity and population structure in a reef-building coral, *Acropora cervicornis:* self-recognition analysis and demographic interpretation. *Evolution* **37:** 437–453.
15. **Curtis, A. S. G., J. Kerr, and N. Knowlton. 1982.** Graft rejection in sponges: genetic structure of accepting and rejecting populations. *Transplantation* **30:** 362–367.
16. **Neigel, J. E., and G. P. Schmahl. 1984.** Phenotypic variation within histocompatibility-defined clones of marine sponges. *Science* **224:** 413–415.
17. **Neigel, J. E., and J. C. Avise. 1985.** The precision of histocompatibility response in clonal recognition in tropical marine sponges. *Evolution* **39:** 724–732.
18. **Tanaka, K., and H. Watanabe. 1973.** Allogenic inhibition in a compound ascidian, *Botryllus primigenus* Oka. I. Processes and features of "non-fusion" reaction. *Cell. Immunol.* **7:** 410–426.
19. **Mukai, H., and H. Watanabe. 1975.** Distribution of fusion incompatibility types in natural populations of the compound ascidian, *Botryllus primigenus. Proc. Jpn. Acad.* **51:** 44–47.
20. **Scofield, V. L., J. M. Schlumpberger, L. A. West, and I. L. Weissman. 1982.** Protochordate allorecognition is controlled by a MHC-like gene system. *Nature* **295:** 499–502.
21. **Hauenschild, V. C. 1954.** Genetische und entwichlungphysiologische Intersuchungen uber Intersexualitat und Gewebevertraglichkeit bei *Hydractinia echinata* Flem. *Wilhelm Roux' Arch. Entwicklungsmech.* **147:** 1–41.
22. **Hauenschild, V. C. 1956.** Uber die Vererbung einer Gewebevertraglichkeits-eigenschaftt bei dem Hydroidpolypen *Hydractinia echinata. Z. Naturforsch.* **11b:** 132–138.
23. **Yund, P. O., and H. M. Parker. 1989.** Population structure of *Hydractinia* sp. nov. C in the Gulf of Maine. *J. Exp. Mar. Biol. Ecol.* **125:** 63–82.
24. **Crozier, R. H. 1986.** Genetic clonal recognition abilities in marine invertebrates must be maintained by selection for something else. *Evolution* **40:** 1100–1101.
25. **Grosberg, R. K., and J. F. Quinn. 1988.** The evolution of allorecognition specificity. Pp. 157–167 in *Invertebrate Historecognition,* R. K. Grosberg, D. Hedgecock, and K. Nelson, eds. Plenum Press, New York.
26. **Ayala, F. J., and C. A. Campbell. 1974.** Frequency-dependent selection. *Ann. Rev. Ecol. Syst.* **5:** 115–138.
27. **Ohno, S. 1969.** The spontaneous mutation rate revisited and the possible principle of polymorphism generating more polymorphism. *Can. J. Genet. Cytol.* **11:** 457–467.
28. **Bodmer, W. F., and A. J. Darlington. 1969.** Linkage and recombination at the molecular level. Pp. 223–265 in *Genetic Organization,* Vol. 1, E. W. Caspari and A. W. Ravin, eds. Academic Press, New York.
29. **Rinkevich, B., and I. L. Weissman. 1987.** A long-term study on fused subclones in the ascidian *Botryllus schlosseri:* the resorption phenomenon (Protochordata: Tunicata). *J. Zool (Lond.)* **213:** 717–733.
30. **Rinkevich, B., and I. L. Weissman. 1987.** The fate of *Botryllus* larvae cosettled with parental colonies: benefical or deleterious consequences? *Biol. Bull.* **173:** 474–488.
31. **Rinkevich, B., and I. L. Weissman. 1989.** Variation in the outcomes following chimera formation in the colonial tunicate *Botryllus schlosseri. Bull. Mar. Sci.* **45:** 213–227.
32. **Weissman, I. L., and B. Rinkevich. 1990.** Allorecognition histocompatibility in a protochordate species: is the relationship to MHC somatic or structural? *Immunol. Rev.* **113:** 227–241.
33. **Shenk, M. A., and L. W. Buss. 1991.** Ontogenetic changes in fusibility in the colonial hydroid *Hydractinia symbiolongicarpus. J. Exp. Zool.* **257:** 80–86.
34. **Grosberg, R. K., and J. F. Quinn. 1986.** The genetic control and consequences of kin recognition by the larvae of a colonial marine invertebrate. *Nature* **332:** 456–459.
35. **Yund, P. O., C. W. Cunningham, and L. W. Buss. 1987.** Recruitment and postrecruitment interactions in a colonial hydroid. *Ecology* **68:** 971–982.
36. **Maynard Smith, J. 1988.** Evolutionary progress and levels of selection. Pp. 219–230 in *Evolutionary Progress,* M. H. Nitecki, ed. University of Chicago Press, Chicago, IL.

Reference: *Biol. Bull.* **182:** 159–162. (February, 1992)

Avoidance of Hypoxia in a Cnidarian Symbiosis by Algal Photosynthetic Oxygen

M. L. RANDS, A. E. DOUGLAS*, B. C. LOUGHMAN, AND R. G. RATCLIFFE

*Department of Plant Sciences and *Department of Zoology, South Parks Road, Oxford 0X1 3RB, U.K.*

The algal symbionts in a variety of invertebrates are widely believed to increase the oxygen tension in the animal tissue by producing photosynthetic oxygen (1). This could be advantageous to the animal by maintaining normoxia in anoxic waters (2–4). Equally, it could be detrimental, through hyperoxia and the generation of toxic oxygen radicals (5), and this may contribute to the recurrent incidence of mass bleaching in tropical cnidarian symbioses over the last decade (6). Here, we use *in vivo* ^{31}P nuclear magnetic resonance spectroscopy (NMR) to assess the effect of photosynthetic oxygen production by the symbiotic alga *Symbiodinium* sp. on the energy metabolism of a sea anemone, *Anemonia viridis* and, by using acidification of the tissues and elevated ADP/ATP ratios as linked indices of anaerobiosis (7), we show unequivocally that photosynthetic oxygen can protect an invertebrate from hypoxia. Illumination prevents the rapid acidification and reduction in ATP that occurs under hypoxic conditions in the dark, and we suggest that this effect could be partly responsible for algal enhancement of coral calcification.

^{31}P NMR spectra of *Anemonia viridis* tentacles showed signals from a range of phosphorylated metabolites including phosphonates, orthophosphate (P_i), and ATP (Fig. 1). The spectra were assigned on the basis of an earlier ^{31}P NMR study of sea anemones (8) and from the characteristic chemical shifts of the signals in the spectra. The intensity of the ATP, ADP, and P_i resonances, as well as the position of the P_i signal, were of particular interest here, and the analysis of the spectra was confined to these regions of the spectrum. The chemical shift of the P_i signal was measured relative to the narrow signal from a capillary containing phosphocreatine; for the present purpose, the accuracy with which this measurement could be made outweighed any disadvantage arising from the overlap of this reference signal with weak endogenous signals from phosphocreatine and phosphoarginine.

Symbiotic tissue showed a high level of ATP when incubated in the dark with a circulating oxygenated medium (Fig. 1a). In contrast, when tissue was incubated in the dark without the circulation of an oxygenated medium, hypoxia developed, and the ATP level fell rapidly, becoming undetectable after 6 h (Fig. 1b). A number of other metabolic changes, all characteristic of the transition to the hypoxic state and well-documented in earlier *in vivo* ^{31}P NMR studies of animal tissue (9–11), were also observed in the hypoxic tentacles. ADP, which was undetectable in the well-oxygenated tissue (Fig. 1a), became measurable during the early stages of hypoxia (Fig. 1c), and the increase in the ADP/ATP ratio to values greater than 1, could be followed for 3 h before the absolute levels of both metabolites became unmeasurable. Breakdown of the nucleotides caused a three-fold increase in the P_i level, and the shift in the position of the P_i signal (see below) reflected the expected acidification of the cytoplasm under hypoxic conditions. Illumination of the tissue reversed all of these spectroscopic changes, and when light was provided continuously, the absence of an external oxygen supply had no effect on either the ATP level or the cytoplasmic pH (Fig. 1d). This striking result is consistent with a number of earlier observations, including: (i) assays of adenylates, which showed that ATP was reduced and ADP/ATP increased in the nonsymbiotic anemone *Bunodosoma cavernata* during hypoxia (12); and (ii) oxygen flux data, which suggested that the symbiotic

Received 30 August 1991; accepted 21 November 1991.

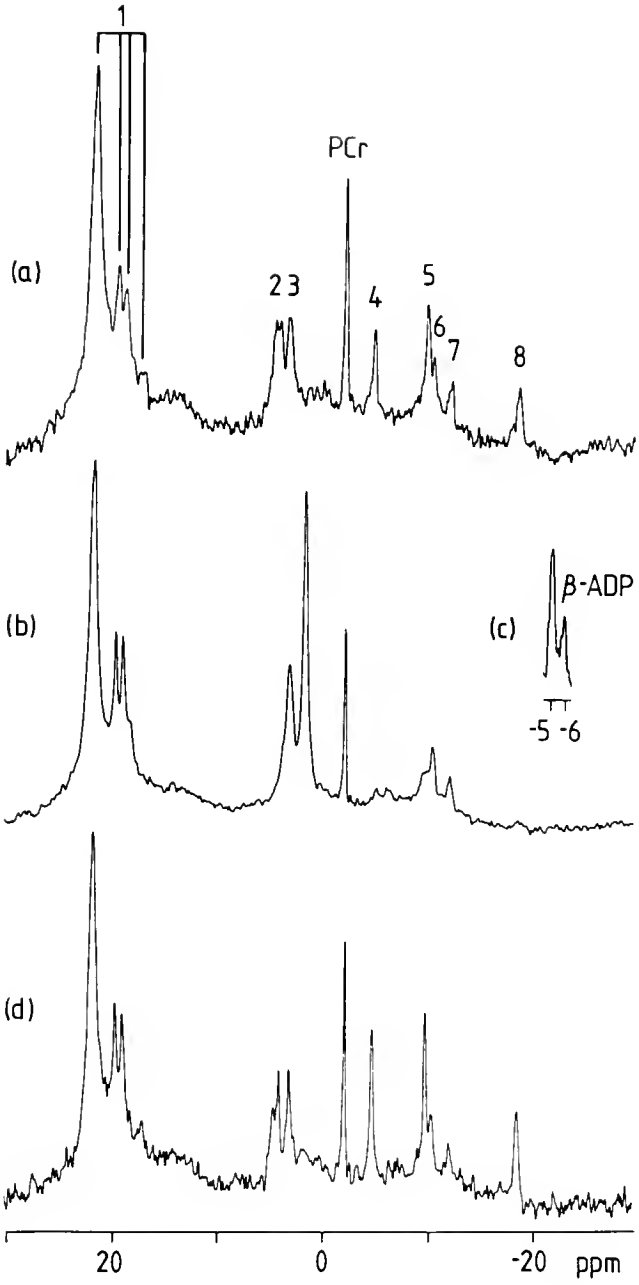

Figure 1. *^{31}P NMR spectra of three different samples of* Anemonia viridis *tentacles: (a) bathed in a circulating oxygenated medium in the dark; (b,c) under hypoxic conditions, i.e., without an external oxygen supply, in the same medium in the dark; and (d) under hypoxic conditions in the light. The spectra were recorded at 121.49 MHz on a Bruker CXP300 NMR spectrometer using a selective frequency ^{31}P probehead. Approximately 50 tentacles from specimens collected from Portsmouth Harbour, U.K., were suspended in an artificial seawater medium (545 mM NaCl, 10 mM KCl, 10 mM Tris, pH 8.3) and packed into a 10 mm NMR tube attached to an experimental arrangement (23) that allowed the suspending medium to be circulated through the tube. Normoxic conditions were maintained with the oxygenated medium flowing at 10 ml min^{-1}, hypoxic conditions were achieved by stopping the flow and allowing the tissue to deplete the oxygen in the small volume (approx. 9.5 ml) of medium in the tube. The tissue was illuminated using a 150W Schott cold light source (KL-1500T) and a fiber optic cable, 1 m long, inserted through the probehead to the NMR tube. This arrangement produced 40 μE m^{-2} s^{-1} P.A.R. around the sample in the probehead. The tissue was maintained at 21–22°C and spectra were recorded in 30-min blocks over a 6-h period using a 45° pulse angle and a 0.5-s recycle time. Spectrum (c) is a 30 min spectrum, recorded early in the hypoxic time-course, while the spectra in (a), (b), and (d) are sums of four 30-min blocks recorded from 4 to 6 h after the start of each experiment. The resonance assignments are: 1, phosphonates, 2, phosphomonoesters; 3, P_i, 4, γ-ATP, 5, α-ATP, 6, NAD(P)(H) and NDP-hexose; 7, NDP-hexose; 8, β-ATP. PCr, phosphocreatine in the chemical shift reference capillary. Chemical shifts are quoted relative to the signal from 85% orthophosphoric acid, but they were measured relative to the signal at −2.44 ppm from the PCr capillary.*

anemone *Anthopleura elegantissima* can avoid oxygen debt when placed under hypoxia in the light (4).

In vivo NMR extends our understanding of the oxygen relations in Cnidaria by allowing changes in intracellular pH and P_i in response to hypoxia to be followed at the same time as changes in ATP and ADP/ATP. The pH dependence of the P_i chemical shift allows cytoplasmic pH values to be deduced *in vivo* from ^{31}P NMR spectra (13), and the intracellular pH in the tentacles was measured using a calibration curve based on the presumed ionic composition of the cnidarian tissue (Fig. 2). In the dark, with oxygen supplied by the circulating medium, the average chemical shift for P_i was 2.94 ± 0.02 ppm (mean ± S.E. from 25 experiments) corresponding to an intracellular pH of ~7.55 in line with the pH values reported for other oxygenated marine invertebrates (9–11,14–16). A similar value, 2.83 ± 0.01 ppm (n = 11), corresponding to an intracellular pH of ~7.35, was obtained in the light in the absence of an external oxygen supply (Fig. 2), but in the dark, the pH fell rapidly, reaching a value of 6.2 or less after 6 h of hypoxia. However, when the hypoxic tissue was illuminated, the intracellular pH returned to its normoxic value within 2 h (Fig. 2). The degree of acidification in hypoxic tissues depends on a number of factors (7), including the conditions under which hypoxia develops (8), but the rapid acidification observed here shows that *Anemonia viridis* has only weak control over its intracellular pH during hypoxia.

It should be noted that the algal symbionts in *A. viridis* represent less than 10% of the total biomass (17,18) and that this was crucial to the success of the NMR experiments for two reasons. First, there was insufficient algal tissue to give detectable signals in the ^{31}P spectrum, allowing the spectrum to be interpreted entirely in terms of contributions from the host tissue. A similar conclusion was reached in a study of *Aiptasia pulchella* (8) and it was confirmed for *Anemonia viridis* by the negligible intensity recorded in a dilute suspension of the isolated *Symbiodinium* sp. (data not shown). Second, the low biomass of the algal symbionts meant that the symbiotic tissue required very little light for photosynthesis, permitting a relatively simple arrangement for illuminating the tissue in the NMR tube. The 40 μEm^{-2}s^{-1} P.A.R. provided by the optical fiber should exceed the compensation point

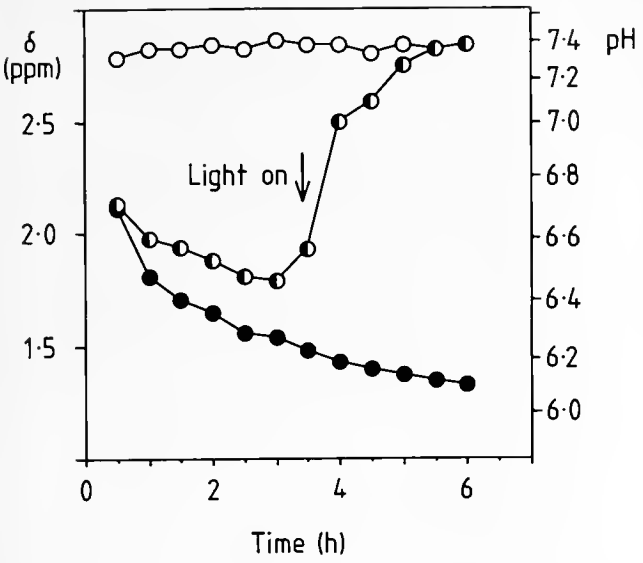

Figure 2. *Time dependence of the chemical shift (δ) of the P_i resonance for* Anemonia viridis *tentacles in the absence of an external oxygen supply: (○) in the light; (●) in the dark; and (◐) initially in the dark followed by illumination. The pH values were deduced from the chemical shift of the tissue P_i resonance using a calibration curve obtained from a solution containing 190 mM KCl, 100 mM NaCl, 0.1 μM $CaCl_2$, 3 mM Na_2HPO_4, 2 mM NaH_2PO_4. The composition of this solution was based on the presumed intracellular ionic composition of cnidarian tissue (24–26), and the calibration curve permitted pH measurements in the range pH 6–8 with an accuracy of ±0.1 pH units. Changes in pH could be detected with an accuracy of ±0.05 pH units.*

for oxygen production in this system (19), and the spectroscopic changes observed on illumination are consistent with the production of at least enough oxygen to meet the respiration demands of the tentacles. In contrast, the very high extinction coefficient of dense algal suspensions and leaf tissues has, to a large extent, prevented the investigation of light-dark transitions in these tissues by NMR (20). Thus the low biomass of the algal symbiont favors the application of *in vivo* NMR and allows the metabolic significance of the photosynthetically derived oxygen to the host to be investigated directly.

Finally, these observations may have implications for the mechanisms underlying calcification in cnidarian corals. Recent respiratory experiments (21) have shown that anthozoan polyps and colonies may actually be hypoxic in the dark under well-stirred, air-saturated conditions due to diffusion limitation of the oxygen supply. Hypoxia inhibits calcium carbonate deposition (22), but because we have shown that this condition can be prevented in a symbiotic tissue by illumination, it may be argued that algal symbionts promote calcification by preventing hypoxia.

Acknowledgments

B. C. Loughman and R. G. Ratcliffe acknowledge the financial support of the Agricultural and Food Research Council, A. E. Douglas acknowledges the support of the Royal Society of London, and M. L. Rands acknowledges the receipt of a studentship from the Science and Engineering Research Council.

Literature Cited

1. **Smith, D. C., and A. E. Douglas. 1987.** *The Biology of Symbiosis.* Edward Arnold, London. 302 pp.
2. **Eaton, J. W., and J. O. Young. 1975.** Studies on the symbiosis of *Phaenocora typhlops* (VEJDOVSKY) (Turbellaria; Neorhabdocoela) and *Chlorella vulgaris,* Var. *vulgaris,* FOTT & NOVAKOVA (Chlorococcales). *Arch. Hydrobiol.* **75:** 50–75.
3. **Boyle, J. E., and D. C. Smith. 1975.** Biochemical interactions between the symbionts of *Convoluta roscoffensis. Proc. R. Soc. Lond. B.* **189:** 121–135.
4. **Shick, J. M., and W. I. Brown. 1977.** Zooxanthellae-produced O_2 promotes sea anemone expansion and eliminates oxygen debt under environmental hypoxia. *J. Exp. Zool.* **201:** 149–155.
5. **Dykens, J. A., and J. M. Shick. 1982.** Oxygen production by endosymbiotic algae controls superoxide dismutase activity in their animal host. *Nature* **297:** 579–580.
6. **Lesser, M. P., W. R. Stochaj, D. W. Tapley, and J. M. Shick. 1990.** Physiological mechanisms of bleaching in coral reef anthozoas: effect of irradience, ultra-violet radiation, and temperature on the activities of protective enzymes against active oxygen. *Coral Reefs* **8:** 225–232.
7. **Hochachka, P. W., and T. P. Mommsen. 1983.** Protons and anaerobiosis. *Science* **219:** 1391–1397.
8. **Steen, R. G. 1986.** Impact of symbiotic algae on sea anemone metabolism: analysis by *in vitro* ^{31}P Nuclear Magnetic Resonance spectroscopy. *J. Exp. Zool.* **240:** 315–325.
9. **Kamp, G., and H. P. Juretschke. 1989.** Hypercapnic and hypocapnic hypoxia in the lugworm *Arenicola marina:* a ^{31}P NMR study. *J. Exp. Zool.* **252:** 219–227.
10. **Raffin, J. P., M. T. Thebault, and J. Y. Legall. 1988.** Changes in phosphometabolites and intracellular pH in the tail muscle of the prawn *Palaemon serratus* as shown by *in vivo* ^{31}P-NMR. *J. Comp. Physiol. B* **158:** 223–228.
11. **Wiseman, R. W., W. R. Ellington, and R. C. Rosanske. 1989.** Effects of extracellular pH and D-lactate efflux on regulation of intracellular pH during isotonic contractions in a molluscan mussel: a ^{31}P Nuclear Magnetic Resonance study. *J. Exp. Zool.* **252:** 228–236.
12. **Ellington, W. R. 1981.** Effect of anoxia on the adenylates and the energy charge in the sea anemone, *Bunodosoma cavernata* (Bosc). *Physiol. Zool.* **54:** 415–422.
13. **Gadian, D. G. 1982.** *Nuclear Magnetic Resonance and its Applications to Living Systems.* Clarendon Press, Oxford. 197 pp.
14. **Zange, J., W. O. Portner, A. W. H. Jans, and M. K. Grieshaber. 1990.** The intracellular pH of a molluscan smooth muscle during a contraction-catch-relaxation cycle estimated by the distribution of [^{14}C] DMO and by ^{31}P-NMR spectroscopy. *J. Exp. Biol.* **150:** 81–93.
15. **Walsh, P. J., D. G. McDonald, and C. E. Booth. 1984.** Acid-base balance in the sea mussel, *Mytilus edulis.* II. Effects of hypoxia and air-exposure on intracellular acid-base status. *Mar. Biol. Lett.* **5:** 359–369.
16. **Ellington, W. R. 1983.** The extent of intracellular acidification during anoxia in the catch muscles of two bivalve molluscs. *J. Exp. Zool.* **227:** 313–317.

17. **Tytler, E. M., and P. Spencer Davies. 1986.** The budget of photosynthetically derived energy in the *Anemonia sulcata* (Pennant) symbiosis. *J. Exp. Mar. Biol. Ecol.* **99**: 257–269.
18. **Harland, A. D., L. M. Fixter, P. Spencer Davies, and R. A. Anderson. 1991.** Distribution of lipids between the zooxanthellae and animal compartment in the symbiotic sea anemone *Anemonia viridis:* wax esters, triglycerides, and fatty acids. *Mar. Biol.* **110:** 13–19.
19. **Dorsett, D. A. 1984.** Oxygen production in the intertidal anemone *Anemonia sulcata*. *Comp. Biochem. Physiol.* **78A:** 225–228.
20. **Callies, R., R. Altenburger, A. Mayer, L. H. Grimme, and D. Leibfritz. 1990.** A new illumination system for *in vivo* NMR spectroscopy. *J. Magn. Reson.* **90:** 561–566.
21. **Shick, J. M. 1990.** Diffusion limitation and hyperoxic enhancement of oxygen consumption in zooxanthellate sea anemones, zoanthids, and corals. *Biol. Bull.* **179:** 149–158.
22. **Crisp, D. J. 1989.** Tidally deposited bands in shells of barnacles and molluscs. Pp. 103–124 in *Origin, Evolution, and Modern Aspects of Biomineralization in Plants and Animals,* R. E. Crick, ed. Plenum Press, New York.
23. **Lee, R. B., and R. G. Ratcliffe. 1983.** Development of an aeration system for use in plant tissue NMR experiments. *J. Exp. Botany* **34:** 1213–1221.
24. **Herrera, F. C., I. Lopez, R. Egea, and P. Zanders. 1989.** Short-term osmotic responses of cells and tissues of the sea anemone, *Condylactis gigantea*. *Comp. Biochem. Physiol. A* **92:** 377–384.
25. **Herrera, F. C., A. Rodriguez, I. Lopez, H. Weitzmann, and I. P. Zanders. 1986.** Characterization of cell ion exchange in the sea anemone *Condylactis gigantea*. *J. Comp. Physiol. B.* **156:** 591–597.
26. **Dunlap, K., K. Takeda, and P. Brehm. 1987.** Activation of a calcium-dependent photoprotein by chemical signalling through gap junctions. *Nature* **325**: 60–62.

The Biological

Bulletin Board

February 1992

What's News at the BB...

•We now offer ***expedited processing*** for Research Notes. We use express mail only, and offer a small emolument to reviewers to provide reviews within two weeks. A carefully prepared Research Note will appear in print in as little as 3.6 months after its submission. See our Research Notes style guidelines outlined in our "Instructions to Authors" section at the beginning of each issue.

• Authors who regularly send manuscripts of high quality to the *Bulletin* will be considered **Preferred Authors.** Preferred Authors benefit from ***expedited processing*** for ALL of their submissions, and receive 200 free reprints and color plates as needed. (Yes, we do color in the *Bulletin*! See the Short Reports of the MBL General Scientific Meetings in our October 1991 issue.)

•**Back and special issues of the *Bulletin* are available:**

—"The Woods Hole Marine Biological Laboratory," by F. R. Lillie, an MBL Centennial supplement—$10

—"The Naples Zoological Station and The Marine Biological Laboratory: One Hundred Years of Biology," an MBL Centennial Supplement—$5

—"Consistency and Variability in Peptide Families," a symposium reprint from October 1989—$9

—Regular single back issues, as available—$30 each

Contact our subscription manager, Christine Showalter, at our Woods Hole office for further information.

Meeting Announcements

•The 20th Annual **Marine Benthic Ecology Meeting** will be held in Newport, Rhode Island, on March 26 to 29, 1992. For further information contact Stanley Cobb, Department of Zoology, University of Rhode Island, Kingston, RI 02881; Tel: 401-792-2372.

•The **International Conference on Molluscan Conservation** will be held at the University of Glasgow, Scotland, on September 10 to 12, 1992. Sessions will include taxonomy, distribution, legislation, and conservation. For further information contact Fred Woodward, International Conference on Molluscan Conservation, Kelvingrove Museum & Art Gallery, Kelvingrove, Glasgow G3 8AG, Great Britian; Tel: (041) 357-3929.

•The international symposium on **Climate Change and Northern Fish Populations** will be held in Victoria, British Columbia, Canada, on October 13 to 16, 1992. Topics include evidence for changes in climate and the resulting effects in freshwater and marine environments; effects of climate on fish populations; economic impacts of climate change on fisheries; and preparing for climate change. For further information contact the Symposium Secretary, Department of Fisheries and Oceans, Pacific Biological Station, Nanaimo, British Columbia, Canada V9R 5K6; Tel: 604-756-7260.

CONTENTS

Volume 182 Number 2

THE BIOLOGICAL BULLETIN

APRIL, 1992

Published by the Marine Biological Laboratory

MBL 1992 Short Courses

MOLECULAR EVOLUTION *August 2 – August 14, 1992*

APPLICATION DEADLINE: JUNE 1, 1992

A series of lectures and discussions exploring multiple approaches to molecular evolution, and a computer laboratory for phylogenetic and sequence analysis. This two week program is designed for a class of 60 established investigators, postdoctoral fellows, and advanced graduate students. *Director: Mitchell L. Sogin, Marine Biological Laboratory.*

METHODS IN COMPUTATIONAL NEUROSCIENCE

August 2 – August 29, 1992

APPLICATION DEADLINE: MAY 15, 1992

For 20 advanced graduate students and postdoctoral fellows in neurobiology, physics, electrical engineering, computer science, and psychology. A background in programming (preferably in C and UNIX) is highly desirable. This course presents the basic techniques necessary to study single cells and neural networks from a computational point of view and is organized around lectures, tutorials, and computer laboratories. *Directors: James M. Bower and Christof Koch, Computation and Neural System Program, California Institute of Technology.*

FUNDAMENTAL ISSUES IN VISION RESEARCH: MOLECULAR AND CELL BIOLOGICAL APPROACHES [sponsored by the National Eye Institute, NIH] *August 16 – August 29, 1992*

APPLICATION DEADLINE: MAY 1, 1992

This laboratory-lecture course is intended for 20 graduate students and postdoctoral fellows currently training in molecular biology, cell biology, and neurosciences who are not currently involved in vision research. The goal of the course is to present, in depth, the exciting theoretical and experimental approaches to fundamental research problems in vision so that the students can evaluate the potential for active research in this field. The faculty will describe and direct laboratories of ongoing research in the tissues of the eye of invertebrates and vertebrates. Costs of attending the course, including travel, housing, and meals at MBL will be supported by a scholarship fund from NEI. *Directors: David S. Papermaster, University of Texas Health Science Center, San Antonio; and John E. Dowling, Harvard University.*

RAPID MEASUREMENT OF NEUROTRANSMITTER SIGNALS IN THE CENTRAL NERVOUS SYSTEM USING *IN VIVO* ELECTROCHEMISTRY *August 19 – August 24, 1992*

APPLICATION DEADLINE: JUNE 1, 1992

This course/workshop is intended for 16 graduate students, post-doctoral researchers, and investigators with interests in neuroscience, pharmacology, and chemoreception who wish to learn the art and practice of *in vivo* electrochemistry as applied to studies of the CNS. The course will address the theory and practice of these techniques, and will encompass a combination of lectures, demonstrations, and hands-on use of these methods and technologies. *Directors: Greg A. Gerhardt and Paul A. Moore, Rocky Mountain Center for Sensor Technology, University of Colorado Health Sciences Center.*

OPTICAL MICROSCOPY AND IMAGING IN THE BIOMEDICAL SCIENCES *September 23 – 30, 1992*

APPLICATION DEADLINE: JULY 1, 1992

Designed primarily for 22 research scientists, physicians, postdoctoral trainees, and advanced graduate students in animal, plant, and medical sciences as well as non-biologists with experience in microscopy and university faculty planning to develop courses on similar topics. The course covers the fundamental theory and practical use of modern optical microscopy. Special attention will be given to different optical techniques and the newest photographic and video methods used in biological and biomedical research. *Directors: Nina Strömgren Allen, Wake Forest University; and Colin S. Izzard, State University of New York at Albany.*

For Further information and application forms, contact:
Florence Dwane, Admissions Coordinator • Office of Sponsored Programs
Marine Biological Laboratory • Woods Hole, MA 02543, USA • (508) 548-3705, ext. 216

THE
BIOLOGICAL BULLETIN

PUBLISHED BY
THE MARINE BIOLOGICAL LABORATORY

APRIL, 1992

Printed and Issued by
LANCASTER PRESS, Inc.
PRINCE & LEMON STS.
LANCASTER, PA

THE BIOLOGICAL BULLETIN is published six times a year by the Marine Biological Laboratory, MBL Street, Woods Hole, Massachusetts 02543.

Subscriptions and similar matter should be addressed to Subscription Manager, THE BIOLOGICAL BULLETIN, Marine Biological Laboratory, Woods Hole, Massachusetts 02543. Single numbers, $30.00. Subscription per volume (three issues), $77.50 ($155.00 per year for six issues).

Communications relative to manuscripts should be sent to Michael J. Greenberg, Editor-in-Chief, or Pamela L. Clapp, Managing Editor, at the Marine Biological Laboratory, Woods Hole, Massachusetts 02543. Telephone: (508) 548-3705, ext. 428. FAX: 508-540-6902. E-mail: pamcl@hoh.mbl.edu.

POSTMASTER: Send address changes to THE BIOLOGICAL BULLETIN, Marine Biological Laboratory, Woods Hole, MA 02543.

Second-class postage paid at Woods Hole, MA, and additional mailing offices.
ISSN 0006-3185

INSTRUCTIONS TO AUTHORS

The Biological Bulletin accepts outstanding original research reports of general interest to biologists throughout the world. Papers are usually of intermediate length (10–40 manuscript pages). A limited number of solicited review papers may be accepted after formal review. A paper will usually appear within four months after its acceptance.

Very short, especially topical papers (less than 9 manuscript pages including tables, figures, and bibliography) will be published in a separate section entitled "Research Notes." A Research Note in *The Biological Bulletin* follows the format of similar notes in *Nature*. It should open with a summary paragraph of 150 to 200 words comprising the introduction and the conclusions. The rest of the text should continue on without subheadings, and there should be no more than 30 references. References should be referred to in the text by number, and listed in the Literature Cited section in the order that they appear in the text. Unlike references in *Nature*, references in the Research Notes section should conform in punctuation and arrangement to the style of recent issues of *The Biological Bulletin*. Materials and Methods should be incorporated into appropriate figure legends. See the article by Lohmann *et al.* (October 1990, Vol. **179:** 214–218) for sample style. A Research Note will usually appear within two months after its acceptance.

The Editorial Board requests that regular manuscripts conform to the requirements set below; those manuscripts that do not conform will be returned to authors for correction before review.

1. ***Manuscripts.*** Manuscripts, including figures, should be submitted in triplicate. (Xerox copies of photographs are not acceptable for review purposes.) The original manuscript must be typed in no smaller than 12 pitch, using double spacing (*including* figure legends, footnotes, bibliography, etc.) on one side of 16- or 20-lb. bond paper, 8½ by 11 inches. Please, no right justification. Manuscripts should be proofread carefully and errors corrected legibly in black ink. Pages should be numbered consecutively. Margins on all sides should be at least 1 inch (2.5 cm). Manuscripts should conform to the *Council of Biology Editors Style Manual*, 5th Edition (Council of Biology Editors, 1983) and to American spelling. Unusual abbreviations should be kept to a minimum and should be spelled out on first reference as well as defined in a footnote on the title page. Manuscripts should be divided into the following components: Title page, Abstract (of no more than 200 words), Introduction, Materials and Methods, Results, Discussion, Acknowledgments, Literature Cited, Tables, and Figure Legends. In addition, authors should supply a list of words and phrases under which the article should be indexed.

2. ***Title page.*** The title page consists of: a condensed title or running head of no more than 35 letters and spaces, the manuscript title, authors' names and appropriate addresses, and footnotes listing present addresses, acknowledgments or contribution numbers, and explanation of unusual abbreviations.

3. ***Figures.*** The dimensions of the printed page, 7 by 9 inches, should be kept in mind in preparing figures for publication. We recommend that figures be about 1½ times the linear dimensions of the final printing desired, and that the ratio of the largest to the smallest letter or number and of the thickest to the thinnest line not exceed 1:1.5. Explanatory matter generally should be included in legends, although axes should always be identified on the illustration itself. Figures should be prepared for reproduction as either line cuts or halftones. Figures to be reproduced as line cuts should be unmounted glossy photographic reproductions or drawn in black ink on white paper, good-quality tracing cloth or plastic, or blue-lined coordinate paper. Those to be reproduced as halftones should be mounted on board, with both designating numbers or letters and scale bars affixed directly to the figures. All figures should be numbered in consecutive order, with no distinction between text and plate figures. The author's name and an arrow indicating orientation should appear on the reverse side of all figures.

4. ***Tables, footnotes, figure legends, etc.*** Authors should follow the style in a recent issue of *The Biological Bulletin* in preparing table headings, figure legends, and the like. Because of the high cost of setting tabular material in type, authors are asked to limit such material as much as possible. Tables, with their headings and footnotes, should be typed on separate sheets, numbered with consecutive Roman numerals, and placed after

the Literature Cited. Figure legends should contain enough information to make the figure intelligible separate from the text. Legends should be typed double spaced, with consecutive Arabic numbers, on a separate sheet at the end of the paper. Footnotes should be limited to authors' current addresses, acknowledgments or contribution numbers, and explanation of unusual abbreviations. All such footnotes should appear on the title page. Footnotes are not normally permitted in the body of the text.

5. ***Literature cited.*** In the text, literature should be cited by the Harvard system, with papers by more than two authors cited as Jones *et al.*, 1980. Personal communications and material in preparation or in press should be cited in the text only, with author's initials and institutions, unless the material has been formally accepted and a volume number can be supplied. The list of references following the text should be headed Literature Cited, and must be typed double spaced on separate pages, conforming in punctuation and arrangement to the style of recent issues of *The Biological Bulletin*. Citations should include complete titles and inclusive pagination. Journal abbreviations should normally follow those of the U. S. A. Standards Institute (USASI), as adopted by BIOLOGICAL ABSTRACTS and CHEMICAL ABSTRACTS, with the minor differences set out below. The most generally useful list of biological journal titles is that published each year by BIOLOGICAL ABSTRACTS (BIOSIS List of Serials; the most recent issue). Foreign authors, and others who are accustomed to using THE WORLD LIST OF SCIENTIFIC PERIODICALS, may find a booklet published by the Biological Council of the U.K. (obtainable from the Institute of Biology, 41 Queen's Gate, London, S.W.7, England, U.K.) useful, since it sets out the WORLD LIST abbreviations for most biological journals with notes of the USASI abbreviations where these differ. CHEMICAL ABSTRACTS publishes quarterly supplements of additional abbreviations. The following points of reference style for THE BIOLOGICAL BULLETIN differ from USASI (or modified WORLD LIST) usage:

A. Journal abbreviations, and book titles, all underlined (for *italics*)

B. All components of abbreviations with initial capitals (not as European usage in WORLD LIST *e.g., J. Cell. Comp. Physiol.* NOT *J. cell. comp. Physiol.*)

C. *All* abbreviated components must be followed by a period, whole word components *must not* (*i.e., J. Cancer Res.*)

D. Space between all components (*e.g., J. Cell. Comp. Physiol.*, not *J.Cell.Comp.Physiol.*)

E. Unusual words in journal titles should be spelled out in full, rather than employing new abbreviations invented by the author. For example, use *Rit Vísindafjélags Islendinga* without abbreviation.

F. All single word journal titles in full (*e.g., Veliger, Ecology, Brain*).

G. The order of abbreviated components should be the same as the word order of the complete title (*i.e., Proc.* and *Trans.* placed where they appear, not transposed as in some BIOLOGICAL ABSTRACTS listings).

H. A few well-known international journals in their preferred forms rather than WORLD LIST or USASI usage (*e.g., Nature, Science, Evolution* NOT *Nature, Lond., Science, N.Y.; Evolution, Lancaster, Pa.*)

6. ***Reprints, page proofs, and charges.*** Authors receive their first 100 reprints (without covers) free of charge. Additional reprints may be ordered at time of publication and normally will be delivered about two to three months after the issue date. Authors (or delegates for foreign authors) will receive page proofs of articles shortly before publication. They will be charged the current cost of printers' time for corrections to these (other than corrections of printers' or editors' errors). Other than these charges for authors' alterations, *The Biological Bulletin* does not have page charges.

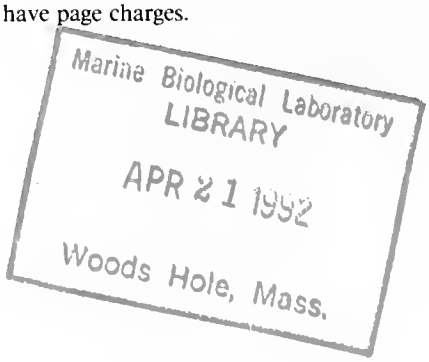

ERRATA

The Biological Bulletin, Volume **181,** Number 3

Page 423, Table III

The following correction should be made in the article by R. K. Zimmer-Faust titled, "Chemical signal-to-noise detection by spiny lobsters" (*Biol. Bull.* **181:** 419–426):

On page 423, in Table III, the last entry in the W_f column, which reads "3.65 ($\pm$ 1.79) $\times$ 10^{-2}" should read, "3.65 ($\pm$ 1.79) $\times$ 10^{-3}." The exponent "$^{-3}$" replaces the exponent "$^{-2}$."

Page 427

The following correction should be made in the article by J. J. O'Brien *et al.,* "Proteins of crustacean exoskeletons: I. Similarities and differences among proteins of the four exoskeletal layers of four brachyurans" (*Biol. Bull.* **181:** 427–441):

On page 427, the first footnote, which reads "Received" should read, "Received 24 April 1991; accepted 17 September 1991."

Page 499

The following correction should be made in the article by S. Soinila and G. J. Mpitsos titled, "Immunohistochemistry of diverging and converging neurotransmitter systems in mollusks" (*Biol. Bull.* **181:** 484–499).

On page 499, the reference to Leonard *et al.,* 1990, which reads "Leonard, J. L., M. Martinez-Padron, J. P. Edstrom, and K. Lukowiak. 1990. Does altering identified gill motor neuron activity alter gill behavior in *Aplysia?* North Holland Publishing Co., Amsterdam" should read, "Leonard, J. L., M. Martinez-Padron, J. P. Edstrom, and K. Lukowiak. 1990. Does altering identified gill motor neuron activity alter gill behavior in *Aplysia?* Pp. 30–37 in *Molluscan Neurobiology,* K. S. Kits, H. Boer, and J. Joose, eds. North Holland Publishing Co., Amsterdam." The line, "Pp. 30–37 in *Molluscan Neurobiology,* K. S. Kits, H. Boer, and J. Joose, eds.," should be added to the reference.

Reference: *Biol. Bull.* **182:** 165–166. (April, 1992)

Carroll M.* Williams

DOROTHY M. SKINNER AND JOHN S. COOK

Biology Division, Oak Ridge National Laboratory, Oak Ridge, Tennessee 37831

In spite of its history of keponed waters,
Virginia is loved by its sons and daughters.
From this land of ham and bourbon barrel
Emerged a Williams, christened Carroll.
A Southerner born, and a Richmond alumn,
He has lived in Cambridge since Kingdom Come.
But like natives of Hong Kong or even Tashkent,
He always retained his partic'lar accent.

In his first stint at Harvard, his doctor's degree
Crowned him Philos'pher of Biology.
He then mastered the art of prescription concoctor
And achieved the degree of a Medical Doctor.
But his expertise with scalpel and suture
Was devoted to insects alone in the future.

All matters insectuous engaged his attention.
From the many, a highlight or two shall we mention.
For example, consider the dry cleaner's plight,
Beleaguered, while cleaning, with insects in flight.
When the kelp flies bugged (or the kelp bugs flew),
The cleaners were frantic, but Carroll knew:
What was driving these people to grief and distraction
Was simply their own cleaning fluid's attraction.

He was later enchanted, but not for too long,
By the siren-sweet sound of *Drosophila's* song.

He made the humble moth *Cecropia*
A scientific cornucopia.
The careful perusal of hormonal data
Called his attention to corpora allata.
Switched on by the cold, just as Carroll was hopin',
They discharged their prothoracicotropin.

Another Stoff with a different style
Is *Cecropia's* hormone juvenile.
To its own secretion it cannot adapt;
The pupa remains as a pupa entrapped.
This leads to a concept that's really quite scary:
Physiological hari kari.

* M stands for Milton, Muriel, Massachusetts, moth, *Manduca*, molting, metamorphosis, mitochondria, muscle, midge, magician, and much more.

Carroll M. Williams died on October 11, 1991. He was one of America's premiere insect physiologists, and he spent his entire career at Harvard University. Over a period of forty years, *The Biological Bulletin* published more than 25 of his seminal papers, and has chosen to honor the memory of this extraordinary scientist with a poetic synopsis of some of the highlights of his career. This poem was delivered by Dorothy Skinner at the banquet that concluded a symposium dedicated to Williams at the 1980 annual meeting of the American Society of Zoologists. Carroll was enraptured by the rendition, and we hope it will convey to its readers some of his spirit and creativity. Scholarly tributes to the career of Dr. Williams will appear in *Developmental Biology* and the *Biographical Memoirs of the National Academy of Sciences.*

A woody factor that development fouls
He obtained from a column of paper towels.
A cost-cutting process was therein conceived;
With the factor eluted, the towels were retrieved.

Are corners required for *Cecropia* cocoons?
Carroll reared the poor beasts inside safe-sex balloons.

With the hypnotic charm of a true Southern preacher,
Carroll was born-to-the-art as a teacher.
He offered a course in Insect Disease.
The prerequisite was: "Can you read Japanese?"

Hungry students with stipends as teaching assistants
Were often hard-pressed just to manage subsistence.
But many were able to keep tummies quiet
With Carroll's tea cakes as their principal diet.

An integral part of his craft professorial
Is the camera work of his cohort Muriel.
In his published work, among the fixtures
Supporting the data are Muriel's pictures.
Surely there can be no finer alliance
Than elegant art wed to elegant science.

We close these lines of appreciation
With a word or two on sub-speciation.
A genetic analogy may not be prudent,
But he transmitted something to each Williams student.
For six-legged studies he set new criteria;
With his standards so high, we disdain the inferia.

Reference: *Biol. Bull.* **182:** 167–168. (April, 1992)

How the Axon Got its Tale

(For K.D.)

DEFOREST MELLON, JR.

Department of Biology, University of Virginia, Charlottesville, Virginia 22901

In early days the axon was unknown and quintessential
'Till Bernstein's brilliant insights gave its secrets new potential.

With pluses out and minuses within the membrane's confines,
There must exist a gradient of concentrated ions.

An impulse in its travels down an axon would exist
Because ionic permeances undergo a twist.

Potassium is high within and sodium without,
And transient membrane breakdown then would foster turnabout.

Short circuit currents would ensue as ions rushed across,
Internal voltage then would fall, and very soon be lost.

But if conductances returned to resting states, anon,
A voltage would arise once more, predicted by Donnan.

This model was impressive as a formal working scheme,
And others came to increment a growing nervous team.

Lucas, Adrian, and Matthews, Gasser, Hartline, Forbes, and Katz
Worked on nerves in many animals, from *Limulus* to rats.

Spikes were soon a-popping in a host of different labs,
As the drive to learn their secrets grew intense and up for grabs.

First, Hodgkin showed us how the nervous impulse moves about:
Local circuits are the answer, sorting currents in and out.

Then Cole and Curtis found that Bernstein's story had some credence,

They showed that spikes in axons come from changes in impedance.

And Hodgkin and his sidekick had the fun of being first
To learn potentials during spikes are actually reversed!

These two then went to Plymouth where, with Katz, they made their camp;
And with their brains predicting gains, used KC's voltage clamp.

They needed nerves of super size to extricate their facts from,
and J.Z. Young surprised them, saying "Squids have giant axons."

These, threaded through with two fine twists of chloride-coated wire
Were quickly held in voltage steps to stimulate their fire.

With capacitative surges voided early at each go,
The resulting current traces now gave signs of ion flow.

Now, sodium was first allowed sole access through its gate,
Then the membrane's charge would switch, a half a millisecond late.

Potassium then rushed across, the other way about,
Until the membrane had reset its voltage in and out.

(Bernstein had it half-right, but he didn't know the sequel:
The channels all are separate—and their latencies aren't equal)

Soon, Moore and Narahashi found a fishy substance which,
When put on axons, blocked the voltage-gated sodium switch.

And TEA when tested in a voltage-clamped condition,
Removed the second ion flow: potassium emission.

Now, these two channels set the tune at every nervous dance
But in the wings are many more, all waiting for their chance.

Nerve terminals need calcium to talk about their states;
Membrane channels are the answer, controlled by voltage gates.

Other channels set the mood for the neurons' current tempers,
Their gates are held in different states by second messengers.

And peptides that a year ago were totally unknown
Are recognized by schoolboys as the latest neurohormone.

So now we know the ins and outs of axon current flow,
How membrane gates are modified to make the impulse go.

The thoughts which built this story through the years, with wire and prose,
Themselves were born of agencies they were destined to disclose.

The dancing spikes thus spin their tale of learning, love, and pain
And turning round, they watch it all come running back again.

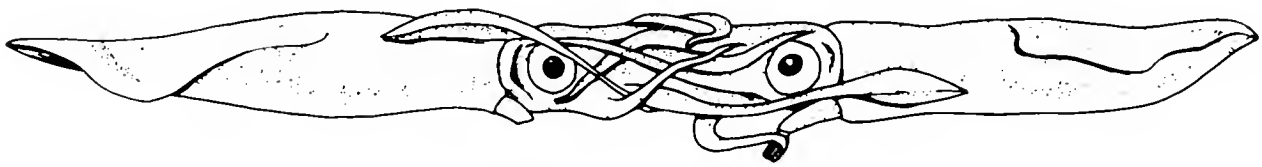

From. Barth, Robert H., and Robert E. Broshears. 1982. The Invertebrate World. *Saunders College Publishing, Philadelphia P. 301.*

Reference: *Biol. Bull.* **182:** 169–176. (April, 1992)

The Culture, Sexual and Asexual Reproduction, and Growth of the Sea Anemone *Nematostella vectensis*

CADET HAND AND KEVIN R. UHLINGER

Bodega Marine Laboratory, P.O. Box 247, Bodega Bay, California 94923

Abstract. *Nematostella vectensis,* a widely distributed, burrowing sea anemone, was raised through successive sexual generations at room temperature in non-circulating seawater. It has separate sexes and also reproduces asexually by transverse fission. Cultures of animals were fed *Artemia* sp. nauplii every second day. Every eight days the culture water was changed, and the anemones were fed pieces of *Mytilus* spp. tissue. This led to regular spawning by both sexes at eight-day intervals. The cultures remained reproductive throughout the year. Upon spawning, adults release either eggs embedded in a gelatinous mucoid mass, or free-swimming sperm. In one experiment, 12 female isolated clonemates and 12 male isolated clonemates were maintained on the 8-day spawning schedule for almost 8 months. Of the female spawnings, 75% occurred on the day following mussel feeding and water change, and 64% of the male spawnings were similarly synchronized under this regime. Fertilization and development occur when gametes from both sexes are combined *in vitro.* At 20°C, the embryos gastrulate within 12–15 hours. Spherical ciliated planulae emerge from egg masses 36–48 hours post-fertilization. The planulae elongate and form the first mesenteric couple, as well as four tentacle buds, by day five. By day seven, they metamorphose and settle as 250–500 μm long, four-tentacled juvenile anemones. More tentacles and all eight macrocnemes are present at 2–3 weeks. Individuals may become reproductively mature in as few as 69 days. *Nematostella vectensis* has the potential to become an important model for use in cnidarian developmental research.

Introduction

Many sea anemones can be maintained for long periods under a variety of conditions including non-circulating water at room temperatures (Stephenson, 1928), and under the latter conditions some species produce numerous asexual offspring by a variety of methods (Cary, 1911; Stephenson, 1929). More recently this trait has been used to produce clones of genetically identical individuals useful for experimentation; *i.e., Haliplanella luciae* (by Minasian and Mariscal, 1979), *Aiptasia pulchella* (by Muller-Parker, 1984), and *Aiptasia pallida* (by Clayton and Lasker, 1984). We now add one more species to this list, namely *Nematostella vectensis* Stephenson (1935), a small, burrowing athenarian sea anemone synonymous with *N. pellucida* Crowell (1946) (see Hand, 1957).

Nematostella vectensis is an estuarine, euryhaline member of the family Edwardsiidae and has been recorded in salinities of 8.96 to 51.54‰ and water temperatures of −1° to 28°C (Williams, 1983). It is a small animal, usually less than 2 cm long and a few millimeters in diameter when found in the field (Williams, 1983). It occurs in England, from Nova Scotia to Georgia on the North American Atlantic coast, from Florida to Louisiana along the shores of the Gulf of Mexico, and from California to Washington on the Pacific coast (Hand, unpub. Louisiana record; Heard, 1982; Kneib, 1985; Williams, 1983). Williams (1983) considered the species vulnerable to extinction in Great Britain, but it is plentifully abundant throughout most of its range and is readily collected. *Nematostella* occurs in soft sediments, in plant debris, and among living plants in permanent pools and tidal creeks in salt marshes. It also occurs subtidally in estuaries in Chesapeake Bay (M. Posey, pers. comm.; Calder, 1972) and in the Indian River in Delaware (Jensen, 1974).

To date we have only the barest outline of the life history of this species. Crowell (1946) and Frank and Bleakney (1976) reported that eggs were discharged in mucoid masses accompanied by numerous nematosomes. Nematosomes, which occur in the coelenteron, are spherical, 15–45 μm, flagellated bodies containing nematocysts and

Received 25 July 1991; accepted 13 January 1992.

are known only from the genus *Nematostella* (Williams, 1979). Frank and Bleakney (1976) reported that planula larvae developed from the eggs, but subsequently disappeared, and Williams (1975) found three, 1.0 mm long planulae that he attributed to *Nematostella* in a pool containing that sea anemone. Rudy and Rudy (1983) kept *N. vectensis* in the laboratory for five years and stated that eggs developed to planulae in three days and to "four-knobbed" juveniles, *i.e.*, with four tentacle buds, in five days. The sexes are separate (Hand, 1957; Frank and Bleakney, 1976; Williams, 1975), and *N. vectensis* reproduces asexually by transverse fission (Lindsay, 1975; Williams, 1976; Frank and Bleakney, 1978).

Even less is known about the natural history of *N. vectensis*. Kneib (1985) has shown that the grass shrimp *Palaemonetes pugio* may prey on this anemone, and Lindsay (1975) and Frank and Bleakney (1978) have given us information on the anemone's diet. We also know that it tolerates extremes of temperature and salinity (Bleakney and Meyer, 1979; Stephenson, 1935) and, at times, may occur in dense populations, *i.e.*, over 5 million in a single pool (Williams, 1983) and 1816 in a 15 cm^2 sample (Bleakney and Meyer, 1979). Little beyond this is known of its natural history.

Here we describe the culture, reproduction, development, and growth of *Nematostella*, as well as some other aspects of its biology. In particular, we show that this anemone reproduces sexually in standing water at room temperature, is readily raised through successive generations, is sexually active throughout the year, and shows no sign of seasonality in its reproduction in the laboratory. This combination of traits—namely asexual reproduction, which allows the development of clones, and sexual reproduction with subsequent development through larval stages to reproductive adults, all under room temperature culture conditions—suggests that this sea anemone should be useful in the study of cnidarian biology, particularly development.

Materials and Methods

In December 1987, we received 12 living *N. vectensis* that had been collected subtidally from the Rhode River, a subestuary of the Chesapeake Bay in Maryland. The largest of these anemones was about 15 mm long when fully extended. The salinity at the time and place of collection was about 12‰. These Rhode River anemones, together with their sexual and asexual descendants, have been maintained in our laboratory and now number several thousand. It is from these cultures that isolated female and male clonemates were reared (see below). We also have cultures of *Nematostella* from England, Nova Scotia, Georgia, California, Oregon, and Washington.

Culture methods

Our cultures were maintained in crystallizing dishes with plastic Petri dish parts as covers. They were kept at room temperatures ranging from 16–26°C, and at a salinity of about 12‰. We did not provide these animals with any substrate, such as silt or fine sediments, nor did we provide aeration to the cultures. The water was changed weekly to bi-weekly, but solitary anemones or cultures of only a few individuals may actually be kept for several weeks in unchanged water. *Nematostella* will tolerate crowding. We have raised about 300 sea anemones to lengths of 2–4 cm in a single 80 × 40 mm dish containing 100 ml of water, and we have reared equal numbers from planulae to young sea anemones, about 1.0 cm long, in 25 ml of water in 51 × 31 mm dishes.

We fed *Artemia* nauplii to our cultures every second day, and cultures have been maintained for more than two years on that diet alone; we have used both San Francisco Bay Brand and Sanders Premium Great Salt Lake *Artemia*. Other foods used were the yolk of hard boiled hens' eggs and veliger larvae of mussels and oysters. These are readily accepted by recently metamorphosed sea anemones. Tissues from *Mytilus edulis* and *M. californianus*, such as the ovary cut into 1–2 mm pieces, are also readily eaten by larger *Nematostella*.

The production of isolated female and male clonemates

The 12 *Nematostella* received from the Rhode River in December 1987 grew rapidly and began producing fertile egg masses in February 1988. From these and subsequent spawnings we reared several hundred *Nematostella* to sexual maturity. To observe spawnings more closely and to control the time of fertilization, we isolated sibling anemones that were several months old. By April 1989 we had isolated 16 mature and reproductively active females and 14 reproductive males. Each animal was held in a 51 × 31 mm dish containing 25 ml of 33% seawater, and each was fed 3–5 drops of concentrated *Artemia* nauplii every second day. Each animal was fed small pieces of *M. californianus* ovary every eighth day, the water in each dish was changed irregularly, and the pattern of spawning was observed.

In time, through asexual reproduction by transverse fission, many of the isolated individuals became clonal groups, and in the period from February 1989 to December 1989, one particular isolated male anemone became a clone of 96 individuals and one female became a clone of 38. From these two clones, we isolated 12 female and 12 male clonemates as above. These isolated anemones were fed several drops of nauplii every second day and two pieces of *M. californianus* ovary every eighth day followed by a water change. We recorded spawnings for these anemones from 12 February to 3 October 1990 (Table I).

Effects of salinity

Because *Nematostella* is euryhaline and because it reproduced frequently for us, we explored the effect of salinity on both sexual and asexual reproduction. We prepared the following concentrations of seawater: 10%, 20%, 33%, 66%, 100%, 125%. The salinity of the 100% seawater was 34‰, and the 125% seawater was prepared by evaporation. We selected 6 groups of 20 anemones each from a culture of about 300, essentially mature, 6-month-old siblings, 2.0–3.0 cm long. Other than the group of 20 that was to stay in 33% seawater, each group was acclimated to the desired final concentration by being successively moved, every four days, through the increasing or decreasing concentrations. We fed these anemones brine shrimp nauplii every second day, and recorded their sexual and asexual reproduction for a sixteen week period, from mid-October 1988, to the end of January 1989.

Results

Sexual reproduction

In our cultures, anemones become sexually mature at three to four months of age and at column lengths of between 1.5 and 3.5 cm. The sexes are separate, and individuals that have been isolated for more than two years continue on as either males or females. We have seen no signs of hermaphroditism or change of sex. In cultures of mixed sexes, spawning frequently occurred in numerous dishes on a given day; *i.e.*, cultures on comparable feeding regimes tended to spawn at the same time. Egg masses formed within females are extruded through the mouth (Fig. 1). The eggs are opaque and creamy white, and they vary in diameter from 170 to 240 μm. The masses consist of a gelatinous-like material which adheres to nearby objects when first extruded. The masses may be small and spherical (up to about 2 or 2.5 mm diameter) or elongate, and in the extreme, more than 5 cm long by 3 mm in diameter (Fig. 2). There may be few eggs, *i.e.*, 5–10, such as reported by Crowell (1946), or there may be many more (the largest egg masses we have seen contained more than 2000 ova). As well as ova, the egg masses contain hundreds, even thousands, of nematosomes. These can be seen rotating in place within the egg mass. In our cultures, sexual reproduction has occurred in every month of the year with no apparent seasonality or correlation with moon phases.

In the first experiment with 16 female and 14 male isolated siblings, we recorded numerous instances when most of both sexes spawned within a few hours of one another, between mid-afternoon and early evening. Females produced from one to three egg masses each spawning, and males released varying amounts of sperm.

In the second experiment, with 12 female and 12 male isolated clonemates, we recorded 322 female and 264 male spawnings; 242 of those by females and 170 of those by males occurred the day after both sexes had eaten mussel and had had their water changed (Table I). Thus 75% of the female spawnings and 64% of the male spawnings occurred on the same days and, as before, within a few hours of one another. Of those spawnings, all 12 females spawned in seven cases, and all 12 males spawned in four. On three occasions, all 12 of both sexes spawned on the same day. On the day after eating mussel, at least one female always spawned, but on three occasions, no male spawned.

Embryology and development

Sperm produced by isolated males can be added to extruded egg masses and development observed. Cleavage leads to translucent blastulae, most of which become invaginate gastrulae 12–15 hours after fertilization at around 20°C (Fig. 3). The gastrulae emerge from the egg mass as 200–250 μm spherical, ciliated planulae 36–48 hours after fertilization. The planulae alternate between periods of swimming and resting and develop an apical tuft of large cilia that becomes obvious by the third day. They change their shape progressively from spherical, to pear-shaped, to elongate, and by five days, some develop four tentacle buds around the mouth (Figs. 4, 5). At four to five days, there are two thickened areas of tissue internally that represent the first mesenteric couple. By the seventh day, many planulae cease swimming, settle to the bottom, and metamorphose into 250–500 μm long juveniles with four tentacles. The metamorphosed young may retain cilia on their columns for more than a month and grow to a length of more than 1 mm before the cilia are lost. During the first few days after metamorphosis, the juveniles glide over the substrate with the aboral end forward, although they no longer rotate about their longitudinal axes as the planulae did. The direction of movement reverses after a few days, and the juveniles then glide with the oral end leading. Most juveniles cease gliding before they are 1 mm long.

The young anemones vary considerably in size, and by 10 days some may already be 1 mm long when fully extended. By two weeks some will have grown to 2 mm (Fig. 6), by three weeks to 4 mm or slightly longer, and, in the extreme, to 2.5 cm long in a month. At 2–3 weeks, a second set of four tentacles develops, and all eight macrocnemes are obvious, although the first couple are much larger than any of the others. This seeming dominance of the first mesenteric couple is a feature that remains obvious for the first several months. Commonly, month-old animals have 12 tentacles, can extend their bodies to 1–2 cm, and possess a few nematosomes. Two-month-old animals are approaching sexual maturity, are 2–5 cm long, may have 16 tentacles, and have usually developed abundant nematosomes. Some mature sexually and spawn at

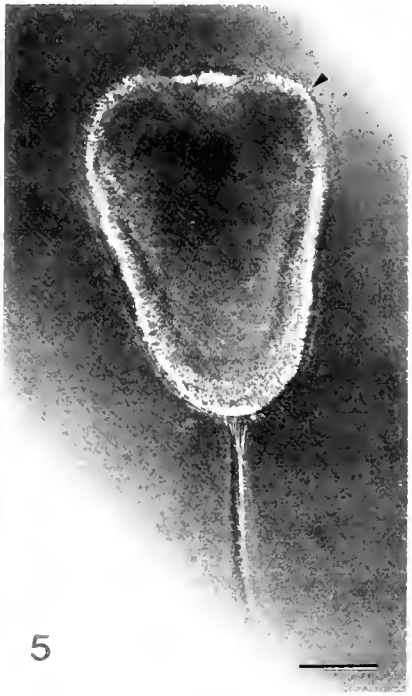

an age of about 10 weeks. Spawning occurred in one culture that was only 69 days post fertilization. Asexual division by transverse fission also becomes common at about 10 weeks. The earliest fission noted was in a seven-week-old individual that was almost 3 cm long. In about five months, heavily fed animals can grow to expanded lengths exceeding 16 cm, with physal diameters of 4–5 mm, and tentacles 2–3 cm long.

In every group of developing sea anemones, we have observed variations in timing and size of individuals. Not all planulae metamorphose to juveniles in seven days, and some delay metamorphosis for at least two weeks. In one instance, planulae remained active for as long as 135 days, and in that time their size decreased such that the last one measured, just six days before it was last seen, was about 100 μm long. Frequently a few planulae, 1% or less, remain active for 1–2 months in bowls with their developing siblings, but we do not know whether these are still capable of metamorphosing.

As well as variations in growth rates, we have observed newly metamorphosed juveniles with two and three tentacles rather than the normal four. At ages of several months to a year or more, there may be large variations in the abundance of nematosomes. Too, some individuals have large physal regions or very long tentacles compared to others, and the frequency of asexual reproduction varies greatly from individual to individual. There also may be much variability in planular size, because the planulae in our cultures seldom exceed 500 μm long, a size substantially less than those reported by Frank and Bleakney (1976) and Williams (1975).

Nematosomes

Nematosomes are equally abundant in both sexes. Those embedded in the egg masses emerge from the matrix along with the emerging planulae. They do not move throughout the water column, but tend to remain rotating near the degenerating matrix of the original egg mass. However, both the egg mass matrix and the nematosomes may remain in the dish with the developing anemones for extended periods. We have had nematosomes remain active for as long as 13 days past the date of spawning, and the gelatinous matrix from the egg mass, although shrinking in size, may remain for a month or more.

Other populations

We have kept cultures from areas other than Chesapeake Bay on feeding and water changing schedules identical to those from Chesapeake Bay. These cultures also tend to spawn synchronously with those from Chesapeake Bay. The development, metamorphosis, and growth of the offspring of those cultures do not differ from those of the Chesapeake Bay anemones.

Salinity

The anemones in 10% and 20% seawater did not do well; we terminated these two cultures at 5 weeks because 18 of the 20 in 10% seawater, and 13 of the 20 in 20% seawater, were deflated and had mesenteries everted through their mouths. There had been one asexual division in the group in 20% seawater. The anemones in the other salinities all produced fertile egg masses and planula larvae, and all planulae, except those in 125% seawater, metamorphosed to young anemones. At the end of 16 weeks (Table II), we discontinued this study. The anemones in 33% seawater had grown to be 4–6 cm long, had spawned four times, and by asexual reproduction had become a group of 29 anemones. The group in 66% seawater did not grow much, and were barely larger than at the initiation of the experiment. These had spawned four times and had become a group of 28 animals. The anemones in 100% seawater had decreased in size, the largest being about 2.5 cm long when fully extended. These anemones had become a group of 26 and had spawned only once. The anemones in 125% seawater also only spawned once, had become a group of 22, and decreased in size, the largest being about 2.0 cm long.

Discussion

Nematostella vectensis is regarded as a small sea anemone, and Williams (1983) stated that, although they may

Figure 1. Spawning female releasing part of an egg mass. Note the remaining unreleased egg mass in colenteron at the arrow. Scale bar: 1.0 cm.

Figure 2. Egg masses from numerous individuals collected from one evening's spawn. Scale bar: 1.0 cm.

Figure 3. Blastulae, early gastrulae and nematosomes *in situ* in an egg mass fertilized 14 hours earlier. Arrow points to a nematosome. Scale bar: 100 μm.

Figure 4. Three day post-fertilization planula with early apical tuft. Scale bar: 100 μm.

Figure 5. Five day post-fertilization planula with fully developed apical tuft and developing tentacle buds. Tentacle bud at arrow. Scale bar: 100 μm.

Figure 6. Two-week-old, four tentacled juvenile anemone. Arrow points to one member of the first couple of mesenteries. Note its size compared to the adjacent smaller primary mesenteries. Scale bar: 1.0 mm.

Table I

Spawning of 12 isolated female and 12 isolated male clonemates of Nematostella vectensis *from 12 February to 3 October 1990*

Females

Day of spawn	Number of spawns of anemone												Total spawns	%
	1	2	3	4	5	6	7	8	9	10	11	12		
Day before eating mussel	3	4	2	3	1	2	4	2	3	3	1	4	32	10
Day of eating mussel	1	0	0	0	1	0	0	0	0	0	1	1	4	1
Day after eating mussel	20	18	20	21	21	22	19	21	21	19	19	21	242	75
Other days	3	3	5	4	3	5	3	2	7	3	2	4	44	14
Sum	27	25	27	28	26	29	26	25	31	25	23	30	322	100

Males

Day of spawn	Number of spawns of anemone												Total spawns	%
	1	2	3	4	5	6	7	8	9	10	11	12		
Day before eating mussel	0	0	1	0	0	0	0	1	0	0	0	0	2	1
Day of eating mussel	6	2	6	6	4	5	6	3	7	5	8	3	61	23
Day after eating mussel	16	13	15	12	16	15	11	13	11	17	16	15	170	64
Other days	1	5	2	1	0	2	2	6	5	1	4	2	31	12
Sum	23	20	24	19	20	22	19	23	23	23	28	20	264	100

All anemones were fed brine shrimp nauplii every second day. Each eighth day they were fed pieces of *Mytilus californianus* ovary and the water was changed. All were mature, 6–10 cm long adults at the initiation of the test and were maintained in 33% seawater.

be up to 6 cm long, they are usually less than 2 cm. We were surprised, therefore, when our laboratory specimens grew to more than twice the maximum size reported previously. All earlier size measurements appear to have been made on recently collected animals, and not well-fed cultured ones. The small size of the sea anemones in the field, relative to the larger sizes in our cultures, must reflect the small amount of food they capture in their native habitats.

The production of gelatinous egg masses by *Nematostella* is a unique feature of this sea anemone, although the eggs of *Halcampa duodecimcirrata,* which are released individually, become surrounded by a jelly envelope after fertilization (Nyholm, 1949). The jelly attaches the eggs to the sandy bottom in which *Halcampa* lives.

We know of no other sea anemone that spawns repeatedly over extended periods, although an annual period of reproductive activity is known for many sea anemones (Jennison, 1979). *N. vectensis* may well have an annual reproductive cycle in nature; but in the laboratory it has spawned repeatedly and on a predictable schedule. We have tried feeding mussel tissue every fourth day to some female clonemates of the anemones on the eight-day cycle. The results led to spawns in an erratic and unpredictable fashion; apparently *N. vectensis* cannot spawn repeatedly at four-day intervals. We now are attempting a seven-day cycle, and early results suggest that predictable spawnings will occur at seven-day intervals.

How the reproductive cycle of *N. vectensis* operates in nature is unknown. Most populations of this anemone

Table II

Asexual reproduction, growth, and spawning during 16 weeks in various concentrations of seawater

Sea water concentration	Initial number	Final number	Largest final size	Number of spawns	Larvae metamorphosed
33%	20	29	6.0 cm	4	yes
66%	20	28	3.5 cm	4	yes
100%	20	26	2.5 cm	1	yes
125%	20	22	2.0 cm	1	no

All anemones were 2.0–3.0 cm long, six-month-old siblings at the initiation of the experiment. All were fed brine shrimp nauplii every second day, and the water was changed every one to two weeks.

live in pools in marshes at tidal elevations that do not necessarily receive fresh water with each tidal cycle, and their food consists of denizens of the pools they inhabit (Lindsay, 1975; Williams, 1976; Frank and Bleakney, 1978). The higher tides generally provide fresh seawater to the pools, and at times that water must carry large amounts of plankton. We wonder whether the pulses of extra food, in the form of the mussel ovary that we supply, may mimic pulses of extra food from the plankton that they receive in nature. Perhaps that pulse of food, along with the change of water, is the key to the release of gametes in *N. vectensis*.

The planula larvae of *N. vectensis*, from the age of about three days onward, are active swimmers, although they do spend long periods immobile on the bottoms of our culture dishes. Some swimming is spontaneous, but if the cultures are disturbed, most of the motionless planulae leave the bottom and swim actively. They swim in a clockwise spiral, as viewed from the oral end of the planula, and while doing this they rotate around their longitudinal axes in a clockwise direction. Widersten (1968) reported similar rotation in several cnidarian larvae, including several species of sea anemones, although he also observed some anemone planulae that rotated either clockwise or counterclockwise. In contrast to the generally clockwise rotation of the sea anemone larvae, he found only counterclockwise rotation in hydrozoan and scyphozoan planulae.

The reversal in the direction of gliding by the juvenile anemones was unexpected and is previously unreported. We presume that the same cilia that move the planulae in an aboral direction later reverse their beat and move the recently metamorphosed anemones in an oral direction. But the juveniles could alternatively be propelled by newly developed cilia.

In the only specific study of nematosomes, Williams (1979) found no correlation between the size of an anemone and the number of its nematosomes, and we agree. He also considered nematosomes to be functionless, and although we find that difficult to accept, their function is certainly not obvious. In his study, Williams also showed that nematosomes removed from anemones had relatively short lives; *i.e.*, only those maintained at low temperature (1.5–3.5°C) lived as long as 55 hours. In sharp contrast, we found that nematosomes would live for 13 days outside of the body of anemones at temperatures around 20°C. Williams (1979) made his observations on material in normal seawater (34‰), whereas our material was in a salinity of about 12‰. Too, we did not artificially free the nematosomes from the anemones. Our observations were on nematosomes contained in egg masses, from which they emerged along with the planulae.

As we noted earlier, *N. vectensis* is a euryhaline sea anemone; it can be found in widely varying salinities. Our own experience in culturing this anemone confirms that we are dealing with a widely tolerant euryhaline, eurythermal sea anemone, and we know of no other sea anemone of equal tolerance. Not only is *N. vectensis* tolerant, but it carries out its full repertoire of sexual and asexual reproduction, development, and growth in a wide range of salinities. When cultured in full strength seawater, or higher salinities, growth seems to be inhibited, and we have not observed successful sexual reproduction and subsequent metamorphoses in salinities greater than 34‰.

Sexual reproduction and the subsequent development in sea anemones have rarely been studied (see review by Stephenson, 1928; also Mergner, 1971; Campbell, 1974; and Fautin *et al.*, 1989). Those species that have been reported upon had all been recently collected, brought in to a nearby laboratory or field station, and subsequently spawned. Fortuitously, investigators on the scene, such as Nyholm (1943, 1949), Chia and Spaulding (1972), Siebert (1973, 1974), Riggs (1988), and Chia *et al.* (1989), have been able to examine some of the events from spawning onwards, although until now there have been no reports of rearing of successive generations of any species. Most studies do not describe development beyond the planula, although those of Spaulding (1972) on *Peachia quinquecapitata*, Chia and Spaulding (1972) on *Tealia crassicornis*, and Siebert (1973) on *Stomphia didemon* are exceptions. Of all the studies of development of sea anemones, we are aware of only two (Clark and Dewell, 1974; Larkman and Carter, 1984) that have provided a close look at fertilization and related events. Those studies, like the others we have cited on matters related to development, were largely made possible by spontaneous spawnings and not as the result of planned or controlled spawnings. Now that we can culture *Nematostella* throughout its life history and can control some of the variation through the use of clonal anemones, we can look closely and repeatedly at all events, from fertilization to spawning. Moreover, the short generation time of two to three months in laboratory-reared *Nematostella* will allow ready genetic analyses. Because *Nematostella* can be cultured away from marine facilities, research on every aspect of its life history can be carried out at inland laboratories, and we believe this sea anemone has the potential to become an important model for research in cnidarian biology.

Acknowledgments

We are grateful to Martin Posey for the material from Chesapeake Bay, and we also owe our thanks to the following for other material: Martin Sheader and Daphne Fautin for specimens from England; Sherman Bleakney for specimens from Nova Scotia; R. T. Kneib for specimens from Georgia; Edward Lyke, Daniel Wickham, and

Pamela Roe for specimens from California; Jon Geller for specimens from Oregon; Eugene Kozloff, Edward Lyke, and Claudia Mills for specimens from Washington. We thank Tzyy-ing Chen, Jennifer Russo, and Eleanor Uhlinger for their help in caring for our animals, and we are grateful for the assistance Beth Clark provided in the preparation of our manuscript. Fred Griffin and Eduardo Almeida each provided invaluable assistance with photography and we thank Wallis Clark for the use of his laboratory's photographic and optical equipment. Comments and suggestions from Wallis Clark, Fred Griffin, and Eleanor Uhlinger have been of great assistance in the development of the manuscript. This work is a result of research sponsored in part by NOAA, National Sea Grant College Program, Department of Commerce, under grant number NA89AA-D-SG138, project number 83-A-N, through the California Sea Grant College. The U.S. Government is authorized to reproduce and distribute reprints for governmental purposes.

Literature Cited

Bleakney, J. S., and K. B. Meyer. 1979. Observations on saltmarsh pools, Minas Basin, Nova Scotia 1965–1977. *Proc. N.S. Inst. Sci.* **29:** 353–371.

Calder, D. 1972. Phylum Cnidaria. Pp. 97–107 in *A Check List of the Biota of Lower Chesapeake Bay*. Special Scientific Report No. 65, Virginia Institute of Marine Science.

Campbell, R. D. 1974. Cnidaria. Pp. 133–199 in *Reproduction of Marine Invertebrates, Vol. 1, Acoelomate and Pseudocoelomate Metazoans*, A. C. Giese and J. S. Pearse, eds. Academic Press, New York.

Cary, L. R. 1911. A study of pedal laceration in actinians. *Biol. Bull* **20:** 81–108.

Chia, F.-S., and J. G. Spaulding. 1972. Development and juvenile growth of the sea anemone *Tealia crassicornis*. *Biol. Bull.* **142:** 206–218.

Chia, F.-S., J. Lützen, and I. Svane. 1989. Sexual reproduction and larval morphology of the primitive anthozoan *Gonactinia prolifera* M. Sars. *J. Exp. Mar. Biol. Ecol.* **127:** 13–24.

Clark, W. H., Jr., and W. C. Dewel. 1974. The structure of the gonads, gametogenesis, and sperm-egg interactions in the Anthozoa. *Am. Zool.* **14:** 495–510.

Clayton, W. S., Jr., and H. R. Lasker. 1984. Host feeding regime and zooxanthellal photosynthesis in the anemone, *Aiptasia pallida* (Verrill). *Biol. Bull.* **167:** 590–600.

Crowell, S. 1946. A new sea anemone from Woods Hole, Massachusetts. *J. Wash. Acad. Sci.* **36:** 57–60.

Fautin, D. G., J. G. Spaulding, and F.-S. Chia. 1989. Cnidaria. Pp. 43–62 in *Reproductive Biology of Invertebrates, Vol. IV, Part A*, K. A. Adiyodi and R. G. Adiyodi, eds. John Wiley & Sons, Chichester.

Frank, P., and J. S. Bleakney. 1976. Histology and sexual reproduction of the anemone *Nematostella vectensis* Stephenson 1935. *J. Nat. Hist* **10:** 441–449.

Frank, P., and J. S. Bleakney. 1978. Asexual reproduction, diet and anomolies of the anemone *Nematostella vectensis* in Nova Scotia. *Can. Field-Nat.* **92:** 259–263.

Hand, C. 1957. Another sea anemone from California and the types of certain California species. *J. Wash. Acad. Sci.* **47:** 411–414.

Heard, R. W. 1982. Guide to common tidal marsh invertebrates of the northern Gulf of Mexico. Mississippi Alabama Sea Grant Consortium. Publ. 79-004, 82 pp.

Jennison, B. L. 1979. Gametogenesis and reproduction cycles in the sea anemone *Anthopleura elegantissima* (Brandt, 1835). *Can. J. Zool.* **57:** 403–411.

Jensen, L. D. 1974. Environmental responses to thermal discharges from the Indian River Station, Indian River, Delaware. Electric Power Research Institute. Report No. 12. Publ. No. 74-049-00-3.

Kneib, R. T. 1985. Predation and disturbance by grass shrimp, *Palaemonetes pugio* Holthuis, in soft-substratum benthic invertebrate assemblages. *J. Exp. Mar. Biol. Ecol.* **93:** 91–102.

Larkman, A. U., and M. A. Carter. 1984. The apparent absence of a cortical reaction after fertilization in a sea anemone. *Tissue & Cell* **16:** 125–130.

Lindsay, J. A. 1975. A salt marsh anemone. *Mar. Aquarist* **6**(8): 43–48.

Mergner, H. 1971. Cnidaria. Pp. 1–84 in *Experimental Embryology of Marine and Freshwater Invertebrates*, G. Reverberi, ed. North Holland Press, Amsterdam.

Minasian, L. L., Jr., and R. N. Mariscal 1979. Characteristics and regulation of fission activity in clonal cultures of the cosmopolitan sea anemone, *Haliplanella luciae* (Verrill). *Biol. Bull.* **157:** 478–493.

Muller-Parker, G. 1984. Photosynthetic-irradiance responses and photosynthetic periodicity in the sea anemone *Aiptasia pulchella* and its zooxanthellae. *Mar. Biol.* **82:** 225–232.

Nyholm, K. G. 1943. Zur Entwicklung und Entwicklungsbiologie der Ceriantharien und Aktinien. *Zool. Bidr. Uppsala* **22:** 87–248.

Nyholm, K. G. 1949. On the development and dispersal of Athenaria actinia with special reference to *Halcampa duodecimcirrata* M. Sars. *Zool. Bidr. Uppsala* **27:** 465–506.

Riggs, L. L. 1988. Feeding behavior in *Aiptasia tagetes* (Duchassaing and Michelotti) planulae: a plausible mechanism for zooxanthellae infection of aposymbiotic planktotrophic planulae. *Caribb. J. Sci.* **24:** 201–206.

Rudy, P., Jr., and L. H. Rudy. 1983. *Oregon Estuarine Invertebrates: An Illustrated Guide to the Common and Important Invertebrate Animals* Fish and Wildlife Service. FWS/OBS-83/16.

Siebert, A. E., Jr. 1973. A description of the sea anemone *Stomphia didemon* sp. nov. and its development. *Pac. Sci.* **27:** 363–376.

Siebert, A. E., Jr. 1974. A description of the embryology, larval development, and feeding of the sea anemones *Anthopleura elegantissima* and *A. xanthogrammica*. *Can. J. Zool.* **52:** 1383–1388.

Spaulding, J. G. 1972. The life cycle of *Peachia quinquecapitata*, an anemone parasitic on medusae during its larval development. *Biol. Bull.* **143:** 440–453.

Stephenson, T. A. 1928. *The British Sea Anemones, Vol. I.* The Ray Society, London.

Stephenson, T. A. 1929. On methods of reproduction as specific characters. *J. Mar. Biol. Assoc. U.K.* **16:** 131–172.

Stephenson, T. A. 1935. *The British Sea Anemones, Vol. II.* The Ray Society, London.

Widersten, B. 1968. On the morphology and development in some cnidarian larvae. *Zool. Bidr. Uppsala* **37:** 139–182.

Williams, R. B. 1975. A redescription of the brackish-water sea anemone *Nematostella vectensis* Stephenson, with an appraisal of congeneric species. *J. Nat. Hist.* **9:** 51–64.

Williams, R. B. 1976. Conservation of the sea anemone *Nematostella vectensis* in Norfolk, England and its world distribution. *Trans. Norfolk Norwich Nat. Soc.* **23:** 257–266.

Williams, R. B. 1979. Studies on the nematosomes of *Nematostella vectensis* Stephenson (Coelenterata, Actiniaria). *J. Nat. Hist.* **13:** 69–80.

Williams, R. B. 1983. *Starlet sea anemone: Nematostella vectensis.* Pp. 43–46 in *The IUCN Invertebrate Red Data Book.* IUCN, Gland, Switzerland.

Reference: *Biol. Bull.* **182:** 177–187. (April, 1992)

Morphology and Development of a Unique Type of Pelagic Larva in the Starfish *Pteraster tesselatus* (Echinodermata: Asteroidea)

LARRY R. McEDWARD

Department of Zoology, University of Florida, Gainesville, Florida 32611

Abstract. Several unusual features characterize the morphology of the pelagic larva of the starfish *Pteraster tesselatus* and its metamorphosis into the juvenile stage: (1) morphogenesis of the supradorsal membrane during metamorphosis by fusion of 15 lobes on the aboral region of the body; (2) absence of brachiolar arms and attachment disk; (3) heterochronic acceleration of development in the water vascular system, and use of podia for attachment to the substratum at settlement; (4) radial (rather than bilateral) symmetry of the larva; and (5) congruent larval and adult axes of symmetry, and a transverse orientation of the adult rudiment within the larva. Collectively, these features demonstrate that *P. tesselatus* has a highly derived mode of development and a larva that is unique among the asteroid echinoderms. In contrast to the current interpretation of this larva as a modified pelagic brachiolaria, I suggest that the unusual larva of *Pteraster* represents an example of an apparently rare evolutionary transition in animal development: the re-evolution of pelagic larval development from benthic brooding.

Introduction

Major evolutionary transitions in the patterns of animal development are rare. Some transitions, such as the change from feeding larval development to nonfeeding larval development, involve such drastic morphological reorganization that the transition is irreversible (Strathmann, 1978). The evolution of pelagic larval development from benthic brooding has not been documented in the echinoderms. This suggests that, once lost from a clade, a pelagic dispersive stage might not be re-evolved. This is an important issue because it bears on the evolutionary flexibility of the marine fauna and the predicted consequences of major environmental change: faunal turnover due to extinction and replacement or adaptive response through modification of development and life history. In this paper I describe the morphology and development of a unique type of pelagic larva from the starfish *Pteraster tesselatus*. The unusual features of this larva are consistent with the hypothesis that it has evolved from benthic brooding, rather than by modification of a pelagic larva (Strathmann, 1974). The significance of this finding is that *Pteraster* could provide a system for elucidating the functional and developmental changes that underlie the transition from benthic to pelagic development.

Starfish in the family Pterasteridae possess an unusual structure known as the supradorsal membrane. In most pterasterids, the supradorsal membrane is a thick (1–2 mm) layer that extends aborally from the lateral margins of the ambulacra to form a secondary covering over the body wall of the arms and disk (Fig. 1). This structure is supported above the body wall by skeletal elements (paxillae) and encloses a space, the nidamental chamber. In *Pteraster tesselatus*, the supradorsal membrane lacks skeletal ossicles, but contains muscles and mucus cells, is perforated by numerous minute spiracles, and possesses a single large osculum (Fig. 1) located in the center of the aboral surface (Ives, 1888; Fisher, 1911, pp. 355–363; Rodenhouse and Guberlet, 1946; Verrill, 1914, pp. 268–269).

The supradorsal membrane has three known functions: respiratory ventilation, defense, and reproduction. Alternating muscular contractions of the supradorsal membrane and the aboral body wall produce rhythmic expansions and contractions of the nidamental chamber. Seawater enters the chamber via ambulacral pores, flows over the respiratory papulae, and exits via the osculum (Johansen and Petersen, 1971; Nance and Braithwaite, 1981).

Received 6 November 1991; accepted 22 January 1992.

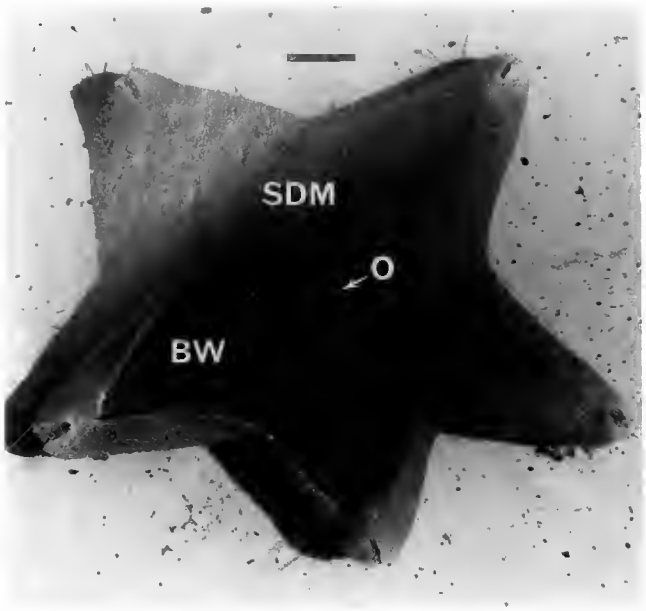

Figure 1. Adult specimen of *Pteraster tesselatus* Ives 1888. Aboral view. Scale bar = 2 cm. Supradorsal membrane (SDM) removed from two arms and part of the disk, exposing the aboral body wall (BW). Osculum (O) located center of aboral surface of supradorsal membrane.

In addition, the supradorsal membrane contains numerous mucous cells associated with the spiracles (Rodenhouse and Guberlet, 1946). Production of tremendous quantities of mucus occurs in association with expulsion of water from the nidamental chamber through the spiracles rather than the osculum. The mucus effectively deters predation by the starfish *Solaster dawsoni* and *Pycnopodia helianthoides*, possibly because of the presence of saponin-like compounds (Nance and Braithwaite, 1979). Finally, the nidamental chamber is used for brood protection (Koren and Danielssen, 1856; McClary and Mladenov, 1988). In many species of pterasterids, young are retained within the nidamental chamber of the mother throughout development to the juvenile stage (*e.g., Pteraster obscurus*, Fisher, 1911, p. 363–368; Verrill, 1914, pp. 274–277; *Pteraster stellifer*, Fisher, 1940, pp. 199–200; *Diplopteraster verrucosus*, Fisher, 1940, pp. 201–203; *Hymenaster praecoquis*, Sladen, 1889, pp. 524–525.

Benthic, brooding development has been considered the rule in pterasterids. Fisher (1940, p. 73) stated that probably all species in the genus *Pteraster* were brooders. However, Chia (1966) reported that *P. tesselatus* spawned eggs, and he provided a brief description of their development as pelagic larvae. In addition, *Pteraster militaris*, which broods embryos (Kaufmann, 1968; McClary and Mladenov, 1989, 1990), also spawns some eggs that presumably develop as pelagic larvae (McClary and Mladenov, 1988). But, beyond the observation that pelagic development occurs within the genus, very little is known about the morphology and development of *Pteraster* larvae.

Here I report the results of a re-examination of the development of *Pteraster tesselatus* in which I either discovered or reinterpreted a number of unusual features: (1) morphogenesis of the supradorsal membrane during metamorphosis, (2) absence of brachiolar arms and attachment disk, (3) heterochronic acceleration of development in the water vascular system, (4) radial symmetry of the larva, and (5) congruent larval and adult axes of symmetry. Because of these features, the larva of *Pteraster tesselatus* is unlike that reported in any other asteroid. This description of the morphology of the pelagic larva and its development into the benthic juvenile will provide the basis for investigating the evolution of this unusual pattern of larval development (McEdward, in prep.).

Materials and Methods

Pteraster tesselatus Ives 1888 (Order Velatida; see Blake, 1987) is a subtidal, often deep-water starfish that occurs along the Pacific coast of North America from central California to the Bering Sea (Lambert, 1981, p. 88). SCUBA was used in the collection of adult starfish from depths of 5–20 m at several sites near the Bamfield Marine Station (48°49′N, 125°08′W) in Barkley Sound, Vancouver Island, British Columbia, Canada, and from depths of 15–30 m near the Friday Harbor Laboratories (48°32′N, 123°0′W) in the San Juan archipelago, Washington. *Pteraster tesselatus* is reproductive during July and August (Chia, 1966; McEdward, pers. obs.).

Females were induced to spawn by intracoelomic injection of 2–5 ml (10^{-4} *M*) of the hormone 1-methyl adenine. Eggs were released within 1–3 h after injection and developed without artificial insemination.

Embryos, larvae, and juveniles were cultured in plastic beakers equipped with mesh bottoms (500 μm mesh). The beakers were suspended from a rack in an aquarium with flowing seawater (see descriptions in Hoeg, 1984; Strathmann, 1987, p. 15). The mesh bottom allowed continuous exchange of seawater between the aquarium and the culture containers. The seawater was not filtered. After the larvae hatched, ≈250–300 healthy larvae were pipetted from each culture into clean mesh-bottom beakers for subsequent rearing.

Light microscope photographs and most of the original observations were made on living embryos, larvae, and juveniles. In some cases, larvae and juveniles were fixed and cleared to render them transparent for observation of internal features, such as the water vascular system and the skeleton. Specimens were fixed in 10% formalin in seawater (10 min), then dehydrated stepwise in ethanol (30%, 50%, 70% twice, 90%, 100%, 2 min each). Contrast was enhanced by staining the specimens with borax car-

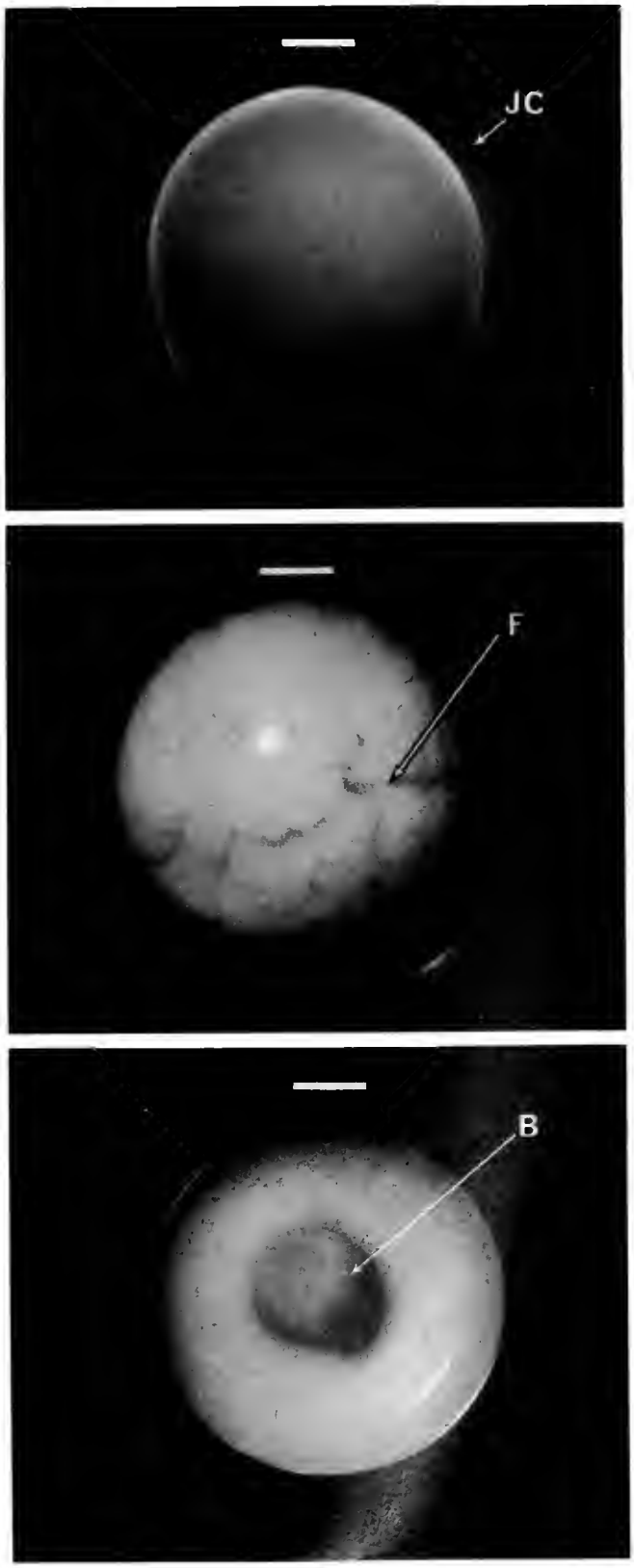

Figure 2. Light micrographs of egg and embryos of *Pteraster tesselatus*. Scale bars = 0.2 mm. (Top) Newly spawned egg. Jelly coat (JC) surrounds the egg. The vitelline layer lies between the jelly and the egg cell membrane but is not visible until after loss of the jelly coat. (Middle) Wrinkled blastula. Age ≈ 36 h. Blastular wall with deep fold (F). Note that this is a preserved specimen and the jelly coat and vitelline layer have swollen. (Bottom) Gastrula. Vegetal view. Age = 2 days. Large blastopore (B) lies at the center of the vegetal pole.

mine (2 min) between the two changes of 70% ethanol. Immediately following dehydration, the specimens were transferred to one of three clearing agents: methyl salicylate (= oil of wintergreen), clove oil, or a mixture of benzyl alcohol and benzyl benzoate (range 1:3–3:1). Clearing was complete within 30 min to 1 h. Specimens were observed and stored in the clearing agent.

Specimens were fixed for scanning electron microscopy in cold 2% osmium tetroxide (1 h) in 0.45 μm filtered seawater, rinsed twice with distilled water, dehydrated through a graded series (30%, 50%, 70%, 15 min each) of ethanol, and stored in 70% ethanol. In preparation for drying, specimens were dehydrated stepwise to absolute ethanol (90%, 100%, 15 min each), then infiltrated with hexamethydisilazane (HMDS, Sigma Chemical Co.) for several hours. Specimens were air-dried at room temperature (Nation, 1983) in a dust-free chamber, sputter coated with gold-palladium, and stored under desiccation.

Results

Pelagic larval development

Eggs were spawned from interradial gonopores into the nidamental chamber and carried out through the osculum of the supradorsal membrane with the exhalant flow of water. Usually between 1–10 eggs were released with each ventilation. The eggs were large, ranging in size from 1.0 to 1.4 mm in diameter (Fig. 2A). They were opaque, yolky, and positively buoyant. Egg color varied among spawns from light yellow to dark red, but was most commonly a rich orange color. There were not obvious correlations among egg color, egg size, or the success of development. The eggs were surrounded by a thick (>100 μm) jelly coat (Fig. 2A). The jelly coat was lost prior to hatching, typically within the first 48 h of development (see Table I for chronology of development).

The cleavage pattern was variable and irregular, not the typical radial pattern characteristic of asteroids. Cleavage led to the formation of a blastula that initially had a smooth wall. With continued division of the blastomeres, the blastular wall was deeply folded to produce a wrinkled blastula (Fig. 2B). Gastrulation occurred within the vitelline envelope and involved the formation of a broad, shallow archenteron with a large blastopore at the vegetal pole (Fig. 2C). Archenteron formation was correlated with the loss of folding of the blastular wall in the vegetal hemisphere of the embryo. Subsequently, the

Table I

Chronology of development in the starfish Pteraster tesselatus *at 11–13°C*

Age (days)	Developmental stage or event
0	Spawning; initiation of development
2	Wrinkled blastula; gastrulation
3	Hatching; ovoid, ciliated, swimming larva
5	Circumferential groove divides larva into two body regions
7	Podia visible within circumferential groove
8	Five marginal bulges form in posterior body region
10	Settlement; ten marginal lobes present, anterior yolky region flattened
11	Five aboral lobes begin to form
13	Aboral lobes well developed
17	Fusion of 15 lobes begins
19	Fusion of lobes complete
20	Some individuals still swimming
28	Supradorsal membrane smooth, no indication of lobes
2 (mo.)	Mouth functional
2.5 (mo.)	Distinct arms extend beyond margin of disk

blastopore was greatly reduced in size, and this occurred in association with a progressive loss of folding of the blastular wall, from the equatorial region of the vegetal hemisphere towards the animal pole. The loss of folding was completed by the time hatching from the vitelline envelope occurred.

Prior to hatching, the eggs and embryos floated at the surface. After hatching, larvae swam actively through the water column. Anterior was defined as the end that was directed forward during swimming. Hatching yielded a simple, ciliated, ovoid larva (1.1–1.2 mm length). Distinct ciliated bands for food capture were absent, and the cilia remained uniformly distributed over the surface of the larva throughout development (Fig. 3A). A larval mouth and functional gut were absent, and the blastopore closed soon after hatching; development was entirely lecithotrophic.

Within 1–2 days of hatching, a circumferential groove (Chia, 1966) formed around the larva, ≈¼–⅓ of the way back from the anterior end (Fig. 3A). The groove divided the larva into two distinct body regions: an anterior region that contained mostly nutritional stores and was resorbed during development, and a posterior region that developed into the juvenile starfish. In striking contrast to most other asteroid larvae, specialized settlement structures (brachiolar arms and attachment disk; see Fig. 7) did not form in the anterior region at any time during development (Figs. 3, 5A).

Shortly after the formation of the circumferential groove, the posterior region of the larva shortened along the anterior-posterior axis. At the same time, five broad marginal bulges formed around the circumference of the larva, immediately posterior to the groove (Fig. 3B). The larva continued to shorten over the next 1–2 days until it was ≈0.9–1.0 mm in length. The posterior region assumed a domed shape that was pentagonal in outline because of the broad marginal bulges. The region of the larva anterior to the groove assumed a flattened, platelike shape (Figs. 3B, 5A).

At about the same time that the marginal bulges first became visible, podia emerged from the groove (Fig. 3B). The podia were distributed around the circumference of the larva in five clusters, each located close to the center of one of the marginal bulges. Within one week of hatching, there was an unpaired terminal podium and two pair of functional podia in each cluster. The first pair of podia

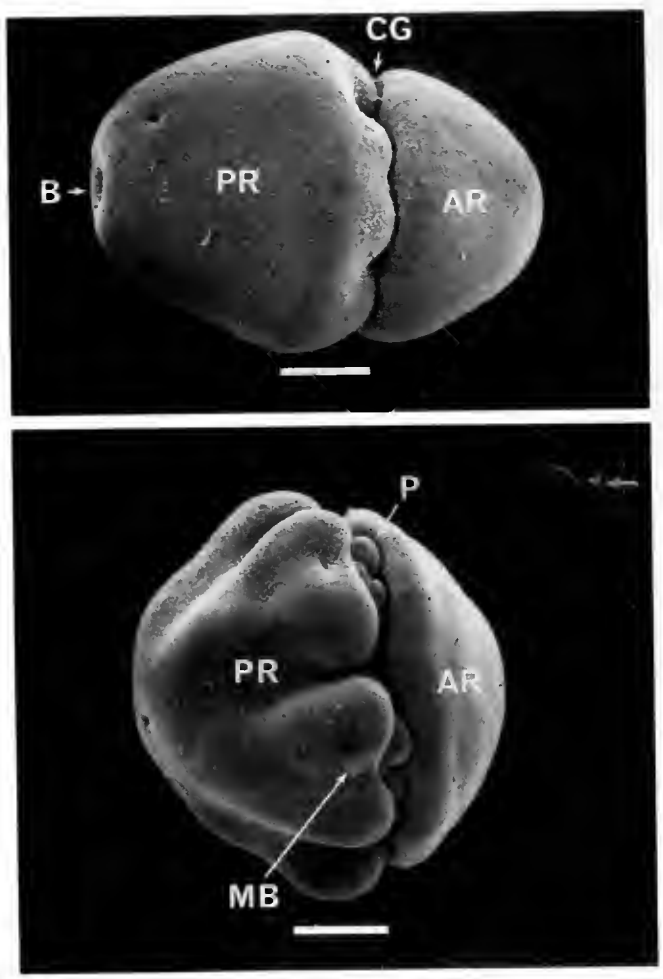

Figure 3. Scanning electron micrographs of pelagic larvae of *Pteraster tesselatus*. Scale bars = 0.2 mm. (Top) Lateral view. Age = 6 days. Circumferential groove (CG) divides the larval body into anterior (AR) and posterior (PR) regions. Note the remnant of the closing blastopore (B) at the posterior end. (Bottom) Lateral view. Age = 8 days. The terminal unpaired podium and the first pair of podia (P) of two ambulacra are visible within the circumferential groove. The bilobed marginal bulges (MB) can be seen just posterior to the groove.

was considerably longer than the second pair. The clusters became less distinct as these podia developed and additional podia formed. Eventually the podia came to be distributed in a ring around the circumference of the larva, within the groove (Fig. 5C).

Settlement and metamorphosis

Because *Pteraster* lacks purely larval structures characteristic of asteroids (*e.g.,* ciliated bands, gut, or brachiolar arms) and does not undergo a well-defined period of metamorphosis, larval and juveniles stages cannot be rigorously defined using morphological or developmental criteria. Therefore, I have used ecological criteria: "larva" refers to the free-swimming, pelagic, dispersive stage of the life cycle and "juvenile" refers to the animal following initial settlement and assumption of the adult orientation on the substratum. In fact, the fully formed juvenile starfish was not achieved until weeks to months after settlement.

Initially larvae swam with the anterior end forward. Later, as the rudiment of the juvenile starfish developed in the posterior end, the orientation of the larval body in the water column changed and the yolky anterior end was directed upward. During settlement, the larva attached to the substratum using podia. However, attachment could only occur when the larva turned on edge because the podia were not long enough to reach around the posterior region to contact the substratum. Upon settlement, the larva placed the flattened, anterior region against the substratum, thereby assuming the definitive orientation of the adult. Settled juveniles were not fixed to the substratum and were capable of moving freely about using the podia. During the first 10 days after settlement, juveniles retained the ability to detach from the bottom and swim. Well-developed juveniles have been obtained from the plankton (F. S. Chia, pers. comm.).

Larvae that settled 2–3 days later than the majority continued to develop at the same rate as the rest, even though they remained planktonic. Likewise, juveniles that resumed swimming after initial settlement continued to develop at the same rate as those remaining on the bottom. Therefore, settlement was not coupled to a rapid, drastic metamorphosis into the juvenile form. In this respect, *Pteraster tesselatus* is similar to other asteroids with pelagic lecithotrophic larvae (*e.g., Solaster endeca,* Gemmill, 1912; *Crossaster papposus,* Gemmill, 1920) that undergo an extensive but prolonged and gradual transformation from larva to juvenile. But in contrast to most asteroid larvae, settlement of *Pteraster* did not involve fixation to the substratum nor a 90° bending (*i.e.,* flexion, *sensu* Gemmill, 1912, p. 19) of the rudiment relative to the larval body. In all other asteroid larvae, the disk of the juvenile starfish lies in a sagittal plane in the posterior part of the larval body, with the oral surface of the juvenile on the left side of the larva (Fig. 4). Settlement involves a bending of the larval body to bring the oral surface of the juvenile disk against the substratum. In *Pteraster,* the presumptive oral surface of the juvenile corresponds to the yolky anterior region of the larva, which corresponds to the animal pole of the embryo (site of polar body formation). The aboral surface of the juvenile disk corresponds to the posterior end of the larva and the vegetal pole (blastopore) of the embryo (Fig. 4). Since the juvenile disk lies in a transverse plane in the larval body, it does not require flexion to attain the definitive orientation with respect to the substratum following settlement.

Morphogenesis of the supradorsal membrane

Near the time of settlement, each of the five marginal bulges developed a central indentation and became strongly bilobed (Fig. 3B). Eventually they divided to yield ten distinct marginal lobes around the juvenile (Fig. 5A, B). Initially, these lobes were simple projections from the larval surface. Later, they assumed a convoluted shape and increased in size, nearly covering the lateral surface of the aboral region of the juvenile disk (Fig. 5B). Simul-

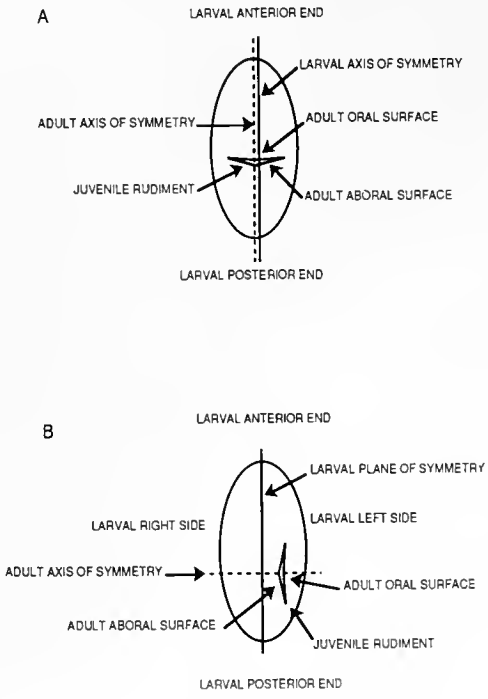

Figure 4. Diagrammatic representation of the location and orientation of surfaces, planes of section, and axes of symmetry in the larval body and rudiment of the juvenile disk of asteroids. Solid line represents the anterior-posterior axis of the larva and the dashed line represents the oral-aboral axis of the juvenile and adult. (A) Longitudinal view of the larva of *Pteraster tesselatus.* (B) Ventral view of a generalized larva representative of all other asteroids.

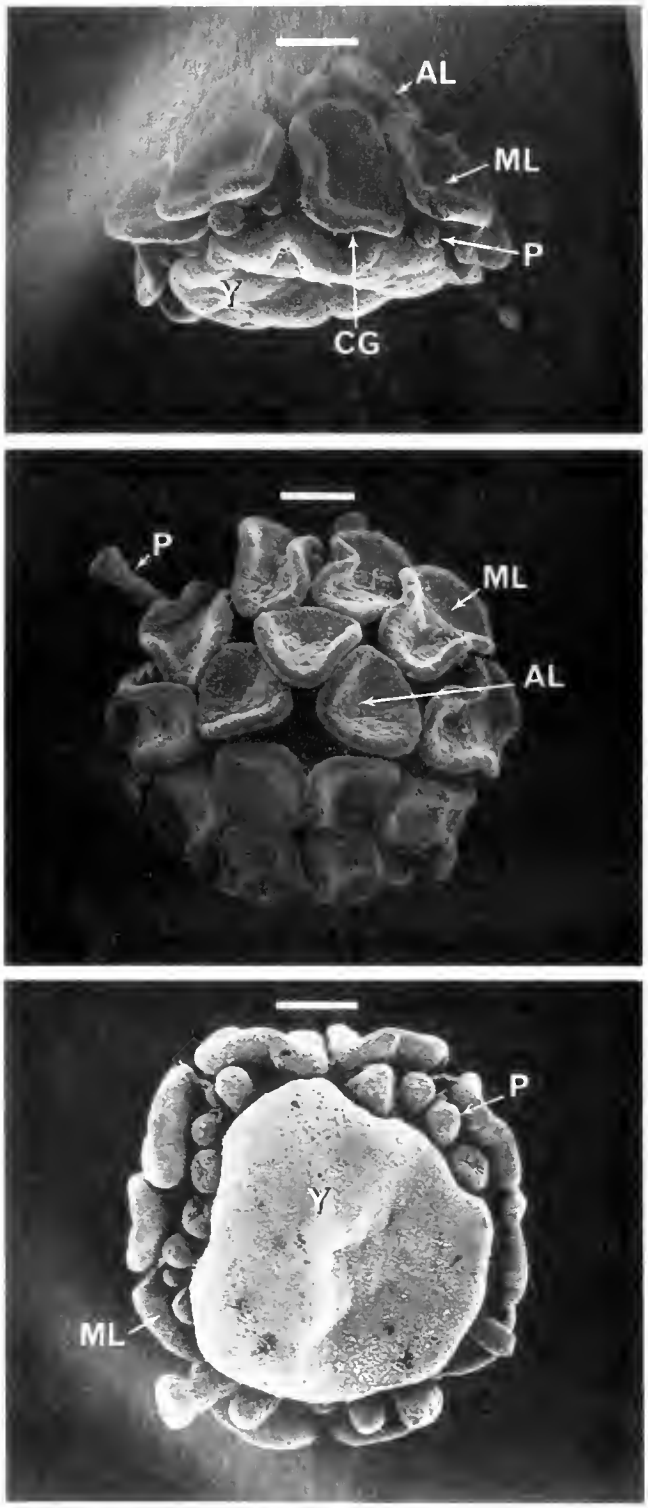

taneously with the splitting of the five marginal bulges to yield ten marginal lobes, an additional five lobes formed at the aboral pole of the juvenile (Fig. 5B). At this stage, the juvenile consisted of an oral yolk plate directed towards the substratum, a ring of podia located on the oral surface of the disk (Fig. 5C), and a developing disk with 15 convoluted lobes on the aboral surface (10 marginal and 5 aboral) (Fig. 5A).

The aboral lobes developed differently in animals from Vancouver Island compared to those from the San Juan archipelago. In animals from the San Juan Islands, the aboral lobes arose from the aboral regions of elongate marginal bulges. The marginal bulges had a triangular shape and gave rise to the three lobes (2 marginal + 1 aboral) from the vertices of the triangle. In contrast, animals from Vancouver Island produced aboral lobes independently of the marginal lobes. A central stalk developed in the center of the aboral pole of the larva and produced five rays. The tips of the rays became bulbous and developed into aboral lobes.

Subsequent development of the lobes led to the formation of the supradorsal membrane. The ten marginal lobes became organized into five sets. The lobes in a set were not derived from the same marginal bulge but instead developed from neighboring bulges. Over a period of two days, the lobes in each set enlarged and then fused along their lateral edges. The aboral lobes fused along their lateral edges and with the top (aboral) edge of the marginal lobes. Later, fusion occurred among all of the lobes to produce a complete secondary covering over the aboral surface of the juvenile starfish (Fig. 6A). At the margin of the disk, the oral edges of the marginal lobes extended beyond the disk to form a skirt around the body. Fusion along the lateral edges of the marginal lobes from adjacent sets (*i.e.*, between lobes derived from the same original marginal bulge) was restricted to the aboral regions, leaving a cleft extending between them from the oral edge of the marginal skirt (Fig. 6A). This cleft was located above the ambulacral cluster of podia and marked the site where the juvenile arms would form later in development. The osculum was formed by the lack of fusion along the central edges of the five aboral lobes, which left a central opening in the supradorsal membrane (Fig. 6B). Within ten days of the start of lobe fusion, the supradorsal membrane was completely smooth, without any visible indication that it had formed from 15 separate elements. Ventilation of the nidamental chamber by muscular pumping of the supra-

Figure 5. Scanning electron micrographs of newly settled juveniles of *Pteraster tesselatus*. Scale bars = 0.2 mm. (Top) Lateral view. Age = 16 days. Convoluted marginal lobes (ML) and aboral lobes (AL) cover the aboral surface of the juvenile. Flattened yolky plate (Y) is located below the circumferential groove (CG) and the podia (P). (Middle) Aboral view. Age = 16 days. Ten marginal (ML) and five aboral lobes (AL) cover the aboral surface. Podia (P) can be seen between some of the marginal lobes and extending beyond the edge of the disk. (Bottom) Oral view. Age = 12 days. The ten marginal lobes (ML) can be seen around the edge of the disk of the juvenile. Podia (P) are arranged in a ring around the yolk plate (Y).

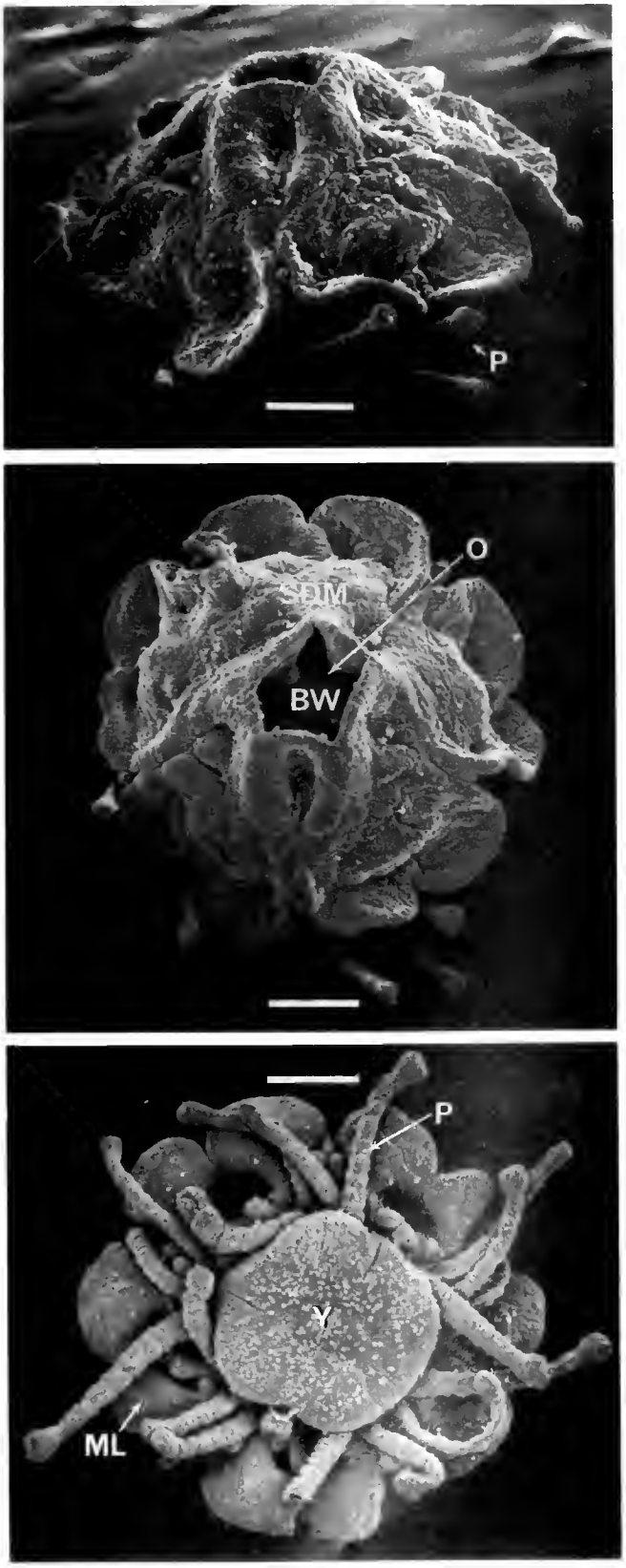

Figure 6. Scanning electron micrographs of juveniles of *Pteraster tesselatus*. Scale bars = 0.2 mm. (Top) Lateral view. Age = 27 days. Aboral surface covered by the supradorsal membrane. Podia (P) extend from under the oral side of the margin of the supradorsal membrane. (Middle) Aboral view. Age = 27 days. Aboral surface covered by a complete supradorsal membrane (SDM) formed from the fusion of the 15 lobes. The aboral body wall (BW) can be seen as the floor of the nidamental chamber through the large central osculum (O). (Bottom) Oral view. Age = 28 days. Remnant of the yolk plate (Y) lies in the center of the disk. The mouth has not formed yet. The free edges of the marginal lobes (ML) define the outer limit of the disk. Numerous podia (P) lie in a circle around the yolk plate. Note that the juvenile arms have not formed yet.

dorsal membrane (as occurs in adults) was not observed in the juveniles, even six months after settlement (diameter ≈ 2.0–2.1 mm). Ciliary activity was detected on the external surface of the juvenile, including the supradorsal membrane, but internal currents that might ventilate the nidamental chamber could not be demonstrated with dye streams. Mucus production was not obvious in juveniles up to ≈9 months after settlement (diameter ≈ 2.1–2.3 mm).

Chronology of larval development

Larvae and juveniles were raised at ambient seawater temperatures that ranged between 11–13°C. The schedule of events during development of the larval and early juvenile stages is listed in Table I. Development was remarkably synchronous throughout all of the cultures and among the larvae from different parents. However, the age at settlement varied greatly. The majority (>80–95%) of the larvae settled initially between days 10–12, but some continued to swim (or resumed swimming) until the third week. As indicated above, the schedule of development was not influenced by the age at which settlement occurred because the development of juvenile structures proceeded normally in swimming larvae. Morphogenesis of the supradorsal membrane was largely completed within 7–10 days following settlement. At the age of 1 month, the juveniles measured ≈1.5–1.8 mm in diameter, and the oral surface was still covered by a remnant of the yolk from the anterior region of the larva (Fig. 6C). The juvenile mouth had not yet formed and would not appear until the end of the second month. There were no indications of the juvenile arms. This resulted in a circular arrangement of the podia (3–4 pair per ambulacral cluster) around the oral surface of the disk. A radial arrangement of podia is evident in most starfish larvae at the time of settlement when the first two pair of podia are developing on the juvenile arms (Fig. 7). Distinct arms were not present in most *Pteraster* juveniles until the third month.

Discussion

Pattern of development in Pteraster tesselatus

The present study confirms the observation by Chia (1966) that *Pteraster tesselatus* has free-swimming larvae

and presumably pelagic development. Eggs were forcefully expelled from the nidamental chamber through the osculum by the ventilatory flow. Eggs and embryos were positively buoyant, as were larvae until close to the time of settlement (8–10 days). Larvae were uniformly ciliated and swam actively near the surface of the water, in the laboratory. Later, larvae swam near the bottom and attached to solid substrata, resulting in settlement from plankton to benthos. *Pteraster* larvae and juveniles have been obtained from the plankton in the San Juan archipelago (F. S. Chia, pers. comm.; R. Emlet, pers. comm; R. Strathmann, pers. comm.).

My observations also confirm the lack of brooding in this species. Chia (1966) did not find any brooded young in the 12 animals that he dissected. I have dissected (*i.e.*, opened or removed the supradorsal membrane) of >50 starfish without finding any evidence of brooding. Likewise, brooding has not been reported for this species by any of the authors investigating other (nonreproductive) aspects of *Pteraster* biology (Fisher, 1911, pp. 355–363; Verrill, 1914, pp. 268–269; Rodenhouse and Guberlet, 1946; Mauzey *et al.*, 1968; Johansen and Petersen, 1971; Nance and Braithwaite, 1979, 1981).

Comparisons with previous descriptions of pterasterid development

The only previous descriptions of morphological development in pterasterids are a preliminary study of development in *Pteraster tesselatus* by Chia (1966) and a brief report on brooding in *P. militaris* (Kaufman, 1968). My observations on *P. tesselatus* confirm many of Chia's descriptions: egg size, egg color, jelly coat, wrinkled blastula, large blastopore that later closes, ovoid early larva, circumferential groove, anterior (= animal) and posterior (= vegetal) body regions, resorption of the anterior region, rudiment development in the posterior region, and the chronology of early development (days 1–6).

However, there are also a number of substantial differences. Chia reported that the arms of the juvenile starfish formed early in development (p. 508): "As soon as the two parts [of the larval body] were clearly distinguishable, five primordial arms of the young seastar appeared simultaneously in the vegetal part of the larval body and the first pair of tube feet appeared on each arm (fig. 5)". According to his chronological description, the arms were formed by day 10 and the podia by day 13. I did not observe arms even after one month (Fig. 6C). Probably the initial five marginal bulges were misinterpreted as the primordial juvenile arms. My observations show that the marginal bulges are well developed by day 9, they are arranged radially around the rudiment of the juvenile disk, and they have clusters of podia associated with them (Fig. 3B).

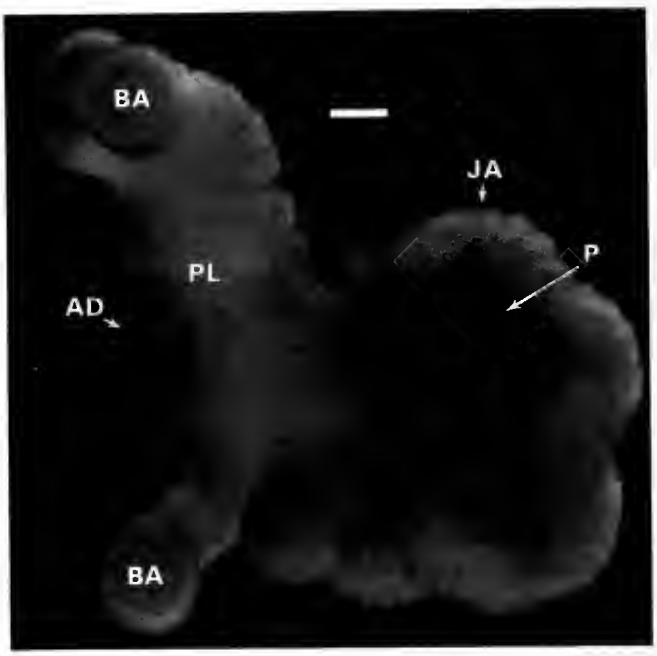

Figure 7. Light micrograph of a late-stage brachiolaria larva of *Henricia sp. (leviuscula?)*. Scale bar = 0.2 mm. Lateral view from the left side of the larva (= oral side of juvenile). Age = 28 days. Brachiolar arms (BA) and attachment disk (AD) located at anterior end on the preoral lobe (PL). Each juvenile arm (JA) has two pairs of developing podia (P) and a terminal unpaired podium on the oral surface. The plane of larval bilateral symmetry is parallel to the plane of the photograph.

I observed that most of the larvae settled between days 10–12. Chia reported that settlement occurred on the 25th day. I attribute this difference to the conditions under which the larvae were raised. A microbial and diatomaceous film developed on the mesh bottoms of my culture containers because they were suspended in unfiltered seawater and were not cleaned except when the larvae hatched (day 3). Larvae settled readily on the filmed mesh, starting on day 10. Both texture and film seem important components of attractive surfaces for larval settlement in *Pteraster*. Larvae never settled on the smooth, but filmed, sides of the culture containers. Furthermore, larvae from the same spawn that were held in closed culture containers, which were cleaned periodically, did not settle until at least one week later than larvae in mesh-bottom containers. I have observed this difference in settlement with the lecithotrophic larvae of other asteroid species that I have cultured in the laboratory: *Solaster stimpsoni, S. dawsoni, S. endeca, Crossaster papposus, Henricia sp. (leviuscula?)*. Chia cultured larvae of *Pteraster tesselatus* in a small glass aquarium (pers. comm.) that probably lacked an attractive surface (film or texture) for settlement.

Differences in the reported time of appearance of the podia (2nd pair: day 25, Chia; day 9 present study) or the number of podia present at a given stage can be explained

by the difficulty of observing the podia; they develop deep within the circumferential groove and are nearly hidden, unless they are extended for exploration of the substratum (Figs. 3B, 5A).

Other differences are less readily explained by culture conditions or interpretation of structures. Chia reported that the yolk mass was absorbed by day 25 and that the mouth of the juvenile was open on day 30. A substantial portion of the yolk plate was present on larvae in my cultures on day 28, and the mouth did not open until a month later. More puzzling is that Chia's description did not mention the marginal or aboral lobes, nor the formation of the supradorsal membrane. These were among the most outstanding features of the development of *Pteraster* larvae in my cultures (Fig. 5A, B). He does describe the aboral epidermis as wrinkled and lacking spines or ossicles. This suggests that the aboral surface was covered by the supradorsal membrane because, in *Pteraster tesselatus,* the supradorsal membrane lacks ossicles. I observed well-developed paxillae, by day 15, in juveniles that had been cleared to make the supradorsal membrane transparent. They should have been visible externally if the supradorsal membrane had not yet formed in Chia's cultures. Further, no mention was made by Chia of the lack of brachiolar structures, the unusual symmetry of the larva, or the orientation of the juvenile rudiment within the larval body.

The striking differences between these two studies raise interesting questions about development within the family Pterasteridae. Development in *Pteraster tesselatus* may be extremely variable, because I observed marked differences in the mode of aboral lobe formation in larvae from different geographic regions. Alternatively, could we have examined two different species? The systematics of the genus *Pteraster* in the northeastern Pacific Ocean has not been examined since the classic works of Fisher (1911) and Verrill (1914), and the family Pterasteridae is not well known (M. Downey, pers. comm.). Clearly, the explanation of the reported differences in development of *P. tesselatus* must await further examination of geographic variation in development and analysis of specific and subspecific systematics. Finally, Chia may have described larvae undergoing abnormal development. He reported that only 2% of the eggs in his cultures developed (Chia, 1966, p. 507), and the larvae in his Figures 3 and 5 do not resemble the larvae that I observed. However, some of these larvae successfully completed development into apparently healthy juvenile starfish.

The development of only one other pterasterid has been described. *Pteraster militaris* broods its young within the nidamental chamber (Koren and Danielssen, 1856). Recently it was shown that only a fraction of the eggs are retained and brooded, the rest are spawned through the osculum into the water column (McClary and Mladenov, 1988). Presumably the spawned eggs develop as pelagic larvae, but their development has not been described.

Development of brooded embryos of *P. militaris* was briefly described by Kaufman (1968). The embryos were divided by a constriction (= circumferential groove) into two hemispherical regions: an oral region consisting of yolk that was eventually resorbed, and an aboral region consisting of the rudiment of the body of the starfish. Five radial (= marginal) bulges developed around the aboral region. Subsequently, ten round tubercles (= marginal lobes) developed from the five radial bulges. Podia developed between the tubercles. Later, five "arms" developed at the aboral end. Kaufman misinterpreted these aboral "arms" as the arms of the juvenile starfish (see his Fig. 2). They are probably equivalent to the five aboral lobes of *Pteraster tesselatus,* and are therefore destined to be incorporated into the supradorsal membrane. Surprisingly, Kaufman did not mention the formation of the supradorsal membrane. He stated that, when the juvenile starfish was 1.5–2.0 mm in diameter (7–10 days after formation of the constriction), the madreporite opened near the center of the aboral surface. I interpret this to be the osculum of the supradorsal membrane. The young emerged from the nidamental chamber of the mother through transient slits in the supradorsal membrane.

P. militaris clearly broods at least some of its young. However, if the embryos were artificially removed from the brood chamber, they could swim via the uniform ciliation and could develop normally (Kaufman, 1968). The free-swimming embryos became benthic at the same stage that larvae of *P. tesselatus* settled. The similarity between these two species suggests that, at least in some cases, there are not major morphological differences between benthic brooding and pelagic larval development within the Pterasteridae.

Unusual features of development in Pteraster tesselatus

The larval development of *Pteraster tesselatus* is very different from what has been observed in other asteroids, including velatids [*e.g., Solaster endeca* (Gemmill, 1912), *Crossaster papossus* (Gemmill, 1920), *Solaster stimpsoni* and *S. dawsoni* (McEdward, unpubl. obs.)], and other orders (see reviews by Hyman, 1955; Fell, 1967; Oguro *et al.,* 1988).

Morphogenesis of the supradorsal membrane. The most striking feature of the development of *Pteraster tesselatus* is the formation of 15 elaborate lobes on the external surface of the posterior region of the larva (Fig. 5A, B). This feature alone makes the pelagic larva of *P. tesselatus* unique among asteroids. The lobes fuse during the transformation of the larva into the juvenile to produce the supradorsal membrane (Fig. 6A, B). It is not surprising that a pterasterid larva has an unusual morphology, given

that metamorphosis involves the formation of a highly specialized structure found only in that family. Why the supradorsal membrane forms so early in development, before other juvenile features such as the arms and the mouth, is not known.

Lack of brachiolar structures. All asteroids, except paxillosids, develop specialized larval attachment structures consisting of the brachiolar arms and disk (Fig. 7) (Oguro *et al.*, 1988). The brachiolar arms are for temporary attachment to the bottom during exploration of the substratum, and the attachment disk is generally used to cement the settled larva to the substratum during metamorphosis (Barker, 1978). *P. tesselatus,* which is a velatid, not a paxillosid, has a larva that does not form brachiolar structures during development (Fig. 3A, B). Instead, podia are used for attachment during settlement.

Accelerated development of the water vascular system. Functional podia developed very early in *Pteraster* (day 7) compared to other species from the same geographic region with pelagic lecithotrophic larval development (*e.g., Solaster stimpsoni* 25–30 days, *S. dawsoni* ≈30 days, *Crossaster papposus* ≈50 days, *Henricia* sp.: 25–35 days; McEdward, unpubl. obs.). Because *Pteraster* reproduces in the summer and all of these other species develop in the early spring, the rapid development of *Pteraster* might be partly the result of higher seawater temperature (11–13°C in summer *vs.* 7–9°C in spring). However, the podia in *Pteraster* not only develop at a younger age, they are also accelerated relative to other juvenile structures such as the arms. In other asteroids with pelagic lecithotrophic larval development, there are generally two pair of podia and an unpaired terminal podium developing in the ambulacrum of each juvenile arm at settlement (Fig. 7). These podia do not become functional until days or weeks later. In contrast, there were several pair of functional podia in *Pteraster* long before the formation of the juvenile arms (Table I; Fig. 6C). Heterochronic acceleration of podial development in *P. tesselatus* provides a means of attaching to solid substrata at settlement in the absence of the typical larval attachment structures, the brachiolar apparatus.

Symmetry of the larva. The pelagic larva of *Pteraster* is radially symmetrical, based on external morphology (Fig. 3A, B) and the arrangement of internal structures (*e.g.*, coelomic cavities and water vascular system, Janies and McEdward, in prep.). All other asteroid larvae that have been described are bilaterally symmetrical (Fig. 7). *P. tesselatus* and *P. militaris* are the only asteroids known to lack a bilateral stage in the life cycle.

Larval and juvenile axes. The disk of the juvenile starfish lies in a transverse plane within the larval body of *Pteraster* (Figs. 3B, 5A) so that the anterior-posterior axis of the larva is parallel to the oral-aboral axis of the juvenile (Fig. 4). The anterior end of the larva corresponds to the oral surface of the juvenile and the posterior end of the larva becomes the aboral surface. The orientation of the juvenile disk within the larva is very different in all other starfish. Typically, the disk lies in a sagittal plane such that the larval and juvenile axes are perpendicular and the oral surface of the juvenile develops on the left side of the larva and the aboral surface develops on the right (Figs. 4, 7) (see review by Hyman, 1955).

Collectively, these features of morphology and development distinguish the pelagic larva of *P. tesselatus* from all other asteroid larvae. The distinctiveness of the *Pteraster* larva raises the question of its evolutionary origin. It has been considered to be a lecithotrophic, modified brachiolaria larva (Chia, 1966; Fell, 1967; Oguro *et al.*, 1988), presumably derived from an ancestor with pelagic development. This interpretation is unlikely because it requires modification of fundamental and highly conservative features of larval morphology and metamorphosis while those features were functional in the life cycle. As an alternative explanation, the unusual larva of *P. tesselatus* might have evolved from an ancestor that brooded its young (Strathmann, 1974). I suggest that most of the unusual features (namely 1, 2, 4, and 5 from the list above) can be interpreted as evidence of a highly derived mode of development associated with the evolution of the specialized form of brooding in the pterasterids. The unique structural modifications of adult pterasterids, which provide a brood chamber for the young, attest to the extreme specializations towards brooding that have evolved in this group. The evolution of this type of brooding probably occurred during the radiation of the pterasterids in the deep sea. Brooding development throughout much of the evolutionary history of the pterasterids could have led to the reduction and eventual loss of larval characteristics in the offspring. For instance, the brachiolar structures were probably lost in association with an entirely benthic life cycle, where settlement structures are not needed. I postulate that the degree of reduction of larval features has been more extensive in pterasterids than in other asteroids. This does not require different selective forces acting on pterasterid development, but rather could simply be a function of differences in the evolutionary duration of the brooding pattern of development in different taxa. The relative stability of environmental conditions in the deep sea over geological time scales could have resulted in greater species longevity for pterasterid brooders compared to brooding asteroids in other taxa in shallow water. The result of extreme reduction and simplification would be highly direct development from the embryonic stage to the juvenile stage (McEdward, 1989, and in prep.; Janies and McEdward, 1991). This would explain nearly all of the unusual features in the development of *Pteraster tesselatus.* Subsequent re-evolution of pelagic development, probably in a shallow-water ancestor of *P. tesselatus,* resulted in a larval form that was distinctly different from

that of all other asteroids. Accelerated podial development was probably a key event in the re-evolution of pelagic development; it resulted in functional attachment structures that replaced the lost brachiolar complex and facilitated settlement to the benthos (McEdward, in prep.).

Acknowledgments

A. O. D. Willows, Director, provided space and facilities at the Friday Harbor Laboratories, and J. McIhnerney, Director, provided space and facilities at the Bamfield Marine Station. S. Carson and G. Gibson helped collect starfish. SEM facilities were provided by the University of Florida, Interdisciplinary Center for Biotechnology Research and the Department of Zoology. A. Griffin, D. Janies, and P. Eliazar assisted with preparation of specimens for SEM and photography. J. Herrera prepared specimens for clearing. Photographic printing was done by D. Harrison. F.-S. Chia, M. Downey, J. Herrera, D. Janies, R. Strathmann, and M. Strathmann discussed ideas or reviewed various drafts of the manuscript. I thank all of these colleagues for their assistance. Funding was provided by the University of Florida Division of Sponsored Research (#89100245, #90012443, and DSR-B), the Department of Zoology, University of Florida, the Friday Harbor Laboratories, University of Washington, and the Bamfield Marine Station, Western Canadian Marine Biological Society.

Literature Cited

Barker, M. F. 1978. Structure of the organs of attachment of brachiolaria larvae of *Stichaster australis* (Verrill) and *Coscinasterias calamaria* (Gray) (Echinodermata: Asteroidea). *J. Exp. Mar. Biol. Ecol.* **33:** 1–36.

Blake, D. B. 1987. A classification and phylogeny of post-Paleozoic sea stars (Asteroidea: Echinodermata). *J. Nat. Hist.* **21:** 481–528.

Chia, F.-S. 1966. Development of a deep-sea cushion star, *Pteraster tesselatus*. *Proc. Cal. Acad. Sci.* **34:** 505–510.

Fell, H. B. 1967. Echinoderm ontogeny. Pp. S60–S85 in *Treatise on Invertebrate Paleontology, Part S, Echinodermata*, R. C. Moore, ed. Geological Society of America and Kansas Univ. Press, Lawrence, Kansas.

Fisher, W. K. 1911. Asteroidea of the North Pacific and adjacent waters. Part 1, Phanerozonia and Spinulosa. *Smithsonian Inst. Bull. U. S. Nat. Mus.* **76:** 419 pp.

Fisher, W. K. 1940. Asteroidea. *Discovery Rep.* **20:** 69–306.

Gemmill, J. F. 1912. The development of the starfish *Solaster endeca* Forbes. *Trans. Zool. Soc. Lond.* **20:** 1–71.

Gemmill, J. F. 1920. The development of the starfish *Crossaster papposus*, Muller and Troschel. *Q. J. Microsc. Sci.* **64:** 155–190.

Hoeg, J. T. 1984. A culture system for rearing marine invertebrate larvae and its application to larvae of rhizocephalan barnacles. *J. Exp. Mar. Biol. Ecol.* **84:** 167–172.

Hyman, L. H. 1955. *The Invertebrates, Vol. 4, Echinodermata.* McGraw-Hill, New York. 763 pp.

Ives, J. E. 1888. On two new species of starfishes. *Proc. Acad. Nat. Sci. Phil.* **40:** 421–424.

Janies, D. A., and L. R. McEdward. 1991. Evolutionary significance of a derived mode of coelom formation in the larva of the starfish, *Pteraster tesselatus*. *Am. Zool.* **31:** 105A.

Johansen, K., and J. A. Petersen. 1971. Gas exchange and active ventilation in a starfish, *Pteraster tesselatus*. *Z. vergl. Physiol.* **71:** 365–381.

Kaufman, Z. S. 1968. The postembryonic period of development of some White Sea starfish. *Sov. J. Mar. Biol.* **18:** 507–510.

Koren, J., and D. C. Danielssen. 1856. Observations sur le développement des astéries. *Fauna Littoralis Norvegiae* **2:** 55–59.

Lambert, P. 1981. *The Sea Stars of British Columbia.* British Columbia Prov. Mus., Victoria. 153 pp.

Mauzey, K. P., C. Birkeland, and P. K. Dayton. 1968. Feeding behavior of asteroids and escape responses of their prey in the Puget Sound region. *Ecology* **49:** 603–619.

McClary, D. J., and P. V. Mladenov. 1988. Brood and broadcast: a novel mode of reproduction in the sea star *Pteraster militaris*. Pp. 163–168 in *Echinoderm Biology*, R. D. Burke, P. V. Mladenov, P. Lambert, and R. L. Parsley, eds. Balkema, Rotterdam.

McClary, D. J., and P. V. Mladenov. 1989. Reproductive pattern in the brooding and broadcasting sea star *Pteraster militaris*. *Mar. Biol.* **103:** 531–540.

McClary, D. J., and P. V. Mladenov. 1990. Brooding biology of the sea star *Pteraster militaris* (O. F. Muller): energetic and histological evidence for nutrient translocation to brooded juveniles. *J. Exp. Mar. Biol. Ecol.* **142:** 183–199.

McEdward, L. R. 1989. Development and evolution of a novel type of starfish larva. *Am. Zool.* **29:** 114A.

Nance, J. M., and L. F. Braithwaite. 1979. The function of mucous secretions in the cushion star *Pteraster tesselatus* Ives. *J. Exp. Mar. Biol. Ecol.* **40:** 259–266.

Nance, J. M., and L. F. Braithwaite. 1981. Respiratory water flow and production of mucus in the cushion star, *Pteraster tesselatus* Ives (Echinodermata: Asteroidea). *J. Exp. Mar. Biol. Ecol.* **50:** 21–31.

Nation, J. L. 1983. A new method using hexamethyldisilazane for preparation of soft insect tissue for scanning electron microscopy. *Stain Technol.* **58:** 347–351.

Oguro, C., M. Komatsu, and Y. T. Kano. 1988. Significance of the nonbrachiolarian type of development in sea-stars. Pp. 241–246 in *Echinoderm Biology*, R. D. Burke, P. V. Mladenov, P. Lambert, and R. L. Parsley, eds. Balkema, Rotterdam.

Rodenhouse, I. Z., and J. E. Guberlet. 1946. The morphology and behavior of the cushion star *Pteraster tesselatus* Ives. *Univ. of Washington. Publ. Biol.* **12:** 21–48.

Sladen, W. P. 1889. Report on the Asteroidea collected by the H.M.S. Challenger. *Challenger Rep., Zool.* **30:** 888 pp.

Strathmann, M. F. 1987. *Reproduction and Development of Marine Invertebrates of the Northern Pacific Coast.* Univ. Washington Press. Seattle, Washington. 670 pp.

Strathmann, R. R. 1974. Introduction to function and adaptation in echinoderm larvae. *Thal. Jugoslav.* **10:** 321–339.

Strathmann, R. R. 1978. The evolution and loss of feeding larval stages of marine invertebrates. *Evolution* **32:** 894–906.

Verrill, A. E. 1914. Monograph of the shallow-water starfishes of the North Pacific coast from the Arctic Ocean to California. *Smithsonian Inst., Harriman Alaska Series* **14:** 408 pp.

Reference: *Biol. Bull.* **182:** 188–194. (April, 1992)

Age of the Mangrove Crab *Scylla serrata* at Colonization by Stalked Barnacles of the Genus *Octolasmis*

WILLIAM B. JEFFRIES[1], HAROLD K. VORIS[2], AND SOMBAT POOVACHIRANON[3]

[1]*Department of Biology, Dickinson College, Carlisle, Pennsylvania 17013;* [2]*Department of Zoology, Field Museum of Natural History, Chicago, Illinois 60605; and* [3]*Phuket Marine Biological Center, Phuket 83000, Thailand*

Abstract. Cyprid larvae of the lepadomorph *Octolasmis* colonize the gill chambers of the edible mangrove crab, *Scylla serrata* (Forskål, 1755), sometimes in debilitating numbers. We set out to determine when, in the life cycle of the host, barnacle infestation begins. A total of 856 mangrove crabs, ranging in size from 10.9 to 132.3 mm carapace width (instars 5 to 18), were collected from natural populations in Phuket, Thailand, and examined for these barnacles. Almost a third harbored one or more barnacles. The smallest crab to host a barnacle was 34.3 mm (instar 10); 233 smaller crabs, representing instars 5–9, had none. Infestations by more than one barnacle were uncommon among crabs of less than 70 mm carapace width (instar 13). The percentage of crabs hosting barnacles increased as the crabs approached sexual maturity, and the magnitude of infestation on individual crabs increased with their size. The distribution of octolasmids on the gills of immature crabs differed from that on mature crabs. In the former, all barnacles were on the inside of the gill surfaces and none were on the outside, whereas in the latter, 11% were on the outside of the gills. The numbers of barnacles on the inside and the outside of the gills is a function of the number of barnacles in the gill chamber. The major inhalant aperture size, and gill chamber size were eliminated as possible factors limiting infestation. Instars 10 and 11 may be suboptimal for infestation by octolasmids because the intermolt time between instars does not allow sufficient time for production of barnacle nauplii. Current data do not permit us to distinguish the relative influences of microhabitat use, host hormonal changes, and behavioral changes on infestation.

Received 16 September 1991; accepted 12 December 1991.

Introduction

Many interesting and diverse symbiotic relationships (*sensu lato,* de Bary, 1879) exist between decapods and metazoans of different phyla. The growth of some rhizocephalans, *e.g., Sacculina* spp., results in parasitic castration of hosts so that male crabs develop some of the secondary sexual and behavioral characteristics of female crabs (Bang, 1983; Cressey, 1983; Overstreet, 1983). Infestation of crab branchial lamellae and subsequently crab egg masses by nemertean worms, *e.g., Carcinomemertes* spp., likely impedes the free flow of water over the gills and results in the predation of host eggs (Humes, 1942). Colonization of crab respiratory surfaces by *Octolasmis* spp. may result in heavy infestations that overwhelm the cleaning capacity of grooming appendages and make respiration difficult (Overstreet, 1983).

As is the case with many edible crab species, the respiratory chambers of the mangrove crab, *Scylla serrata* (Forskål, 1755), are inhabited by stalked barnacles, which occupy space on the gills normally available for respiratory exchange of oxygen and carbon dioxide. To colonize the crabs, octolasmid cyprid larvae collect on the host just prior to molt and transfer from the old exoskeleton to the newly molted crab at the time of ecdysis (Jeffries *et al.,* 1989). Following attachment, the cyprid metamorphoses to the adult barnacle body form and is sessile thereafter. Because they are sessile, these barnacles cannot recolonize crabs that have molted. Thus for a barnacle to achieve reproductive success, there must be a sufficient interval between crab molts for the cyprid to attach, metamorphose to the adult form, reach sexual maturity, copulate, oviposit, and release nauplii.

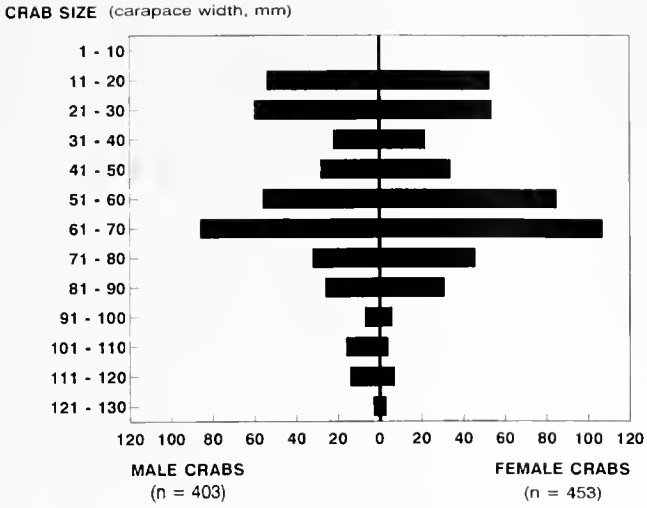

Figure 1. The size distributions for 403 male and 453 female mangrove crabs (*Scylla serrata*) collected from mangrove areas in the immediate vicinity of Phuket, Thailand.

Some small crabs also harbor octolasmids, *e.g., Uca minax*, with a carapace width of 38 mm (Williams, 1965) was reported to bear *Octolasmis müilleri* (Coker, 1902), (Pearse, 1936). In a survey of the decapods of Sabah, Malaysia (unpublished), we noted that three different crab species, all small, harbored *Octolasmis angulata* in their branchial chambers: 2 male *Pilumnus scabriusculus* (Adams & White), 32.1 and 36.3 mm, respectively; 1 male *Pilumnus vespertilio* (Fabricius, 1793), 23.2 mm; and 1 male *Actaeodes* sp., 26.9 mm. These observations, together with the observation that smaller *S. serrata* had few or no octolasmids, prompted us to ask whether host size might be a consideration in the mangrove crab-octolasmid symbiosis.

The purpose of this research was to determine the stage and time in the life cycle of the mangrove crab when *Octolasmis* spp. colonize its gill chambers. Specifically, we sought to identify the youngest crab instars that harbor *Octolasmis*, and to compare the number and distribution of barnacles on their gills with those on mature crabs.

Materials and Methods

During 1990 and 1991, *S. serrata* were collected from shallow seas adjacent to mangroves, mostly within 2 km of the town of Phuket, Thailand, for study at the Phuket Marine Biological Center. The very small instars were caught by hand, whereas larger crabs were caught in baited traps. The crabs were sexed, weighed, and their carapace lengths and widths measured (Heasman, 1980). They were preserved in formalin and stored in 70% ethanol for later examination. The crabs were examined for *Octolasmis* cyprids, juveniles, adults with distinct ovaries, and gravid adults. The exact location (left or right gill chamber, gill number, inside or outside gill surface, proximal, medial, or distal region of gill), and the length of the capitulum of each barnacle were recorded using the methods previously employed (Jeffries *et al.*, 1982). A dissecting microscope was used to determine the reproductive status of the barnacles.

Results

A total of 856 *S. serrata* were examined; 403 were males and 453 females. The carapace width of the male and female crabs ranged from 10.9 to 125.5 mm and from 11.2 to 132.3 mm, respectively. The size distributions of the male and female crabs examined were very similar (Fig. 1).

Of the 6648 barnacles observed, 168 were cyprids, 3670 were *Octolasmis cor*, 1758 were *Octolasmis angulata*, and the remainder were too small to identify. Except where noted, all stages and both species were pooled in the analysis because the focus of this paper is on barnacle colonization relative to crab age. In a subsequent paper about the ecology of barnacles resident on mangrove crabs, we will address the differences between the two species. That subject deserves individual treatment because opinion is divided on whether *S. serrata* branchial chambers bear several varieties of *Octolasmis cor* (Monod, 1922; Newman, 1960) or two species, *O. cor* and *O. angulata*, as we assert.

The percentage of crabs that harbored barnacles was very low (<5%) for crabs of less than 50 mm carapace width, whereas the incidence of infestation rose sharply as crab size increased above 50 mm (Fig. 2).

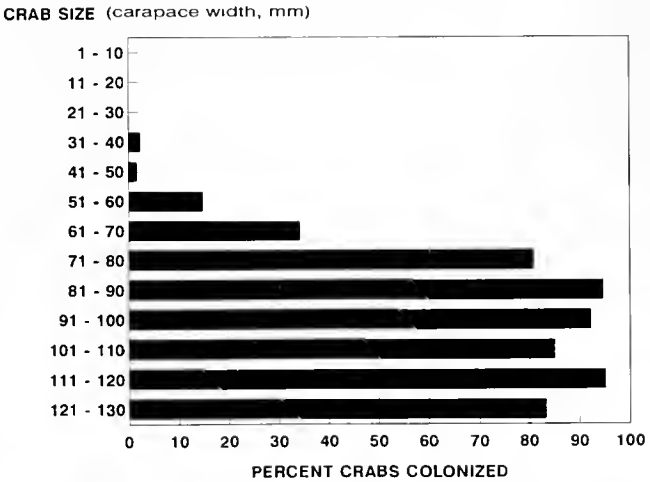

Figure 2. The percentage of mangrove crabs (*Scylla serrata*) of different sizes with one or more octolasmid barnacles present in a gill chamber. The 856 crabs range in size from 10.9 to 132.3 mm in carapace width.

Of the 856 crabs examined for barnacles, 260 (30.4%) had one or more barnacles in their gill chambers. Of these, 134 crabs were males and 126 were females. The percentage of male crabs harboring barnacles (33.3%) was only slightly greater than for female crabs (27.8%), and both males and females showed increased numbers of barnacles with increased carapace width (Fig. 3).

The smallest crab in the sample bearing a barnacle in its gill chamber was a male with a carapace width of only 34.3 mm (instar number 10; Ong, 1966). The solitary octolasmid (*O.* sp.) was found on the inside of the seventh gill; it was reproductively immature and had a capitular length of 0.86 mm. The next smallest crab to have a barnacle in its gill chamber was a female with a carapace width of 43.1 mm (instar 11; Ong, 1966). This crab had a single cyprid on the inside of the sixth gill. The carapace widths of all other barnacle-bearing crabs were more than 50.0 mm, corresponding to instar 12 or greater.

Two male crabs with carapace widths of 51.3 mm were the next smallest crabs to harbor single barnacles. One crab had a cyprid, whereas the other was the smallest crab to possess a sexually mature *Octolasmis cor,* measuring 1.72 mm in capitular length, with a distinct ovary indicating that it was potentially reproductively active.

The smallest crab with multiple barnacles, a female, had a carapace width of 54.5 mm; it harbored two *O. cor* with distinct ovaries and capitular lengths of 1.86 and 2.43 mm. Figure 2 shows that the incidence of barnacles increased on crabs between 60 and 70 mm, but most crabs below 70 mm had no more than 5 barnacles. One notable exception was a female crab with a carapace width of 60.4 mm and 95 barnacles. This crab was also the smallest crab to harbor ten or more barnacles (Fig. 3). The 95 barnacles ranged in size from 0.57 to 2.57 mm in capitular length ($\bar{X}$ = 1.66 mm). Of the 95 barnacles, 38 had distinct ovaries, and the smallest of these had a capitular length of 1.43 mm. Eleven were gravid with ovigerous lamellae, and the smallest of these was 1.72 mm in capitular length. Of five bearing nauplius I larvae about to hatch (stage N; Lewis, 1975), the smallest was also 1.72 mm in capitular length. This crab was exceptionally small for the level of infestation, and the next smallest crab with 10 or more barnacles had only 11; its carapace width was 67.3 mm.

The distribution of barnacles (n = 6648) between the left and right chambers did not differ significantly from 50:50 (Binomial test, $P < .01$), and thus the left and right chambers were pooled for the following distribution comparisons.

To explore possible differences in patterns of colonization among crabs of different sizes, the 260 infected crabs were divided into two groups: those with carapace widths below 70 mm (n = 87) and those above 70 mm (n = 173). This division point was selected on the basis of observed infestation levels (Fig. 3) and the knowledge that 70 mm (instar 14) likely corresponds to the beginning of crab sexual maturity. Among female mangrove crabs of instar 14, the ovaries are considerably developed and easy to see grossly as was reported for female *Callinectes sapidus* (Rathbun, 1896) following the penultimate molt (Johnson, 1980).

All 303 barnacles found on the 87 crabs with carapace widths of less than 70 mm were located on the inside surface of the gills (Table 1). This distribution is significantly different (df = 1, χ^2 = 38.8, $P < .001$) from that

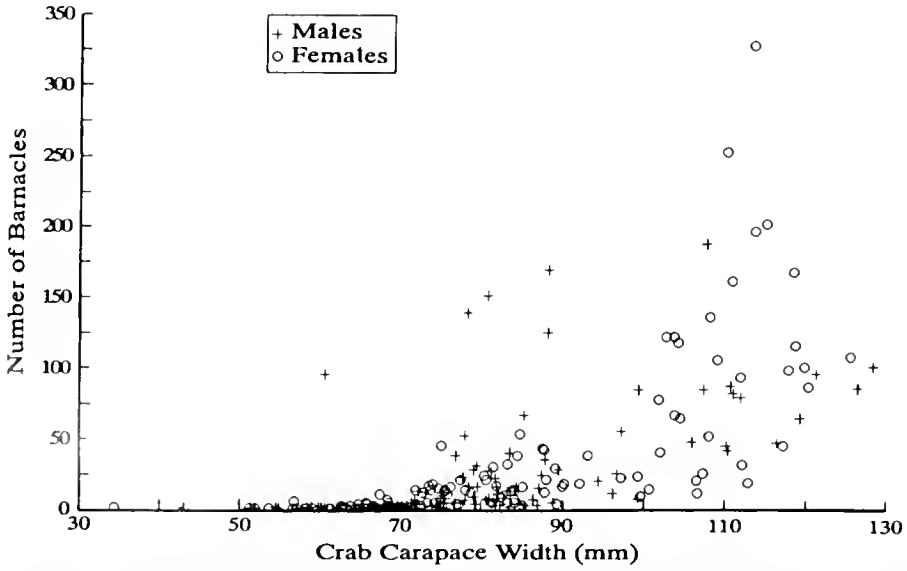

Figure 3. The relationship between the crab carapace width and the number of octolasmid barnacles present in the gill chambers for 134 male and 126 female mangrove crabs (*Scylla serrata*).

Table I

The distribution of barnacles over the inside and outside surfaces of the gills of the 87 crabs with carapace widths less than 70 mm

Gill number	Inside of gills				Outside of gills				In + Out totals
	Proximal	Medial	Distal	Totals	Proximal	Medial	Distal	Totals	
1	1	4	0	5	0	0	0	0	5
2	0	0	0	0	0	0	0	0	0
3	9	22	0	31	0	0	0	0	31
4	33	32	1	66	0	0	0	0	66
5	27	38	1	66	0	0	0	0	66
6	26	42	5	73	0	0	0	0	73
7	16	31	2	49	0	0	0	0	49
8	5	8	0	13	0	0	0	0	13
Totals =	117	177	9	303	0	0	0	0	303
								On Rakers	1
								Total =	304

observed for the 173 crabs with carapace widths of greater than 70 mm, where 5609 barnacles were found on the inside surface of the gills and 723 (11%) were found on the outside (Table II). The smallest crab having a barnacle attached to the outside surface of its gills had a carapace width of 76.8 mm, and the inside surface of the gills in that chamber had a total of 20 barnacles. The smallest crab having multiple barnacles attached to the outside surface of its gills had a carapace width of 78.2 mm, and the numbers of barnacles on the inside and outside surfaces of the gills were 64 and 2 in the left chamber, and 61 and 3 in the right chamber.

For the 87 crabs less than 70 mm, and the 173 above 70 mm in carapace width, the distribution of barnacles on the inside of gills 1 through 8 (Tables I, II) did not differ significantly ($df = 7$, $\chi^2 = 6.1$, $P > .05$). Nor did the distribution of barnacles along the length of the gills (proximal, medial, and distal) on the inside surface differ significantly ($df = 2$, $\chi^2 = 2.4$, $P > .05$) between the crabs above and below 70 mm.

The distribution of barnacles on the inside *versus* the outside of the gills among all 260 crabs with barnacles (data from Tables I and II combined) showed significant differences. The distribution of barnacles on the inside *versus* the outside, and over gills 1 through 8, differed significantly ($df = 7$, $\chi^2 = 525.9$, $P < .001$). In addition, the distribution of barnacles along the length of the gills (proximal, medial, and distal) on the inside *versus* the outside surface differed significantly ($df = 2$, $\chi^2 = 87.3$, $P > .001$). Whether on the inside or outside surface of the gills, barnacles in this sample were least common on the distal third of the gills. On the inside surface, the medial section of the gill was the most densely populated, whereas on the outside surface, the proximal portion of the gills was the most populated.

Discussion

These data support four major conclusions about colonization of mangrove crabs by barnacles: (1) juvenile crabs are virtually free of octolasmids; (2) as crabs approach sexual maturity, the percentage of crabs hosting octolasmids increases; (3) the level of barnacle infestation of individual crabs increases with crab size; and (4) the distribution of octolasmids on the gills of immature crabs is different from that on mature crabs. Our discussion will focus on possible explanations for these findings.

In this study we found that 233 crabs, representing instars 5 through 9 (Ong, 1966), did not host a single barnacle. Several previous studies of decapods and their symbionts also have suggested size thresholds for infestation. Although the intertidal shore crab, *Hemigrapsus oregonensis* (Dana, 1851), of either sex, mature or not, may become infested with juvenile nemertean worms, *Carcinonemertes epialti* Coe, 1902, a threshold carapace width of 8 mm exists; above that threshold, both the incidence of infestation and the average burden of worms increase dramatically with increasing host size (Kuris, 1978). Also, juveniles of the edible dungeness crab, *Cancer magister,* below 20 mm carapace width are not infested by *Carcinonemertes errans,* whereas worm burdens increase with crabs above 20 mm (Wickham, 1980). Metacercariae of the trematode, *Spelotrema excellens* Nicoll, were found in 103 of 115 specimens of the portunid crab, *Carcinus maenas* (L.). Twelve crabs with carapace widths of less than 15 mm were not parasitized, whereas all above 15 mm were parasitized, and there was a significant correlation between the crab carapace width and the intensity of infection (Threlfall, 1968).

These studies suggest that size thresholds do exist among the host decapods in such symbiotic relationships. However, there has been very little critical examination of the

Table II

The distribution of barnacles over the inside and outside surfaces of the gills of the 173 crabs with carapace widths greater than 70 mm

Gill number	Inside of gills				Outside of gills				In + Out totals
	Proximal	Medial	Distal	Totals	Proximal	Medial	Distal	Totals	
1	37	36	4	77	1	1	23	25	102
2	5	4	6	15	14	13	9	36	51
3	162	398	45	605	16	18	2	36	641
4	607	691	33	1331	87	41	0	128	1459
5	431	564	39	1034	209	95	10	314	1348
6	579	577	43	1199	72	73	2	147	1346
7	322	633	66	1021	11	18	2	31	1052
8	144	171	12	327	0	6	0	6	333
Totals =	2287	3074	248	5609	410	265	48	723	6332
								On Rakers	12
								Total =	6344

possible effects of host ontogenetic changes on symbiosis involving Crustacea. This is important because the way that symbionts interact with different host ontogenetic stages can contribute to our understanding of the mechanisms underlying the symbiotic relationships.

For the relationship between *S. serrata* and *Octolasmis* spp., we have considered the following possible influences on the observed non-random distributions: ontogenetic differences in physical barriers such as the size of the major incurrent respiratory apertures, and gill chamber size; duration of intermolt period; crab macrohabitat distribution; crab microhabitat distribution; and crab behavior.

In order to be a limiting factor, the incurrent respiratory apertures of the crab would have to be small enough to exclude cyprid larvae. The average length and diameter of 10 preserved *Octolasmis* cyprids was 0.82×0.35 mm. By comparison, the average width and height of the major apertures of five of the smallest crabs (carapace width 10–19 mm) examined in this study was 1.9×1.0 mm. Clearly, crab intake aperture size is not a limiting factor to cyprid larvae trying to enter the branchial chambers of *S. serrata*.

If space in the gill chamber were a major factor in limiting the occurrence of barnacles on immature crabs, we would expect the numbers of barnacles on crabs to increase steadily with increased crab size. This does not seem to be the case. For example, two crabs with carapace widths of 60.4 and 61.4 mm had large populations of barnacles, although their sizes are at the threshold where colonization is just beginning (Fig. 3).

For the length of the crab intermolt period to strictly limit the effective colonization by barnacles, the crab intermolt period must be shorter than the total time necessary for the cyprid to attach, metamorphose, reach sexual maturity, become gravid, and release nauplius I larvae. This is the case because post-metamorphic barnacles are sessile, and when a crab molts, individual barnacles remain attached to the crab exuviae and are unable to recolonize a host. Thus there is the potential for a fine-tuned host/symbiont relationship predicated on the intermolt time period of the host and the time the symbiont requires to complete its life cycle.

Earlier work provided an estimate of 24 h for *Octolasmis* cyprid attachment to metamorphosis, an estimated daily growth rate of 0.336 mm in capitular length (Jeffries *et al.*, 1985), and demonstrated that the major colonization of crabs by cyprids occurs immediately after ecdysis (Jeffries *et al.*, 1989). In this study, the capitular length of the smallest *Octolasmis cor* (1.72 mm) observed with ovigerous lamellae compares favorably with the 1.6 mm specimen reported with mature eggs by Matheswari and Fernando (1989), and exceeds the 1.14 mm gravid specimen of *O. mülleri* reported by Jeffries and Voris (1983). On average, the capitular length of the newly metamorphosed barnacle is 0.57 mm, and thus it takes about 3.4 days to reach 1.72 mm at the daily growth rate of 0.336 mm. Hence, the time from cyprid attachment to a gravid barnacle at oviposition with ovigerous lamellae is about 4.4 days.

The development time from oviposition to the release of nauplius I larvae is unpublished for octolasmids, but it has been reported for other lepadomorphs. For *Ibla quadrivalvis* Cuv., it was 16 to 17 days at 23°C (Anderson, 1964), and for *Pollicipes polymerus*, it averaged 25.4 days at 12 to 16°C (Lewis, 1975). Because seawater temperatures at the *S. serrata* collection sites near Phuket, Thailand, range from 27 to 31°C, it is very likely that for *O. cor* the required time from oviposition to release of nauplius I larvae is no more than 14 days, and may be as little as one week. Thus, the time required for *O. cor* to attach and reproduce is likely no more than 18.4 days (4.4 plus 14) and may be as little as 11.4 days (4.4 plus 7).

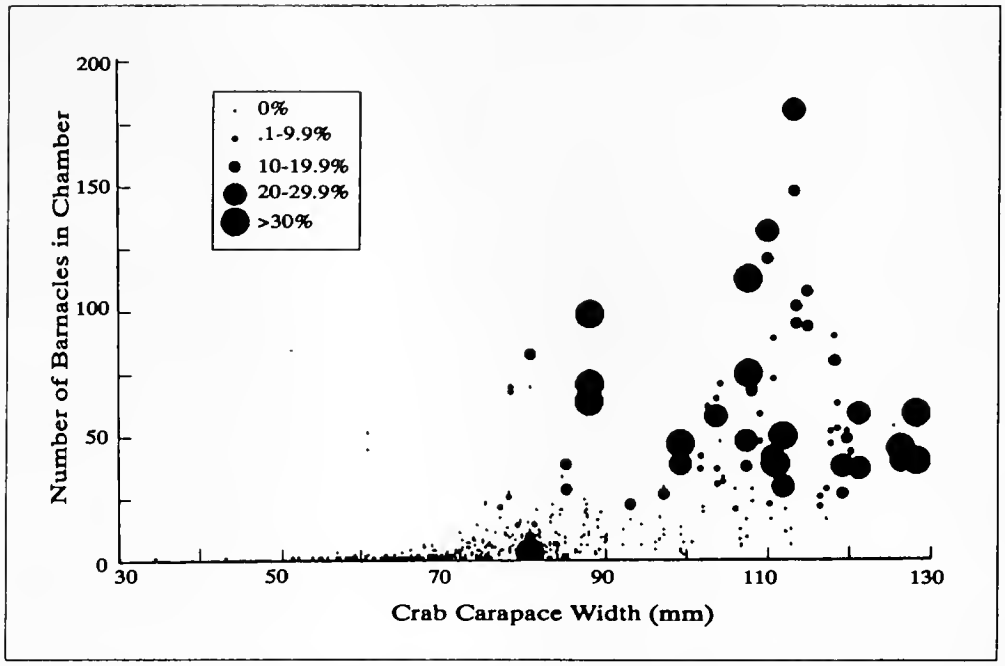

Figure 4. Of the 260 crabs with barnacles, 435 of the 520 gill chambers contained one or more barnacles. For each chamber, the size of the crab is plotted against the number of barnacles present in the chamber. The symbol size indicates the percentage of the barnacles present on the outside surface of the gills in increments of 10%.

S. serrata instar 9 crabs range in size from 26 to 33 mm in carapace width and have an intermolt period of at least 15 days (Ong, 1966). The absence of any barnacles on the 233 crabs of instars 5 to 9 in this study may be attributable to barnacle avoidance because the intermolt period is too short to allow for barnacle reproduction.

Crab instars 10 to 11 range from 33 to 48 mm in carapace width and have minimum intermolt periods of 16 and 22 days, respectively. According to our earlier calculations, these are minimum time periods that octolasmids require to produce offspring and they would not allow individuals to produce multiple broods, thus limiting fecundity (Jeffries *et al.*, 1985). In this study, the fact that only a small fraction of instars 10 and 11 harbored barnacles (Fig. 2) and none had heavy infestations (Fig. 3) is consistent with the idea that these crab instars represent suboptimal substrata.

Instars 12 and above have carapace widths greater than 45 mm and intermolt periods of 30 days or more. Such intermolt periods are sufficient to allow for the production of multiple broods. This is consistent with our observations that the incidence of infestation increases among crabs above 50 mm carapace width (Fig. 2) and is further supported by the observation that one crab of 60.4 mm carapace width (instar 13) had 95 barnacles (Fig. 3), many of which harbored nauplius 1 larvae.

In this study, mangrove crabs of different sizes—juveniles and adults—were collected at the same time in the same shallow water mangrove macrohabitat, thus diminishing the possibility of a difference in availability of cyprids to potential hosts at the macrohabitat level.

Differences in infestation rates among successive instars of *S. serrata* might be the result of ontogenetic changes in microhabitat use, shifts in host hormone levels (chemotaxis), or behavioral changes. However, we cannot discriminate among these factors on the basis of current information. For example, it was reported that juvenile mangrove crabs use shelter under existing bottom debris in open areas (Heasman, 1980), whereas older crabs use burrows. But we do not know whether this difference has an impact on mangrove crab colonization by *Octolasmis* cyprid larvae.

The differences observed in the distribution of barnacles on the inside and outside of the gills in crabs less than and those greater than 70 mm carapace width (Tables I, II) could be due to a density-dependent response to crowding on the inside surface of the gills, or it could be due to a lack of space in the chamber on the outside surface of the gills. The former explanation is better supported by our data. If space on the outside of the gills controlled colonization, we would expect larger crabs with modest numbers of barnacles (*e.g.*, 5 to 20) to have barnacles on both the inside and outside surface of their gills. This is not the case. Barnacles are only found on the outside gill surfaces in significant numbers when the inside surface has 20 or more barnacles, regardless of crab size (Fig. 4).

These non-random, species-specific distributions suggest the next generation of research questions to be addressed.

Acknowledgments

We thank the staff of the Phuket Marine Biological Center for their logistical support and the use of their facilities. In particular, we are grateful to the Director, Mr. Udom Bhatia, for his generous cooperation. Special thanks are due to Mr. Boonchoy Kuoyratanakul, a fisherman who collected most of the crabs and Mr. Saengdee Chailert who received crabs from fishermen for us. We thank Helen Voris for numerous helpful editorial comments. Support from the Dickinson College Board of Advisors and the Faculty Research Fund, and the Field Museum of Natural History Research Fund made this investigation possible.

Literature Cited

Anderson, D. T. 1965. Embryonic and larval development and segment formation in *Ibla quadrivalvis* Cuv. (Cirripedia). *Aust. J. Zool.* **13:** 1–15.

Bang, F. B. 1983. Crustacean disease responses. Pp. 113–153 in *The Biology of the Crustacea, Vol. 6,* Anthony J. Provenzano, Jr., ed. Academic Press, Inc. New York.

Cressey, R. F. 1983. Crustaceans as parasites of other organisms. Pp. 251–273 in *The Biology of the Crustacea, Vol. 6,* Anthony J. Provenzano, Jr., ed. Academic Press, Inc. New York.

de Bary, A. 1879. *Die Erscheinung Der Symbiose,* Karl J. Trubner, Strassburg.

Heasman, M. P. 1980. Aspects of the general biology and fishery of the mud crab *Scylla serrata* (Forskål) in Moreton Bay, Queensland. Ph.D. Thesis No. 2210, University of Queensland. 506 pp.

Humes, A. G. 1942. The morphology, taxonomy, and bionomics of the nemertean genus *Carcinonemertes. Illinois Biol. Monogr.* **18:** 1–105.

Jeffries, W. B., and H. K. Voris. 1983. The distribution, size and reproduction of the pedunculate barnacle, *Octolasmis mülleri* (Coker, 1902) on the blue crab, *Callinectes sapidus* (Rathbun, 1896). *Fieldiana Zool. N. S.* **16:** 1–10.

Jeffries, W. B., H. K. Voris, and C. M. Yang. 1982. Diversity and distribution of the pedunculate barnacle *Octolasmis* in the seas adjacent to Singapore. *J. Crustacean Biol.* **2**(4): 562–569.

Jeffries, W. B., H. K. Voris, and C. M. Yang. 1985. Growth of *Octolasmis cor* (Aurivillius, 1892) on the gills of *Scylla serrata* (Forskål, 1755). *Biol. Bull.* **169:** 291–296.

Jeffries, W. B., H. K. Voris, and C. M. Yang. 1989. A new mechanism of host colonization: pedunculate barnacles of the genus *Octolasmis* on the mangrove crab *Scylla serrata. Ophelia* **31:** 51–58.

Johnson, P. T. 1980. Histology of the blue crab, *Callinectes sapidus.* Praeger Publishers, New York.

Kuris, A. M. 1978. Life cycle, distribution and abundance of *Carcinonemertes epialti,* a nemertean egg predator of the shore crab, *Hemigrapsus oregonensis,* in relation to host size, reproduction and molt cycle. *Biol. Bull.* **154:** 121–137.

Lewis, C. A. 1975. Development of the gooseneck barnacle *Pollicipes polymerus* (Cirripedia: Lepadomorpha): fertilization through settlement. *Mar. Biol.* **32:** 141–153.

Matheswari, R., and S. A. Fernando. 1989. Fecundity of epizoic barnacles. *Indian J. Inv. Zool. Aqua. Biol.* **1**(2): 31–35.

Monod, T. 1922. Sur un *Dichelaspis* de Madagascar, commensal de *Scylla serrata* (Forskål). *Extrait du Bulletin de la Societe Zoologique de France* **XLVI:** 264–269.

Newman, W. A. 1960. Five pedunculate cirripeds from the western pacific, including two new forms. *Crustaceana* **1:** 100–116.

Ong, K. S. 1966. Observations on the post-larval life history of *Scylla serrata,* Forskål, reared in the laboratory. Malays. Agric. J. **45**(4): 429–443.

Overstreet, R. M. 1983. Metazoan Symbionts of Crustaceans. Pp. 155–250 in *The Biology of Crustacea. Vol. 6,* Anthony J. Provenzano, Jr., ed. Academic Press, Inc. New York.

Pearse, A. S. 1936. Estuarine animals at Beaufort, North Carolina. *J. Elisha Mitchell Sci. Soc.* **52**(2): 174–222.

Threlfall, W. 1968. Note on metacercariae of *Spelotrema excellens* Nicoll in *Carcinus maenas* (L.). *J. Exp. Mar. Biol. Ecol.* **2:** 154–155.

Wickham, D. E. 1980. Aspects of the life history of *Carcinonemertes errans* (Nemertea: Carcinonemertidae), an egg predator of the crab *Cancer magister. Biol. Bull.* **159:** 247–257.

Williams, A. B. 1965. Marine decapod crustaceans of the Carolinas. *Fish. Bull. U. S. Fish Wildlife Serv.* **1:** 1–298.

Reference: *Biol. Bull.* **182:** 195–209. (April, 1992)

Architectural and Mechanical Properties of the Black Coral Skeleton (Coelenterata: Antipatharia): A Comparison of Two Species

KIHO KIM*, WALTER M. GOLDBERG**, AND GEORGE T. TAYLOR

Florida International University, Department of Biological Sciences, University Park, Miami, Florida 33199

Abstract. Black coral skeletons are laminated composites, composed primarily of chitin fibrils and non-fibrillar protein. This paper examines mechanical properties of the composite and the architecture of the chitin component. Two species are shown to differ significantly in their tensile strength and fibril structure. The skeleton of *Antipathes salix*, a Caribbean species of commercial value, is stiffer, harder, darker, more dense, and more hydrophobic than *Antipathes fiordensis* from New Zealand. The chitin fibrils constitute a greater proportion of the skeleton in *A. salix*, where they are helically wound in an anticlockwise pattern within layer. Adjacent layers of skeleton are arranged with relatively small layer-to-layer fibril biases. There is no evidence of "helicoidal" structure in this skeleton. The fibrils in *A. fiordensis* are also wound anticlockwise within layer, but with rather large fibril biases between layers, giving the appearance of a meshwork. Large-scale helicoidal patterns with apparent rotations of 180° characterize this material. Skeletal architecture is compared with the cuticle of insects and other arthropods. The skeletons of both species exhibit spines characteristic of the Antipatharia. We suggest that these have a significant reinforcing effect on the strength of the skeleton, contributing to an overdesign for the habitat in which these organisms presently occur.

Introduction

Black corals are well known as articles of commerce in the jewelry and curio trade dating from at least the time of the ancient Greeks (Hickson, 1924). The skeleton can be polished to an onyx-like luster, but because it is organic, it can also be bent and molded while being heated. Consequently, this material is highly prized in the jewelry trade, and collection pressure has resulted in the listing of black corals in the Convention for the International Trade in Endangered Species (CITES) (Wood and Wells, 1988). Collection pressure notwithstanding, certain species of black coral may constitute a substantial part of the fauna on deep reefs and in other more geographically restricted habitats. In the Fiordland district on the southwest coast of New Zealand's south island, for example, the endemic black coral, *Antipathes fiordensis* Grange is the dominant macrobenthic organism in depths of 10–20 m (Grange, 1985, 1990). Similarly, *Antipathes salix* Pourtalès, is one of the more commonly occurring black coral species in the Caribbean, although it is most often restricted to coral reef slopes below 30–40 m. Yet in spite of their commoness in some areas, rarity or endangerment in others, and their historical and commercial value, black corals remain among the least known of colonial coelenterates. Almost nothing is known about the architectural and material properties of black coral skeleton, which may determine not only its commercial value, but its ecological functions as well. This paper is the first attempt to elucidate and compare the structural and mechanical properties of black coral skeleton, using as examples the geographically disparate congeners *A. fiordensis* and *A. salix*.

Materials and Methods

Colonies of *A. fiordensis* were collected by SCUBA divers at Doubtful Sound, New Zealand, in 10–20 m depth, and *A. salix* at Cay Sal Bank, Bahamas, in 30–40 m. Liv-

Received 21 October 1991; accepted 24 January 1992.

* Current address: State University of New York at Buffalo, Department of Biological Sciences, Buffalo, New York, 14260.

** To whom correspondence should be addressed.

ing tissue was removed by jets of fresh water, and the remaining skeletal material was stored dry at 4°C.

Microscopy

Skeletal material was examined both before and after treatment with a variety of agents. Some skeleton was examined after standard double fixation (3% glutaraldehyde and 1% osmium tetroxide) and double staining (saturated uranyl acetate in 50% methanol and 0.3% lead citrate). However, because the fibrils comprising the skeleton of both species are embedded in an amorphous, resistant matrix, observation of fibrillar orientation or structure often required chemical treatment. Unfixed material was placed in concentrated formic acid for 24–48 h at room temperature to cause swelling and delamination of the skeletal layers (Goldberg, 1991). Using watchmaker's forceps, narrow strips of the outer skeleton were torn away along the long axis. Formic acid-treated material was washed and dehydrated in graded ethanols and embedded in Spurr resin. Thin sections were taken at parallel, 45° and perpendicular to the long axis of the branch. Additional material was examined after deproteination with 1 *N* KOH (24 h, 105°C; Hackman and Goldberg, 1971). Sections were stained with 2% phosphotungstic acid (PTA) in 10% ethanol (Bouligand, 1972) and examined using a Phillips EM 300 transmission electron microscope (TEM) operated at 60 kV. Fine structural observations of fibril orientation by scanning electron microscopy (SEM) could not be made without etching the smooth surface of formic acid-treated material with 1.0 M $NaBH_4$ in 1.0 M NaOH (4 h, 70°C). The delaminated, etched skeleton was dried after ethanol dehydration and coated with Au/Pd prior to examination in an ISI Super 3A SEM. We also prepared fracture cross-sections for SEM from acid-treated material. Samples of untreated, as well as formic acid-treated, and KOH-treated skeleton were examined in the light microscope. One micron sections of Spurr-embedded material were either stained with Toluidine blue, or viewed unstained using polarized light and/or phase-contrast microscopy. We also examined unembedded, aqueous mounts, and epoxy-embedded thick sections ground and polished with graded abrasives.

Material properties

Measurements of density and Young's modulus were performed on skeleton rehydrated in artificial seawater (ASW). To estimate minimum time required for rehydration, skeletal pieces of various diameters and lengths were dried overnight at 70°C, and cooled in a desiccator. The dry skeletons were weighed, placed in ASW (~37‰, room temperature), then surface-dried and re-weighed daily. When weights for three consecutive days were within 0.5%, hydration was considered complete and the gravimetric change was noted as the water content. The rehydrated piece was surface-dried and placed in a graduated cylinder (accurate to 0.01 ml). Density was calculated as weight of the skeleton divided by the volume of water displaced.

Mechanical properties were determined using samples 6–10 cm long and 0.7–1.5 mm in diameter, embedded in methyl methacrylate at both ends prior to rehydration. We were limited to branches less than 1.5 mm in diameter because larger branches pulled out of the plastic before failing. The plastic ends were loaded under tension using an Instron 1011 strength tester fitted with a 5 kg cross head travelling at a constant rate of 50 mm/min. The Young's modulus (E) was calculated using the formula, $E = FL/AdL$, where F and dL are the amount of force applied to the branch and the change in its length at failure, respectively. The length of the skeleton (L) is the distance between the two methyl methacrylate blocks, while A is the cross sectional area of the sample. Because the skeleton was never perfectly cylindrical and often tapered toward the apex, an average cross sectional area was estimated by assuming the taper was linear from one end to the other. Hardness was measured on both the Moh's and Vicker's scale. Moh's is a qualitative scale in which 10 minerals are used as standards ranging from talc (1) to diamond (10). Hardness is based on the ability of one material to scratch another. The Vicker's scale is a more quantitative measure of microhardness, which measures the impression made using a pyramid-shaped diamond forced into the surface of a material. Microhardness is expressed as Vickers Hardness Numbers according to the formula $VHN = 1854P/d^2$ (kg mm^{-2}), where P is the load in grams and d is the mean length of the indentation in microns (*cf.*, Hillerton *et al.*, 1982). Testing was performed both parallel and perpendicular to the long axis of hydrated and unhydrated skeleton using a Leco-DM 400F hardness tester with an applied load of 10 g.

Skeletal chemistry

Protein content and amino acid composition were determined after hydrolysis in 4 *N* methanesulfonic acid (105°C, 20 h) (Simpson *et al.*, 1976) using a JEOL 5AH amino acid analyzer with a ninhydrin-based detection system. Protein was expressed as total ninhydrin reactivity. Chitin was estimated from the amino sugar content, corrected for deacetylation. Dry skeletal powder was extracted using chloroform:methanol (2:1, V:V) on a shaker for 48 h at room temperature. The powder was washed in methanol (3×), dried overnight, and re-weighed to estimate lipid content.

Results

Microscopy

The external surfaces of antipatharian skeletons are distinguished by the presence of spines. Both the spine morphology and pattern of spination clearly distinguish the two species, and correspond with skeletal characters given by Grange (1988, 1990) and Opresko (1972). The skeleton of *A. fiordensis* is marked by rows of numerous, smooth, slender spines 200–350 μm long in addition to shorter, branched secondaries (Fig. 1). In contrast, spines in *A. salix* are relatively uniform, compressed cones 90–100 μm long, that become nodose during maturation (Fig. 5, inset). As is typical of antipatharians (Opresko, 1972), the spines are organized into spiralling rows along the long axis of the skeleton (Fig. 5). There are no secondary spines in this species.

In light microscopic cross sections of *A. fiordensis*, the growing tip can be distinguished clearly from more mature portions of the skeleton, as a region that stains intensely with Toluidine blue (Fig. 9). The skeleton increases in thickness and in length by adding thin *growth layers* or *lamellae*. These range in thickness from 0.1 to 1.0 μm when measured between the spines (Fig. 14). The lamellae become thinner as they approach and add a layer to the spines. Most of the layers are separated from each other by a subtle discontinuity in optical density. However, at irregular intervals, material that stains more intensely with Toluidine blue separates sets of skeletal lamellae. These deposits, which are also osmiophilic, are visually interpreted as *growth rings*. Growth ring structure has been described by Goldberg (1991). Ring timing in this species will be considered elsewhere (Grange and Goldberg, in prep.).

Strongly birefringent patterns are observed when thin pieces of formic acid-treated skeleton are examined with polarized light microscopy. These patterns appear to result from the chitin fibrils because subsequent deproteination by KOH, albeit incomplete (see skeletal chemistry section below), does not appreciably affect the birefringence of either species. Light microscopic observation of *A. fiordensis* skeleton suggests that the fibrils form anticlockwise helices around the long axis of the branch. Interpretation of the longitudinal pattern is influenced by the presence of numerous spines that serve as convergence points for the fibrils within layers. The spines are numerous enough to obscure the surface fibril pattern, making an accurate assessment of its overall direction difficult. A view through several lamellae creates the appearance of a meshwork (Fig. 10), indicating a layer-to-layer change in the fibrillar winding pattern.

Visualization of *A. fiordensis* chitin microfibrils (hereafter referred to simply as fibrils) by transmission electron microscopy requires treatment with formic acid, or formic acid followed by KOH. In transverse section, the fibrils constituting a lamella appear to be sub-parallel and woven. At intervals, the fibrils are sparse, and it is here that the lamellae separate with KOH or formic acid (Fig. 14, inset). Although chemical treatment removes the electron-opaque material that defines a lamella, it is clear that there are several sublayers of fibrils within each of them. Sections of formic acid-treated material cut at 45° to the skeletal long axis show tracts of fibrils within several adjacent lamellae. Most of the tracts appear to intersect at angles, giving them a twisted or cable-like appearance (Fig. 15). This pattern may be expected from helically wound fibrils in successive layers that are out of phase. There are no lamellae that clearly display fibrils with a preferred orientation, and there are no differences in fibril pattern when material is sectioned transversely. There are irregularly spaced regions of skeleton displaying parabolic or arced patterns, suggesting a systematic, gradual rotation of fibrils among adjacent lamellae (Fig. 15 and inset). However, these are not as obvious in the electron microscope as they are in the light microscope (see below).

Longitudinal preparations indicate that fibrils intersect and overlap one another, displaying gradual changes in orientation (Fig. 16). In some of our preparations there are abrupt changes in orientation particularly in the spines, where fibrils within layer are perpendicular to the long axis. In addition, we note again that each lamella is composed of multiple sublayers with different orientations. Because some of these sublayers may only be 10 nm thick (Figs. 14, inset; 15), thin sections of 90 nm may cut through more than one set of fibrils. Thus the TEM pattern that appears to show intersecting fibrils, may be an artefact. In the SEM, the surface pattern of fibrils within layer is clearer (Fig. 2). Spines are responsible for the large changes in orientation at the top and bottom of the figure. Figure 2 is a surface view of the multiple layers shown in Figure 10. Fibrils appear to fan out between spines but actually wind helically in the longer run.

If the etched surfaces of adjacent layers are examined using SEM, large fibrillar biases (*i.e.*, large angular deviations) can be seen resulting from layer to layer changes in fibril direction. In Figure 4, for example, 30 to 40° changes occur in adjacent lamellae. Up to 45° changes occur between layers in this species. The fracture pattern also suggests a change in fibril orientation, resulting in layers that fracture in different directions (Fig. 3). Perhaps the most revealing view of this complexly arranged skeleton is the ground thick section shown in Figure 11. This transverse section shows that the skeleton is organized into large-scale patterns that are difficult to see at the electron microscopic level. The cable-like arrangements of fibrils appear to be a limited, thin-sectional view of mul-


1

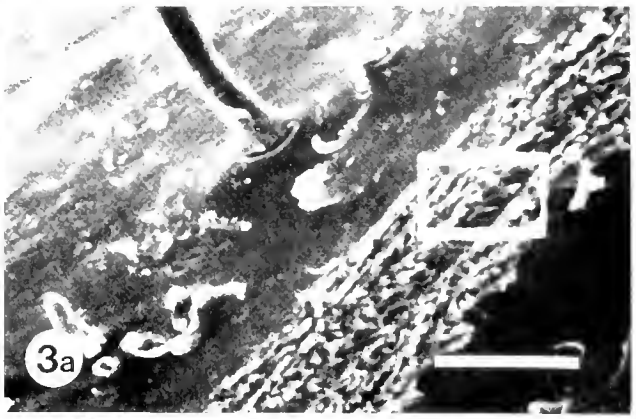
3a


3b

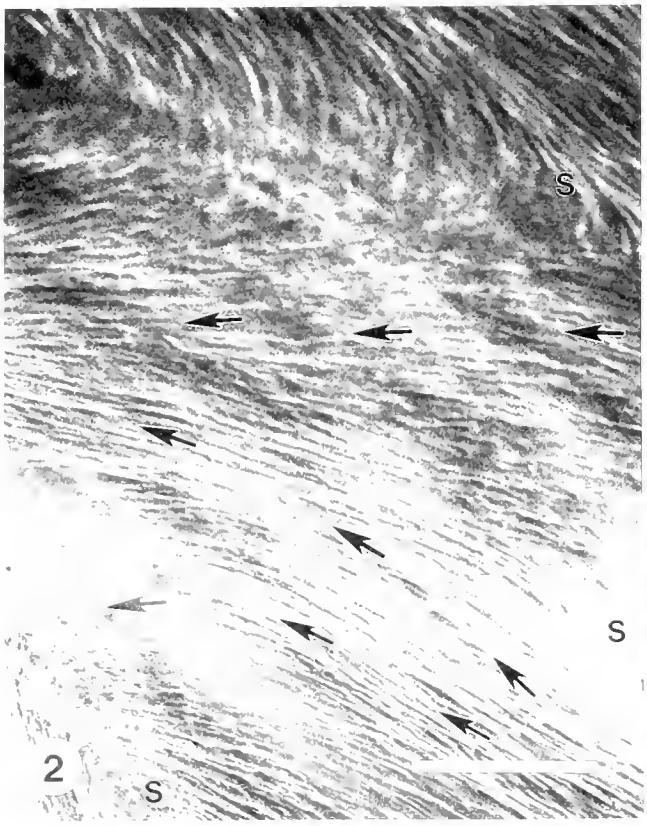
S
S
2
S


4

tiple layers, each of which has small deviations in fibril orientation. Constructive superimposition of fibrillar tracts with similar orientation (but not parallel), give rise to darker tracts of fibrils in polarized light. Regions between tracts give rise to lighter, diffuse areas, representing regions of abrupt change in fibril orientation in successive layers of skeleton. Thus, large (10–20 μ), irregularly spaced helicoids are formed that appear to rotate through 180° (Fig. 15).

Light microscopic cross sections of *A. salix* skeleton are striking in their apparent uniformity compared to *A. fiordensis*. This appearance is due to several factors. First, there are no ontogenetic differences in the staining properties of the skeleton. Instead, clusters of lamellae alternately stain ortho- and metachromatically with Toluidine blue (Fig. 12). Second, the skeleton lacks the irregular deposits of osmiophilic material seen as growth rings in the New Zealand species (compare Figs. 12 and 9). Growth rings in *A. salix* are very subtle and appear in unstained material as slight but regular differences in spacing between clusters of lamellae. This subtle structural distinction all but disappears on staining with Toluidine blue. Electron microscope observations suggest that rings correspond to a particular arrangement of fibrils (see below). This is a structural distinction in the formation of growth rings in the two species. In *A. fiordensis*, rings are osmiophilic and non-fibrillar (Goldberg, 1991). Polarized light examination of KOH treated *A. salix* branches suggest that the fibrils are wound around the long axis of the skeleton following the gradual, left handed spiral pattern of the spines. Fibrillar tracts between spines tend to be more densely packed than they are around and within the spines themselves (Fig. 13) in contrast to *A. fiordensis*. Fibrils in successive layers reinforce this pattern resulting in alternately opaque and translucent zones of birefringence parallel to the skeletal axis. This pattern suggests the absence of large fibril biases as in *A. fiordensis*.

Transverse sections of *A. salix* skeleton (TEM) are organized into a series of light and dark bands that vary in their specific characteristics, and range in thickness from 0.1 to 1.9 μm. Individual lamellae appear to correspond to these bands. The darkest regions consist of densely packed fibrils arranged in parallel within a matrix with a strong affinity for PTA. These grade into bands of intermediate electron opacity that constitute the largest volume of skeletal cross section. The intermediate bands may contain fibrils in a number of planes, including parallel. The lightest bands appear to be narrow (0.1–0.2 μm) regions where fibrils are obliquely arranged (Fig. 17). Although it is difficult to determine with certainty, growth rings appear to correspond to the juxtaposition of light and dark bands within a series of lamellae (Fig. 18). Fibrils in longitudinal sections occur in bands that remain parallel for relatively long distances, and vary in their electron opacity (Fig. 19). This structure corresponds to a section through a band of intermediate electron opacity as seen in cross section (*e.g.*, upper part of Fig. 18), where fibrils occur with minor variations in orientation.

Fracture preparations more clearly show the parallel structure of the lamellae in *A. salix* (Fig. 6). These result from the smaller fibril biases between lamellae in this species (compare with Fig. 3). In SEM preparations the surface fibrils appear to be arranged in a chevron-like pattern (Fig. 7). However, our overall view of the surface fibril pattern in this species is limited due to its less tractable response to chemical and physical manipulation. While formic acid separates the skeleton into layers (Fig. 6, inset), individual lamellae do not separate well, even with mechanical assistance. Additionally, because of the relative uniformity of fibril distribution, phase contrast and polarized light microscopy is not useful in determining the fibril pattern over long distances. Scanning electron microscopy is more successful in showing between-layer changes in fibril orientation over short distances, although etching with borohydride is not as effective in revealing surface fibril patterns in this species. Changes in fibril orientation do occur between layers, however, the fibril biases are small (<20°) compared to *A. fiordensis* (compare Figs. 4 and 8).

Material properties

The Young's modulus is a measure of stiffness or rigidity derived from a simple elastic behavior of materials

Figures 1–4. SEM preparations of *Antipathes fiordensis*.

Figure 1. Branch surface and its numerous and prominent spines; scale bar = 500 μm.

Figure 2. Borohydride-etched branch surface showing complex pattern resulting from counterclockwise winding of surface fibrils (arrows) around numerous spines (s), and the three-dimensional pattern of fibrils in spines themselves. The spine at the top of the figure depicts the change in orientation of fibrils at its base; scale bar = 10 μm.

Figure 3. Fracture pattern of formic acid-treated skeleton. 3b (scale bar = 5 μm) corresponds to the boxed area in 3a (scale bar = 50 μm). Large fibril biases between layers result in lamellae that fracture in different directions; arrows depict fibril orientation within the indicated layer.

Figure 4. Fibril biases of up to 45° (arrows) are encountered when comparing surface fibrils of successive lamellae (formic acid-borohydride preparation); scale bar = 10 μm.

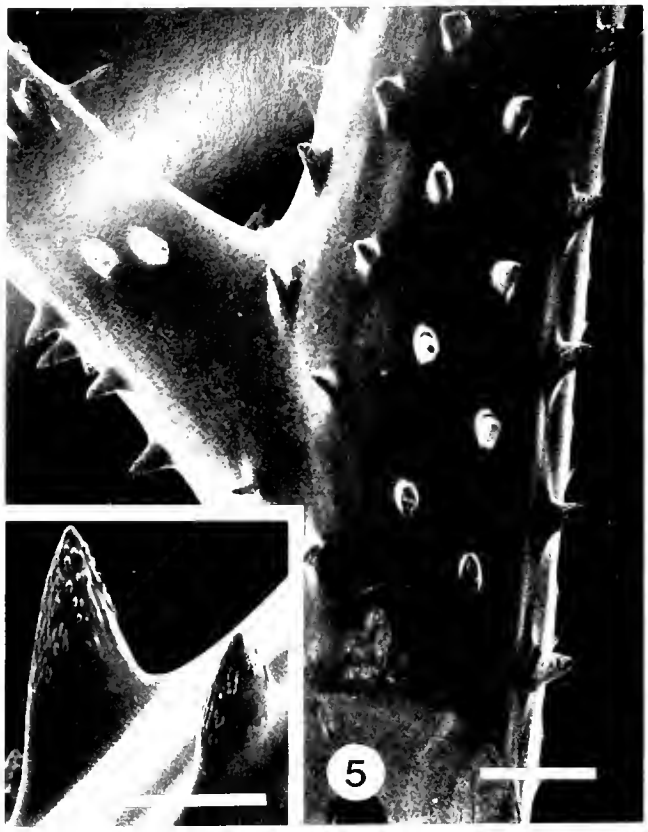
5

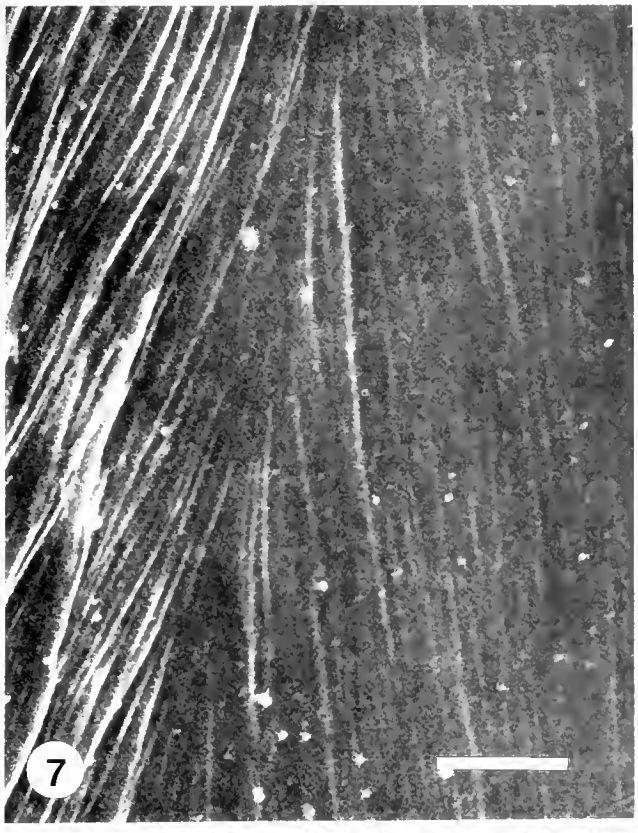
7


6


8

in which stress is proportional to strain, although this proportionality rarely occurs in most materials of biological origin (Hepburn and Chandler, 1980). We calculated Young's modulus from the sigmoidal load-deformation curve of the antipatharian skeleton (*e.g.*, Fig. 20). A small initial lag occurs as the specimen straightens under tension. This is followed by a linear region typically constituting >80% of the distance between the points of origin and failure. The terminal plastic region, where the greatest amount of deformation occurs just before failure, typically constitutes less than 12% of the stress-strain relationship. There is little deviation in the slope of the plastic region, and failure almost always occurs at the test grips. Moduli were calculated using only the linear portion of the curve, and again, using the slope of a line drawn between the origin and the point of failure. Only minor differences were noted. However, we also found that using only the linear portion was more prone to operator error. The moduli reported here were determined by the second method, which gives the average slope of the entire stress-strain relationship. This method is therefore more conservative compared to those determined solely from the slope of the more limited, linear portions of the load-deformation curve (see Bassin *et al.*, 1979; Vincent and Hillerton, 1979).

The material properties of the two antipatharians are very different (Table I, Fig. 21). In addition to being stiffer (more rigid), the skeleton of *A. salix* is more resistant to deformation under tension than *A. fiordensis* ($P < 0.0001$, for both cases). Higher density (12%) is also characteristic of *A. salix*, as is greater hardness. Hardness is a complex measure of material strength and plasticity. Although there are no absolute standards for hardness, a comparative measurement adds an additional perspective for this little-known material. The differences in skeletal hardness are not resolved on the Moh's scale because both skeletons, wet or dry, have hardnesses of 3, *i.e.*, both skeletons are only hard enough to scratch calcite. However, calcite is more readily scratched using *A. salix*, indicating that it is slightly harder than *A. fiordensis*. Microhardness testing further refines this observation, suggesting that *A. salix* is approximately 17% harder and less variable along both axes of testing compared to *A. fiordensis* (Table I).

Skeletal chemistry

We used amino acid analysis to estimate the relative proportions of skeletal chitin and protein. Standard methods of colorimetric analysis (*e.g.*, Lowry or Bradford) consistently underestimate protein levels. Chitin can not be estimated gravimetrically after "deproteination" with KOH because a variable amount of protein remains associated with the chitin after treatment. Table II summarizes these results. The skeletal tips are composed primarily of protein and chitin. Extractable lipid is both low and variable in the two species. The percent protein is greater in *A. fiordensis* ($P < 0.025$) and, conversely, there is a greater proportion of chitin in *A. salix* ($P < 0.05$). Overall, there are few differences in the amino acid composition of the skeletons (data not shown). When sequentially treated with formic acid and aqueous borohydride, some 6 to 9% of the protein is lost (Table III). Although there are some differences in protein composition resulting from this chemical treatment, the most significant change is the total destruction of tryptophan. The dominant amino acids, glycine, alanine, and histidine, are unaffected, as are the levels of glucosamine (*i.e.*, chitin). The principal effect of this reagent is the visual enhancement of chitin fibrils in the scanning electron microscope (see below).

Discussion

There are a number of commonalities between arthropod cuticle and antipatharian skeleton. Some of the general similarities in chemical composition have been described recently (Holl *et al.*, 1992). Arthropod cuticle also provides the basis of morphological comparison or contrast, because it is the most commonly studied example of chitin-protein architecture. Like antipatharian skeleton, cuticle is a composite material constructed of chitin fibrils embedded in an amorphous protein matrix. Cuticle is generally considered as a laminated structure with chitin fibrils lying in parallel within each layer. Layer-to-layer changes in fibril orientation have been characterized, ranging from the rare, totally uniform fibril orientation, to a helicoidal arrangement. Helicoids, as originally described by Bouligand (1965), are optical artefacts of arced

Figures 5–8. SEM preparations of *Antipathes salix*.

Figure 5. Branch surface showing spiral pattern of spines; scale bar = 200 μm. Inset: spines are laterally compressed and nodose; scale bar = 50 μm.

Figure 6. Fracture pattern showing parallel orientations of adjacent lamellae; scale bar = 5 μm. Inset: formic acid treatment does not separate adjacent lamellae, but separates the skeleton into thicker layers, possibly corresponding to growth rings; scale bar = 50 μm.

Figure 7. Surface fibrils, revealed by borohydride-formic acid treatment, are more unidirectional compared to *A. fiordensis*, and form convergent, chevron-like tracts; scale bar = 10 μm.

Figure 8. Adjacent lamellae display relatively small fibril biases; mean direction is depicted by arrows; treatment as in Figure 7; scale bar = 10 μm.

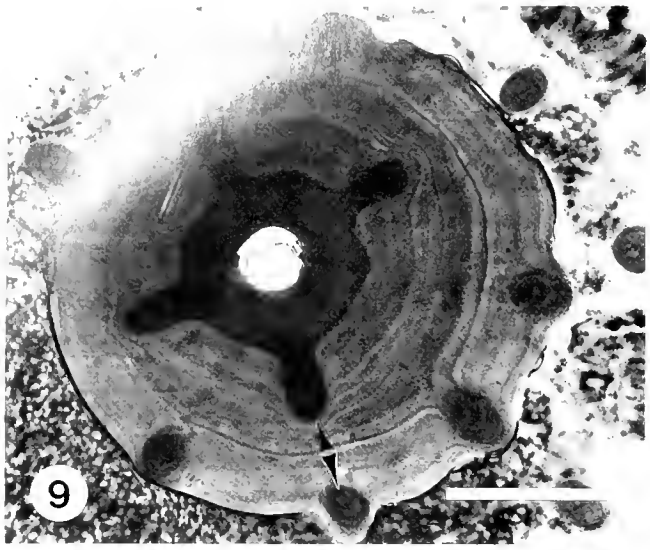
9

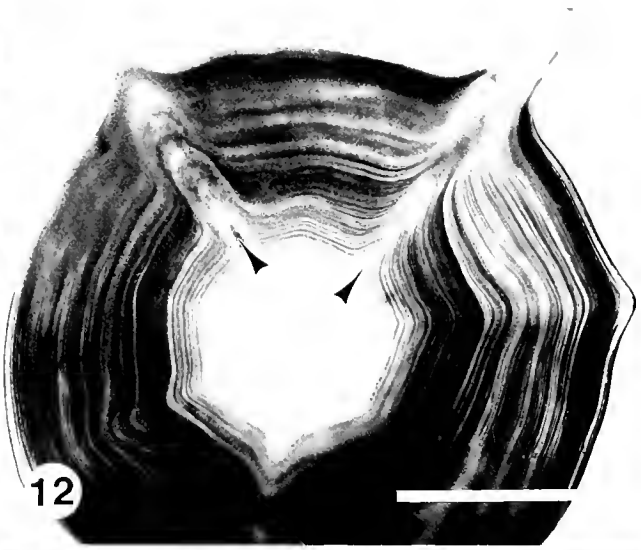
12

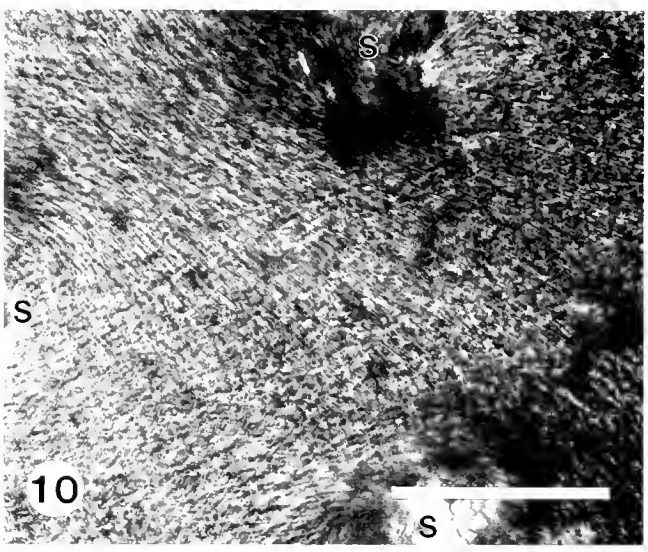
S
S
S
10

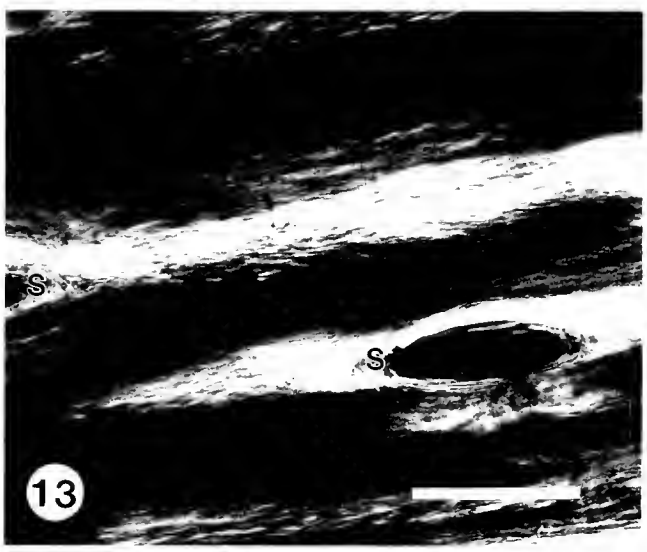
S
S
13

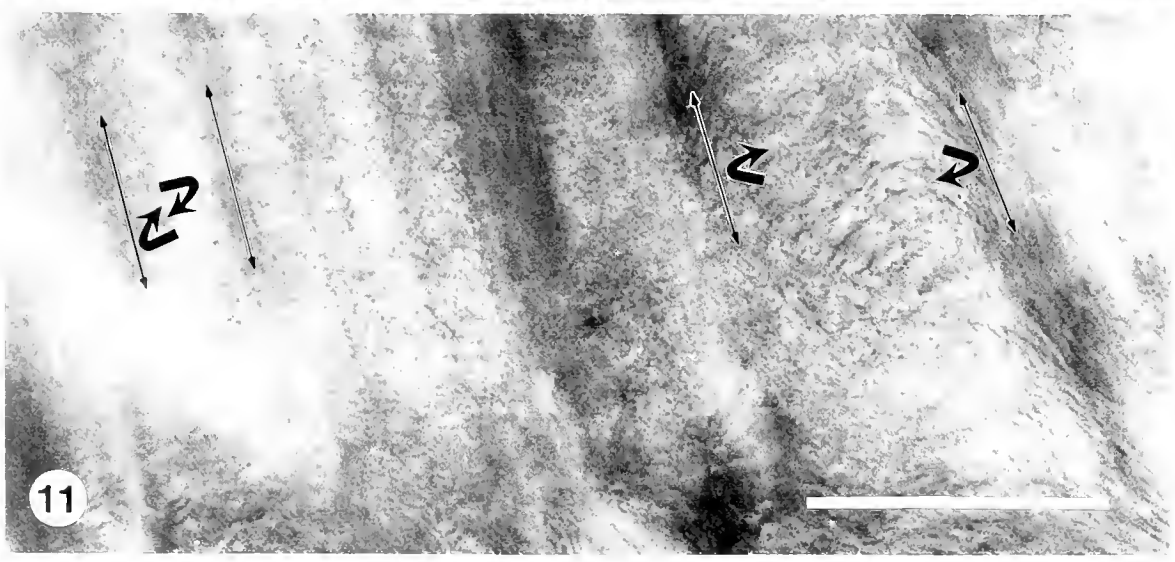
11

or parabolic fibril patterns when multiple layers of parallel fibrils are viewed obliquely or transversely. Helicoids are formed by adjacent fibril layers that appear to rotate gradually from parallel. There are several variations on this theme. Growth layers, consisting of parallel chitin fibrils formed during the day, alternate with helicoidal layers deposited at night in some insect groups (Neville and Luke, 1969). A "plywood" type of architecture can be formed by some insects when parallel layers abruptly change direction on each successive day by about 90°. Alternatively, a pseudo-orthogonal "plywood" cuticle can be formed by more gradual changes in orientation of daily parallel fibril layers. In the latter case, helicoidal layers may rotate gradually through 90° or 180° before a daily parallel layer is deposited. Finally, some insects may not deposit a daily parallel layer of chitin fibrils at all, thus producing the appearance of continuous rotation (Neville, 1967, 1970; Barth, 1973). The helicoidal model is the most common explanation of cuticular structure, especially among insects (*cf.*, Filshie, 1982; Neville, 1984; Hughes, 1987) and crustaceans (*cf.*, Bouligand, 1971; Giraud-Guille, 1984; Compere and Goffinet, 1987). Chitin helicoids have also been described from a whelk periostracum (Hunt and Oates, 1984) and the test of a tunicate (Gubb, 1975). While the helicoidal model has gained wide acceptance, agreement is not universal. Important exceptions to the parallel fibril model include the presence of vertical fibrils supporting the horizontal lamellae in some arthropods (*cf.*, Hepburn and Chandler, 1976). Others have more generally disputed the helicoidal model, suggesting that the layers of fibrils are indeed curved and are not artefactual (Dennell, 1973; Dalingwater, 1975). Helically wound and crossed chitin fibrils occur in certain insect groups but scant attention is paid to them in the modern literature.

Both antipatharian skeletons are composed of helically wound fibrils. They are unlike the crossed fibrillar chitin described from insects, which form alternating layers of left and right handed helices (Neville, 1967). Figure 22 is a composite model of fibril structure, based on our microscopic observations. *Antipathes salix* skeleton is a comparatively simple structure composed of layers with small deviations in fibril orientation. Regions of parallel fibril and sub-parallel orientation are common. Regions of abrupt change in fibril orientation may constitute optical discontinuities that appear as growth rings, but helicoidally arranged layers as such, are absent. *Antipathes fiordensis* skeleton is much more complex. Fibrils within layer exhibit a more "active" pattern. There is a considerable degree of angular change from one layer to the next, as shown in both transverse and longitudinal sections. The helicoidal arrangement of the skeleton cannot be depicted easily because the pattern is obscured by the helically wound fibrils, the pattern of spination, and the irregular thickness of skeletal layers. If these factors are taken into account, the skeleton corresponds most closely to a type D insect cuticle (Barth, 1973) characterized by a helicoidal rotation of approximately 180° between parallel (in this case low angle, cable-like) fibrils.

A helical arrangement of the fibrils provides some flexibility while preventing explosion and localized buckling under multiaxial stress (Wainwright *et al.*, 1976). However, in many helically wound structures there is a danger of delamination caused by the incompatibility of strain

Figures 9–11. Light microscope preparations of *Antipathes fiordensis*.

Figure 9. Transverse 1-μm thick section showing intensely stained (Toluidine blue) young skeleton, followed by lightly stained region marked by irregular, dark growth rings. Spines at the periphery (arrowheads) are obliquely sectioned; scale bar = 100 μm.

Figure 10. Formic acid-treated skeletal peel (unstained) examined with a combination of polarizing and phase contrast optics shows the intersecting pattern of fibrils from several skeletal layers. Surface fibrils converge around the bases of the spines (s); the long axis of the skeleton is parallel to the scale bar. Scale = 50 μm.

Figure 11. Polished transverse section showing irregularly spaced, large scale helicoids. Cable-like fibrils with acute angles constitute the helicoid boundaries (straight arrows). Apparent rotation of successive fibril layers form the helix-like structures depicted by curved arrows. Fibrils converge with a longitudinally sectioned spine at the bottom of the figure; scale bar = 50 μm.

Figures 12–13. Light microscopic preparations of *Antipathes salix*.

Figure 12. Transverse 1-μm thick section showing differential orthochromatic (dark layers) and metachromatic (light layers) staining with Toluidine blue. The skeleton of this species is composed of multiple lamellae, but does not have distinct, differentially staining growth rings; the incremental growth of spines (arrowheads) is also shown; scale = 100 μm.

Figure 13. Formic acid-treated skeletal peel (unstained) examined with a combination of polarizing and phase contrast optics shows both convergent and parallel fibrils arranged in birefringent light and dark bands. In contrast to the New Zealand species, the fibrils tend to be more densely arranged between spines (s). This view through multiple lamellae suggests that large fibril biases are not a prominent feature of this species; the long axis of the skeleton is parallel to the scale bar; scale = 50 μm.

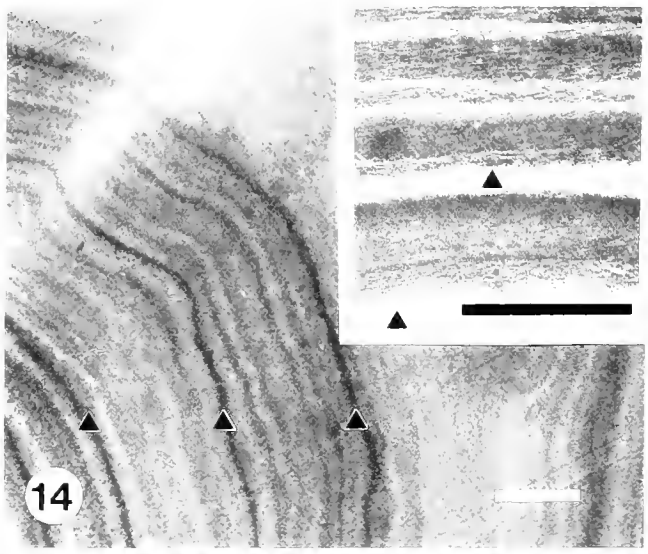

14

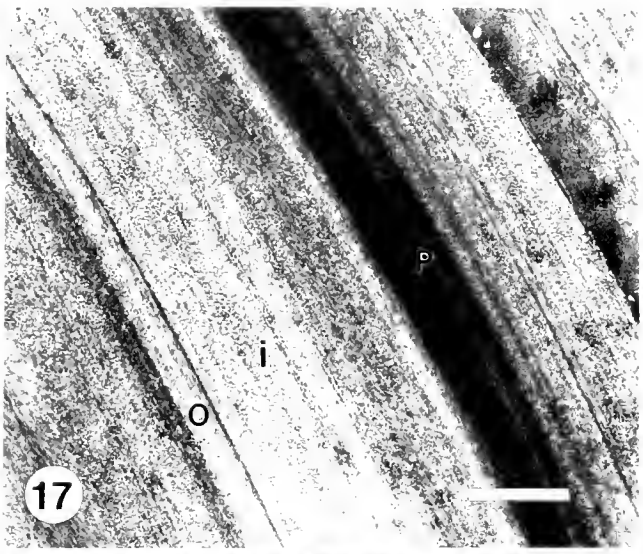

17

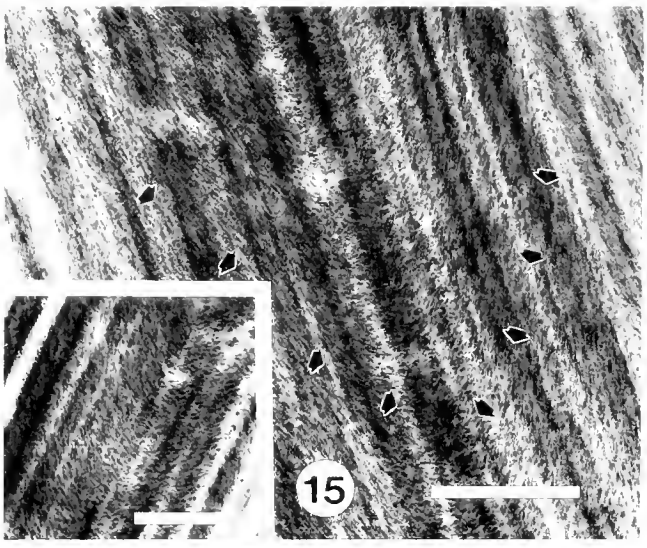

15

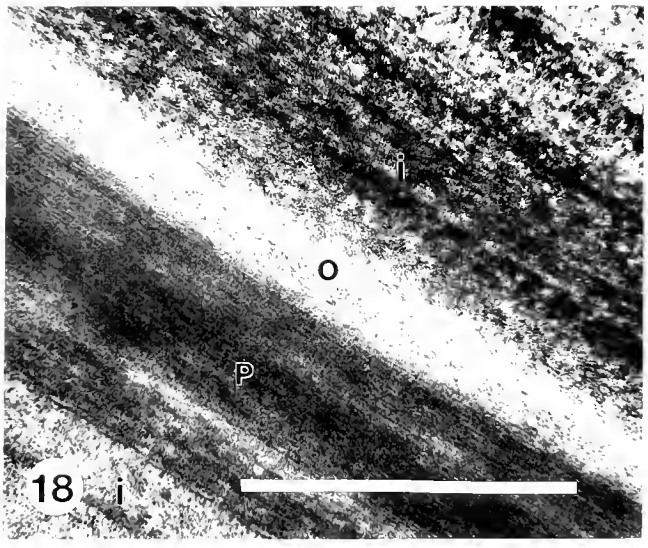

18 i

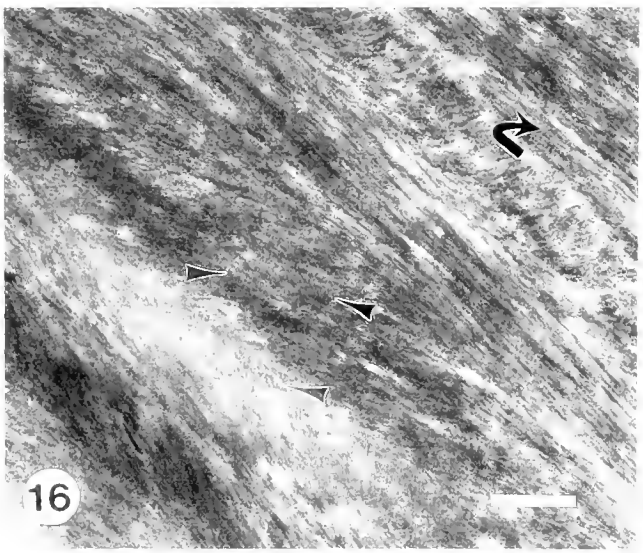

16

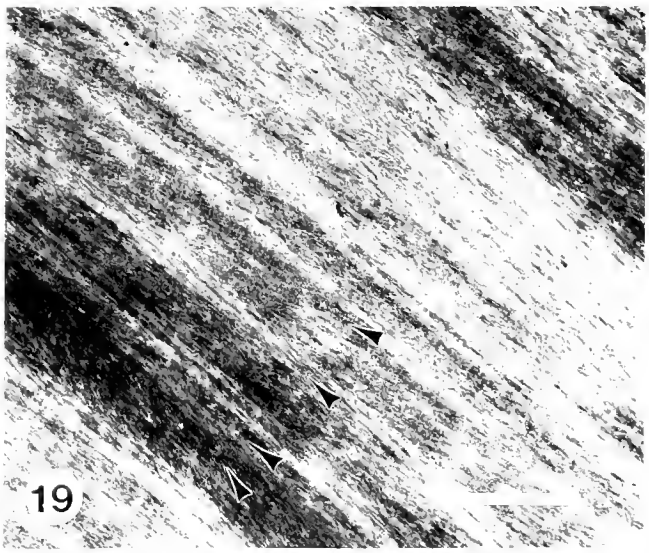

19

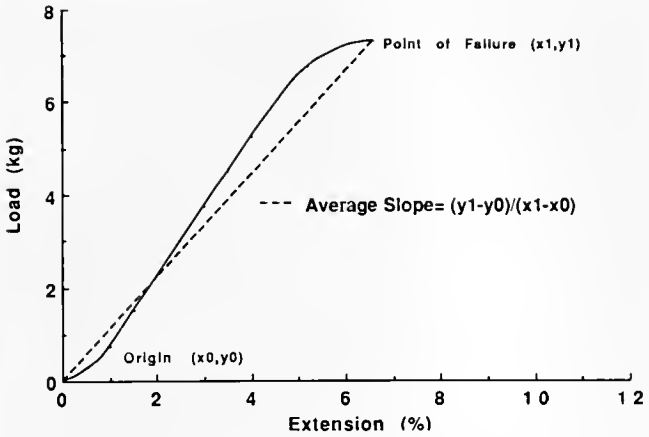

Figure 20. Typical load-deformation curve (solid line) from antipatharian skeleton depicting the method of calculating Young's modulus from the average slope (dashed line) of the stress-strain relationship. Extensibility is the percent elongation of the specimen at failure.

between adjacent layers with different fibril orientations (Wainwright *et al.*, 1976). One way of dealing with this is to allow only small angular differences between fibrils in adjacent layers as in certain types of helicoidally arranged insect cuticle. However, in antipatharian skeleton, the layers are not simple laminated structures. Because the spines are cemented and inserted layer upon layer, the helically wound skeleton is fixed at multiple points. We hypothesize that the spines increase the surface area for cementing one skeletal layer to the next. Moreover, they may play an important role as continuous rivets, preventing delamination from shear forces produced by skeletal bending and torsion. If this suggestion is correct, the presence of spines should reduce or eliminate the requirement of small fibril biases between helically wound layers.

In addition to differences in fiber patterns, there are a number of other disparities inherent in the diversity among the insect cuticles that make mechanical comparisons with black coral skeletons difficult. There are male-female differences, maturational differences, and regional differences within single cuticles. There are also differences in technique among investigators, some of whom have apparently performed mechanical testing without taking water content into account (see review by Vincent, 1980). The data given by Vincent show, not surprisingly, that stiffness values in insect cuticle vary from 1×10^6 Nm^{-2} to 17 GN m^{-2}, with a mean of 1.8 GN m^{-2} for all 28 cases. While the Young's modulus of the black corals studied here fall in line with the mean, the stiffest of insect cuticle can be as stiff as compact bone (see Hepburn and Joffe, 1976; Vincent and Hillerton, 1979). It is doubtful that antipatharian skeleton from a comparable number of species will be found with a comparable range of values.

In a composite structure, the fibrils can be expected to stiffen the more deformable matrix by reinforcing it. The degree of reinforcement should increase quickly with increasing volume to about 10–20%, irrespective of the fibril orientation, after which gains in stiffness become dispro-

---

Figures 14–16. Transmission electron microscope preparations of *Antipathes fiordensis*. Scale bars = 1.0 μm.

Figure 14. Transverse section of doubly fixed, doubly stained skeleton. Lamellae or growth layers are defined by weak osmiophilia or subtle changes in electron opacity (between triangles). Growth rings are perceived as darker or thicker regions of osmium deposition (triangles). Inset: treatment with formic acid and KOH removes protein matrix and osmiophilic material (triangles). Lamellae are composed of fibrils in a variety of orientations, and tend to separate where the fibrils may be diffuse or absent (transverse section).

Figure 15. Formic acid-treated, PTA-stained skeleton sectioned at 45°; skeletal layers consist of light and dark bands. The more prominent dark, cable-like fibrils are interpreted to result from the optical intersection of helically wound fibril layers; light regions are areas where fibrils appear to undergo rotation. Portions of larger scale helicoids, resulting from regular change in fibril bias in successive lamellae, can be seen by focusing on the overall pattern of apparent curvature (arrows). Inset: detail of a partial helicoid.

Figure 16. Formic acid-treated longitudinal section showing gradually intersecting (arrowheads) and abrupt changes in fibril orientation (curved arrow). The latter can be due to the presence of spines (compare with Fig. 2), or a section through more than one layer of fibrils; PTA stain.

Figures 17–19. Transmission electron microscope preparations of *Antipathes salix*. Scale bars = 1.0 μm.

Figure 17. Transverse section showing lamellae with differing fibrillar orientations and electron opacities. O = zone of obliquely oriented fibrils; P = region of parallel fibrils; and i = intermediate zone. Fibril orientations parallel to the long axis of the skeleton are prominent in this species.

Figure 18. Detail of cross section showing electron opaque lamella with parallel orientation followed by narrow, electron-lucent zone of obliquely oriented fibrils and zone of intermediate electron opacity with several changes in fibril orientation; symbols as above.

Figure 19. Longitudinal section showing parallel and sub-parallel orientation (arrowheads) of fibrillar tracts (compare with Fig. 7). All preparations doubly fixed; PTA stained.

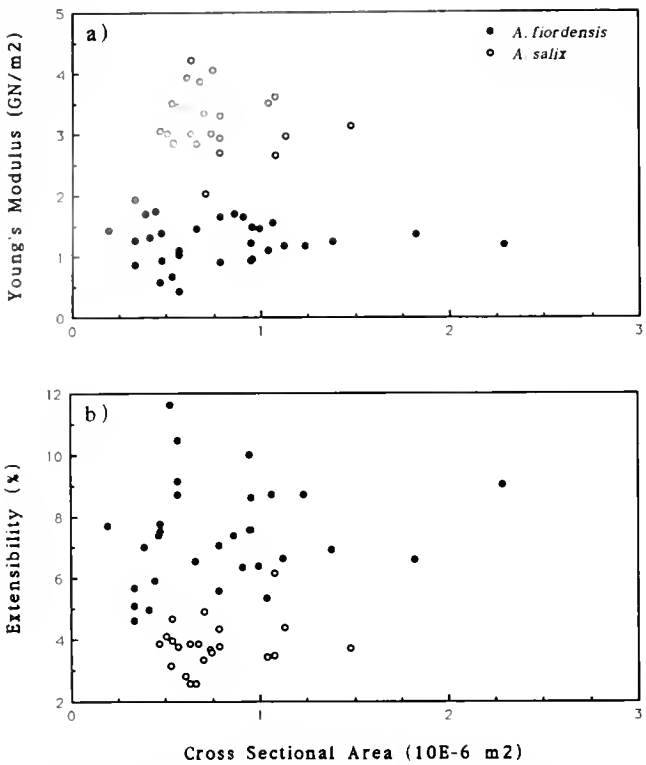

Figure 21. Scattergrams of (a) Young's modulus and (b) extensibility of the skeleton in *Antipathes fiordensis* and *A. salix* plotted against cross-sectional area. Young's modulus is determined from the average slope of the load-deformation curve (see text); extensibility is the percent elongation of the specimen at failure. The small degree of overlap in the data reflects significant differences in mechanical properties. Statistics are given in Table I.

portionately smaller (Wainwright *et al.*, 1976). Insect cuticle is highly variable in its chitin content, ranging from 4 to 60% (Vincent, 1980). In stiff cuticle, the chitin content tends to be 30 to 40% of the dry weight, while in more pliant cuticle, the chitin content tends to be higher, on the order of 50–60% of dry weight (Vincent, 1980; Hillerton, 1984). Black coral skeleton examined thus far contains a relatively low proportion of chitin, ranging from 6 to about 15% (Goldberg, 1978; this paper), and corresponds to published Young's modulus values for stiff cuticle. Although it is not yet possible to allocate mechanical properties to specific components of the skeleton, the greater chitin content of *A. salix* (~29% more than the mean of *A. fiordensis*) is within the overall range of chitin values where the difference may account for at least some of the increased skeletal stiffness.

The antipatharians are less rigid than a number of other biological materials, including wood, bone, mollusk shell, and some insect cuticle, while having a density higher than wood, lower than shell or bone, but about the same as insect cuticle (Wainwright *et al.*, 1976; Table 5.3). The ratio of Young's modulus to density (E/p) is the specific modulus, a means of assessing the stiffness per unit weight of materials. High values of specific stiffness are often considered superior to low values because they enable construction of stiffer and lighter structures. However, for antipatharians, greater flexibility per unit of density should be more important than stiffness. Thus antipatharians have a lower specific modulus compared to insect cuticle values given in Wainwright *et al.*, by having a lower modulus with about the same density (E/p = 5.1–7.9 for 2 insects, and 1.0–2.3 for *A. fiordensis* and *A. salix*, respectively). If the Young's modulus given for *Cirripathes* sp. ($E = 0.3$ GN m^{-2}) in Wainwright *et al.* (1976) is combined with our density measurement of 1.1 in *C. luetkeni* Brook from the Bahamas (see Goldberg, 1976 for description), a skeleton of even lower specific modulus results (E/p = 0.27). The Young's moduli of the two *Antipathes* species differ by more than twofold, but range from 4.1 to 10.7 times stiffer than that reported for *Cirripathes* sp. by Wainwright *et al.* (1976). Antipatharians of this genus, unlike the ones we studied, are unbranched and whip-

Table I

Material properties of antipatharian skeletons

Properties	*Antipathes fiordensis*	*Antipathes salix*	Test statistics
I) Young's Modulus (GN/m^2)	1.24 (0.360); n = 31	3.20 (0.511); n = 23	$\chi^2 = 38.89$; $P < 0.0001$
II) Extensibility (mm/cm)	7.37 (1.667); n = 31	3.84 (0.783); n = 23	$\chi^2 = 36.95$; $P < 0.0001$
III) Density (g/cm^3)	1.25 (0.096); n = 15	1.40 (0.058); n = 25	$\chi^2 = 19.45$; $P < 0.0001$
IV) Hardness (Mohs)	3	3	
V) Microhardness (HV)			
i) Long Axis	18.2 (1.473); n = 3	22.1 (0.378); n = 3	$\chi^2 = 3.857$; $P < 0.05$
ii) Short Axis	20.3 (3.342); n = 3	22.8 (0.987); n = 3	$\chi^2 = 0.429$; $P > 0.05$

Means and standard deviations (in parentheses) are provided along with numbers of observations (n). The Kruskal-Wallis One-Way ANOVA by ranks (Chi-squares corrected for ties) were calculated to note differences between the two species.

Table II

Chemical composition of antipatharian skeletal tips

Properties	*Antipathes fiordensis*	*Antipathes salix*	Test statistics
I) Water content (% dry wt.)	21.1 (0.59); n = 15	19.6 (0.72); n = 25	$\chi^2 = 20.63$; $P < 0.0001$
II) Chitin content (% org. wt.)	10.4 (2.20); n = 8	14.7 (1.25); n = 3	$\chi^2 = 5.04$; $P < 0.05$
III) Protein content (% org. wt.)	55.4 (2.93); n = 8	51.3 (0.58); n = 3	$\chi^2 = 6.00$; $P < 0.025$
IV) Lipid content (% dry wt.)	0.32 (0.70); n = 25	0.22 (0.503); n = 25	$\chi^2 = 0.32$; $P > 0.05$

Means are followed by standard deviations (in parentheses) along with numbers of observations (n). Kruskal-Wallis One-Way ANOVA by ranks (Chi-squares corrected for ties) were calculated to note differences between the two species.

like, often forming corkscrew-like shapes on cliff faces of the reef. The low Young's modulus may structurally reflect this idiosyncrasy. Unfortunately, the correlative architectural properties of this genus are unknown.

Mechanical properties of gorgonian skeleton have been reported (Goldberg *et al.*, 1984; Jeyasuria and Lewis, 1987; Esford and Lewis, 1990), and although the two systems differ structurally and chemically (collagen instead of chitin, and distinct amino acid composition among other differences) the Young's moduli of the two black corals fall within the range (1.1–9.3 GN m^{-2}) reported for the tips of 13 gorgonians by Esford and Lewis (1990). Interestingly, they found that stiffer axes were typical of species from deeper water but unlike antipatharians, gorgonian skeletons from such environments are often calcified.

Table III

Organic composition of skeletal powder after formic acid and sodium borohydride treatment compared to untreated materials

	Antipathes fiordensis	*Antipathes salix*
Amino acids		
ASP	−6.8 (*)	5.9 (**)
THR	−9.6	0.8
SER	−2.4 (ns)	6.2 (*)
GLU	6.8	10.7
PRO	−14.7	9.5
GLY	2.6 (ns)	5.3 (*)
VAL	−13.7	−18.4
MET	−40.0	−10.0
ILE	−18.6	−11.7
LEU	0.1	4.3
TYR	−13.5 (ns)	−17.3 (*)
PHE	−39.1 (**)	−14.5 (ns)
HIS	8.1 (**)	7.6 (*)
TRP	−100.0 (**)	−100.0 (*)
LYS	−56.2	−48.2
ARG	−10.6	0.1
Protein	−6.1 (ns)	−8.7 (*)
Chitin	8.4 (ns)	13.7 (*)

(ns) not significant; (*) $P < 0.05$; (**) $P < 0.025$.

Changes are noted as percent decreases (negative values) or increases (positive values) from organic composition of untreated skeleton. All values are means of three trials and statistical differences were analyzed as in previous tables.

There is a growing body of evidence showing a relationship between skeletal mechanics and ecological function. In organisms with flexible skeletons, orientation to flow can maximize efficiency of suspension feeding and minimize drag forces (reviewed by Wainwright *et al.*, 1976). In certain gorgonian corals, adaptation to flow may be recorded in the skeleton as a change in preferred orientation of fan-like species (Wainwright and Dillon, 1969; Grigg, 1972; Velimirov, 1976). In branched gorgonians the skeleton can be reinforced perpendicular to the direction of flow, by deposition of carbonate (Wainwright and Koehl, 1976; Wainwright *et al.*, 1976). Preferred orientation occurs in the Antipatharia (Warner, 1981), and there is a degree of it exhibited in *A. fiordensis*. Colonies near the mouths of the fiords, are subjected to more consistent current fields, resulting in more fan-shaped colonies. Otherwise, this species tends to branch in multiple planes (Grange, 1988). In addition, the skeleton is often elliptical in cross section, especially in the thicker branches, with the compressed sides facing the predominant current flow. In *A. salix*, there is no obvious structural asymmetry, and the colonies tend to be branched in many planes. Antipatharians generally require low rheological environments. Unlike other cnidarians, the polyps have no structural protection from the abrasive forces associated with strong current. The muscular systems of the polyps and tentacles are so poorly developed that a modest contraction is their only apparent defense against such forces (Goldberg and Taylor, 1989). Transplant experiments into relatively shallow water further suggest that abrasion is a major source of mortality (Grigg, 1965). Thus the substantial structural and mechanical properties of the black coral skeleton seem to be overdesigned for the deeper and hydrodynamically more docile zones in which antipatharians are generally found. It

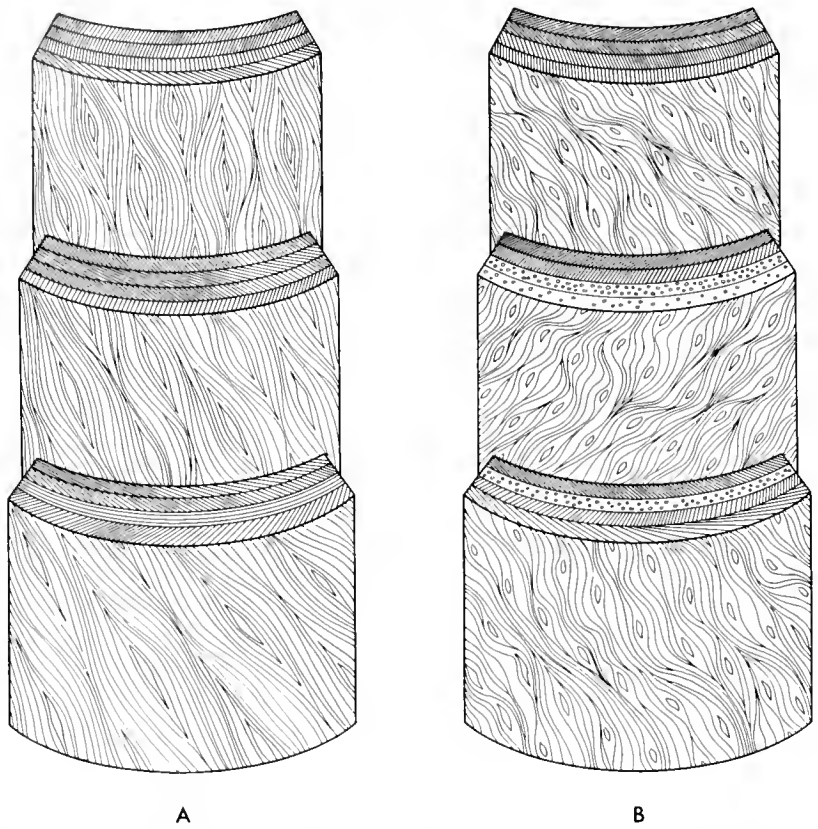

Figure 22. Composite sketch of fibril patterns. (A) *Antipathes salix* is shown with surface fibrils helically wound in an anticlockwise direction. The gradual change in the rotational sense of the winding pattern is shown in successive longitudinal sections. Spines are shown as the centers of the fibrillar pattern. Transverse sections through adjacent layers depict gradual, angular changes in fibril orientation as well as layers with little or no change. (B) *Antipathes fiordensis* is depicted with a swirling pattern of fibrils that generally tend anticlockwise. The more numerous spines are shown as focal points for the surface fibril pattern. Abrupt layer-to-layer changes in fibril orientation are characteristic of this species. No two adjacent layers have the same fibril pattern.

seems counterintuitive to find such stiff skeletons in zones of relatively low velocity water movement.

While the fit between ecological function and skeletal design is unclear, the distinction between the two species studied has shown that *Antipathes salix* is darker, harder, more dense, more hydrophobic, and stiffer than *A. fiordensis*. These material differences appear to reflect the more considerable commercial value of *A. salix* in the jewelry trade.

Acknowledgments

We thank W. Faulkner of Telectronics Pacemakers Corp. for his assistance with microhardness testing and R. Nutt for the illustrations. Both K. Gordon (Biology) and C. Levy (Mechanical Engineering) at FIU contributed substantially to the mechanical analysis. We also thank K. Gordon, K. Grange, and two anonymous reviewers for helpful comments on the manuscript. This work was supported by NSF grant OCE-8613884 (to W.G.). New Zealand coral material was obtained with the assistance of K. Grange and R. Singleton of DSIR, Wellington, and the support of the U.S.-New Zealand Cooperative Science Program, as well as funds from DSIR. The Florida Institute of Oceanography provided ship time and facilities to support the collection of Bahamian coral material. Collecting permits from the Governments of New Zealand and the Bahamas are also gratefully acknowledged.

Literature Cited

Bassin, M., G. M. Brodsky, and H. Wolkoff. 1979. *Statics and the Strength of Materials,* 3rd Ed. McGraw-Hill, Toronto.

Barth, F. G. 1973. Microfiber reinforcement of an arthropod cuticle. Laminated composite material in biology. *Z. Zellforsch.* **144:** 409–433.

Bouligand, Y. 1965. Sur une architecture torsadée répandue dans les nombreuses cuticles d'arthropodes. *C.R. hebd. Seances Acad. Sci. Paris* **261:** 3665–3668.

Bouligand, Y. 1971. Les orientations fibrillaires dans le squelette des Arthropods 1. L'example des crabes, l'arrangement torsadé des strates. *J. Microsc. (Paris)* **11:** 441–472.

Bouligand, Y. 1972. Twisted fibrous arrangements in biological materials and cholesteric metaphases. *Tissue & Cell* **4:** 189–217.

Compere, P., and G. Goffinet. 1987. Aspects ultrastructureaux et fonctionnels de diverses régions cuticulaires non minéralisées d'un crustacé décapode, *Carcinus maenas*. *Ann. Soc. R. Zool. Belg.* **117:** 159–173.

Dalingwater, J. E. 1975. The reality of arthropod cuticular laminae. *Cell Tissue Res.* **163:** 411–413.

Dennell, R. 1973. The structure of the cuticle of the shore crab, *Carcinus maenas*. *Zool. J. Linn. Soc.* **52:** 159–163.

Esford, L. E., and J. C. Lewis. 1990. Stiffness of Caribbean gorgonians (Coelenterata, Octocorallia) and Ca/Mg content of their axes. *Mar Ecol. Prog. Ser.* **67:** 189–200.

Filshie, B. K. 1982. Fine structure of the cuticle of insects and other arthropods. Pp. 281–312 in *Insect Ultrastructure*, Vol. 1, R. King and H. Akai, eds. Plenum Press, New York.

Giraud-Guille, M. M. 1984. Fine structure of the chitin-protein system in the crab cuticle. *Tissue & Cell* **16:** 75–92.

Goldberg, W. M. 1976. A comparative study of the chemistry and structure of gorgonian and antipatharian coral skeletons. *Mar. Biol.* **35:** 253–267.

Goldberg, W. M. 1978. Chemical changes accompanying maturation of the connective tissue skeletons of gorgonian and antipatharian corals. *Mar. Biol.* **49:** 203–210.

Goldberg, W. M. 1991. Chemistry and structure of skeletal growth rings in the black coral *Antipathes fiordensis* (Cnidaria, Antipatharia). *Hydrobiologia* **216:** 403–409.

Goldberg, W. M., J. Makemson, and S. B. Colley. 1984. *Entocladia endozoica* sp. nov., a pathogenic chlorophyte: structure, life history, physiology and effect on its coral host. *Biol. Bull.* **166:** 368–383.

Goldberg, W. M., and G. T. Taylor. 1989. Cellular structure and ultrastructure of the black coral *Antipathes aperta*: 1. Organization of the tentacular epidermis and nervous system. *J. Morphol.* **202:** 239–253.

Grange, K. R. 1985. Distribution, standing crop, population structure and growth rates of black coral in the southern fiords of New Zealand. *NZ J. Mar. Freshw. Res.* **19:** 467–475.

Grange, K. R. 1988. Redescription of *Antipathes aperta*. Totton, (Coelenterata: Antipatharia), an ecological dominant in the southern fiords of New Zealand. *NZ J. Zool.* **15:** 55–61.

Grange, K. R. 1990. *Antipathes fiordensis*, a new species of black coral (Coelenterata: Antipatharia) from New Zealand. *NZ J. Zool.* **17:** 279–282.

Grigg, R. 1965. Ecological studies of black coral in Hawaii. *Pac. Sci* **19:** 244–260.

Grigg, R. W. 1972. Orientation and growth in sea fans. *Limnol. Occanogr.* **17:** 185–192.

Gubb, D. 1975. A direct visualization of helicoidal architecture in *Carcinas macnas* and *Halocynthia papillosa* by scanning electron microscopy. *Tissue & Cell* **7:** 19–32.

Hackman, R. H., and M. Goldberg. 1971. Studies on the hardening and darkening of insect cuticles. *J. Insect Physiol.* **17:** 335–347.

Hepburn, H. R., and H. D. Chandler. 1976. Material properties of arthropod cuticles: the arthrodial membranes. *J Comp. Physiol* **109:** 177–198.

Hepburn, H. R., and H. D. Chandler. 1980. Materials testing of arthropod cuticle preparations. Pp. 1–44. in *Cuticle Techniques in Arthropods*, T. A. Miller, ed. Springer-Verlag, New York.

Hepburn, H. R., and I. Joffe. 1976. On the material properties of insect exoskeletons. Pp. 209–235 in *The Insect Integument*, H. R. Hepburn, ed., Elsevier, New York.

Hickson, S. J. 1924. *An Introduction to the Study of Recent Corals.* Manchester University Press, Longmans, Green & Co., London. 257 p.

Hillerton, J. E. 1984. Cuticle: mechanical properties. Pp. 626–637 in *Biology of the Integument 1. Invertebrates*, J. Bereiter-Hahn, A. G. Matolsky, and K. S. Richards, eds. Springer-Verlag, New York.

Hillerton, J. E., S. E. Reynolds, and J. F. V. Vincent. 1982. On the indentation hardness of insect cuticle. *J. Exp. Biol.* **96:** 45–52.

Holl, S. M., J. Schaefer, W. M. Goldberg, K. J. Kramer, T. D. Morgan, and T. L. Hopkins. 1992. Comparison of black coral skeleton and insect cuticle by a combination of carbon-13 NMR and chemical analyses. *Arch. Biochem. Biophys.* **292:** 107–111.

Hughes, P. M. 1987. Insect cuticular growth layers seen under the scanning electron microscope: a new display method. *Tissue & Cell.* **19:** 705–712.

Hunt, S., and K. Oates. 1984. Chitin helicoids accompany protein helicoids in the periostracum of a whelk, *Buccinum*. *Tissue & Cell* **16:** 565–575.

Jeyasuria, P., and J. C. Lewis. 1987. Mechanical properties of the axial skeletons on gorgonians. *Coral Reefs* **5:** 213–219.

Neville, A. C. 1967. Chitin orientation in cuticle and its control. *Adv. Insect Physiol.* **4:** 213–286.

Neville, A. C. 1970. Cuticle ultrastructure in relation to the whole insect. *Symp. R. Entomol. Soc. Lond.* **5:** 17–39.

Neville, A. C. 1984. Cuticle: organization. Pp. 611–625 in *Biology of the Integument 1. Invertebrates*, J. Bereiter-Hahn, A. G. Matolsky, and K. S. Richards, eds. Springer-Verlag, New York.

Neville, A. C., and B. M. Luke. 1969. A two-system model for chitin-protein complexes in insect cuticles. *Tissue & Cell* **1:** 689–707.

Opresko, D. M. 1972. Redescription and reevaluations of the antipatharians described by L. F. De Pourtales. *Bull. Mar. Sci.* **22:** 950–1017.

Simpson, R. J., M. R., Neuberger, and T. Y. Liu. 1976. Complete amino analysis of protein from a single hydrolysate. *J. Biol. Chem.* **251:** 1936–1940.

Velimirov, B. 1976. Variation in growth form of *Eunicea cavolinii* Koch (Octocorallia) related to water movement. *J. Exp. Mar. Biol. Ecol.* **21:** 109–117.

Vincent, J. F. V. 1980. Insect cuticle: a paradigm for natural composites. *Symp. Soc. Exp. Biol.* **34:** 183–210.

Vincent, J. F. V., and J. E. Hillerton. 1979. The tanning of insect cuticle—a critical review and a revised mechanism. *J. Insect Physiol.* **25:** 653–658.

Wainwright, S. A., and J. R. Dillon. 1969. On the orientation of sea fans (genus *Gorgonia*). *Biol. Bull.* **136:** 130–139.

Wainwright, S. A., and M. A. R. Koehl. 1976. The nature of flow and the reaction of benthic Cnidaria to it. Pp. 5–21 in *Coelenterate Ecology and Behavior*, G. O. Mackie, ed. Plenum Press, New York.

Wainwright, S. A., W. D. Biggs, J. D. Currey, and J. M. Gosline. 1976. *Mechanical Design in Organisms.* Edward Arnold Publ. Ltd., London. 423 pp.

Warner, G. F. 1981. Species descriptions and ecological observations of black corals (Antipatharia) from Trinidad. *Bull. Mar. Sci.* **31:** 147–163.

Wood, E. M., and S. M. Wells, 1988. The Marine Curio Trade: Conservation Issues. A report for the Marine Conservation Society, Herefordshire, England. Pp. 1–120.

Reference: *Biol. Bull.* **182:** 210–220. (April, 1992)

Adult Plasticity and Rapid Larval Evolution in a Recently Isolated Barnacle Population

PETER T. RAIMONDI

The Marine Science Institute and Department of Biological Sciences, University of California, Santa Barbara, California 93106

Abstract. *Balanus amphitrite*, a common barnacle species, was introduced into the landlocked Salton Sea in 1943 or 1944. In 1949, *Balanus amphitrite* from the Salton Sea was classified as the subspecies, *Balanus amphitrite saltonensis*, based upon morphological differences between Salton Sea and coastal individuals. This classification was maintained following an investigation of the *Balanus amphitrite* complex in 1975. Such a designation implies that the morphological divergence is underlain by genetic differences. Using field and laboratory transplantations, I tested the alternative hypothesis that the observed morphological divergence in the adult stage of *Balanus amphitrite* was the result of phenotypic plasticity. The results show that the divergence in the examined adult characters is in fact due to environmentally induced phenotypic plasticity. There were also phenotypic differences between larvae from the Salton Sea and those from coastal habitats that only became apparent during experimentation with the adult stage. Here, however, experimental results suggest that the divergence was due to an evolutionary process, probably selection. These results also provide the basis for two slightly precautionary conclusions: (1) the observation that individuals living in typical and novel habitats differ cannot even weakly indicate a cause for the difference, and (2) a consideration of the divergence of populations is incomplete if all of the life history stages of the organism are not studied.

Introduction

One of the continuing challenges in evolutionary ecology is to determine the genetic contribution to phenotypic variation among populations. Two general, and non-independent processes can cause such phenotypic differentiation (Gould and Johnson, 1972; Berven *et al.*, 1979; Falconer, 1989); implicitly assumed in both cases is that, within a species, all individuals share a common ancestor and, therefore, are derived from the same ancestral genotype. First, populations may evolve differently (*evolution*). Second, even when the gene frequencies of two populations do not differ, phenotypic differences may result from plasticity in some traits (*phenotypic plasticity;* see Smith-Gill, 1983; West-Eberhard, 1989 for a discussion of the forms of phenotypic plasticity). The two processes may also interact to produce phenotypic variation among populations.

The distinction between phenotypic differentiation by evolutionary mechanisms and differentiation resulting from phenotypic plasticity cannot be made on the grounds that the latter has a non-genetic basis (West-Eberhard, 1989). Phenotypically plastic responses (to the environment) have as much genetic basis as do other less plastic characters, and plasticity is therefore a trait subject to evolutionary change (Bradshaw, 1965; Williams, 1966; Schlichting, 1986; Macdonald *et al.*, 1988; West-Eberhard, 1989). The distinction is simply that evolution is a characteristic of populations, whereas plasticity is a characteristic of individuals (after Lewontin, 1957). Thus, for populations in which individuals exhibit no plasticity, phenotypic modification as a response to the environment is possible only at the level of the population (across generations). In contrast, for populations in which individuals exhibit plastic characters, phenotypic modification in response to the environment is possible at the level of the individual (within a generation).

Either as untidy noise in complicated genetic systems as it was once regarded (see West-Eberhard, 1989), or as a selectable trait (Schlichting, 1986), plasticity is important to measure. This is because without determining the contribution of phenotypic plasticity, the adaptive significance

Received 13 May 1991; accepted 6 January 1992.

of phenotypic variation cannot be assessed (Berven *et al.*, 1979). In this study I investigated whether evolutionary change or phenotypic plasticity was responsible for the observed phenotypic variation between two Californian populations of the barnacle, *Balanus amphitrite*. One population was from a typical coastal (harbor) habitat in San Diego, California, the other was recently isolated in a novel environment, the Salton Sea.

The Salton Sea is a recently formed landlocked body of saline water, the largest body of water in California. Its average size is 55 by 24 kilometers, but the dimensions vary considerably (Carpelan, 1961a). The genesis and recent history of the Salton Sea have created an environment that is in many ways different from an open marine environment (Carpelan, 1961b) and yet supports a simple, but fascinating, community of introduced marine species. In 1904–1905, a series of floods on the Colorado and Gila rivers breached the headworks of an irrigation channel. For two years these rivers, which normally drain into the Gulf of California, emptied into the Salton Sink, a landlocked sub-sea level basin in southeastern California, and thus formed the Salton Sea. Since 1907, when the headworks were repaired, the level of the Salton Sea has been maintained by irrigation water, and its salinity has risen from 3.65‰ (Carpelan, 1961b) to about 43‰ (Anonymous, 1989); the latter value is between 5 and 8‰ greater than is typical for ocean water. The visibility (usually less than 1 m in the Salton Sea), ionic composition, chlorinity, pH, dissolved oxygen, and temperature fluctuations (10–36°C) of Salton Sea water differ from those of ocean water (Carpelan, 1961b; Raimondi, pers. obs.); because it is an inland body of water, tidal fluctuations in the Salton Sea are trivial.

Balanus amphitrite was first noticed in the Salton Sea in about 1943–1944. Apparently *B. amphitrite* individuals were transported from the San Diego area by air during Naval exercises, as adults on mooring buoys or ropes (Cockerall, 1945; Newman and Abbott, 1980), or as larvae in the bilge water of Naval flying boats (Hilton, 1945). By late 1944 they were ubiquitous: ". . . they were already multiplying so fast that a stick or board only had to be in the water a few days before a crust of minute barnacles started to form." (from Hilton, 1945). "Barnacles now seem to outnumber all other forms of life, both vertebrate and invertebrate, found in the Salton Sea." (from Cockerall, 1945).

In 1949, the Salton Sea population was described as the subspecies *Balanus amphitrite saltonesis* (Rogers, 1949). Subspecific designation was supported by a monograph by Henry and Mclaughlin (1975) on the barnacles of the *Balanus amphitrite* complex; the authors distinguished between *Balanus amphitrite amphitrite* and *Balanus amphitrite saltonensis* on the basis of a multivariate analysis of 15 morphological characters of individuals taken from the field. However, Newman and Abbott (1980) suggested that because the Salton Sea form was also found in a population from Wilmington Harbor (Pacific coast), the difference was ecotypic. Flowerdew (1985) has recently recommended, based upon an electrophoretic investigation of 31 alleles at 11 loci, that the subspecies designation for the Salton Sea population be removed. He found that the values from both indices of *genetic identity* (I) and *genetic distance* (D) were in the range of variation expected between conspecific populations (Nei, 1972). He also concluded that there was no "significant genetic differentiation" of *Balanus amphitrite saltonensis* from *Balanus amphitrite amphitrite*. This implies that no evolutionary divergence could have occurred between the populations, which is incorrect. Nonsignificant I and D values should only be viewed as not refuting the null hypothesis that there is no divergence between populations for the tested alleles (Richardson *et al.*, 1986). Indeed, there are cases of apparently separate (good) species showing no electrophoretic divergence (Avise *et al.*, 1975).

My initial interest was to determine whether the *observed* morphological divergence between Salton Sea and coastal adults (Henry and Mclaughlin, 1975) was due to environmental factors. As the samples used in this initial study came from field collections, there was no way to determine the contribution of the environment to the divergence. In the present study I made no attempt to evaluate any adult character other than those that had been described as differing between the two populations. This was because: (1) I was interested in determining the basis for the differentiating characters, and (2) the selection of additional characters would have been largely unmotivated, because, unlike larvae (see following), when adults from different populations were reared under experimental conditions, they could not be distinguished.

While evaluating the mechanisms determining adult morphological divergence, I found a number of differences in the larvae of the two populations. The basis of these differences was also examined.

Materials and Methods

Study organism, sites, and general methods

Balanus amphitrite is a moderately sized bay barnacle [average basal diameter is between 15 and 20 mm (Newman and Abbott, 1980)], with a virtually world-wide distribution (Henry and Mclaughlin, 1975). Like most thoracican barnacles, it is a simultaneous hermaphrodite (Strathmann, 1987), and fertilized eggs are brooded in the mantle cavity of the parent until they become at least stage one nauplius larvae, when they are expelled into the water. In acorn barnacles such as *Balanus amphitrite*, there are typically seven larval stages (Strathmann, 1987): six naupliar stages (feeding) followed by the final cyprid

stage (non-feeding). All stages are potentially planktonic, but stage one nauplii will often stay within the mantle cavity of the parent, making stage two nauplii the first planktonic stage (Raimondi, pers. obs.).

Adults were collected from three locations: (1) Salton Sea, near North Shore, (2) Mission Bay, California, and (3) Beaufort, North Carolina (larvae from these individuals represented a second coastal population). After collection, individuals were maintained in the laboratory at a water temperature of 20–23°C, and were fed a mixed diet of brine shrimp and the diatom, *Skeletonium costatum* (see Rittschof *et al.*, 1984). As individuals died, new ones were brought in from the field so that 300–500 adults per population were maintained at all times. Adults were induced to expel brooded larvae by a combination of overfeeding and direct bright light. Expelled larvae could then be attracted by a light source and collected.

Larvae were grown in culture at 27–28°C on a diet of *Skeletonium costatum* (see Rittschof *et al.*, 1984, for details of culturing techniques). Larvae from each population were grown in separate containers (usually 3000–5000 per population in 10 l of seawater). The larvae from each of these rearing events were called a batch. Usually, batches of larvae from all populations were reared simultaneously. With this protocol, individuals could not be considered replicates for among-population comparisons, because the effect of batches could not be separated from the effect of populations. Hence, for the examined larval characters, the average value for the individuals within each batch was used as the replicate unit.

All of the larvae used in the experiments described below were reared at the Duke University Marine Laboratory in Beaufort, North Carolina. Upon metamorphosis to the cyprid stage, individuals were collected and shipped live in cold packs, via overnight delivery, to the University of California at Santa Barbara.

Adult characters

As stated, Henry and Mclaughlin (1975) compared the Salton Sea population with coastal populations using a multivariate analysis of 15 morphological characters. The statistical difference between populations was largely due to six ratios of four measurements of the tergum (Table I, Fig. 1). To determine the contribution of environmental factors to the morphological divergence, as manifested in these ratios, I did the following experiment. [The best method of determining whether the morphological divergence between populations was due to environmental differences would have been to reciprocally transplant newly settled individuals from one location to the other (Mission Bay to Salton Sea, and vice versa). Legally and ethically this could not be done].

Cyprids from both the Salton Sea and Mission Bay brood stocks (see above) were allowed to settle on 10×10 cm clay tiles in the laboratory and raised to maturity on those tiles in two environments: "lab," and "lagoon" (the rationale for having two experimental habitats is given below). The density of settlers was about 1 cm^{-2}. Lab individuals were grown under laboratory conditions in the running unfiltered seawater system at the University of California at Santa Barbara. Water temperature during the experiment was about 20°C. Lagoon individuals were raised at the same time as the lab individuals shallow salt water lagoon (approximately 10 hectacres in size) on the campus of the University of California at Santa Barbara, however the water temperature in the lagoon during the experiment varied between 25 and 28°C. The lagoon is separated from the ocean by a sandy barrier through which water, but not plankton, can pass. Salinity in both environments was 32–33‰ during the experiment. No spontaneous (additional) settlement of *Balanus amphitrite* occurred in either the lab or lagoon.

Lab individuals were fed a mixture of brine shrimp and *Skeletonium* (see above); lagoon individuals fed upon the natural plankton in the lagoon. When the lab and lagoon individuals had grown to 6 to 8 mm basal diameter, they were collected. Individuals of the same size were also collected from both the Salton Sea and Mission Bay; these were the "field populations" in all comparisons. In summary, there were six populations of barnacles: Mission Bay—field, lab, and lagoon; and Salton Sea—field, lab, and lagoon.

From the several hundred individuals reared or collected from each population, 19–54 were randomly and sequentially selected, and from each the tergum was removed and placed individually in a small container of bleach. This procedure removed all tissue from the calcareous mass. Differences in sample size reflect differences among populations in the variability associated with measurements (see Sokal and Rohlf, 1981). Each tergum was drawn using dissecting microscopic and camera lucida projection. From the drawings, measurements of the four tergal dimensions were made and tergal ratios were calculated (Table Ia). Ratios were compared among populations using a multivariate analysis of variance. Ratios were used so the analysis would be comparable to that done in the original work by Henry and Mclaughlin (1975), which described the morphological divergence. However, there are convincing arguments that the use of ratios in morphometric analyses might lead to spurious interpretation of data (Atchley *et al.*, 1976). For this reason, I also compared populations using the four characters (not the ratios, Table Ib) in a multivariate analysis of covariance, as advocated by Atchley *et al.* (1976).

Two experimental habitats were tested because plasticity can be a heritable trait, and the degree of expressible plasticity, if any, might therefore have differed between populations. At the extreme, one population might be

plastic for the examined characters and the other might not be. With only one experimental habitat, there would have been no *a priori* way to control for this possibility. In the following discussion I assume that phenotypic plasticity, if any, will be in the form of phenotypic modulation (Smith-Gill, 1983); this is a reasonable assumption for characters like the ones examined (Table 1). Suppose that, in addition to the field populations, there were only the lab populations, and that *a posteriori* analyses indicated: (1) no difference in the examined characters between the Salton Sea and Mission Bay lab populations, (2) no difference between the lab populations and the Mission Bay field population, and (3) that the lab and Mission Bay field populations were all different from the Salton Sea field population. Under this scenario there would be no basis to support the hypothesis that the Salton Sea population was plastic for the examined characters but the Mission Bay population was not, over the alternative hypothesis that both populations were plastic and that lab conditions are similar to conditions in Mission Bay. With the inclusion of a second experimental habitat in the design, the former hypothesis could be ruled out if the Mission Bay lagoon population differed (in the examined characters) from the Mission Bay lab and field populations. If such differences were not observed, then plasticity in the examined characters would not be supported for in the Mission Bay population. A problem could arise if lab, lagoon, and Mission Bay habitats were all similar in the characteristic that induced the plastic response. The test of this would be the comparison of Salton Sea lab and lagoon populations. As the Salton Sea population, in this hypothetical case, was already shown to be plastic, if the examined characters did not differ between the two experimental populations it would suggest that the two habitats were similar in a critical way. Other possibilities concerning the degree of plasticity between populations could be addressed following similar logical steps.

Larval characters

Three characteristics of the cultured larvae differed between the Salton Sea and Mission Bay populations: (1) cyprid pigmentation—Salton Sea cyprids were unpigmented and white, whereas Mission Bay cyprids were greenish-brown, (2) cyprid length—Salton Sea cyprids were larger than those from Mission Bay, and (3) duration in naupliar stages—individuals from the Salton Sea took longer to become cyprids than did individuals from Mission Bay. I did the experiment described below to assess the contribution of environmental factors to the divergence in these larval characters and to correct for a limitation of my initial observations: I did not know if Mission Bay larvae were representative of coastal larvae in general. Although Henry and Mclaughlin (1975) surveyed adult characteristics for a number of *Balanus amphitrite* populations and found that coastal individuals were similar, there have been no comparisons of larval characteristics across populations for this species. Hence, I knew that Mission Bay adults were representative of typical coastal populations for the examined characters, but I had no idea about the scale of phenotypic differentiation among populations of larvae.

I compared cyprid length and pigmentation (color), and duration in the naupliar larval stages, of individuals from the Salton Sea, Mission Bay, and Beaufort, North Carolina, that were reared in a laboratory under identical environmental conditions. Beaufort larvae were compared to ones from Mission Bay to determine the extent of divergence between geographically well-separated coastal populations (*i.e.,* Atlantic *vs.* Pacific populations). Two categories of larvae were used in experimentation: G1 and G2. G1 larvae were progeny of adults brought from the field to the lab and used as brood stock. To minimize the effect of the parental environment, the first release of larvae, which may have developed within the brooding adults in the field, was not used. Some of the G1 larvae were raised to maturity under laboratory conditions and their progeny, G2 larvae, were also examined as a further control of residual parental effects. No G2 Beaufort larvae were cultured because comparisons of Mission Bay G1 and Beaufort G1 larvae indicated that these two coastal populations did not differ for the examined larval characters.

There are two general methods for defining and measuring color (from Chamberlin and Chamberlin, 1980): (1) visual comparison with a standard that is accepted as a reference, and (2) instrumental measurement of the fundamental make-up of the constituent parts of the color in terms of the relative contribution of absorption and reflectance of each wavelength. Both methods were used.

For each batch of cyprids, 2000–3000 from each population were put in separate test tubes (cyprids from each population in one test tube) and chilled to 6°C. This procedure did not damage the larvae, and it caused them to congregate in the bottom of the tubes. The color of the mass of cyprids was then compared to standards contained in the *Methuen Handbook of Colour* (Kornerup and Wanscher, 1978). No statistics are possible for this type of color definition, therefore the Methuen coding will be reported for reference.

To quantify an aspect of coloration, microspectrophotometry was performed on two batches of each larval population. In initial sampling I found that there was divergence in light transmittance between Salton Sea and coastal populations in the range of 450 to 700 nanometers. For logistical reasons I decided to concentrate comparisons on a particular wavelength and chose 510 nanometers. Transmittance was measured through a 40 × 40

Table Ia

Morphological characters used in the multivariate analysis of variance (MANOVA; explanation for the two tests is found in the text). See Figure 1

1) The width of the tergal spur (sw)/the length of the basal margin (bm).
2) The distance from the basiscutal angle to the margin of the spur (aw)/the length of the tergal spur (sl).
3) sl/sw.
4) aw/sw.
5) aw/bm.
6) sl/bm.

Table Ib

Morphological characters used in the multivariate analysis of covariance (MANCOVA). Basal margin (bm) was used as the covariate. See Figure 1

1) The width of the tergal spur (sw).
2) The distance from the basiscutal angle to the margin of the spur (aw).
3) The length of the tergal spur (sl).

μm section in the middle of each cyprid. Light intensity was standardized prior to each measurement.

Cyprid length was measured with a compound microscope and micrometer. The final larval character that was examined, the rate of larval development, required individuals to be drawn from culture and viewed microscopically. This process can damage larvae and potentially can introduce bacteria or ciliates to the culture. To minimize the risk of larval damage or culture contamination, cultures were checked only once each day to determine the developmental stage of the larvae.

Results

Adult characters

Tergal plate ratios or dimensions (Table Ia–b, Fig. 1) for the six populations were compared in MANOVA and MANCOVA procedures and there was a significant difference between populations (Table II). There were no qualitative differences between the results of the two analyses (MANOVA, MANCOVA), indicating that the use of ratios would not, for this data set, lead to spurious interpretations. Comparisons among populations clearly showed where the differences were (Table II). The field populations (Salton Sea *vs.* Mission Bay) were different from each other, as also shown by Henry and Mclaughlin (1975), and were different from all other populations. However, when grown under similar conditions, there was no difference between Salton Sea and Mission Bay individuals: Mission Bay and Salton Sea lab populations were not significantly different, nor were Mission Bay and Salton Sea lagoon populations. Also, the two lab populations (pooled for comparison) were different from the two lagoon populations (also pooled). Examples of the plates can be seen in Figure 2. Particular attention should be directed to the tergal spur (see Fig. 1 for a detailed diagram of the tergum). These results indicate that the phenotypic differences between field populations in the Salton Sea and Mission Bay are the result of phenotypic plasticity and not genetic divergence.

Plasticity itself is a trait that can be selected (Schmalhausen, 1949; Bradshaw, 1965; Schlichting, 1986), and it could be argued that individuals from one of the two locations (Salton Sea and Mission Bay): (1) might not be plastic, or (2) might not be as plastic as individuals from the other location (Schlichting, 1986). If individuals from one location were not plastic for the examined characters, then there would be no statistical difference between lab, lagoon, and field populations. For individuals from both locations, there were highly significant differences among all experimental populations (Table II). Thus, there is no doubt that individuals from both locations are phenotypically plastic. No conclusive answer may be given to the question of whether one population is more plastic than the other because the degree of plasticity in individuals from the two locations was not directly examined. However, the data suggest that individuals from the two locations are similar in their plasticity (in the examined characters) because there were no differences between

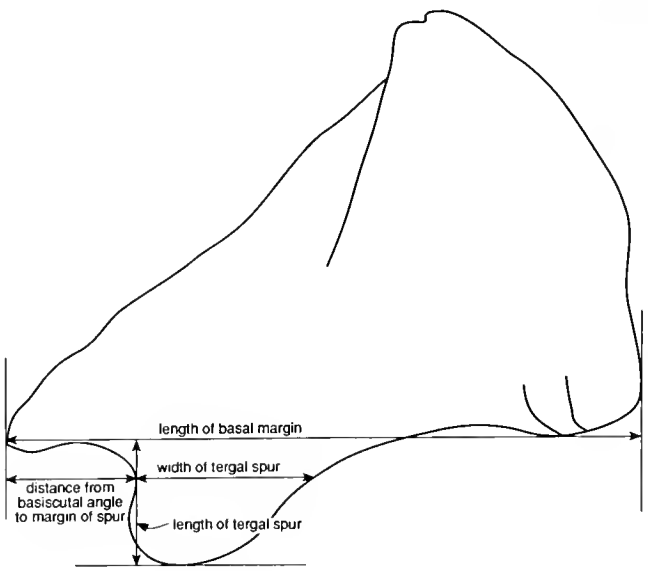

Figure 1. The morphological measurements made on tergal plates: (1) The length of the basal margin, (2) the length of the tergal spur, (3) the width of the tergal spur, (4) the distance from the basiscutal angle to the margin of the spur (see Table I for examined ratios).

Table II

Multivariate (MANOVA & MANCOVA) comparisons of tergal plate measurements between six populations of Balanus amphitrite *(Table 1a–b, Fig. 1)*

	MANOVA		
Pillai trace statistic	DF	F-STAT	*P*-VALUE
1.035	30, 790	6.878	<0.0001
	MANCOVA		
Pillai trace statistic	DF	F-STAT	*P*-VALUE
0.818	15, 474	11.846	<0.0001

	COMPARISONS		
Population comparisons	MANOVA *P*-VALUE	MANCOVA *P*-VALUE	Conclusion
1) Mission Bay field *vs.* Salton Sea field	<0.0001	<0.0001	Populations differ
2) Mission Bay lab *vs.* Salton Sea lab	0.594	0.869	No difference between populations
3) Mission Bay lagoon *vs.* Salton Sea lagoon	0.340	0.247	No difference between populations
4) Mission Bay field *vs.* both lab populations	<0.0001	<0.0001	Populations differ
5) Salton Sea field *vs.* both lab populations	<0.0001	<0.0001	Populations differ
6) Mission Bay field *vs.* both lagoon populations	<0.0001	<0.0001	Populations differ
7) Salton Sea field *vs.* both lagoon populations	<0.0001	<0.0001	Populations differ
8) Both lab populations *vs.* both lagoon populations	<0.0001	<0.0001	Populations differ

Populations: Mission Bay field (n = 26), Salton Sea field (n = 45), Mission Bay lab (n = 28), Salton Sea lab (n = 26), Mission Bay lagoon (n = 21), Salton Sea lagoon (n = 19), both lab populations (pooled n = 54), both lagoon populations (pooled n = 40). Because eight comparisons were made (for each model) the critical P-VALUE for the population comparisons should be 0.05/8 = 0.0063.

reared Salton Sea and Mission Bay individuals in *both* experimental habitats.

Larval characters

For each of the measured parameters, larvae from the Salton Sea differed from the other two populations, which were similar. Differences in pigmentation can result from differences in food type, however, in these experiments food type was constant among populations of parent stock and larvae. The most noticeable difference between Salton Sea cyprids and coastal ones was the lack of pigmentation in the former. Coastal cyprids were consistently green-brown, whereas those from the Salton Sea were white [Number of batches: Salton Sea G1 (8), Salton Sea G2 (2), Mission Bay G1 (7), Mission Bay G2 (2), Beaufort G1 (5)]. As compared to the Methuen color standards (Kornerup and Wanscher, 1978), the color of individuals from the Salton Sea was white (standard 3A1), while that for individuals from either of the coastal populations was olive (standards 3F8–3F4). Individuals from the two coastal populations were indistinguishable on the basis of color. The results from a microspectrophotometric analysis at 510 nanometers substantiated the finding that pigmentation differed between individuals from the Salton Sea and coastal populations (Table III, Fig. 3).

Cyprid length also differed between Salton Sea and coastal populations, which were similar (Table IV, Fig. 4). The third measured parameter was the time between release of larvae by an adult and the metamorphosis from the 6th naupliar larval stage to the cyprid stage (Fig. 5). No analysis was performed on these data as there was no way to meet an often unrecognized shared assumption of parametric and nonparametric statistics: similarity of distributions among groups (Day and Quinn, 1989). Naupliar duration was invariant among all populations except Salton Sea G1, and therefore there is no way to homogenize variance terms. However, it should be obvious without a probability value that naupliar duration was longer for the Salton Sea populations than for the coastal populations.

In all cases where it was examined, within a population there was no statistical difference between G1 and G2 cyprids indicating that residual environmental effects did not affect the results (Figs. 3–5).

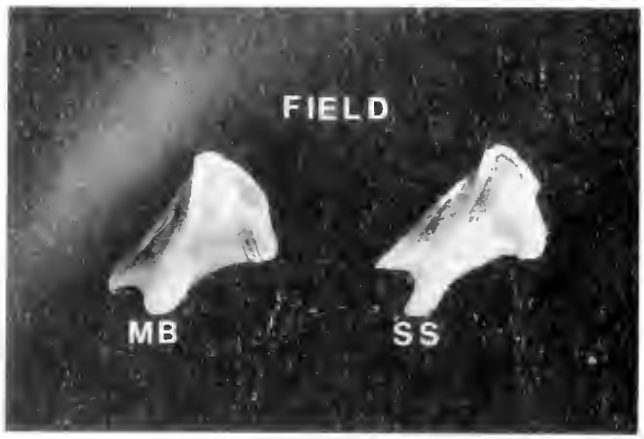

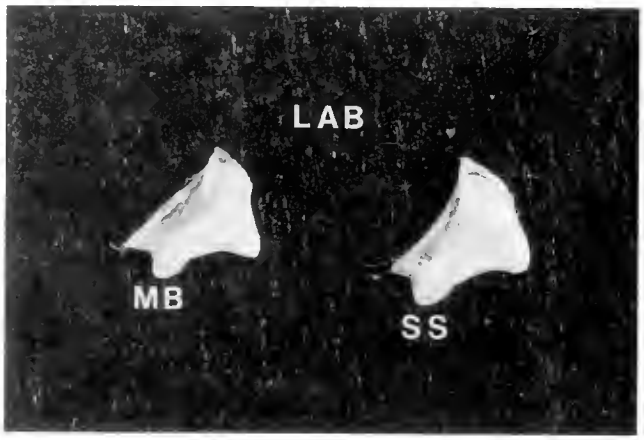

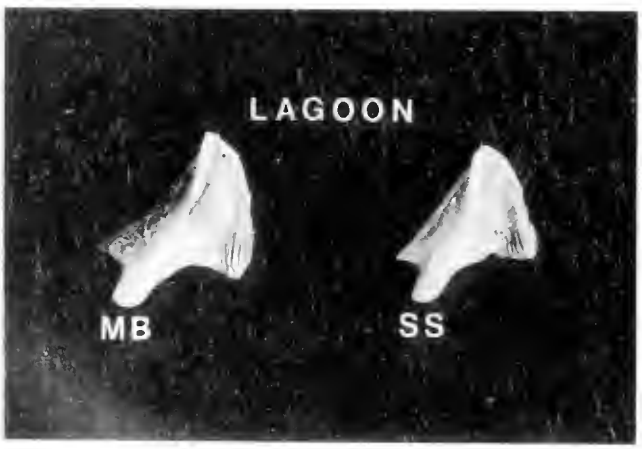

Figure 2. Tergal plates: (Top) Field populations: Mission Bay (left), Salton Sea (right). (Middle) Lab populations: Mission Bay (left), Salton Sea (right). (Bottom) Lagoon populations: Mission Bay (left), Salton Sea (right).

Discussion

The linkage of evolutionary arguments to ecological observations has been rather severely criticized in recent years. These criticisms are in two forms. First, the assignment of specific evolutionary mechanisms to phenotypic divergence has been questioned on the logical grounds that most investigators postulating such mechanisms did not properly test alternative hypotheses (Connell, 1980; Underwood, 1990; but see Roughgarden, 1983). The second criticism has been directed at investigators who failed to consider genetic constraints when proposing evolutionary explanations for ecological data (Gould and Lewontin, 1979; Lande, 1979, 1982; Templeton, 1981; Lynch, 1984). For an examination of phenotypic divergence of an isolated population in a novel environment, like *Balanus amphitrite* in the Salton Sea, understanding these criticisms is crucial because phenotypic modification of individuals in the novel environment is the expected result of *either* evolutionary or plastic processes (see Endler, 1986). Hence, the observation that individuals differ between coastal habitats and the Salton Sea cannot even

Table III

A comparison of transmittance of light at 510 nanometers through cyprids from five populations: (1) Salton Sea G1, (2) Salton Sea G2, (3) Mission Bay G1, (4) Mission Bay G2, and (5) Beaufort G1

ANOVA Source	df	MS	F	*P*
Population	4	38.65	15.28	0.0052
Residual	5	2.53		

For all populations, two batches of cyprids were examined. *A-posteriori* comparisons are shown in Figure 3.

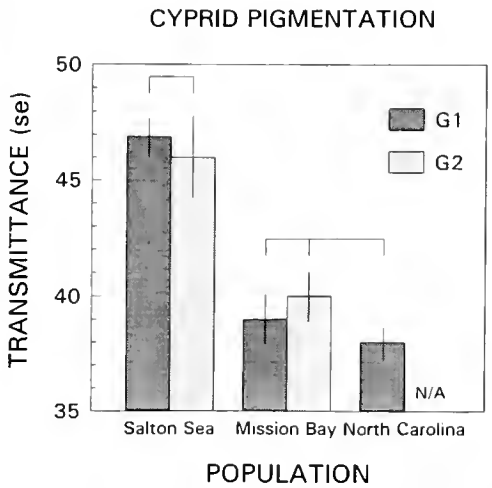

Figure 3. Transmittance of visible light, 510 nm, through cyprids of three populations (no G2 Beaufort cyprids were cultured). Groups not connected by horizontal lines differ at $P < 0.05$ [ANOVA with Tukey procedure, see Table III]. Error bars are ± one standard error of the mean.

Table IV

A comparison of cyprid lengths from five populations: (1) Salton Sea G1 (8 batches), (2) Salton Sea G2 (2 batches), (3) Mission Bay G1 (7 batches), (4) Mission Bay G2 (2 batches), and (5) Beaufort G1 (5 batches)

ANOVA Source	df	MS	F	*P*
Population	4	1954.16	20.25	<0.001
Residual	19	96.49		

A-posteriori comparisons are shown in Figure 4.

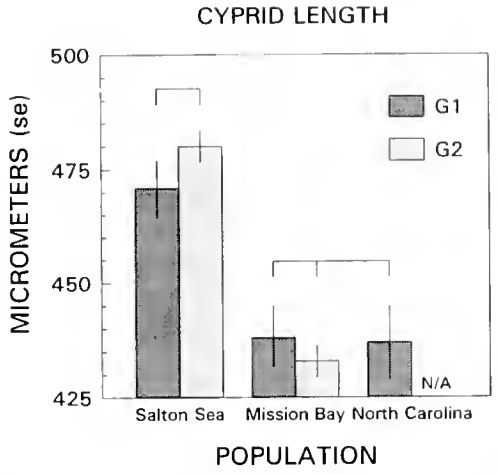

Figure 4. Lengths of cyprids of three populations (no G2 Beaufort cyprids were cultured). Groups not connected by horizontal lines differ at $P < 0.05$ [ANOVA with Tukey procedure, see Table IV]. Error bars are ± one standard error of the mean.

weakly indicate a cause for the difference. The underlying causes for phenotypic divergence in such populations can be determined only through properly designed experiments.

The first goal of this investigation was to determine experimentally if the observed morphological divergence between adult *Balanus amphitrite* in the Salton Sea and those in coastal populations was due to evolutionary or plastic processes. Like Henry and Mclaughlin (1975), I too found that field populations of adult *Balanus* differed for a number of characteristics. However, these differences disappeared when individuals from the two locations were reared in similar environmental conditions (laboratory or lagoon). This is unequivocal evidence that the divergence in the examined characters was due to phenotypic plasticity.

During the investigation of adult characteristics, I found that larvae from the Salton Sea differed from those from Mission Bay. In subsequent experiments, I also found that Salton Sea larvae differed from ones from another coastal population, Beaufort, North Carolina, and that individuals from the two coastal populations did not differ in any examined larval character. The latter result is important because it indicates that widely separated but coastal populations have not diverged for the examined characters. However, it should be noted that coastal populations of bay or harbor species like *Balanus amphitrite* are probably never completely isolated because of transport of adults and larvae by ships (Carlton, 1985). The phenotypic differences between the Salton Sea and coastal populations persisted, undiluted, after two generations in the laboratory, suggesting that the differences are underlain by genetic variation. Genetic crosses are needed to confirm this suggestion (Falconer, 1989), however, *in vivo* crosses would have been confounded by the possibility of self-fertilization (Patel and Crisp, 1961), and *in vitro* crosses that were attempted were unsuccessful.

Assuming that there is a genetic basis for the phenotypic differences found between Salton Sea and coastal larvae, what mechanism may be responsible for the divergence? Only two mechanisms seem plausible: selection and genetic drift, and of these I contend that selection is more likely because there is evidence that there has been no genetic drift. If genetic drift were responsible for the divergence in larval characters for individuals in the Salton Sea then: (1) the Salton Sea population must be isolated from coastal populations, (2) the genes coding for the characters that have diverged must be subject to very little selection (stablizing selection), and (3) the effective population size of the Salton Sea population must have at some time been small (after Falconer, 1989).

If these conditions were all met, then evolution by genetic drift would probably occur. This would likely be

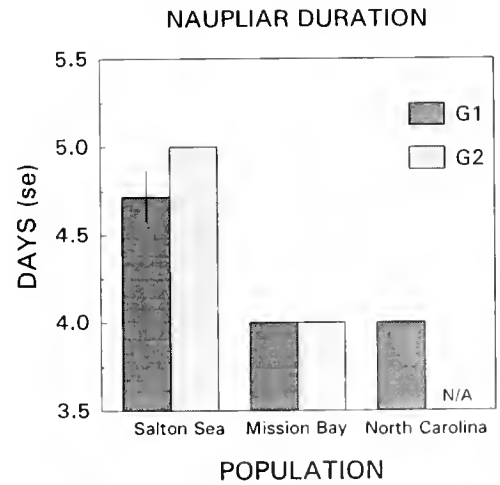

Figure 5. Time between release of larvae from adults and the metamorphosis from the 6th naupliar stage to the cyprid stage (no G2 Beaufort cyprids were cultured). Number of batches: Salton Sea G1 (8), Salton Sea G2 (2), Mission Bay G1 (7), Mission Bay G2 (2), and Beaufort G1 (5). Error bars are ± one standard error of the mean.

reflected in an electrophoretic comparison of allozymes between the Salton Sea and conspecific populations because many of the genes coding for these enzymes would probably be (effectively) selectively neutral (Falconer, 1989). In such a comparison, Flowerdew (1985) found no evidence for either divergence in allelic proportions or loss of heterozygosity for the Salton Sea population of *Balanus amphitrite*. This indicates that significant genetic drift has not occurred in the Salton Sea population. The most likely reason that drift has not occurred is that the inoculation population of the barnacle was not small enough to promote a significant loss of heterozygosity [heterozygosity is lost at a rate of $1/2N_e$ per generation, where N_e = effective population size (Lande, 1980)], and that after the introduction its size increased explosively (Cockerall, 1945; Hilton, 1945).

What selective agents could have caused the divergence of larval characters in Salton Sea *Balanus amphitrite?* As mentioned in the introduction, water in the Salton Sea differs from that in typical oceanic habitats in a number of ways. One that may be important in the present discussion is clarity. Ultraviolet (UV) radiation is harmful to many marine organisms (Jokiel, 1980), and there is a positive relationship between penetration by ultraviolet radiation and water clarity (Jerlov, 1950). Pigmentation has been proposed as an adaptive defense in marine organisms against damage by solar ultraviolet radiation (Ireland and Scheuer, 1979; Yentsch and Yentsch, 1982; Dunlop *et al.*, 1986). I suggest that pigmentation may have been lost by cyprids in the Salton Sea because, in part, the potential for damage by UV radiation in its chronically turbid water is much lower than in coastal water.

The other two characters showing divergence were cyprid length and naupliar duration (the series of naupliar stages constituting the planktonic period prior to metamorphosis to the cyprid stage). Naupliar duration was longer and the resulting cyprids were larger for individuals from the Salton Sea than for those from coastal populations. The increase in cyprid size probably is, at least in part, due to the increase in naupliar period, the period during which larvae feed and grow. In other organisms, larval period is positively correlated with size at metamorphosis, and it has been hypothesized that larval period and the stability of larval habitat should be positively related (Petranka and Sih, 1987; Travis *et al.*, 1987; Newman, 1988). Applied to *Balanus amphitrite*, this hypothesis would require that the Salton Sea be a more stable environment for larvae than coastal bays and harbors. Effectively this would mean that the negative slope of the relationship between larval duration and successful settlement would be less extreme for larvae in the Salton Sea. This seems possible given that predation on larvae, interspecific competition among larvae, maximum distance from hard substrate, and the intensity of storms and currents advecting larvae away from favorable areas for settlement, should all be less for larvae in the Salton Sea.

One of many alternatives to the preceding hypothesis is that longer naupliar periods may be an adaptation to retard a temperature-driven accelerated development rate that would be detrimental to larvae in the Salton Sea. Culture temperature has a dramatic positive effect on the rate of larval development for *Balanus amphitrite* (Rittschof, pers. comm.; Raimondi, pers. obs.), and temperature in the Salton Sea during the period of maximum larval abundance averages between 31 and 36°C (Carpelan, 1961b; Linsley and Carpelan, 1961). I noticed many coastal larvae reared at temperatures above 30°C whose morphology appeared to be intermediate between naupliar stages (Raimondi, unpubl. data). Such larvae have no further development, and their incomplete metamorphoses may result from temperature-driven differences in the maximum rate of development of independent physiological processes. Hence, Salton Sea larvae could show slower development than coastal larvae when reared at 27–28°C because of adaptations to control development at 31–36°C.

Conclusion

The primary aim of this study was to determine whether evolutionary change or phenotypic plasticity was responsible for the observed phenotypic divergence of a population of *Balanus amphitrite* recently introduced and isolated in the Salton Sea. Clearly, divergence in the examined adult characters was due to environmentally induced plasticity. In contrast, there is strong support for the hypothesis that the observed divergence in larval characters was due to an evolutionary process, probably selection. These results are not evidence for a general ontogenetic difference in the way organisms respond to a changing or novel environment. I suspect that there are some unexamined divergent adult traits between populations that are underlain by genetic differences, and some divergent larval ones that are not. However, it is clear that the consideration of divergence between populations is incomplete if all life history stages of the organism are not studied. In the present example I would have found no evidence for genetic divergence between the Salton Sea and coastal populations of *Balanus amphitrite* if only the adult morph had been studied. My final comment is a precautionary one. There has been an historic fascination with examining the causes of phenotypic divergence in isolated populations by considering them as experimental populations. Perhaps this is because they resemble experimental treatments on a larger scale (both temporal and spatial) and with more ecological realism than is possible in manipulations. This is flawed thinking, because there is no

provision for eliminating alternative hypotheses. For *Balanus amphitrite* isolated in a novel environment, the Salton Sea, phenotypic divergence was the expected result of either of two processes: evolution of phenotypic plasticity. Only through experimental manipulations could the responsible process be determined, and then only on a trait-by-trait basis.

Acknowledgments

I am particularly thankful to Dr. Daniel Morse for his intellectual and financial support in all phases of this research. This study would not have been done without his invaluable contributions. I also thank C. Amsler, M. Carr, J. Connell, A. Constable, J. Endler, M. Hart, M. Keough, C. Lively, D. Macmillan, C. and D. Reed, S. Schuster, J. Smissen, and D. Stellar for valuable discussions or laboratory assistance. I also thank D. Rittschof and A. Schmidt of Duke University Marine Laboratory for their expertise and assistance in cultivation of larvae. This research was supported in part by a grant to Dr. Daniel Morse by the Oceanic Biology Program of the U. S. Navy Office of Naval Research (Grant # N00014-88-K-0288).

Literature Cited

Anonymous. 1989. In *The Los Angeles Times,* April 3, 1989.

Atchley, W. R., C. T. Gaskins, and D. Anderson. 1976. Statistical properties of ratios. I. Empirical results. *Syst. Zool.* **25:** 137–148.

Avise, J. C., J. J. Smith, and F. J. Ayala. 1975. Adaptive differentiation with little genic change between two native California minnows. *Evolution* **29:** 411–426.

Berven, K. A., D. E. Gill, and S. J. Smith-Gill. 1979. Countergradient selection in the green frog, *Rana clamitans. Evolution* **33:** 609–623.

Bradshaw, A. D. 1965. Evolutionary significance of phenotypic plasticity in plants. *Adv. Genet.* **13:** 115–155.

Carlton, J. T. 1985. Transoceanic and interoceanic dispersal of coastal marine organisms: the biology of ballast water. *Oceanogr. Mar. Biol. Annu. Rev.* **23:** 313–371.

Carpelan, L. H. 1961a. History of the Salton Sea. *State of California Department of Fish and Game Fish Bulletin* **113:** 9–13.

Carpelan, L. H. 1961b. Physical and chemical characteristics (of the Salton Sea). *State of California Department of Fish and Game Fish Bulletin* **113:** 17–32.

Chamberlin, G. J., and D. G. Chamberlin. 1980. *Colour: its Measurement, Computation and Application.* Heyden & Son, London.

Cockerall, T. D. A. 1945. The Colorado desert of California: its origin and biota. *Transactions Kans. Acad. Sci.* **48**(1): 1–39.

Connell, J. H. 1980. Diversity and the coevolution of competitors, or the ghost of competition past. *Oikos* **35:** 131–138.

Day, R. W., and G. P. Quinn. 1989. Comparisons of treatments after an analysis of variance in ecology. *Ecol. Monogr* **59:** 433–463.

Dunlop, W. C., B. E. Chalker, and J. K. Oliver. 1986. Bathymetric adaptations of reef-building corals at Davies reef, Great Barrier Reef, Australia. III. UV-B absorbing compounds. *J. Exp. Mar. Biol. Ecol.* **104:** 239–448.

Endler, J. A. 1986. *Natural Selection in the Wild.* Princeton University Press, Princeton, New Jersey.

Falconer, D. S. 1989. *Introduction to Quantitative Genetics.* Third edition. Longman Scientific & Technical, New York.

Flowerdew, M. W. 1985. Indices of genetic identity and distance in three taxa within the *Balanus amphitrite* Darwin complex (Cirripedia, Thoracica). *Crustaceana* **49:** 7–15.

Gould, S. J., and R. F. Johnson. 1972. Geographic variation. *Annu. Rev. Ecol. Syst.* **3:** 457–498.

Gould, S. J., and R. C. Lewontin. 1979. The spandrels of San Marco and the Panglossian paradigm: a critique of the adaptationist programme. *Proc. R. Soc. Lond. (B)* **205:** 581–598.

Henry D. P. and P. A. Mclaughlin. 1975. The barnacles of the *Balanus amphitrite* complex (Cirripedia, Thoracica). *Zool. Verh.* **141:** 3–254.

Hilton, J. 1945. Where barnacles grow on the sage. *Desert Magazine* **8**(5): 4–6.

Ireland, C., and P. J. Scheuer. 1979. Photosynthetic marine molluscs: *in vivo* ^{14}C incorporation into metabolites of the sacoglossan *Placobranchus ocellatus. Science* **205:** 922–923.

Jokiel, P. J. 1980. Solar ultraviolet radiation and coral reef epifauna. *Science* **207:** 1069–1071.

Jerlov, N. G. 1950. Ultra-violet radiation in the sea. *Nature* **166:** 111–112.

Kornerup, A., and J. H. Wanscher. 1978. *Methuen Handbook of Colour,* 3rd edition. Eyre Methuen, London.

Lande, R. 1979. Quantitative genetic analysis of multivariate evolution applied to brain: body size allometry. *Evolution* **33:** 402–416.

Lande, R. 1980. Genetic variation and phenotypic evolution during allopatric speciation. *Am. Nat.* **116:** 463–479.

Lande, R. 1982. A quantitative genetic theory of life history evolution. *Ecology* **63:** 607–615.

Lewontin, R. C. 1957. The adaptation of populations to varying environments. *Cold Springs Harbor Symp. Quant. Biol.* **22:** 395–408.

Linsley, R. H., and L. H. Carpelan. 1961. Invertebrate fauna (of the Salton Sea). *State of California Department of Fish and Game Fish Bulletin* **113:** 43–61.

Lynch, M. 1984. The limits to life history evolution in *Daphnia. Evolution* **38:** 465–482.

Macdonald, S., C. C. Chinnappa, and D. M. Reid. 1988. Evolution of phenotypic plasticity in the *Stellaria longipes* complex: comparisons among cytotypes and habitats. *Evolution* **42:** 1036–1046.

Nei, M. 1972. Genetic distances between populations. *Am. Nat.* **106:** 283–292.

Newman, R. A., and D. P. Abbott. 1980. Cirripedia: the barnacles. Pp. 504–535 in *Intertidal Invertebrates of California,* R. H. Morris, D. P. Abbott, and E. C. Haderlie, ed. Stanford University Press, Stanford, California.

Newman, R. A. 1988. Adaptive plasticity in development of *Scaphiopus couchii* in desert ponds. *Evolution* **42:** 774–783.

Patel, B., and D. J. Crisp. 1961. Relation between the breeding and moulting cycles in cirripedes. *Crustaceana* **2:** 89–107.

Petranka, J. W., and A. Sih. 1987. Habitat duration, length of larval period, and the evolution of complex life cycle of a salamander, *Ambystoma texanum. Evolution* **41:** 1347–1356.

Richardson, B. J., P. R. Baverstock, and M. Adams. 1986. *Allozyme Electrophoresis: A Handbook for Animal Systematics and Population Studies.* Academic Press Australia, Sydney.

Rittschof, D., E. S. Branscomb, and J. D. Costlow. 1984. Settlement and behavior in relation to flow and surface in larval barnacles. *Balanus amphitrite* Darwin. *J. Exp. Mar. Biol. Ecol.* **82:** 131–146.

Rogers, F. L. 1949. Three new species of *Balanus amphitrite* from California. *J. Entomol. Zool.* **41:** 23–32.

Roughgarden, J. R. 1983. Competition and theory in community ecology. *Am. Nat.* **122:** 583–601.

Schlichting, C. D. 1986. The evolution of phenotypic plasticity in plants. *Annu. Rev. Ecol. Syst.* **17:** 667–693.

Schmalhausen, I. I. 1949. *The Theory of Stabilizing Selection.* Blakiston, Philadelphia.

Smith-Gill, S. J. 1983. Developmental plasticity: developmental conversion *versus* phenotypic modulation. *Am. Zool.* **23:** 47–55.

Sokal, R. R., and F. J. Rohlf. 1981. *Biometry,* Second edition. W. H. Freeman, San Fransisco, California.

Strathmann, M. F. 1987. *Reproduction and Development of Marine Invertebrates of the Northern Pacific Coast.* University of Washington Press, Seattle, Washington.

Templeton, A. R. 1981. The evolution of life histories under pleiotrophic constraints and r-selection. *Theor. Popul. Biol.* **18:** 279–289.

Travis, J., S. B. Emerson, and M. Blouin. 1987. A quantitative-genetic analysis of larval life history traits in *Hyla crucifer. Evolution* **41:** 145–156.

West-Eberhard, M. J. 1989. Phenotypic plasticity and the origins of diversity. *Annu. Rev. Ecol. Syst.* **20:** 249–278.

Williams, G. C. 1966. *Adaptation and Natural Selection.* Princeton University Press, Princeton, New Jersey.

Yentsch, C. S., and C. M. Yentsch. 1982. The attenuation of light by marine phytoplankton with specific reference to the absorbtion of near-UV radiation. Pp. 691–706 in *The Role of Solar Ultraviolet Radiation in Marine Ecosystems,* J. Calkins, ed. Plenum Press, New York.

Underwood, A. J. 1990. Experiments in ecology and management: their logics, functions, and interpretations. *Aust. J. Ecol.* **15:** 365–389.

Reference: *Biol. Bull.* **182**: 221–230. (April, 1992)

Intercolony Coordination of Zooid Behavior and a New Class of Pore Plates in a Marine Bryozoan

DANIEL F. SHAPIRO

Section of Ecology and Systematics, Cornell University, Ithaca, New York, 14853.

Abstract. This paper describes a mixed allorecognition interaction between adjoining colonies of the encrusting cheilostome bryozoan *Membranipora membranacea,* in which characteristics of both intercolony fusion and intercolony rejection occur simultaneously. Intercolony coordination of zooid behavior was assayed by applying electrical stimuli to one colony of a colony pair while observing the behavior of the adjoining colony. Retraction of feeding structures (lophophores) by the unstimulated colony indicated intercolony coordination of behavior. Naturally occurring and artificially created pairs of genotypically identical and genotypically distinct colonies were examined. Additionally, colony borders were examined for the presence of pore plates, structures that physiologically link zooids within colonies. Contact between genetically identical colonies (isocontact) always resulted in a characteristic border morphology, characteristic pore plates, and intercolony coordination of zooid behavior. Contact between genotypically distinct colonies (allocontact) always resulted in a characteristic border morphology and in the formation of characteristic pore plates of a type never before described. However, only colonies that were young when they first came into contact showed coordinated behavior. Intercolony coordination of zooid behavior is probably the result of neural connections made through pore plates. Intercolony behavioral coordination between young genotypically distinct colonies is peculiar, because the colonies simultaneously show characteristics of physiological integration (coordinated behavior) and tissue rejection (borders and pore plates characteristic of contact between genetically distinct tissues). This interaction shows that the presence of the morphological characteristics of intercolony rejection does not always imply a lack of physiological integration between colonies.

Received 4 June 1990; accepted 13 January 1992.

Introduction

Colonial marine invertebrates such as sponges, cnidarians, bryozoans, and ascidians are capable of indeterminate asexual growth. As a result, contact between conspecific and heterospecific colonies is extremely common on most marine hard substrata where space is limiting (Dayton, 1971; Stebbing, 1973a; Jackson, 1977; Osman, 1977). Many of these colonial invertebrates have highly discriminating immune systems capable of allorecognition—the ability to distinguish between genetically identical and genetically distinct tissue (for review see Grosberg, 1988). If genotypically identical, or closely related (*e.g.,* sibling) colonies come into contact, they commonly fuse into a single colony. If genotypically distinct colonies come into contact, tissue rejection typically follows, and fusion does not occur (Sabbadin, 1982; Scofield *et al.,* 1982; Chaney, 1983; Rinkevich and Loya, 1983a; Shenk and Buss, 1991).

Recent work describing allorecognition responses of colonial marine invertebrates has revealed a diversity of interactions ranging from intercolony fusion to intercolony rejection. Colonies of the hydroid *Hydractinia symbiolongicarpus* may fuse permanently, fuse and then later reject, or reject with the subsequent production of aggressive hyperplasitic stolons (Buss and Grosberg, 1990; Shenk and Buss, 1991). In ascidians, allorecognition responses include permanent fusion, fusion followed by separation, fusion followed by complete resorption of one colony, rejection with little further interaction, and rejection with necrosis of the tissues of one or both colonies (Koyama and Watanabe, 1982; Scofield and Nagashima, 1983; Rinkevich and Weissman, 1987, 1989).

All of the above examples involve either different intensities of rejection or a temporal separation between fusion and rejection. This paper describes a mixed interaction between colonies of the encrusting cheilostome

bryozoan *Membranipora membranacea* involving simultaneous evidence of physiological fusion and tissue rejection. Zooids within bryozoan colonies are physiologically integrated through a nerve net that traverses the calcified zooidal walls through pore plates (Thorpe *et al.*, 1975; Lutaud, 1977, 1979), distinctive structures in the zooidal wall where there is a concentration of several open pores (Silen, 1944; Banta, 1969). The most obvious display of physiological integration of zooids within a bryozoan colony is the coordination of the lophophore retraction response. In response to a localized disturbance to one or a few zooids, all of the zooids within a colony simultaneously retract their feeding structures (lophophores). I have observed that when genotypically distinct colonies of *M. membranacea* come into contact, intercolony coordination of lophophore retraction is frequently observed. Yet, the intercolony borders of these same colonies show no morphological characteristics of fusion.

Because of the mixed nature of this interaction, I will avoid the terms fusion and rejection. Fusion in bryozoans is commonly associated with physiological integration (Stebbing, 1973b; Humphries, 1979; Nielsen, 1981; Chaney, 1983); consequently, the term fusion could also be applied to colonies that show physiological integration, but lack any morphological characteristics of fusion. To avoid this ambiguity, I will refer to contact between genetically distinct tissues as "allocontact", and I will refer to contact between genetically identical tissues as "isocontact." The physiological consequences and morphology of these interactions can then be described separately.

M. membranacea occurs naturally in dense monospecific populations where contact between conspecifics is extremely common, if not unavoidable. Larvae of *M. membranacea* disperse in the plankton for up to four weeks (Yoshioka, 1982), thus naturally settled adjoining colonies are unlikely to be siblings. Consequently, the majority of intercolony interactions are between unrelated colonies. However, contact between genotypically identical tissues occasionally occurs when a single colony grows into contact with itself after either growing around some object or fusion resulting from damage to the colony (pers. obs.). I will (1) examine how intercolony coordination is related to the size and age at which genotypically distinct colonies first come into contact, (2) compare the morphology of the borders between genotypically distinct colonies to those between genotypically identical colonies, and (3) examine both types of borders for pore plates that could facilitate intercolony coordination of zooid behavior.

Materials and Methods

Animal collection

Research was conducted at Friday Harbor Laboratories (FHL), San Juan Island, Washington, and at the University of California, Los Angeles. At FHL, colonies of *Membranipora membranacea* that had settled on black acrylic panels suspended from the FHL dock, as well as colonies collected from the field, were used in this study. Colonies were collected from the field by haphazardly selecting bryozoan-encrusted blades of the kelp *Laminaria* sp. from Turn Island and transporting them back to FHL where the kelp blades were hung from the FHL dock. In California, *M. membranacea* colonies were collected from kelp beds off the coast of Malibu, California. Bryozoan encrusted blades of the kelp *Macrocystis pyrifera* were haphazardly removed from the upper parts of kelp fronds on, and just below, the surface of the water. Blades were then transported back to the laboratory where they were maintained in a recirculating seawater system.

Intercolony coordination of lophophore retraction

To ensure that a given intercolony border was between two colonies descended from different larvae rather than previously separated parts of a colony decended from a single larva, I used only colony pairs for which I could locate both ancestrulae. The ancestrula is a pair of morphologically distinct zooids that develop from the larva after settlement and metamorphosis (Fig. 1A). Ancestrular zooids are easily distinguished from younger asexually produced zooids because they are rounder, more heavily calcified, and together are distinctively heart shaped (Fig. 1B). Unless indicated otherwise, whenever I mention colony pairs, I will be referring to pairs of colonies descended from separate larvae.

To test for intercolony coordination of lophophore retraction, I stimulated colony pairs electrically. A stimulus was applied to one of the two colonies. A colony-wide lophophore retraction response in the adjoining unstimulated colony was used as an indication of intercolony behavioral coordination. Electrical stimuli were applied with an electrode placed on the surface of the colony. All stimuli were at, or just above, the threshold stimulus (a single square pulse between 5 and 10 volts for 5–10 ms) required to elicit a colony-wide lophophore retraction response. In addition to electrical stimuli, mechanical stimuli were applied to pairs of very small colonies (less than 10 mm^2) to eliminate the possibility that intercolony coordination was an artifact resulting from electrical conduction of the stimulus through the water or across the colony surface. Mechanical stimuli were applied by lightly touching a dissecting needle to one of the colonies on the edge opposite the intercolony border.

To determine whether the non-stimulated colony of a pair of behaviorally coordinated colonies was responding to the physical retraction of the lophophores of the adjoining colony, I retested 20 coordinated colony pairs after first making a fine cut with a razor blade along the border

between the adjoining colonies. Cuts were made so that no lophophores along the intercolony borders were damaged.

To determine whether coordination was bidirectional, a stimulus was applied to one colony of a pair until I had obtained 20 behaviorally coordinated and 20 non-coordinated pairs. A second stimulus was then applied to the other colony of each pair.

The frequency of intercolony behavioral coordination in a natural population of *M. membranacea* was measured at Friday Harbor by sampling three blades of *Laminaria*. Both sides of 5 × 10 cm rectangles were censused 5 cm from each edge of the blade at 25, 50, 75, 100, and 125 cm from the base of each blade (where the stipe meets the blade). Each colony was recorded as being solitary or in contact with other colonies. If a colony was in contact with another colony, it was tested for intercolony coordination of lophophore retraction. In all, 1301 colonies were sampled.

Intercolony coordination and size at first contact

To determine the relationship between colony size at first contact and intercolony coordination, 92 pairs of *M. membranacea* colonies were cultured on black acrylic panels in Friday Harbor. Panels were cleared at least once a week of all other organisms. Each colony monitored was in contact with only one other colony. The size of each colony at the time of first intercolony contact was determined by tracing each colony on acetate paper and calculating the area of the tracing using a video-integrated image analysis system. Following contact, all colony pairs were tested for intercolony coordination of lophophore retraction one to three times each week for five weeks.

Additional data on the relationship between intercolony coordination and colony size at first contact were obtained for *M. membranacea* colonies in California. Densities of *M. membranacea* in California tend to be higher than in Friday Harbor (pers. obs.). As a result, data could be obtained for adjoining colonies that were typically smaller at first contact than those observed in Friday Harbor. In all, 230 colony pairs were selected from 10 different *Macrocystis* blades. Colonies were selected to give a maximum range of values for size at first contact. Because of high colony density, colony "pairs" were sometimes in serial contact with other colonies (forming linear groups of 3, 4, or more colonies). However, no colony was ever in contact with more than two other colonies, and a single colony was never used more than once. Colonies were examined using a dissecting microscope, and all measurements were made with an ocular micrometer.

Because I was unable to culture colonies in California, direct measurements of colony size at first contact were not possible. Instead, I estimated colony size at first contact by measuring the intercolony ancestrula distance (Fig. 3). Because the ancestrula marks the site of larval settlement and metamorphosis, I assumed that the distance between the ancestrulae of two colonies would be directly correlated to the size of the colonies at first contact. Additionally, it seemed likely that colonies would not become coordinated immediately upon contact, but would instead require a period of time for the formation of intercolony physiological connections. Consequently, for each colony pair I also estimated how long colonies had been in contact by measuring the intercolony border length (Fig. 3). Because the length of the border between colonies increases as both colonies grow, I assumed that the length of the intercolony border would be directly correlated to how long the colonies had been in contact. After making these measurements, colonies were tested for intercolony coordination of lophophore retraction.

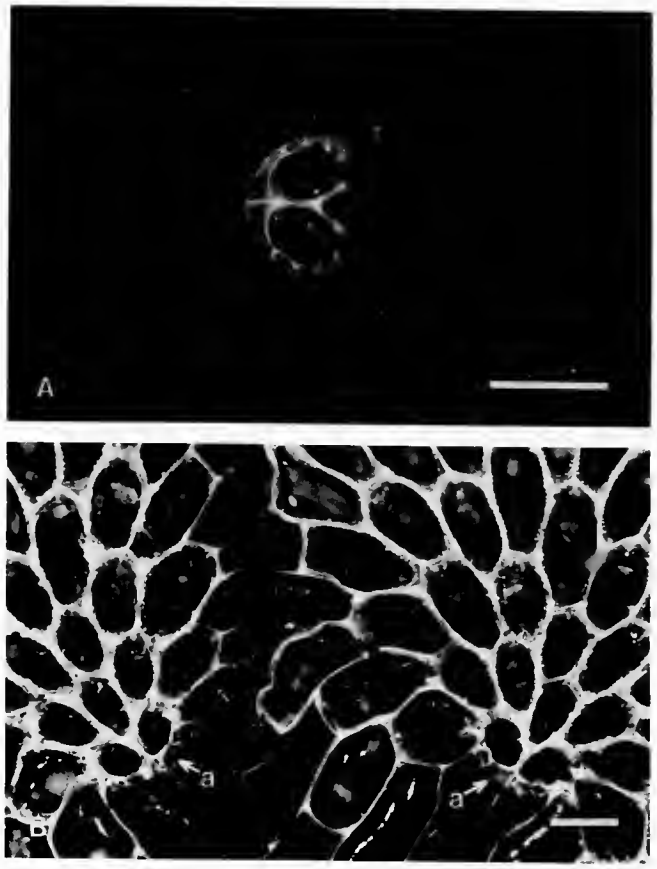

Figure 1. A. The founding ancestrula of a colony shortly after larval settlement and metamorphosis. B. Ancestrulae and intercolony border of a pair of colonies that have grown into contact. Small bubble-like structures visible along the intercolony border are allocontact pore plates. Abbreviation: a, ancestrula. Size bars = 0.5 mm.

Transplant experiment

Although unlikely, I cannot be sure that naturally settled adjoining colonies are not genetically similar siblings

that have settled in close proximity. To determine whether behavioral coordination can occur between colonies that are clearly not siblings, I paired *M. membranacea* colonies from Turn Island with colonies from Rocky Point, San Juan Island, a site approximately 10 miles northwest from Turn Island. Bryozoan encrusted blades of the red alga *Iridea* were collected from the two sites. I removed 48 small colonies (<25 mm^2) from the algal blades by gently stretching the blade until the colony detached. Twenty-four colony pairs, each consisting of one colony from Turn Island and one colony from Rocky Point, were then placed on acrylic panels. After 24 h, colonies had attached to the panels that were subsequently suspended below the FHL docks. Following contact, all colony pairs were tested for intercolony coordination of lophophore retraction twice each week for four weeks.

Size reduction experiment: allocontact and isocontact

To distinguish the effects of colony age from those of colony size and to establish unambiguous examples of isocontact between completely separated parts of a single colony, I reduced large colonies growing on acrylic panels at Friday Harbor to pairs of smaller subcolonies. Using a razor blade to cleanly cut a square of the appropriate size in the colony, I created pairs of either small or large square subcolonies that were 16 mm^2 or 100 mm^2, respectively. All other parts of the colony were then scraped off the panel with a small spatula. A 1-mm strip of space was also scraped between each colony pair.

Allocontact pairs were created by making subcolonies on both sides of the intercolony border between pairs of non-coordinated colonies (after testing for behavioral coordination). In all, eight small and seven large allocontact pairs were established. Isocontact pairs were created by reducing single colonies into two smaller subcolonies. In all, seven small and eight large isocontact pairs were established. In addition to providing an unambiguous example of isocontact, this latter treatment also served as a control for possible effects of damage on the establishment of behavioral coordination, because adjoining parts of a single colony should become physiologically integrated when they meet. Regeneration and growth of the cut borders was rapid; all colony pairs had grown back into contact in approximately a week. After subcolonies had grown into contact, I tested for intercolony behavioral coordination.

Pore plates

A scanning electron microscope was used to examine isocontact borders (n = 2) and allocontact borders of coordinated (n = 2) and non-coordinated (n = 2) colony pairs for the presence of pore plates. Colonies growing on *Laminaria* were collected at Friday Harbor. For isocontact, only single colonies that had grown around some object and back into contact with itself were used; for allocontact, only colonies with both ancestrulae present were used. Colonies were prepared by dissolving away the tissues of colonies in 2.5% sodium hypochlorite for 12 h to expose the calcium carbonate skeleton.

Isocontact and allocontact borders of naturally occurring colonies were also examined histologically for pore plates. I examined isocontact borders (n = 3) and allocontact borders between behaviorally coordinated (n = 6) and non-coordinated (n = 6) colony pairs collected in California. Approximately 2–3 mm long sections of borders, along with the kelp substrate, were removed with a razor blade. Samples were first fixed in 3% glutaraldehyde in 0.1 *M* sodium cacodylate buffer, pH 7.4 for 1 h, and then in 4% osmium in 0.1 *M* sodium cacodylate buffer for an additional hour. Samples were then dehydrated in a graded series of ethanol dilutions, treated with propylene oxide, and infiltrated overnight in Medcast low viscosity embedding medium. After polymerizing overnight at 70°C, samples were sectioned (approximately 3 μ thick) and viewed using a light microscope.

Results

Intercolony coordination of lophophore retraction

A cut between behaviorally coordinated colony pairs always completely eliminated intercolony coordination of lophophore retraction. Thus, colonies were not responding to the physical disturbance created by the retraction of the lophophores of adjoining colonies.

For all behaviorally coordinated colony pairs tested, intercolony coordination was always bidirectional. Stimulation of either colony resulted in a colony-wide lophophore retraction response in the non-stimulated colony. Unstimulated colonies of non-coordinated pairs always failed to respond regardless of which colony was stimulated. No colony pairs were found in which information flow was unidirectional.

Intercolony coordination of behavior is frequently observed in natural populations. Of the 1301 colonies sampled from *Laminaria* blades, 568 (44%) were in contact with another colony. Of these, 408 (72%) were behaviorally coordinated with at least one neighbor.

Intercolony coordination and size at first contact

Intercolony coordination of zooids was observed most frequently when two colonies were small at the time of first contact (Fig. 2). When the areas of each colony in a pair at the time of first contact were summed, the combined area of colony pairs with coordinated behavior (n = 15; mean = 1.02 cm^2, S.D. = 1.51) was significantly smaller than the combined area of colony pairs that were

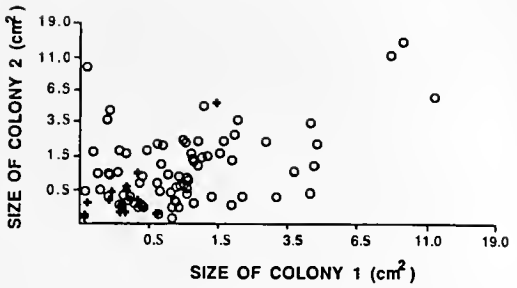

Figure 2. Colony size at first contact and intercolony behavior for 92 colony pairs cultured on acrylic panels. Each colony is plotted by the size of each colony in the pair at the time of initial intercolony contact. One colony of each pair was arbitrarily designated colony 1 and the other colony 2; + = coordinated colony pair, o = non-coordinated colony pair. Note that data are plotted on a logarithmic scale.

not coordinated (n = 77; mean = 3.05 cm^2, S.D. = 3.76; t-test of ln transformed data, $P < 0.001$). In all pairs that became behaviorally coordinated, there was a short period (approximately a week) following initial contact during which colonies were not behaviorally coordinated. Coordinated behavior of the one outlying pair in Figure 2 was observed on only a single occasion, suggesting either human error or that the pair was anomalous.

There was a significant relationship between intercolony coordination and both the estimated size at first contact (intercolony ancestrula distance; $\chi^2 = 46.82$, $P < 0.0001$) and the estimated length of time in contact (intercolony border length; $\chi^2 = 22.22$, $P < 0.0001$) for colony pairs from California. Data were analyzed using multiple logistic regression with intercolony ancestrula distance and intercolony border length as independent variables and behavior, coordinated or not coordinated, as the binary dependent variable. As the estimate of colony size at first contact increased, the probability of intercolony coordination decreased (Fig. 3). Although many colony pairs with small intercolony ancestrula distances (*e.g.* < 7 mm) were not coordinated, the majority of these also had small intercolony border lengths relative to the coordinated colony pairs.

Transplant experiments

Of the 24 colony pairs composed of one colony from Turn Island and one colony from Rocky Point, 20 remained attached to the acrylic panels and grew into contact. Of these, 13 (65%) showed intercolony coordination of zooid behavior within two weeks, thus demonstrating that coordinated behavior can occur between colonies that are clearly not related. For all colony pairs that became coordinated, there was a brief period (approximately one week) following initial intercolony contact when colonies were not coordinated.

Size reduction experiment: allocontact and isocontact

In the size reduction experiment, none of the allocontact colony pairs became behaviorally coordinated, regardless of size. Thus, if colonies are genotypically distinct, age rather than size appears to be the most important factor determining whether intercolony coordination occurs. All isocontact colony pairs did become behaviorally coordinated, regardless of size.

Isocontact borders were morphologically distinct from allocontact borders. Isocontact borders were straight and fully calcified, and zooids distal to the area of first contact aligned to form a single growing edge (Fig. 4A). Allocontact borders were clearly distinct from isocontact borders. Allocontact borders were not as straight as isocontact borders and were uncalcified or only lightly calcified, and each colony maintained a separate growing edge (Fig. 4B).

Pore plates

All isocontact and all allocontact borders (both from coordinated and non-coordinated colony pairs) contained structures (Figs. 5, 6) that clearly resemble the previously described bryozoan pore plates, transverse pore plates, lateral pore plates, and fusion pore plates (Silen, 1944; Banta, 1969; Chaney, 1983). Transverse and lateral pore plates are located respectively in the transverse and lateral zooidal walls that separate adjoining zooids within the same colony (Figs. 5A, B; 6A). Fusion pore plates are found in the walls between two colonies that have fused into a single colony (Chaney, 1983). Pore plates are round (lateral and fusion pore plates) to elliptical (transverse pore

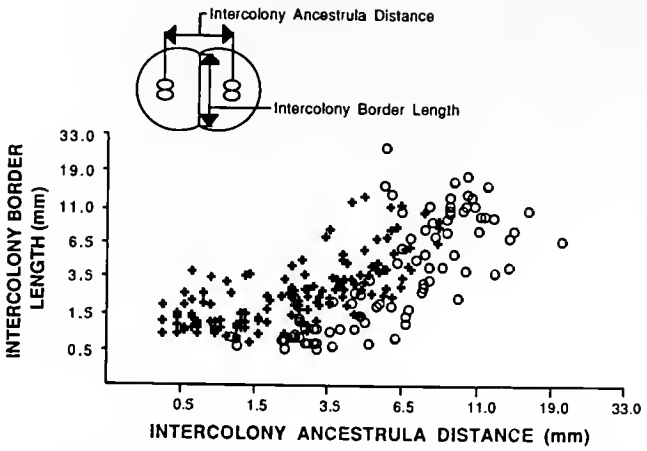

Figure 3. Intercolonial ancestrula distance, intercolonial border length and intercolonial behavior for 230 colony pairs from *Macrocystis* blades. For each colony pair intercolony ancestrula distance (estimate of size at first contact) is plotted against intercolony border length (estimate of time since first contact); + = coordinated colony pair, o = non-coordinated colony pair. Note that data are plotted on a logarithmic scale.

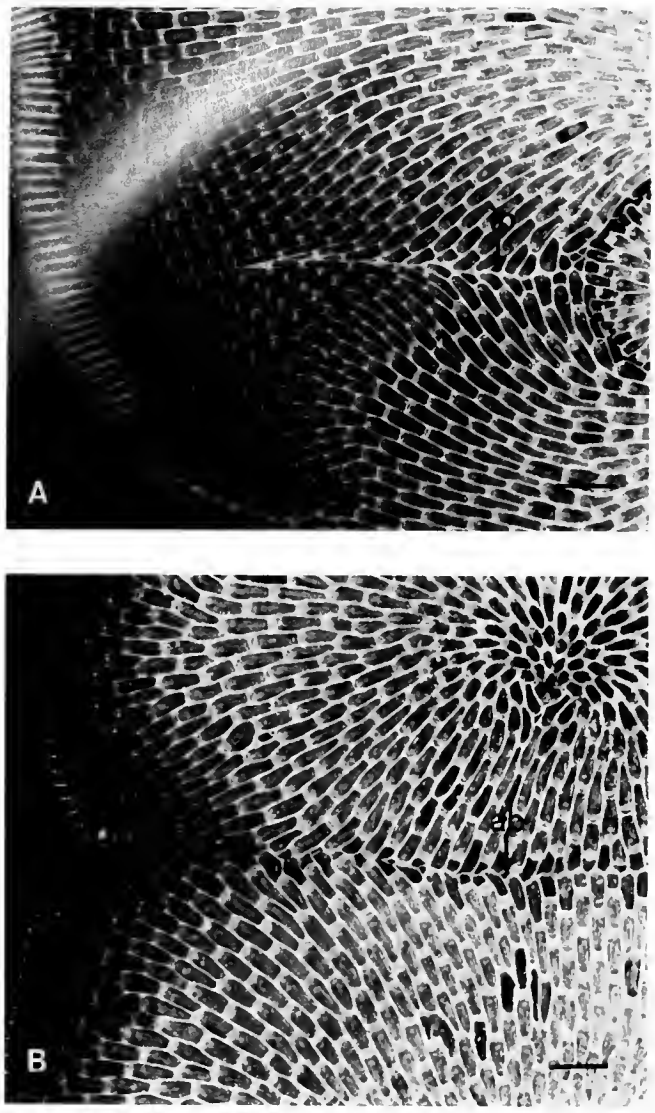

Figure 4. A. Isocontact border between genotypically identical tissues of a colony that has grown around another colony and back into contact with itself. B. Allocontact border between genotypically distinct colonies. Abbreviations: ab, allocontact border; ib, isocontact border; Size bars = 1.0 mm.

plates) in shape and slightly raised to form a perforated calcium carbonate dome or lens, the base of which is attached to the zooidal wall (Fig. 5A–C).

Pore plates found in isocontact borders, herein referred to as "isocontact pore plates" (Figs. 5C, 6B), were similar to lateral pore plates in that they consisted of a single round perforated dome. However, whereas lateral pore plates tended be of a uniform size and regularly spaced in lateral walls, isocontact pore plates were variable in size and occurred irregularly, occasionally in groups, in the walls formed between genotypically identical colonies.

Pore plates found in allocontact borders, herein referred to as "allocontact pore plates" (Figs. 5D; 6C, D) were found in the borders between both coordinated and non-coordinated colonies. Whereas all previously described pore plates consist of a single perforated calcium carbonate dome, allocontact pore plates were composed of two perforated calcium carbonate domes placed base to base forming a single sphere embedded in the intercolony border. Allocontact pore plates also differed from other pore plates in that they generally had three or fewer pores. In contrast, other types of pore plates generally had four or more pores. There were no obvious morphological differences between allocontact pore plates of coordinated and non-coordinated colonies.

Discussion

The results of this study show that allorecognition responses following contact between colonies of the bryozoan *Membranipora membranacea* vary depending on the genetic similarity and age of interacting colonies. Contact between genetically identical colonies is always characterized by an isocontact border, isocontact pore plates, and coordinated behavior of zooids. Contact between genotypically distinct colonies is always characterized by allocontact borders and allocontact pore plates. However, only colonies that are young when they first come into contact, show coordinated behavior.

Intercolony coordinated behavior appears to be the result of intercolony neural integration. Thorpe *et al.* (1975) demonstrated the presence of electrical signals that conducted across colonies of *M. membranacea* at the same rate as the spread of lophophore retractions. Electrical signals similar to those described by Thorpe *et al.* (1975) have been found to pass between behaviorally coordinated colonies but not between non-coordinated colonies (Shapiro and Mackie, unpub. data), providing direct evidence of intercolony neural linkage.

The presence of pore plates provides morphological evidence for intercolony neural linkage. The time required for the formation of isocontact or allocontact pore plates following initial intercolony contact would explain why colonies did not become coordinated immediately upon contact and why colonies with short intercolony border lengths did not show coordinated behavior. However, the presence of allocontact pore plates does not necessarily indicate behavioral coordination because allocontact pore plates were also found between non-coordinated colony pairs. Thus, there may be morphological differences on a finer scale (*e.g.*, presence or absence of functional nerves) between the allocontact pore plates of behaviorally coordinated and non-coordinated colonies.

Allocontact pore plates represent a new, morphologically distinct class of pore plates never before described in the Bryozoa. This is the first time pore plates between unrelated bryozoan colonies have been described. Chaney

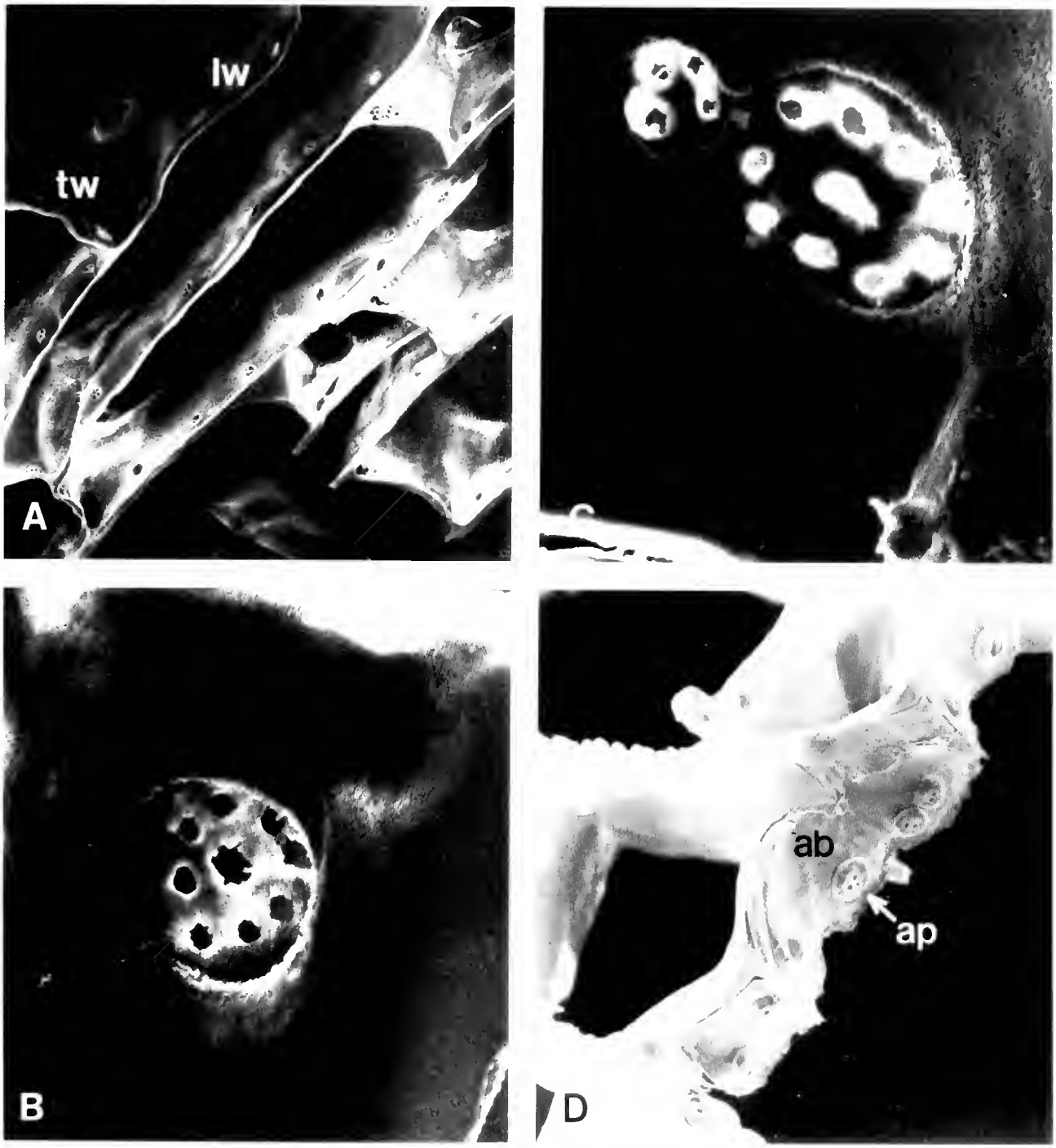

Figure 5. Scanning electron micrographs of the different types of pore plates found in *Membranipora membranacea*. A. Basal view of calcified zooidal walls showing transverse and lateral pore plates between zooids within a colony. (100 ×). B. Lateral pore plate between zooids within a colony (500 ×). C. Isocontact pore plates (500 ×). D. Allocontact border showing allocontact pore plates (100 ×). Abbreviations: ab, allocontact border; ap, allocontact pore plate; lw, lateral wall; tw, transverse wall.

(1983) examined the borders between unrelated colonies of the cheilostome bryozoan *Thalamoporella californica*, but found no evidence of pore plates. However, Chaney (1983) did find pore plates between sibling colonies of *T. californica*. These pore plates, which he called fusion pore plates, consisted of a single rather than a double calcium

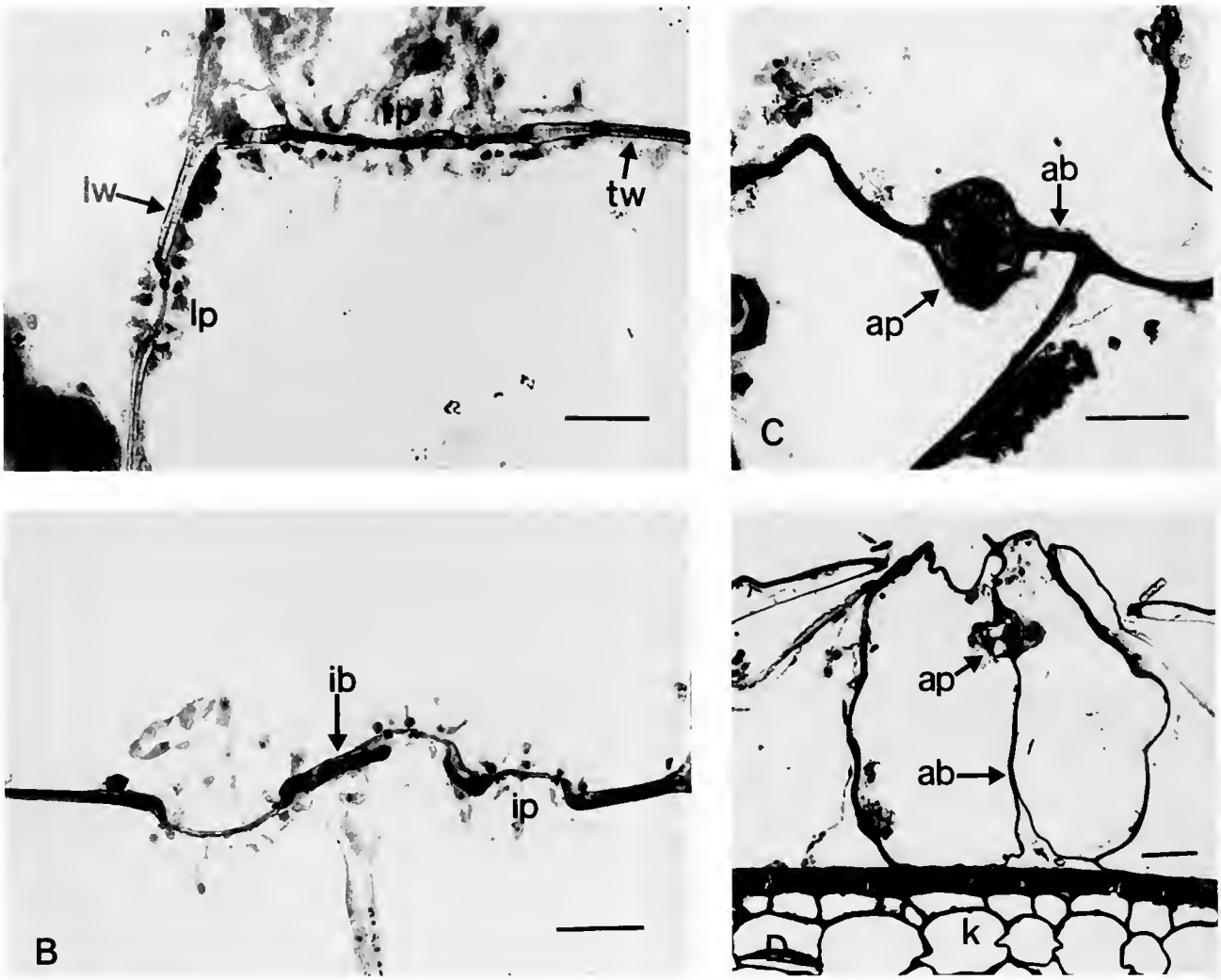

Figure 6. Light micrographs of the different types of pore plates found in *Membranipora membranacea*. Sections A through C were made parallel to the plane of the colony. A. Transverse and lateral pore plates between zooids within a colony. B. Isocontact plates. C. Allocontact plate. D. Section perpendicular to allocontact border and plane of colony showing an allocontact plate. Abbreviations: ab, allocontact border; ap, allocontact plate; ib, isocontact border; ip, isocontact plate; k, kelp; lw, lateral zooidal wall; tp, transverse pore plate; tw, transverse zooidal wall. Size bars = 20 μm.

carbonate dome and thus resemble the isocontact pore plates described in this study and not allocontact pore plates. Additionally, fusion pore plates, like isocontact pore plates, were variable in size and occurred irregularly in the walls formed by contact between two colonies. *T. californica* larvae settle within hours of release from the parental colony (Chaney, 1983), thus indicating the potential for substantial inbreeding in natural populations (Jackson, 1986). Consequently, although sexually produced, sibling colonies may be nearly genetically identical. Thus, fusion pores plates are probably the same as isocontact pore plates, both being characteristic of contact between genetically similar tissues.

It is usually assumed that colony pairs that have the morphological characteristics of fusion are physiologically integrated, and unfused colonies are not (Humphries, 1979; Stebbing, 1973b; Buss, 1982; Chaney, 1983). However, assays for physiological integration are rarely performed (Hidaka, 1985; Rinkevich and Loya, 1983a, b). When Rinkevich and Loya (1983a) used SEM to examine the allocontact borders between colonies of the Red Sea coral *Stylophora pistillata* with the morphological characteristics of fusion, they found that the colonies were not physiologically connected. In contrast, this study has demonstrated that *M. membranacea* colonies with the morphological characteristics of rejection can be physi-

ologically connected. Thus, unless adequate tests are performed, it may not always be safe to use morphological evidence of fusion or rejection to imply the presence or absence of physiological integration.

Allorecognition responses are important in intra- and interspecific interactions. Rejection responses to contact with colonies often result in the induction of aggressive structures used to fight, damage, or surround neighboring colonies (*e.g.,* Ivker, 1972; Francis, 1973; Rinkevich and Loya, 1983a; Sebens and Miles, 1988; Harvell and Padilla, 1990). On the other hand, fusion responses may benefit interacting colonies by increasing competitive ability, increasing fecundity, decreasing probability of mortality, or decreasing age of first reproduction (Buss, 1982). However, it may be erroneous to always associate fusion with cooperation and rejection with aggression. Rinkevich and Weissman (1987, 1989) found that fusion between genotypically distinct ascidian colonies frequently resulted in partial or total resorption of one of the colonies at a cost to both colonies. Thus, in this case fusion is apparently an aggressive interaction. In contrast, the results of the present study indicate the potential for cooperation between colonies that do not appear to have fused.

Intercolony behavioral coordination may be an adaptation that benefits small colonies by reducing the probability of mortality. Mortality of many marine invertebrates, including bryozoans, is size dependent, with small colonies having a higher probability of mortality (Jackson, 1985; Yund and Parker, 1989; Harvell *et al.,* 1990). Coordinated behavior between small *M. membranacea* colonies may benefit each colony by enabling colonies to receive and transmit signals that act as "warnings" of possible sources of damage or mortality. Such cooperative behavior is consistent with theory predicting that cooperation will be more likely to evolve between sessile organisms that interact repeatedly (Axelrod and Hamilton, 1981; Buss, 1981).

It could also be argued that intercolony behavioral coordination is a non-adaptive trait that results from the inability of young colonies to distinguish between genetically identical and genotypically distinct tissues. There are several examples of colonial marine invertebrates that will fuse when young but not when older (*e.g.,* Hidaka, 1985; Shenk and Buss, 1991). It is not known what causes changes in fusibility, although immunological incompetence of young colonies has been suggested (Hidaka, 1985). However, if immature, genotypically distinct colonies of *M. membranacea* were simply treating adjoining colonies as genotypically identical, intercolony borders and pore plates should resemble isocontact borders and isocontact pore plates. Instead, typical allocontact borders and allocontact pore plates were formed between all genotypically distinct behaviorally coordinated colonies implying that colonies had recognized their neighbors as being genotypically distinct.

Acknowledgments

I thank Jim Morin for generously providing lab space and materials in California and Andrea Huvard for instructing me in the techniques of light microscopy. This manuscript benefited from comments by Liz Francis, Jim Morin, Drew Harvell, Josh Nowlis, Jordan West, Staci Eisner, and an anonymous reviewer. Discussions with Liz Francis were extremely helpful in organizing the final draft. This research was supported in part by the Lerner-Gray Fund for Marine Research and NSF-OCE-8817498 to C. Drew Harvell. I also thank Dennis Willows for providing space and facilities at Friday Harbor Laboratories.

Literature Cited

Axelrod R., and W. D. Hamilton. 1981. The evolution of cooperation. *Science* **211:** 1390–1396.

Banta, W. C. 1969. The body wall of cheilostome Bryozoa, II. Interzooidal communication organs. *J. Morphol.* **129:** 149–170.

Buss, L. W. 1981. Group living, competition, and the evolution of cooperation in a sessile invertebrate. *Science* **213:** 1012–1014.

Buss, L. W. 1982. Somatic cell parasitism and the evolution of somatic tissue compatibility. *Proc. Natl. Acad. Sci. USA* **79:** 5337–5341.

Buss, L. W., and R. K. Grosberg. 1990. Morphogenetic basis for phenotypic differences in hydroid competitive behavior. *Nature* **343:** 63–66.

Chaney, H. W. 1983. Histocompatibility in the cheilostome bryozoan *Thalamoporella californica. Trans. Am. Microsc. Soc.* **102:** 319–332.

Dayton, P. K. 1971. Competition, disturbance, and community organization: the provision and subsequent utilization of space in a rocky intertidal community. *Ecol. Monogr.* **41:** 351–389.

Francis, L. 1973. Clone specific segregation in the sea anemone *Anthopleura elegantissima. Biol. Bull.* **144:** 64–72.

Grosberg, R. K. 1988. The evolution of allorecognition specificity in clonal invertebrates. *Q. Rev. Biol.* **63**(4): 377–412.

Harvell, C. D., and D. K. Padilla. 1990. Inducible morphology, heterchrony, and size hierarchies in a marine bryozoan. *Proc. Natl. Acad. Sci. USA* **87:** 508–512.

Harvell, C. D., H. Caswell, and P. Simpson. 1990. Density effects in a colonial monoculture: experimental studies with a marine bryozoan (*Membranipora membranacea* L.). *Oecologia* **82:** 227–237.

Hidaka, M. 1985. Tissue compatibility between colonies and between newly settled larvae of *Pocillopora damicornis. Coral Reefs* **4:** 111–116.

Humphries, E. M. 1979. Selected features of growth in *Parasmittina nitida.* Pp. 195–218 in *Advances in Bryozoology,* G. P. Larwood and M. B. Abbott, eds. Academic Press, New York.

Ivker, F. 1972. A hierarchy of histo-incompatability in *Hydractinia echinata. Biol. Bull.* **143:** 162–174.

Jackson, J. B. C. 1977. Competition on marine substrata: the adaptive significance of solitary and colonial strategies. *Am. Nat.* **111:** 743–767.

Jackson, J. B. C. 1979. Overgrowth competition between encrusting cheilostome ectoprocts in a Jamaican cryptic reef environment. *J. Anim. Ecol.* **48:** 805–823.

Jackson, J. B. C. 1985. Distribution and ecology of clonal and aclonal benthic invertebrates. In *Population Biology and Ecology of Clonal*

Organisms, J. B. C. Jackson, L. W. Buss, and R. E. Cook, eds. Yale University Press, New Haven and London.

Jackson, J. B. C. 1986. Modes of dispersal of clonal and aclonal benthic invertebrates: consequences for species' distributions and genetic structure of local populations. *Bull. Mar. Sci.* **39:** 588–606.

Koyama, H., and H. Watanabe. 1982. Colony specificity in the ascidian, *Perophora sagamiensis. Biol. Bull.* **162:** 171–181.

Lutaud, G. 1977. The bryozoan nervous system. In *The Biology of Bryozoans,* R. M. Woollacott and R. L. Zimmer, eds. Academic Press, New York and London.

Lutaud, G. 1979. Étude ultrastructurale du plexus colonial et recherche de connexions nerveuses interzoidiales chez le bryozoaire chilostome *Electra pilosa* (Linné). *Cah. Biol. Mar.* **20:** 315–324.

Nielson, C. 1981. On morphology and reproduction of *Hippodiplosia insculpta* and *Fenestrulina malusii* (Bryozoa, Cheilostomata). *Ophelia* **20**(1): 91–125.

Osman, R. W. 1977. The establishment and development of a marine epifaunal community. *Ecol. Monogr.* **47:** 37–63.

Rinkevich, B., and Y. Loya. 1983a. Intraspecific competitive networks in the Red Sea coral *Stylophora pistillata. Coral Reefs* **1:** 161–172.

Rinkevich, B., and Y. Loya. 1983b. Oriented translocation of energy in grafted reed corals. *Coral Reefs* **1:** 243–247.

Rinkevich, B., and I. L. Weissman. 1987. A long-term study on fused subclones in the ascidian *Botryllus schlosseri:* the resorption phenomenon (Protochordata: Tunicata). *J. Zool. Lond.* **213:** 717–733.

Rinkevich, B., and I. L. Weissmann. 1989. Variation in the outcome following chimera formation in the colonial tunicate *Botryllus schlosseri. Bull. Mar. Sci.* **45**(2): 213–227.

Sabbadin, A. 1982. Formal genetics of ascidians. *Am. Zool.* **22:** 765–773.

Scofield, V. L., J. M. Schlumpberger, L. A. West, and I. L. Weissman. 1982. Protochordate allorecognition is controlled by a MHC-like gene system. *Nature* **295:** 499–502.

Scofield, V. L., and L. S. Nagashima. 1983. Morphology and genetics of rejection reactions between oozoids from the tunicate *Botryllus schlosseri. Biol. Bull.* **165:** 733–744.

Sebens, K. P., and J. Miles. 1988. Sweeper tentacles in a gorgonian octocoral: Morphological modifications for interference competition. *Biol. Bull.* **175:** 378–387.

Shenk, M. A., and L. W. Buss. 1991. Ontogenetic changes in fusibility in the colonial hydroid *Hydractinia symbiolongicarpus. J. Exp. Zool.* **257:** 80–86.

Silen, L. 1944. On the formation of the interzoidal communications of the Bryozoa. *Zool. Bidr. Upps.* **22:** 433–488.

Stebbing, A. R. D. 1973a. Competition for space between the epiphytes of *Fucus serratus* L. *J. Mar. Biol. Assoc. UK* **53:** 247–261.

Stebbing, A. R. D. 1973b. Observations on colony overgrowth and spatial competition. Pp. 173–183 in *Living and Fossil Bryozoa,* G. P. Larwood, ed. Academic Press, London and New York.

Thorpe, J. P., G. A. B. Shelton, and M. S. Laverack. 1975. Electrophysiology and coordinated responses in the colonial bryozoan *Membranipora membranacea* (L.). *J. Exp. Biol.* **62:** 115–121.

Yoshioka, P. M. 1982. Role of planktonic and benthic factors in the population dynamics of the bryozoan *Membranipora membranacea. Ecology* **63**(2): 457–468.

Yund, P. O., and H. M. Parker. 1989. Population structure of the colonial hydroid *Hydractinia* sp. nov. C in the Gulf of Maine. *J. Exp. Mar. Biol. Ecol.* **125:** 63–82.

Reference: *Biol. Bull.* **182**: 231–240. (April, 1992)

Antipredator Defenses in Tropical Pacific Soft Corals (Coelenterata: Alcyonacea). I. Sclerites as Defenses Against Generalist Carnivorous Fishes

KATHRYN L. VAN ALSTYNE[1], CHAD R. WYLIE,
VALERIE J. PAUL, AND KAREN MEYER

University of Guam Marine Laboratory, UOG Station, Mangilao, Guam 96923

Abstract. Calcified sclerites are common in many invertebrate species and are frequently used as taxonomic indicators; however, little is known about the function of sclerites. To determine whether sclerites could function as antipredator defenses, we conducted field assays in which sclerites from the Indo-Pacific soft corals *Sinularia maxima, S. polydactyla,* and *S.* sp. were incorporated into an artificial diet and offered to a natural assemblage of fishes in the field. Sclerites from both the tips and bases of all three species of *Sinularia* reduced feeding by a natural assemblage of generalist carnivorous fishes off Guam by 27–44%; however, sclerites from the bases of the colonies were 18–51% more deterrent than tip sclerites. The greater effectiveness of sclerites from the bases of the colonies was largely attributable to their high concentrations. Sclerites in the tips of the colonies occurred in mean concentrations from 24 to 58% by dry weight and were generally less than 0.5 mm in length. Sclerites in the bases of the colonies were larger and occurred in average concentrations of 82–88%. *Sinularia* sclerites were increasingly effective as feeding deterrents with increasing concentration at concentrations less than 30–50% by dry weight. The effectiveness of sclerites as deterrents leveled off at higher concentrations. Sclerite morphology was also important in determining antipredator activity. Although sclerites can play a role in predator deterrence, they can also function in the structural support of colonies. Thus, the sizes, shapes, and abundances of sclerites at different locations within colonies will be determined by their functions at particular locations as well as constraints upon their use or production.

Received 11 July 1991; accepted 23 January 1992.

[1] Present Address: Department of Biology, Kenyon College, Gambier, Ohio 43022.

Introduction

Soft corals are frequently a conspicuous component of shallow, Indo-Pacific tropical reef communities despite the abundance of carnivorous fishes. For example, on Guam, soft corals have been reported to provide ~95% of the total living animal cover on some reefs (Wylie and Paul, 1989). On New Guinean reefs, soft corals constitute approximately 50% of the living cover between depths of 0 and 5 m (Tursch and Tursch, 1982).

The persistence of soft corals and gorgonians in areas with high levels of predation has previously been attributed to their production of predator-deterrent secondary metabolites (Coll *et al.,* 1983; LaBarre *et al.,* 1986; Pawlik *et al.,* 1987; Wylie and Paul, 1989); but, soft corals and gorgonians also produce sclerites or spicules that could potentially serve as antipredator defenses (Harvell and Suchanek, 1987; Sammarco *et al.,* 1987; Harvell *et al.,* 1988; Harvell and Fenical, 1989). Mineral-hardened spicules are common within a number of invertebrate groups including sponges, cnidarians, platyhelminth worms, mollusks, echinoderms, and ascidians (Kingsley, 1984). However, despite the widespread occurrence of sclerites within marine invertebrates, little is known about the function of these structures, in particular, their ability to deter feeding by potential predators.

Only in recent studies has the role of sclerites as antipredator defenses been explored. When incorporated into an artificial diet, sclerites of the gorgonian sea whip *Pseudopterogorgoria acerosa* deterred feeding by carnivorous fishes in field assays in Belize (Harvell *et al.,* 1988). Scler-

ites of the Caribbean gorgonian *Gorgonia ventalina* deter feeding by natural assemblages of fishes in the field and by the gorgonian specialist *Cyphoma gibbosum* (Van Alstyne and Paul, in press). Toxicity of soft corals to the mosquito fish *Gambusia affinis* was negatively correlated with the degree of armament of the polyps in the Nephthedidae and negatively correlated with the degree of mineralization of the coenenchyme in 14 species of *Sinularia* (Sammarco *et al.*, 1987). Alcyonarian sclerites are extremely variable in size and morphology and are frequently used as taxonomic characters (*e.g.*, Bayer, 1956, 1961; Bayer *et al.*, 1983). Seasonal fluctuations in collagen levels in the organic matrix of sclerites indicate that these structures are dynamic and may undergo seasonal cycles of demineralization and remineralization (Kingsley *et al.*, 1990).

In this paper, we provide direct experimental evidence that sclerites from the alcyonian soft corals *Sinularia* spp. serve as antipredator defenses to generalist carnivorous fishes in the field. Soft corals of the genus *Sinularia* are widely distributed throughout the Indo-Pacific region (Verseveldt, 1977, 1980), and are an important component of shallow coral reef communities on Guam (Gawel, 1977). *Sinularia* spp. generally have a lobate morphology with an upper portion that contains polyps, and a lower sterile stalk (Verseveldt, 1977). The surface of the lobes contains small club-shaped sclerites, rods, and spindles (Verseveldt, 1980). We also document differences in sclerite morphologies and densities within soft coral colonies and explore the consequences of these differences in deterring feeding by fishes.

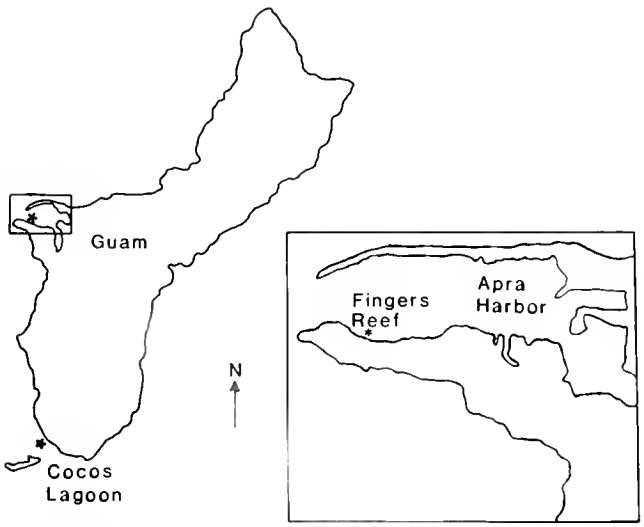

Figure 1. Locations of the Fingers Reef and Cocos Lagoon study sites on Guam.

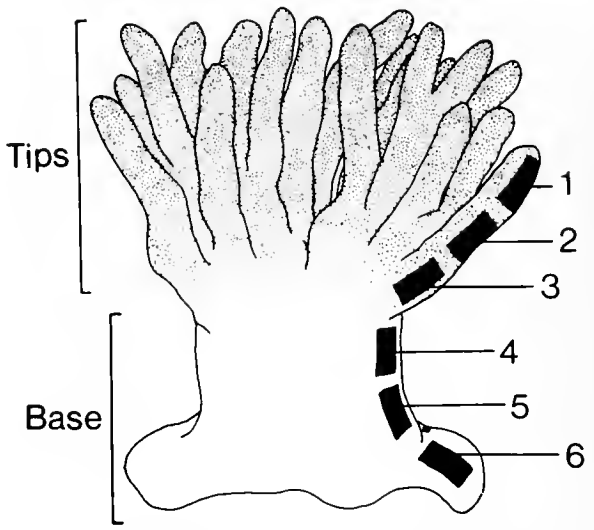

Figure 2. Sampling locations within an individual *Sinularia* colony. Three transects of six samples each were made from the tips of the colony to the base of the colony. Transects ran from the most distal tips of the colonies (location 1) to the point of attachment at the base of the colony (location 6).

Materials and Methods

Study sites

Sinularia maxima, S. polydactyla, and *S.* sp. were collected from a patch reef in Cocos Lagoon, Guam, USA (Fig. 1). This reef has been previously described by Paul and Van Alstyne (1987) and Wylie and Paul (1989). It is a small patch reef, ~35 m × 50 m, that is composed mainly of dead *Acropora.* Soft corals comprise ~10% of the cover of the reef (Wylie, 1988).

All feeding experiments took place on Fingers Reef in Apra Harbor, Guam. The reef at Fingers (Fig. 1) is composed of a diverse assemblage of scleractinian corals, as well as many unidentified species of *Sinularia.* Numerous species of herbivorous and carnivorous fish inhabit this reef. The fishes that were observed to feed on ropes during feeding experiments included sergeant majors (*Abudefduf* spp.), damselfish (*Amblyglyphidodon curacao*), wrasses (*Cheilinus fasciatus, Gomphosus varius, Halichoeres trimaculatus*), and triggerfish (*Balistapus undulatus*).

Quantification of sclerite concentrations

Five soft corals each of *Sinularia maxima, S. polydactyla,* and *S.* sp. were collected from Cocos Lagoon. Six samples of ~2 cm (height) × 1 cm (length) × 1 cm (width) were removed from each of three "transects" of each colony. The transects ran from the most distal part of the tips to the point of attachment at the base (Fig. 2). These samples areas will be referred to as locations #1 (most

distal tip sample) through #6 (base sample closest to the attachment point of the colony). Eighteen samples were taken from each of the 15 colonies. Sclerites concentrations from each sample were quantified as described in Van Alstyne and Paul (in press).

An analysis of variance was used to test for differences in mean sclerite concentrations among species, among individuals within a species, among transects within an individual, and among locations. A mixed model ANOVA was conducted with the factors being (1) species, (2) individuals nested within species, (3) transects nested within individuals, and (4) locations along the transects from the tips to the bases of the colonies. The analysis was conducted with an SPSSPC + statistical package.

Measurement of sclerites

Sclerites from the samples taken above were used to obtain measurements of sclerite sizes within colonies. Measurements of maximum sclerite length were made from 100 to 200 sclerites from each sample using a video image analysis system. All of the sclerites in at least two randomly selected fields from each of three subsamples from each sample were measured to the nearest μm at magnifications ranging from 60× to 500× using a JAVA computer program.

Sclerite masses were estimated by using a log-log regression of sclerite masses to lengths. To obtain the regression, 15–20 sclerites from each species were measured to the nearest μm with a video image analysis system and then weighed to the nearest 0.01 mg. The regression equations for each species were: *S. maxima:* $\text{mass(g)} = e^{-26.85+3.10*\ln[\text{length}(\mu\text{m})]}$ ($n = 20$, $r^2 = 0.696$, $P < 0.05$), *S. polydactyla:* $\text{mass(g)} = e^{-18.80+2.15*\ln[\text{length}(\mu\text{m})]}$ ($n = 20$, $r^2 = 0.802$, $P < 0.05$), *S.* sp: $\text{mass(g)} = e^{-20.00+2.41*\ln[\text{length}(\mu\text{m})]}$ ($n = 15$, $r^2 = 0.960$, $P < 0.05$).

Extraction of sclerites for feeding assays

Approximately 15 individuals each of 3 soft coral species were collected from Cocos Lagoon. Tissues at the bases of the soft corals were separated from the tips and lobes (*sensu* Wylie and Paul, 1989). The polyp-bearing, top 10–15 cm of the colonies will hereafter be referred to as the tips (Fig. 2). The pieces from all individuals of a species were combined and extracted twice in 1:1 methylene chloride:methanol. The organic extracts were removed, and the remaining soft coral pieces were dried, then digested in bleach until no organic material remained. The sclerites were rinsed five to eight times in tap water, then once with acetone, and dried. Examination of sclerites using light microscopy and scanning electron microscopy showed no signs of sclerite deterioration due to the extraction process.

Two-choice feeding experiments

Sclerites from soft coral tips and bases were incorporated into an artificial diet consisting of 2.5 g carrageenan (Sigma #C-1013), 4 g of paraffin wax, and 70 ml water, heated in a microwave oven for 75 s. After the wax/carrageenan mixture was heated, ~50 g of squid homogenate (250 ml water:500 g squid) and sclerites were added. Concentrations of sclerites used in these feeding experiments are listed in Table I. These values are within the ranges of concentrations measured in bases and tips of *Sinularia* spp. in this study. Controls consisted of the artificial diet without sclerites. The diet was then poured into stainless steel potato slicers that were composed of a 7 × 7 grid of 1 cm × 1 cm squares that were ~1 cm high. Prior to the addition of the diet, black plastic o-rings (⅜ in OD, ¼ in ID) were placed in each cube in the potato slicer. After the diet had gelled, it was removed from the mold and attached to ropes to be placed out in the field. The diet was presented to fishes on 50 cm long pieces of 3 strand, ¼ in yellow polypropylene rope in which four 3-cm long safety pins were attached equidistantly along the top 30–40 cm of the rope (Fig. 3).

The ropes were placed on the reef in pairs by attaching them to pieces of coral. All experiments were done on Fingers Reef in Apra Harbor, Guam, at a depth of 5–8 m. Pairs of ropes were placed on the reef and removed when at least four of the eight pieces of artificial diet on the two ropes had been completely consumed. Each experiment consisted of 17–21 pairs of ropes. Differences in consumption were compared with a Wilcoxon Signed Ranks test ($\alpha = 0.05$).

Feeding experiments at Fingers Reef consisted of the following paired experiments: (1) comparisons of feeding rates on control diet *versus* diet containing either tip sclerites or base sclerites at natural concentrations (Table I), (2) comparisons of feeding rates on control diet and diet containing either tip or base sclerites at 10%, 25%, or 50% by dry weight, and (3) comparisons of diet containing tip sclerites at natural concentrations with diet containing base sclerites at natural concentrations. Each of the experiments described above was conducted with all three species of *Sinularia*.

Table I

Concentrations (as percent of dry weight) of sclerites used in feeding assays

	Tips	Bases
Sinularia maxima	31%	81%
S. polydactyla	41%	76%
S. sp.	47%	82%

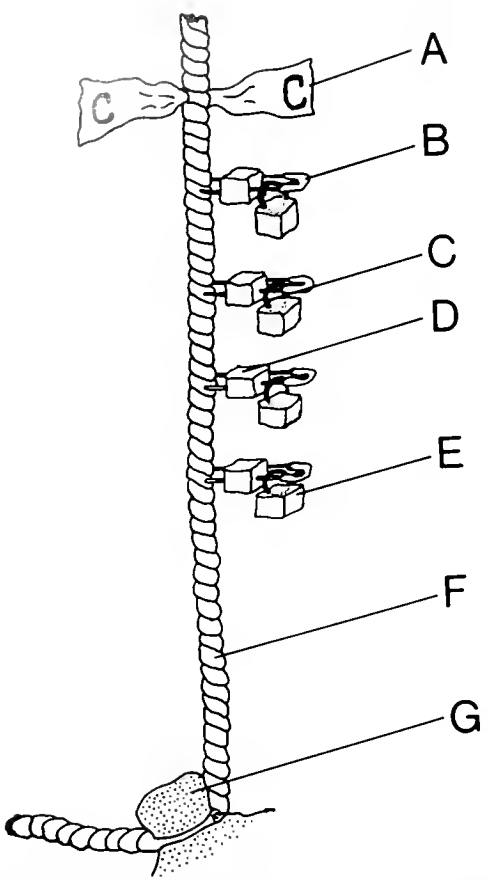

Figure 3. Rope used in a feeding assay. The assay consisted of attaching an o-ring (C) embedded within a piece of artificial diet (E) to a safety pin (B). The safety pins were attached to a 0.5 m piece of 3-strand polypropylene rope (F) and were buoyed with small pieces of neoprene (D). The ropes were attached in the field to pieces of coral (G). Ten-cm pieces of labelled surveyor's tape (A) were used to distinguish ropes containing different types of diet. A single rope held only one type of diet.

Four-choice feeding experiments

To determine the relative effects of sclerite morphologies and concentrations on feeding deterrence, fishes were offered artificial diets containing two types of sclerites (tip and base) at two different concentrations (tip concentrations and base concentrations). Thus, fishes were offered tip sclerites at natural tip concentrations, tip sclerites at natural base concentrations, base sclerites at natural tip concentrations, and base sclerites at natural base concentrations. Separate experiments were conducted for each of the three *Sinularia* species.

Artificial diets were attached to polypropylene ropes and offered to fishes in the field in the same manner as described for the two-choice experiments, with the exception that a set of four ropes were offered instead of a pair of ropes. Each of the four ropes contained one of the four diets described above; each of the four types of diet was presented in each replicate (n = 19 or 20). Ropes were removed and the number of pieces of each diet remaining on each rope were counted after fishes had consumed at least half of the sixteen pieces of diet in the set. Statistical analyses were conducted with a two-way Kruskal-Wallis test. Factors used in the analysis were sclerite type and sclerite concentration.

Results

Distribution and abundance of sclerites

Dry weight concentrations of sclerites differed among the three species of *Sinularia* and among locations within the colonies (Table II). In general, sclerite concentrations (as % of dry weight) increased from the tips of the colonies to their bases (Fig. 4). Mean concentrations at the tips of the colonies ranged from 24% in *S. polydactyla* to 58% in *S.* sp. Mean concentrations of sclerites in the most basal portion of the colonies ranged from 82% in *S. maxima* to 88% in *S.* sp.

The size distributions of sclerites also showed considerable intra-colony variation. Almost all of the sclerites in the most distal tips of the colonies of the three species of soft corals were less than 0.5 mm in length (Figs. 5–7). However, in *S.* sp., the majority of the mass of the sclerites in the most distal tips were comprised of sclerites that were greater than 0.5 mm long; the largest fraction by mass was 1.0–1.5 mm long (Fig. 5). In the most distal tips of *S. polydactyla,* approximately 55% of the sclerite mass was comprised of sclerites less than 0.5 mm in length (Fig. 6); and, in *S. maxima,* all of the mass of the sclerites in the most distal tips was in the <0.5 mm category (Fig. 7).

Larger sclerites increased in abundance in the more basal portions of the colonies of all three soft coral species (Figs. 5–7). Even in the most basal samples, sclerites less than 0.5 mm long were numerically abundant; however, they made up only a small fraction of the total sclerite

Table II

Analysis of variance of sclerite concentrations in Sinularia *spp.*

Source	df	SS	MS	F	*P*
Species	2	12,130	6,065	10.39	0.000
Individual (species)	12	8,363	697	1.19	0.288
Transect (individual)	10	6,483	648	1.11	0.355
Location	5	55,625	11,124	19.06	0.000
Error	240	140,071	584		
Total	269	222,672			

A mixed model ANOVA was conducted with the factors being (1) species, (2) individuals nested within species, (3) transects nested within individuals, and (4) locations along the transects from the tips to the bases of the colonies.

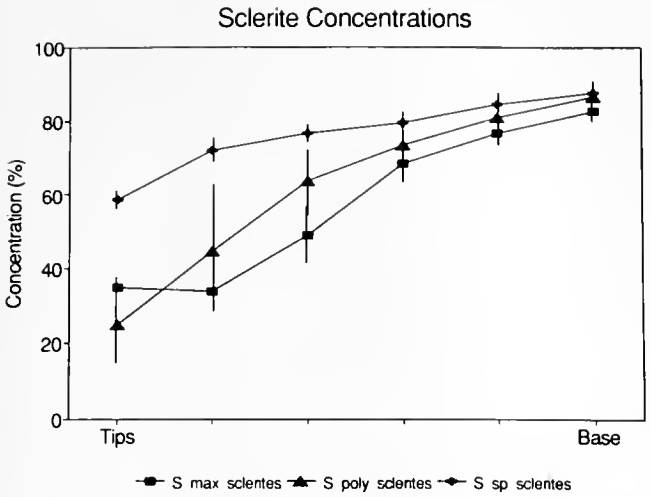

Figure 4. Sclerite concentrations (as % of dry weight) within colonies of *Sinularia* spp. Samples were obtained from five colonies of each of the three species. The samples correspond with locations 1 (tips) through 6 (base) shown in Figure 2. Horizontal bars represent ± 1 SD.

mass. In the most basal samples, the largest fractions of sclerites by mass were in the 1.0–1.5 mm size class in *S. maxima* (Fig. 7) and in the 1.5–2.0 mm size class in *S. polydactyla* (Fig. 6) and *S.* sp. (Fig. 5). Thus, in all three species of *Sinularia* examined in this study, sclerites increased in both size and concentration from the tips of the colonies to the bases.

Sclerites in *S. maxima* ranged in length from 0.06 to 5.0 mm. The largest sclerites in *S. maxima* were elongated spindles with complex tubercles (*sensu* Bayer *et al.*, 1983). The small sclerites (<0.5 mm long) were rods with volcano-like processes and wart clubs (*sensu* Bayer *et al.*, 1983). Wart clubs were proportionately more abundant in the tips than the bases of *S. maxima*. The large sclerites (>0.5 mm long) of *S. polydactyla* were comprised primarily of spindles with complex tubercles. Most of the spindles were straight; however, a few were bent. The small sclerites were either thorn clubs or rods with volcano-like processes. Sclerites from *S. polydactyla* ranged in length from 0.08 to 5.0 mm. In *S.* sp., the larger sclerites were comprised of spindles with complex tubercles, thorn stars, and thorn scales. The spindles were frequently bent and occasionally bifurcated on one end. The tubercles on the spindles of *S.* sp. were smaller than those on *S. maxima* and *S. polydactyla*. The smaller sclerites were rods and thorn clubs. Sclerites from *S.* sp. ranged in length from 0.08 to 4.6 mm.

Effectiveness of sclerites as feeding deterrents

At natural concentrations, all of the sclerites from the bases and the tips of all three species of *Sinularia* were significantly ($P < 0.05$) deterrent to fishes at Fingers Reef (Fig. 8). The addition of sclerites from the tips of *Sinularia* spp. reduced feeding by 33–44%, whereas sclerites from the bases of the colonies reduced feeding by 27–33%.

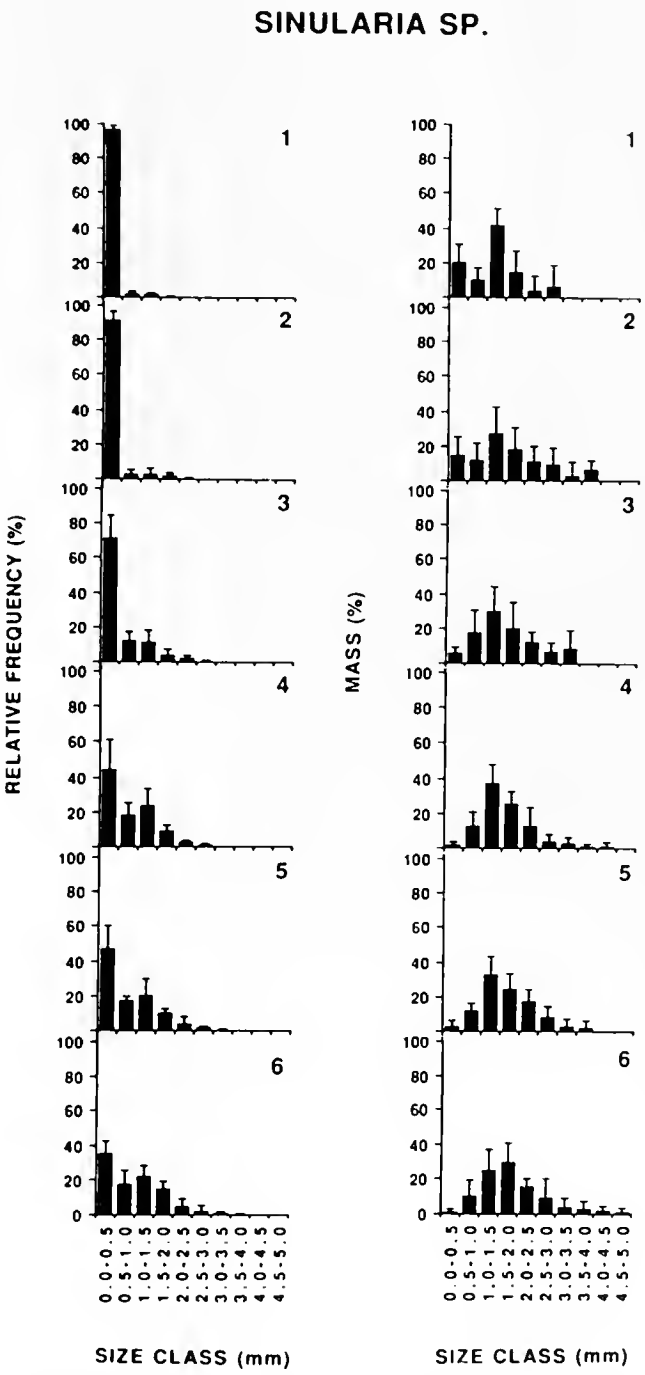

Figure 5. Relative frequencies and masses of sclerites within ten length classes from six locations within colonies of *Sinularia* sp. Samples were taken along transects from the tips of the colonies (location 1) to the bases of the colonies (location 6). The values for each size class are means from five colonies ± 1 SD.

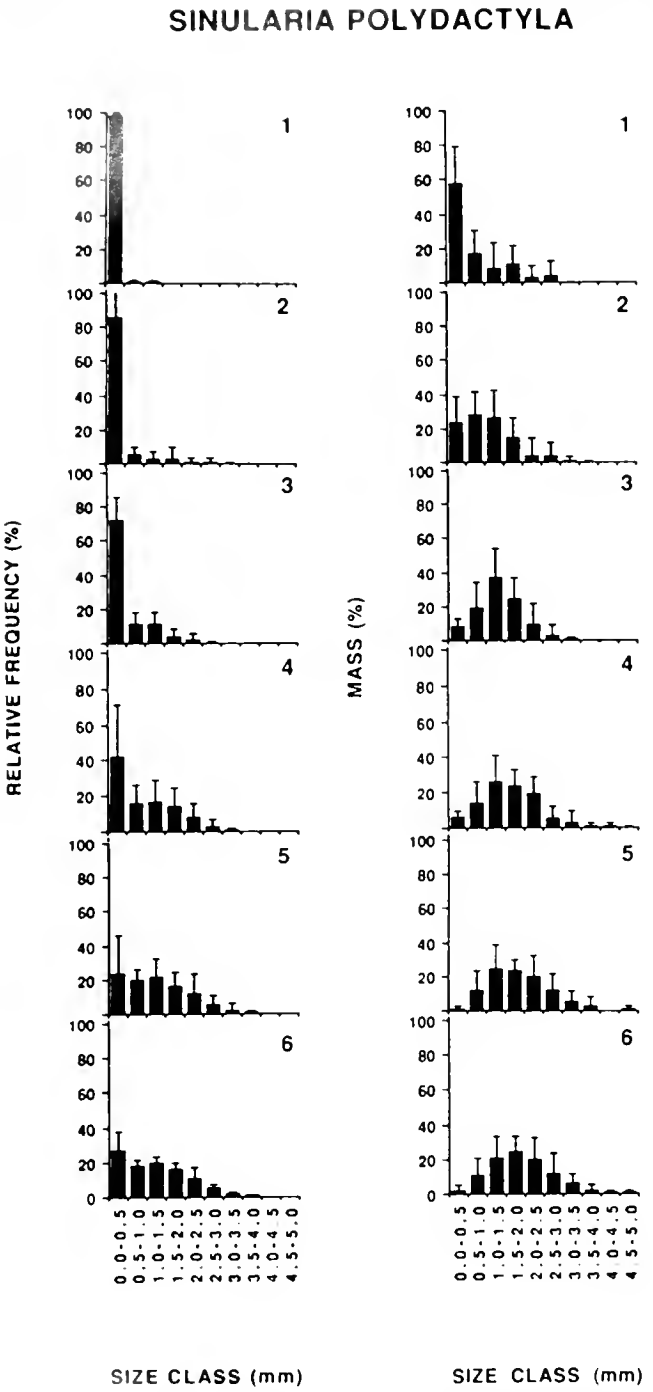

Figure 6. Relative frequencies and masses of sclerites within ten length classes from six locations within colonies of *Sinularia polydactyla*. Samples were taken along transects from the tips of the colonies (location 1) to the bases of the colonies (location 6). The values for each size class are means from five colonies ± 1 SD.

The ability of *Sinularia* sclerites to deter feeding was dependent upon the concentration of sclerites added to the artificial diet. At the low concentrations of 10% by dry weight, none of the sclerites from either bases or tips were significantly deterrent (Figs. 9, 10). Artificial diets containing sclerites from the bases of the colonies at 10% by dry weight were consumed at approximately equal rates

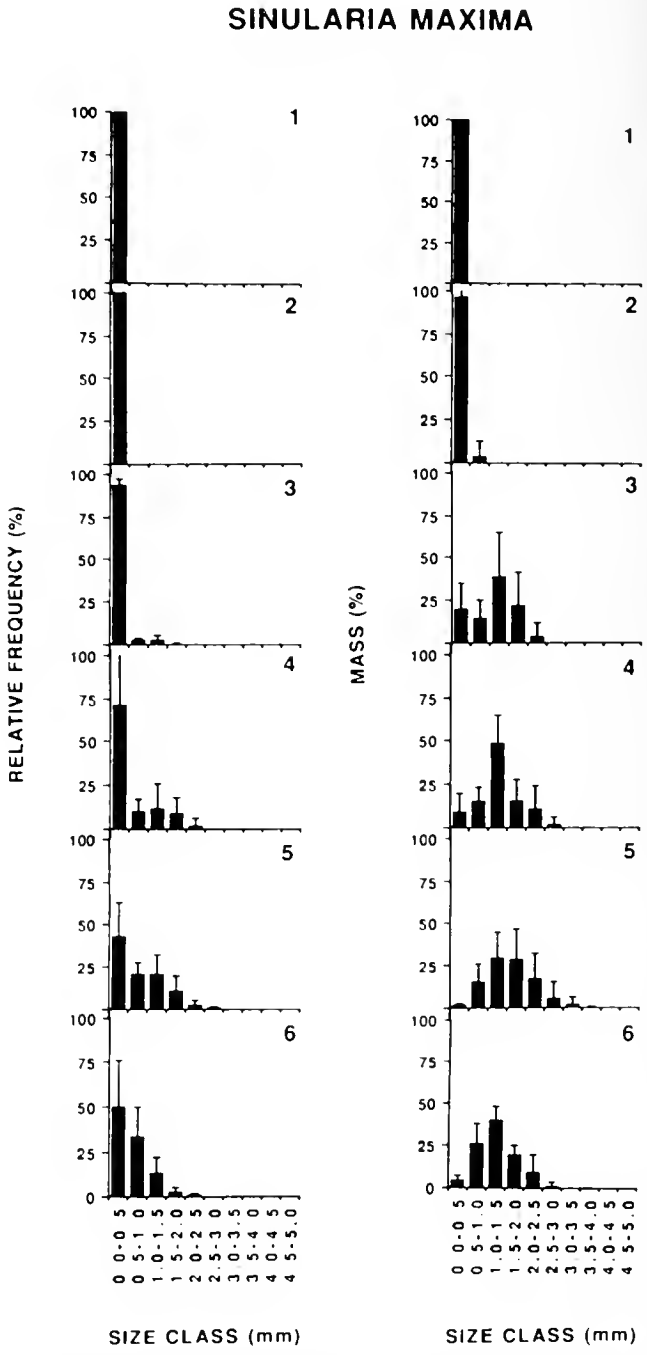

Figure 7. Relative frequencies and masses of sclerites within ten length classes from six locations within colonies of *Sinularia maxima*. Samples were taken along transects from the tips of the colonies (location 1) to the bases of the colonies (location 6). The values for each size class are means from five colonies ± 1 SD.

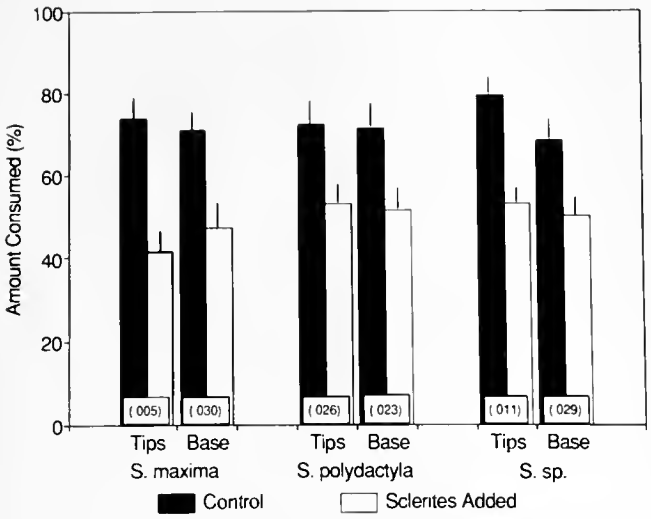

Figure 8. Mean amount consumed by generalist fishes at Fingers Reef of artificial diet with sclerites from *Sinularia* spp. (white bars) and without sclerites (dark bars). Numbers in parentheses at the bases of the bars are *P* values from Wilcoxon Signed Ranks tests for paired comparisons.

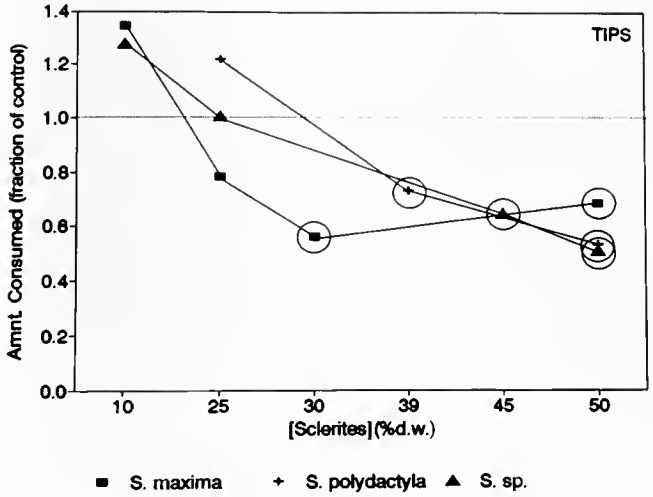

Figure 10. Feeding deterrence of *Sinularia* tip sclerites towards generalist carnivorous fishes at different sclerite concentrations. Points represent the mean feeding rate on artificial diet with sclerites relative to control diet lacking sclerites. Each value represents the results of a single two-way choice experiment. Circled points denote experiments in which sclerites were significantly deterrent ($P < 0.05$).

to artificial diet lacking sclerites (Fig. 9); artificial diets containing tip sclerites from *S. maxima* and *S.* sp. at 10% by dry weight were consumed at a greater rate than the control diets (Fig. 10). The relative consumption rate of artificial diets with sclerites relative to control diets lacking sclerites decreased with increasing sclerite concentration. All of the sclerites except those from the bases of *S.* sp. were significantly deterrent ($P < 0.05$) at concentrations greater than 25% by dry weight; *S.* sp. base sclerites were not significantly deterrent ($P > 0.05$) at 50% by dry weight, but were deterrent at 82% by dry weight.

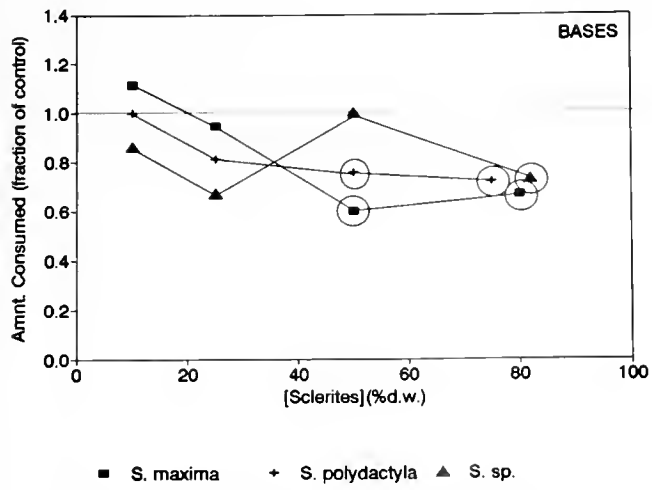

Figure 9. Feeding deterrence of *Sinularia* base sclerites towards generalist carnivorous fishes at different sclerite concentrations. Points represent the mean feeding rate on artificial diet with sclerites relative to control diet lacking sclerites. Each value represents the results of a single two-way choice experiment. Circled points denote experiments in which sclerites were significantly deterrent ($P < 0.05$).

Intracolony differences in sclerite effectiveness

When directly tested in paired feeding experiments, sclerites from the bases of the colonies were more effective feeding deterrents than sclerites from the tips of the colonies (Fig. 11). The amount of feeding on artificial diets

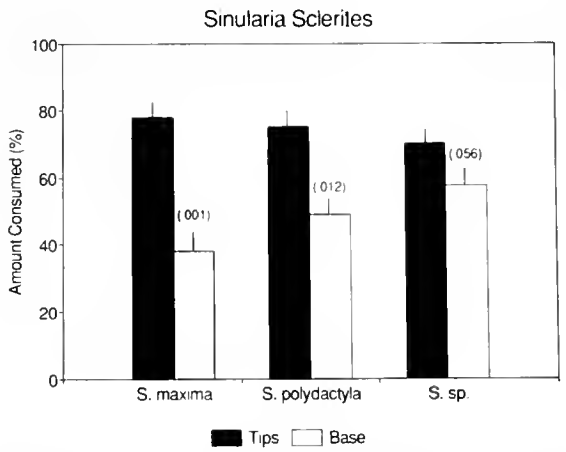

Figure 11. Mean amount consumed by generalist carnivorous fishes of artificial diet containing tip (dark bars) and base (white bars) sclerites in paired feeding experiments (n = 19 to 20). Numbers in parentheses are *P* values from Wilcoxon Signed Ranks tests for paired comparisons.

containing sclerites from the bases of the colonies was 18% (in *S.* sp.) to 51% (in *S. maxima*) lower than the consumption of diets containing tip sclerites.

Because both the morphologies and concentrations of sclerites differ between the bases and tips of the colonies, differences in the deterrence of tip and base sclerites could result from differences in the sizes and shapes of the sclerites or from differences in their amounts. To sort out the relative contributions of sclerite morphology and concentration to predator deterrence, experiments were conducted in which fishes were offered four choices of foods simultaneously: diet containing tip sclerites at tip concentrations, diet containing tip sclerites at base concentrations, diet containing base sclerites at tip concentrations, and diet containing base sclerites at base concentrations. These experiments demonstrated that the ability of sclerites to deter feeding was dependent upon both the morphology of the sclerites and their concentrations; however, concentration is a more important factor than morphology in *Sinularia* spp. (Table III). Feeding rates were higher on artificial diets containing sclerites at the lower tip concentrations than the higher base concentrations, regardless of sclerite type (Fig. 12). In *S. maxima*, the smaller tip sclerites were less effective deterrents than the larger base sclerites at high concentrations, but were only slightly less effective at low concentrations. In *S. polydactyla*, tip sclerites were more effective deterrents than base sclerites at both high and low concentrations. In *S.* sp., tip and base sclerites were equally effective at low concentrations; however, at high concentrations, tip sclerites were less effective deterrents.

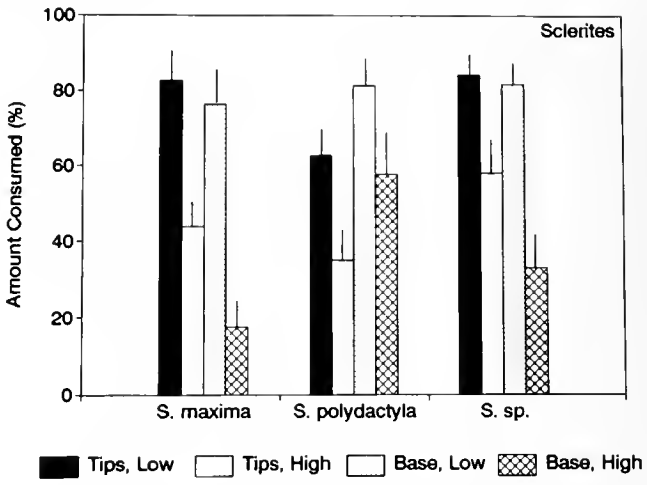

Figure 12. Results of four-way feeding experiments. Vertical bars represent mean feeding rates on tip or base sclerites at natural tip (low) or natural base (high) concentrations. Vertical lines represent ± 1 SE. Statistical analyses are presented in Table III.

Discussion

This and other studies have clearly demonstrated the potential for a defensive role for alcyonarian sclerites. We have shown that sclerites from three species of *Sinularia* in Guam, when incorporated into an artificial diet, reduced feeding by generalist carnivorous fishes in the field (Fig. 4). Similar studies with sclerites from the Caribbean gorgonians *Pseudopterogorgia acerosa* (Harvell *et al.*, 1988) and *Gorgonia ventalina* (Van Alstyne and Paul, in press) have also demonstrated that sclerites can deter feeding in the field. However, not all alcyonarian sclerites are deterrent at natural concentrations. For example, sclerites from the white whip, *Junceela* sp., naturally occur at concentrations of ~45% by dry weight, a similar concentration to those found in *Sinularia;* but, *Junceela* sclerites are not deterrent towards carnivorous fishes at natural dry weight concentrations (Paul and Van Alstyne, in prep.).

Invertebrate spicules and sclerites vary widely in size, shape, and concentration. We have demonstrated that, in these three species of *Sinularia*, concentration is more important than morphology in determining the ability of sclerites to deter the generalist predators of Guam. *Sinularia* sclerites were increasingly effective as deterrents until concentrations of about 30–50% by dry weight, at which point deterrence leveled off (Figs. 9, 10). The level at which maximum effectiveness was reached was determined by the sizes and shapes of the sclerites. The differ-

Table III

Results of two-way Kruskal-Wallis tests on data from four choice feeding experiments

	Location of sclerites		Concentration of sclerites		Location* concentration	
Species	H	*P*	H	*P*	H	*P*
Sinularia maxima	2.696	0.096	29.13	0.000	1.265	0.260
Sinularia polydactyla	7.057	0.008	9.136	0.003	0.071	0.786
Sinularia sp.	1.972	0.156	17.39	0.000	1.238	0.265

Data are presented in Figure 12.

ences in deterrence of sclerites from the tips and bases of the colonies (Fig. 11) was primarily a result of concentration differences of sclerites in these two regions (Table III), not of morphological differences between tip and base sclerites.

Although differences in the sizes and shapes of sclerites between the tips and the bases of the colonies had a lesser impact on the relative effectiveness of structural defenses than sclerite concentration, sclerite morphology is still an important determinant of feeding deterrence. Differences in sclerite morphologies between the tips and bases of *S. polydactyla* colonies significantly affected feeding by fishes off Guam (Table III). Two components of sclerite morphology may influence their effectiveness as feeding deterrents: size and shape. The effects of sclerite morphology may be more important when making interspecific comparisons of deterrence. For example, sclerites from *Junceela* sp. do not deter feeding by fishes at Fingers Reef (Paul and Van Alstyne, in prep.). These *Junceela* sclerites are similar in size and concentration to many of the smaller *Sinularia* sclerites, but, they differ in shape (Paul and Van Alstyne, in prep.). Sclerite shape probably has a significant effect on function, particularly in determining the ability of the sclerite to deter potential predators.

Although our experiments have demonstrated that *Sinularia* sclerites can deter feeding by fishes, predator deterrence may not be the primary function of these structures. Spicules from marine invertebrates also play a role in structural support for colonies, increasing the stiffness of connective tissues by acting like reinforcing fibers (Koehl, 1982). Small sclerites tend to increase colony stiffness more than large sclerites; however, stiffness, like predator deterrence, increases with increasing sclerite concentration (Koehl, 1982). Further work is needed to clarify the structural and defensive functions of invertebrate spicules.

The differences in sclerite morphologies and concentrations within *Sinularia* colonies may reflect differences in the function of sclerites in different locations within the colony or differences in constraints upon sclerite use. Sclerites are most concentrated in the bases of the colonies (Fig. 4), making the bases less susceptible to attack than the tips (Fig. 12, 13, Table III). However, it is the tips of the colonies that receive the majority of attacks by predators (Wylie and Paul, 1989). The lack of high levels of sclerites in the colony tips may reflect constraints on sclerite use. The presence of large quantities of sclerites may interfere with the functioning of the soft coral polyps, which are found only in the tips of the colonies. Alternatively, sclerites in the bases of the colonies may serve primarily as structural support rather than predator deterrents. The presence of high concentrations of predator-deterrent extracts in the tips of the colonies (Wylie and Paul, 1989; Van Alstyne *et al.*, in prep.) supports the hypothesis that sclerite concentrations in the tips of colonies are under functional constraints.

Acknowledgments

The authors are grateful to D. Carandang-Liberty, K. Foster, K. Kuetzing, H. Sanger, and K. Sonada for the many hours spent attaching o-rings onto safety pins. We are also grateful to these individuals and the attendees of the UOG POETS club for spending many more hours taking the o-rings off safety pins. We are indebted to D. Carandang-Liberty, K. Foster, B. Irish, L. Meyer, H. Sanger, and K. Sonada for their assistance with the field experiments. We also thank S. Murray of the California State University at Fullerton for use of his image analysis system, J. Smith of CSUF for advice on statistical analyses, and A.O.D. Willows and the staff of the Friday Harbor Laboratories for the use of the scanning electron microscopy facilities. This manuscript greatly benefitted from the comments of two anonymous reviewers. This research was funded by NIH grant GM 38624 to VJP and a Guyer postdoctoral fellowship from the University of Wisconsin to KLV. This is contribution number 311 of the University of Guam Marine Laboratory.

Literature Cited

Bayer, F. M. 1956. Octocorallia. Pp. F166–F231 in *Treatise on Invertebrate Paleontology, Part F, Coelenterata*, R. C. Moore, ed. University of Kansas Press, Lawrence, KS.

Bayer, F. M. 1961. The shallow water Octocorallia of the West Indian region. *Studies on the Fauna of Curacao and Other Caribbean Islands* **12:** 1–373.

Bayer, F. M., M. Grasshoff, and J. Verseveldt. 1983. *Illustrated Trilingual Glossary of Morphological and Anatomical Terms Applied to Octocorallia.* E. J. Brill, Leiden. 75 pp.

Coll, J. C., D. M. Tapiolas, B. F. Bowden, L. Webb, and H. Marsh. 1983. Transformation of soft coral (Coelenterata: Octocorallia) terpenes by *Ovula ovum* (Mollusca: Prosobranchia). *Mar. Biol.* **74:** 35–40.

Gawel, M. J. 1977. The common shallow-water soft corals (Alcyonacea) of Guam. M.Sc. Thesis, University of Guam, Agana, Guam. 201 pp.

Harvell, C. D., and W. Fenical. 1989. Chemical and structural defenses of Caribbean gorgonians (*Pseudopterogorgia* spp.): intracolony localization of defense. *Limnol. Oceanogr.* **34:** 380–387.

Harvell, C. D., W. Fenical, and C. H. Greene. 1988. Chemical and structural defenses of Caribbean gorgonians (*Pseudopterogorgia* spp.) I: Development of an *in situ* feeding assay. *Mar. Ecol. Prog. Ser.* **49:** 287–294.

Harvell, C. D., and T. H. Suchanek. 1987. Partial predation on tropical gorgonians by *Cyphoma gibbosum* (Gastropoda). *Mar. Ecol. Prog. Ser.* **38:** 37–44.

Kingsley, R. J. 1984. Spicule formation in the invertebrates with special reference to the gorgonian *Leptogorgia virgulata*. *Am. Zool.* **24:** 883–891.

Kingsley, R. J., M. Tsuzaki, N. Watabe, and G. L. Mechanic. 1990. Collagen in the spicule organic matrix of the gorgonian *Leptogorgia virgulata*. *Biol. Bull.* **179:** 207–213.

Koehl, M. A. R. 1982. Mechanical design of spicule-reinforced connective tissue. *J. Exp. Biol.* **98:** 239–268.

LaBarre, S., J. C. Coll, and P. W. Sammarco. 1986. Defensive strategies of soft corals (Coelenterata: Octocorallia) of the Great Barrier Reef. II: The relationship between toxicity and feeding deterrence. *Biol. Bull.* **171:** 625–636.

Paul, V. J., and K. L. Van Alstyne. 1987. Chemical defense and chemical variation in some tropical Pacific species of *Halimeda* (Halimedaceae; Chlorophyta). *Coral Reefs* **6:** 263–269.

Pawlik, J. R., M. T. Burch, and W. Fenical. 1987. Patterns of chemical defense among Caribbean gorgonian corals: a preliminary survey. *J. Exp. Mar. Biol. Ecol.* **108:** 55–66.

Sammarco, P. W., S. LaBarre, and J. C. Coll. 1987. Defensive strategies of soft corals (Coelenterata: Octocorallia) of the Great Barrier Reef: III. The relationship between icthyotoxicity and morphology. *Oecologia* **74:** 93–101.

Tursch, B., and A. Tursch. 1982. The soft coral community on a sheltered reef quadrat at Laing Island (Papua New Guinea). *Mar. Biol.* **68:** 321–332.

Van Alstyne, K. L., and V. J. Paul. 1992. Chemical and structural antipredator deterrents in the sea fan *Gorgonia ventalina:* effects against generalist and specialist predators. *Coral Reefs* In press.

Verseveldt, J. 1977. Octocorallia from various localities in the Pacific Ocean. *Zool. Verhand. Leiden* **150:** 1–52.

Verseveldt, J. 1980. A revision of the genus *Sinularia* May (Octocorallia, Alcyonacea). *Zool. Verh. Leiden* **178:** 1–165.

Wylie, C. R. 1988. Chemical defenses in three species of *Sinularia* (Coelenterata, Alcyonacea): effects against the predator *Cheatodon unimaculatus* (Perciformes). M.Sc. Thesis, University of Guam, Mangilao, Guam. 38 pp.

Wylie, C. R., and V. J. Paul. 1989. Chemical defenses in three species of *Sinularia* (Coelenterata, Alcyonacea): effects against generalist predators and the butterflyfish *Chaetodon unimaculatus* Bloch. *J. Exp. Mar. Biol. Ecol.* **129:** 141–160.

Reference: *Biol. Bull.* **182:** 241–247. (April, 1992)

Characterization of Two Novel Neuropeptides From the Sea Cucumber *Holothuria glaberrima*

LUCY DÍAZ-MIRANDA[1], DAVID A. PRICE[2], MICHAEL J. GREENBERG[2], TERRY D. LEE[3], KAREN E. DOBLE[2], AND JOSÉ E. GARCÍA-ARRARÁS[1]

[1]*Department of Biology, University of Puerto Rico, Río Piedras, Puerto Rico 00931;* [2]*The Whitney Laboratory, St. Augustine, Florida 32086; and* [3]*Division of Immunology, Beckman Research Institute of the City of Hope, Duarte, California 91010*

Abstract. Two peptides were purified from intestinal extracts of a sea cucumber, *Holothuria glaberrima,* by high pressure liquid chromatography (HPLC). The peptides were detected by a radioimmunoassay (RIA) based on an antiserum raised to the molluscan peptide, pGlu-Asp-Pro-Phe-Leu-Arg-Phe-NH_2 (pQDPFLRFamide). Automated sequencing and mass spectrometry indicate that the isolated peptides are: Gly-Phe-Ser-Lys-Leu-Tyr-Phe-NH_2 (GFSKLYFamide) and Ser-Gly-Tyr-Ser-Val-Leu-Tyr-Phe-NH_2 (SGYSVLYFamide). These are the first peptides to have been isolated from a member of the echinoderm class Holothuroidea.

The antiserum used in the RIA of the peptides was also employed in localizing immunoreactive nerve cells and fibers in the intestine of *H. glaberrima.* The immunohistochemical results suggest that these peptides might be responsible for the FMRFamide-like immunoreactivity reported earlier. Sequence similarities between GFSKLYFamide, SGYSVLYFamide, and a pair of peptides previously isolated from starfish lead us to propose that all four molecules are members of a family of peptides acting as neurotransmitters in echinoderms.

Introduction

Very few echinoderm neuropeptides have been characterized. For example, the sequence of the first neuropeptide detected in this phylum—*i.e.,* gonad-stimulating substance (GSS) from starfish (Chaet and McConnaughy, 1959)—is still unknown (references in Cobb, 1988). Recently, FMRFamide-like immunoreactivity was detected in the nervous system of the starfish *Asterias rubens,* and immunoreactive nerve fibers were found in the area of the tube feet, suggesting that FMRFamide might be regulating the process of locomotion (Elphick *et al.,* 1989). Subsequently, two novel neuropeptides from the starfish *A. rubens* and *A. forbesi* were identified: GFNSALM-Famide and SGPYSFNSGLTFamide, and the previously reported FMRFamide-like immunoreactivity in *A. rubens* was attributed to these peptides (Elphick *et al.,* 1991).

Peptide immunoreactivity has also been demonstrated in members of another echinoderm class, the Holothuroidea. For example, cholecystokinin (CCK)-like immunoreactivity occurs in neurons and in a plexus of fibers in the intestines of *Holothuria mexicana, Holothuria glaberrima,* and *Stichopus badionotus* (García-Arrarás *et al.,* 1991a). Similarly, FMRFamide-like immunoreactivity was reported in cells and fibers of the intestine of *H. glaberrima* (García-Arrarás *et al.,* 1991b). The location of these immunoreactive substances suggests that they have a role in the regulation of digestive physiology, and indeed peptides of the CCK family do induce a partial relaxation of the intestinal musculature (García-Arrarás *et al.,* 1991a). These results notwithstanding, none of the endogenous peptides in the nervous system of sea cucumbers had been identified before the present study was undertaken.

In this report, we describe the isolation and characterization of two peptides from the digestive system of *H. glaberrima.* In addition, we provide histochemical evidence for the presence of these peptides in the enteric nervous system of the sea cucumber.

Materials and Methods

Specimens of *H. glaberrima* (10–15 cm in length) were collected from the rocky intertidal zone of the north coast

Received 10 October 1991; accepted 27 January 1992.

of Puerto Rico. The animals were either used immediately or, in some cases, maintained in marine aquaria at the Department of Biology of the University of Puerto Rico.

Digestive system extracts

Four extracts of sea cucumber digestive systems were prepared as follows. First, 13 to 25 animals were sectioned with a razor blade, just posterior to the calcareous ring. The body wall was slit open, and the intestinal tract, including the esophagus and the small and large intestine, together with adherent pieces of hemal vessel and respiratory tree, were removed. The tissue (37–113 g wet weight) was placed in a fourfold excess of acetone and left at −20°C for 48 h. The supernatant was then filtered through Whatman #1 paper, and the acetone and part of the water were removed on a rotary evaporator. The aqueous portion was acidified to 0.02 *M* acetic acid, centrifuged at 2500 × *g*, and the supernatant dried in a Speed-Vac (Savant). The dried sample was reconstituted in aqueous 0.1% trifluoroacetic acid (TFA), centrifuged, and filtered.

Purification

The reconstituted sample was pumped onto a Brownlee C8 reverse phase column (Aquapore RP300: 220 × 4.6 mm or Prep 10 Aquapore Octyl 100 × 10 mm), according to the procedure described by Price *et al.* (1990a). Once loaded, the column was rinsed with aqueous solvent (0.1% TFA) until the UV absorbance fell to near baseline. The eluting solvent was rapidly changed (by a step or 1 min gradient) to 20 or 30% of organic solvent (80% acetonitrile containing 0.1% TFA), whereupon a linear gradient was started with a 1%/min increase in the organic solvent up to 50 or 60% organic. Half-minute fractions were collected, and 2 μl aliquots were taken from each fraction for the RIA.

Further purification was also done on Brownlee C8 RP-300 columns (220 × 2.1 mm or 220 × 4.6 mm). The columns were developed, either with TFA/acetonitrile gradients as above, or with aqueous 0.05% heptafluorobutyric acid (HFBA) and 80% acetonitrile containing 0.05% HFBA.

Radioimmunoassay (RIA)

A rabbit antiserum (Q2), raised against pQDP-FLRFamide coupled to thyroglobulin (Price *et al.*, 1990b), was diluted 1:500 for use in the RIA. Iodinated pQYPFLRFamide served as the tracer.

Sequencing and spectrometry

The most immunoreactive fraction within each pure peak was analyzed. The fraction was divided in half: one half was dried in a Speed-Vac for FABms, and the other half (about .1 ml) was applied (in 3 portions with intermediate drying) directly to a pre-conditioned glass-fiber filter disk containing 3 mg of Polybrene. The disk was placed in the sequencer (Applied Biosystems 470A gas-phase sequencer with an on-line 120a PTH analyzer), and the PTH-amino acid derivatives in each cycle were identified by their retention times and quantitated by comparison of the peak areas to standards (performed by B. Parten, University of Florida Interdisciplinary Center for Biotechnology Research, Protein Sequencing Core Facility, Gainesville). The FABms analysis was carried out on a JEOL HX100HF magnetic sector mass spectrometer, as described in Bulloch *et al.* (1988).

Synthetic peptide

The peptides GFSKLYFamide and SGYSVLYFamide were synthesized on an Applied Biosystems synthesizer by the Protein Chemistry Laboratory of the University of Florida's Interdisciplinary Center for Biotechnology Research; t-Boc protecting groups were used. The peptides were deprotected and removed from the resin with trifluoromethanesulfonic acid (Applied Biosystems protocol), purified by HPLC, and quantified by amino acid analysis (Hitachi 835 analyzer).

Immunohistochemistry

For the histochemical study, the procedure described by García-Arrarás *et al.* (1991a) was followed. In brief, isolated portions of the large and small intestines of *H. glaberrima* were fixed in picric acid-formaldehyde mixture overnight at 4°C. The tissue sections (10–12 μm) were treated with antiserum Q2 (1:500) or with an antiserum against FMRFamide (#8 3i 2s; 1:500) (García-Arrarás *et al.*, 1991b). As a control, the Q2 antiserum was incubated with 10 μg/ml of GFSKLYFamide, FMRFamide (Peninsula), or FLRFamide (Sigma) for 24 h before being applied to the tissue sections.

Results

Fractionation of extracts

Each of the four gut extracts was fractionated with a somewhat different series of HPLC steps. We discovered, finally, that the simplest way to purify the immunoreactive peptides was to select the immunoreactive fractions after each step, and to run them back through the same column under the same conditions (Fig. 1). This finding was certainly not expected. The method works because the extract behaves anomalously; *i.e.*, the immunoreactive peaks shift to an ever earlier elution time during each successive step of purification (*e.g.*, compare Figs. 1C2 and 1C3). Moreover, even the order of elution of the immunoreactive

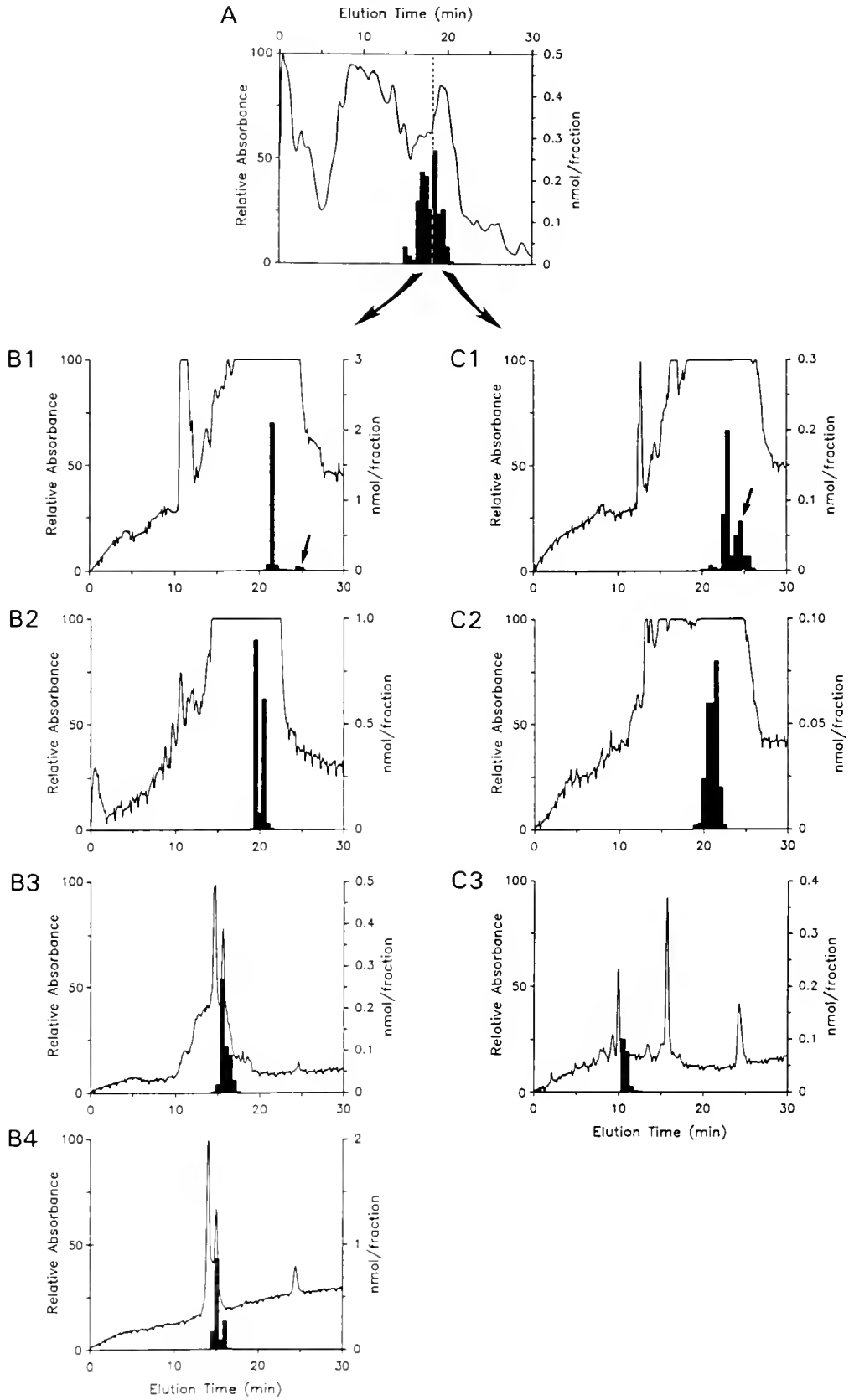
A
Elution Time (min)
Relative Absorbance
nmol/fraction
B1
B2
B3
B4
C1
C2
C3
Elution Time (min)

peaks changes (Fig. 1). This relative shift in elution position was clearly observed in all but the first of the four extracts.

One peptide, already purified from the first extract, was readily and unambiguously identified as GFSKLYFamide when we obtained its molecular ion (860.4) and sequence (Fig. 2a). The calculated value of the amide of this sequence is 860.5, whereas that of the free acid is 861.5. Thus the molecular ion confirmed the presence of the C-terminal amide, which had been inferred from the immunoreactivity; in contrast, the PTH derivatives of phenylalanine and its amide are indistinguishable in normal Edman sequencing. The first extract contained other minor immunoreactive peaks; one of these was analyzed by FABms and sequenced; this product, found again in the fourth extract, will be described further below.

From the second extract, we obtained a molecular ion (934.6) and the partial sequence of a second peptide, SGXSVLXFamide (where X could be either tyrosine or methionine sulfone). The first peptide (GFSKLYFamide) did not appear in this extract.

The third extract contained two immunoreactive peaks. Using mass spectrometry, we again identified GFSKLYFamide (860 molecular ion) and SGXSVLXFamide (934 molecular ion).

The fractionation of the fourth extract was undertaken to resolve the ambiguities left after the first three, and the HPLC runs leading to the purification of the two most immunoreactive peaks are shown in Figure 1.

The first HPLC step in this last purification yielded a broad, irregular peak of immunoreactivity (Fig. 1A). From the earlier half of this, we succeeded, after four steps, in purifying a peak (at 15 min in Fig. 1B4) that sequenced as SGYSVLYF (Fig. 2B). The calculated molecular ion for this peptide—with its C-terminal amidated—is 934.5, and this is in good agreement with the molecular ion (934.6) found earlier. The small immunoreactive peak at 16 min in Figure 1B4 had the same sequence as the main peak, so it is probably just a tail of the main peak.

From the later half of the initial broad immunoreactive peak obtained in the first step of the purification (Fig. 1A), two peaks were resolved in the second (Fig. 1C1). The major (and earlier-eluting) of these peaks co-eluted with synthetic GFSKLYFamide.

The second peak, eluting at 23.5–25 min, was pooled with a similar small peak that had eluted a few minutes after SGYSVLYFamide (see arrows in Figs. 1B1 and 1C1). After purification (not shown), these pooled minor peaks yielded the sequence GFSXLYF, which corresponds to that of the synthetic peptide, except that no lysine (or other PTH derivative) appeared in cycle 4. This peak had a molecular ion of 958, which is 98 larger than that expected for the lysine containing amidated peptide. A peak with the same relative elution time, and a similar molec-

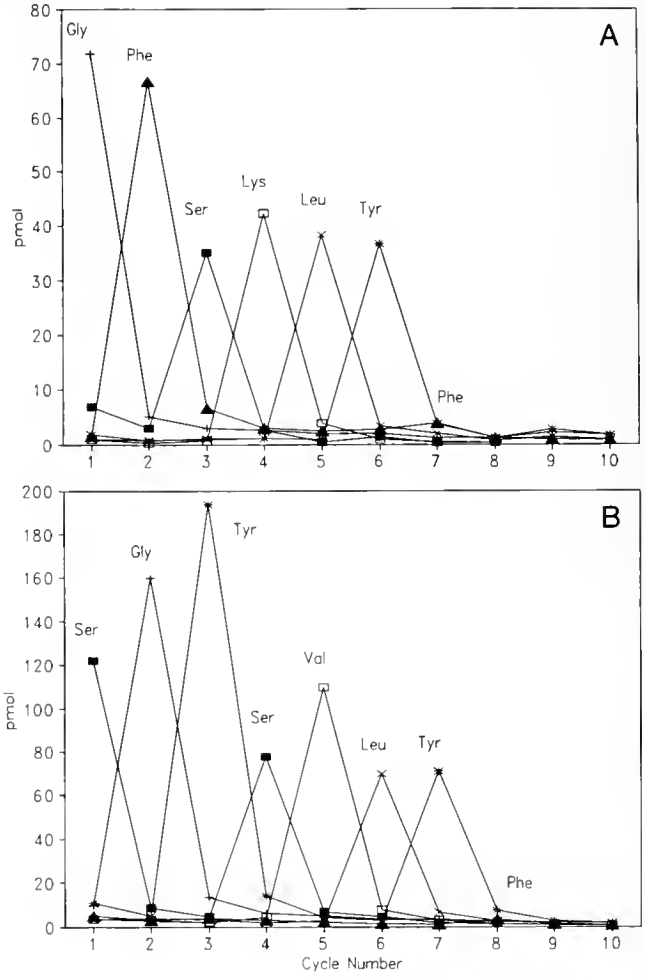

Figure 2. Amino acid sequences of the purified peptides. The yields of the pertinent PTH amino acid derivatives at each cycle are plotted and the amino acid assigned to each position is shown. (A) The peptide having an 860 molecular ion. (B) The peptide having a 934 molecular ion.

Figure 1. HPLC fractionation of a sea cucumber gut extract. The ultraviolet absorbance at 210 nm (solid line) and the immunoreactivity (histogram) are shown for each HPLC run. The initial fractionation (A) was done on a Prep10 Octyl column (10 × 100 mm; 4 ml/min) with a 30 min gradient from 16 to 40% acetonitrile in water with 0.1% trifluoroacetic acid. Subsequent runs (B1-4; C1-3) were done on an RP-300 column (2.1 × 220 mm; 0.5 ml/min) with the same gradient. The arrows in B1 and C1 indicate peaks that were pooled and subsequently purified (not shown; see text). The full scale absorbance in the top trace is 2.0 and is 0.5 AU in all the subsequent traces.

ular ion (958.6) and sequence, had also appeared in the first extract, as briefly noted above.

We suspect that the peptide GFSXLYFamide has a derivatized lysine side chain. For example, a peptide with the lysine amino group amidated by hexanoic acid would give such a molecular ion, and such a derivative could occur naturally in the sea cucumber. It is more likely, however, that the derivative is a substituted oxazolidine ring, formed by the condensation, with the lysine, of two molecules of acetone (58 + 58) with the loss of a water (−18). This derivatization would add 98 to the molecular weight of the peptide. In summary, this peptide may very well be an artifact of the purification.

Synthetic peptides

The synthetic peptides GFSKLYFamide and SGYSVLYFamide were purified by HPLC after deprotection. Each peptide co-eluted with its natural counterpart on HPLC. An amino acid analysis of GFSKLYFamide gave the following composition: Gly 1.05, Phe 1.75, Ser 1.0, Lys 1.1, Leu 1.25, and Tyr 1.05. The composition of SGYSVLYFamide was: Gly 1.00, Phe .90, Ser 2.03, Leu 1.11, Tyr 1.99, Val 1.33.

Q2 immunoreactivity

The tissue distribution of immunoreactivity to Q2 (the antiserum used in the characterization of GFSKLYFamide and SGYSVLYFamide) was determined by immunohistochemistry. Results with antibodies Q2 and #8 (the latter an antiserum against FMRFamide) were similar. Cells and fibers located in the outer connective tissue (serosa) of the small and large intestine were labeled, as were single fiber-like projections in the submucosal layer (Fig. 3). In addition, a strong nerve plexus was observed in the mesentery next to the muscular layer. This nerve plexus was continuous with the serosal nerve plexus. In contrast to the FMRFamide-like immunoreactivity (García-Arrarás *et al.*, 1991b), Q2 also labeled a group of cells located in the submucosal layer of the intestines, similar to what has been described as morula cells (Hetzel, 1963, 1965), but this reaction does not seem to be specific.

When the Q2 antiserum was preabsorbed with GFSKLYFamide (12 μM), no immunoreactivity to Q2 was observed in the cells and fibers of the mesentery, serosa, or submucosa; but the morula cells continued to be labeled. These results suggest that other antibodies in the Q2 serum recognize unrelated substances. The peptides FMRFamide (17 μM) and FLRFamide (17 μM) were also used for preabsorption of Q2, but they could not completely block the observed immunoreactivity of the cells and nerve fibers in the serosa, or of the nerve fibers in the submucosa. The Q2 immunoreactivity of the morula cells was not blocked, whether the antiserum was preabsorbed with FMRFamide or with FLRFamide.

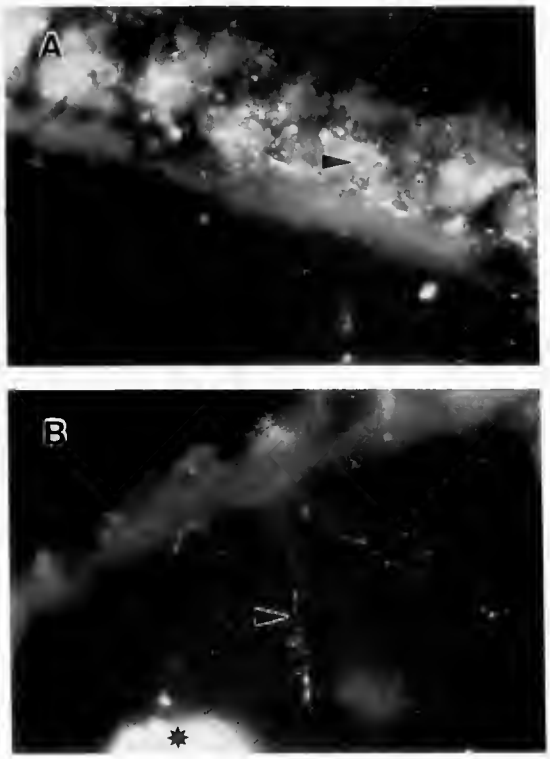

Figure 3. Transverse sections of the large intestine of *H. glaberrima* showing Q2-like immunoreactivity. A. Immunoreactive nerve fibers at the level of the serosa and longitudinal muscle. Most of these fibers were associated with the longitudinal muscle (arrowhead). B. Arrowhead points at one immunoreactive fiber extending throughout the submucosa layer. Asterisk: endogenous fluorescence. Magnification: A. ×405; B. ×270.

Discussion

We have purified two peptides from gut extracts of the sea cucumber *H. glaberrima*, using high pressure liquid chromatography for separation and radioimmunoassay for detection. These peptides—GFSKLYFamide and SGYSVLYFamide—were completely characterized by microsequencing and mass spectrometry, and are the first to have been isolated from the echinoderm class Holothuroidea.

Two related peptides were isolated earlier from another echinoderm class, the Asteroidea: *i.e.*, GFNSALMFamide and SGPYSFNSGLTFamide from the starfishes *Asterias forbesi* and *A. rubens* (Table I; Elphick *et al.*, 1991). These peptides, like those of the sea cucumber reported here, were detected on the basis of their binding to an antiserum, Q2, raised against pQDPFLRFamide (Price *et al.*, 1990b). In both studies, furthermore, the Q2 antiserum was originally selected because the aim was to characterize putative FMRFamide-related peptides (FaRPs) that had been

Table I

Amino acid sequences of SxLxFamide[1] peptides isolated from Echinodermata

CLASS Species	Sequence	Ref.
HOLOTHUROIDEA		
Holothuria glaberrima	Gly-Phe-**SER**-Lys-**LEU**-Tyr-**PHE**-NH_2	2
	Ser-Gly-Tyr-**SER**-Val-**LEU**-Tyr-**PHE**-NH_2	
ASTEROIDEA		
Asterias forbesi	Gly-Phe-Asn-**SER**-Ala-**LEU**-Met-**PHE**-NH_2	3
A. rubens	Ser-Gly-Pro-Tyr-Ser-Phe-Asn-**SER**-Gly-**LEU**-Thr-**PHE**-NH_2	

[1] Ser-x-Leu-x-Phe-NH_2, where the positions "x" can be occupied by any residue.
[2] This report.
[3] Elphick *et al.*, 1991.

identified by immunocytochemistry (Elphick *et al.*, 1989; García-Arrarás *et al.*, 1991b).

FaRPs, defined liberally, have now been isolated from many animal groups, including coelenterates, nematodes, annelids, arthropods, and even vertebrates (reviewed by Price and Greenberg, 1989; Greenberg and Price, 1992), and a penultimate arginyl residue is not only a common feature of this extended family, but has been shown to be critical for physiological activity (*e.g.*, see Kobayashi and Muneoka, 1986). Antiserum Q2 should have identified most FaRPs that might have been present in our extracts, but in fact, not one of the four neuropeptides sequenced from echinoderms has the penultimate arginine. Our results, therefore, when taken together with the evidence obtained from the starfish (Elphick *et al.*, 1991), suggest that authentic FaRPs are absent from the Echinodermata.

If the above assertion is correct, we must account for the FMRFamide-like immunoreactivity described in sea cucumbers (García-Arrarás *et al.*, 1991b) and in starfish (Elphick *et al.*, 1989). In the sea cucumber *H. glaberrima*, immunoreactivity to FMRFamide has been reported in the radial nerves, in nerve plexuses of the esophagus, and in the enteric nervous system (García-Arrarás *et al.*, 1991b). The distribution of immunoreactivity observed with the Q2 antibody in the gut of *H. glaberrima* is similar, if not identical, to that observed with antibodies against FMRFamide. The localization of Q2-binding to nerve cells and fibers in the sea cucumber intestine suggests that the peptides recognized by this antibody occur in the enteric nervous system of holothurians, and that they may be involved in neural transmission or modulation.

The story in the starfish *Asterias rubens* is similar: *i.e.*, FMRFamide-like immunoreactivity was detected in the radial nerve cords, the circumoral nerve ring, and the subepithelial nerve plexus of the tube feet (Elphick *et al.*, 1989), and this immunoreactivity has been attributed to the two isolated peptides from the starfishes by Elphick *et al.* (1991). In conclusion, the FMRFamide-like immunoreactivity previously reported in both echinoderm classes might be due to the presence of the isolated peptides reacting with the anti-FMRFamide serum.

As Table I illustrates, the two sea cucumber peptides have five of seven residues in common, and the two starfish peptides have five of eight identical; but the most similar sea cucumber and starfish peptides share only four of eight residues. The clear unifying feature of these four echinoderm peptides is the C-terminal sequence SxLx-Famide, where the positions indicated by "x" can be occupied by any other residue. We therefore propose that this periodic sequence of serine, leucine, and phenylalanine defines a novel family of peptides present in the Echinodermata.

Acknowledgments

This research was supported by funds from the Resource Center for Sciences and Engineering, the Patricia Robert Harris Fellowship to LDM, the Grass Foundation (to the Whitney Lab), the National Science Foundation (BNS-8801538 to JGA), and the National Institute of Health (HL28440 to MJG). We would like to thank the Protein Chemistry Core Facility of the University of Florida for peptide sequencing and peptide synthesis, and we also acknowledge the help of the Interdisciplinary Center for Biotechnology Research (ICBR) of the University of Florida. We are very grateful to Mr. Dietmar Nieves and Ms. Lynn Milstead for their excellent assistance with the preparation of figures.

Literature Cited

Bulloch, A. G. M., D. A. Price, A. D. Murphy, T. D. Lee, and H. N. Bowes. 1988. FMRFamide peptides in *Helisoma:* identification and physiological actions at a peripheral synapse. *J. Neurosci.* **8:** 3459–3469.

Chaet, A. B., and R. A. McConnaughy. 1959. Physiologic activity of nerve extracts. *Biol. Bull.* **117:** 407–408.

Cobb, J. L. S. 1988. Neurohumors and neurosecretion in echinoderms: a review. *Comp. Biochem. Physiol.* **91C:** 151–158.

Elphick, M. R., D. A. Price, T. D. Lee, and M. C. Thorndyke. 1991. The SALMFamides: a new family of neuropeptides isolated from an echinoderm. *Proc. Roy. Soc. B* **243:** 121–127.

Elphick, M. R., R. H. Emson, and M. C. Thorndyke. 1989. FMRFamide-like immunoreactivity in the nervous system of the starfish *Asterias rubens*. *Biol. Bull.* **177:** 141–145.

García-Arrarás, J. E., I. Torres-Avillán, and S. Ortíz-Miranda. 1991a. Cells in the intestinal system of holothurians (Echinodermata) express cholecystokinin-like immunoreactivity. *Gen. Comp. Endocrinol.* **83:** 233–242.

García-Arrarás, J. E., I. Enamorado-Ayala, I. Torres-Avillán, and V. Rivera. 1991b. FMRFamide-like immunoreactivity in cells and fibers of the holothurian nervous system. *Neurosci. Letters* **132:** 199–202.

Greenberg, M. J., and D. A. Price. 1992. Relationships among the FMRFamide-like peptides. *Prog. Brain Res.* (in press).

Hetzel, H. R. 1963. Studies on holothurian coelomocytes. I. A survey of coelomocyte types. *Biol. Bull.* **125:** 289–301.

Hetzel, H. R. 1965. Studies on holothurian coelomocytes. II. The origin of coelomocytes and the formation of brown bodies. *Biol. Bull.* **128:** 102–112.

Kobayashi, M., and Y. Muneoka. 1986. Structural requirements for FMRFamide-like activity on the heart of the prosobranch *Rapana thomasiana*. *Comp. Biochem. Physiol.* **84C:** 349–352.

Price, D. A., and M. J. Greenberg. 1989. The hunting of the FaRPs: the distribution of FMRFamide-related peptides. *Biol. Bull.* **177:** 198–205.

Price, D. A., K. E. Doble, T. D. Lee, S. M. Galli, B. M. Dunn, B. Parten, and D. H. Evans. 1990a. The sequencing, synthesis, and biological actions of an ANP-like peptide isolated from the brain of the killifish *Fundulus heteroclitus*. *Biol. Bull.* **178:** 279–285.

Price, D. A., W. Lesser, T. D. Lee, K. E. Doble, and M. J. Greenberg. 1990b. Seven FMRFamide-related and two SCP-related cardioactive peptides from *Helix*. *J. Exp. Biol.* **154:** 421–437.

Reference: *Biol. Bull.* **182:** 248–256. (April, 1992)

Giant Axons and Escape Swimming in *Euplokamis dunlapae* (Ctenophora: Cydippida)

G. O. MACKIE[1], C. E. MILLS[2], AND C. L. SINGLA[1]

[1]*Biology Department, University of Victoria, Victoria, British Columbia, V8W 2Y2, Canada, and*
[2]*Friday Harbor Laboratories, University of Washington, Friday Harbor, Washington 98250*

Abstract. *Euplokamis dunlapae* responds to anterior stimulation by reversing the beat direction of its comb plate cilia and swimming rapidly backwards. It responds to posterior stimulation by swimming forwards at an accelerated rate. Video playback and laser monitoring were used to analyze changes in the pattern of ciliary beating, while electrical activity was recorded extracellularly. Escape responses occur with latencies of less than 150 ms and involve greatly increased ciliary beat frequencies. Giant axons run longitudinally along each of the eight comb rows, as shown by optical and electron microscopy. They form chains of overlapping neurons, with diameters of about 12 μm in life, and conducting at over 50 cm $\cdot$ s^{-1} as recorded with an extracellular electrode placed directly over the chain. The giant neurons are synaptically linked with smaller neurites of the general ectodermal nerve plexus, with each other, and with the ciliated cells of the comb plates. They appear to constitute a single system mediating rapid conduction of signals in either direction, but a full analysis was not attempted for lack of sufficient material. Electro-physiological examination of two other ctenophores (*Pleurobrachia* and *Beroë*) gives no indication of rapid conduction pathways, and these forms probably lack giant axons.

Introduction

Several cydippid and lobate ctenophores have the ability to reverse the direction of the power stroke of their comb plate cilia. In the best-studied example, *Pleurobrachia* (Tamm and Moss, 1985; Moss, 1986; Moss and Tamm, 1986, 1987), reversals occur unilaterally as part of feeding behavior, and make the animal rotate on its axis. Reversals can also occur simultaneously in all the comb rows, causing the animal to swim backwards. Several cases of reverse swimming have been reported (reviewed by Tamm, 1982), but none have been studied in detail. We here describe the responses of an unusual and interesting cydippid ctenophore, *Euplokamis dunlapae,* that responds rapidly to stimulation by forward and reverse swimming. A novel feature of these responses is that they appear to be mediated in part by giant axons that run under the comb rows.

A taxonomic account of *Euplokamis dunlapae* (Fig. 1). is given by Mills (1987). The species is probably the most abundant midwater ctenophore in the Strait of Georgia and adjacent fjord systems, reaching its greatest density at 250 m; however, specimens are rare above 100 m, and only very infrequently found at the surface (Mackie and Mills, 1983; Mackie, 1985). They are too fragile to be collected and brought to the surface in nets. Thus, opportunities to study them have been few. In 1984 we obtained enough specimens for a study of their prehensile tentilla (Mackie *et al.,* 1988). In 1990 and 1991 we obtained five more specimens, on which this account is based. Having so few specimens necessarily limited the scope of the study, but they were in good physiological condition, and there is no reason to doubt the generality of the findings.

Materials and Methods

Specimens of *Euplokamis dunlapae* Mills 1987 were collected off the dock at the Friday Harbor Laboratories and kept in wide-mouthed glass bottles at 8°C until used. Material for electron microscopy was fixed in 2.5% glutaraldehyde in 0.4 *M* Millonig's phosphate buffer at pH 7.4 for 1 h at room temperature, rinsed, and osmicated

Received 3 January 1991; accepted 12 December 1991.

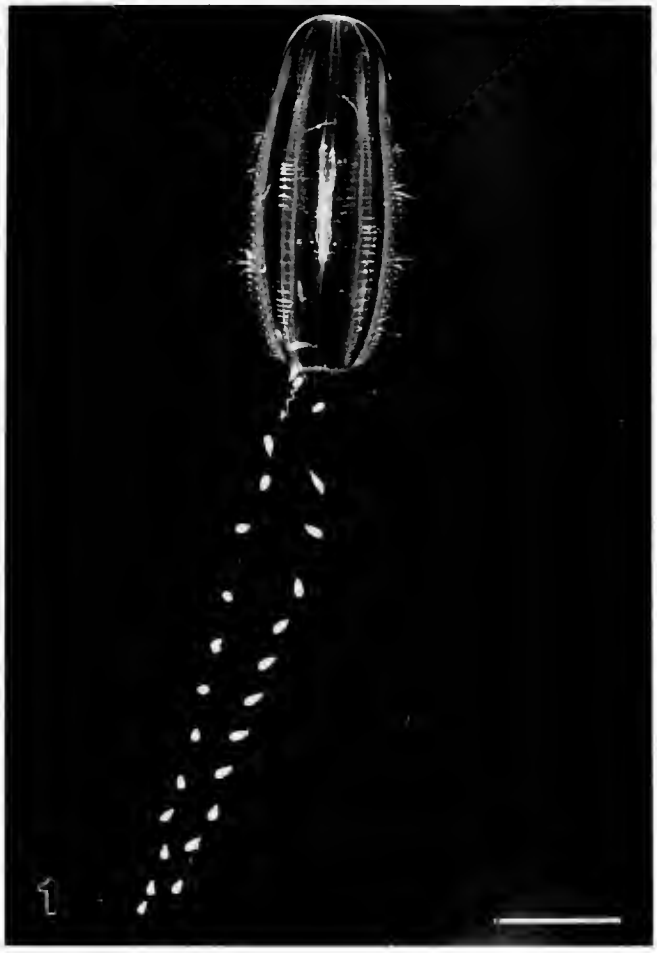

Figure 1. *Euplokamis dunlapae* swimming in an aquarium, oral end up. Scale bar: 5 mm.

in 1% osmium tetroxide in the same buffer at 4°C for 1 h. Specimens invariably disintegrated during fixation despite every precaution. Fortunately, intact fragments of comb rows, along with some attached underlying tissue, could be retrieved from the debris and processed for electron microscopy. The tissue was dehydrated through graded ethanols and propylene oxide and embedded in Epon 812. Thick sections were stained with Richardson's stain. Thin sections were treated with uranyl acetate and lead citrate. Because the tissues were extremely fragile, we could not prepare whole mounts of living material for examination by Nomarski or phase contrast microscopy. Figure 2, showing giant axons in an intact, living animal, was taken through a dissecting microscope illuminated with a double substage mirror, with the mirror angles arranged to give shadows along the edges of the axons.

Behavior of free-swimming specimens was observed in a 15-l tank, illuminated from the sides, and with a dark background. A Sony CCD video camera (HVM-200), fitted with a Nikon 105 mm macro lens, was used in conjunction with a VCR with frame-by-frame playback for analysis of responses. Recordings of electrical activity were made from specimens pinned down in a Sylgard-lined Pyrex pie dish placed on top of a doughnut-shaped Cambion cooling stage, which allowed light to enter from below. Temperature was maintained at 12°C. Fine polyethylene suction electrodes were attached directly to the body surface using minimal suction to keep them attached. Signals were amplified with capacity-coupled amplifiers and displayed on a digital oscilloscope; conventional extracellular recording procedures were used. Stimuli were delivered through paired metal wires insulated to near the tip. Movement of comb plates was monitored; we used a ruby laser (Spectra Physics Model 155) to project a narrow beam of light across the comb row, and a photomultiplier (International Light 270C) to detect purturbations of the beam caused by the ciliary movement. Laser monitoring of ciliary beating in molluscan veligers is described by Arkett *et al.* (1987). The method, as used here, allowed us to distinguish forward from reverse power strokes by the polarity of the waves recorded.

Histology and Ultrastructure

The comb rows of *Euplokamis* resemble those of other ctenophores as reviewed by Tamm (1982). Each plate consists of thousands of cilia springing from "polster" cells, which are packed with large mitochondria. We have confirmed that gap junctions are present between the polster cells as first reported by Hernandez-Nicaise (1974). The comb plates are richly innervated by fine nerve fibers running among the bases of the polster cells. These fine neurites have diameters in the range of 0.7–2.5 μm ($\bar{X}$ = 1.2, SD = 0.4, n = 13). They appear to represent part of the general ectodermal nerve plexus. This system is well known in *Pleurobrachia* from the investigations of Hernandez-Nicaise (1973a, 1974). Moss (1986) has shown that ciliary reversals in *Pleurobrachia* are mediated by a diffuse conduction system running in the ectoderm, presumably the nerve plexus described by Hernandez-Nicaise in whole or part.

Where *Euplokamis* differs from other known ctenophores is in its possession of bipolar giant axons running along each comb row. These can be seen under the dissecting microscope in the intact, living animal (Fig. 2), and at higher magnifications in thick epon sections (Fig. 3) and electron micrographs (Fig. 4). They are present in all eight comb rows and run roughly down the midline of each comb row from one end to the other. Their cell bodies lie between the comb plates, and there appears to be one cell body between each pair of comb plates. They evidently form a chain of cells arranged end to end, with

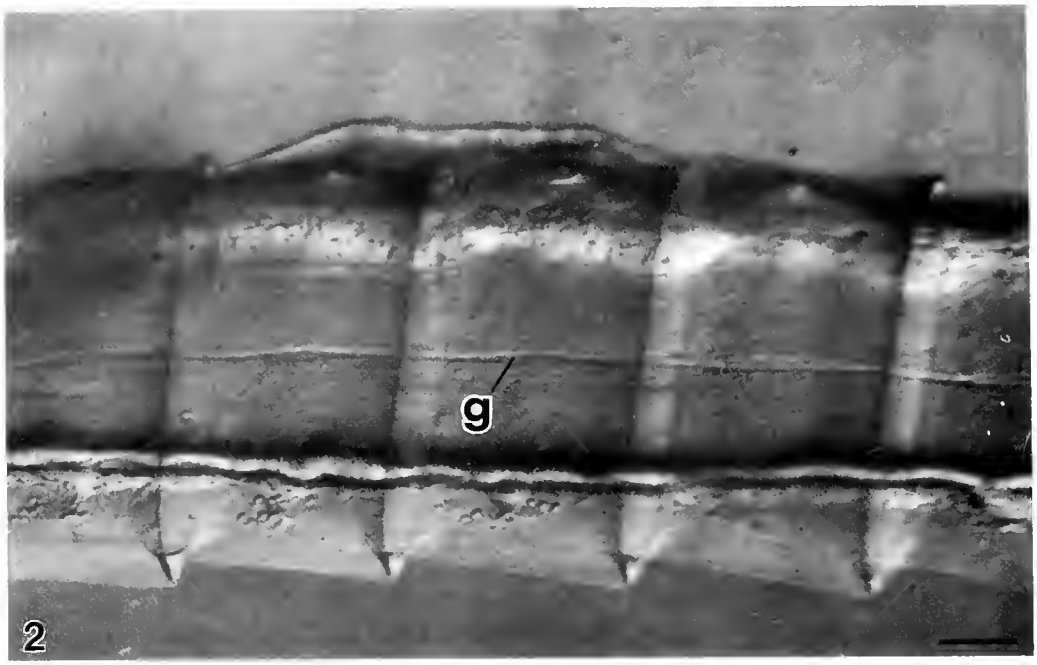

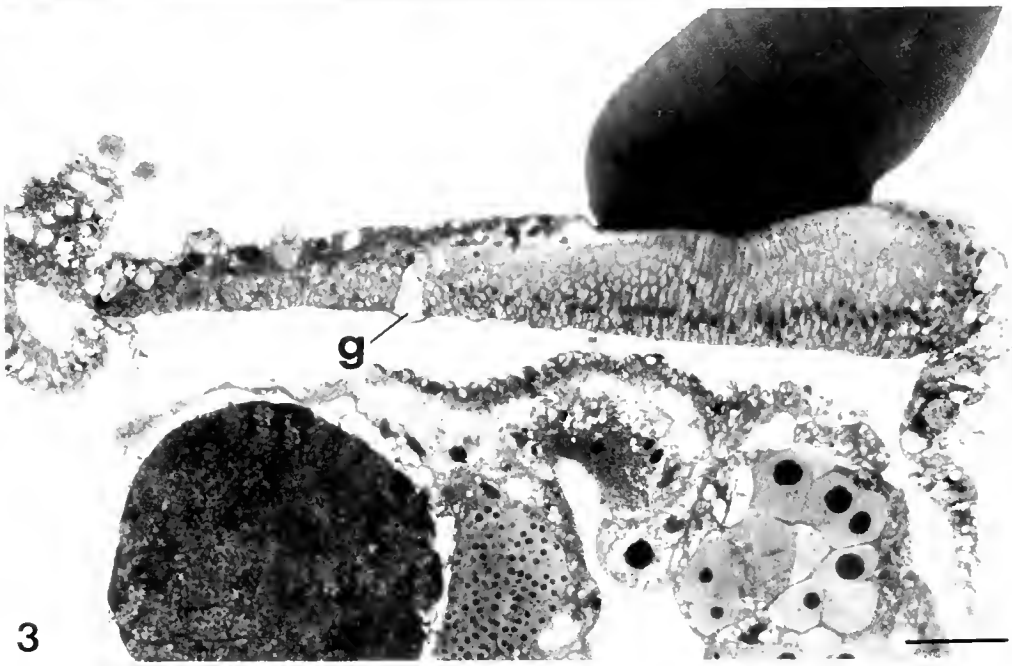

Figure 2. Surface view of a sub-tentacular comb row in living animal, showing four comb plates whose cilia are laid down flat on the surface, and giant axon chain (g). Scale bar: 100 μm.

Figure 3. One (1.0) μm section cut transversely but at a slight angle through a comb plate showing massed cilia (dark mass, upper right) arising from polster cells, and giant axons (g). Gametes are seen in the underlying endodermal canal. Scale bar: 50 μm.

some overlap. In typical sections, one or two axon profiles, but not more, are seen, showing that the neurites must be quite short, probably less than 400 μm. In their thicker regions, they show diameters of approximately 8.5–12.0 μm ($\bar{X}$ = 9.7, SD = 1.02, n = 10), but they taper towards the ends. Allowing for shrinkage during fixation and embedding, the axons are probably at least 12 μm in the living animal, which is also suggested by measurements

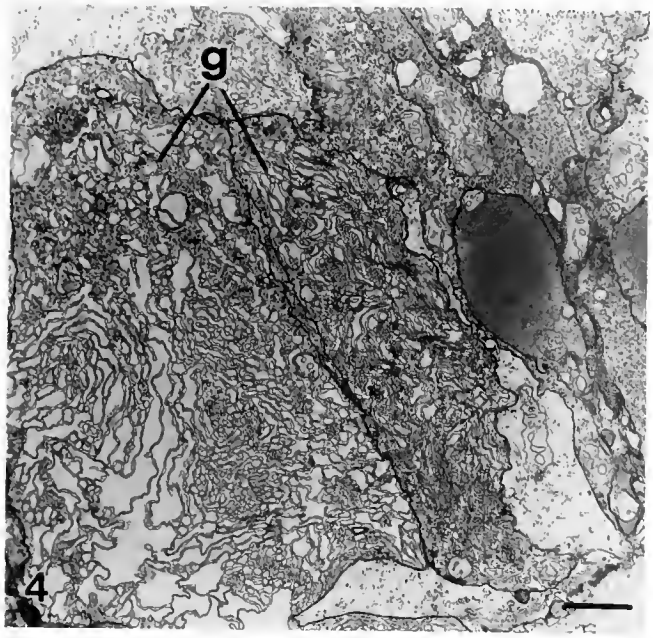

Figure 4. Low power electron micrograph showing cross sections of giant axons (g) surrounded by polster cell bases. Scale bar: 2 μm.

on living preparations. There appears to be only one nucleus per cell; it is long and thin and causes only a slight swelling in the cell body region.

The axoplasm of the giant axons is remarkable for its richly developed smooth endoplasmic reticulum, which appears to form a continuous network of fine canals throughout the entire cell. The axoplasm also contains conspicuous bundles of microtubules. Rows of 100-nm dense-cored vesicles have been seen associated with these bundles (Fig. 5). The area around the nucleus does not differ markedly from other parts of the axoplasm. There is little indication of active protein synthesis. The nucleolus is not prominent, and there is little rough endoplasmic reticulum. Mitochondria and Golgi bodies (one is seen in Fig. 6) are distributed along the whole length of the axon.

We have seen no gap junctions in the nervous system (nor are there any reports of such in the ctenophore literature), but we have observed synapses between neurites of all sizes. There are synapses between fine neurites and giants, and between giants in areas of overlap (Fig. 6). Synapses also occur between these neurons and polster cells (Fig. 7). The synapses resemble those seen in the tentilla of *Euplokamis* (Mackie *et al.*, 1988), as well as those described in other ctenophores. They are characterized by "presynaptic triads" (Hernandez-Nicaise, 1973b, 1974) consisting of a mitochondrion embraced by a flattened ER cisterna with an accompanying row of small (50 nm) synaptic vesicles.

Behavior of Free-Swimming Specimens

When left to its own devices in a large tank, *Euplokamis* shows bouts of forward "cruising" swimming, interspersed with periods of quiescence. During cruising, ciliary metachronal waves run down the comb rows with a frequency of about 5 Hz, driving the animal forward (mouth leading). A specimen 15 mm long cruises at about 2 $cm \cdot s^{-1}$. The tentacles trail behind, partially extended and with their tentilla coiled. When swimming stops, the body swings around passively so that the mouth points up and the tentacles hang down. The animal can hang in this posture with its cilia either arrested or beating irregularly and infrequently. Swimming animals will go into reverse if they hit the walls of the tank, but otherwise they swim forward steadily in the cruising mode.

Stimulation by touch or by an electric shock on any part of the surface alters the pattern of swimming. If the stimulus is applied at the front, for instance on the lips, the animal rapidly changes the direction of the ciliary power stroke in all eight comb rows, goes into reverse, and swims backward for one or two body lengths, pauses, and then resumes forward cruising behavior. During backward swimming, velocities of about 4 $cm \cdot s^{-1}$ were observed, with elevated metachronal beat frequencies. Using frame-by-frame playback on the VCR, the first signs of interruption of the ciliary beat pattern were generally seen within four frames (<130 ms) following the stimulus, with the actual change in the direction of movement occurring one or two frames (<67ms) later.

When stimuli are applied at the rear (statocyst) end, the animal responds by accelerated forward swimming: within four frames (<130 ms) the metachronal rhythm suddenly increases as in the backward escape response, but with no change in the direction of the power stroke, so the animal darts forward rapidly at a velocity of about 5.5 $cm \cdot s^{-1}$. After several seconds, it slows to the normal cruising speed.

During both backward and forward escape swimming, the tentacles contract. The first signs of contraction are seen at about the same time as the first signs of change in the pattern of ciliary beating.

Animals that have been left to swim around the tank without interference respond to stimuli with great alacrity, but after repeated stimulation, responses become less intense and latencies tend to increase.

Electrophysiology

Propagation along the comb rows

If a recording electrode is placed directly over the giant axon chain at any point along its length, and an electrical stimulus is delivered further along the comb row, a pattern

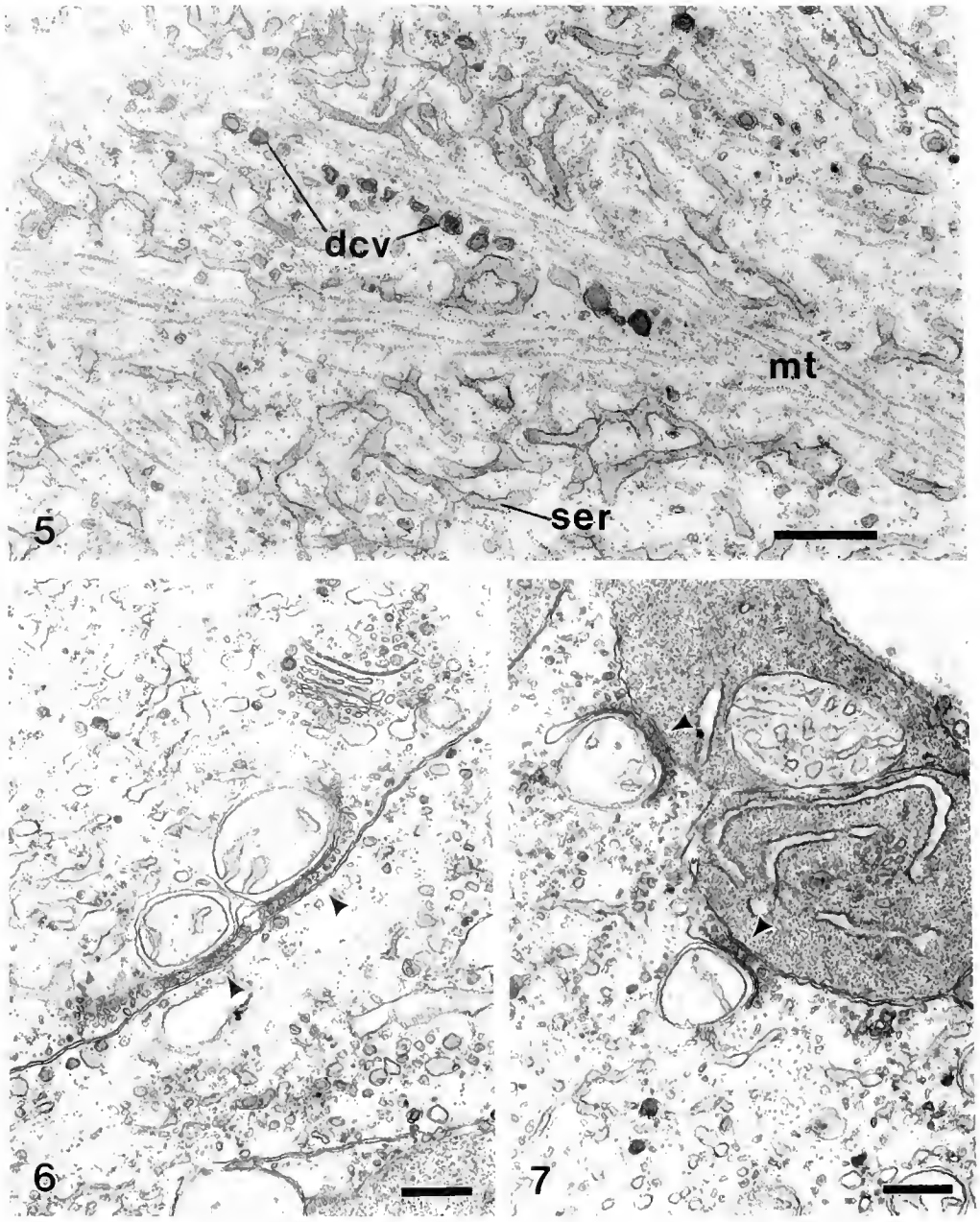

Figure 5. Axoplasm of giant axon cut longitudinally showing dense-cored vesicles (dcv) aligned along microtubule bundle (mt) and richly developed smooth endoplasmic reticulum (ser). Scale bar: 0.5 μm.

Figures 6, 7. Synapses (arrowheads) between giant axons (6) and from giant axon to polster cell (7). Scale bars: 0.5 μm.

of electrical potentials is recorded, which has two readily separable components (Fig. 8). The first component is a small (150 μV), sharp, spikey event conducted at 51–56 $cm \cdot s^{-1}$ ($\bar{X}$ = 53.4, SD = 1.95, n = 10). This event is presumably the extracellular correlate of an action potential propagated in the giant axon chain. The signal is lost when the recording electrode is moved even slightly to one side or the other of the giant axon. The second component is a larger, complex, and variable series of positive and negative-going potentials that presumably represent responses in the ciliated polster cells. This component may be brief or it may take the form of flurries lasting several hundred milliseconds. We were not able to analyze these events in detail, but assume that they include

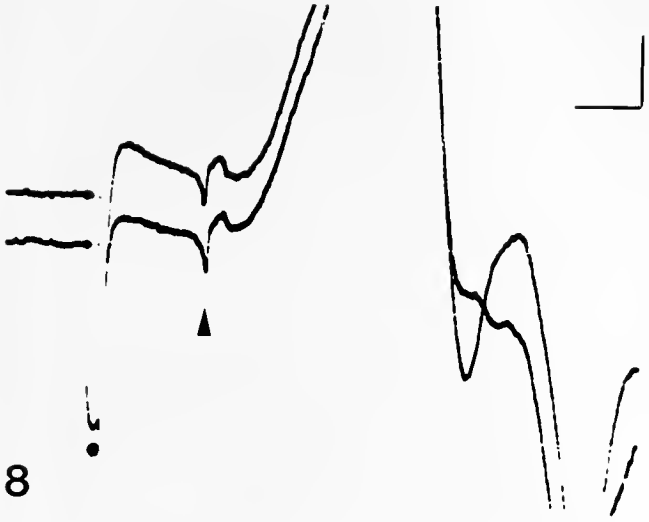

Figure 8. Recording with an electrode placed directly over the giant axon row, two successive sweeps in same position. Following electrical stimulation further along the comb row in the aboral direction (black spot marks shock artifact), a rapidly conducted, sharp, spikey event (arrowhead) is recorded, followed by a much larger, complex, and variable series of potential changes. Scale bar: 10 ms, 200 μV.

summed synaptic events and regenerative events in the polster cells, which, with some of their cilia, were partially engulfed by the electrode. The large biphasic events, which reach amplitudes in the millivolt range, would presumably correspond to the calcium spikes described by Moss and Tamm (1986, 1987) in *Pleurobrachia.*

The interval between the arrival of the giant nerve spike at the recording electrode and the start of the polster cell depolarization is quite variable, ranging from 5 to 20 ms ($\bar{X}$ = 12.2 ms, SD = 5.5, n = 7). This may mean that the polster cell depolarization is not initiated at the recording site, but is propagated from an unknown and more or less distant site. Consequently, unless the nerve spike is actually recorded, it is impossible to give an accurate or even consistent estimate of conduction velocity in the nervous system. In spite of this, measurements of the latency between stimulus and polster cell response can give a rough figure (here termed "apparent conduction velocity") serving for comparative purposes in any one location. These estimates assume that conduction always takes place along the most direct route measured between stimulus and recording points, but this too needs verification.

Apparent conduction velocities along the midline of the comb row were reduced to 75% of their original value after a single cut through the giant axon chain. Apparent conduction velocity decreased progressively with further cuts at different levels, reaching 55% of the original value after the axon chain had been destroyed over most of its length. At this point, it must be assumed that excitation was travelling in the general epidermal nerve plexus. The apparent conduction velocity along the comb rows after destruction of giant axons is close to the value obtained for conduction across the ectoderm in regions devoid of giant axons, the mean velocity being 12 $cm \cdot s^{-1}$ (SD = 3.07, n = 17, three specimens). Incisions into the comb row tissue did not reduce apparent conduction velocities unless they intersected the giant axons. The fact that several incisions must be made through the giant axon chain at different levels along the comb row to bring the apparent conduction velocity down to the non-giant velocity is consistent with the idea that impulses can enter the giant axons from a diffuse nerve net at numerous points along the giant axon chain.

Simultaneous recording of polster cell depolarizations and ciliary beat patterns

Animals pinned down in a small dish continue to show normal cruising swimming with a metachronal wave frequency of about 5 Hz (Fig. 9). Using the laser beam method of monitoring ciliary beating, we could, in a few cases, detect the exact moment at which this pattern was interrupted following stimulation and determine the interval between this change and the onset of the electrical response in the polster cells (Figs. 10, 11). The giant axon spike is not seen in these records, as the recording electrode was not placed directly over the midline of the comb row. In Figure 10, following stimulation at the oral end of a comb row, the cilia switched to the reverse pattern of beating 122 ms after the stimulus, and 85 ms after the start of the electrical response recorded from polster cells adjacent to the laser-monitoring site. Beat frequency was 25 Hz immediately after the change of gait, but the frequency declined quickly, and the cilia shortly switched back to beating in the forward cruising mode at 5 Hz. The response latency of 122 ms recorded by this method is consistent with the value of <130 ms obtained from the video-playback analysis.

When the stimulating and recording positions were reversed and a shock was delivered at the aboral end of the comb row, a forward escape swimming response was obtained (Fig. 11). Regular, slow metachronal beating changed suddenly to rapid forward beating starting 143 ms after the shock, and 107 ms after the first component of the electrical response recorded from adjacent polster cells. After two beats at the equivalent of 17 Hz, the frequency declined to 8 Hz and later (off the record) to 5 Hz, as normal cruising was resumed. We could not repeat these experiments enough times to allow a proper statistical analysis and cannot say, therefore, whether the response latency is consistently shorter in the case of reverse escape swimming than in forward, nor how this may vary

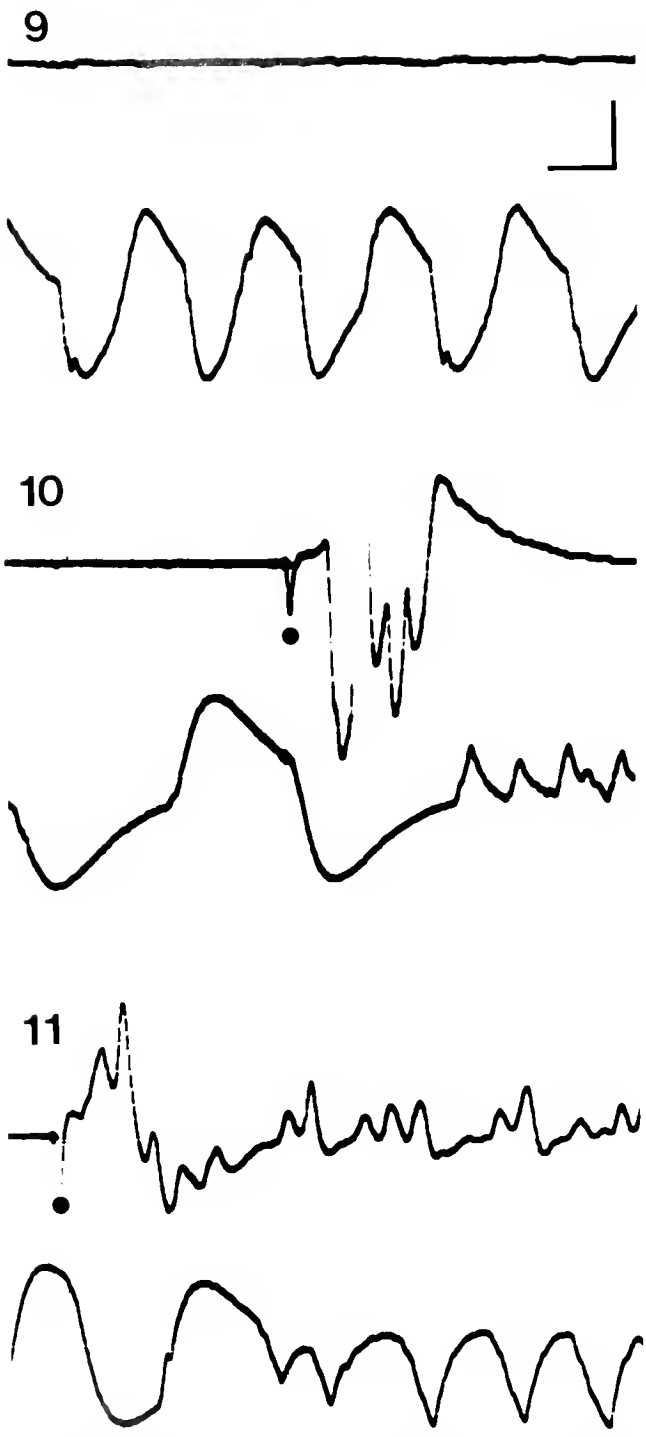

Figures 9, 10, and 11. In each figure, the upper trace is a record of electrical activity from a comb plate while the lower is a laser beam record of the ciliary beating at the same spot. Figure 9 is a control (no stimulus). Figure 10 shows the response to a shock delivered orally of the recording electrode. Small upward events on the laser record correspond to reverse ciliary beats. Figure 11 shows the response to shock delivered aborally. Small downward events on the laser record correspond to fast forward beats. Spots mark shock artifacts. Scale bars: 100 ms, 500 μV (upper trace) (9); 50 ms, 500 μV (10); 50 ms, 200 μV (11).

with position along the comb row. In both cases, however, the response latency can clearly be less than 150 ms.

The cilia generally appear to switch directly from one mode of beating to another without a break, but in some cases a short period of inactivity was observed before the new pattern emerged. During these periods, the cilia appeared to be in the "laydown" position described for *Pleurobrachia* (Moss and Tamm, 1986), but this needs to be verified.

Comparison with other species

We know of no previous reports of giant axons in the comb rows of ctenophores. We have looked at living specimens of *Pleurobrachia bachei* and *Beroë sp.* using the optical arrangement that enabled us to see the giant axons in *Euplokamis* (Fig. 2) and could see no comparable structures. We have cut some sections of *Pleurobrachia* and examined them under the EM with the same result, confirming Hernandez-Nicaise (1973a, 1974), who found only small-diameter neurites. Electrophysiological recordings from *Beroë*, made in the same way and at the same temperature (12°C) as *Euplokamis*, show the complex responses associated with excitation of the polster cells but no preceding neural event. Presumably the nerves conducting the excitation are too small and scattered to give a clear extracellular signal. The response latency is also much longer than in *Euplokamis*, with apparent conduction velocities lying in the range of 21–25 $cm \cdot s^{-1}$. This is similar to the mean value of 25 $cm \cdot s^{-1}$ recorded for *Beroë ovata* at 22°C by Hernandez-Nicaise *et al.* (1980). Apparent conduction velocities in *Pleurobrachia* are even slower, in the range of 11–16 $cm \cdot s^{-1}$. It would appear that rapid conduction is peculiar to *Euplokamis* and is presumably made possible by the giant axons found in this species.

Discussion

Giant axons have evolved in many invertebrate groups as mediators of rapid responses serving either for escape or food capture. Such rapid movements are generally muscular, but there is no reason why a streamlined animal swimming by means of powerful cilia should not have undergone selection for fast pathways mediating its locomotory responses. Such appears to be the case with *Euplokamis*. While many details of the ciliary control mechanism remain to be elucidated, there can be little doubt that the giant axons have evolved to bring about rapid changes in ciliary beat frequency and direction in the context of escape. The finding of giant axons in a ctenophore, though interesting, is not likely to require any drastic reconsideration of ctenophore phylogeny and relationships. We agree with Bullock (1984) that giant

fibers have probably evolved independently in many groups.

The giant axons appear to be fairly short, thick, mononucleate structures forming a chain with some overlap. They synapse with each other, suggesting that they constitute a single pathway. They also synapse with elements of the diffuse nerve net, and can be regarded as a specialized pathway within this net, recalling a similar situation in certain hydrozoan coelenterates (Mackie, 1989). Ultrastructurally, the axons are rather unusual. They have an extremely rich smooth endoplasmic reticulum that appears to form a continuous canal network throughout the entire cell. Such a system could serve for intracellular transport (Droz *et al.*, 1975), but we also see EM images of vesicles lined up along microtubule bundles (*e.g.*, Fig. 5), which is suggestive of mechanoenzyme-driven transport (Vallee *et al.*, 1989).

We are not yet in a position to explain exactly how ctenophores control the frequency of ciliary beating or the direction of the power stroke, though much progress has been made in recent years with *Pleurobrachia*. In this genus, the process can be explained without resorting to a dual innervation model (Moss and Tamm, 1986). Moderate depolarization of the polster cells is associated with increased rates of beating in the normal (forward) direction. Larger depolarizations sufficient to cause a regenerative response (calcium spike) are associated with arrest (laydown) and with accelerated beating in the reverse direction. The comb plates can pass fairly abruptly from accelerated reverse to accelerated forward beating, although a period of intermediate beating may intervene. Thus, depending simply on the number and time relationships of input events at a single set of synapses, the polster cells could be maintained at any level of depolarization or spike frequency required for the various locomotory gaits. Moss and Tamm, however, found evidence of two types of excitatory post-synaptic potentials, suggesting that there may actually be two functionally distinct neuronal excitatory pathways, one associated with a short latency response and moderate depolarization of the polster cells, and the other with a more delayed response and facilitating excitatory post-synaptic potentials that generate spikes and cause ciliary arrest or reversal. Recall, in this context, that three subsets of neurites were described in the ectodermal plexus of *Pleurobrachia* from ultrastructural and pharmacological studies (Hernandez-Nicaise, 1974). Pharmacological evidence of two subsets was also presented by Satterlie (1978).

At first sight, our physiological findings on *Euplokamis* favor the dual innervation theory because they show that the direction in which the cilia beat depends on the direction from which the excitation is coming. The easiest way of explaining this observation would be to assume that there are two separate diffuse nerve nets, one receiving sensations from the front and one from the back, and exciting the comb plates in different ways. If so, however, there should be two sets of giant axons, one associated with each net, but this is not the case. The giants appear to constitute a single series in each comb row, adjacent giants being interconnected by synapses. If this is the case, then there is only one cilio-motor innervation, and the giants are part of it, providing the final common pathway for information from all parts of the animal. In this scenario, the way the comb plates respond might depend on impulse frequency differences associated with the excitation of receptors at the two ends, transmitted through the common excitatory pathway. Frequency coding in a single conducting system provides the basis for two sorts of behavior in the sea anemone *Actinia* (McFarlane and Lawn, 1991). However, other explanations are possible, and as the evidence needed to decide between them is not yet available, further speculation on this question is inappropriate. Very probably, however, the control system in *Euplokamis* will prove to be a modified version of the *Pleurobrachia* system, and as *Pleurobrachia* is a rugged and common surface-living species, it is probably better suited for use in exploring these questions than our fragile and elusive midwater species.

Acknowledgments

We thank Dennis Willows, Director of the Friday Harbor Laboratories, for space and laboratory facilities and Colin Hermans for help collecting specimens. Tony Moss kindly made available portions of his doctoral dissertation. This research was funded by the Natural Sciences and Engineering Research Council of Canada.

Literature Cited

Arkett, S. A., G. O. Mackie, and C. L. Singla. 1987. Neuronal control of ciliary locomotion in a gastropod veliger (*Calliostoma*). *Biol. Bull.* **173:** 513–526.

Bullock, T. H. 1984. Comparative neuroethology of startle, rapid escape and giant fiber-mediated responses. Pp. 1–13 in *Neural Mechanisms of Startle Behavior*, R. C. Eaton, ed. Plenum, New York.

Droz, B., A. Rambourg, and H. L. Koenig. 1975. The smooth endoplasmic reticulum: structure and role in the renewal of axonal membrane and synaptic vesicles by fast axonal transport. *Brain. Res.* **93:** 1–13.

Hernandez-Nicaise, M.-L. 1973a. Le système nerveux des Cténaires I. Structure et ultrastructure des réseaux epithéliaux. *Z. Zellforsch.* **137:** 223–250.

Hernandez-Nicaise, M.-L. 1973b. The nervous system of ctenophores III. Ultrastructure of synapses. *J. Neurocytol.* **2:** 249–263.

Hernandez-Nicaise, M.-L. 1974. Système nerveux et intégration chez les Cténaires: etudes ultrastructurale et comportementale. Doctoral dissertation. Université Claude-Bernard (Lyon I).

Hernandez-Nicaise, M. L., G. O. Mackie, and R. W. Meech. 1980. Giant smooth muscle cells of *Beroë*. *J. Gen. Physiol.* **75:** 79–105.

Mackie, G. O. 1985. Midwater macroplankton of British Columbia studied by submersible PISCES IV. *J. Plankt. Res.* **7:** 753–777.

Mackie, G. O. 1989. Evolution of cnidarian giant axons. Pp. 395–407 in *Evolution of the First Nervous Systems*, P. A. V. Anderson ed. Plenum, New York.

Mackie, G. O., and C. E. Mills. 1983. Use of the PISCES IV submersible for zooplankton studies in coastal waters of British Columbia. *Can. J. Fish. Aquat. Sci.* **40:** 763–776.

Mackie, G. O., C. E. Mills, and C. L. Singla. 1988. Structure and function of the prehensile tentilla of *Euplokamis* (Ctenophora, Cydippida). *Zoomorphology* **107:** 319–337.

McFarlane, I. D., and I. D. Lawn. 1991. The senses of sea anemones: responses of the SS1 nerve net to chemical and mechanical stimuli. *Hydrobiologia* **216/217:** 599–604.

Mills, C. E. 1987. Revised classification of the genus *Euplokamis* Chun, 1880 (Ctenophora: Cydippida: Euplokamidae n. fam.) with a description of the new species *Euplokamis dunlapae*. *Can. J. Zool.* **65:** 2661–2668.

Moss, A. G. 1986. The control of ciliary comb plate beating in the ctenophore *Pleurobrachia*. Doctoral dissertation. Boston University.

Moss, A. G., and S. L. Tamm. 1986. Electrophysiological control of ciliary motor responses in the ctenophore *Pleurobrachia*. *J. Comp. Physiol.* **158:** 311–330.

Moss, A. G., and S. L. Tamm. 1987. A calcium regenerative potential controlling ciliary reversal is propagated along the length of ctenophore comb plates. *Proc. Natl. Acad. Sci. USA* **84:** 6476–6480.

Satterlie, R. A. 1978. Feeding mechanisms in the ctenophore *Pleurobrachia pileus*. *Biol. Bull.* **155:** 464.

Tamm, S. L. 1982. Ctenophora. Pp. 266–358 in *Electrical Conduction and Behaviour in 'Simple' Invertebrates*, G. A. B. Shelton, ed. Clarendon Press, Oxford.

Tamm, S. L., and A. G. Moss. 1985. Unilateral ciliary reversal and motor responses during prey capture by the ctenophore *Pleurobrachia*. *J. Exp. Biol.* **114:** 443–461.

Vallee, R. B., H. S. Shpetner, and B. M. Paschal. 1989. The role of dynein in retrograde axonal transport. *Trends Neurosci.* **12:** 66–70.

Reference: *Biol. Bull.* **182**: 257–264. (April, 1992)

Phase Shift of a Tidal Rhythm by Light-Dark Cycles in the Semi-Terrestrial Crab *Sesarma pictum*

MASAYUKI SAIGUSA

Okayama University, College of Liberal Arts & Sciences, Tsushima 2-1-1, Okayama 700, Japan

Abstract. The larval release activity of the semi-terrestrial crab *Sesarma pictum* was monitored for three-week periods under laboratory conditions of constant and cyclic light. Under conditions of constant dim light, the rhythm for the first ten days was unimodal (larval release just after the nocturnal high tide) and then became bimodal (no apparent synchrony with the tides or with other members of the population) for the remainder of the experimental period. On the other hand, in photoperiods similar to those in the field, the rhythm was maintained; the phase was bimodal and the timing of larval release was delayed 1–2 h from the predicted times of high water in the habitat. When the photoperiod was advanced or delayed, the tidal rhythm was phase-shifted accordingly. The photoperiod does entrain the release rhythm to bimodal tidal cycle. So the phase-shift of a tidal rhythm by 24-h LD cycles is a very difficult phenomenon to explain.

Introduction

In their natural habitats, intertidal and estuarine animals are exposed, not only to the day-night cycle (24 h), but also to the rhythmic ebb and flow of the tides, which include 12.4-h, 24.8-h, and 15-day components. Having adapted to such an environment, marine organisms often show a complex activity pattern with circadian, circatidal, and circa-semilunar frequencies; the dominant rhythmicity is circadian in some species, and circatidal or semilunar in others (see reviews by Neumann, 1981; DeCoursey, 1983).

Compared with the terrestrial animals, information about the biological timing systems is relatively limited in marine animals. This paucity of information is partly due to the complexity of environmental cycles. In addition, most biological timings have been investigated in locomotor activities. The noisy nature of these activities, and the individual variability in the responses to environmental cycles, have made the analyses difficult in most aquatic animals. For example, when the locomotor activity of the fiddler crab *Uca crenulata* was monitored in constant light or 24-h light-dark conditions, half of the experimental crabs only showed a rhythmic activity; the activity of the remaining half was random (Honegger, 1973).

Clearly demarcated biological rhythms have been reported in the swimming activity of some marine crustaceans (Enright, 1963, 1972). The records of their activity have demonstrated predominantly circatidal rhythms that were not affected by light-dark cycles in the laboratory. Animals do entrain or respond to simulated tidal stimuli, such as wave action in the isopod *Excirolana* (Enright, 1965), or cycles of hydrostatic pressure in the amphipods *Synchelidium* (Enright, 1962) and *Corophium* (Morgan, 1965).

Precise biological timings also often develop in reproductive phenomena, and this has been observed in a variety of marine animals, including the polychaete *Platynereis* (Hauenschild, 1960), the intertidal midge *Clunio* (Hashimoto, 1976; Neumann, 1976), and many species of Crustacea (Branford, 1978; DeCoursey, 1979, 1983). The larval release behavior of the estuarine terrestrial crab *Sesarma haematocheir* is also synchronized with environmental light and tidal cycles, showing a unimodal tidal rhythm that coincides with the times of nocturnal high water (Saigusa, 1982, 1985). A phase jump is involved in the timing process, so that this tidal rhythm appears at 15-day intervals. Experimental analyses indicated that the timing is endogenously controlled, and that the phase of the rhythm can be shifted by artificial 24-h light-dark (LD) cycles (Saigusa, 1986). An important problem is the timing mechanism underlying the tide-synchronized biological rhythm, the phase of which is shifted by day-night cycles.

In this paper, ovigerous females of *Sesarma pictum* were used for experiments, because larval release activity in

Received 27 March 1990; accepted 21 January 1992.

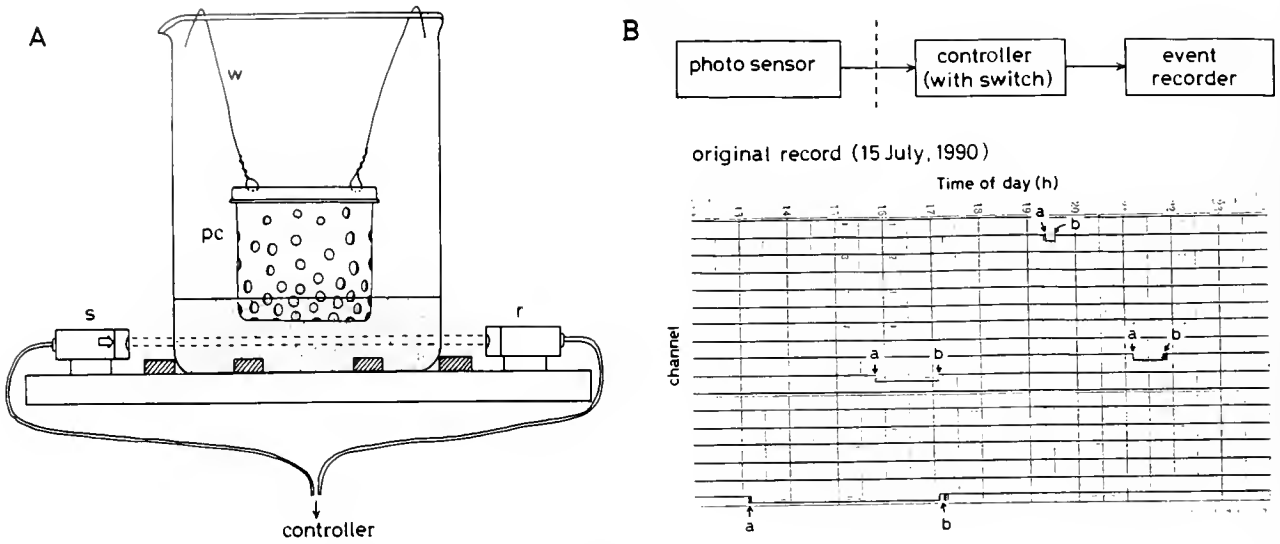

Figure 1. System for recording the larval release activity of *Sesarma pictum* females. A. The apparatus used to detect the time of day of larval release. w: fine wire. pc: plastic cage to confine an ovigerous crab. s and r: infrared source and receiver (E3S-2E4, Omron Co. Ltd., Japan). The glass beaker illustrated here is the larger one (13.5 cm diameter; see text). B. An example of an original record showing 4 out of 17 females releasing their larvae (a part of the data illustrated in Figure 2). The output of the sensor unit was monitored by an event recorder (R17-H12T, Fuji Electric Co. Ltd., Japan) through a controller (S3S-A-10, Omron). a: time of larval release by a female. b: time when that female was removed from the experimental chamber with her beaker. Simultaneously, a new beaker with a plastic cage that confined another ovigerous female was placed in each apparatus.

this species has a tidal rhythm with a bimodal phase (12.5-h period) that has no apparent circadian component. The present paper asks whether this tidal rhythm is also affected by the day-night cycle, and it discusses possible mechanisms for this influence.

Materials and Methods

Sesarma pictum inhabits banks above the water's edge in the intertidal zone. Male and female crabs spend the winter hibernating in burrows dug into the bank, but they become active in the latter half of April. In early summer (June–July), the females incubate their eggs in their folded abdomens, where the embryos are ventilated by movements of the pleopods. When embryonic development is completed, the females enter the water to liberate their zoea larvae. The larval release behavior has not been observed in the field because it is not carried out at the water's edge, as is that of *S. haematocheir* (Saigusa, 1982, 1985). Rather, the ovigerous females of *S. pictum* enter the water at about high tide, and then soon disappear in the depths; possibly they release their larvae in the water near the shore.

Ovigerous females were collected from the seacoast at Kasaoka, Okayama Prefecture. The crabs occur in narrow crevices between rocks on the bank; they were stimulated to emerge with a thin stick, and were then captured by hand. Once suitable numbers had been collected, they were brought into the laboratory and placed in aquaria (70 cm long, 40 cm wide, and 25 cm high). The aquaria had a shallow pool of diluted seawater (salinity at about 20‰) at the bottom, and hiding places (moistened with fresh water) made of boards set above the surface of water. The crabs were fed every few days. The experimental rooms were equipped with controlled light and temperature. Temperature was at 23 ± 1.5°C; luminous intensity was about 700–1200 lux at the floor with the light on, and less than 0.01 lux in the dark phase. Only two experiments were carried out under continuous light, and in these cases the luminous intensity was at 0.5–1.0 lux, or 100–300 lux, respectively.

The eggs (*i.e.*, embryos with egg capsules) of each female were checked by eye every day, and those crabs carrying embryos that seemed likely to hatch within a few days were individually set in a recording apparatus placed in the same room (Fig. 1A). With this apparatus, the time of larval release could be monitored without any change in the ambient lighting conditions. The day of hatching is difficult to predict; the only indication that hatching is imminent is the brownish green color of the embryos (mainly caused by yolk consumption). The larval release behavior of *S. pictum* was observed in the laboratory, and was generally not as vigorous as that of *S. haematocheir*. The female repeatedly flexed her abdomen inward and made associated movements of the pleopods bearing embryos. These pumping

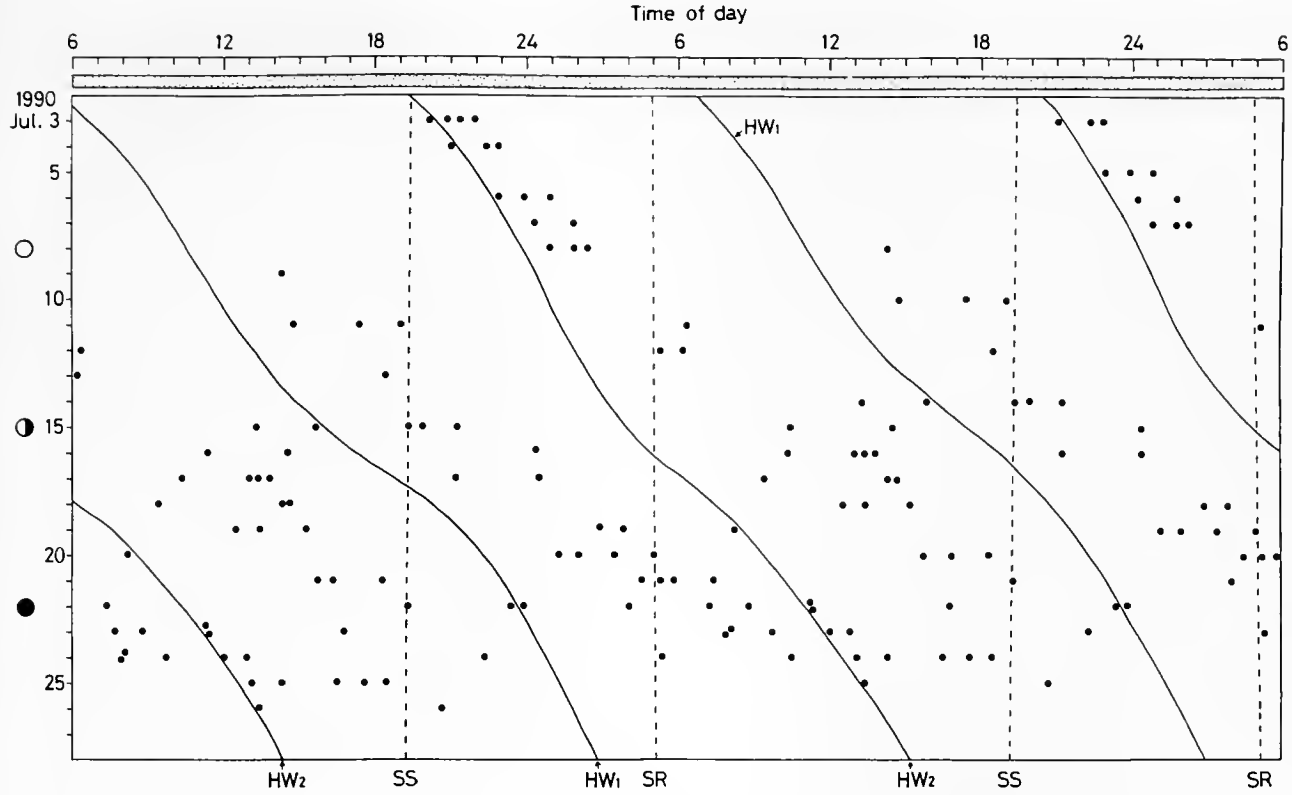

Figure 2. Time of day of larval release monitored under a regime of continuous light (LL: 0.5–1.0 lux) and no tidal influence in the laboratory. All of the ovigerous females were collected in the field on 3 July 1990; black dots indicate the time of day of larval release by those females. For comparison, environmental cycles in the field are characterized by the times of sunset (SS) and sunrise (SR), by the curves connecting predicted time of day of high tides (HW_1 and HW_2), and by the phase of the moon (○: full moon, ◑: the last quarter of the moon, ●: new moon). The entire record is duplicated on the right and displaced upwards one day, so that each day's data can be matched with those of the following day. Eighty (80) females were used in this experiment.

movements swept clouds of newly hatched zoeae away from the female.

The larval release recording system consisted of a sensor unit (infrared source and receiver) placed inside the experimental room, and a controller unit placed outside. Each ovigerous female was confined in a separate, small plastic cage (6 cm in diameter and 8 cm in height) with many holes drilled in the bottom and sides. As Figure 1A shows, the cage was suspended by a fine wire from the rim of a glass beaker containing diluted, clean seawater (salinity at about 20‰). The experimental procedures for monitoring the larval release activity of *S. pictum* were basically the same as those for *S. haematocheir* (Fig. 1B), and they have already been described elsewhere (Saigusa, 1986).

For each female, one of two kinds of glass beakers was selected to hold her plastic cage: a bigger one (13.5 cm in diameter), or a smaller one (11 cm in diameter). The selection was made to ensure that the photoelectric switch would respond and was based on the size of the egg sponge carried by the female. Moreover, because the ovigerous female of *S. pictum* has a smaller carapace (1.6–2.5 cm) than *S. haematocheir,* the amount of seawater in the larger beaker was reduced to 0.5 l, and to 0.3–0.4 l in the smaller one. The number of ovigerous females used in each experiment is described in the figure legends or in the text. (Some females were released into the aquaria before being confined to cages. Because the time of the release of those females was not monitored, such releases were not included in the figures.) The animals were not fed after they had been confined in the recording apparatus.

Results

The females used in the present experiments were randomly collected from the field; thus, some crabs seemed ready to release larvae within a few days, whereas others carried eggs that seemed to have commenced incubation just one or two days before. The larval release by these females was completed within three weeks after the collection, suggesting that females incubate their embryos for about 2–3 weeks.

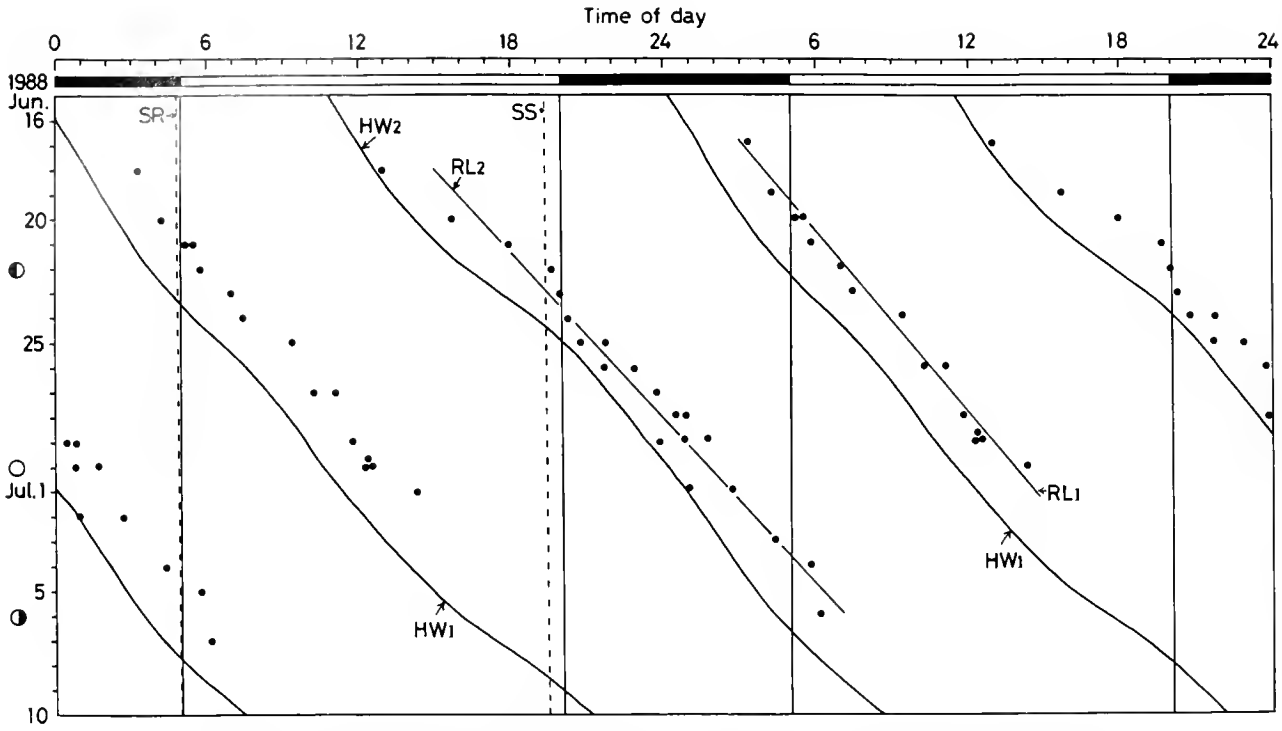

Figure 3. Daily timing of larval release by *Sesarma pictum* monitored under the conditions of a 24-h light-dark (LD) cycle in the laboratory. Forty crabs were used. Date of collection: 16 June 1988. Vertical lines indicate the times of light-off and light-on in the chamber, respectively. SS and SR are the times of sunset and sunrise in nature. Diagonal curves (HW_1 and HW_2) connect the times of high water in the field. Diagonal lines (RL_1 and RL_2) are least squares regression lines fitted to each phase of the tidal rhythm. The period length of each phase (τ) is estimated from the slope (a) of its regression line (τ = 24h + a). The slopes of RL_1 and RL_2 are 0.75 and 0.84, respectively. The regression lines are based on those data obtained after the phase shift was considered to have been completed.

The first experiment was designed to determine whether an endogenous component is involved in the larval release activity and, if so, whether this component corresponds to the day-night cycle or to tidal cycle at the local habitat. For these purposes, the larval release activity of the population (80 specimens) was monitored under constant, very dim light (LL) conditions for more than three weeks following collection. As indicated in Figure 2, the larval release activity persisted under these conditions. For the first 10 days, the phase of the rhythm was unimdal (24.5-h period) and the larval release roughly coincided with the nocturnal high tides. The release rhythm then became bimodal (12.5-h period), but no apparent synchrony with the tides, or with other members of the population, appeared for the remainder of the experimental period. A similar experiment, with 40 individuals under stronger luminous intensity (100–300 lux), also had the same tendency (not illustrated).

To examine the effect of light regime, experiments were then conducted with a 15-h light: 9-h dark photoperiod; *i.e.*, the phase of the cycle was set to be similar to that in the field. The effects of cyclic light were markedly different from those illustrated in Figure 2: the timing of the larval release was closely correlated with the tidal cycles (high water) for at least three weeks (Fig. 3). The phase of this rhythm is clearly bimodal (12.5-h period). Least squares regression lines fitted to each phase of the rhythm (RL_1 and RL_2) showed that the timing of release monitored in the laboratory was delayed 1–2 h from the predicted times of high water in the habitat. The correlation of larval release with the tidal cycle in the habitat of the crabs continued throughout the experiment. Another experiment, with 50 females and the same light conditions, was performed on 1–20 July 1987; the results were the same as those of Figure 3 (not illustrated). A comparison of Figures 2 and 3 suggests that a 24-h natural light-dark cycle maintains the normal tidal phase of a population rhythm.

Next, I examined whether the phase of the tidal rhythm can be affected if the phase of the experimental cyclic light is shifted from the natural day-night cycles. The following experiments were made to confirm this point quantitatively. In Figure 4, the phase of the artificial day-night cycle was advanced relative to the natural light cycle, by 6.25 h at lights-on, and by 7 h at lights-off. After some days had elapsed, the time of release shifted ahead of the predicted high water curves. This suggests an advanced

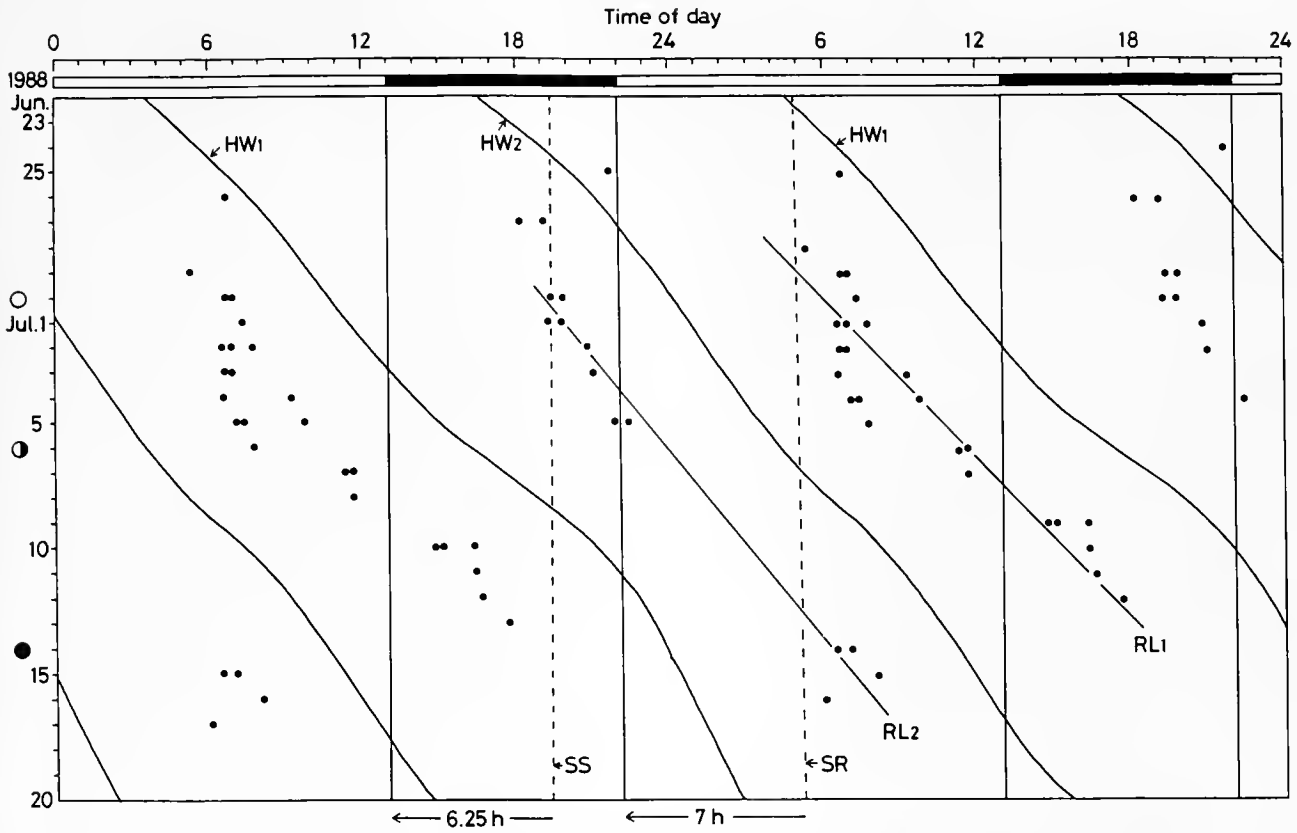

Figure 4. Time of day of larval release monitored under a 24-h light-dark regime (LD 15:9), the phase of which was *changed* by 6–7 h with respect to the natural conditions. Times of light-off and light-on in the artificial light cycles are shown by vertical lines (light-on at 22:00, light-off at 13:00), and times of sunset and sunrise are marked by the broken lines. RL_1 and RL_2 indicate least squares regression lines applied to the new phase after the shift; *i.e.*, the data from 29 June–13 July for RL_1, and those of 30 June–17 July for RL_2. Other symbols are the same as in Figure 2. Collection of crabs: 23 June 1988. The slopes of RL_1 and RL_2 are 0.76 and 0.80, respectively. Fifty animals were used in the experiment.

phase-shift. The magnitude of the shifts in the two phases were somewhat different; *i.e.*, whereas the time difference between HW_1 and RL_1 was 5–6 h, that between HW_2 and RL_2 was 4–5 h. The phase differences between the rhythms in both Figures 2 and 3, corresponded to the time lag between the natural day-night and the artificial 24-h LD cycles.

Another experiment was also meant to verify that the magnitude of the phase-shift of the tidal rhythm is dependent on the phase difference between natural and artificial day-night cycles. In this case, the experiment asked whether the phase can be delayed. One hundred females were used in these experiments, and the light regime was shifted by 5 h at lights-on and by 5.7 h at lights-off. In this experiment, the data suggest that, after about 10 days, a delayed phase-shift occurred (Fig. 5). Another experiment, in which 35 animals received the same treatment (23 July to 7 August 1987), clearly demonstrated a similar phase delay (not illustrated). Figure 5 also shows that the phase of the population rhythm remained stable with respect to the phase of high water, for at least the next 2–3 weeks, with no notable desynchronization of the individuals. The time lag between HW_1 and RL_1 was 5.5–7 h, and between HW_2 and RL_2 it was 5.5–6.5 h. The duration of the phase delay could not be determined in these experiments, because the number of the females incubating the next clutch diminished.

The experiments described above were performed with crabs collected on different dates. Uncertainties remained, therefore, about whether a light cycle can actually phase-shift a tidal rhythm, and if so, whether advancing or delaying the photoperiod truly corresponds to the change in the tidal rhythm. To meet this question, about 200 ovigerous females were collected from the field on 3–4 July 1991, and randomly separated in the laboratory into two groups of similar size. One group was exposed to an artificial 24-h LD cycle, the phase of which was similar to the natural LD cycle (Fig. 6A); the other group was exposed to an artificial LD cycle that was advanced 4–5 h from the natural light cycle (Fig. 6B).

In the control experiment (Fig. 6A), the larval release occurred just after the time of high tides in the field. The

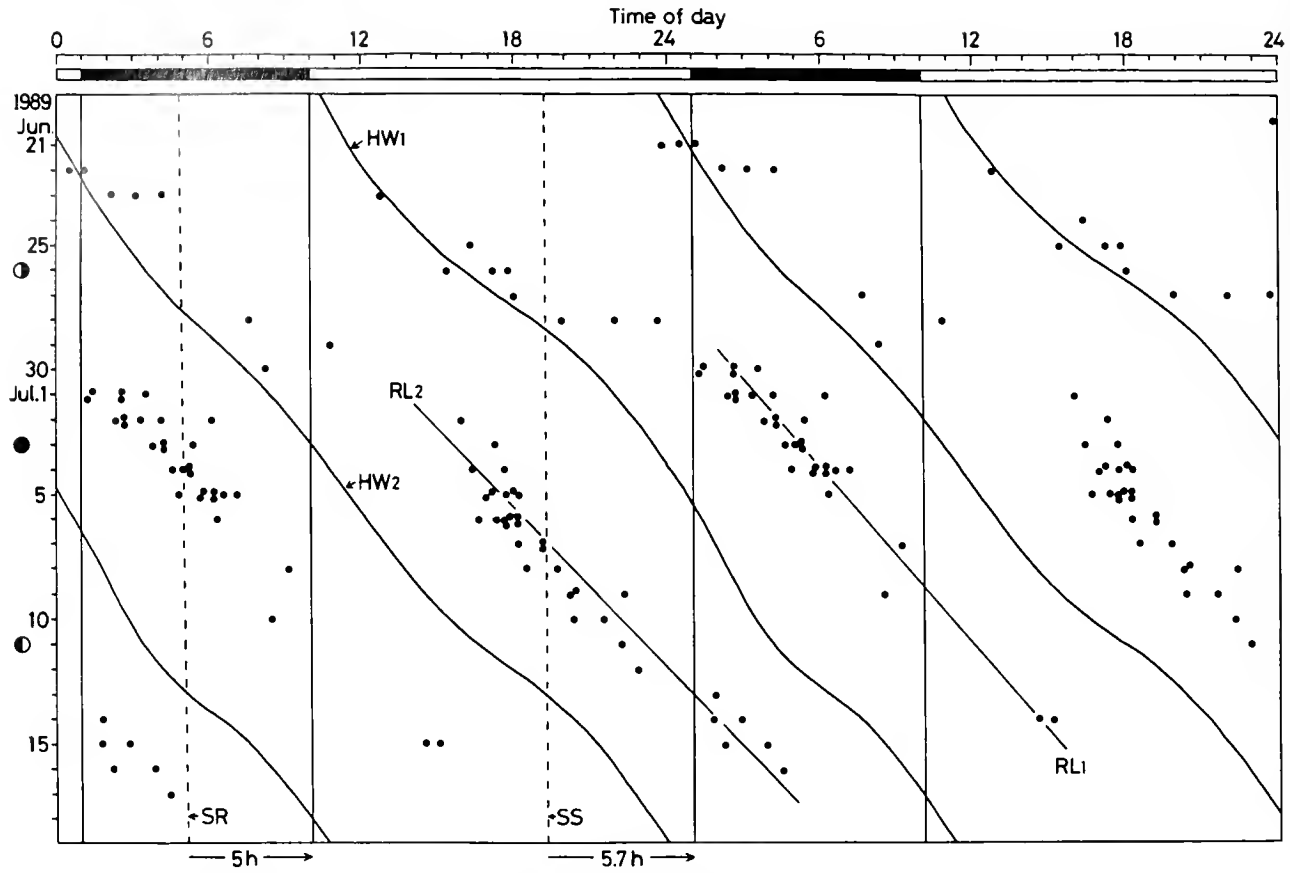

Figure 5. Time of day of larval release monitored under a 24-h light-dark regime (LD 15:9), the phase of which was *delayed* by 5–6 h from the natural light cycle. Times of light-on and light-off were 1:00 and 10:00, respectively. All of the crabs were collected on 21 June 1989. Some of the females incubated a second clutch in the laboratory, and the larval release activity of those crabs was also monitored. The estimated slope of RL_1 and RL_2 is 0.85 and 0.86, respectively. ◑: the last quarter of the moon, ●: new moon, ◐: the first quarter. About 100 females were used in the experiment.

phase of this rhythm was clearly bimodal. These features were the same as those in Figure 3. The crabs exposed to the light cycle that had been advanced (Fig. 6B) also showed a bimodal tidal rhythm, but a week had elapsed, and the time of release shifted ahead of the time of high tides. The time lag between the activity after 10 July and high tide (HW_2) showed an advancing phase-shift of about 4 h.

No clear indication of a semilunar component (*i.e.*, a semi-monthly fluctuation in the number of females releasing larvae per day) was found in these results. Neither was a 24-h solar day (*i.e.*, circadian) component detected, at least in the activity pattern itself.

Discussion

The purpose of devising experiments in constant light (*e.g.*, Fig. 2) is to demonstrate a free-running rhythm. Certainly the larval release was roughly correlated with the time of nocturnal high tides for the first 10 days, and then the rhythm became bimodal. However, no apparent synchrony with the tides, or other individuals in the population, was seen for the latter half of the experimental period; so no free-running rhythm was clearly evident in Figure 2.

In most studies of rhythmic behavior, activities that are carried out repeatedly by each individual are monitored throughout the investigation. In this work, however, each crab released larvae just once during a three-week experimental period; so no free-running rhythm was evident. A possible explanation of the data in Figure 2 is, therefore, that the constant light increased the variability of the free-running period in each individual, desynchronizing the population rhythm.

The first question arising here is related to the environmental cues that entrain the tidal rhythm of this species. Circa-tidal rhythms are known to respond to stimuli correlated with on-shore tides, and not to day-night cycles. Enright (1965) showed that cycles of water turbulence can effectively entrain the circa-tidal rhythm of the isopod

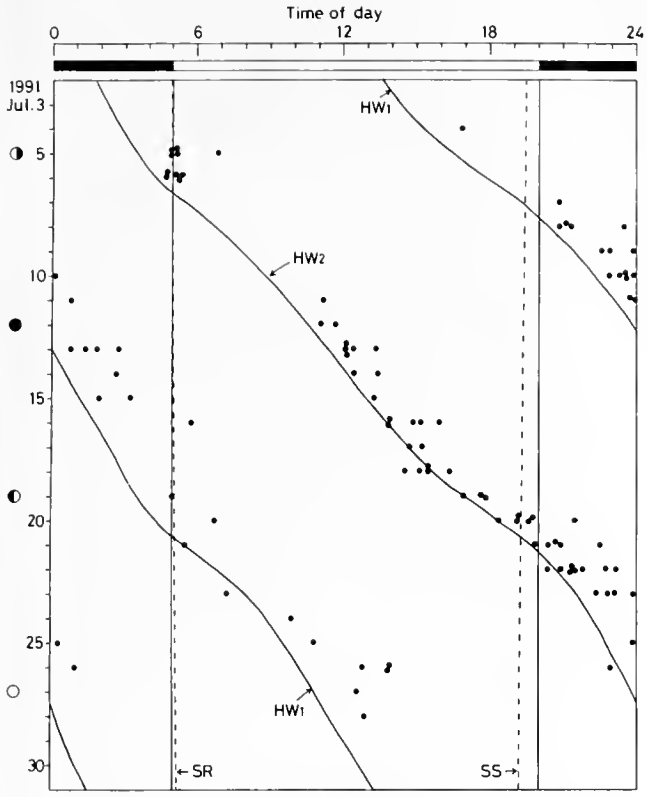

Figure 6A. Time of day of larval release monitored under a 24-h LD cycle (LD 15:9), the phase of which was *similar* to that of the field. Date of collection: 3–4 July 1991. About 100 animals were used in the experiment. Symbols were the same as in Figure 2.

Excirolana. Cyclical or non-cyclical changes of hydrostatic pressure have been shown to cause behavioral responses in the amphipods (Enright, 1962; Morgan, 1965). However, all the experimental data obtained in this study (Figs. 2–5 and 6A, B) have demonstrated that a light regime actually takes part in the phase shift. The 24-h LD cycle may be the zeitgeber of the *Sesarma pictum* tidal rhythm. In the field, however, this rhythm is not likely to be entrained solely by the 24-h LD cycle.

The tidal rhythm of *Sesarma haematocheir* was entrained by 24.5-h artificial moonlight cycles administered in the dark period of a 24-h LD cycle (Saigusa, 1988, 1989). In view of these studies, the *S. pictum* larval release rhythm could be entrained by more than one environmental cue. A 24-h LD cycle is one zeitgeber, but others remain unknown. The habitat of *S. pictum* is restricted to the bank along the shoreline, so tidally correlated factors, such as the periodic fluctuations of water turbulence on the shore, should also be considered.

The second, and central, question posed in this paper is the effect of light on the tidal rhythm of *S. pictum*. If the results of Figures 4 and 5, and those of Figure 2, were regarded as arising from substantially similar mechanisms, there would be no need to assume a phase shift caused by the environmental light cycle. In this case, one possible explanation is that light cycles exert some superficial influence on the phase of the tidal rhythm irrespective of timing mechanisms, causing abnormal phasing of the rhythm. However, the results of Figure 6A and B would completely deny such a possibility; a photoperiod does entrain larval release rhythm to a bimodal tidal cycle. Because a 24-h LD cycle can evoke a phase shift of the tidal rhythm, then the difficulty is understanding the timing mechanism involved.

Many investigators have found that behavioral and physiological events in marine organisms not only coincide with the tidal cycle, but are also correlated with the day-night cycle to produce activity patterns with simultaneous daily and tidal components (Naylor, 1958; Barnwell, 1966; Palmer and Round, 1967; Honegger, 1973; Benson and Lewis, 1976). Accordingly, recent interpretations have included two types of internal clocks: one of circatidal frequency, and the other of circadian frequency (Naylor, 1958; Barnwell, 1966, 1968; Palmer and Round, 1967; Benson and Lewis, 1976; Webb, 1976). For example, two internal clocks were proposed to explain noc-

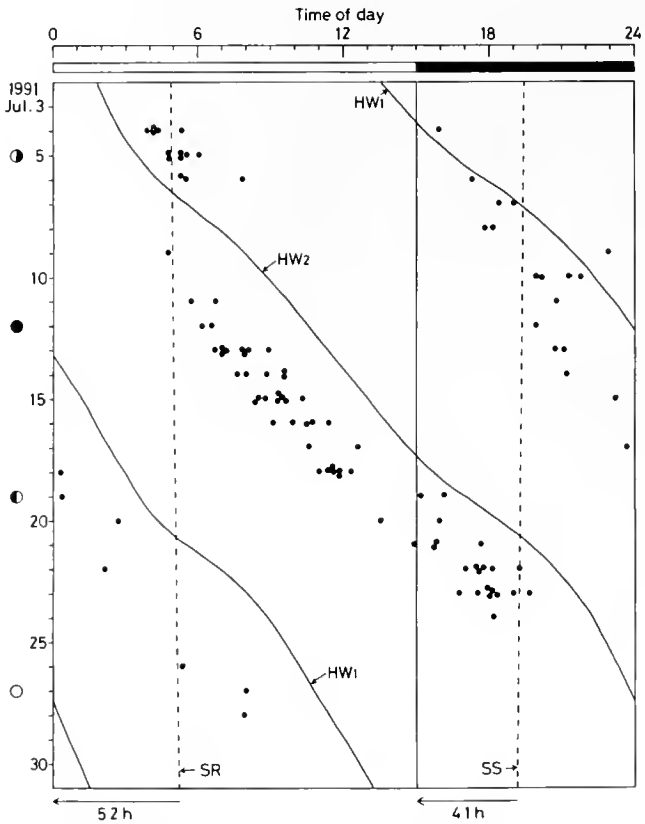

Figure 6B. Time of day of larval release recorded in a 24-h LD cycle (LD 15:9), the phase of which was *advanced* by 4–5 h from that of the field. Date of collection was the same as in Figure 6A. Times of light-on and light-off were at 0:00 and 15:00, respectively. One hundred and five animals were used in the experiment.

turnal locomotion in the amphipod *Talorchestia* (Benson and Lewis, 1976). One of these, a circadian clock, controls the nocturnal phase of the activity, and the other, a circa-tidal clock, inhibits the activity around the time of nocturnal high water.

The phenomenon reported in this paper, *i.e.*, phase shift of the tidal rhythm appearing under cyclic light (Figs. 4, 5, and 6B), could not be explained in terms of an interaction between circa-tidal and hidden circadian rhythms operating simultaneously within individuals. The reason is based on the understanding that a circa-tidal rhythm is only the expression of a circadian rhythm which, as a result of an adaptation to marine environment, has slightly modified its internal period and is responsible to tide-correlated zeitgebers, too. Yet clearly, the circa-tidal rhythm of *S. pictum* cannot be explained in terms of a hypothesis requiring that those tide-correlated zeitgebers affect a circadian (bimodal) rhythm directly, changing its internal period to that of a bimodal tidal cycle.

The nocturnal release rhythm of *S. haematocheir* was, therefore, accounted for by a hypothesis similar to the mechanisms proposed by Pittendrigh and coworkers (Pittendrigh, 1960, 1981; Pittendrigh and Bruce, 1959) (see Saigusa, 1986 and 1988, for details). In that model, when the driven oscillator is delayed until dawn, it leaps back to dusk. However, if one wants to explain the effect of light by the mechanism that was applied to *S. haematocheir*, then one would have to assume that the driving oscillator can control the phase of the driven oscillator which has a different period. Perhaps such an assumption is not realistic. Thus, the phase-shift of a tidal rhythm by 24-h LD cycle is a very difficult phenomenon to explain.

Acknowledgments

I thank Mr. A. Bettchaku, Faculty of Education, Okayama University, who helped me to collect crabs in the field.

Literature Cited

Barnwell, F. H. 1966. Daily and tidal patterns of activity in individual fiddler crab (Genus *Uca*) from the Woods Hole region. *Biol. Bull.* **130:** 1–17.

Barnwell, F. H. 1968. The role of rhythmic systems in the adaptation of fiddler crabs to the intertidal zone. *Am. Zool.* **8:** 569–583.

Benson, J. A., and R. D. Lewis. 1976. An analysis of the activity rhythm of the sand beach amphipod, *Talorchestia quoyana*. *J. Comp. Physiol.* **105:** 339–352.

Branford, J. R. 1978. The influence of daylength, temperature and season on the hatching rhythm of *Homarus gammarus*. *J. Mar. Biol. Assoc. U.K.* **58:** 639–658.

DeCoursey, P. J. 1979. Egg-hatching rhythms in three species of fiddler crabs. Pp. 399–406 in *Cyclic Phenomena in Marine Plants and Animals*, E. Naylor and R. G. Hartnoll, ed. Pergamon Press, Oxford.

DeCoursey, P. J. 1983. Biological timing. Pp. 107–162 in *The Biology of Crustacea, Vol. 7: Behavior and Ecology*, F. J. Vernberg and W. B. Vernberg, ed. Academic Press, Washington.

Enright, J. T. 1962. Pressure sensitivity of an amphipod. *Science* **133:** 758–760.

Enright, J. T. 1963. The tidal rhythm of activity of a sand-beach amphipod. *Z. Vergl. Physiol.* **46:** 276–313.

Enright, J. T. 1965. Entrainment of a tidal rhythm. *Science* **147:** 864–867.

Enright, J. T. 1972. A virtuoso isopod. Circa-lunar rhythms and their tidal fine structure. *J. Comp. Physiol.* **77:** 141–162.

Hashimoto, H. 1976. Non-biting midges of marine habitats (Diptera: Chironomidae). Pp. 377–414 in *Marine Insects*, L. Cheng, ed. North-Holland Publishing Company, Amsterdam.

Hauenschild, C. 1960. Lunar periodicity. Pp. 491–497 in *Biological Clocks. Cold Spring Harbor Symposia on Quantitative Biology*, Vol. 25, New York.

Honegger, H.-W. 1973. Rhythmic motor activity responses of the California fiddler crab *Uca crenulata* to artificial light conditions. *Mar. Biol.* **18:** 19–31.

Morgan, E. 1965. The activity rhythm of the amphipod *Corophium volutator* (Pallas) and its possible relationship to changes in hydrostatic pressure associated with the tides. *J. Anim. Ecol.* **34:** 731–746.

Naylor, E. 1958. Tidal and diurnal rhythms of locomotory activity in *Carcinus maenas* (L.). *J. Exp. Biol.* **35:** 602–610.

Neumann, D. 1976. Adaptations of chironomids to intertidal environments. *Annu. Rev. Entomol.* **21:** 387–414.

Neumann, D. 1981. Tidal and lunar rhythms. Pp. 351–380 in *Biological Rhythms. Handbook of Behavioral Neurobiology*, Vol. 4, J. Aschoff, ed. Plenum Press, London.

Palmer, J. D., and F. E. Round. 1967. Persistent, vertical-migration rhythms in benthic microflora. VI. The tidal and diurnal nature of the rhythm in the diatom *Hantzschia virgata*. *Biol. Bull.* **132:** 44–55.

Pittendrigh, C. S. 1960. Circadian rhythms and the circadian organization of living systems. Pp. 159–184 in *Biological Clocks. Cold Spring Harbor Symposia on Quantitative Biology*, Vol. 25, New York.

Pittendrigh, C. S. 1981. Circadian systems: general perspective. Pp. 57–80 in *Biological Rhythms. Handbook of Behavioral Neurobiology*, Vol. 4, J. Aschoff, ed. Plenum Press, London.

Pittendrigh, C. S., and V. G. Bruce. 1959. Daily rhythms as coupled oscillator systems and their relation to thermoperiodism and photoperiodism. Pp. 475–505 in *Photoperiodism and Related Phenomena in Plants and Animals*, R. B. Withrow, ed. American Association for the Advancement of Science, Washington.

Saigusa, M. 1982. Larval release rhythm coinciding with solar day and tidal cycles on the terrestrial crab *Sesarma*. *Biol. Bull.* **162:** 371–386.

Saigusa, M. 1985. Tidal timing of larval release activity in non-tidal environment. *Jpn. J. Ecol.* **35:** 243–251.

Saigusa, M. 1986. The circa-tidal rhythm of larval release in the incubating crab *Sesarma*. *J. Comp. Physiol.* **159:** 21–31.

Saigusa, M. 1988. Entrainment of tidal and semilunar rhythms by artificial moonlight cycles. *Biol. Bull.* **174:** 126–138.

Saigusa, M. 1989. A circadian rhythm in tidal environment: larval release activity of the terrestrial crab *Sesarma*. Pp. 175–186 in *Circadian Clocks and Ecology*, T. Hiroshige and K. Honma, ed. Hokkaido University Press, Sapporo.

Webb, H. M. 1976. Interactions of daily and tidal rhythms. Pp. 129–135 in *Biological Rhythms in the Marine Environment*, P. J. DeCoursey, ed. University of South Carolina Press, Columbia.

Reference: *Biol. Bull.* **182**: 265–269. (April, 1992)

Effects of Hypoxia and Anoxia on Larval Settlement, Juvenile Growth, and Juvenile Survival of the Oyster *Crassostrea virginica*

S. M. BAKER AND R. MANN

Virginia Institute of Marine Science, The College of William and Mary, Gloucester Point, Virginia, 23062

Abstract. The effects of hypoxia (1.5 mg O_2 l^{-1}, 20% of air saturation) and anoxia (<0.07 mg O_2 l^{-1}, <1% of air saturation) on oyster (*Crassostrea virginica*) larval settlement, juvenile growth, and juvenile survival were studied. Settlement was reduced significantly ($P < 0.05$) in hypoxic treatments, as compared to normoxic treatments (7.3 mg O_2 h^{-1}, 100% of air saturation), and almost no settlement took place in anoxic treatments. After 96 h, 38% and 4% of the larvae placed in hypoxic and anoxic treatments had settled, while 79% settled in normoxic treatments. In the first 144 h after settlement, juveniles in hypoxic treatments grew one third as much as those in normoxic treatments, while juveniles in anoxic treatments did not grow at all. Median mortality times of recently settled juveniles in hypoxic and anoxic treatments were 131 h and 84 h, respectively. We conclude that hypoxic and anoxic waters have potentially detrimental effects on oyster settlement and recruitment.

Introduction

Chesapeake Bay exhibits episodes of oxygen depletion concomitant with seasonal salinity and temperature stratification (Taft *et al.*, 1980; Officer *et al.*, 1984). Oxygen depletion is usually restricted to areas below the pycnocline, but wind stress frequently tilts the pycnocline (Carter *et al.*, 1978; Malone *et al.*, 1986) irrigating shallow areas, where oyster reefs occur, with hypoxic or anoxic water from deeper areas (May, 1973; Sanford et al., 1990). The pycnocline remains tilted for from several hours to two or three days (Malone *et al.*, 1986; Sanford *et al.*, 1987). These events often coincide with the timing of settlement and recruitment of the oyster, *Crassostrea virginica* Gmelin. Reduced settlement or complete settlement failure in localized areas has been attributed to incidents of pycnocline tilting (May, 1973; Abbe, 1986).

Previous studies have demonstrated that tolerance of larval and adult oysters to hypoxia and anoxia increases with developmental stage and body size. Larval stages and juvenile oysters (16 mm height) survive anoxia from hours to days (Widdows *et al.*, 1989), while adult oysters survive periods of unsuitable conditions lasting days or weeks (Galtsoff, 1964; Stickle *et al.*, 1989).

Little is known about the tolerance of settling oyster larvae or recently settled juvenile oysters to hypoxia and anoxia. These stages are pivotal to subsequent recruitment into the population. The objectives of this study, therefore, were to examine the effects of hypoxia and anoxia on settlement of oyster pediveliger larvae and on the growth and survival of recently settled juvenile oysters.

Received 26 August 1991; accepted 25 November 1991.

Contribution No. 1707 from the Virginia Institute of Marine Science, School of Marine Science, The College of William and Mary.

Materials and Methods

Experimental apparatus

All experiments were performed at 25°C and 21‰ S. Temperature was maintained by controling laboratory temperature and by a circulating water bath in which the experimental chambers were immersed. Three 4-liter flasks of 0.45 μm filtered seawater containing algae (*Isochrysis galbana*) at a concentration of 20,000 cells ml^{-1} were bubbled with air, a mixture of oxygen and nitrogen, or nitrogen. The target oxygen concentrations were 7.3 mg O_2 l^{-1} (100% of air saturation), 1.5 mg O_2 l^{-1} (20% of air saturation), and less than 0.07 mg O_2 l^{-1} (<1% of air saturation). These treatments will be referred to as

normoxia, hypoxia, and anoxia, respectively, although the latter of these conditions is more correctly termed 'microxia.' Although carbon dioxide was not included in the latter two treatments, pH did not differ significantly ($P < 0.05$, ANOVA) among the three treatments.

Flow-through chambers were constructed to hold larval and juvenile oysters during experimental trials. Each chamber was a 20 ml glass vial closed with a rubber stopper pierced by two 20 gauge needles. Inflow needles were fitted with inverted pipette tips. Outflow needles were cut off even with the bottom of the stoppers and covered with 202 μm Nitex mesh, fine enough to retain pediveliger larvae. Chambers within the same treatment were connected in series as depicted in Figure 1. Stainless steel tubing (1 mm bore) was used throughout. The flow rate through the chambers was about 233 ml h^{-1}, and water residence time in the system was 1 h or less. The flasks of seawater and algae were replaced every 12 h with identical flasks that had been bubbled with the appropriate gases for at least 2 h prior to replacement.

Oxygen concentration at the outflow of each treatment was measured daily with a Strathkelvin Instruments (SI) oxygen sensor (1302) held in a SI microcell (MC100) and coupled to a SI oxygen meter (781) and chart recorder. The oxygen sensor was calibrated daily with air-saturated water and a 0% oxygen solution of sodium borate and crystalline sodium sulfite. Normoxic, hypoxic, and anoxic treatments were consistently maintained at 85–100%, 15–22% and 0–1% of full air saturation, respectively. Outflow concentrations of oxygen did not differ measurably from the inflow concentrations.

Larval settlement experiments

Oyster (*Crassostrea virginica*) pediveliger larvae were reared by the Virginia Institute of Marine Science oyster hatchery at Gloucester Point, Virginia. Oyster shell settlement substrates were conditioned in seawater for 24 h prior to each experiment to develop a settlement-inducing bacterial coating (Fitt *et al.*, 1990). One conditioned oyster shell was placed in each chamber, with the rough side up. Fifty larvae were counted into each chamber with a Drummond Captrol III microdispensor. Only actively swimming larvae were used.

Two chambers were removed daily from each treatment; they were not replaced. Settlement was calculated by expressing the number of settled oyster larvae as a percentage of the total number of larvae introduced into the chamber. The data from the two chambers were pooled as one replicate for that exposure time. The entire larval settlement experiment was repeated five times, resulting in five replicates of normoxic treatments, and three replicates each of hypoxic and anoxic treatments.

Larval settlement data were arcsine transformed, and analysis of variance was performed for each exposure time to test the null hypothesis that the means of the three treatments were equal. For those exposure times in which the null hypothesis was rejected, the Tukey multiple comparison test was performed to determine between which treatment means differences existed (Zar, 1984). Means and standard deviations were back transformed for report in Figure 2.

Juvenile growth and survival experiments

Unless otherwise noted, the term "juvenile" is used in this paper to refer to those oysters 144 h post settlement or less. Oyster pediveliger larvae were allowed to settle on conditioned oyster shells for 2 h just prior to commencement of the experiments. Non-settled larvae were washed off after 2 h. One oyster shell with settled larvae was placed in each chamber, with the rough side up. Two chambers were removed daily from each treatment; they were not replaced. Twenty-five randomly selected live juvenile oysters from each of the two chambers were measured with a compound microscope and an ocular micrometer. Growth was measured as the amount of new shell in the dorsal-ventral axis (height). Mortality was recorded as the proportion of dead juveniles among 50 randomly selected juveniles from each chamber. The data from the two chambers were pooled as one replicate for that exposure/post settlement time. The entire juvenile growth and survival experiment was repeated four times, resulting in four replicates of normoxic treatments, and three replicates each of hypoxic and anoxic treatments.

Growth data were log transformed, and the residuals were examined for homoscedasticity. Analysis of variance was performed to test significance and linearity of the growth regressions. Student's t test was used to determine differences between the normoxic and hypoxic growth regression coefficients and regression elevations (Zar, 1984).

Survival data for juvenile oysters were arcsine transformed. Analysis of variance was performed for each exposure/post settlement time to test the null hypothesis that the means of the three treatments were equal. For those exposure/post settlement times in which the null hypothesis was rejected, the Tukey multiple comparison test was performed to determine between which treatment means differences existed (Zar, 1984). Means and standard deviations were back transformed for report in Figure 4.

Results

Larval settlement

In normoxic treatments at 24 h, the mean settlement of oyster larvae was 38% (Fig. 2). The percentage of settled larvae increased 10–20% per day, and was 79% at 96 h. In the hypoxic treatments, settlement was 18% at 24 h

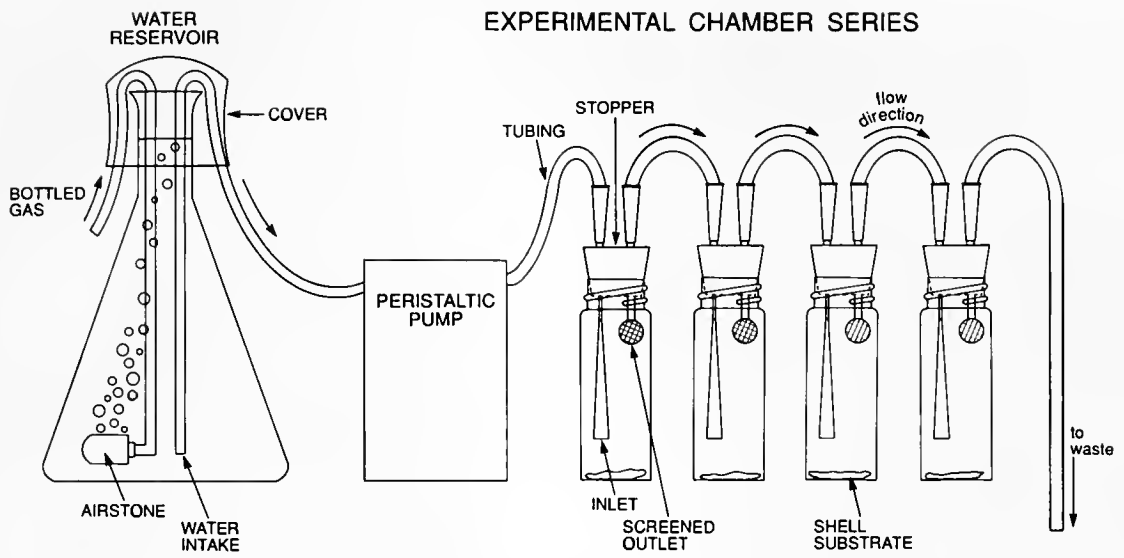

Figure 1. The experimental apparatus. Four chambers of one treatment are shown. Flasks of seawater were bubbled with air, a mix of oxygen and nitrogen, or nitrogen. The equilibrated seawater was pumped through chambers containing settlement substrate and pediveliger larvae or juveniles of the oyster *Crassostrea virginica*. Flow-through chambers were immersed in a circulating water bath of 25°C. (Not drawn to scale.)

and 38% at 48 h. After 48 h, hypoxic treatments had no further settlement. In anoxic treatments, settlement was 4% at 24 h, with no subsequent settlement. At 24 h, anoxic and normoxic treatment means were significantly different ($P < 0.05$), and at 48 h, the anoxic treatment mean was significantly different ($P < 0.05$) from both the hypoxic and normoxic treatment means. At 72 and 96 h, all three treatment means were significantly different ($P < 0.05$) from each other.

Juvenile growth

Regressions of log transformed juvenile oyster growth data from normoxic and hypoxic treatments were linear and significant. The regression coefficients of the normoxic and hypoxic treatments were not significantly different; however, the regression elevations were significantly different ($P < 0.05$) from each other (Fig. 3). Juveniles in the normoxic treatments grew over 255 μm of new shell

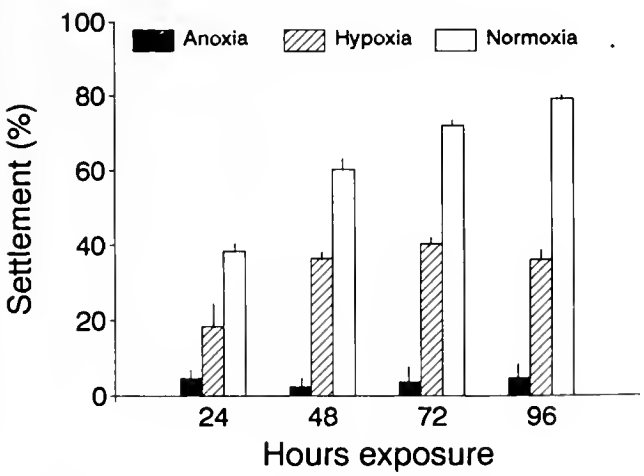

Figure 2. Relation between percentage settlement of oyster (*Crassostrea virginica*) pediveliger larvae and duration of normoxic (7.3 mg O_2 l^{-1}), hypoxic (1.5 mg O_2 l^{-1}), and anoxic (<0.07 mg O_2 l^{-1}) treatments. (Means + SD; normoxia n = 5; hypoxia n = 3; anoxia n = 3.)

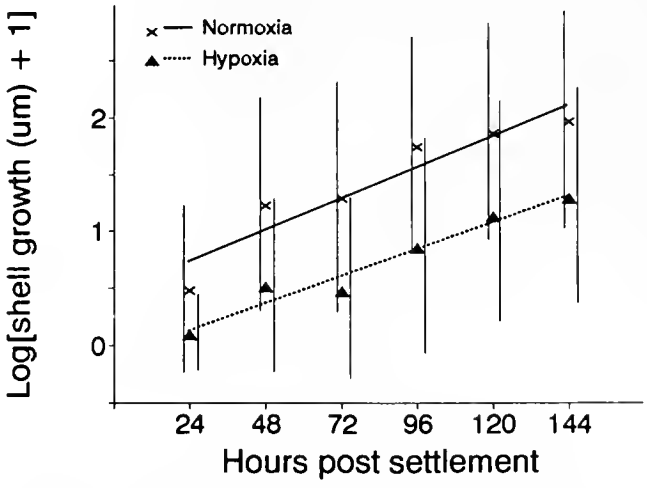

Figure 3. Log of growth of *Crassostrea virginica* juveniles (initial shell height 290 μm) in normoxic (7.3 mg O_2 l^{-1}), hypoxic (1.5 mg O_2 l^{-1}), and anoxic (<0.07 mg O_2 l^{-1}) treatments in relation to hours post settlement. (Means ± SD; normoxia n = 175 for each mean marker; hypoxia n = 125 for each mean marker.)

in 144 h, nearly doubling in length. Juveniles in hypoxic treatments grew only 77 μm of new shell in 144 h, approximately one third as much as those in normoxic treatments. Juveniles in anoxic treatments did not increase in shell height.

Juvenile survival

Juvenile oyster survival was similar in all three treatments for the first 72 h (Fig. 4). At 96 h and 120 h, the anoxic treatment mean was significantly different ($P < 0.05$) from both hypoxic and normoxic treatment means. All three treatment means were significantly different ($P < 0.05$) from each other at 144 h. Juveniles in the anoxic treatments had a median mortality time (time to 50% mortality) of 84 h. Mortality of juveniles in anoxic treatments was 100% by 144 h. Juveniles in the hypoxic treatments had a median mortality time of 131 h. Normoxic treatments, in contrast, had a mean of only 13% mortality at 144 h.

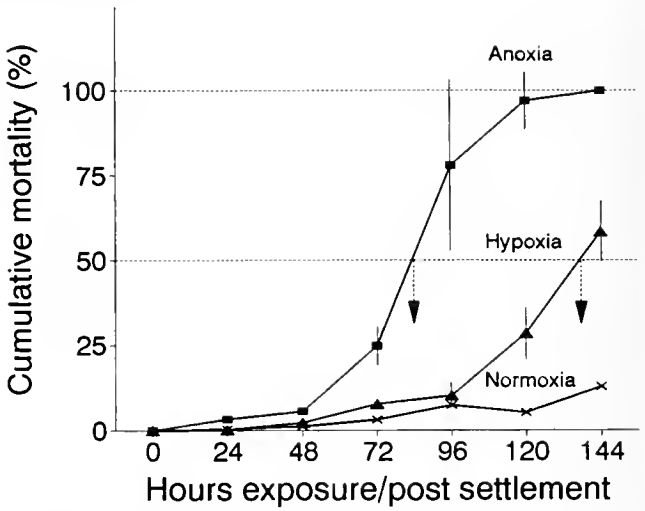

Figure 4. Relation between cumulative mortality of *Crassostrea virginica* juveniles and duration of normoxic (7.3 mg O_2 l^{-1}), hypoxic (1.5 mg O_2 l^{-1}), and anoxic (<0.07 mg O_2 l^{-1}) treatments. Arrows indicate median mortality times. Where no standard deviation is shown, the standard deviation is smaller than the mean marker. (Means ± SD; normoxia n = 4; hypoxia n = 3; anoxia n = 3)

Discussion

Under hypoxic and anoxic conditions, oyster pediveliger larvae significantly reduce energetically costly activities, thereby reducing total metabolism and oxygen requirements (Widdows *et al.*, 1989). The results of this study indicate that settlement is another costly activity that oyster pediveliger larvae avoid when in oxygen-limiting environments.

In a recent paper on the effects of hypoxia and anoxia on *Mytilus edulis* larvae, Wang and Widdows (1991) report that moderate hypoxia has little effect on larval settlement. Settlement of mussel pediveliger larvae onto adult byssus filaments is approximately 12% after two days in conditions of 8.2 mg O_2 l^{-1} (20.0 kPa pO_2, 98% of air saturation at 15°C and 31‰), 2.4 mg O_2 l^{-1} (5.91 kPa pO_2, 29% of air saturation), or 1.3 mg O_2 l^{-1} (3.16 kPa pO_2, 15% of air saturation). An oxygen concentration of 0.6 mg O_2 l^{-1} (1.38 kPa pO_2, 7% of air saturation) shows 1% settlement. Settlement of *C. virginica* appears to be more sensitive to moderate hypoxia than mussel settlement. While settlement of mussel larvae is unchanged in treatments of 8.2 mg O_2 l^{-1} down to 1.3 mg O_2 l^{-1} (Wang and Widdows, 1991), oyster larval settlement was significantly reduced by oxygen concentrations of 1.5 mg O_2 l^{-1} or less. The estimated oxygen concentration at which settlement after two days is 50% of that in normoxic treatments is 0.9 mg O_2 l^{-1} (10% of air saturation) for mussel larvae (Wang and Widdows, 1991) compared to 1.4 mg O_2 l^{-1} (20% of air saturation) for oyster larvae. While oysters are entirely sessile once they have settled, post larval mussels migrate repeatedly before arriving at a final settlement site (Lane *et al.*, 1985). Larval mussels, therefore, do not need to be as discriminating as oyster larvae when selecting a suitable settlement habitat.

In other aspects of their physiology, oyster larvae are less sensitive to oxygen deprivation than are mussel larvae. For example, the oxygen concentration at which the respiration rate is 50% of the normoxic rate is 2.3 mg O_2 l^{-1} (5.7 kPa pO_2, 28% of air saturation) for mussel pediveliger larvae (Wang and Widdows, 1991) and 0.9 mg O_2 l^{-1} (2.3 kPa pO_2, 11% of air saturation at 22°C and 12‰) for oyster pediveliger larvae (Widdows *et al.*, 1989). The 10°C difference in temperature at which the mussel (Wang and Widdows, 1991) and oyster (this paper) settlement experiments were performed, and the resulting differences in metabolic rates, may have contributed to the discrepancy observed in oxygen sensitivity of mussel and oyster larval settlement. At 15°C, mussel pediveliger larvae have a normoxic oxygen uptake of 75 pmol O_2 h^{-1} $larva^{-1}$ (Wang and Widdows, 1991), while at 22°C, oyster pediveliger larvae have an oxygen uptake of 400 pmol O_2 h^{-1} $larva^{-1}$ (Widdows *et al.*, 1989).

As discussed earlier, pediveliger larvae reduce energetically costly activities during hypoxic exposure, such as ingestion, digestion, and growth, thereby reducing oxygen demand. Under hypoxic conditions, there is a marked decline in the proportion of pediveliger larvae feeding and in ingestion rates (Widdows *et al.*, 1989). Mussel pediveliger larvae also exhibit depressed feeding rates and growth in hypoxic conditions (Wang and Widdows, 1991). The reduction of juvenile oyster growth in hypoxic treatments and complete lack of growth in anoxic treatments

observed in this study may have resulted from a cessation of feeding.

In this study, juvenile oysters had a median mortality time of 84 h in anoxia. This indicates that, like oyster larvae and adults, recently settled juvenile oysters are capable of anaerobic metabolism. Widdows *et al.* (1989) report median mortality times in anoxia of 11, 18, and 51 h for oyster prodissoconch, veliconch, and pediveliger larvae, and 150 h for juveniles 16 mm in shell height. The data for recently settled juveniles are consistent with the trend of increasing anoxic tolerance with developmental stage and body size. The increased median survival time in later stages is associated with an ability to reduce energy use, measured as heat dissipation, under anoxic conditions (Widdows *et al.,* 1989). The degree of heat dissipation reduction by recently settled juvenile oysters in anoxia is expected to be between that of the pediveliger larvae and 16 mm juveniles studied by Widdows *et al.* (1989).

Further studies on feeding, heat dissipation, and oxygen uptake are required to understand more clearly the effects of anoxia and hypoxia on settling pediveliger larvae and recently settled juvenile oysters. The present study does demonstrate that hypoxic and anoxic conditions have detrimental effects on larval settlement, juvenile growth, and juvenile survival. Oyster distribution may be influenced by anoxia and hypoxia, especially in those areas that experience prolonged (longer than 48 to 72 h) or severe (anoxic) pycnocline tilt events. Pycnocline tilt events may control recruitment into the adult population directly, because of larval settlement failure and juvenile mortality, and indirectly, because of a reduction in the growth rate of juveniles.

Acknowledgments

This study was supported by funds from the National Oceanic and Atmospheric Administration to RM and the International Women's Fishing Association to SMB. We thank the staff of the VIMS oyster hatchery for the provision of larvae. P. Baker, B. Barber, L. Schaffner, R. I. E. Newell, and two anonymous reviewers made helpful comments on the manuscript.

Literature Cited

Abbe, G. R. 1986. A review of some factors that limit oyster recruitment in Chesapeake Bay. *Am. Malacol. Bull., Special Edition No.* 3: 59–70.

Carter, H. H., R. J. Regier, E. W. Schiemer, and J. A. Michael. 1978. The summertime vertical distribution of dissolved oxygen at the Calvert Cliffs generating station: a physical interpretation. Chesapeake Bay Institute, The Johns Hopkins University, Special Report 60: 1–95.

Fitt, W. K., S. L. Coon, M. Walch, R. M. Weiner, R. R. Colwell, and D. B. Bonar. 1990. Settlement behavior and metamorphosis of oyster larvae (*Crassostrea gigas*) in response to bacterial supernatants. *Mar. Biol.* **106:** 389–394.

Galtsoff, P. S. 1964. The American Oyster *Crassostrea virginica* Gmelin. *Fish. Bull. Fish Wildlife Ser.* **64:** 1–480.

Lane, D. J. W., A. R. Beaumont, and J. R. Hunter. 1985. Byssus drifting and the drifting threads of the young post-larval mussel *Mytilus edulis*. *Mar. Biol.* **84:** 301–308.

Malone, T. C., W. M. Kemp, H. W. Ducklow, W. R. Boynton, J. H. Tuttle, and R. B. Jonas. 1986. Lateral variation in the production and fate of phytoplankton in a partially stratified estuary. *Mar. Ecol. Prog. Ser.* **32:** 149–160.

May, E. B. 1973. Extensive oxygen depletion in Mobile Bay, Alabama. *Limnol. Oceanogr.* **18**(3): 353–366.

Officer, C. B., R. B. Biggs, J. L. Taft, L. E. Cronin, M. A. Tyler, and W. R. Boynton. 1984. Chesapeake Bay anoxia: origin, development, and significance. *Science* **223:** 22–27.

Sanford, L. P., K. G. Sellner, and D. L. Breitburg. 1990. Covariability of dissolved oxygen with physical processes in the summertime Chesapeake Bay. *J. Mar. Res.* **48:** 567–590.

Sanford, L., K. Sellner, and M. Bundy. 1987. Moored measurements of dissolved oxygen in the Chesapeake Bay during the summer of 1987. AGU Ocean Sciences Meeting, New Orleans, LA, 1987.

Stickle, W. B., M. A. Kapper, L.-L. Liu, E. Gnaiger, and S. Y. Wang. 1989. Metabolic adaptations of several species of crustaceans and molluscs to hypoxia: tolerance and microcalorimetric studies. *Biol. Bull.* **177:** 303–312.

Taft, J. L., E. D. Hartwig, and R. Loftus. 1980. Seasonal oxygen depletion in Chesapeake Bay. *Estuaries* 3(4): 242–247.

Wang, W. X., and J. Widdows. 1991. Physiological responses of mussel larvae *Mytilus edulis* to environmental hypoxia and anoxia. *Mar. Ecol. Prog. Ser.* **70:** 223–236.

Widdows, J., R. I. E. Newell, and R. Mann. 1989. Effects of hypoxia and anoxia on survival, energy metabolism, and feeding of oyster larvae (*Crassostrea virginica,* Gmelin). *Biol. Bull.* **177:** 154–166.

Zar, J. H. 1984. *Biostatistical Analysis.* Prentice-Hall, Englewood Cliffs, New Jersey.

Reference: *Biol. Bull.* **182:** 270–277. (April, 1992)

Developmental Changes in Ionic and Osmotic Regulation in the Dungeness Crab, *Cancer magister*

A. CHRISTINE BROWN[1] AND NORA B. TERWILLIGER

Oregon Institute of Marine Biology, University of Oregon, Charleston, Oregon 97420, and Department of Biology, University of Oregon, Eugene, Oregon 97403

Abstract. The ontogeny of osmoregulation and specific ion regulation was studied in the megalopa, 1st instar juvenile, 5th instar juvenile and adult of *Cancer magister*. Hemolymph Na^+, Cl^-, K^+, Mg^{++}, and Ca^{++} concentrations and osmolality were measured after 8-h exposure to 100%, 75%, and 50% seawater at 10°C and 20°C. The ability to hyperosmotically regulate is present in the megalopa, and ontogenic changes occur in both ionic and osmotic regulation. First instar juvenile crabs, which are exposed to the greatest extremes of salinity and temperature in the field, are less able to osmoregulate than are the other three stages examined. Changes in Na^+, Cl^-, and K^+ concentrations parallel total osmolality in all four stages. Hemolymph Mg^{++} concentrations in megalopa and juveniles acclimated to 100% seawater are more than twice that of the concentration in the adult; after 8 h in 50% seawater, the megalopa and juvenile Mg^{++} concentrations decrease to the level of the strongly regulated adult Mg^{++} concentration. Ca^{++} is strongly regulated by megalopas and adult crabs exposed to reduced salinity compared to the two juvenile stages. Diminished predation pressure and high food availability are proximate factors that may outweigh short-term osmoregulatory stress encountered on the tideflats during development of the juvenile crab.

Introduction

Estuarine invertebrates vary greatly in their abilities to deal with changes in ambient salinity. The effects of environmental salinity on the internal osmolality and specific ion regulation of adult estuarine crustaceans have been investigated in numerous studies (for review, see Mantel and Farmer, 1983). Ontogeny of osmoregulation and ion regulation has been comprehensively studied in branchiopod crustaceans, especially the anostracan brine shrimp, *Artemia* (for review, see Conte, 1984). Comparable information about larval, post-larval, and juvenile decapod crustacean osmoregulation is relatively limited (Kalber, 1970; Foskett, 1977; Young, 1979; Read, 1984; Rabalais and Cameron, 1985; Charmantier *et al.*, 1988; Charmantier and Charmantier-Daures, 1991), and there are almost no data available regarding specific ion regulation during decapod crustacean development (Charmantier *et al.*, 1984a,b,c; Felder *et al.*, 1986).

The Dungeness crab, *Cancer magister*, inhabits the cold waters of the Pacific Northwest coast of North America and uses different portions of the estuarine and nearshore waters during its life cycle. Along the Oregon coast, embryos hatch from December through March (Reed, 1969; Lough, 1976). The newly hatched larvae go through five zoeal stages, all of which are planktonic in ocean waters, moving as far as 200 miles offshore. The transitional stage, an actively swimming planktonic megalopa, reenters the coastal and estuarine waters from mid April through early July (Lough, 1976). The megalopas then metamorphose into 1st instar juveniles that join the benthic community. Throughout the summer, juvenile crabs in the estuary are found in high numbers on the tideflats, while the adult crabs occur mainly in the deeper channels. Summer tidal changes in salinity and temperature, extending over a period of 6–8 h, are much greater on the tideflats than in the estuarine channels. Adults of *C. magister* do not migrate up into brackish waters for long periods as does *Callinectes sapidus*, the East and Gulf coast blue crab, but remain in the lower half of the bay, moving back and forth into nearshore waters.

Received 26 August 1991; accepted 21 January 1992.

[1] Present Address: Department of Biology, Lake Forest College, Lake Forest, IL 60045.

Previous studies on osmotic and ionic regulation in *Cancer magister* reported that adult crabs were weak hyperosmoregulators after 72–96 h exposure to dilute concentrations of seawater (Jones, 1941; Alspach, 1972; Engelhardt and Dehnel, 1973; Hunter and Rudy, 1975). These authors found that in reduced salinity, adult crabs were able to strongly hyporegulate magnesium and hyperregulate calcium. Hemolymph sodium, chloride, and potassium were hyperregulated but not as strongly as calcium. None of these studies examined the responses of larval, megalopa, or juvenile *C. magister* to changes in salinity.

In this paper, we ask how adults of *C. magister* respond osmotically to ecologically relevant short term tidal cycle changes in salinity. We also investigate whether the adult osmotic response pattern is present in the megalopa and juvenile stages or whether there is an ontogeny of osmotic regulatory abilities. Finally, we compare specific ion regulation during these life stages to see whether regulatory abilities for individual ions occur differentially during ontogeny.

Materials and Methods

Animals

Megalopas of *Cancer magister* (Dana) were collected with a dip net from the surface waters of Coos Bay, Oregon, from April through June of 1989. Because the megalopas molt within 48–72 h after collection, they were used in experiments within two days. In the laboratory, megalopas were kept in glass and wood aquaria (10 gallons) with running aerated seawater pumped on an incoming tide from near the mouth of Coos Bay. Salinity was 30–33‰, and water temperature was 10–12°C. Megalopas were not fed.

Juvenile crabs were raised from field-caught megalopas and were maintained in similar aquaria with running seawater and aeration. Adult males of *C. magister,* collected from the Coos Bay channel using crab pots, were kept in large holding tanks (260 gallons) with running seawater and aeration at the same temperature and salinity as megalopas and juveniles. Both juveniles and adults were fed 3–5 times a week on mussels, fish, and squid. Feeding was stopped 24 h prior to experiments to ensure a post-absorptive state in the crabs and to avoid their fouling the experimental chamber.

Protocol and sampling

Experiments were run on intermolt animals with juvenile intermolt stage based on time elapsed since the preceding molt. Thus, intermolt 1st instar juveniles were available in April–June, 5th instar juveniles in September–November, and adults in December–February.

Megalopas (approx. 3 mm carapace width), 1st instar juveniles (6–8 mm carapace width), 5th instar juveniles (25–33 mm carapace width), and adults (larger than 120 mm carapace width) were exposed to test conditions at varied temperatures and salinities for a period of 8 h. Hemolymph samples were taken immediately thereafter for osmotic and ionic analyses. Test conditions included 100% seawater (32‰, obtained on an incoming tide at the mouth of Coos Bay), 75% seawater, and 50% seawater (Coos Bay seawater diluted with glass distilled water) maintained at both 10°C and 20°C. Glass aquaria (one gallon) were used for the experimental chambers. About 250 megalopas or 1st instar juveniles and 2 or 3 5th instar juveniles were placed in each aquarium. Adults were kept one to an aquarium for the duration of the experiments.

Hemolymph was taken from the megalopas by puncturing the heart with a glass micro-capillary pipette. Juveniles and adults were bled by puncturing the arthrodial membrane at the base of a walking leg; 1st instar juveniles were bled with micro-capillary pipettes, 5th instar juveniles and adults were bled with needle and syringe. Hemolymph obtained from all individuals in each experimental aquarium was pooled in order to collect a single sample of sufficient volume for both osmotic and ionic analyses. In figure legends 1–6, n refers to the number of separate pooled samples on which analyses were performed (megalopa, n = 1–3; 1st and 5th instar juveniles, n = 2–3; adult, n = 8). Seawater samples from each aquarium were collected. Samples were immediately frozen and stored at −73°C for subsequent osmotic and ionic analyses.

Osmotic and ionic analyses

Osmolality of seawater and hemolymph samples was measured using a Wescor 5500 vapor pressure osmometer. Chloride concentration was measured using a Buchler-Cotlove chloridometer. Magnesium concentration was measured colorimetrically after the method of Sky-Peck (1964). That is, samples were deproteinized with 5% trichloroacetic acid and reacted with thiazole yellow in the presence of excess base. The absorbance at 540 nm was measured with a Beckman DU-70 spectrophotometer. Sodium, calcium, and potassium ion activities were measured with a Radiometer Ion 83 ion meter in mV mode and the following electrodes: Radiometer G502 sodium Selectrode, Microelectrodes Inc. MI-420 sodium microelectrode, Radiometer F2112 calcium Selectrode, and Orion 90-19 potassium electrode. The reference electrode in all cases was an Orion 90-02 double junction reference electrode with an NH_4Cl outer chamber filling solution and a AgCl saturated inner chamber filling solution. Samples were diluted 1:100 in the appropriate ionic strength adjustment solution. Prior to the analysis of samples, cal-

ibration for measurement of each ion species was done with salt solutions of known concentration spanning the expected range of values.

Data analysis

Results are expressed as mean ± S.E. (n = number of observations). Three-way analysis of variance (ANOVA) was used to test for significance among treatments (developmental stage, salinity, and temperature). Subsequent multiple comparisons of means were performed using the Tukey-Kramer method. Statistical significance was accepted at $P < 0.05$.

Results

Estuarine salinity and temperature were measured in areas where the different developmental stages of *C. magister* were abundant in order to set limits for these parameters in laboratory studies. The tideflat environment of juveniles ranges from 10°C at high tide to 25°C when the tide has receded and tideflats are exposed during early- to mid-morning low tides in summer. At the same time, salinity drops from 32 to 16‰ as the freshwater lens on the surface passes down the flats. In the channels where adults are found, summer water temperature (10–15°C) and salinity (32–20‰) are much more stable. Winter water temperature is consistently low (10–12°C). Winter range of salinity (32–16‰) at depth in the estuary varies as widely as salinity on the summer tideflats owing to the increased fresh water input from rain.

Osmoregulation

After 8-h exposure to 100% seawater, the megalopa, 1st instar juvenile, 5th instar juvenile, and adult are isosmotic with the ambient seawater (Fig. 1). In 75% seawater, the hemolymph osmolalities of all four stages are significantly lower than in 100% seawater, yet they are all hyperosmotic relative to 75% seawater. In 50% seawater, the hemolymph osmolalities of all four stages are significantly lower than in 75% seawater, and all are significantly hyperosmotic compared with 50% seawater. The 1st juvenile is least able to maintain hemolymph osmolality in dilute seawater compared to the other stages examined. The crabs are less able to osmoregulate in warmer water. Hemolymph osmolalities of the adult and 5th instar juvenile are significantly lower at 20°C than at 10°C in both 75% and 50% seawater; megalopa hemolymph osmolality is also lower at 20°C than at 10°C in 50% seawater.

Ionic regulation

The hemolymph chloride concentration in all four stages in 100% seawater is hypoionic compared with ambient seawater (Fig. 2). In 75% seawater the adult becomes

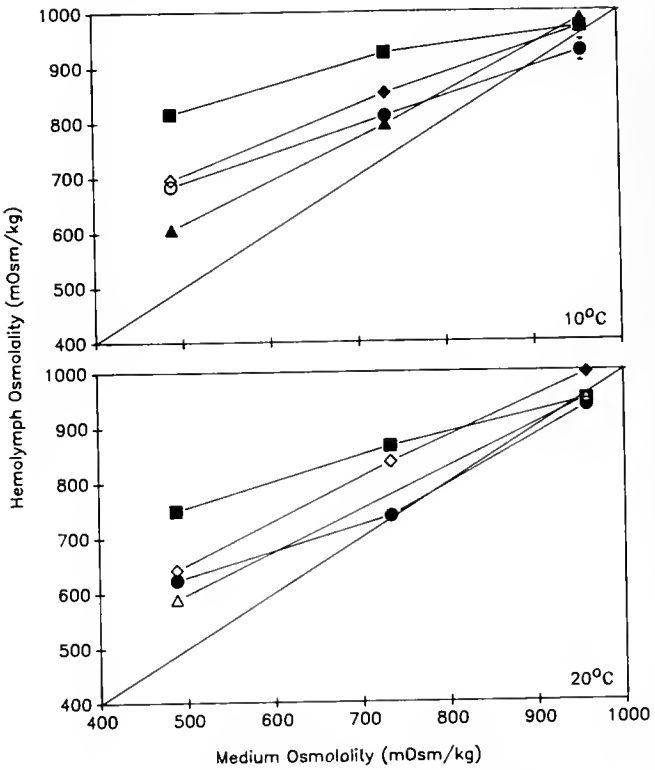

Figure 1. Hemolymph osmolality of *Cancer magister* as a function of medium osmolality for ♦, megalopa (n = 1–3); ▲, 1st instar juvenile (n = 2–3); ●, 5th instar juvenile (n = 2–3); ■, adult (n = 8). Solid symbols, n > 2, standard error bars drawn; open symbols, n ≤ 2, mean.

nearly isoionic compared with the seawater and has significantly lower hemolymph chloride concentration at 20°C than at 10°C. In 50% seawater the adult hemolymph chloride concentration is hyperionic and is lower at 20°C than at 10°C. The hemolymph chloride concentrations of the megalopa and of the 5th instar juvenile are also temperature sensitive in 75% seawater. In 50% seawater the megalopa and 1st instar juvenile hemolymph chloride concentrations are the same as the ambient seawater chloride, while that of the 5th instar juvenile is significantly higher than that of the megalopa and 1st instar juvenile and lower than that of the adult.

Hemolymph sodium ion activity (Fig. 3) in all four stages shows essentially the same pattern as hemolymph chloride. In 100% seawater all four stages are hypoionic with respect to ambient seawater sodium. In 75% seawater the megalopa, 1st instar juvenile, and 5th instar juvenile hemolymph sodium ion activities are significantly less than in 100% seawater, while the adult hemolymph sodium ion activity is not significantly changed. In 50% seawater the megalopa and 1st instar juvenile hemolymphs are isoionic to ambient sodium, whereas the 5th instar juvenile hemolymph sodium is intermediate between the younger stages and the adult. There is no significant effect

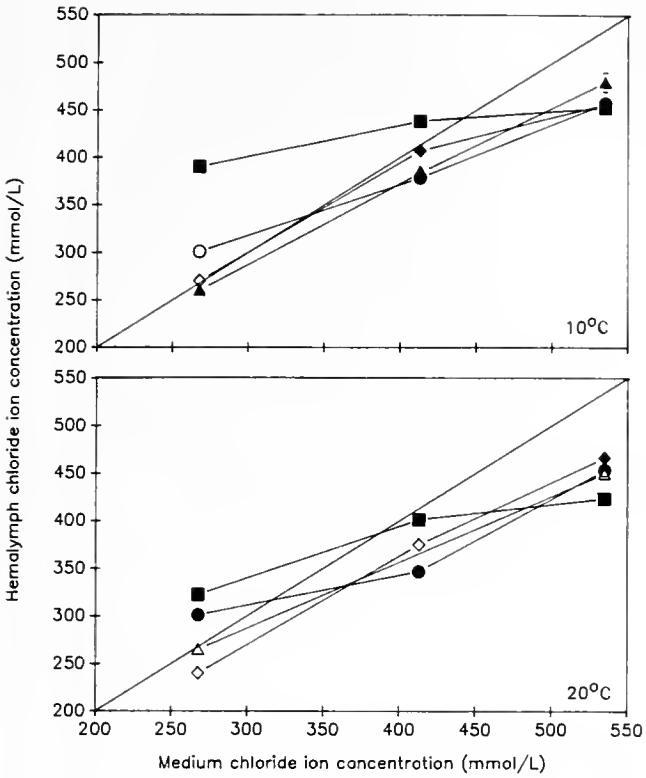

Figure 2. Hemolymph chloride ion concentration of *Cancer magister* as a function of medium chloride ion concentration for ♦, megalopa (n = 1–3); ▲, 1st instar juvenile (n = 2–3); ●, 5th instar juvenile (n = 2–3); ■, adult (n = 8). Solid symbols, n > 2, standard error bars drawn; open symbols, n ≤ 2, mean.

of temperature on the hemolymph sodium ion activity in any of the stages.

There is no significant effect of temperature on hemolymph potassium ion activity (Fig. 4). The megalopa shows no significant change in hemolymph potassium ion activity. The adult, 1st instar juvenile, and 5th instar juvenile hemolymph potassium ion activities, however, are significantly less in 75% and 50% seawater than in 100% seawater.

In contrast to the concentrations of chloride, sodium, and potassium, that of magnesium is strongly hyporegulated in adult hemolymph in all salinity treatments (Fig. 5). In 100% seawater the megalopa, 1st instar juvenile, and 5th instar juvenile hemolymph magnesium concentrations are significantly higher than the adult. As salinity decreases, magnesium concentration in these three stages also decreases until, in 50% seawater, there is no difference in the hemolymph magnesium concentration among all four stages. The only stage in which magnesium regulation shows a significant temperature sensitivity is the 5th instar juvenile in 100% seawater.

In 100% seawater the hemolymph calcium ion activities in all four stages are not significantly different from the ambient seawater calcium ion activity (Fig. 6). The hemolymph calcium ion activities of the megalopa and adult do not change significantly with salinity. The 1st instar juvenile and 5th instar juvenile, however, have significantly lower hemolymph calcium ion activities in 75% and 50% seawater than in 100% seawater. Overall there is no significant effect of temperature on hemolymph calcium ion activity.

Discussion

Different developmental stages in the life cycle of *Cancer magister* have distinctly different patterns of hemolymph osmotic and ionic regulation when exposed to reduced salinity. The values for hemolymph osmolality and ionic concentrations in the present study were obtained after an 8-h exposure time, the duration of a tidal cycle, which is physiologically and ecologically relevant for these crabs. Furthermore, the general trends for osmotic and ionic regulation reported in the long-term 72–96 h equilibrium exposures (Jones, 1941; Alspach, 1972; Engelhardt and Dehnel, 1973; Hunter and Rudy, 1975) are apparent after the 8-h exposure time used here. We find, just as the

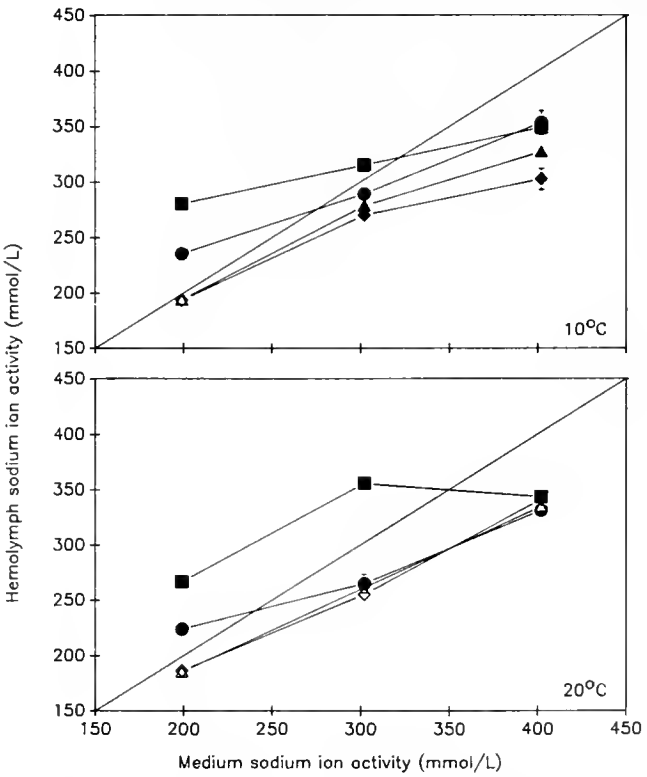

Figure 3. Hemolymph sodium ion activity of *Cancer magister* as a function of medium sodium ion activity for ♦, megalopa (n = 1–3); ▲, 1st instar juvenile (n = 2–3); ●, 5th instar juvenile (n = 2–3); ■, adult, (n = 8). Solid symbols, n > 2, standard error bars drawn; open symbols, n ≤ 2, mean.

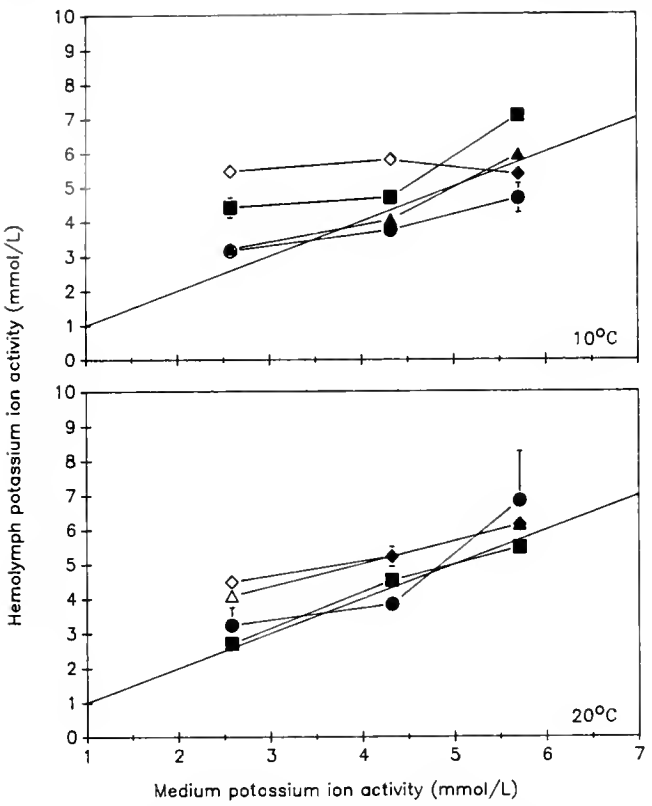

Figure 4. Hemolymph potassium ion activity of *Cancer magister* as a function of medium potassium ion activity for ♦, megalopa (n = 1–3); ▲, 1st instar juvenile (n = 2–3); ●, 5th instar juvenile (n = 2–3); ■, adult (n = 8). Solid symbols, n > 2, standard error bars drawn; open symbols, n ≤ 2, mean.

earlier equilibrium studies reported, that the hemolymph of adult *C. magister* is weakly hyperosmoregulated in water less concentrated than normal ocean seawater; chloride, sodium, and potassium are somewhat hyperregulated in reduced salinity, magnesium is very strongly hyporegulated and calcium is strongly hyperregulated. Compared with adults of four other species within the genus *Cancer* for which data are available (see Charmantier and Charmantier-Daures, 1991, for review), *C. magister* adults are the strongest osmoregulators. For example, *Cancer antennarius* has a hemolymph osmolality only 15 mOsm/kg above ambient seawater osmolality in approximately 53% seawater at 15–20°C (Jones, 1941) compared with *C. magister* hemolymph osmolality of 250 mOsm/kg above ambient seawater in 50% seawater at 20°C.

Ontogeny of osmoregulation

Studies on the larvae, post-larvae, and juveniles of a number of decapod crustacean species indicate that most larvae and post-larvae can maintain hemolymph osmolality above that of ambient seawater, either by hyperosmoconforming or by weakly hyperosmoregulating (see Charmantier *et al.*, 1988). In such cases, metamorphosis often marks a profound change in osmoregulation from larval to adult patterns. Many decapods that are hyperosmoconforming or weakly hyperosmoregulating over a wide range of salinities in the premetamorphic stages undergo a change to become either (a) strongly hyperosmoregulating in low salinity and osmoconforming in high salinity in the adult, as in *Clibanarius vittatus, Homarus gammarus, Homarus americanus,* and *Cancer irroratus* (Young, 1979; Thuet *et al.*, 1988; Charmantier *et al.*, 1988; Charmantier and Charmantier-Daures, 1991) or (b) hyper-hypoosmoregulating in the adult, as in *Sesarma reticulatum, Uca subcylindricum,* and *Penaeus japonicus* (Foskett, 1977; Rabalais and Cameron, 1985; Charmantier *et al.*, 1988). Less frequently described are species in which the larvae have a greater osmoregulatory ability than the adult, *i.e., Hepatus epheliticus* and *Libinia emarginata,* but a switch still occurs around the time of metamorphosis (Kalber, 1970). *Macrobrachium petersi* is a case in which both larvae and adults are strong osmoregulators, but the different stages vary in their capacity to hypo or hyperosmoregulate (Read, 1984). To date the

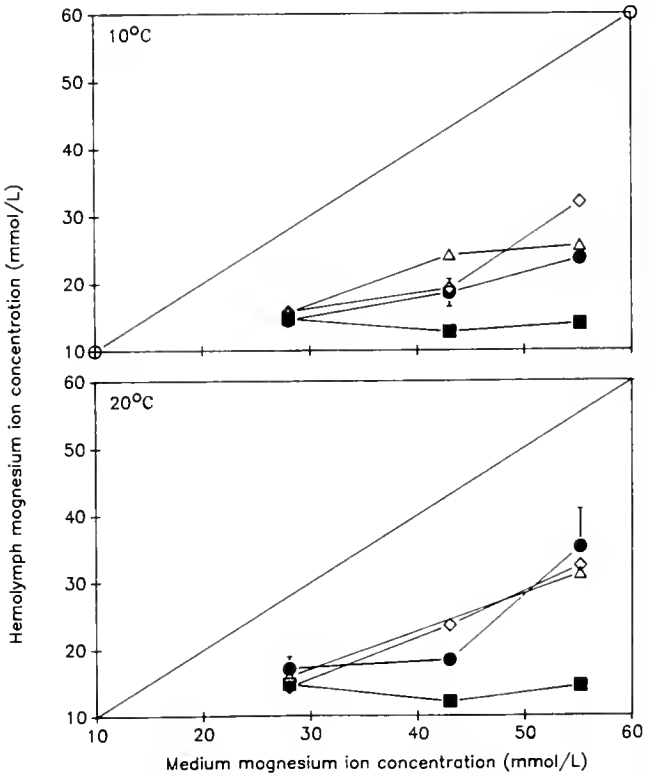

Figure 5. Hemolymph magnesium ion concentration of *Cancer magister* as a function of medium magnesium ion concentration for ♦, megalopa (n = 2); ▲, 1st instar juvenile (n = 2); ●, 5th instar juvenile (n = 2–3); ■, adult (n = 8). Solid symbols, n > 2, standard error bars drawn; open symbols, n ≤ 2, mean.

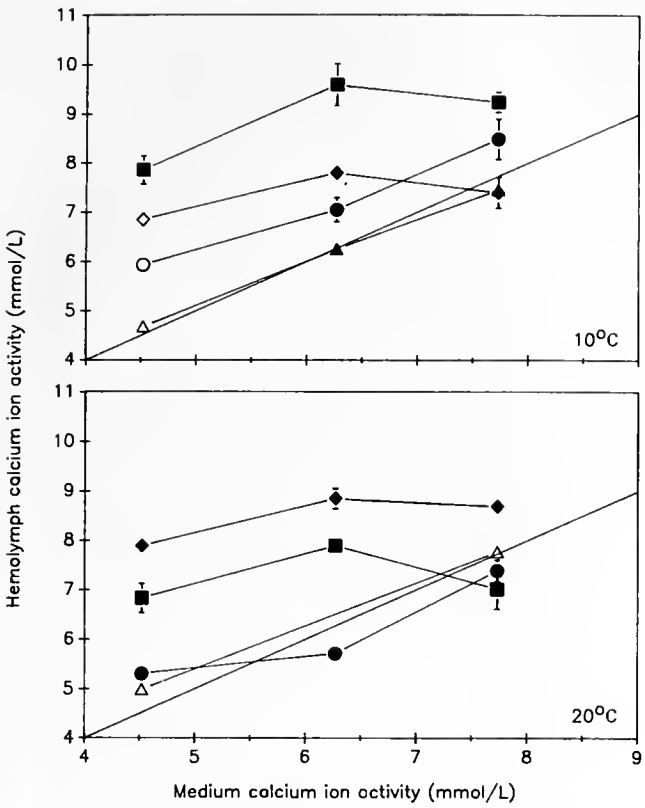

Figure 6. Hemolymph calcium ion activity of *Cancer magister* as a function of medium calcium ion activity for ♦, megalopa (n = 1–3); ▲, 1st instar juvenile (n = 2–3); ●, 5th instar juvenile (n = 2–3); ■, adult (n = 8). Solid symbols, n > 2, standard error bars drawn; open symbols, n ≤ 2, mean.

only decapod species whose osmoregulatory pattern does not change during development is *Callianassa jamaicense* var. *louisianensis*. Its larvae remain in the hyposaline burrow habitat of the adult, and all stages show limited hyperosmoregulation in dilute media, although the adult can hyperregulate a bit more strongly than the zoeae (Felder, 1978; Felder *et al.*, 1986).

In the present study, there is a marked change in osmoregulation at metamorphosis from megalopa to 1st instar juvenile in *C. magister*. Interestingly, the juvenile *C. magister* is less able to regulate over the short 8-h exposure than is the megalopa (Fig. 1). As development proceeds, however, osmoregulatory ability becomes more like that of the adult. A correlation between ontogeny of osmoregulation and changes in habitat salinity has been observed for several species (for review, see Charmantier *et al.*, 1988). This correlation does not hold as an explanation for the observed patterns of osmoregulation in the different stages of *C. magister*. The 1st instar juvenile, the stage least able to osmoregulate, is found in high numbers on the mudflats where it encounters extremes of low salinity and high temperature. Other factors, such as the short duration of exposure to these extremes and behavioral responses, must play a role in environmental distribution. Both juvenile and adult *C. magister* become inactive in low salinities. This behavior may enable the juveniles to endure the low salinity portion of the tide cycle on the mudflat without great expenditure of energy while experiencing protection from heavy predation by adult crabs and fish concentrated during low tide in the deeper channels. As the tide rises, juveniles on the mudflats are able to immediately resume active foraging; proximity to high food availability may offset the short term osmoregulatory stresses experienced during low tide.

Several factors may be responsible for the diminished ability of the 1st instar juvenile to osmoregulate. Although megalopas, 1st, and 5th instar juveniles all have gills that function in ion transport based on silver staining (Brown, unpub. obs.), there are no data available on the ratio of gill surface area to total body volume in these stages. The carapace of the 1st instar juvenile is about twice as wide as in the megalopa, and the juvenile weighs twice as much; if the gill surface area has not increased proportionately, this might explain the diminished osmoregulatory capacity of the juveniles. Also important are the efficiency of salt transport at the gill and the amount of area on the gill associated with that salt transport (see Conte, 1984). Felder *et al.* (1986) have shown differences in Na^+/K^+ ATPase activity in the different prehatch stages of *Callianassa jamaicense* var. *louisianensis* and have demonstrated the presence of salt transport type tissue on the brancheostegites of the zoeae. *Homarus gammarus* post-larvae, which have greater osmoregulatory capacities compared with larval stages, show a marked increase in gill Na^+/K^+ ATPase and carbonic anhydrase activities (Thuet *et al.*, 1988). It is possible that the juvenile stages of *C. magister* initially have lower Na^+/K^+ ATPase activity levels or a different relative proportion of salt transporting tissue than the megalopas.

Ontogeny of ion regulation

This is the first report of an ontogenic change in specific ion regulation in brachyuran crabs. The data show that specific ions are regulated differently by megalopa, juvenile, and adult *C. magister*. At metamorphosis from megalopa to 1st instar juvenile, there are shifts in specific ion regulatory patterns that do not parallel changes in hemolymph osmolality. Ion regulation in 5th instar juvenile is more like that in adult than that in 1st instar juvenile; the fifth instar juvenile is beginning to show the adult pattern of ion regulation but does not regulate to the same extent as the adult.

Hemolymph levels of sodium, chloride, and potassium parallel stage-specific changes in hemolymph osmolality as salinity decreases. Sodium and chloride are the two

main inorganic ion constituents in the hemolymph and appear to be the major components in osmotic regulation in the different developmental stages.

Two aspects of developmental changes in specific ion regulation are particularly striking. First, hemolymph magnesium concentrations in megalopas and in 1st and 5th instar juveniles in 100% seawater are twice as high as in the adult, when none of the other ions show any differences between stages in 100% seawater. Second, calcium is strongly hyperregulated in megalopa and adult hemolymph, as salinity decreases, compared to the two juvenile stages studied.

Adults of all species of crustaceans that have been examined maintain hemolymph magnesium well below the magnesium concentration of the ambient water, except when they are in extremely dilute water. Engelhardt and Dehnel (1973) stated that "hyporegulation of magnesium is the most universal feature of ionic regulation in crustacean blood." Adult *C. magister* excrete magnesium in urine formed in the antennal gland; the urine to hemolymph ratio of magnesium is nearly 4:1 in 100% seawater (Hunter and Rudy, 1975; Holliday, 1980). In the early stages of crustaceans, the antennal gland may not be fully developed and functional (Waite, 1899; Conte, 1984), and this may account for the high hemolymph magnesium in megalopa and juvenile crabs. Low hemolymph magnesium levels have often been associated with high levels of activity or a greater extent of terrestriality in crustaceans. According to Robertson (1960), decapod species with hemolymph magnesium concentrations less than 50% that of seawater are more active than those with higher hemolymph magnesium concentrations. In fact, high magnesium concentrations are often used to anaesthetize marine invertebrates. The totally aquatic *C. magister* megalopa is an extremely active animal, however, capable of swimming very rapidly for extended periods. The 1st instar juvenile, which like the megalopa has more than twice the adult's hemolymph magnesium, is also considerably more active than the adult. Gross (1964) discusses magnesium regulation at length in relation to the extent of terrestriality of various crab species. Mantel and Farmer (1983) note that grapsids and other species of semi-terrestrial and terrestrial decapods all have low hemolymph magnesium concentrations. Because all stages in the life cycle of *C. magister* are aquatic, the change from higher to lower magnesium concentration we observe during development is not related to changes in extent of terrestriality. In summary, the high magnesium in the hemolymph of the megalopa and juvenile and the developmental changes in magnesium levels are consistent with neither of these hypotheses, activity level or terrestriality.

Calcium regulation in *C. magister* adults has been previously reported (Alspach, 1972; Engelhardt and Dehnel, 1973; Hunter and Rudy, 1975). The strong regulation of calcium by the megalopa and weak regulation by the juveniles is noteworthy. The low levels of calcium in the hyposaline-exposed 1st and 5th instar juveniles may reflect their overall decreased ability to regulate ions.

In summary, tidal cycle changes in salinity and temperature have a strong effect on hemolymph osmolality and ionic concentration in megalopas, juveniles, and adults of *C. magister*. There are ontogenic changes in both ionic and osmotic regulation in *C. magister*. Calcium and magnesium regulation change markedly during development from megalopa to adult crab. Both of these ions have strong effects on the oxygen affinity and the cooperativity of hemocyanin from a variety of crustacean species (Larimer and Riggs, 1964; Miller and Van Holde, 1974; Truchot, 1975). The changes in hemolymph calcium and magnesium levels during the development of *C. magister* may be involved in modulating the oxygen-binding properties of the hemocyanin. This hypothesis is currently under investigation.

Acknowledgments

This study was supported by NSF DMB 85-11150 and DCB 89-08362 (NBT) and the Lerner-Grey Fund for Marine Research (ACB). This is Oregon Institute of Marine Biology Contribution Number 91-002.

Literature Cited

Alspach, G. S. 1972. Osmotic and ionic regulation in the Dungeness crab, *Cancer magister* Dana. Ph.D. thesis, Oregon State University, Corvallis, Oregon.

Charmantier, G., M. Charmantier-Daures, and D. E. Aikens. 1984a. Neuroendocrine control of hydromineral regulation in the American lobster *Homarus americanus* H. Milne-Edwards 1837 (Crustacea, Decapoda) 1. Juveniles. *Gen. Comp. Endocrinol.* **54:** 8–19.

Charmantier, G., M. Charmantier-Daures, and D. E. Aikens. 1984b. Neuroendocrine control of hydromineral regulation in the American lobster *Homarus americanus* H. Milne-Edwards 1837 (Crustacea, Decapoda) 2. Larval and postlarval stages. *Gen. Comp. Endocrinol.* **54:** 20–34.

Charmantier, G., P. Thuet, and M. Charmantier-Daures. 1984c. La regulation osmotique et ionique chez *Homarus gammarus* (L.) (Crustacea: Decapoda). *J. Exp. Mar. Biol. Ecol.* **76:** 191–199.

Charmantier, G., M. Charmantier-Daures, N. Bouaricha, P. Thuet, D. E. Aiken, and J.-P. Trilles. 1988. Ontogeny of osmoregulation and salinity tolerance in two decapod crustaceans: *Homarus americanus* and *Penaeus japonicus*. *Biol. Bull.* **175:** 102–110.

Charmantier, G., and M. Charmantier-Daures. 1991. Ontogeny of osmoregulation and salinity tolerance in *Cancer irroratus;* elements of comparison with *C. borealis* (Crustacea, Decapoda). *Biol. Bull.* **180:** 125–134.

Conte, F. P. 1984. Structure and function of the crustacean larval salt gland. *Int. Rev. Cytol.* **91:** 45–106.

Engelhardt, F. R., and P. A. Dehnel. 1973. Ionic regulation in the Pacific edible crab, *Cancer magister* (Dana). *Can. J. Zool.* **51:** 735–743.

Felder, D. L. 1978. Osmotic and ionic regulation in several western Atlantic Callianassidae (Crustacea, Decapoda, Thalassinidae). *Biol. Bull.* **154:** 409–429.

Felder, J. M., D. L. Felder, and S. C. Hand. 1986. Ontogeny of osmoregulation in the estuarine ghost shrimp *Callianassa jamaicense* var. *louisianensis* Schmitt (Decapoda, Thalassinidea). *J. Exp. Mar. Biol. Ecol.* **99:** 91–105.

Foskett, J. K. 1977. Osmoregulation in the larvae and adults of the grapsid crab *Sesarma reticulatum* Say. *Biol. Bull.* **153:** 505–526.

Gross, W. J. 1964. Trends in water and salt regulation among aquatic and amphibious crabs. *Biol. Bull.* **127:** 447–466.

Holliday, C. W. 1980. Magnesium transport by the urinary bladder of the crab, *Cancer magister*. *J. Exp. Biol.* **85:** 187–201.

Hunter, K. C., and P. P. Rudy, Jr. 1975. Osmotic and ionic regulation in the Dungeness crab, *Cancer magister* Dana. *Comp. Biochem. Physiol.* **51A:** 439–447.

Jones, L. L. 1941. Osmotic regulation in several crabs of the Pacific coast of North America. *J. Cell. Comp. Physiol.* **18:** 79–91.

Kalber, F. A. 1970. Osmoregulation in decapod larvae as a consideration in culture techniques. *Helgol. Wiss. Meeresunters.* **20:** 697–706.

Larimer, J. L., and A. F. Riggs. 1964. Properties of hemocyanins. I. The effects of calcium ions on the oxygen equilibrium of crayfish hemocyanin. *Comp. Biochem. Physiol.* **13:** 35–46.

Lough, R. G. 1976. Larval dynamics of the Dungeness crab, *Cancer magister,* off the central Oregon coast, 1970–1971. *Fish. Bull.* **74:** 353–375.

Mantel, L. H., and L. L. Farmer. 1983. Osmotic and ionic regulation. Pp. 53–161 in *The Biology of Crustacea, vol. 5, Internal Anatomy and Physiological Regulation,* L. H. Mantel, ed. Academic Press, New York, London.

Miller, K. I., and K. E. Van Holde. 1974. Oxygen binding in *Callianassa californiensis* hemocyanin. *Biochemistry* **13:** 1668–1674.

Rabalais, N. N., and J. N. Cameron. 1985. The effects of factors important in semi-arid environments on the early development of *Uca subcylindrica*. *Biol. Bull.* **168:** 147–160.

Read, G. H. L. 1984. Intraspecific variation in the osmoregulatory capacity of larval, post larval, juvenile and adult *Macrobrachium petersi* (Hilgendorf). *Comp. Biochem. Physiol.* **78A:** 501–506.

Reed, P. H. 1969. Culture methods and effects of temperature and salinity on survival and growth of Dungeness crab (*Cancer magister*) larvae in the laboratory. *J. Fish. Res. Board Can.* **26:** 389–397.

Robertson, J. D. 1960. Osmotic and ionic regulation. Pp. 317–339 in *Physiology of Crustacea, Vol. 1,* T. H. Waterman, ed. Academic Press, New York.

Sky-Peck, H. H. 1964. Determination of magnesium in serum and urine. *Clin. Chem.* **10:** 391–398.

Thuet, P., M. Charmantier-Daures, and G. Charmantier. 1988. Relation entre osmoregulation et activites d'ATPase Na^+–K^+ et d'anhydrase carbonique chez larves et postlarves de *Homarus gammarus* (L.) (Crustacea: Decapoda). *J. Exp. Mar. Biol. Ecol.* **115:** 249–261.

Truchot, J.-P. 1975. Factors controlling the *in vitro* and *in vivo* oxygen affinity of the hemocyanin in the crab *Carcinus maenas* (L.). *Respir. Physiol.* **24:** 173–189.

Waite, F. C. 1899. The structure and development of the antennal glands in *Homarus americanus* Milne-Edwards. *Bull. Mus. Comp. Zool. Harv.* **35:** 151–210 and plates.

Young, A. M. 1979. Osmoregulation in larvae of the striped hermit crab *Clibanarius vittatus* (Bosc) (Decapoda: Anomura; Diogenidae). *Estuarine Coastal Mar. Sci.* **9:** 595–601.

Reference: *Biol. Bull.* **182**: 278–287. (April, 1992)

Visual Rhythms in Stomatopod Crustaceans Observed in the Pseudopupil

THOMAS W. CRONIN

Department of Biological Sciences, University of Maryland Baltimore County, Baltimore, Maryland 21228

Abstract. Many aspects of visual function in animals are influenced by the operation of endogenous rhythms. Using techniques of intracellular optical physiology, I investigated visual rhythms in two species of stomatopod crustaceans (mantis shrimps): *Squilla empusa*, a species active throughout the day and night, and *Gonodactylus oerstedii*, which is strictly diurnal. Reflectance from within the deep pseudopupil of the compound eyes and its change upon stimulation with light were monitored in individual animals in constant conditions for up to two weeks. Both species expressed circadian rhythms in visual function. In *S. empusa*, the pupillary response was much stronger during subjective night; little or no response could be elicited during subjective day. In this species, an endogenous rhythm caused pupillary reflectance to increase during subjective day. Rhythms in *G. oerstedii* were of lower amplitude than in *S. empusa* and were more difficult to detect. The differences between these species, together with the results of other comparative research on visual rhythms in arthropods, suggest that circadian, rhythmic processes are involved in optimizing nocturnal eyes for maximum sensitivity and dynamic range.

Introduction

Endogenous rhythms in visual function are common among animals. Diverse rhythmic phenomena associated with vision occur in both vertebrate and invertebrate species. For example, in the vertebrates, events known to be under endogenous control include photoreceptor membrane shedding (LaVail, 1976), retinomotor movements (reviewed in Levinson and Burnside, 1981; Burnside and Nagle, 1983), and synthesis of mRNA coding for opsin (Korenbrot and Fernald, 1989). Invertebrate visual systems also express rhythmicity in membrane shedding (Nässel and Waterman, 1979; Horridge *et al.*, 1981; Williams, 1982) or preparation for shedding (Chamberlain and Barlow, 1984). Visual rhythms apparently unique to invertebrates include cyclic changes in ERG amplitude (*e.g.*, Aréchiga and Wiersma, 1969; Page and Larimer, 1975; Barlow, 1983; Fleissner and Fleissner, 1985), in rates of action potential production (Jacklet, 1969), and, particularly in arthropods, migration of screening pigment in secondary pigment cells (Welsh, 1930; Kleinholz, 1937; Page and Larimer, 1975; see reviews of Stavenga, 1979, and Autrum, 1981).

In many cases, circadian changes in sensitivity are due primarily to variations in the quantum catch by the photoreceptor cells, produced by alterations either in associated structures such as secondary pigment cells or in the amount of photoreceptor membrane per cell. But in some species, the actual photoreceptor cells can undergo rhythmic changes that affect their ability to respond to the capture of a photon by rhodopsin. For example, in *Limulus polyphemus*, circadian events alter electrophysiological properties of individual photoreceptor cells (Kaplan and Barlow, 1980; Barlow *et al.*, 1987; Kass and Renninger, 1988).

The photoreceptor cells of many arthropod species are independently capable of adjusting their sensitivity to light by mobilizing granules of primary pigment, producing a phenomenon known as the pupillary response (Kirschfeld and Franceschini, 1969; see review of Stavenga, 1979). Arthropod pupillary responses may be observed noninvasively by monitoring light reflected from the deep pseudopupil of the compound eye (Stavenga and Kuiper, 1977; Bernard and Stavenga, 1979; Cronin, 1989); as the pigment granules migrate inwards in response to photic stimulation, reflectance rises. Circadian changes in pseudopupillary appearance and level of reflectance have been

Received 24 October 1991; accepted 13 January 1992.

observed in many arthropod compound eyes (Stavenga, 1977; see review of Stavenga, 1979). The rhythms are apparently due to circadian events in secondary pigment cells, under nervous (Page and Larimer, 1975) or neuroendocrine (Smith, 1948; Page and Larimer, 1975; Hernández-Falcón *et al.*, 1987) control. True pupillary responses, however, are caused by translocations of primary pigments, within the actual photoreceptor cells, in direct response to photic stimulation (Stavenga, 1979). Do these responses also express circadian rhythms? If so, the eyes may be optimized for sensitivity and dynamic range at a particular phase of the diel cycle, under rhythmic control.

In earlier work with the squilloid stomatopod crustacean *Squilla empusa,* I found that it was difficult or impossible to elicit any changes in reflection from the deep pseudopupil during the day, whereas nocturnal stimulation produced large, highly repeatable reflectance increases (Cronin, 1989). In contrast, the gonodactyloid stomatopod species *Gonodactylus oerstedii* and *Pseudosquilla ciliata* expressed pupillary responses no matter when they were stimulated. In this report, I describe experiments testing whether there is a rhythmic component to pupillary function in *S. empusa* and *G. oerstedii.* The results suggest that rhythmic events strongly alter the pupillary responses of *S. empusa* and have a weaker influence on those of *G. oerstedii.*

Materials and Methods

Adult animals were used in all experiments. Work with *Squilla empusa* was carried out at the Duke University Marine Laboratory in Beaufort, North Carolina. Animals were collected locally and maintained either in running seawater tables exposed to indirect, natural daylight through windows along two sides of the room (ambient photoperiod experiments) or in small containers containing natural seawater placed in a chamber with a controlled light:dark cycle (reversed photoperiod experiments). Animals were fed fresh oyster and shrimp meat. Experiments with *Gonodactylus oerstedii* took place in Baltimore, using animals collected in the Florida Keys. These animals were kept in aquaria filled with artificial seawater in a 12 h:12 h light:dark cycle, and were fed frozen shrimp.

Reflectance from the deep pseudopupil was monitored using the techniques of intracellular optical physiology, described in detail in Bernard and Stavenga (1979) and Cronin (1989). Dorsal surfaces of animals were attached, using Scutan dental plastic, to a moveable platform which was then submersed in seawater. During each experiment, water in the experimental chamber (which contained about 1200 ml) was changed occasionally, at irregular times. Animals were not fed during an experiment.

Once mounted, each experimental animal was aligned so that the pseudopupil of either the dorsal or ventral half of the eye (see photographs in Cronin, 1986, and Cronin, 1989) was centered within the field of view of an incident-light, photometric microscope. The entire apparatus was housed in a dark box with a black curtain covering the front, and experiments took place in a room that was completely blacked out and isolated from external sources of light. The central region of the pseudopupil under study, which appeared to glow dully when viewed by eye, was isolated using an adjustable field diaphragm. Reflectance from the pseudopupil was monitored as described in Cronin (1989), using light of wavelengths >720 nm (Schott RG720 longpass filter, used with *Squilla*) or >800 nm (Schott RG800 longpass filter, used with *Gonodactylus*); this source of light illuminated the eye continually throughout each experiment, and by itself caused no measurable pupillary response. At 20- or 30-min intervals, a stimulating exposure automatically was provided, produced by passing light from a 150-W Xenon arc through a monochromator (Oriel 7250 with 500-nm blazed grating), counterrotating 10-cm diameter neutral density wedges, and a linear polarizing filter. All stimuli were confined to the ommatidia contributing to the pseudopupil under study, and were at a wavelength of 500 nm (half bandwidth of 10 nm). They were produced by opening a Uniblitz electromagnetic shutter under the control of a microcomputer, and lasted for 5 min (*Squilla empusa*) or 30 s (*Gonodactylus oerstedii*). Measurements of light reflected from the pseudopupil commenced before each exposure and continued until well afterwards, and data were stored on the microcomputer's hard disk for later analysis. The response for each stimulus was defined as the average reflectance during the final 20% of the stimulation's duration, divided by the average reflectance before stimulus onset and following a period in the dark equal to the duration of the stimulus itself (see also Cronin and King, 1989). Responses are plotted as the percentage change in reflectance relative to the average dark levels.

In some cases, the sensitivity of the pupillary response was measured by providing a series of stimulating intensities over a range of 3.5 to 3.8 density units at steps of 0.5 units. Each series was produced under microcomputer control, by rotating the neutral density wedges to a series of preprogrammed settings. The intensity of the stimulating source was measured for each experiment using a calibrated PIN-10DP/SB photodiode (United Detector Technology) placed at the position of the animal's eye.

Results

Earlier work with *Squilla empusa* had revealed that the ability of an animal to express pupillary responses apparently varied with time. Results of an experiment designed to detect rhythms in responsiveness are shown in Figure 1. The animal, a male of body length (rostrum–telson)

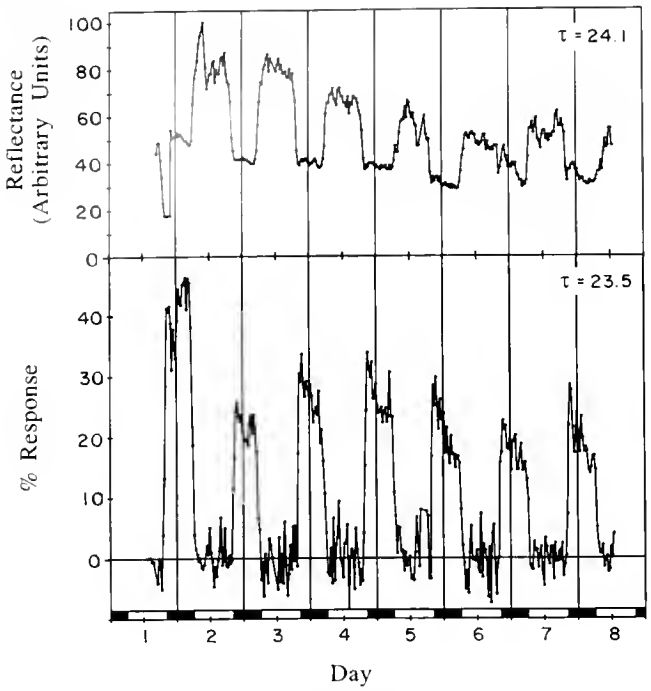

Figure 1. Light reflectance from the deep pseudopupil (Reflectance; top panel) and percentage change in reflectance on stimulation (% Response; bottom panel) in an adult male individual of *Squilla empusa* maintained in constant conditions. Measurements were made at 30-min intervals for a total of 327 intervals, from 7 to 14 July 1987. Stimuli were at 500 nm, at a quantal intensity of 2.9×10^{11} quanta cm^{-2} s^{-1}. The reflectance was measured as described in the text for 1 min before each 5-min stimulation; average values are plotted on a scale normalized to the largest value obtained. Percent response was calculated as described in the text. Vertical lines are drawn at successive midnights. The light and dark bands on the abscissa represent times of natural sunrise and sunset (Eastern Daylight Time). The period (τ) of each rhythm, in h, is given in the top right corner of its panel. Each time series was analyzed using Enright's periodogram technique (Enright, 1965). Periodogram amplitudes were computed at 0.1-h intervals for periods from 10 h to 30 h. The value given on the graph is that of the period in this 20-h range having the greatest amplitude.

85 mm, was placed in constant darkness in the apparatus at midday on the first day and stimulated each 30 min for the next 7 days.

The results of the experiment of Figure 1 are typical of those of most experiments. Rhythmical variations occurred both in the level of the pupillary response and in the reflectance from the pseudopupil in the absence of stimulation. During the subjective day, pseudopupillary reflectance remained high, and little or no measurable reflectance change occurred in response to the light stimulus—the variations that were observed were due to apparently random fluctuations. However, near the time of natural sunset, reflectance from the deep pseudopupil diminished, and large increases in reflectance occurred upon stimulation. Within 1 to 2 h, the reflectance rise during stimulation changed from near zero to greater than 20%. Concurrently, baseline pseudopupillary reflectance decreased by up to 50%. Near the time of subjective dawn, the change in reflectance during stimulation dropped once more to near zero, again over a period of 1 to 2 h, while the baseline reflectance quickly rose to its daytime level. This rhythmical pattern was typical of that expressed in animals maintained under the ambient photoperiod. The period of the rhythm was estimated using Enright's periodogram technique (Enright, 1965); both rhythms had periods near 24 h (see Fig. 1; the difference between the two periods is meaningless with time series of this length).

It is conceivable that the observed rhythms in baseline reflectance and responsiveness were expressions of a single phenomenon; the pupillary mechanism could rhythmically assume its fully light-adapted state during the day, thus increasing reflectance and losing its ability to adapt further to light. Two types of observations argue against this interpretation of the data. First, the two rhythms did not have exactly inverse forms. Baseline reflectance tended to change less abruptly than did the level of response, and on some days its changes were not precisely in phase with the changes in response level. More convincingly, some animals expressed rhythms in responsiveness with little or no circadian change in the baseline reflectance. For example, in the experiment of Figure 2, the baseline re-

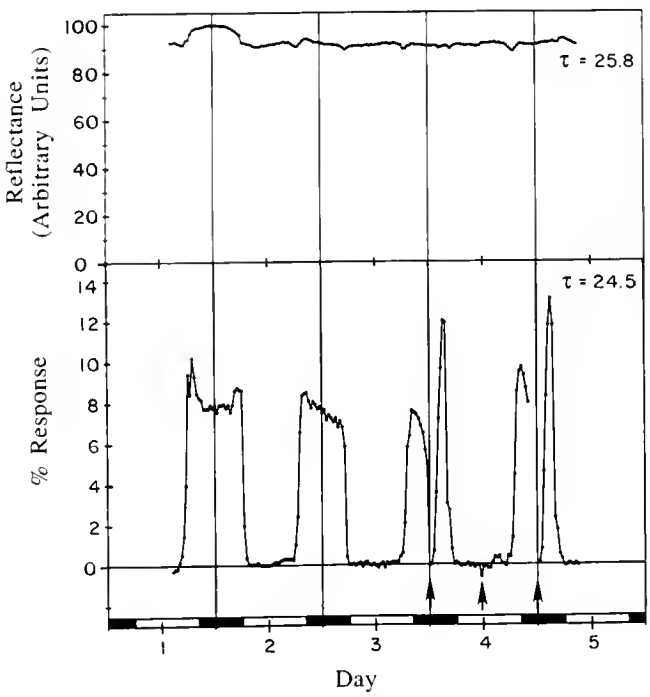

Figure 2. Results obtained from a male *Squilla empusa* maintained in constant conditions from 19 to 23 July 1987. Three series of stimuli of increasing intensities were given, at the times indicated by arrows, for determination of response-*versus*-intensity functions (see text). Except during these series, stimulation was at a quantal intensity of 1.05×10^{11} quanta cm^{-2} s^{-1}. Otherwise as in Figure 1.

flectance varied only slightly over four days. The only changes were a small increase during first dark phase and transient changes on each successive dusk and dawn. These results strongly suggest that the ability of the pupillary mechanism itself to respond to light varies rhythmically. Changes in baseline reflectance could not result from a rhythmical responsiveness to the constant 720-nm light used to monitor reflectance, for such a rhythm should produce increasing pseudopupillary reflectance at night, when responsiveness is greatest. I therefore conclude that although the two rhythms observed in Figure 1 may be intimately linked, they are expressions of separate events within the ommatidia. Once again, periodogram analysis suggests that the rhythms of Figure 2 are circadian. Periodogram analysis is particularly unreliable for time series as short as that of Figure 2, but inspection of the forms of the rhythms clearly confirms that their periods are near 24 h.

The onset of responsiveness at dusk occurs by a smooth transition (Fig. 3). Although successive responses increase in size, the time each takes to reach its plateau phase is similar. It is not primarily the rate of the response that alters, therefore, but the actual amplitude of the reflectance change. The increasing sizes of the responses during the dusk transition mimic the increasing responses that occur with increasing intensity, when the eye is maximally sensitive (Cronin, 1989). The dusk transition, therefore, appears to be a time of rapidly increasing sensitivity of the pupillary mechanism.

The rhythms of responsiveness in these experiments retained phases that appeared to be tightly linked to the external diel cycle, and there remained the possibility that external timing cues were reaching the experimental animals. This possibility was tested by placing an animal in an isolated chamber subjected to a light:dark cycle phased differently from the ambient cycle of sunrise and sunset; lights were switched on at 1800 (Eastern Daylight Time) and off at 0600 each day. Following 12 days of exposure to this "inverted" photoperiod, an animal was placed in constant conditions. Rhythms both of the pupillary response and the baseline reflectance were now observed to be in phase with the imposed cycle. Responsiveness increased, and baseline reflectance decreased, during the entrained dark period between 6 am and 6 pm. To avoid repeatedly stressing the animal by mounting it for study, its visual rhythms were not experimentally defined before imposing the reversed photoperiod. Nevertheless, this was the only case in which maximum responses were ever observed during the astronomical day, so it is reasonable to conclude that the rhythms had been entrained by the exposure to the "inverted" photoperiod. Such results also demonstrate that the rhythms observed in the earlier experiments were not in response to exogenous cues. As before, the periods of the rhythms were very near 24 h (Fig. 4).

Response-*versus*-intensity functions were obtained from the individuals studied in Figures 2 and 4 during both the subjective night and the subjective day. The

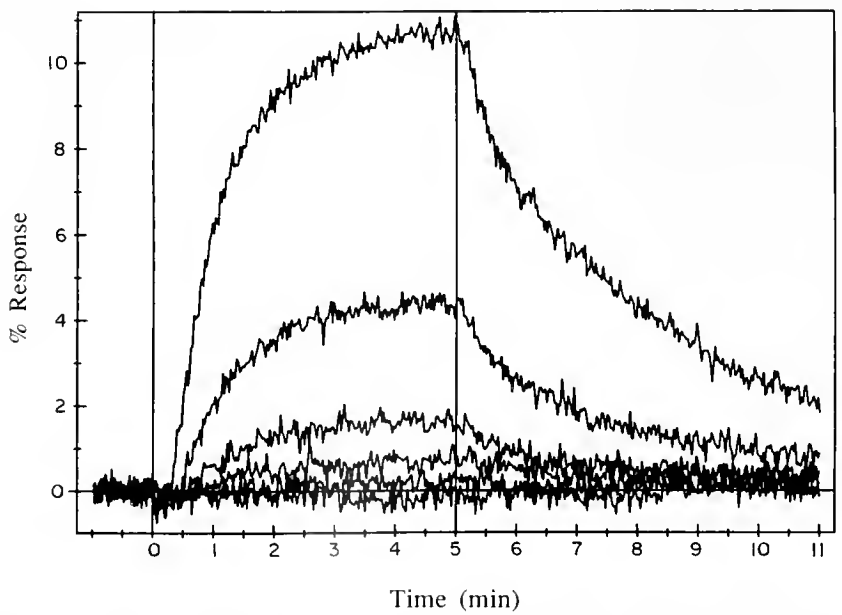

Figure 3. Changes in reflectance from the deep pseudopupil of the animal used in the experiment of Figure 2, during the onset of the nocturnal increase in responsiveness. The 6 traces were obtained at 30-min intervals, beginning at 1535 EDT (lowest trace) and ending at 1805 (highest trace) on 19 July 1987. Percent response is computed relative to the average reflectance in the 1 min prior to stimulation. Vertical lines are drawn at the beginning (0 min) and end (5 min) of the stimulation interval.

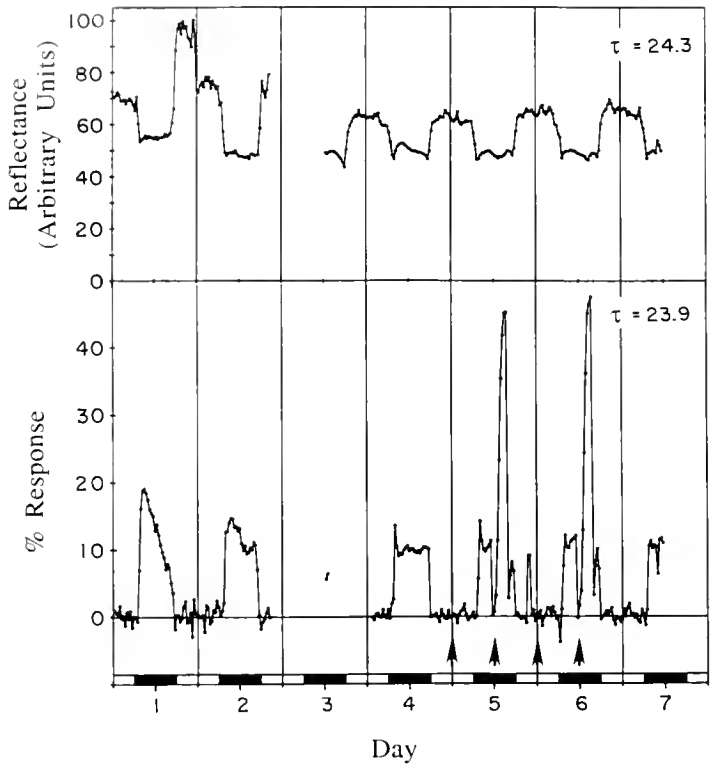

Figure 4. Results obtained from a female *Squilla empusa* maintained in constant conditions from 1 to 11 July 1988. Prior to the experiment, the animal was kept in a controlled light:dark cycle as described in the text; the light and dark bands on the abscissa indicate the times of light and dark of the entraining cycle. Arrows indicate times of the beginnings of series during which stimulation was increased during each half hour. At all other times, stimulation was at a quantal intensity of 1.02×10^{11} quanta cm^{-2} s^{-1}. Gaps in the record indicate times of missing data due to equipment failure; otherwise as in Figure 1.

functions were obtained by stimulating the eye on 8 or 9 successive 30-min intervals with stimuli increasing at steps of 0.5 log units, ultimately providing a maximum quantal intensity of 3.44×10^{12} quanta cm^{-2} s^{-1} (experiment of Fig. 2) or 2.62×10^{13} quanta cm^{-2} s^{-1} (experiment of Fig. 4).

All nighttime series produced response-*versus*-intensity functions of similar shape, with maximal reflectance increases near 13% (Fig. 5A) or 45% (Fig. 5B). In contrast, the daytime response level remained near 0, rising at most to about 3% of the height of the nighttime peak at the maximum stimulation intensity. It appears, in fact, that the maximum pupillary response that can be generated is greatly reduced during the day. To test this conjecture would require stimuli far more intense than what was available in these experiments. The highest intensities to which the animal was exposed during these series were up to 100 times the usual test exposure; somewhat surprisingly, these produced no obvious phase shifts in subsequent cycles of the rhythms (Figs. 2 and 4).

In the earlier work with gonodactyloid stomatopod species (Cronin, 1989; Cronin and King, 1989), no particular diel variation in the pupillary responses was noticed. Nevertheless, it seemed likely that gonodactyloids could possess rhythms similar to those of *Squilla*, but perhaps more subtle in their form. This possibility was tested with *Gonodactylus oerstedii*, using an overall experimental design like that employed with *Squilla empusa*, except that in these cases entrainment was imposed entirely by artificial cycles of light and dark. The pupillary response is much more rapid in *G. oerstedii* than in *S. empusa*, so I used briefer, more frequent stimuli in these experiments. Results of two experiments, representing the range of observed experimental outcomes, are displayed in Figures 6 and 7.

In the experiment of Figure 6, reflectance from the pseudopupil prior to stimulation showed a clear circadian rhythm. Here, the form was rather different from what was obtained using *S. empusa*. Soon after the expected time of lights-out, reflectance from the deep pseudopupil slowly increased, ultimately becoming about 10% greater than during the subjective day. Beginning near midday in the entrainment cycle, this elevated reflectance once more declined. A rhythm in pupillary responsiveness was

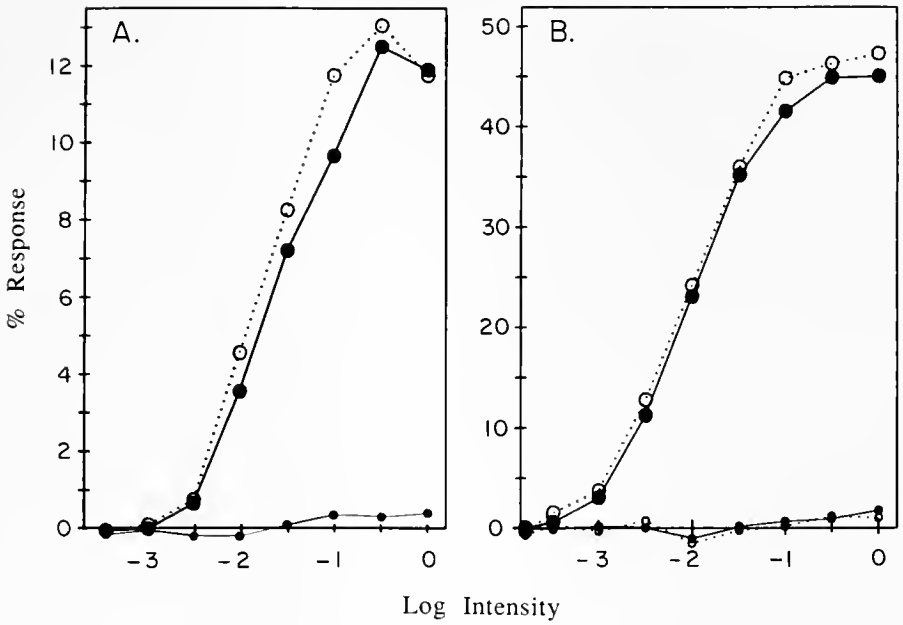

Figure 5. Response-*versus*-intensity functions obtained during the experiments of Figure 2 (A) and Figure 4 (B). Functions were obtained at the times indicated by arrows on those figures; large circles indicate results obtained during subjective night and small circles, during subjective day. Open circles correspond to the first series and closed circles to the second. Photic intensities are relative to 3.44×10^{12} quanta cm^{-2} s^{-1} in panel (A) or 2.62×10^{13} quanta cm^{-2} s^{-1} in panel (B).

more difficult to detect, although on average, responses did appear to be slightly larger at subjective night. Periodogram analysis of the data suggests the presence of circadian cycles in both the baseline reflectance data and the responsiveness data (Fig. 6).

The experiment of Figure 7 revealed the strongest expression of circadian rhythms in responsiveness that I observed in over 20 experiments with *G. oerstedii*. Amplitudes of the pupillary response were about twice as large during subjective day as during subjective night, thus having the opposite form of those expressed by *S. empusa*. The pupillary response was present both during the day and night. In this case, however, there was no evidence of a circadian cycle in pupillary reflectance.

Discussion

As demonstrated here, rhythms with a circadian period can readily be observed through observations of pseudopupils in compound eyes of stomatopod crustaceans. In the squilloid species, *Squilla empusa*, two parallel rhythms of high amplitude are usually observed: a cycle in baseline reflectance from the pseudopupil in the absence of stimulation, and a cycle in the amplitude of the pupillary response to light stimulation. In some experiments, the gonodactyloid *Gonodactylus oerstedii* expressed the baseline reflectance rhythm, although at lower amplitude than *S. empusa*. Rhythms in responsiveness in *G. oerstedii* were more difficult to detect than in *S. empusa*, but they could be observed in some individuals.

The rhythms that were observed were robust. They persisted and maintained their form, frequently with a high amplitude, for a week or more in constant conditions. The rhythms were clearly circadian; their periods were consistently revealed to be near 24 h either by inspection or by periodogram analysis of the data. The rhythm in responsiveness expressed by *S. empusa* was particularly impressive for its rapid rise each subjective evening and its equally rapid fall in the morning.

During the day, the sensitivity of the pupillary response decreased by at least three orders of magnitude. These changes are greater than observed in *Limulus polyphemus*, in which both the electroretinogram (ERG) and single-cell sensitivities decrease by about 1.5 log units (Barlow *et al.*, 1977, 1987). Other arthropods, however, have sensitivity changes between the day and night states about as large as those of *S. empusa*. In the crayfish *Cherax destructor*, dark-adapted single photoreceptor cells are more than two log units more sensitive at night (Bryceson, 1986), while the simple eyes of scorpions rhythmically gain nearly four log units of sensitivity each night (review: Fleissner and Fleissner, 1985). In its natural habitat, *S. empusa* probably lacks a pupillary response during the day. The maximum intensities of stimulation used in producing the response-*versus*-intensity functions of Fig-

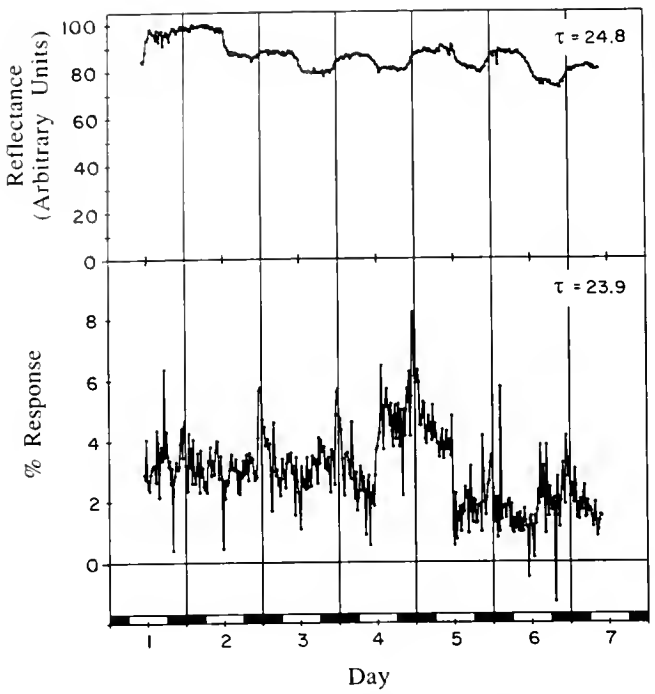

Figure 6. Results obtained from a female *Gonodactylus oerstedii* maintained in constant conditions from 22 to 28 January 1988. The animal was kept in a controlled light:dark cycle, indicated by the light and dark bands on the abscissa, prior to the experiment. Stimulation was at 500 nm, at intervals of 20 min, and at a quantal intensity of 1.57×10^{12} quanta cm^{-2} s^{-1}. Otherwise as in Figure 1.

ure 4, on the order of 10^{13} quanta cm^{-2} s^{-1}, are similar to intensities an animal would experience at a depth of only a few meters in the coastal waters it inhabits (Forward *et al.*, 1988). During the daylight phase of the rhythm, such intensities produced no apparent response.

If these circadian rhythms are to be properly phased to the diel cycle, they must be entrainable by cycles of light and dark. Animals apparently do entrain completely to a novel light:dark cycle within 12 days, as suggested by the results of the experiment of Figure 4. Presumably, photoreceptors for this entrainment are either within the compound eyes or exist elsewhere in the animal. In fact, many invertebrate species entrain their circadian rhythms using extraocular pathways (see review of Bennett, 1979). In crayfish, and probably other decapod crustaceans, photic entrainment of circadian rhythms can be achieved by retinal illumination (Larimer and Smith, 1980), but such entrainment may also involve photoreceptors of the 6th abdominal ganglion (Fuentes-Pardo and Inclán-Rubio, 1987) or other regions of the CNS (Page and Larimer, 1976; Larimer and Smith, 1980). In particular, the work of Page and Larimer (1976) demonstrated that the caudal photoreceptors (in the 6th abdominal ganglion) are not required for entrainment. In contrast to decapod crustaceans, *S. empusa* lacks this caudal photoreceptor (Wilkens and Larimer, 1976), and no other extraretinal photoreceptors have yet been described in stomatopods. If entrainment is mediated solely by the compound eyes, the spatially limited stimuli of these experiments (which were restricted to the ommatidia of the pseudopupil of one part of a single eye) must have been insufficient to induce observable phase changes. Nevertheless, intense stimuli like those used to measure the response-*versus*-intensity functions produce no obvious phase shifts, implying that there may be a role for extraocular photoreception in rhythm entrainment in stomatopods.

What underlying events take place within the compound eyes to bring about the rhythms observed in this study? Changes in the level of baseline reflectance can be effected in several ways (Stavenga, 1979). External to the receptor cells, these include reorganization of optical structures or associated pigment cells, movement of pigment in secondary pigment cells, and masking or unmasking of a tapetum. Within the photoreceptors, changes in reflectance could be caused by alterations in rhabdom size or microvillar organization, or by events within the

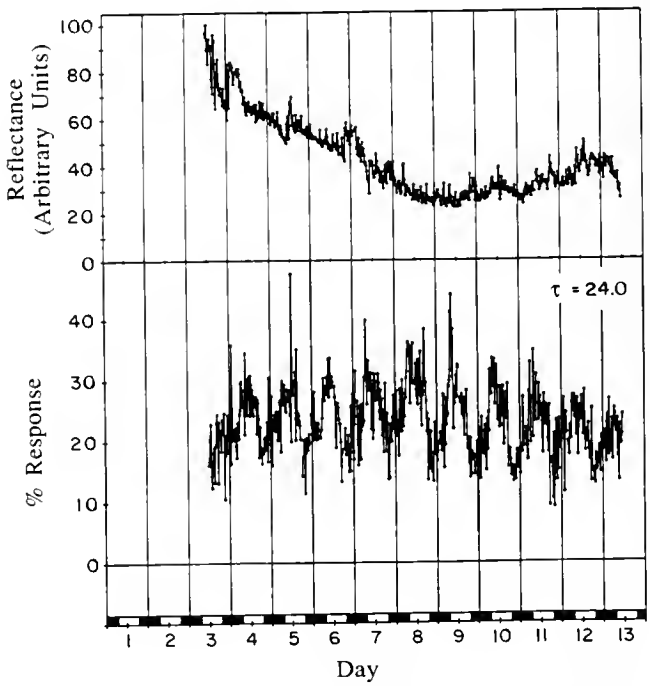

Figure 7. Results obtained from a male *Gonodactylus oerstedii* maintained in constant conditions from 31 January to 12 February 1991. The animal was kept in a controlled light:dark cycle, indicated by the light and dark bands on the abscissa, prior to the experiment. Data from the first two days of the experiment are not plotted, due to repeated animal movement and equipment failure. Stimulation was at 500 nm, at intervals of 20 min, and at a quantal intensity of 1.97×10^{12} quanta cm^{-2} s^{-1}. Periodogram analysis of the data of the upper panel (pupillary reflectance) produced a slowly rising periodogram with a spike peak at 27.1 h; because the analysis produced no clear maximum, the value of τ is not given on the figure. Otherwise as in Figure 1.

cytoplasm of retinular cells, such as rearrangement of the perirhabdomal palisade or movements of pigment granules.

Ommatidial reorganization no doubt accounts for much of the circadian change in the appearance of the pseudopupil of *Limulus polyphemus* (Stavenga, 1979), but more recent work suggests that the retinular cell pigment itself migrates under circadian control (Kier and Chamberlain, 1990). Long-term studies of anatomical changes in stomatopod eyes do not exist. In work with the Mediterranean species *Squilla mantis,* Schiff (1974) stated that during dark adaptation, rhabdoms increase in length and decrease in diameter; simultaneously, the crystalline cone contracts. Schönenberger (1977) also observed the contraction of the crystalline cone during dark adaptation, and noted that the distal pigment cells reorganize at that time. Within the photoreceptor cells, granules of primary pigment line up in neat rows, encircling the rhabdom as it dark adapts. These changes occur during diurnal dark adaptation, following prolonged exposure to daylight, at times when *Squilla empusa* reveals no light-sensitive pupillary responses and no evidence of dark adaptation following stimulation. At present, it is uncertain whether these two species of *Squilla* differ in their ability to respond to light during the day, whether the two sets of studies involve different phenomena, or whether prolonged exposure to light during the day can in fact produce reversible light-adaptation via the pupillary mechanism.

While cyclic restructuring of ommatidia or translocation of secondary pigment could produce rhythmic changes in baseline reflectance, events effecting major alterations in the level of the pupillary response must occur within the actual photoreceptor cells. In apposition eyes like those of stomatopods, the pupillary response is produced by radial translocation of granules of primary pigment residing in the photoreceptors (Stavenga, 1979; King and Cronin, 1989). Reflectance changes may be produced in superposition compound eyes, however, by events in secondary pigment cells (Bernard *et al.,* 1984; Weyrauther, 1986). Compared to the responses in stomatopod eyes, these changes are slow and have considerable inertia—the process continues, or remains saturated, long after stimulation ceases.

Migration of primary pigment is directly under the control of the retinular cell, and, at least in crustaceans, is thought not to be influenced by hormones (Ludolph *et al.,* 1973). In another arthropod, *Limulus polyphemus,* rhythmic neural input does influence the position of primary pigment (Kier and Chamberlain, 1990); similar processes may act in crustacean eyes. The pupillary response requires the presence of calcium ions (Kirschfeld and Vogt, 1980; Frixione and Aréchiga, 1981; Howard, 1984). Since excitation of arthropod photoreceptor cells is also dependent upon intracellular increases in calcium concentration (see review of Fein and Payne, 1989), the absence of the pupillary response during the day could imply that electrophysiological responses of the photoreceptors are also abolished at that time. However, this is unlikely to be the case; Kirschfeld and Vogt (1980) showed that in fly photoreceptors, it is possible to block pigment migration without changing retinal electrical responses. In work with mutant flies, Lo and Pak (1981) also observed that electrophysiological responses could remain in the absence of pigment migration. The processes of pigment translocation and membrane depolarization, while both calcium-dependent, are therefore not completely parallel. The diurnal loss of pupillary responsiveness in *Squilla empusa* could represent another example of the decoupling of these two processes. Experiments are desirable in which the electrical and pupillary responses are monitored simultaneously in this species.

Despite having radically different anatomies, the compound eyes of *S. empusa* and *Limulus polyphemus* are, to some extent, analogous in the functioning of their pupillary responses. Both express rhythmic changes in reflectance from the deep pseudopupil, and both show changes in this reflectance only at night (see Stavenga, 1979). Interestingly, demands on their visual systems throughout the course of each day may also be analogous. Neither species is entirely inactive during the day, but mating of *Limulus,* a behavior involving vision (Barlow *et al.,* 1982), occurs mostly during twilight or night (Barlow *et al.,* 1986). Indeed, nocturnal vision in *Limulus* is extraordinary, enabling the detection of high-contrast targets under starlight (Barlow *et al.,* 1982). Activity cycles of *Squilla empusa* have yet to be examined in the field, but in the laboratory, at least, this species is most active during the night (pers. obs.), and the congener, *Squilla mantis,* is clearly nocturnal (Froglia and Giannini, 1989). The ocular design of *S. empusa* is that of a nocturnal animal (Cronin, 1986). It is plausible that the rhythms in visual function described in this paper are characteristic physiological properties of a nocturnal compound eye. In fact, throughout the arthropods, regardless of eye type, all high-amplitude rhythms in visual physiological function yet described are in nocturnal species. Besides *Limulus,* these include scorpions (simple eyes, rhythm in ERG amplitude and sensitivity: reviewed in Fleissner and Fleissner, 1985), crayfish (superposition compound eye, rhythm in ERG amplitude and sensitivity: Aréchiga and Wiersma, 1969; Page and Larimer, 1975; Bryceson, 1986), and cockroach (apposition compound eye, rhythm in ERG amplitude: Wills *et al.,* 1986).

G. oerstedii, unlike *S. empusa,* is active only from dawn to dusk (Dominguez and Reaka, 1988). At evening twilight, it seals off the entrance to its burrow and remains enclosed all night. Its eyes are optimized for photopic function; indeed, the specialized spectral receptor classes

in its eyes require reasonably bright light to operate at all (Cronin and Marshall, 1989; see also Marshall *et al.*, 1991). Because the eye is used primarily for vision when photon capture is not limiting, strong rhythmic cycles in visual function may be unnecessary.

The expression of high-amplitude circadian visual rhythms in a primarily nocturnal species like *S. empusa*, and their absence in the diurnal *G. oerstedii*, could therefore reveal fundamental differences in function between compound eyes designed for nocturnal (or continuous) *versus* diurnal function. If so, the rhythms observed in this study by monitoring light reflectance from deep pseudopupils are a manifestation of more pervasive underlying alterations that must occur to maintain visual function at day and night. The study of rhythmic cycles of sensory function, and in particular their underlying significance and control, deserves more attention.

Acknowledgments

This material is based on work supported by the National Science Foundation under Grants No. BNS-8518769 and BNS-8917183. I thank D. G. Stavenga and L. Kass for their comments on an earlier version of the manuscript.

Literature Cited

Aréchiga, H., and C. A. G. Wiersma. 1969. Circadian rhythm of responsiveness in crayfish visual units. *J. Neurobiol.* **1:** 71–85.

Autrum, H. 1981. Light and dark adaptation in invertebrates. Pp. 1–91 in *Handbook of Sensory Physiology, Vol VII/6C,* H. Autrum, ed. Springer, Berlin, Heidelberg, New York.

Barlow, R. B., Jr. 1983. Circadian rhythms in the *Limulus* visual system. *J. Neurosci.* **3:** 856–870.

Barlow, R. B., Jr., S. J. Bolanowski, Jr., and M. L. Brachman. 1977. Efferent optic nerve fibers mediate circadian rhythms in the *Limulus* eye. *Science* **197:** 86–89.

Barlow, R. B., Jr., L. C. Ireland, and L. Kass. 1982. Vision has a role in *Limulus* mating behavior. *Nature* **296:** 65–66.

Barlow, R. B., Jr., E. Kaplan, G. H. Renninger, and T. Saito. 1987. Circadian rhythms in *Limulus* photoreceptors. I. Intracellular studies. *J. Gen. Physiol.* **89:** 353–378.

Barlow, R. B., Jr., M. K. Powers, H. Howard, and L. Kass. 1986. Migration of *Limulus* for mating: relation to lunar phase, tide height, and sunlight. *Biol. Bull.* **171:** 310–329.

Bennett, M. F. 1979. Extraocular light receptors and circadian rhythms. Pp. 641–663 in *Handbook of Sensory Physiology, Vol. VII/6A,* H. Autrum, ed. Springer, Berlin, Heidelberg, New York.

Bernard, G. D., E. D. Owens, and A. V. Hurley. 1984. Intracellular optical physiology of the eye of the moth *Amyelois. J. Exp. Biol.* **138:** 155–179.

Bernard, G. D., and D. G. Stavenga. 1979. Spectral sensitivities of retinular cells measured in intact, living flies by an optical method. *J. Comp. Physiol.* **134:** 95–107.

Bryceson, K. P. 1986. Diurnal changes in photoreceptor sensitivity in a reflecting superposition eye. *J. Comp. Physiol. A* **158:** 573–582.

Burnside, B., and B. Nagle. 1983. Retinomotor movements of photoreceptors and retinal pigment epithelium: mechanisms and regulation. Pp. 67–109 in *Progress in Retinal Research, Vol 2,* N. Osborne and G. Chader, eds. Pergamon, Oxford, New York.

Chamberlain, S. C., and R. B. Barlow, Jr. 1984. Transient membrane shedding in *Limulus* photoreceptors: control mechanisms under natural lighting. *J. Neurosci.* **4:** 2792–2810.

Cronin, T. W. 1986. Optical design and evolutionary adaptation in crustacean compound eyes. *J. Crust. Biol.* **6:** 1–23.

Cronin, T. W. 1989. Application of intracellular optical techniques to the study of stomatopod crustacean vision. *J. Comp. Physiol. A* **164:** 737–750.

Cronin, T. W., and C. A. King. 1989. Spectral sensitivity of vision in the mantis shrimp, *Gonodactylus oerstedii,* determined using non-invasive optical techniques. *Biol. Bull.* **176:** 308–316.

Cronin, T. W., and N. J. Marshall. 1989. Multiple spectral classes of photoreceptors in retinas of gonodactyloid stomatopod crustaceans. *J. Comp. Physiol. A* **166:** 261–275.

Dominguez, J. H., and M. Reaka. 1989. Temporal activity patterns in reef-dwelling stomatopods: a test of alternative hypotheses. *J. Exp. Mar. Biol. Ecol.* **117:** 47–69.

Enright, J. T. 1965. The search for rhythmicity in biological time-series. *J. Theoret. Biol.* **8:** 426–468.

Fein, A., and R. Payne. 1989. Phototransduction in *Limulus* ventral photoreceptors: roles of calcium and inositol trisphosphate. Pp. 171–185 in *Facets of Vision,* D. G. Stavenga and R. C. Hardie, eds. Springer, Berlin, Heidelberg, New York.

Fleissner, G., and G. Fleissner. 1985. Neurobiology of a circadian clock in the visual system of scorpions. Pp. 351–375 in *Neurobiology of Arachnids,* F. G. Barth, ed. Springer, Berlin, Heidelberg, New York.

Forward, R. B., Jr., T. W. Cronin, and J. K. Douglass. 1988. The visual pigments of crabs. II. Environmental adaptations. *J. Comp. Physiol. A* **162:** 479–490.

Frixione, E., and H. Aréchiga. 1981. Ionic dependence of screening pigment migrations in crayfish retinal photoreceptors. *J. Comp. Physiol.* **144:** 35–43.

Froglia, C., and S. Giannini. 1989. Field observations on diel rhythms in catchability and feeding of *Squilla mantis* (L.) (Crustacea, Stomatopoda) in the Adriatic Sea. Pp. 221–228 in *Biology of Stomatopods,* E. A. Ferrero, ed. Mucchi, Modena.

Fuentes-Pardo, B., and V. Inclán-Rubio. 1987. Caudal photoreceptors synchronize the circadian rhythms in crayfish. I. Synchronization of ERG and locomotor circadian rhythms. *Comp. Biochem. Physiol.* **86A:** 523–527.

Hernández-Falcón, J., E. Moreno-Sáenz, J. M. Farías, and B. Fuentes-Pardo. 1987. Role of the sinus gland in crayfish circadian rhythmicity. I. Pseudopupil circadian rhythm. *Comp. Biochem. Physiol.* **87A:** 111–118.

Horridge, G. A., J. Duniec, and L. Marcelja. 1981. A 24-hour cycle in single locust and mantis photoreceptors. *J. Exp. Biol.* **91:** 307–322.

Howard, J. 1984. Calcium enables photoreceptor pigment migration in a mutant fly. *J. Exp. Biol.* **113:** 471–475.

Jacklet, J. W. 1969. Circadian rhythm of optic nerve impulses recorded in darkness from isolated eye of *Aplysia. Science* **164:** 562–563.

Kaplan, E., and R. B. Barlow, Jr. 1980. Circadian clock in *Limulus* brain increases response and decreases noise of retinal photoreceptors. *Nature* **286:** 393–395.

Kass, L., and G. H. Renninger. 1988. Circadian change in function of *Limulus* ventral photoreceptors. *Visual Neurosci.* **1:** 3–11.

Kier, C. K., and S. C. Chamberlain. 1990. Dual controls for screening pigment movement in photoreceptors of the *Limulus* lateral eye: circadian efferent input and light. *Visual Neurosci.* **4:** 237–255.

King, C. A., and T. W. Cronin. 1989. Ultrastructural evidence for pupillary response in stomatopod photoreceptors: Cytoskeleton and orientation of pigment granules. *Invest. Ophthalmol. Visual Sci.* **30** (suppl):292.

Kirschfeld, K., and N. Franceschini. 1969. Ein Mechanismus zur Steuerung des Lichtflusses in den Rhabdomeren des Komplexauges von Musca. *Kybernetik* **6:** 13–22.

Kirschfeld, K., and K. Vogt. 1980. Calcium ions and pigment migration in fly photoreceptors. *Naturwissenschaften* **67:** 516–517.

Kleinholz, L. H. 1937. Studies in the pigmentary system of crustacea. II. Diurnal movements of the retinal pigments of Bermudan decapods. *Biol. Bull.* **72:** 176–189.

Korenbrot, J. I., and R. D. Fernald. 1989. Circadian rhythm and light regulate opsin mRNA in rod photoreceptors. *Nature* **337:** 454–457.

Larimer, J. L., and J. T. F. Smith. 1980. Circadian rhythm of retinal sensitivity in crayfish: modulation by the cerebral and optic ganglia. *J. Comp. Physiol.* **136:** 313–326.

LaVail, M. 1976. Rod outer segment disc shedding in relation to cyclic lighting. *Exp. Eye Res.* **23:** 277–280.

Levinson, G., and B. Burnside. 1981. Circadian rhythms in teleost retinomotor movements. *Invest. Ophthalmol. Visual Sci.* **20:** 294–303.

Lo, M. C., and W. L. Pak. 1981. Light-induced pigment granule migration in the retinular cells of *Drosophila melanogaster*. Comparison of wild type with ERG-defective mutants. *J. Gen. Physiol.* **77:** 155–175.

Ludolph, C., D. Pagnanelli, and M. I. Mote. 1973. Neural control of migration of proximal screening pigment by retinular cells of the swimming crab, *Callinectes sapidus*. *Biol. Bull.* **145:** 159–170.

Marshall, N. J., M. F. Land, C. A. King, and T. W. Cronin. 1991. The compound eyes of mantis shrimps (Crustacea, Hoplocarida, Stomatopoda). II. Colour pigments in the eyes of stomatopod crustaceans: polychromatic vision by serial and lateral filtering. *Phil. Trans. R. Soc. Ser. B* **334:** 57–84.

Nässel, D. R., and T. H. Waterman. 1979. Massive diurnally modulated photoreceptor membrane turnover in crab light and dark adaptation. *J. Comp. Physiol.* **131:** 205–216.

Page, T. L., and J. L. Larimer. 1975. Neural control of circadian rhythmicity in the crayfish. II. The ERG amplitude rhythm. *J. Comp. Physiol.* **97:** 81–96.

Page, T. L. and J. L. Larimer. 1976. Extraretinal photoreception in entrainment of crustacean circadian rhythms. *Photochem. Photobiol.* **23:** 245–251.

Schiff, H. 1974. A discussion of light scattering in the *Squilla* rhabdom. *Kybernetik* **14:** 127–134.

Schönenberger, N. 1977. The fine structure of the compound eye of *Squilla mantis* (Crustacea, Stomatopoda). *Cell Tissue Res.* **176:** 205–233.

Smith, R. I. 1948. The role of the sinus glands in retinal pigment migration in grapsoid crabs. *Biol. Bull.* **95:** 169–185.

Stavenga, D. G. 1977. Optics of compound eyes and circadian pigment movements studied by pseudopupil observations *in vivo*. *Biol. Bull.* **153:** 446.

Stavenga, D. G. 1979. Pseudopupils of compound eyes. Pp. 357–439 in *Handbook of Sensory Physiology, Vol. VII/6A*, H. Autrum, ed. Springer, Berlin, Heidelberg, New York.

Stavenga, D. G., and J. W. Kuiper. 1977. Insect pupil mechanisms. I. On the pigment migration in the retinula cells of hymenoptera. *J. Comp. Physiol.* **113:** 55–72.

Welsh, J. H. 1930. Diurnal rhythm of the distal pigment cells in the eyes of certain crustaceans. *Proc. Natl. Acad. Sci.* **16:** 386–395.

Weyrauther, E. 1986. Do retinula cells trigger the screening pigment migration in the eye of the moth *Ephestia kuehniella? J. Comp. Physiol. A* **159:** 55–60.

Wilkens, L. A., and J. L. Larimer. 1976. Photosensitivity in the sixth abdominal ganglion of decapod crustaceans: a comparative study. *J. Comp. Physiol.* **106:** 69–75.

Williams, D. S. 1982. Ommatidial structure in relation to turnover of photoreceptor membrane in the locust. *Cell Tissue Res.* **225:** 595–617.

Wills, S. A., T. L. Page, and C. S. Colwell. 1986. Circadian rhythms in the electroretinogram of the cockroach. *J. Biol. Rhythms.* **1:** 25–37.

CONTENTS

Volume 182 Number 3

THE BIOLOGICAL BULLETIN

JUNE, 1992

Published by the Marine Biological Laboratory

THE BIOLOGICAL BULLETIN

PUBLISHED BY
THE MARINE BIOLOGICAL LABORATORY

JUNE, 1992

Printed and Issued by
LANCASTER PRESS, Inc.
PRINCE & LEMON STS.
LANCASTER, PA

THE BIOLOGICAL BULLETIN

THE BIOLOGICAL BULLETIN is published six times a year by the Marine Biological Laboratory, MBL Street, Woods Hole, Massachusetts 02543.

Subscriptions and similar matter should be addressed to Subscription Manager, THE BIOLOGICAL BULLETIN, Marine Biological Laboratory, Woods Hole, Massachusetts 02543. Single numbers, $30.00. Subscription per volume (three issues), $77.50 ($155.00 per year for six issues).

Communications relative to manuscripts should be sent to Michael J. Greenberg, Editor-in-Chief, or Pamela L. Clapp, Managing Editor, at the Marine Biological Laboratory, Woods Hole, Massachusetts 02543. Telephone: (508) 548-3705, ext. 428. FAX: 508-540-6902. E-mail: pamcl@hoh.mbl.edu.

POSTMASTER: Send address changes to THE BIOLOGICAL BULLETIN, Marine Biological Laboratory, Woods Hole, MA 02543.

Second-class postage paid at Woods Hole, MA, and additional mailing offices.
ISSN 0006-3185

INSTRUCTIONS TO AUTHORS

The Biological Bulletin accepts outstanding original research reports of general interest to biologists throughout the world. Papers are usually of intermediate length (10–40 manuscript pages). A limited number of solicited review papers may be accepted after formal review. A paper will usually appear within four months after its acceptance.

Very short, especially topical papers (less than 9 manuscript pages including tables, figures, and bibliography) will be published in a separate section entitled "Research Notes." A Research Note in *The Biological Bulletin* follows the format of similar notes in *Nature*. It should open with a summary paragraph of 150 to 200 words comprising the introduction and the conclusions. The rest of the text should continue on without subheadings, and there should be no more than 30 references. References should be referred to in the text by number, and listed in the Literature Cited section in the order that they appear in the text. Unlike references in *Nature*, references in the Research Notes section should conform in punctuation and arrangement to the style of recent issues of *The Biological Bulletin*. Materials and Methods should be incorporated into appropriate figure legends. See the article by Lohmann *et al.* (October 1990, Vol. **179**: 214–218) for sample style. A Research Note will usually appear within two months after its acceptance.

The Editorial Board requests that regular manuscripts conform to the requirements set below; those manuscripts that do not conform will be returned to authors for correction before review.

1. ***Manuscripts.*** Manuscripts, including figures, should be submitted in triplicate. (Xerox copies of photographs are not acceptable for review purposes.) The original manuscript must be typed in no smaller than 12 pitch, using double spacing (*including* figure legends, footnotes, bibliography, etc.) on one side of 16- or 20-lb. bond paper, 8½ by 11 inches. Please, no right justification. Manuscripts should be proofread carefully and errors corrected legibly in black ink. Pages should be numbered consecutively. Margins on all sides should be at least 1 inch (2.5 cm). Manuscripts should conform to the *Council of Biology Editors Style Manual*, 5th Edition (Council of Biology Editors, 1983) and to American spelling. Unusual abbreviations should be kept to a minimum and should be spelled out on first reference as well as defined in a footnote on the title page. Manuscripts should be divided into the following components: Title page, Abstract (of no more than 200 words), Introduction, Materials and Methods, Results, Discussion, Acknowledgments, Literature Cited, Tables, and Figure Legends. In addition, authors should supply a list of words and phrases under which the article should be indexed.

2. ***Title page.*** The title page consists of: a condensed title or running head of no more than 35 letters and spaces, the manuscript title, authors' names and appropriate addresses, and footnotes listing present addresses, acknowledgments or contribution numbers, and explanation of unusual abbreviations.

3. ***Figures.*** The dimensions of the printed page, 7 by 9 inches, should be kept in mind in preparing figures for publication. We recommend that figures be about 1½ times the linear dimensions of the final printing desired, and that the ratio of the largest to the smallest letter or number and of the thickest to the thinnest line not exceed 1:1.5. Explanatory matter generally should be included in legends, although axes should always be identified on the illustration itself. Figures should be prepared for reproduction as either line cuts or halftones. Figures to be reproduced as line cuts should be unmounted glossy photographic reproductions or drawn in black ink on white paper, good-quality tracing cloth or plastic, or blue-lined coordinate paper. Those to be reproduced as halftones should be mounted on board, with both designating numbers or letters and scale bars affixed directly to the figures. All figures should be numbered in consecutive order, with no distinction between text and plate figures. The author's name and an arrow indicating orientation should appear on the reverse side of all figures.

4. ***Tables, footnotes, figure legends, etc.*** Authors should follow the style in a recent issue of *The Biological Bulletin* in preparing table headings, figure legends, and the like. Because of the high cost of setting tabular material in type, authors are asked to limit such material as much as possible. Tables, with their headings and footnotes, should be typed on separate sheets, numbered with consecutive Roman numerals, and placed after

the Literature Cited. Figure legends should contain enough information to make the figure intelligible separate from the text. Legends should be typed double spaced, with consecutive Arabic numbers, on a separate sheet at the end of the paper. Footnotes should be limited to authors' current addresses, acknowledgments or contribution numbers, and explanation of unusual abbreviations. All such footnotes should appear on the title page. Footnotes are not normally permitted in the body of the text.

5. ***Literature cited.*** In the text, literature should be cited by the Harvard system, with papers by more than two authors cited as Jones *et al.*, 1980. Personal communications and material in preparation or in press should be cited in the text only, with author's initials and institutions, unless the material has been formally accepted and a volume number can be supplied. The list of references following the text should be headed Literature Cited, and must be typed double spaced on separate pages, conforming in punctuation and arrangement to the style of recent issues of *The Biological Bulletin*. Citations should include complete titles and inclusive pagination. Journal abbreviations should normally follow those of the U. S. A. Standards Institute (USASI), as adopted by BIOLOGICAL ABSTRACTS and CHEMICAL ABSTRACTS, with the minor differences set out below. The most generally useful list of biological journal titles is that published each year by BIOLOGICAL ABSTRACTS (BIOSIS List of Serials; the most recent issue). Foreign authors, and others who are accustomed to using THE WORLD LIST OF SCIENTIFIC PERIODICALS, may find a booklet published by the Biological Council of the U.K. (obtainable from the Institute of Biology, 41 Queen's Gate, London, S.W.7, England, U.K.) useful, since it sets out the WORLD LIST abbreviations for most biological journals with notes of the USASI abbreviations where these differ. CHEMICAL ABSTRACTS publishes quarterly supplements of additional abbreviations. The following points of reference style for THE BIOLOGICAL BULLETIN differ from USASI (or modified WORLD LIST) usage:

A. Journal abbreviations, and book titles, all underlined (for *italics*)

B. All components of abbreviations with initial capitals (not as European usage in WORLD LIST *e.g., J. Cell. Comp. Physiol.* NOT *J. cell. comp. Physiol.*)

C. *All* abbreviated components must be followed by a period, whole word components *must not* (*i.e., J. Cancer Res.*)

D. Space between all components (*e.g., J. Cell. Comp. Physiol.*, not *J Cell.Comp.Physiol.*)

E. Unusual words in journal titles should be spelled out in full, rather than employing new abbreviations invented by the author. For example, use *Rit Vísindafjélags Islendinga* without abbreviation.

F. All single word journal titles in full (*e.g., Veliger, Ecology, Brain*).

G. The order of abbreviated components should be the same as the word order of the complete title (*i.e., Proc.* and *Trans.* placed where they appear, not transposed as in some BIOLOGICAL ABSTRACTS listings).

H. A few well-known international journals in their preferred forms rather than WORLD LIST or USASI usage (*e.g., Nature, Science, Evolution* NOT *Nature, Lond., Science, N.Y.; Evolution, Lancaster, Pa.*)

6. ***Reprints, page proofs, and charges.*** Authors receive their first 100 reprints (without covers) free of charge. Additional reprints may be ordered at time of publication and normally will be delivered about two to three months after the issue date. Authors (or delegates for foreign authors) will receive page proofs of articles shortly before publication. They will be charged the current cost of printers' time for corrections to these (other than corrections of printers' or editors' errors). Other than these charges for authors' alterations, *The Biological Bulletin* does not have page charges.

Reference: *Biol. Bull.* **182:** 289–297. (June, 1992)

Evidence for a Programmed Circannual Life Cycle Modulated by Increasing Daylengths in *Neanthes limnicola* (Polychaeta: Nereidae) From Central California

PETER P. FONG[1] AND JOHN S. PEARSE

Biology Board of Studies and Institute of Marine Sciences, University of California, Santa Cruz, California, 95064

Abstract. Timing of parturition, fecundity, and life span were determined in laboratory cultures of the semelparous, self-fertilizing, viviparous polychaete *Neanthes limnicola*. Worms were exposed to fixed daylengths (short—8h light: 16h dark; neutral—12h:12h; long—16h:8h), switched between different fixed daylengths, and switched from fixed daylengths to increasing or decreasing daylengths. Timing of parturition was synchronized when under neutral daylength, but became asynchronous under both short and long daylength, as well as when any of the fixed daylength was followed by decreasing daylengths. Worms under neutral daylength had the highest fecundities and shortest life spans, while those under long days had the lowest fecundities and longer life spans. When fixed daylength (short, neutral, long) was followed by increasing daylengths, timing of parturition was synchronized, fecundity was high, and life span shortened. These and earlier published experiments on the influence of seasonally changing photoperiods indicate that the life cycle of the estuarine *N. limnicola* is programmed to be completed in somewhat less than a year, and that seasonally changing photoperiods modulate it to determine the optimal time of parturition.

Introduction

Photoperiodic control of reproduction has been demonstrated for many organisms (reviewed by Saunders, 1982; Gwinner, 1986). Most experimental work has focussed on the effects of fixed daylength on annual reproductive rhythms (*e.g.*, for annelids: Garwood and Olive, 1982; Olive and Pillai, 1983; Clark, 1988; Schierwater and Hauenschild, 1990). However, seasonally changing photoperiod also has profound effects on the timing of reproduction (Goss, 1982, 1984; Pearse *et al.*, 1986). Such is the case for *Neanthes limnicola* (Johnson, 1901), a viviparous, self-fertilizing hermaphroditic polychaete that gives birth mainly during the spring (late February–May) in the brackish-water creeks flowing into Monterey Bay, California (Smith, 1950; Fong and Pearse, 1992). This semelparous worm responds to seasonally changing photoperiod by giving birth to young in spring light regimes when maintained under either in-phase or 6 months out-of-phase light conditions. Worms in culture live for 6 months to 2 years and still reproduce mainly in spring light regimes (Fong and Pearse, 1992). These findings suggested to us that the worms must "see" either one or more critical daylengths, or increasing daylengths mimicking spring light regimes, to complete sexual maturation. The present paper reports on experiments that examined the effects of constant fixed daylength, and fixed daylengths followed by increasing or decreasing daylengths, on the timing of parturition, on fecundity, and on life span in culture of *N. limnicola*. These experiments revealed evidence for an endogenous, circannual rhythm that responds to increasing daylengths.

Materials and Methods

We have maintained worms and their offspring in the laboratory since October 1987 when approximately 20 adults were collected from Watsonville Slough, California (36°45′N; 121°45′W). Worms used in all experiments

Received 17 September 1991; accepted 18 February 1992.

[1] Present address: Department of Physiology, Wayne State University, Detroit, MI 48201.

were born in the laboratory as a result of self-fertilizations from lab-reared adults. Although worms in the field are usually born in the spring, birth date in the laboratory can be controlled by manipulating seasonally changing daylengths (Fong and Pearse, 1992). Juvenile worms were reared singly, initially in small, plastic petri dishes, then transferred to 80 × 100 mm pyrex culture dishes with lids (1 worm/dish). All culture dishes were maintained at laboratory air temperature (Fig. 1), and a salinity of 15‰. Worms were fed brine shrimps once per week, and the culture media was changed 1–2 days after each feeding. As worms grew and matured they were monitored daily for signs of reproduction. About 10 days before giving birth, the body wall of the adult becomes greenish and semi-transparent, and developing embryos are easily seen moving through the coelomic fluid. At birth, juvenile worms emerge through fissures in the degenerating body wall of the dying adult. Occasionally, adult worms with normal body size and reproductive morphology produced no young. Because they looked and behaved normally before parturition, these worms (n = 7) were included in all statistical analyses. Parturition date, life span (days adults spent in culture) and fecundity (numbers of young produced) were recorded for each birth. All experiments (treatments and numbers of worms used) are summarized in Table I. For statistical analysis of parturition dates, sequential numerical values were assigned to each date in each experiment; the value of 1 was assigned to the date of the first parturition, 2 to the following calendar day, etc. (*e.g.,* in experiment A the first parturition occurred on 2 April 1989 and was given the value 1, 3 April = 2, and 5 May = 33, etc.). Analysis of variance was used to compare mean parturition dates, life span, and fecundity (see Fong, 1991, for full analysis).

Fixed daylength (experiment A)

Immediately after birth (Aug–Sept 1988), each of the 108 worms was placed in one of three light-tight wooden boxes (n = 36/box) illuminated with fluorescent lights (General Electric F40 daylight) at fixed photoperiods of either long (L:D 16h:8h), neutral (12h:12h), or short (8h:16h) daylengths. The northern distribution of *N. limnicola* extends to Vancouver Island, where extreme daylengths of 16h:8h and 8h:16h occur in June and December, respectively. In central California, extreme daylengths are approximately 14.5h:9.5h and 9.5h:14.5h. After 3 months, some of the worms in each light treatment were removed from their boxes and switched into one of the other two light regimes (for example, 24 worms were removed from the neutral daylength box, and 12 each were placed under short and long daylengths; symbolized by neutral → short and neutral → long). The remainder of the worms were maintained under their initial fixed-daylength light regimes. Of the 108 worms, 27 (25%) died during the experiments either before or after shifting light regimes (Table I).

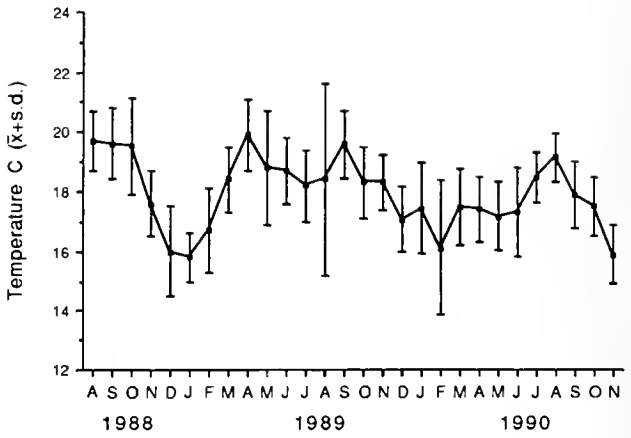

Figure 1. Monthly air temperature ($\bar{x}$ + S.D.) at Long Marine Laboratory from daily records.

Fixed daylength followed by increasing daylengths (experiment B) or by decreasing daylengths (experiment C)

In experiment B, 60 worms (all born on 4 May 1989) were divided equally among 3 fixed daylength light regimes of long (L:D 16:8), neutral (12:12), or short (8:16) daylength. After 3 months, roughly half of the worms in each light treatment were switched into a room where daylengths would be increasing for almost 5 months, (light regimes corresponding to February–June), controlled by a mechanical warehouse clock switch (Astronomic Time Switch, R.W. Cramer & Co., Type SY Model SOL). The lights were turned on and off at local sunrise and sunset 6 months out of phase with ambient photoperiod. The early February light regime was approximately (L:D) 10:14, thus worms initially exposed to neutral daylength (12:12) saw a shorter, but increasing daylength for the first 6 weeks after shifting. Those initially exposed to long (16:8) daylength also saw shorter, but increasing daylengths. Only worms initially exposed to short (8:16) daylength saw longer and increasing daylengths. The other half of the worms in each treatment were maintained in their original fixed-daylength light regimes (control). Of the 60 worms, 17 (28%) died either before or after shifting (Table I).

In experiment C, 60 worms (born 30 July–5 August 1989) were kept in phase (decreasing daylength) for about 1 month after birth, then divided equally and maintained as above in either short, neutral, or long daylengths for 7 weeks. In late September, 10 worms from each treatment were transferred to a room where daylengths (controlled by another time switch) would be decreasing (in phase)

Table I

Mean parturition dates, mean numbers of young, and mean days in culture of Neanthes limnicola *in all experiments*

Experiment name	Photoperiod treatment	Date adults born	n surviving	Mean parturition date	Mean # young (+S.D.)	Mean life span (+S.D.)
A. Fixed daylength	short	22 Aug 88	6	4 May	100.6 (60.4)	252.6 (18.0)
	neutral	22–28 Aug 88	8	12 July	163.8 (44.3)	318.5 (141.8)
	long	22 Aug 88	10	11 July	114.4 (44.5)	313.3 (38.5)
	short → neutral	22 Aug 88	7	3 June	124.4 (41.0)	281.4 (92.3)
	short → long	22 Aug 88	7	10 June	124.1 (49.5)	286.4 (59.8)
	neutral → short	28 Aug 88	11	11 May	153.7 (25.7)	254.2 (15.1)
	neutral → long	28 Aug. 14 Sept 88	12	10 Aug	99.91 (56.1)	340.2 (97.1)
	long → short	22 Aug 88	9	11 July	139.7 (55.8)	309.6 (55.8)
	long → neutral	22 Aug 88	11	15 Aug	92.3 (77.4)	349.9 (102.6)
	Independent of shifting					
	initially short		20	28 May	117.2 (48.8)	274.4 (64.2)
	initially neutral		31	1 July	135.5 (51.7)	304.0 (98.6)
	initially long		30	24 July	113.9 (60.0)	325.6 (72.8)
	Pooled					
	pooled short + neutral		51	18 June	128.3 (50.9)	292.4 (87.3)
	pooled long		30	24 July	113.9 (60.0)	325.6 (72.8)
B. Fixed → increasing daylength	short	4 May 89	6	1 Apr	87.2 (68.7)	332.6 (141.5)
	neutral	4 May 89	7	1 Apr	143.4 (66.0)	330.3 (18.7)
	long	4 May 89	4	23 May	64.6 (56.9)	385.0 (113.0)
	short → inc	4 May 89	7	29 Nov (=May light regime)	105.8 (48.5)	209.4 (21.5)
	neutral → inc	4 May 89	10	14 Dec (=June light regime)	115.5 (35.8)	223.3 (8.1)
	long → inc	4 May 89	9	12 Jan (=July light regime)	152.8 (46.5)	253.1 (7.4)
C. Fixed → decreasing daylength	short	5 Aug 89	9	22 July	89.22 (55.9)	350.7 (116.1)
	neutral	5 Aug 89	9	27 April	108.9 (36.7)	265.0 (5.1)
	long	30 July 89	5	14 Aug	39.4 (41.2)	380.4 (32.7)
	short → dec	5 Aug 89	10	20 Aug	89.2 (40.4)	377.3 (131.8)
	neutral → dec	5 Aug 89	8	20 May	106.3 (18.5)	288.3 (25.4)
	long → dec	30 July 89	8	22 June	77.87 (30.2)	327.3 (37.6)
	Independent of shifting					
	initially short		19	6 Aug	89.2 (46.9)	364.7 (121.9)
	initially neutral		17	8 May	107.6 (28.7)	275.9 (21.0)
	initially long		13	13 July	63.1 (38.4)	347.7 (43.7)

Parturition dates are dates on which adults gave birth. Daylengths are: short daylength = (L:D 8h:16h), neutral daylength = (12h:12h), long daylength = (L:D 16h:8h). Short → neutral indicates cultures which were initiated in (8:16), then after 3 months shifted into 12:12, etc. inc = increasing daylengths; dec = decreasing daylengths.

for about 3 months. On 23 December 1989, worms were placed in constant short daylengths (8:16) where they remained until they gave birth. Control worms (n = 10 for each light treatment) were maintained in their original fixed-daylength light regimes. Of the 60 worms, 11 (18%) died during the experiment (Table I).

Results

Fixed daylength (experiment A)

Photoperiod significantly affected the timing of parturition in *Neanthes limnicola* (one-way ANOVA of mean parturition date, $F_{8,72} = 2.08$, $P = 0.04$). Worms maintained in constant short and neutral → short daylengths gave birth on average in the ambient spring (May), and those in short → neutral and short → long in the ambient late spring (June) (Table I, Fig. 2). Worms maintained in constant neutral (12:12) also gave birth in the ambient spring, but parturition dates were separated by 10–11 months (Fig. 2); thus the mean parturition date was in July. Those worms that encountered long daylengths initially, gave birth in July and August on average (Table I, Fig. 2). Four significant comparisons were made between groups (Fisher's Least Significant Difference test, $P < 0.05$), and all involved groups that saw either short or neutral daylengths initially, compared with those that saw long daylengths at any stage. In each case, exposure to long daylength resulted in worms giving birth significantly

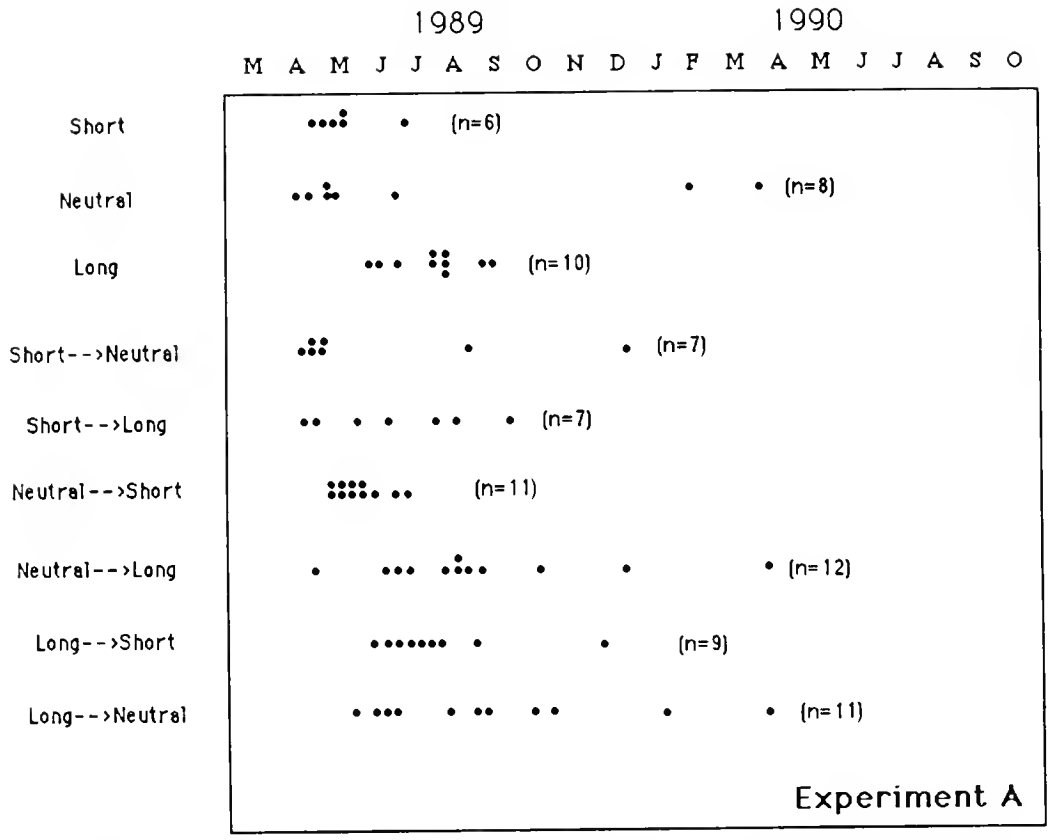

Figure 2. Parturition dates of *Neanthes limnicola* in various conditions of fixed daylength (experiment A). Each point represents a parturition. Daylengths are short = (L:D 8:16), neutral = (L:D 12:12), and long = (L:D 16:8). Short → neutral indicates cultures initiated in short daylength, then shifted into neutral daylength, etc. Adults that gave birth were themselves born in August–September 1988.

later in the calendar year, and spread over an extended period. Despite significant differences in the timing of parturition, photoperiod did not significantly affect life span (one-way ANOVA, $F_{8,72} = 1.75$ $P = 0.10$), but did have a significant effect on fecundity (one-way ANOVA, $F_{8,72} = 2.20$ $P = 0.04$). Highest fecundities were recorded in worms that saw either constant neutral ($\bar{x} = 163.8$, n = 8) or neutral → short ($\bar{x} = 153.7$, n = 11) daylengths (Table I). Lowest fecundity was in the long → neutral treatment ($\bar{x} = 92.27$, n = 11); 4 of these 11 worms had good reproductive morphology, but produced no young.

The initial daylengths to which worms were exposed (*i.e.*, independent of shifting) had a significant effect on timing of parturition (one-way ANOVA of mean parturition date, $F_{2,78} = 3.03$, $P = 0.05$); worms in short and neutral daylengths gave birth in the spring and early summer ($\bar{x}_{short}$ = 28 May, $\bar{x}_{neutral}$ = 1 July, Table I), but worms that initially saw long daylengths gave birth in the midsummer ($\bar{x}_{long}$ = 24 July; Fisher's LSD, $P < 0.05$ for both comparisons). However, no significant difference in life span or fecundity exists among these photoperiodic groups.

Increasing daylength experiments (experiment B)

The timing of parturition was affected by increasing daylength (one-way ANOVA of mean parturition date, $F_{5,37} = 7.79$, $P = 0.0001$). Worms that saw increasing daylength gave birth in late spring-early summer light regimes ($\bar{x}_{short \rightarrow inc}$ = 29 November = May light regime, $\bar{x}_{neutral \rightarrow inc}$ = 14 December = June light regime, $\bar{x}_{long \rightarrow inc}$ = 12 January = July light regime; Table I), and in each treatment, most of the parturition dates were clustered within 1–2 months of each other (Fig. 3). Worms in constant neutral daylength showed a trend similar to those that saw increasing daylengths, giving birth in the ambient spring ($\bar{x}$ = 1 April) with all births clustered within 2 months of each other (Fig. 3). Most worms in constant short daylength gave birth from October 89 to May 1990 ($\bar{x}$ = 1 April); one worm lived in culture until November 1990, had good reproductive morphology, but produced no young. Of the four worms in constant long daylength, three gave birth from June to September 1990 ($\bar{x}$ = 22 Aug.); one worm lived until late December 1989 but produced no young. In the latter two light treatments, no consistent pattern of parturition timing was evident.

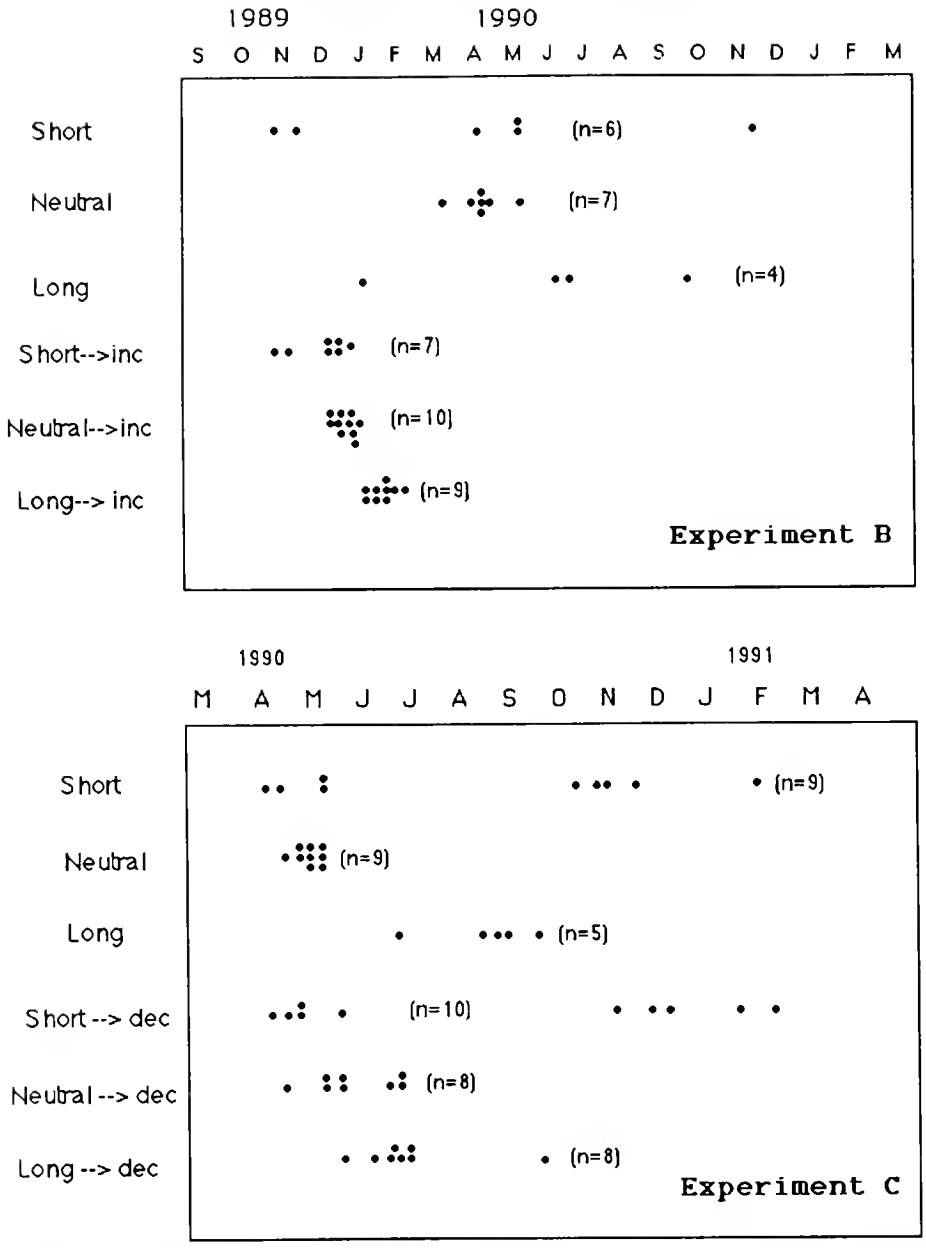

Figure 3. Parturition dates of *Neanthes limnicola* exposed to constant short (L:D 8:16), neutral (12:12), or long (16:8) daylength, initial fixed daylength followed by increasing daylength (upper: experiment B), and initial fixed daylength followed by decreasing daylength (lower: experiment C). Worms exposed to increasing daylengths were 6 months out of phase with ambient daylength, thus parturition dates in October, November, December, and January were actually in light regimes corresponding to April, May, June, and July.

Three months of fixed daylength followed by increasing daylength had a significant effect on life span (Table I; one-way ANOVA, $F_{5,37} = 7.73$, $P = 0.0001$). Worms that saw increasing daylength spent the shortest time in culture, and all three pair-wise comparisons of fixed (control) versus increasing daylengths (*e.g.*, fixed short daylength versus short → increasing daylength) showed significant differences (Fisher's LSD, $P < 0.05$ for all three comparisons).

Increasing daylength had a significant effect on fecundity (one-way ANOVA, $F_{5,37} = 7.79$, $P = 0.05$), yet there was no consistent trend (Table I). The highest mean fecundity recorded was in cultures that experienced long → increasing daylengths ($\bar{x} = 152.77$), even though these worms lived from 77 to 132 days less than all three of the fixed-daylength treatments (Fig. 4). High mean fecundity ($\bar{x} = 143.4$) also was recorded in constant neutral

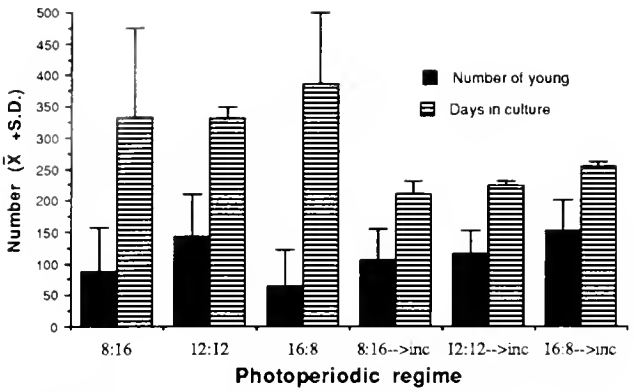

Figure 4. Fecundity (number of young born) and life span (days in culture) in experimental light regimes of experiment B. inc: increasing daylengths.

daylength, but the lowest mean fecundities were in constant long ($\bar{x}$ = 64.75) and constant short ($\bar{x}$ = 87.16) daylengths.

Comparison of pooled constant daylength (constant short, neutral, and long) with pooled increasing daylength showed a significant difference in life span. Worms that saw increasing daylengths independent of their initial fixed daylength, reproduced at a younger age than those in constant daylength ($\bar{x}_{constant}$ = 344 days, n = 17, $\bar{x}_{increasing}$ = 230 days, n = 26; t = 5.83, df = 41, P = 0.0001).

Decreasing daylength experiment (experiment C)

Seven weeks of fixed daylength followed by two months of decreasing daylength, and then constant short daylength had a significant effect on the timing of parturition (Table I; one-way ANOVA of mean parturition date, $F_{5,43}$ = 2.83, P = 0.02). Cultures in neutral and neutral → decreasing daylength reproduced in the ambient spring and showed much tighter reproductive synchrony than cultures in other light treatments, which reproduced later in the year, on average, and with much greater spread in the parturition dates (Fig. 3).

Life span was affected by decreasing daylengths (Table I; one-way ANOVA, $F_{5,43}$ = 2.76, P = 0.03). Those worms in cultures maintained at neutral and neutral → decreasing daylengths took the shortest time to reproduce ($\bar{x}_{neutral}$ = 265 days, $\bar{x}_{neutral \rightarrow decreasing}$ = 288 days).

Decreasing daylengths affected fecundity (Table I; one-way ANOVA, $F_{5,43}$ = 2.50, P = 0.04). Highest fecundities were recorded in cultures at neutral ($\bar{x}$ = 108.9 young) and neutral → decreasing ($\bar{x}$ = 106.3 young), even though on average, worms in both these treatments had a shorter life span than worms in cultures in other light treatments. Worms in long daylength had the longest life span, but produced the fewest young ($\bar{x}$ = 39.4).

Initial fixed daylength treatments, independent of shifting, had a significant effect on all three parameters. Mean parturition dates are significantly different (one-way ANOVA, $F_{2,46}$ = 5.99, P = 0.004); worms initially exposed to neutral daylengths had a mean parturition date in spring ($\bar{x}$ = 8 May) whereas those initially exposed to short daylength gave birth in spring and fall ($\bar{x}_{short}$ = 6 August) and those in long daylength reproduced in the summer and fall ($\bar{x}_{long}$ = 13 July) (Fig. 3; Fisher's LSD, $P < 0.05$ for both comparisons). Correspondingly, worms exposed to neutral daylength initially have shorter life spans than those exposed initially to either short or long daylength ($\bar{x}_{neutral}$ = 276 days, $\bar{x}_{short}$ = 365 days, $\bar{x}_{long}$ = 348 days; one-way ANOVA, $F_{2,46}$ = 5.92, P = 0.005; Fisher's LSD, $P < 0.05$ for both comparisons). Fecundity was also significantly affected (one-way ANOVA, $F_{2,46}$ = 4.77; P = 0.01); worms initially exposed to neutral daylength produced significantly more young ($\bar{x}$ = 107.64) than worms initially exposed to long ($\bar{x}$ = 63.07; Fisher's LSD, $P < 0.05$), but not to short ($\bar{x}$ = 89.21) daylengths.

Discussion

We have shown that seasonally changing photoperiod controls the timing of parturition in *Neanthes limnicola* from central California (Fong and Pearse, 1992). In the field, worms give birth mainly in late winter–spring (late February–May), and in the laboratory, parturition can be shifted to late summer–fall when the worms had been reared under seasonally changing photoperiods 6 months out of phase with ambient. In California, winter–spring light regimes increase from about (9.5:14.5 L:D) on 21 December to about (14.5:9.5 L:D) on 21 June. Thus, most worms experience increasing daylengths for 2–5 months before giving birth.

In the present study, worms exposed to increasing daylengths (corresponding to changes in light regimes from February to June) after 3 months of either fixed short, neutral, or long daylengths gave birth within 3–5 months, independent of the initial fixed daylengths to which they were exposed. That increasing daylengths act to synchronize parturitions in *N. limnicola* corresponds to our earlier findings (Fong and Pearse, 1992).

Parturition also was synchronized when the worms were exposed to fixed, neutral (12:12) daylength: nearly all gave birth at 9–11 months of age in all three experiments. In experiment A, most worms in neutral daylength gave birth at 8–10 months of age, but two worms gave birth 10–12 months later in the following late winter–spring. The latter two worms may have missed the "gate-open period," which specifies a time interval in which worms may initiate a rapid phase of oocyte growth (Olive, 1984), and had to wait another full cycle for it to reopen (see below). However, these worms never saw any changes in photoperiod with which to gauge time and synchronize reproduction. Laboratory temperatures did vary, but with little

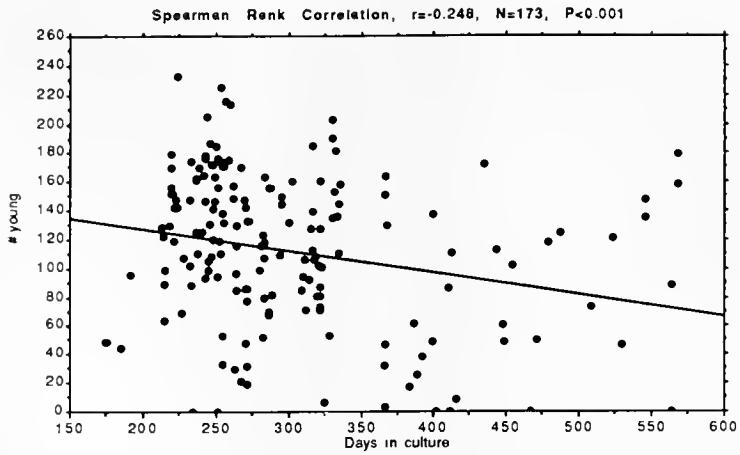

Figure 5. Regression of number of young on days in culture. Data are combined from all three experiments.

pattern by which the animals could seasonally synchronize activities (Fig. 1). Parturition by most worms under fixed, neutral daylength was in April–June 1989 in experiment A, following increasing temperatures, and in April–May 1990 in experiments B and C, following a period of little temperature change. Previous experiments with *N. limnicola* (Fong and Pearse, 1992) showed that temperature had no effect on the timing of parturition in worms exposed to seasonally changing daylength from birth.

Constant short (8:16) and long (16:8) daylength had no consistent effect on parturition synchrony but tended to desynchronize parturition especially when long daylength was combined (either before or after) with neutral daylength. Short and long daylengths also had a detrimental effect on fecundity. However, the disruptive effect of long daylength on reproductive timing and fecundity was mitigated when followed by increasing daylengths.

Decreasing daylengths did not synchronize parturition and no consistent trend was evident. Moreover, parturient synchronization was not as tight among worms in neutral → decreasing daylengths as it was in constant neutral daylengths (Fig. 3).

Exposure to different photoperiodic regimes affected fecundity. The highest fecundity in any experimental treatment was found in fixed neutral daylength (experiment A), and the lowest in long daylength (experiment C). Nevertheless, fecundities in the present experiments, in general, were lower than those previously recorded in *N. limnicola* exposed to seasonally changing daylengths continuously from birth (Fong and Pearse, 1992). Thus, a seasonal cycle of decreasing and increasing daylengths may be necessary for maximum fecundity.

Fecundity is a component of fitness. The finding that photoperiod can strongly influence fecundity and hence fitness has also been shown by Chu and Levin (1989) in the spionid polychaete *Streblospio benedicti*. In the case of *N. limnicola*, parturition during periods of increasing daylength appears to select for higher fecundity.

Although both fecundity and life span of *Neanthes limnicola* varied with photoperiod, life span varied inversely with fecundity (Fig. 5). Worms that saw short → increasing and long → increasing daylength (experiment B) had a shorter life span in culture but higher fecundity than the constant short- and constant long-daylength controls (Fig. 4). Likewise in experiment C, worms in neutral and neutral → decreasing daylengths had the highest fecundity but the shortest life span. The worm that gave birth to the most young (232) in all of our experiments lived 224 days, whereas two of the longest-lived worms (564 days each) produced only 88 and 0 young (Fig. 5). These results are inconsistent with life history theory that life span, growth, and fecundity are positively correlated (*e.g.*, Bell, 1980), but consistent with our previous findings (Fong and Pearse, 1992), and indicate that *N. limnicola* can reach maximum reproductive potential in half its lifetime. Consequently, these animals spend the later part of their lives in maintenance, waiting for a "gate-open period," before proceeding with reproduction. This conclusion indicates that the photoperiodic control resulting in seasonality of parturition in spring-early summer is under strong selection.

Our experiments reported here demonstrate that in *Neanthes limnicola* (1) parturition occurs with near-maximum fecundity in about 8–11 months under fixed, neutral photoperiod, (2) parturition is delayed and asynchronous, and fecundity is lowered under short, long, or decreasing photoperiods, and (3) parturition is earlier, synchronous, and only slightly below maximum fecundity when given seasonally increasing photoperiods after an initial 3-month exposure to either short, neutral, or long photoperiod. Moreover, changes in temperature cannot account for the synchrony displayed by the animals held

under neutral photoperiod (see above). These results from the neutral photoperiod treatments suggest that the animals are programmed to complete their life cycle, from birth to metamorphosis and parturition, in late winter and spring. The slight extension (up to 4 months) of the annual rhythm over the underlying 8–11 month endogenous rhythm is probably the result of modifying effects of seasonally changing photoperiod. This situation is similar to that described by Olive and Garwood (1983) for *Nereis diversicolor* in northern England. Worms maintained under constant temperatures and daylengths become sexually mature at the same time as worms in the field. Oocyte growth in *N. diversicolor* proceeds at the same rate at 5°, 10°, 15°, or 20°C, thus the duration of oogenesis is fixed, and the timing of its completion depends on the time of its initiation. At 5° and 10°C, two cycles of reproductive activity occur at intervals somewhat less than 1 year apart. At 15°C, all worms become sexually mature within 1 year of collection. This pattern of reproductive activity suggests an endogenous, gated reproductive rhythm of circannual periodicity, initiated at birth, which free-runs for 1–3 years (Olive and Garwood, 1983; Olive, 1984). No evidence for an exogenous, entraining zeitgeber has yet been found, however.

Carpet beetles (*Anthrenus verbasci*) appear to have a similar endogenous, circannual rhythm of pupation. Beetle larvae maintained in constant darkness at either 22.5° or 25°C, show one pulse of pupation following their first winter diapause, then emerge the following spring. But, larvae held at either 17.5° or 20°C have two peaks of pupation separated by about 41 weeks (Blake, 1959).

The main component of photoperiod that seems important for maintaining reproductive synchrony in populations of *Neanthes limnicola* is increasing daylength, as is normally experienced in the winter and spring. Not only did increasing daylength synchronize reproduction in our experiments reported here, but earlier experiments showed that the life cycle of *N. limnicola* could be shifted out of phase when the animals were held in seasonally changing photoperiods out of phase with ambient (Fong and Pearse, 1992). Similar experiments have shown that both a fall reproductive diapause in the shrimp *Heptacarpus pictus* (Custer, 1986) and gametogenesis in the sea star *Pisaster ochraceus* (Pearse and Eernisse, 1982; Pearse *et al.*, 1986) can be shifted by shifting the phase of the seasonally changing photoperiods, but these reproductive cycles remain unaffected when the animals are maintained under fixed long, neutral, or short daylengths. From the experiments with *P. ochraceus*, Pearse *et al.* (1986) suggested that an underlying endogenous rhythm was synchronized by changing photoperiod. However, unlike *N. limnicola* and *H. pictus*, which live only 1–2 years, individuals of *P. ochraceus* live decades or more, spawning year after year; photoperiodism maintains synchrony among individuals of *P. ochraceus* over many years, while it maintains synchrony within successive generations of *N. limnicola* and *H. pictus*.

In most examples of photoperiodism, including those of seasonal reproductive activity, one or more "critical daylengths" appear to trigger events leading to synchronization (Saunders, 1982). The sea urchin *Strongylocentrotus purpuratus*, a marine example, is gametogenic and full of gametes when under photoperiods less than 12 h, but gametogenesis is repressed under longer daylengths (Bay-Schmith and Pearse, 1987). Thus, gametogenesis is initiated in the fall when daylength drops below 12 h and slows down in the spring when daylength exceeds 12 h. Such examples are the basis for "hour-glass," "circadian," or similar models explaining photoperiodism (Saunders, 1982; Gwinner, 1986); critical processes require a minimum amount of light each day (hour-glass), or a particular length of time between two lighted periods (circadian), to activate a photoperiodic response. However, these models are inadequate for explaining how changing daylengths, but not fixed daylengths of any length [(or expected combinations such as short → long (experiment A)], might synchronize activities such as parturition in *Neanthes limnicola*, diapause in *Heptacarpus pictus*, or gametogenesis in *Pisaster ochraceus* (or antler shedding in reindeer, Goss, 1982, 1984). Rather, the organisms need to be able to measure daylength and compare it with earlier daylengths before initiating a photoperiodic response. As pointed out by Pearse *et al.* (1986), new models and insights are needed to explain how changing daylengths can act to synchronize seasonal activities with an underlying circannual endogenous rhythm.

Acknowledgments

We thank V.B. Pearse, A.T. Newberry, R. I. Smith, D. McHugh, and two anonymous reviewers for critiquing the manuscript. M.E. Steele coordinated the daily lab checking schedule, and J. Blaney, G. Allison, M. Paddack, S. Davis, E. Sanford, and D. Ghiglione helped maintain cultures. Facilities at Long Marine Laboratory were made available through the Institute of Marine Sciences, University of California, Santa Cruz, and its director Dr. W. Doyle. This work was supported by graduate student research funds from the Biology Board of Studies, and seed funds from the Graduate Division, University of California, Santa Cruz; the Society for Sigma Xi; the Dr. Earl H. and Ethel M. Myers Oceanographic and Marine Biology Trust; and the Friends of Long Marine Laboratory. The research was done by the senior author in partial fulfillment of the requirements for the Ph.D. degree at the University of California, Santa Cruz.

Literature Cited

Bay-Schmith, E., and J. S. Pearse. 1987. Effect of fixed daylength on the photoperiodic regulation of gametogenesis in the sea urchin *Strongylocentrotus purpuratus*. *Int. J. Invert. Rep. Dev.* **11:** 287–294.

Bell, G. 1980. The costs of reproduction and their consequences. *Am. Nat.* **116:** 45–76.

Blake, G. M. 1959. Control of diapause by an 'internal clock' in *Anthrenus verbasci* (L) (Col., Dermestidae). *Nature* **183:** 126–127.

Chu, J.-W., and L. Levin. 1989. Photoperiod and temperature regulation of growth and reproduction in *Streblospio benedicti* (Polychaeta: Spionidae). *Int. J. Invert. Rep. Dev.* **15:** 131–142.

Clark, S. 1988. A two phase photoperiodic response controlling the annual gametogenic cycle in *Harmothoe imbricata* (L) (Polychaeta: Polynoidae). *Int. J. Invert. Rep. Dev.* **14:** 245–266.

Custer, D. M. 1986. The tidepool shrimp *Heptacarpus pictus:* population dynamics at Pigeon Point, California and the effects of photoperiod on growth and reproduction. M.Sc. Thesis, University of California, Santa Cruz. 72 pp.

Fong, P. P. 1991. Environmental control of reproduction in California Nereidae (Annelida: Polychaeta). Doctoral Dissertation, University of California, Santa Cruz. 181 pp.

Fong, P. P., and J. S. Pearse. 1992. Photoperiodic regulation of parturition in the self-fertilizing viviparous polychaete *Neanthes limnicola* from central California. *Mar. Biol.* **112:** 81–89.

Garwood, P. R., and P. J. W. Olive. 1982. The influence of photoperiod on oocyte growth and its role in the control of the reproductive cycle of the polychaete *Harmothoe imbricata* L. *Int. J Invert. Rep. Dev.* **5:** 161–166.

Goss, R. J. 1982. Control of deer antler cycles by photoperiod. Pp. 1–13 in *Antler Development in Cervidae*, R. D. Brown, ed. Caesar Kleberg Wildlife Research Institute, Kingsville, Texas.

Goss, R. J. 1984. Photoperiodic control of antler cycles in deer VI. Circannual rhythms on altered day lengths. *J. Exp. Zool.* **230:** 265–271.

Gwinner, E. 1986. *Circannual Rhythms: Endogenous Annual Clocks in the Organization of Seasonal Processes.* Springer-Verlag, Berlin. 154 pp.

Olive, P. J. W. 1984. Environmental control of reproduction in Polychaeta. *Fortschr. Zool.* **29:** 17–38.

Olive, P. J. W., and P. R. Garwood. 1983. The importance of long term endogenous rhythms in the maintenance of reproductive cycles of marine invertebrates: a reappraisal. *Int. J. Invert. Reprod. Dev.* **6:** 339–347.

Olive, P. J. W., and G. Pillai. 1983. Reproductive biology of the polychaete *Kefersteinia cirrata* Keferstein (Hesionidae). II. The gametogenic cycle and evidence for photoperiodic control of oogenesis. *Int. J Invert. Reprod. Dev.* **6:** 307–315.

Pearse, J. S., and D. J. Eernisse. 1982. Photoperiodic regulation of gametogenesis and gonadal growth in the sea star *Pisaster ochraceus*. *Mar. Biol.* **67:** 121–125.

Pearse, J. S., D. J. Eernisse, V. B. Pearse, and K. A. Beauchamp. 1986. Photoperiodic regulation of gametogenesis in sea stars, with evidence for an annual calendar independent of fixed daylength. *Am. Zool.* **26:** 417–431.

Saunders, D. S. 1982. Photoperiodism in animals and plants. Pp. 65–82 in *Biological Timekeeping*, J. Brady, ed. Cambridge University Press, Cambridge.

Schierwater, B., and C. Hauenschild. 1990. A photoperiod determined life-cycle in an oligochaete worm. *Biol. Bull.* **178:** 111–117.

Smith, R. I. 1950. Embryonic development in the viviparous nereid polychaete, *Neanthes lighti* Hartman. *J. Morphol.* **87:** 414–466.

Reference: *Biol. Bull* **182**: 298–304. (June, 1992)

Ultrastructural Study of an Endogenous Energy Substrate in Spermatozoa of the Sea Urchin *Hemicentrotus pulcherrimus*

MASATOSHI MITA[1,*] AND MASARU NAKAMURA[2]

[1]*Department of Biochemistry, Teikyo University School of Medicine, Itabashi-ku, Tokyo 173, and*
[2]*Department of Zoology, Faculty of Medicine, Teikyo University, Hachioji, Tokyo 192-03, Japan*

Abstract. The morphology of the midpiece in spermatozoa of the sea urchin *Hemicentrotus pulcherrimus* was investigated ultrastructurally with particular emphasis on an endogenous substrate providing energy for motility. The midpiece was composed of a single toroidal mitochondrion surrounding the flagellum. Several lipid bodies (0.1–0.2 μm in diameter) were contained in the space between the mitochondrial outer and inner membranes. Following incubation with seawater, spermatozoa began to swim and the lipid bodies became small and finally disappeared, coincident with a decrease in the level of phosphatidylcholine (PC), an endogenous substrate for energy metabolism. In contrast, during incubation in 100 m*M* K^+-seawater, in which spermatozoa are immotile, there was no decrease in the level of PC and the lipid bodies remained intact. These results strongly suggest that the PC available for use in energy metabolism is located in the lipid bodies within mitochondria in the midpieces of *H. pulcherrimus* spermatozoa.

Introduction

Spermatozoa are stored for months as immotile cells in male sea urchins (Gray, 1928; Rothschild, 1959). Upon spawning in seawater, flagellar movement begins and respiration is activated, in close association with Na^+-dependent acid extraction (Nishioka and Cross, 1978; Christen *et al.*, 1982; Lee *et al.*, 1983; Bibring *et al.*, 1984). Internal alkalization leads to activation of dynein ATPase, resulting in the initiation of motility (Christen *et al.*, 1983).

The energy for flagellar motility of spermatozoa of the sea urchin *Hemicentrotus pulcherrimus* is produced by the oxidation of endogenous phospholipids (Mohri, 1957; Mita and Yasumasu, 1983a). Similar findings have been obtained in many other sea urchins, such as *Echinus esculentus* (Rothschild and Cleland, 1952), *Arbacia lixula* (Mohri, 1964), and *Strongylocentrotus intermedius* (Kozhina *et al.*, 1978). The spermatozoa of *H. pulcherrimus* are generally composed of various phospholipids and cholesterol (Mita and Ueta, 1988, 1989). Triacylglycerol (TG) and glycogen are present in trace amounts (Mita and Yasumasu, 1983a; Mita and Ueta, 1988). The phospholipids include phosphatidylcholine (PC), phosphatidylserine, phosphatidylethanolamine, and cardiolipin. Following incubation with seawater, the level of PC decreases, with no change in the levels of other phospholipids (Mita and Ueta, 1988, 1990; Mita *et al.*, 1990), indicating that PC may be a substrate for energy metabolism in sea urchin spermatozoa. This preferential hydrolysis of PC is related to the properties of phospholipase A_2. The phospholipase A_2 in *H. pulcherrimus* spermatozoa has high substrate specificity for PC (Mita and Ueta, 1990), which may therefore be used specifically for energy metabolism.

Recently, PC has been shown to be abundant in *H. pulcherrimus* sperm midpieces (Mita *et al.*, 1991). Following the initiation of motility, the PC content of sperm midpieces decreases significantly, while that in sperm heads and tails does not change (Mita *et al.*, 1991). Phospholipase A_2 activity is also distributed in the midpieces (Mita *et al.*, 1991). Thus, PC available for use in energy metabolism is located in the midpieces. It has also been reported that the midpieces of *Brissopsis lyrifera* (Afzelius and Mohri, 1966) and *Echinarachinus parma* (Summers and Hylander, 1974) contain a single mitochondrion and lipid globules. The lipid globules are spherical and located in the posterior region between the base of the mitochon-

Received 28 August 1991; accepted 18 February 1992.
* To whom reprint requests should be addressed.

drion and the plasma membrane (Afzelius and Mohri, 1966). Although similar lipid globules have not been observed in spermatozoa of other sea urchin species, it has been reported that lipid bodies are present in *A. punctulata* (Longo and Anderson, 1969) and *A. lixula* (Cosson and Gulik, 1982) spermatozoa. The lipid body differs from the lipid globules, because the former is located inside the mitochondrion and it is relatively smaller than lipid globules (Longo and Anderson, 1969; Cosson and Gulik, 1982). In the present study, the midpieces of *H. pulcherrimus* spermatozoa were examined ultrastructurally to clarify further the energy metabolism of sea urchin spermatozoa.

Materials and Methods

Materials

Spawning of stored spermatozoa of the sea urchin *H. pulcherrimus* was induced by injecting 0.5 *M* KCl into the coelomic cavity. Semen was always collected freshly as "dry sperm" and kept undiluted on ice.

Incubation of spermatozoa

Dry sperm were diluted 100-fold in artificial seawater (ASW) consisting of 458 m*M* NaCl, 9.6 m*M* KCl, 10 m*M* $CaCl_2$, 49 m*M* $MgSO_4$, and 10 m*M* Tris-HCl, pH 8.2. After dilution and incubation at 20°C, the sperm suspension was centrifuged at 3000 × *g* for 5 min at 0°C. In 100 m*M* K^+-seawater, Na^+ was substituted for K^+.

Determination of PC concentration

Total lipids were extracted from spermatozoa using the method of Bligh and Dyer (1959). PC levels were determined by high-performance thin-layer chromatography, as described previously (Macala *et al.*, 1983; Mita and Ueta, 1988). PC content consumed during incubation for 1 h was calculated from the absolute value of PC before and after incubation.

Oxygen consumption

Oxygen consumption in a sperm suspension was measured polarographically with an oxygen consumption recorder (MD-1000, Iijima Electronics MFG Co., Japan). Twenty-five μl of dry sperm were incubated in 2.5 ml of ASW in the closed vessel of the oximeter at 20°C.

Preparation for electron microscopy

Dry sperm were diluted 100-fold in ASW and incubated at 20°C. At appropriate intervals, the spermatozoa were prefixed in 2.5% glutaraldehyde ASW solution for 40–60 min at 4°C; a volume of sperm suspension was mixed with the same volume of cold 5% glutaraldehyde in 80% ASW. The prefixed spermatozoa were rinsed with cold ASW and post-fixed with 1% OsO_4 in ASW for 2 h at 4°C. Samples were washed in distilled water, and then immersed in saturated aqueous uranyl acetate for 1 h for block staining. After dehydration in a graded series of ethanol solutions, the specimens were embedded in epoxy resin and ultrathin sections were cut on a Reichert Ultracut ultramicrotome. After staining the specimens with lead citrate, we used a Hitachi 7000 or JEM 100 CX electron microscope to observe them.

Results

In longitudinal sections through spermatozoa of *H. pulcherrimus*, the midpiece was observed to consist of a single toroidal mitochondrion (Fig. 1). The midpiece did not contain the lipid globules observed in the spermatozoa of *B. lyrifera* (Afzelius and Mohri, 1966) and *E. parma* (Summers and Hylander, 1974). A region between the mitochondrial outer and inner membranes—intramembrane space—was dilated in a band nearest the flagellum

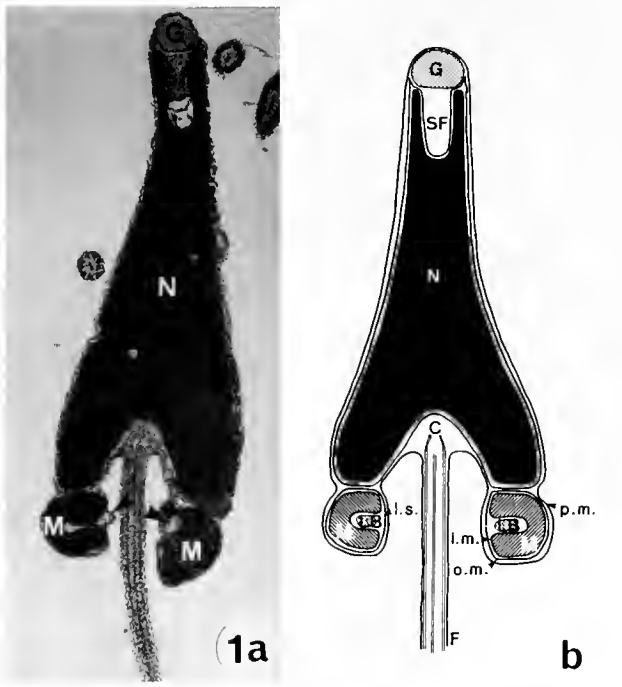

Figure 1. Longitudinal section (a) and schematic representation (b) of a spermatozoon of *Hemicentrotus pulcherrimus*. Arrow heads show lipid bodies (LB). C: proximal centriole, F: flagellum, G: acrosomal granule, M: mitochondrion, N: nucleus, o.m.: mitochondrial outer membrane, p.m.: plasma membrane, SF: subacrosomal fossa, i.s.: intramembrane space. ×19,700.

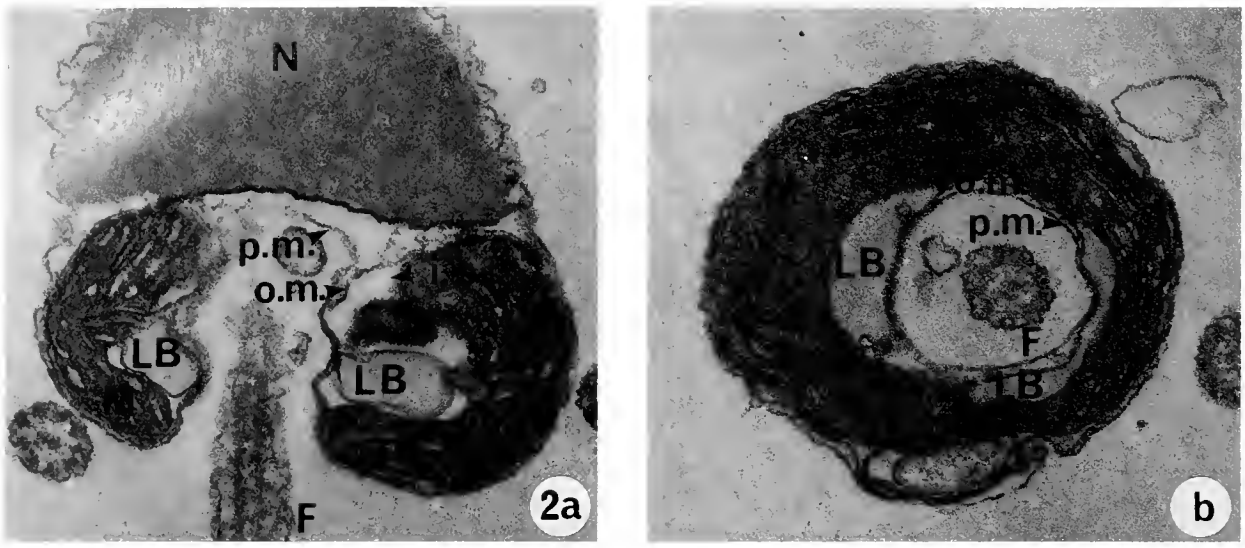

Figure 2. Longitudinal (a) and transverse (b) sections through the mitochondrial region of spermatozoa before incubation in seawater. F: flagellum, i.m.: inner mitochondrial membrane, i.s.: intramembrane space, LB: lipid body, M: mitochondrion, N: nucleus, o.m.: outer mitochondrial membrane, p.m.: plasma membrane. ×58,800.

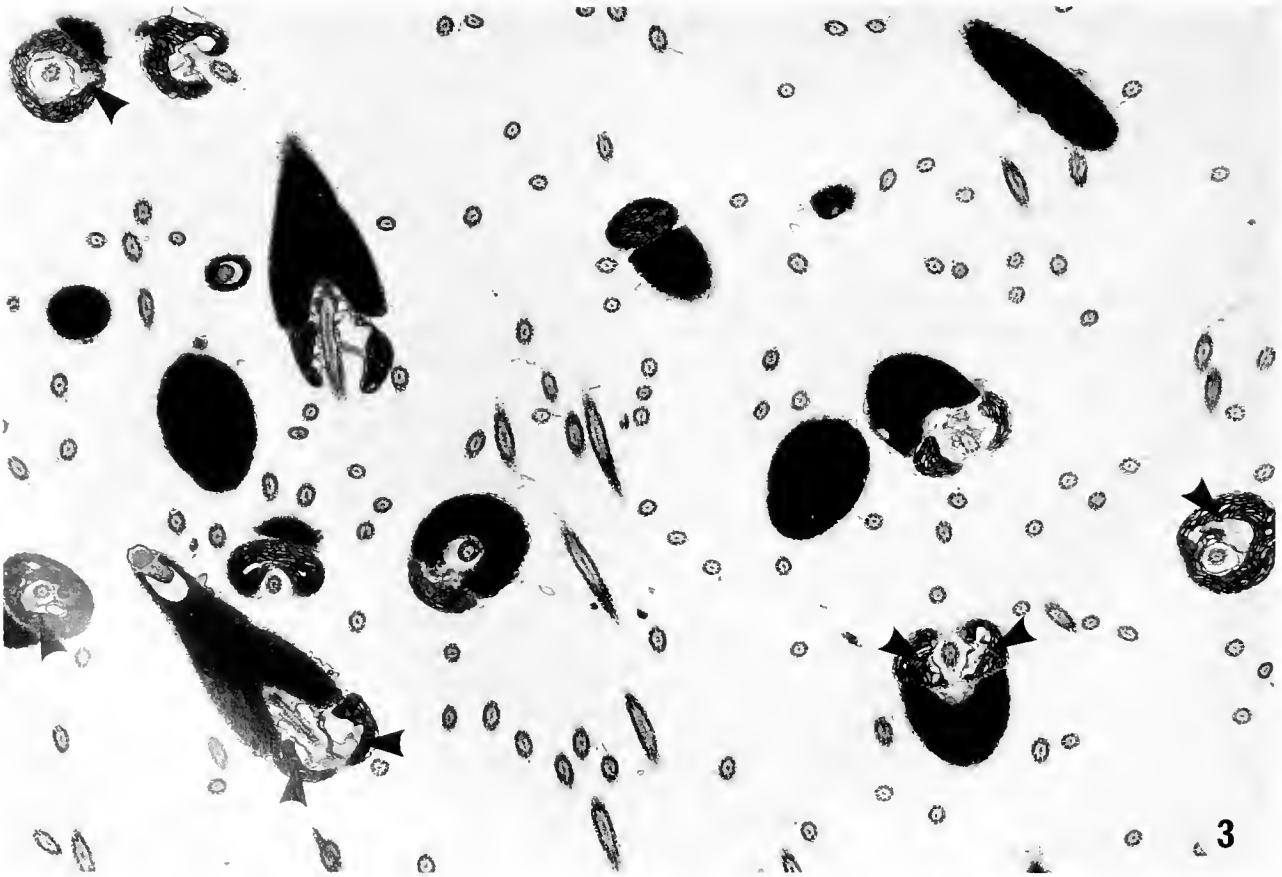

Figure 3. Electron micrograph of spermatozoa before incubation with seawater. Arrow heads show lipid bodies. ×11,800.

and contained low-electron-density lipid bodies (Fig. 2). These lipid bodies were irregular in profile and about 0.1–0.2 μm in diameter. All of the spermatozoa in semen contained the lipid bodies within their mitochondria (Fig. 3). The same lipid bodies were also observed in spermatozoa present in the testis (data not shown).

When dry sperm were diluted and incubated in ASW, spermatozoa began to swim and the amount of sperm PC decreased (Fig. 4). About 6 μg of PC was consumed in 10^9 spermatozoa following incubation for 1 h (Table I). In addition to PC consumption, respiration was activated and about 0.27 μmol O_2/h/10^9 spermatozoa was consumed. These findings confirm the previous observations (Mita and Ueta, 1988, 1990). Longitudinal and transverse sections of the midpieces of spermatozoa were examined following incubation in ASW. After 5 min of incubation, changes were noted in the structure of the inner ring of the mitochondrion. Although lipid bodies were still present, they had shrunk. In addition, a gap was observed to have opened between the plasma membrane and the mitochondrial outer membrane (Fig. 5b, e). After 30 min of incubation, the inclusion bodies and the inner ring of the mitochondrion had disappeared (Fig. 5c, f). Various structural features of the mitochondrion, such as the number of cristae and the thickness of the membranes, did not change during incubation in ASW.

Because sea urchin spermatozoa incubated in high K^+-seawater are immotile and their respiration extremely low (Schackmann *et al.*, 1981; Mita and Yasumasu, 1983b, 1984), the effect of a high-K^+ environment on the lipid bodies of the midpiece was examined. After incubation in 100 m*M* K^+-seawater for 1 h at 20°C, neither oxygen nor PC was consumed by the spermatozoa (Table I), and the lipid bodies of the midpiece remained intact (Fig. 6a, b). Thus, the disappearance of the lipid bodies was correlated with the decrease in the level of PC.

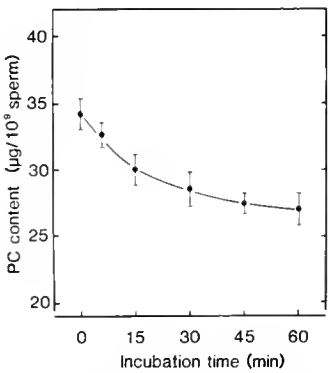

Figure 4. The change in level of phosphatidylcholine (PC) in sea urchin spermatozoa following incubation in seawater. Each value is the mean of four separate experiments. Vertical bars show S.E.M.

Table I

Phosphatidylcholine and oxygen consumption in sea urchin spermatozoa

Conditions	PC consumption (μg/h/10^9 sperm)	O_2 consumption (μmol O_2/h/10^9 sperm)
Seawater	6 ± 1	0.27 ± 0.02
100 m*M* K^+-seawater	N.D.	<0.01

Dry sperm were diluted 100-fold in either seawater or 100 m*M* K^+-seawater and incubated for 1 h at 20°C. Values are means ± S.E.M. obtained from four separate experiments. N.D., not detectable.

Discussion

The present study demonstrated lipid bodies in the intramembrane space of the mitochondrion in the sperm midpiece of *H. pulcherrimus* (Fig. 1). Following incubation of spermatozoa in seawater, these lipid bodies disappeared gradually (Fig. 5), although they still remained after incubation in 100 m*M* K^+-seawater (Fig. 6). These observations were correlated with changes in the level of intracellular PC (Fig. 4), suggesting that PC available for use in energy metabolism is related to the lipid bodies within the mitochondria of the midpiece. Similar lipid bodies have been observed in the spermatozoa of *A. punctulata* (Longo and Anderson, 1969) and *A. lixula* (Cossin and Glik, 1982). It has also been reported that *A. lixula* spermatozoa obtain energy for movement from the oxidation of endogenous phospholipid (Mohri, 1964). These findings also support the hypothesis that the lipid bodies within mitochondria are reservoirs of endogenous PC substrate in sea urchin spermatozoa.

We also showed that about 6 μg of PC was consumed in 10^9 spermatozoa following incubation for 1 h (Fig. 4, Table I). Because this amount was only $^1/_5$ of the total PC, the remaining $^4/_5$ of cellular PC may be membrane-bound and therefore inaccessible as an energy substrate for motility. About 0.27 μmol O_2/h/10^9 spermatozoa were consumed (Table I). This degree of oxygen consumption is enough to account for the consumed PC, as mentioned previously (Mita and Yasumasu, 1983; Mita *et al.*, 1990). Presumably, the fatty acid liberated from PC in the lipid bodies is metabolized through β-oxidation to produce ATP.

Unfortunately, there is little direct evidence to indicate whether the content of the lipid bodies is, in fact, PC. A cytochemical study would be useful to identify PC in the lipid bodies, although an antibody against PC would be difficult to prepare because PC is a common membrane component. We are now investigating the role and characteristics of the lipid bodies to provide useful insights

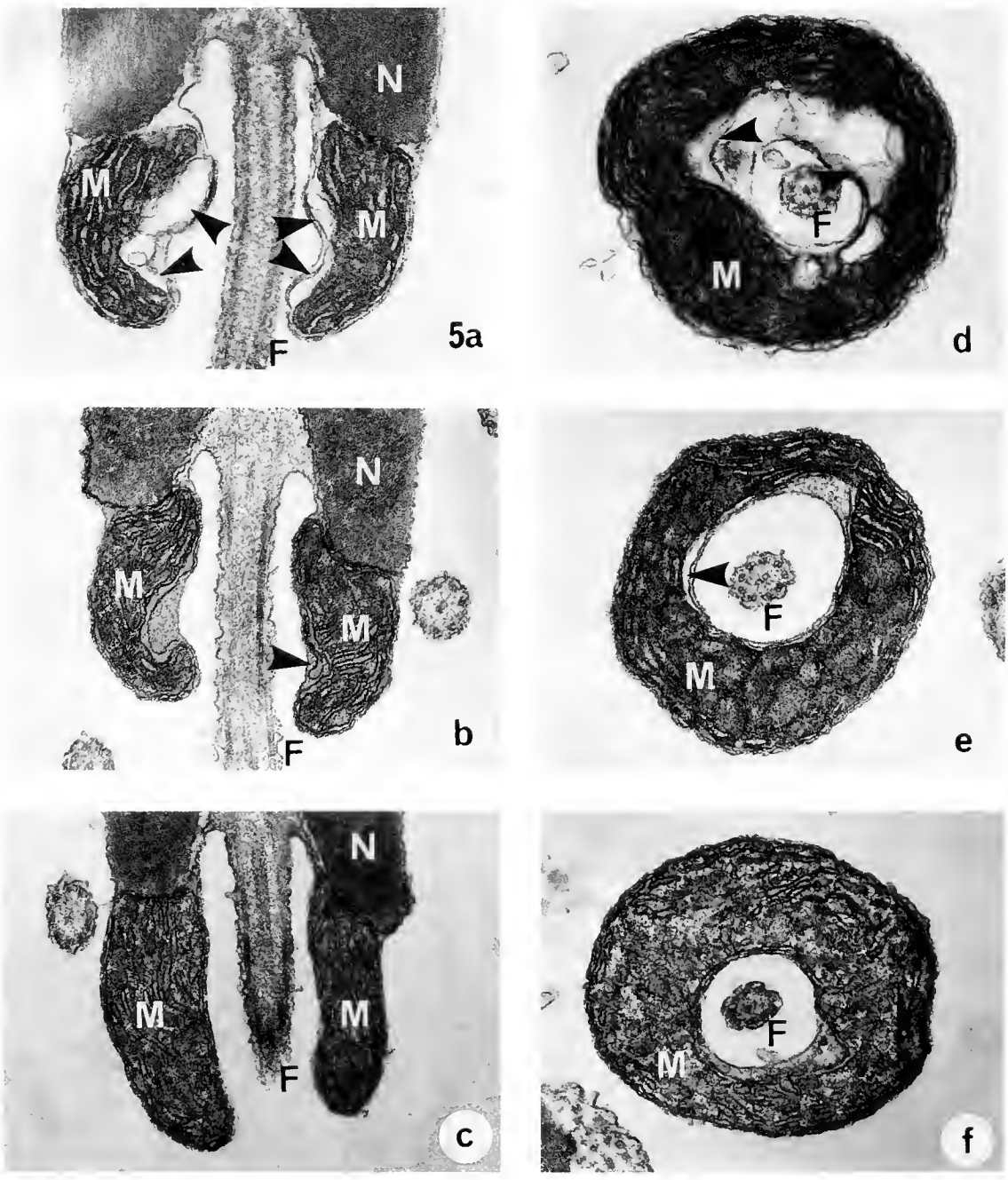

Figure 5. Longitudinal (a–c) and transverse (d–f) sections through the mitochondrial region of spermatozoa before (a, d) and after incubation in seawater for 5 min (b, e) and 30 min (c, f). Arrow heads show lipid bodies. F: flagellum, M: mitochondrion, N: nucleus. ×42,500.

into the direct mechanism of energy metabolism in sea urchin spermatozoa.

In contrast to the PC used in *H. pulcherrimus*, *Glyptocidaris crenularis* spermatozoa use TG as a substrate for energy metabolism (Mita, 1991). There are several lipid globules at the bottom of the midpiece in *G. crenularis* spermatozoa (Mita and Nakamura, 1992), similar to those in the spermatozoa of *B. lyrifera* (Afzelius and Mohri, 1966) and *E. parma* (Summers and Hylander, 1974). After incubating *G. crenularis* spermatozoa with seawater, both the number and the size of the lipid globules decreased, coincident with a decrease in the TG level.

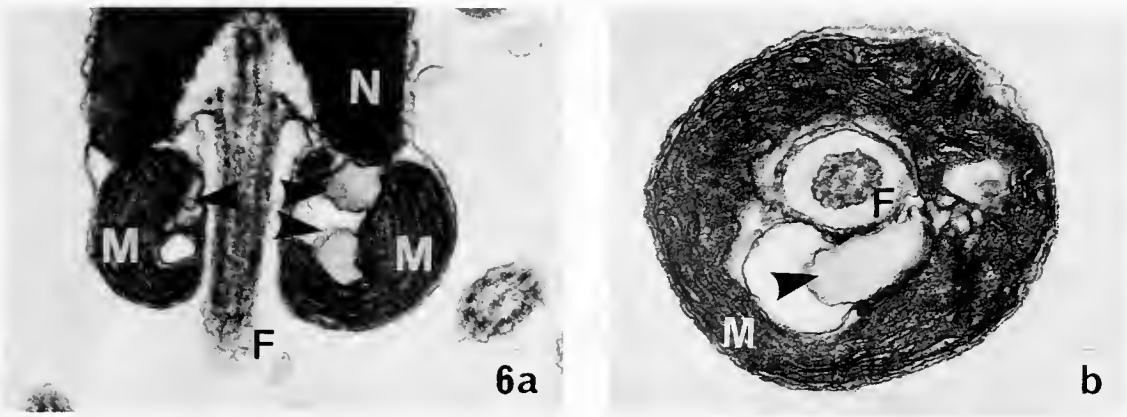

Figure 6. Longitudinal (a) and transverse (b) sections through the mitochondrial region of spermatozoa after incubation in 100 m*M* K^+-seawater for 1 h. Arrow heads show lipid bodies. F: flagellum, M: mitochondrion, N: nucleus. ×42,500.

However, neither TG (Mita and Ueta, 1988) nor lipid globules (Fig. 1) are present in *H. pulcherrimus* spermatozoa. Thus it appears that TG is related to the lipid globules.

Acknowledgments

The authors are grateful to Dr. N. Ueta, Teikyo University School of Medicine, for his encouragement and valuable advice, and to Dr. N. Usui, Teikyo University School of Medicine, and Dr. Y. Nagahama, National Institute for Basic Biology, for their valuable comments. Thanks are also extended to Dr. S. Nemoto and the staff of the Tateyama Marine Laboratory, Ochanomizu University, for their assistance in collecting the sea urchins. This work was supported in part by a Grant-in-Aid (03740396) from the Ministry of Education, Science and Culture of Japan.

Literature Cited

Afzelius, B. A., and H. Mohri. 1966. Mitochondria respiring without exogenous substrate: a study of aged sea urchin spermatozoa. *Exp. Cell Res.* **42:** 10–17.

Bibring, T. J., J. Baxandall, and C. C. Harter. 1984. Sodium-dependent pH regulation in active sea urchin sperm. *Dev. Biol.* **101:** 425–435.

Bligh, E. G., and W. J. Dyer. 1959. A rapid method of total lipid extraction and purification. *Can. J. Biochem. Physiol.* **37:** 911–917.

Christen, R., R. W. Schackmann, and B. M. Shapiro. 1982. Elevation of intracellular pH activates sperm respiration and motility of sperm of the sea urchin *Strongylocentrotus purpuratus*. *J. Biol. Chem.* **257:** 14,881–14,890.

Christen, R., R. W. Schackmann, and B. M. Shapiro. 1983. Metabolism of sea urchin sperm. Interrelationships between intracellular pH, ATPase activity, and mitochondrial repiration. *J. Biol. Chem.* **258:** 5392–5399.

Cosson, M. P., and A. Gulik. 1982. Description of the mitochondria-axoneme junction in sea urchin spermatozoa: presence of a flagellar necklace. *J. Ultrastruct. Res.* **79:** 47–57.

Gray, J. 1928. The effect of dilution on the activity of spermatozoa. *J. Exp. Biol.* **5:** 337–344.

Kozhina, V. P., T. A. Terekhova, and V. I. Stretashev. 1978. Lipid composition of gametes and embryos of the sea urchin *Strongylocentrotus intermedius* at early stages of development. *Dev. Biol.* **62:** 512–517.

Lee, H. C., C. Johnson, and D. Epel. 1983. Changes in internal pH associated with initiation of motility and acrosome reaction of sea urchin sperm. *Dev. Biol* **95:** 31–45.

Longo, F. J., and E. Anderson. 1969. Sperm differentiation in the sea urchins *Arbacia punctulata* and *Strogylocentrotus purpuratus*. *J. Ultrastruct. Res.* **27:** 486–509.

Macala, L. J., R. K. Yu, and S. Ando. 1983. Analysis of brain lipids by high performance thin-layer chromatography and densitometry. *J. Lipid Res* **24:** 1243–1250.

Mita, M., and I. Yasumasu. 1983a. Metabolism of lipid and carbohydrate in sea urchin spermatozoa. *Gamete Res.* **7:** 133–144.

Mita, M., and I. Yasumasu. 1983b. Effect of Na^+-free seawater on energy metabolism in sea urchin spermatozoa with special reference to coenzyme A and carnitine derivatives. *Gamete Res.* **7:** 259–267.

Mita, M., and I. Yasumasu. 1984. The role of external potassium ion in activation of sea urchin spermatozoa. *Dev. Growth Differ.* **26:** 489–495.

Mita, M., and N. Ueta. 1988. Energy metabolism of sea urchin spermatozoa, with phosphatidylcholine as the preferred substrate. *Biochim. Biophys. Acta* **959:** 361–369.

Mita, M., and N. Ueta. 1989. Fatty chain composition of phospholipids in sea urchin spermatozoa. *Comp. Biochem. Physiol.* **92B:** 319–322.

Mita, M., N. Ueta, T. Harumi, and N. Suzuki. 1990. The influence of egg-associated peptide on energy metabolism in sea-urchin spermatozoa: the peptide stimulates preferred hydrolysis of phosphatidylcholine and oxidation of fatty acid. *Biochim. Biophys. Acta* **1035:** 175–181.

Mita, M., and N. Ueta. 1990. Phosphatidylcholine metabolism for energy production in sea urchin spermatozoa. *Biochim. Biophys. Acta* **1047:** 175–179.

Mita, M., T. Harumi, N. Suzuki, and N. Ueta. 1991. Localization and characterization of phosphatidylcholine in sea urchin spermatozoa. *J. Biochem.* **109:** 238–242.

Mita, M. 1991. Energy metabolism of spermatozoa of the sea urchin *Glyptocidaris crenularis*. *Mol. Reprod. Dev.* **28:** 280–285.

Mita, M., and M. Nakamura. 1992. Lipid globules at the midpieces of *Glyptocidaris crenularis* spermatozoa and its relation to energy metabolism. *Mol. Reprod. Dev.* (in press).

Mohri, H. 1957. Endogenous substrates of respiration in sea-urchin spermatozoa. *J. Fac. Sci. Tokyo Univ. IV* **8:** 51–63.

Mohri, H. 1964. Phospholipid utilization in sea-urchin spermatozoa. *Pubb. Staz. Zool. Napoli* **34:** 53–58.

Nishioka, D., and N. Cross. 1978. The role of external sodium in sea urchin fertilization. Pp. 403–413 in *Cell Reproduction: In Honor of D. Mazia*, E. R. Dirksen, D. M. Prescott, and S. F. Fox, eds. Academic Press, New York.

Rothschild, Lord, and K. W. Cleland. 1952. The physiology of sea-urchin spermatozoa. The nature and location of the endogenous substrate. *J. Exp. Biol.* **41:** 66–71.

Rothschild, Lord. 1956. The physiology of sea-urchin spermatozoa. Action of pH, dinitrophenol, dinitrophenol + versene, and usnic acid or O_2 uptake. *J. Exp. Biol.* **33:** 155–173.

Schackmann, R. W., R. Christen, and B. M. Shapiro. 1981. Membrane potential depolarization and increase intracellular pH accompanying the acrosome reaction of sea urchin sperm. *Proc. Natl. Acad. Sci. USA* **78:** 6066–6070.

Summers, D. G., and B. L. Hylander. 1974. An ultrastructural analysis of early fertilization in the sand dollar, *Echinarachnius parma*. *Cell Tissue Res.* **150:** 343–368.

Reference: *Biol. Bull.* **182**: 305–323. (June, 1992)

Studies on the Structure and Function of the Larval Kidney Complex of Prosobranch Gastropods

BRIAN R. RIVEST

Department of Biological Sciences, State University of New York at Cortland, Cortland, New York 13045

Abstract. The larval kidneys of prosobranch gastropods have long been assumed to be involved in handling wastes, but with little supporting evidence. In this study, the larval kidneys of *Searlesia dira* and *Nucella canaliculata* were studied with light, electron, and fluorescence microscopy. They consist of three cell types: (1) a large external absorptive cell swollen with heterophagosomes and possessing an endocytotically active external surface; (2) an internal crystal cell with numerous vacuole-bound crystals of a calcium salt and with morphologically complex canaliculi; (3) an internal pore cell characterized by slit-pores that lead to subsurface cisternae, a tubular network, and one or two ciliated ducts that open into the hemocoel. Empirical evidence indicates that the absorptive cell rapidly takes up and stores albumen proteins from the capsular fluid. Absorptive cells were found in 17 of 19 species tested, representing three prosobranch orders, but were not found in 2 opisthobranch or 1 pulmonate species. We hypothesize that the absorptive cells have become specialized for the uptake of capsular albumen prior to the functional differentiation of the gut. However, the nutritional importance of the absorbed albumen proteins and the functions of the crystal and pore cells are presently unknown. No evidence for an excretory function was found for the larval kidney complex; it may be a vestigial protonephridium, the components of which have become disorganized and functionally altered.

Introduction

Larval kidneys are prominent structures found in the neck region in many prosobranch embryos. They have long been considered to excrete actively or to accumulate waste products (Bobretzky, 1877; Heymons, 1893; Glaser, 1904; Pelseneer, 1911; Franc, 1940). The hypothesis that these structures are organs of accumulation is attractive because it explains the large cells as an adaptation for encapsulated development (Pelseneer, 1911; Eisawy and Sorial, 1974). Embryos might better sequester their wastes than pollute the surrounding capsular fluid.

Prosobranch larval kidneys have been described as paired, laterally located uni- or multicellular structures that protrude from the region behind the velum, and are usually considered to be of ectodermal origin (Casteel, 1904; Portmann, 1930; Franc, 1941). Bobretzky (1877), Conklin (1897), Glaser (1904), and D'Asaro (1966) described them as enlarged ectodermal cells that either released excretory granules or were completely cast off before hatching. In *Ocenebra aciculata*, Franc (1940) found the larval kidneys to consist of a larger outer vacuolated cell overlying a smaller internal cell containing green vacuoles. He tried unsuccessfully to demonstrate experimentally an excretory function of the larval kidneys. However, he did find what he described as yolk platelets in the larger external cell of *O. aciculata* and *Thais haemastoma* (Franc, 1940, 1941). Although Franc realized that the presence of yolk would suggest that larval kidneys were involved in something other than excretion, he retained the classical assumption that they were organs of waste accumulation and hypothesized that the yolk supplied the energy used for waste acquisition (Franc, 1941).

Although the presence of larval kidneys in prosobranch embryos has been reported by numerous authors, they are poorly understood. The material accumulated in the enlarged ectodermal cells of the larval kidneys has not been identified, although Glaser (1904) claimed that an aqueous extraction of larval kidney cells contained dilute urea. Furthermore, little is known of the ultrastructure of prosobranch larval kidneys. In this study I describe the ultrastructure of the three cells that make up the larval

Received 30 December 1991; accepted 17 March 1992.

kidney in the marine snail *Searlesia dira* and the ontogeny of these cells, from the early trochophore to the mid-veliger stage. Similar observations of the larval kidneys of *Nucella canaliculata* are included. Morphological and experimental evidence shows that the large size of the larval kidneys is due to endocytotically absorbed albumen proteins, not stored waste products. Twenty other species of gastropods were tested for larval kidneys that absorb dissolved proteins from the surrounding fluid.

Materials and Methods

Collection of egg masses and egg capsules

Most egg masses or capsules used in this study were collected in intertidal or subtidal areas around San Juan Island, Washington, or were obtained from animals maintained in aquaria at the Friday Harbor Laboratories. Egg capsules of *Ocenebra japonica* were collected on oyster flats in southern Puget Sound, Washington, and those of *Nucella lapillus* at York Beach, Maine.

Specimen preparation for light and electron microscopy

Searlesia dira and *Nucella canaliculata* embryos to be examined with scanning electron microscopy were removed from their capsules, rinsed in filtered seawater, relaxed with 7.5% magnesium chloride and fixed for one to two hours at room temperature in 2% osmium tetroxide in 1.25% sodium bicarbonate at pH 7.2 (Wood and Luft, 1965). The embryos were then rinsed in distilled water, dehydrated in ethanol, critical point dried, mounted, and coated with gold. The embryos were examined with an ETEC Autoscan or a JEOL JSM-35 scanning electron microscope.

Satisfactory fixation of larval kidney cells for transmission electron microscopy was difficult. Fixatives that appeared suitable for adjacent ectoderm and subjacent endoderm often produced fixation artifacts in the larval kidney, particularly in the outer absorptive cell. The heterophagosomes of this voluminous cell appeared particularly sensitive to the osmolarity of the fixative. The larval kidneys of *Searlesia dira* were most satisfactorily fixed in a cacodylate buffered glutaraldehyde solution containing ruthenium red, a method modified from Cavey and Cloney (1972). Embryos removed from their capsules and rinsed with seawater were placed in 2% glutaraldehyde in a solution buffered by 0.2 *M* sodium cacodylate adjusted to 1000–1100 mOsM with sucrose and containing 0.05% ruthenium red and 0.002 *M* calcium chloride. Final pH was adjusted to 7.4. This fixative did not work well for the larval kidneys of *Nucella canaliculata*, which showed better preservation using a 3% glutaraldehyde solution containing 0.1 *M* sodium cacodylate and 0.001 *M* calcium chloride and adjusted to 1000–1100 mOsM with sodium chloride. This worked satisfactorily for light microscopy but produced severe artifacts at the ultrastructural level.

The embryos were postfixed in 2% osmium tetroxide in freshly mixed 1.25% sodium bicarbonate (pH 7.2) for one hour at room temperature. The embryos were then dehydrated and embedded in EPON (Luft, 1961).

One micrometer thick sections for light microscopy were stained with a mixture of Azure II and methylene blue in 0.5% sodium borate (Richardson *et al.*, 1960). Serial thin sections for transmission electron microscopy were stained with uranyl acetate and lead citrate (Reynolds, 1963) and examined with a Philips EM-300 electron microscope.

The *Searlesia dira* developmental stages that were sectioned included early trochophores prior to or just after the initiation of nurse egg feeding, late trochophores near or just after the end of nurse egg feeding, early veligers with the cephalopedal elements elevated from the main embryonic body and the mantle fold near the anterior end, and mid-veligers with greater differentiation of the cephalopedal elements and a small mantle cavity. The *Nucella canaliculata* developmental states that were sectioned included late trochophores, early veligers, and mid-veligers.

Exposure of embryos to test solutions

To study the uptake of material by the larval kidneys, embryos were initially exposed to isosmotic solutions of ferritin. Later experiments included placing embryos in isosmotic solutions containing fluorescein, bovine serum albumin (BSA), capsular albumen, fluoresceinisothiocyanate labelled BSA (FITC-BSA, Sigma Chemical Company), and/or FITC-capsular albumen.

The capsular albumen proteins of *Searlesia dira* were labelled with FITC as follows: (1) seventy capsules less than three weeks old (before the embryos had begun to feed on the nurse eggs) were opened in 4°C filtered seawater containing 10 μg/ml of the antibiotic rifampicin. The albumen was separated from the embryos and nurse eggs by using a 152 μm Nitex screen. (2) The seawater-diluted albumen was centrifuged to remove any debris. (3) The supernatant was placed in dialysis tubing on a bed of Aquacide (CalBiochem) to extract water and concentrate the proteins. (4) The protein content of the solution was estimated by spectrophotometrically measuring absorbance at 280 mμ and assuming the extinction coefficient of capsular albumen is 6.2 (intermediate between the extinction coefficients of BSA and human serum albumin). (5) Sufficient $NaHCO_3$ was added to make a 0.1 *M* solution with a pH of about 9.2. (6) FITC (approximately one-tenth the weight of the estimated protein in the solution) was dissolved in one drop of 0.5 *N* NaOH, then the buffered albumen solution was added. (7) The

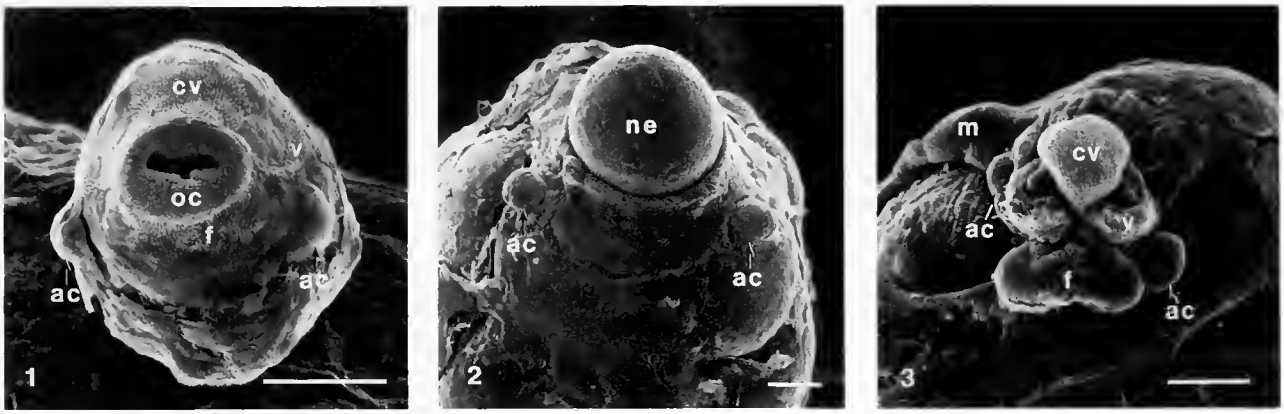

Figure 1. SEM of a *Searlesia dira* embryo shortly after the onset of feeding on nurse eggs showing the protruding absorptive cells of the larval kidneys.

Figure 2. SEM of an older feeding stage of *S. dira* fixed while swallowing a nurse egg. The absorptive cells are larger and protrude further from the embryo's surface.

Figure 3. SEM of an *S. dira* intracapsular veliger showing the developing cephalopedal structures and the bulbous nature of the left absorptive cell.

Scale bars represent 100 μm; ac, absorptive cell of the larval kidney; cv, cephalic vesicle; f, foot; oc, oral cilia; m, mantle margin; ne, nurse egg; v, velum.

mixed solutions were incubated at 20°C for 20 h. (8) Unreacted FITC was removed by adding 50 mg powdered charcoal per mg FITC, spinning the charcoal down after 30 min and repeating this step. (9) The pH was adjusted to that of seawater with 0.1 *N* HCl and the final solution was dialyzed against seawater for four hours. This solution contained approximately 0.37 mg/ml protein, as determined spectrophotometrically.

Embryos were transferred to a test solution at 12°C after first being removed from their capsules and rinsed in filtered seawater. After periods of 10 min to 4 h, the embryos were rinsed again in seawater and examined using light, fluorescence, or transmission electron microscopy.

To examine the nature of the crystals found in one of the inner cells of *Searlesia dira* larval kidneys, live and heat-killed embryos were examined with polarized light while exposed to one of the following solutions: Millonig's phosphate buffer at pH 3.5 to 7.5; 0.1 *M* glycine at pH 9.2; buffered (pH 8.5) and unbuffered (pH 3.0) 10% formalin in seawater; 0.1 *M* EGTA (pH 9.0) in seawater; 100% ethanol; 10% Triton-X 100 in distilled water; saturated aqueous calcium chloride. Some live embryos were placed in a 2% alizarin red S solution in seawater for 48 h.

Some *Searlesia dira* embryos at the early veliger stage of development were micro-injected in the hemocoel behind the velum with an isosmotic ferritin solution. After 10 to 60 min, these embryos were fixed and prepared for examination with transmission electron microscopy.

Larval kidney histochemistry

The periodic acid-Schiff reaction was performed on 10 μm thick serial paraffin sections of *Searlesia dira* embryos fixed in Carnoy's fixative (Humason, 1972). As a control for glycogen, some sections were incubated in saliva at 37°C for 1 h before applying the PAS technique. The hexamine silver method (Pearse, 1972) was used to test for urates in paraffin sections of embryos fixed in 100% ethanol or Carnoy's fixative.

Results

Searlesia dira

External morphology of the larval kidneys. The two larval kidneys develop laterally on the embryo just posterior to the mouth (Fig. 1). They are discernible as protrusions on live embryos within four weeks of oviposition at 12°C, before the embryos have begun to feed on nurse eggs. At this early trochophore stage, the larval kidneys are circular in outline and 40 to 50 μm in diameter. During the one to two and a half weeks that the embryos are feeding on nurse eggs and for a week or two afterwards, the larval kidneys enlarge, bulging outward from the embryo (Fig. 2). As they enlarge they become more hemispherical, but their shape and size varies among embryos.

After nurse egg feeding has ended, the cephalopedal elements grow out from the previously roundish embryo. At this point the larval kidneys are on the neck region of these veligers, posterior to the developing velar lobes but anterior to the forming mantle cavity. The right larval kidney has typically become elongate in the dorso-ventral axis, extending dorsally from the midlateral line. In contrast, the left larval kidney has become more bulbous, protruding at the level of, or slightly ventral to, the left lateral midline (Fig. 3).

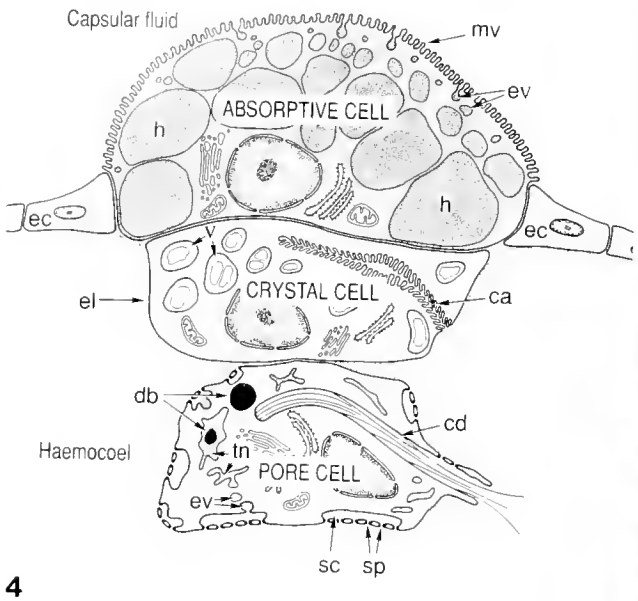

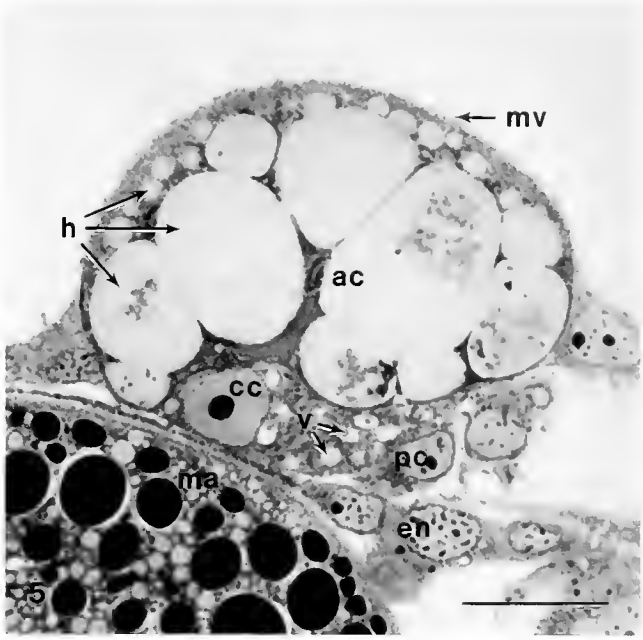

Figure 4. Schematic drawing of a section through the three cells making up a larval kidney complex in a *Searlesia dira* veliger. Proportions are not relative. The crystals in the vacuoles of the crystal cell dissolve during fixation and were not seen in sections.

Figure 5. One micrometer thick section of the larval kidney complex in *S. dira*. The pore cell can only be positively identified in fixed material with TEM.

Scale bar represents 25 μm; ac, absorptive cell; ca, canaliculus; cc, crystal cell; cd, ciliated duct (one of two); db, dark body; ec, ectoderm; el, external lamina; en, endoderm; ev, endocytotic invaginations and vesicles; h, heterophagosomes; ma, macromere of swallowed nurse egg; mv, microvilli; pc, pore cell; tn, tubular network; sc, subsurface cisternae; sp, split pores; v, vacuoles.

The larval kidneys have achieved their maximum size by the time the advancing mantle margin begins to form the mantle cavity. The elongate right larval kidney can be up to 100 μm long and 35 μm wide, while the more spherical left larval kidney may reach 80 μm in diameter. The larval kidneys have no distinctive coloration, but appear more yellowish-white than adjacent ectodermal cells. Both larval kidneys maintain their relative shape, position, and size during the intracapsular veliger phase of development. During the intracapsular metamorphosis that follows, the larval kidneys diminish in size until they are no longer discernible before the end of velar lobe resorption. There is no evidence suggesting that the larval kidneys fall off or spontaneously release their contents into the lumen of the capsule. There is also no evidence of a pore near the larval kidney as reported in *Ilyanassa obsoleta* (Tomlinson, 1987).

Ultrastructure of the larval kidneys of Searlesia dira. Each larval kidney is a complex of three cells: absorptive, crystal, and pore cells. An exception was found in one sectioned embryo that had a small second crystal cell adjacent to the main one. Absorptive cells are named after their ability to absorb external proteins. Crystal cells have been reported in prosobranch larval kidneys by Portmann (1930) and Fioroni (1985). Larval kidney pore cells have surface specializations similar to pore cells found in molluscan connective tissue (Sminia and Boer, 1973), although they are called rhogocytes by Fioroni *et al.* (1984). Each cell type is identifiable in thin sections of the prefeeding trochophores, the earliest stage examined. Figure 4 schematically illustrates the distinctive features of these three cells in an early veliger.

Absorptive cell. The absorptive cell is the outermost and largest of the three cells that comprise the larval kidney complex (Figs. 4, 5). The external surface of the absorptive cell is exposed to the capsular fluid surrounding the embryo. Morphological and experimental evidence indicate that it is a surface active in receptor-mediated endocytosis. It is elaborated into numerous microvilli up to 1.8 μm long that have endocytotic vesicles forming around their bases (Fig. 6). Adjacent endocytotic vesicles apparently fuse shortly after their formation, and the resulting small heterophagosomes fuse with larger, deeper heterophagosomes. The size of the absorptive cell may be due mostly to a few large heterophagosomes, which can reach 35 μm in diameter. In live embryos, large heterophagosomes can easily be detected in the absorptive cell with light microscopy; they appear refractile and colorless.

When embryos are soaked in a ferritin solution for 10 min or more, ferritin is found in endocytotic vesicles and heterophagosomes (Fig. 6). Thus, the heterophagosomes contain material brought into the cell by endocytosis. In untreated embryos, the contents of the heterophagosomes appear fairly uniform with scattered granules, fibrils, or membranous structures. The density of the contents varies among the heterophagosomes within a cell. This appears to be due to differences in concentration of the contents, not to a segregation of material brought into the cell. This is supported by the fact that ferritin is eventually found in all the heterophagosomes in treated embryos. After an embryo has soaked 20 min in a reddish ferritin solution at 15–18°C, the absorptive cell takes on a light reddish color. This color is restricted to small heterophagosomes in the external cortex of the cell. After another 30 min in the solution, the color can be perceived in larger heterophagosomes deeper inside the cell. After an hour or more, the absorptive cells are deep red. This contrasts with the rest of the ectoderm which has remained translucent and colorless. There is also no concentration of ferritin in cells lining the gut.

The heterophagosomes comprise an estimated 80–90% of the absorptive cell's volume when the cell has reached its maximum size. The nucleus is usually centrally located, surrounded by heterophagosomes that indent the nuclear membrane. Few organelles occur in the apical cytoplasm; Golgi cisternae, mitochondria, and dense concentrations of rough ER are found laterally and basally. The ground cytoplasm appears more electron-dense than that of adjacent ectodermal cells or the subjacent crystal cell (Fig. 7, upper right).

The heterophagosomes showed a positive periodic-acid Schiff reaction which did not change after incubation of sections with saliva. This indicates the presence of a carbohydrate or carbohydrate-protein complex, but not of glycogen (Humason, 1972). Also, glycogen was not seen in electron micrographs. Tests for urates were negative, and no crystals or large granules were found in the heterophagosomes or cytoplasm. The heterophagosomes contained a few myelinic bodies, but these were uncommon and probably fixation artifacts. Experimental evidence (described below) indicates that the heterophagosomes contain albumen proteins taken in from the capsular fluid.

Crystal cell. The crystal cell is subjacent to the absorptive cell (Figs. 4, 5, 7). The plasmalemmae of these two cells are closely apposed, although occasionally small intercellular spaces are found. Junctional complexes between them were not found. The crystal cell covers most of the inner surface of the absorptive cell.

In live embryos, the crystal cell can be discerned under the absorptive cell because of its crystals. These crystals can be seen most easily in early veliger stages. They are irregularly shaped and usually occur singly within vacuoles, but may be in clusters of up to five crystals. The crystals measure up to 5 μm in diameter and are birefringent under polarized light. There are from 20 to 60 crystals in each crystal cell in early veligers. The crystals are solubilized, as determined by the loss of birefringence, within 2–5 min in heat killed embryos in pH 3.5 Millonig's phosphate buffer or in pH 9.0 0.1 *M* EGTA in seawater. They quickly dissolved when live embryos were fixed in unbuffered pH 3.0 10% formalin, but not in buffered pH 8.5 formalin. The crystals were not solubilized within 10 min in phosphate buffers with a pH from 5.0 to 7.5, in pH 9.2 0.1 *M* glycine, in ethanol, or in live embryos in the EGTA solution. The crystals quickly dissolved in 1 *N* NaOH and in a 10% solution of the detergent Triton-X 100 as soon as the vacuoles containing the crystals broke open. However, in 10% Triton-X 100 made up in a saturated calcium chloride solution, the crystals dissolved more slowly after the vacuoles were lysed. In live embryos that were soaked in a filtered 2% alizarin red S solution in seawater for 24 h, the normally lightly greenish-yellow crystals were reddish, as was the growing edge of the shell.

The distinctive features of the crystal cell in sectioned material are the presence of numerous membrane-bound vacuoles and a complex canaliculus. The vacuoles are few and small in pre-feeding trochophores (Fig. 8), but they become larger and more numerous as development proceeds (Fig. 7). The vacuoles originally contained the crystals that were solubilized during fixation. The appearance of the vacuolar contents varies with the fixation used, but they generally appear light under light and electron microscopy. In material fixed in cacodylate buffered glutaraldehyde with ruthenium red and post-fixed in osmium tetroxide, the contents include small granules, fibrils, and membranous or myelinic bodies. Larger electron-dense granules are occasionally found, especially when osmium tetroxide is used as the primary fixative. These may be the remnants of partially dissolved crystals.

The canaliculus that also characterizes the crystal cell is morphologically complex and ends blindly. Its development is associated with the development of a ciliated duct in the pore cell. In the early trochophore, the opening of the canaliculus faces the pore cell in an area surrounded by a zonula adherens between these two cells (Fig. 8). At this stage there is no communication between the lumen of the canaliculus and the nearby hemocoel. The walls of the canaliculus possess numerous plications and microvilli that protrude into the lumen, vastly increasing the surface area of the canaliculus. Cilia arising from a duct in the pore cell extend into the lumen of the canaliculus. The canaliculus can extend for most of the length of the crystal cell before it ends. It has many short side branches, and it may bifurcate near its blind end. As development proceeds, the plications and microvilli become more nu-

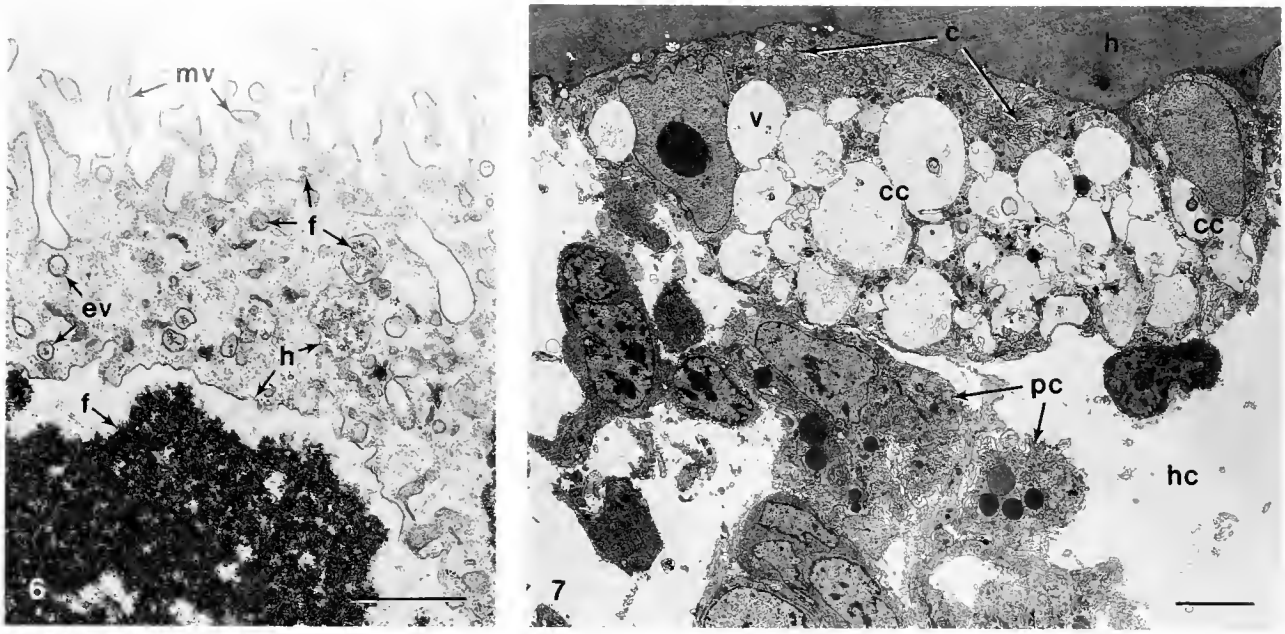

Figure 6. TEM of the external border of an absorptive cell in a *Searlesia dira* trochophore that had been soaked in a ferritin solution for 2 h prior to fixation, illustrating the endocytotic uptake of ferritin and its accumulation in heterophagosomes. Scale bar represents 1 μm.

Figure 7. TEM showing two crystal cells, a pore cell and the inner edge of the absorptive cell in a larval kidney of an early *S. dira* veliger. Most larval kidney complexes have only one crystal cell. The pore cell at this stage has little contact with the crystal cell, and has become branched. Scale bar represents 5 μm.

c indicates the canaliculus; cc, crystal cell; ev, endocytotic vesicles; f, ferritin; h, heterophagosomes of absorptive cell; hc, hemocoel; mv, microvilli; pc, pore cell; v, vacuole.

merous and more cilia grow into the canaliculus from the pore cell as the canaliculus becomes longer (Fig. 9). Occasional invaginations of coated membrane in the canalicular wall and nearby coated vesicles suggest receptor-mediated endocytotic uptake of material from the canalicular lumen.

By the time the embryo has developed into an early veliger, the crystal cell has lost its close association with the pore cell. These two cells still adjoin each other in a small area, but junctional complexes between them are no longer found. With the separation of these cells, the cilia from the pore cell no longer extend into the canaliculus of the crystal cell. Both the canaliculus of the crystal cell and ciliated duct of the pore cell now open into the hemocoel. However, the lumen of the canaliculus has become generally occluded by plications and microvilli. These structures fill the canalicular opening so that it is reduced to a web of anastomosing slits (Fig. 10). Only at one or two sites inside the cell does the lumen of the canaliculus open up into spaces that are lined by microvilli (Fig. 11). At these locations, the contents of the lumen appear finely granular. Elsewhere there is very little space within the walls of the canaliculus. Even the finger-like side branches contain long microvilli that fill the lumen. A transverse section of these filled branches appears as two concentric rings of unit membrane (Fig. 11).

Pore cell. The pore cell is the inner most of the three cells which comprise the larval kidney complex. It is characterized by slit-pores on the cell surface leading to subsurface cisternae, an extensive network of membranous tubules, and one or two ciliated ducts that eventually open into the hemocoel.

In the prefeeding trochophore, the pore cell is discoid and adheres closely to the hemocoelic side of the much larger crystal cell (Fig. 8). It is relatively undifferentiated, having few if any slit-pores and little tubular network. At this stage about six cilia arising from a shallow invagination have grown into the canaliculus of the crystal cell. The invagination deepens and the cilia become more numerous as the cell continues to differentiate (Fig. 9). As the crystal cell and pore cell become less closely associated, the cilia may extend into the hemocoel.

As the pore cell enlarges and differentiates, it grows away from the crystal cell into the hemocoel and becomes branched. As seen by Nomarski differential interference contrast microscopy, the branches attenuate into filopodia that extend toward the esophagus or to nearby ectodermal

cells. The cell body is thus suspended in the hemocoel underneath the crystal cell.

The cell surface develops slightly flattened, interdigitating finger-like processes that lie over spaces called subsurface cisternae (Skelding and Newell, 1975) (Figs. 12–14). The subsurface cisternae are typically around 200 to 300 nm deep, but their width varies considerably and in relation to the number of processes that form their roof. Although subsurface cisternae eventually develop under most of the cell surface, they are not interconnected.

The interdigitations are separated by slit-pores of a uniform 22.5 to 24.0 nm width that connect the subsurface cisternae with the hemocoel. The gap may contain fibrous material, but there was no evidence suggesting that the slit-pore is spanned by a diaphragm or membrane. An external lamina covers the surface of the pore cell, although in many preparations it has separated from the cell surface, possibly a result of fixation (Fig. 14). A dense material lies beneath the plasmalemma on either side of the slit-pores (Figs. 12, 13).

The floor of the subsurface cisternae consists of an endocytotically active plasmalemma. Invaginations of coated membrane pinch off to form vesicles that contain material brought in through the slit-pores (Fig. 14). The slit-pores could be a site of filtration, although particles as large as ferritin injected into the hemocoel pass through the slit-pores into the subsurface cisternae and are taken up by endocytotic vesicles (Fig. 15). The external lamina, however, may act as a partial barrier to the passage of ferritin because the density of ferritin within the subsurface cisternae was less than that in the hemocoel.

An extensive tubular network is found throughout the cytoplasm of the pore cell. This anastomosing network contains material taken in from the subsurface cisternae by endocytosis. Ferritin injected into the hemocoel is found within 10 to 15 min in endocytotic vesicles and the tubular network (Fig. 15). In non-injected embryos, a very fine fibrillar material is found adjacent to coated membranes in the subsurface cisternae, in endocytotic vesicles, and in some parts of the tubular network (Fig. 16).

Some inflated parts of the tubular network contain dark bodies. The dark bodies appear homogeneous and consist of a finely granular material. Small dark bodies may be surrounded by regions of the lumen of the tubular network (Fig. 16, near top), but this is not true with large dark bodies (Figs. 7, 15, 16, near bottom, and 17). Dark bodies are apparently formed by a condensation of material taken up endocytotically from the subsurface cisternae and channeled into the cell by the tubular network. Although the dark bodies appear electron dense in the transmission electron microscope, they are colorless and refractile in live embryos.

Golgi complexes are often found near enlarged regions of the tubular network (Fig. 17). Small vesicles about 80 nm in diameter frequently found near the Golgi cisternae may arise from the ends of the Golgi cisternae and fuse with the tubular network.

During development, the ciliated inpocketing of the pore cell deepens until the cilia arising from the proximal end of the duct no longer extend distally beyond the duct opening into the hemocoel. A second ciliated duct develops, apparently separate from any association with a canaliculus in the crystal cell. Regardless, it is morphologically indistinguishable from the first duct. As development of these ducts proceeds, additional cilia form, both at the proximal ends and scattered along the walls. Transverse sections of each duct reveal from 10 to 70 cilia. The number becomes greater in distal regions of the ducts and with greater cell differentiation. Occasional inpocketings of coated membrane indicate a low level of endocytotic activity. The duct walls are surrounded by a continuous plasmalemma for most of their length, but are perforated by a few slit-pores in a some distal areas (Fig. 16). In contrast to the other slit-pores, these are openings between the duct lumen and the hemocoel. When present, there are usually only one to five slit-pores in a transverse section through a ciliated duct. Even when they are more numerous, they have never been seen to occur around more than one third of the periphery of the duct, nor do they occur along much of the duct length. Presumably, the beating of the cilia in the duct could draw hemolymph in through the slit-pores. However, no ferritin was found in the ciliated ducts of embryos that had been injected with ferritin fifteen minutes before fixation.

The internal walls of the duct occasionally possess slit-pores leading to subsurface cisternae (Fig. 16). These structures have the same morphology as those on the peripheral cell surface and show some endocytotic activity, but are not common.

In the mid-veliger stage, prior to the formation of a mantle cavity into which the cephalopedal elements can be withdrawn, the distal region of each ciliated duct is found in a tubular outgrowth from the pore cell. The walls of this tube may be as thin as 0.3 μm, but are only occasionally perforated by slit-pores even though some slit-pores leading to subsurface cisternae are found on the hemocoelic surface of the tube. As in the more proximal regions of the duct, some cilia arise within this tubular section. The ciliated ducts' opening into the hemocoel has no morphological specializations, although cilia originating from within and around the opening extend into the hemocoel.

The branches of the pore cell containing the ciliated ducts do not appear to be extending towards a particular point within the embryo. The distal tubular sections of the ducts and their openings were found in a variety of locations: just beneath nearby ectodermal cells, internally

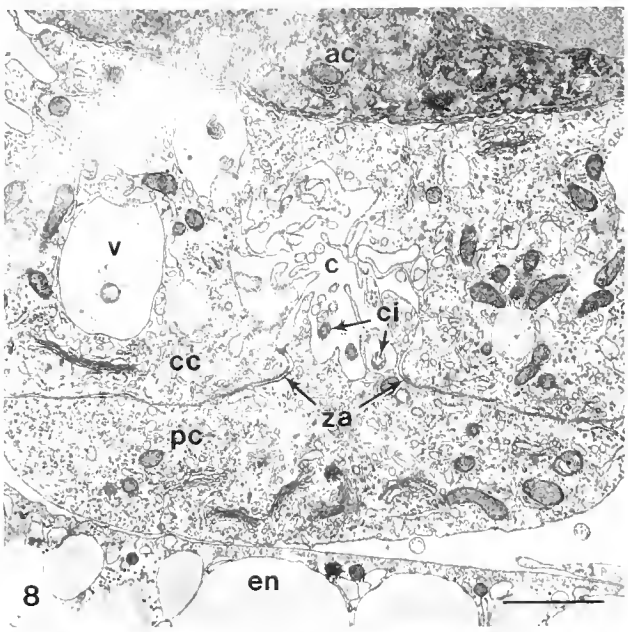

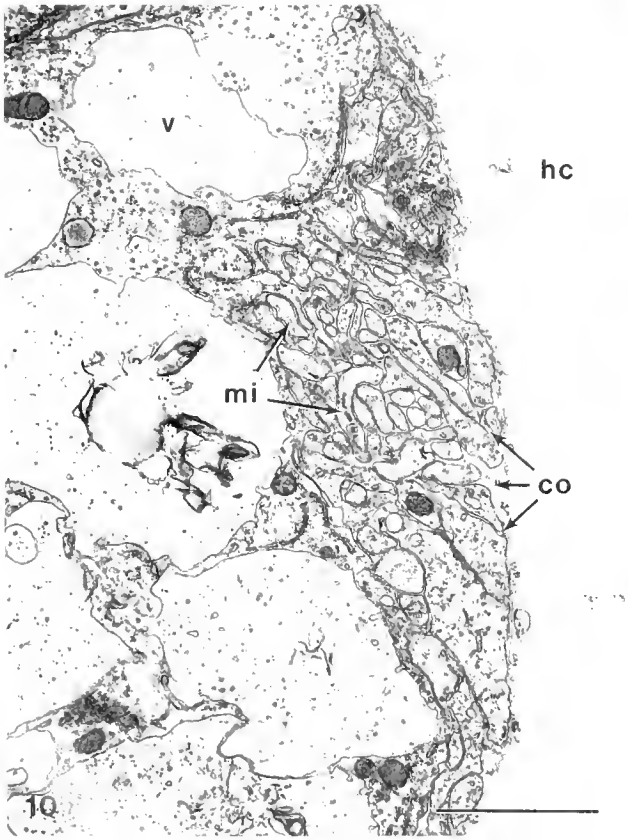

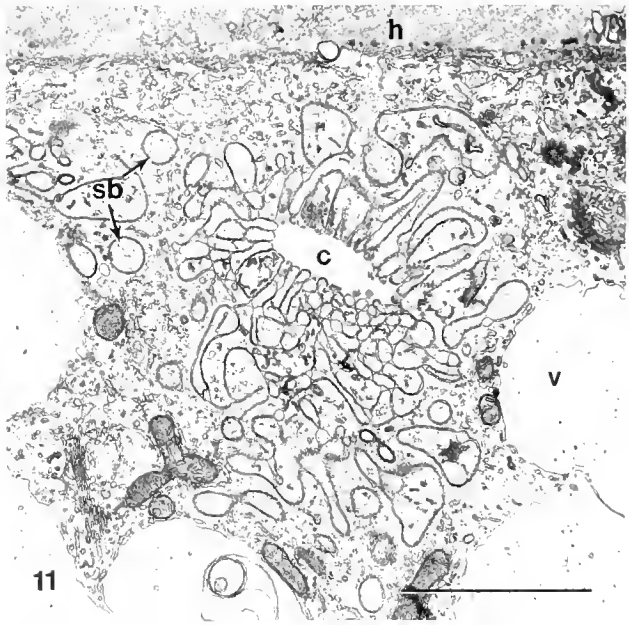

Figure 8. TEM showing the close association of the developing ciliated duct of the pore cell with the canaliculus of the crystal cell in an early trochophore of *Scarlesia dira*

Figure 9. TEM of the same association seen in Figure 8, but in an older trochophore. Numerous cilia arising from the duct in the pore cell extend into the canaliculus of the crystal cell.

Figure 10. TEM of the opening of the crystal cell's canaliculus into the hemocoel in an early *S. dira* veliger. The opening of the canaliculus is no longer obstructed by the pore cell, but plications and microvilli from the canalicular wall reduce the opening to a web of anastomosing slits.

closer to the esophagus, or at some point between the esophagus and ectoderm.

In living early veligers, the ciliated ducts could be observed with Nomarski differential interference contrast microscopy. This stage was most suitable for observations because the larval kidneys were on the transparent neck region of the embryo. As seen in sections, the branching pattern and location of the pore cell relative to the crystal cell varied among embryos and between sides of the same embryo. Cilia within the ducts were seen actively beating, but those that extended for most of their length into the hemocoel beat irregularly and slowly. Occasionally the beat of the cilia would stop, at which time the ducts could not be discerned. In some preparations where the embryos were favorably oriented, two ciliated ducts within a single pore cell could be distinguished. However, only one could be discerned in most.

Uptake of fluorescein-labelled proteins by the absorptive cell. The initial endocytotic uptake and concentration of ferritin by absorptive cells raised questions regarding the kinds of material that normally would be removed from the capsular fluid by the these cells. If the larval kidneys were a storage site for wastes or foreign molecules picked up from the capsular fluid, then the absorptive cells may have reacted to the apoferritin protein coat as an exogenous molecule and removed it from the external milieu. To determine if the absorptive cells take up the endogenous albumen proteins to which they are normally exposed, embryos were soaked in a solution of FITC-labelled capsular albumen proteins for 10 min to 4 h, then rinsed with seawater. Under UV epi-illumination, the absorptive cells on these treated embryos fluoresced, whereas no other cells did at a visible level (Figs. 18, 19). This was true for all developmental stages examined, from early prefeeding trochophores with absorptive cells barely protruding from the embryo, to late veligers with absorptive cells that were diminishing in size. No cells in control embryos examined immediately upon removal from their capsules fluoresced.

Absorptive cells on embryos soaked in FITC-BSA fluoresced in a manner indistinguishable from those exposed to FITC-conjugated capsule albumen proteins. Therefore, FITC-BSA was used for many observations on *Searlesia dira* as well as other species. Some embryos, particularly trochophores during the nurse egg feeding stage of development, had swallowed enough of the FITC-BSA solution so that the gut lumen fluoresced. However, the level of this fluorescence was comparable to that of the soaking solution, which was low relative to the brilliance of the absorptive cells.

The absorptive cells did not take up unconjugated fluorescein in quantities visible even after soaking for 24 h. Furthermore, no fluorescence was seen in the absorptive cells when glucose, urea, BSA, capsular albumen, or ferritin was added to the fluorescein solution, even when the ferritin was taken up at levels detectable at the light level.

Contrary to the absorptive cells, the crystal cells did fluoresce in embryos that had been exposed to fluorescein solutions. In contrast to FITC-conjugated proteins, fluorescein entered the embryos so that the hemocoel fluoresced. However, the fluorescence of the crystal cell was greater than that of the hemocoel. Approximately 50% of the fluorescing crystal cells possessed an internal structure, possibly the canaliculus, whose fluorescence was markedly brighter than the rest of the cell. It was around 5 to 6.5 μm wide and 30 to 35 μm long, traversing about two-thirds of the cell. Although this is up to twice the diameter of the canaliculus visualized in sectioned material, no other structure in the cell more closely approximates these dimensions. The vacuoles containing the crystals were not distinguishable in these treated embryos under UV epi-illumination.

The pattern of fluorescence in the absorptive cells of the embryos exposed to FITC-BSA depended on the length of time of exposure and on the time since they were removed from the FITC-BSA. After 10 min of exposure, fluorescence could be detected in a few small heterophagosomes lying beneath the plasmalemma. With increasing time of exposure, fluorescence was seen in many more small heterophagosomes, in larger heterophagosomes further inside the cell and with greater intensity. The larger internal heterophagosomes were dimly fluorescent within 2 h, and brightly fluorescent after 4 h. After 7 h, the fluorescence in the larger heterophagosomes was uneven, suggesting a heterogeneity of protein concentrations within those structures. In embryos that were exposed to FITC-BSA for 3 h and then placed in normal seawater, few fluorescent small heterophagosomes were seen after another 3 h, with most of the fluorescence restricted to larger heterophagosomes. The fluorescence from the FITC-BSA taken in during the 3-h exposure was still present in the larger heterophagosomes three days later, the longest embryos survived after excapsulation. The fluorescence did not appear to diminish in intensity,

Figure 11. TEM of a cross section of a canaliculus in the pore cell of an *S. dira* early veliger. The lumen of the canaliculus is surrounded and often occluded by microvilli. There are numerous finger-like side branches of the canaliculus, each of which is filled by a microvillus.

Scale bars represent 2 μm; ac, absorptive cell; c, canaliculus; cc, crystal cell; cd, ciliated duct; ci, cilia; co, openings of ciliated duct; en, endoderm; h, heterophagosome of absorptive cell; hc, hemocoel; mi, microvilli; pc, pore cell; sb, side branches of the canaliculus each filled by a microvillus; v, vacuole; za, zonula adherens.

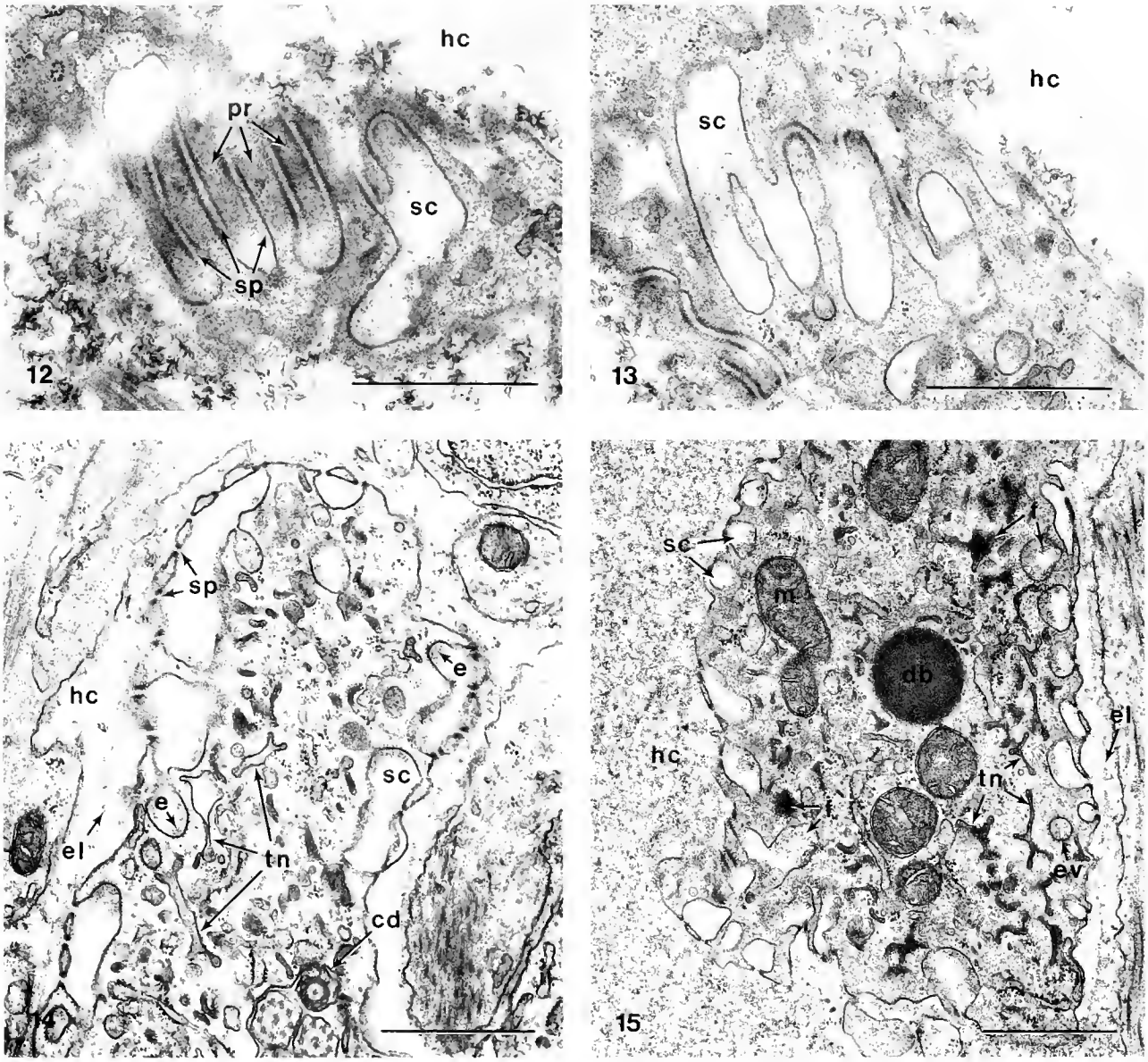

Figures 12 and 13. TEMs of two sequential grazing sections of the surface of the pore cell in *Scarlesia dira*, illustrating how the interdigitations of finger-like processes form uniform 23 nm wide slit-pores and subsurface cisternae.

Figure 14. TEM of a pore cell in an *S. dira* early veliger, showing the extensive tubular network and endocytotic vesicles forming from the floor of the subsurface cisternae.

Figure 15. TEM of the pore cell of an *S. dira* early veliger whose hemocoel had been injected with ferritin 15 min prior to fixation. The ferritin solution still fills the hemocoel. Ferritin has entered the subsurface cisternae and was taken up in endocytotic vesicles which then fused with the tubular network.

Scale bars represent 1 μm; cd, ciliated duct; db, dark body; e, endocytotic invagination; el, external lamina; ev, endocytotic vesicle; f, ferritin; hc, hemocoel; m, mitochondrion; pr, cell processes; sc, subsurface cisternae; sp, slit-pore; tn, tubular network.

nor did it appear in other cells. However, within 15 h of exposure to FITC-BSA, the fluorescence was not clearly confined to the heterophagosomes; the cytoplasm of the absorptive cell also fluoresced, although dimly. This may indicate that labelled material is passed to the cytoplasm, that some heterophagosomes had burst, or that digestion of the FITC-BSA was releasing fluorescein which was diffusing into the cytoplasm.

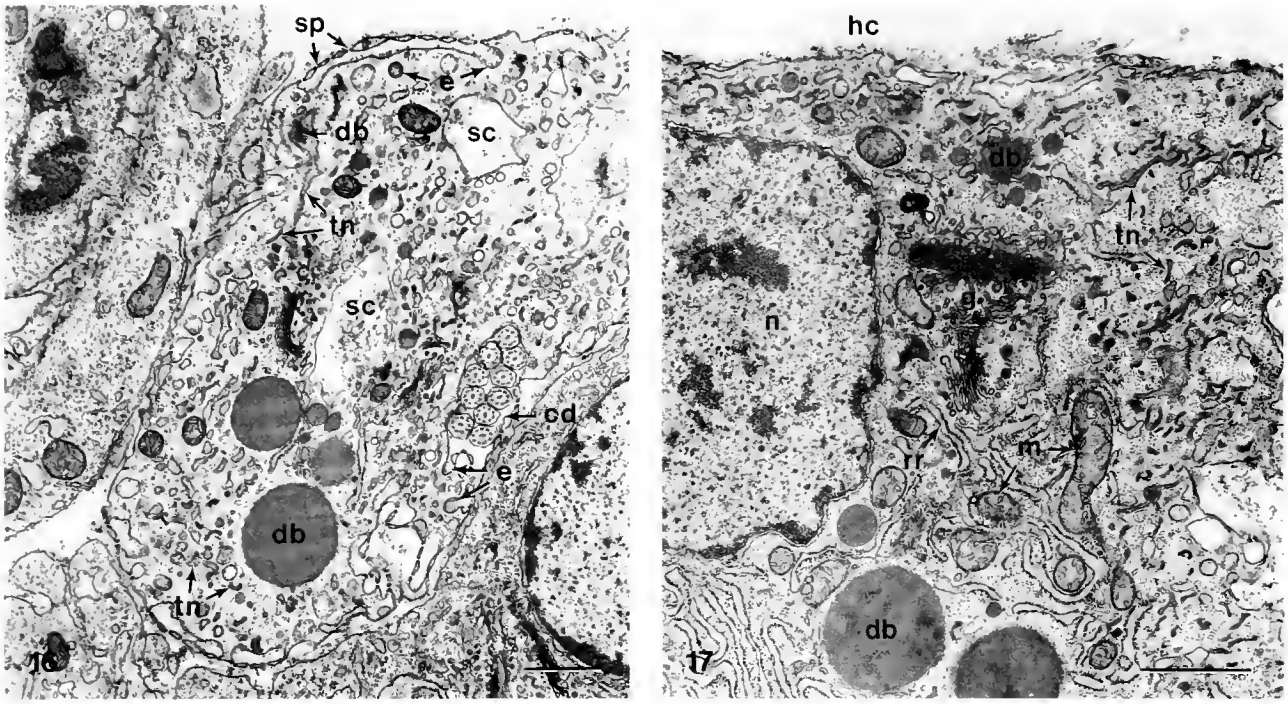

Figure 16. TEM showing the ciliated duct, endocytotic activity and dark bodies in the pore cell of a *Searlesia dira* early veliger. Note the early stage of dark body formation within the tubular network near the upper surface of the cell and the slit-pores within the ciliated duct.

Figure 17. TEM of the pore cell of an early trochophore of *S. dira* showing a large Golgi complex near a small dark body (near the upper cell surface) that is surrounded by smaller membrane-bound vesicles of similarly electron-dense material. Membranes are not always clearly seen around large dark bodies, as is evident at the bottom of this figure.

Scale bars represent 1 μm; cd, ciliated duct; db, dark body; e, endocytotic invaginations or vesicles; g, Golgi complex; hc, hemocoel; m, mitochondria; n, nucleus; rr, rough endoplasmic reticulum; sc, grazing sections of subsurface cisternae; sp, slit-pores; tn, tubular network.

Nucella canaliculata

As in all other species examined, the larval kidney complexes in *N. canaliculata* are located laterally in the neck region. They are first discernible in live embryos about the time the cephalic vesicle begins to enlarge on early trochophores. They increase rapidly in size and are prominent structures on late trochophores (Fig. 20). They reach their maximum size by the early veliger stage, a stage by which all nurse eggs have been eaten and the viscous capsular albumen has been absorbed or eaten.

The *N. canaliculata* absorptive cells become the largest cells in the embryo. They are larger than absorptive cells in any other species examined in this study except for those in *N. lamellosa*, which are comparable in size. They are hemispherical to almost spherical in shape. Their diameter can reach 300 μm, which means the two absorptive cells can comprise approximately 20% of the tissue volume of the embryo. The absorptive cells are fragile; their plasmalemmae are easily ruptured by handling of the embryos or by osmotic shock, slowly releasing intact heterophagosomes that may adhere to the outside of the cell (Fig. 21).

Only a general ultrastructural examination of the *N. canaliculata* larval kidney was completed because a satisfactory fixative was not found. Early trochophores through late veliger stages were sectioned for examination with light microscopy, but only the late trochophore stage was serially thin sectioned for TEM. The larval kidney in *N. canaliculata* consists of the same arrangement of an absorptive cell, a crystal cell and a pore cell as found in *S. dira*. The cytology of the absorptive cell in *N. canaliculata* is also similar. The external plasmalemma with its microvilli (Fig. 21) is endocytotically active. The heterophagosomes are heterogeneous in their density at both the light (Fig. 22) and TEM level. Rosettes of glycogen are present in the cytoplasm. Ferritin is rapidly taken in and stored in heterophagosomes, as is FITC-BSA (Fig. 23). These cells are endocytotically active throughout the intracapsular veliger phase of development. The crystal and pore cells differentiate in association with each

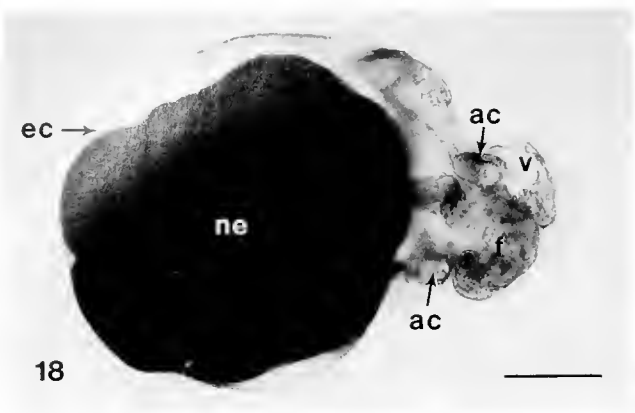

Figure 18. Light photomicrograph of a live *Searlesia dira* early veliger that had been soaked in a solution of FITC-capsular albumen for 3 h.

Figure 19. Epifluorescence photomicrograph of the same veliger seen in Figure 18, showing the bright absorptive cells that accumulated the fluorescein-labelled protein.

Scale bar represents 100 μm; ac, absorptive cell; ec, ectoderm; f, foot; ne, swallowed nurse eggs; v, velum.

other and develop the same ultrastructures they do in *S. dira*.

Presence of absorptive cells in different gastropod species. Embryos and some larvae from the three gastropod subclasses were tested for the presence of larval kidney absorptive cells. The species examined normally hatch either as veligers or postmetamorphic juveniles. Embryos were removed from their capsules, rinsed in seawater and placed in an FITC-BSA solution for at least 1 h before being examined under UV epi-illumination. Posthatching veligers of several species were obtained from cultures for testing.

In all seven prosobranch species tested that hatch as veligers, paired absorptive cells were found in prehatching stages (Table I). After hatching, veligers lost their absorptive cells within two or three days. Crystal cells were also detected in *Oenopota levidensis* veligers with polarized light. These cells were no longer detectable after the absorptive cells were resorbed during the second to third day after hatching.

Of the twelve prosobranch species tested that hatch as juveniles, only ten had embryos possessing paired absorptive cells (Table I). In these species, the absorptive cells were resorbed or at least did not protrude from the embryos after intracapsular metamorphosis. *Littorina sitkana* and *Petaloconchus montereyensis* embryos were the only prosobranchs that did not show absorptive cells at some stage. The capsules of *L. sitkana* contain albumen, but those of *P. montereyensis* possess little or none as they are packed with nurse eggs. None of the opisthobranch or pulmonate embryos had absorptive cells.

Discussion

Lack of evidence of waste accumulation

Marine prosobranchs are basically ammoniotelic, although uric acid may be found in various tissues (Nicol, 1960; Duerr, 1968). The larval kidneys, however, do not contain uric acid. The histochemical tests for urates in *Searlesia dira* and *Nucella canaliculata* embryos were negative, and there was no ultrastructural evidence for urates like that seen in terrestrial snails by Bouillon and Vandermeerssche (1962) and Pecheco (1971). The lack of uric acid and the positive PAS staining of the absorptive cells indicates that their large size is due to polysaccharides or polysaccharide-protein complexes and is unlikely due to accumulation of waste products.

Although no evidence for excretory activity by the larval kidneys was found during this study, previous reports indicating such a function may have been a consequence of several factors. First, these complexes of cells were called larval kidneys without any apparent definitive elucidation of their function, thus possibly biasing others as to their supposed role. Second, the delicate nature of the absorptive cells and the difficulty in fixing them well for ultrastructural studies help explain some of the observations of 'excretory' activity that have been reported. These large cells often break open, releasing intact heterophagosomes, before other structures visibly deteriorate in embryos removed from their capsules. Thus, the "excretory granules" seen by D'Asaro (1966, p. 895) emanating from the larval kidneys of *Thais haemastoma* and what Portmann (1930) thought were escaping waste-ladened wandering cells in *Buccinum undatum* embryos were likely to be heterophagosomes spilling from ruptured absorptive cells. The fragility of these cells may be due to the proteins they have accumulated causing osmotic shock when the embryos are removed from their capsules. This may be why these cells are difficult to fix well for ultrastructural study. The exocytosis cited as evidence for excretion by the absorptive cells in *Nucella lapillus* (Fioroni, 1985; Fioroni *et al.*, 1985) is similar to that seen in poorly fixed embryos

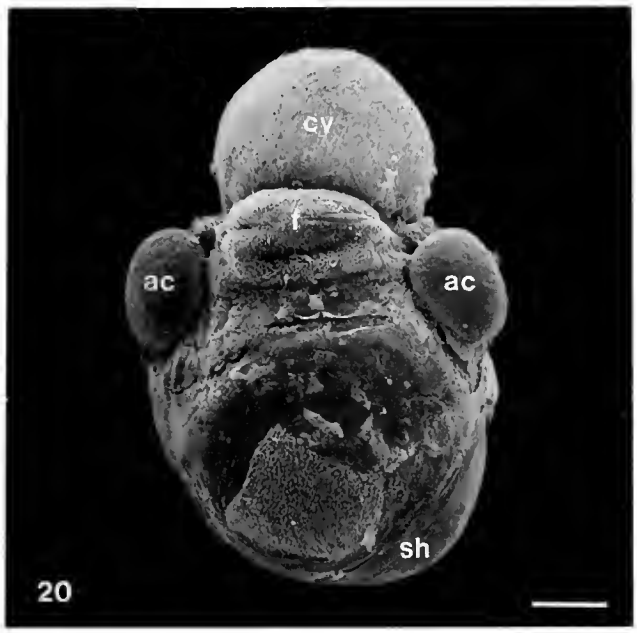

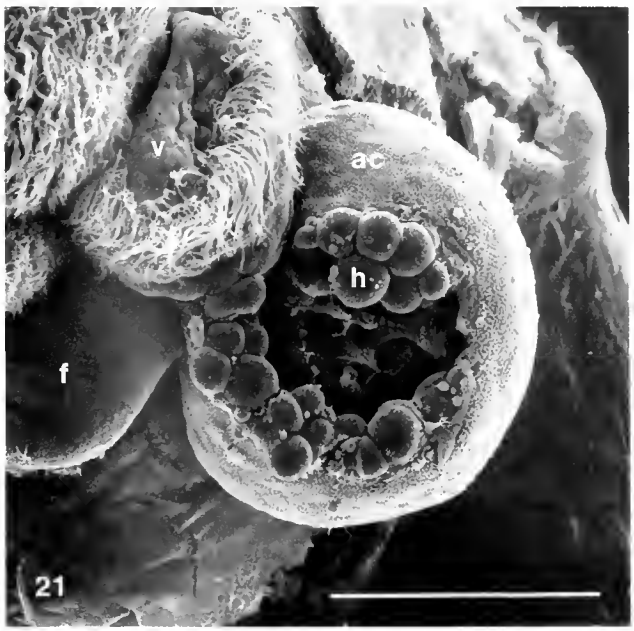

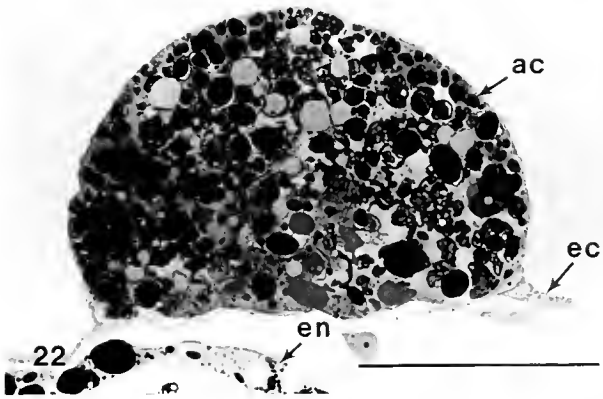

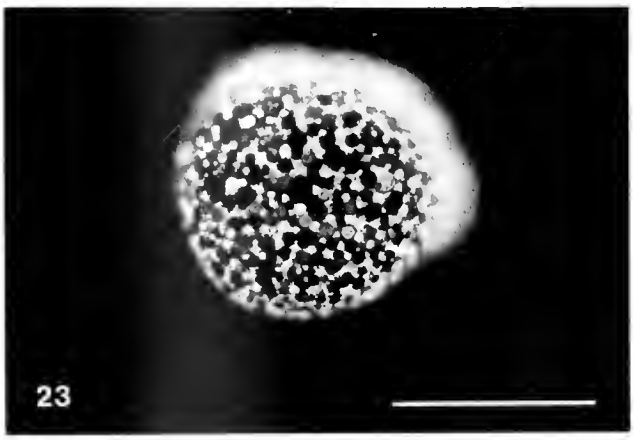

Figure 20. SEM of a *Nucella canaliculata* late trochophore showing the large size of the absorptive cells.

Figure 21. SEM of an absorptive cell on an early veliger of *N. canaliculata*. The cell has broken open revealing heterophagosomes. Microvilli are evident covering the external surface of the cell.

Figure 22. A light photomicrograph of a 1-μm thick section of an absorptive cell in an early veliger of *N. canaliculata*. Although the heterophagosomes are evident, the internal ultrastructure of the cell was greatly affected by fixation artifacts.

Figure 23. An epifluorescence photomicrograph of an absorptive cell on a live *N. canaliculata* early veliger that had been soaked for 1 h in a solution containing FITC-BSA. Heterophagosomes are clearly visible, with their level of fluorescence differing according to the amount of FITC-BSA they contain.

Scale bars represent 100 μm; ac, absorptive cell; cv, cephalic vesicle; ec, ectoderm; en, endoderm; f, foot; h, heterophagosome; sh, shell; v, velum.

of *S. dira* and *N. canaliculata*. It would seem illogical to describe the larval kidneys as specialized organs for encapsulated development that accumulate waste and then release it into the capsular fluid that bathes the embryos.

Absorptive cell

The absorptive cell is the only cell of the larval kidney complex that is exposed to the capsular fluid. It is clear from the experimental exposure of *S. dira* embryos to ferritin and FITC-capsular albumen that the absorptive cells rapidly take up protein from the external milieu by endocytosis and store it in heterophagosomes.

The early differentiation of the absorptive cells is consistent with the hypothesis that the albumen is an important source of nutrition for which capsulemates compete. The earlier an embryo has functional absorptive cells the

Table I

The presence of paired, laterally located fluorescent ectodermal absorptive cells in gastropod embryos or larvae exposed to FITC-BSA

Species (hatching stage*)	Fluorescing cells	Developmental stages tested
PROSOBRANCHIA		
Mesogastropoda		
Lacuna variegata (V)	+	Prehatching and 2-day-old veligers
Littorina sitkana (J)	–	Veligers
Petaloconchus montereyensis (J)	–	Before, during, and just after feeding on nurse eggs
Calyptraea fastigiata (V)	+	Late trochophore
Crepidula fornicata (V)	+ (weak)	Prehatching veligers
Crepidula adunca (J)	+	Early to late shell formation
Trichotropis cancellata (V)	+	Prehatching to 3-day-old veligers
Lamellaria sp. (V)	+	Prehatching veligers
Neogastropoda		
Nucella canaliculata (J)	+	Trochophores to late veligers
Nucella emarginata (J)	+	Trochophores, late veligers
Nucella lamellosa (J)	+	Trochophores to late veligers
Nucella lapillus (J)	+	Trochophores to early veligers
Nucella luna (J)	+	Trochophores to early veligers
Ocenebra japonica (J)	+	Early veligers
Ceratostoma foliatum (J)	+	Early trochophores
Amphissa columbiana (V)	+ (weak)	Prehatching veligers
	–	4 days post-hatching
Searlesia dira (J)	+	Trochophores to late veligers
Neptunea lyrata (J)	+	Late trochophores
Oenopota levidensis (V)	+	0–2-day-old veligers
	–	Veligers older than 2 days
OPISTHOBRANCHIA		
Onchidoris bilamellata (V)	–	1–2 days posthatching
Tritonia diomedea (V)	–	Prehatching veligers
PULMONATA		
Lymnaea stagnalis (J)	–	Before and during intracapsular albumen ingestion phase

* V = veliger; J = crawling juvenile.

greater are its chances of getting a larger share of the albumen in the capsule. The larval kidneys may be present as early as before (Franc, 1940) or just after (Eisawy and Sorial, 1974) the end of gastrulation. In living *S. dira* and *N. canaliculata* embryos, the absorptive cells are visible with light microscopy and are increasing in volume by the early trochophore stage. The cells reach their maximum size by the early veliger stage, a time by which no viscous albumen remains in the capsular fluid. There are great differences in absorptive cell sizes among prosobranch species, but this does not necessarily mean differences in the amount of albumen available. In species with smaller absorptive cells, the absorbed proteins may be passed to the rest of the embryo more rapidly or sooner than in species with larger absorptive cells.

It appears that when the larval kidneys of *S. dira* and *N. canaliculata* diminish in size they are totally resorbed, but the cytology of post-resorption stages has not been examined. No ultrastructural evidence of lysosomal activity was found in *S. dira* absorptive cells up through mid-veliger, the oldest stage examined. Resorption occurs during intracapsular metamorphosis in all the neogastropod species examined in this study that hatch as juvenile snails. However, Conklin (1897, p. 143) said the larval kidneys in *Crepidula fornicata* embryos "appear to be pinched off completely" and in *C. adunca*, Moritz (1939) said they were rolled off by the advancing mantle edge on the left side and by the larval heart on the right. In my examinations of these two species and on the confamilial *Calyptraea fastigiata*, the larval kidneys became almost spherical and then were easily dislodged when the capsules were opened. Observations through the clear walls of carefully handled capsules never revealed cast off absorptive cells. Rather, they were resorbed.

For species that hatch as veligers, the time of absorptive cell resorption varies. In *Thais savignyi* (Eisawy and Sorial, 1974) and *T. haemastoma* (Belisle and Byrd, 1980), they are resorbed before hatching. If the primary function of the absorptive cell is the uptake of capsular albumen during encapsulated development, then they are no longer needed after hatching. However, some species retain their absorptive cells for a few days after hatching. Tests with FITC-BSA indicate that the veligers of *Lacuna variegata*, *Trichotropis cancellata*, and *Oenopota levidensis* have

functional absorptive cells for at least two or three days after hatching. Similarly, the larval kidneys of *Trivia europea* persist after hatching, but only for a short time (Lebour, 1931). Thus, the absorptive cells appear to be principally an adaptation for intracapsular development.

The tests using FITC-BSA on a few opisthobranch and pulmonate species did not reveal structures that absorbed and concentrated proteins as did the prosobranch absorptive cells. Opisthobranch veligers may have an unpaired ectodermal larval or secondary kidney that consists of several types of cells near the anus (Bonar and Hadfield, 1974; Bickell and Chia, 1979). The veligers of *Aeolidia papillosa* are reported to possess protonephridia (Bartolomaeus, 1989). In pulmonates, some albumen is taken up generally during early embryogenesis by endocytosis, but most of the albumen is ingested after the gut becomes functional (Raven, 1946, 1975). Thus, prosobranch absorptive cells, as specialized embryonic ectodermal structures for the uptake of capsular albumen, may be unique among the invertebrate phyla.

Crystal cell

Although the function of the absorptive cell appears to be the uptake and storage of capsular albumen, the functions of the crystal and pore cells are less clear. The association of the crystal cell with most of the absorptive cell's internal surface suggests that the functions of these cells may be related, but evidence for this is presently lacking. The association may simply reveal an ancestral relationship.

In the crystal cell, vacuoles containing the crystals increase in number as the embryos develop. The crystals are likely to be made of a calcium salt. They are possibly calcium carbonate, for they were more soluble in acids than bases, were quickly dissolved in a solution of EGTA, which chelates Ca^{++} ions (Schmid and Reilley, 1957), and were stained by alizarin red S, which stains bone (Emmel and Cowdry, 1964) and calcium carbonate (Buddemeir and Kinzie, 1976). The crystals are in a readily soluble form, as indicated by their rapid dissolution after vacuolar membrane breakdown in non-salt-saturated solutions. The vacuolar membrane clearly protects the integrity of the crystals. The EGTA solutions did not affect the crystals in live embryos, but quickly dissolved those in heat-killed embryos. Although the crystals are more likely to contain calcium than uric acid, which dissolve more readily in high pH solutions (Thorpe, 1930), the function of sequestering calcium is unclear.

Endocytotic activity along the canaliculus in the crystal cell suggests that the contents of the vacuoles may originate from the canalicular lumen. However, the evidence indicates a very low level of endocytotic activity, and vacuoles are formed both before and after the separation of the pore cell and crystal cell when the canaliculus is first open to the hemocoel. Thus the relationship between the function of the canaliculus and crystal formation is uncertain. The canaliculi in the parietal cells of the vertebrate gastric mucosa are implicated in ion transport for HCl secretion (Ito and Winchester, 1963). However, the canaliculi in the crystal cells of *S. dira* are unlikely to be heavily involved in ion transport, for they lack the close association with numerous mitochondria that is characteristic in cells that do (Lawn, 1960; Copeland, 1967; Sardet *et al.*, 1979). Although the large surface area of the canaliculus due to the numerous microvilli and plications suggests a membrane-dependent function, the restricted nature of the lumen indicates an impeded movement of material either into or out of the canaliculus.

In experiments exposing *S. dira* embryos to solutions of fluorescein, the crystal cells fluoresced brightly. How the fluorescein is concentrated and what role the canaliculi play in the concentrating mechanism remains unknown.

Crystal cells have been reported in several other prosobranch embryos (Portmann, 1930; Franc, 1940; Fioroni, 1966, 1985). Franc (1940) described a vacuolated cell lying under the large external larval kidney cell in the embryos of *Oceanebra aciculata*. As in *S. dira*, the cell increased in size and became filled with vacuoles, but the vacuoles in *O. aciculata* became greenish in older developmental stages. In most of the species listed in Table I, the larval kidney cells had a yellowish color with the crystals in the crystal cells being a dark yellow to yellow-green. However, in additional observations on embryos of *Oceanebra* (either *O. interfossa* or *O. lurida*), the crystal cells were greenish-yellow with green granules (pers. obs.). There was no green color in young embryos, nor was there any green color elsewhere in the capsule. Therefore, the pigment likely was synthesized *de novo*.

Pore cell

Pore cells are a conspicuous cell type in the connective tissue of gastropods and bivalves (Sminia and Boer, 1973). There are also pore cells, referred to as nephrocytes or podocytes, in the blood spaces of decapod gill shafts (Wright, 1964; Strangways-Dixon and Smith, 1970; Foster and Howse, 1978; Taylor and Greenway, 1979). 'Nephrocyte' is an appropriate label for these cells if the material they remove from the hemolymph is an excretory product, but pore cells have also been implicated in the production of blood pigments in mollusks (Sminia and Boer, 1973; Skelding and Newell, 1975). Calling them 'pore cells' aptly describes their distinctive morphological features without implying function, whereas calling them 'podocytes' is misleading because of their morphological and functional differences with vertebrate kidney podocytes (Bloom and Fawcett, 1968).

In *S. dira* pore cells, material from the hemolymph passes through the slit-pores and is taken into the pore cell by endocytotic vesicles that form from the basal membranes of the subsurface cisternae. The external lamina may act as a filter, for in experimentally injected *S. dira* embryos the density of ferritin molecules inside the subsurface cisternae was markedly less than that in the hemocoel. Additional filtration is unlikely at the slit-pores, because their gaps are much wider than the diameter of the ferritin molecules. Furthermore, a membrane or diaphragm like that found in the nephrocytes of shrimp gills (Foster and Howse, 1978) was not seen spanning the slit-pores in *S. dira*. The material taken in by endocytosis is transferred to an extensive network of tubules, where it appears to be condensed to form large dark-staining bodies. A similar ultrastructure is found in pore cells in the gill blood vessels of a land crab, *Holthuisana transversa* (Taylor and Greenway, 1979). In general, pore cells appear to remove material from the hemolymph. However, the nature of this material and its fate remains to be elucidated.

A characteristic of the pore cells of *S. dira* and *N. canaliculata* that has not been found in pore cells in other species is the ciliated ducts. In *S. dira*, only the first of the two ciliated ducts develops in association with the canaliculus of the crystal cell, but eventually the two ducts are indistinguishable. They both originate near the cell center, contain a similar number of cilia, possess some slit-pores leading to the hemocoel somewhere along their length, and open into the hemocoel. The duct lumens in most places are only slightly wider than the cilia they contain. Movement of the cilia could move fluid down and out of the ducts. However, the low number of slit-pores to the hemocoel in the duct walls would result in a low flow rate. Indeed, no ferritin was found in ducts in injected embryos.

Comparison with protonephridia

It is logical to compare the 'larval kidneys' of *S. dira* and *N. canaliculata* to protonephridia because of their name, their bilateral location, and the fact that protonephridia have been described in other prosobranch, opisthobranch, and pulmonate gastropods, in chitons, and in bivalves (Erlanger, 1894; Brandenburg, 1966; Bartolomaeus, 1989; Ruthensteiner and Schaefer, 1991). This comparison is especially attractive in light of the pore cells' ciliated ducts with their slit-pore perforations to the hemocoel being so similar in morphology to many protonephridia. Although protonephridia are diverse in details of their morphology (Goodrich, 1945; Brandenburg, 1966, 1975; Wessing and Polenz, 1974; Wilson and Webster, 1974; Ruppert and Smith, 1988), they basically consist of a terminal cell or cells with one or more cilia within a cytoplasmic tube that leads to a channel cell or tubule that opens externally. The beating of the cilia draws hemolymph into the tubule through a weir of slits formed in some species by the interdigitation of microvilli from both the terminal and channel cells (Brandenburg, 1975; Kummel, 1975).

It is clear that the larval kidneys of *S. dira* and *N. canaliculata* are not functional protonephridia because a filtration weir never develops and the ciliated ducts lead not to the external milieu, but to the haemocoel. However, it is possible that the larval kidneys may have evolved from protonephridia and that the components have become disorganized and functionally altered. If this is so, the pore cell probably evolved from a protonephridial terminal cell. The pore cell's ciliated ducts are reminiscent of protonephridial 'flames,' and the slit-pores and subsurface cisternae are similar to that seen in a section of the terminal cell of the trochophore of *Pomatoceros triqueter* (Wessing and Polenz, 1974, Fig. 2b). The crystal and absorptive cells may have evolved from channel cells. The canaliculus may be the last remnant of the crystal cell's ancestral duct, with no such vestige remaining in the highly altered absorptive cell.

The presence of larval protonephridia may represent the ancestral condition in mollusks (Bartolomaeus, 1989), but gastropod embryos undergoing encapsulated development experience an environment different from the open-ocean surroundings experienced during development of their free-spawning, more primitive relatives. The egg capsules with their intracapsular fluid presumably create an osmotic environment different from that of seawater. This is supported by two observations made during this study. One is the fixation artifacts seen. These artifacts suggested an osmotic problem and were diminished when fixatives with osmolarities higher than seawater were used. The second is the bursting of the absorptive cells when embryos were carefully excapsulated into seawater. This was most noticeable in species where these cells are particularly large, and is presumably due to the osmotic imbalance between the concentrated proteins within the heterophagosomes and the seawater. Because protonephridia are reported to be involved in osmoregulation (Braun *et al.*, 1969) and the filtration and reabsorption of macromolecules from coelomic fluid (Smith and Ruppert, 1988), it would seem logical for encapsulation to reduce the selective pressures that maintain protonephridia as osmoregulatory organs. It is thus possible that the larval kidneys described herein may represent rudimentary protonephridia. The lack of organization among the components is not surprising if the need for functional protonephridia is lacking. The vestigial eyes of cave fish show a similar disorganization of components (Remane, 1971). The functions of the larval kidneys' cells also have changed. The pore and crystal cells have functions that

are presently unknown, and may simply be vestigial structures. The absorptive cell, however, has taken on a new role. It does not accumulate wastes as previously thought (*e.g.*, Franc, 1940), but is specialized for the acquisition of capsular albumen.

An ultrastructural study of the ontogeny of the larval kidney complex in *Nassarius reticulatus* might shed light on this question of homology, for Ruthensteiner and Schaefer (1991) found in their light microscopical study protonephridia with what appears to be an enlarged absorptive cell adjacent to the excretory pore. A similar study on the early ontogeny of the larval kidney complex of *S. dira* or *N. canaliculata* might help reveal the germ layer origins of the component cells and their homology with cells in other protonephridia. Investigators have described the larval kidneys as being ectodermal or also part mesodermal (Heymons, 1893; Conklin, 1897; Casteel, 1904; Pelseneer, 1911; D'Asaro, 1966). The absorptive cell in *S. dira* embryos is probably derived from an ectodermal cell for it has junctional complexes with the surrounding unspecialized ectodermal cells. However, the origins of the inner two cells is unclear. If they are protonephridial in nature, then they may be ectodermal (Goodrich, 1945). However, the pore cells in *S. dira* larval kidneys have similarities with pore cells in the connective tissues of other gastropods and bivalves (Sminia and Boer, 1973), which suggests that they may be mesodermal in origin. It should be noted here that protonephridial terminal cells (presumably ectodermal in origin) in the larvae of the polychaete *Sabellaria* transform into a podocyte (presumably a mesodermal cell) in the coelomic lining at metamorphosis (Smith and Ruppert, 1988), indicating that caution must be exercised in making assumptions about germ layer affinities (Ruppert and Smith, 1988).

Nutritional role of capsular albumen and other suggested functions

Although albumen in prosobranch egg capsules does not appear to be bactericidal (Rivest, 1981; Pechenik *et al.*, 1984), it may serve several other functions. It may be important physically by increasing the viscosity of the intracapsular fluid relative to seawater so that embryos can maneuver and feed on nurse eggs (Rivest, 1983). It may be important osmotically by protecting embryos from osmotic shock (Pechenik, 1983) or by aiding hatching (Hertling, 1928). The albumen, containing proteins and carbohydrates and sometimes lipid (Bayne, 1968; Stöckmann-Bosbach and Althoff, 1989), also can have nutritive value for prosobranch embryos. It can influence the developmental stage that hatches (Giglioli, 1955) or the size at hatching (Rasmussen, 1951; Rivest, 1986). Its nutritional value is suggested also by its endocytotic uptake in early cleavage stages (Elbers and Bluemink, 1960; Fioroni, 1977) and by the presence of a special transitory albumen digestive sac in the embryonic gut of some species (Portmann, 1955; Portmann and Sandmeier, 1965). In the closely allied pulmonates, protein gains in the growing embryo are positively correlated with protein losses in the capsular fluid (Morrill, 1964). Thus, it is apparent that regardless of its other functions, the proteinaceous albumen can be important nutritionally.

The albumen taken up by the absorptive cells in prosobranch larval kidneys is presumably used for embryonic nutrition, but the nutritional significance of this absorbed albumen is presently unknown. Assuming that the abortive cells' volume is due primarily to absorbed albumen proteins, the fact that these cells in *N. canaliculata* can comprise 20% of an embryo's tissue volume suggests that in this species the larval kidneys may procure a significant quantity of albumen. It would be difficult to empirically examine this in *Nucella* unless techniques for culturing encapsulated embryos improve. Although early embryos of *Conus pennaceus* can be reared to the veliger stage outside their capsules with no apparent detrimental effect (Perron, 1981), young *Nucella* embryos do not survive very long once removed from their capsule (Pechenik *et al.*, 1984; Stöckmann-Bosbach, 1988; pers. obs.).

Acknowledgments

This study benefitted from the advice of R. R. Strathmann, the late R. L. Fernald, the late C. G. Reed, C. Gabel, E. M. Eddy, and R. A. Cloney, who piqued my curiosity about prosobranch larval kidneys. E. Ruppert made numerous constructive criticisms on the manuscript, especially regarding the possible vestigial nature of the larval kidneys. R. Shimek provided *Oenopota levidensis* veligers, and R. Palmer provided *Nucella lima* egg capsules. The director of the Friday Harbor Laboratories kindly provided use of the laboratories' facilities. This study was supported in part by National Institutes of Health grants 5-T01-HD00266-10 and 1-T32-HD07183-01 and National Science Foundation grant OCE 7818608 (to R. R. Strathmann).

Literature Cited

Bartolomaeus, T. 1989. Larvale Nierenorgane bei *Lepidochiton cinereus* (Polyplacophora) und *Aeolidia papillosa* (Gastropoda). *Zoomorphology* **108:** 297–307.

Bayne, C. J. 1968. Histochemical studies on the egg capsules of eight gastropod molluscs. *Proc. Malacol. Soc. Lond.* **38:** 199–212.

Belisle, B. W., and W. Byrd. 1980. *In vitro* egg activation and maturation, and ultrastructural analysis of development in the marine prosobranch, *Thais haemastoma*. *Trans. Am. Microsc. Soc.* **99:** 111–127.

Bickell, L. R., and F. S. Chia. 1979. Organogenesis and histogenesis in the planktotrophic veliger of *Doridella steinbergae* (Opisthobranchia: Nudibranchia). *Mar. Biol.* **52:** 291–313.

Bloom, W., and D. W. Fawcett. 1968. *A Textbook of Histology, 9th ed.* W. B. Saunders Co., Philadelphia.

Bobretzky, N. 1877. Studien über die embryonal Entwicklung der Gastropoden. *Arch. Mikrobiol. Anat. Bd.* **13:** 95–169.

Bonar, D. B., and M. G. Hadfield. 1974. Metamorphosis of the marine gastropod *Phestilla sibogae* Bergh (Nudibranchia: Aeolidacea) I. Light and electron microscopic analysis of larval and metamorphic stages. *J. Exp. Mar. Biol. Ecol.* **16:** 227–255.

Bouillon, J., and G. Vandermeerssche. 1962. Electron microscope observations of the excretory organ of the pulmonary molluscs. *5th Int. Cong. Electron Microsc., Philadelphia* **2:** WW14–15.

Brandenburg, J. 1966. Die Reusenformem der Cyrtocyten. *Zool. Beit.* **12:** 346–417.

Brandenburg, J. 1975. The morphology of the protonephridia. *Fortsch. Zool* **23:** 1–17.

Braun, G., G. Kümmel, and J. A. Mangos. 1966. Studies on the ultrastructure and function of a primitive excretory organ, the protonephridium of the rotifer *Asplanchna priodonta*. *Pflügers Arch.* **289:** 141–154.

Buddemeir, R. W., and R. A. Kinzie, III. 1976. Coral growth. *Oceanogr. Mar. Biol. Ann. Rev.* **14:** 183–225.

Casteel, D. B. 1904. The cell-lineage and early larval development of *Fiona marina*, a nudibranch mollusk. *Proc. Acad. Natl Sci. Phil. Ser. 3* **56:** 325–405.

Cavey, M., and R. Cloney. 1972. Fine structure and differentiation of ascidian muscle. I. Differentiated caudal musculature of *Distaplia occidentalis* tadpoles. *J. Morphol.* **138:** 349–374.

Conklin, E. G. 1897. The embryology of *Crepidula*. *J. Morphol.* **13:** 1–226.

Copeland, D. E. 1967. A study of salt secreting cells in the brine shrimp (*Artemia salina*). *Protoplasma* **63:** 363–384.

D'Asaro, C. N. 1966. The egg capsules, embryogenesis, and early organogenesis of a common oyster predator, *Thais haemastoma* (Gastropoda: Prosobranchia). *Bull. Mar. Sci* **16:** 884–914.

Duerr, F. G. 1968. Excretion of ammonia and urea in seven species of marine prosobranch snails. *Comp. Biochem. Physiol* **26:** 1051–1059.

Eisawy, A. M., and A. E. Sorial. 1974. Egg capsules and development of *Thais savignyi* Deshayes. *Bull. Inst. Oceanogr. Fish., Cairo* **4:** 237–258.

Elbers, P. F., and J. G. Bluemink. 1960. Pinocytosis in the developing egg of *Limnaea stagnalis* L. *Exp. Cell Res.* **21:** 619–622.

Emmel, V. M., and E. V. Cowdry. 1964. *Laboratory Technique in Biology and Medicine.* The Williams and Wilkens Co., Baltimore.

Erlanger, R. 1894. Zur Bildung des Mesoderms bei der *Paludina vivipara*. *Morph. Jb.* **22:** 113–118.

Fioroni, P. 1966. Zur Morphologie und Embryogenese des Darmtraktes und der transitorischen Organe bei Prosobranchiern (Mollusca, Gastropoda). *Rev. Suisse Zool* **73:** 621–876.

Fioroni, P. 1977. On the peripheric resorption of albumen in gastropods and its significance for general embryology. *Zool. Jb. Anat. Bd* **98:** 181–202.

Fioroni, P. 1985. Struktur und Funktion der larvalen Zellen des Cephalopodiums bei jungen intrakapsulären Larven von *Nucella lapillus* (Gastropoda, Prosobranchia). *Zool Beitr. N. F.* **29:** 103–117.

Fioroni, P., G. Sundermann, and D. P. Scheidegger. 1984. Die Ultrastruktur der freien Rhogocyten bei intrakapsulären Veligern von *Nucella lapillus* (Gastropoda, Prosobranchia, Stenoglossa). *Zool. Anz.* **212:** 193–202.

Fioroni, P., D. P. Scheidegger, and G. Sundermann. 1985. Die Ultrastruktur der Larvalnierne bei intrakapsulären Larven von *Nucella lapillus* (Gastropoda, Prosobranchia, Stenoglossa). *Zool. Jb. Anat.* **113:** 145–164.

Foster, C. A., and H. D. Howse. 1978. A morphological study on gills of the brown shrimp, *Penaeus aztecus*. *Tissue Cell.* **10:** 77–92.

Franc, A. 1940. Recherches sur le développement d'*Ocinebra aciculata* Lamark. *Bull. Biol. France Belgique* **74:** 327–345.

Franc, A. 1941. Sur les reins larvaires de certains Mollusques prosobranches. *C. R. Soc. Biol. Paris* **135:** 1487–1489.

Giglioli, M. E. 1955. The egg masses of the Naticidae (Gastropoda). *J. Fish. Res. Board Can.* **12:** 287–327.

Glaser, O. 1904. Excretory activities in the nuclei of gastropod embryos. *Am. Nat.* **38:** 513–516.

Goodrich, E. S. 1945. The study of nephridia and genital ducts since 1895. *O. J. Microsc. Sci.* **86:** 113–392.

Hertling, H. 1928. Beobactungen und Versuche an den Eiern von *Littorina* und *Lacuna*. Bedeutung der Eihüllen. Entwicklung im natürlichen und abgeänderten Medium. *Wiss. Meers. Abt. Helgoland* **17:** 1–49.

Heymons, R. 1893. Zur Entwicklungsgeschicte von *Umbrella mediterranea*, Lam. *Z. Wiss. Zool.* **56:** 245–298.

Humason, G. L. 1972. *Animal Tissue Technique, 3rd ed.* W. H. Freeman and Co., San Francisco.

Ito, S., and R. J. Winchester. 1963. The fine structure of the gastric mucosa in the bat. *J. Cell Biol.* **16:** 541–577.

Kummel, G. 1975. The physiology of protonephridia. *Fortsch. Zool.* **23:** 18–32.

Lawn, A. M. 1960. Observations on the fine structure of the gastric parietal cells of the rat. *J. Biophys. Biochem. Cytol.* **7:** 161–166.

Lebour, M. 1931. The larval stages of *Trivia europea*. *J. Mar. Biol. Assoc. U. K.* **17:** 819–831.

Luft, J. H. 1961. Improvements in epoxy resin embedding methods. *J. Biophys. Biochem. Cytol* **9:** 409–414.

Moritz, C. E. 1939. Organogenesis in the gasteropod *Crepidula adunca* Sowerby. *Univ. Calf. Publ. Zool.* **43:** 217–248.

Morrill, J. B. 1964. Protein content and dipeptidase activity of normal and cobalt-treated embryos of *Lymnaea palustris*. *Acta Embryol. Morphol. Exp.* **7:** 131–142.

Nicol, J. A. C. 1960. *The Biology of Marine Animals.* Interscience Publishers, New York.

Pearse, A. G. E. 1972. *Histochemistry, Vol. II, 3rd ed.* The Williams and Wilkens Co., Baltimore.

Pecheco, J. 1971. Fine structure of concretions in the kidney epithelium of *Pomacea urceus* (Gastropoda: Prosobranchia). *Acta Biol. Venez.* **7:** 443–458.

Pechenik, J. 1983. Egg capsules of *Nucella lapillus* (L.) protect against low-salinity stress. *J. Exp. Mar. Biol. Ecol.* **71:** 165–179.

Pechenik, J. A., S. C. Chang, and A. Lord. 1984. Encapsulated development of the marine prosobranch gastropod *Nucella lapillus*. *Mar. Biol* **78:** 223–229.

Pelseneer, R. 1911. Recherches sur l'embryologie des gastropodes. *Acad. R. Belg. Mem. Cl. Sci. Collect* **3:** 1–167.

Perron, F. E. 1981. Larval growth and metamorphosis of *Conus* (Gastropoda: Toxoglossa). *Pac. Sci.* **35:** 25–38.

Portmann, A. 1930. Die Larvenniern von *Buccinum undatum* L. *Z. Zell. Mikro. Anat.* **10:** 401–410.

Portmann, A. 1955. La métamorphose "abritée" de *Fusus* (Gast. Prosobranches). *Rev. Suisse Zool.* **62:** 236–252.

Portmann, A., and E. Sandmeier. 1965. Die Entwicklung von Vorderdarm, Macromeren und Enddarm unter dem Einfluss von Nähreiern bei *Buccinum*, *Murex* und *Nucella* (Gastrop. Prosobranchia). *Rev. Suisse Zool.* **72:** 187–204.

Rasmussen, E. 1951. Faunistic and biological notes on marine invertebrates II. The eggs and larvae of some Danish Marine Gastropods. *Vidensk. Medd. Dan. Naturhist. Foren.* **113:** 201–249.

Raven, C. P. 1946. The development of the egg of *Lymnaea stagnalis* L. from the first cleavage till the trochophore stage, with special reference to its "chemical embryology." *Arch. Neerl. Zool.* **7:** 353–434.

Raven, C. P. 1975. Development. Pp. 367–400 in *Pulmonates*, V. Fretter and J. Peake, eds. Academic Press, New York.

Remane, A. 1971. *Die Grundlagen des natürlichen Systems, der vergleichenden Anatomie und der Phylogenetik.* Otto Koeltz, Koenigstein-Taunus (reprint of the 1956 ed. published by Geest & Portig, Leipzig).

Reynolds, E. S. 1963. The use of lead citrate at high pH as an electron-opaque stain in electron microscopy. *J. Cell Biol.* **17:** 208–211.

Richardson, K. C., L. Jarrett, and E. H. Finke. 1960. Embedding in epoxy resins for ultrathin sectioning in electron microscopy. *Stain Technol.* **35:** 313–323.

Rivest, B. R. 1981. Nurse egg consumption and the uptake of albumen in the embryonic nutrition of marine snails. Ph.D. dissertation. University of Washington, Seattle.

Rivest, B. R. 1983. Development and the influence of nurse egg allotment on hatching size in *Searlesia dira* (Reeve, 1846) (Prosobranchia: Buccinidae). *J. Exp. Mar. Biol. Ecol.* **69:** 217–241.

Rivest, B. R. 1986. Extra-embryonic nutrition in the prosobranch gastropod *Urosalpinx cinerea* (Say, 1822). *Bull. Mar. Sci.* **39(2):** 498–505.

Ruppert, E. E., and P. R. Smith. 1988. The functional organization of filtration nephridia. *Biol. Rev.* **63:** 231–258.

Ruthensteiner, B., and K. Schaefer. 1991. On the protonephridia and 'larval kidneys' of *Nassarius* (*Hinia*) *reticulatus* (Linnaeus) (Caenogastropoda). *J. Moll. Stud.* **57:** 323–329.

Sardet, C., M. Pisam, and J. Maetz. 1979. The surface epithelium of teleostean fish gills. Cellular and junctional adaptations of the chloride cell in relation to salt adaptation. *J. Cell Biol.* **80:** 96–117.

Schmid, R. W., and C. N. Reilley. 1957. New complexon for titration of calcium in the presence of magnesium. *Anal. Chem.* **29:** 264–268.

Skelding, J. M., and P. F. Newell. 1975. On the functions of the pore cells in the connective tissue of terrestrial pulmonate molluscs. *Cell Tissue Res.* **156:** 381–390.

Sminia, T., and H. H. Boer. 1973. Haemocyanin production in pore cells of the snail *Lymnaea stagnalis*. *Z. Zellforsch.* **145:** 443–445.

Smith, P. R., and E. E. Ruppert. 1988. Nephridia. In *Ultrastructure of the Polychaeta* W. Westheide and C. O. Hermans, eds. *Microfauna Marina* **4:** 231–262.

Stöckmann-Bosbach, R. 1988. Early stages of the encapsulated development of *Nucella lapillus* (Linnaeus) (Gastropoda, Muricidae). *J. Moll. Stud.* **54:** 181–196.

Stöckmann-Bosbach, R., and J. Althoff. 1989. A correlated morphological and biochemical study of capsular fluid of *Nucella lapillus* (Gastropoda: Prosobranchia: Muricidae). *Mar. Biol.* **102:** 283–289.

Strangways-Dixon, J., and D. S. Smith. 1970. The fine structure of gill 'podocytes' in *Panulirus argus* (Crustacea). *Tissue Cell* **2:** 611–624.

Taylor, H. H., and P. Greenway. 1979. The structure of the gills and lungs of the arid-zone crab, *Holthuisana* (*Austrothelphusa*) *transversa* (Brachyura: Sundathelphusidae) including observations on arterial vessels within the gills. *J. Zool., Lond.* **189:** 359–384.

Thorpe, E. 1930. *A Dictionary of Applied Chemistry.* Longmans, Green and Co., London.

Tomlinson, S. G. 1987. Intermediate stages in the embryonic development of the gastropod *Ilyanassa obsoleta*: a scanning electron microscope study. *Int. J. Invert. Reprod. Dev.* **12:** 253–280.

Wessing, A., and A. Polenz. 1974. Structure, development and function of the protonephridia in trochophores of *Pomatoceros triqueter* (Annelida, Polychaeta, Sedentaria). *Cell Tissue Res.* **156:** 21–33.

Wilson, R. A., and L. A. Webster. 1974. Protonephridia. *Biol. Rev.* **49:** 127–160.

Wood, R. L., and J. H. Luft. 1965. The influence of buffer systems on fixation with osmium tetroxide. *J. Ultrastruct. Res.* **12:** 22–45.

Wright, K. A. 1964. The fine structure of the nephrocyte of the gills of two marine decapods. *J. Ultrastruct. Res.* **10:** 1–13.

Reference: *Biol. Bull.* **182**: 324–332. (June, 1992)

Temperature Stress Causes Host Cell Detachment in Symbiotic Cnidarians: Implications for Coral Bleaching

RUTH D. GATES, GAREN BAGHDASARIAN, AND LEONARD MUSCATINE

Department of Biology, University of California, Los Angeles, California 90024

Abstract. During the past decade, acute and chronic bleaching of tropical reef corals has occurred with increasing frequency and scale. Bleaching, *i.e.*, the loss of pigment and the decrease in population density of symbiotic dinoflagellates (zooxanthellae), is often correlated with an increase or decrease in sea surface temperature. Because little is known of the cellular events concomitant with thermal bleaching, we have investigated the mechanism of release of zooxanthellae by the tropical sea anemone *Aiptasia pulchella* and the reef coral *Pocillopora damicornis* in response to cold and heat stress. Both species released intact host endoderm cells containing zooxanthellae. The majority of the released host cells were viable, but they soon disintegrated in the seawater leaving behind isolated zooxanthellae. The detachment and release of intact host cells suggests that thermal stress causes host cell adhesion dysfunction in these cnidarians. Knowledge of the cellular entity released by the host during bleaching provides insight into both the underlying release mechanism and the way in which natural environmental stresses evoke a bleaching response.

Introduction

Most tropical corals and sea anemones (Phylum Cnidaria) contain large populations of symbiotic dinoflagellates (zooxanthellae). The zooxanthellae are located in vacuoles within the host endoderm cells (Glider *et al.*, 1980; Trench, 1987) where they mediate the flux of carbon and nutrients between the host and the environment (Muscatine, 1990).

Zooxanthellae-cnidarian symbioses are normally stable; that is, they have a relatively constant ratio of zooxanthellae to host biomass (Drew, 1972). During the past decade, however, ecologists have observed that relatively small changes in the physical parameters of the marine environment can dramatically influence the stability of these symbioses (Glynn, 1990). Cnidarian bleaching and mortality have often been correlated with unusually high or low sea surface temperatures in tropical oceans worldwide (Brown and Suharsono, 1990; Coles and Fadlallah, 1990; Glynn, 1990; Williams and Bunkley-Williams, 1990). Bleaching has been attributed to a reduction in the amount of chlorophyll *a* (Coles and Jokiel, 1977; Kleppel *et al.*, 1989; Porter *et al.*, 1989; Szmant and Gassman, 1990) and accessory pigments (Kleppel *et al.*, 1989) per zooxanthella cell, a decline in the population density of the zooxanthellae (Fisk and Done, 1985; Hoegh-Guldberg and Smith, 1989), or both (Glynn and D'Croz, 1990; Lesser *et al.*, 1990). Loss of zooxanthellae *per se* has been described extensively at the organismic level (Jaap, 1979; Gates, 1990; Glynn and D'Croz, 1990; Goreau and Macfarlane, 1990; Hayes and Bush, 1990; Jokiel and Coles, 1990; Lesser *et al.*, 1990; Szmant and Gassman, 1990), yet few investigators have addressed the underlying cellular mechanism (see O'Brien and Wyttenbach, 1980; Sandeman, 1988; Lesser *et al.*, 1990) or the morphology of the cellular entity released. Insight into these features is essential for an understanding of how sea surface temperature anomalies or other environmental stresses destabilize zooxanthellae-cnidarian symbioses.

Zooxanthellae could be released by any of five mechanisms (Fig. 1), four of them resulting in the release of morphologically characteristic cellular entities. The five mechanisms are: (a) exocytosis of zooxanthellae from the host cell, resulting in the release of isolated algae (Steen and Muscatine, 1987); (b) apoptosis (programmed cell death) and (c) necrosis, both resulting in the release of

Received 17 January 1992; accepted 17 March 1992.

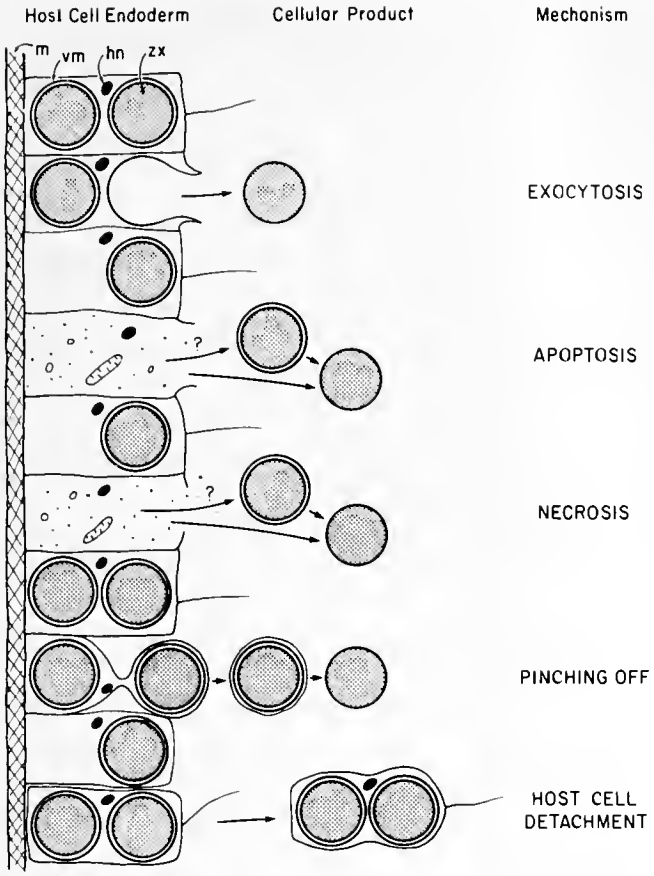

Figure 1. A schematic representation of five potential mechanisms by which zooxanthellae could be released from the endoderm of cnidarians, and the cellular entities associated with each mechanism. m, mesoglea; vm, host vacuolar membrane; hn, host cell nucleus; zx, zooxanthella (shaded for clarity of presentation).

zooxanthellae associated with remnants of the host cell (Searle *et al.*, 1982); (d) pinching off of the distal portion of the host cell, resulting in the release of zooxanthellae surrounded by the vacuolar and pinched off plasma membrane (Glider, 1983); and (e) detachment of endoderm cells from the host and release of these intact cells containing their complement of zooxanthellae.

Because cnidarians can be readily bleached in the laboratory by brief exposure to low (Steen and Muscatine, 1987; Muscatine *et al.*, 1991) or high (Hoegh-Guldberg and Smith, 1989; Glynn and D'Croz, 1990) seawater temperature, the mechanism of bleaching and the morphology of the cellular entities released can be investigated experimentally. This approach, together with scanning electron microscopy of endoderm of the Hawaiian sea anemone *A. pulchella* after experimental cold shock, revealed profiles that were interpreted as evidence of exocytosis of zooxanthellae (Steen and Muscatine, 1987). Indeed, examination of the cellular entities released 24 h after cold stress revealed abundant isolated zooxanthellae.

In this paper, we describe the cellular entity released by *A. pulchella* and the Hawaiian coral *Pocillopora damicornis* immediately after a brief exposure to low or high temperature. *P. damicornis* is one of several coral genera that have undergone extensive bleaching in the tropical eastern Pacific during the elevated temperature of the El Niño-southern oscillation event (Glynn, 1990), and during upwelling and seasonal low temperatures (see Discussion in Glynn and D'Croz, 1990; see also Walker *et al.*, 1982). Both species can be bleached in the laboratory, and bleaching is due to a reduction in zooxanthellae population density (Glynn and D'Croz, 1990; Muscatine *et al.*, 1991). Observations of the cellular entities released at hourly intervals during, and shortly after, both cold and heat stress, showed clearly that temperature stress causes detachment and release of intact endoderm cells containing zooxanthellae. Soon after release, the host cells disintegrate in the environment, leaving isolated zooxanthellae.

Materials and Methods

Animal collection and maintenance

A. pulchella and *P. damicornis* were collected at 1 meter depth on Checker Reef adjacent to the Hawaii Institute of Marine Biology (HIMB), Coconut Island, Oahu, Hawaii. Habitat temperatures range annually from 21–22°C to 26–27°C (Jokiel and Coles, 1977). *P. damicornis* colonies were placed in running seawater and used for experiments at HIMB within three days of collection. *A. pulchella* was transported to the University of California at Los Angeles, maintained in an aquarium at 25°C on a 12 h light/dark regime, and fed twice a week on *Artemia* nauplii. Prior to experiments, the anemones were starved for 24 h in an incubator (Precision Scientific Model 8) at 25°C on a 12 h light/dark cycle at 40 μmole quanta $m^{-2} \cdot s^{-1}$.

Temperature treatments

All experiments were carried out in darkness following the protocol of Muscatine *et al.* (1991).

Cold stress. Individuals of *A. pulchella* were incubated in Petri dishes (35 × 10 mm) containing 4 ml of 0.45 μm Millipore filtered seawater (MFSW) chilled to 12°C. After 2.5 h, the chilled seawater was removed and replaced with seawater at 25°C. Anemones were maintained at 25°C in an incubator in darkness for 14 h. The cellular entities released to the seawater were then collected and processed as described below.

Small branches of *P. damicornis* (2–3 cm length) were removed from each coral colony and placed in beakers containing 25 ml of MFSW chilled to 12°C (for the protein assay, corals were cold stressed at 14°C). After 4 h, the

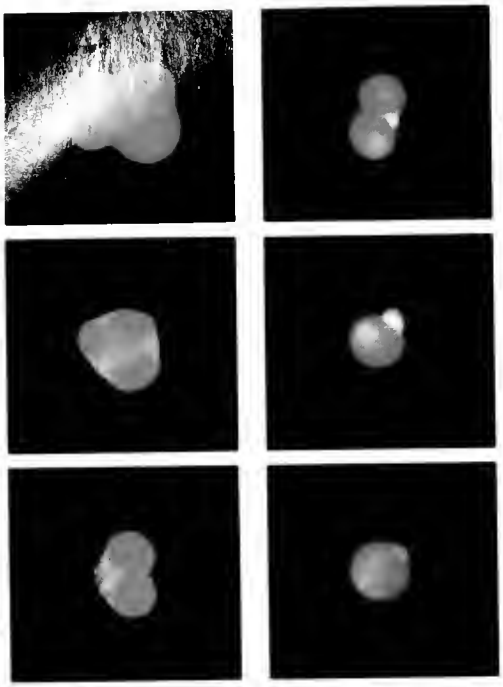

Figure 2. Left panel: photomicrographs of the host cells released to the seawater by *Aiptasia pulchella* in response to cold stress, stained for viability with fluorescein diacetate (×4000). Right panel: photomicrographs of the host cells released to the seawater by *Pocillopora damicornis* in response to cold stress, stained with the DNA specific fluorochrome Hoechst 33258 (×4000).

branches were immediately transferred to beakers containing 25 ml of MFSW at ambient temperature (23–24°C). The beakers were placed in the seawater tables for ambient temperature control and the coral tissue and seawater in the beakers was sampled after 12 h. Controls for both species were treated identically to experimental animals but were maintained at ambient seawater temperature (25°C for *A. pulchella* and 23–24°C for *P. damicornis*) for 16–16.5 h.

Heat stress. Individuals of *A. pulchella* were placed in Petri dishes (35 × 10 mm) containing 4 ml of MFSW warmed to 32°C. Small branches of *P. damicornis* (2–3 cm length) were placed in beakers containing 25 ml MFSW pre-heated to 32°C. The animals were maintained at this temperature for up to 16 h. The water surrounding experimental specimens was examined microscopically at hourly intervals and the cellular entity released to the seawater removed and treated as described below. Control animals of both species were maintained at ambient seawater temperature (25°C for *A. pulchella* and 23–24°C for *P. damicornis*) over the experimental time period.

Staining and epifluorescence microscopy

The cellular entities released during and after temperature stress were collected with a fine bore mouth suction pipette and deposited onto coverslips coated with poly-L-lysine (0.1% in distilled water). The entities were stained for viability with the fluorogenic dye fluorescein diacetate (Sigma Chemical Co., stock solution 15 mg/ml in acetone; working solution 0.04 ml in 9.96 ml 0.1 *M* sodium phosphate, 3% sodium chloride, 0.004% calcium chloride, pH 7.4). The coverslips were rinsed twice in phosphate buffer, mounted and viewed under epifluorescence with an Olympus BH-2 microscope. Non-specific esterases in viable cells hydrolyze non-polar fluorescein diacetate to polar molecular fluorescein (Schupp and Erlandsen, 1987). Additional coverslips were treated for 30 min with the DNA specific fluorochrome Hoechst 33258 (Reynolds *et al.*, 1986; Sigma Chemical Co., stock solution 5 mg/ml in distilled water; working solution 0.04 ml stock in 9.96 ml 0.1 *M* sodium phosphate, 3% sodium chloride, 0.004% calcium chloride). The coverslips were dipped in phosphate buffer, mounted, and viewed with epifluorescence microscopy.

Maceration and electron microscopy

The cellular entities released after cold stress were compared to isolated endoderm cells obtained by maceration of control anemones and corals. *A. pulchella* tissue was macerated using 0.05% collagenase (Type 1, Sigma Chemical Co.) and *P. damicornis* tissue was dissociated using calcium-free artificial seawater (Gates and Muscatine, 1992). Endoderm cells released by maceration and the cellular entities released to the seawater as a result of temperature stress were collected with a mouth pipette and transferred onto poly-L-lysine coated coverslips. The coverslips were immersed in 3% glutaraldehyde in 0.1 *M* sodium cacodylate buffer (pH 7.4) for 1 h, rinsed twice in 0.1 *M* sodium cacodylate buffer and post-fixed in 1% osmium tetroxide in 0.1 *M* sodium cacodylate for 30 min. After dehydration in 30, 50, 70, 90, 95, and 100% (×3) ethanol, the coverslips and attached cells were immersed in hexamethyldisilazane (Applied Sciences, Inc.) for 5 min (Nation, 1983), dried in air, and then mounted on aluminum stubs. The stubs were coated with gold and viewed on a Cambridge 360 scanning electron microscope, with an accelerating voltage of 10 kV.

For transmission electron microscopy, the endoderm cells released by maceration of *P. damicornis* tissue and the cellular entities released as a result of temperature stress were collected and centrifuged (Eppendorf model 5414, full speed for 30 s) in microfuge tubes (Gilson, 1.5 ml). The pellets were fixed as described for scanning electron microscopy. After partial dehydration by sequential 30 min treatments in 30, 50, and 70% ethanol, the 70% ethanol was drained from the tube and immediately replaced with 2% agar. After the agar solidified, the tube was cut away from the agar plug containing either cold-

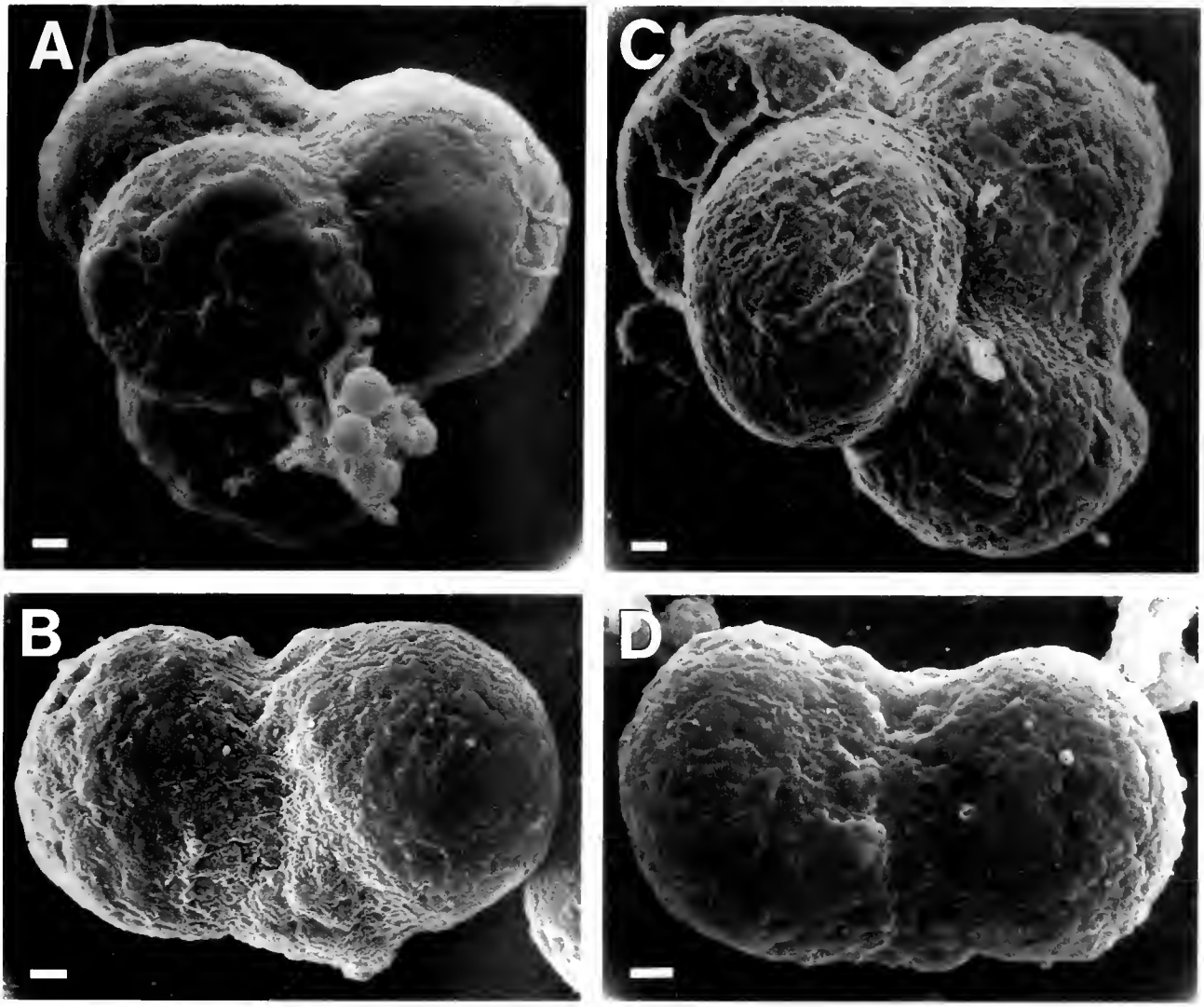

Figure 3. Scanning electron micrographs of individual host cells released by *Aiptasia pulchella* (A) and *Pocillopora damicornis* (B) in response to cold stress, and those obtained from *A. pulchella* (C) and *P. damicornis* (D) by tissue maceration. Bar = 1 μm.

stressed or macerated cells and dehydration completed through 90, 95, and 100% (×3) ethanol. The preparations were embedded via propylene oxide into epoxy resin (Spurr). Thin sections were cut using a Sorvall 6000 ultramicrotome, stained with lead acetate, and viewed on a JEOL transmission electron microscope.

Protein determination

To investigate the loss of animal protein to the seawater as a result of temperature stress, the seawater was removed from the Petri dishes of cold stressed and control *A. pulchella* and homogenized in a teflon-glass tissue grinder. Sodium dodecyl sulphate (SDS, 1% in seawater) was added to each homogenate to a final concentration of 0.05% (modified from McAuley, 1986). For *P. damicornis* a 4 ml sub-sample was removed from 25 ml seawater samples, homogenized, and treated with SDS as described above. Each sample was incubated at room temperature for 45 min to solubilize protein in the seawater and host cell membranes associated with released algae. The algae were pelleted by centrifugation (Damon/IEC model HN-S for 4 min at 3000 rpm) and the supernatant put aside for protein analysis as described below. Each algal pellet was resuspended in a known volume of MFSW and the total number of algae assessed using a hemacytometer.

Two 1 ml samples were removed from each supernatant and the amount of protein assessed spectrophotometrically using the method of Hartree (1972). To ensure that protein in the seawater samples was animal in origin and

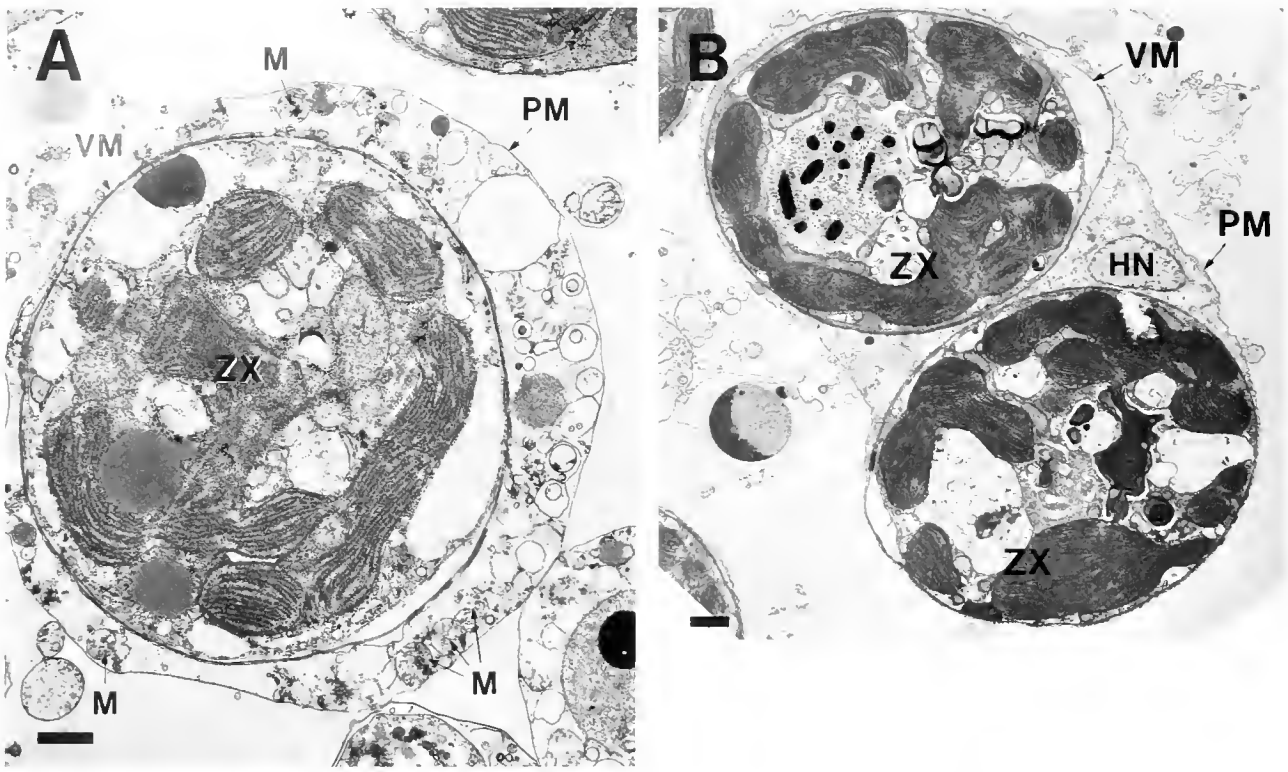

Figure 4. Transmission electron micrographs of host cells released by *Pocillopora damicornis* in response to cold stress (A), and tissue maceration (B). HN, host cell nucleus; ZX, zooxanthella; VM, vacuolar membrane; PM, host cell plasma membrane; and M, mitochondria; Bar = 1 μm.

not secreted by the algae during the 16.5-h experimental period, control algae were isolated from anemones using homogenization and centrifugation. The resulting algal pellets were washed twice in MFSW and treated for 45 min with 0.05% SDS to solublize any animal protein associated with the algal cells. After two more washes and re-suspension in MFSW, the number of algae present was assessed using a hemacytometer. Algal suspensions were cold stressed (with controls) as described for whole animals. SDS was added to a final concentration of 0.05% and the samples were left at room temperature for 45 min. The algae were removed by centrifugation and counted again to determine if cells had lysed during the incubation. The remaining supernatant was assayed for protein as before.

Results

The entities released during and after temperature stress appeared to be intact host cells. Those released after cold stress settled at the bottom of the container. In contrast, those released after heat stress accumulated at the surface of the water. Unlike the former, the latter were extremely difficult to collect and handle. They were too fragile to manipulate for electron microscopy, but we were able to view them by epifluorescence microscopy. After staining with fluorescein diacetate and Hoechst 33258, these cells were identical in profile to those released after cold stress. Host cells released in both cases appeared to be viable, with fluorescence restricted to the narrow compartment of the host cell cytoplasm that surrounded from one to five zooxanthellae (Fig. 2, left panel). Fluorescein diacetate was either not taken up by the zooxanthellae, or it was taken up but masked by the intense red autofluorescence of the zooxanthellae chlorophylls and the yellow autofluorescence of the zooxanthellae accumulation bodies. Staining with the bisbenzamide dye Hoechst 33258 revealed a single nucleus within each of these cells (Fig. 2, right panel).

When viewed with scanning electron microscopy, the cells released as a result of low temperature stress exhibited a morphology that was similar to endoderm cells released from both *P. damicornis* and *A. pulchella* by maceration (Fig. 3). In both cases, the host cell nucleus was visible under the plasma membrane. This observation suggested that entities released by thermal stress were intact cells and not "pinched off" products. Transmission electron microscopy confirmed the similarity, and clearly revealed the host cell plasma membrane, the vacuolar membrane surrounding the zooxanthellae, the host cell nucleus, and

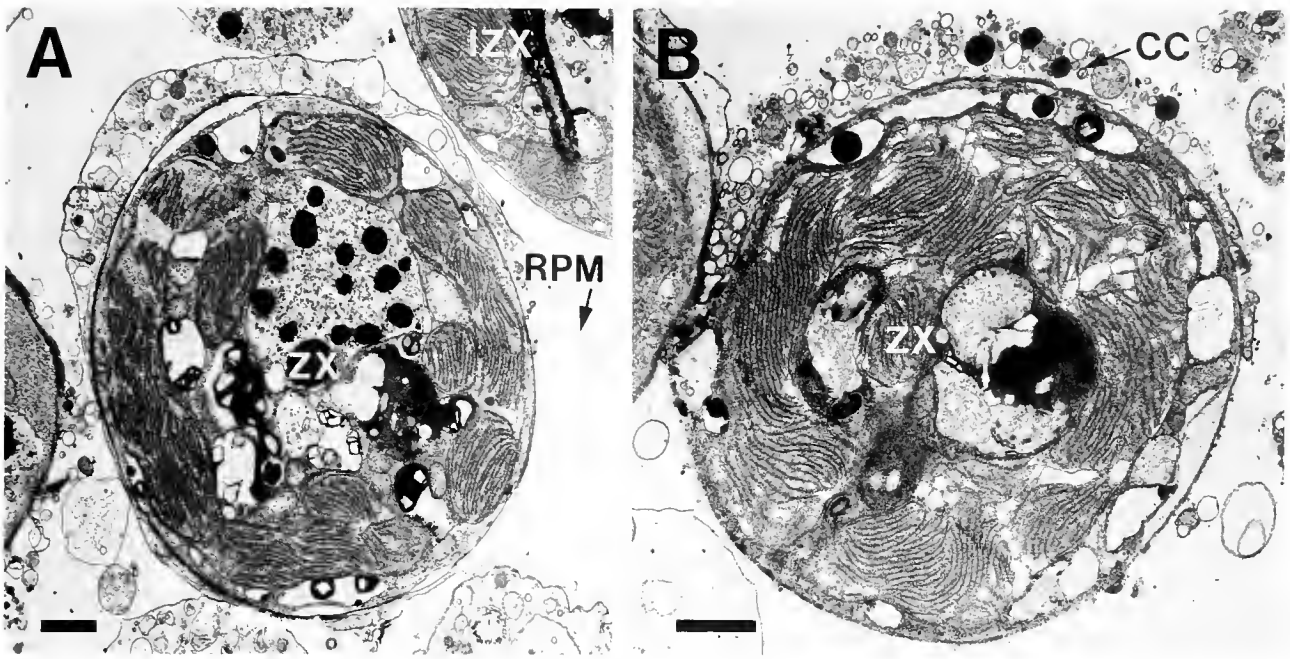

Figure 5. Transmission electron micrographs showing degradation of the host cells released by *Pocillopora damicornis* in response to cold stress. After dissociation from the epithelium, the host cell plasma membrane ruptures (A) and the cytoplasmic constituents are free to disperse in the seawater (B). ZX, zooxanthella; RPM, ruptured host cell plasma membrane; CC, host cell cytoplasmic constituents; IZX, isolated zooxanthella. Bar = 1 μm.

mitochondria (Fig. 4). Once released as a result of temperature stress, the host cells degraded rapidly. The host cell plasma membrane ruptured, the cytoplasmic components dispersed, and the vacuolar membrane disappeared completely, leaving isolated algae in the seawater (Fig. 5).

The release of intact host cells by *A. pulchella* and *P. damicornis* after thermal stress was further indicated by a significant positive correlation between the number of algae released and the total soluble protein detected in the surrounding medium after the host cells disintegrated (Fig. 6). Zooxanthellae and soluble protein released by unstressed control animals was modest (*A. pulchella*) or negligible (*P. damicornis*). Protein released by isolated zooxanthellae was below the limits of detection, and cell counts confirmed that isolated zooxanthellae had not lysed during the incubation (data not shown).

Discussion

The results of this investigation show that transient low and high temperature stress in darkness causes a reduction in the population density of zooxanthellae in *A. pulchella* and *P. damicornis*. Quantitative aspects of this reduction are described elsewhere (Steen and Muscatine, 1987; Muscatine *et al.*, 1991). This reduction is caused largely by detachment of host cells containing zooxanthellae. The profiles observed by Steen and Muscatine (1987), and interpreted as exocytosis of zooxanthellae, may have been incidentally evoked by low temperature, or by other stimuli, but neither exocytosis, apoptosis, necrosis, nor pinching off appear to be primary mechanisms of thermal bleaching by the cnidarians observed in this investigation. Loss of host cells may explain why investigators observe loss of protein by bleached corals in excess of that accounted for by loss of zooxanthellae alone (Porter *et al.*, 1989; Glynn and D'Croz, 1990; Szmant and Gassman, 1990). Despite loss of cells, the hosts survive the treatment.

Release of zooxanthellae appears to be a two-phase process. Time-lapse video of *A. pulchella* during and after low temperature shock reveals that host cells containing zooxanthellae first dissociate from the endoderm and accumulate in the coelenteron where they form pellets or remain as loose cells. Then, during the rewarming period, the pellets and cells are periodically propelled by cilia and muscles through the actinopharynx to the external medium (Hoegh-Guldberg, 1989; Muscatine *et al.*, 1991). A protocol using gradual change in temperature also revealed host cell detachment. However, this protocol was dismissed in favor of the precipitous change in temperature because the former required a more lengthy and complex sampling regime.

We speculate that the dissociation of host cells from the endoderm is caused by host cell adhesion dysfunction.

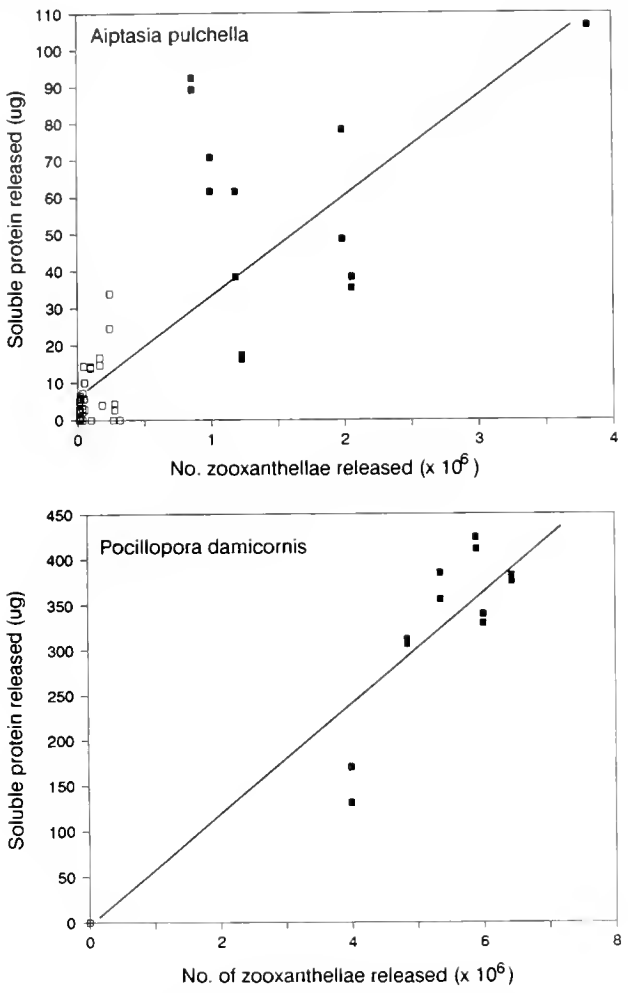

Figure 6. Appearance of soluble protein in the incubation medium concomitant with release of zooxanthellae by *Aiptasia pulchella* and *Pocillopora damicornis*. Control (open squares), cold stressed (closed squares). Line fit with linear regression (Zar, 1984), for *A. pulchella*, $r = 0.81$ ($y = 6.6012 + (2.71 \cdot 10^{-5})x$). For *P. damicornis*, $r = 0.96$ ($y = 10.2124 + (6.28 \cdot 10^{-5})x$).

The effect of high and low temperature stress on cell adhesion and cytoskeletal organization has been investigated extensively in other systems. Cell adhesion dysfunction may result from temperature-induced membrane thermotropism (Melchior and Steim, 1976; Quinn, 1989) and passive influx of ions (Grisham and Barnett, 1973; Larsen *et al.*, 1988), especially calcium which, in turn, may cause the collapse of actin and the intermediate filaments vimentin and cytokeratin (Van Bergen en Henegouwen, 1985; Coakley, 1987; Wachsberger and Coss, 1989; Cress *et al.*, 1990; Walter *et al.*, 1990). Cytoskeletal elements are co-located with the cytoplasmic domain of cell adhesion molecules (Hirano *et al.*, 1987). As elements of the cytoskeleton and cell adhesion proteins function as a whole to maintain the integrity of epithelia, disruption of the former may cause dysfunction of the latter (Takeichi, 1988). Alternatively, temperature stress may cause denaturation of proteins involved in cell adhesion (Watson and Morris, 1987; Suzuki and Choi, 1990).

Although we have described the cellular entities released after thermal stress in darkness, and a probable underlying mechanism, low salinity (Goreau, 1964; Egana and Disalvo, 1982) and sedimentation (Acevedo and Goenaga, 1986) also evoke bleaching. Moreover, at high temperature, the bleaching response in some cnidarians is thought to be exacerbated by high irradiance (Coles and Jokiel, 1978), ultraviolet radiation (Harriot, 1985; Jokiel and York, 1982; Lesser *et al.*, 1990), and active oxygen (Lesser and Shick, 1990). These other types of stress cause decreased zooxanthellae population density, but the mechanism of bleaching in each instance is still unknown. It may be fundamentally different from that observed in thermal bleaching. For example, we speculate that low salinity may cause the cnidarians to lose zooxanthellae by the mechanical disruption caused by hypoosmotic shock (*i.e.*, necrosis). We suggest that bleaching be defined more rigorously in terms of both the environmental stress, and the morphology of the cellular entity released. Studies are now under way to determine if host cell detachment after thermal stress is a general phenomenon or specific to selected cnidarian genera.

Acknowledgments

We thank Alicia Thompson and Birgitta Sjostrand for assisting with electron microscopy, Gordon Grau for providing an epifluorescence microscope at HIMB, and the Office of Naval Research (Grant #NOOO14-89-J-3246 to L.M.) and the National Science Foundation (Grant #OCE-8723090 to L.M.) for research support.

Literature Cited

Acevedo, R., and C. Goenaga. 1986. Note on coral bleaching after a chronic flooding in southwestern Puerto Rico. *Caribb. J. Sci.* **22:** 225.

Brown, B. E., and Suharsono. 1990. Damage and recovery of coral reefs affected by El Nino related seawater warming in the Thousand Islands, Indonesia. *Coral Reefs* **8:** 63–170.

Coakley, W. T. 1987. Hyperthermia effects on the cytoskeleton and on cell morphology. *Soc. Exp. Biol.* **41:** 187–211.

Coles, S. J., and Y. H. Fadlallah. 1990. Reef coral survival and mortality at low temperatures in the Arabian Gulf: new species-specific lower temperature limits. *Coral Reefs* **9:** 231–237.

Coles, S. L., and P. L. Jokiel. 1977. Effects of temperature on photosynthesis and respiration in hermatypic corals. *Mar. Biol.* **43:** 209–216.

Coles, S. L., and P. L. Jokiel. 1978. Synergistic effects of temperature, salinity and light on the hermatypic coral *Montipora verrucosa*. *Mar. Biol.* **49:** 187–195.

Cress, A. E., J. A. Majda, J. R. Glass, D. E. Stringer, and E. W. Gerner. 1990. Alteration of cellular adhesion by heat shock. *Exp. Cell Res.* **190:** 40–46.

Drew, E. A. 1972. The biology and physiology of alga-invertebrate symbioses. II. The density of symbiotic algal cells in a number of hermatypic corals and alcyonarians from various depths. *J. Exp. Mar. Biol. Ecol.* **9:** 71–75.

Egana, A. C., and L. H. DiSalvo. 1982. Mass expulsion of zooxanthellae by Easter Island corals. *Pac. Sci.* **36:** 61–63.

Fisk, T. A., and T. J. Done. 1985. Taxonomic and bathymetric patterns of bleaching in corals, Myrmidon Reef (Queensland). *Proc. Fifth Int. Coral Reef Cong.* **6:** 149–154.

Gates, R. D. 1990. Seawater temperature and sublethal coral bleaching in Jamaica. *Coral Reefs* **8:** 193–198.

Gates, R. D., and L. Muscatine. 1992. Three methods for isolating viable anthozoan endoderm cells with their intracellular symbiotic dinoflagellates. *Coral Reefs* (in press).

Glider, W. V. 1983. The biology of the association of *Symbiodinium microadriaticum* with *Aiptasia pallida:* an anemone-alga symbiosis. Ph.D. Thesis, University of Nebraska. 102 pp.

Glider, W. V., D. Phipps, and R. L. Pardy. 1980. Localization of symbiotic dinoflagellate cells within tentacle tissue of *Aiptasia pallida* (Coelenterata, Anthozoa). *Trans. Am. Microsc. Soc.* **99:** 426–438.

Glynn, P. 1990. Coral mortality and disturbances to coral reefs in the tropical eastern Pacific. Pp. 55–126 in *Global Ecological Consequences of the 1982–83 El-Nino Southern Oscillation,* P. W. Glynn, ed. Elsevier, Amsterdam.

Glynn, P., and L. D'Croz. 1990. Experimental evidence for high temperature stress as the cause of El Nino-coincident coral mortality. *Coral Reefs* **8:** 181–192.

Goreau, T. F. 1964. Mass expulsion of zooxanthellae from Jamaican reef communities after Hurricane Flora. *Science* **145:** 383–386.

Goreau, T. J., and A. H. Macfarlane. 1990. Reduced growth rate of *Montastrea annularis* following the 1987–1988 coral-bleaching event. *Coral Reefs* **8:** 211–216.

Grisham, C. M., and R. E. Barnett. 1973. The role of lipid-phase transitions in the regulation of the (sodium + potassium) adenosine triphosphatase. *Biochemistry* **12:** 2635–2637.

Harriot, V. J. 1985. Mortality rates of scleractinian corals before and during a mass bleaching event. *Mar. Ecol. Prog. Ser.* **21:** 81–88.

Hartree, E. F. 1972. Determination of protein: a modification of the Lowry method that gives a linear photometric response. *Anal. Biochem.* **48:** 422–427.

Hayes, R. L., and P. G. Bush. 1990. Microscopic observations of recovery in the reef-building scleractinian coral, *Montastrea annularis,* after bleaching on a Cayman reef. *Coral Reefs* **8:** 203–209.

Hirano, S., A. Nose, K. Hatta, A. Kawakami, and M. Takeichi. 1987. Calcium-dependent cell-cell adhesion molecules (Cadherins): subclass specificities and possible involvement of actin bundles. *J. Cell Biol.* **105:** 2501–2510.

Hoegh-Guldberg, O. 1989. The regulatory biology of plant-animal endosymbiosis. Ph.D. Thesis, University of California at Los Angeles. 309 pp.

Hoegh-Guldberg, O., and G. J. Smith. 1989. The effect of sudden changes in temperature, light, and salinity on population density and export of zooxanthellae from the reef corals *Seriatopora hystrix* and *Stylophora pistillata. J. Exp. Mar. Biol. Ecol.* **129:** 279–303.

Jaap, W. 1979. Observations on zooxanthellae expulsion at Middle Sambo Reef, Florida Keys. *Bull. Mar. Sci.* **29:** 414–422.

Jokiel, P. L., and S. L. Coles. 1977. Effects of temperature on the mortality and growth of Hawaiian reef corals. *Mar. Biol.* **43:** 201–208.

Jokiel, P. L., and S. L. Coles. 1990. Response of Hawaiian and other Indo-Pacific reef corals to elevated temperature. *Coral Reefs* **8:** 155–162.

Jokiel, P. L., and R. H. York. 1982. Solar ultraviolet photobiology of the reef coral *Pocillopora damicornis* and symbiotic zooxanthellae. *Bull. Mar. Sci.* **32:** 301–315.

Kleppel, G. S., R. E. Dodge, and C. J. Reese. 1989. Changes in pigmentation associated with the bleaching of stony corals. *Limnol. Oceanogr.* **34:** 1331–1335.

Larsen, T., S. Solberg, R. Johansen, and L. Jorgensen. 1988. Effect of cooling in the intracellular concentrations of Na^+, K^+ and Cl^- in cultured human endothelial cells. *Scand. J. Lab. Invest.* **48:** 565–571.

Lesser, M. P., and J. M. Shick. 1990. Photoadaptation and defenses against oxygen toxicity in zooxanthellae from natural populations of symbiotic cnidarians. *J. Exp. Mar. Biol. Ecol.* **134:** 129–141.

Lesser, M. P., W. R. Stochaj, D. W. Tapley, and J. M. Shick. 1990. Bleaching in coral reef anthozoans: effects of irradiance, ultraviolet radiation, and temperature on the activities of protective enzymes against active oxygen. *Coral Reefs* **8:** 225–232.

McAuley, P. J. 1986. Isolation of viable uncontaminated *Chlorella* from green hydra. *Limnol. Oceanogr.* **31:** 222–224.

Melchior, D., and J. M. Steim. 1976. Thermotropic transitions in biomembranes. *Ann. Rev. Biophys. Bioeng.* **5:** 205–238.

Muscatine, L. 1990. The role of symbiotic algae in carbon and energy flux in reef corals. Pp. 75–87 in *Coral Reefs,* Z. Dubinsky, ed. Elsevier, Amsterdam.

Muscatine, L., D. Grossman, and J. Doino. 1991. Release of symbiotic algae by tropical sea anemones and corals after cold shock. *Mar. Ecol. Prog. Ser.* 77: 233–243.

Nation, J. L. 1983. A new method using hexamethyldisilazane for preparation of soft insect tissue for scanning electron microscopy. *Stain. Technol.* **56:** 347–351.

O'Brien, T. L., and C. R. Wyttenbach. 1980. Some effects of temperature on the symbiotic association between zoochlorellae (Chlorophyceae) and the sea anemone *Anthopleura xanthogrammica. Trans. Am. Microsc. Soc.* **99:** 221–225.

Porter, J. W., W. K. Fitt, H. J. Spero, C. S. Rogers, and M. W. White. 1989. Bleaching in reef corals: physiological and stable isotope responses. *Proc. Natl. Acad. Sci. USA* **86:** 9342–9346.

Quinn, P. J. 1989. Principles of membrane stability and phase behavior under extreme conditions. *J. Bioenergetics Biomembranes* **21:** 3–19.

Reynolds, C. P., A. T. Black, and J. N. Woody. 1986. Sensitive method for detecting viable cells seeded into bone marrow. *Cancer Res.* **46:** 5878–5881.

Sandeman, I. M. 1988. Coral bleaching at Discovery Bay, Jamaica: a possible mechanism for temperature-related bleaching. Pp. 46–48 in *Mass Bleaching of Corals in the Caribbean: A Research Strategy.* Research report 88-2, J. Ogden and R. Wicklund, eds. NOAA Undersea Research Program, Rockville, MD.

Schupp, D. G., and S. L. Erlandsen. 1987. A new method to determine *Giardia* cyst viability: correlation of fluorescein diacetate and propidium iodide staining and animal infectivity. *Appl. Environ. Microbiol.* **53:** 704–707.

Searle, J., J. F. R. Kerr, and C. J. Bishop. 1982. Necrosis and apoptosis: distinct modes of cell death with fundamentally different significance. *Pathol. Annu.* **17:** 229–259.

Steen, R. G., and L. Muscatine. 1987. Low temperature evokes rapid exocytosis of symbiotic algae by a sea anemone. *Biol. Bull.* **172:** 246–263.

Suzuki, M., and B. H. Choi. 1990. The behavior of the extracellular matrix and the basal lamina during the repair of cryogenic injury in the adult rat cerebral cortex. *Acta. Neuropathol.* **80:** 355–361.

Szmant, A., and N. J. Gassman. 1990. The effects of prolonged "bleaching" on the tissue biomass and reproduction of the reef coral *Montastrea annularis*. *Coral Reefs* **8:** 217–224.

Trench, R. K. 1987. Dinoflagellates in non-parasitic symbiosis. Pp. 530–570 in *Biology of Dinoflagellates*, F. J. R. Taylor, ed. Blackwell, Oxford.

Takeichi, M. 1988. The cadherins: cell-cell adhesion molecules controlling animal morphogenesis. *Development* **102:** 639–655.

Van Bergen en Henegouwen, P. M. P., W. J. R. M. Jordi, G. Van Dongen, F. C. S. Ramaekers, H. Amesz, and W. A. M. Linnemans. 1985. Studies on a possible relationship between alterations in the cytoskeleton and induction of heat shock protein synthesis in mammalian cell. *Int. J. Hyperthermia* **11:** 69–83.

Wachsberger, P. R., and R. A. Coss. 1989. Acrylamide sensitization of the heat response of the cytoskeleton and cytotoxicity in attaching and well-spread synchronous Chinese hamster ovary cells. *Cell Motility Cytoskel.* **13:** 67–82.

Walker, N. D., II. H. Roberts, L. J. Rouse, Jr., and O. K. Huh. 1982. Thermal history of reef-associated environments during a record cold-air outbreak event. *Coral Reefs* **1:** 83–87.

Walter, M. F., N. S. Petersen, and H. Biessman. 1990. Heat shock causes the collapse of the intermediate filament cytoskeleton in *Drosophila* embryos. *Dev. Genet.* **11:** 270–279.

Watson, P. F., and G. J. Morris. 1987. Cold shock injury in animal cells. *Symp. Soc. Exp. Biol.* **41:** 311–340.

Williams, E. H., Jr., and L. Bunkley-Williams. 1990. The world-wide coral reef bleaching cycle and related sources of coral mortality. *Atoll Res. Bull.* **335:** 1–71.

Zar, J. H. 1984. *Biostatistical Analysis*, 2nd ed. Prentice Hall, New Jersey.

Reference: *Biol. Bull.* **182:** 333–340. (June, 1992)

Modulation of Crayfish Hearts by FMRFamide-related Peptides

A. JOFFRE MERCIER[1] AND RUNE T. RUSSENES

Department of Biological Sciences, Brock University, St. Catharines, Ontario L2S 3A1 Canada

Abstract. The present study examines effects of FMRFamide-related peptides (FaRPs) on crayfish heart. Lobster peptides F_1 (TNRNFLRFamide) and F_2 (SDRNFLRFamide) increase the rate and amplitude of heart beat in hearts isolated from *Procambarus clarkii*. Thresholds for these effects were between 10^{-10} and 10^{-9} *M* for F_2 and between 10^{-9} and 10^{-8} *M* for F_1. FMRFamide and FLRFamide elicited similar cardioexcitatory effects, but at thresholds of approximately 10^{-7} *M*. Thus, the amino-terminal extensions "TNRN" and "SDRN" enhance the excitatory actions of FMRFamide and FLRFamide. SchistoFLRFamide (PDVDHVFLRFamide) and leucomyosuppressin (pQDVDHVFLRFamide) markedly decrease the rate of cardiac contractions at 10^{-9} to 10^{-8} *M* and can suppress the cardiac rhythm for one minute or more at 10^{-7} *M*. The amino-terminal extensions of these two peptides, therefore, are necessary for inhibition of heart rate. Both of these peptides cause an initial reduction in contraction amplitude, but contractions subsequently increase in the presence of schistoFLRFamide. Thus, crayfish hearts are sensitive to several FMRFamide-related peptides, but the sites and mechanisms of action remain to be determined.

Introduction

Since the discovery of the neuropeptide FMRFamide (Phe-Met-Arg-Phe-NH_2) in the bivalve mollusk *Macrocallista nimbosa* (Price and Greenberg, 1977), FMRFamide-related peptides (FaRPs) have been reported in numerous invertebrate and vertebrate species (*e.g.*, Boer *et al.*, 1980; Dockray *et al.*, 1983; Watson *et al.*, 1984; Grimmelikhuijzen and Graff, 1985; Lehman and Price, 1987; Li and Calabrese, 1987; Elphick *et al.*, 1989; Robb *et al.*, 1989; Krajniak and Price, 1990). It is now recognized that FaRPs represent members of a very large family of neuropeptides that is widely distributed throughout the animal kingdom (Greenberg and Price, 1983; Price and Greenberg, 1989).

In crustaceans, FMRFamide-like immunoreactivity (FLI) has been found throughout most of the nervous system, but the highest amounts are present in the pericardial organs (POs) (Koberski *et al.*, 1987; Marder *et al.*, 1987; Krajniak, 1991; Mercier *et al.*, 1991b). Because the POs are located in the pericardial sinus just outside the heart (Maynard, 1960), and because they release cardioactive hormones (*e.g.*, Cooke and Sullivan, 1982; Kravitz *et al.*, 1980), the heart is likely to be an important target for crustacean FaRPs. So far, only two FaRPs have been sequenced and identified in extracts of the lobster POs, although other FMRFamide-like immunoreactive material is present (Trimmer *et al.*, 1987). These two peptides have the sequences TNRNFLRFamide (F_1) and SDRNFLRFamide (F_2). Both of these peptides excite isolated hearts of lobsters (Kravitz *et al.*, 1987) and blue crabs (Krajniak, 1991). However, the effects of these and other FaRPs on crustacean hearts have not been thoroughly investigated.

The primary aim of the present study was to examine in greater detail the cardio-regulatory effects of lobster peptides F_1 and F_2. The effects of these two peptides were studied on isolated crayfish hearts. To examine the relationship between amino acid sequence and biological activity, the effects of F_1 and F_2 were compared with those of FMRFamide, FLRFamide, and two FaRPs with significantly different amino-terminal extensions: leucomyosuppressin (LMS), with the sequence pQDVDHVFLRFamide (Holman *et al.*, 1986) and SchistoFLRFamide (Sch), with the sequence PDVDHVFLRFamide

Received 16 September 1991; accepted 26 March 1992.

[1] To whom correspondence should be addressed.

(Robb *et al.*, 1989). The crayfish heart was sensitive to all of the compounds tested.

Materials and Methods

Crayfish were obtained commercially and were maintained in aerated freshwater tanks at 14.5°C on a mixed vegetable diet.

Synthetic peptides were applied to spontaneously active crayfish hearts. The dorsal carapace, containing the heart and pericardium, was dissected from crayfish weighing approximately 3 g and was pinned to a Sylgard-lined dish with the ventral side up. The pericardial membrane was severed and pinned at each side to allow the bathing fluid access to the heart. The recording chamber, which had a volume of 0.5 ml, was perfused with crayfish saline (van Harraveld, 1936), which had the following constituents (in m*M*): Na^+, 205; Cl^-, 232; K^+, 5.3; Ca^{++}, 13.5; Mg^{++}, 2.5; HEPES, 5.0 (pH 7.4). Saline was added to the chamber at a rate of 3.0 ml min^{-1} using a peristaltic pump and was removed at the other end of the chamber by suction. The entire preparation was superfused continuously in this manner. The temperature was maintained at 14–16°C, but did not vary by more than 1°C during any one experiment. Heart preparations were viable for up to 8 h.

Contractions were recorded by connecting the sternal artery to a tension transducer using two insect pins that were hooked at one end and glued to the transducer at the other end. The artery and heart were stretched until the maximum contraction amplitude was obtained. Contractions were displayed on a Grass Model 7B Polygraph. The rate and amplitude of contractions were measured manually over intervals of either 30 s or 1 min.

Peptides were applied by changing the perfusate to a solution containing a selected peptide concentration. Peptides were present in the bathing chamber for 8–10 min; 10 min was chosen arbitrarily as the maximum time of exposure. In a few cases, it was obvious that the maximal effect of the peptide had already occurred, and washout was begun after 8 min. The maximal effect of the peptides generally occurred well before this time, except for the increased amplitude caused by SchistoFLRFamide (see Results).

During washout, the effects of the peptides began to subside within 5 min and had completely worn off within 20–30 min. In many cases (*e.g.*, Fig. 7), the effects wore off more rapidly. Each peptide was tested by starting with the lowest concentration (10^{-12} *M*) and subsequently increasing the dosage in 10-fold increments until the entire response range had been tested. Successive doses were always given after the previous dose was completely washed out. Three successive applications of 1×10^{-9} *M* F_2 onto the same preparation yielded virtually identical effects each time. The results reported here were obtained from a total of 37 preparations. In all but six experiments, each peptide was tested on one preparation only. The number of preparations used for testing each peptide is indicated in the figure legends.

SchistoFLRFamide and leucomyosuppressin were obtained from Peninsula Laboratories Ltd. (Belmont, California). Peptides F_1 and F_2 were synthesized by Dr. D. McCormack (Rochester, Minnesota) and were a gift from Dr. M. Schiebe. FMRFamide, FLRFamide, and all other chemicals were obtained from Sigma Chemical Co. (St. Louis, Missouri).

In each case, the error value reported is the standard error of the mean. Statistical significance of differences between mean values was determined using a Student's *t* Test (Furguson, 1971).

Results

Of the six neuropeptides tested, four elicited responses that were exclusively cardio-excitatory. FMRFamide, FLRFamide, F_1, and F_2 increased both the rate and amplitude of contractions of isolated *Procambarus* hearts. Figure 1 shows representative examples of the effects of these four peptides, at doses that elicited approximately equivalent responses. The onset of such responses usually

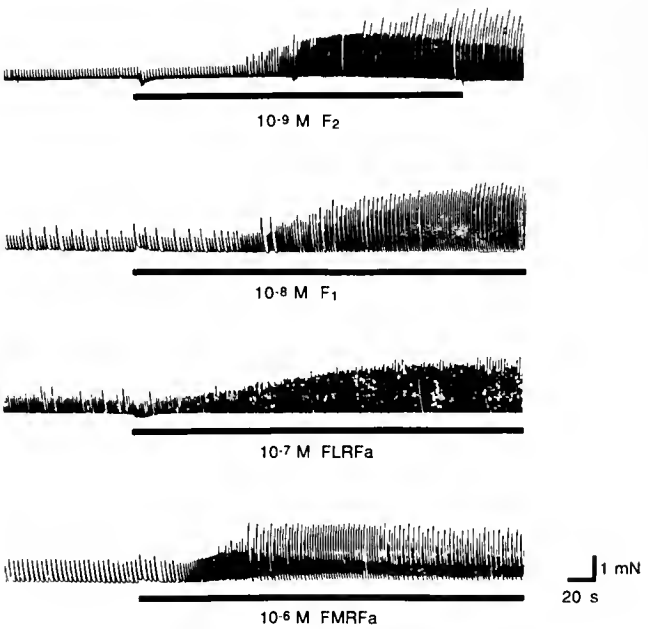

Figure 1. Effects of excitatory FaRPs on crayfish heart contractions. Each panel shows chart recordings of spontaneous contractions. Peptides, at the concentrations indicated, were present in the bathing solution during the periods indicated by the thick horizontal bars. The recordings were obtained from different preparations. (Abbreviations: FLRFa for FLRFamide, FMRFa for FMRFamide, F_1 and F_2 as in text.)

occurred within 60–90 s after the peptide entered the bathing chamber, and the lag-time was shorter at higher peptide concentrations. The effects on heart rate and contraction amplitude were always completely reversed by 20–30 min of washing in normal saline (data not shown). None of these four peptides elicited any inhibitory effects.

Log dose-response curves, constructed for the four excitatory peptides (Fig. 2), were based on the responses of five to six preparations in each case. Responses were expressed as the percentage change in contraction rate and the percentage change in amplitude by comparing the maximal effect of each peptide with the average contraction rate, or contraction amplitude, during the 3 min period immediately preceding peptide application. Peptides F_1 and F_2 caused a more pronounced increase in the amplitude of the contractions than on their rate. For FLRFamide and FMRFamide, however, the percentage change in amplitude was similar to the change in rate in each case.

Differences in the relative potencies of the peptides were more prominent for the effect on contraction amplitude (Fig. 2A) than for the effect on rate (Fig. 2B). A comparison of the effects on contraction amplitude gave the following results. F_2 was the most potent peptide, with a threshold concentration between 10^{-10} and 10^{-9} *M*. A comparison of the effects of 10^{-9} *M* F_2 and 10^{-5} *M* FMRFamide suggests that F_2 was up to 10,000 times more potent than FMRFamide. F_1 was the next most potent peptide, with a threshold between 10^{-9} and 10^{-8} *M*, and was approximately 1000 times more potent than FMRFamide (based on the effects of 10^{-8} *M* F_1 and 10^{-5} *M* FMRFamide). FLRFamide was about 10 times more potent than FMRFamide (based on the effects of 10^{-7} *M* FLRFamide and 10^{-6} *M* FMRFamide), but the threshold concentrations for both appeared to be between 10^{-8} and 10^{-7} *M*. FMRFamide gave a relatively broad log-dose *versus* response curve, which rose steadily over the concentration range of 10^{-8} to 10^{-5} *M*, while the other peptides appeared to reach saturation within slightly narrower concentration ranges.

Differences in relative potency were not as marked when comparing the effects of the excitatory peptides on contraction rate (Fig. 2B). F_2 and F_1 had approximately equivalent effects on heart rate, but both compounds were about 100 times more potent than FLRFamide and FMRFamide. The log-dose *versus* response curves for FLRFamide and FMRFamide were very similar.

SchistoFLRFamide (Sch) and leucomyosuppressin (LMS) had inhibitory effects on cardiac contractions at concentrations of 10^{-9} to 10^{-7} *M* (Figs. 3–5). The rate of spontaneous contractions was reduced consistently by both peptides. At 10^{-7} *M*, contractions were completely suppressed for a period lasting 1 min or longer, after which

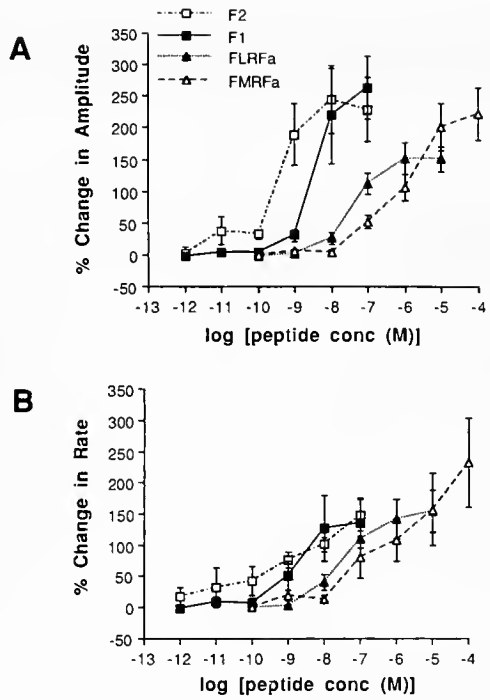

Figure 2. Log-dose *versus* response curves for the effects of excitatory FaRPs on the amplitude of cardiac contractions (A) and on heart rate (B). The percentage change in rate or in amplitude was determined by comparing the maximum value obtained in the presence of the peptide from the average value during the three minutes prior to peptide application:

$$\% \text{ change} = [(\text{peak value} - \text{initial value})/\text{initial value}] \times 100.$$

Each point represents the mean value for five preparations in the case of F_2 and for six preparations in all other cases. Error bars depict standard errors of the means. (Abbreviations are as in Fig. 1.)

contractions resumed at a rate that was lower than before peptide application (Figs. 3, 4, and 6A). Dose-response curves, based on the maximal reduction in rate, were markedly similar for these two peptides (Fig. 5A). The threshold for inhibition of heart rate was between 10^{-10} and 10^{-9} *M*.

Effects of Sch and LMS on the amplitude of contractions were more complex. For most preparations, such as the one represented in Figure 4, the contractions that persisted in the presence of either Sch or LMS were initially reduced in amplitude. This type of effect was observed in 4 of 6 preparations exposed to Sch and in 6 of 8 preparations exposed to LMS. Figure 3 is an example of recordings from a preparation in which no substantial reduction in contraction amplitude occurred during exposure to LMS. When observed, reductions in contraction size were usually transient. Approximately 2–4 min after peptide exposure began, 10^{-7} *M* Sch caused a substantial increase in contraction size above the level observed prior

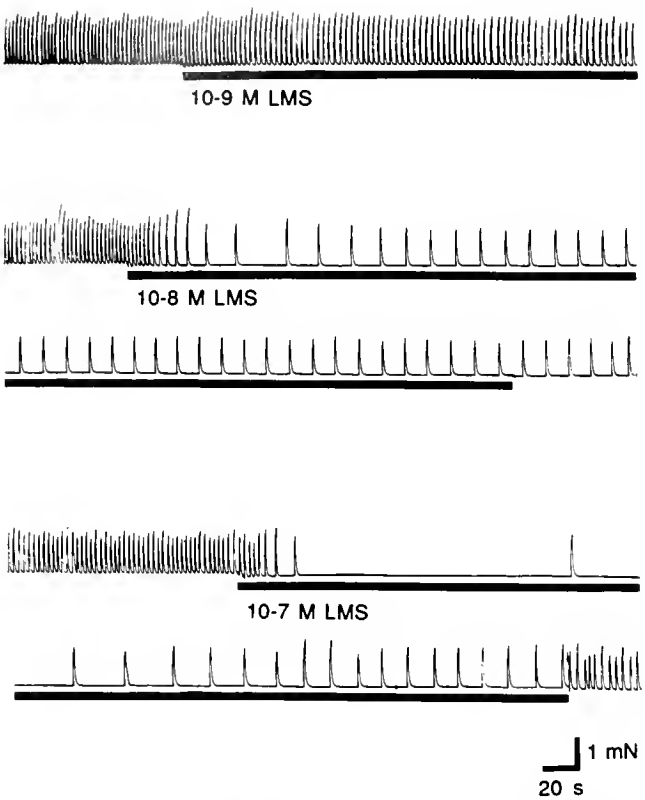

Figure 3. Effects of LMS on heart contractions. Each panel shows chart recordings of spontaneous cardiac contractions. LMS was present in the bathing solution during the periods indicated by the thick horizontal bars at the concentrations indicated. The recordings were all from the same preparation.

to peptide exposure (Fig. 4). Thus, the effect of Sch on contraction amplitude appeared to be biphasic.

Log-dose *versus* response curves for the initial effect of LMS and Sch on contraction amplitude were obtained by comparing responses 1 min after the peptide entered the bath with the average amplitude over a 2-min period prior to peptide exposure (Fig. 5B). (The change in contraction size was expressed as a percentage of the amplitude during the period prior to peptide application.) The dramatic reduction in contraction size at 10^{-7} *M* was due mainly to the fact that this dose completely suppressed contractions in most preparations. Log-dose *versus* response curves for the increase in amplitude that occurred later were obtained by comparing the average contraction amplitude during the 2-min period before peptide application with the highest average amplitude over a 1-min period during exposure to the peptide or during the first 5 min of the wash-out period (Fig. 5C). On average, contraction amplitudes doubled in 10^{-8} *M* Sch and tripled in 10^{-7} *M* Sch. In contrast, 10^{-7} *M* LMS caused only a 25% increase in contraction size.

The increase in contraction amplitude caused by Sch developed more slowly than did the reduction in contraction rate. Figure 6A shows the time course of the effects of 10^{-8} *M* Sch for an individual preparation. In this case, heart rate began to decline within 2 min of peptide exposure and reached its lowest value 6 min later. Contraction amplitude, however, did not begin to rise until 6 min after the peptide entered the bath and required an additional 8 min to reach its maximal level. In experiments with six preparations exposed to 10^{-7} *M* Sch, the mean time for the maximal inhibition of heart rate (1.3 ± 0.36 min) was shorter than the mean time for the maximal increase in amplitude (10.9 ± 2.0 min), and the difference in means was statistically significant ($t = 5.56$; $P < 0.01$).

In contrast, the increased amplitude caused by F_2 occurred rapidly and usually coincided with the maximal increase in rate, as in the example shown in Figure 6B. Mean times for the maximal rate (2.7 ± 0.68 min) and amplitude (3.1 ± 0.99) for five preparations were not significantly different ($t = 0.93$; $P > 0.4$). As in the example shown in Figure 6B, the heart rate often declined rapidly from the peak value, even though F_2 was still present in the bathing solution. Contraction amplitude, however, remained elevated until the peptide was removed.

As a first step toward examining potential interactions between FaRPs, the effect of a mixture of F_2 and Sch was studied. We were particularly interested in determining

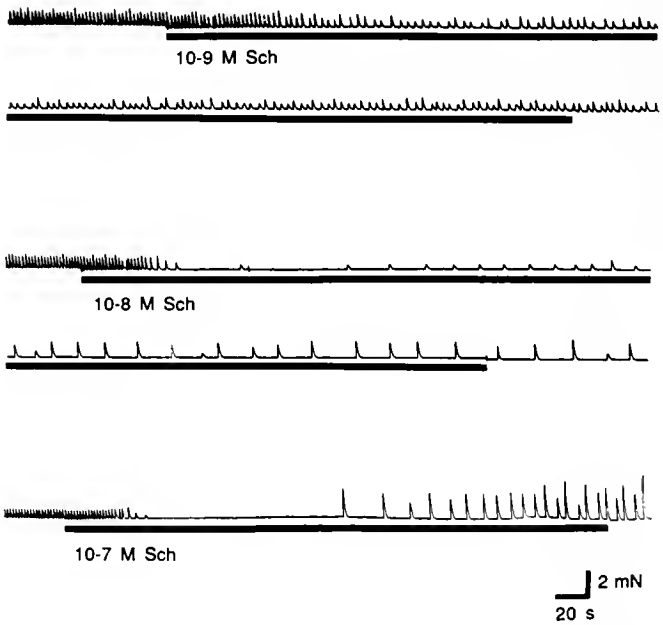

Figure 4. Effects of Sch on heart contractions. Each panel shows chart recordings of spontaneous cardiac contractions. Sch was present in the bathing solution during the periods indicated by the thick horizontal bars at the concentrations indicated. The recordings were all from the same preparation.

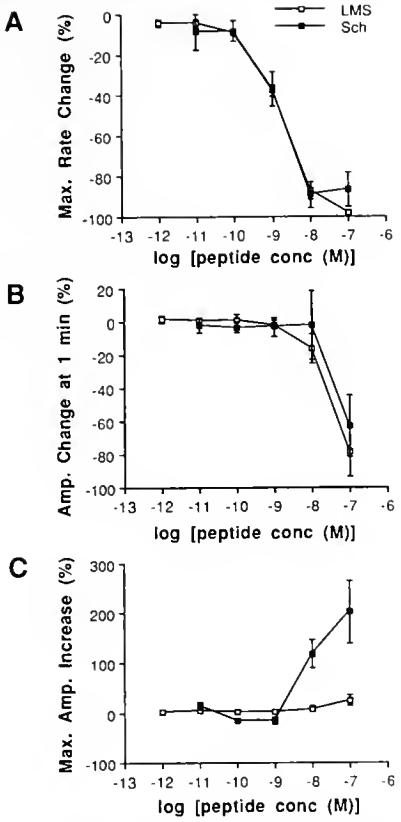

Figure 5. Log-dose *versus* response curves for effects of LMS and Sch on heart rate (A), on the amplitude of contractions after 1 min of peptide exposure (B) and on the maximum amplitude of contractions during peptide exposure or in the first 5 min of the wash-out period (C). The change in rate or in amplitude was determined by comparing the value obtained in response to the peptide with the average value prior to peptide application and was expressed as a percentage of the initial value as in Figure 2. Effects on heart rate (A) were determined using the minimum heart rate during peptide exposure. Each point represents the mean value obtained from eight preparations exposed to LMS and from six preparations exposed to Sch. Error bars depict standard errors of the means.

whether the chronotropic action of one peptide might predominate or, alternatively, whether the two substances might produce an "additive" response. Figure 7 illustrates the responses of an individual preparation in which 10^{-8} M F_2 caused a rapid 60% increase in heart rate and 10^{-8} M Sch decreased heart rate by about 50%. A mixture of the two peptides produced a heart rate that increased only slightly and was comparatively stable. Subsequent application of F_2 showed that the heart was capable of responding to this peptide as before. Thus, these two peptides exert chronotropic actions that are mutually antagonistic and tend to cancel each other out when combined. Sch did not antagonize the effect of F_2 on contraction size and may even have potentiated it (Fig. 7). This experiment was performed six times with qualitatively similar results

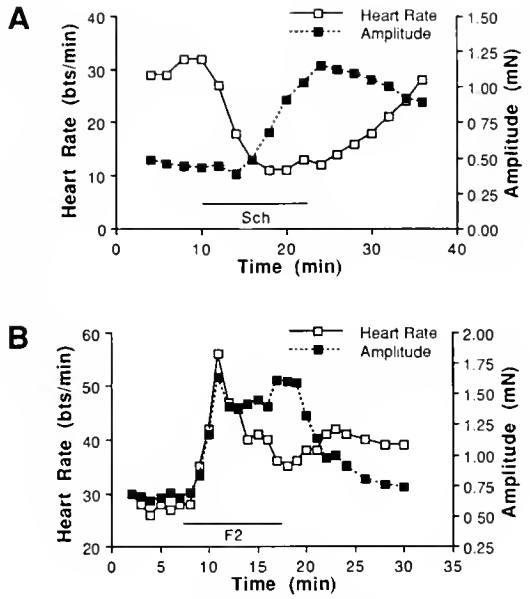

Figure 6. Time course for the effects of Sch (A) and F_2 (B) on the rate and amplitude of cardiac contractions. The peptides were present in the bathing solution at concentrations of 10^{-8} M during the periods indicated by the horizontal bars. The data for (A) and (B) were obtained from the same experimental preparation.

in each case. Sch always antagonized the chronotropic effect of F_2 but not its inotropic effect. Thus, while F_2 is chronotropically and inotropically excitatory, and Sch is chronotropically inhibitory, a mixture of these FaRPs can produce a response that is predominantly inotropic.

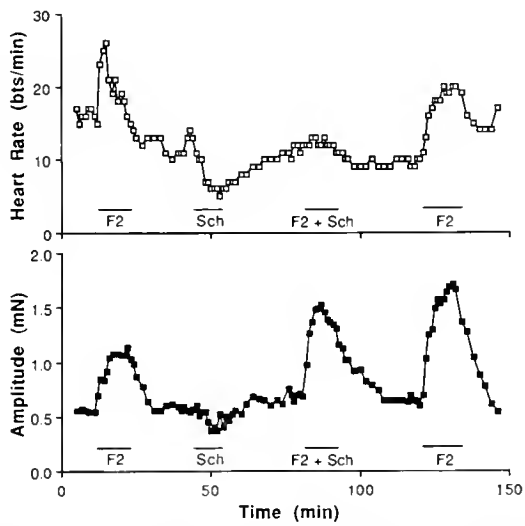

Figure 7. The effect of a mixture of F_2 and Sch on the rate (upper panel) and amplitude (lower panel) of cardiac contractions. The data were obtained from a single preparation. Peptides were present in the bathing solution at 10^{-8} M at the times indicated by the horizontal bars.

Discussion

FaRPs have been reported to modulate the activity of hearts from several types of invertebrates, including mollusks (*e.g.*, Painter and Greenberg, 1982; Price *et al.*, 1990), insects (Cuthbert and Evans, 1989; Robb *et al.*, 1989), leeches (Li and Calabrese, 1987), and crustaceans (Kravitz *et al.*, 1987; Krajniak, 1991). Some FaRPs elicit responses that are mainly excitatory, others elicit responses that are primarily inhibitory, and others are reported to elicit mixed or biphasic responses (Cuthbert and Evans, 1989). The type of response depends on the chemical structure of the peptide and on the invertebrate species (Painter and Greenberg, 1982).

The present study did not investigate the sites or mechanisms of action of the various FaRPs tested. Changes in rate are most likely to result from effects on the cardiac ganglion, which sets the overall rhythm for cardiac contractions (Maynard, 1960). Changes in the amplitude of contractions could be due to changes in the number or frequency of nerve impulses per burst produced in the cardiac motor neurons (Maynard, 1960), or they could result from direct effects on the cardiac muscle cells, as in *Limulus* (Watson *et al.*, 1985).

It should be noted, however, that the POs, which contain several cardioexcitatory agents (*e.g.*, Cooke and Sullivan, 1983), were still present in the preparations used for study. We cannot exclude the possibility that the applied peptides act by inducing the release of other agents from the POs. Such hormone-induced release of hormones from the same neurosecretory organ has not been reported for any of the pericardial substances and seems unlikely. In addition, the inhibitory effects of Sch and of LMS are qualitatively similar to those reported in insect hearts, which lack POs (Cuthbert and Evans, 1989; Robb *et al.*, 1989).

F_1 and F_2 exert purely excitatory effects on hearts of *Procambarus*, increasing both the rate and amplitude of spontaneous contractions. F_1 and F_2, respectively, are up to 1,000 and 10,000 times more potent than FMRFamide when comparing inotropic responses. Similar results have been obtained with isolated hearts of the blue crab, *Callinectes sapidus* (Krajniak, 1991) and of the lobster, *Homarus americanus* (Kravitz *et al.*, 1987). F_1 is also 1000 times more potent than FMRFamide in exciting the semi-isolated heart of the locust, *Schistocerca gregaria* (Cuthbert and Evans, 1989). Thus, arthropod hearts appear to be more sensitive to N-terminally extended analogues of FLRFamide than to FMRFamide. FMRFamide and FLRFamide are both excitatory, but the addition of the amino acid sequence thr-asn-arg-asn- or of ser-asp-arg-asn- to the amino terminal of the tetrapeptide-phe-leu-arg-phe-NH_2 effectively increases the potency of the peptide. Similar structure-activity relationships have been reported for the locust extensor tibiae nerve-muscle preparation (Cuthbert and Evans, 1989) and for neuromuscular synapses on crayfish abdominal extensor muscles (Mercier *et al.*, 1990).

The sensitivity of hearts from *Homarus* (Kravitz *et al.*, 1987), *Callinectes* (Krajniak, 1991), and *Procambarus* to F_1 suggests that F_1 or closely related peptides are common cardioexcitatory hormones in decapods. F_1 and F_2 were originally isolated from lobster POs (Trimmer *et al.*, 1987) and have not been positively identified in any other tissues to date. The POs of *Procambarus clarkii*, however, appear to contain cardioexcitatory FaRPs that are very similar to F_1 and F_2 (Mercier *et al.*, 1991a, b).

The crayfish heart was also sensitive to Sch and LMS, which have markedly different N-terminal extensions than the other FaRPs studied. The primary effect of Sch and of LMS appears to be a reduction in heart rate, which occurs at a threshold concentration between 10^{-10} and 10^{-9} *M* for both peptides. Similar thresholds have been reported for inhibition of locust hearts (Robb *et al.*, 1989) and oviducts (Lange *et al.*, 1991) by Sch, and for inhibition of cockroach hindguts (Holman *et al.*, 1986) and locust hearts (Cuthbert and Evans, 1989) by LMS. Because FLRFamide excites the crayfish heart, the inhibitory effects observed in the present study must be due to the presence of the N-terminal extensions PDVDHV- and pQDVDHV- on Sch and LMS, respectively.

In contrast, Krajniak (1991) has reported that LMS causes cardioexcitation in *Callinectes*. The effect was observed in a single preparation and has a threshold 10,000 times higher than that of F_1. Such an observation might reflect species-dependent differences in the target tissues, but this possibility requires further study.

Reduction in the amplitude of contractions was not observed as consistently with crayfish hearts as with insect preparations (Cuthbert and Evans, 1989; Lange *et al.*, 1991). The large increase in contraction size at higher Sch concentrations was distinct from the inhibitory effect in that it developed much more slowly. In addition, the large increase in amplitude was only produced by Sch, whereas both Sch and LMS could inhibit heart rate. This indicates that Sch activates a receptor that is not activated by LMS. This might seem surprising, in view of the high degree of homology between the two peptides, which differ by only the N-terminal amino acid. It is possible, however, that at the low concentrations, both peptides activate the same receptor or receptor class (one responsible for reducing heart rate), and that a different class of receptor is activated at higher concentrations of Sch (causing the increase in amplitude). This hypothesis is consistent with the high similarity between the log-dose *versus* response curves for the effects of Sch and LMS on contraction rate (Fig. 5A).

The reason for the delayed inotropic effect of Sch is not clear. One possibility may be that the peptide is hydrolyzed beginning at the N-terminal end. This would gradually produce a peptide more closely resembling FLRFamide, which, at 10^{-7} *M*, caused a substantial increase in contraction size (Figs. 1, 2). The combination of Sch with an excitatory FaRP (F_2) was capable of increasing the amplitude of contractions without increasing heart rate (Fig. 7). Thus, if hydrolysis were to cause an accumulation of an excitatory FaRP, the combination of Sch and its breakdown product would be expected to produce a response similar to that observed after several minutes of exposure to Sch (Figs. 4, 6A). Such an explanation, however, is speculative, and others are possible.

Responses to mixtures of excitatory and inhibitory agents may be of some physiological significance. Increases in cardiac output (the fluid volume ejected by the heart per minute) during physical activity (*e.g.*, McMahon *et al.*, 1979) and hypoxia (*e.g.*, Burnett, 1979; McMahon and Wilkens, 1975) generally involve changes in both heart rate and stroke volume (the amount of fluid ejected per beat). In some cases, however, stroke volume increases independently of heart rate (Taylor, 1976; McMahon and Wilkens, 1977; Taylor and Butler, 1978), and the mechanisms that underly such an effect are not known (McMahon and Burnett, 1990). It is tempting to speculate that a mixture of peptides like F_2 and Sch, which is capable of increasing the amplitude of contractions independently of rate, might be involved. Tension recordings, however, do not provide a direct measure of stroke volume or of cardiac output. In addition, crayfish POs do not contain Sch or LMS (Mercier *et al.*, 1991b), and none of the neurohormones isolated from POs to date decreases heart rate. More research aimed at identifying neuropeptides and examining their effects may provide a better understanding of how stroke volume and cardiac output are regulated.

Acknowledgments

This work was supported by a grant to AJM from the Natural Sciences and Engineering Research Council of Canada. We thank Pat Quigley for assistance in analyzing data for some of the experiments and Dr. Ian Orchard for commenting on a draft of the manuscript. Dr. R. Baines also provided some helpful suggestions.

Literature Cited

Boer, H. H., L. P. C. Schot, J. A. Veenstra, and D. Reichelt. 1980. Immunocytochemical identification of neural elements in the central nervous systems of a snail, some insects, a fish and a mammal with an antiserum to the molluscan cardio-excitatory tetrapeptide FMRF-amide. *Cell Tissue Res.* **213:** 21–27.

Burnett, L. 1979. The respiratory function of hemocyanin in the spider crab *Libinia emarginata* and the ghost crab *Ocypode quadrata* in normoxia and hypoxia. *J. Exp. Zool.* **210:** 289–300.

Cooke, I. M., and R. E. Sullivan. 1982. Hormones and neurosecretion. Pp. 205–290 in *The Biology of Crustacea*, D. E. Bliss, H. L. Atwood, and D. C. Sandeman, eds. Academic Press, New York.

Cuthbert, B. A., and P. D. Evans. 1989. A comparison of the effects of FMRFamide-like peptides on locust heart and skeletal muscle. *J. Exp. Biol.* **144:** 395–415.

Dockray, G. J., J. R. Reeve, Jr., J. Schively, R. J. Gayton, and C. S. Barnard. 1983. A novel active pentapeptide from chicken brain identified by antibodies to FMRFamide. *Nature* **305:** 328–330.

Elphick, M. R., R. H. Emson, and M. C. Thorndyke. 1989. FMRFamide-like immunoreactivity in the nervous system of the starfish *Asterias rubens*. *Biol. Bull.* **177:** 141–145.

Furguson, G. A. 1971. *Statistical Analysis in Psychology and Education*, McGraw Hill, New York. Pp. 146–159.

Greenberg, M. J., and D. A. Price. 1983. Invertebrate neuropeptides: native and naturalized. *Ann. Rev. Physiol.* **45:** 271–288.

Grimmelikhuijzen, C. J. P., and D. Graff. 1986. Isolation of <Glu-Gly-Arg-Phe-NH_2 (AnthoRFamide), a neuropeptide from sea anemones. *Proc. Natl. Acad. Sci. USA* **83:** 9817–9821.

Holman, G. M., B. J. Cook, and R. J. Nachman. 1986. Isolation, primary structure and synthesis of leucomyosuppressin, an insect neuropeptide that inhibits spontaneous contractions of the cockroach hindgut. *Comp. Biochem. Physiol.* **85C:** 324–333.

Kobierski, L. A., B. S. Beltz, B. A. Trimmer, and E. A. Kravitz. 1987. FMRFamide-like peptides of *Homarus americanus*: distribution, immunocytochemical mapping, and ultrastructural localization in terminal varicosities. *J. Comp. Neurol.* **266:** 1–15.

Krajniak, K. G. 1991. The identification and structure-activity relations of a cardioactive FMRFamide-related peptide from the blue crab *Callinectes sapidus*. *Peptides* **12:** 1295–1302.

Krajniak, K. G., and D. A. Price. 1990. Authentic FMRFamide is present in the polychaete *Nereis virens*. *Peptides* **11:** 75–78.

Kravitz, E. A., S. Glusman, R. M. Harris-Warrick, M. S. Livingstone, T. Schwarz, and M. F. Goy. 1980. Amines and a peptide as neurohormones in lobsters: actions on neuromuscular preparations and preliminary behavioural studies. *J. Exp. Biol.* **89:** 159–175.

Kravitz, E. A., L. Kobierski, B. A. Trimmer, and M. F. Goy. 1987. Peptide F_1: a myoactive lobster peptide related to FMRFamide. *Soc. Neurosci. Abstr.* **13:** 1257.

Lange, A. B., I. Orchard, and V. A. TeBrugge. 1991. Evidence for the involvement of a SchistoFLRF-amide-like peptide in the neural control of locust oviduct. *J. Comp. Physiol. A* **168:** 383–391.

Lehman, H. K., and D. A. Price. 1987. Localization of FMRFamide-like peptides in the snail *Helix aspersa*. *J. Exp. Biol.* **131:** 37–53.

Li, C., and R. L. Calabrese. 1987. FMRFamide-like substances in the leech. III. Biochemical characterization and physiological effects. *J. Neurosci.* 7: 595–603.

Marder, E., R. L. Calabrese, M. P. Nusbaum, and B. Trimmer. 1987. Distribution and partial characterization of FMRFamide-like peptides in the stomatogastric nervous systems of the rock crab, *Cancer borealis*, and the spiny lobster, *Panulirus interruptus*. *J. Comp. Neurol.* **259:** 150–163.

Maynard, D. M. 1960. Circulation and heart function. Pp. 161–226 in *Physiology of Crustacea*, Vol. 1, T. H. Waterman, ed. Academic Press, New York.

McMahon, B. R., and L. E. Burnett. 1990. The crustacean open circulatory system: a reexamination. *Physiol. Zool.* **63:** 35–71.

McMahon, B. R., D. G. McDonald, and C. M. Wood. 1979. Ventilation, oxygen uptake, and haemolymph oxygen transport following enforced

exhaustive activity in the Dungeness Crab *Cancer magister*. *J. Exp. Biol.* **80**: 271–285.

McMahon, B. R., and J. L. Wilkens. 1975. Respiratory and circulatory responses to hypoxia in the lobster *Homarus americanus*. *J. Exp. Biol.* **62**: 637–655.

McMahon, B. R., and J. L. Wilkens. 1977. Periodic respiratory and circulatory performance in the red rock crab *Cancer productus*. *J. Exp. Zool.* **202**: 363–374.

Mercier, A. J., I. Orchard, M. Skerrett, and V. TeBrugge. 1991a. FMRFamide-related peptides from crayfish pericardial organs. *Soc. Neurosci. Abstr.* **17**: 200.

Mercier, A. J., I. Orchard, and V. TeBrugge. 1991b. FMRFamide-like immunoreactivity in the crayfish nervous system. *J. Exp. Biol.* **156**: 519–538.

Mercier, A. J., M. Schiebe, and H. L. Atwood. 1990. Pericardial peptides enhance synaptic transmission and tension in phasic extensor muscles of crayfish. *Neurosci. Lett.* **111**: 92–98.

Painter, S. D., and M. J. Greenberg. 1982. A survey of the responses of bivalve hearts to the molluscan neuropeptide FMRFamide and to 5-hydroxytryptamine. *Biol. Bull.* **162**: 311–332.

Price, D. A., and M. J. Greenberg. 1977. Purification and characterization of a cardioexcitatory neuropeptide from the central ganglia of a bivalve molluscs. *Prep. Biochem.* **7**: 261–281.

Price, D. A., and M. J. Greenberg. 1989. The hunting of the FaRPs: the distribution of FMRFamide-related peptides. *Biol. Bull.* **177**: 198–205.

Price, D. A., W. Lesser, T. D. Lee, K. E. Doble, and M. J. Greenberg. 1990. Seven FMRFamide-related and two SCP-related cardioactive peptides from *Helix*. *J. Exp. Biol.* **154**: 421–437.

Robb, S., L. C. Packman, and P. D. Evans. 1989. Isolation, primary structure and bioactivity of SchistoFLRF-amide, a FMRF-amide-like neuropeptide from the locust, *Schistocerca gregaria*. *Biochem. Biophys. Res. Comm.* **160**: 850–856.

Taylor, A. C. 1976. The respiratory responses of *Carcinus maenas* to declining oxygen tension. *J. Exp. Biol.* **65**: 309–322.

Taylor, E. W., and P. J. Butler. 1978. Aquatic and aerial respiration in the shore crab *Carcinus maenas* (L.), acclimated to 15°C. *J. Comp. Physiol.* **127**: 315–323.

Trimmer, B. A., L. A. Kobierski, and E. A. Kravitz. 1987. Purification and characterization of FMRFamide-like immunoreactive substances from the lobster nervous system: isolation and sequence analysis of two closely related peptides. *J. Comp. Neurol.* **266**: 16–26.

van Harreveld, A. 1936. A physiological solution for freshwater crustaceans. *Proc. Soc. Exp. Biol. Med.* **34**: 428–432.

Watson, W. H., J. R. Groome, B. M. Chronwall, J. Bishop, and T. L. O'Donohue. 1984. Presence and distribution of immunoreactive and bioactive FMRFamide-like peptides in the nervous system of the horseshoe crab, *Limulus polyphemus*. *Peptides* **5**: 585–592.

Watson, W. H., III, T. Hoshi, J. Colburne, and G. J. Augustine. 1985. Neurohormonal modulation of the *Limulus* heart: amine actions on neuromuscular transmission and cardiac muscle. *J. Exp. Biol.* **118**: 71–84.

Reference: *Biol. Bull.* **182**: 341–347. (June, 1992)

Quantitative Analysis by Reverse Phase High Performance Liquid Chromatography of 5-Hydroxytryptamine in the Central Nervous System of the Red Swamp Crayfish, *Procambarus clarkii*

GUNDERAO K. KULKARNI AND MILTON FINGERMAN

Department of Ecology, Evolution, and Organismal Biology, Tulane University, New Orleans, Louisiana 70118

Abstract. The concentrations of 5-hydroxytryptamine (5-HT) in central nervous organs of the red swamp crayfish, *Procambarus clarkii,* were determined by reverse phase high performance liquid chromatography (RP-HPLC) with electrochemical detection. The quantity ranged between 54 and 168 pg/mg wet weight of tissue. The amount is highest in the brain, followed in decreasing order by the thoracic ganglia, subesophageal ganglion, eyestalks, and abdominal nerve cord. Significant increases in the levels of 5-HT in the eyestalks, brain, subesophageal ganglion, and thoracic ganglia occurred in crayfish exposed for three days to continuous light on a white background, whereas the 5-HT levels in these tissues decreased in crayfish kept in darkness. Electrical stimulation of central nervous organs *in vitro* produced significant decreases in the levels of 5-HT. Fenfluramine (5-HT releaser), 5,6-DHT (5-HT neurotoxin), and reserpine (5-HT depletor) induced significant decreases in the 5-HT levels in the portions of the central nervous system tested.

Introduction

The biogenic amines, norepinephrine, dopamine, histamine, octopamine, 5-hydroxytryptamine (5-HT), and gamma aminobutyric acid, function as neurotransmitters in various animals (Werman, 1966; Gerschenfeld, 1973; Krnjevic, 1974; Fingerman, 1985), and have been found in crustacean central nervous organs (Beltz and Kravitz, 1983; Elofsson, 1983; Laxmyr, 1984; Fingerman, 1985; Sandeman *et al.,* 1988). Aréchiga *et al.* (1990) showed that the species used in this study, the red swamp crayfish *Procambarus clarkii,* contains, in the lamina ganglionaris of its eyestalks, a set of axons with 5-HT-like immunoreactivity. These investigators also found that the responsiveness of the retinal photoreceptors of this crayfish to light is enhanced by exposure to 5-HT, both *in vivo* and *in vitro.* With respect to other crayfishes, 5-HT-containing neurons have been reported in the optic lobes and proto-, deuto-, and tritocerebral regions of the brain of *Pacifastacus leniusculus* (Myhrberg *et al.,* 1979; Elofsson, 1983), *Orconectes virilis* (Sandeman and Sandeman, 1987), and *Cherax destructor* (Sandeman *et al.,* 1988).

Kulkarni *et al.* (1991) have shown that 5-HT stimulates oocyte maturation in *Procambarus clarkii.* This observation and the earlier study of Aréchiga *et al.* (1990) have led us to determine, for the first time, the quantity of 5-HT in the central nervous system of this crayfish. In addition, we have determined the effects, on the 5-HT concentration in components of the central nervous system of (1) continuous exposure to light or darkness, (2) *in vitro* electrical stimulation, and (3) pharmacological agents known to affect 5-HT levels in vertebrates.

Received 21 October 1991; accepted 26 March 1992.

Materials and Methods

Animals

Red swamp crayfish, *Procambarus clarkii,* were purchased from a local seafood dealer and maintained in the laboratory at 24°C in a recirculating freshwater system. They were acclimatized to the laboratory conditions (12:12 L:D) for at least two days before being used in an experiment. Medium sized (carapace length 40–50 mm), intermolt (Stage C_4, Reddy *et al.,* 1990) crayfish of both

sexes were used. The crayfish were fed commercial crayfish food. Fiddler crabs, *Uca pugilator*, were obtained from the Gulf Specimen Co., Panacea, Florida, and acclimatized for three days to the laboratory conditions under 12:12 L:D in a recirculating artificial seawater system.

Tissue preparation and homogenization for 5-HT determinations

In this section and the following two, we describe the procedure for determining the 5-HT concentrations in the components of the central nervous system of crayfish maintained in the stock tanks. The eyestalks, brain, subesophageal ganglion, thoracic ganglia, and abdominal nerve cord of 100 crayfish were dissected out as rapidly as possible in cold Van Harreveld's crayfish physiological saline (van Harreveld, 1936). These components were then distributed, ten per tube, in tubes containing 1 ml of 0.4 *M* perchloric acid and sonicated in four cycles of 30 s each with a sonicator (Biosonik-II, Bronwill Scientific) equipped with narrow probe for small volumes. The homogenates were centrifuged (10,000 × *g*) for 15 min at 4°C. The pH of the supernatant, after decanting, was adjusted to 6.0 with 2 *M* potassium carbonate, and the mixture was again centrifuged for 10 min; the supernatants were used for further purification. The wet weight of each tissue was recorded. The averages for the ten determinations of the 5-HT contents of each nervous system component were then calculated.

Purification and analysis of the sample

The supernatants were filtered and purified on a weakly acid cation exchanger column, Amberlite IRP-64 (Hansson and Rosengren, 1978). The column was glass, 30 mm long with 5 mm i.d., equipped with a Millipore HV 0.45 μm filter (Nihon Millipore Kogyokk) at the bottom and filled with 300 μl of the resin. The supernatant from each 1 ml extract was divided into two 500 μl aliquots, and each aliquot was loaded separately onto the resin at a rate of 50 μl/min. The 5-HT adsorbed onto the resin from each aliquot was eluted with 500 μl of 1.2 *N* HCl. The two eluted fractions were combined for faster analysis of only one sample rather than two, and we obtained high recovery which was always in the range of 80–82%. The data presented have been corrected to reflect the recovery percentage. The remaining samples were stored at −70°C (Hansson and Rosengren, 1978; Elofsson, *et al.*, 1982).

A Waters RP-HPLC unit, Model 501, fitted with a U6K universal LC injector and a 3.9 × 150 mm 5 μm silica C-18 steel column with a small guard column, coupled to a Waters electrochemical detector (Model 460) was used for the quantitative analysis of 5-HT in the samples. Five aliquots (25 μl) of each sample were run, and the results were averaged. The variation among samples was less than 10%. The elution reagent was methane sulphonic acid (40 m*M*) and phosphoric acid (30 m*M*) in 17% methanol, pH 2.5, and was thoroughly degassed before use (Hansson and Rosengren, 1978; Elofsson *et al.*, 1982; Nässel and Laxmyr, 1983). The pressure applied was 1500 psi with a flow rate of 1 ml/min. The detector was a glassy carbon electrode, and the working potential was set at +0.75 V against the reference electrode. The 5-HT concentrations were determined by comparing the peak height in the elution profile of the sample with that of the standards, and are presented as pg/mg of wet tissue. One additional criterion, other than elution time, was used to identify the 5-HT peak in the samples. Before analysis, we added a small amount (10 μg/ml) of synthetic 5-HT to the samples. In no case did the sample peak show any inhomogeneity due to the addition of 5-HT to the biological material when compared with the peak of the standard. With this analytical system we could detect as little as 25 pg of 5-HT.

Calibration curve

The calibration curve was prepared as follows. To nine clean glass tubes, each containing 2 ml of 0.4 *M* perchloric acid, was added a known amount of 5-HT creatinine sulfate monohydrate (0–51.2 ng/ml free base) and 10^{-5} *M* 3,4-dihydroxybenzylamine hydrobromide (DHBA) (internal standard). The samples were loaded onto the ion exchange column (Amberlite IRP-64) and treated as above. Samples (100 μl) were collected and 25 μl of the eluate was injected onto the RP-HPLC column. The peak heights were recorded and fitted in a graph against the concentration of 5-HT free base. The retention time, with 1 ml/min flow rate and at 1500 psi, was 8.8–8.9 min for 5-HT and 3.8 min for DHBA (Fig. 1).

Experimental protocols

The 5-HT content in the central nervous organs of the crayfish were initially determined using specimens that had been exposed for 2 days to 12:12: L:D. In addition, 20 equal-sized crayfish were held continuously for an additional three days either under a fluorescent light (450–500 lux) or in darkness. After these three days, all of the central nervous organs from ten crayfish were dissected out for 5-HT determinations. In addition, the central nervous organs were removed from the rest of these crayfish and homogenized in 2 ml of crab physiological saline (Cooke *et al.*, 1977), pH 7.4. These extracts were then centrifuged (10,000 × *g*) at 4°C, and the supernates were bioassayed for red pigment-dispersing activity in eyestalkless fiddler crabs, *Uca pugilator*, of 10–15 mm carapace width. The pigment in the erythrophores of these eyestalkless crabs was initially maximally concentrated. The erythrophores were staged according to the method

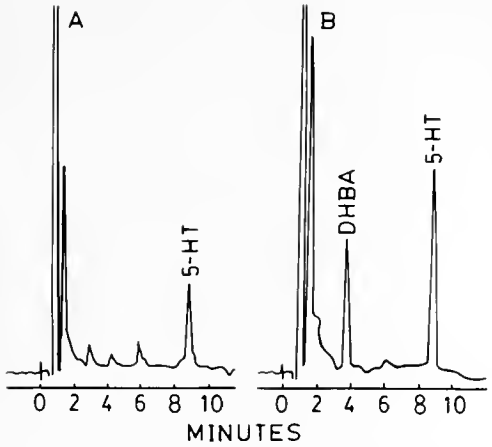

Figure 1. Chromatograms of (A) brain supernatant of *Procambarus clarkii* and (B) aqueous standard containing 5-HT and DHBA. Column: 5 μm silica C-18 steel. Mobile phase: methane sulphonic acid and phosphoric acid in methanol. Detector: glassy carbon electrode at +0.75 V potential. Retention time for 5-HT 8.8–8.9 min and for DHBA 3.8 min.

of Hogben and Slome (1931) wherein stage 1 indicates maximal pigment concentration, stage 5 maximal pigment dispersion, and stages 2, 3, and 4 the intermediate conditions. The Hogben and Slome stages for the experimental and control animals were then used to calculate Standard Integrated Responses (SIR) of the erythrophores of *Uca pugilator* to the nervous tissue extracts of *Procambarus clarkii* according to the method of Fingerman *et al.* (1967). Briefly, when pigment dispersion occurs, the sum of the Hogben and Slome stages recorded for the duration of the experiment for the control group is substracted from the corresponding sum for the experimental group. The difference is the SIR. The SIR integrates the amplitude, which is based on the observed Hogben and Slome stages, and duration of the response of the erythrophores. A dose of 50 μl containing the tissue extract equivalent to either one eyestalk, brain, subesophageal, or thoracic ganglion was injected into each crab.

For experiments involving *in vitro* electrical stimulation, the entire optic tract, including the major ganglia and sinus gland, was removed from the eyestalk and maintained in 50 μl physiological saline. The remaining nervous tissue from the brain to the end of thoracic nerve cord was also dissected out intact and carefully placed in 100 μl of physiological saline. Electrical stimulation of the isolated tissue was performed as described in detail by Quackenbush and Fingerman (1984). Briefly, the eyestalk tissue was held in place with a suction electrode attached to the stump of the optic nerve, whereas the central nerve tract, from the brain to the end of the thoracic nerve cord, was held in place by a suction electrode attached at the brain end. The stimulation given via the suction electrode was 5 pps, 4 ms delay, with pulses of 40 ms duration and varying voltage (10, 15, 20, and 25 V). Stimulation was delivered by a stimulator (Model S44) with a stimulus isolation unit (Model SIU 5A; both from the Grass Instrument Co.) After a stimulation bout of 2 min, the nervous tissues were homogenized in 0.4 *M* perchloric acid and processed for 5-HT determination as described above. A total of 75 crayfish were used, divided equally among one group of unstimulated controls and four groups of voltage stimulated preparations.

Experiments on the effects of pharmacological agents, such as fenfluramine (5-HT releaser, Consolo *et al.*, 1979), fluoxetine (5-HT potentiator, Wong *et al.*, 1975), 5,6-dihydroxytryptamine (5,6-DHT) (5-HT neurotoxin, Baumgarten *et al.*, 1982), and reserpine (5-HT depletor, Myhrberg *et al.*, 1979; Elofsson *et al.*, 1982), on the levels of 5-HT in the central nervous tissues of *Procambarus clarkii*, were performed according to the procedure of Myhrberg *et al.* (1979). Crayfish were divided into 5 groups of 15 each. The first group received physiological saline alone and served as the control. The crayfish in the second through fifth groups were administered various concentrations (10–25 μg/g body weight) of either fenfluramine, fluoxetine, 5,6-DHT, or reserpine. All injections were given once in a dose of 50 μl, and the crayfish were sacrificed after 2 h and their nervous tissues removed and processed for 5-HT analysis as described earlier.

Fenfluramine hydrochloride, 5,6-DHT, reserpine, and Amberlite IRP-64 were purchased from Sigma. Fluoxetine hydrochloride was a gift from Lilly Research Laboratories, whereas the 5-HT creatinine sulfate monohydrate and DHBA were purchased from Aldrich. All drugs were dissolved in isosmotic crayfish physiological saline.

The data obtained from these experiments were analyzed statistically by calculating the standard error for each of the means (SEM).

Results

The measurements quantifying 5-HT in the central nervous organs, eyestalks, brain, subesophageal ganglion, thoracic ganglia, and abdominal nerve cord of crayfish maintained under laboratory conditions (12:12 L:D; 24°C) in recirculating freshwater for two days are summarized in Figure 2. The 5-HT concentration was highest in the brain (168 pg/mg) and lowest in the abdominal nerve cord (54 pg/mg), with the eyestalk, subesophageal ganglion, and thoracic ganglia having intermediate concentrations. Because the concentration of 5-HT in the abdominal nerve cord is small relative to the rest of the central nervous organs, only eyestalks, brains, subesophageal ganglia, and thoracic ganglia were used in the rest of the experiments.

The pigment in the erythrophores of the crayfish (*P. clarkii*) that were illuminated while on a white background

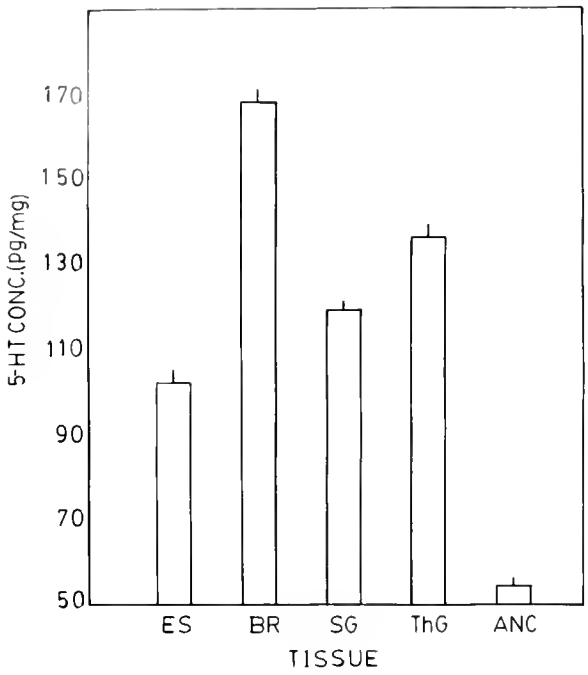

Figure 2. 5-HT concentration in pg/mg of tissue, assayed by HPLC and electrochemical detection, in eyestalks (ES), brain (BR), subesophageal ganglion (SG), thoracic ganglia (ThG), and abdominal nerve cord (ANC) of *Procambarus clarkii*. Error bars are SEM for ten separate extracts of tissue pooled from ten animals each.

was concentrated, whereas the red pigment of the crayfish kept in darkness was dispersed. The 5-HT concentrations in the eyestalks, brain, subesophageal ganglion, and thoracic ganglia of crayfish held under continuous light for three days on a white background increased significantly (Fig. 3). The corresponding red pigment-dispersing SIR values evoked in the fiddler crabs by these extracts also increased. In contrast, both the 5-HT levels and the SIR values in the eyestalks, brains, subesophageal ganglia, and thoracic ganglia of crayfish held in darkness showed significant decreases when compared to the controls (Fig. 3).

In the experiments in which eyestalk, neural ganglia, and the central nerve tract (from brain to the end of the thoracic nerve cord) were electrically stimulated with various voltages (10, 15, 20, and 25 V), 25 V was found to be most effective. The data in Figure 4 are for tissues stimulated with 25 V. The stimulation produced significant decreases in the concentration of 5-HT in all the tissues, with the maximum decrease occurring in the eyestalks (−37.4%) and the minimum in the thoracic ganglia (−22.8%). Furthermore, when extracts of the electrically stimulated tissues were bioassayed for red pigment-dispersing activity in crabs, it was found that the SIR values evoked by these extracts were significantly decreased in comparison to the tissue extracts from the control crayfish. Interestingly, the percentage decrease in 5-HT content decreased progressively in the tissues along the central nervous chain from the brain to the thoracic ganglia.

Of the concentrations tested, the smallest concentrations that produced significant effects on the 5-HT level after 2 h were 15 μg/g body weight of fenfluramine, 10 μg/g body weight of 5,6-DHT, and 15 μg/g body weight of reserpine. Fenfluramine induced a significant decrease of 5-HT from all of the nervous tissues (Fig. 5). The decrease was maximum in the eyestalks and least in the thoracic ganglia. None of the concentrations (10–25 μg/g body weight) of fluoxetine produced any significant effect on the 5-HT concentration in any of the tissues. 5,6-DHT and reserpine produced significant decreases in the 5-HT concentration of all the nervous tissues tested. The maximum decrease was produced in the eyestalks, whereas the minimum decrease occurred in the thoracic ganglia.

Discussion

Histochemical studies by means of fluorescence microscopy have revealed the presence of yellow-fluorescing

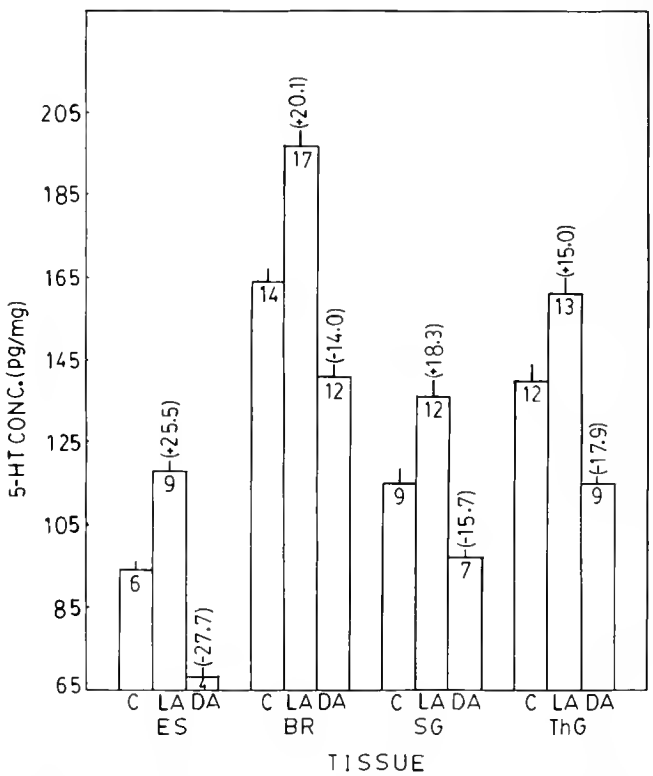

Figure 3. 5-HT concentration in eyestalks (ES), brain (BR), subesophageal ganglion (SG) and thoracic ganglia (ThG) of *Procambarus clarkii* exposed for three days to continuous light (light adapted, LA) or held in total darkness (dark adapted, DA). Error bars are SEM of ten separate extracts of tissues pooled from ten animals each. Figures in parentheses are percent change from the 12:12 L:D control (C) and those in the columns are the red pigment-dispersing Standard Integrated Responses (SIR) of the erythrophores of eyestalkless fiddler crabs, *Uca pugilator*, to extract of that tissue of *Procambarus clarkii*.

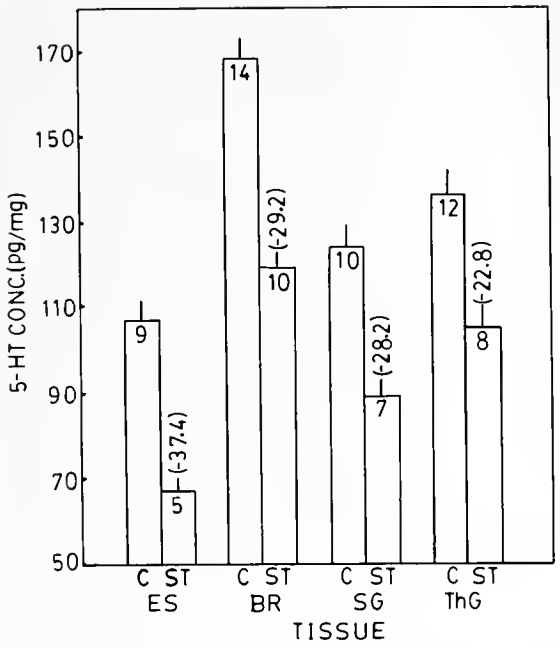

Figure 4. Effect of 25 V electrical stimulation (ST) for 2 min on the concentration of 5-HT in eyestalks (ES), brain (BR), subesophageal ganglion (SG), and thoracic ganglia (ThG) of *Procambarus clarkii*. Error bars are SEM of ten separate extracts of tissues pooled from ten animals each. Figures in parentheses denote percent change from the control (C) and those in columns are the red pigment-dispersing Standard Integrated Responses (SIR) of the erythrophores of eyestalkless fiddler crabs, *Uca pugilator*, to extracts of that particular tissue of *Procambarus clarkii*.

cells, indicative of 5-HT, in the eyestalks, brain and ventral nerve cord of the crayfishes, *Astacus astacus* (Elofsson *et al.*, 1966) and *Pacifastacus leniusculus* (Myhrberg *et al.*, 1979). The identification of biogenic amines and the determination of their concentrations in arthropods had earlier depended on fluorometric methods. Those methods required relatively large tissue samples and yielded readings only in the microgram or nanogram range. The advent of HPLC technology enabled investigators to analyze the 5-HT content of tissues from small arthropods with only moderate amounts of biogenic amines, and the sensitivity has been extended down to the picogram level.

A comparison of the amount of 5-HT present in various tissues of the central nervous system of the red swamp crayfish, *Procambarus clarkii*, revealed distinct differences among them (Fig. 2). These experiments provide, for the first time, data on the amount of 5-HT in different nervous tissues of this crayfish. The level of 5-HT found in the eyestalks (102 pg/mg) of *Procambarus clarkii* is comparable to the value reported by Elofsson *et al.* (1982) for the eyestalks (100 pg/mg) of another crayfish, *Pacifastacus leniusculus*, whereas the brain (168 pg/mg) of *Procambarus clarkii* contained slightly more 5-HT than the brain (150 pg/mg) of *Pacifastacus leniusculus* (Elofsson *et al.*, 1982), but like *Pacifastacus* the 5-HT level in the brain of *Procambarus* is higher than in the eyestalk.

The 5-HT levels in all nervous tissues of crayfish held for three days under constant illumination on a white background were higher than the corresponding values for the crayfish held for three days in complete darkness, and the values of the control crayfish held under 12:12 L:D (Fig. 3). Furthermore, the red pigment-dispersing SIR values for the erythrophores of the eyestalkless fiddler crabs, *Uca pugilator*, that received the extracts of eyestalks, brain, subesophageal ganglion, and thoracic ganglia of the light adapted crayfish were also significantly higher than the corresponding SIR values evoked by the nervous tissues of the dark adapted crayfish or by those of the controls. Earlier studies with the fiddler crab, *Uca pugilator*, and dwarf crayfish, *Cambarellus shufeldti*, had revealed that 5-HT functions as a neurotransmitter that stimulates the release of red pigment-dispersing hormone (Rao and Fingerman, 1970, 1975). The changes that occurred in the 5-HT concentrations in the central nervous organs of the crayfish in darkness or in constant illumination on a white background presumably reflect this role of 5-HT in releasing the color change hormone. The red pigment of the crayfish kept in light on a white background was concentrated. The central nervous tissues of these crayfish on

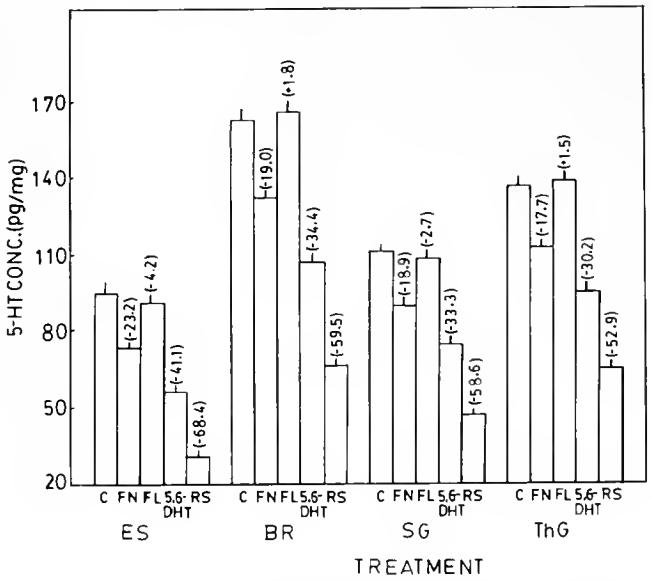

Figure 5. Effects of pharmacological agents on the concentration of 5-HT in eyestalks (ES), brain (BR), subesophageal ganglion (SG), and thoracic ganglia (ThG) of *Procambarus clarkii*. Error bars are SEM of ten separate extracts of tissues pooled from ten animals each. Values in parentheses show the percent change from the control (C). 5,6-DHT = 5,6-dihydroxytryptamine, 10 μg/g body weight; FN = fenfluramine, 15 μg/g body weight; FL = fluoxetine, 25 μg/g body weight; RS = reserpine, 15 μg/g body weight. The volume of drug solution or saline injected was 50 μl. The tissues were removed from the crayfish 2 h after the injections were given.

a white background not only contained higher 5-HT levels than the tissues of the control crayfish, but also evoked higher red pigment-dispersing SIR values, observations that are consistent with a pigment-dispersing hormone releasing role of 5-HT. Presumably, because the red pigment was concentrated, neither 5-HT nor pigment-dispersing hormone was being used, thereby accounting for the increased levels of both substances. Earlier, Fingerman *et al.* (1964) reported the presence of erythrophorotropic hormones in the eyestalks and brain of juveniles and adults of *Procambarus clarkii*. They observed that the injection of an extract containing one-third of an organ complement per dose significantly evoked pigment migration in eyestalkless animals. More recently, McCallum *et al.* (1988, 1989) confirmed the previous findings of Fingerman *et al.* (1964) by isolating and sequencing the pigment-dispersing hormone (PDH), which is an octadecapeptide, from the eyestalks of *Procambarus clarkii*.

Rao and Fingerman (1975) later reported that 5-HT, when injected into the dwarf crayfish *Cambarellus shufeldti*, dispersed the red pigment in the erythrophores, as in the fiddler crab, but was ineffective when tested *in vitro* on isolated chromatophore-bearing pieces of the crayfish carapace. In crayfish on a white background with their red pigment concentrated, 5-HT turnover would presumably have decreased because, with the red pigment concentrated, 5-HT would not be used to stimulate release of red pigment-dispersing hormone, so a rise in the intraneuronal concentration of this neurotransmitter would occur. On the other hand, because darkness fosters red pigment dispersion, crayfish in darkness would be using the intraneuronal stores of 5-HT to effect red pigment dispersion and would, according to the hypothesis, have a lower intraneuronal concentration of 5-HT than crayfish on a white background under light, which the present data show is indeed the case.

Previously, Berlind and Cooke (1970) reported the release of a neurosecretory peptide hormone from the pericardial organs of the spider crabs *Libinia emarginata* and *Libinia dubia* following electrical stimulation. Later, Quackenbush and Fingerman (1984) found that electrical stimulation of the isolated eyestalks of the fiddler crab, *Uca pugilator*, releases chromatophorotropic peptides from the sinus gland. Recently, Kulkarni and Fingerman (1991) also used *Uca pugilator* to show that the distal retinal pigment light-adapting hormone is released by electrical stimulation of isolated eyestalk neuroendocrine tissues. The data presented in Figure 4 clearly show that 25 V stimulation reduced the 5-HT levels in the central nervous tissues of *Procambarus clarkii*. Furthermore, the stimulation appears also to have reduced the amount of stored red pigment-dispersing hormone in the central nervous system because the extracts of the stimulated tissues produced lesser SIR values for red pigment dispersion than did the tissues of the unstimulated controls. In their studies, both Quackenbush and Fingerman (1984) and Kulkarni and Fingerman (1991) bioassayed only the bathing fluid and not the actual stimulated tissue. In the present study, the stimulated tissues were extracted and bioassayed for red pigment-dispersing activity by injecting the extracts into eyestalkless crabs, *Uca pugilator*.

Fenfluramine (5-HT releaser), 5,6-DHT (5-HT neurotoxin), and reserpine (5-HT depletor) decreased the amount of 5-HT in the central nervous system, although their modes of action are different (Fig. 5). However, the 5-HT potentiator fluoxetine had no appreciable effect on the 5-HT concentration. These findings are consistent with earlier 5-HT depletion studies in which reserpine was used with crustaceans. Myhrberg *et al.* (1979), using the histochemical fluorescence method of Falck and Hillarp, and Elofsson *et al.* (1982), using HPLC, both found that reserpine decreases the 5-HT content of nervous tissues in the crayfish, *Pacifastacus leniusculus*. Likewise, the 5-HT content of the brain and eyestalks of *Uca pugilator* decreased after injection of reserpine and 5,6-DHT (Fingerman *et al.*, 1974).

Acknowledgments

This research was supported by Grant No. I-1435-88 from BARD, The United States-Israel Binational Agricultural Research & Development Fund. We thank Mr. Chayan Chakraborti for his technical assistance.

Literature Cited

Aréchiga, H., E. Bannelos, E. Frixione, A. Picones, and L. Rodriguez-Sosa. 1990. Modulation of crayfish retinal sensitivity by 5-hydroxytryptamine. *J. Exp. Biol.* **150:** 123–143.

Baumgarten, J. G., S. Jenner, A. Bjorklund, M. P. Klemm, and H. G. Schlossberger. 1982. Serotonin neurotoxins. Pp. 249–277 in *Biology of Serotonergic Transmission*, N. N. Osborne, ed. John Wiley & Sons, New York.

Beltz, B. S., and E. A. Kravitz. 1983. Mapping of serotonin-like immunoreactivity in the lobster nervous system. *J. Neurosci.* **3:** 585–602.

Berlind, A., and I. M. Cooke. 1970. Release of neurosecretory hormone as peptide by electrical stimulation of crab pericardial organs. *J. Exp. Biol.* **53:** 679–686.

Consolo, S., M. Ladinsky, A. S. Tirelli, V. Crunelli, S. Samanian, and S. Garattini. 1979. Increase in rat striatal acetylcholine content by d-fenfluramine, a serotonin releaser. *Life Sci.* **25:** 1975–1981.

Cooke, I. M., B. A. Haylett, and T. M. Weatherby. 1977. Electrically elicited neurosecretory and electrical responses of the isolated crab sinus gland in normal and reduced calcium salines. *J. Exp. Biol.* **70:** 125–149.

Elofsson, R. 1983. 5-HT-like immunoreactivity in the central nervous system of the crayfish, *Pacifastacus leniusculus*. *Cell Tiss. Res.* **232:** 221–236.

Elofsson, R., T. Kauri, S. O. Nielsen, and J. O. Stromberg. 1966. Localization of monoaminergic neurons in the central nervous system of *Astacus astacus* Linné (Crustacea). *Z. Zellforsch. Mikroskop. Anat.* **107:** 343–360.

Elofsson, R., L. Laxmyr, E. Rosengren, and C. Hansson. 1982. Identification and quantitative measurements of biogenic amines and DOPA in the central nervous system and haemolymph of the crayfish, *Pacifastacus leniusculus* (Crustacea). *Comp. Biochem. Physiol.* **71C:** 191–205.

Fingerman, M. 1985. The physiology and pharmacology of crustacean chromatophores. *Am. Zool.* **25:** 233–252.

Fingerman, M., W. E. Julian, M. A. Spirtes, and R. M. Kostrzewa. 1974. The presence of 5-hydroxytryptamine in the eyestalks and brain of the fiddler crab *Uca pugilator*, its quantitative modification by pharmacological agents, and possible role as a neurotransmitter in controlling the release of red pigment-dispersing hormone. *Comp. Gen. Pharmac.* **5:** 299–303.

Fingerman, M., K. R. Rao, and C. K. Bartell. 1967. A proposed uniform method of reporting response values for crustacean chromatophorotropins: the standard integrated response. *Experientia* **23:** 962–964.

Fingerman, M., Y. Yamamoto, and C. W. Jacob. 1964. Differences between the chromatophore systems of juvenile and adult specimens of the crayfish *Procambarus clarkii*. *Am. Zool.* **4:** 164.

Gerschenfeld, H. M. 1973. Chemical transmission in invertebrate central nervous systems and neuromuscular junctions. *Physiol. Rev.* **53:** 1–119.

Hansson, C., and E. Rosengren. 1978. Quantitative analysis of 5-hydroxytryptamine in biological material by high performance liquid chromatography and electrochemical detection. *Anal. Lett.* **B11:** 901–912.

Hogben, L., and D. Slome. 1931. The pigmentary effector system-VI. The dual character of endocrine co-ordination in amphibian colour change. *Proc. R. Soc. Lond.* **108B:** 10–53.

Krnjevic, K. 1974. Chemical nature of synaptic transmission in vertebrates. *Physiol. Rev.* **54:** 418–540.

Kulkarni, G. K., and M. Fingerman. 1991. Release of black pigment-dispersing hormone and distal retinal pigment light-adapting hormone upon electrical stimulation of the isolated eyestalk neuroendocrine complex of the fiddler crab, *Uca pugilator*. *Comp. Biochem. Physiol.* **99C:** 47–52.

Kulkarni, G. K., R. Nagabhushanam, G. Amaldoss, R. G. Jaiswal, and M. Fingerman. 1991. 5-hydroxytryptamine stimulation of the ovary in the crayfish, *Procambarus clarkii*. *Am. Zool.* **31:** 115A.

Laxmyr, L. 1984. Biogenic amines and DOPA in the central nervous system of decapod crustaceans. *Comp. Biochem. Physiol.* **77C:** 139–143.

McCallum, M. L., K. R. Rao, and J. P. Riehm. 1989. A comparison of the effects of two pigment-dispersing hormones on the crayfish *Procambarus clarkii*. *Am. Zool.* **29:** 217.

McCallum, M. L., K. R. Rao, J. P. Riehm, C. J. Mohrherr, and W. T. Morgan. 1988. Isolation of a β-PDH analog from the crayfish, *Procambarus clarkii*. *Biol. Bull.* **177:** 225–229.

Myhrberg, H. E., R. Elofsson, R. Aramant, N. Klemm, and L. Laxmyr. 1979. Selective uptake of exogenous catecholamines into nerve fibres in crustaceans. A fluorescence histochemical investigation. *Comp. Biochem. Physiol.* **62C:** 141–150.

Nässel, D. R., and L. Laxmyr. 1983. Quantitative determination of biogenic amines and DOPA in the CNS of adult and larval blowflies, *Calliphora erythrocephala*. *Comp. Biochem. Physiol.* **75C:** 259–265.

Quackenbush, L. S., and M. Fingerman. 1984. Regulation of the release of chromatophorotropic neurohormones from the isolated eyestalk of the fiddler crab, *Uca pugilator*. *Biol. Bull.* **166:** 237–250.

Rao, K. R., and M. Fingerman. 1970. Action of biogenic amines on crustacean chromatophores, II. Analysis of the responses of erythrophores in the fiddler crab, *Uca pugilator*, to indolealkylamines and an eyestalk hormone. *Comp. Gen. Pharmacol.* **1:** 117–126.

Rao, K. R., and M. Fingerman. 1975. Action of biogenic amines on crustacean chromatophores, IV. Analysis of the synergistic erythrophoric pigment dispersion evoked by 5-hydroxytryptamine and lysergic acid diethylamide in the dwarf crayfish, *Cambarellus shufeldti*. *Comp. Biochem. Physiol.* **51C:** 53–58.

Reddy, T. S. N., G. K. Kulkarni, L. Glade, and M. Fingerman. 1990. Molt stages of the red swamp crayfish, *Procambarus clarkii*. *Am. Zool.* **30:** 109A.

Sandeman, R. E., and D. C. Sandeman. 1987. Serotonin-like immunoreactivity of giant olfactory interneurons in the crayfish brain. *Brain Res.* **403:** 371–374.

Sandeman, D. C., R. E. Sandeman, and A. R. Aitken. 1988. Atlas of serotonin-containing neurons in the optic lobes and brain of the crayfish, *Cherax destructor*. *J. Comp. Neurol.* **269:** 465–478.

van Harreveld, A. 1936. A physiological solution for fresh water crustaceans. *Proc. Soc. Exp. Biol. Med.* **34:** 428–432.

Werman, R. 1966. Criteria for identification of a central nervous system transmitter. *Comp. Biochem. Physiol.* **18:** 745–766.

Wong, D. T., F. P. Bymaster, J. S. Horng, and B. B. Molloy. 1975. A new selective inhibitor for uptake of serotonin into synaptosomes of rat brain: 3-(p-trifluoromethylphenoxy)-N-methyl-3-phenylpropylamine. *J. Pharmacol. Exp. Ther.* **193:** 804–811.

Reference: *Biol. Bull.* **182**: 348–365. (June, 1992)

New Interpretation of a Nudibranch Central Nervous System Based on Ultrastructural Analysis of Neurodevelopment in *Melibe leonina*. I. Cerebral and Visceral Loop Ganglia

LOUISE R. PAGE

Department of Biology, University of Victoria, Victoria, British Columbia, Canada V8W 2Y2

Abstract. Development of the 'cerebropleural' ganglia in the dendronotid nudibranch *Melibe leonina* (Gould, 1852) was examined by electron microscopy of semi-serial sections through larval stages. Although comparative neuroanatomical studies suggest that the paired cerebropleurals of nudibranchs are formed by fusion of cerebral and pleural ganglia, plus all other ancestral ganglia of the visceral loop, my study indicates that the pleural ganglia are not part of these compound ganglionic masses. In *Melibe* larvae, the cerebral, optic, and rhinophoral ganglia, arise from pre-trochal cephalopedal ectoderm. At hatching stage, the visceral loop extends from the two cerebral ganglia, is non-ganglionated, and forms a complete circuit beneath the esophagus. Ganglia that subsequently develop along the visceral loop, which were identified as subintestinal, visceral, supraintestinal, and possibly right parietal ganglia, arise from placodes of visceropallial ectoderm that show torsional displacements. In addition, a cluster of neurons, presumed to be osphradial, lies close to the rim of the right mantle fold. Detorsion of the visceral loop is accomplished by migration of subintestinal neurons along the visceral loop fiber tract, not by visceral loop shortening. Localized elongation of a different segment of this fiber tract during metamorphosis displaces the visceral ganglion to the left, where it fuses with subintestinal and left cerebral ganglia.

Introduction

More than a century of comparative neuroanatomical studies on opisthobranchs have revealed a wide range of ganglionic fusions and cephalization within this gastropod group (Russell, 1929; Hoffmann, 1936; others reviewed by Bullock, 1965; Schmekel, 1985). In species showing evidence of fusions, homologous ganglionic regions have been inferred by extrapolation from the layout of distinct ganglia, connectives, and peripheral nerves found in presumably more primitive species. Although these interpretations have been largely accepted by most contemporary gastropod systematists and neurophysiologists, they are nevertheless conjectural (see Dorsett, 1986). This is particularly true for nudibranchs, in which ganglia of the central nervous system (CNS) show extreme consolidation. Ambiguity about homologous ganglionic regions reduces the taxonomic value of neuroanatomical characters and contributes to the uncertainty about phyletic origins and relationships of the opisthobranchs (see Minichev, 1970; Minichev and Starobogatov, 1978; Gosliner, 1981, 1991; Gosliner and Ghiselin, 1984; Haszprunar, 1985b, Schmekel, 1985). Furthermore, possible misconceptions about ganglionic fusion patterns can confound comparative neurobiological studies—a lamentable situation for an animal group that is otherwise very amenable to neuroethological investigation (see Kandel, 1979; Willows, 1985–1986).

Studies of gangliogenesis in prosobranch gastropods indicate that the CNS typically develops from a similar groundplan, with various derived conditions arising later in ontogeny [compare studies of Crofts (1937) and Moritz (1939) with those of Honegger (1974) and Demian and Yousif (1975)]. This groundplan, in which discrete ganglia are interconnected in a specific pattern, is not greatly altered during the subsequent development of some prosobranchs, and it appears also in Gosliner's (1981) proposal for the ancestral opisthobranch nervous system.

Received 6 November 1991; accepted 5 March 1992.

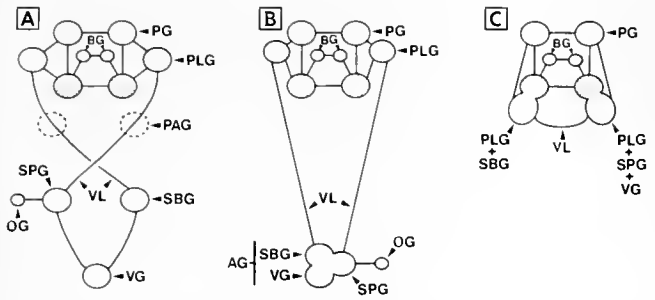

Figure 1. Opisthobranch central nervous systems showing varying degrees of cephalization, ganglionic fusions, and euthyneury. Dorsal views; cerebral ganglia stippled. A. Possible ancestral condition (adapted from Gosliner, 1981); distinct parietal ganglia found in some extant opisthobranchs. B. *Aplysia californica* (adapted from Kriegstein, 1979a, b). C. aeolid nudibranch (adapted from Russell, 1929); note visceral loop emerging from ganglionic mass projecting posteriorly from cerebral ganglia. AG = abdominal ganglion; BG = buccal ganglia; OG = osphradial ganglion = PG = pedal ganglion; PAG = parietal ganglion; PLG = pleural ganglion; SBG = subintestinal ganglion; SPG = supraintestinal ganglion; VG = visceral ganglion; VL = visceral loop.

Reasoning from studies of a variety of opisthobranchs, Gosliner (1981) suggested that the common ancestor of this group had paired cerebral, pleural, and pedal ganglia interconnected around the esophagus, a long streptoneurous visceral loop (twisted due to torsion) punctuated by subintestinal, supraintestinal, and visceral ganglia, and an osphradial ganglion connected to the supraintestinal ganglion (Fig. 1A). Extant opisthobranchs also have a pair of buccal ganglia, and some species have an extra ganglionic pair, called the parietals, located anterior to the intestinals. Developmental studies on the anaspidean *Aplysia californica* have shown that all ganglia of Gosliner's ancestral opisthobranch appear during early larval development, but the visceral and intestinal ganglia fuse eventually to form what is called the abdominal ganglion (Fig. 1B) (Kriegstein, 1977a, b; Schacher *et al.*, 1979a, b). These results suggest that the true pattern of ganglionic fusions among other opisthobranchs might be revealed by studies of neurodevelopment.

The adult CNS of nudibranchs, which shows only three pairs of distinct ganglia surrounding the esophagus, is much more consolidated than that of aplysiids. The ganglia have been identified traditionally as the pedals, buccals, and cerebropleurals, with the latter incorporating the cerebral and pleural ganglia plus all other ganglia of the visceral loop (Fig. 1C). Developmental studies of nudibranchs have indeed shown that the cerebropleurals are constructed ontogenetically from precursor ganglia, but there are three different interpretations for the location and identity of these precursor ganglia (Thompson, 1958; Tardy, 1970, 1974; Bickell and Chia, 1979; Bickell and Kempf, 1983; Kempf *et al.*, 1987). Much of this confusion may stem from limited resolution provided by histological sections.

To address the controversy regarding the ontogeny of the cerebral and visceral loop ganglia in nudibranchs, I have cut semi-serial, ultrathin sections through sequential larval stages of the dendronotid nudibranch *Melibe leonina*. A review of the genus has been given recently by Gosliner (1987). General features of larval and metamorphic development in this species were described from histological sections by Bickell (now Page) and Kempf (1983). The interpretation of gangliogenesis given in the present paper and the following companion paper (Page, 1992) differs from that described in the earlier study.

Materials and Methods

Adults of *Melibe leonina* and their egg masses were collected from Patricia Bay, Vancouver Island, Canada.

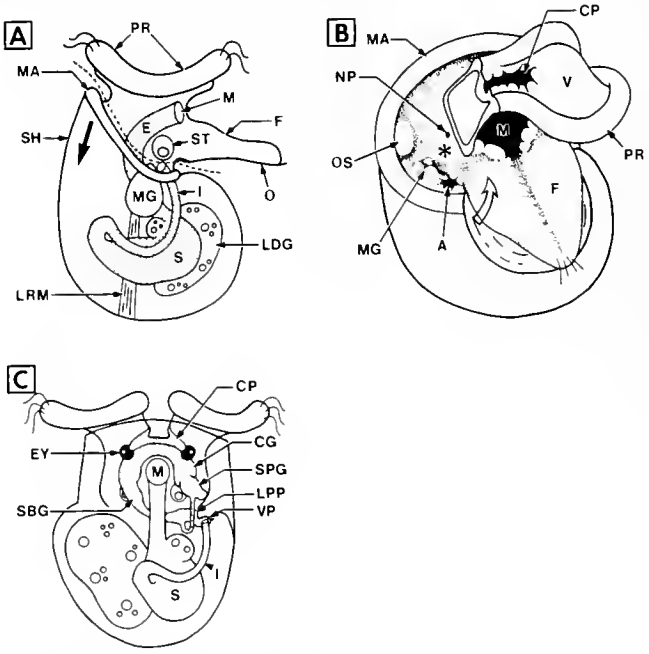

Figure 2. Veliger larvae of *Melibe leonina*. A. Lateral view, prior to mantle retraction, showing basic anatomy; gut is stippled. Broken line passes along floor of mantle cavity and demarcates cephalopedal mass from visceropallial mass. Arrow indicates displacement of mantle at mantle retraction. B. Oblique, antero-ventral view of young veliger; right velar lobe cut away to reveal mantle fold lining right mantle cavity. Swellings in mantle fold are osphradial neurons (OS) and apices of mantle gland (MG). The asterisk marks position of right pallial placode; open arrow indicates a site *beneath* the foot, where the left pallial placode is located. Note invagination of left cephalic plate (CP) within pre-trochal ectoderm. C. Dorsal view of veliger shortly after mantle retraction showing positions of cerebral ganglia and components of visceral loop (developing CNS stippled). Mantle gland omitted for clarity. A = anus; CG = cerebral ganglion; CP = cephalic plate; EY = eye; E = esophagus; F = foot; I = intestine; LDG = left digestive gland; LPP = left pallial placode; LRM = larval retractor muscle; M = mouth; MA = shell-secreting cells of mantle; MG = mantle gland; NP = nephrocyst pore; O = operculum; PR = prototroch (cilia not shown in 2B); S = stomach; SBG = subintestinal ganglion; SH = shell; SPG = supraintestinal ganglion; ST = statocyst; V = velar lobe; VP = visceral placode.

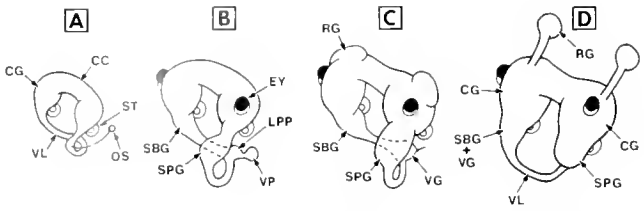

Figure 3. Summary sketches of developing ganglia of cephalic plate and visceral loop in *Melibe leonina;* postero-lateral views from right side. A. newly hatched larva. B. larva at mantle retraction stage. C. late larval stage. D. metamorphic stage. CC = cerebral commissure; CG = cerebral ganglion; EY = eye; LPP = left pallial placode; OS = osphradial neurons; RG = rhinophoral ganglion; SBG = subintestinal ganglion; SPG = supraintestinal ganglion; ST = statocyst; VG = visceral ganglion; VL = visceral loop; VP = visceral placode.

Larvae that hatched from egg masses laid in the field or laboratory were reared according to the method of Bickell and Kempf (1983). Under laboratory conditions and a rearing temperature of 12 to 14°C, larvae required a minimum of 5 weeks to complete pre-metamorphic development.

Larvae were anaesthetized as described by Bickell and Kempf (1983), and were fixed according to the method of Bickell and Chia (1979).

The area of the larval body containing developing ganglia was thin sectioned in whole or part with a diamond knife, and batches of eight to ten sections were collected on uncoated copper grids (150 mesh size). The grids were first washed in acetone and distilled water, then passed briefly through the flame of an alcohol burner; this eases the pick-up of floating sections, possibly by reducing the hydrophobicity of the grid surface. To discourage the tendency of sections to float towards the grid periphery, grids were bent slightly so that sections were lifted onto a convex grid surface without excess water. The central areas of wet sections were teased over openings between grid bars with an eyebrow hair mounted on an orange stick. With this method, two to six whole sections per grid could be viewed, with each gridload of sections representing approximately 0.8 μm of tissue thickness. Sections were stained for 90 min in aqueous 2% uranyl acetate and 8 min in 0.2% lead citrate at room temperature.

Initially, a general picture of the CNS within each specimen was reconstructed by photographing one section per two to three grids at a magnification of 873× on the negative with a Philips EM300. This gave a panoramic view of the section but still allowed resolution of small fiber tracts. Subsequently, areas showing important structural features were photographed at higher magnification from these and intervening grids.

The following larval stages were thin sectioned: newly hatched, 6 days old, just prior to mantle retraction (larval shell at full size but mantle fold not yet retracted), onset of mantle retraction, complete mantle retraction, hypertrophy of retracted mantle fold, and late stage larva with ceratal rudiments. Characteristics of the mantle fold were used to stage larvae because these can be recognized before sectioning (Bickell and Kempf, 1983). Stages fixed immediately after shell loss, and at 5 and 10 h after shell loss, were cut into serial 1 μm thick sections and stained with methylene blue and Azure II in sodium borax (Richardson *et al.,* 1960). All larval stages were also thick sectioned to corroborate gross features seen in ultrathin sections.

Results

General

Planktotrophic veliger larvae of *Melibe leonina* consist of two major parts: a cephalopedal mass, which includes the ciliated velar lobes, distal esophagus, and foot; and a visceropallial mass, which consists of the remainder of the gut encased by the mantle (pallium) (Fig. 2A). The mantle is derived from the embryonic shell gland and consists of a squamous epithelium lining the inner wall of the shell and a peripheral rim of large cells that secrete larval shell material. Epithelium extending from the shell-secreting cells to the cephalopodium is called the mantle fold, although it is unclear if this is also derived from the shell gland. In newly hatched *Melibe* larvae, the mantle fold is only a few cells wide and thus the mantle cavity it

Figure 4. Cross section through newly hatched larva passing through cerebral ganglia (CG), cerebral commissure (CC), and cephalic apical organ (AO). The prototroch (PR) is indented over the mouth. Arrow indicates position of osphradial nerve (enlarged in inset) within the right mantle fold (MF). Orientation arrows: D = dorsal; V = ventral; L = left; R = right. Scale, 10 μm.

Figure 5. Cross section through newly hatched larva showing part of cerebral commissure (CC) extending into left cerebral ganglion (CG). Arrow indicates cilia within apical organ cell. Scale, 2 μm.

Figure 6. Cross section through apex of 6-day-old larva showing cephalic plates (CP) invaginated from pre-trochal ectoderm. PR = prototroch. Scale, 10 μm.

Figure 7. Frontal section through left side of larva at onset of mantle retraction showing multilayered, invaginated cephalic plate (CP) overlying cerebral ganglion (CG). Arrowhead indicates mitotic cell; arrow indicates ingressing cephalic plate cells. V = velar lobe. Scale, 5 μm.

Figure 8. Frontal section through right side of larva at onset of mantle retraction showing eye (EY) overlying dorsal area of cerebral ganglion (CG). CC = cerebral commissure. Scale, 5 μm.

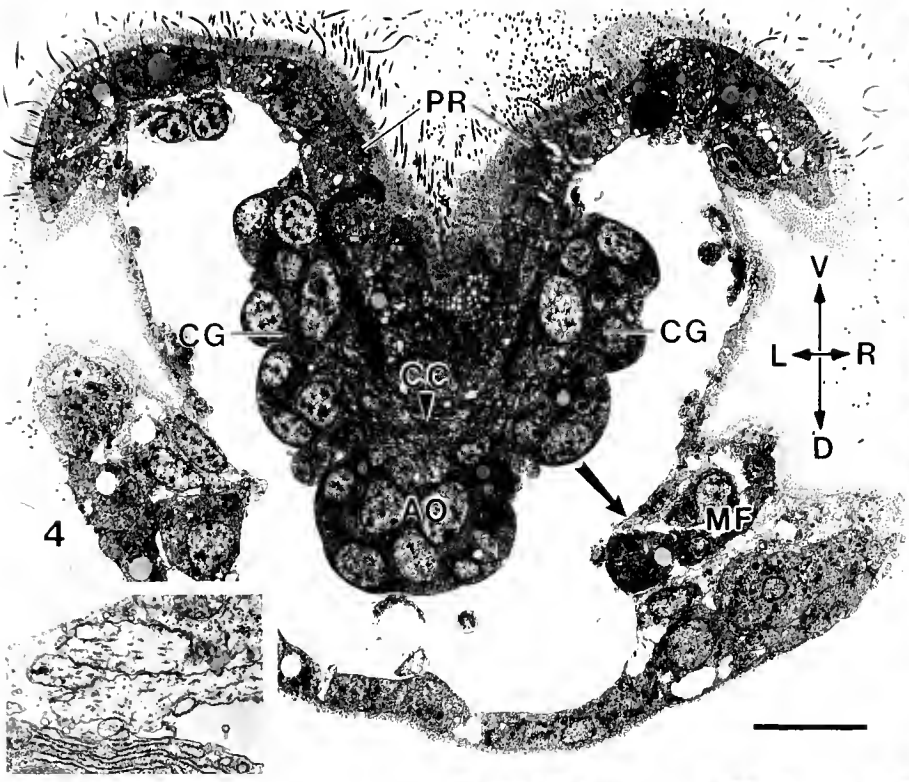
PR
CG
CG
CC
V
L
R
D
AO
MF
4

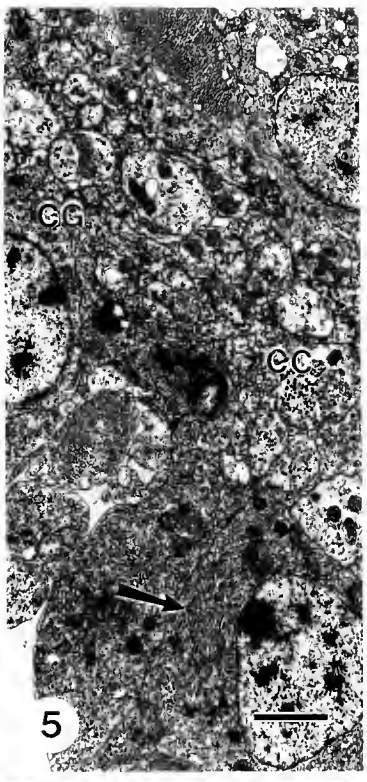
CG
CC
5

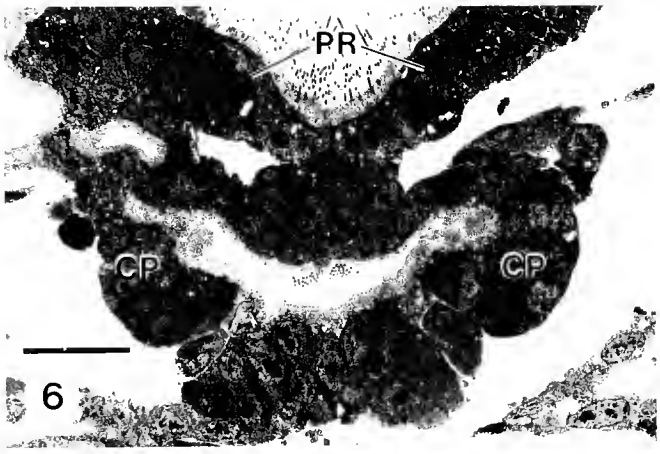
PR
CP
CP
6


V
CP
CG
7

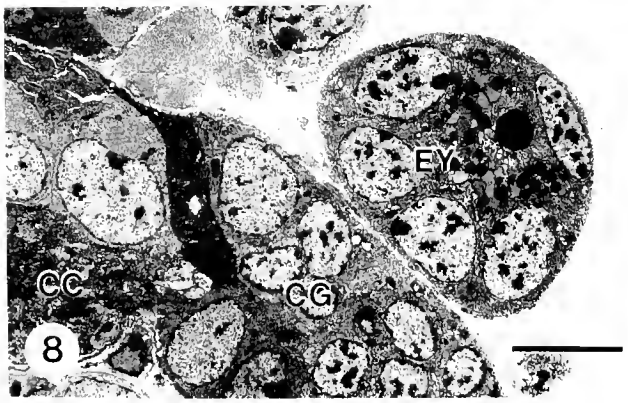
EY
CC
CG
8

defines is extremely shallow. The anus opens into the mantle cavity on the right ventro-lateral side, indicating slightly less than 90° torsion of the gut (Fig. 2B).

The shell growth that occurs during the first half of larval life is accompanied by a deepening of the right side of the mantle cavity, which extends from the anus over to the dorsal side (Fig. 2B). The left mantle cavity, which extends from the anus along the ventral aspect of the larva, remains shallow. It is important to note that the right mantle fold in partially torted *Melibe* larvae is equivalent to the left mantle fold of gastropods showing full 180° of torsion. It is this side that retains the various components of the pallial complex (ctenidium, osphradium, kidney) in monotocardian prosobranchs.

Midway through the larval phase of *Melibe,* shell secretion is arrested and the mantle fold detaches from the shell aperture and retracts posteriorly. The future post-metamorphic dorsum and cerata are formed from retracted mantle fold.

Two days after metamorphic shell loss, the basic characteristics of the adult nervous system are evident. The post-metamorphic CNS is formed by consolidation of many ganglionic primordia that arise during larval development by cellular ingression from thickened placodes of ectoderm. Neurogenic ectodermal cells often show mitotic figures.

To identify ganglionic primordia in *Melibe,* the locations of their respective neurogenic ectodermal placodes were compared to those that give rise to specific ganglia in prosobranchs. For these comparisons, it is important to distinguish three main areas of larval ectoderm, as illustrated in Figure 2. Ectoderm of the cephalopedal mass is subdivided into pre- and post-trochal areas by the band of large velar ciliated cells (the prototroch) that runs around the periphery of the velar lobes (Fig. 2B). The distinction between cephalopedal and visceropallial ectoderm is less distinct, but the latter shows torsional displacement whereas cephalopedal ectoderm does not. The pores of the left and right nephrocysts (large terminal cells of protonephridia) provide a convenient marker for the posterior limit of cephalopedal ectoderm (Fig. 2B). The nephrocysts do not exhibit torsional displacement in young larvae, although the left member is pulled further posteriorly than the right during mantle retraction. The anus and mantle gland (previously called larval kidney cell) lie posterior to the nephrocysts and show evidence of torsion (Figs. 2A, B).

The development and post-metamorphic fate of ganglia derived from pre-trochal cephalopedal ectoderm and from ectodermal placodes within the visceropallium are described below. Results are summarized by the diagrams in Figures 2C and 3. The companion paper (Page, 1992) describes ganglionic derivatives of post-trochal cephalopedal ectoderm.

Pre-trochal cephalopedal ganglia

Two placodes of neurogenic ectoderm, called cephalic plates, flank the mid-sagittal plane of the pre-trochal cephalopedal zone (Fig. 2B). Cells ingressing from the cephalic plates form the paired cerebral ganglia, eyes, optic ganglia, and rhinophoral ganglia.

In newly hatched veligers, each cerebral ganglion consists of neuronal cells clustered around a neuropile that is continuous with the fiber tract of the cerebral commissure. In cross sections, the cerebral ganglia and commissure form a horseshoe shaped complex (Fig. 4), perched above the distal esophagus, that parallels the trajectory of the prototroch where it arches above the mouth. The peculiar cells of the cephalic apical organ, which have an internal vacuole containing many cilia, are located on the dorsal side of the cerebral commissure (Fig. 5).

The paired cephalic plate placodes that overlie the cerebral ganglia are invaginated only slightly at hatching, but 6 days later the invaginations have deepened and are connected by a trough (Fig. 6). By the time of mantle retraction, the two invaginated cephalic plate lobes are composed of multiple layers of cells that sit as caps overhanging the ventro-lateral borders of the enlarging cerebral ganglia (Fig. 7). These cells ingress individually or in small clusters to the cerebral ganglia. Evidence of ingression is most prominent along the medial side of each invaginated cephalic plate lobe (Fig. 7).

Two eyes, each with a spherical lens and pigment granules, appear on the dorso-lateral surface of each cerebral ganglion prior to mantle retraction (Fig. 8). The eyes form adjacent to protuberances of the cerebral ganglia, which become the optic ganglia. The rhinophoral ganglia, which also arise from the cephalic plate, appear as mounds of cells on the cerebral ganglia of late stage larvae. During

---

Figure 9. Cross section through newly hatched larva at a level just beneath the foot showing where the visceral loop completes its subesophageal trajectory. Area within left box enlarged in Figure 10; area within right box enlarged in Figure 11. A = anus; E = esophagus; LPP = left pallial placode; LRM = larval retractor muscle; MA = shell-secreting mantle cells; MG = mantle gland. Scale, 10 μm.

Figure 10. Left limb of visceral loop (arrows) extending towards right side beneath esophagus (E). Scale, 2 μm.

Figure 11. Right limb of visceral loop (R) leaving mantle gland (MG) to merge with left limb (L). A = anus. Scale, 2 μm.

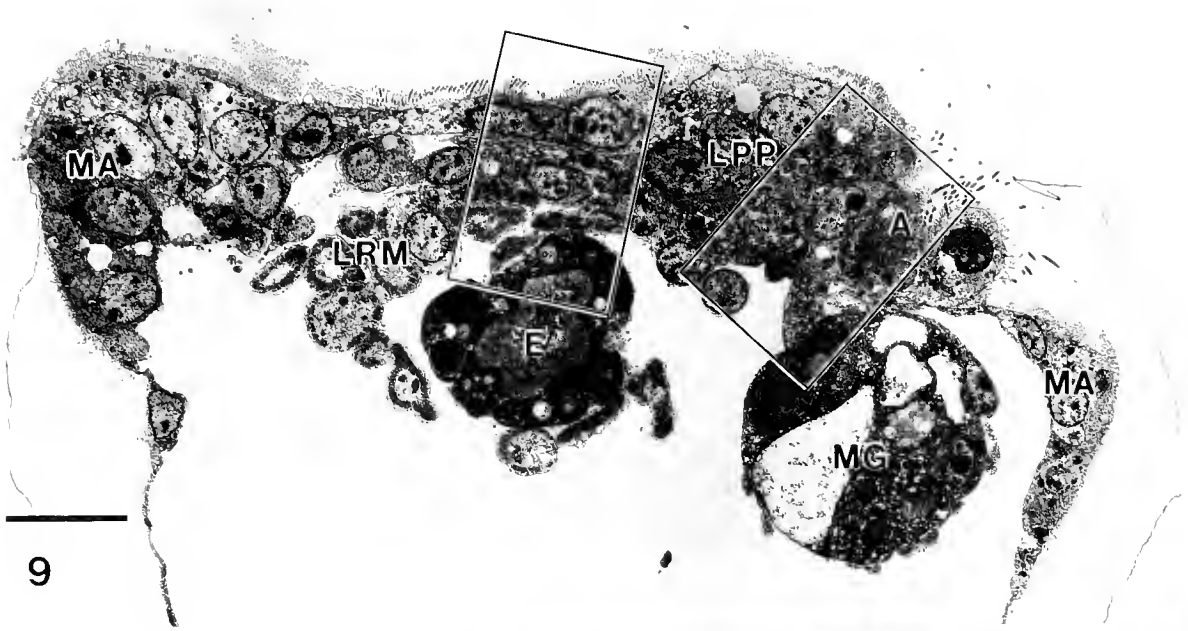
MA
LRM
E
LPR
A
MA
MG
9

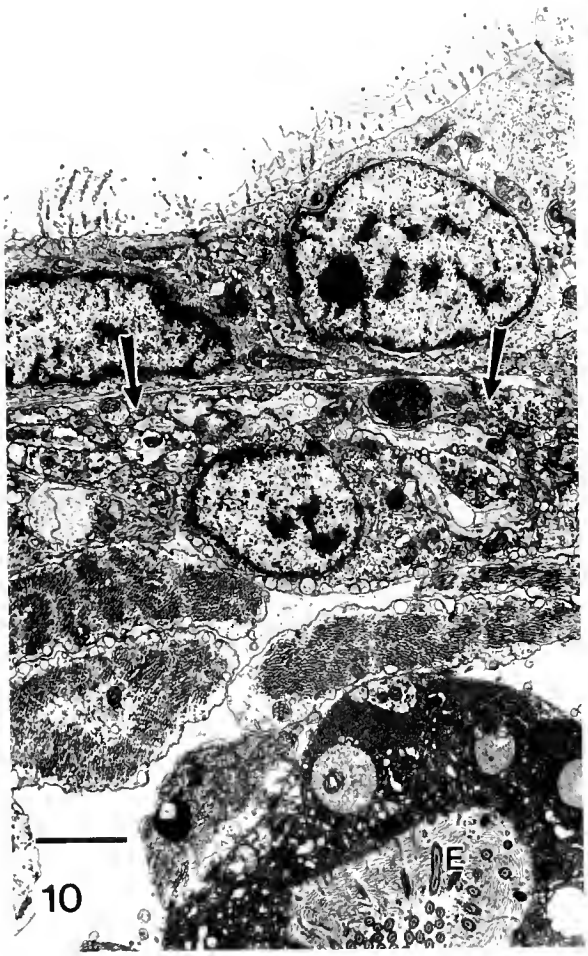
E
10


A
L
R
MG
11

metamorphosis, the rhinophoral ganglia are carried distally within the expanding oral hood (Bickell and Kempf, 1983).

Visceral loop ganglia

To minimize confusion, I will define my nomenclature for the visceral loop ganglia because varying schemes have been used by past authors. I use the terminology of Bullock (1965), in which the most anterior ganglia of the typical gastropod visceral loop are called left and right pleurals (Fig. 1A). These are followed by the sub- and supraintestinals and finally the unpaired visceral ganglion. The supraintestinal ganglion gives rise to a nerve extending to the osphradial ganglion. A second osphradial ganglion linked to the subintestinal ganglion is a characteristic restricted to diotocardian prosobranchs. In some pulmonates and opisthobranchs, but not in prosobranchs, extra ganglionic swellings are located anterior to the intestinal ganglia; these are called parietal ganglia. The visceral loop is long and twisted (streptoneurous) in many prosobranchs and a few opisthobranchs, but is short or untwisted (euthyneurous) in most extant opisthobranchs.

Sections through newly hatched larvae of *Melibe* show that the left and right limbs of the visceral loop fiber tract emerge directly from the neuropiles of their respective cerebral ganglia. The left limb swings beneath the esophagus to merge with the right limb at a point just medial to the anus (Figs. 9–11). The visceral loop is complete but nonganglionated at this initial larval stage and consists of at least 20 axons.

Figure 12 is a cross section through the left side of a newly hatched veliger, close to where the visceral loop on that side emerges from the cerebral ganglion. The section gives the impression that post-trochal ectodermal cells are ingressing from the left mantle fold toward the base of the cerebral ganglion. However, higher magnification reveals myofilaments within these subepidermal cells (Fig. 13); they are not ingressing pleural or parietal neurons. Differentiating subepidermal muscle cells are present in the same location on the right side of the larva. Indeed, the nuclear regions of many other fully and partially differentiated muscle cells are concentrated within the cephalopedal area of young larvae; these cannot be distinguished from neuronal elements in histological sections.

Right limb of visceral loop and osphradial neurons

After travelling a short distance posteriorly from the right cerebral ganglion, the right limb of the visceral loop in newly hatched veligers associates with a placode of thickened ectoderm that I call the right pallial placode (Fig. 14). The right pallial placode lines the deepest part of the right mantle cavity, immediately beneath the pore of the ipsilateral nephrocyst (Fig. 2B). At least one neuron originating from the right pallial placode is fully differentiated at hatching stage and is filled with many vesicles (Fig. 14). From this point, a small nerve extends anteriorly between the epithelial cells and underlying basal lamina of the mantle fold (Figs. 4 inset, 15). At least some of the axons forming this nerve arise from a cluster of sparsely ciliated neurons located close to the antero-lateral periphery of the right mantle fold. These neurons are associated with a mucous cell and their location corresponds to that of the osphradium and osphradial ganglion in prosobranch larvae (Figs. 2B, 15, 16). The fate of these osphradial neurons after mantle retraction requires further study. I failed to find them in sections of larvae fixed after onset of mantle retraction.

At least some of the neurons ingressing from the right pallial placode must be homologues of supraintestinal neurons, because they form a ganglion at the intersection of the visceral loop and osphradial nerve. However, the series of sections shown in Figures 17–20 reveal that this ganglion receives neurons from two ingression sites within the right pallial placode. These two sites may be sources of right parietal and supraintestinal neurons. However, an alternative interpretation is given in the discussion, and until this issue is clarified I will refer to the ganglion arising from the right pallial placode as the supraintestinal ganglion.

Figure 12. Cross section through left side of newly hatched larva close to where visceral loop (VL) emerges from cerebral ganglion (CG). Arrow indicates subepidermal cell (enlarged in Fig. 13) lying between mantle fold ectoderm (MF) and cerebral ganglion. MC = mantle cavity; ST = statocyst. Scale, 2 μm.

Figure 13. Detail from Figure 12 showing myofilaments (arrows) within subepidermal cell. Scale, 0.5 μm.

Figure 14. Cross section through newly hatched larva showing right limb of visceral loop (VL) deflecting towards right pallial placode (RPP). Asterisk marks neuron with many vesicles. Scale, 1 μm.

Figure 15. Mantle fold ectoderm on right side of 6-day-old larva showing differentiating osphradial neuron (asterisk) adjacent to axons of osphradial nerve (arrowheads). Arrow indicates vesicles that are enlarged in the inset. Scale, 1 μm; inset, 0.3 μm.

Figure 16. Frontal section through larva just prior to mantle retraction showing osphradial neurons (OS) and associated mucous cell (arrow) beneath shell-secreting periphery of mantle (MA). Supraintestinal ganglion (SPG) enlarged in Figure 19. H = hemocoel; N = nephrocyst; RPP = right pallial placode. Scale, 10 μm.

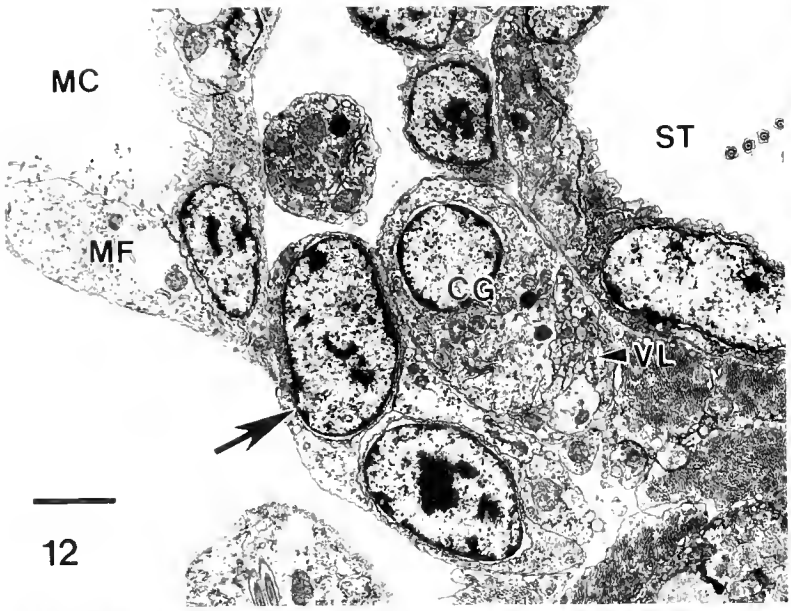

12

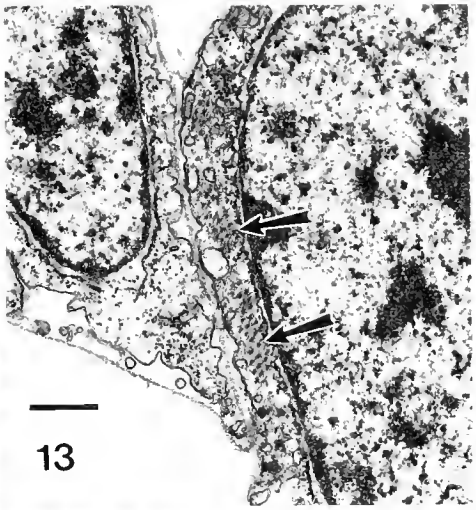

13

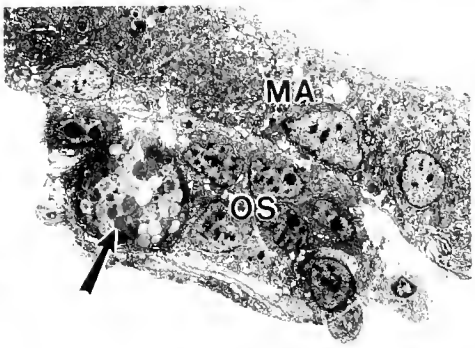

H

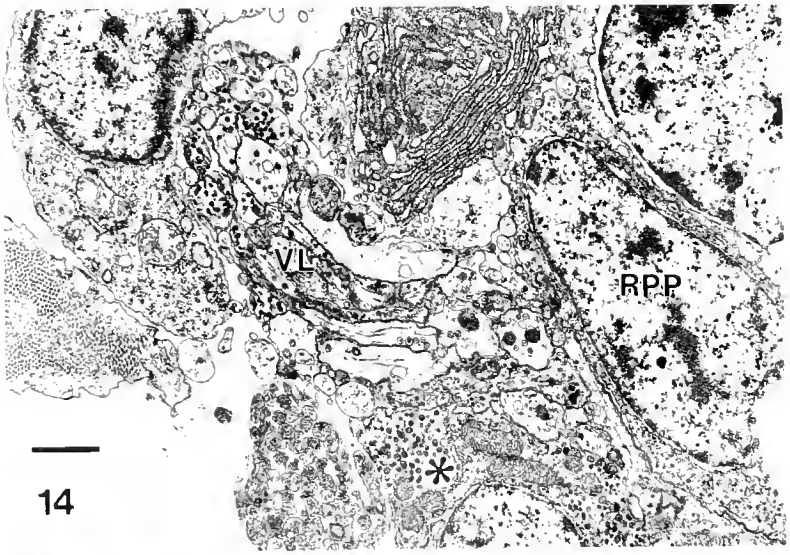

14

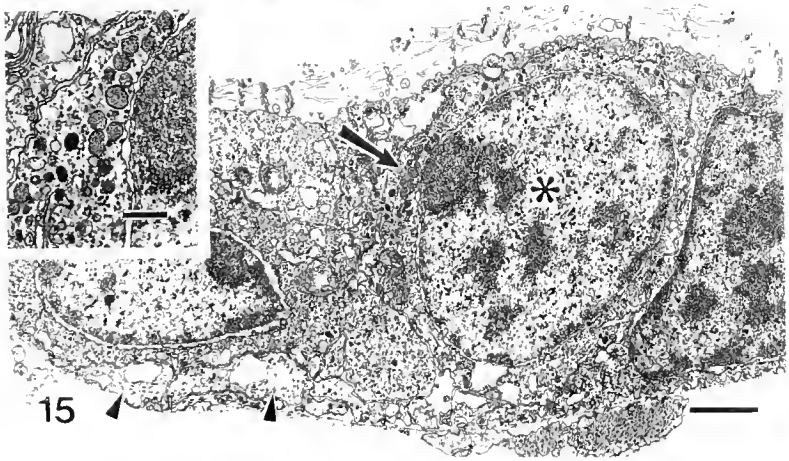

15

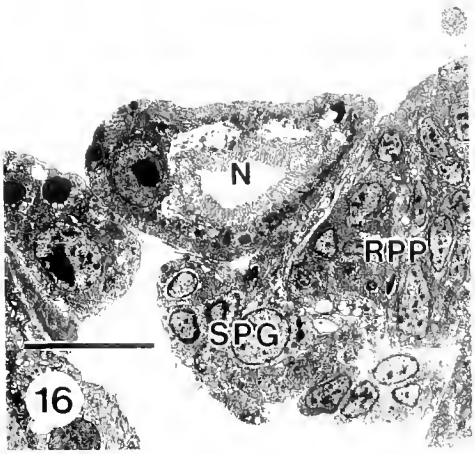

16

Immediately after leaving the supraintestinal ganglion, the right limb of the visceral loop passes to the very large mantle gland that bulges into the hemocoel from the right mantle fold ectoderm (Fig. 20). This structure has been called the larval kidney complex, but evidence of an excretory role is weak and its ultrastructure is more consistent with a secretory function. The largest cell of the mantle gland, along with several associated secretory cells and the muscle fibers that invest the complex, are innervated by axons extending from the intimately associated visceral loop fiber tract.

In young larvae, the right limb of the visceral loop travels ventrally along the mantle gland until merging with the left limb (Fig. 11). However, the visceral loop lifts away from the mantle gland when the latter is displaced posteriorly during mantle retraction (Fig. 21). Although the peripheral rim of the mantle fold is pulled a great distance posteriorly during mantle retraction, the right pallial placode continues to be closely associated with the supraintestinal ganglion (Fig. 22). The ganglion lies lateral to the esophagus but projects dorsally.

Left limb of visceral loop and visceral ganglion

At the hatching stage, mantle ectoderm to the left of the anus is thickened by presumptive neurons. I call this the left pallial placode, because it is part of the left mantle fold. However, due to torsion, the placode is located toward the right side of the ventral aspect of the larval body (Figs. 2B, 9, 10). During later development, the left pallial placode is the only recognizable source of neurons along the entire left limb of the visceral loop in all larval stages examined. Furthermore, the only axons that leave this portion of the visceral loop extend to larval muscles, not to the ectoderm. Nevertheless, during subsequent development, cells are distributed along the entire left limb of visceral loop with a concentration appearing where the visceral loop emerges from the left cerebral ganglion (Fig. 23). These cells appear to be subintestinal neurons that originated from the left pallial placode on the right, ventrolateral side of the body and that migrated along the subesophageal trajectory of the visceral loop toward the left cerebral ganglion. Unlike the supraintestinal ganglion, which projects dorsally from the right cerebral ganglion (Fig. 22), the concentration of subintestinal neurons projects ventrally from the left cerebral ganglion (Fig. 23).

I could find no morphological evidence of a distinct ingression site for left parietal neurons.

The visceral placode, which is neurogenic visceropallial ectoderm for neurons of the future visceral ganglion, becomes recognizable at 6 days after shell loss. The visceral and left pallial placodes are contiguous. Figures 24–27, which is a series of frontal sections through a larva at onset of mantle retraction, show the positions of these two placodes and their relationship to the visceral loop. Note that the right limb of the visceral loop extends to the left pallial placode, not to the visceral placode.

During later development, the left limb of the visceral loop becomes progressively denuded of cells, presumably because most subintestinal neurons have migrated toward the left cerebral ganglion. Nevertheless, a small clump of neurons is apparent at the junction of the left and right limbs of the visceral loop and from this point, a prominent visceral nerve extends into the base of the visceral placode (Figs. 28–30). Ingressing visceral neurons do not form a ganglion immediately beneath the visceral placode. My observations suggest that visceral neurons migrate along the visceral nerve to form a consolidated ganglion on the visceral loop.

By the end of the larval phase, there are three neuronal concentrations along the visceral loop fiber tract: the supraintestinal ganglion behind the right cerebral ganglion, the subintestinal ganglion behind the left cerebral ganglion, and the visceral ganglion immediately adjacent to the anus (Fig. 3C). At this stage, the two intestinals have begun to fuse with their respective cerebral ganglia, but the visceral ganglion remains separate. Histological sections through metamorphic stages show that the visceral ganglion is relocated to the left side during the hours after shell loss, where it fuses with the left cerebral and subintestinal ganglionic mass (Figs. 3D; 31–33).

Discussion

It has been known since the last century that molluscan neurons are ectodermal derivatives (see reviews by Raven,

Figures 17–20. Series of frontal sections through right pallial placode (RPP) and supraintestinal ganglion (SPG) of a larva just prior to mantle retraction. N = nephrocyst.

Figure 17. Arrow indicates presumptive neurons ingressing from right pallial placode to underlying ganglion. Scale, 2 μm.

Figure 18. Slightly deeper section showing no neuronal ingression. Scale, 2 μm.

Figure 19. Second site of neuronal ingression (arrow) coinciding with emergence of osphradial nerve (arrowheads) from the visceral loop (VL). Scale, 2 μm.

Figure 20. Visceral loop (VL) travelling from supraintestinal ganglion to mantle gland (MG). Scale, 2 μm.

Figure 21. Longitudinal section through supraintestinal ganglion (SPG) at full mantle retraction stage showing visceral loop (arrow) dissassociated from mantle gland (MG). Scale, 5 μm.

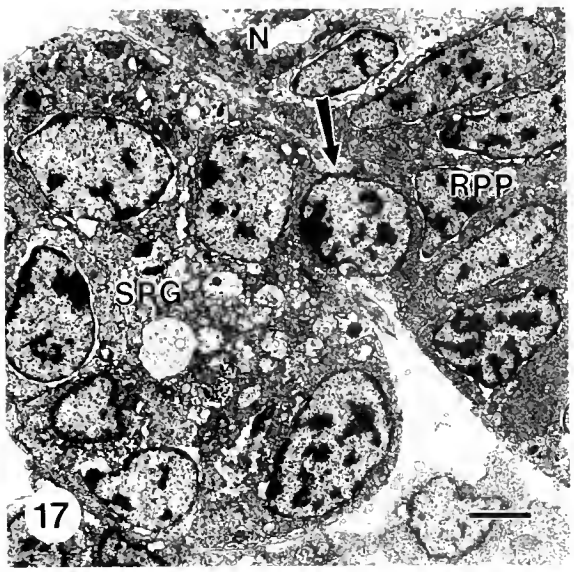
N
RPP
SPG
17

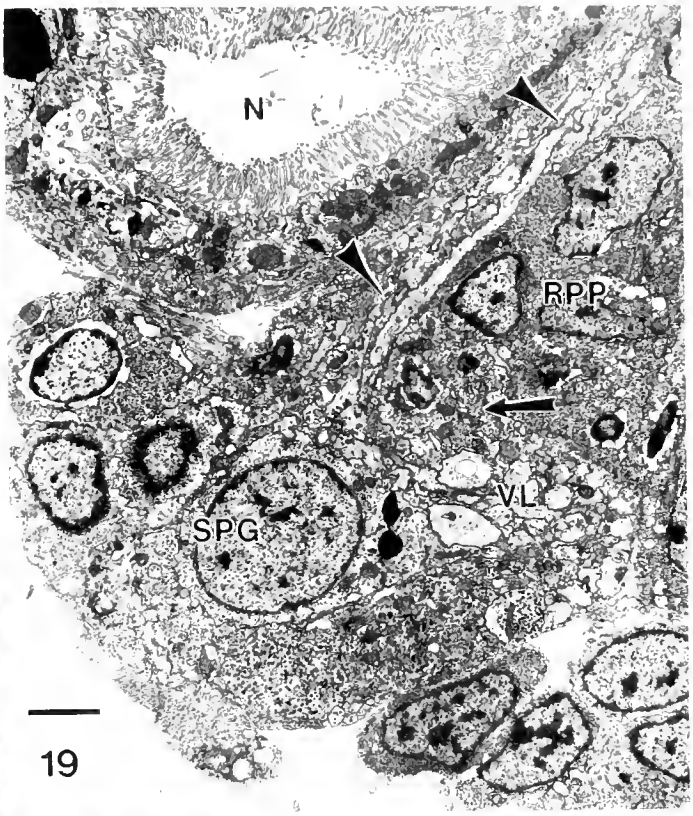
N
RPP
VL
SPG
19

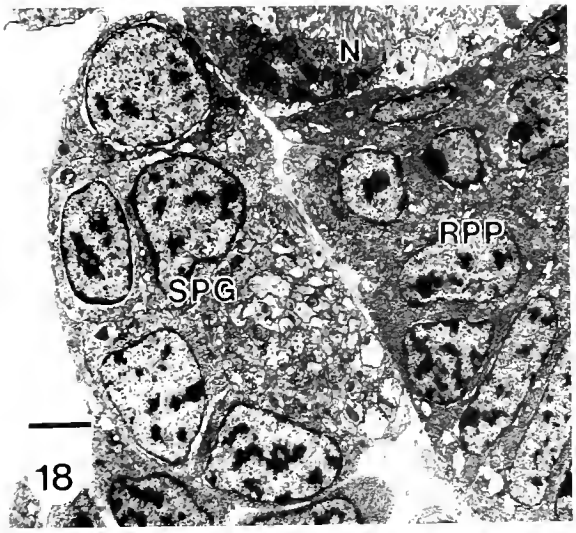
N
RPP
SPG
18


RPP
SPG
VL
MG
20

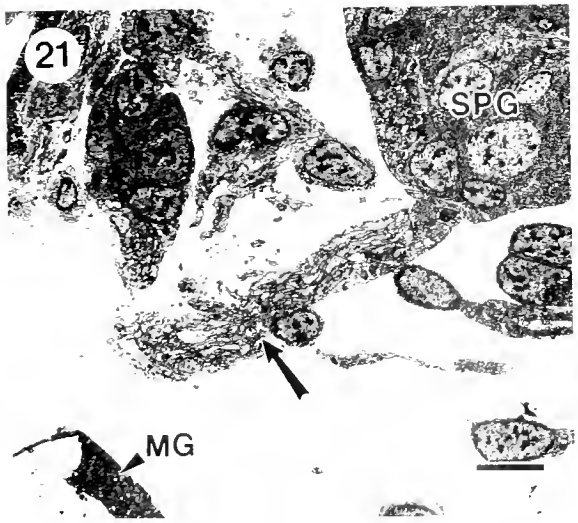
21
SPG
MG

1958; Moor, 1983). Furthermore, comparison of various histological accounts of prosobranch neurogenesis indicate that primordia of each ganglionic type arise from stereotypic locations within the ectoderm of the veliger (Smith, 1935; Crofts, 1937; Moritz, 1939; Creek, 1951; Régondaud, 1961, 1964; D'Asaro, 1969; Cumin, 1972; Guyomarc'H-Cousin, 1974; Honegger, 1974; Demian and Yousif, 1975). Cerebral ganglia always arise from the intravelar cephalic plates and intestinal, visceral, and osphradial ganglia arise from characteristic areas of visceropallial ectoderm. This phenomenon is particularly unambiguous in those gastropods that retain separate central ganglia through metamorphosis. Nevertheless, these sites appear to be a highly conserved feature of early gastropod neurogenesis, regardless of the final, species-specific form of the adult CNS (illustrated well by studies of Honegger, 1974; Demian and Yousif, 1975). Therefore, it is appropriate to identify ganglionic primordia in *Melibe* by comparing their ectodermal ingression sites to those described for the ganglia of other gastropods, particularly prosobranchs. Adjustments for variable degrees of torsional displacement among these species are made possible by the position of the anus relative to the cephalopedal mass.

Using *in situ* hybridization and immunofluorescence techniques, McAllister *et al.* (1983) found that mRNA for egg laying hormone (ELH) and related peptides in the opisthobranch *Aplysia californica* is located in neurosecretory bag cells located adjacent to the abdominal (intestinovisceral) ganglion, and also in a small number of central ganglia neurons. In veligers, cells containing this mRNA are "distributed throughout the entire length of the inner surface of the body wall, with one particularly dense cluster of cells expressing ELH-related mRNA along the body cavity close to the head." From this description, it cannot be determined if presumptive ELH-containing neurons, destined for central ganglia, are indeed located within typical ectodermal proliferative zones for these ganglia. The bag cell neurons, unlike neurons forming initial primordia of central ganglia in developing gastropods, do not begin to ingress from the ectoderm until after metamorphosis and their definitive position is outside the abdominal ganglion proper. Therefore, the observations of McAllister *et al.* (1983) do not contradict the notion that primordia of CNS ganglia arise initially from stereotypical ectodermal locations on the veliger body.

Pre-trochal cephalopedal ganglia

Derivation of cerebral ganglia from pre-trochal (intravelar) ectoderm, specifically the cephalic plates, was first described in early cell lineage studies of gastropods (see Conklin, 1897) and has been confirmed by many subsequent analyses (reviewed by Raven, 1958; Moor, 1983; Verdonk and van den Biggelaar, 1983). As suggested by Thompson (1958), invagination of the cephalic plates during cerebral gangliogenesis may fulfill a need for increased ectodermal surface area during rapid mitoses of cephalic plate cells.

Tardy (1970, 1974) has stated that the invaginated cephalic plates in the nudibranch *Aeolidiella alderi* are the source of both cerebral and pleural neurons. According to his interpretation, the ganglia formed from the two cephalic plates are fused cerebropleural ganglia, each having a dorsal lobe corresponding to the pleural component and a ventral lobe corresponding to the cerebral component. In young *Melibe* larvae, each developing cerebral ganglion also has a small dorsal protuberance, but these develop into the optic ganglia. The pleural ganglia of *Melibe* develop from a pair of post-trochal ectodermal placodes, as described in the following paper.

Presumptive neurons within the cephalic plate ectoderm of *Melibe* ingress singly or in small clusters throughout the larval phase; they do not separate en masse from the ectoderm during later development as suggested by Tardy (1970; 'telencephalization') for the nudibranch *Aeolidiella alderi*.

Visceral loop and osphradial neurons

The fiber tract of the visceral loop forms a complete circuit beneath the esophagus from the time *Melibe* larvae hatch from the egg mass. This fiber tract is probably established by axons from cerebral neurons, because many differentiated cerebral neurons are present at the hatching stage and the cerebral neuropiles are continuous with the visceral loop fiber tract. With the exception of several osphradial neurons and one neuron associated with the right pallial placode, differentiated neurons are not associated with the visceral loop at the hatching stage. A visceral loop arising directly from the cerebral ganglia is found in Caudofoveata, Solenogastres, Monoplacophora, and Polyplacophora, and may be the ancestral state for the molluscan nervous system (Salvini-Plawen, 1985).

Ganglia identifications

In *Melibe* larvae, all primordial ganglia associated with the visceral loop originate from visceropallial ectoderm and show some degree of torsional displacement. In prosobranchs, these characteristics apply to the intestinal and visceral ganglia, with the osphradium and osphradial ganglion also arising from visceropallial ectoderm. The pleural ganglia of prosobranchs ingress from post-trochal cephalopedal ectoderm and do not show torsional displacement (Smith, 1935; Crofts, 1937; Guyomarc'H-Cousin, 1974; Honegger, 1974; Demian and Yousif, 1975). Moritz (1939) is alone in describing a slight asymmetrical positioning for pleural ganglia in *Crepidula adunca*. I must

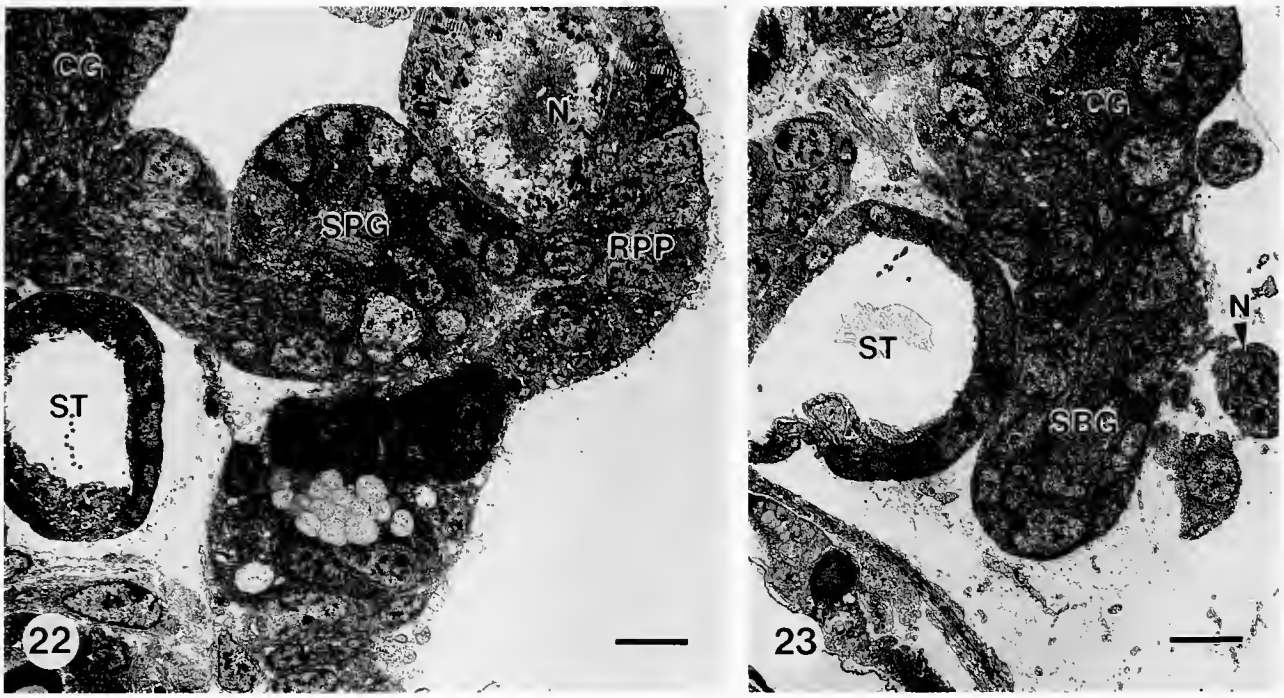

Figure 22. Longitudinal section through a larva after completing mantle retraction showing supraintestinal ganglion (SPG) projecting dorsally from right cerebral ganglion (CG). N = nephrocyst; RPP = right pallial placode; ST = statocyst. Scale, 5 μm.

Figure 23. Longitudinal section through same larva showing concentration of subintestinal neurons (SBG) projecting ventrally from left cerebral ganglion (CG). N = ciliated tube of nephrocyst; ST = statocyst. Scale, 5 μm.

conclude that pleural neurons are not associated with the visceral loop of *Melibe* and, therefore, are not part of the adult 'cerebropleural' ganglia.

A pentaganglionate visceral loop (not including the pleural ganglia), consisting of paired parietal ganglia in addition to paired intestinal and unpaired visceral ganglia, has been called a major synapomorphy of opisthobranchs and pulmonates (Haszprunar, 1985b, 1988), even though five distinct visceral loop ganglia are rarely found among adults of this group. It is assumed that ganglionic fusions have masked the pentaganglionate condition in most Euthyneura. In support of this, Tardy (1970, 1974) and Régondaud (1961, 1964) claimed to resolve five visceral loop ganglia in a transient developmental stage of a nudibranch opisthobranch and basommatophoran pulmonate, respectively. However, the visceral loop of developing euthyneurans is short and, in *Melibe* at least, passes through a prolonged stage in which cells are distributed along the entire left limb. I argue that individual CNS ganglia cannot be defined solely by the criterion of an apparent local concentration of neuronal cells, but each must have a distinct site of neuronal ingression from the ectoderm. Only in this way can homologous ganglia be recognized in developmental stages of different gastropods. Using this criterion, which usually requires ultrastructural examination, I found only four ganglionic ingression sites along the visceral loop of *Melibe* larvae: subintestinal neurons arise from the left pallial placode; visceral neurons arise from the visceral placode; and two neuronal ingression sites were resolved for the right pallial placode, one of which must be the source of supraintestinal neurons (see below).

The neurons that differentiate from the right mantle fold ectoderm, close to its shell-secreting periphery, can be identified as osphradial by their position and because they are linked to the right limb of the visceral loop by a nerve tract. There are many descriptions of an osphradium or osphradial ganglion in larvae of prosobranchs (Thiriot-Quiévreux, 1974; Demian and Yousif, 1975; others reviewed by Fretter and Graham, 1962) and opisthobranchs that retain a mantle cavity through metamorphosis (Smith, 1967; Kriegstein, 1977a, b). However, osphradial neurons have not been identified previously in nudibranch larvae, although Kempf *et al.* (1987) found a neuron close to the edge of the right mantle fold in the nudibranch, *Tritonia diomedea*, that labelled with a monoclonal antibody to small cardioactive peptide B.

From the time of hatching, the osphradial neurons of *Melibe* are associated with a mucous cell, which suggests that the structure is homologous to the osphradial sensory

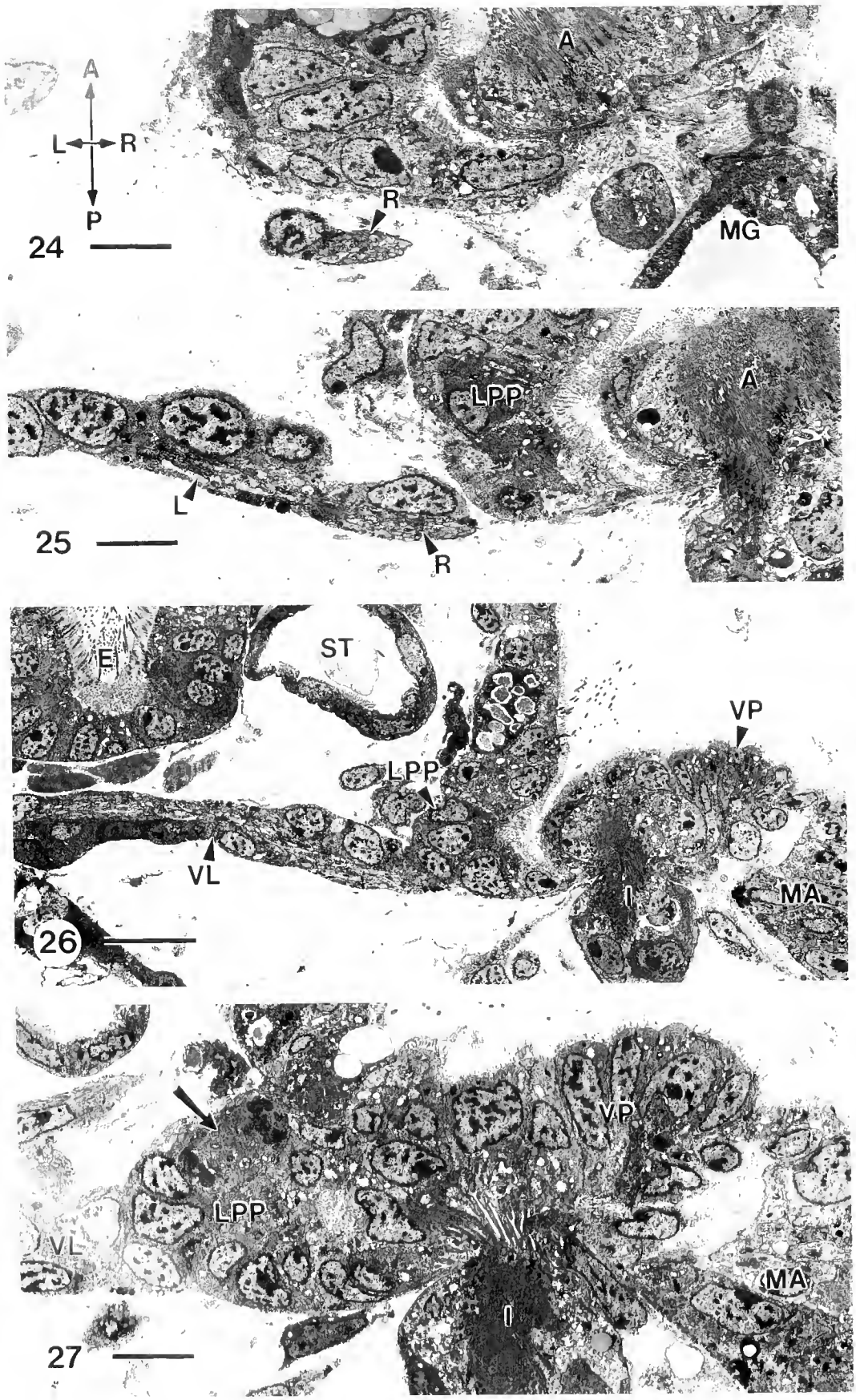
A
L
R
P
24
A
R
MG
25
LPP
A
L
R
E
ST
VP
LPP
VL
I
MA
26
VP
LPP
VL
I
MA
27

epithelium of other gastropods. If this is the case, then is there an osphradial ganglion? Present data are insufficient to answer this question, but two possibilities can be suggested. First, if the osphradial ganglion of gastropods is generated from neurons that ingress from the osphradial sensory epithelium, as proposed by Demian and Yousif (1985), then this process does not occur during the ontogeny of *Melibe* and there is no osphradial ganglion. Consequently, the two ingression sites within the right pallial placode can be interpreted as the source of right parietal and supraintestinal neurons, respectively. Alternatively, these two ingression sites may generate neurons homologous to those of the supraintestinal and osphradial ganglia in other gastropods, in which case there is no evidence of a right parietal ganglion. The latter possibility may seem unlikely, and yet patelloid limpets (archeogastropods) have a streak of sensory epithelium along the distal mantle skirt that is connected by a nerve to a much more proximally located osphradial ganglion with overlying osphradium (Haszprunar, 1985a). Comparative developmental studies on opisthobranchs having both osphradium and osphradial ganglion could help resolve this uncertainty.

It might be argued that the more anterior of the two neuronal ingression sites within the right pallial placode is better identified as the source of right pleural neurons. However, this interpretation would require that neurons of the left pleural ganglion arise from the left pallial placode, which is obviously in a post-torsional location on the right, ventro-lateral side of the larva. No other ectodermal placode is associated with the left limb of the visceral loop in any larval stage that I examined. Furthermore, neurons that accumulate behind the left cerebral ganglion project ventrally, reflecting their post-torsional heritage. Therefore, the alternative interpretation is unacceptable because pleural ganglia are not affected by torsion in gastropods (see Fretter and Graham, 1962; Bullock, 1965). It follows that pleural ganglia must be derived from ectoderm of the cephalopedal mass and their morphogenesis is described in the companion paper.

Asymmetry of the visceral loop

The larval digestive tract of *Melibe* is torted by less than 90°, so partial torsion of visceropallial neurogenic placodes is expected. However, the visceropallial placodes exhibit differing amounts of torsion. The left pallial placode, which generates subintestinal neurons, is actually located on the right side in a position showing marked torsional displacement; it is far removed from the left nephrocyst. By contrast, torsional displacement of the right pallial placode (and the osphradial neurons) is minimal, particularly in young veligers. This placode is located immediately adjacent to the right nephrocyst. The visceral placode, like the digestive tract, exhibits approximately 60° of torsion. Consequently, all sites of pallial neurogenic ectoderm are located toward the right side of the larva, and the visceral loop is asymmetrical but never actually streptoneurous. A similar pattern of non-uniform torsion of the visceral loop was described by Crofts (1937, p. 250) for larvae of the archaeogastropod *Haliotis tuberculata*, following the initial (90°) phase of torsional twisting. Régondaud (1961, 1964) found that the visceral loop of *Lymnaea stagnalis* (Pulmonata) is only partially torted and its asymmetrical trajectory is comparable to that of *Melibe* larvae.

Cephalization and detorsion

Cephalization in gastropods is the anterior concentration of ganglia, particularly those of the visceral loop. Euthyneury is the uncrossing of the twisted visceral loop and displacement of ganglia to their pre-torsional sides; it is essentially a reversal of torsion as it affects the nervous system. Cephalization and euthyneury are believed to be prominent trends among opisthobranch and pulmonate gastropods (reviewed by Bullock, 1965; Schmekel, 1985).

Naef (1911) appears to have originated the idea that euthyneury is due to shortening of the visceral loop. He suggested that shortening concentrates the ganglia in the head, thereby pulling them out of the body area subject to torsion. This notion was more recently reiterated by Tardy (1970). Naef's theory is false because observations

---

Figures 24–27. Series of frontal sections through larva at onset of mantle retraction showing merger of right and left limbs of visceral loop and left pallial and visceral placodes. Orientation arrows: A = anterior; P = posterior; L = left; R = right.

Figure 24. Right limb of visceral loop (R) extending toward left from mantle gland (MG). A = anus. Scale, 5 μm.

Figure 25. Merger of right and left limbs of visceral loop (R and L, respectively) adjacent to anus (A) and left pallial placode (LPP). Scale, 5 μm.

Figure 26. Left limb of visceral loop (VL) associated with left pallial placode (LPP). Section grazes through periphery of visceral placode (VP) adjacent to terminal intestine (I). E = esophagus; MA = mantle; ST = statocyst. Scale, 10 μm.

Figure 27. Left pallial placode (LPP) with mitotic cell (arrow) and visceral placode (VP). I = intestine; MA = mantle; VL = visceral loop. Scale, 5 μm.

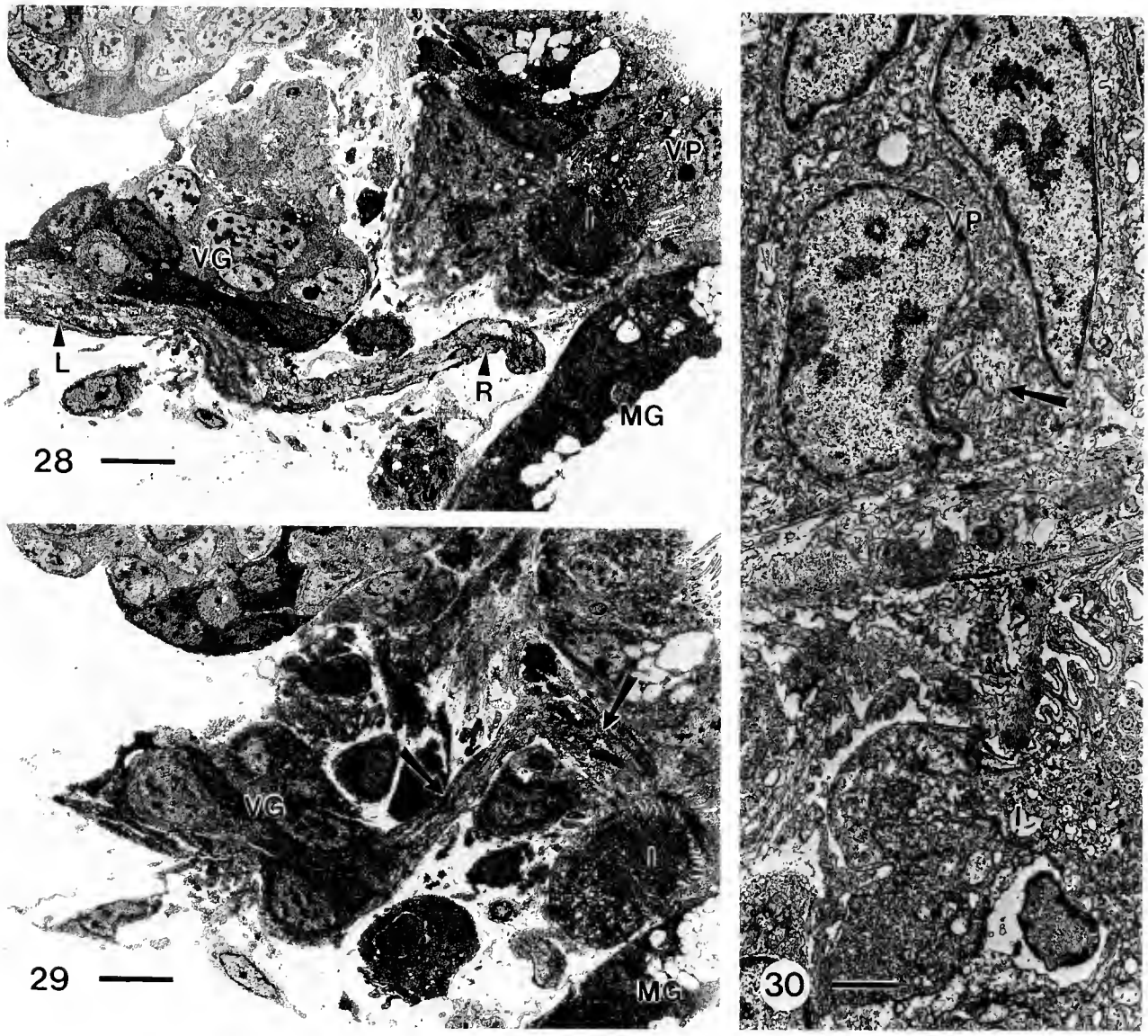

Figure 28. Frontal section through larva at mantle fold hypertrophy stage showing merger of right and left limbs of visceral loop (R and L, respectively) adjacent to intestine (I). MG = mantle gland; VG = visceral ganglion; VP = visceral placode. Scale, 5 μm.

Figure 29. Slightly deeper section showing visceral nerve (arrows) extending around distal intestine (I) from visceral ganglion (VG) towards visceral placode. Scale, 5 μm.

Figure 30. Visceral nerve (arrow) within base of visceral placode (VP). I = intestine. Scale, 1 μm.

on *Melibe* and *Lymnaea stagnalis* (Régondaud, 1961, 1964) show that visceral loop ganglia differentiate from torted visceropallial ectoderm, as they do in prosobranchs. Nevertheless, the concept of visceral loop shortening as the cause of euthyneury is popular (see Fretter and Graham, 1962; Bulloch, 1965). It might be envisioned that visceral loop ganglia become concentrated against the cerebral ganglia of their respective pre-torsional sides as threaded beads pushed together during shortening of a convoluted string. However, as pointed out previously by Régondaud (1961) for *Lymnaea*, and also seen in *Melibe* and *Aplysia californica* (Kriegstein, 1977a, b), all visceral loop ganglia differentiate within close proximity along a short visceral loop. This loop simply remains short in cephalized species, while the rest of the body elongates after metamorphosis. Instructions to elongate are given instead to peripheral nerves. This is more than a semantic point if cephalization is to provide a mechanism for eu-

thyneury, because visceral loop ganglia of *Melibe* and *Lymnaea* are close together *and* torted at the outset of gangliogenesis.

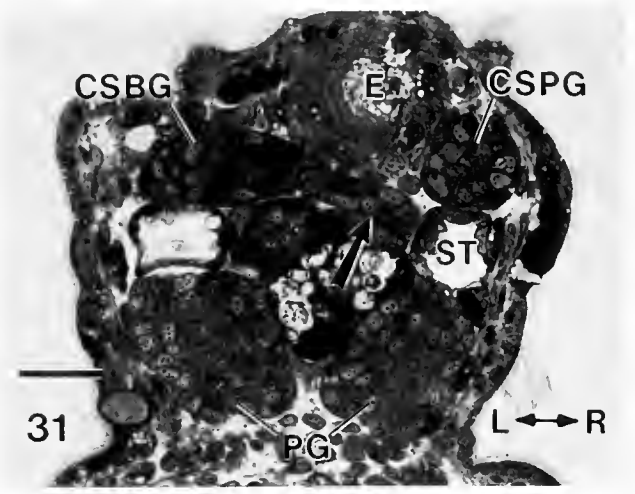

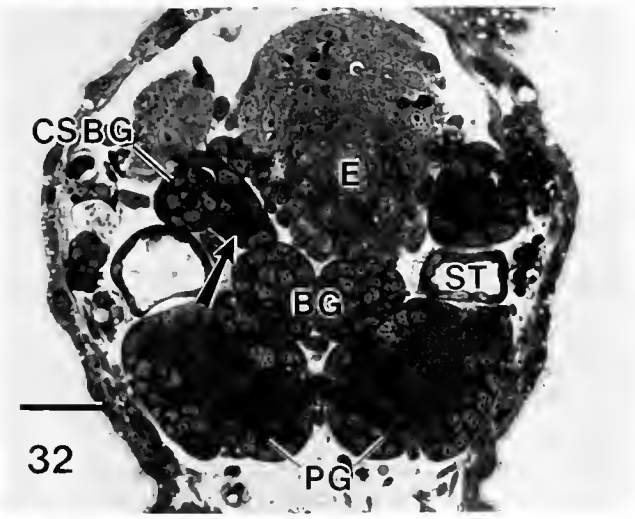

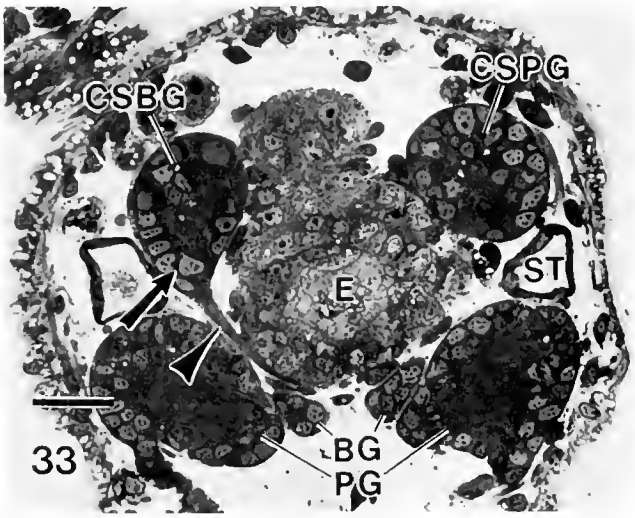

I propose that euthyneury in *Melibe* can be explained by two factors. First, half of the hypothesized detorsion is fictional because ganglia differentiate from visceropallial ectoderm that never shows more than partial torsion. Second, existing evidence suggests that subintestinal neurons, which arise from visceropallial ectoderm showing marked torsional displacement (unlike supraintestinal neurons), move toward the left cerebral ganglion by active migration along the visceral loop fiber tract. Other evidence that neurons migrate along existing connectives during gastropod neurogenesis comes from the study of McAllister *et al.* (1983), who found evidence that bag cells migrate along the visceral loop in juveniles of *Aplysia californica*. Active, leftward migration of subintestinal neurons contributes to both cephalization and detorsion without involving a length change of the visceral loop.

Similarly, visceral neurons appear to migrate along the nerve linking visceral placode and visceral loop during later larval development. However, it is unlikely that active migration of neurons is responsible for the final displacement of the visceral ganglion to the left side during metamorphosis, because the movement is rapid and involves all visceral neurons simultaneously. Instead, metamorphic movement of the visceral ganglion may be accomplished by differential lengthening of various connectives and commissures linking the CNS ganglia. Lengthening is restricted to the pedal and parapedal commissures and the segment of visceral loop extending between the supraintestinal and visceral ganglia (elongation of the latter is still minimal compared to that which occurs after metamorphosis in *Aplysia californica*). Therefore, when the larval body expands rapidly after shell loss, the visceral ganglion is pulled to the left because its tether to the left side of the CNS remains short, whereas that connecting it to the right side lengthens. Displacement of the visceral ganglion to the left side 'overshoots' detorsion.

Conclusions

Results of this study suggest that the paired 'cerebropleural' ganglia of *Melibe leonina* are, in reality, a fusion

Figures 31–33. Histological cross sections through metamorphic stages showing movement of visceral ganglion (arrow) from right to left sides of post-larva. Orientation arrows: L = left; R = right. BG = buccal ganglia; E = esophagus; CSBG = left cerebral + subintestinal ganglia; CSPG = right cerebral + supraintestinal ganglia; PG = pedal ganglia; ST = statocyst. Scales, 25 μm.

Figure 31. Immediately after shell loss.

Figure 32. Five hours after shell loss.

Figure 33. Ten hours after shell loss. Visceral ganglion has fused with left cerebral + subintestinal ganglionic complex. Arrowhead indicates visceral loop fiber tract.

of cerebral, subintestinal, and visceral ganglia on the left side, and cerebral, supraintestinal, and possibly parietal and osphradial ganglia on the right side.

The basic configuration of the post-metamorphic CNS and the pattern of peripheral nerves among many non-dorid nudibranchs are generally similar to that of *Melibe leonina*. Among dendronotaceans, Dorsett (1978) extended this to include similarities at the level of individual neurons, despite differences in adult body form. Therefore, my conclusions about the identity and fate of visceral loop ganglia may apply to many other non-dorid nudibranchs. However, small differences in adult neuroanatomy may signify large morphogenetic differences. Even among members of the genus *Melibe*, Gosliner (1987) has documented differences in relative size and surface texture of CNS ganglia. Development of visceral loop ganglia in aeolids such as *Phestilla sibogae*, in which the dorsum and cerata are derived from epipodial ectoderm rather than pallial ectoderm (Bonar and Hadfield, 1974; Bonar, 1976), may be quite different from that in *Melibe*.

Dorid nudibranchs form a cohesive group with features that distinguish them from other nudibranchs (Minichev, 1970; Schmekel, 1985), including anatomical details of the CNS and pattern of peripheral nerves. Ganglionic regions in the CNS of dorids requires separate neurodevelopmental analysis.

Acknowledgments

I am grateful for the encouragement and support provided by Dr. G. O. Mackie, who financed this study with a grant from the Natural Science and Engineering Research Council of Canada.

Literature Cited

Bickell, L. R., and F. S. Chia. 1979. Organogenesis and histogenesis in the planktotrophic veliger of *Doridella steinbergae* (Opisthobranchia: Nudibranchia). *Mar. Biol* **52:** 291–313.

Bickell, L. R., and S. C. Kempf. 1983. Larval and metamorphic morphogenesis in the nudibranch *Melibe leonina* (Mollusca: Opisthobranchia). *Biol. Bull.* **165:** 119–138.

Bonar, D. B. 1976. Molluscan metamorphosis: a study in tissue transformation. *Am. Zool.* **16:** 573–591.

Bonar, D. B., and M. G. Hadfield. 1974. Metamorphosis of the marine gastropod *Phestilla sibogae* Bergh (Nudibranchia: Aeolidacea). I. Light and electron microscopic analysis of larval and metamorphic stages. *J. Exp. Mar. Biol. Ecol* **16:** 227–255.

Bullock, T. H. 1965. The Mollusca. Pp. 1273–1515 in *Structure and Function in the Nervous Systems of Invertebrates*, v.2, T. H. Bullock and G. A. Horridge, eds. Freeman Press, San Francisco.

Conklin, E. G. 1897. The embryology of *Crepidula*. *J. Morphol.* **13:** 1–226.

Creek, G. A. 1951. The reproductive system and embryology of the snail *Pomatias elegans* (Muller). *Proc. Zool. Soc. Lond* **121:** 599–640.

Crofts, D. R. 1937. The development of *Haliotis tuberculata*, with special reference to the organogenesis during torsion. *Phil. Trans. R. Soc. Lond B* **228:** 219–268.

Cumin, R. 1972. Normentafel zur Organogenese von *Limnaea stagnalis* (Gastropoda, Pulmonata) mit besonderer Berücksichtigung der Mitteldarmdrüse. *Rev. Suisse Zool.* **79:** 709–774.

D'Asaro, C. N. 1969. The comparative embryogenesis and early organogenesis of *Bursa corrugata* and *Distorsia clathrata*. *Malacologia* **9:** 349–389.

Demian, E. S., and F. Yousif. 1975. Embryonic development and organogenesis in the snail *Marisa cornuarietis* (Mesogastropoda: Ampullariidae). V. Development of the nervous system. *Malacologia* **15:** 29–42.

Dorsett, D. A. 1978. Neurons controlling foot and mantle movements in *Armina californica*. *Mar. Behav. Physiol.* **5:** 307–324.

Dorsett, D. A. 1986. Brains to cells: the neuroanatomy of selected gastropod species. Pp. 101–187 in *The Mollusca*, K. M. Wilbur, ed. V.9, *Neurobiology and Behavior*, part 2, A. O. D. Willows, ed. Academic Press, New York.

Fretter, V., and A. Graham. 1962. *British Prosobranch Molluscs: Their Functional Anatomy and Ecology*. Ray Society, London.

Gosliner, T. M. 1981. Origins and relationships of primitive members of the Opisthobranchia (Mollusca: Gastropoda). *Biol. J. Linn. Soc.* **16:** 197–225.

Gosliner, T. M. 1987. A review of the genus *Melibe* (Opisthobranchia: Dendronotacea) with descriptions of two new species. *Veliger* **29:** 400–414.

Gosliner, T. M. 1991. Morphological parallelism in opisthobranch gastropods. *Malacologia* **32:** 313–327.

Gosliner, T. M., and M. Ghiselin. 1984. Parallel evolution in opisthobranch gastropods and its implications for phylogenetic methodology. *Syst. Zool.* **33:** 255–274.

Guyomarc'H-Cousin, C. 1974. Etude descriptive de l'organogénèse du système nerveux chez *Littorina saxatilis* (Olivi) Gastéropode Prosobranche. *Ann. Embryol. Morphog.* **4:** 349–364.

Haszprunar, G. 1985a. The fine morphology of the osphradial sense organs of the Mollusca. I. Gastropoda, Prosobranchia. *Phil. Trans. R. Soc. Lond. B* **307:** 457–496.

Haszprunar, G. 1985b. The Heterobranchia—a new concept of the phylogeny of the higher Gastropoda. *Zeitsch. Zool. Syst. Evol.* **23:** 15–37.

Haszprunar, G. 1988. On the origin and evolution of major gastropod groups, with special reference to the Streptoneura. *J. Moll. Stud* **54:** 367–441.

Hoffmann, H. 1936. Opisthobranchia. Pp. 641–864 in *Klassen und Ordnungen des Tierreichs*, H. G. Bronns, ed. Akad. Verlagsges., Leipzig.

Honegger, T. 1974. Die Embryogenese von *Ampullarius* (Gastropoda, Prosobranchia). *Zool. Jahr. Abt. Anat. Ontog. Tiere* **93:** 1–76.

Kandel, E. R. 1979. *Behavioral Biology of* Aplysia. Freeman, San Francisco.

Kempf, S. C., B. Masinovsky, and A. O. D. Willows. 1987. A simple neuronal system characterized by a monoclonal antibody to SCP neuropeptides in embryos and larvae of *Tritonia diomedea* (Gastropoda, Nudibranchia). *J. Neurobiol.* **18:** 217–236.

Kriegstein, A. R. 1977a. Development of the nervous system of *Aplysia californica*. *Proc. Natl. Acad. Sci. USA* **74:** 375–378.

Kriegstein, A. R. 1977b. Stages in the post-hatching development of *Aplysia californica*. *J. Exp. Zool.* **199:** 275–288.

McAllister, L. B., R. H. Scheller, E. R. Kandel, and R. Axel. 1983. *In situ* hybridization to study the origin and fate of identified neurons. *Science* **222:** 800–808.

Minichev, Y. S. 1970. On the origin and system of nudibranchiate molluscs (Gastropoda, Opisthobranchia). *Monitore Zool. Ital.* (N.S.) **4:** 169–182.

Minichev, Y. S., and Y. I. Starobogatov. 1978. On the systematic arrangement of euthyneuran snails. *Malacol. Rev.* **11:** 67–68.

Moor, B. 1983. Organogenesis. Pp. 123–177 in *The Mollusca,* K. M. Wilbur, ed., v.3, *Development,* N. H. Verdonk, J. A. M. van den Biggelaar, and A. S. Tompa, eds. Academic Press, New York.

Moritz, C. E. 1939. Organogenesis in the gasteropod *Crepidula adunca* Sowerby. *Univ. Calif. Berkeley Publ. Zool.* **43:** 217–248.

Naef, A. 1911. Studien zur generellen Morphologie der Mollusken, 1. Ueber Torsion und Asymetrie der Gasteropoden. *Ergb. Fortsch. Zool.* 3: 73–164.

Page, L. R. 1992. New interpretation of a nudibranch central nervous system based on ultrastructural analysis of neurodevelopment in *Melibe leonina.* II. Pedal, pleural, and labial ganglia. *Biol. Bull.* **182:** 366–381.

Raven, C. P. 1958. *Morphogenesis: the Analysis of Molluscan Development* Pergamon Press, Oxford.

Régondaud, J. 1961. Formation du système nerveux et torsion chez *Lymnaea stagnalis* L. (Mollusque Gastéropode). *C. R. Hebd. L'Acad. Sci.* **252:** 1203–1205.

Régondaud, J. 1964. Origine embryonnaire de la cavité pulmonaire de *Lymnaea stagnalis* L. Considérations particulières sur la morphogénèse de la commissure viscérale. *Bull. Biol. Fr. Belgique* **98:** 433–471.

Richardson, K. C., L. Jarrett, and E. H. Finke. 1960. Embedding in epoxy resins for ultrathin sectioning in electron microscopy. *Stain Technol.* **35:** 313–323.

Russell, L. 1929. The comparative morphology of the elysioid and aelidioid types of the molluscan nervous system, and its bearing on the relationships of the ascoglossan nudibranchs. *Proc. Zool. Soc. Lond.* **14:** 197–233.

Salvini-Plawen, L. v. 1985. Early evolution and the primitive groups. Pp. 59–150 in *The Mollusca,* K. M. Wilbur, ed., v.10, *Evolution,* E. R. Trueman and M. R. Clarke, eds. Academic Press, New York.

Schacher, S., E. R. Kandel, and R. Woolley. 1979a. Development of neurons in the abdominal ganglion of *Aplysia californica.* I. Axosomatic synaptic contacts. *Dev. Biol.* **71:** 163–175.

Schacher, S., E. R. Kandel, and R. Woolley. 1979b. Development of neurons in the abdominal ganglion of *Aplysia californica* II. Nonneural support cells. *Dev. Biol.* **71:** 176–190.

Schmekel, L. 1985. Aspects of evolution within the Mollusca. Pp. 221–267 in *The Mollusca,* K. M. Wilbur, ed., v.10, *Evolution,* E. R. Trueman and M. R. Clarke, eds. Academic Press, New York.

Smith, F. G. W. 1935. The development of *Patella vulgata. Phil. Trans. R. Soc. Lond. B***225:** 95–125.

Smith, S. T. 1967. The development of *Retusa obtusa* (Montagua) (Gastropoda, Opisthobranchia). *Can. J. Zool.* **45:** 737–764.

Tardy, J. 1970. Contribution à l'étude des métamorphoses chez les nudibranches. *Ann. Sci. Nat. Zool. Paris* **12:** 299–370.

Tardy, J. 1974. Morphogenèse du système nerveux chez les mollusques nudibranches. *Haliotis* **4:** 61–75.

Thiriot-Quiévreux, C. 1974. Anatomie interne de véligères planctoniques de Prosobranches Mésogastropodes au stade proche de la métamorphose. *Thal. Jugoslav.* **10:** 379–399.

Thompson, T. E. 1958. The natural history, embryology, larval biology, and post-larval development of *Adalaria proxima* (Alder and Hancock) (Gastropoda, Opisthobranchia). *Phil. Trans. R. Soc. Lond. B***242:** 1–58.

Verdonk, N. H., and J. A. M. van den Biggelaar. 1983. Early development and the formation of the germ layers. Pp. 91–122 in *The Mollusca* K. M. Wilbur, ed., v.3, *Development,* N. H. Verdonk, J. A. M. van den Biggelaar, and A. S. Tompa, eds. Academic Press, New York.

Willows, A. O. D. ed. 1985–1986. *The Mollusca,* K. M. Wilbur, ed., v.8 and 9, *Neurobiology and Behavior,* parts 1 and 2, Academic Press, New York.

Reference: *Biol. Bull.* **182**: 366–381. (June, 1992)

New Interpretation of a Nudibranch Central Nervous System Based on Ultrastructural Analysis of Neurodevelopment in *Melibe leonina*. II. Pedal, Pleural, and Labial Ganglia

LOUISE R. PAGE

Department of Biology, University of Victoria, Victoria, British Columbia, Canada V8W 2Y2

Abstract. Electron microscopical analysis of semi-serial sections through larval stages of the dendronotid nudibranch *Melibe leonina* (Gould, 1852) revealed paired placodes of neurogenic ectoderm at the base of the foot. The location of these laterocephalic placodes corresponds to descriptions of the ectodermal site generating pleural neurons in prosobranchs. In *Melibe*, there are two sites of neuronal ingression within each laterocephalic placode. Neurons ingressing from one of these sites join the cerebral ganglia, and their initial axons extend into the cerebrobuccal connectives or run distally along the esophagus. I identify these neurons as homologues of labial ganglia neurons in archeogastropods. However, neurons derived from the second ingression site within each laterocephalic placode join the pedal ganglia. Pedal ganglia are present in hatching veligers and are linked to the cerebral ganglia by cerebropedal connectives associated with the statocyst nerves. A second connective between each cerebral and pedal ganglia appears at the onset of neuronal ingression from the laterocephalic placodes. Peripheral axons branching from this second pair of connectives are associated with laterocephalic neurons that ingress to the pedal ganglia. I argue that these are pleural neurons, meaning that the pleural ganglia in *Melibe* are uncoupled from the visceral loop.

Introduction

The nervous systems of opisthobranch gastropods have proven highly amenable to neurophysiological investigations (reviewed in Kandel, 1979; Willows, 1985–1986), and have been used to support or criticize phylogenetic theories for this taxonomically difficult subclass (Guiart, 1901; Russell, 1929; Boettger, 1954; Gosliner, 1981; Haszprunar, 1985, 1988; Schmekel, 1985). As a result, the neuroanatomy and neurophysiology of this group is the subject of a large body of literature, with the former studies extending back to the last century. It might be expected that the basic structure of opisthobranch central nervous systems (CNS) would be thoroughly understood. In fact, homologous ganglionic regions within the often highly consolidated nervous systems of opisthobranchs are essentially best guesses based on comparisons of adult neuroanatomy in primitive and derived species.

In some opisthobranchs, distinct pleural ganglia are linked by connectives to ipsilateral cerebral and pedal ganglia, and are also the first pair of ganglia along an elongate visceral loop bearing additional ganglia. This arrangement conforms to the basic design for the gastropod nervous system (reviewed by Bullock, 1965; Dorsett, 1986). However, separate pleural ganglia are not distinguishable in most extant opisthobranchs. In nudibranchs, it is always assumed that the pleurals have fused with the cerebral ganglia to form a pair of cerebropleural ganglia (see Guiart, 1901; Hoffmann, 1936; Boettger, 1954; Schmekel, 1985). This interpretation seems entirely logical because the visceral loop enters the posterior lobes of the 'cerebropleural' ganglia, and each 'cerebropleural' ganglion is often linked to the ipsilateral pedal ganglion by two connectives (Fig. 1). Presumably, the more posterior of these two connectives is the pleuropedal, and the anterior connective is the cerebropedal. However, in my previous study of gangliogenesis in the nudibranch *Melibe leonina*, I found no evidence of pleural ganglia associated with either the visceral loop or cerebral ganglia. All ganglia of the visceral loop in *Melibe* arise from ectoderm of the visceropallium and show torsional displacement, whereas

Received 6 November 1991; accepted 5 March 1992.

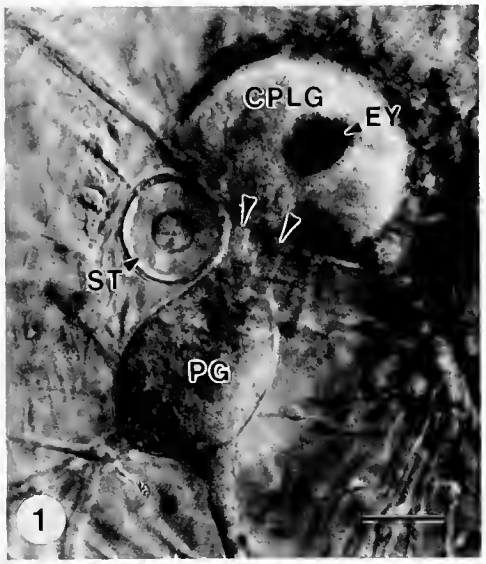

Figure 1. Light micrograph of the central nervous system of *Melibe leonina* at 48 h after metamorphic shell loss (lateral view). Traditionally, the two ganglia have been called cerebropleural (CPLG) and pedal ganglia (PG). Note the two connectives (large arrowheads) with statocyst (ST) associated with posterior connective. EY = eye. Scale 25 μm.

the pleural ganglia of gastropods are not affected by torsion.

If the pleural ganglia are not part of the visceral loop in *Melibe*, then where are they? Ultrastructural study of semi-serial thin sections through larval stages of this nudibranch, suggests that the pleural ganglia are fused with the pedal ganglia. This interpretation differs from that of an earlier developmental study by Bickell (now Page) and Kempf (1983), based on histological sections. Evidence of labial ganglia in larvae of *Melibe* was a second unexpected result. These are distinct ganglia in some archaeogastropods and a pyramidellid, but not in other adult gastropods (Fretter and Graham, 1949, 1962). The labial ganglia in larval *Melibe* fuse with the ventral side of the cerebral ganglia prior to metamorphosis.

All members of the genus *Melibe* are characterized by an oral hood, an expansion of the circumoral cephalic epidermis that is used to capture prey (Gosliner, 1987). This structure appears to be homologous to the smaller oral veil of other dendronotacean nudibranchs. Nevertheless, the large size of the oral hood may have modified gangliogenesis in *Melibe*, relative to that in other nudibranchs, particularly ganglia arising from cephalopedal ectoderm. Therefore, the generality of this new model for nudibranch CNS structure must be tested by further studies on other species.

Materials and Methods

Methods for rearing and anaesthetizing larvae of *Melibe leonina* were described by Bickell and Kempf (1983); the fixation method was that of Bickell and Chia (1979). The technique for semi-serial thin sectioning and the larval stages examined were described in the first paper of this duet (Page, 1992).

Results

As justified in the previous paper (Page, 1992), ganglionic primordia were identified by the locations of their neurogenic ectoderm, as compared to those described for the ganglia of prosobranchs. Trajectories of associated connectives, commissures, and peripheral axon tracts were also very useful for identifying ganglia derived from posttrochal cephalopedal ectoderm. The sketch in Figure 2 shows approximate positions of neurogenic ectoderm for pedal, pleural, and labial ganglia in veligers that have completed mantle retraction (approximately midway through the larval phase).

Pedal ganglia and cerebropedal connectives

In hatching veligers, an axon tract emerges from the ventral aspect of each cerebral ganglion, extends past the ipsilateral statocyst, and associates with a small cluster of subepidermal pedal cells. The axon tracts are the left and right cerebropedal connectives and the bilaterally symmetrical cell clusters within the foot are anlagen of the pedal ganglia (Fig. 3). The statocyst nerves, which each leave their respective statocyst in company with a blind, ciliated static duct, combine with the ipsilateral cerebropedal connective as the two join the cerebral ganglion (Fig. 4). Therefore, the cerebropedal connectives can be

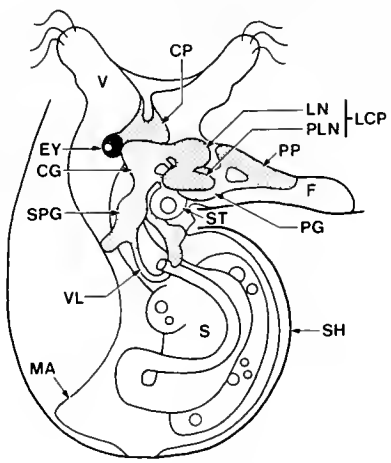

Figure 2. Right lateral view of *Melibe leonina* larva shortly after mantle retraction showing developing CNS (scant stippling) and approximate locations of neurogenic ectoderm (dense stippling). The laterocephalic placodes (LCP) include zones of ingression for both labial and pleural neurons (LN and PLN, respectively). CG = cerebral ganglion; CP = cephalic plate; EY = eye; F = foot; MA = mantle fold; PG = pedal ganglion; S = stomach; SH = shell; SPG = supraintestinal ganglion; ST = statocyst; V = velar lobe; VL = visceral loop.

identified in all larval and post-larval stages by their association with the statocysts and statocyst nerves. In young larvae, the cerebropedal connective is the only axon tract extending between each cerebral and pedal ganglion. In post-metamorphic animals, the cerebropedal connective becomes the more posterior of two connectives extending between each of these ganglia (Fig. 1).

Within each pedal ganglion of hatching veligers, the fiber tract of the cerebropedal connective breaks up into small bundles (Fig. 5) that extend independently to the overlying pedal ectoderm.

During subsequent development, the pedal ganglia enlarge greatly by addition of cells ingressing from paired ectodermal placodes (pedal placodes) extending down each side of the ventral surface of the foot. Sites of cellular ingression appear to be restricted to where the peripheral axon tracts run into the pedal ectoderm (Fig. 6). These peripheral tracts become the anterior, medial, and posterior pedal nerves of post-metamorphic animals.

The left and right pedal ganglia become connected by a pedal commissure by mantle retraction stage, and a parapedal commissure is distinguishable in histological sections of metamorphic animals.

Pleural ganglia

In 6-day-old larvae, a pair of thickened ectodermal placodes has appeared where the two sides of the foot merge with the head, just beneath the origin of the velar lobes and lateral to the mouth and statocysts (Figs. 7, 8, 9). The placode on the right side is larger than that on the left, but the positions of the two are bilaterally symmetrical (Fig. 7). These laterocephalic placodes are immediately proximal to the pedal placodes that give rise to pedal ganglion neurons, and the right laterocephalic placode is separated from the right pallial placode by the nephrocyst pores. Therefore, the laterocephalic placodes are components of post-trochal cephalopedal ectoderm.

On each side, the visceral loop and cerebropedal connective travel past the ipsilateral laterocephalic placode, shortly after these fiber tracts emerge from their respective cerebral ganglion (Fig. 9). However, neither tract associates in any way with the adjacent laterocephalic placode in 6-day-old larve. Placodal ectodermal cells do not begin to ingress until shortly before mantle retraction.

Sections through larvae at 6 days after hatching suggest that the base of each laterocephalic placode is constricted by underlying muscle fibers (Fig. 9). The adjacent membranes of both the muscle and placodal cells are thrown into folds (Fig. 10), and the two are connected by numerous adherens junctions. Furthermore, the manner in which the ectodermal cells are contorted suggests that their basal ends are being pulled toward the pedal placode located more distally along the foot (Fig. 8).

Each laterocephalic placode eventually delivers neurons to the developing CNS from two separate sites of cellular ingression. Neurons arising from the more ventro-medial of these sites fuse with the ipsilateral cerebral ganglion; these are homologues of labial ganglia (see following section of Results). Neurons ingressing from the second, more lateral site fuse with the ipsilateral pedal ganglion and represent the pleural ganglion on each side. Onset of cellular ingression from the laterocephalic placodes is correlated with the appearance of the second connective extending between each cerebral and pedal ganglion. I identify these as the cerebropleural connectives; they lie anterior to the previously formed cerebropedal connectives. The positions of the labial and pleural ganglia in *Melibe* larvae, relative to other components of the CNS, is shown in Figure 11.

For an unknown reason, ingression of cells from the two laterocephalic placodes does not occur symmetrically on both sides of the larva. Labial neurons begin ingression on the left side before ingression starts on the right side. Conversely, the timetable for ingression of pleural neurons on the right side may be slightly ahead of that on the left side, although this appearance may actually result from fewer pleural neurons ingressing from the left compared to the right placode (the left laterocephalic placode is smaller than the right). Nevertheless, in larvae examined after full mantle retraction, concurrent ingression of both labial and pleural neurons is evident on both sides.

The series of micrographs in Figures 12 to 15 show an early stage in the development of the right pleural ganglion and reveal its relationship to the cerebropleural connective

Figure 3. Low magnification electronmicrograph of slightly oblique cross section through newly hatched larva of *Melibe leonina* showing right pedal ganglion (PG; enlarged in Fig. 5) located distal to the statocysts (ST) within the foot (F), and the upper extremity of the right pallial placode (RPP). E = esophagus; MA = shell secreting cells of mantle; N = nephrocysts. Scale 10 μm.

Figure 4. Cross section through base of right cerebral ganglion (CG) in newly hatched larva showing close association between statocyst nerve (SN) and cerebropedal connective (CPC) where they merge with the cerebral neuropile (NP). SD = static duct. Scale 3 μm.

Figure 5. Pedal ganglion (PG) of newly hatched larva beneath ectoderm of foot (F). Arrows indicate three small axon bundles. Scale 3 μm.

Figure 6. Portion of pedal ganglion (PG) and overlying pedal placode (PP; label is on mitotic cell) at mantle fold hypertrophy stage. Ingressing pedal neurons (arrowheads) are associated with peripheral axon tract (arrow). Scale 3 μm.

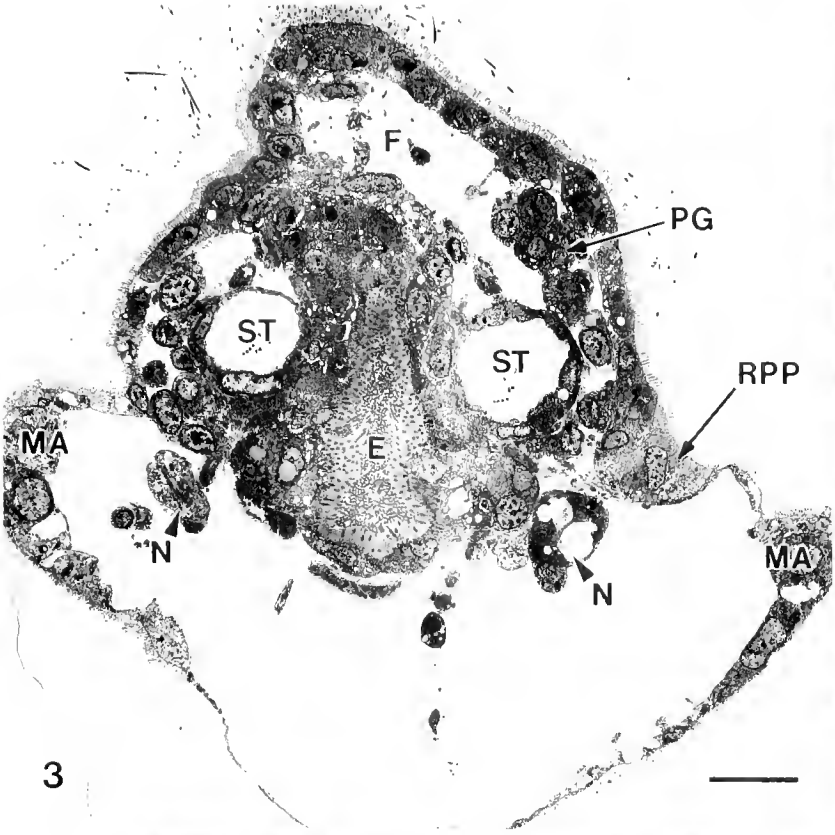
F
PG
ST
ST
RPP
MA
E
N
N
MA
3

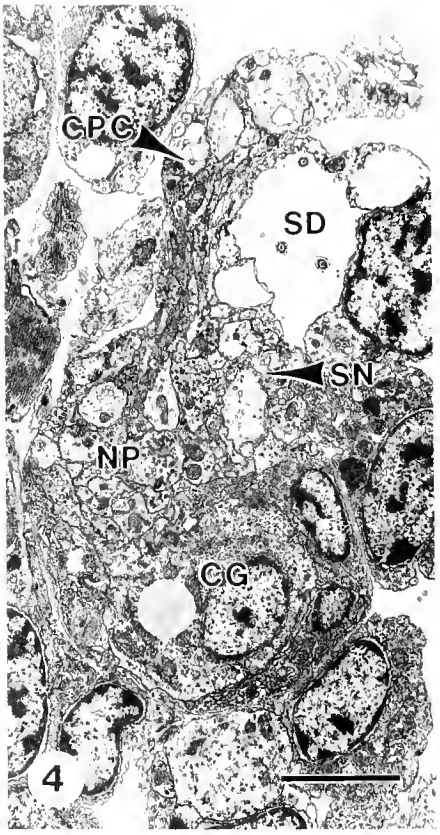
CPC
SD
SN
NP
CG
4

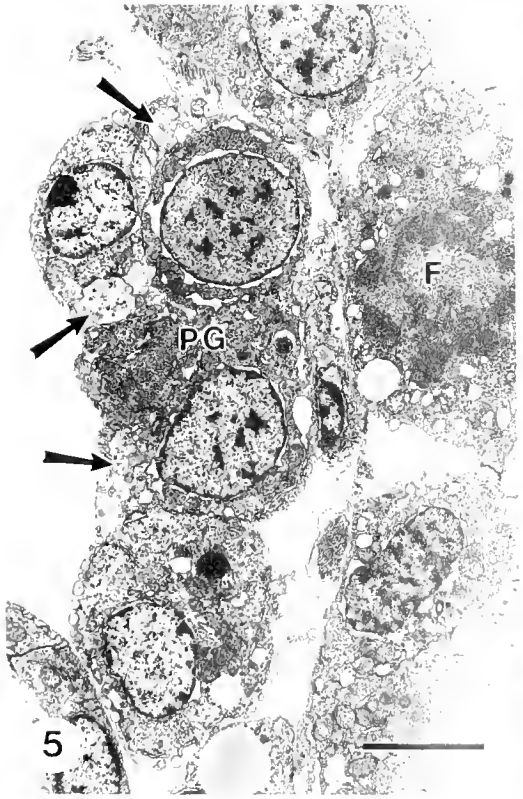
F
PG
5

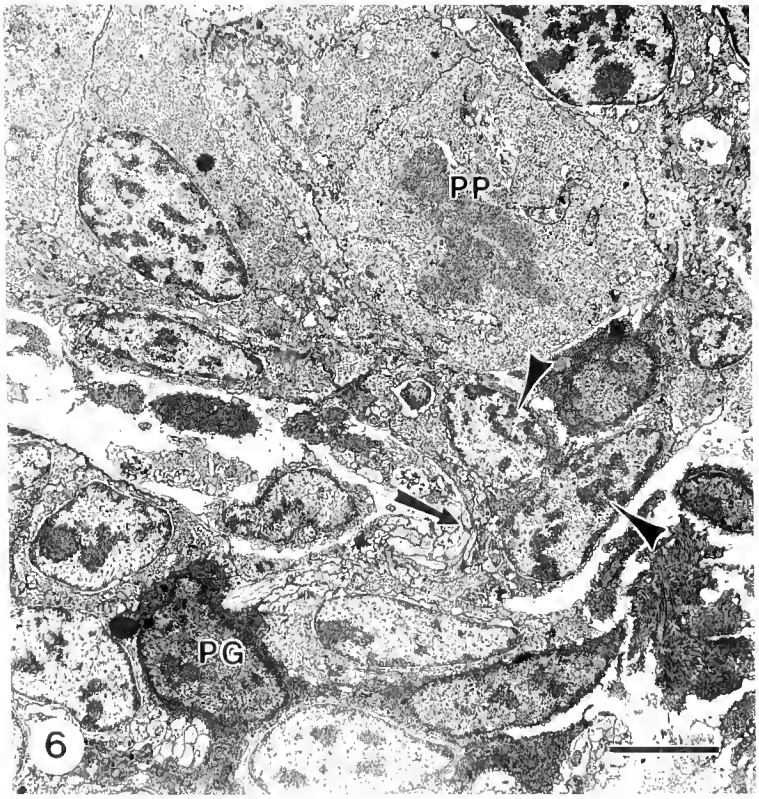
PP
PG
6

and pedal ganglion. Figure 12 passes through the laterocephalic placode adjacent to the statocyst. An enlarged area of this section (Fig. 13) reveals that the right cerebropedal connective, associated with the statocyst nerve, has emerged from the cerebral ganglion, whereas the fiber tract of the cerebropleural connective is still associated with the antero-ventral extremity of the cerebral ganglion. In Figure 14, the cerebropleural connective is leaving the cerebral ganglion and the fiber tract is bifurcating. In Figure 15, a bulge of neurons is evident on the anterior border of the pedal ganglion; this is the anlage of the right pleural ganglion. The cerebropedal connective is entering the pedal ganglion and the main body of the cerebropleural fiber tract is deflecting medially. Axons forming the other branch of the previous bifurcation of the cerebropleural connective are emerging from the pleural ganglion at two sites. These peripheral axon tracts extend to the adjacent laterocephalic placode and are associated with ingressing pleural neurons (Fig. 15). Later in larval development, at least one of the two peripheral axon tracts extending to each laterocephalic placode is joined by axons that appear to arise from the cerebropedal connective.

The cerebropleural connective lengthens after its initial formation and the boundary between pleural and pedal ganglia is indistinguishable in late stage larvae.

Labial neurons have not begun to ingress from the right laterocephalic placode at onset of mantle retraction, although this process is evident on the left side as described in the following section.

Labial ganglia

The series of micrographs shown in Figures 16 to 19 were taken from the left side of the same larva shown in Figures 12 to 15. They illustrate the early formation of the left labial ganglion from an ingression site within the laterocephalic placode that is distinct from the ingression site for pleural neurons.

In Figure 16, the cerebropedal connective has left the cerebral ganglion but the cerebropleural connective is still within the antero-ventral extremity of this ganglion. Immediately after the cerebropleural connective has left the cerebral ganglion, the ganglion acquires a prominent lateral extension of neurons (Fig. 17) that is continuous with the laterocephalic placode (Fig. 19). These neurons are clearly fusing with the cerebral ganglion, and evidence from a slightly older developmental stage (see below) indicates they are homologues of the labial ganglia found in archeogastropods.

Figures 17 and 18 show a second site of neuronal ingression from the laterocephalic placode, located slightly beneath and lateral to that for labial neurons. These are ingressing pleural neurons associated with a small tract of axons that branched from the cerebropleural connective. The pleural neurons are extending toward the pedal ganglion, but unlike the right pedal ganglion of this larva, the left pedal ganglion has not yet acquired a prominent bulge of pleural neurons.

The micrographs in Figures 20 to 25 show the trajectories of initial axons elaborated by labial ganglion neurons on the left side. At the time of fixation, this larva had completed mantle retraction and mantle fold cells had begun proliferation prior to forming the definitive dorsal epidermis. Figure 20 passes through an area comparable to that of the younger stage shown in Figure 16. In addition to the cerebropedal and cerebropleural connectives, the cerebrobuccal connective is prominent and extends to a thickening of the ventral esophageal wall that is neurogenic ectoderm for the left buccal ganglion. A subsequent section through the base of the cerebrobuccal connective (Fig. 21) shows a group of axons that originated from the fiber tract of the cerebrobuccal connective, plus two other axon tracts that both originated from labial neurons (Figs. 22, 23). One of the labial axon tracts merges with the tract extending from the cerebrobuccal connective (Fig. 21), whereas the other labial tract extends directly into the cerebral ganglion (not shown). The combined labial and cerebrobuccal axons form a peripheral nerve that extends distally along the wall of the esophagus (Fig. 22), forming synapses on esophageal cells just inside the mouth (labial nerve; Figs. 24, 25).

Animals sectioned immediately after metamorphic shell loss show a prominent plug of neuronal cell bodies within the ventro-lateral aspect of each cerebral ganglion, anterior to the connectives. This corresponds to the site where labial neurons have joined the cerebral ganglia. The labial

Figure 7. Low magnification electron micrograph of a cross section through a 6-day-old larva. Boxed areas contain left and right laterocephalic placodes (LCP), which are enlarged in Figures 8 and 9, respectively. Note size difference between two placodes. Orientation arrows: L = left; R = right; D = dorsal; V = ventral. E = esophagus; M = mouth; N = nephrocysts; ST = statocysts. Scale 10 μm.

Figure 8. Left LCP. Note how bases of placodal cells are flexed in direction of foot (arrow). M = muscle fiber. Scale 3 μm.

Figure 9. Right LCP. Note adjacent cerebropedal connective (CPC) and visceral loop (VL) emerging from cerebral ganglion. Muscle fibers (M) underly placodal cells. Asterisk marks position of nephrocyst duct in slightly deeper section. MF = right mantle fold. Scale 3 μm.

Figure 10. Base of right LCP. Arrowheads indicate processes from underlying muscle fiber (M) extending to convoluted basal lamina of placodal ectoderm. Scale 1 μm.

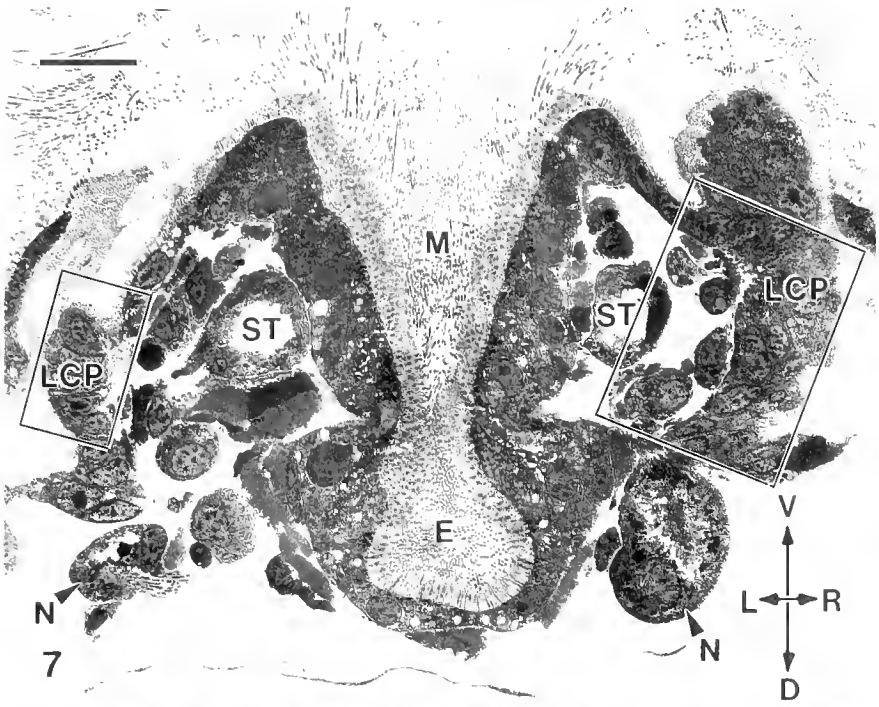

7

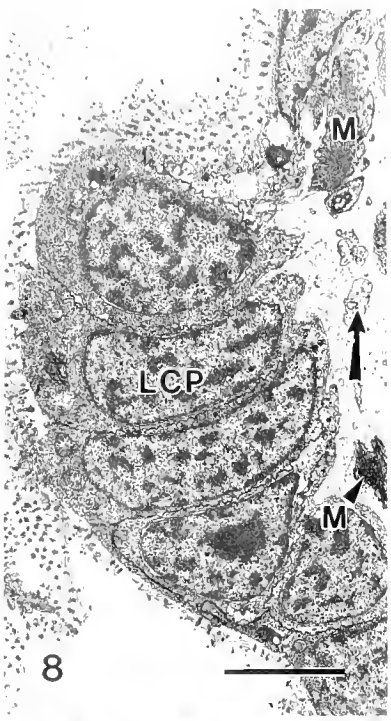

8

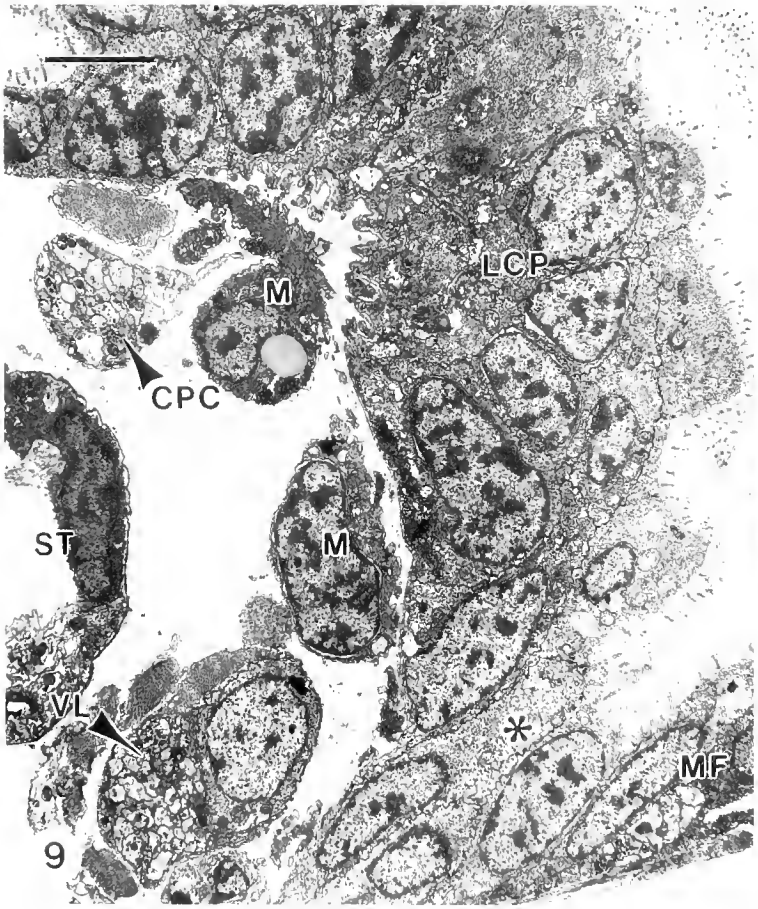

9

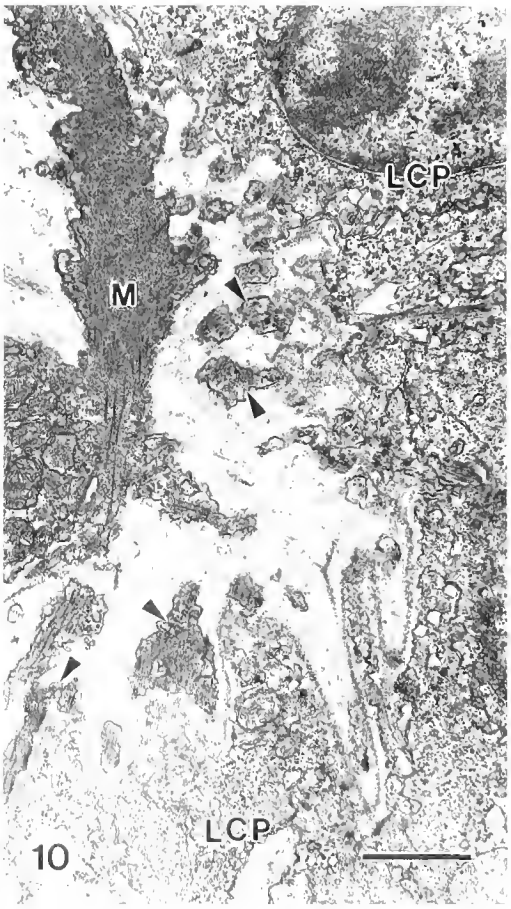

10

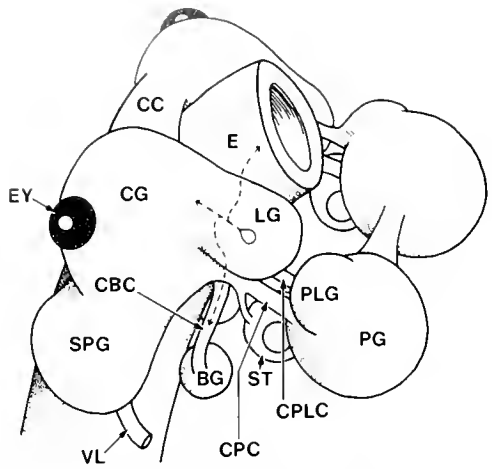

Figure 11. Reconstruction of cephalopedal ganglia and supraintestinal ganglion in larva of *Melibe leonina*, right, ventro-lateral view. Ganglia and connectives labelled on right side only. For clarity, rhinophoral ganglia are omitted and connectives over the statocysts are elongated. Broken lines show initial axon tracts of labial neurons (all tracts do not necessarily arise from single neurons). BG = buccal ganglion; CBC = cerebrobuccal connective; CC = cerebral commissure; CG = cerebral ganglion; CPC = cerebropedal connective; CPLC = cerebropleural connective; E = esophagus; EY = eye; LG = labial ganglion; PG = pedal ganglion; PLG = pleural ganglion; ST = statocyst; VL = visceral loop.

nerve becomes the nerve labelled C1 in adult *Melibe* by Hurst (1968). This nerve innervates the oral tube and lips.

Discussion

Identifications of ganglia

Pedal ganglia. The pedal ganglia in *Melibe leonina*, like those in other gastropods, arise from proliferative ectoderm along ventro-lateral zones of the larval foot. Ingressing pedal neurons are associated with axons that extend from the intraganglionic fiber tract of each cerebropedal connective, to the overlying neurogenic ectoderm of the pedal placode. These axon tracts become peripheral nerves after metamorphosis. A similar association between ingressing neurons and peripheral axon tracts was observed for pleural and visceral ganglia.

In *Aplysia californica*, the number of neurons within all central ganglia continue to increase after metamorphosis (Cash and Carew, 1989), and results of McAllister *et al.* (1983) and Hickmott and Carew (1991) suggest that added neurons come from the body wall. Jacob (1984) and McAllister *et al.* (1983) proposed that ingressing neurons in larvae and juveniles of this species migrate along connective tissue strands or muscle fibers to reach their definitive locations within the CNS. Alternatively, observations on *Melibe* larvae suggest that ingressing neurons may be guided to developing ganglia by migrating along peripheral axon tracts. After metamorphosis, these tracts continue to connect the CNS with the often distant body wall, and are therefore ideally suited to guide later ingressing neurons to appropriate central ganglia.

Pleural ganglia. My identification of pleural ganglia in *Melibe* larvae, and their developmental fate, is probably the most controversial part of this analysis and therefore requires detailed justification.

Histological studies of neurogenesis in prosobranchs and pulmonates have shown that the ectodermal placode giving rise to pleural neurons is post-trochal (Smith, 1935; Crofts, 1937; Régondaud, 1961, 1964; D'Asaro, 1969; Cumin, 1972; Honegger, 1974; Guyomarc'H Cousin, 1974; Demian and Yousif, 1975; Raven, 1975). Nevertheless, Tardy (1970, 1974), studying the nudibranch *Aeolidiella alderi* by means of histological sections, claimed that both cerebral and pleural neurons are derived from pre-trochal cephalic plate ectoderm, so that cerebral and pleural ganglia are fused from the outset. Smith (1967) suggested the same for the cephalaspid *Retusa obtusa*, and Jacob (1984) also claimed a common site of origin for cerebral and pleural ganglia in *Aplysia californica*.

If previous studies have correctly identified a post-trochal ectodermal ingression site for pleural neurons in prosobranchs and pulmonates, then I reject the notion of a common origin for cerebral and pleural neurons in opisthobranchs. Conklin's (1897) monumental study of cell

Figures 12 to 15. Series of frontal sections through right laterocephalic placode (LCP) showing cerebropleural connective and pleural ganglion.

Figure 12. Right LCP immediately beneath velar lobe (V) and opposite the statocyst (ST). Boxed area enlarged in Figure 13. CG = cerebral ganglion; CP = cephalic plate; PG = periphery of pedal ganglion. Scale 5 μm.

Figure 13. Detail from Figure 12 showing cerebropedal connective (CPC) with associated statocyst nerve (SN); cerebropleural connective (CPLC) is still within cerebral ganglion (CG). Scale 2 μm.

Figure 14. Same area in slightly deeper section showing cerebropleural connective (CPLC) emerging from cerebral ganglion (CG). Arrow indicates axons branching from CPLC. Scale 2 μm.

Figure 15. Subsequent section showing anlage of pleural ganglion (PLG) perched atop pedal ganglion (PG). Note fiber tracts of cerebropedal and cerebropleural connectives (CPC and CPLC, respectively). Axons that branched from CPLC in Figure 14 are emerging from pleural ganglion at two points (arrows). Note pleural neurons (PL) ingressing from laterocephalic placode (LCP). CG = cerebral ganglion; ST = statocyst. Scale 2 μm.


CP
V
CG
LCP
PG
ST
12


CG
CPLC
CPC
SN
13

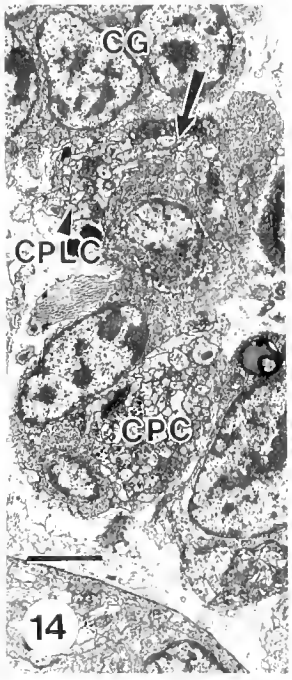
CG
CPLC
CPC
14

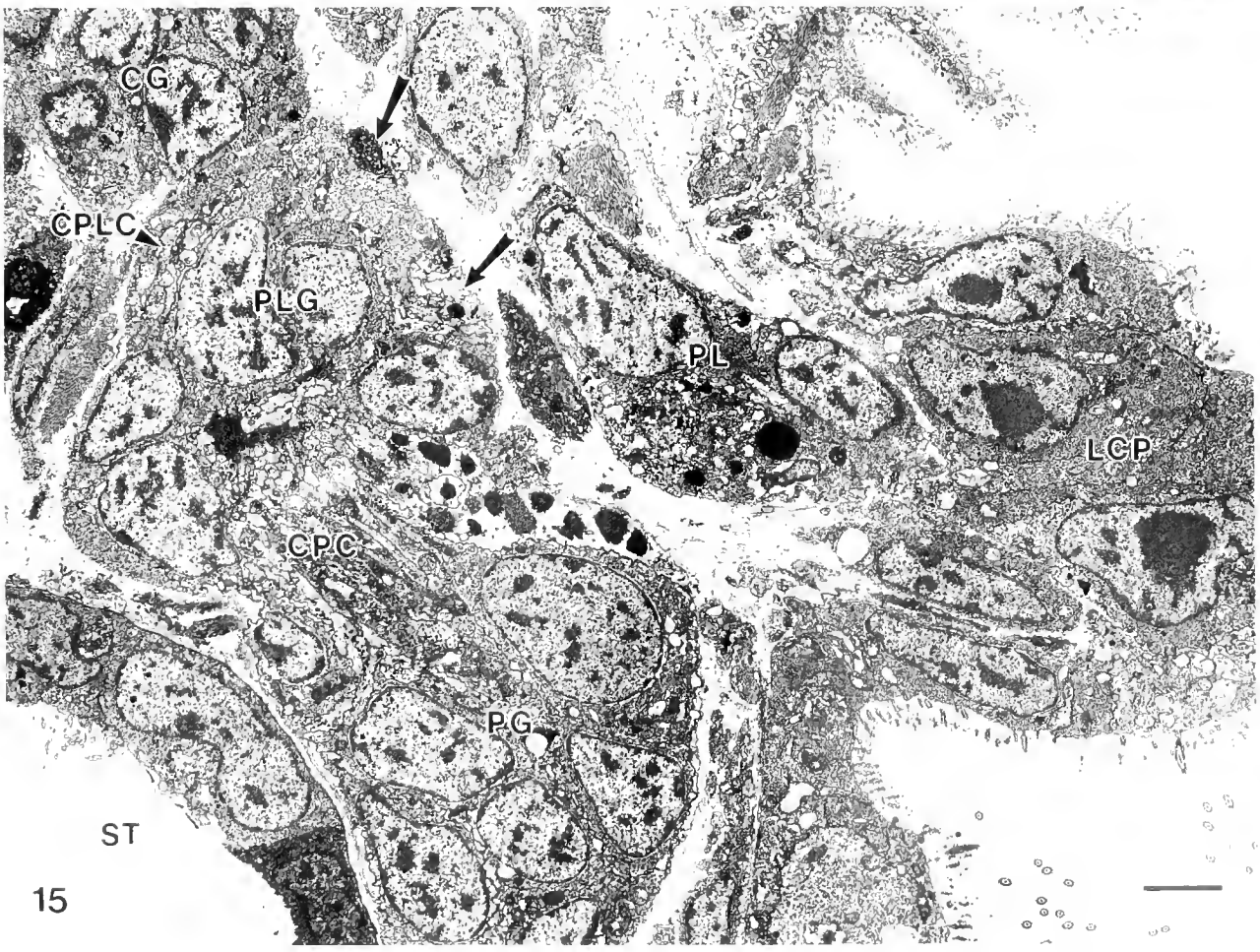
CG
CPLC
PLG
PL
LCP
CPC
PG
ST
15

lineage in the prosobranch gastropod, *Crepidula*, showed that the cephalic plates are derived from the first quartet of embryonic micromeres, whereas post-trochal ectoderm is derived from subsequent micromere quartets. This has been confirmed by many other studies (reviewed by Raven, 1958; Verdonk and van den Biggelaar, 1983), including Casteel's (1904) cell lineage study on the nudibranch *Fiona marina*. Therefore, none of the neurons ingressing from the cephalic plate in opisthobranchs can be homologous to pleural neurons ingressing from post-trochal ectoderm in other gastropods.

The ectodermal proliferation placode for pleural neurons must be located within the cephalopedal mass, rather than the visceropallial mass, because the pleural ganglia of gastropods do not show torsional displacement. The exact location of the paired ectodermal placodes for the pleural ganglia in a variety of prosobranchs has been described as: the sides of the head, base of the foot, opposite the statocysts or within the pleural groove. Even in *Littorina saxatilis*, a caenogastropod with an epiathroid adult nervous system (pleural ganglia close to cerebrals), the pleural ganglia arise from the base of the foot (Guyomarc'H-Cousin, 1974). In *Melibe*, the location described by these phrases corresponds to the post-trochal, laterocephalic placodes.

Jacob (1984), who used ^{3}H-thymidine autoradiography to study neurogenesis in *Aplysia californica*, suggests that pleural neurons arise from the velar lobes. However, the velar proliferation placode shown in her Figure 4a is clearly the large ciliated cells of the prototroch, with the subvelar ridge (metatroch) immediately below. What Jacobs (1984) interprets as velar cells migrating to the cerebral, and ultimately the pleural ganglia (see her Fig. 5a), may be the area where the prototroch arches over the mouth, closely approaching the cerebral ganglia (see Fig. 4 in the companion paper, Page, 1992). However, Jacob's figure 5b also shows ^{3}H-thymidine labelling in a protruding placode of ectodermal cells, lateral to the statocyst, that corresponds in appearance and location to a laterocephalic placode in *Melibe* larvae.

Appropriate location within post-trochal cephalopedal ectoderm is only one of several clues that help identify the ectodermal ingression site for pleural neurons in *Melibe* larvae. Another is the correlation between the onset of cellular ingression from this site and the appearance of the second pair of connectives extending in front of the statocysts from the cerebral ganglia. These connectives are clearly not the earlier formed cerebropedal connectives associated with the statocyst nerve. Furthermore, the two peripheral axon tracts extending to each laterocephalic placode branch from this second pair of connectives, which are presumably the cerebropleural connectives. These two axon tracts may correspond to the anterolateral and dorsal 'pedal' nerves described in adult *Melibe rosea* by De Vries (1963). Based on peripheral projection patterns, De Vries (1963) believed that the anterolateral nerve in *Melibe rosea* represents part of the ancestral anterior pleural nerve.

The size difference between left and right laterocephalic placodes correlates with a similar size difference between left and right dorsal 'pedal' nerves in adults of *Melibe* and other non-dorid nudibranchs. This difference, in turn, may relate to unilateral innervation of the penis by the right member of this nerve pair. Similarly, Régondaud (1961) noted that the right-side ectodermal placode for generating pleural neurons in *Lymnaea stagnalis* is larger than that of the left side. The pleural ganglia in *Lymnaea* are associated with the visceral loop and do not fuse with other ganglia during development.

I cannot readily explain the slight timing differences for developmental events involving the left and right laterocephalic placodes. Possibly, the temporal asymmetries are somehow related to the size difference between the two placodes and the unilateral innervation of the penis from the right side. Whatever the reason, similar developmental asynchronies involving bilaterally homologous structures are not unusual among mollusks, even for structures not affected by torsion. Examples include the cephalic tentacles of some prosobranchs, the statocysts of *Buccinum*, and the ctenidia of the bivalve, *Ostrea* (reviewed by Moor, 1983).

The slight temporal differences for developmental events involving the left and right laterocephalic placodes are dwarfed by the much greater difference between the onset of neuronal ingression from the pedal placodes and that from the laterocephalic placodes. Presumptive neu-

Figures 16 to 19. Series of frontal sections through left side of larva at onset of mantle retraction showing labial ganglion developing from left laterocephalic placode.

Figure 16. Cerebropedal connective (CPC) associated with statocyst nerve (SN), and cerebropleural connective (CPLC; enlarged in inset) still within anteroventral extremity of cerebral ganglion (CG). CP = cephalic plate; ST = statocyst. Scale 5 μm; inset 0.5 μm.

Figure 17. Subsequent section showing left LCP and labial ganglion (LG) projecting laterally from cerebral ganglion (CG). Arrow indicates cerebropleural connective, which is enlarged in inset. Ingressing pleural neurons (PL) are enlarged in Figure 18. PG = pedal ganglion; ST = statocyst; V = velar lobe. Scale 5 μm; inset 0.5 μm.

Figure 18. Ingressing pleural neurons (PL) associated with axons (arrowheads). Scale 5 μm.

Figure 19. Arrow indicates mitotic labial ganglion neuron ingressing from LCP. CG = cerebral ganglion; PG = pedal ganglion; ST = statocyst; V = velar lobe. Scale 5 μm.

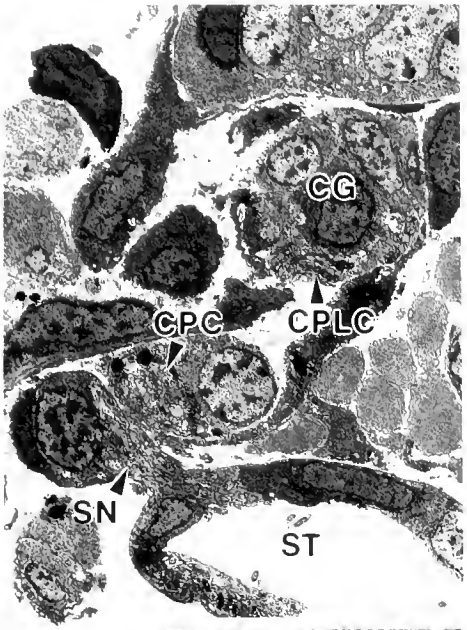

16

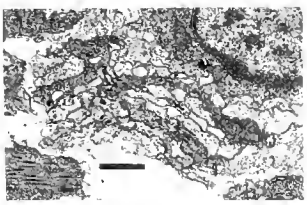

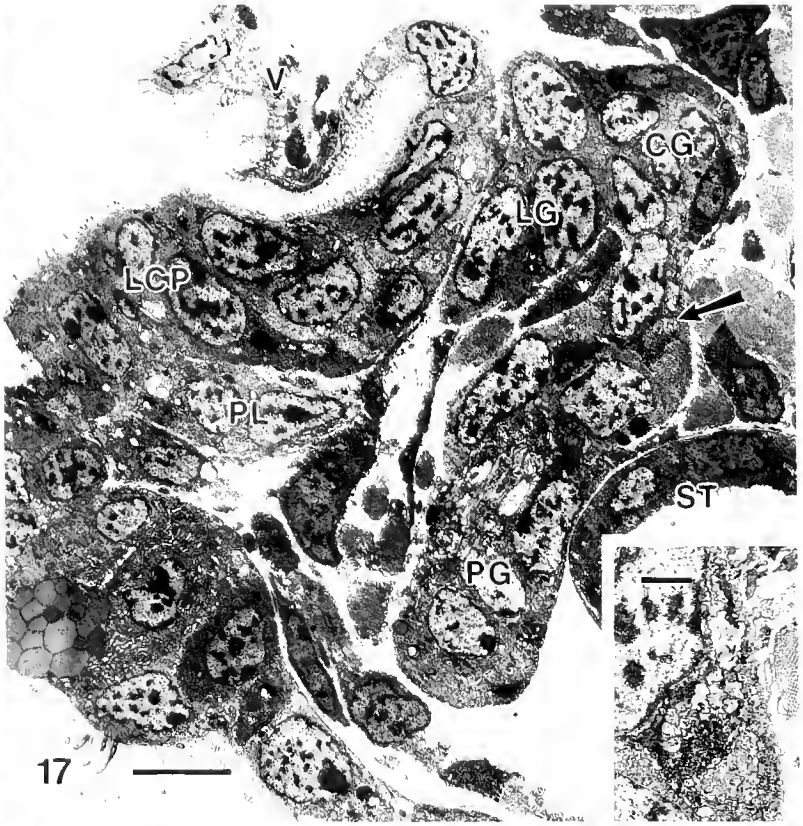

17

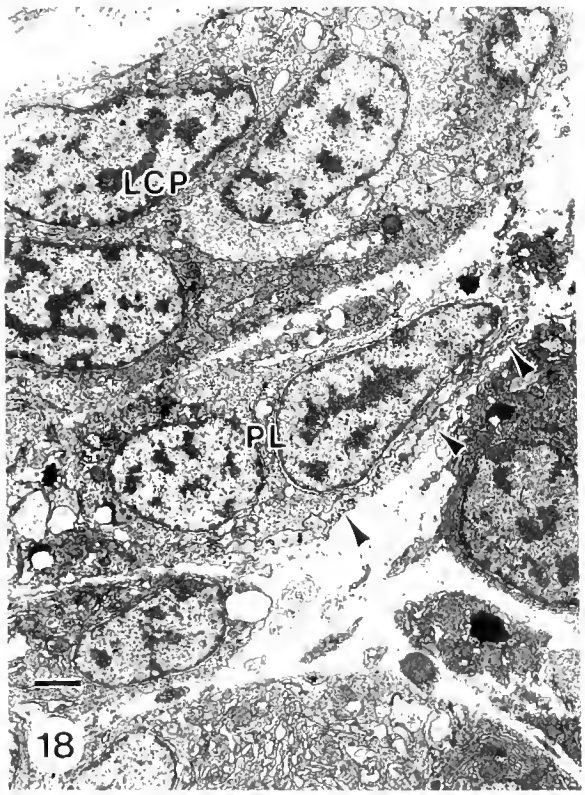

18

19

rons begin to ingress from the pedal placodes even before hatching, whereas laterocephalic neurons do not begin to leave the ectoderm until the latter part of the shell-secreting phase. This marked difference further attests to the separate identity of neurons arising from laterocephalic and pedal placodes.

The notion that the pleural ganglia are primarily pallial in nature has become rather entrenched in the malacological literature. Although these ganglia certainly contribute to the innervation of the mantle in adult gastropods, they are not derived developmentally from visceropallial ectoderm, and Crofts (1937) observed that the pleural nerves ("external pallial nerves") extending into the mantle folds in *Haliotis* are not established until the long-lasting second phase of torsion is complete. If this were not the case, the trajectory of these nerves would be skewed by torsion.

If my arguments are accepted for the identity of the visceral loop fiber tract and associated ganglia (Page, 1992), and for the pleural ganglia in *Melibe* larvae, then one must also accept a conclusion that is unprecedented in previous developmental or neuroanatomical studies of gastropods: the cell bodies of the pleural neurons in *Melibe* have become uncoupled from the visceral loop. This conclusion is actually not so startling, because the visceral loop appears to be established by axons extending from the cerebral ganglia, with other ganglia applied later. A visceral loop (lateral cords), arising directly from the cerebral ganglia, is thought to be the ancestral condition of the gastropod nervous system and is exhibited by monoplacophorans, caudofoveates, solenogastres, and polyplacophorans (see Bullock, 1965; Salvini-Plawen, 1985; Wingstrad, 1985); none of these groups have pleural ganglia. In *Melibe*, and probably all gastropods, it is inappropriate to think of the visceral loop as an initiative of the pleural ganglia. Furthermore, uncoupling of pleural ganglia from the visceral loop is no less bizarre than the complex restructuring of the visceral loop and ganglia that occurs during development of ampullarid prosobranchs (Honegger, 1974; Demian and Yousif, 1975).

Circumstantial support for the reality of pleuropedal ganglia among other dendronotid nudibranchs comes from neuroanatomical and neurophysiological data on *Tritonia diomedea* and *T. hombergi* (Willows *et al.*, 1973; Dorsett, 1974), and on *Armina californica* (Dorsett, 1978). The dorsum and branchial tufts (cerata) of tritoniids are derived from larval mantle fold ectoderm (Thompson, 1962; Kempf and Willows, 1977). Mantle fold ectoderm also gives rise to the intestinal and visceral ganglia, which fuse to the cerebral ganglia, so it is not surprising that some neurons effecting branchial tuft withdrawal are located within the lobes projecting posteriorly from the cerebral ganglia (traditionally called the pleural lobes). However, two other effector neurons for branchial tufts are located in each 'pedal' ganglion. Extrapolating from the fact that axons of pleural neurons project into pallial tissues in shelled gastropods, it is possible that these neurons have a pleural ganglion ancestry. It is interesting to note that one of these neuronal pairs (L and RPd1), particularly that of the right side, is occasionally found within the ipsilateral cerebral ganglionic mass; that is, in the expected position if pleural ganglia were not uncoupled from the visceral loop. During the development of *Melibe*, I found that both the visceral loop and the pedal ganglia are positioned equidistant from the laterocephalic placodes in 6-day-old larvae. A relatively minor developmental miscue might easily deflect individual pleural neurons towards the visceral loop, rather than the pedal ganglion. Morphological evidence suggests that contracting muscle fibers underlying the laterocephalic placodes may pull placodal cells toward the pedal ganglion, and therefore away from the visceral loop fiber tract.

As in tritoniids, Dorsett (1978) found neurons in the pedal ganglia of *Armina californica* that control movements of the 'mantle' periphery (this species lacks cerata).

Figures 20 to 25. Series of frontal sections through left side of larva at mantle fold hypertrophy stage showing anlage of labial ganglion (LG) and trajectory of labial axons. Sections proceed distally along esophagus toward mouth.

Figure 20. Anteroventral portion of left cerebral ganglion (CG) with developing cerebrobuccal connective (large arrowheads) extending to buccal placode (BP) in ventral wall of esophagus (E). CPC = cerebropedal connective; CPLC = cerebropleural connective; PG = periphery of pedal ganglion; SN = statocyst nerve; ST = statocyst. Scale 5 μm.

Figure 21. Cerebral ganglion end of cerebrobuccal connective showing two bundles of labial axons (arrows), one of which is extending toward axons of cerebrobuccal connective (CBC). Scale 1 μm.

Figure 22. Arrow indicates axons arising from labial ganglion neurons (LG; enlarged in Fig. 23). Note labial nerve (LN) adjacent to wall of esophagus (E). Scale 3 μm.

Figure 23. Detail from Figure 22 showing an axon (arrowheads) arising from a labial ganglion neuron (LG). Scale 0.5 μm.

Figure 24. Section passing just inside mouth showing labial ganglion (LG) continuous with laterocephalic placode (LCP). Arrowheads indicate ingressing pleural neurons. Boxed area, enlarged in Figure 25, includes labial nerve. E, esophagus; PPG = pleuropedal ganglion. Scale 5 μm.

Figure 25. Detail from Figure 24 showing labial nerve with probable synapse (arrowhead) onto esophageal cell (E). Scale 0.5 μm.

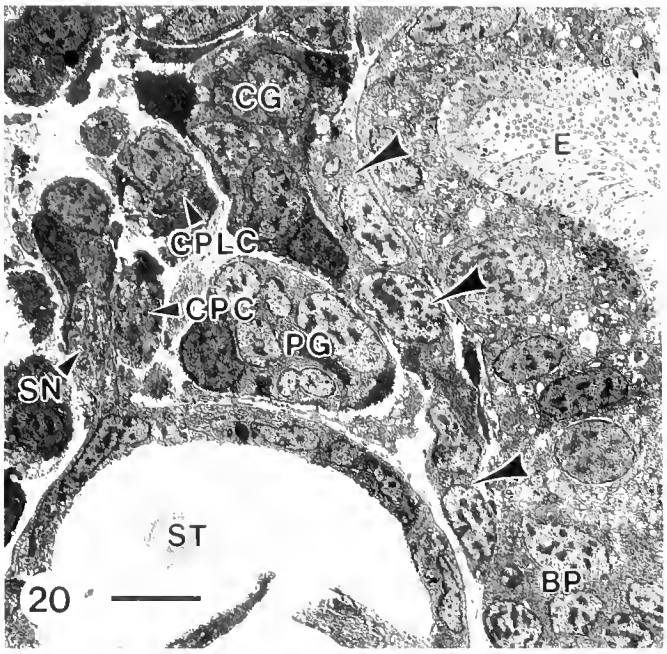
CG
E
CPLC
CPC
PG
SN
ST
BP
20

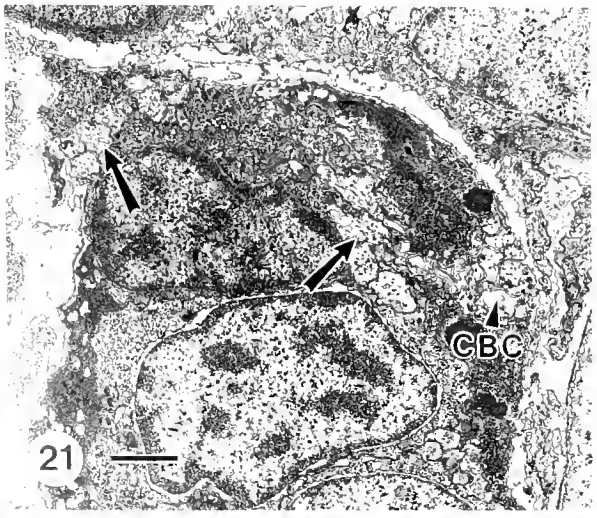
CBC
21


LN
LG
E
22

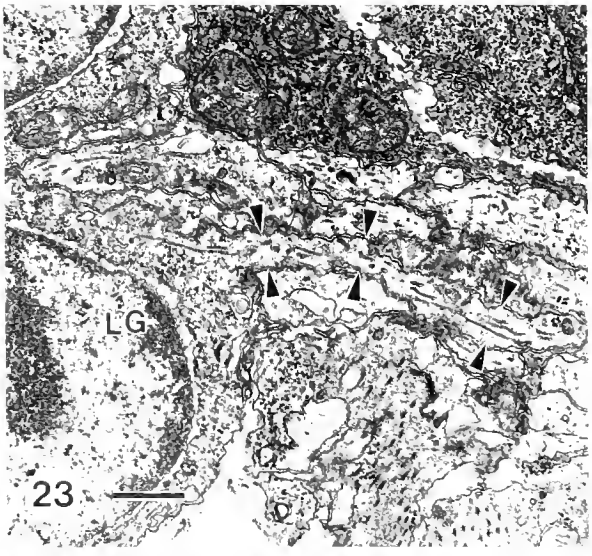
LG
23

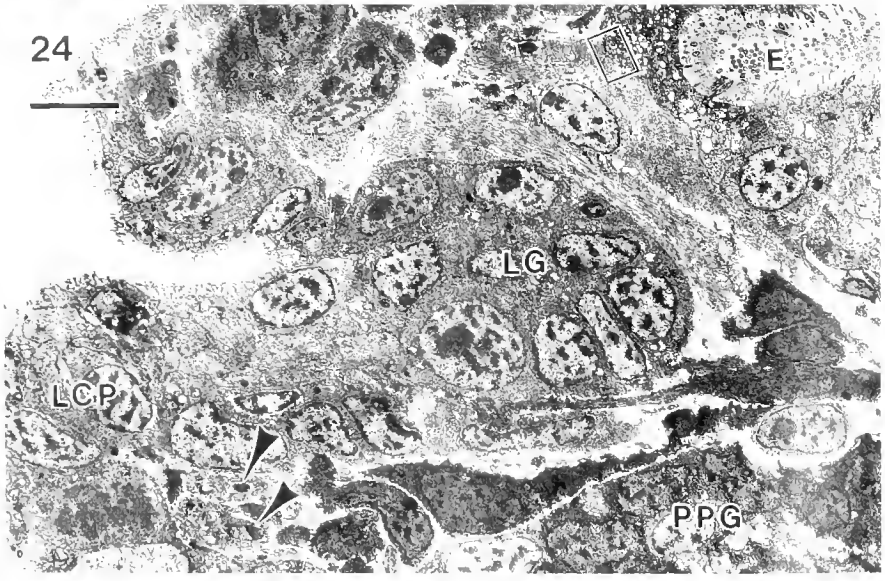
24
E
LG
LCP
PPG


E
25

Some of these, or other pedal neurons, also control movements of the foot or oral veil. These efferents can be stimulated by tactile stimuli to the foot or mantle margins.

Walters *et al.* (1983) described a conspicuous cluster of mechanosensory neurons within the undisputed pleural ganglia of *Aplysia californica*. Collectively, these primary mechanosensory neurons are sensitive to tactile stimuli applied along the entire length of the foot, including the 'parapodia' (epipodial folds). Therefore, the receptive field for pleural sensory neurons in *Aplysia* corresponds approximately to the location of larval neurogenic ectoderm for presumed pleural neurons in *Melibe*.

Labial ganglia. Unlike pleural neurons, ingressing labial neurons fuse with the ipsilateral cerebral ganglion in *Melibe*. Separate labial ganglia, which are linked beneath the buccal mass by a labial commissure and which give rise to labial nerves innervating the oral lips and buccal musculature, are found in some archaeogastropods and a pyramidellid (Fretter and Graham, 1949, 1962). They are thought to be absent or fused to the cerebral ganglia in other gastropods.

In archaeogastropods such as *Haliotis*, the cerebrobuccal connectives are routed through the labial ganglia before arriving at the buccal ganglia (see Fretter and Graham, 1962). This design can be recognized in the relationship between cerebrobuccal and labial nerve tracts in larval *Melibe*, and is the major justification for labelling these ganglia as homologues of archaeogastropod labial ganglia.

Audesirk (1979) and Audesirk and Audesirk (1980) investigated two adjacent clusters of mechanoreceptive neurons within each cerebral ganglion of *Tritonia diomedea*. The two clusters have distinct axonal projections and neurophysiological characteristics, but both are located where the labial ganglia are fused to the cerebral ganglia in *Melibe* (ventro-lateral side of each cerebral ganglion, anterior to the connectives to the pedal ganglia). One of the clusters sends axons out each ventral cerebral nerve (labelled CN4 in *Tritonia* but clearly equivalent to CN1 of *Melibe*) and also into the adjacent cerebrobuccal connective; a trajectory that is consistent with my observations on initial labial axons in *Melibe* larvae. These mechanoreceptors respond to pressure or stretch of the oral tube or jaw closer muscles (Audesirk, 1979). The second category of mechanoreceptive neurons sends axons out cerebral nerves extending to the oral veil and a pedal nerve extending to the anterior foot (Audesirk and Audesirk, 1980). Although further data are needed, I consider it very possible that cerebral nerves innervating the oral veil in *Tritonia* and the oral hood in *Melibe* are also established by labial neurons.

It might be argued that the labial ganglia are better identified as the pleural ganglia in *Melibe*. They arise from a pair of post-trochal ectodermal sites of appropriate location for pleural neurons and they fuse with the cerebral ganglia, which the traditional interpretation dictates for the pleural ganglia of opisthobranchs. However, the trajectory of axons arising from labial neurons is inappropriate for pleural neurons.

Critique of previous neurodevelopmental models

All previous accounts of sequential neurodevelopment in nudibranchs have been histological, yet this method cannot reveal with certainty all neuronal ingression sites from ectodermal proliferation placodes or trajectories of early connectives and axon tracts. Uncertainty resulting from limited resolution has resulted in three different models (more including variations) for the pattern of neurogenesis in nudibranchs. These earlier models, plus the current model generated from ultrastructural study of *Melibe leonina* larvae, are illustrated schematically in Figure 26 and are discussed below.

The groundbreaking study of nudibranch organogenesis was done by Thompson (1958) on the lecithotrophic veliger of the dorid nudibranch, *Adalaria proxima*. Thompson identified cerebral, optic, pedal, pleural, and buccal ganglia in *Adalaria* (Fig. 26A). The intestinal and visceral ganglia escaped notice, possibly because they may fuse precociously to the cerebrals in this lecithotrophic veliger. Alternatively, Tardy (1970) has suggested that Thompson misidentified visceral loop ganglia as the buccal ganglia.

According to Thompson (1958), the pleural ganglia of *Adalaria* are large neuronal masses located within the base of the foot, and they fuse with the cerebrals at metamorphosis. The 'anterolateral propodial ganglia' described by Chia and Koss (1989) and Arkett *et al.* (1989) for the dorid nudibranch *Onchidoris bilamellata* have a similar size and location to the ganglia identified as the pleurals in *Adalaria*. Further study is needed to determine if these are indeed pleural ganglia, or alternatively, the labial ganglia.

Tardy (1970, 1974) proposed that both cerebral and pleural neurons arise from the cephalic plate in *Aeolidiella alderi*, thereby producing cerebropleural ganglia that are fused from the beginning (Fig. 26B). As discussed earlier, this contradicts observations made on many other species. Tardy also recognized buccal ganglia in *Aeolidiella alderi*, but his description of their early development is highly anomolous. Many studies, including this one on *Melibe*, have found that neurogenic ectoderm for buccal ganglia is located within the ventral wall of the distal esophagus (Smith, 1935; Creek, 1951; D'Asaro, 1969; Guyomarc'H-Cousin, 1974; Honegger, 1974; Demian and Yousif, 1975), but Tardy (1974; p. 315 and Fig. 2E) shows the location of buccal neurogenic ectoderm as lateral to the mouth, proximal to the pedal placodes, and adjacent to the statocysts. I suggest that these are the laterocephalic placodes. Tardy also described a pair of ganglia that arise from the ectoderm of the oral tentacles, but only after metamorphosis.

Having rejected Tardy's (1970, 1974) interpretation for the origin of pleural ganglia in nudibranchs, my colleagues and I identified the ganglia directly behind the cerebrals as the pleural ganglia in previous histological studies on the dorid *Doridella steinbergae* (Bickell and Chia, 1979) and on *Melibe leonina* (Bickell and Kempf, 1983). Kempf *et al.* (1987) gave the same interpretation for the larval CNS of the dendronotid *Tritonia diomedea*, except they also resolved a visceral ganglion (Fig. 26C). This model is superficially attractive because it produces an adult CNS with ganglionic regions that conform to the traditional interpretation based on comparative neuroanatomical studies of adult opisthobranchs (Fig. 27A). However, this model fails to explain why the left 'pleural ganglion' in the larva projects ventrally relative to the right, when pleural ganglia should not be involved in torsional displacements. I now believe that these ganglia are the intestinals.

Figure 26D shows my current interpretation of ganglionic regions within the late larval nervous system of *Melibe leonina*. The subsequent pattern of ganglionic fusions produces a CNS with ganglionic regions that differ from the traditional interpretation. The differences are illustrated in Figure 27.

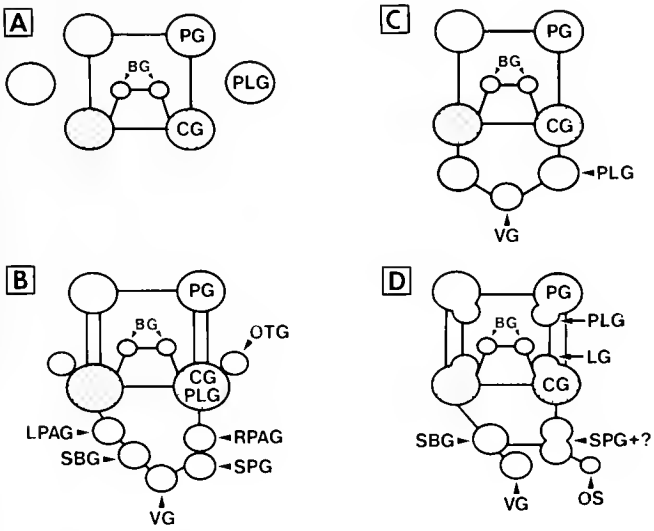

Figure 26. Four interpretations of the developing nudibranch CNS. Relative lengths of connectives and sizes of ganglia are not accurate; optic and rhinophoral ganglia not shown. (A) Thompson (1958) for *Adalaria proxima*. (B) Tardy (1970, 1974) for *Acolidiella alderi*. (C) Bickell and Chia (1979) for *Doridella steinbergae* and Bickell and Kempf (1983) for *Melibe leonina*; visceral ganglion added by Kempf *et al.* (1987) for *Tritonia diomedea*. (D) present study on *Melibe leonina*. Abbreviations: BG = buccal ganglia; CG = cerebral ganglion; LG = labial ganglion; LPAG = left parietal ganglion; OS = osphradial neurons; OTG = oral tentacle ganglion; PG = pedal ganglion; PLG = pleural ganglion; RPAG = right parietal ganglion; SBG = subintestinal ganglion; SPG = supraintestinal ganglion; VG = visceral ganglion.

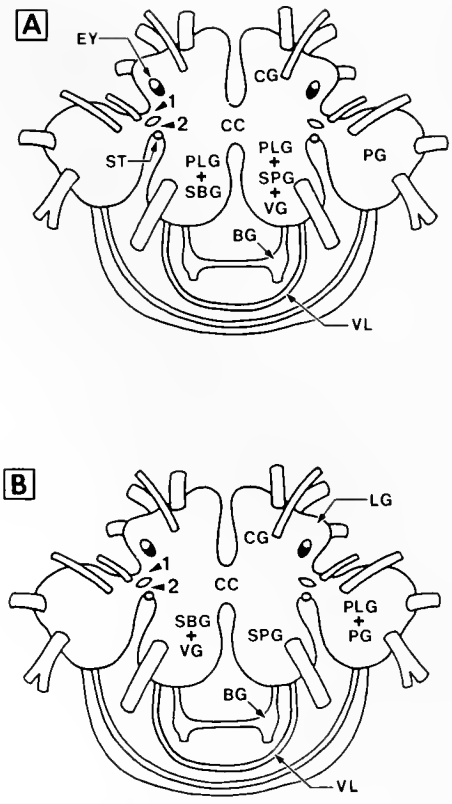

Figure 27. Interpretations of ganglionic regions in adult CNS of *Melibe leonina* (optic and rhinophoral ganglia not shown). (A) Traditional Model. Arrowhead no. 1 indicates cerebropedal connective; arrowhead no. 2 indicates pleuropedal connective. (B) Revised Model. Arrowhead no. 1 indicates cerebropleural connective; arrowhead no. 2 indicates cerebropedal connective. BG = buccal ganglion; CC = cerebral commissure; CG = cerebral ganglion; EY = eye; LG = labial ganglion (ventrally located); PG = pedal ganglion; PLG = pleural ganglion; SBG = subintestinal ganglion; SPG = supraintestinal ganglion; VG = visceral ganglion; VL = visceral loop.

Thoughts on phylogeny

Questions about phyletic relationships among opisthobranchs and about opisthobranch origins continue to be debated. Uncertainties stem from the large degree of morphological variation within the group and many instances of apparent parallelism (Ghiselin, 1965; Gosliner, 1981, 1991; Gosliner and Ghiselin, 1984). Nervous systems have a reputation for conservatism and are therefore valued as phyletic characters. It might be hoped that opisthobranch nervous systems could help unmask relationships otherwise hidden by superficial morphological differences or convergences. To date, proposed phylogenies have considered only adult neuroanatomical characters, with emphasis given to the length and detorsion of the visceral loop, and extent of ganglionic fusions. Using the latter criterion, Russell (1929) argued convincingly that nudibranchs are unlikely ancestors for sacoglossans. Nevertheless, Ghiselin (1965), among others, believes that

most of these characters show polyphyletic trends, and the extensively fused nervous systems of many adult opisthobranchs offer few other unambiguous clues to assist in phylogenetic reconstructions. However, ultrastructural study of neurodevelopment has revealed much more about an opisthobranch nervous system than is apparent from adult CNS structure. Indeed, the new developmental data about homologous ganglionic regions in *Melibe* raise serious questions about the validity of adult-based neuroanatomical interpretations given for other opisthobranchs.

In a revision of gastropod systematics, Salvini-Plawen and Haszprunar (1987) and Haszprunar (1988) argued that a hypoathroid or dystenoid nervous system (fused or semi-fused pleural and pedal ganglia) is a diagnostic character for the archaeogastropod grade. Based partly on the assumption that opisthobranch pleural ganglia are fused to the cerebrals (epiathroid nervous system; typical of caenogastropods), when not distinct in adults, Haszprunar (1985, 1988) proposed a primitive caenogastropod ancestor for the Opisthobranchia. Gosliner (1981) came to the same conclusion based on a suite of many criteria. It is therefore surprising to find a hypoathroid nervous system in a nudibranch, although the pleural ganglia of *Aplysia californica* are also very close to the pedal ganglia (well illustrated by fig. 4 of Cash and Carew, 1989). These observations contradict Haszprunar's proposed criterion for the archaeogastropod grade and undermine the notion of an epiathroid nervous system for all opisthobranchs. The possibility that the condition in *Melibe* is merely an exceptional, secondarily derived state, possibly related to the unusual oral hood of this genus, must be determined.

I have identified pleural neurons in *Melibe*, partly on the assumption that the two connectives between 'cerebral' and 'pedal' ganglia are cerebropedal and cerebro-pleural-pedal connectives. This dictum for gastropod CNS organization is supported by a large body of comparative anatomical data, but its universality is certainly not proven. Again, ultrastructural studies of development for a variety of gastropod groups are needed.

To date, labial ganglia have been identified in adults of some archaeogastropods (reviewed by Fretter and Graham, 1962), a pyramidellid (Fretter and Graham, 1949; pyramidellids have strong opisthobranch affinities), and in larvae of the nudibranch *Melibe leonina*. However, if the subcerebral commissure is evidence of labial ganglia fused to cerebral ganglia, as suggested by Bullock (1965), then labial ganglia are present also in other opisthobranchs and in pulmonates. Neither labial ganglia nor a subcerebral commissure have been found among caenogastropods, nor have they been reported in developmental stages of this group.

In conclusion, the nervous system of *Melibe* shares major plesiomorphous characters (pleuropedal ganglia, labial ganglia) with that of archaeogastropods. Although the uncoupling of the pleural ganglia from the visceral loop is an apomorphy not suspected previously for any other gastropod, the *Melibe* nervous system is not readily derived from the epiathroid nervous system typical of extant caenogastropods. The validity of these speculations must await further comparative studies.

Acknowledgments

It is a pleasure to thank Dr. G. O. Mackie for encouragement and financial support, and Dr. D. H. Paul for discussions of this topic. The study was funded by a grant from the Natural Science and Engineering Research Council of Canada to GOM.

Literature Cited

Arkett, S. A., F. S. Chia, J. I. Goldberg, and R. Koss. 1989. Identified settlement receptor cells in a nudibranch veliger respond to specific cue. *Biol. Bull.* **176:** 155–160.

Audesirk, T. E. 1979. Oral mechanoreceptors in *Tritonia diomedea*. I. Electrophysiological properties and location of receptive fields. *J. Comp. Physiol.* **A130:** 71–78.

Audesirk, G., and T. E. Audesirk. 1980. Complex mechanoreceptors in *Tritonia diomedea*. I. Responses to mechanical and chemical stimuli. *J. Comp. Physiol.* **A141:** 101–109.

Bickell, L. R., and F. S. Chia. 1979. Organogenesis and histogenesis in the planktotrophic veliger of *Doridella steinbergae* (Opisthobranchia: Nudibranchia). *Mar. Biol.* **52:** 291–313.

Bickell, L. R., and S. C. Kempf. 1983. Larval and metamorphic morphogenesis in the nudibranch *Melibe leonina* (Mollusca: Opisthobranchia). *Biol. Bull.* **165:** 119–138.

Boettger, C. 1954. Die Systematik der euthyneuren Schnecken. *Zool. Anz. Leipzig* (suppl.) **17:** 253–279.

Bullock, T. H. 1965. The Mollusca. Pp. 1273–1515 in *Structure and Function in the Nervous Systems of Invertebrates*, V. 2, T. H. Bullock and G. A. Horridge, eds. Freeman Press, San Francisco.

Cash, D., and T. J. Carew. 1989. A quantitative analysis of the development of the central nervous system in juvenile *Aplysia californica*. *J. Neurobiol.* **20:** 25–47.

Casteel, D. B. 1904. The cell-lineage and early larval development of *Fiona marina*, a nudibranch mollusc. *Proc. Acad. Nat. Sci. Philadelphia* **56:** 325–405.

Chia, F. S., and R. Koss. 1989. The fine structure of a newly discovered propodial ganglia of the veliger larva of the nudibranch *Onchidoris bilamellata*. *Cell Tissue Res.* **256:** 17–26.

Conklin, E. G. 1897. The embryology of *Crepidula*. *J. Morphol.* **13:** 1–226.

Creek, G. A. 1951. The reproductive system and embryology of the snail *Pomatias elegans* (Muller). *Proc. Zool. Soc. Lond.* **121:** 599–640.

Crofts, D. R. 1937. The development of *Haliotis tuberculata*, with special reference to the organogenesis during torsion. *Phil. Trans. R. Soc. Lond.* **B228:** 219–268.

Cumin, R. 1972. Normentafel zur Organogenese von *Limnaea stagnalis* (Gastropoda, Pulmonata) mit besonderer Berücksichtigung der Mitteldarmdrüse. *Rev. Suisse Zool.* **79:** 709–774.

D'Asaro, C. N. 1969. The comparative embryogenesis and early organogenesis of *Bursa corrugata* and *Distorsia clarthrata*. *Malacologia* **9:** 349–389.

Demian, E. S., and F. Yousif. 1975. Embryonic development and organogenesis in the snail *Marisa cornuarietis* (Mesogastropoda: Am-

pullariidae). V. Development of the nervous system. *Malacologia* **15:** 29–42.

De Vries, J. B. 1963. Contribution to the morphology and histology of the nudibranch *Melibe rosea* Rang. *Ann. Univ. Stellenbosch* **38** (ser. A): 105–153.

Dorsett, D. A. 1974. Neuronal homologies and the control of branchial tuft movements in two species of *Tritonia*. *J. Exp. Biol.* **61:** 639–654.

Dorsett, D. A. 1978. Neurons controlling foot and mantle movements in *Armina californica*. *Mar. Behav. Physiol.* **5:** 307–324.

Dorsett, D. A. 1986. Brains to cells: the neuroanatomy of selected gastropod species. Pp. 101–187 in *The Mollusca*, K. M. Wilbur, ed. V.9, *Neurobiology and Behavior*, part 2, A. O. D. Willows, ed. Academic Press, New York.

Fretter, V., and A. Graham. 1949. The structure and mode of life of the Pyramidellidae, parasitic opisthobranchs. *J. Mar. Biol. Assoc. U.K.* **28:** 493–532.

Fretter, V., and A. Graham. 1962. *British Prosobranch Molluscs: Their Functional Anatomy and Ecology*. Ray Society, London.

Ghiselin, M. 1965. Reproductive function and the phylogeny of opisthobranch gastropods. *Malacologia* **3:** 327–378.

Gosliner, T. M. 1981. Origins and relationships of primitive members of the Opisthobranchia (Mollusca: Gastropoda). *Biol. J. Linn. Soc.* **16:** 197–225.

Gosliner, T. M. 1987. A review of the genus *Melibe* (Opisthobranchia; Dendronotacea) with descriptions of two new species. *Veliger* **29:** 400–414.

Gosliner, T. M. 1991. Morphological parallelism in opisthobranch gastropods. *Malacologia* **32:** 313–327.

Gosliner, T., and M. Ghiselin. 1984. Parallel evolution in opisthobranch gastropods and its implications for phylogenetic methodology. *Syst. Zool.* **33:** 255–274.

Guiart, J. 1901. Contribution à l'étude des gastéropodes opisthobranchs et en particulier de céphalaspides. *Mem. Soc. Zool. Fr.* **14:** 5–219.

Guyomarc'H-Cousin, C. 1974. Étude descriptive de l'organogénèse du système nerveux chez *Littorina saxatilis* (Olivi) Gastéropode Prosobranche. *Ann. Embryol. Morphog.* **4:** 349–364.

Haszprunar, G. 1985. The Heterobranchia—a new concept of the phylogeny of the higher Gastropoda. *Z. Zool. Syst. Evol.* **23:** 15–37.

Haszprunar, G. 1988. On the origin and evolution of major gastropod groups with special reference to the Streptoneura. *J. Moll. Stud.* **54:** 367–441.

Hicknott, P. W., and T. J. Carew. 1991. An autoradiographic analysis of neurogenesis in juvenile *Aplysia californica*. *J. Neurobiol.* **22:** 313–326.

Hoffmann, H. 1936. Opisthobranchia. Pp. 641–864 in *Klassen und Ordungen des Tierreichs*, v.3, H. G. Bronns, ed. Acad. Verlagsges., Leipzig.

Honegger, T. 1974. Die Embryogenese von *Ampullarius* (Gastropoda, Prosobranchia). *Zool. Jahrb. Abt. Anat. Ontogenie Tiere* **93:** 1–76.

Hurst, A. 1968. The feeding mechanism and behaviour of the opisthobranch *Melibe leonina*. *Symp. Zool. Soc. Lond.* **22:** 151–166.

Jacob, M. H. 1984. Neurogenesis in *Aplysia californica* resembles nervous system formation in vertebrates. *J. Neurosci.* **4:** 1225–1239.

Kandel, E. R. 1979. *Behavioral Biology of* Aplysia. Freeman, San Francisco.

Kempf, S. C., B. Masinovsky, and A. O. D. Willows. 1987. A simple neuronal system characterized by a monoclonal antibody to SCP neuropeptides in embryos and larvae of *Tritonia diomedea* (Gastropoda, Nudibranchia). *J. Neurobiol.* **18:** 217–236.

Kempf, S. C., and A. O. D. Willows. 1977. Laboratory culture of the nudibranch *Tritonia diomedea* Bergh (Tritoniidae: Opisthobranchia) and some aspects of its behavioral development. *J. Exp. Mar. Biol. Ecol.* **30:** 261–276.

McAllister, L. B., R. H. Scheller, E. R. Kandel, and R. Axel. 1983. *In situ* hybridization to study the origin and fate of identified neurons. *Science* **222:** 800–808.

Moor, B. 1983. Organogenesis. Pp. 123–177 in *The Mollusca*, K. M. Wilbur, ed., v.3, *Development*, N. H. Verdonk, J. A. M. van den Biggelaar, and A. S. Tompa, eds. Academic Press, New York.

Page, L. R. 1992. New interpretation of a nudibranch central nervous system based on ultrastructural analysis of neurodevelopment in *Melibe leonina* I. Cerebral and visceral loop ganglia. *Biol. Bull.* **182:** 348–365.

Raven, C. P. 1958. *Morphogenesis: The Analysis of Molluscan Development*. Pergamon Press, Oxford.

Raven, C. P. 1975. Development. Pp. 367–400 in *Pulmonates*, Vol. 1, V. Fretter and J. Peake, eds. Academic Press, New York.

Régondaud, J. 1961. Formation due système nerveux et torsion chez *Lymnaea stagnalis* L. (Mollusque Gastéropode). *C.R. Hebd. Seances L'Acad. Sci.* **252:** 1203–1205.

Régondaud, J. 1964. Origine embryonnaire de la cavité pulmonaire de *Lymnaea stagnalis* L. Considérations particulières sur la morphogénèse de la commissure viscérale. *Bull. Biol. Fr. Belg.* **98:** 433–471.

Russell, L. 1929. The comparative morphology of the elysioid and aeolidioid types of the molluscan nervous system, and its bearing on the relationships of the ascoglossan nudibranchs. *Proc. Zool. Soc. Lond.* **14:** 197–233.

Salvini-Plawen, L. v. 1985. Early evolution and the primitive groups. Pp. 59–150 in *The Mollusca*, K. M. Wilbur, ed., V.10, *Evolution*, E. R. Trueman and M. R. Clarke, eds. Academic Press, New York.

Salvini-Plawen, L. v., and G. Haszprunar. 1987. The Vetigastropoda and the systematics of the streptoneurous gastropods (Mollusca). *J. Zool. Lond.* **A211:** 747–770.

Schmekel, L. 1985. Aspects of evolution within the Mollusca. Pp. 221–267 in *The Mollusca*, K. M. Wilbur, ed., v.10, *Evolution*, E. R. Trueman and M. R. Clarke, eds. Academic Press, New York.

Smith, F. G. W. 1935. The development of *Patella vulgata*. *Phil. Trans. R. Soc. Lond.* **B225:** 95–125.

Smith, S. T. 1967. The development of *Retusa obtusa* (Montagua) (Gastropoda, Opisthobranchia). *Can. J. Zool.* **45:** 737–764.

Tardy, J. 1970. Contribution à l'étude des métamorphoses chez les nudibranches. *Ann. Sci. Nat., Zool., Paris* **12:** 299–370.

Tardy, J. 1974. Morphogenèse du système nerveux chez les mollusques nudibranches. *Haliotis* **4:** 61–75.

Thompson, T. E. 1958. The natural history, embryology, larval biology, and post-larval development of *Adalaria proxima* (Alder and Hancock) (Gastropoda, Opisthobranchia). *Phil. Trans. R. Soc. Lond.* **B242:** 1–58.

Thompson, T. E. 1962. Studies on the ontogeny of *Tritonia hombergi* Cuvier (Gastropoda Opisthobranchia). *Phil. Trans. R. Soc. Lond.* **B245:** 172–218.

Verdonk, N. H., and J. A. M. van den Biggelaar. 1983. Early development and the formation of the germ layers. Pp. 91–122 in *The Mollusca*, K. M. Wilbur, ed., v.3, *Development*, N. H. Verdonk, J. A. M. van den Biggelaar, and A. S. Tompa, eds. Academic Press, New York.

Walters, E. T., J. H. Byrne, T. J. Carew, and E. R. Kandel. 1983. Mechanoafferent neurons innervating tail of *Aplysia*. I. Response properties and synaptic connections. *J. Neurophysiol.* **50:** 1522–1542.

Willows, A. O. D., ed. 1985–1986. *The Mollusca*, K. M. Wilbur, ed. v.8 and 9, *Neurobiology and Behavior*, parts 1 and 2. Academic Press, New York.

Willows, A. O. D., D. A. Dorsett, and G. Hoyle. 1973. The neuronal basis of behavior in *Tritonia*. I. Functional organization of the nervous system. *J. Neurobiol.* **4:** 207–237.

Wingstrad, K. G. 1985. On the anatomy and relationships of recent Monoplacophora. *Galathea Rep.* **16:** 7–94.

Reference: *Biol. Bull.* **182**: 382–390. (June, 1992)

Control of Cilia in the Branchial Basket of *Ciona intestinalis* (Ascidacea)

DWIGHT BERGLES* AND SIDNEY TAMM

Boston University Marine Program, Marine Biological Laboratory, Woods Hole, Massachusetts 02543

Abstract. We investigated arrest and inactivation responses of stigmatal cilia in the branchial basket of the ascidian, *Ciona intestinalis*. Using an improved preparation of living tissue for microscopic imaging of ciliary responses, we found that Ca-ionophore A23187 in seawater + 50 m*M* Ca caused actively beating cilia to assume the upright inactive posture, while A23187 in seawater + 100 m*M* Ca caused transient (5–10 s) stigma-wide arrests in which the cilia lie flat against the stigmatal walls. Both responses are therefore Ca dependent, but the inactive state has a lower threshold for Ca than does arrest. Membrane permeant cAMP analogues induced >40% of the quiescent cilia within a stigma to begin beating.

Saponin-extracted models of stigmatal cilia were developed to study the ionic and molecular control of ciliary activity in *Ciona*. Extracted cilia were stimulated to beat vigorously for >45 min by ATP-containing reactivation solution (RS). Addition of 10^{-5} to 10^{-3} *M* Ca to reactivation solution caused the cilia to stand upright (inactivate), but not to arrest. The calmodulin antagonists trifluoperazine and calmidazolium (100 μM) restored active beating when included in RS + 50–100 μM Ca, thereby reversing Ca-dependent inactivation. Addition of bovine brain calmodulin to RS + 100 μM Ca did not cause arrest of reactivated cilia. RS + 100 μM cAMP + 1 m*M* 3-isobutyl-1-methyl-xanthine or the catalytic subunit of c-AMP-dependent protein kinase increased both the proportion and vigor of reactivated beating. Addition of 100 μM Ca to the RS + cAMP + IBMX solution caused reactivated cilia to vibrate or twitch in an upright position, suggesting that Ca and cAMP have antagonistic effects on stigmatal cilia.

Received 13 December 1991; accepted 27 March 1992.

* Present address: Department of Molecular & Cellular Physiology, Beckman Center, Stanford University School of Medicine, Stanford, California 94305-5426.

Abbreviations. B-cAMP, N6-benzoyl-cAMP; M-cAMP, N6-monobutryl-cAMP; ES, extraction solution; WS, wash solution; RS, reactivation solution; TFP, trifluoperazine; IBMX, 3-isobutyl-1-methyl-xanthine; TAME, Nα-p-tosyl-L-arginine methyl ester, PKA, c-AMP-dependent protein kinase.

Introduction

The activity of cilia and flagella is regulated in many organisms, reflecting the important role of these organelles in locomotion, suspension feeding, gas exchange, mucous and gamete transport, and sperm chemotaxis. Well-known examples of ciliary and flagellar responses to stimuli include reorientation of beat direction in ciliate protozoa (Eckert *et al.*, 1976; Machemer, 1986), arrest of lateral cilia of lamellibranch gills (Murakami and Takahashi, 1975; Tsuchiya, 1977; Walter and Satir, 1978), inhibition of velar cilia of molluscan larvae (Carter, 1926), activation of *Mytilus* abfrontal cilia (Stommel, 1984), *Beroë* macrocilia (Tamm, 1988), and sperm flagella (Brokaw, 1987), changes in waveform of sea urchin sperm flagella (Brokaw *et al.*, 1974; Brokaw, 1979) and *Chlamydomonas* flagella (Hyams and Borisy, 1978; Bessen *et al.*, 1980), and reversal of direction of wave propagation in trypanosome flagella (Holwill and McGregor, 1976). Many of these axonemal responses are known to be triggered by depolarization-induced changes in intracellular Ca or alterations in cyclic nucleotide levels (Machemer, 1986; Brokaw, 1987; Otter, 1989; Stephens and Stommel, 1989; Preston and Saimi, 1990; Bonini *et al.*, 1991).

Tunicates show periodic interruptions in the beating of cilia that line openings (stigmata) of the branchial basket and generate the feeding current (Fedele, 1923; MacGinitie, 1939). These temporary ciliary arrests occur spontaneously, in response to general disturbances, or when undesirable material enters the branchial siphon (Bone

and Mackie, 1982), and are usually accompanied by quick contractions of siphons and mantle ("squirts") (MacGinitie, 1939). Previous studies on the ascidian branchial basket showed that ciliary arrests are: (1) induced by depolarizing stimuli, (2) controlled by identified neurons in the central ganglion, (3) mediated by cholinergic synapses, (4) correlated with action potentials recorded from the stigmatal ciliated cells, and (5) dependent on external Ca (Takahashi *et al.*, 1973; Mackie *et al.*, 1974; Arkett, 1987; Arkett *et al.*, 1989). Ascidian stigmatal cilia also undergo an "inactive" state in which they stand in an upright position before resuming normal beating (Takahashi *et al.*, 1973; Mackie *et al.*, 1974; Arkett, 1987).

Despite the evidence suggesting that ascidian cilia are controlled by mechanisms similar to those operating in other systems, neither Ca dependence of arrest or inactivation responses, nor the possible role of cyclic nucleotides in ciliary activity has been investigated directly in any tunicate.

We have addressed these questions in the ascidian *Ciona intestinalis* by devising an improved method for microscopic imaging of motile responses of living cilia, and by developing the first detergent-extracted, ATP-reactivated cell models of stigmatal cilia. These new advances enable direct tests of the ionic and biochemical basis of control of ciliary motility in *Ciona* and are valuable complements to other studies on regulation of sperm flagellar motility in *Ciona* (Brokaw, 1987). A preliminary report of this work has appeared (Bergles and Tamm, 1989).

Materials and Methods

Organism

Specimens of *Ciona intestinalis* (5–10 cm long) were obtained from Marine Resources at the Marine Biological Laboratory and kept in baskets immersed in running seawater, or were simply removed from the sides of laboratory sea-tables in which they had settled and grown. *Ciona* specimens were used within a week after removal from their substrate, because the branchial basket often deteriorated after the animals were detached.

Perfusion slides of living stigmatal cilia

Ciona were pinned laterally against a Sylgard-coated dish, and the tunic was sliced open and pulled back. The branchial cavity was opened by cutting longitudinally along the length of the endostyle, then across between the two siphons. The branchial basket was removed by cutting the many trabeculae connecting the basket to the mantle. The excised branchial basket was pinned flat in a Sylgard-lined petri dish of normal seawater and kept on ice at 0°C. Prior to experimentation, the branchial basket was further subdivided into small rectangular pieces, about 1 × 5 mm, by cutting between the longitudinal bars with fine iridectomy scissors. Tissue was used within 2–4 h after its removal from the animal.

In the final preparation, a piece of branchial basket was pipetted onto a microscope slide that had been ringed by a 15 × 50 mm rectangular ridge of petroleum jelly (Vaseline). The tissue was stretched out near the center of this rectangular well with the pharyngeal side facing upward. The ends of the piece were then pressed down against the slide by fine stainless steel pins anchored in dabs of Vaseline that had previously been placed on the dry slide. A square coverslip was placed over the tissue, mounted near the center of the rectangular well, leaving room on either side of the coverslip to add and withdraw solution from the well during perfusion.

Cell models

Small rectangular pieces of branchial basket were placed in 0.1% saponin, 1% DMSO, 20 m*M* EGTA, 150 m*M* KCl, 10 m*M* $MgCl_2$, 30 m*M* PIPES, pH 7 (extraction solution, ES) in a glass well for 4–9 min at room temperature. Tissue was transferred to a second well containing 2 m*M* ATP, 1 m*M* DTT, 10 m*M* EGTA, 150 m*M* KCl, 10 m*M* $MgCl_2$, 30 m*M* PIPES, pH 7 (reactivation solution, RS), or to the same solution without ATP (wash solution, WS). The tissue pieces were then mounted on perfusion slides for observations. Extraction and reactivation of living pieces mounted on perfusion slides was not feasible due to distortion of the tissue by muscular contractions induced by ES.

The effects of ions or reagents on ciliary reactivation were estimated as follows (Table 1). Twenty-five to 100 stigmata with clearly observable cilia were observed for each tissue piece. A rating of ++++ indicates that >95% of the cilia in each stigma were beating vigorously. Ratings of +++, ++, and + indicate that 75–95%, 50–75%, and 15–50% of the cilia in each stigma were beating, respectively, typically at decreasing frequencies. A rating of ± indicates that 5–15% of the cilia were active, and a negative rating indicates that <5% were beating. All treatments were repeated on at least five different preparations of branchial basket pieces.

Reagents and solutions

Calmidazolium and norepinephrine were obtained from Calbiochem-Behring Corp. (San Diego, California); sodium metavanadate was obtained from Mallinckrodt Inc. (St. Louis, Missouri). Calmodulin (bovine brain), cAMP (bovine brain), protein kinase catalytic subunit (bovine heart), and all other chemicals were obtained from Sigma Chemical Co. (St. Louis, Missouri). Ca-EGTA

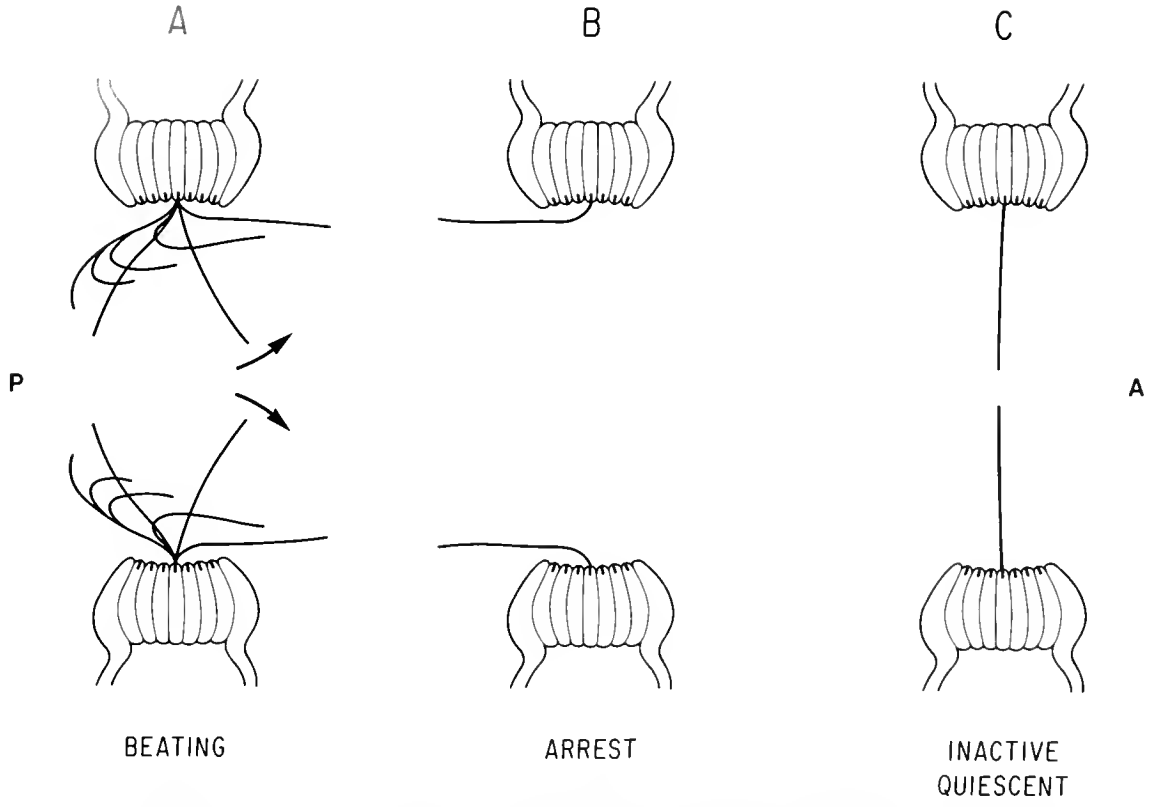

Figure 1A–C. Diagram of three different states of *Ciona* stigmatal cilia, as viewed in cross section of a stigma to show ciliary profiles. For clarity, only one of the cilia arising from the seven ciliated cells is shown. The branchial cavity (P) is to the left, the atrial (cloacal) cavity (A) is to the right in all figures. Based on our observations and Takahashi *et al.* (1973), Mackie *et al.* (1974), and Arkett (1987). (A) Active cilia beat with the effective stroke directed towards the atrial chamber (arrows), propelling water out of the pharynx. The recovery stroke occurs in three dimensions, out of the plane of the power stroke. Metachronal waves (not shown) travel at right angles to the effective stroke. (B) Arrested cilia lie flat against the stigmatal walls, inclined in a posture beyond the end of the recovery stroke (stigmata open). (C) Following arrest, cilia stand upright in an inactive posture (stigma closed) before active beating resumes. Quiescent cilia also remain in this position.

buffers were prepared according to Salmon and Segall (1980).

Light microscopy

Perfusion slides were viewed with Zeiss brightfield or phase-contrast optics (16×/0.40 NA or 40×/0.75 NA objectives), and images were recorded with a DAGE 67M video camera (Dage-MTI, Michigan City, Indiana 46360) on a VHS videocasette recorder allowing still-field playback (GYYR model 2051, Anaheim, California 92802). Beat frequency was determined by repetitive counting of the number of video fields (1/60 s) per beat cycle. Photographs of still-fields from a video monitor were taken with an Olympus OM-2N camera on Kodak Tech Pan (2415) 35 mm film.

Results

Stigmatal ciliary system

The anatomy and motility of the stigmatal ciliary system of *Ciona* and other ascidians have been described previously (MacGinitie, 1939; Takahashi *et al.*, 1973; Mackie *et al.*, 1974; Arkett, 1987), and are reviewed briefly here.

The branchial slits or stigmata are lined with seven rows of laterally flattened cells, each bearing a single row of cilia (Fig. 1). The ciliated cells are stacked side-by-side in clusters that abut end-to-end, forming a continuous ciliated band around the inside of a stigma. Neurons run within the blood sinus and make synaptic contacts onto the bases of the ciliated cells, which are coupled by gap junctions (Mackie *et al.*, 1974; Arkett *et al.*, 1989).

The stigmatal cilia beat outward from the branchial cavity towards the atrial cavity, generating a water current that enters the branchial (incurrent) siphon, passes through the branchial basket, and flows out the atrial siphon (Fig. 1A). Ciliary beating is coordinated into dexioplectic metachronal waves that travel unidirectionally around the stigmatal openings (Fig. 2A).

In response to mechanical, electrical, or chemical stimulation, all the cilia lining a stigma perform a single rapid reverse stroke and lie flat against the stigmatal walls for 1–2 s in an arrest position inclined beyond the end of the normal recovery stroke (Fig. 1B). Ciliary arrest halts water flow into the pharynx and leaves the stigmata completely open, allowing muscular contractions to "squirt" water out of the branchial siphon.

Following an arrest, the cilia gradually rise to an upright position, closing the stigmatal opening (Fig. 1C). The cilia remain in this straight "inactive" state for a few seconds before beating resumes and normal metachrony is re-established.

In both excised pieces of branchial basket and exposed intact baskets, some stigmata are always observed with cilia that stand upright in an "inactive" posture for long periods. It is not known whether this long-lasting inactive state was, in any case, preceded by an arrest; but a direct transition from beating to the inactive position has never been reported (Takahashi *et al.*, 1973; Mackie *et al.*, 1974; Arkett, 1987). Upon stimulation, inactive cilia as well as beating cilia perform an arrest response together (Takahashi *et al.*, 1973; Mackie *et al.*, 1974).

Effects of calcium ionophore

Perfusion of pieces of branchial basket with 100 μM A23187 in normal seawater for 15–30 min had no noticeable effect on stigmatal ciliary activity. Addition of 50 mM $CaCl_2$ to both the bath and the ionophore suspension caused most of the cilia to assume an upright inactive position (stigmata closed) within 5 s after perfusion of ionophore. Cilia remained in this posture for as long as observed (up to 5 min). The addition of 100 mM $CaCl_2$ to the bath and ionophore suspension resulted in stigma-wide ciliary arrests throughout the field of view within 5 s after perfusion of A23187 (Fig. 2). Ciliary arrests lasted less than 5–10 s, after which the cilia moved to the inactive position and remained upright for 15–30 s before resuming beating. When larger pieces of branchial basket were used, arrests were accompanied by vigorous muscular contractions.

Perfusion of normal seawater containing 50 mM or 100 mM Ca without A23187 but with solvent (0.1% ethanol/DMSO) did not elicit arrests or inactivations.

Membrane-permeant cAMP analogues

To investigate the possible role of cAMP-regulated processes (*i.e.*, activation of PKA) in stigmatal ciliary responses, we applied membrane-permeant cAMP analogues to branchial basket pieces on perfusion slides.

We directed our attention to stigmata where most of the cilia were standing upright in a long-lasting inactive state. Perfusion of 1–10 mM N6-benzoyl-cAMP (B-cAMP) or N6-monobutyryl-cAMP (M-cAMP) in normal seawater caused many of the quiescent cilia to beat with normal metachronal coordination within 1–3 min. In most cases, more than 40% of the cilia became active. A greater number of quiescent cilia became active in stigmata where some of the cilia were already beating prior to perfusion with B-cAMP or M-cAMP. No significant activation of cilia was observed after perfusion of the solvent carrier (0.1% ethanol) in seawater without cAMP analogues.

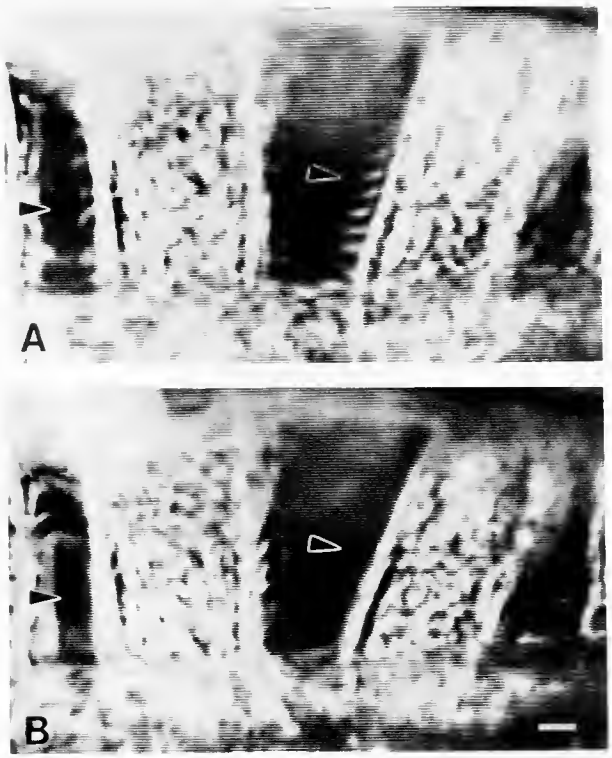

Figure 2. Ca ionophore-induced arrest of stigmatal cilia. (A) In seawater, metachronal waves of ciliary activity are evident on the stigmatal wall (arrowhead). (B) Perfusion of A23187 in seawater + 100 mM Ca causes ciliary arrest (arrowhead). Video prints; scale bar, 20 μm.

Cell models

Extraction and reactivation. Treatment of pieces of branchial basket in ES for 4–9 min stopped most stigmatal cilia in a more or less upright position. The cilia projected as tufts from clusters of swollen stigmatal cells, and there were gaps between the ciliary tufts of adjacent cell groups. Transfer of tissue to WS did not activate beating; the cilia remained in a relatively upright posture (Fig. 3A). Shorter extraction times (2–3 min) resulted in very slow ciliary beating (<2 Hz) in WS; the cilia usually stopped in the inactive position within 5–10 min. Thin-section electron microscopy of tissue extracted for 7 min showed partial

or complete removal of ciliary membranes from most of the stigmatal cilia, while non-extracted tissue prepared by the same procedure had intact ciliary membranes (not shown).

Transfer of extracted branchial basket tissue to RS resulted in vigorous beating of 50–70% of the stigmatal cilia. Ciliary reactivation typically lasted more than 45 min. Beating sometimes dislodged or displaced the ciliated cells from the fragile stigmatal wall, causing them to "swim" through the solution. Normal metachronal waves were not present. Separated tufts of cilia often beat independently, and displayed unicellular metachrony as reported for reactivated lateral cilia on separated cell groups of *Modiolus demissus* gills (Child and Tamm, 1963).

Reactivated beating was also observed by perfusing RS through a slide of extracted branchial basket in WS (Fig. 3B). RS perfusion caused the cilia to beat hesitantly at first with a restricted range of motion, then rapidly and fully within 10–20 s. Reactivated cilia often reached a steady-state frequency similar to that of living cells (10–14 Hz). Long stretches of cilia sometimes beat nearly synchronously to form common wavefronts (Fig. 3B).

Vanadate inhibition. RS + 20 μM vanadate, a potent inhibitor of dynein ATPase (Gibbons *et al.*, 1978), did not reactivate ciliary beating. Norepinephrine (5 mM) in RS + vanadate restored reactivated beating, reversing vanadate inhibition of motility (Table I).

Ca sensitivity. ES-treated pieces of branchial basket showed normal reactivation of ciliary beating when placed in wells of 10^{-7} to 10^{-6} M free Ca (Ca-EGTA buffer). However, RS + 10^{-5} to 10^{-3} M Ca caused the majority of cilia to assume an upright inactive posture, but never an arrest position (Table I). A gradual decrease in Ca sensitivity for eliciting inactivation was observed with longer times in ES; extraction times of more than 9 min often yielded cilia that did not inactivate in response to Ca.

To check whether a transient Ca-induced arrest response might have been missed in depression wells, RS + 10^{-4} to 10^{-3} M Ca was perfused into a slide containing a piece of extracted branchial basket in WS. No momentary arrest response was observed before the cilia assumed a rigidly straight inactive position.

Various approaches were tried to elicit arrests in RS + 10^{-5} to 10^{-3} M Ca. For example, a cocktail of protease inhibitors (1 mg/ml trypsin inhibitor; 0.5 mg/ml leupeptin; 1 mM TAME; 0.2 mg/ml PMSF, 1 mg/ml BSA) were included in both ES and RS to prevent possible proteolysis of putative Ca sensors or proteins required to mediate arrest. Different detergents (Brij-58, Brij-35, Triton-X 100) were tried in place of saponin to preclude the extraction of Ca-binding proteins (*i.e.*, calmodulin). In another series of experiments, K acetate was substituted for KCl in both ES and RS. None of these modifications resulted in ciliary arrests in RS + 10^{-4} M Ca. We did note, however, that reactivation was consistently better in solutions containing KCl rather than K acetate (Table I).

Calmodulin. Addition of calmodulin antagonists, 100 μM trifluoperazine (TFP) or 100 μM calmidazolium to RS + 50–100 μM Ca restored reactivated beating, thereby reversing Ca-dependent inactivation (Table I). TFP typically gave more consistent results than did calmidazolium. Chlorpromazine (100 μM) did not significantly reverse the inactivation of cilia in RS + Ca. These results indicate that calmodulin mediates Ca-dependent inactivation of stigmatal cilia.

Addition of 65 μg/ml bovine brain calmodulin to RS + 100 μM Ca did not elicit an arrest of cilia in tissue initially bathed in WS or RS (Table I).

cAMP and PKA

RS + 100 μM cAMP and 1 mM IBMX, a cyclic nucleotide phosphodiesterase inhibitor substantially increased both the proportion and vigor of ciliary reactivation compared to tissue incubated in RS alone (Table I). Thus cAMP and Ca exert opposing effects on ciliary reactivation. In RS containing 100 μM cAMP + 100 μM Ca, cilia vibrated or twitched rapidly in a rigid inactive position. Addition of 28 μg/ml catalytic subunit of PKA to RS likewise improved the extent of ciliary reactivation to more than 95% in most cases (Table I).

Discussion

Calcium and arrest

The role of Ca in triggering a variety of ciliary and flagellar motor responses is well documented (Eckert and Murakami, 1972; Naitoh and Kaneko, 1972; Tsuchiya, 1977; Hyams and Borisy, 1978; Walter and Satir, 1978; Gibbons and Gibbons, 1980; Brokaw and Nagayama, 1985; Nakamura and Tamm, 1985; Satir, 1985; Stommel and Stephens, 1985; Machemer, 1986; Brokaw, 1987, 1991; Tamm, 1988; Otter, 1989).

Although arrest of stigmatal cilia in ascidians has long been suspected to be Ca-dependent (Takahashi *et al.*, 1973; Mackie *et al.*, 1974), direct evidence for this has been lacking. Our finding that Ca ionophore in the presence of 100 mM Ca elicits arrest of *Ciona* stigmatal cilia strongly argues for the Ca-dependency of this response. However, these experiments were performed on pieces of branchial basket tissue, and stigmatal cilia have been shown to be under neuronal control (Mackie *et al.*, 1974; Arkett, 1987). Therefore, our results could also be explained by ionophore-mediated influx of Ca at presynaptic sites mediating nervous control of ciliary arrest, without requiring Ca influx into the ciliated cells themselves.

To directly test whether ciliary motility in ascidians is regulated by Ca, we prepared the first ATP-reactivated

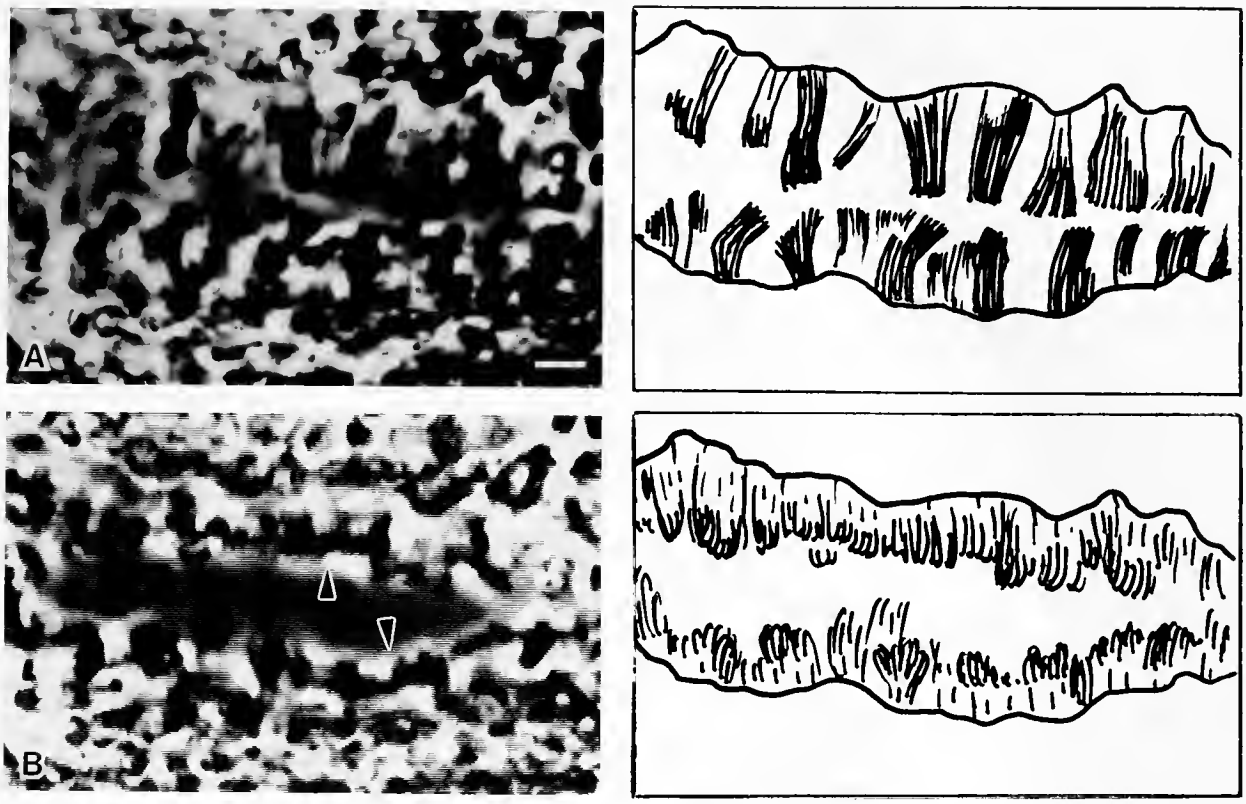

Figure 3. Stigmatal cell models. Cilia lining a stigma are shown on the left and diagrammed on the right. (A) A single stigma in WS. Tufts of immotile cilia (black) stand upright, projecting from the refractile wall of the stigma into the stigmatal space. In the diagram, the wall (edge) of the stigma is indicated by the irregular horizontal lines. (B) The same stigma after perfusion of RS. The cilia beat vigorously and, to a large extent, synchronously, giving rise to common wavefronts (arrowheads). As a result, the stigma is more open than in A. The stigmatal wall does not change (compare outlines of stigma in diagrams). Scale bar, 10 μm, *A, B*.

models of stigmatal ciliated cells. We were unable to elicit ciliary arrest in our saponin-permeabilized models at any Ca concentration used (10^{-5} to $10^{-3}M$ Ca in RS). Instead, the axonemes stopped in an upright inactive position without passing through an arrest.

We were concerned that our permeabilization procedure, or possibly subsequent proteolysis, might have removed or destroyed critical control factors or Ca-binding proteins (*i.e.*, calmodulin) necessary for demonstrating Ca-sensitivity of arrest in cell models. For example, extraction of calmodulin from sea urchin sperm and protist cilia leads to modification or loss of Ca control of axonemal motor responses (Brokaw and Nagayama, 1985; Izumi and Miki-Noumura, 1985; Izumi and Nakaoka, 1987). Extraction and incubation procedures may also modify the calmodulin-binding affinity of the axoneme (Brokaw, 1991). In addition, some detergents commonly used to make cell models (*i.e.*, Triton-X 100) are potent inhibitors of both calmodulin and calmodulin-dependent cyclic nucleotide phosphodiesterase (Sharma and Wang, 1981).

However, our attempts to restore presumed Ca sensitivity of ciliary arrest in models by trying different detergents, extraction times, protease inhibitors, or addition of exogenous bovine brain calmodulin, were uniformly unsuccessful. Nevertheless, the variable sensitivity of the inactivation response of models to Ca, particularly after longer extraction times (more than 9 min in ES), suggests that the absence of Ca-sensitive arrest in our models may be due to loss or modification of an as yet unidentified factor.

Calcium and inactivation

The upright inactive posture of stigmatal cilia is clearly Ca-dependent: reactivated cilia are inactivated by 10^{-5} to 10^{-3} *M* Ca, and cilia on living tissue are inactivated by Ca ionophore in the presence of a lower Ca concentration (50 m*M*) than that leading to arrest (100 m*M*, see above). These findings suggest that inactivation has a lower threshold to intracellular Ca than does arrest.

Inactive cilia of cell models in RS + Ca were induced to beat by the addition of a calmodulin antagonist, either

Table 1

Effects of various compounds on reactivation of ciliary motility in cell models

Solution	Ciliary activity
WS	–
RS (KCl)*	++(+)
RS (K Acetate)	++
RS + 20 μM Vanadate	
RS + 20 μM Vanadate + 5 mM Norepinephrine	+++
RS + 10 μM Ca^{2+}	+
RS + 50 μM Ca^{2+}	±
RS + 100 μM Ca^{2+}	–
RS + 100 μM Ca^{2+} + PIs	–
RS + 100 μM Ca^{2+} + 100 μM Trifluoperazine	+++
RS + 100 μM Ca^{2+} + 100 μM Calmidazolium	++
RS + 100 μM Ca^{2+} + 100 μM Chlorpromazine	±
RS + 100 μM Ca^{2+} + Calmodulin (65 μg/ml)	–
RS + 100 μM cAMP + 1 mM IBMX	++++
RS + 100 μM Ca^{2+} + 100 μM cAMP	– vibrating
RS + PKAcs (28 μg/ml)	++++

* Standard RS used below.

Plus and minus ratings indicate relative degrees of ciliary activity (see Materials and Methods); minus indicates that nonbeating cilia were in an upright inactive position.

Abbreviations: WS, wash solution; RS, reactivation solution; IBMX, isobutylmethylxanthine; PIs, protease inhibitors; PKAcs, catalytic subunit of protein kinase.

TFP or calmidazolium. This suggests that Ca-induced inactivation of *Ciona* stigmatal cilia is mediated by calmodulin. Other Ca-dependent ciliary motor responses, such as arrest of mussel gill lateral cilia (Reed *et al.*, 1982; Stommel, 1984), activation of *Mytilus* gill abfrontal cilia (Stommel, 1984), and reorientation of ciliary beat direction in some cell models of *Paramecium* (Otter *et al.*, 1984; Izumi and Nakaoka, 1987) and *Tetrahymena* (Izumi and Miki-Noumura, 1985), are also partially or completely inhibited by anti-calmodulin drugs.

Ca may exert its effects on ciliary motility by activating calmodulin-dependent protein kinase (C kinase) or phosphatase (calcineurin), thus changing the phosphorylation levels of axonemal regulatory proteins (Nakaoka and Ooi, 1985; Tash, 1989; Hamasaki *et al.*, 1989; Bonini *et al.*, 1991). Because the catalytic subunit of PKA did not inactivate reactivated *Ciona* stigmatal cilia, but rather enhanced motility, the mechanism by which Ca-calmodulin is presumed to inactivate stigmatal cilia may involve a dephosphorylation reaction.

The transient inactive state exhibited by *Ciona* cilia after every arrest resembles the transient inactivation of *Paramecium* cilia that occurs after depolarization-induced Ca-dependent reversal of beat direction, before the beat cycle is renormalized (Machemer, 1986). Voltage-clamp experiments with *Paramecium* showed that an inactive state, or frequency minimum, also intervenes between normal beating and the onset of stimulus-induced ciliary reversal. In *Paramecium*, a transient inactivation response therefore precedes and follows the Ca-dependent ciliary reversal response, suggesting that inactivation may be caused by a Ca concentration slightly elevated above normal resting level (Machemer, 1986). The transient inactive state following the arrest of *Ciona* cilia may also reflect an intermediate level of internal Ca concentration. The epaulette cilia of echinoplutei larvae sometimes undergo a similar upright inactive state after Ca-dependent reversed beating (Mogami *et al.*, 1991).

Finally, a recent study of Ca-induced asymmetry of ATP-reactivated flagellar bending waves of sea urchin sperm indicates the existence of two separate Ca responses, mediated by high-affinity and lower-affinity Ca sensors (Brokaw, 1991).

cAMP and quiescence

Cyclic nucleotides (cAMP, cGMP) also play a role in regulating ciliary and flagellar motility: in particular, cAMP is typically involved in initiating and maintaining ciliary and flagellar beating (Opresko and Brokaw, 1983; Stommel and Stephens, 1985; Takahashi *et al.*, 1985; Murofushi *et al.*, 1986; Brokaw, 1987; Murakami, 1987a,b; Stephens and Stommel, 1989; Tash, 1989; Bonini *et al.*, 1991).

Neuronal activation of quiescent lateral cilia on *Mytilus* gill is due to 5 HT-triggered augmentation of cellular cAMP levels, leading to cAMP-dependent protein kinase-mediated phosphorylation of axonemal dynein light chains (Stephens and Prior, 1990). Quiescence of lateral cilia is thus believed to reflect lowered cAMP concentration and resultant dephosphorylation of dynein polypeptides. Phosphorylation of axonemal dynein polypeptides has also been reported in other systems (Hamasaki and Satir, 1989; Chilcote and Johnson, 1990; Dey and Brokaw 1991; Stephens and Prior, 1991).

We found that membrane-permeant cAMP analogs stimulate the beating of *Ciona* stigmatal cilia held in a long-lasting inactive state (termed quiescence). Moreover, reactivated beating of stigmatal ciliary models is improved by cAMP and IBMX, or the addition of the catalytic subunit of protein kinase to RS. Reactivation of *Mytilus* lateral ciliary models is also improved by the presence of the catalytic subunit, which can override Ca arrest (Stommel, 1984; Stommel and Stephens, 1985; Stephens and Stommel, 1989). These findings suggest that the quiescence (long-lasting inactivation) of *Ciona* cilia is physiologically similar to the quiescence of *Mytilus* lateral cilia; *i.e.*, that increased cAMP levels may also be responsible for maintaining the activity of *Ciona* stigmatal cilia via cAMP-dependent phosphorylation of regulatory axonemal polypeptides.

Although their underlying biochemical mechanisms seem to be similar, the postures of quiescent *Mytilus* lateral cilia and quiescent *Ciona* sigmatal cilia are quite different. Lateral cilia rest at the end of the recovery stroke, whereas stigmatal cilia stand upright, midway between the effective and recovery strokes.

Ciona cilia thus remain upright during both the transient inactive state and the quiescent or long-lasting inactive state. However, quiescence differs from inactivation, not only by its longer duration, but also by the apparent absence of a preceding arrest.

cAMP and Ca act antagonistically on *Mytilus* lateral cilia, as well as on several other ciliary and flagellar systems (see Brokaw, 1987; Stephens and Stommel, 1989; Bonini *et al.*, 1991). Moreover, cAMP or cAMP-dependent protein kinase can override the Ca effect and activate beating of Ca-arrested cilia (Murakami and Takahashi, 1975; Murakami, 1983; Stommel and Stephens, 1985). Our finding, that adding Ca and cAMP to RS causes rapid vibration or twitching of stigmatal cilia in the straight inactive position, indicates a similar antagonism between cAMP-mediated activation of beating and Ca-induced inactivation (rather than arrest) of cilia.

In conclusion, we have developed an *in vitro* preparation of *Ciona* branchial basket cilia which allows investigation for the first time of the ionic and molecular control of ciliary motility in tunicates. Further studies using improved models should provide more detailed and quantitative information for comparison to other systems.

Acknowledgments

We thank Dr. Ray Stephens, MBL, for helpful discussions and advice, and Signhild Tamm for electron microscopy. Dorothy Hahn patiently and skillfully processed these words. This research fulfilled the requirements for Independent Work of Distinction by DB at the Boston University Marine Program, and was supported by NIH grant GM 27903 to SLT.

Literature Cited

Arkett, S. A. 1987. Ciliary arrest controlled by identified central neurons in a urochordate (Ascidiacea). *J. Comp. Physiol. A* **161:** 837–847.

Arkett, S. A., G. O. Mackie, and C. L. Singla. 1989. Neuronal organization of the ascidian (Urochordata) branchial basket revealed by cholinesterase activity. *Cell Tiss. Res.* **257:** 285–294.

Bergles, D. E., and S. L. Tamm. 1989. Calcium-sensitive ATP-reactivated models of *Ciona intestinalis* branchial basket cilia. *Biol Bull.* **177:** 313.

Bessen, M., R. B. Fay, and G. B. Witman. 1980. Calcium control of waveform in isolated flagellar axonemes of *Chlamydomonas*. *J. Cell Biol.* **86:** 446–455.

Bone, Q., and G. O. Mackie. 1982. Urochordata. Pp. 473–535 in *Electrical Conduction and Behaviour in 'Simple' Invertebrates*, G. A. B. Shelton, ed. Oxford University Press, Oxford, U.K.

Bonini, N. M., T. C. Evans, L. A. P. Miglietta, and D. L. Nelson. 1991. The regulation of ciliary motility in *Paramecium* by Ca^{2+} and cyclic nucleotides. Pp. 227–272 in *Advances in Second Messenger and Phosphoprotein Research*, vol 23, P. Greengard and G. A. Robison, eds. Raven Press, New York.

Brokaw, C. J. 1979. Calcium-induced asymmetrical beating of Triton-demembranated sea urchin sperm flagella. *J. Cell Biol.* **82:** 401–411.

Brokaw, C. J. 1987. Regulation of sperm flagellar motility by calcium and cAMP-dependent phosphorylation. *J. Cell Biochem.* **35:** 175–184.

Brokaw, C. J. 1991. Calcium sensors in sea urchin sperm flagella. *Cell Motil. Cytoskel.* **18:** 123–130.

Brokaw, C. J., R. Josslin, and L. Bobrow. 1974. Calcium ion regulation of flagellar beat symmetry in reactivated sea urchin spermatozoa. *Biochem. Biophys. Res. Commun.* **58:** 795–800.

Brokaw, C. J., and S. M. Nagayama. 1985. Modulation of the asymmetry of sea urchin sperm flagellar by calmodulin. *J. Cell Biol.* **100:** 1875–1883.

Carter, G. S. 1926. On the nervous control of the velar cilia of the nudibranch veliger. *J. Exp. Biol.* **4:** 1–26.

Chilcote, T. J., and K. A. Johnson. 1990. Phosphorylation of *Tetrahymena* 22 S dynein. *J Biol. Chem.* **265:** 17257–17266.

Child, F. M., and S. L. Tamm. 1963. Metachronal ciliary coordination in ATP-reactivated models of *Modiolus* gills. *Biol. Bull.* **25:** 373–374.

Dey, C. S., and C. J. Brokaw. 1991. Activation of *Ciona* sperm motility: phosphorylation of dynein polypeptides and effects of a tyrosine kinase inhibitor. *J. Cell Sci* **100:** 815–824.

Eckert, R., and A. Murakami. 1972. Calcium dependence of ciliary activity in the oviduct of the salamander *Necturus*. *J. Physiol.* **226:** 699–711.

Eckert, R., Y. Naitoh, and H. Machemer. 1976. Calcium in the bioelectric and motor functions of *Paramecium*. *Symp. Soc. Exp. Biol.* **30:** 233–255.

Fedele, M. 1923. Le attivita dinamiche ed i rapporti nervosi nella vita dei Dolioli. *Publ. Staz. Zool. Napoli* **4:** 129–239.

Gibbons, I. R., M. P. Cosson, J. A. Evans, B. H. Gibbons, B. Houck, K. H. Martinson, W. S. Sale, and W.-J. Y. Tang. 1978. Potent inhibition of dynein adenosine triphosphatase and of the motility of cilia and sperm flagella by vanadate. *Proc. Natl. Acad. Sci. USA* **75:** 2220–2224.

Gibbons, B. H., and I. R. Gibbons. 1980. Calcium-induced quiescence in reactivated sea urchin sperm. *J Cell Biol.* **84:** 13–27.

Hamasaki, T., T. J. Murtaugh, B. H. Satir, and P. Satir. 1989. *In vitro* phosphorylation of *Paramecium* axonemes and permeabilized cells. *Cell Motil Cytoskel.* **12:** 1–11.

Hamasaki, T., and P. Satir. 1989. *Paramecium* dynein contains a phosphorylatable 29 kDa light chain. *Cell Motil. Cytoskel.* **11:** 189A.

Holwill, M. E. J., and J. L. McGregor. 1976. Effects of calcium, on flagellar movement in the trypanosome *Crithidia oncopelti*. *J Exp. Biol.* **65:** 229–242.

Hyams, J. S., and G. G. Borisy. 1978. Isolated flagellar apparatus of *Chlamydomonas*: characterization of forward swimming and alteration of waveform and reversal of motion by calcium ions *in vitro*. *J. Cell Sci.* **33:** 235–253.

Izumi, A., and T. Miki-Noumura. 1985. *Tetrahymena* cell model exhibiting Ca-dependent behavior. *Cell Motil.* **5:** 323–331.

Izumi, A., and Y. Nakaoka. 1987. cAMP-mediated inhibitory effect of calmodulin antagonists on ciliary reversal of *Paramecium*. *Cell Motil.* **7:** 154–159.

MacGinitie, G. E. 1939. The method of feeding of tunicates. *Biol Bull* **77:** 443–447.

Machemer, H. 1986. Electromotor coupling in cilia. Pp. 205–250 in *Membrane Control of Cellular Activity*, H. C. Lüttgau, ed. Gustav Fischer Verlag, New York.

Mackie, G. O., D. H. Paul, C. M. Singla, M. A. Sleigh, and D. E. Williams. 1974. Branchial innervation and ciliary control in the ascidian *Corella*. *Proc. R. Soc. Lond. B* **187:** 1–35.

Mogami, Y., K. Fujima, and S. A. Baba. 1991. Five different states of ciliary activity in the epaulette of echinoplutei. *J. Exp. Biol.* **155:** 65–75.

Murakami, A. 1983. Control of ciliary beat frequency in *Mytilus*. *J. Submicrosc. Cytol.* **15:** 313–316.

Murakami, A. 1987a. Control of ciliary beat frequency in the gill of *Mytilus*. I. Activation of the lateral cilia by cyclic AMP. *Comp. Biochem. Physiol.* **86C:** 273–279.

Murakami, A. 1987b. Control of ciliary beat frequency in the gill of *Mytilus*. II. Effects of saponin and Brij-58 on the lateral cilia. *Comp. Biochem. Physiol.* **86C:** 281–287.

Murakami, A., and K. Takahashi. 1975. The role of calcium in the control of ciliary movement in *Mytilus*. II. The effects of calcium ionophores x537A and A23187 on the lateral gill cilia. *J. Fac. Sci. Univ. Tokyo IV* **13:** 251–256.

Murofushi, H., K. Ishiguro, D. Takahashi, J. Ikeda, and H. Sakai. 1986. Regulation of sperm flagellar movement by protein phosphorylation and dephosphorylation. *Cell Motil.* **6:** 83–88.

Naitoh, Y., and H. Kaneko. 1972. Reactivated Triton-extracted models of *Paramecium*: modification of ciliary movement by calcium ions. *Science* **176:** 523–524.

Nakamura, S., and S. L. Tamm. 1985. Calcium control of ciliary reversal in ionophore-treated and ATP-reactivated comb plates of ctenophores. *J. Cell Biol.* **100:** 1447–1454.

Nakaoka, Y., and H. Ooi. 1985. Regulation of ciliary reversal in Triton-extracted *Paramecium* by calcium and cyclic adenosine monophosphate. *J. Cell Sci.* **77:** 185–195.

Opresko, L. K., and C. J. Brokaw. 1983. cAMP-dependent phosphorylation associated with activation of motility of *Ciona* sperm flagella. *Gamete Res.* **8:** 201–218.

Otter, T. 1989. Calmodulin and the control of flagellar movement. Pp. 281–298 in *Cell Movement, vol 1 The Dynein ATPases*, F. D. Warner, P. Satir, and I. R. Gibbons, eds. Alan R. Liss, New York.

Otter, T., B. Satir, and P. Satir. 1984. Trifluoperazine-induced changes in swimming behavior of *Paramecium*: evidence for two sites of drug action. *Cell Motil.* **4:** 249–267.

Preston, R. R., and Y. Saimi. 1990. Calcium ions and the regulation of motility in *Paramecium*. Pp. 173–200 in *Ciliary and Flagellar Membranes*, R. A. Bloodgood, ed. Plenum, New York.

Reed, W., S. Lebduska, and P. Satir. 1982. Effects of trifluoperazine upon the calcium dependent ciliary arrest response of freshwater mussel gill lateral cells. *Cell Motil.* **2:** 405–427.

Salmon, E. D., and R. R. Segall. 1980. Calcium-labile mitotic spindles isolated from sea urchin eggs (*Lytechinus variegatus*). *J. Cell Biol.* **86:** 355–365.

Satir, P. 1985. Switching mechanisms in the control of ciliary motility. *Mod. Cell Biol.* **4:** 1–46.

Sharma, R. K., and J. H. Wang. 1981. Inhibition of calmodulin-activated cyclic nucleotide phosphodiesterase by Triton X-100. *Biochem. Biophys. Res. Commun.* **100:** 710–715.

Stephens, R. E., and E. W. Stommel. 1989. Role of cyclic adenosine monophosphate in ciliary and flagellar motility. Pp. 299–316 in *Cell Movement, vol 1 The Dynein ATPases*, F. D. Warner, P. Satir, and I. R. Gibbons, eds. Alan R. Liss, New York.

Stephens, R. E., and G. Prior. 1990. Cyclic AMP-dependent dynein light chain phosphorylation in neuronally-controlled mussel gill cilia. *J. Cell. Biol* **111:** 295a.

Stephens, R. E., and G. Prior. 1991. Cyclic AMP-dependent phosphorylation of dynein alpha-heavy chains in *Mytilus edulis* sperm flagella. *Biophys. J.* **59:** 567A.

Stommel, E. W. 1984. Calcium activation of mussel gill abfrontal cilia. *J. Comp. Physiol. A* **155:** 457–469.

Stommel, E. W., and R. E. Stephens. 1985. Cyclic AMP and calcium in the differential control of *Mytilus* gill cilia. *J. Comp. Physiol. A* **157:** 451–459.

Takahashi, D., H. Murofushi, K. Ishiguro, J. Ikeda, and H. Sakai. 1985. Phosphoprotein phosphatase inhibits flagellar movement of Triton models of sea urchin spermatozoa. *Cell Struct. Funct.* **10:** 327–337.

Takahashi, D., S. A. Baba, and A. Murakami. 1973. The "excitable" cilia of the tunicate *Ciona intestinalis*. *J. Fac. Sci. Univ. Tokyo IV* **13:** 123–137.

Tamm, S. L. 1988. Calcium activation of macrocilia in the ctenophore *Beroë*. *J. Comp. Physiol. A* **163:** 23–31.

Tash, J. S. 1989. Protein phosphorylation: the second messenger signal transducer of flagellar motility. *Cell Motil. Cytoskel.* **14:** 332–339.

Tsuchiya, T. 1977. Effects of calcium ions on Triton-extracted lamellibranch gill cilia: ciliary arrest in a model system. *Comp. Biochem. Physiol.* **56A:** 353–361.

Walter, M. F., and P. Satir. 1978. Calcium control of ciliary arrest in mussel gill cells. *J. Cell Biol.* **79:** 110–120.

Reference: *Biol. Bull.* **182**: 391–400. (June, 1992)

Slow Photic and Chemical Induction of Bioluminescence in the Midwater Shrimp, *Sergestes similis* Hansen

MICHAEL I. LATZ* AND JAMES F. CASE

Department of Biological Sciences and Marine Science Institute, University of California, Santa Barbara, California 93106

Abstract. The initial luminescent response to photic stimulation of dark-maintained specimens of the midwater shrimp, *Sergestes similis* Hansen, differed from the conventional counterillumination response. Animals were initially unresponsive to light; bioluminescence was only induced after a latency of 3 min. Maximum intensity was reached after approximately 25 min. During the induction process, light emission from the anterior light organs was frequently observed prior to output from the posterior organ. Once luminescence was induced, responses exhibited the typical fast kinetics of the counterillumination response and changes in light organ output occurred synchronously.

Visual input was necessary to maintain this state. Dark readaptation of counterilluminating animals resulted in a return to the slow response kinetics characteristic of untested animals. Because eyestalk ablation or crushing caused immediate production of luminescence in previously untested animals, the slow induction did not involve the ability of the light organs to produce light.

Serotonin was effective in stimulating bioluminescence in intact animals; the induction of light emission proceeded at a rate similar to that for photic stimulation. Other putative neurotransmitters, including norepinephrine, acetylcholine, GABA, and L-glutamic acid, did not stimulate bioluminescence. Isolated light organs exhibited high background levels of light emission, which were unchanged by serotonin treatment. However, serotonin was effective in stimulating luminescence in animals with ablated eyestalks. These results suggest a dual control system involved in the induction and maintenance of bioluminescence in *S. similis*.

Received 31 October 1991; accepted 6 March 1992.

* Present address: Marine Biology Research Division 0202, Scripps Institution of Oceanography, University of California, San Diego, La Jolla, California 92093.

Abbreviations: ACh, acetylcholine; GABA, gamma aminobutyric acid; PCA, p-chloroamphetamine; 5-MT, 5-methoxytryptamine.

Introduction

Marine organisms are vulnerable to predation by upwards-viewing predators that scan for prey silhouetted against downwelling illumination. In some midwater animals, this vulnerability may be reduced by luminescent countershading, or counterillumination, in which downward-directed bioluminescence replaces oceanic light absorbed or reflected by the animal's body (Clarke, 1963; Herring, 1982; Young, 1983). For counterillumination to be optimally effective, light emission must match the spectrum, intensity, and direction of ambient light, so that bioluminescence effectively replaces ambient downward-directed illumination. Strong experimental evidence for a counterillumination role of luminescence exists for midwater squids, fishes, and crustaceans (reviewed by Young, 1983).

Bioluminescence by the decapod shrimp, *Sergestes similis* Hansen, functions in this manner (Warner *et al.*, 1979), counterilluminating the body by matching the spectral distribution (Herring, 1983; Widder *et al.*, 1983), intensity (Warner *et al.*, 1979), and angular distribution (Latz and Case, 1982) of oceanic downwelling illumination. Light emission by *S. similis* associated with counterillumination is stimulated only by downward-directed illumination and can be maintained for long periods (Warner *et al.*, 1979). In the dark, no luminescence is produced for counterillumination.

Little is known of the physiological control of counterillumination. Luminescence by *S. similis* is regulated by visual input; when the eyes are masked, light emission

is absent. Luminescent response latencies to visual stimulation of only a few seconds are consonant with either neural or hormonal control (Warner *et al.*, 1979). Bioluminescence originates from modified portions of the hepatopancreas, the organs of Pesta (Dennell, 1940; Herring, 1981). The mechanism of control of light emission by the organs of Pesta is unclear because the light organs have neither been shown to be innervated nor luminescence to be electrically or chemically excitable (Herring, 1976, 1981).

In other midwater animals, bioluminescence used for counterillumination appears to be under neural control. In squids, morphological and physiological evidence supports direct neural control (Arnold and Young, 1974; Dilly and Herring, 1974; Herring, 1977). The photophores and caudal organs of myctophid fishes are under neural control, even though the chemical basis remains obscure. They are richly innervated and electrically or neurally excitable (reviewed by Herring, 1982).

The present study documents a previously undescribed aspect of counterillumination by *S. similis:* the slow initial induction of luminescence in previously untested, dark-maintained animals, which occurs prior to the counterillumination response. This induction can be mimicked by chemical treatment with the neurotransmitter serotonin. The slow kinetics of photic and chemical induction compared to the typical counterillumination response suggest different mechanisms controlling these responses. Results support the hypothesis that a blood-born factor, perhaps via a neurosecretory pathway, is involved in the induction process.

Materials and Methods

Adult specimens of *Sergestes similis* were collected at night from depths of 75–200 m in the Santa Barbara Basin, near Santa Barbara, California, using a midwater trawl. Trawl contents were recovered under dark conditions on moonless nights and sorted under dim red light. Animals were placed in chilled seawater, brought into the laboratory within 3 h of collection, and were maintained in 100-l aquaria with flow-through, sand-filtered seawater (10°C). All tests were performed within one week of collection, during which time animals remained in good physiological condition and exhibited low mortality. Only actively swimming specimens were used for testing. Except for brief exposure to dim red light during handling, animals remained in constant darkness and were not fed.

For testing, specimens were loosely restrained by a clamp around the cephalothorax and placed in a sealed, clear acrylic chamber (1.75 × 2.5 × 10 cm) filled with 10°C seawater (Fig. 1A). Bioluminescence was induced by downward-directed illumination conducted by a fiber optic light guide from a tungsten-halogen source (Dolan-Jenner Inc.) to a 465 nm interference filter (Ditric Optics, half band width 9.4 nm) and diffused by two opal ground glass plates. Light intensity was regulated by neutral density filters (Rolyn Optics) and measured by a United Detector Technology Inc. 40× Optometer. Stimulus duration was controlled by an electro-mechanical shutter (Vincent Associates) (Fig. 2). Stimulus intensities were comparable to light intensities of $<1 \times 10^{-6}$ to 5×10^{-2} μW cm^{-2} present at daytime depths frequented by *S. similis* in the Santa Barbara Basin (Clarke, 1966).

Photomultiplier recordings

For these long-term experiments, the seawater in the acrylic chamber containing the restrained animal was exchanged at a rate of approximately 50 ml min^{-1}. The apparatus for light stimulation was as described above. Bioluminescence was detected by an EMI 9781B photomultiplier operating at −550 V and fitted with an electromechanical shutter (Fig. 2). The photomultiplier was located 10 cm beneath the animal. The stimulus light and the photomultiplier were isolated by a pair of rotating light choppers (Rofin) producing 5 ms light pulses at 100 Hz, synchronized 180° out of phase with each other and positioned one above and one below the experimental chamber. Consequently, the photomultiplier viewed the specimen in the dark interval between light pulses delivered to the specimen. The test animal perceived the light stimulus as a continuous source, because the chopping rate was greater than the critical flicker fusion frequency of marine crustaceans, which is typically below 60 Hz (Waterman, 1961). The chopped photomultiplier signal was led through a Keithley 427 Current Amplifier, rectified by a Keithley Autoloc 840 Amplifier referenced to the chopping frequency, and displayed on a Grass 79D Polygraph. A photodiode monitored the filtered light stimulus and registered stimulus presentations on the polygraph record.

Specimens in the chamber were acclimated in the dark for at least 20 min following handling under dim red light. They were then subjected to light stimuli ranging from 2×10^{-5} to 4×10^{-4} μW cm^{-2}.

The intensity of bioluminescence was measured from the polygraph record as amount of baseline shift corrected for dark current, and expressed as photomultiplier anode current. The apparatus was not calibrated for luminescent output in irradiance units.

Image intensification

Bioluminescence from restrained animals was viewed from below with an image intensifier (EMI Type 9912, four-stage, maximum radiant power gain 10^6 at 440 nm), fitted with a 75 mm f/1.9 objective lens, by means of a first-surface mirror positioned beneath the chamber at

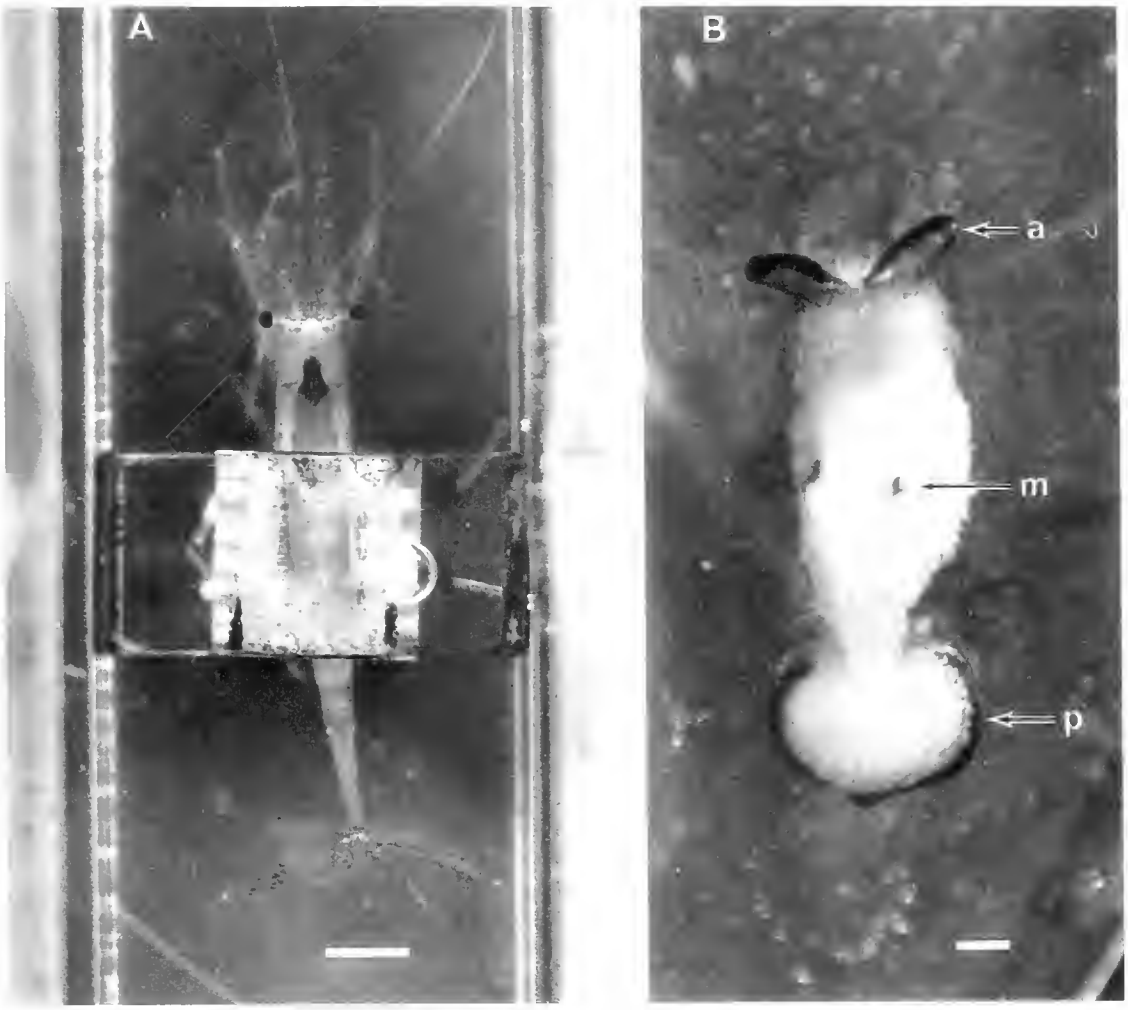

Figure 1. Views of intact and dissected preparations of *Sergestes similis*. (A) Dorsal view of living intact specimen restrained in testing chamber. Specimen was loosely clamped about the midregion of the body during experimentation. Immediately anterior to the clamp is the hepatopancreas and foregut. The chamber was superfused with chilled (10°C) filtered seawater. Scale bar = 5 mm. (B) Ventral view of isolated hepatopancreas showing locations of luminous tissue. Dark pigmentation characteristic of the luminous tissue (arrows) is associated with the (a) anterolateral pair of organs of Pesta, (m) lateral midgastric pair of organs, and (p) posterior fringe organ. Scale bar = 1 mm.

an angle of 45°. Typical operating voltage was 34 kV. The anode phosphor of the image intensifier was viewed by a Panasonic newvicon video camera with a 25 mm f/0.95 objective lens, and images were recorded on videotape together with a time and video frame reference. The apparatus for stimulus illumination was as described above.

The chamber containing a restrained animal was positioned in the dark in the experimental apparatus. During experiments, the stimulus intensity was either 1×10^{-5} or 2×10^{-4} μW cm^{-2}. At one-minute intervals, the stimulus was briefly extinguished to permit documentation of bioluminescence.

Chemical stimulation

The physiological basis of the slow photic induction of bioluminescence was further investigated with tests of putative invertebrate neurotransmitters. For this study, specimens of *S. similis* were collected during the day from the Santa Barbara Basin and thereafter maintained in darkness and handled under dim red light. Intact live animals were restrained in the test chamber. In some cases, the hepatopancreas tissue with attached light organs was isolated by dissection, pinned in a clear dish layered with Sylgard, and placed in the test chamber. In some specimens, both eyestalks were ablated at their bases with iridectomy scissors prior to chemical testing. Bioluminescence

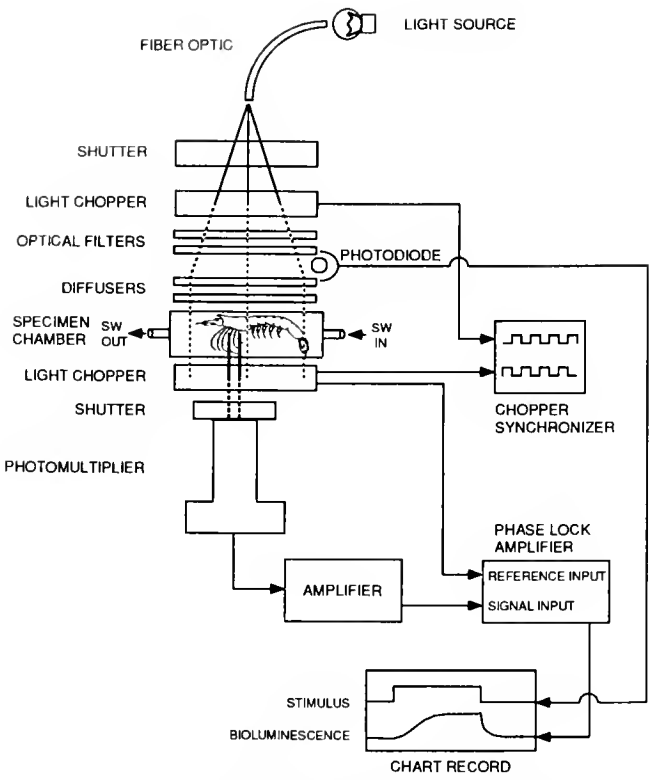

Figure 2. Schematic of experimental apparatus used to measure the intensity of bioluminescence during counterillumination. The specimen in the testing chamber superfused with chilled seawater (SW) was subjected to a diffuse downward-directed illumination of controlled intensity and wavelength, pulsed at approximately 100 Hz by a light chopper (dashed lines above specimen). Downward-directed luminescence (solid lines below specimen) was chopped (dashed lines below specimen) by a second light chopper, synchronized 180° out of phase with the stimulus chopper, and was detected by a photomultiplier. The second light chopper prevented the stimulus illumination from reaching the detector. The bioluminescence signal was amplified, rectified by a lock-in amplifier, and displayed on a chart recorder along with a stimulus record obtained from a photodiode monitoring the stimulus illumination. Not drawn to scale.

cence was detected from below the chamber by an EMI 9701B photomultiplier operating at −750 V and fitted with an electromechanical shutter. The photomultiplier signal was amplified by a Keithley 427 Current Amplifier and displayed on a Grass 79D Polygraph. Levels of light emission were expressed as PMT anode current, without radiometric calibration.

The action of neurotransmitters was assayed with intact specimens or isolated hepatopancreas tissue containing the organs of Pesta. The following solutions were prepared in filtered seawater: 1×10^{-3} *M* acetylcholine (ACh), 1×10^{-3} *M* gamma aminobutyric acid (GABA), 1×10^{-3} *M* L-glutamic acid, 1×10^{-3} *M* norepinephrine, and 5.7×10^{-4} *M* serotonin creatinine phosphate (5-hydroxytryptamine). In addition, the following combinations of serotonin and serotonin-specific chemicals were tested: 5.7×10^{-4} *M* serotonin plus 1.5×10^{-5} *M* cinanserin (Squibb 10,643 cinnamanilide hydrochloride), a serotonin antagonist; 5.7×10^{-4} *M* serotonin plus 1.3×10^{-3} *M* fluoxetine, a serotonin uptake inhibitor; 10^{-4} g/ml p-chloroamphetamine (PCA), a serotonin releasing agent; and 1×10^{-3} *M* 5-methoxytryptamine (5-MT), the precursor to serotonin (see Fuller, 1982). The control consisted of filtered seawater alone. All solutions were prepared in advance and frozen in glass vials in 50 ml aliquots until time of use. For testing, vials were thawed and solutions equilibrated to 10°C prior to filling the experimental chamber. Intact specimens or isolated hepatopancreas tissue were then immersed in the test solution. Permeability of solutions to the site of action was not considered to be a problem with this protocol because it has been successfully used on euphausiids and shrimps treated with serotonin, cinanserin, and other compounds (Herring, 1976; Herring and Locket, 1978).

The kinetics of the luminescent responses were described according to the following terms: latency, the time period from presentation or termination of stimulus to beginning of response; half rise, time from stimulus presentation to half maximum response amplitude; half decay time, time from stimulus termination to half maximum response amplitude. Unless otherwise stated, values are stated as mean ± standard error of the mean.

Parametric statistical tests included the two-sample T test and one-factor analysis of variance, while the Mann-Whitney U test and Kruskal-Wallis test were used for nonparametric comparisons. All statistical tests were performed using Statview software (Abacus Concepts, Inc.).

Results

Photic stimulation

The luminescent response of restrained specimens of *Sergestes similis* to photic stimulation depended upon the degree of recent light exposure. Previously untested animals responded differently from counterilluminating specimens.

The typical counterillumination response to a dim photic stimulus (Fig. 3A) displayed a latency of 2 s and reached half maximum intensity within 13 s (Table I). Generally, steady-state emission was achieved within 25 s. Luminescent intensity remained stable while the stimulus was maintained. Upon termination of the stimulus, luminescence was rapidly extinguished after a latency of 1 s (Table I). The kinetics of the counterillumination responses in the present study were similar to those previously measured (Warner *et al.*, 1979).

These responses were not present in previously untested, dark acclimated specimens of *S. similis*. There was a latency period of several minutes during which no lu-

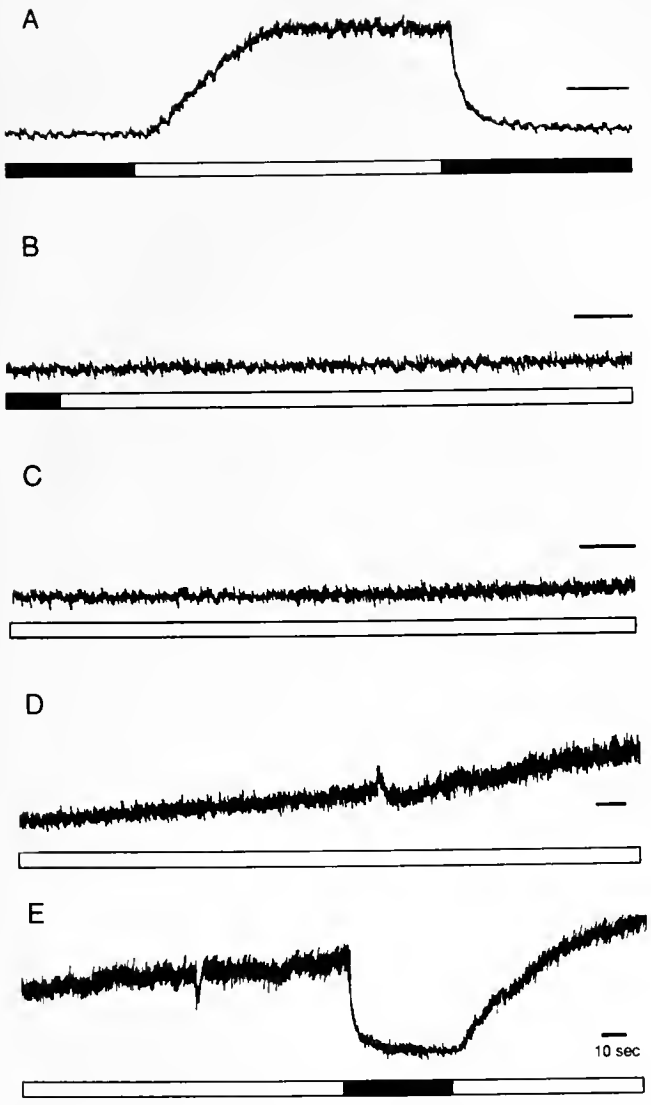

Figure 3. Comparison of counterillumination and slow photic induction of bioluminescence. For each trace of the chart recorder record, the upper trace is the bioluminescence record, with an upward deflection indicated increasing levels of light emission; the lower trace monitors stimulus illumination, with a solid bar indicating no photic stimulus and a clear bar representing stimulus "on." (A) Counterillumination in response to stimulus illumination of 1×10^{-3} μW cm^{-2}. Steady luminescence was produced only when the light stimulus was present, and was rapidly extinguished at the end of stimulation. (B–E) Slow photic induction of bioluminescence in a previously untested, dark-acclimated animal, illuminated by a maintained light stimulus with an intensity of 2×10^{-4} μW cm^{-2} (clear bar). Dim bioluminescence slowly increased in intensity until termination of the stimulus midway through (E) (dark bar), which produced a rapid extinguishing of luminescence. The subsequent photic stimulus (clear bar) resulted in rapid "on" kinetics similar to those of counterillumination in (A).

minescence was produced; subsequently, light emission slowly increased (Fig. 3). Based on photomultiplier measurements, light emission was first detected 3.3 ± 0.7 min (range 2–5 min) after stimulus initiation. Luminescence reached half maximum intensity after 12 min; maximum steady light output occurred after approximately 25 min of illumination (Table I).

Image intensification confirmed that light emission originated from the organs of Pesta (Figs. 1B, 4). Based on observations of 31 previously untested animals, luminescence was induced in the anterior organs 2.4 ± 0.3 min (mean ± standard error) after presentation of the light stimulus, and in the posterior organs 3.6 ± 0.5 min after the beginning of stimulation. Even though there was no statistical significance to the earlier onset of emission by the anterior organs (paired-sample t test, t = 0.86, $P > 0.20$), this trend was observed in more than 60% of the specimens tested. In most cases, the anterior light organs were the brightest, and light emission from the midgastric organs was very dim if detected at all.

Once luminescence was induced, an animal was capable of subsequent responses with fast kinetics typical of the counterillumination response. Termination of the initial photic stimulus resulted in a rapid extinguishing of luminescence (Fig. 3E) after a latency of 1 s. The kinetics of the induction "off" response did not significantly differ from those of the counterillumination "off" response (Table I). All subsequent photic stimulation resulted in light emission with rapid response kinetics. An "on" response latency of 2 s and time to maximum intensity of 25 s was similar to those of conventional counterillumination responses. Image intensifier observations under these conditions indicated that once luminescence was induced, the light organs invariably responded synchronously to stimulus "on" and "off."

Photic stimulation was needed not only for induction of the counterillumination response, but also to maintain this state. Preliminary observations indicated that after 1 h of darkness, a previously counterilluminating animal underwent a new induction process similar to those of untested specimens. Subsequent to this, counterillumination was regained.

Eye glow, indicative of the dark-adapted eye state (Ball *et al.*, 1986), was observed prior to testing in 5 of 6 dark-maintained specimens, but was absent after testing. Animals adapted to a light intensity of 1×10^{-2} μW cm^{-2} (an intensity higher than that present in their depth range: Clarke, 1966) did not exhibit eye glow (0 of 4 specimens), suggesting that the eye is light adapted at this level of illumination. The threshold for light adaptation was not determined.

Chemical stimulation

Serotonin was the only neurotransmitter tested that was effective in producing bioluminescence (Fig. 5). Maximum levels of light emission from intact animals immersed in 5.7×10^{-4} M serotonin were significantly dif-

Table I

Kinetics of the luminescent responses of Sergestes similis

Condition	"On" latency (s)*	Half rise time (s)*	"Off" latency (s)†	Half decay time (s)†
Induction	198.0 ± 39.0 (4)	750.0 ± 86.6 (3)	1.3 ± 0.8 (2)	2.5 ± 1.5 (2)
Counterillumination	2.2 ± 0.2 (11)	12.8 ± 1.2 (11)	0.9 ± 0.1 (10)	1.6 ± 0.1 (11)

* Mean values for induction and counterillumination conditions are significantly different (Two-sample T test, $t \geq 9.497$, $P < 0.001$).
† No significant difference between means for test conditions ($t \leq 1.584$, $P > 0.10$).
Values represent means with standard errors of the mean; number of observations given in parentheses.

ferent from seawater controls (Mann-Whitney U test, U = 42, $P < 0.01$). The average temporal response consisted of a latency of 6.0 ± 0.5 min followed by a slow increase to maximum intensity that was reached in 26.7 ± 3.5 min (Fig. 6B). These response kinetics are similar to those for luminescent induction by photic stimulation.

Treatment with the neurotransmitters acetylcholine, GABA, L-glutamic acid, and norepinephrine did not result in levels of bioluminescence significantly different from seawater controls (Mann-Whitney U-test, $P > 0.1$) (Fig. 5).

The specificity of serotonin in stimulating bioluminescence was further investigated (Fig. 5). A solution of serotonin and fluoxetine, a serotonin uptake inhibitor, did not produce significantly higher levels of light emission compared to serotonin alone (Mann-Whitney U test, U = 18, $P > 0.5$), nor did a solution of serotonin and cinanserin, a serotonin antagonist, produce significantly lower levels of light emission (Mann-Whitney U test, U = 18, $P > 0.1$). There was no difference in the response latencies for these conditions from that of serotonin alone (Kruskal-Wallis test, $P > 0.05$). Treatment with PCA, a serotonin releasing agent, and 10^{-3} *M* 5-MT, a serotonin agonist, did not result in significant production of luminescence (Mann-Whitney U-test, $P > 0.2$).

Isolated hepatopancreas tissue containing the light organs produced background levels of luminescence that were significantly higher than for intact animal seawater controls (Fig. 5, 6C) (Mann-Whitney U-test, U = 55, $P < 0.01$). Treatment of the isolated tissue with serotonin did not significantly alter the control glowing (Mann-Whitney U-test, U = 25, $P > 0.5$).

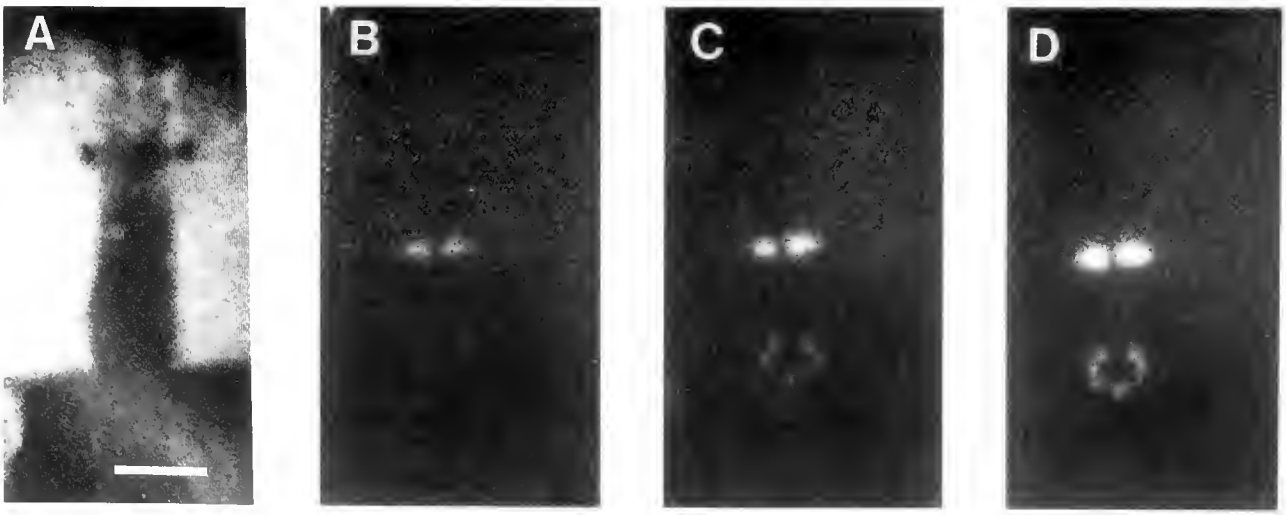

Figure 4. Image intensifier views of slow photic induction of bioluminescence. Photographs of ventral views of an animal were made from single fields of the video record. (A) View of cephalothorax of an intact restrained specimen (clamp at bottom) under dim red light illumination. Anterior end is up. Bioluminescence was observed (B) 2 min, (C) 3 min, and (D) 6.5 min after the beginning of maintained light stimulation, showing emission initially from the anterior organs of Pesta, and then dimmer emission from the posterior light organ. For (B–D) the stimulus light was briefly extinguished for photographic documentation. Scale bar in (A) = 5 mm.

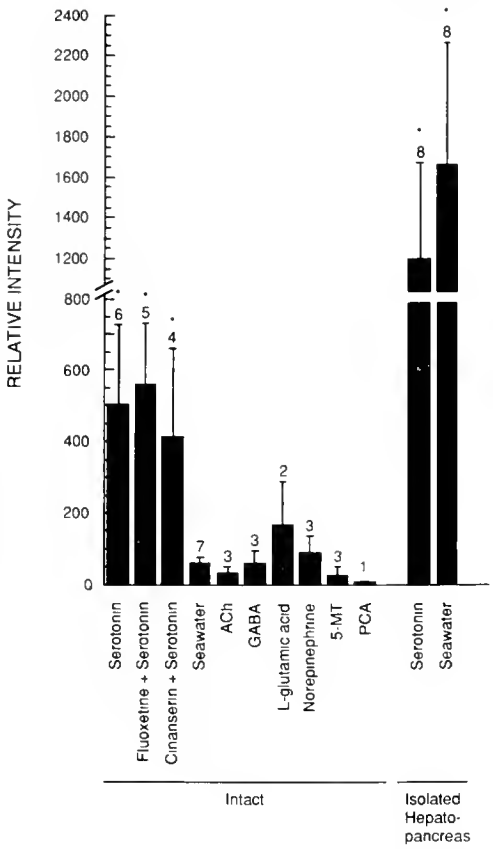

Figure 5. The effect of chemical treatment on bioluminescence. For each experiment, the maximum relative intensity of light emission in the initial 35 min of stimulation was determined. Concentrations of solutions are given in Materials and Methods. Mean intensities with standard errors of the mean are shown for each condition; the number of treatments is displayed above each bar. An (*) indicates that the experimental treatment produced bioluminescence significantly different from seawater control levels in intact animals (Mann-Whitney U test, $P < 0.05$).

Effect of eyestalk manipulation

Squeezing or ablating the eyestalks of previously untested animals immediately evoked luminescence. It was not possible to obtain response latency values as the PMT shutter was closed during the eyestalk manipulation. However, when the shutter was opened 5 s following the procedure, light emission was present.

Serotonin treatment was effective in animals with ablated eyestalks (Fig. 7). In one experiment, eyestalkless animals treated with serotonin produced a higher intensity of light emission than the serotonin-stimulated luminescence of intact specimens (Mann-Whitney U test, U = 40, $P < 0.01$). Squeezing a single eyestalk of intact serotonin-induced luminescing animals immediately increased light emission by more than a factor of 2 (n = 3).

Discussion

The responses to light of previously untested, dark-maintained specimens of *Sergestes similis* clearly differed from the typical counterillumination responses ascribed to this species (Warner *et al.*, 1979). Previously untested animals generated no detectable luminescence for several minutes after initial photic stimulation; subsequently, light emission increased to a maximum and steady level approximately 25 min later. However, once induced, subsequent luminescent responses displayed the rapid kinetics typical of the counterillumination response. The different

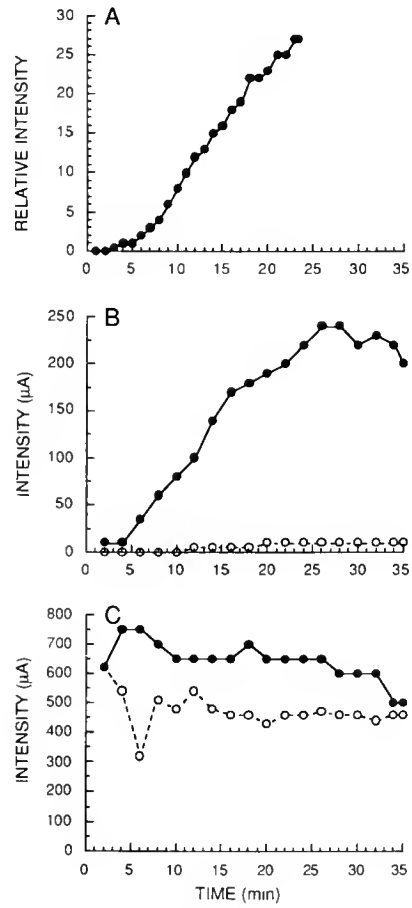

Figure 6. The comparison of slow induction of bioluminescence by photic and serotonin stimulation. The intensity of emission is shown as a function of time of stimulation. (A) The response of an uninduced dark-adapted specimen to initial photic stimulation with a light intensity of 4×10^{-4} μW cm^{-2}. Bioluminescence is expressed in relative units. (B–C) Luminescent responses (expressed as PMT anode current in μA) to treatment with 5.7×10^{-4} *M* serotonin and seawater controls. (B) Responses of intact animals. Serotonin was effective in producing a slow rise in light emission (solid circles), while seawater was ineffective (open circles). (C) Tests with isolated hepatopancreas tissue containing the luminescent organs of Pesta. Serotonin treatment (solid circles) did not increase luminescence above initial high background levels. Seawater control levels (open circles) were higher than controls for intact animals (open circles in B).

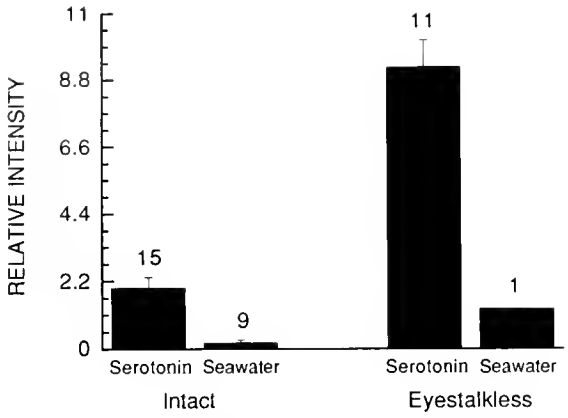

Figure 7. The effect of bilateral eyestalk ablation on bioluminescence. The mean intensity of maximum light emission produced in the first 35 min of stimulation is shown along with standard errors of the mean. All serotonin treatments were significantly different from seawater controls (Mann-Whitney U test, $P < 0.01$). The serotonin response of eyestalkless animals was significantly different from that of intact specimens (Mann-Whitney U test, $P < 0.01$).

kinetics of the induction and counterillumination responses suggest dual control mechanisms regulating light emission.

One mechanism for control of bioluminescence in *S. similis* may involve a neuronal pathway. Evidence for neural control includes: (1) the immediate production of luminescence upon eyestalk ablation of previously untested animals, and (2) the immediate increase in light emission following pinching of an eyestalk of an actively luminescing specimen.

The kinetics of the counterillumination response in *S. similis* are consonant with those of neurally controlled systems. Direct electrical stimulation of the spinal cord of myctophid fishes results in luminescent response latencies of 15 s or less (Anctil, 1972; Barnes and Case, 1974). Intact counterilluminating myctophids exhibit average response latencies of 1 to 18.5 s (Case *et al.*, 1977), with a half rise time of 12 s and a half decay time of 1–2 s (Young *et al.*, 1979). Even though at present there is no morphological evidence for innervation of the organs of Pesta of *S. similis* (Herring, 1981), the kinetics of the counterillumination response of *S. similis* (half rise time of 12.8 s, half decay time of 1.6 s) are similar to those of the neurally controlled myctophid control system.

The long latency and slow increase in emission intensity during the induction process suggest a different control mechanism active during this period. Several features of the induction process support the involvement of a blood-born or neurosecretory pathway: (1) Photic induction of bioluminescence occurred at a similar rate to chromatophore pigment dispersion in crustaceans, where an increase in illumination causes release of erythrophore pigment dispersing hormone (reviewed by Rao, 1985). (2) Bioluminescence is stimulated by serotonin, which is a known crustacean hormone releasing factor (reviewed by Rao, 1985; Fingerman, 1987). (3) The loss of the counterillumination state in *S. similis* after dark re-adaptation may be due to the clearing of a blood-born substance, similar to the return to the dark-adapted state of the crustacean eye via gradual clearing of light-adapting hormone from the hemolymph (Brown *et al.*, 1952). Initial observations confirmed that eye glow in untested specimens of *S. similis*, which indicated a dark-adapted eye state (Ball *et al.*, 1986), was absent after testing, indicating a change to the light-adapted eye state. (4) The induction process did not appear to involve the light-producing ability of the photogenic cells, because the light organs of uninduced specimens produced immediate luminescence upon squeezing or ablating the eyestalks.

A bioluminescence induction process has not been described for other counterilluminating midwater animals. Some species of shallow-living leiognathid fishes of the Indo-Pacific exhibit an initial slow rise in light emission, proportional to the previous period of dark adaptation, although this is due to chromatophore modulation of light organ transparency rather than physiological regulation of the production of luminescence (McFall-Ngai and Morin, 1991; McFall-Ngai, pers. comm.). Perhaps a more analogous phenomenon is arousal in the firefly *Photuris*, which, if stimulated during daytime, requires 15 to 30 s before flashes can be generated. During this period, the light organ glows with increasing intensity and, finally, flashing capability is established just after a rapid quenching of the glow (Case and Buck, 1963).

The adaptive significance of an uninduced state and the slow induction of bioluminescence is obscure. *S. similis* does perform diurnal vertical migrations (*e.g.*, Clarke, 1966; Pearcy and Forss, 1969; Omori and Gluck, 1979) during which it apparently follows a particular isolume (Clarke, 1966). Continuous exposure to dim downwelling illumination would serve to maintain animals in the active counterilluminating condition. On moonless nights, when levels of downwelling illumination would be undetectable and counterillumination unnecessary, animals would revert to the uninduced condition. This might prevent inadvertent luminescent responses to the luminescent displays of other animals and thereby reduce the chance of being detected by predators. Although *S. similis* can respond to light pulses as short as 2 s in duration (Warner *et al.*, 1979), it is not known if it responds to shorter duration stimuli typical of luminescent flashes.

The role of light in the induction of counterillumination in *S. similis* differs from light pulses that produce bursts of luminescence in some organisms. For the shrimp *Thalassocaris* (Herring and Barnes, 1976), copepod *Metridia longa* (Lapota *et al.*, 1986), ostracods (Tsuji *et al.*, 1970;

Morin, 1986), and pyrosomes (Bowlby *et al.*, 1990) a photic stimulus acts as a trigger to release luminescent behavior. In contrast, the long time course of luminescent induction in *S. similis* suggests a longer-term change in physiological state occurring during the induction process.

Salient features of the *S. similis* luminescent system are similar to those of euphausiids. In euphausiids, light emission is stimulated by bright light or strobe illumination after a latency of several minutes. Serotonin is the only neurotransmitter that stimulates light emission in euphausiids, with a latency of 5 to 15 min (reviewed by Herring and Locket, 1978). This response occurs only in intact animals; isolated photophores treated with serotonin do not luminesce (Herring and Locket, 1978). Although the euphausiid control system has not been fully elucidated, it is believed to involve control of blood flow through the photophores by innervated sphincters (Harvey, 1977; Herring and Locket, 1978).

Serotonin is present in the tissues of many marine invertebrates (reviewed by Walker, 1984), and has been detected in the eyestalks, cerebral ganglia (brain), ventral nerve cord, and hemolymph of crustacea (*e.g.*, Fingerman *et al.*, 1974; Elofsson *et al.*, 1982; Laxmyr, 1984). It is well known to act on the crustacean neuromuscular junction by increasing neurotransmitter release (reviewed by Kravitz *et al.*, 1985). Serotonin also acts on neurosecretory cell terminals in the sinus gland of the crustacean eyestalk. It mediates the release of a putative neurodepressing hormone, a putative molt-inhibiting hormone, the hyperglycemic hormone, and a red chromatophore pigment dispersing hormone from neurosecretory cells in the eyestalk (reviewed by Rao, 1985; Fingerman, 1987). The pigment dispersing hormone is effective only in intact animals; direct treatment of serotonin on erythrophores in isolated legs or carapace has no effect (Nagabhushanam *et al.*, 1987; reviewed by Fingerman, 1987). This hormone also acts to cause migration of the retinal distal pigment to the light-adapted state (Kleinholz, 1975).

There are no marine luminescent systems in which direct hormonal control of light emission has been demonstrated. Direct innervation of squid and euphausiid light organs occurs even when the photophores receive a rich blood supply through an extensive capillary network (Arnold and Young, 1974; Herring and Locket, 1978). Control of leiognathid bioluminescence through muscular shutters may be fine-tuned through the action of chromatophores with slow response times (McFall-Ngai and Morin, 1991), which are presumably under neural control.

The present data suggest at least two sites involved in the control of bioluminescence in *S. similis*. The eyestalk contains the photoreceptors that detect downward-directed illumination, and associated efferent neural or neurosecretory cells. The responses of eyestalkless animals to serotonin suggest an additional control site, possibly located in the central ganglia. Furthermore, spontaneous light emission from isolated light organs suggests inhibitory control of light emission. The close coupling of vision and bioluminescence in *S. similis* may be achieved via a hormonal component simultaneously active in the visual and luminescent systems.

Acknowledgments

We are most grateful for the assistance of S. Willason, K. Johnson, T. Frank, and M. Jess during nocturnal collecting, M. Jess, D. Rupp, and G. Hallock with manuscript preparation, and P. Herring, J. Morin, and M. Grober for comments on the manuscript. Cinanserin was a gift of E.R. Squibb and Sons, Inc. Supported by Office of Naval Research contracts N00014-75-C-0242 (to JFC), N00014-89-J-1477 (to MIL), and University of California faculty research funds.

Literature Cited

Anctil, M. 1972. Stimulation of bioluminescence in lanternfishes (Myctophidae). II. *Can. J. Zool.* **50:** 233–237.

Arnold, J. M., and R. E. Young. 1974. Ultrastructure of a cephalopod photophore. I. structure of the photogenic tissue. *Biol. Bull.* **147:** 507–521.

Ball, E. E., L. C. Kao, R. C. Stone, and M. F. Land. 1986. Eye structure and optics in the pelagic shrimp *Acetes sibogae* (Decapoda, Natantia, Sergestidae) in relation to light-dark adaptation and natural history. *Phil. Trans. R. Soc. Lond. B* **313:** 251–270.

Barnes, A. T., and J. F. Case. 1974. The luminescence of lanternfish (Myctophidae): spontaneous activity and responses to mechanical, electrical, and chemical stimulation. *J. Exp. Mar. Biol. Ecol.* **15:** 203–221.

Bowlby, M. R., E. A. Widder, and J. F. Case. 1990. Patterns of stimulated bioluminescence in two pyrosomes (Tunicata: Pyrosomatidae). *Biol. Bull* **179:** 340–350.

Brown, F. A., M. Fingerman, and M. N. Hines. 1952. Alterations in the capacity for light and dark adaptation of the distal retinal pigment of *Palaemonetes*. *Physiol. Zool.* **25:** 230–239.

Case, J. F., and J. Buck. 1963. Control of flashing in fireflies. II. Role of central nervous system. *Biol. Bull.* **125:** 234–250.

Case, J. F., J. Warner, A. T. Barnes, and M. Lowenstine. 1977. Bioluminescence of lantern fish (Myctophidae) in response to changes in light intensity. *Nature* **265:** 179–181.

Clarke, W. D. 1963. Function of bioluminescence in mesopelagic organisms. *Nature* **198:** 1244–1246.

Clarke, W. D. 1966. Bathyphotometric studies of the light regime of organisms of the deep scattering layers. A.E.C. Research and Development Rep. UC-48, Biology and Medicine. 47 pp.

Dennell, R. 1940. On the structure of the photophores of some decapod crustacea. *Discovery Rep.* **20:** 307–382.

Dilley, P. N., and P. J. Herring. 1974. The ocular light organ of *Bathothauma lyromma* (Mollusca: Cephalopoda). *J. Zool. Lond.* **172:** 81–100.

Elofsson, R., L. Laxmyr, E. Rosengren, and Ch. Hanson. 1982. Identification and quantitative measurements of biogenic amines and DOPA in the central nervous system and haemolymph of the crayfish *Pacifastacus* leniusculus (Crustacea). *Comp. Biochem. Physiol.* **71C:** 195–201.

Fingerman, M. 1987. The endocrine mechanisms of crustaceans. *J. Crustacean Biol.* **7:** 1–24.

Fingerman, M., W. E. Julian, M. A. Spirtes, and R. M. Kostrezewa. 1974. The presence of 5-hydroxytryptamine in the eyestalks and brain of the fiddler crab *Uca pugilator*, its quantitative modification by pharmacological agents, and possible role as a neurotransmitter in controlling the release of red pigment-dispersing hormone. *Comp. Gen. Pharmacol.* **5:** 299–303.

Fuller, R. W. 1982. Drugs acting on serotonergic neuronal systems. Pp. 221–247 in *Biology of Serotonergic Transmission*, N. N. Osborne, ed. John Wiley & Sons, New York.

Harvey, B. J. 1977. Circulation and dioptric apparatus in the photophores of *Euphausia pacifica*: some ultrastructural observations. *Can. J. Zool.* **55:** 884–889.

Herring, P. J. 1976. Bioluminescence in decapod crustacea. *J. Mar. Biol. Assoc. U.K.* **56:** 1029–1047.

Herring, P. J. 1977. Luminescence in cephalopods and fish. *Symp. Zool. Soc., Lond.* **38:** 127–159.

Herring, P. J. 1981. The comparative morphology of hepatic photophores in decapod crustacea. *J. Mar. Biol. Assoc. U.K.* **61:** 723–737.

Herring, P. J. 1982. Aspects of the bioluminescence of fishes. *Oceanogr. Mar. Biol. Ann. Rev.* **20:** 415–470.

Herring, P. J. 1983. The spectral characteristics of luminous marine organisms. *Proc. R. Soc. Lond.* **220:** 183–217.

Herring, P. J., and A. T. Barnes. 1976. Light-stimulated bioluminescence of *Thalassocaris crinita* (Dana) (Decapoda, Caridea). *Crustaceana* **31:** 107–110.

Herring, P. J., and N. A. Locket. 1978. The luminescence and photophores of euphausiid crustaceans. *J. Zool., Lond.* **186:** 431–462.

Kleinholz, L. H. 1975. Purified hormones from the crustacean eyestalk and their physiological specificity. *Nature* **258:** 256–257.

Kravitz, E. A., B. Beltz, S. Glusman, M. Goy, R. Harris-Warrick, M. Johnston, M. Livingstone, T. Schwartz, and K. King Siwicki. 1985. The well-modulated lobster. The roles of serotonin, octopamine, and proctolin in the lobster nervous system. Pp. 339–360 in *Model Neural Networks and Behavior*, A. I. Selverston, ed. Plenum Press, New York.

Lapota, D., J. R. Losee, and M. L. Geiger. 1986. Bioluminescence displays induced by pulsed light. *Limnol. Oceanogr.* **31:** 887–889.

Latz, M. I., and J. F. Case. 1982. Light organ and eyestalk compensation to body tilt in the luminescent midwater shrimp, *Sergestes similis*. *J. Exp. Biol.* **98:** 83–104.

Laxmyr, L. 1984. Biogenic amines and dopa in the central nervous system of decapod crustaceans. *Comp. Biochem. Physiol.* **77C:** 139–143.

McFall-Ngai, M., and J. G. Morin. 1991. Camouflage by disruptive illumination in Leiognathids, a family of shallow-water, bioluminescent fishes. *J. Exp. Biol.* **156:** 119–137.

Morin, J. G. 1986. "Firefleas" of the sea: luminescent signaling in marine ostracode crustaceans. *The Florida Entomol.* **69:** 105–121.

Nagabhushan, R., R. Sarojini, and S. M. Kandharkar. 1987. Action of biogenic amine on crustacean chromatophores. Analysis of response of erythrophores in the prawn *Caridina rajadhari* to serotonin. *J. Anim. Morphol. Physiol.* **34:** 83–88.

Omori, M., and D. Gluck. 1979. Life history and vertical migration of the pelagic shrimp *Sergestes similis* off the Southern California coast. *Fish. Bull.* **77:** 183–198.

Pearcy, W. G., and C. A. Forss. 1969. The oceanic shrimp *Sergestes similis* off the Oregon coast. *Limnol. Oceanogr.* **14:** 755–765.

Rao, K. R. 1985. Pigmentary Effectors. Pp. 395–462 in *The Biology of Crustacea, Vol. 9. Integument, Pigments and Hormonal Processes*, D. E. Bliss, and L. H. Mantel, eds. Academic Press, Orlando, FL.

Tsuji, F. I., R. V. Lynch, and Y. Haneda. 1970. Studies on the bioluminescence of the marine ostracod crustacean *Cypridina serrata*. *Biol. Bull.* **139:** 386–401.

Walker, R. J. 1984. 5-Hydroxytryptamine in invertebrates. *Comp. Biochem. Physiol.* **79C:** 231–235.

Warner, J. A., M. I. Latz, and J. F. Case. 1979. Cryptic bioluminescence in a midwater shrimp. *Science* **203:** 1109–1110.

Waterman, T. H. 1961. Light sensitivity and vision. Pp. 1–64 in *The Physiology of Crustacea*, T. H. Waterman, ed. Academic Press, New York.

Widder, E. A., M. I. Latz, and J. F. Case. 1983. Marine bioluminescence spectra measured with an optical multichannel detection system. *Biol. Bull.* **165:** 791–810.

Young, R. E. 1983. Oceanic bioluminescence: an overview of general functions. *Bull. Mar. Sci.* **33:** 829–845.

Young, R. E., C. F. E. Roper, and J. F. Walters. 1979. Eyes and extraocular photoreceptors in midwater cephalopods and fishes: their roles in detecting downwelling light for counterillumination. *Mar. Biol.* **51:** 371–380.

Reference: *Biol. Bull.* **182**: 401–408. (June, 1992)

Evidence for Ammonia as a Natural Cue for Recruitment of Oyster Larvae to Oyster Beds in a Georgia Salt Marsh

W. K. FITT[1] AND S. L. COON[2]

[1]*Department of Zoology, University of Georgia, Athens, Georgia 30602 and* [2]*Department of Microbiology and Center of Marine Biotechnology, University of Maryland, College Park, Maryland 20742*

Abstract. Competent veliger larvae of the oysters *Crassostrea virginica* and *C. gigas* exhibited settlement behavior when exposed to ammonia (NH_3). The threshold for this response decreased with increasing larval age. The response of veligers to adult-conditioned seawater was correlated with the concentration of NH_3 in the seawater. Although the concentrations of NH_3 found in marsh water flowing over oyster beds on Sapelo Island, Georgia, were never high enough to elicit settlement behavior from oyster larvae, the concentrations found near the substrate were sufficient to induce settlement behavior in older larvae of *C. virginica*. In addition, dilution occurs during sampling in the field and may lead one to underestimate, by a factor of 1.7 to 3.5, the actual concentration of NH_3 associated with surfaces. In conclusion, NH_3 may be an important environmental cue triggering settlement behavior of larval oysters, which, along with other substrate cues, leads to cementation and metamorphosis.

Introduction

As a prelude to attachment and metamorphosis, veliger larvae of oysters exhibit a set of specific behavioral responses known as settlement behavior. This behavior is induced by a variety of chemicals, including L-3,4-dihydroxyphenylalanine (L-DOPA) which is known to activate larval endogenous dopaminergic neural pathways (Coon *et al.*, 1985; Bonar *et al.*, 1990). Recent laboratory experiments showed that ammonia (NH_3) also induces settlement behavior of oyster larvae that are competent to undergo metamorphosis (see Coon *et al.*, 1990a), but by a different mechanism, possibly involving pH-induced depolarization of nerve cells (Coon *et al.*, 1990a,b). A similar mechanism is thought to be involved in the ammonia and bacterial induction of settlement and metamorphosis of echinoid larvae (Gilmour, 1991; pers. com.). Although most organisms release ammonia as a by-product of metabolism, and the anaerobic muds characterizing oyster habitats usually contain high concentrations of ammonia, the potential importance of ammonia from these sources for settlement of oysters is not known. The presence of bacterial films on surfaces is often correlated with oyster settlement and metamorphosis, suggesting that one or more cues associated with either the bacteria or their released metabolites is important for recruitment (Galtsoff, 1964; Crisp, 1967; Weiner *et al.*, 1989; Bonar *et al.*, 1990). In addition, marine bacteria isolated and grown in laboratory cultures release soluble cues that induce settlement and metamorphosis of oyster larvae (Fitt *et al.*, 1989, 1990). A variety of analyses of supernatants from cultures of *Shewanella colwelliana*, a bacterial species known to enhance oyster recruitment, showed that their ability to induce settlement behavior of oyster larvae was correlated with the concentration of NH_3, not with that of melanin nor of any other catechol-related intermediates (Coon and Fitt, unpub.).

Oysters are gregarious, and although many attempts have been made to elucidate factors responsible for the settlement and metamorphosis of larvae around and on adults, the responsible chemical cues have not yet been conclusively identified (Cole and Knight-Jones, 1949; Knight-Jones, 1952; Crisp, 1967; Hidu, 1969; Veitch and Hidu, 1971; Keck *et al.*, 1971; Hidu *et al.*, 1978). Because oysters and oyster reefs release ammonia (Mann, 1979;

Received 2 December 1991; accepted 6 March 1992.

Boucher and Boucher-Rodoni, 1985, 1988; Dame *et al.*, 1985, 1989), such release by congeners may trigger the initial 'search behavior' portion of settlement and metamorphosis (see Coon *et al.*, 1990a, for model). Oyster larvae exposed to adult extrapallial fluid exhibit "setting behavior" within 10 min of exposure, the rapid response characteristic of larval responses to NH_3, but not to catecholamines (Hidu *et al.*, 1978, Coon *et al.*, 1990b). In addition, larvae induced with adult fluids have a higher percentage attachment on shells than larvae exposed only to seawater (Hidu *et al.*, 1978). Seawater that has been conditioned by adult oysters also significantly increases setting rates on cultch (in Hidu *et al.*, 1978). Whether adult and juvenile oysters can produce enough NH_3 to induce settlement behavior, and whether larvae respond to adult-produced NH_3, has not previously been determined.

Another important but unanswered question is whether enough ammonia is present on oyster reefs to affect larval settlement behavior. The highly productive salt marshes of the east coast of the United States are characterized by organically rich mud containing partially decomposed plant material. Oyster larvae are recruited to established oyster reefs in these biologically rich and complex environments. High concentrations of ammonia have been measured from salt-marsh oyster habitats (Stevens, 1983; Boucher and Boucher-Rodoni, 1985; Dame *et al.*, 1985, 1989), but these levels are typically 5–100 times lower than those needed for induction of settlement behavior by newly competent larvae (*cf.* Coon *et al.*, 1990b). However, oyster larvae (Fitt *et al.*, 1989; Coon *et al.*, 1990a), as well as other invertebrate larvae (Knight-Jones, 1953; Bayne, 1965; Rittschoff *et al.*, 1984, 1986; Fitt and Hofmann, 1985; Crisp, 1988; Hadfield, 1977), become more sensitive to morphogens as they age. For instance, the threshold concentration of L-DOPA to which larvae of the oyster *Crassostrea gigas* will respond decreases from 10^{-5} *M* in early competency to 10^{-6} *M* three to four weeks after the onset of competence (Coon and Fitt, unpub.). In addition, during settlement, competent veligers inevitably encounter crevices and boundary layers on and near surfaces where concentrations of chemicals originating from these substrates are higher than those in the surrounding seawater. No one, to our knowledge, has attempted to look for chemical inducers of settlement of oyster larvae in micro-habitats on oyster reefs.

We therefore hypothesized that oysters and oyster reefs may produce high enough concentrations of NH_3 to trigger settlement behavior of oyster larvae. We have tested this by quantifying NH_3 levels in and around oyster reefs and comparing these with the responses of larvae of *Crassostrea virginica* and *C. gigas* to NH_3. In addition, we investigated the decline, with larval age, in the threshold concentration of NH_3 required to induce settlement behavior. We report here that the concentration of NH_3 measured in the extensive oyster bed habitats on Sapelo Island, Georgia, overlaps the response range of competent veliger larvae, suggesting that ammonia may be an inducer of settlement behavior in nature.

Materials and Methods

Laboratory experiments

Larvae of the Pacific oyster *Crassostrea gigas* (Thunberg) were obtained from the Coast Oyster Company of Quilcene, Washington, and those of the American oyster *C. virginica* from either Horn Point Environmental Laboratory, University of Maryland, St. George Oyster Company, Piney Point, Maryland, or Virginia Institute of Marine Science, Gloucester Point, Virginia. The larvae were maintained in the laboratory as detailed in Coon *et al.* (1990a).

Settlement behavior in veliger larvae of oysters includes a well-characterized series of stereotyped maneuvers (Coon *et al.*, 1990a). These include swimming with the foot extended forward, followed by crawling on the substrate in a progression of increasingly localized behaviors, including reduced crawling speed and increased frequency of turns. This behavior is initiated in competent veliger larvae upon exposure to an appropriate soluble chemical cue, and after perception of additional substrate cues may result in cementation to the substrate. Settlement behavior of competent larvae was monitored as previously described (Coon *et al.*, 1990a). Between 20 and 50 larvae were assayed in each well of 24-well tissue culture plates (Falcon #3047) in a final volume of 1.0 ml at 20°C. Typically, six replicate wells were monitored for each experimental condition. Settlement behavior of larvae actively extending their foot was monitored in each well using a dissecting microscope every 5 min, for a 1-min interval over a 30–60 min period. Responses to concentrations of NH_4Cl (pH 7.8–8.0) ranging from 300 μM to 9 m*M* were determined with 19–30-day-old competent larvae of *C. virginica*. Competent veliger larvae are defined as being able to respond to external stimuli to trigger settlement behavior and metamorphosis. This typically develops in veliger larvae between 14–21 days post-fertilization and is usually characterized by a well-developed foot and black eye-spots. All veliger larvae used in experiments possessed well-developed eye spots (Coon *et al.*, 1990a).

Some experiments were designed to monitor the settlement behavior of competent veligers in response to adult-conditioned seawater. Adult oysters (4–10 cm in length) were scrubbed 1–2 days before the experiment with a toothbrush and 10% hypochlorite solution to remove algae, invertebrates, and bacterial films. Cleaned oysters were rinsed repeatedly to remove hypochlorite, and were allowed to sit in fresh seawater for 24–48 h.

They were then placed in acid-washed glass petri dishes containing 100 ml of 0.45 μm Millipore-filtered Instant Ocean to begin the experiment. After 12–48 h, adult-conditioned seawater was removed from the petri-dish and assayed for NH_3 concentration and its ability to induce larval settlement behavior.

Field experiments

Field work was conducted in oyster beds (=reefs) in South End Creek, adjacent to the Marine Institute of the University of Georgia on the southern end of Sapelo Island, Georgia. These oyster reefs, like many on the Georgia coast, are characterized by high densities of oysters that line the creek banks and bottoms in intertidal portions of the marsh. Settlement of larvae onto these reefs occurs sporadically throughout the spring, summer, and early fall. This particular tidal creek drains a diked marsh, and contains numerous oyster reefs along its 0.75-mile course connecting it to Doboy Sound. Water samples were taken during late spring (May 1990), summer (June 1990 and 1991, August 1991), and early fall (October 1989).

The characteristics of the marsh water overlying the oyster reefs were determined from 5–10 l water samples collected hourly for 26 h during the diurnal tidal cycle 19–20 May 1990. Temperature and pH were measured simultaneously with a portable temperature-compensated pH meter immediately after collection of the water. A refractometer was used to determine salinity, and oxygen was measured with a calibrated YSI oxygen electrode within 5 min of collection. Duplicate subsamples (5 ml) were taken for ammonia determination (below). Tide height at each collection time was calculated using a marked rope weighted at one end, calibrated to the lowest and highest water level.

Water samples for determination of natural levels of ammonia associated with the oyster reefs were collected with adjustable pipettors from three general habitats on the oyster reef. First, the interface between creekwater and the oyster reef was sampled at both high and low tides from a canoe. Second, water was collected from tidepools surrounded by oyster reefs. Third, small bodies of water surrounding exposed oysters were sampled. In each habitat, water was collected with the pipettors during low tide from three sources: (1) horizontal and vertical surfaces of adult and juvenile shells, with the resulting data combined into a category called 'shell surface'; (2) crevices between oyster shells; and (3) open water near, or above, live oyster reefs. In addition, some water samples were taken from crevices and surfaces of submerged adult oysters during an incoming tide (5–10 cm below the surface). Samples, either 250 or 100 μl, were diluted with deionized distilled water before being assayed for total ammonia (NH_3-NH_4^+) as detailed below. Because the sampling procedures disturb natural nutrient gradients, replicate samples were taken from a similar habitat (*i.e.*, shell surface, crevice between shells) at the same sampling location, but not at exactly the same position. In all cases, care was taken not to disturb the water around oysters before collection.

Collecting water samples from shell surfaces and crevices inevitably involves dilution of the immediate surface water by the adjacent seawater. To estimate this dilution effect during sampling, duplicate water samples of volumes between 25 and 1000 μl were collected from the same surfaces. Ammonia was analyzed as described below and plotted against volume sampled. A theoretical boundary layer concentration was calculated by extrapolating the data back to a zero volume sample (by linear regression). A dilution factor was calculated by dividing the total NH_3-NH_4^+ concentration at the theoretical zero ml volume by the concentration sampled.

Ammonia determination

Total NH_3-NH_4^+ concentration was measured by a modification (Wilkerson and Trench, 1986) of the phenol-hypochlorite method (Liddicoat *et al.*, 1975). Absorbance of replicate samples were read on a spectrophotometer at 640 nm after a minimum 1 h incubation in the dark to allow color development. Ammonia (NH_3) concentration was calculated from standard tables relating pH, salinity, and temperature to the proportion of NH_3 from the total NH_3-NH_4^+ content (Bower and Bidwell, 1978).

Results

Larval response to ammonia

Older larvae of *C. virginica* responded to lower concentrations of NH_3 than newly competent larvae (Fig. 1). The dose-response curves showed the typical peak in maximum number of larvae exhibiting settlement behavior in less than 10 min at the highest concentrations tested (*cf.* Coon *et al.*, 1990b), extending to 20 min or longer as the concentration of NH_3 decreased (Fig. 1). The lowest concentration of NH_3 eliciting larval settlement behavior (8.2 ± 3.3%, mean ± S.D., of larvae responding, n = 6) that was higher than controls (0%, n = 6) was 7.1 μ*M* (Fig. 2).

Larval response to adult-conditioned water

Competent larvae of both *C. gigas* and *C. virginica* exhibited settlement behavior when exposed to adult-conditioned seawater (Figs. 2, 3). The level of larval response was similar to that expected from the amount of NH_3 found in the adult-conditioned seawater (Fig. 2). In addition, the larval response to adult-conditioned water increased in a predictable fashion when the NH_3 concentration in oyster-conditioned water was increased by rais-

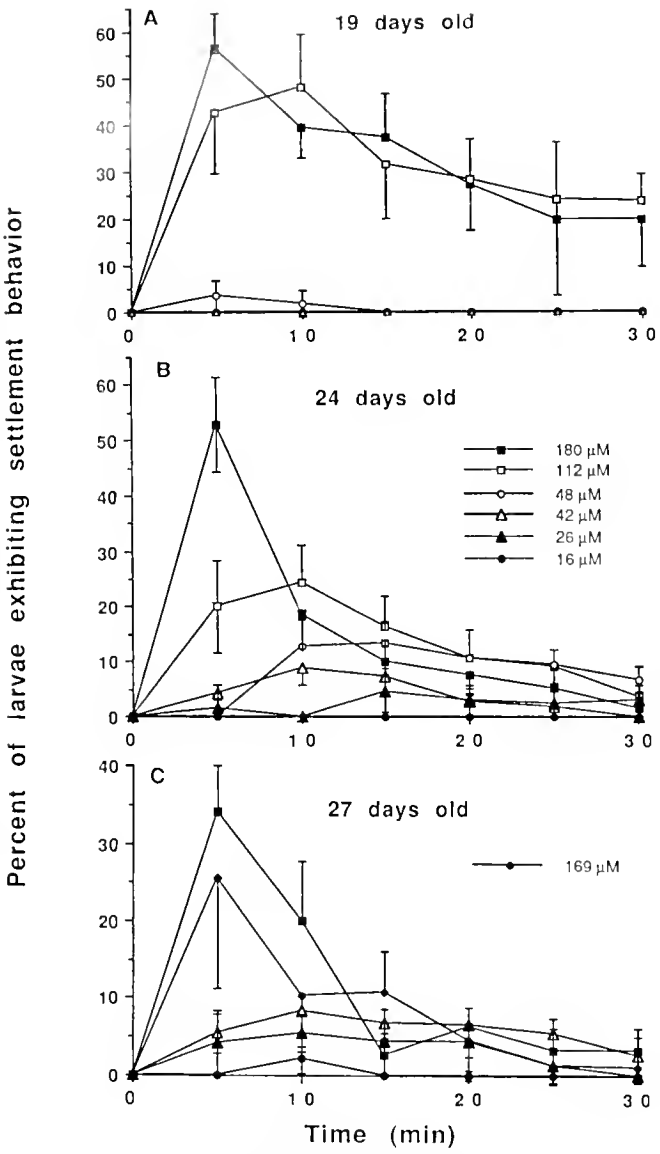

Figure 1. Percent of *Crassostrea virginica* exhibiting settlement behavior when exposed to various concentrations of NH_4Cl as a function of exposure time. All experiments were conducted at pH 7.8–8.0. Concentrations of NH_3 were approximately: solid squares = 180 μM NH_3; diamonds = 169 μM NH_3; open squares = 112 μM NH_3; open circles = 48 μM NH_3; open triangles = 42 μM NH_3; closed triangles = 26 μM NH_3; closed circles = 16 μM NH_3. Data are means ± S.D., n = 6.

ing the pH of the conditioned water from 7.4 to 8.0, and decreased by lowering the pH from 7.4 to 7.1 (Fig. 3).

Ammonia levels in an oyster bed

Total NH_3-NH_4^+ concentration in surface (0–20 cm) creek water over an oyster bed on Sapelo Island in May 1990, varied with tide height and time of day (Fig. 4). Total NH_3-NH_4^+ levels were inversely correlated with tide height, pH, and oxygen (Fig. 4). Highest concentrations of total NH_3-NH_4^+ were measured during low tide, when oxygen levels and pH were lowest. The total NH_3-NH_4^+ concentrations in these samples did not exceed 20 μM, and ammonia (NH_3) was less than 1 μM. The highest NH_3 concentrations in creek water were on an incoming tide during the daytime (Fig. 4B). There were two low points in NH_3 concentration: (1) at peak high tide, when total NH_3-NH_4^+ was at its lowest in the seawater entering the creek from Doboy Sound; and (2) on the outgoing tide, when pH decreased relatively faster than the total NH_3-NH_4^+ concentration increased (Fig. 4B).

When water samples were taken next to oyster shells, in moving water on an incoming tide, NH_3 concentrations were similar to that of the creek water overlying the oyster bed (Table I: 1, 2A3). However, water sampled from surfaces and between shells at low tide when the flow was minimal often had higher levels of NH_3 and total NH_3-NH_4^+ than the overlying creek water (Table I:1). Values

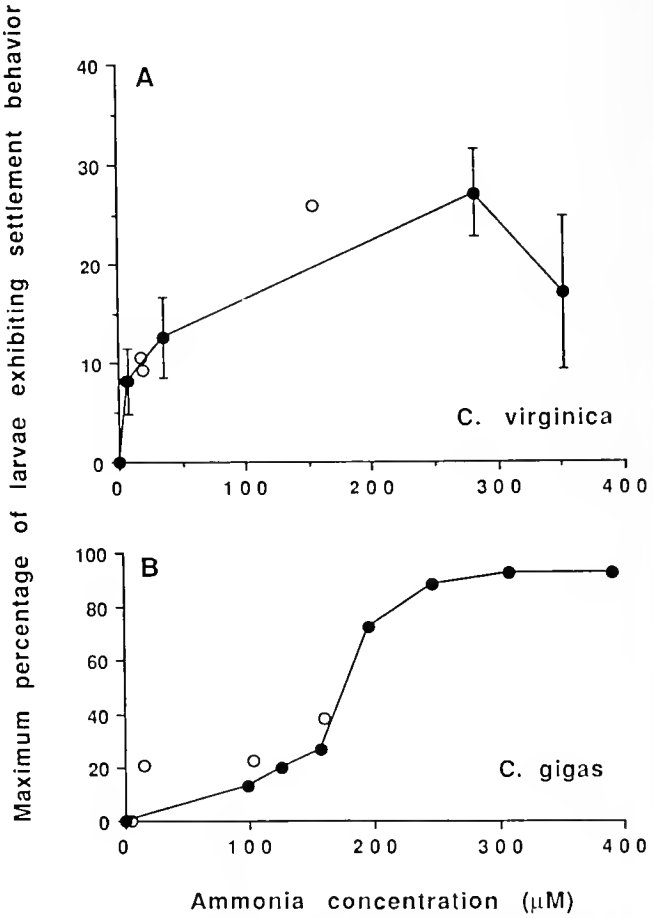

Figure 2. Maximum percent of larvae exhibiting settlement behavior in response to either NH_4Cl (filled circles) or adult-conditioned water (open circles). (A) *Crassostrea virginica*, (30 days old), (B) *C. gigas*, newly competent larvae (19 days old). Data are means ± S.D. (n = 6) of the maximum response, seen between 0 and 20 min, depending on the concentration of NH_4Cl.

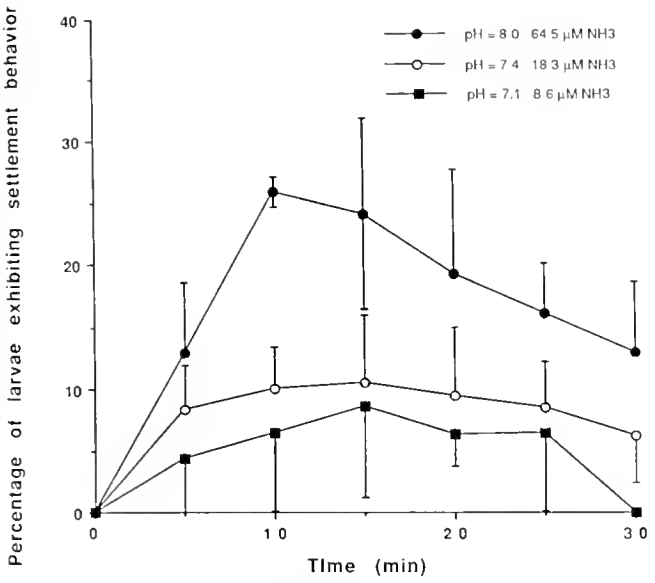

Figure 3. Percent of *Crassostrea virginica* exhibiting settlement behavior in response to adult-conditioned seawater as a function of exposure time. pH was adjusted before the experiment began in order to manipulate the NH_3 concentration, as noted in the text. Data are means ± S.D. (n = 6).

in Table 1:1 are from August 1991; values from June 1991 were similar to those found in August 1991. Samples taken at earlier dates were lower, probably due to dilution from surrounding water resulting from the larger volumes sampled (>1.0 ml), or due to seasonal differences. The highest concentrations of total NH_3-NH_4^+ were recorded between oyster shells (crevices), and include numerous samples exceeding 300 μM and a maximum concentration of 422 μM total NH_3-NH_4^+. The highest average ammonia (NH_3) values were recorded on 2 August 1991 around oysters exposed on an incoming tide (mean = 6.6 ± 3.2 S.D. μM NH_3, range 3.9 to 11.2 μM, n = 9). Six out of 16 samples taken from shell crevices on this date had concentrations of NH_3 greater than 7.1 μM. Although the total NH_3-NH_4^+ concentrations were higher on some samples on the previous afternoon, NH_3 concentration was always lower than 7.1 μM, because the pH of the outgoing tide was so low.

Dilution factor

As smaller volumes were sampled from a surface of an oyster shell, the measured total NH_3-NH_4^+ concentration increased (Fig. 5). The calculated dilution factor varied with sample volume, and was about 1.5 for volumes ≥ 250 μl using a 1000 μl pipettor (Fig. 5), and 3.5 for 100 μl samples using a 100 μl pipettor (data not shown). These dilution factors will obviously vary with type of habitat and substrate sampled. Control samples from >1 cm away from a shell surface showed no significant difference in ammonia concentration with sample volume. The highest concentrations of NH_3 measured in the oyster beds (Table 1) are well within the minimum range needed for induction of settlement behavior of older larvae of *C. virginica* (Fig. 2, above). Environmental concentrations of NH_3 associated with some shell surfaces, calculated using these dilution factors, exceeded 30 μM, far surpassing the minimum values needed to elicit larval settlement behavior.

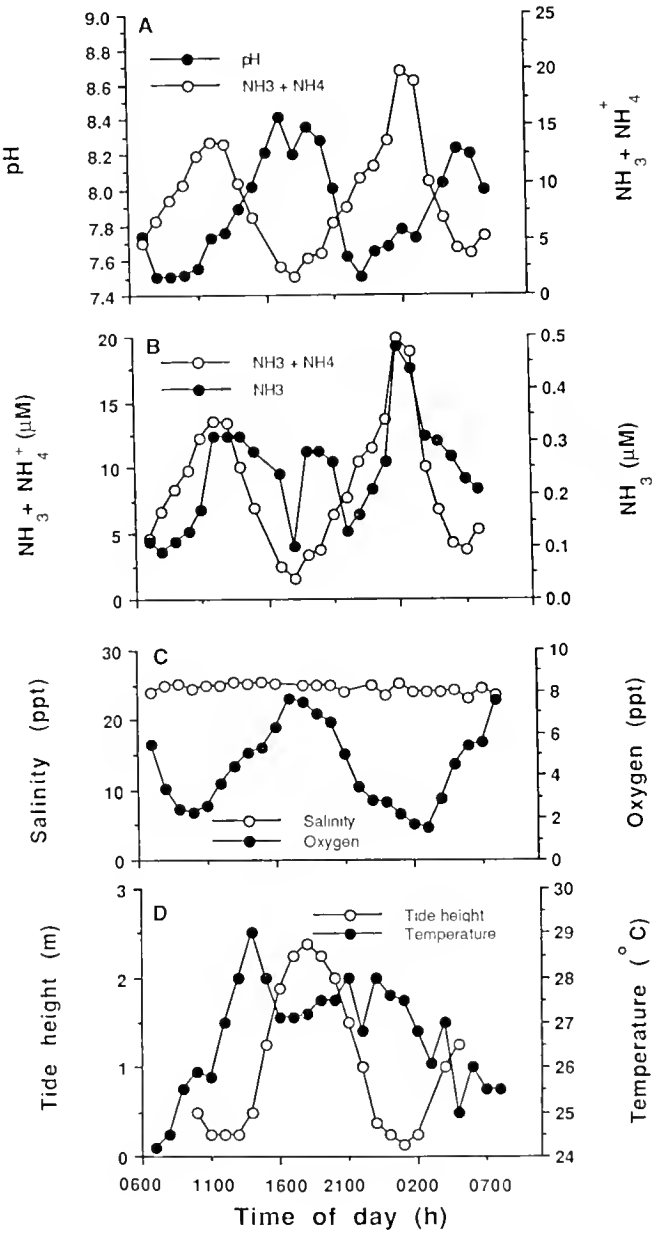

Figure 4. Characteristics of creek water from Sapelo Island on 19–20 May 1990 in relation to time of day. (A) Total NH_3-NH_4^+ and pH. (B) NH_3 and total NH_3-NH_4^+. (C) Salinity and oxygen. (D) Tide height and temperature.

Table I

Concentration of total NH_3-NH_4^+ [μM, means ± S.D. (n)], and the range of corersponding concentrations of NH_3 (μM) in oyster bed habitats on Sapelo Island

	Ambient seawater	Shell surface	Shell crevice
I. 1 August 1991 (250 µl samples)			
A. Morning low tide (incoming tide), pH = 7.4–7.7			
1. Creek	43.2 ± 2.6 (7)	52.1 ± 5.3 (14)	70.5 ± 32.5 (11)
Range (NH_3):	0.8–0.9	0.9–1.2	0.9–3.2
2. Pool 1	101.0 ± 1.7 (3)	111.3 ± 12.9 (3)	165.4 ± 66.3 (8)
Range (NH_3)	2.0–2.0	2.0–2.5	2.0–5.4
B. Afternoon low tide (outgoing tide), pH = 7.3–7.4			
1. Pool 1	81.9 ± 7.8 (4)	76.5 ± 3.5 (2)	142.6 ± 56.8 (9)
Range (NH_3):	0.7–0.9	0.7–0.8	0.9–2.6
2. Pool 2	199.4 ± 14.0 (2)	203.0 ± 11.3 (2)	270.7 ± 82.7 (6)
Range (NH_3):	1.9–2.1	2.0–2.1	2.1–4.2
3. Exposed oysters	n.d.	n.d.	256.6 ± 55.5 (5)
Range (NH_3):	n.d.	n.d.	1.7–3.3
II. 2 August 1991 (100 µl samples)			
A. Morning low tide (incoming tide), pH = 7.8–8.0			
1. Pool 1	72.8 (1)	n.d.	101.3 ± 38.4 (7)
Range (NH_3):	2.8	n.d.	3.2–7.2*
2. Exposed oysters	n.d.	n.d.	169.9 ± 83.0 (9)
Range (NH_3):	n.d.	n.d.	3.9–11.2*
3. Between tides (reef underwater)	20.9 ± 6.7 (5)	18.2 ± 1.1 (2)	21.7 ± 2.1 (9)
Range (NH_3):	0.5–1.1	0.7–0.7	0.7–1.0

* Six out of 16 water samples taken from these habitats had a high enough concentration of NH_3 (≥7.1 μM) to induce settlement behavior of veliger larvae.

n.d. = no data.

Discussion

Our goal in this study was to determine whether NH_3 levels in nature are high enough to induce settlement behavior of veliger larvae of oysters. The data show that concentrations of NH_3 close to oyster shells in oyster beds at Sapelo Island reach concentrations at least as high as the minimum concentration of NH_3 needed to induce settlement behavior of larvae of *C. virginica*. In addition, adult oysters produced enough NH_3 in laboratory experiments to induce settlement behavior. These results suggest that NH_3 concentrations in or near boundary layers of surfaces in oyster beds may be at least partially responsible for triggering settlement behavior in nature.

The highest values for total NH_3-NH_4^+ were found during afternoon low tides in the summer, when temperatures are typically highest in the marsh (Table I). However, the interaction of pH of the ambient seawater and total NH_3-NH_4^+ (Fig. 4, Table I) combined to give concentrations of NH_3 that were higher on incoming than outgoing tides. If competent oyster larvae are present in the water column, and if NH_3 is one of the cues to which they respond in nature as suggested in this study, then one might expect oyster larvae to settle during incoming tides rather than on outgoing tides. An alternative scenario might find competent larvae in areas of quiescent water on oyster reefs during low tide, where levels of NH_3 may become very high. There are currently no convincing data indicating that part of the tidal cycle, or time of day, when oyster larvae tend to set.

Other chemical cues also trigger settlement behavior of oyster larvae. A number of catecholamines, including L-DOPA and norepinephrine, induce classic veliger settlement behavior and subsequent metamorphosis (Coon *et al.*, 1985, 1990a). Treatment with methylamine and other weak bases also induces settlement behavior (Coon *et al.*, 1990b). None of these compounds has been found in oyster beds, but there is evidence from experiments in salt marshes that other soluble cues may exist and play a role in oyster settlement. Zimmer-Faust (1990) and Tamburri (1990) found differences in larval swimming behavior in marsh water containing sub-threshold concentrations of NH_3. The relationship between these changes in swimming behavior and the specific behaviors involved in settlement (*e.g.*, foot extension, crawling, and turning) are unclear. While these other soluble cues may be important in oyster recruitment, their identity and characteristics are virtually unstudied.

Chemical induction of settlement behavior modifies veliger movement in such a way as to bring competent larvae into physical contact with potential substrates for

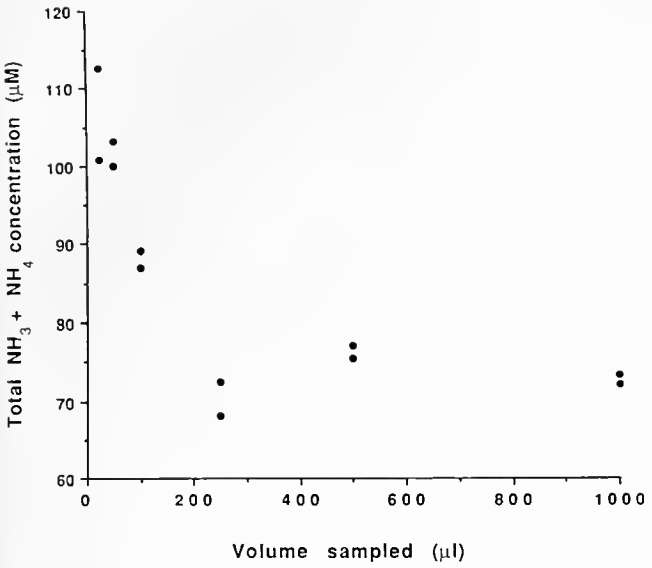

Figure 5. Relation of total NH_3-NH_4^+ measured to volume of water sampled from oyster-shell surfaces on Sapelo Island using a 1000 μl pipettor.

attachment and metamorphosis. Researchers have speculated for years about the characteristics of substrates suitable for oyster attachment and metamorphosis, but only the presence of other larvae or adults (Cole and Knight-Jones, 1949; Knight Jones, 1952; Crisp, 1974) and biofilms (Crisp and Ryland, 1960; Galtsoff, 1964; Weiner *et al.*, 1989) have convincingly correlated with higher oyster set. The molecular factors associated with conspecifics in nature are not known, but as shown here may involve the production of ammonia. Our data show that larval behavior can be altered by changing the availability of NH_3 in adult-conditioned water by changing pH. Others have found a settlement-behavior inductive factor in adult-conditioned water, but have been unable to identify it (references in Hidu *et al.*, 1978).

Settlement of oyster larvae involves two basic steps. (1) Settlement behavior triggered by soluble cues that act to bring the larvae in contact with surfaces, and (2) cementation and subsequent metamorphosis triggered by unknown cues associated with surfaces (Coon *et al.*, 1990a). The latter appear to be related to biofilms, but few experiments have addressed this relationship (*cf.* Walch *et al.*, 1987; Labare and Weiner, 1990). Many of the early results showing more set on cultch coated with oyster extracts than control cultch (references in introduction) may have been due to higher numbers of resulting bacteria, and thus higher concentrations of NH_3 as well.

Ammonia-induced settlement behavior does not by itself result in subsequent attachment and metamorphosis in laboratory experiments (Coon *et al.*, 1990b; unpub.). Experiments demonstrating this were performed in plastic cell-culture plates, previously shown to be sub-optimal setting surfaces for oyster larvae (Coon *et al.*, 1990a). Because larvae that are induced with NH_3 characteristically habituate to that stimulus in less than 30 min and then resume normal swimming behavior (Coon *et al.*, 1990b), we hypothesize that, in the laboratory, they do not spend enough time in contact with this substrate to induce settlement. Such a phenomenon may also occur in competent larvae in nature, where the importance of selecting among a variety of settlement sites may be crucial to survival. Such a process may be part of the mechanism by which veliger larvae settle on premium substrates, such as congener shells, more frequently than suboptimal substrates, such as mud. The substrate factors important in triggering final attachment and metamorphosis are not currently known.

Acknowledgments

The authors thank the following oyster hatcheries for veliger larvae: Coast Oyster Company of Quilcene, Washington; Horn Point Environmental Laboratory, University of Maryland; St. George Oyster Company, Piney Point, Maryland; and Virginia Institute of Marine Science, Gloucester Point, Virginia. We thank Doug Haymans, Dr. Abdelmonem Khalil, and students in the 1990 Ecological Physiology course at the University of Georgia for help in collecting some of the data presented in this paper and thank Dr. Dick Zimmer-Faust for information on his current research. We also thank the staff at the University of Georgia Marine Institute on Sapelo Island for logistical support of the field work. Portions of this work were supported by the Sea Grant Program of Georgia, and the National Science Foundation (DCB-9108074 to WKF). Contribution #191, Center of Marine Biotechnology, University of Maryland.

Literature Cited

Bayne, B. L. 1965. Growth and the delay of metamorphosis of the larvae of *Mytilus edulis* (L.) *Ophelia* **2:** 1–47.

Bonar, D. B., S. L. Coon, M. Walch, R. M. Weiner, and W. K. Fitt. 1990. Control of oyster settlement and metamorphosis by endogenous and exogenous chemical cues. *Bull. Mar. Sci.* **46:** 484–498.

Boucher, G., and R. Boucher-Rodoni. 1985. Fluctuations des nutriments au cours de la maree sur les parcs ostreicoles de la riviere Penze (Nord-Finistere). *Hydrobiologia* **123:** 251–261.

Boucher, G., and R. Boucher-Rodoni. 1988. *In situ* measurement of respiratory metabolism and nitrogen fluxes at the interface of oyster beds. *Mar. Ecol. Prog. Ser.* **44:** 229–238.

Bower, C. E., and J. P. Bidwell. 1978. Ionization of ammonia in seawater: effects of temperature, pH, and salinity. *J. Fish. Res. Board Can.* **35:** 1012–1016.

Cole, H. A., and E. W. Knight-Jones. 1949. The setting behaviour of larvae of the European flat oyster, *Ostrea edulis* L. and its influence on methods of cultivation and spat collection. *Fishery Invest., Lond. Ser. II.* **17:** 1–39.

Coon, S. L., D. B. Bonar, and R. M. Weiner. 1985. Induction of settlement and metamorphosis of the Pacific oyster, *Crassostrea gigas* (Thunberg), by L-DOPA and catecholamines. *J. Exp. Mar. Biol. Ecol.* **94:** 211–221.

Coon, S. L., W. K. Fitt, and D. B. Bonar. 1990a. Competence and delay of metamorphosis in the Pacific oyster, *Crassostrea gigas*. *Mar. Biol.* **106:** 379–387.

Coon, S. L., M. Walch, W. K. Fitt, R. M. Weiner, and D. B. Bonar. 1990b. Ammonia induces settlement behavior in oyster larvae. *Biol. Bull.* **179:** 297–303.

Crisp, D. J. 1967. Chemical factors inducing settlement in *Crassostrea virginica* (Gmelin). *J. Anim. Ecol.* **36:** 329–335.

Crisp, D. J. 1974. Factors influencing the settlement of marine invertebrate larvae. Pp. 177–265 in *Chemoreception in Marine Organisms*, P. T. Grant and A. M. Mackie, eds., Academic Press, London.

Crisp, D. J. 1988. Reduced discrimination of laboratory-reared cyprids of the barnacle *Balanus amphitrite amphitrite* Darwin, Crustacea Cirripedia, with a description of a common abnormality. Pp. 409–432 in *Marine Biodeterioration*, M. F. Thompson, R. Sarojini, and R. Nagabushanam, eds., Oxford and IBH Publ. Co., New Delhi.

Crisp, D. J., and J. S. Ryland. 1960. Influence of filming and of surface texture on the settlement of marine organisms. *Nature* **185:** 119.

Dame, R. F., T. G. Wolaver, and S. M. Libes. 1985. The summer uptake and release of nitrogen by an interstitial oyster reef. *Neth. J. Sea Res.* **19:** 265–268.

Dame, R. F., J. D. Spurrier, and T. G. Wolaver. 1989. Carbon, nitrogen and phosphorus processing by an oyster reef. *Mar. Ecol.* **54:** 249–256.

Fitt, W. K., and D. K. Hofmann. 1985. Chemical induction of settlement and metamorphosis of planulae and buds of the reef-dwelling coelenterate *Cassiopeia andromeda*. *Proc. 5th Intl. Coral Reef Congr.* **5:** 239–244.

Fitt, W. K., M. P. Labare, W. C. Fuqua, M. Walch, S. L. Coon, D. B. Bonar, R. R. Colwell, and R. M. Weiner. 1989. Factors influencing bacterial production of inducers of settlement behavior of larvae of the oyster *Crassostrea gigas*. *Microb. Ecol.* **17:** 287–298.

Fitt, W. K., S. L. Coon, M. Walch, R. M. Weiner, R. R. Colwell, and D. B. Bonar. 1990. Settlement behavior and metamorphosis of oyster larvae of *Crassostrea gigas* in response to bacterial supernatants. *Mar. Biol.* **106:** 389–394.

Galtsoff, P. S. 1964. The American oyster, *Crassostrea virginica* Gmelin. *Fish. Bull. Fish. Wildlife Serv. U. S.* **64:** 1–480.

Gilmour, T. H. J. 1991. Induction of metamorphosis of echinoid larvae. *Am. Zool.* **31:** 105A.

Hadfield, M. G. 1977. Chemical interactions in larval settling of a marine gastropod. Pp. 403–413 in *Marine Natural Products Chemistry*, D. J. Faulkner and W. H. Fenical, eds., Plenum Publ. Corp., NY.

Hidu, H. 1969. Gregarious setting in the American oyster *Crassostrea virginica* Gmelin. *Chesapeake Sci.* **10:** 85–92.

Hidu, H., W. G. Valleau, and F. P. Veitch. 1978. Gregarious setting in European and American oysters—response to surface chemistry *vs.* waterborne pheromones. *Proc. Natl. Shellfisheries Assoc.* **68:** 11–16.

Keck, R., D. Maurer, J. D. Kauer, and W. A. Sheppard. 1971. Chemical stimulants affecting larval settlement in the American oyster. *Proc. Natl. Shellfisheries Assoc.* **61:** 24–28.

Knight-Jones, E. W. 1952. Reproduction of oysters in the Rivers Crouch and Roach, Essex, during 1947, 1948, and 1949. *Fishery Invest., Lond. Ser. II.* **18:** 1–48.

Knight-Jones, E. W. 1953. Decreased discrimination during setting after prolonged planktonic life in larvae of *Spirorbis borealis* (Serpulidae). *J. Mar. Biol. Assoc. U.K.* **32:** 337–345.

Labare, M. P., and R. M. Weiner. 1990. Interactions between *Shewanella colwelliana*, oyster larvae, and hydrophobic organophosphate pesticides. *Applied Environ. Microbiol.* **56:** 3817–3821.

Liddicoat, M. I., I. S. Tibbits, and E. Butler. 1975. The determination of ammonia in seawater. *Limnol. Oceanogr.* **20:** 131–132.

Mann, R. 1979. Some biochemical and physiological aspects of growth and gametogenesis in *Crassostrea gigas* and *Ostrea edulis* grown at sustained elevated temperatures. *J. Mar. Biol. Assoc. U.K.* **59:** 95–110.

Rittschof, D., E. S. Branscomb, and J. D. Costlow. 1984. Settlement and behavior in relation to flow and surface in larval barnacles, *Balanus amphitrite* Darwin. *J. Exp. Mar. Biol. Ecol.* **82:** 131–146.

Rittschof, D., J. Maki, R. Mitchell, and J. D. Costlow. 1986. Ion and neuropharmacological studies of barnacle settlement. *Neth. J. Sea Res.* **20:** 269–275.

Stevens, S. A. 1983. Ecology of Intertidal Oyster Reefs: Food, Distribution, and Carbon/Nutrient Flow. Ph.D. Dissertation, University of Georgia, 112 pp.

Tamburri, M. N. 1990. Oyster larvae settle to waterborne chemical factors released by adult conspecifics and by bacteria films. *Am. Zool.* **30:** 97A.

Veitch, F. P., and H. Hidu. 1971. Gregarious setting in the American oyster *Crassostrea virginica* Gmelin: I. Properties of a partially purified "setting factor." *Chesapeake Sci.* **12:** 173–178.

Walch, M., M. P. Labare, R. M. Weiner, R. R. Colwell, W. K. Fitt, and D. B. Bonar. 1987. Use of specific bacterial biofilms and their products to enhance spat set of the oysters *Crassostrea virginica* and *C. gigas*. *J. Shellfish Res.* **7:** 179–180.

Weiner, R. M., M. Walch, M. P. Labare, D. B. Bonar, and R. R. Colwell. 1989. Effect of biofilms of the marine bacterium *Alteromonas colwelliana* (LST) on set of the oysters *Crassostrea gigas* (Thunberg, 1793) and *C. virginica* (Gmelin, 1791). *J. Shellfish Res.* **8:** 117–123.

Wilkerson, F. P., and R. K. Trench. 1986. Uptake of dissolved inorganic nitrogen by the symbiotic clam *Tridacna gigas* and the coral *Acropora* sp. *Mar. Biol.* **93:** 237–246.

Zimmer-Faust, R. K. 1990. Settlement behavior of larvae is revealed using computer-video motion analysis. *Am. Zool.* **30:** 98A.

Reference: *Biol. Bull.* **182**: 409–415. (June, 1992)

Proline Synthesis During Osmotic Stress in Megalopa Stage Larvae of the Blue Crab, *Callinectes sapidus*

RONALD S. BURTON

Program in Evolutionary Biology, Department of Biology, University of Houston, Houston, Texas 77204-5513

Abstract. The free amino acid (FAA) pool of individual *Callinectes sapidus* megalopas acclimated to 100% seawater averaged over 56% larger than that of 50% seawater acclimated megalopas. Most of the difference was due to a four-fold increase in proline concentration at the higher salinity. In 100% seawater, proline comprises 64% of the total FAA pool in megalopas; this contrasts with the role of proline in adult tissues where it never exceeds 25% of the total FAA pool. Metabolic tracer studies using ^{14}C-glucose and ^{14}C-glutamate as radiolabelled precursors showed that *de novo* synthesis of proline was very low unless induced by hyperosmotic stress. The induction of the synthetic pathway was inhibited by cycloheximide, a protein synthesis inhibitor. These results suggest that the induction of proline synthesis is regulated by the synthesis of either one of the enzymes catalyzing the three steps in the glutamate to proline pathway or a protein acting to stimulate the activity of one of those enzymes.

Introduction

The adjustment of intracellular free amino acid (FAA) concentrations plays an important role in acclimation to salinity change in Crustacea and a diversity of other marine invertebrate taxa (see reviews by Florkin and Schoffeniels, 1969; Gilles, 1975, 1979; Schoffeniels, 1976). High intracellular FAA concentrations apparently function to balance high inorganic ion concentrations in the hemolymph of animals exposed to elevated salinity. Only a few non-essential amino acids such as alanine, proline, and glycine are major contributors to the response and show rapid, quantitatively important, changes in concentration following changes in environmental salinity. One or more of these FAA typically obtain intracellular concentrations in excess of 0.1 *M* in seawater-acclimated Crustacea where the total FAA pool may account for as much as 50% of the total intracellular osmolyte pool (Bowlus and Somero, 1979).

While changes in FAA pool sizes have been widely documented, relatively little is known about the regulation of FAA concentrations during osmotic stress. The most widely cited hypothesis involves the direct action of inorganic ions on a key enzyme, glutamate dehydrogenase (GDH, EC 1.4.1.2), which catalyzes the reductive amination of α-ketoglutarate to form glutamate (see Gilles, 1979; Gilles and Pequeux, 1983; Hochachka and Somero, 1984). Increasing medium salinity is postulated to result in increases in intracellular NaCl concentrations that may directly stimulate GDH activity, resulting in the synthesis of glutamate. Because glutamate is the amino group donor for synthesis of alanine and aspartate (and probably glycine) and a direct precursor for proline, the increased glutamate synthesis could drive, by mass action, the synthesis of these other FAAs. Other key enzymes in FAA synthesis are unaffected by changes in inorganic ions (*e.g.*, transaminases), while some involved in FAA catabolism are inhibited by increased inorganic ion concentrations (*e.g.*, serine hydrolyase). Combined, these effects are thought to alter the synthesis/catabolism balance for FAA and result in their accumulation.

Unfortunately, while data continue to support the occurrence of *de novo* synthesis of FAA in response to hyperosmotic stress (*e.g.*, Burton, 1986), few data directly support the above model for regulation of FAA synthesis. The effect of NaCl and other inorganic ions on glutamate dehydrogenase activity *in vitro* has proven to be complex at best, and some investigators now propose that the major change leading to FAA accumulation is not increased synthesis, but rather reduced FAA catabolism (Gilles, 1979; Gilles and Pequeux, 1983). However, Burton (1986,

Received 19 November 1991; accepted 10 March 1992.

1991a, b) has shown that in the euryhaline intertidal copepod *Tigriopus californicus*, detectable proline synthesis is observed only during hyperosmotic stress. After proline accumulates for approximately 24 h, proline synthesis is effectively turned off. This is in contrast to other FAAs (such as alanine, glutamate, and aspartate), which are synthesized continuously under a variety of salinity regimes. Clearly, proline synthesis is not simply driven by mass action following increased glutamate production because glutamate production occurs under all salinity conditions and glutamate pool size does not change markedly during hyperosmotic stress. Similarly, regulation of the proline pool cannot be the result of changes in proline catabolism alone, because such a model could not account for the fact that ^{14}C-labelling of glutamate (from labelled bicarbonate) occurs under constant salinity (50% or 100% SW), while no labelling of proline is observed under these conditions (Burton, 1986). These data are in direct conflict with the mass action synthesis model discussed above.

Recently, by using *in vivo* translation inhibitor studies, we have shown that the induction of proline synthesis in *T. californicus* in response to hyperosmotic stress requires protein synthesis (Burton, 1991b). By providing ^{14}C-(U)-L-glutamate as a proline precursor, evidence was obtained that the ultimate site of action for protein synthesis inhibitors was in the three-step pathway between glutamate and proline. This work suggests that hyperosmotic stress induces the synthesis of one or more of the enzymes in the glutamate to proline biosynthetic pathway or a protein that stimulates the activity of these enzymes. Given that this mechanism for the regulation of FAA metabolism has not been previously documented among marine Crustacea, it was of interest to determine the generality of our *T. californicus* work by performing similar studies on other, taxonomically distant, crustacean species.

Several criteria were important in choosing an appropriate study system for testing the mechanism of induction of proline synthesis. First, the test organism should be a euryhaline osmoconformer where adjustment of FAA concentrations function in salinity acclimation. Second, because proline is only a minor constituent of the FAA pool in some species, a species was needed in which proline was known to be an important contributor to the FAA pool. Finally, for analytic convenience, we sought a small organism because smaller quantities of tracer isotopes are necessary for metabolic studies. One system meeting these criteria is the blue crab, *Callinectes sapidus*, an abundant portunid that experiences substantial salinity variation in its natural estuarine habitat along the Texas coast. The participation of FAA in osmotic acclimation of adult *C. sapidus* has previously been studied (Gerard and Gilles, 1972; Engel, 1977), and proline was found to be a major contributor to the osmolyte pool in each tissue studied. While adult *C. sapidus* is too large for the *in vivo* radiotracer studies needed to address mechanisms of proline synthesis, *C. sapidus* megalopas (dry weight of approximately 0.4 mg) are locally abundant and easily maintained in the lab. In the work described below, osmotically induced changes in FAA concentrations are documented in *C. sapidus* megalopas and the role of protein synthesis in regulating these changes is assessed via *in vivo* application of the protein synthesis inhibitor cycloheximide.

Materials and Methods

C. sapidus megalopas were collected with a hand-pulled beam trawl in shallow water (<1.5 meter) along the sandy Gulf coast beach of Galveston Island, Texas, in early June to August 1991. Ambient salinities ranged from 17 to 37 ppt. Animals were maintained at room temperature (23°C) and acclimated for 3–5 days at 17 ppt (50% seawater = 50% SW) and 34 ppt (100% SW) before being exposed to experimental treatments. Animals were fed commercial flake fish food (Tetramin) during acclimation. *C. sapidus* megalopas were initially identified by comparing them to the description presented in Costlow and Bookout (1959). Numerous megalopas molted to the first crab stage in our aquaria within a few days of capture; these were identified as *C. sapidus* as described in Williams (1984).

Procedures for studying the incorporation of labelled precursors into the FAA pool in individuals of *C. sapidus* were as follows: prior to exposure to precursor-laced medium, animals were pretreated for 1 h with an antibiotic mixture ("AM 4" of Provasoli *et al.*, 1959) in filtered (0.2 μ), buffered (30 m*M* HEPES) commercial (Instant Ocean) artificial seawater (SW) of appropriate salinity. The effectiveness of this antibiotic mixture in preventing contaminating bacterial growth was previously tested (Burton, 1991a). Radioactive precursor, ^{14}C-(U)-L-glutamate, (Sigma Chemical Company, 229.4 mCi/mmol) or ^{14}C-(U)-D-glucose, (Sigma Chemical Company, 255 mCi/mmol) was added to a small volume (5 μCi/150 μl) of medium of appropriate salinity; all media contained the antibiotic mixture. Experimental treatments involving the translation inhibitor cycloheximide also used a 1-h pretreatment period (with antibiotics and cycloheximide) prior to salinity transfer. Transfers between pretreatment and treatment media were carried out by pipetting individual megalopas onto filter paper and then moving them (with a fine forceps) into 1.5 ml microcentrifuge tubes containing the desired treatment medium. Up to six megalopas were treated together in a single tube. Handling was identical for controls and treatments and did not directly result in any mortality. Osmotic concentrations of artificial SW solutions were routinely determined with a hand refractometer and checked with a vapor pressure osmometer (Wescor Model 5500).

Following experimental exposures (typically 3–6 h), animals were individually sacrificed and FAA extracted in 100 μl of 80% ethanol and then dried under vacuum. Samples were resuspended in 60 μl of 0.1 *M* sodium bicarbonate and then reacted with 40 μl of dansyl chloride in acetone (0.5 mg/ml) for 90 min at room temperature to fluorescently label primary and secondary amino groups. FAA analysis was carried out on dansyl derivatives of the FAA using reverse-phase high pressure liquid chromatography (HPLC) (C18 "Hypersil" 5 μ 4.6 × 250 mm cartridge column, Alltech Assoc.) with fluorescence detection; peaks representing FAA were quantified with a computing integrator and were individually collected directly into minivials for liquid scintillation counting (see Burton, 1986, for further HPLC details). Although glycine, taurine, alanine, and proline derivatives were completely resolved, there was some difficulty in resolving dansyl-glutamate from dansyl-aspartate; data for the combined glutamate/aspartate peak are presented here as "glutamate." To determine whether the confounding of glutamate and aspartate would have a significant effect on estimates of glutamate specific activity, one sample from each experimental treatment was analyzed by one-dimensional thin-layer chromatography (TLC), as follows. Three samples and one lane of dansyl-FAA standards (Sigma Chemical) were spotted in four lanes on a 5 × 20 cm polyamide 6 TLC plate (Baker Chemical). Chromatograms were run in a chloroform-t-amyl alcohol-acetic acid (70:30:3) solvent system until the solvent front migrated 15 cm. Glutamate and aspartate pool sizes were qualitatively assessed under UV illumination, and distribution of radiolabel was determined by a 48–72-h autoradiographic exposure. In most cases, the aspartate spot was too faint to be detected by eye. Subsequently, chromatographic regions in the sample lanes corresponding to aspartate and glutamate standards were cut out and eluted for scintillation counting. In all tests, the bulk of the label (minimum 75%) was recovered in the glutamate region. Because none of our qualitative results are significantly affected by reducing the counts recovered in glutamate by such a factor, we concluded that pooling the glutamate and aspartate peaks via HPLC did not introduce significant error into the results presented here.

Levels of FAA measured by HPLC are presented here in units of nanomoles/larva. The mean (±S.E.) wet weight of a larva was 1.37 ± 0.04 mg; dry weight was 0.39 ± 0.02 mg. Although the reported values can, therefore, be converted to more common units (*e.g.*, mmoles/kg tissue water, or mmoles/g dry weight), the fact that whole megalopas were homogenized would make it difficult to compare the values presented here to values reported for adult tissues. This is because our wet weights include gut water content, and our dry weights consist primarily of exoskeleton rather than actual FAA-containing tissue.

Results

FAA pool of Callinectes sapidus *megalopas acclimated to 50% and 100% SW*

Following collection from ambient 100% SW, groups of megalopas were acclimated to 100% and 50% SW for five days as described above. Results of FAA analyses are shown in Figure 1. In 50% SW, taurine and glycine are the dominant FAAs, comprising approximately 42% and 25% of the measured pool, respectively. The total FAA pool of 100% SW acclimated animals averaged over 56% larger than that of 50% SW acclimated animals (one-tailed *t*-test, $P = 0.022$). The only amino acid that contributed significantly to the increased pool was proline (taurine and glutamate actually showed relatively minor but statistically significant decreases); in 100% SW, proline comprised over 64% of the FAA pool.

Incorporation of radiolabelled glucose into the FAA pool

Megalopas were presented with ^{14}C-(U)-D-glucose (5 μCi/150 μl of medium) under three salinity treatments: constant 50% SW (involved transfer between media of the same salinity), constant 100% SW, and immediately following hyperosmotic transfer from 50% to 100% SW. Larvae were sampled at two time points: 3 h and 6 h after treatment. After 3 h of hyperosmotic stress, concentrations of the five FAAs measured had not increased significantly above the 50% SW control (taurine showed a small but statistically significant drop). Although FAA concentrations had not yet changed, analysis of radiotracer incorporation shows evidence of significant changes in FAA metabolism. Although 80–90% of all recovered radioactivity in FAA is in the alanine pool under each salinity treatment, only proline showed significant variation in specific activity among treatments (Fig. 2). Under either constant salinity treatment, proline specific activity av-

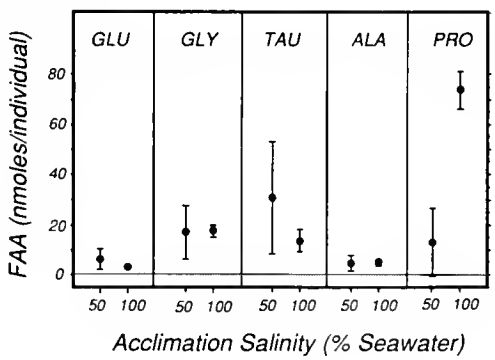

Figure 1. FAA concentrations in individual *Callinectes sapidus* megalopas acclimated to 50% and 100% SW for five days following collection from ambient 100% SW. Error bars are 95% confidence intervals (n = 5 and 6 to the two treatments, respectively).

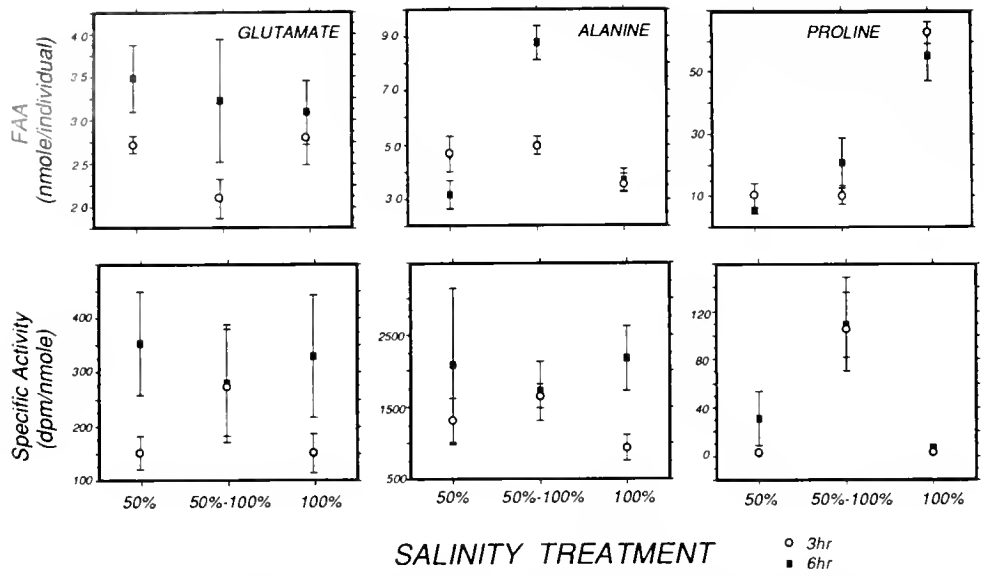

Figure 2. FAA concentrations and specific activities in individual *Callinectes sapidus* megalopas subjected to three treatments: acclimated to 50% and transferred to 50% SW or 100% SW, or acclimated to 100% SW and transferred to 100% SW. ^{14}C-(U)-D-glucose was added and animals were sampled at 3 and 6 h. Four to six individuals were analyzed per treatment. Error bars are ±1 S.E.M. Note scale differences among panels.

eraged less than 2 dpm/nmole while that of glutamate, a direct proline precursor, averaged 95 dpm/nmole, nearly two orders of magnitude higher (note that because aspartate was lumped with glutamate and all counts appear to be in glutamate, this specific activity is an underestimate of true glutamate activity); this fact indicates that proline is essentially not being synthesized *de novo* from glucose carbon under constant salinity conditions. In contrast, proline specific activity in the hyperosmotic stress treatment increased dramatically (to approximately 50% of the glutamate specific activity in the same treatment), indicating the induction of proline biosynthesis by the hyperosmotic stress treatment. Hence, although glutamate and alanine specific activities were not significantly influenced by the salinity treatments, proline specific activity increased by two orders of magnitude within 3 h of hyperosmotic stress. Glycine and taurine showed no label incorporation in any treatment and are omitted from Figure 2.

By 6 h, a significant concentration increase was detected for alanine in the stress treatment over 50% SW controls; while mean proline concentration increased by a factor of four, inter-individual variance was large and the mean difference was not statistically significant (Fig. 2). Again only the specific activity of proline was elevated over constant salinity controls.

Incorporation of radiolabelled glutamate into the FAA pool

Megalopas were presented with ^{14}C-(U)-L-glutamate (5 μCi/150 μl of medium) under both constant salinity (100% SW) and hyperosmotic stress conditions (50–100% SW transfer) to further ascertain that induction of proline synthesis involves the regulation of the glutamate to proline pathway. The high salinity control was employed because if proline is being synthesized under constant salinity conditions, it should be most evident in high salinity where proline pool sizes are large. Results are presented in Figure 3. Although the size of the glutamate pool was slightly larger in the control *versus* the osmotic stress conditions (two-tailed *t*-test, $P < 0.01$), radiolabel recovered in glutamate and glutamate specific activity did not differ. This indicates that a comparable pool of labelled glutamate was available for proline synthesis under both sets of conditions (if anything, slightly more glutamate was available under the control conditions). In contrast, even though the proline pool is significantly larger in control animals ($P < 0.02$), label recovered in the pool and proline specific activity is lower under control conditions ($P < 0.001$ for each measure). Hence, while some label is observed in proline under constant salinity conditions, the near-zero specific activity suggests that the flux from glutamate to proline under these conditions is very low. In fact, if glutamate is the primary precursor of the proline pool, a flux from glutamate to proline should lead to equilibration of the specific activities of the two pools. Paired *t*-tests show that glutamate and proline have different specific activities (within each individual) under control conditions ($P < 0.01$), but not following the 4-h hyperosmotic stress treatment ($P > 0.1$).

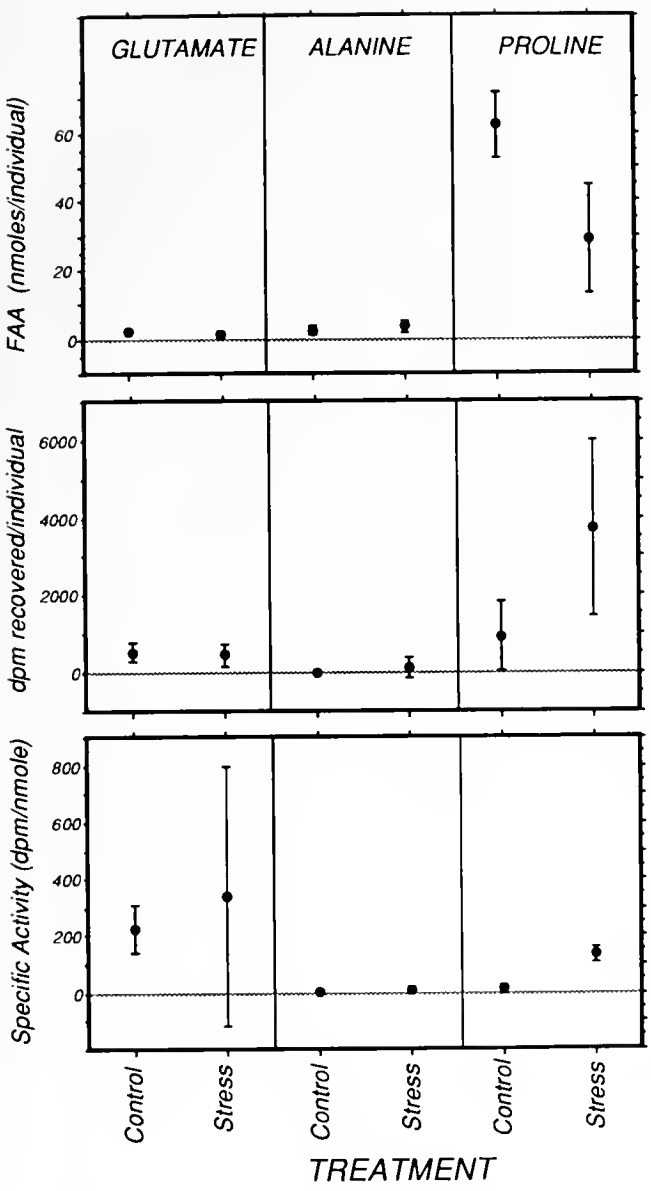

Figure 3. FAA concentrations and specific activities in individual *Callinectes sapidus* megalopas acclimated to 100% SW and transferred to 100% SW (Control) and acclimated to 50% SW and transferred to 100% SW (Stress) for 4 h in the presence of ^{14}C-(U)-L-glutamate. Error bars are 95% confidence intervals (n = 6 individuals per treatment).

Effects of the protein synthesis inhibitor cycloheximide on FAA synthesis

Because the results above clearly demonstrate the induction of proline synthesis from glutamate during response to hyperosmotic stress, we used cycloheximide (CHX) as a protein synthesis inhibitor to address the role of protein synthesis in this induction. Paired groups of megalopas were exposed to hyperosmotic stress, with one group being treated with CHX. Results are shown in Figure 4. Levels of glutamate, labelling of the glutamate pool, and glutamate specific activity do not differ between control and CHX treatments. In contrast, all three measures of proline were affected. Although the size of the proline pool was only slightly decreased by CHX (one-tailed *t*-test, $P < 0.05$), both label recovered in proline and proline specific activity were dramatically reduced by CHX treatment ($P < 0.005$). Interestingly, alanine pool sizes increased by over 40% in the CHX treatment ($P < 0.05$). Neither glycine nor taurine pool sizes were significantly influenced by CHX treatment ($P > 0.25$, data not shown). The magnitude of this change is not enough to compensate for reduced proline synthesis, but it does indicate that

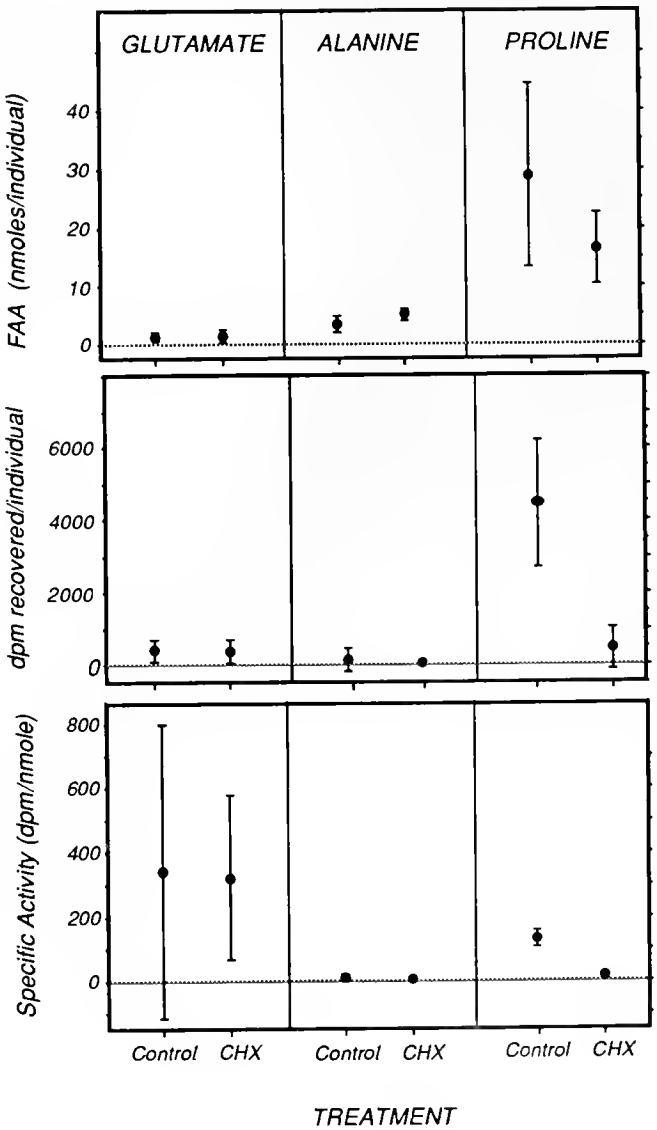

Figure 4. FAA concentrations and specific activities in individual *Callinectes sapidus* megalopas acclimated to 50% SW for 3 days and transferred to 100% SW for 4 h in the presence of ^{14}C-(U)-L-glutamate. CHX groups were pretreated with 10 m*M* cycloheximide for 1 h. Error bars are 95% confidence intervals (n = 6 individuals per treatment).

CHX treatment was specifically inhibitory to proline (but not alanine) synthesis.

Discussion

Although the role of proline accumulation in the hyperosmotic response is variable among the Crustacea, such an accumulation of proline is wide-spread among taxa, having been observed among bacteria (Le Rudulier *et al.*, 1984), fungi (Ho and Miller, 1978), and metaphytes (Boggess *et al.*, 1976), as well as among marine invertebrates (Florkin and Schoffeniels, 1969; Gilles, 1975, 1979; Schoffeniels, 1976). The mechanisms underlying proline accumulation may include protein degradation, uptake from the medium, and *de novo* synthesis. The role of each mechanism varies among taxa: for example, among microorganisms, gram-positive bacteria appear to regulate the synthesis or degradation of proline, whereas gram-negative bacteria achieve accumulation primarily via uptake from the medium (Csonka, 1989).

There is substantial variation among species with regard to the importance of proline in the FAA pool during hyperosmotic response (Claybrook, 1983). Among the Crustacea, proline is insignificant in the FAA pools of some species but the dominant contributor to the FAA pool in others. Furthermore, different tissue types vary dramatically in composition of the FAA pool. While proline is a major contributor to the pool in most adult *C. sapidus* tissues (Gerard and Gilles, 1972), it never accounted for more than 25% of the FAA pool in seawater-acclimated animals. In contrast, our data indicate that proline is the predominant FAA in megalopas, comprising over 50% of the FAA pool. Whether such ontogenetic changes in the composition of the FAA pool are common to other Crustacea has yet to be studied.

The regulation of FAA metabolism in response to osmotic stress among the Crustacea and other marine invertebrates is poorly understood. As discussed above and in Burton (1991a, b), models of direct inorganic ion effects on specific enzymes in FAA metabolism appear to be insufficient to explain the regulation of proline synthesis for two reasons. (1) Patterns of incorporation of radioactive precursors into proline indicate that rate of proline synthesis is nearly undetectable unless induced by hyperosmotic stress (Burton, 1986). (2) Because ^{14}C-labelled glutamate was provided as a precursor and inhibition of protein synthesis prevented proline synthesis which occurred in the absence of inhibitor, we can conclude that protein synthesis inhibition acts somewhere in the glutamate to proline pathway. Based on available information from bacteria and yeast, three gene loci encode the enzymes: γ-glutamyl kinase, γ-giutamyl phosphate reductase, and pyrroline-5-carboxylate reductase (Hayzer and Leisinger, 1980; Tomenchok and Brandriss, 1987). Although work on the proline biosynthetic pathway has not yet progressed to the genetic level among metazoans, available data suggests that homologous gene-enzyme systems are present (Smith *et al.*, 1980; Wakabayashi and Jones, 1983).

The results presented here for *C. sapidus* megalopas are similar to those obtained by Burton (1986, 1991b) for the copepod *Tigriopus californicus* in suggesting that proline synthesis is specifically induced by increases in environmental salinity rather than simply driven by changes in the synthetic rate of a precursor (*i.e.*, glutamate). As in the *T. californicus* system, induction of proline synthesis appears to be dependant on protein synthesis. In both systems, the inhibition of protein synthesis with cycloheximide decreased proline synthesis and accumulation during hyperosmotic stress but significantly increased alanine accumulation. Two possible explanations for the enhanced alanine accumulation follow: (1) By directly preventing the incorporation of alanine and other amino acids into protein, cycloheximide might lead to measurable increases in components of the FAA pool. (2) By preventing the induction of proline synthesis, cycloheximide increases the availability of alanine precursors (*e.g.*, glutamate), thereby stimulating alanine synthesis. In *T. californicus*, cycloheximide treatment resulted in significant incorporation of ^{14}C-label from glutamate into alanine (presumably via glutamate catabolism to malate and then pyruvate, a direct alanine precursor), supporting the latter explanation. This effect was not observed in *C. sapidus*, so the validity of the two hypotheses cannot be resolved with the data available. It should be noted, however, that of the five FAA monitored (glutamate, glycine, taurine, alanine, and proline), only alanine showed increased levels in response to cycloheximide treatment. This suggests that the former hypothesis alone is unlikely to account for the observed pattern of FAA accumulation when protein synthesis is inhibited.

The similarities between proline regulation in *C. sapidus* megalopas and *T. californicus* suggest that the induction of proline synthesis by hyperosmotic stress might be a common regulatory mechanism among the Crustacea. Protein synthesis is clearly required for the induction of proline synthesis in both species. While one must be cautious about generalizing on the basis of only two species, our results suggest a need for molecular tools to determine if the responsible protein is an enzyme in the pathway itself or a regulatory protein of some sort that stimulates existing enzymes to initiate proline synthesis.

Acknowledgments

I thank L. Kordos, J. Bishop, and H. Nguyen for collecting the crab megalopas, and H. Nguyen for technical assistance. J. Bishop and two anonymous reviewers provided thoughtful comments on the manuscript. This work

was supported by Texas Sea Grant, NSF Grant DCB-8811227, and the University of Houston Coastal Center.

Literature Cited

Boggess, S. F., C. R. Stewart, D. Aspinall, and L. G. Paleg. 1976. Effect of water stress on proline synthesis from radioactive precursors. *Plant Physiol.* **58:** 398–401.

Bowlus, R. D., and G. N. Somero. 1979. Solute compatibility with enzyme function and structure: rationales for the selection of osmotic agents and end-products of anaerobic metabolism in marine invertebrates. *J. Exp. Zool.* **208:** 137–152.

Burton, R. S. 1986. Incorporation of ^{14}C-bicarbonate into the free amino acid pool during hyperosmotic stress in an intertidal copepod. *J. Exp. Zool.* **238:** 55–61.

Burton, R. S. 1991a. Regulation of proline synthesis during osmotic stress in the copepod *Tigriopus californicus*. *J. Exp. Zool.* **259:** 166–173.

Burton, R. S. 1991b. Regulation of proline synthesis in osmotic response: effects of protein synthesis inhibitors. *J. Exp. Zool.* **259:** 272–277.

Claybrook, D. L. 1983. Nitrogen metabolism. Pp. 163–213 in *The Biology of Crustacea. Vol. 5*, L. H. Mantel, ed. Academic Press, New York.

Costlow, J. D., Jr., and C. G. Bookout. 1959. The larval development of *Callinectes sapidus* Rathbun reared in the laboratory. *Biol. Bull.* **116:** 373–396.

Csonka, L. N. 1989. Physiological and genetic responses of bacteria to osmotic stress. *Microbiol. Rev.* **53:** 121–147.

Engel, D. W. 1977. Comparison of the osmoregulatory capabilities of two portunid crabs, *Callinectes sapidus* and *C. similis*. *Mar. Biol.* **41:** 275–279.

Florkin, M., and E. Schoffeniels. 1969. *Molecular Approaches to Ecology.* Academic Press, New York. 203 pp.

Gerard, J. F., and R. Gilles. 1972. The free amino acid pool in *Callinectes sapidus* (Rathbun) tissues and its role in the osmotic intracellular regulation. *J. Exp. Mar. Biol. Ecol.* **10:** 125–136.

Gilles, R. 1975. Mechanisms of ion and osmoregulation. Pp. 259–347 in *Marine Ecology, Vol. 2, Part 1*, O. Kinne, ed. John Wiley and Sons, London.

Gilles, R. 1979. Intracellular organic osmotic effectors. Pp. 111–154 in *Mechanisms of Osmoregulation in Animals*, R. Gilles, ed. John Wiley and Sons, New York.

Gilles, R., and A. Pequeux. 1983. Interactions of chemical and osmotic regulation with the environment. Pp. 109–177 in *The Biology of Crustacea, Vol. 8*, F. J. Vernberg and W. B. Vernberg, eds. Academic Press, New York.

Hayzer, D. J., and Th. Leisinger. 1980. The gene-enzyme systems of proline biosynthesis in *Escherichia coli*. *J. Gen. Microbiol.* **118:** 287–293.

Ho, K. H., and J. J. Miller. 1978. Free proline content and sensitivity to desiccation and heat during yeast sporulation and spore germination. *Can. J. Microbiol.* **24:** 312–320.

Hochachka, P. W., and G. N. Somero. 1984. *Biochemical Adaptation.* Princeton University Press, Princeton. 537 pp.

Le Rudulier, D., A. R. Strom, A. M. Dandekar, L. T. Smith, and R. C. Valentine. 1984. Molecular biology of osmoregulation. *Science* **224:** 1064–1068.

Provasoli, L., K. Shiraishi, and J. R. Lance. 1959. Nutritional idiosyncrasies of *Artemia* and *Tigriopus* in monoxenic culture. *Annals N. Y. Acad. Sci.* **77:** 250–261.

Schoffeniels, E. 1976. Adaptations with respect to salinity. *Biochem. Soc. Symp.* **41:** 179–204.

Smith, R. J., S. J. Downing, J. M. Phang, R. F. Lodato, and T. T. Aoki. 1980. Pyrroline-5-carboxylate synthase activity in mammalian cells. *Proc. Natl. Acad. Sci. USA* **77:** 5221–5225.

Tomenchok, D. M., and M. J. Brandriss. 1987. Gene-enzyme relationships in the proline biosynthetic pathway of *Saccharomyces cerevisiae*. *J. Bacteriol.* **169:** 5364–5372.

Wakabayashi, Y., and M. E. Jones. 1983. Pyrroline-5-carboxylate synthesis from glutamate by rat intestinal mucosa. *J. Biol. Chem.* **258:** 3865–3872.

Williams, A. B. 1984. *Shrimps, Lobsters, and Crabs of the Atlantic Coast of the Eastern United States, Maine to Florida.* Smithsonian Institution Press, Washington, DC. 550 pp.

Reference: *Biol. Bull.* **182**: 416–423. (June, 1992)

Behavioral Regulation of Hemolymph Osmolarity Through Selective Drinking in Land Crabs, *Birgus latro* and *Gecarcoidea lalandii*

CHRISTIAN A. COMBS, NICOLE ALFORD, ANGELA BOYNTON, MARK DVORNAK, AND RAYMOND P. HENRY

Department of Zoology and Wildlife Science, 101 Cary Hall, Auburn University, Alabama 36849

Abstract. Drinking behavior in *Birgus latro* and *Gecarcoidea lalandii* was videotaped under controlled laboratory conditions. *B. latro* displayed the drinking behavior typically observed in nature, spooning up water with the chelae (Lister, 1888; Gross, 1955). *G. lalandii* is documented for the first time displaying this same behavior; however it obtained water primarily through immersion. Under normal hydrated conditions (hemolymph osmolarities < 1050 mOsm) *B. latro* showed no preference for drinking fresh or seawater. When dehydrated (hemolymph osmolarities > 1050 mOsm) *B. latro* altered its drinking behavior and showed a distinct preference for freshwater. This strategy resulted in restoration of original hemolymph osmolarities and wet weights and was accomplished through periods of intensive drinking activity. Conversely, *G. lalandii* never experienced true dehydration; rather, the hemolymph became hyperosmotic compared with control animals. This species preferred freshwater both under normal and hemoconcentrated conditions. *G. lalandii* was also able to osmoregulate behaviorally and was able to restore hemolymph osmolarities to normal concentrations via immersion in freshwater following experimentally induced hemoconcentration. Possible physiological and ecological reasons for the differences in water uptake strategies and preferences are discussed.

Introduction

The transition from the aquatic to the terrestrial environment was both problematic and beneficial for crabs. Although oxygen was more readily available and there were new resources to exploit, certain morphological, physiological, and behavioral strategies were required to overcome the barrier of desiccation and concomitant increase in hemolymph ion concentrations. Changes in hemolymph ion concentrations can profoundly affect many physiological processes in crustaceans including respiration, acid-base status, intracellular fluid volume, nitrogenous waste elimination, and enzyme function (Harris, 1977; Burrgren and McMahon 1981, 1988; Morris *et al.*, 1988; Wheatly *et al.*, 1984; Wood *et al.*, 1986; for reviews see Huggins and Munday, 1968; Schoffeniels, 1976; Gilles and Pequeux, 1981; Mangum, 1981; Taylor, 1982; Yancey *et al.*, 1982). In land crabs, dehydration and changes in hemolymph concentration are resisted using combinations of adaptations such as immersion, burrowing, water storage in the body or branchial chambers, evolutionary reduction in gill size, urine reprocessing, excretion of nitrogenous waste as urea or uric acid, and drinking (Bliss and Mantel, 1968; Bliss, 1979; Mantel and Farmer, 1983; Powers and Bliss, 1983; Wolcott and Wolcott, 1985, 1991; Greenaway, 1988; Greenaway *et al.*, 1988; T. G. Wolcott, 1988; D. L. Wolcott, 1991).

Drinking, or spooning up water with the chelae to the mouthparts, has been documented in *Gecarcoidea natalis*, *Geograpsus grayi*, *Cardisoma guanhumi* (Gross *et al.*, 1966), *C. carnifex* (Greenaway, 1988), *Gecarcoidea lalandii* (this paper), and in *Birgus latro* (Lister, 1888). Fresh and seawater are available to most land crabs, but it is not known precisely how the more terrestrial species use the two to regulate the concentration of their hemolymph. These crabs inhabit islands in the Indo-Pacific region where rainfall is seasonal and water sources other than the ocean may become scarce at certain times of year (Gross, 1964). This study examines the drinking preference of two of the more strictly terrestrial crabs, *Birgus*

Received 9 September 1991; accepted 26 February 1992.

latro (Anomura) and *Gecarcoidea lalandii* (Brachyura), when hemolymph concentrations are normal and hemoconcentrated (with possible dehydration).

Materials and Methods

Animal collection and maintenance

Specimens of both species, *Birgus latro* (500–2100 g) and *Gecarcoidea lalandii* (65–220 g) were obtained from the islands of Palau and Pohnpei and were shipped via air-freight in damp burlap inside coolers or ice chests. They were maintained in isolated Nalgene tanks (*B. latro*) or fabricated wooden pens with plexiglass partitions (*G. lalandii*) in a dark room at approximately 25°C. All were fed coconut, lettuce, and apples every other day, and were given either dechlorinated tapwater or seawater (35–40 ppt, as determined with a refractometer) depending on the subsequent testing regime.

Protocol

Observation chambers were constructed using standard 75 and 115 l aquaria fitted with a false bottom of plexiglass to facilitate viewing and minimize water spillage. Two circular holes were cut side-by-side in the false bottom to allow access to a pair of glass preparation dishes (115 × 50 mm, Fisher) that were secured with silicone to the aquarium floor. The tops of the dishes were flush with the plexiglass platform, simulating pools of water. The chamber was darkened on three sides to isolate each crab. The uncovered end of the aquaria permitted head-on viewing of both bowls. A plexiglass cover with air holes for ventilation was secured to each tank to prevent escape.

Drinking behavior of animals was recorded for individuals displaying hemolymph osmotic concentrations typically found for crabs sampled in the field (<1050 mOsm) (as reported by Henry and Cameron, 1981; Greenaway, 1988) and after hemoconcentration with possible dehydration (hemolymph osmolarity > 1050 mOsm). The former condition was maintained by allowing crabs to drink ad libitum from both fresh and seawater. Hemoconcentration was achieved through a combination of water deprivation and allowing access to only hypersaline water (>35 ppt). Animals were weighed daily and were not allowed to lose more than 12% of their initial wet weight, a value that was within the maximal tolerable levels of dehydration as reported by Kormanik and Harris (1981) and Burggren and McMahon (1981). Hemolymph osmolality was measured concurrently to determine at what point values exceeded 1050 mOsm, after which an experiment was begun.

Individual crabs were randomly assigned their initial condition, normal or hemoconcentrated. Behavior of each individual was recorded under both normal and hemoconcentrated conditions, allowing at least a 48 h recovery period between experiments.

All crabs were allowed to adjust to the chambers for 24 h prior to observation/videotaping, while remaining on their water regime. Immediately preceding an observation period, crabs were weighed to the nearest 0.1 g on a top loading balance (Sartorius), and a blood sample (0.1 ml) was taken from the infrabranchial sinus. The water in each chamber was replaced with 225 ml of seawater (35 ppt) and 225 ml of fresh (deionized) water was placed randomly in either the right or left dish. The crabs were then recorded for 12 h (1800–0600 h) using a Panasonic VHS Recorder Model AG-HT3. After 12 h, the crabs were weighed, blood samples were drawn, and the water volume remaining in each bowl was measured to the nearest 1.0 ml. Evaporative water loss was quantified using duplicate bowls of freshwater and seawater placed in an empty chamber. Temperature and relative humidity were also recorded using a ExTech Instruments Digital Humidity/Temperature Meter.

Hemolymph samples were placed in microcentrifuge tubes and kept on ice. After being sonicated at 20 watts for 10 s with a Microson Cell Disruptor CM-1 convertor (Heat Systems—Ultrasonics, Inc.), the samples were centrifuged for 1 min using a Micro-Centrifuge Model 235B (Fisher). Osmolarity was determined on 10 μl samples of serum using a Wescor 5100C Vapor Pressure Osmometer.

Quantification of the number of drinks, time spent drinking, and time spent immersed in the water bowl were determined from video tape analysis. An individual drink was considered to be a cheliped sweep from the water to the mouth and subsequent sweep by the maxillae over the cheliped to remove the water (Lister, 1888). Time spent drinking was designated as the time of the first cheliped sweep to the time of the last cheliped sweep. Immersion time was considered to be the amount of time that a crab had part of its carapace submerged in a water bowl.

Statistics

Paired *t*-tests were used to determine if there were differences between water preferences within hemolymph concentration treatments, weight differences between hemolymph concentrations, and starting and ending hemolymph concentrations between treatments. Analysis of variance (ANOVA) was used to determine if there were differences between the preferences of crabs for drinking freshwater or seawater between hemolymph concentration conditions in each species. To reduce biases inherent in individual animals, only individuals that were tested at both hemolymph conditions were included in the statistical analysis. Scheffe's multiple comparisons test was used to compare means of the variables between normal and

hemoconcentrated treatments. All data were tested for normality using the Wilkes-Shapiro test and can be assumed to be normally distributed unless specified. All statistical analyses were accomplished with the SAS™ statistical computer package (SAS Inst., Inc., 1982).

Results

Strategies of water uptake

The two species employed different strategies of water uptake both to maintain a normal hemolymph osmotic condition and to reduce hemolymph concentrations in response to hemoconcentration (often accompanied by dehydration in *B. latro*). *B. latro* used cheliped drinking as the only means of water uptake, spending 100% of their drinking time in that behavior; immersion in the water bowls was not employed, although the bowls could have accommodated at least portions of their bodies. The observed drinking behavior was virtually identical to that reported previously by Lister (1888). *G. lalandii*, however, was observed in cheliped drinking behavior only 2% of the time; the remainder of the time in contact with water was spent with all or part of the carapace immersed in the water bowl. When this species did engage in cheliped drinking, the behavioral pattern was similar to that seen in *B. latro*.

Normal water uptake and response to hemoconcentration

All specimens of *B. latro* that began an experiment in a normal hemolymph concentration state (848 ± 22 mOsm) were able to maintain that state over the 12 h observation period (*t*-test: $P > 0.81$) (Fig. 1). Under normal conditions, *B. latro* spent an average of 61 min engaged in drinking, performing 660 individual cycles of cheliped sweeps during a 12-h experiment. This species showed no preference for fresh or seawater, either with respect to the percent of the total drinks taken from each bowl (*t*-test: $P > 0.73$), the time spent drinking from each bowl (*t*-test: $P > 0.2$), or the percent of volume that was drunk (*t*-test: $P > 0.2$) (Fig. 2).

When individuals were hemoconcentrated prior to an experiment (1171 ± 51 mOsm), both the overall drinking behavior and the drinking preference were altered. Animals in a hemoconcentrated condition increased their total drinking time by over four-fold to 273 min, taking an average of 2702 individual drinks during that time. These animals displayed a distinct preference for freshwater for all three variables measured: total drinks, time of drinking, and volume consumed (*t*-test: $P < 0.01$) (Fig. 2). In addition, the drinking preferences were different between the two osmotic states (ANOVA: $P < 0.01$) with all control crabs exhibiting the same preference and all hemoconcentrated crabs exhibiting the same preference (Scheffe: $P < 0.05$). This behavior led to a significant difference in osmolarity changes before and after the 12-h tests between the normal and hemoconcentrated treatments (*t*-test: $P < 0.02$), with the hemoconcentrated animals reducing their average osmolarity by 18% to 948 ± 26 mOsm. In addition, differences in weight before and after the 12-h tests were significantly different between control and hemoconcentrated animals (*t*-test: $P < 0.01$) with normal animals averaging only a 5 ± 12 g weight gain while hemoconcentrated animals gained 75 ± 16 g (Fig. 1). Therefore, *B. latro* compensated for hemoconcentration via water gain, indicating that initial hemoconcentration was accompanied by dehydration.

All specimens of *Gecarcoidea lalandii* that began an experiment in a normal hemolymph concentration state (947 ± 31 mOsm) were also able to maintain that state over the 12-h observation period (*t*-test: $P > 0.77$) (Fig. 3). On average, specimens of *G. lalandii* that began an experiment in a hemoconcentrated state (1168 ± 27 mOsm) were able to reduce their hemolymph concentration back to control levels (*t*-test: $P > 0.30$) over the 12-h observation period. Freshwater was significantly preferred over seawater at both osmotic states (*t*-test: $P < 0.05$ and $P < 0.1$, respectively) when immersion time was used as an indicator of behavioral osmoregulation (Fig. 4). Moreover, there is a significant difference in the amount of time spent immersed in seawater between the two osmotic states, with more time being spent in seawater when individuals started the experiments hemoconcentrated (ANOVA: $P < 0.05$, Scheffe: $P < 0.05$). The data for number of cheliped drinks and time spent cheliped drinking were not normally distributed, but freshwater was overwhelmingly preferred at both hydration states (Fig. 4) for the small amount of time, 2%, this species spent cheliped drinking. End-volume differences in the drinking bowls were not examined in this species due to the propensity of the animals to splash water out of the bowls while entering and exiting from them. This obscured any differences that might have been due to their drinking or absorbing water. Differences in weight before and after the 12-h tests were not significantly different between control and hemoconcentrated animals (*t*-test: $P > 0.25$). Therefore, *G. lalandii* did not compensate for hemoconcentration by water gain but rather appeared to reduce hemolymph ion concentrations through ion exchange via immersion in the ambient water.

Discussion

Both *Birgus latro* and *Gecarcoidea lalandii* can osmoregulate behaviorally, by selecting drinking water of the appropriate salinity, under laboratory conditions. Using this strategy they were able to maintain hemolymph

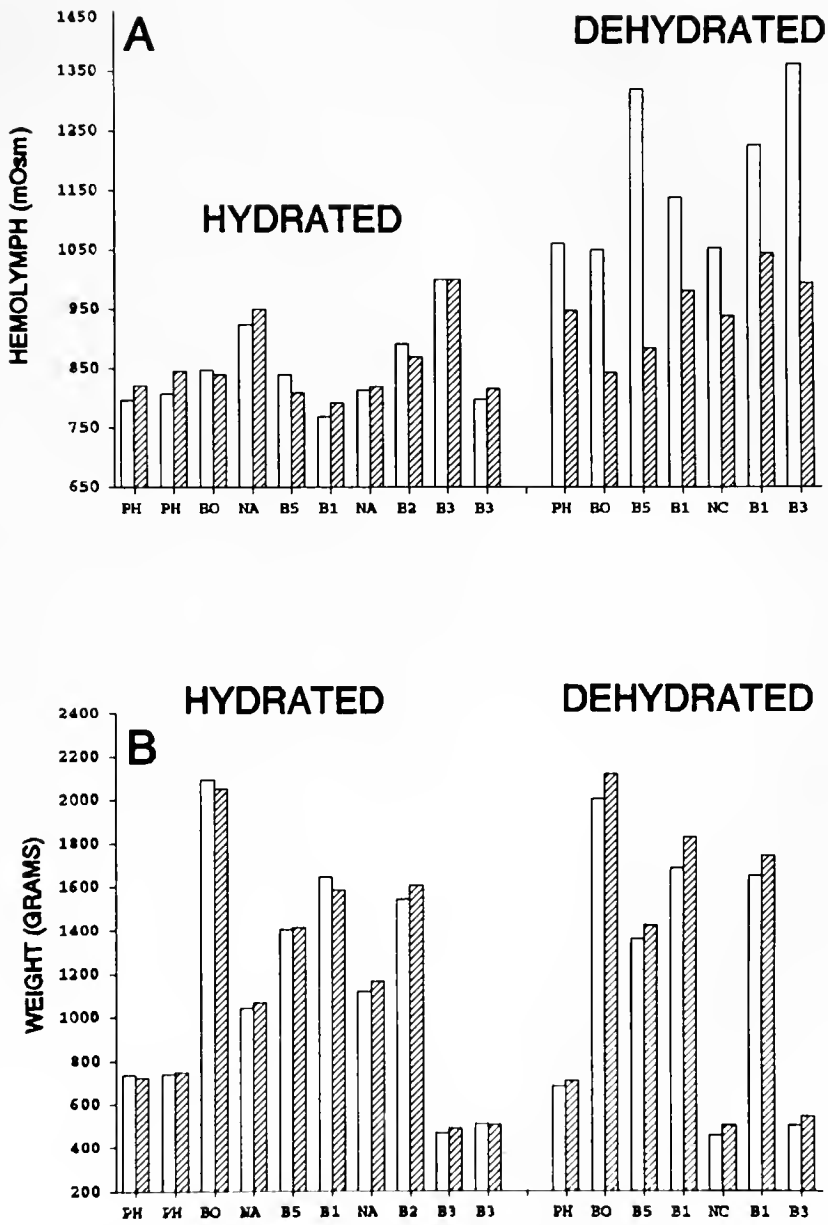

Figure 1. (A) Hemolymph concentrations (mOsm), and (B) weight (g), before (open bars) and after (shaded bars) 12-hour tests involving *Birgus latro*. Left-hand regions of figure are tests with initially normal hemolymph concentrations (<1050 mOsm) and right-hand regions are tests with initially concentrated hemolymph osmolarities (>1050 mOsm). X-axis labels identify individual specimens.

concentration and wet weight at normal hydrated levels during 12-h test periods. When hemoconcentrated, both species could reduce their hemolymph osmolarities to normal levels. This was accomplished by ion exchange in *G. lalandii*, whereas *B. latro* took on water to dilute the hemolymph.

Gross (1955) first documented the ability of *B. latro* to osmoregulate behaviorally. The present study indicated somewhat different results for drinking preference than did Gross (1955). In our study, specimens of *B. latro* at normal hemolymph concentrations (hypoosmotic to seawater) showed no preference for either fresh or seawater; rather, they precisely regulated their hemolymph osmolarity through piecemeal drinking of both water types. In contrast, Gross (1955) reported that hydrated crabs preferred freshwater, but did drink some seawater. Our results coincide with those of Gross (1955) in that dehydrated crabs (hemolymph concentrations hyperosmotic to seawater) preferred freshwater. The difference in results between the two studies may be a result of the manner by

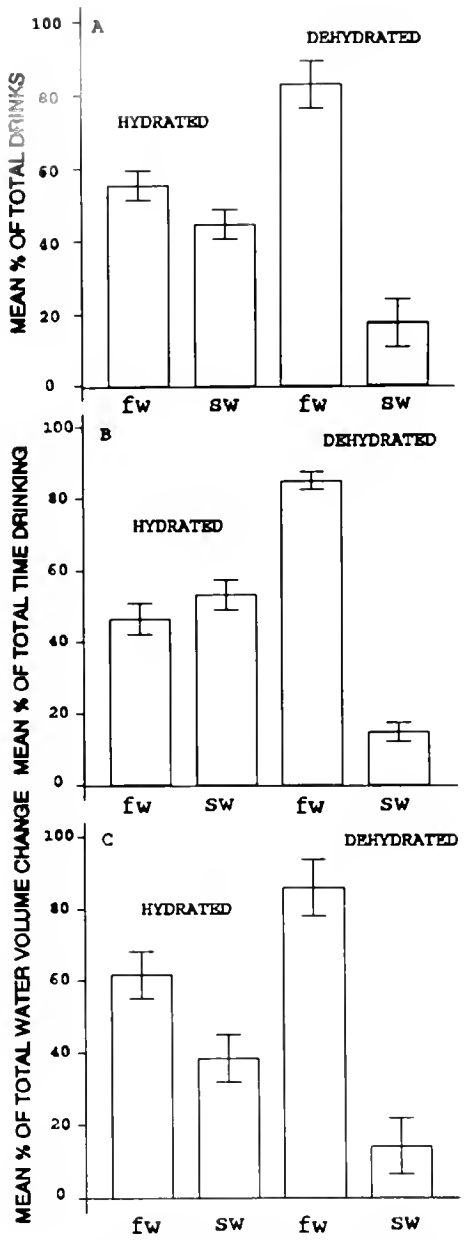

Figure 2. Drinking preference for freshwater or seawater according to initial hemolymph concentration (hydrated and dehydrated) during 12-hour tests involving *Birgus latro* (n = 5). Drinking preference is expressed as (A) mean percentage of total drinks, (B) mean percentage of total time spent drinking, (C) mean percentage of total volume change from water bowls (normalized for evaporative water loss).

which the quantification of the drinking preference was obtained. Gross (1955) quantified drinking behavior indirectly. Drinking behavior was monitored by etchings made on Kymograph drums caused by depressions of platforms over drinking bowls (see Gross, 1955, 1957 and Gross and Holland, 1960 for details). These etchings were then used to quantify drinking bouts. Precautions were taken in his study to reduce recording of behavior other than drinking, but because these recordings were unattended it is unclear whether all the behavior recorded was actually drinking. Our study had the distinct advantage of directly viewing all of the animals' behavior, thereby allowing differentiation of drinking and exploratory behaviors, which enabled precise quantification of drinking behavior.

Birgus latro usually inhabits sand burrows or piles of decaying vegetation during the day and forages at night when ambient temperatures are cooler (Gross, 1964). These crabs employ both physiological and behavioral means of osmoregulation, although the main method appears to be behavioral avoidance of desiccation (Gross, 1964) along with uptake of water by drinking from inland pools. *Birgus latro* also uses a suite of physiological adaptions for osmoregulation. *B. latro* can reabsorb salts from the urine (Harris and Kormanik, 1981; Greenaway and Morris, 1989) and it has evolved the ability to excrete uric acid and therefore waste less water in nitrogen elimination (Bliss and Mantel, 1968; Kormanik and Harris, 1981; Greenaway and Morris, 1989). During periods of dehydration, specimens of *B. latro* continue to produce isosmotic urine and maintain intracellular fluid volume while sacrificing extracellular stores (Burggren and McMahon, 1981; Harris and Kormanik, 1981). The large abdomen is the water storage site in *B. latro* (Harris and Kormanik, 1981) and becomes quite distended when fully hydrated, but only a small volume of water is stored in the branchial cavity relative to other terrestrial crabs (Wood and Boutilier, 1985). In addition, the gills are highly reduced (Cameron, 1981), thus limiting evaporative water loss, and they are used as exchange sites for ions, water, and carbon dioxide with oxygen uptake taking place at the primitive lung (Greenaway *et al.*, 1988). Thus, it seems that *B. latro*'s ability to differentiate between water of different salinities and its precise regulation of hemolymph concentration through piecemeal drinking augment its suite of other behavioral and physiological mechanisms and help to explain its high degree of terrestriality.

Birgus latro has never been observed drinking seawater directly from the ocean, although tracks have been found on dunes close to the shoreline (Gross, 1964), and Grubb (1971) reported anecdotal evidence of coconut crabs visiting the ocean. Considering the evidence presented in this study as well as in Gross (1955), *B. latro* might use the ocean as a water source under certain conditions. Field studies investigating the natural behavior of these crabs, particularly on some of the dry Pacific atolls, would help bring the findings of this study into context with the natural strategies these animals employ to osmoregulate behaviorally.

Gecarcoidea lalandii usually inhabits dry inland burrows (Bliss, 1968) and probably relies on intermittent access to dew and rain, along with soil water, for water up-

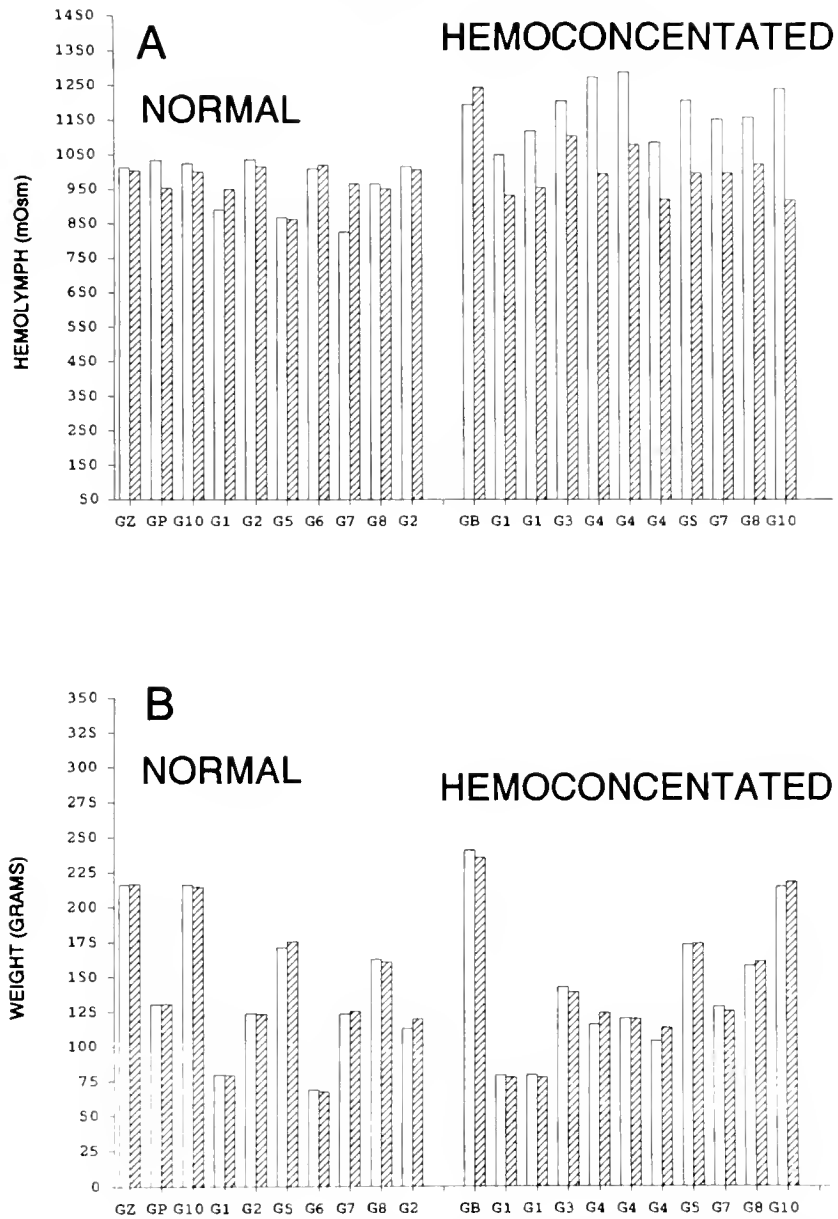

Figure 3. (A) Hemolymph concentrations (mOsm), and (B) weight (g), before (open bars) and after (shaded bars) 12-hour tests involving *Gecarcoidea lalandii*. Left-hand regions of figure are tests with initially normal hemolymph concentrations (<1050 mOsm) and right-hand regions are tests with initially concentrated hemolymph osmolarities (>1050 mOsm). X-axis labels identify individual specimens.

take (Wolcott, 1988). Although it is a highly terrestrial crab, its gills are not as reduced as those of *B. latro* (Cameron, 1981) and are therefore more subject to evaporative water loss. In this study, specimens of *G. lalandii* preferred to immerse themselves in, and drink from, freshwater regardless of initial blood condition. This contrasts with the water uptake strategy employed by their cogener *G. natalis*, which prefers to drink (Gibson-Hill, 1947). This is the first quantification of drinking preference for this species. The preference for freshwater is not surprising considering the recent work of Wolcott and Wolcott (1985, 1991) who showed that other brachyurans (*Gecarcinus lateralis* and *Ocypode quadrata*) can reabsorb salts through urine reprocessing in the branchial chamber. Perhaps this and other physiological and behavioral osmoregulatory strategies explain why brachyurans do not need to rely heavily on seawater for their water budget. Wolcott and Wolcott (1988) conclude that *G. lateralis* inhabiting the island of Bermuda seldom if ever comes in contact with seawater except when spawning. Further, they conclude

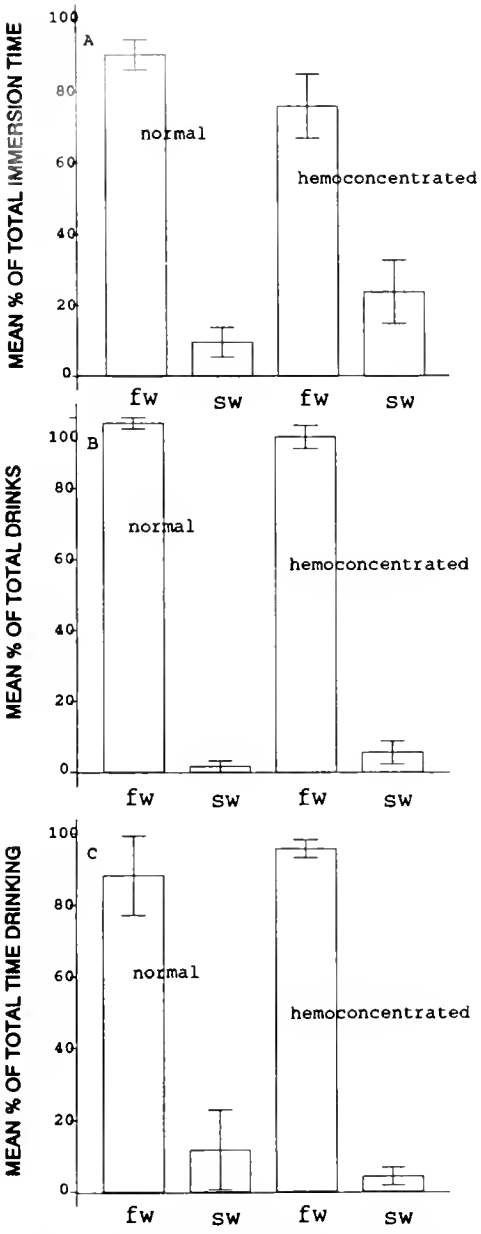

Figure 4. Drinking preference for freshwater or seawater according to initial hemolymph concentration (hydrated and dehydrated) during 12-hour tests for *Gecarcoidea lalandii* (n = 5). Drinking preference is expressed as (A) mean percentage of total immersion time, (B) mean percentage of total number of cheliped drinks, (C) mean percentage of total time spent cheliped drinking.

that most of the drinking water available to land crabs on Bermuda is freshwater, even near the edge of the shore. Brachyurans living on some islands in the Indo-Pacific region however, face seasonal paucity of freshwater (Gross 1964), but their behavior during these times has yet to be reported.

Land crabs in general are euryhaline (Mantel and Farmer, 1983) and can withstand a wide range of hemolymph concentrations. Restoration of hemolymph osmolarities to normal levels after dehydration occurs quickly in both species but by different methods. This phenomenon may be a result of the natural unavailability of water sources (other than the ocean) at certain times of year thus forcing animals to rehydrate quickly after desiccation whenever favorable situations occur. This is evidenced by the amazing amount of time (5 h av.) and activity (>2500 individual cheliped drinking cycles) expended by *B. latro* in rehydrating itself after desiccation. In contrast, *B. latro* spent an average of only 1 h per night drinking, performing only about 500 individual cheliped drinking cycles when hydrated.

G. lalandii preferred to immerse itself rather than drink in order to obtain water, although it did occasionally drink. The reason for this difference in strategy is unclear, but it could have both a physiological and ecological basis. *B. latro* experienced both hemoconcentration and dehydration (*i.e.*, weight loss) when deprived of water. This suggests that some tissue water loss occurs, most probably from the large abdomen, in addition to a reduction in hemolymph volume. Therefore, it is possible that *B. latro* drinks to replenish tissue water content. *G. lalandii,* however, appears only to undergo hemoconcentration, and this may be related to the fact that this species lacks an obvious store of tissue water. As a consequence, hemolymph volume may be sacrificed to maintain tissue water content, and the major function of immersion may be to alleviate a hemolymph ion load, which can be done readily across the gills. Thus, the different strategies of rehydration may be in answer to two different physiological stresses.

The decrease in time devoted to obtaining water via immersion *versus* cheliped sweeps (2.5 min average following desiccation and 1.3 min average when hydrated per 12-h test session) may also decrease the risk of predation in *G. lalandii,* which is smaller and potentially more vulnerable than *B. latro.*

Further research involving behavioral osmoregulation may investigate the feedback mechanisms of internal and external osmoreceptors. Internal receptors that monitor blood osmolality have not yet been found. However, in other species, hormones produced by cells in the optic ganglia, brain, and thoracic ganglia affect the movement of salts and water across the gills, renal organ membranes, and gastrointestinal wall (Hill and Wyse, 1989). Greenaway (1988) speculated that *B. latro* has osmoreceptors on the chelae or mouth parts. It is quite possible that *B. latro* and *G. lalandii* also have internal blood osmotic receptors and that feedback mechanisms involving hormones and external osmoreceptors enable it to choose water of the appropriate salinity to maintain normal blood osmolalities. Future work involving manipulation of blood osmolality and testing with the video protocol we have established might initiate understanding of the

mechanisms that enable *B. latro* and *G. lalandii* to osmoregulate behaviorally.

Acknowledgments

We gratefully thank Lynn M. Robison, Dr. James West, Dr. Robert Lishak, and John Newman for their contributions to this investigation and to Dr. Lawrence Wit for contributing laboratory space and for advice and criticism. Supported by NSF DCB 88-01926 to RPH, by funds from the NSF Research Experience for Undergraduates (REU) program, and by the Alabama Agricultural Experiment Station (AAES 15-923248).

Literature Cited

Bliss, D. E. 1968. Transition from water to land in decapod crustaceans. *Am. Zool.* **8:** 355–392.

Bliss, D. E. 1979. From sea to tree: saga of a land crab. *Am. Zool.* **19:** 385–410.

Bliss, D. E., and L. H. Mantel. 1968. Adaptations of crustaceans to land: a summary and analysis of new findings. *Am. Zool.* **8:** 673–685.

Burggren, W. W., and B. R. McMahon. 1981. Hemolymph oxygen transport, acid-base status, and hydromineral regulation during dehydration in three terrestrial crabs, *Cardisoma, Birgus*, and *Coenobita*. *J. Exp. Zool.* **218:** 53–64.

Burggren, W. W., and B. R. McMahon. 1988. *Biology Of The Land Crabs.* Cambridge University Press, Cambridge.

Cameron, J. N. 1981. Brief introduction to the land crabs of the Palau Islands: stages in the transition to air breathing. *J. Exp. Zool.* **218:** 1–5.

Gibson-Hill, C. A. 1947. Field notes on the terrestrial crabs. *Bull. Raffles Mus.* **18:** 43–52.

Gilles, R., and A. Pequeux. 1981. Cell volume regulation in crustaceans: relationship between mechanisms for controlling the osmolarity of extracellular and intracellular fluids. *J. Exp. Zool.* **215:** 351–362.

Greenaway, P. 1988. Ion and water balance. Pp. 211–248 in *Biology of the Land Crabs*, W. W. Burggren, and B. R. McMahon, eds. Cambridge University Press, Cambridge.

Greenaway, P., and S. Morris. 1989. Adaptations to a terrestrial existence by the robber crab, *Birgus latro* L. III. Nitrogenous excretion. *J. Exp. Biol.* **143:** 333–346.

Greenaway, P., S. Morris, and B. R. McMahon. 1988. Adaptations to a terrestrial existence by the robber crab *Birgus latro*. II. *In vivo* respiratory gas exchange and transport. *J. Exp. Biol.* **140:** 493–509.

Gross, W. J. 1955. Aspects of osmotic regulation in crabs showing the terrestrial habitat. *Am. Nat.* **89:** 205–222.

Gross, W. J. 1957. A behavioral mechanism for osmotic regulation in a semi-terrestrial crab. *Biol. Bull.* **113:** 268–274.

Gross, W. J. 1964. Water balance in anomuran land crabs on a dry atoll. *Biol. Bull.* **126:** 54–68.

Gross, W. J., and P. V. Holland. 1960. Water and ionic regulation in a terrestrial hermit crab. *Physiol. Zool.* 33: 21–28.

Gross, W. J., R. C. Lasiewski, M. Dennis, and P. Rudy, Jr. 1966. Salt and water balance in selected crabs of Madagascar. *Comp. Biochem. Physiol.* **17:** 641–660.

Grubb, P. 1971. Ecology of terrestrial decapod crustaceans of Aldabra. *Phil. Trans. Roy. Soc. Lond.* **260:** 411–416.

Harris, R. R. 1977. Urine production rate and water balance in the terrestrial crabs *Gecarcinus lateralis* and *Cardisoma guanhumi*. *J. Exp. Biol.* **68:** 57–67.

Harris, R. R., and G. A. Kormanik. 1981. Salt and water balance and antennal gland function in three Pacific species of terrestrial crab (*Gecarcoidea lalandii, Cardisoma carnifex, Birgus latro*). II. The effects of desiccation. *J. Exp. Zool.* **218:** 107–116.

Henry, R. P., and J. N. Cameron. 1981. A survey of blood and tissue nitrogen compounds in terrestrial decapods of Palau. *J. Exp. Zool.* **218:** 83–88.

Hill, R. W., and G. A. Wyse. 1989. *Animal Physiology*, 2nd. ed. Harper and Row, New York. 656 pp.

Huggins, A. K., and K. A. Munday. 1968. Crustacean metabolism. *Adv. Comp. Biochem. Physiol.* **3:** 271–378.

Kormanik, G. A., and R. R. Harris. 1981. Salt and water balance and antennal gland function in three Pacific species of terrestrial crab (*Gecarcoidea lalandii, Cardisoma carnifex, Birgus latro*). I. Urine production and salt exchanges in hydrated crabs. *J. Exp. Zool.* **218:** 97–109.

Lister, J. J. 1888. On the natural history of christmas island, in the Indian Ocean. *Proc. Zool. Soc. Lond.* **2:** 512–531.

Mantel, L. H., and L. L. Farmer. 1983. Osmotic and ionic regulation. Pp. 53–161 in *The Biology of Crustacea*, Vol. 5., L. H. Mantel and D. E. Bliss, eds. Academic Press, New York.

Mangum, C. P. 1981. 1983. Oxygen transport in the blood. Pp. 373–362 in *The Biology of Crustacea*, Vol. 5, L. H. Mantel and D. E. Bliss, eds. Academic Press, New York.

Morris, S., P. Greenaway, and B. R. McMahon. 1988. Adaptations to a terrestrial existence by the robber crab *Birgus latro*. I. An *in vitro* investigation of blood gas transport. *J. Exp. Biol.* **140:** 477–491.

Powers, L. W., and Bliss, D. E. 1983. Terrestrial adaptions. Pp. 271–334 in *The Biology of Crustacea*, Vol. 8, F. J. Vernberg and W. B. Vernberg, eds. Academic Press, New York.

Schoffeniels, E. 1976. Adaptations with respect to salinity. *Biochem. Soc. Symp.* **41:** 179–204.

Taylor, E. W. 1982. Control and co-ordination of ventilation and circulation in crustaceans: responses to hypoxia and exercise. *J. Exp. Biol.* **111:** 103–121.

Wheatly, M. G., W. W. Burggren, and B. R. McMahon. 1984. The effects of temperature and water availability on ion and acid-base balance in hemolymph of the land hermit crab *Coenobita clypeatus*. *Biol. Bull.* **166:** 427–445.

Wolcott, D. L., 1991. Nitrogen excretion is enhanced during urine recycling in two species of terrestrial crab. *J. Exp. Zool.* **259:** 181–187.

Wolcott, T. G., 1988. Ecology. Pp. 55–95 in *Biology of the Land Crabs*, W. W. Burggren, and B. R. McMahon, eds. Cambridge University Press, Cambridge.

Wolcott, T. G., and D. L. Wolcott. 1985. Extrarenal modification of urine for ion conservation in ghost crabs, *Ocypode quadrata* (Fabricus). *J. Exp. Mar. Biol. Ecol.* **91:** 93–107.

Wolcott, T. G., and D. L. Wolcott. 1988. Availability of salts is not a limiting factor for the land crab *Gecarcinus Lateralis* (Freminville). *J. Exp. Mar. Biol. Ecol.* **120:** 199–219.

Wolcott, T. G., and D. L. Wolcott. 1991. Ion conservation by reprocessing of urine in the land crab *Gecarcinus lateralis* (Freminville). *Physiol. Zool.* **64:** 344–361.

Wood, C. M., and R. G. Boutilier. 1985. Osmoregulation, ionic exchange, blood chemistry, and nitrogenous waste excretion in the land crab *Cardisoma carnifex*: a field and laboratory study. *Biol. Bull.* **169:** 267–290.

Wood, C. M., R. G. Boutilier, and D. J. Randall. 1986. The physiology of dehydration stress in the land crab, *Cardisoma carnifex*: respiration, ionoregulation, acid-base balance and nitrogenous waste excretion. *J. Exp. Biol.* **126:** 271–296.

Yancey, P. H., M. E. Clark, S. C. Hand, R. D. Bowlus, and G. N. Somero. 1982. Living with water stress: evolution of osmolyte systems. *Science* **217:** 1214–1222.

Reference: *Biol. Bull.* **182**: 424–434. (June, 1992)

Causes and Consequences of Fluctuating Coelomic Pressure in Sea Urchins

OLAF ELLERS[1] AND MALCOLM TELFORD[2]

[1]*Department of Zoology, University of California, Davis, California 95616 and*
[2]*Department of Zoology, University of Toronto, Toronto, Ontario M5S 1A1, Canada*

Abstract. We measured coelomic pressure in sea urchins to determine whether it was high enough to support a pneu hypothesis of growth. In *Strongylocentrotus purpuratus* the pressure was found to fluctuate rhythmically about a mean of −8 Pa, and was negative for 70% of the time. This is at variance with the theoretically required positive pressures of the pneu hypothesis. Furthermore, there were no sustained significant differences between the pressure patterns of fed and starved urchins, presumed to be growing and not growing, respectively. The rhythmical fluctuations in pressure were caused by movements of the lantern which changed the curvature and tension of the peristomial membrane. We developed a mathematical and morphological model relating lantern movements, membrane tension, and pressure, that correctly predicts the magnitude of the fluctuations. Pressures predicted by the model depend also on coelomic volume changes. In *Lytechinus variegatus* simultaneous retraction of the podia, which causes expansion of the ampullae, resulted in an 8.8 Pa increase in coelomic pressure, relative to the pressure during simultaneous podial protraction.

Introduction

For some seventy-five years, the growth and shape of sea urchins have, with few exceptions, been attributed to a similarity with internally pressurized tensile structures. D'Arcy Thompson (1917) remarked on the similarity of shape between sea urchins and water droplets on a glass plate. A water-filled balloon resting on a table (Fig. 1) provides an analogous form. This basic idea has been invoked repeatedly to explain both growth and form. Moss and Meehan (1968) suggested that growth of the gut and gonads increased coelomic pressure and this caused growth in the test. Likening echinoids to inflated structures (pneus), Seilacher (1979) argued that variations in shape among regular and irregular echinoids could be explained by forces from the tube feet and by the occurrence of internal "tethers" of calcite or collagen. Dafni and Erez (1982), Dafni (1983, 1985, 1986), and Baron (1988), all assumed the existence of positive internal pressure in sea urchins, and explained morphogenesis in terms of the resulting stress patterns and the action of forces from other sources such as podia, internal muscles, and mesenteries.

Although internal fluid pressure is usually not relevant in the functional analysis of solid structures, there are engineering designs in which it does play an important role. While designing underwater storage vessels that require a minimum of wall materials, Royles *et al.* (1980) were impressed by the similarity of their theoretically derived shapes and some sea urchins (most notably *Echinus esculentus*). The design of such "constant strength" or "buckle-free" structures involves balancing pressure differences (positive or negative) across the vessel wall with forces in the wall. It is tempting to interpret the convergence on an echinoid form as indicative of an underlying similarity in the balance of forces. Royles *et al.* (1980) actually coined the expression of "Echinodome" for these structures.

The obvious and crucial question—what is the magnitude of the internal pressure in echinoids—has not been answered. Dafni (1985, 1986) attempted to manipulate forces acting on the growing test and isolated plates, but provided no measurements of pressure. Reporting the only pressure measurements, Baron (1991) recorded fluctuating coelomic pressures in an echinoid. With the aid of a finite element method he developed a complicated tensile growth model which, although elegantly refined, is still fundamentally a pneu hypothesis. According to his model,

Received 21 October 1991; accepted 27 March 1992.

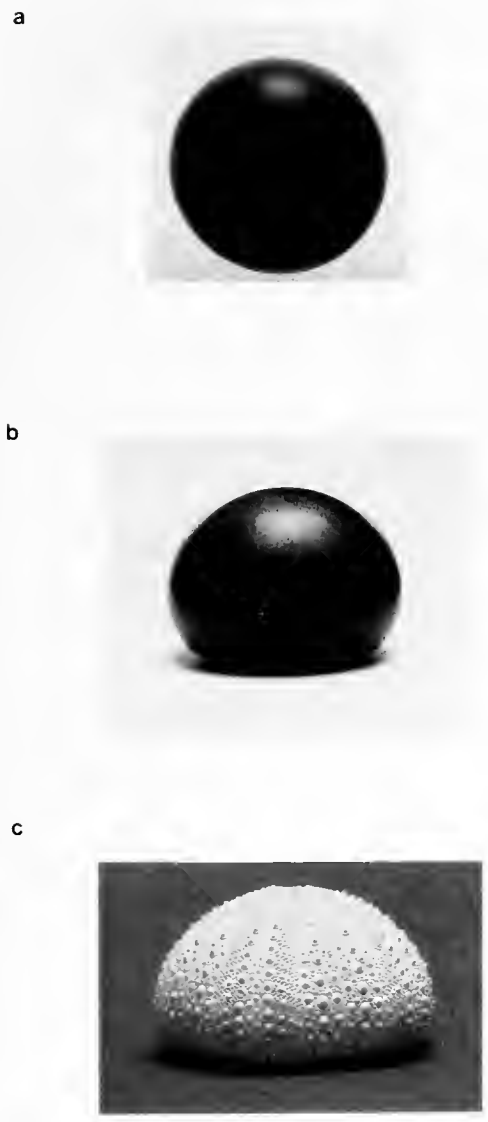

Figure 1. (a) A balloon filled with water in water; (b) a balloon filled with water in air; and (c) an urchin test. Note the similarity of shape between the (b) and (c). The difference in shape between (a) and (b) illustrates the importance of self-weight forces. There are no self-weight forces on a water-filled balloon in water since the water inside and outside are equally dense. In urchins, the internal volume also has no effective weight: thus the downward forces result only from the underwater weight of the calcite or the pull of tube feet. The weight forces are balanced by internal pressure resulting from tension in the membrane. None of these structures are pneus because they are not air-filled, but (a) and (b) certainly, and (c) possibly, form their shape as a result of forces analogous to those in a pneu, including internal pressurization.

growth can occur only during periods of positive internal pressure.

In this paper we describe a technique for measuring coelomic pressure in sea urchins and report the results of two series of experiments. The first series was undertaken to determine whether there was sufficient positive pressure to support the pneu hypothesis of growth. For this, we compared pressures in sea urchins (*Strongylocentrotus purpuratus*) fed *ad libitum* and presumed to be actively growing, with pressures in starved animals, presumably not growing (Ebert, 1968). After measuring the fluctuating pressures, we investigated the possible morphological and physical causes of the pressure patterns. This led to development of a model relating pressure changes to alterations in curvature in the peristomial membrane during protraction and retraction of the lantern. In the second series of experiments we examined the effect of volume changes, resulting from the alternate extension and retraction of podia, on coelomic pressure in *Lytechinus variegatus*. We consider the interaction of volume changes and behavior of the peristomial membrane in explaining the observed pattern of coelomic pressures in sea urchins.

Materials and Methods

Experimental animals

Specimens of *Strongylocentrotus purpuratus* collected subtidally at Bodega Bay, California, and maintained in running seawater, were divided into two lots. The first was fed *ad libitum* with kelp (*Macrocystis* sp.) and the second was starved. There were no significant differences in the size of urchins in the fed (33.0–81.4 mm, n = 27) and unfed (41.9–82.6 mm, n = 25) groups. Size was estimated by a volume approximation which was (height $\times$ diameter)^2. Pressure measurements were performed during a three-week period, starting two months after the beginning of these feeding regimes. *Lytechinus variegatus* (53.9–68.1 mm diameter) was collected at Long Key, Florida, and maintained on natural substrate with dead leaves of *Thalassia testudinum*, for 12 to 72 h before experimental use.

Pressure measurement

Internal pressure was measured by mounting the urchins on a vertical, 14 gage, hypodermic needle passing through the peristomial membrane. The needle was connected to one side of a P305D differential, moving membrane, pressure transducer (Validyne Corporation, Northridge, California) fitted with a nickel plated 3–20 membrane to read pressures up to $\pm$550 Pa. The other side of the transducer was open to the seawater surrounding the experimental animal.

Calibration of pressure transducer

The system was calibrated before each series of measurements. Calibrations and all experiments were performed in a two-chambered Plexiglas aquarium. At the start, seawater levels in the two chambers were equilibrated via a connecting valve. After closure of the valve, the water

level in one chamber (positive side of transducer) was raised by increments of 1.1 mm by the gradual immersion of a Plexiglas box propelled by a threaded drive mechanism. At each step the voltage output at 1-s intervals was averaged over a 30-s period by a Dynamic Signal Analyzer (Hewlett-Packard #3561A). Initial calibrations were continued to a total pressure head of about 22 mm of seawater (220 Pa). Later calibrations extended only to 11 mm of seawater, which adequately covered the range of pressures commonly encountered. Calibration readings were taken as pressure increased and as it decreased back to zero. Linear regression of transducer output (mv) and pressure, fitted by least squares, was used to convert experimental readings to pressure. For field experiments in Florida, the system was simplified. The Plexiglas box and threaded drive assembly was replaced by a pipetting technique in which 15-ml aliquots of seawater were added sequentially and then removed from the reference chamber.

Estimate of errors in pressure measurements

Due to uncertainty in the measurement of the pressure head against which the transducer was calibrated, the range of bias in the slope of the calibration curve was less than 0.1%. The precision range of the slope was ±10% because of day-to-day variation. Additionally, in the worst case, the 8-bit digitizer recorded only to the nearest 1.7 Pa, and there was drift in the zero; a combined imprecision range of ±3 Pa resulted. The accuracy can be expressed as ±(10.1% + 3) Pa.

We were concerned that urchins might leak, thus artificially relieving high positive or negative pressures. We ruled out this possibility by injecting the urchins with food coloring and by coloring the liquid in the transducer. We observed no color leakage, except at very much higher pressures than those reported in this experiment.

Internal pressure could also be artificially relieved by flow through the needle into the tiny space vacated as the metal membrane of the transducer shifted while making the measurement. This possibility was minimized by use of a "low volume" pressure transducer. To test this potential error, we set up an experiment in which we could simulate the pressure measurement and watch what happened to the pressure and volume. The urchin was replaced by a rubber tube filled with dyed seawater, closed at one end, and attached to a 5 mm diameter graduated pipet that was open to the atmosphere at the other end. With fluid in the pipet levelled to measure 40 Pa, we inserted the needle through the rubber hose. There was no detectable motion of the water level in the pipet, indicating that volume changes due to the transducer motion were less than 3 μl; in a 60 mm diameter urchin, this volume change could be accommodated by a 10 μm upward or downward motion of the lantern involving a strain of 5×10^{-6} in the peristomial membrane, an amount that has a negligible effect on pressure in the coelom.

Experimental procedure

Each urchin, when mounted on the needle, rested on a small platform. The podia reached the platform but could not reach the sides or the floor of the aquarium. During the course of an experiment the transducer output was sampled at 5.12 Hz and digitized. The trace was displayed by the signal analyzer simultaneously with a frequency spectrum. The data were transferred in 200-s sections to an Apple Mac II equipped with a "LabVIEW" GPIB interface card (National Instruments, Austin, Texas). For each urchin, data were recorded for 10 min. The zero point of the transducer was checked after each measurement was completed, and the needle was detached and syringed to remove any coagulated coelomic fluid. Diameter and height of each specimen was measured by calipers. The water in the experimental chamber was replaced after each group of five specimens to minimize changes in water temperature.

The procedure for *L. variegatus* was similar except that a 10 min section of data was transferred directly into the computer, and the light level was manipulated to induce podial movements. For each of ten urchins, room lights and fiber-optic microscope lights directed at the urchin were alternately switched on and off every 2 min. When the lights were on, the podia retracted; when the lights were off, they extended.

Data analysis

For *S. purpuratus* specimens, each 200 s trace was scanned and the following information was compiled: (i) seconds below zero pressure; (ii) the mean pressure; (iii) the standard deviation of pressure; (iv) the maximum pressure; (v) the minimum pressure; (vi) the mean of positive pressures; (vii) the standard deviation of positive pressures; (viii) the mean of negative pressures; (ix) the standard deviation of negative pressures. Two-way analyses of variance by trace and by feeding regime were performed on these data. Additional *t*-tests were performed to compare fed and starved animals by successive traces. A Fourier transform of the third 200-s trace for each specimen gave the amplitude and periodicity of rhythmic pressure fluctuations. Using the first 200-s trace (during which the needle was inserted), a discriminant functions analysis was performed to see whether fed and unfed individuals could be identified from their initial pressure patterns. We performed a stepwise regression to determine which variables to include in the discriminant functions analysis. The discriminant model is

$$Y = b + a_1x_1 + a_2x_2 + a_3x_3 \cdots a_9x_9, \qquad (1)$$

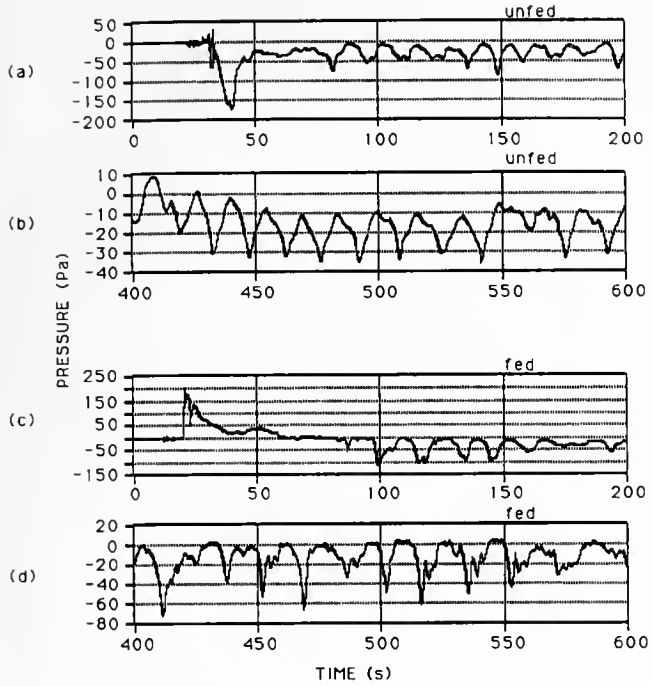

Figure 2. (a) Pressure-time trace for an unfed urchin during the first 200 s of the experiment. The large negative pressure pulse, characteristic of unfed urchins, occurred just after the needle was inserted through the peristomial membrane. (b) Pressure-time trace for an unfed urchin 400–600 s after the start of the experiment. This trace shows the characteristic, rhythmic fluctuations of pressure associated with movements of the lantern. (c) Pressure-time trace for a fed urchin during the first 200 s of the experiment, showing the characteristic, positive pressure pulse as the needle was inserted through the peristomial membrane. (d) Pressure-time trace for a fed urchin 400–600 s after the start of the experiment, showing rhythmical changes with lantern movements. Differences in the traces for starved and fed urchins (a and c) were statistically significant; during the third 200-s traces (b and d) the differences were not significant.

where y is equal to -1 if an urchin is fed, and is equal to $+1$ if an urchin is unfed. The nine variables descriptive of the pressure traces are x_1 to x_9. The fitted slopes are a_1 to a_9 and b is the intercept.

For *L. variegatus* the average level of pressure was measured for each 2-min segment except the first, which was assumed to be a settling-down period. A paired *t*-test was done on the average pressures to compare the lights-off periods with the immediately ensuing lights-on periods.

Results

Description of the pressure traces

Pressure traces for *S. purpuratus* characteristically fluctuated at a frequency of 0.055 Hz with a S.D. of 0.021 Hz (n = 167 traces). This corresponds to an average period of 18 s, and the range of periods corresponding to the above S.D. is 13–29 s.

When the needle was inserted through the peristomial membrane, there was usually a negative or positive pressure peak (Fig. 2) that often went off-scale on the recording equipment, and that differed significantly from the fluctuations in the second and third traces as shown by the maxima and minima in Table I. Over several minutes the pressure tended toward, and eventually stabilized at, an average mean pressure of -8.2 Pa with a S.D. of 11 Pa (n = 52 urchins). According to our error estimate, zero lies in the range $\pm (8.2 \times 10\% + 3)$ Pa: a *t*-test shows that the worst-case zero of -3.8 Pa is significantly different from -8.2 Pa with a S.E. of 1.4 Pa ($P < 0.01$). The average S.D. of the pressure was 10 Pa with S.D. of 6.4 Pa (n = 52). The pressure was below zero 70% of the time.

Urchins fed *ad libitum*, and those receiving food only via occasional cannibalism, had very different initial pressure responses (Fig. 2). Well-fed urchins had pressures that tended to increase initially. Unfed urchins had pressures that tended to decrease initially. All of the variables except S.D. differed significantly in the first 200-s trace (Table I). Step-wise regression of variables for the first trace indicated that the mean of the positive pressures and the minimum pressure ($r^2 = 0.41$, slope significantly non-zero, $P < 0.001$) correctly predicted whether the animals were fed or unfed 83% of the time.

There were no significant correlations between urchin volume and any of the nine descriptive variables in any traces for fed urchins, nor in the first 200-s trace for unfed urchins. However, in subsequent traces from unfed urchins, five of the variables (mean, S.D., minimum, mean negative, and S.D. of negative pressures) were correlated with test size (Table II).

Podial movements and pressure

When the lights were turned off, *L. variegatus* protracted its podia and the coleomic pressure decreased. When the lights were turned on, podia retracted and the coelomic pressure increased (Fig. 3). Coelomic pressure

Table I

Results of t*-tests showing statistically significant differences between fed and starved* Strongylocentrotus purpuratus *for the nine variables descriptive of coelomic pressure during the three successive 200 s traces*

Variable	Trace 1	Trace 2	Trace 3
Seconds below zero	**	n.s.	n.s.
Mean pressure	***	n.s.	n.s.
S.D. pressure	n.s.	n.s.	n.s.
Maximum pressure	**	n.s.	n.s.
Minimum pressure	***	n.s.	n.s.
Mean +ve pressure	***	n.s.	n.s.
S.D. +ve pressure	***	n.s.	n.s.
Mean −ve pressure	**	n.s.	n.s.
S.D. −ve pressure	**	n.s.	n.s.

(n.s. not significant; $^{**}P \leq 0.01$; $^{***}P \leq 0.001$).

Table II

Correlation coefficients between body size and statistical variables descriptive of pressure traces from unfed Strongylocentrotus purpuratus

Variable	Trace 1	Trace 2		Trace 3	
Seconds below zero	n.s.	—	n.s.	—	n.s.
Mean pressure	n.s.	−0.4	*	−0.5	*
S.D. pressure	n.s.	0.4	*	0.4	*
Maximum pressure	n.s.	—	n.s.	—	n.s.
Minimum pressure	n.s.	−0.4	*	−0.5	**
Mean +ve pressure	n.s.	—	n.s.	—	n.s.
S.D. +ve pressure	n.s.	—	n.s.	—	n.s.
Mean −ve pressure	n.s.	−0.5	*	−0.6	**
S.D. −ve pressure	n.s.	0.4	*	0.4	*

(n.s. not significant; $*P \leq 0.05$; $**P \leq 0.01$). Note: There were no correlations between any of these variables and body size in fed urchins.

during the lights-on period was 8.8 Pa higher than the mean pressure during the immediately subsequent lights-off period ($P < 0.0001$; n = 20; 10 urchins, 2 paired samples each).

Discussion

The fluctuating coelomic pressures observed in this study were predominantly negative. In the wide range of animals surveyed by Trueman (1975), most reported pressures are positive, the highest being 10^4 Pa in the lugworm, *Arenicola marina*. In soft-walled pressure vessels, the internal pressure can only be zero or positive relative to the outside. At zero relative pressure, the body wall is limp and any process tending to a negative internal pressure will cause the membrane to collapse and fold, thus reducing the pressure to zero (Clark and Cowey, 1958). Negative pressures are possible in systems in which the walls have flexural stiffness, as is the case with some skeletal and muscular tissues. Trueman (1975) reported pressures of −500 Pa from underneath the foot of *Patella* sp. during the passage of pedal waves. Negative pressures have also been generated inside the gastropod foot (Voltzow, 1986) and by the suckers of an octopus (Kier and Smith, 1990; Smith, 1991). Many soft-bodied animals have some hard, stiff parts, while many primarily hard-bodied organisms have some soft, flexible membranes. Sea urchins, having a hard test and large peristomial membrane, are examples of the latter.

There are several processes that could influence coelomic pressures in sea urchins, but some of them do not produce pressures of the observed magnitude. However, we found two processes of great importance: the exertion of force on the coelomic fluid (for instance, by the peristomial membrane) and the movement of water into the coelomic space (as in the simultaneous retraction of the podia). Before considering these two in more detail, we show why a number of the other possibilities are not significant.

Causes of pressure in urchins

Pressure is a force magnitude per area. In non-accelerating fluids, at each point in the fluid there is a balance of forces in all directions. Gravitational pressure, p_g, at a given depth is

$$p_g = \rho g d, \tag{2}$$

where ρ is the density of seawater, g the acceleration due to gravity, and d the depth (atmospheric pressure is not included). We measured the difference between pressures inside and outside the urchin. Because the two locations were at the same depth, hydrostatic, gravitational pressures are irrelevant, and the remaining discussion refers only to relative transmural pressures.

Sound or sudden impacts from waves could also cause internal pressure. The rhythmic, 20-s pressure patterns we observed cannot be sound because there was no such rhythm when the needle was removed from the urchin. Nevertheless, in the ocean, sudden coelomic pressures from impact forces such as waves and sound are possible and might have implications for behavior, mechanical functioning, or even pressure-regulated growth of urchins. These phenomena have not been investigated.

Hydrodynamic forces are unlikely to be of importance in explaining pressures inside urchins, because rates of flow are very slow. Hanson and Gust (1986) measured rhythmic flows inside urchin coeloms that have the same periodicity (20 s) as the pressure pulses we measured. Thus, fluid dynamic pressures cannot be immediately ruled out in explaining the observed pressure patterns. Expected pressures from flow are less than or equal to the dynamic pressure, p_d, which is

$$p_d = \frac{\rho}{2} u^2, \tag{3}$$

where ρ is the density of seawater, and u is the velocity of flow (Vogel, 1981). In our experimental observations,

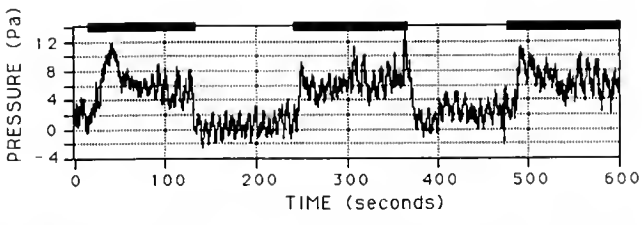

Figure 3. The pressure pattern in *Lytechinus variegatus* when lights are alternately turned on and off at 2-min intervals (black bar indicates lights on). The podia protracted when the light was off and retracted when the light was turned on.

the standard deviation of pressure was 10 Pa. This would correspond to a minimum flow of 100 mm s^{-1}. Because Hanson and Gust (1986) observed a maximum flow of 1.5 mm s^{-1}, we conclude that the pressures we observed were not due to flow.

Tension in a curved, stretched membrane can be another cause of pressure differentials. According to Laplace's law (see Popov, 1976; Wainwright *et al.*, 1976; Vogel, 1988; or Ellers and Telford, 1991), the pressure drop across such a membrane or a flexible body wall depends on its tension and radius of curvature. The pressure inside the membrane will be positive with respect to external pressure when the membrane is inwardly concave. In a cylinder the pressure difference, Δp, across the membrane is

$$\Delta p = \frac{T}{r}, \tag{4}$$

where r is the radius of curvature and T the tension in the membrane. The tension, T, is the stress times the thickness of the material. More generally, in a three-dimensional shape such as a sphere or ellipsoid, two radii of curvature are involved, so that at every point on the surface

$$\Delta p = \frac{T_1}{r_1} + \frac{T_2}{r_2}, \tag{5}$$

where T_1 is the tangential tension in one direction with radius of curvature r_1, and T_2 is the tangential tension in an orthogonal direction, with radius of curvature r_2 (modified from Timoshenko and Woinowsky-Krieger, 1959, p. 435). Both negative and positive differences can occur across a membrane, depending on whether its radii of curvature are positive or negative.

If the several coelomic compartments in echinoids (somatocoels, hydrocoel, axocoel, and peripharyngeal coelom) (Hyman, 1955; Smith, 1984) are bounded by stretched membranes, there is potential for a diversity of pressure relationships between them. We found no reason to suspect that there are more than two functionally pressurized spaces, the water-vascular system and the coelom proper. Injection of red dye confirmed a separate peripharyngeal space, but the membrane is flaccid and flimsy and could not support separate pressurization. The only stretched membranes are found in the peristome, periproct, and water vascular system.

Pressure and peristomial membrane

The peristomial membrane is a circular sheet composed of cross-fiber collagen arrays and circular and radial muscles (Hyman, 1955). In some species, it contains calcite plates or spicules (Smith, 1984; Candia Carnevali *et al.*, 1990). It is joined to the test at the distal edge, and to the lantern centrally. Thus the shape of the membrane is like a washer: flat, with a hole in the middle. No one has studied the deformation of this membrane as the lantern protracts and retracts, but from our pressure measurements and the general rules about membranes given above, we can make predictions about its curvature.

Curvature of the membrane depends on the relative pressure difference across it. As the lantern protracts, the pressure inside becomes negative relative to ambient. From Laplace's law, we know that a negative internal pressure implies that the membrane is convex on the coelomic side. Conversely, a positive internal pressure would imply that the membrane is concave on the coelomic side. The same is true for the periproctal membrane. In species in which the periproct is flexible, its shape might indicate a positive or negative internal pressure. These predictions hold only if the membranes have low flexural stiffness. Often flexural stiffness may be conferred by catch-collagen or ossicles. If the membranes are flexurally very stiff, then they may produce negative or positive pressures regardless of their curvature, just as the test does not reverse its curvature as internal pressure changes from positive to negative. It should be a goal of future studies to determine the flexural stiffness of such membranes.

Regardless of the membrane curvature and flexural stiffness, protractor and retractor muscles controlling the motion of the lantern exert forces that cause tension in the peristomial membrane and thus a pressure drop across it. We observed the lantern moving in and out during our pressure measurements, and the 20-s pressure rhythm appeared to match its protraction and retraction. Jensen (1985) suggests that the role of such lantern movements is to stir the coelomic fluid, thus facilitating distribution of nutrients and respiratory gases.

Pressure and podial movements

When many podia simultaneously retract, water previously in the podia will be stored in the ampullae, thus effectively moving water into the coelomic space. If the peristomial membrane and periproct do not move compensatorily outward, and if there is negligible flow via the madreporite, the pressure in the coelom must rapidly increase. In fact, because of the incompressibility of water, if there is no volume regulation the urchin must either spring a leak or the pressure would become so great that the podia could not retract. Fechter (1965) recognized this problem. He calculated that the volume made available when the peristomial membrane moves outward is sufficient to compensate for the volume of water moved into the coelomic space when all podia simultaneously contract. Further, he showed that the size of the peristomial membrane was more closely correlated with the number of podia than with test size. Finally, he demon-

strated only very small flows via the madreporite during simultaneous podial retraction. We observed that simultaneous podial retraction caused an 8.8 Pa pressure increase in the coelom. Fechter (1965), working with *Echinus esculentus*, reported an increase of 200 Pa.

Although the madreporite is not involved in volume-related pressure regulation, Fechter (1965) concluded that it was involved in non-volume-related changes due to gravitational, hydrostatic pressure. We believe that Fechter's conclusion must be wrong, but first we will present his experimental evidence. Fechter glued the madreporite shut and performed two manipulations. (1) He increased the hydrostatic, gravitational pressure by increasing the depth at which the urchin was kept. When the external pressure increased the podia collapsed. (2) He pulled the lantern outward, decreasing the pressure in the coelom, and again the tube feet collapsed.

In the second case, the madreporite could not relieve the induced pressure change because, according to Fechter's own results, it allows insufficient flow. We argue, instead, that pulling the peristomial membrane outwards causes a volume flow from the podia into the ampullae. In the first case, when hydrostatic pressure increases, it does so with negligible volume change. Therefore, although the increase in hydrostatic pressure may be sufficient to cause the podia to collapse, it would do so only if the pressure was being relieved by a flow from the podia into the ampullae. But because this pressure change is gravitational, it is not associated with a volume change, and therefore even the tiniest flow from the podia into the ampullae will immediately relieve the pressure difference.

The only way we can explain Fechter's results is if there was an air bubble in the coelom that would have diminished in size with increasing gravitational pressure, therefore causing flow from the podia into the ampullae. Such air bubbles sometimes form in urchins that have been in air for some time. Fechter dried the madreporite with a stream of hot air, before gluing it shut. Perhaps this procedure explains his results. We suggest that, contrary to Fechter's conclusion, his experiments do not show that the madreporite functions to accommodate hydrostatic gravitational pressures. Furthermore, such a function is unnecessary because volume changes caused by hydrostatic pressure would be accommodated by miniscule flows and deformation of tissues.

Although accommodation of hydrostatic, gravitational pressure is unnecessary, there are other types of pressure that might require the coelomic pressure to be maintained independent of the water-vascular system, and perhaps the madreporite has such a role. For instance, the pressure fluctuations we observed (±10 Pa) could have caused the podia to malfunction because these pressures would be exerted on the ampullae inside the coelom. But such fluctuations can only cause podia to extend or retract if they cause the ampullae to expand or contract, which would happen only if volume changes were associated with the pressure fluctuations. Additionally, the deformation of a membrane depends on its stiffness and on radius of curvature [as in equations (4) and (5), above]. The radius of curvature of the ampullae is much smaller than that of the peristomial membrane, and therefore we expect much smaller deformations in the ampullae. That the ampullae have a smaller radius of curvature than the peristomial membrane may be a design requirement of echinoderm water-vascular systems.

The digestive tract is another potential source of pressure change. When full, the stomach will take up more room in the coelom, and the peristomial membrane must move outwards to relieve the volume increase. Similarly, flows into and out of the mouth, or in the siphon, may cause volume fluctuations that could cause pressure changes if the peristomial membrane does not move compensatorily. Further, without compensation by the peristomial membrane, defecation may lower coelomic pressure because it tends to reduce the volume of gut contents.

Finally, several authors have described ruffled sacs hanging externally from the peristomial membrane (Hyman, 1955; Smith, 1984), the supposed function of which is either as gills or pressure regulators for the peripharyngeal coelom. However, no experimental data about their function have been presented. We saw no evidence that these sacs expanded or contracted while the coelomic pressure fluctuated. Furthermore, their openings are far too small to allow sufficient flow to regulate coelomic volume.

A model of forces causing a pressure drop across the peristomial membrane

The forces causing protraction of the lantern, and thus tension in the peristomial membrane, come from lantern protractor and retractor muscles and from the submerged weight of the lantern. These forces must be estimated. Andrietti *et al.* (1990) report 3 g (0.03 *N*) for lantern weight minus buoyancy in a specimen of *Paracentrotus lividus*. They also report forces of 40 g (0.4 *N*) exerted by lantern protractors and forces of 10 g (0.1 *N*) exerted by lantern retractor muscles. Because *P. lividus* rarely exceeds 70 mm diameter (Mortensen, 1977), it is similar in size to *S. purpuratus* and *L. variegatus*, and the forces should be comparable.

The assumed geometry of the lantern, test and peristomial membrane are shown in Figure 4a. The forces on the peristomial membrane are: (1) a vertical force, f_v, exerted by the lantern weight and the lantern muscles; (2) forces from the pressure difference across the membrane; and (3) the reactive, tensile force exerted on the membrane

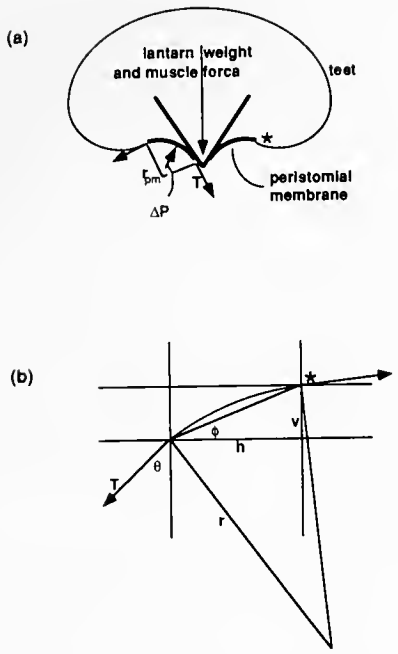

Figure 4. (a) Location of the peristomial membrane in an urchin. The star in both figures marks the point of attachment to the edge of the peristome. (b) Geometric model of the peristomial membrane. The angle θ, and the radius of curvature of the membrane are not independent. Zero vertical displacement occurs when the membrane is horizontal.

by the test. The vertical force, f_v, exerts a force, f_m, in the membrane,

$$f_m = \frac{f_v}{\cos(\theta)}, \tag{6}$$

where θ is the angle between the vertical and a tangent at the central margin of the membrane (at the point of attachment of the peristomial membrane to the teeth) (Fig. 4b). The force, f_m, on the membrane corresponds to a tension, $\mathbb{T}$, (force per length) in the membrane of

$$\mathbb{T} = \frac{f_m}{(2\pi r_t)}, \tag{7}$$

where r_t is the radius of the central margin of the peristomial membrane. From Laplace's equation (4)

$$\Delta p = \frac{\mathbb{T}}{r_{pm}}, \tag{8}$$

where r_{pm} is the radius of curvature of the membrane. In using equation (4) rather than (5) we make two simplifying assumptions: that a second horizontal radius of curvature can be ignored, and that the curve formed by a vertical cross section of the peristomial membrane has a single radius of curvature at every point. In reality this curve may have variable radii of curvature. A more realistic model would add an unjustifiable degree of complexity for the present context. The two-dimensional approach used here should give results of the correct order of magnitude.

The radius of curvature of the peristomial membrane, r_{pm}, for a given protraction of the lantern, v, and a given horizontal, peristomial radius, h, can be derived from the geometry shown in Figure 4b. The radius of curvature is

$$r_{pm} = \frac{h}{2\cos(\arctan(v/h))\cos(\theta + \arctan(v/h))}. \tag{9}$$

Substituting through equations 6, 7 and 8,

$$\Delta p = \frac{f_v \cos(\arctan(v/h))\cos(\theta + \arctan(v/h))}{\pi h r_t \cos(\theta)}, \tag{10}$$

which is shown in Figure 5. This graph shows that many possible combinations of pressure, protraction, and θ are possible when only the force balance on the membrane is considered. Initially, this may seem counterintuitive. Intuition suggests that as the lantern protracts, the internal pressure should get more and more negative relative to outside as the membrane pulls more and more on the constant volume of water inside the urchin. That this pressure pattern is not implied in Figure 5 reflects the fact

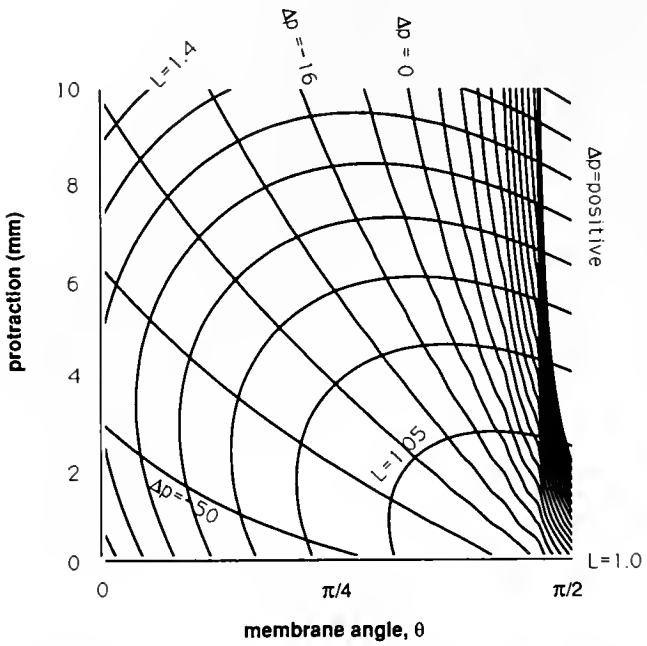

Figure 5. Contour plot of theoretical predictions from the geometric, force balance model of the peristomial membrane (see Fig. 4 and text for details). Elongation of the peristomial membrane and pressure across it are functions of the membrane angle at the central edge, θ, and protraction, v, given a downward force of the teeth and lantern muscles on the membrane, f_v. This graph shows that many combinations of θ and v are possible at a given pressure across the membrane. Which θ, v path the membrane follows as the lantern protracts depends on the volume of the urchin and the properties of the peristomial membrane.

that the force balance makes no assumption about the volume of water inside the urchin, nor about the material properties of the peristomial membrane.

To understand a fluctuating pattern of pressure becoming increasingly negative as the lantern protracts, examine the change in length of the peristomial membrane. The length of the membrane, the distance along its vertical arc from the attachment point at the test to its attachment point at the teeth, is

$$\mathbb{L}_{pm} = r_{pm}(\pi - 2(\theta + \phi)) \qquad (11)$$

(the angle ϕ is shown in Fig. 4b).

By examining the contour plots of pressure drop, and peristomial membrane length (Fig. 5), it is possible to imagine what is happening as the lantern moves. As it protracts, the peristomial membrane elongates, and, assuming constant coelomic volume, the internal pressure must decrease. Initially, assume that the membrane starts at the point, $\theta = \pi$ radians (the membrane is straight and horizontal). As the lantern protracts, the line representing the motion of the lantern must move towards higher v (protraction) and towards lower θ on the graph, to stay in the region of negative pressure and simultaneously to increase the length of the peristomial membrane. Increase in the length of the peristomial membrane helps to compensate for volume changes that would otherwise occur because it can arch upward, effectively compensating for the volume of the lantern pulled downward.

According to Figure 5, the tendency to decrease θ while increasing v, initially causes Δp to become negative quickly because many pressure contour lines must be crossed, but, after even a little protraction, it is possible for the lantern to protract and follow an isobar. This may be an explanation for the plateaus often observed at the peaks of fluctuations in the pressure trace. A path followed by the lantern could be specified by two functions of time, θ(time) and v(time), which we call a "θ, v" path. This path, represented by an imaginary line in Figure 5, will depend on the constraints imposed by the degree of constancy of the coelomic volume and the material properties of the peristomial membrane. We plan to develop this theoretical model further in the future and obtain measurements of the motion of the lantern, the constancy of the coelomic volume, and the material properties of the peristomial membrane.

This crude, initial model serves to explain some aspects of the relationship between pressure and the behavior of the structures that cause it. The pressures are of the correct order of magnitude to have been caused by lantern muscles. The mean negative pressure observed (−8 Pa) is small enough that it could have been caused by the weight of the lantern. If the podia simultaneously retract, or if the stomach is full, thus raising the coelomic volume, this model shows that the lantern can still protract with only a change in the θ, v path. Finally, it is reasonable to calculate the pressure based solely on what the peristomial membrane is doing, because the pressure inside the urchin's coelom is the same everywhere, and thus if any other structure were contributing, it would have to be balanced by tension in the peristomial membrane.

Implications of the observed pressures for the pneu theory

In keeping with the pneu hypothesis, we expected continuously positive internal pressure in sea urchins. Instead we found fluctuating positive and negative pressures, with an overall mean below zero. Clearly, the original version of the pneu hypothesis must be rejected on the basis of these measurements.

Baron (1991) also recognized the problem for the pneu hypothesis when he found fluctuating pressures. He developed a modified version of the hypothesis that preserves the spirit of the original (Thompson, 1917) but incorporates new rules for growth of the skeleton. Baron (1991) proposed that skeletal plates grow at their margins whenever they are in tension, and that growth is directly proportional to tensile stress. Instead of the term "pneu," he called this a "tensile growth model." These growth rules necessitated development of a finite element analysis to determine the expected stresses in the skeleton caused by internal pressure and other forces, such as those from tube feet. From these analyses Baron (1991) was able to generate urchin-like shapes using a computer. Making several alternative assumptions about internal pressure, he examined their effect on the shapes produced by his model. In these simulations, he found that a pressure fluctuating about a mean of 30 Pa, with a S.D. of 30 Pa, generated a shape indistinguishable from that produced with a constant pressure of 30 Pa. Based on this finding, he thereafter simulated urchin shapes using constant pressures.

Baron's (1991) assumptions can be compared with our more extensive pressure measurements. For his standard growth situation he assumed a pressure of 30 Pa, and the other pressure used was 15 Pa. We observed an average pressure of −8 Pa. Under fluctuating pressure regimes he assumed a negative pressure for at most 17% of the time, whereas we observed it for 70% of the time. Baron's (1991) model allowed growth whenever the skeleton was in tension due to internal pressure. This implies that during periods of no growth, the pressure must be lower. But we found that in well-fed, growing (Ebert, 1968) and starved, possibly shrinking, urchins (Levitan, 1988; 1989), the mean pressures were equal after the initial pressure surges in the first 200-s traces (Table I).

The discrepancies between our observations and Bar-

on's (1991) assumptions have two possible implications: that our specimens were abnormal, or that his assumptions do not reflect the pressure patterns in real urchins. In the latter case, it may be that the spirit of the pneu hypothesis is wrong, or that Baron's (1991) version does not incorporate exactly the right assumptions. These possibilities can only be resolved by further experiments and more refined theories.

At present, the most detailed predictions of urchin shape, based on Baron's (1991) tensile growth model, deal only with regular urchins. A challenge to all models is the great diversity of forms that must be generated, including flattened sand dollars (Clypeasteroida), heart urchins (Spatangoida), and the bizarre flask-shaped pourtalesiids (Holectypoida).

Acknowledgments

This work was supported by University of California, Davis, Agricultural Experiment Station Project no. 5134-H and a U. C. Davis, Bodega Marine Laboratory Travel Grant to O. Ellers; and a Natural Sciences and Engineering Research Council of Canada Grant (#A4696) to M. Telford. We thank Bodega Marine Laboratory for use of their facilities. We specially thank K. Brown for her organizational help and H. Fastenau for diving to collect the urchins and subsequently caring for and feeding them. We thank J. Swanson and the staff of Keys Marine Laboratory, Florida, for the use of their facilities and help in collecting urchins. Thanks also to M. Martinez and K. Driver who assisted in some of the experiments and to D. Levitan who critically read the manuscript.

Literature Cited

Andrietti, F., M. D. Candia Carnevali, I. C. Wilkie, G. Lanzavecchia, G. Melone, and F. C. Celentano. 1990. Mechanical analysis of the sea-urchin lantern: the overall system in *Paracentrotus lividus*. *J. Zool. Lond.* **220**: 345–366.

Baron, C. J. 1988. Do mechanical forces explain patterns of growth and form in sea urchins? A finite element analysis. *Proc. Int. Echinoderms Conf., Victoria, Canada* **1987:** 786.

Baron, C. J. 1991. The structural mechanics and morphogenesis of extant regular echinoids having rigid tests. Ph. D. Dissertation, University of California, Berkeley. 269 pp.

Candia Carnevali, M. D., F. Bonasoro, F. Andrietti, and G. Melone. 1990. Functional morphology of the peristomial membrane of regular sea urchins: structural organization and mechanical properties in *Paracentrotus lividus*. Pp. 207–216. in *Echinoderm Research*. De Ridder, Dubois, Lahaye and Jangoux, eds. Balkema, Rotterdam.

Clark, R. B., and J. B. Cowey. 1958. Factors controlling the change of shape of certain nemertean and turbellarian worms. *J. Exp. Biol.* 35: 731–748.

Dafni, J. 1983. Aboral depressions in the tests of the sea urchin *Tripneustes cf. gratilla* (L.) in the gulf of Eilat, Red Sea. *J Exp. Mar. Biol. Ecol.* **67**: 1–15.

Dafni, J. 1985. Effect of mechanical stress on the calcification pattern in regular echinoid skeletal plates. *Proc. Int. Echinoderms Conf., Galway* **1984:** 233–236.

Dafni, J. 1986. A biomechanical model for the morphogenesis of regular echinoid tests. *Paleobiology* **12**(2): 143–160.

Dafni, J., and J. Erez. 1982. Differential growth in *Tripneustes gratilla* (Echinoidea). *Proc. Int. Echinoderms Conf., Tampa Bay* **1981:** 71–75.

Ebert, T. A., 1968. Growth rates of the sea urchin *Strongylocentrotus purpuratus* related to food availability and spine abrasion. *Ecology* **49:** 1075–1091.

Ellers, O., and M. Telford. 1991. Forces generated by the jaws of clypeasteroids (Echinodermata: Echinoidea). *J. Exp. Biol.* **155:** 585–603.

Fechter, H. 1965. Über die Funktion der Madreporenplatte der Echinoidea. *Z. Verg. Physiol.* **51**: 227–257.

Hanson, J. L., and G. Gust. 1986. Circulation of perivisceral fluid in the sea urchin *Lytechinus variegatus*. *Mar. Biol.* **92**(1): 125–134.

Hyman, L. H. 1955. *The Invertebrates: Echinodermata. The Coelomate Bilateria*. Volume IV. McGraw-Hill, New York. 763 pp.

Jensen, M. 1985. Functional morphology of test, lantern, and tube feet ampullae system in the flexible and rigid sea urchins (Echinoidea). *Proc. Int. Echinoderms Conf., Galway* **1984:** 281–288.

Kier, W. M., and A. M. Smith. 1990. The morphology and mechanics of octopus suckers. *Biol. Bull.* **178:** 126–136.

Levitan, D. R. 1988. Density-dependent size regulation and negative growth in the sea urchin *Diadema antillarum* Philippi. *Oecologia* **76:** 627–629.

Levitan, D. R. 1989. Density-dependent size regulation in *Diadema antillarum*: effects on fecundity and survivorship. *Ecology* **70**(5): 1414–1424.

Mortensen, Th. 1977. *Handbook of the Echinoderms of the British Isles*. Dr. W. Backhuys, Uitgever, Rotterdam. 471 pp.

Moss, M. L., and M. M. Meehan. 1968. Growth of the echinoid test. *Acta Anatom.* **64:** 409–444.

Popov, E. P. 1976. *Mechanics of Materials*, 2nd ed. Prentice-Hall, Englewood Cliffs, NJ. 590 pp.

Royles, R., A. B. Sofoluwe, M. M. Baig, and A. J. Currie. 1980. Behavior of underwater enclosures of optimum design. *Strain* January, 1980, pp. 12–20.

Seilacher, A. 1979. Constructional morphology of sand dollars. *Paleobiology* **5**(3): 191–221.

Smith, A. B. 1984. *Echinoid Palaeobiology*. George Allen and Unwin, London. 190 pp.

Smith, A. M. 1991. Negative pressure generated by octopus suckers: a study of the tensile strength of water in nature. *J. Exp. Biol.* **157**: 257–271.

Thompson, D. W. 1917. *On Growth and Form*. Cambridge University Press, London.

Timoshenko, S., and S. Woinowsky-Krieger. 1959. *Theory of Plates and Shells*, 2nd ed. McGraw-Hill, New York. 580 pp.

Trueman, E. R. 1975. *The Locomotion of Soft-bodied Animals*. Edward Arnold, London. 200 pp.

Vogel, S. 1981. *Life in Moving Fluids*. Willard Grant Press, Boston. 352 pp.

Vogel, S. 1988. *Life's Devices*. Princeton University Press, Princeton, NJ. 367 pp.

Voltzow, J. 1986. Changes in pedal intramuscular pressure corresponding to behavior and locomotion in the marine gastropods *Busycon contrarium* and *Haliotis kamptschatkana*. *Can. J. Zool.* **64**(10): 2288–2293.

Wainwright, S. A., W. D. Biggs, J. D. Currey, and J. M. Gosline. 1976. *Mechanical Design in Organisms*. Princeton University Press, Princeton, NJ. 423 pp.

Appendix 1

List of theoretical variables

Δp, pressure drop across a membrane
T, tension in the membrane
r, radius of curvature
T_1, tangential tension in one direction in the membrane,
r_1, radius of curvature associated with T_1
T_2, tangential stress in the direction perpendicular to T_1
r_2, radius of curvature associated with T_2
p_g, gravitational pressure, (not including atmospheric pressure)
d, water depth
ρ, density of seawater
g, acceleration due to gravity
p_d, dynamic pressure
u, speed of flow
f_v, vertical force exerted on the membrane by the lantern weight and muscles
f_m, is the tangential force in the membrane at the membrane's attachment to the teeth
θ, angle of membrane's attachment to the lantern (see Fig. 5b), same as tangential angle defined by f_m
$\mathbb{T}$, tension in the membrane
r_t, radius of the central margin of the peristomial membrane
r_{pm}, radius of curvature of the peristomial membrane
v, lantern protraction distance
h, horizontal distance from the central margin to the distal margin of the peristomial membrane.
$\mathbb{L}$, arc length of the peristomial membrane
ϕ, see diagram in Figure 5b.
θ, v path—the combination of θ and v used by the membrane as it protracts

Reference: *Biol. Bull.* **182**: 435–443. (June, 1992)

Hydrogen Sulfide Reduction of Symbiont Cytochrome c_{552} in Gills of *Solemya reidi* (Mollusca)[a]

DAVID W. KRAUS[b,c], JEANNETTE E. DOELLER[b], AND JONATHAN B. WITTENBERG

Department of Physiology and Biophysics, Albert Einstein College of Medicine, 1300 Morris Park Avenue, Bronx, New York, 10461

Abstract. The gill of the protobranch clam *Solemya reidi* houses a dense population of intracellular symbiotic chemoautotrophic sulfur-oxidizing bacteria that fix carbon dioxide into sugars and supply the carbon nutrition of the host. The gill is divided into a bacteriocyte (cells with intracellular symbionts) domain and a domain of mitochondria-rich, symbiont-free ciliated cells. Optical spectra, recorded separately from each domain, are dominated by hemoglobin. Only oxygenated and deoxygenated hemoglobin were detected in the gill. In sharp contrast to the gill of the congener *Solemya velum*, ferric hemoglobin sulfide was not detected, suggesting that this species, if formed, is short lived. The spectral contribution of hemoglobin may be cancelled or subtracted in difference spectra. Difference spectra of each gill domain in nitrogen minus the same tissue in air show a complement of reduced cytochromes, demonstrating that both symbiont and mitochondrial cytochromes are reduced by endogenous substrate. Difference spectra of the bacteriocyte domain exposed to hydrogen sulfide (air containing 1.4 torr hydrogen sulfide minus air) show only the contribution of reduced symbiont cytochrome c_{552}. The extent of reduction increases monotonically with ambient p_{H_2S}, suggesting that, by analogy with some free-living sulfur-oxidizing bacteria, cytochrome c_{552} is near the point of entry of electrons into the symbiont electron transport chain. Difference spectra of muscle or of the ciliated domain under these same conditions show reduced cytochrome c_{550}, cytochrome b and cytochrome oxidase, suggesting that host mitochondria may accept electrons from hydrogen sulfide.

Received 30 December 1991; accepted 2 March 1992.

[a] Part of this work was presented at the American Society of Zoologists meeting, December, 1990.

[b] Present address: Department of Biology, University of Alabama at Birmingham, Birmingham, Alabama, 35243.

[c] To whom correspondence should be sent.

Introduction

Sulfide-oxidizing symbiotic associations between invertebrate hosts and chemoautotrophic bacteria were first recognized in members of the dense animal communities found at deep ocean hydrothermal vents (reviewed in Jones, 1985), and subsequently have been found in a number of animal species inhabiting coastal and deep sediments with disequilibrium mixtures of oxygen and sulfide (reviewed in Southward, 1987; Fisher, 1990; Childress and Fisher, 1992). The bacterial symbionts oxidize sulfide or other reduced compounds and fix carbon dioxide into nutrients that are translocated to the host (Fisher and Childress, 1986). The gigantic size of some symbiont-harboring animals attests to the effectiveness of the symbiotic association.

Symbionts in association with mollusks (clams, mussels, and a snail) are housed intracellularly in specialized cells—bacteriocytes—of the large and extensively modified gill. Within each cell they must be supplied with large influxes of hydrogen sulfide and oxygen, but must be protected from excessive hydrogen sulfide that would inhibit bacterial terminal oxidases and host mitochondrial cytochrome oxidase (Nicholls, 1975; Wilson and Erecinska, 1978; see Somero *et al.*, 1989, and Childress and Fisher, 1992, for reviews). This condition must be met in the naturally occurring steady state where hydrogen sulfide entry is matched by utilization, and the cytoplasmic concentration of hydrogen sulfide, and possibly oxygen, is probably very low (in the micromolar range; Childress, 1987; Wittenberg and Kraus, 1991). These cytoplasmic concentrations of hydrogen sulfide and oxygen may not be sufficient to support the fluxes of hydrogen sulfide and

oxygen to the symbiont, and we suggest that cytoplasmic sulfide-reactive and oxygen-reactive hemoglobins may facilitate diffusion of their ligands through the cytoplasm (Doeller *et al.*, 1988; Kraus and Wittenberg, 1990; Wittenberg and Kraus, 1991).

Hemoglobin is a nearly constant feature of symbioses between mollusks and sulfide-oxidizing chemoautotraphic bacteria (Wittenberg, 1985) and may reach concentrations as high as 1.5 m*M* in the bacteriocyte (Kraus and Wittenberg, 1990; for a possible exception see Dando *et al.*, 1986). Two abundant, high oxygen affinity, cytoplasmic hemoglobins have been isolated from the symbiont-containing gills of *Lucina pectinata* (formerly named *Phacoides pectinatus*) (Read, 1962, 1965). One of these, hemoglobin I, a monomer, reacts reversibly with oxygen but also reacts rapidly and reversibly with hydrogen sulfide in the presence of oxygen to form ferric hemoglobin sulfide (Kraus and Wittenberg, 1990; Kraus *et al.*, 1990). It may be called "sulfide-reactive." The other, the "oxygen-reactive" hemoglobin, is most probably an $alpha_2beta_2$ tetramer made up of hemoglobins II and III (Kraus and Wittenberg, 1990; Kemling *et al.*, 1991). It reacts reversibly solely with oxygen. These two hemoglobins may deliver their respective ligands to the symbiont.

Two cytoplasmic hemoglobins occur in nearly equal concentrations in the symbiont-harboring gill of *Solemya velum*, congeneric with *Solemya reidi* of this study (Doeller *et al.*, 1983, 1988). Approximately half the total hemoglobin within the bacteriocyte domain of living gill filaments reacts reversibly to form ferric hemoglobin sulfide in the presence of sulfide and oxygen; the balance remains oxygenated (Doeller *et al.*, 1988). We infer that the hemoglobins of *Solemya velum*, like those of *Lucina*, may deliver their ligands hydrogen sulfide or oxygen to the symbiont.

Here we present optical spectra of the symbiont-harboring bacteriocyte and the mitochondria-rich ciliated domains of the gill of *Solemya reidi*, and compare these spectra with those of additional symbiont-free tissues. We find that, in contrast to the gill of the congeneric species *Solemya velum*, and in contrast to purified *Lucina pectinata* hemoglobin, the gill of *Solemya reidi* never displays the spectrum of ferric hemoglobin sulfide. Optical spectra ascribed to the bacterial symbiont, weakly apparent in other species, are seen with remarkable clarity in the gill of *Solemya reidi*.

Materials and Methods

Animals

Solemya reidi individuals were collected by Van Veen grab sampling at the Hyperion sludge outfall in Santa Monica Bay, California, from a depth of 50–100 m, and were maintained in cold (5–10°C) seawater. Animals were 3–5 cm long, and gill wet weight averaged 1.5 g. Experiments were completed within 3 weeks of animal collection.

Optical spectrophotometry

Optical spectra were acquired with a Cary model 14 recording spectrophotometer equipped with a Cary scattered transmission accessory and an Aviv digital data acquisition and analysis system (Aviv Associates, Lakewood, New Jersey). Optical spectra were recorded from 650 to 350 nm at 0.5 nm intervals. Experiments were performed at room temperature (22–24°C). This is well above the habitat temperature of *Solemya reidi* from the collection site (<10°C).

Optical spectra of gills and other tissue

Gills of *Solemya reidi* were excised and rinsed in 0.25 μm millipore-filtered seawater. Individual gill filaments were cut from the central ligament of the gill. For some experiments, filaments were divided along the chitinous rod to separate the small ciliated mitochondria-rich domain from the larger bacteriocyte domain. Whole gill filaments or filament domains, each about 40 μm thick (see micrographs in Powell and Somero, 1985; Fisher and Childress, 1986), were placed as a continuous overlapping layer, two to three filaments or about 80 to 120 μm thick on a gas-permeable membrane window (MEM 213, 25 μm thick, General Electric Corp., Schenectady, New York). The layer was covered with a second membrane, and the assembly placed in the previously described gas perfusion cuvette (see Doeller *et al.*, 1988). Each gill preparation was used for no longer than four hours, and for each new experiment, filaments were freshly cut from the gill. Other tissues, foot, adductor and pallial muscles, hypobranchial gland, and nerve trunks or ganglia were examined as thin layer samples. Pallial muscles, if cut free, contract and become thick. A useful preparation was obtained by leaving a portion of the mantle with its fringing pallial muscle attached to a fragment of the valve. A window cut in the valve allowed the light beam to pass through the muscle. A single layer of parafilm (American Can Co., Greenwich, Connecticut) was used to attenuate the Cary reference beam and partially balance light scattering.

Gas delivery

Mixtures of air, oxygen, nitrogen, and carbon monoxide were prepared using a Tylan mass flow controller (Carson, California). Gas mixtures were humidified and passed through the 5 ml spectrophotometer cuvette at a flow rate of 100 ml/min. Hydrogen sulfide was added to the humidified gas mixture from a glass syringe driven by a syringe pump (Harvard).

Protocol

For each experiment, tissue hemoglobin was first oxygenated and then deoxygenated by equilibration of the tissue with air and nitrogen, respectively. Optical spectra were recorded after each equilibration. The difference between these spectra was dominated by the contribution of the difference: oxyhemoglobin minus deoxyhemoglobin. The magnitude of this difference, together with an estimate of the tissue thickness, provided an estimate of hemoglobin concentration in each tissue sample. Subsequently, the samples of each tissue were exposed to mixtures of air and nitrogen in declining increments of 10% air, from 100% air to 0% air, and spectra were recorded at each step. The p_{O_2} at which hemoglobin in each sample was just detectably deoxygenated was noted and was used in subsequent experiments with hydrogen sulfide to minimize spontaneous sulfide oxidation. This oxygen pressure, which is influenced by hemoglobin oxygen affinity, rate of oxygen consumption and tissue thickness, was typically near 30 torr (20% air) for gill preparations and near 90–105 torr (60–70% air) for pallial muscle preparations.

Hydrogen sulfide concentration in the natural environment of *Solemya reidi* is large and variable, 0.1–3 m*M* hydrogen sulfide (Childress and Lowell, 1982), but the animal may control the concentration of sulfide in the ventilatory water current by changing the construction of the burrow and its own placement within the burrow. The partial pressure range of hydrogen sulfide used in most these experiments (0.2–2 torr) is equivalent to 30–300 μM dissolved hydrogen sulfide (Millero, 1986). These concentrations are near the range reported to support sulfide-dependent carbon fixation by *Solemya velum* gill (200 μM; Cavanaugh, 1983a) or sulfide-dependent carbon dioxide net uptake by *Solemya reidi* (50–200 μM; Anderson *et al.*, 1987).

Hemoglobin isolation

Hemoglobin was purified following the general methods of Schuder *et al.* (1979) and Appleby *et al.* (1983), with modifications introduced by Kraus and Wittenberg (1990). The procedure involved extraction of the powdered sample under an atmosphere of carbon monoxide and argon, followed by molecular exclusion and ion exchange chromatography. All steps were carried out under carbon monoxide-saturating conditions to maintain hemoglobin in a carbon monoxide-ligated state until isolation was complete. This minimizes oxidation of ferrous *Solemya* hemoglobin and obviates cross-linking of hemoglobin to itself and other tissue components.

Results

Hemoglobin identification and concentration

Cytoplasmic hemoglobin dominates the optical spectra of the bacteriocyte and ciliated domains of the gill, as well as of all other tissues examined, including foot, adductor and pallial muscles, hypobranchial gland, and nervous tissues. In each tissue, optical difference spectra of tissues equilibrated with nitrogen minus the same tissue equilibrated with air display well-resolved features at 412, 435, 540, and 580 nm, diagnostic for hemoglobin (the difference spectrum of the gill bacteriocyte domain is shown in Fig. 1A). These maxima are the same as those in the deoxyhemoglobin minus oxyhemoglobin difference spectrum of purified *Solemya reidi* hemoglobin. The concentration of hemoglobin in several tissues (Table I) was calculated from the difference in optical density at 435 nm and 412 nm in these difference spectra, taking tissue thickness estimated with a dissecting microscope and using the extinction coefficient $\Delta EmM = 135$, obtained from the dominant fraction of hemoglobin isolated from *Solemya reidi* gills. Hemoglobin concentration calculated from difference spectra reflects only the hemoglobin that reversibly binds oxygen. Hemoglobin concentrations *in situ* are comparable with values obtained using hemoglobin isolated from samples of whole gills and of remaining tissues combined (Table I) and with the concentration of hemoglobin reported by Powell and Arp (1989) for gills of *Solemya reidi* (130 μM).

Optical spectra of the bacteriocyte domain of the gill

Exposure to sulfide: hemoglobin. We now examine the spectral changes induced by exposing the bacteriocyte domain of the gill to hydrogen sulfide. The bacteriocyte domain was first equilibrated with 20% air, sufficient oxygen to just saturate the hemoglobin in these samples, then hydrogen sulfide (about 0.2 torr) was added to the humidified gas. During equilibration with sulfide, absorbance was recorded continuously at either 420 nm or 430 nm, wavelengths near the maxima of ferric hemoglobin sulfide or deoxyhemoglobin, respectively. Absorbance exhibited a monotonic change with time, reaching an asymptote within 80 ± 30 s (n = 6). At steady state, an optical spectrum was recorded. Sulfide partial pressure was then increased incrementally to 2 torr, with the same procedure repeated at each step. Difference spectra of gills in 20% air containing sulfide minus gills in 20% air alone did not produce any feature that could be ascribed to sulfide ligation to hemoglobin (see Doeller *et al.*, 1988; Kraus and Wittenberg, 1990), but instead revealed an apparently single spectral entity with characteristics of a reduced minus oxidized cytochrome c_{552}, discussed below. Thus, we cannot detect the formation of ferric hemoglobin sulfide in the bacteriocyte domain of the gill of *Solemya reidi*.

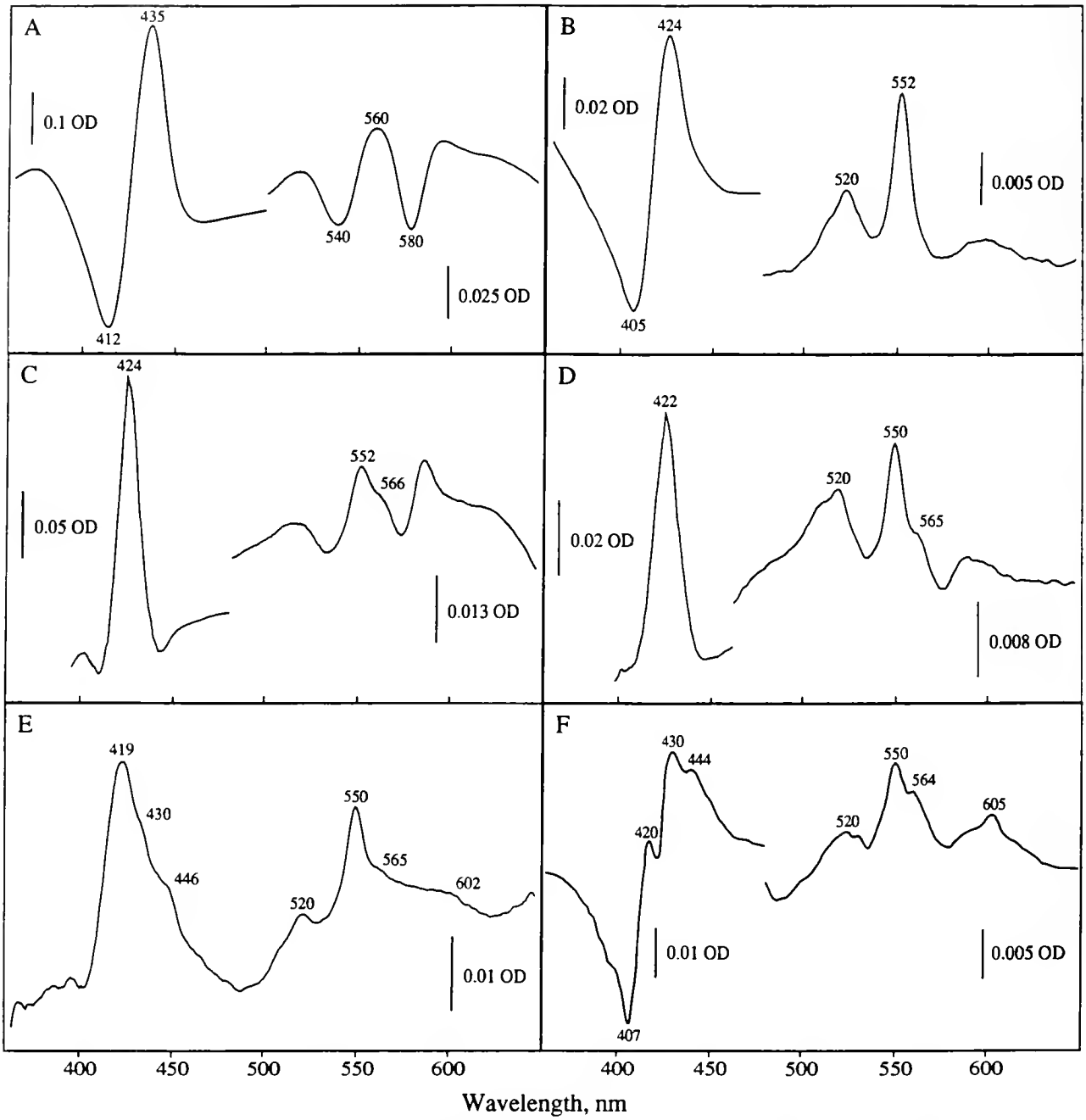

Figure 1. Optical difference spectra of living *Solemya reidi* tissues. Designated wavelength maxima are discussed in detail in text. Traces in the visible region have been amplified four-fold in Figures 1A–C, 2.5-fold in Figure 1D, and two-fold in Figure 1E.

A. Bacteriocyte domain of gill filaments equilibrated with nitrogen minus the same sample equilibrated with air. The contribution of deoxyhemoglobin minus oxyhemoglobin dominates the difference spectrum, with diagnostic maxima at 412, 435, 540, and 580 nm.

B. Bacteriocyte domain of gill filaments equilibrated with 20% air containing 1.4 torr sulfide minus the same sample equilibrated with 20% air. The dominant spectral species is identified as a reduced minus oxidized cytochrome c_{552}, ascribed to bacterial cytochrome c_{552}.

C. Bacteriocyte domain of gill filaments equilibrated with nitrogen minus the same sample equilibrated with 20% air, from which a difference spectrum of purified deoxyhemoglobin minus oxyhemoglobin, computed to be equivalent to the hemoglobin content in gills, was subtracted. The wavelength maxima indicated were confirmed in the second derivative of this difference spectrum. Features are ascribed to bacterial cytochrome c_{552} and to a cytochrome *b* (566 nm). The feature at 586 nm is not identified.

Table I

Approximate hemoglobin concentration in tissues of Solemya reidi, *determined in living tissues and from hemoglobin extracted from tissue*

Tissue	Hemoglobin concentration, μM
I. Living tissue[a]	
bacteriocyte domain of gills	450 ± 90 (21)[b]
ciliated domain of gills	120 ± 15 (4)
pallial muscle	330 (2)
hypobranchial gland	540 (2)
II. Hemoglobin extraction	
whole gill	180
combined symbiont-free tissue (foot, pallial muscle, hypobranchial gland)	170

[a] Tissue thickness was estimated with a dissecting microscope at 80 μm for bacteriocyte domain, 125 μm for ciliated domain, 300 μm for pallial muscle and 100 μm for hypobranchial gland.

[b] Numbers are given as average ± standard deviation (number of repetitions).

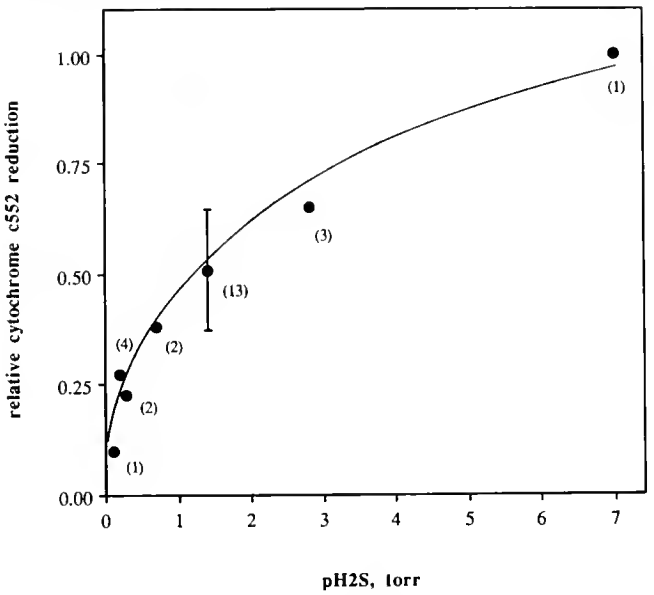

Figure 2. Relative reduction of cytochrome c_{552} in the bacteriocyte domain of living *Solemya reidi* gill filaments as a function of ambient partial pressure of hydrogen sulfide in air. Relative reduction is calculated from difference spectra as described in text. Half-reduction of cytochrome c_{552} occurs near 1.4 torr p_{H_2S}. Numbers in parentheses represent number of experiments.

Exposure to sulfide: cytochrome c_{552}. The optical contribution of hemoglobin did not change in the presence of hydrogen sulfide, either aerobically or anaerobically. Consequently, the spectral contribution of oxyhemoglobin cancels in the difference spectrum: gills in 20% air containing sulfide minus gills in 20% air alone. The remaining spectrum in the bacteriocyte domain (Fig. 1B), characterized by sharp features at 405, 424, 520, and 552 nm, is identified as the difference: reduced minus oxidized cytochrome c_{552} (Pettigrew and Moore, 1987). This is unequivocally distinguishable from mitochondrial cytochrome *c* with maxima in the direct reduced spectrum at 520 and 550 nm (see Figs. 1D, E; Pettigrew and Moore, 1987), and may be ascribed to the symbiont (see Discussion). Thus, hydrogen sulfide causes reduction of symbiont cytochrome c_{552} in the gill of *Solemya reidi*, without detectable change in other heme proteins. We note that reduction of cytochrome c_{552} was not detected in gills exposed to 300 μ*M* thiosulfate in seawater (data not shown). This may reflect the lack of uptake of thiosulfate into bacteriocyte cytoplasm.

The relative extent of reduction of cytochrome c_{552} in the bacteriocyte domain of aerobic gills increases monotonically with p_{H_2S} from zero in the absence of sulfide to a limit near 7 torr p_{H_2S} (Fig. 2). Relative reduction was calculated from the magnitude of the optical density differences 424 nm minus 405 nm and, separately, 552 nm minus 540 nm in difference spectra similar to Figure 1B (gills in 20% air containing sulfide minus gills in 20% air), normalized to a constant amount of hemoglobin in the optical path so as to allow comparison of samples of different thickness. Hemoglobin content was estimated from difference spectra similar to Figure 1A (gills in nitrogen minus gills in air) obtained from the same tissue sample. Reduction of cytochrome c_{552} was taken as maximal at p_{H_2S} = 7 torr and minimal in the absence of hydrogen

D. Ciliated domain of gill filaments equilibrated with nitrogen minus the same sample equilibrated with 40% air, from which a difference spectrum of purified deoxyhemoglobin minus oxyhemoglobin, computed to be equivalent to the hemoglobin content in gills, was subtracted. The wavelength maxima indicated were confirmed in the second derivative of this difference spectrum. Features are ascribed to mitochondrial cytochrome c_{550} and cytochrome *b*.

E. Ciliated domain of gill filaments equilibrated with 40% air containing 1.4 torr hydrogen sulfide minus the same sample equilibrated with 40% air. The wavelength maxima indicated were confirmed in the second derivative of this difference spectrum. Features are ascribed to mitochondrial cytochrome c_{550}, cytochrome *b*, and cytochrome oxidase.

F. Pallial muscle equilibrated with 70% air containing 1.4 torr hydrogen sulfide minus the same sample equilibrated with 70% air. Features are ascribed to mitochondrial cytochromes.

sulfide. Half reduction of cytochrome c_{552} occurred near 1.4 torr p_{H_2S}.

Exposure to nitrogen: cytochromes. The spectral contribution of reduced cytochromes in the optical spectrum of the gill is obscured by the spectral contribution of hemoglobin. Accordingly, the hemoglobin content of each sample was estimated and the equivalent difference spectrum: deoxyhemoglobin minus oxyhemoglobin, was subtracted from the difference spectrum: gills in nitrogen minus gills in air. The remaining spectral contribution (Fig. 1C) is dominated by bacterial cytochromes because mitochondria are sparse. The features at 552 and 424 nm correspond to the bacterial cytochrome c_{552}. The shoulder near 566 nm may tentatively be attributed to a cytochrome *b*. The feature at 586 nm remains unidentified.

Exposure to nitrogen plus sulfide: cytochrome c_{552}. Maximal reduction of cytochrome c_{552} was observed in gills exposed to nitrogen containing 1.4 torr hydrogen sulfide, demonstrated in the difference spectrum between this condition and gills in air (data not shown). Reduction of cytochrome c_{552} in gills exposed to nitrogen alone (Fig. 1C) represented only 81 ± 6% (n = 10) of maximum. It follows that symbiont cytochrome c_{552} is largely reduced in nitrogen alone, but is reduced still further in the presence of hydrogen sulfide. We note that the optical density differences (424 nm minus 405 nm and 552 nm minus 540 nm) are the same in gills exposed to 1.4 torr hydrogen sulfide in the presence of nitrogen and in gills exposed to 7 torr hydrogen sulfide in air, indicating that maximal reduction was achieved in each instance.

Optical spectra of the ciliated domain of the gill

Exposure to nitrogen: cytochromes. Cytoplasmic hemoglobin, at a concentration roughly one third that of the bacteriocyte domain (Table I), dominates the optical spectrum of the symbiont-free ciliated domain of the gill. A reduced minus oxidized difference spectrum (Fig. 1D) was constructed by subtracting the expected spectral contribution of cytoplasmic hemoglobin from the difference spectrum: gills in nitrogen minus the same tissue in air or 40% air. Clearly resolved spectral features at 422, 520, and 550 nm may be ascribed to mitochondrial cytochrome *c*, identified by comparison with the difference of reduced minus oxidized horse heart cytochrome *c*, which has features at 419, 520, and 550 nm (Pettigrew and Moore, 1987). The 550 nm feature in the ciliated domain difference spectrum is consistently distinct from the 552 nm feature seen in the bacteriocyte domain difference spectrum (Fig. 1B). The shoulder at 565 nm may be reasonably ascribed to mitochondrial cytochrome *b* (ubiquinone-cytochrome *c* oxidoreductase).

Exposure to sulfide: cytochromes. We next examine the spectral change produced by exposing the air-equilibrated ciliated domain to 1.4 torr hydrogen sulfide. The difference spectrum (Fig. 1E) is very similar to that of partially reduced minus oxidized mitochondria. Features at 419, 520, and 550 nm may again be ascribed to cytochrome *c*. Features at 446 and 602 nm may be ascribed to cytochrome oxidase. Small features near 430 and 565 nm may be ascribed to cytochrome *b*. All of these features become more prominent with increased hydrogen sulfide to 2.8 torr (data not shown).

Exposure to nitrogen plus sulfide: cytochromes. Further reduction of mitochondrial cytochromes by hydrogen sulfide in nitrogen compared to nitrogen alone was not observed. The optical difference: gills in nitrogen containing 1.4 torr hydrogen sulfide minus gills in nitrogen alone was relatively featureless and exhibited no peaks ascribed to mitochondrial cytochromes (data not shown).

Optical spectra of pallial muscle

Exposure to sulfide: cytochromes. The pink-colored pallial muscle is another example of symbiont-free tissue with cytoplasmic hemoglobin. In the difference spectrum of a thin piece of pallial muscle equilibrated with 70% air containing 1.4 torr hydrogen sulfide minus the same sample in 70% air alone, the spectrum of hemoglobin cancels and the remaining difference spectrum suggests reduction of a full complement of mitochondrial cytochromes: cytochrome c_{550}, cytochrome *b* and cytochrome oxidase (Fig. 1F).

Discussion

The protobranch mollusk *Solemya reidi* lives in burrows in strongly reducing sediments, with hydrogen sulfide concentrations reaching 3 m*M*. It is quite mobile and may seek appropriate sulfide concentrations (Reid, 1980; Childress and Lowell, 1982). There is no sulfide-binding protein in the circulating blood and the sulfide concentration in gills of freshly captured specimens is close to environmental (Childress, 1987), suggesting that symbionts take up hydrogen sulfide and oxygen directly across the gill. Without question, symbionts use hydrogen sulfide. Sulfide stimulates oxygen and carbon dioxide consumption of *Solemya reidi* (Anderson *et al.*, 1987) and carbon fixation in isolated gills of *Solemya velum* (Cavanaugh, 1983a). We note that on a per sulfur basis, sulfide is much more effective in stimulating carbon dioxide fixation than thiosulfate: approximately 14-fold more effective in whole *Solemya reidi* (recalculated from Anderson *et al.*, 1987), and 6-fold more effective in isolated *Solemya velum* gills (recalculated from Cavanaugh, 1983a).

The gill of *Solemya reidi* is comprised of a few hundred individual filaments held together at a central ligament and arranged in parallel somewhat like pages of a book. Each filament is divided into two major domains by a chitinous skeletal rod located near the outer edge: a rel-

atively small outer domain of mitochondria-rich ciliated cells and a much larger inner domain comprised largely of bacteriocytes (Yonge, 1939; Reid, 1980; Powell and Somero, 1985). Ciliated cells near the outer edge drive the flow of water between filaments and across the face of the inner domain. Electron micrographs of *Solemya reidi* (Powell and Somero, 1985) and of the related species *Solemya velum* (Cavanaugh, 1983b; Doeller, 1986) show that cells in the ciliated domain are densely packed with mitochondria and are free of bacteria. Conversely, bacteriocytes are densely packed with bacteria; mitochondria are sparse. Separation of the two cell types occurs also in gills of several lamellibranch mollusks of the family Lucinidae (Giere, 1985), including *Lucina pectinata* (J. B. Wittenberg, unpub.). In this study we take advantage of the separation of bacteriocyte and mitochondria-rich domains to study each separately.

Cytochromes of the bacterial partner are singularly well resolved in optical spectra of the bacteriocyte domain of the *Solemya reidi* gill. Difference spectra of the bacteriocyte domain exposed to a low concentration of hydrogen sulfide in the presence of air are dominated by the spectral contribution of a hemeprotein characterized by a prominent alpha-band centered at 552 nm and identified as a *c*-type cytochrome by the positions of its wavelength maxima, 424, 520, and 552 nm (Fig. 1B). It may be called cytochrome c_{552}. Cytochromes *c* characterized by maxima between 551 and 553 nm are conspicuous components of many sulfur-oxidizing bacteria (Pettigrew and Moore, 1987). They are not known in eukaryote tissues and are easily distinguished from mitochondrial cytochrome c_{550}, observed, for instance, in the ciliated domain of the gill and the pallial muscle (Fig. 1D, E, and F). Narrow spectral bandwidths in the observed spectrum (Fig. 1B) and the absence of features not related to cytochrome c_{552} (other than a small perturbation near 600 nm) suggest strongly that hydrogen sulfide, in the presence of oxygen, has reduced a single spectrally demonstrable species, bacterial cytochrome c_{552}. The extent of this reduction is a monotonic function of ambient p_{H_2S} (Fig. 2), suggesting, but by no means proving, that hydrogen sulfide is the immediate or near immediate reductant for symbiont cytochrome c_{552}. Reduction of cytochromes by sulfide might proceed by direct electron transfer (Wilson and Erecinska, 1978) as it does in the free-living bacterium *Thiobacillus denitrificans* (Sawhney and Nicholas, 1978), or it could be mediated by flavocytochromes *c* (reviewed in Pettigrew and Moore, 1987). Reduction of *Solemya reidi* symbiont cytochrome c_{552} finds a strong parallel in the free-living sulfur-oxidizing bacteria, where soluble *c*-type cytochromes occurring in the periplasmic space are considered the main point of transfer of electrons from external reduced sulfur compounds into the bacterial cytochrome chain (Kelly, 1982, 1985, 1988; Pettigrew and Moore, 1987).

Cytochrome c_{552} in the bacteriocyte domain of the gill is also reduced under anaerobic conditions in the absence of hydrogen sulfide. In this case, a cytochrome *b* and perhaps other cytochromes are reduced as well (Fig. 1C), and we cannot define an unique path of electron flow. Nor do we assert that the cytochrome c_{552} reduced anaerobically in the absence of sulfide is the same species as that reduced by sulfide. Our data indicate that symbiont cytochrome c_{552} is largely reduced by endogenous substrate under anaerobic conditions, but exhibits further reduction by hydrogen sulfide under these conditions. We find a possible analogy in the thiosulfate-oxidizing bacterium *Thiobacillus versutus* (A2), which has two *c*-type cytochromes, c_{551} and $c_{552.5}$, each with two separately titratable oxidation/reduction centers with widely different midpoint potentials (Lu and Kelly, 1984; Lu *et al.*, 1984). Transfer of electrons at two different potentials from thiosulfate to cytochrome *c* of the bacterial electron transport chain is mediated by this multi-heme complex (Lu and Kelly, 1984; Lu *et al.*, 1984). The additional reduction of symbiont cytochrome c_{552} in *Solemya reidi* gills by hydrogen sulfide, over and above that in nitrogen alone, indicates that cytochrome c_{552} may have two oxidation/reduction centers as well.

The symbiont-free ciliated domain of the gill, made anaerobic, displays the expected spectrum of the reduced mitochondrial electron transport chain, with features ascribable to cytochrome *c*, cytochrome *b*, and cytochrome oxidase (Fig. 1D). The ultimate reductant in this instance must be endogenous substrate.

The mitochondria-rich tissues, pallial muscle with singularly well-resolved spectra and the ciliated domain of the gill, exposed to hydrogen sulfide in the presence of air, exhibit spectra of reduced mitochondria, once again with features ascribed to cytochrome *c*, cytochrome *b*, and cytochrome oxidase (Fig. 1E, F). A simple explanation is that hydrogen sulfide is serving as the reductant for the respiratory chain. Indeed, isolated gill mitochondria from *Solemya reidi* are known to oxidize sulfide with production of ATP (Powell and Somero, 1986; O'Brien and Vetter, 1990). The inference from these studies is that electrons from hydrogen sulfide enter the mitochondrial electron transport chain at the level of cytochrome *c*, with oxidative phosphorylation only at the cytochrome oxidase site (Complex IV). An alternative explanation of our observations is that hydrogen sulfide may bind to and inhibit cytochrome oxidase, with a spectral signature not easily distinguished from normal oxidation/reduction (Wilson and Erecinska, 1978). This also would lead to net observed cytochrome reduction, in this instance by endogenous substrate. Possibly both processes occur simultaneously.

Hemoglobin, presumably located in the host cell cytoplasm, is abundant in the symbiont-containing bacteriocytes of the *Solemya reidi* gill and occurs as well in the symbiont-free ciliated domain of the gill, foot, pallial and adductor muscles, hypobranchial gland, and nervous tissue (Table 1). Hemoglobin concentration in these tissues is comparable to the myoglobin content of many hard-working muscles (Schuder *et al.*, 1979). The concentration of hemoglobin in the bacteriocyte domain of the gill is in the upper part of the range reported for other symbiont-housing molluscan gills (Wittenberg, 1985).

Only oxygenated and deoxygenated hemoglobin were detected in the bacteriocyte domain of the *Solemya reidi* gill and in other tissues (*e.g.*, Fig. 1A). Ferric hemoglobin sulfide, that is ferric hemoglobin with sulfide ligated to the heme iron atom in the distal position, was not detected under any conditions. This stands in sharp contrast to the behavior of hemoglobin in the living gill of the congeneric species *Solemya velum*, where about half of the gill hemoglobin is rapidly and reversibly converted to ferric hemoglobin sulfide when the gill is exposed to low concentrations of hydrogen sulfide in aerated seawater (Doeller *et al.*, 1988). The behavior of hemoglobin in the *Solemya reidi* bacteriocyte also stands in contrast to the reaction of the "sulfide-reactive" hemoglobin, Hb I, isolated from the symbiont-containing gill of the lucinid clam *Lucina pectinata* (Kraus and Wittenberg, 1990). Oxygenated *Lucina* Hb I reacts rapidly with hydrogen sulfide at micromolar concentration to form ferric hemoglobin sulfide. We propose that in these three symbioses, sulfide-reactive gill hemoglobin functions to deliver either hydrogen sulfide or reducing equivalents to the symbiont. As one working hypothesis, we offer that the observed large difference in the steady-state concentration of ferric hemoglobin sulfide in the two *Solemya* gills reflects very different rates of chemical reaction. Extraordinary slow dissociation of sulfide from ferric *Lucina* hemoglobin sulfide ($k_{off} = 2 \times 10^{-4}\ s^{-1}$; implying a turnover time of 5000 s) suggests that delivery of sulfide cannot be achieved by simple dissociation of the ligand. Instead, we suggest reduction of ferric hemoglobin sulfide near the peribacterial membrane surface may precede ligand delivery (Kraus and Wittenberg, 1990; Wittenberg and Kraus, 1991). We consider that this latter step may be rate-limiting in the gill of *Solemya velum* but not of *Solemya reidi*. Reduction of the major hemoglobin of the *Solemya reidi* gill, when ferric, is very much more rapid than the corresponding reduction of ferric *Lucina* hemoglobin sulfide in the presence of excess sulfide (Kraus and Doeller, unpub.). Perhaps rapid reductive removal of ferric hemoglobin in the *Solemya reidi* gill prevents accumulation of ferric hemoglobin sulfide in the tissue. As an alternative hypothesis, we offer that *Solemya reidi* gill hemoglobin may function in the transfer of reducing equivalents from sulfide to symbiont. This function is suggested by the rapid reduction of ferric *Solemya reidi* hemoglobin by hydrogen sulfide and by the lack of formation of ferric *Solemya reidi* hemoglobin sulfide *in vitro* (under the same conditions as those that lead to the formation of ferric *Lucina* hemoglobin sulfide; Kraus and Doeller, unpub.).

In summary, bacterial symbionts of the *Solemya* gill use hydrogen sulfide as the sole environmental source of reducing equivalents. We show here that symbiont bacterial cytochrome c_{552} is extensively reduced when the gill is exposed to hydrogen sulfide, and that hydrogen sulfide is the immediate or near immediate reductant for this cytochrome. This finds a strong parallel in free-living, sulfide-oxidizing bacteria that are considered to accept electrons from reduced sulfur compounds at the level of cytochrome *c*, supporting oxidative phosphorylation at the level of the terminal oxidase and reverse electron flow to NAD (reviewed in Kelly, 1982, 1985, 1988; Pettigrew and Moore, 1987). Only oxyhemoglobin and deoxyhemoglobin are detected in the gill of *Solemya reidi*, in sharp contrast to the congener *Solemya velum* where ferric hemoglobin sulfide constitutes about half of the hemoglobin in gills exposed to hydrogen sulfide and oxygen. *Solemya reidi* gill hemoglobin may participate in the symbiosis by rapid formation and reduction of ferric hemoglobin sulfide, or by transfer of electrons from sulfide to symbiont.

Acknowledgments

This work was supported in part by research grants DMB 87-03328 and DCB 90-17722 from the National Science Foundation (to JBW), in part by USPHS research grant HL19299 (to Dr. B. A. Wittenberg), and in part by the University of Alabama at Birmingham Faculty Research Grant (to DWK). Animals used in this study were collected on a cruise of the Point Sur, supported by research grant OCE 86-10514 from the National Science Foundation (to Dr. J. J. Childress). J. B. Wittenberg is a Research Career Program Awardee 1-K6-733 of the United States Public Health Service, National Heart, Lung and Blood Institute. We extend special thanks to Drs. C. R. Fisher and J. J. Childress for the invitation to DWK and JED to participate in the *Solemya reidi* collecting cruise, to the captain and crew of the Point Sur for their help in the collection of *Solemya reidi*, to Dr. R. G. B. Reid for supplying specimens of *Solemya reidi* for preliminary experiments, and to Dr. B. A. Wittenberg for continuing discussions.

Literature Cited

Anderson, A. E., J. J. Childress, and J. A. Favuzzi. 1987. Net uptake of CO_2 driven by sulphide and thiosulfate oxidation in the bacterial symbiont-containing clam *Solemya reidi*. *J. Exp. Biol.* **133**: 1–31.

Appleby, C. A., J. D. Tjepkema, and M. J. Trinick. 1983. Hemoglobin in a nonleguminous plant. *Parasponia:* possible genetic origin and function in nitrogen fixation. *Science* **220:** 951–953.

Cavanaugh, C. M. 1983a. Symbiotic chemoautotrophic bacteria in marine invertebrates from sulphide-rich habitats. *Nature* **302:** 58–61.

Cavanaugh, C. M. 1983b. Chemoautotraphic bacteria in marine invertebrates from sulfide-rich habitats: a new symbiosis. Pp. 699–708 in *Endocytobiology, Vol. II., Intracellular Space as Oligogenetic Ecosystem,* H. E. A. Schenk and W. Schwemmler, eds. Walter de Gruyter and Co., Berlin.

Childress, J. J. 1987. Uptake and transport of sulfide in marine invertebrates. In *Comparative Physiology: Life in Water and on Land,* P. Dejours, L. Bolis, C. R. Taylor, and E. R. Weibel, eds. *Fidia Research Series* **9:** 231–239. Liviana Press, Padova.

Childress, J. J., and C. R. Fisher. 1992. The biology of hydrothermal vent animals: physiology, biochemistry and autotrophic symbioses. *Oceanogr. Mar. Biol. Ann. Rev.* **30:** in press.

Childress, J. J., and W. Lowell. 1982. The abundance of a sulfide-oxidizing symbiosis (the clam *Solemya reidi*) in relation to interstitial water chemistry. *Eos* **63:** 957.

Dando, P. R., A. J. Southward, and E. C. Southward. 1986. Chemoautotrophic symbionts in the gills of the bivalve mollusc *Lucinoma borealis* and the sediment chemistry of its habitat. *Proc. R. Soc. Lond. B* **227:** 227–247.

Doeller, J. E. 1986. A study of the gill hemoglobin in the nearly gutless bivalve *Solemya velum* Say (Protobranchia). Ph.D. Dissertation, Clemson University, SC.

Doeller, J. E., D. W. Kraus, and J. M. Colacino. 1983. The presence of hemoglobin in *Solemya velum* (Bivalvia, Protobranchia). *Am. Zool.* **23:** 976.

Doeller, J. E., D. W. Kraus, J. M. Colacino, and J. B. Wittenberg. 1988. Gill hemoglobin may deliver sulfide to bacterial symbionts of *Solemya velum* (Bivalvia, Mollusca). *Biol. Bull.* **175:** 388–396.

Fisher, C. R. 1990. Chemoautotrophic and methanotrophic symbioses in marine invertebrates. *Rev. Aquatic Sci.* **2:** 399–436.

Fisher, C. R., and J. J. Childress. 1986. Translocation of fixed carbon from symbiotic bacteria to host tissues in the gutless bivalve *Solemya reidi. Mar. Biol.* **93:** 59–68.

Giere, O. 1985. Structure and position of bacterial endosymbionts in the gill filaments of *Lucinidae* from Bermuda (Mollusca, Bivalvia). *Zoomorphology* **105:** 296–301.

Jones, M. L. (ed). 1985. Hydrothermal vents of the eastern Pacific: an overview. *Bull. Biol. Soc. Wash.* **6:** 1–547.

Kelly, D. P. 1982. Biochemistry of the chemolithotrophic oxidation of inorganic sulphur. *Phil. Trans. R. Soc. Lond. B* **298:** 499–528.

Kelly, D. P. 1985. Physiology of the thiobacilli: elucidating the sulphur oxidation pathway. *Microbiol. Sci.* **2:** 105–109.

Kelly, D. P. 1988. Oxidation of sulfur compounds. In *The Nitrogen and Sulfur Cycles,* Cole, J. A. and S. J. Ferguson, eds. *Symp. Soc. Gen. Microbiol* **42:** 65–98.

Kemling, N., D. W. Kraus, J. D. Hockenhull-Johnson, J. B. Wittenberg, S. N. Vinogradov, and P. Martin. 1991. Crystallization of a complex of hemoglobin components II and III of the symbiont-harboring clam *Lucina pectinata. J. Mol. Biol.* **222:** 463–464.

Kraus, D. W., and J. B. Wittenberg. 1990. Hemoglobins of the *Lucina pectinata*/bacteria symbioses. I. Molecular properties, kinetics and equilibria of reactions with ligands. *J. Biol. Chem.* **265:**16,043–16,053.

Kraus, D. W., J. B. Wittenberg, L. Jing-Fen, and J. Peisach. 1990. Hemoglobins of the *Lucina pectinata*/bacteria symbioses. II. An electron paramagnetic resonance and optical spectral study of the ferric proteins. *J. Biol. Chem.* **265:** 16,054–16,059.

Lu, W.-P., and D. P. Kelly. 1984. Purification and characterization of two essential cytochromes of the thiosulphate-oxidizing multi-enzyme system from *Thiobacillus* A2 (*Thiobacillus versutus*). *Biochim. Biophys. Acta* **765:** 106–117.

Lu, W.-P., R. K. Poole, and D. P. Kelly. 1984. Oxidation-reduction potentials and spectral properties of some cytochromes from *Thiobacillus versutus* (A2). *Biochim. Biophys. Acta* **767:** 326–334.

Millero, F. J. 1986. The thermodynamics and kinetics of the hydrogen sulfide system in natural waters. *Mar. Chem.* **18:** 121–147.

Nicholls, P. 1975. The effect of sulphide on cytochrome *aa*3 isosteric and allosteric shifts of the reduced alpha-peak. *Biochim. Biophys. Acta* **396:** 24–35.

O'Brien, J., and R. D. Vetter. 1990. Production of thiosulphate during sulphide oxidation by mitochondria of the symbiont-containing bivalve *Solemya reidi. J. Exp. Biol.* **149:** 133–148.

Pettigrew, G. W., and G. R. Moore. 1987. *Cytochromes c. Biological Aspects.* Springer-Verlag, NY, Pp. 1–282.

Powell, M. A., and A. J. Arp. 1989. Hydrogen sulfide oxidation by abundant nonhemoglobin heme compounds in marine invertebrates from sulfide-rich habitats. *J. Exp. Zool.* **249:** 121–132.

Powell, M. A., and G. N. Somero. 1985. Sulfide oxidation occurs in the animal tissue of the gutless clam, *Solemya reidi. Biol. Bull.* **169:** 164–181.

Powell, M. A., and G. N. Somero. 1986. Hydrogen sulfide oxidation is coupled to oxidative phosphorylation in mitochondria of *Solemya reidi. Science* **233:** 563–566.

Read, K. R. H. 1962. The hemoglobin of the bivalved mollusc, *Phacoides pectinatus* (Gmelin). *Biol. Bull.* **123:** 605–617.

Read, K. R. H. 1965. The characterization of the hemoglobins of the bivalve mollusc *Phacoides pectinatus* (Gmelin). *Comp. Biochem. Physiol.* **15:** 137–158.

Reid, R. G. B. 1980. Aspects of the biology of a gutless species of *Solemya* (Bivalvia: Protobranchia). *Can. J. Zool.* **58:** 386–393.

Sawhney, V., and D. J. D. Nicholas. 1978. Sulfide-linked nitrite reductase from *Thiobacillus denitrificans* with cytochrome oxidase activity: purification and properties. *J. Gen. Microbiol.* **106:** 119–128.

Schuder, S., J. B. Wittenberg, B. Haseltine, and B. A. Wittenberg. 1979. Spectrophotometric determination of myoglobin in cardiac and skeletal muscle: separation from hemoglobin by subunit-exchange chromatography. *Anal. Biochem.* **92:** 473–481.

Somero, G. N., J. J. Childress, and A. E. Anderson. 1989. Transport, metabolism, and detoxification of hydrogen sulfide in animals from sulfide-rich marine environments. *Rev. Aquatic Sci.* **1:** 591–614.

Southward, E. C. 1987. Contribution of symbiotic chemoautotrophs to the nutrition of benthic invertebrates. Pp. 84–116 in *Microbes in the Sea,* M. A. Sleigh, ed. Ellis Horwood, Chichester.

Wilson, D. F., and M. Erecinska. 1978. Ligands of cytochrome *c* oxidase. *Methods Enzymol.* **53:** 191–201.

Wittenberg, J. B. 1985. Oxygen supply to intracellular bacterial symbionts. In *Hydrothermal Vents of the Eastern Pacific: An Overview,* M. L. Jones, ed. *Bull. Biol. Soc. Wash.* **6:** 1–547.

Wittenberg, J. B., and D. W. Kraus. 1991. Hemoglobins of eukaryote/prokaryote symbioses. Pp. 323–330 in *Structure and Function of Invertebrate Oxygen Carriers,* S. N. Vinogradov and O. H. Kapp, eds. Springer-Verlag, New York.

Yonge, C. M. 1939. The protobranchiate molluscs: a functional interpretation of their structure and evolution. *Phil. Trans. Roy. Soc. Lond. B* **230:** 79–147.

Reference: *Biol. Bull.* **182:** 444–453. (June, 1992)

Oxygen- and Nitrogen-Dependent Sulfur Metabolism in the Thiotrophic Clam *Solemya reidi*

DAVID B. WILMOT[1] AND RUSSELL D. VETTER

Marine Biology Research Division, 0202, Scripps Institution of Oceanography, University of California, San Diego, La Jolla, California 92093

Abstract. We investigated aerobic and anaerobic thiotrophic metabolism by the gutless clam *Solemya reidi* and its intracellular symbiotic bacteria. Mean environmental sulfide concentrations in porewater next to animals varied from a high of 888 μM to a low of 17 μM in different sediment samples, while mean thiosulfate concentrations were very low (1–13 μM). The blood of freshly collected clams contained up to 300 μM thiosulfate but little sulfide ($\leq$12 μM). In experimental incubations, clams were able to take up thiosulfate, yet under no conditions could the animals concentrate thiosulfate above external concentrations. Thiosulfate accumulation in the blood during incubations was the result of aerobic but not anaerobic sulfide oxidation by the animals. This finding and previous observations of the presence of high concentrations of thiosulfate in the blood of field-caught clams indicate that the animal portion of the symbiosis normally functions aerobically. The intact symbiosis exhibited nitrate and nitrite respiration under anoxic conditions. Nitrate respiration was stimulated by sulfide, as well as thiosulfate, while nitrite respiration was only stimulated by sulfide. Nitrate respiration also occurred when whole animals were under oxic conditions. Respiration measurements showed that the bacterial symbionts were capable of direct sulfide oxidation. Sulfide-stimulated oxygen consumption by bacterial preparations from the gills of mud-maintained clams reached a maximum rate at 25 μM sulfide and showed no apparent inhibition at sulfide concentrations up to 1 mM sulfide.

Introduction

Solemya reidi is a gutless, marine protobranch bivalve that lives in reduced sediments such as sewage outfall zones and pulp mill effluent sites (Reid, 1980; Reid and Bernard, 1980). The clam contains intracellular, chemolithotrophic bacterial symbionts within specialized cells in its gills (Felbeck, 1983). The bacteria use the energy from the oxidation of reduced sulfur compounds to fix and reduce CO_2 and subsequently translocate the fixed carbon to symbiont-free tissues of the animal, resulting in a net autotrophic existence of the symbiosis (Felbeck, 1983; Fisher and Childress, 1986; Anderson *et al.*, 1987). This autotrophic, sulfur-dependent mode of nutrition is called thiotrophy (Vetter, 1991).

Based on experiments done at high sulfide concentrations, Powell and Somero (1985) concluded that sulfide oxidation occurs in the animal tissue of *S. reidi* and not in the symbiotic bacteria. The authors identified intracellular, ferric iron-containing granules (originally called sulfide-oxidizing bodies, referred to as granules in this manuscript) and based upon a colorimetric assay suggested that granules were responsible for sulfide oxidation in *S. reidi* (Powell and Somero, 1985). The products of this oxidation were not identified. Subsequent studies revealed that isolated mitochondria of *S. reidi* are also capable of sulfide oxidation and that the mitochondria couple sulfide oxidation to aerobic respiration and ATP production (Powell and Somero, 1986; O'Brien and Vetter, 1990). The mitochondria oxidize sulfide exclusively to thiosulfate (O'Brien and Vetter, 1990). In addition, high concentrations of thiosulfate are found in the blood of field-caught animals and clams experimentally exposed to sulfide (Anderson *et al.*, 1987). These findings suggested that the mitochondria may also have a role in sulfide detoxification.

Current models propose that the detoxification of sulfide is an oxygen-dependent process that occurs only in the animal tissues of *S. reidi* (reviewed by Somero *et al.*, 1989). The oxidation results in the production of thio-

Received 17 April 1991; accepted 27 March 1992.

[1] Present address: Ocean Studies Board, HA-550, National Research Council, 2101 Constitution Ave., NW, Washington, DC 20418.

sulfate. Thiosulfate is subsequently transported by the animal to the bacteriocyte where it is further oxidized by the bacteria, again by an oxygen-dependent respiratory process.

Aspects of this model describing thiotrophic metabolism are not proven or they are inaccurate because of a lack of direct experimental evidence or the technical difficulties in early experiments. First, there is little information on the environmental sulfide conditions in the clam's habitat. Although the bulk sulfide concentrations in sediment samples are highly variable, ranging from low micromolar concentrations up to 22 m*M* (Childress and Lowell, 1982; Vetter *et al.*, 1989), the concentration near the animals is not known. Data suggest that the optimal sulfide concentrations for the animals are 100 μM or below (Anderson *et al.*, 1987, 1990). In addition, the concentrations of other possible substrates (including thiosulfate, which is found in the blood of freshly caught clams) in the animals' burrows are not known.

Second, bacterial symbionts may be important agents of direct sulfide oxidation in the symbiosis in the presence of environmental sulfide concentrations. Recent experiments in our laboratory have shown that enriched bacterial suspensions show stimulation of $^{14}CO_2$ uptake in the presence of 500 μM sulfide and exhibit nitrate and nitrite respiration under anoxic conditions in the presence of 200 μM sulfide (Dr. Barbara Javor, pers. comm.). In addition, *in vivo* measurements of spectral changes of intracellular hemoglobins (Doeller *et al.*, 1988) and *in vitro* accumulations of elemental sulfur in isolated gill ctenidia exposed to oxygen and sulfide (Vetter, 1990) suggest that sulfide and oxygen enter the bacteriocyte directly from the seawater.

Third, the effect of anoxic conditions on sulfur metabolism of the host and symbionts needs additional study. Anderson *et al.* (1990) have shown that animal tissues of *S. reidi* maintain aerobic metabolism in the presence of sulfide concentrations up to 100 μM, but they switch to anaerobic metabolism (fermentation) in the presence of oxygen at higher sulfide concentrations. This switch is due to poisoning of cytochrome *c* oxidase and aerobic respiration (Anderson *et al.*, 1990). Whole animal experiments under conditions of low O_2 or at sulfide concentrations above 250 μM showed a loss of net autotrophy, suggesting that bacterial metabolism was inhibited (Anderson *et al.*, 1987). However, the anaerobic sulfide-oxidizing capacity of the symbionts was never measured and the clams were incubated in surface seawater that does not typically contain the alternate electron acceptor nitrate that some sulfur-oxidizing bacteria can use for anaerobic respiration. Thus, the absence of net autotrophy observed could be due to the absence of nitrate. Net CO_2 uptake might be enhanced at high sulfide concentrations or at low O_2 concentrations under conditions promoting anaerobic respiration in the bacteria.

High nitrate reductase activity has been observed in *S. reidi* (Felbeck *et al.*, 1983). However, this enzyme was proposed to be involved only in assimilatory nitrate reduction. The bacterial symbionts of the clam *Lucinoma aequizonata* might use an anaerobic metabolic strategy (Cary *et al.*, 1989), and recently nitrate respiration has been demonstrated in the symbionts of *L. aequizonata* (U. Hentschel, pers. comm.) and *S. reidi* (Javor, pers. comm.). The sulfur metabolism of the whole clam under oxic and anoxic conditions in the presence of nitrate needs to be investigated.

This investigation was designed to address the following questions about sulfide and thiosulfate metabolism in the *S. reidi* symbiosis. (1) Is thiosulfate present in the mud around the clam and what causes thiosulfate to accumulate in clam blood? (2) Can the bacteria oxidize sulfide directly, and do bacteria and granules compete for sulfide? (3) Can the intact symbiosis use nitrate and nitrite as alternate electron acceptors?

Materials and Methods

Experimental animals

Specimens of *Solemya reidi* were collected at the Hyperion sewage outfall in Santa Monica Bay, California, at a depth of 100 to 140 m using a modified Van Veen grab. The animals were maintained in mud from their habitat in a flowing seawater aquarium. The aquarium was kept dark at 8°C to mimic natural conditions. All experimental incubations were done with animals maintained less than 30 days, with most animals maintained less than 14 days. Clam size varied from 32 to 42 mm. An effort was made to use similar size animals within experiments. Nitrate and nitrite respiration experiments (Figs. 1, 2) have all values normalized to a wet gill weight of 420 mg/clam. Blood values (Tables I, II, III) are not normalized to size or gill weight. The values represent the concentrations measured.

Whole clam sulfur use experiments (oxic and anoxic) were done with aquarium-maintained animals that had been pre-incubated for a minimum of 48 h in oxygenated seawater (dark at 8°C) without sulfur substrates. This preincubation allowed the animals to remove reduced sulfur compounds from their blood (see Results). All incubations were performed in a glass, water-jacketed incubation chamber with 500 ml of filtered seawater at 10°C. Whole clam nitrate and nitrite respiration experiments were done with aquarium-maintained animals immediately after removal from the mud. Incubations were done in ground-glass stoppered bottles with 100 ml filtered seawater at 10°C. All anoxic incubations were done in seawater sparged with argon for 10 min. The chambers were sealed

except for sampling, and argon was blown over the opening during sampling.

Sulfur compound sampling and analysis

Concentrations of sulfide, thiosulfate, sulfite, and glutathione were measured by HPLC using the monobromobimane (bimane) technique (Newton and Fahey, 1987; Vetter *et al.,* 1989). For porewater samples, the sediment surrounding individual animals was collected and immediately placed in 50-ml test tubes and centrifuged in a clinical centrifuge at approximately 2500 RPM. Aliquots of 100 μl were immediately derivatized with bimane. The reaction of bimane with the sample rapidly derivatized all reduced thiols and prevented further oxidation. Blood samples were collected by carefully cutting the membrane that connects the two valves and opening the animal. Seawater was wiped away, and the mantle was cut at the exhalent opening. Aliquots of 100 μl blood were immediately derivatized with bimane. Water samples from whole animal incubations were collected and 100 μl aliquots were immediately derivatized with bimane. Fluorescence of the bimane-derivatized samples was measured as previously described (Wilmot and Vetter, 1990).

Bacterial enrichments

Suspensions of bacterial symbionts were obtained by gently homogenizing the gills of aquarium-maintained clams in a glass homogenizer in filtered (0.45 μ*M*) seawater buffered with 10 m*M* MOPS (3-[N-morpholino]propanesulfonic acid), pH 7.5. The homogenate was centrifuged at low speed (53 × *g*) at 4°C for 5 min, pelleting the large cellular debris. Filtration of the suspension through 15-μm or 28-μm Nitex filters separated the bacteria (approximately 1 μm diameter) from the larger subcellular particles. The filtrate was centrifuged a second time at 1925 × *g* at 4°C for 5 min, which pelleted the bacteria and granules while leaving the mitochondria in the supernatant. The pellet was washed and resuspended in MOPS-buffered seawater. The Percoll gradient technique (Distel and Felbeck, 1988; Wilmot and Vetter, 1990) was not effective in separating the bacteria from other subcellular particles. Light microscopy was used to confirm that preparations did not contain nuclei and large cellular debris. Because mitochondria are too small to detect by casual observation, the bacterial preparation was tested for contamination by measuring ATP production. There was no external ATP produced, indicating that either no mitochondria were present or they could not function in seawater. Bacterial preparations had a final concentration of 36–38 mg wet gill tissue/ml seawater.

Bacterial enrichments were also made from clams that had been starved for 21 days. These animals were placed in oxygenated seawater containing no sulfur substrates or nitrate and kept at 8°C in the dark. The seawater was changed at least once a day. The bacterial suspensions were prepared exactly as described above.

Protein determination

Total protein of bacterial suspensions was measured by the method of Hartree (1972).

Nitrite determination

Seawater samples (1 ml) were collected and nitrite determined using a modification of the colorimetric method of Strickland and Parsons (1977). Due to interference by thiols, several modifications were necessary. Briefly, we had to solve the problem of interference by sulfide and thiosulfate. This was accomplished by precipitating the thiols.

Respiration measurements

All incubations were carried out in a Strathkelvin respiration chamber at 15°C. The respiration chamber was thermally jacketed and contained a stir bar that allowed homogeneous incubation at a constant temperature. Oxygen consumption was measured with a Clark-type oxygen electrode (Strathkelvin Instruments) modified to reduce interference by H_2S (O'Brien and Vetter, 1990).

Results

Sediment porewater and blood sulfur compounds

To determine which reduced sulfur compounds were available to the clams, we sampled the sediment porewater surrounding individual clams and in the blood of these clams. The major sulfur compound in sediment porewater was sulfide (Table I). Extremely low concentrations of thiosulfate were measured, but no sulfite or glutathione was present. Mean sulfide concentrations were highly variable between sediment samples at different sites (ranging from a low of 17 μ*M* to a high of 888 μ*M*). Variability within sediment samples was considerably less.

Although sulfide was the major reduced sulfur compound in the seawater surrounding the animals and thiosulfate concentrations were extremely low, clam blood contained high concentrations of thiosulfate (Table I). The blood of the animals also contained low concentrations of sulfide and sulfite (≤12 μ*M*). The cellular thiol compound, glutathione, remained relatively constant throughout sampling and was used as an indicator that hemolymph samples were not diluted by seawater. Nitrite was not present in either the sediment porewater or blood from freshly collected animals (data not shown).

To determine how fast thiosulfate and sulfide could be cleared from the blood of freshly collected animals from

Table I

Sulfur compounds from sediment porewater and blood of freshly collected Solemya reidi

Sample	n	Sulfur compounds (μM)			
		Sulfide	Thiosulfate	Sulfite	Glutathione
Pore water					
May 1987	6	385 ± 321	11 ± 19	ND	ND
June 1987	6	17 ± 5	1 ± 0	ND	ND
July 1990	6	38 ± 30	13 ± 2	0	0
September 1990 #1	4	20 ± 8	3 ± 1	0	0
September 1990 #2	6	888 ± 60	5 ± 4	0	0
Blood					
May 1987	6	4 ± 11	297 ± 120	ND	ND
June 1987	6	1 ± 0	111 ± 31	ND	ND
July 1990	7	11 ± 6	29 ± 17	<1	74 ± 27
September 1990 #1	4	8 ± 3	149 ± 35	9 ± 5	28 ± 13
September 1990 #2	5	12 ± 3	232 ± 89	9 ± 4	57 ± 21

June, 1987, data previously published (Vetter *et al.*, 1989). Values are mean ± standard deviation.
"ND" represents value not determined.

a single grab, 20 clams were placed in oxic seawater containing no reduced sulfur substrates. The removal of thiols from the blood of the clams is shown in Table II. An initial thiosulfate concentration of 274 ± 106 μM decreased to 17 ± 11 μM in 12 h and to zero in 24 h. Low concentrations of sulfide and sulfite were also cleared from the blood within 12 h while glutathione concentrations remained relatively constant.

Aerobic and anaerobic metabolism of sulfide and thiosulfate by whole animals

Sulfide and thiosulfate uptake and metabolism under oxic conditions were investigated using aquarium-maintained clams. Incubations with whole clams were for either 2 or 4 h. The animals were incubated in 500 ml filtered seawater at 10°C in the presence of either sulfide or thiosulfate.

Table II

Clearance of sulfur compounds from the blood of freshly collected Solemya reidi *during an incubation in sulfide-free, oxygenated seawater*

Sample	n	Sulfur compounds (μM)			
		Sulfide	Thiosulfate	Sulfite	Glutathione
T = 0 h	4	9 ± 1	274 ± 106	13 ± 1	19 ± 24
T = 6 h	4	17 ± 8	66 ± 44	27 ± 10	27 ± 29
T = 12 h	4	0 ± 0	17 ± 11	0 ± 0	9 ± 0
T = 24 h	4	0 ± 0	0 ± 0	2 ± 3	11 ± 2
T = 96 h	4	0 ± 0	0 ± 0	0 ± 0	18 ± 5

Values are mean ± standard deviation.

Whole clams incubated with sulfide (100 μM) showed very little sulfide or sulfite accumulation in the blood during the 2-h experiment (Table III). However, high concentrations of thiosulfate in the blood were observed. To examine the possibility that thiosulfate was actively transported by the clam, a thiosulfate ratio representing the ratio of the seawater thiosulfate concentration at the end of each incubation to the thiosulfate concentration in the blood at the end of each incubation was calculated. The thiosulfate ratio under oxic conditions was 1:300. Glutathione concentrations did not show any consistent pattern.

Similar experiments were performed by incubating clams with thiosulfate. Under these conditions, the clams did not concentrate thiosulfate in their blood above the concentration in the surrounding seawater during 2- and 4-h incubations with two thiosulfate concentrations (50 and 250 μM) (Table III). The thiosulfate ratio for either concentration was never greater than 1:1. Virtually no sulfide or sulfite was observed in the blood and glutathione again showed no consistent patterns.

We also investigated whole animal sulfide and thiosulfate metabolism under anoxic conditions. In these experiments, whole clams were incubated in seawater that was sparged with argon. Anoxic conditions were maintained throughout the incubations.

Anoxic incubations of clams with sulfide (100 μM) showed little sulfide or sulfite accumulation in the blood (Table III). However, unlike oxic incubations, blood thiosulfate concentrations did not increase substantially (24 μM as compared to 300 μM during anoxic incubations).

Thiosulfate was removed from the seawater and appeared in the blood of animals incubated under anoxic

Table III

Sulfur compounds from blood of Solemya reidi *after oxic and anoxic incubations with sulfide and thiosulfate. All incubations were in 500 ml seawater at 10°C*

Incubation conditions	n	Sulfur compounds (μM)				Thiosulfate ratio*
		Sulfide	Thiosulfate	Sulfite	Glutathione	
Sulfide						
Oxic—2 h						
Control	4	0 ± 0	18 ± 1	0 ± 0	13 ± 10	
100 μM	6	1 ± 1	300 ± 217	1 ± 1	15 ± 5	1:300
Anoxic—2 h						
Control	4	8 ± 3	8 ± 5	4 ± 3	9 ± 7	
100 μM	6	6 ± 2	24 ± 23	7 ± 1	33 ± 19	1:24
Thiosulfate						
Oxic—2 h						
Control	3	2 ± 2	5 ± 3	4 ± 1	9 ± 10	
250 μM	3	4 ± 1	136 ± 0	7 ± 3	38 ± 9	1:0.8
Oxic—4 h						
250 μM	3	3 ± 2	152 ± 4	6 ± 4	38 ± 2	1:0.9
Oxic—2 h						
Control	4	2 ± 2	22 ± 13	12 ± 4	28 ± 20	
50 μM	4	3 ± 5	35 ± 11	9 ± 9	16 ± 4	1:0.8
250 μM	4	0 ± 0	157 ± 17	3 ± 2	11 ± 1	1:0.8
Anoxic—2 h						
Control	3	2 ± 2	5 ± 3	4 ± 1	9 ± 10	
250 μM with 5 mM nitrate	3	6 ± 2	158 ± 63	4 ± 1	14 ± 12	1:0.7
250 μM w/out 5 mM nitrate	3	3 ± 2	116 ± 33	4 ± 2	25 ± 19	1:0.5

Sulfur compound values are mean ± standard deviation.

* The thiosulfate ratio represents the ratio of the seawater concentration at the end of each incubation to the concentration in the blood. The concentration of thiosulfate in the seawater at the end of the sulfide incubations was below the limits of detection, thus a value of 1 μM was assigned. Controls represent animals after oxic or anoxic incubations without a reduced sulfur substrate (either sulfide or thiosulfate).

conditions both with and without nitrate (Table III). The pattern of blood thiols under anoxic conditions was similar to that for oxic conditions. Thiosulfate was not concentrated in the blood above the concentrations of the surrounding seawater under any of the incubation conditions.

Sulfide and thiosulfate stimulated nitrate/nitrite respiration

The intact symbiosis exhibited nitrate respiration under oxic and anoxic conditions in the presence of sulfide and thiosulfate (Fig. 1a, b). In the presence of 5 mM nitrate, nitrite accumulated in filtered seawater during 3-h oxic incubations with whole clams in the presence of 150 μM sulfide and 250 μM thiosulfate (Fig. 1a). Two different controls were run to confirm that nitrate respiration was being carried out by the symbiotic bacteria. First, 5 mM nitrate was added to filtered seawater containing 150 μM sulfide without clams. No nitrite accumulated in the seawater (not shown). Second, 5 mM nitrate was added to filtered seawater containing clams and no sulfide (Fig. 1a). Blood nitrite concentrations at the end of the 3-h incubations were 158 ± 80 μM (n = 4) and 52 ± 16 μM (n = 4) for sulfide- and thiosulfate-incubated clams, respectively.

Anoxic incubations were also performed. Whole clams had the potential for nitrate respiration under anoxic conditions (Fig. 1b). Three different controls were run. First, 5 mM nitrate was added to filtered, deoxygenated seawater containing 150 μM sulfide without clams. No nitrite accumulated in the seawater (Fig. 1b). Second, no nitrate was added to filtered, deoxygenated seawater containing 250 μM thiosulfate with clams. No nitrite accumulated in the seawater (data not shown). Finally, 5 mM nitrate was added to filtered, deoxygenated seawater containing 150 μM sulfide with clams that had their gills removed. Very little nitrite (2.0 ± 0.2 μM) accumulated in the seawater (Fig. 1b). Blood nitrite concentrations at the end of 3-h incubations were 214 ± 103 μM (n = 4) and 189 ± 80 μM (n = 4) for sulfide- and thiosulfate-incubated clams, respectively.

Five mM nitrate concentrations are not environmentally realistic. Because nitrite accumulation (*versus* nitrate disappearance) was measured and nitrite only accumulated in the presence of excess nitrate, it was essential that excess nitrate be available to the clams during the entire

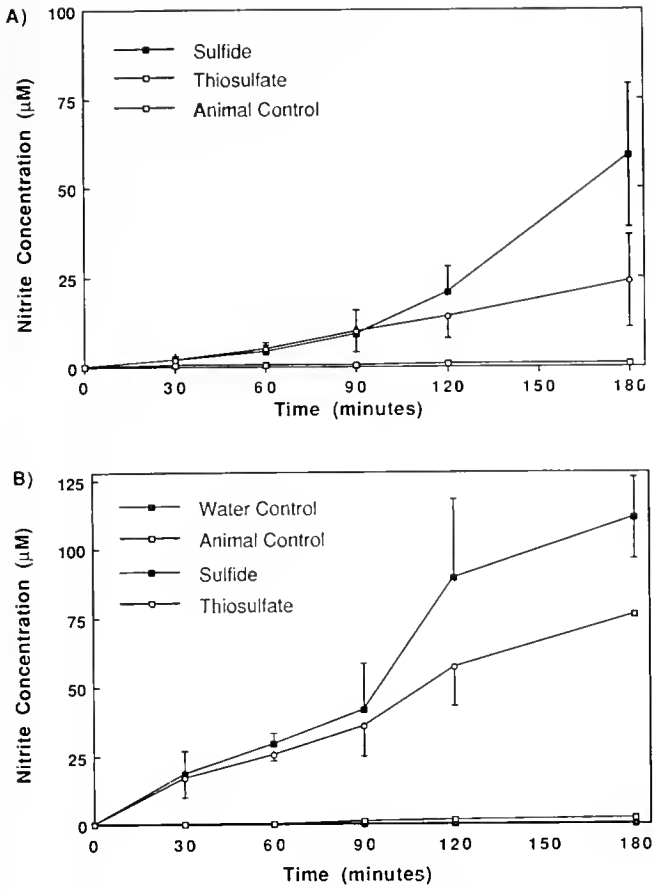

Figure 1. Nitrate respiration of whole *Solemya reidi* during 3-h incubations in oxic and anoxic buffered seawater at 10°C. (A) Nitrite accumulation in oxic seawater during incubations containing 5 mM nitrate and either 150 μM sulfide (mean ± standard deviation of 4 incubations) or 250 μM thiosulfate (mean ± standard deviation of 4 incubations). The animal control represents seawater containing 5 mM nitrate, animals, and no sulfide. (B) Nitrite accumulation in anoxic seawater during incubations containing 5 mM nitrate and either 150 μM sulfide (mean ± standard deviation of 4 incubations) or 250 μM thiosulfate (mean ± standard deviation of 4 incubations). The water control represents seawater containing 5 mM nitrate, 150 μM sulfide, and no animals. The animal control represents seawater containing 5 mM nitrate, 150 μM sulfide, and 4 animals with their gills removed. Clam size ranged from 32 to 42 mm and all values are normalized to a wet gill weight of 420 mg/clam.

3-h incubation. However, whole animal nitrate respiration (nitrite accumulation) rates similar to those presented above were found when clams were incubated in 500 μM and 50 μM nitrate for short incubations (only single experiment—data not shown). Similar results have also been found for bacterial preparations (Javor, pers. comm.).

The intact symbiosis showed nitrite respiration under anoxic conditions in the presence of sulfide but not thiosulfate (Fig. 2). In the presence of 150 μM sulfide, 100 μM nitrite was removed from filtered seawater by whole clams incubated anoxically. An initial nitrite concentration of 101.5 ± 2.8 μM decreased to 69.9 ± 6.0 μM during a 3-h incubation. Two different controls were run to confirm that nitrite respiration, like nitrate respiration, was being carried out by the symbiotic bacteria. First, 100 μM nitrite was added to filtered, deoxygenated seawater containing 150 μM sulfide and no clams. The seawater nitrite concentration did not decrease (Fig. 2). Second, nitrite was added to filtered, deoxygenated seawater containing no reduced sulfur compound and three clams. Again, the seawater nitrite concentration did not decrease (data not shown). Blood nitrite concentrations at the end of 3-h incubations were 5.3 ± 2.5 μM and 17.3 ± 4.6 μM for sulfide and thiosulfate incubations, respectively.

Sulfide-stimulated oxygen consumption by bacterial symbionts

The whole animal experiments could not directly address the question of whether the bacteria could carry out respiratory sulfide oxidation. To determine if the symbionts could respire sulfide aerobically, we measured azide-sensitive (respiratory) and azide-insensitive (non-respiratory) oxygen consumption of bacterial suspensions in the presence of different sulfide concentrations. The bacterial suspensions contained granules because they could not be separated from the bacteria. The suspensions oxidized a wide range of sulfide concentrations with maximal respiration rates at 25 μM sulfide (Fig. 3a). A pairwise comparison of values at 25 μM and all higher concentrations using the Mann-Whitney U test (Zar, 1984) found no significant difference between 25 μM and any higher values ($P > 0.05$). However, the number of repli-

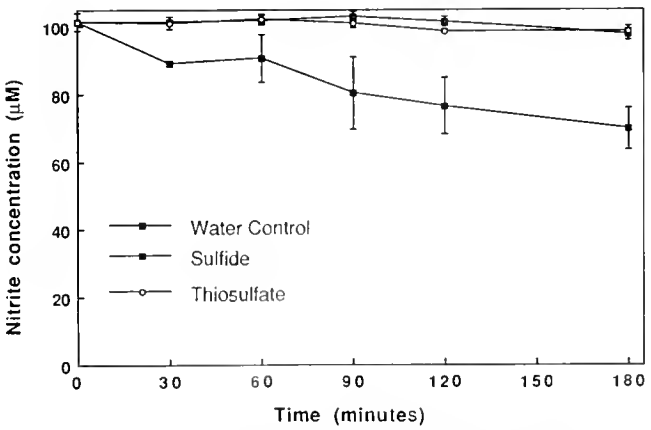

Figure 2. Nitrite respiration of whole *Solemya reidi* during 3-h incubations in anoxic buffered seawater at 10°C. Nitrite disappearance in seawater during incubations containing either 200 μM sulfide (mean ± standard deviation of 4 incubations) or 200 μM thiosulfate (mean ± standard deviation of 4 incubations). The water control represents seawater containing 100 μM nitrite, 150 μM sulfide, and no clams. Clam size ranged from 32 to 42 mm and all values are normalized to a wet gill weight of 420 mg/clam.

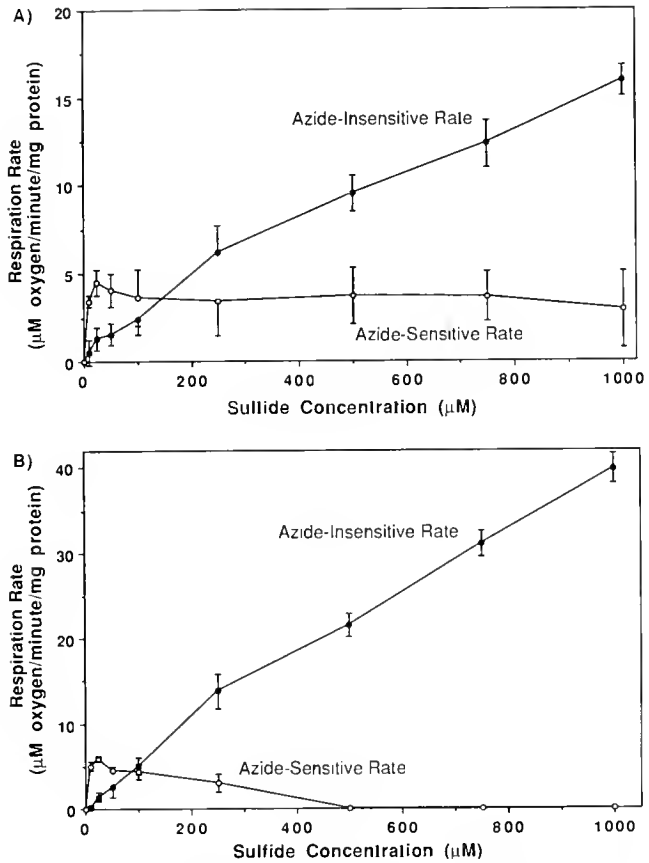

Figure 3. Sulfide-stimulated oxygen consumption in buffered seawater at 15°C by bacterial enrichments from (A) the gills of mud-maintained *Solemya reidi* or (B) the gills of clams maintained in oxygenated seawater that contained no reduced sulfur compounds or nitrate for 21 days. Data points represent means and standard deviations from three experiments (n = 3). See Materials and Methods for clam size and bacterial density.

cates (n = 3) is not sufficient for a robust statistical determination. Thus, aerobic respiration was apparently not inhibited by sulfide concentrations up to 1 m*M*. However, the azide-insensitive oxygen consumption rate increased over the range of sulfide concentrations tested. The maximal rate for azide-insensitive consumption was above 1 m*M*. The data in Figure 3a are the combination of the means from multiple measurements in three different experiments (each experiment was done with one bacterial preparation consisting of many clams).

Similar respiration experiments were conducted on bacterial suspensions from clams that were maintained in oxygenated seawater without an external reduced sulfur source or nitrate for three weeks. The gills of these animals were dark (no yellow sulfur globules). The total number of bacteria or a bacteria to granule ratio was not determined. However, it has been observed that starved clams have more granules than healthy clams (pers. obs.). The bacterial suspensions from these gills showed a different pattern for azide-sensitive and insensitive oxidation rates (Fig. 3b). Azide-sensitive aerobic respiration again had a maximum rate at 25 μM, but appeared to be inhibited at higher concentrations with complete inhibition at 500 μM and greater sulfide concentrations. The azide-insensitive rate increased with increasing sulfide concentrations and was more than double that found in the bacterial enrichments from animals freshly removed from mud based on total protein of the suspensions. The data in Figure 3b are the combination of three different experiments.

Discussion

Analysis of sediment porewaters showed that sulfide was typically the only reduced sulfur compound available to *S. reidi* and that concentrations ranged from below 20 μM to nearly 1 m*M*. Because the clams actively pump water from above the sediment through their burrows, sulfide concentrations in the water that is in contact with the gills may be significantly lower. Porewater thiosulfate was present in extremely low concentrations, and the clams were unable to accumulate thiosulfate in the blood above the external concentration. Thus, it appears that porewater thiosulfate is of little importance as an energy source in the intact symbiosis.

Similar to Anderson *et al.* (1987), we observed high concentrations of thiosulfate in the blood of field caught animals and animals experimentally incubated in the presence of sulfide. Our data show that thiosulfate present in the blood of freshly collected clams results from host oxidation of sulfide and not from uptake of porewater thiosulfate. Because thiosulfate accumulates in the blood during oxic incubations with sulfide but not during anoxic incubations, molecular oxygen must be required for sulfide oxidation to thiosulfate. It is most likely that aerobic respiration of sulfide by mitochondria is responsible for thiosulfate production (O'Brien and Vetter, 1990). Thiosulfate is cleared from the blood by the bacteria within bacteriocytes. However, the relative importance of this energy source *versus* direct uptake of sulfide across the gill is not known.

Two clearly different types of sulfide oxidation occurred in our bacterial enrichments. The first, true respiration, represents electron transport chain (ETS)-linked bacterial sulfide oxidation and it is completely azide-sensitive. The ETS-linked type showed a high capacity to oxidize sulfide at low concentrations (maximal rate by 25 μM). The second, which is azide-insensitive, represents non-enzymatic oxidation by ferric iron catalysis (hematin) in granules (Powell and Arp, 1989) and autocatalysis by sulfur (Chen and Morris, 1972).

Non-enzymatic, heat-stable catalysis of sulfide oxidation has been observed in a variety of animal tissues (re-

viewed by Beauchamp *et al.*, 1984) and specifically in a thiotrophic symbiosis (Wilmot and Vetter, 1990). It has been shown that ferric iron-containing compounds such as hematin and ferritin are responsible for the non-enzymatic catalysis in mammals (Sörbo, 1958; Baxter and van Reen, 1958; Baxter *et al.*, 1958). The benzyl viologen (BV) assay used to determine which components of the *S. reidi* symbiosis carried out sulfide oxidation (Powell and Somero, 1985) measures non-enzymatic ferric iron catalysis in the presence of high (1–5 m*M*) sulfide (Powell and Arp, 1989). It does not measure ETS-linked activity because high sulfide concentrations inhibit the oxidation. Thus, it is not surprising that early studies using the BV assay concluded that the bacteria and mitochondria did not oxidize sulfide (Powell and Somero, 1985).

Although we have shown that the bacteria are capable of sulfide oxidation, it is not clear whether the bacteria encounter sulfide or if it is first oxidized by mitochondria or electron-dense granules. Several lines of evidence suggest that the bacteria normally oxidize sulfide as well as thiosulfate *in vivo*. First, the bacteria are oriented close to the outside and are separated from the seawater by a thin epithelial cell that contains few mitochondria or electron-dense granules (Felbeck, 1983; Gustafson and Reid, 1988). Because the bacteria are not packed close to the blood space, which contains the mitochondrial product of sulfide oxidation, it does not seem likely that thiosulfate is the only sulfur substrate available to the bacteria. Second, isolated gill ctenidia can oxidize sulfide without a host blood supply (Vetter, 1990). The ctenidia produce elemental sulfur and protein, which seems to indicate that sulfide and oxygen are taken directly across the gill (Vetter, 1990). Third, the bacteriocytes of *S. reidi* and *S. velum* contain intracellular hemoglobin that can bind sulfide as ferric hemoglobin sulfide (Doeller *et al.*, 1988; Krause and Wittenberg, 1990). Fiber-optic spectroscopy of intact gills indicated that ferric hemoglobin sulfide was present in the bacteriocyte region of the gill.

The data presented above do not provide direct proof that the bacteria within a bacteriocyte oxidize sulfide. Javor (pers. comm.) has recently observed that bacterial suspensions from *S. reidi* respire nitrate under oxic and anoxic conditions in the presence of sulfide and thiosulfate. Similarly, in this study, the symbionts respired nitrate that entered the bacteriocyte, either from the blood, or directly from seawater in the presence of sulfide and thiosulfate. The product of the anaerobic respiration, nitrite, was excreted from the bacteriocyte in the presence of excess nitrate and accumulated in the blood and seawater. In marine denitrifying bacteria, nitrate is often reduced only to nitrite (Goering and Cline, 1970) and the nitrite accumulates outside the cells (Payne and Riley, 1969). If nitrate concentrations become low or are exhausted, the nitrite can be taken back up by the bacteria and further reduced.

In the absence of nitrate, the intact symbiosis respired nitrite in the presence of sulfide only. This has also been observed for bacterial suspensions from *S. reidi* (Javor, pers. comm.). The nitrite, like the nitrate, either enters the bacteriocyte from the blood or directly from seawater. More importantly, these data provide the best available evidence that the bacteria within bacteriocytes oxidize sulfide. These results suggest that sulfide oxidation is coupled to complete denitrification, but that thiosulfate oxidation is coupled to the first step only. Anaerobic sulfide oxidation by the bacteria may be an important detoxification mechanism when the clam is depleted of oxygen. In addition, because aerobic nitrate respiration has been described for several bacteria (Robertson and Kuenen, 1984; Lloyd *et al.*, 1987) denitrification may occur when nitrate (and sulfide) is present and oxygen concentrations are low.

Although the symbionts are capable of denitrification, and the bacteria have access to nitrate and nitrite when each is present in seawater, we do not know the concentrations that are available to the animals in the natural environment. The water flow across the sludge field is strong and the oxygen concentrations and water chemistry are similar to the surrounding areas (approximately 100–175 μM O_2) (B. Thompson, pers. comm.). At neighboring hydrographic stations in the Santa Monica Bay area, the ammonia concentrations range from 0.5 to 2.0 μM, while sediment porewaters typically are 100–1000-fold higher (Eppley, 1986). Nitrifying bacteria are active in these waters (Ward *et al.*, 1982) and nitrate values at a depth equal to the sludge field are $\geq$20 μM (Williams, 1986). Nitrate is not present below the top 2 cm of sediment at Whites Point outfall near the Hyperion outfall (J. Gieskes, pers. comm.). It can be assumed that as the clams pump water from above the sediment through their burrows, they are probably exposed to oxygen and nitrate simultaneously, but the ratio of oxygen to nitrate is unknown.

When the data presented here are integrated with previous studies (Felbeck, 1983; Powell and Somero, 1985, 1986; Fisher and Childress, 1986; Anderson *et al.*, 1987, 1990; Doeller *et al.*, 1988; Krause and Wittenberg, 1990; O'Brien and Vetter, 1990), a more complete picture emerges of how the symbiosis may be functioning under different environmental conditions. Maximum net autotrophy occurs in the presence of external sulfide concentrations of 100 μM (Anderson *et al.*, 1987). Because seawater is near pH 8.1 at 100 μM total sulfide, approximately 3 μM sulfide as H_2S diffuses into animal cells (Millero, 1986). Assuming an internal pH near pH 7.5, the maximal internal free sulfide (H_2S) concentration is approximately 20 μM, which is very close to the aerobic sulfide-oxidizing maximum for both isolated mitochon-

dria (O'Brien and Vetter, 1990) and bacteria. Aerobic metabolism is maintained by animal tissues in the presence of external sulfide concentrations up to 100 μM. At higher concentrations, the onset of anaerobic pathways is evident (Anderson *et al.*, 1990).

Sulfide oxidation can occur by at least two processes: sulfide respiration by mitochondria and bacteria, and non-enzymatic catalysis by metal containing granules, and autocatalysis by sulfur. The mitochondria oxidize sulfide only to thiosulfate which accumulates in the clam's blood (O'Brien and Vetter, 1990). The oxidation is oxygen-dependent and can yield ATP (Powell and Somero, 1986). Presumably, the bacteria oxidize sulfide to elemental sulfur and polysulfides and ultimately to sulfate. Bacterial sulfide respiration can occur aerobically when oxygen is available or possibly anaerobically when nitrate (or nitrite) is available as an alternate electron acceptor. The importance of nitrate (nitrite) respiration is unknown. In addition, the thiosulfate produced by the mitochondria can be further oxidized by the bacteria. The importance of the non-enzymatic oxidation of sulfide is unknown.

We have shown the metabolic potential for the use of nitrate and nitrite as alternate electron acceptors in the intact symbiosis. Future studies must determine the environmental concentrations of nitrate, nitrite, and oxygen and the relevance of anaerobic respiration to the symbiosis. If oxidized nitrogen compounds are present, they are likely in the oxygen-containing water drawn into the burrow by the clams. Thus, conditions that limit oxygen availability would also limit nitrate. A reasonable hypothesis may be that a switch to anaerobic nitrogen respiration by the symbionts is a tactic by the symbiosis to save oxygen for host metabolism during times of low oxygen.

Acknowledgments

We gratefully acknowledge the captains and crews of the research vessels *RV Robert Gordon Sproul* and *RV Point Sur*, especially Louis Zimm, without whom this work would not have been possible. We would like to thank Dr. George Somero for reviewing the manuscript, the laboratories of H. Felbeck and J. Childress for assisting on cruises and providing collecting opportunities, and John O'Brien for his many hours of assistance at sea and in the laboratory. Special thanks is due Ron Kaufmann for helpful discussions regarding data analysis and Dr. Barbara Javor for reviewing the manuscript and for her laboratory assistance and stimulating discussions during these studies. This work was supported by NSF grant OCE86-10513 (to G. N. Somero and R. D. Vetter) and ONR grant N00014-87-0012 (to R. D. Vetter).

Literature Cited

Anderson, A. E., J. J. Childress, and J. Favuzzi. 1987. Net uptake of CO_2 driven by sulfide and thiosulfate oxidation in the bacterial symbiont-containing clam *Solemya reidi*. *J. Exp. Biol.* **133:** 1–31.

Anderson, A. E., H. Felbeck, and J. J. Childress. 1990. Aerobic metabolism is maintained in animal tissue during rapid sulfide oxidation in the symbiont-containing clam *Solemya reidi*. *J. Exp. Zool.* **256:** 130–134.

Baxter, C. F., and R. van Reen. 1958. Some aspects of sulfide oxidation by rat-liver preparations. *Biochim. Biophys. Acta* **28:** 567–573.

Baxter, C. F., R. van Reen, P. B. Pearson, and C. Rosenberg. 1958. Sulfide oxidation in rat tissues. *Biochim. Biophys. Acta* **27:** 584–591.

Beauchamp, R. O., Jr., J. S. Bus, J. A. Popp, C. J. Boreiko, and D. A. Andjelkovich. 1984. A critical review of the literature on hydrogen sulfide toxicity. *Crit. Rev. Toxicol.* **13**(1): 25–97.

Cary, S. C., R. D. Vetter, and H. Felbeck. 1989. Habitat characterization and nutritional strategies of the endosymbiont-bearing bivalve *Lucinoma aequizonata*. *Mar. Ecol. Prog. Ser.* **55:** 31–45.

Chen, K. Y., and J. C. Morris. 1972. Kinetics of oxidation of aqueous sulfide by O_2. *Envir. Sci. Technol.* **6**(6): 529–537.

Childress, J. J., and W. Lowell. 1982. The abundance of a sulfide-oxidizing symbiosis (the clam *Solemya reidi*) in relation to interstitial water chemistry. *Am. Zool.* **63:** A45.

Distel, D. L., and H. Felbeck. 1988. Pathways of inorganic carbon fixation in the endosymbiotic-bearing lucinid clam *Lucinoma aequizonata*. Part I, Purification and characterization of the endosymbiotic bacteria. *J. Exp. Biol.* **247:** 1–10.

Doeller, J. E., D. W. Kraus, J. M. Colacino, and J. B. Wittenberg. 1988. Gill hemoglobin may deliver sulfide to bacterial symbionts of *Solemya velum* (Bivalvia, Mollusca). *Biol. Bull.* **175:** 388–396.

Eppley, R. W. 1986. People and the plankton. Pp. 289–303 in *Lecture Notes on Coastal and Estuarine Studies*, Vol. 15, *Plankton Dynamics of the Southern California Bight*, R. W. Eppley, ed. Springer-Verlag, New York.

Felbeck, H. 1983. Sulfide oxidation and carbon fixation by the gutless clam *Solemya reidi* an animal-bacterial symbiosis. *J. Comp. Physiol.* **152:** 3–11.

Fisher, C. R., and J. J. Childress. 1986. Translocation of fixed carbon from symbiotic bacteria to host tissue in the gutless bivalve, *Solemya reidi*. *Mar. Biol.* **93:** 59–68.

Goering, J. J., and J. C. Cline. 1970. A note on denitrification in seawater. *Limnol. Oceanogr.* **15:** 306–308.

Gustafson, R. G., and R. G. B. Reid. 1988. Association of bacteria with larvae of the gutless protobranch bivalve *Solemya reidi*. *Mar. Biol.* **97:** 389–401.

Hartree, E. F. 1972. Determination of protein: a modification of the Lowry method that gives a linear photometric response. *Anal. Biochem.* **48:** 422–427.

Kraus, D. W., and J. B. Wittenberg. 1990. Hemoglobins of the *Lucina pectinata*/bacteria symbiosis I. Molecular properties, kinetics and equilibria of reactions with ligands. *J. Biol. Chem.* **265:** 16043–16053.

Lloyd, D., L. Boddy, and J. P. Davies. 1987. Persistence of bacterial denitrification capacity under aerobic conditions: the rule rather than the exception. *FEMS Microbiol. Ecol.* **45:** 185–190.

Millero, F. J. 1986. The thermodynamics and kinetics of the hydrogen sulfide system in natural waters. *Mar. Chem.* **18:** 121–147.

Newton, G. L., and R. C. Fahey. 1987. Purification of thiols from biological samples. *Meth. Enzymol.* **143:** 96–100.

O'Brien, J., and R. D. Vetter. 1990. Production of thiosulfate during sulphide oxidation by mitochondria of the symbiont-containing bivalve *Solemya reidi*. *J. Exp. Biol.* **149:** 133–148.

Payne, W. J., and P. S. Riley. 1969. Suppression by nitrate of enzymatic reduction of nitric oxide. *Proc. Soc. Exp. Biol. Med.* **132:** 258–260.

Powell, M. A., and G. N. Somero. 1985. Sulfide oxidation occurs in the animal tissue of the gutless clam, *Solemya reidi*. *Biol Bull* **169:** 164–181.

Powell, M. A., and G. N. Somero. 1986. Hydrogen sulfide oxidation is coupled to oxidative phosphorylation in mitochondria of *Solemya reidi*. *Science* **233:** 563–566.

Powell, M. A., and A. J. Arp. 1989. Hydrogen sulfide oxidation by abundant nonhemoglobin heme compounds in marine invertebrates from sulfide-rich habitats. *J. Exp. Zool.* **249:** 121–132.

Reid, R. G. B. 1980. Aspects of the biology of a gutless species of *Solemya* (Bivalvia: Protobranchia) *Can. J. Zool.* **58:** 386–393.

Reid, R. G. B., and F. R. Bernard. 1980. Gutless bivalves. *Science* **208:** 609–610.

Robertson, L. A., and J. G. Kuenen. 1984. Aerobic denitrification: a controversy revived. *Arch. Microbiol.* **139:** 351–354.

Somero, G. N., J. J. Childress, and A. E. Anderson. 1989. Transport, metabolism and detoxification of hydrogen sulfide in animals from sulfide-rich marine environments. *Crit. Rev. Aquat. Sci* **1:** 591–614.

Sörbo, B. 1958. On the oxidation of thiosulfate from inorganic sulfide by rat tissue and heme compounds. *Biochim. Biophys. Acta* **27:** 324–329.

Strickland, J. D. H., and T. R. Parsons. 1977. A practical handbook of seawater analysis, 2nd ed. *Bull. Fish. Res. Board Can.* **167:** 1–310.

Vetter, R. D. 1990. Cultured gill filaments from *Solemya reidi*: a model system for the study of thiotrophic symbioses. Pp. 349–352 in *Endocytobiology IV*, P. Nardon, V. Gianinazzi-Pearson, A. M. Grenier, L. Margulis, and D. C. Smith, eds. Institute National de le Recherche Agronoique, Paris, France.

Vetter, R. D. 1991. Symbiosis and the evolution of novel trophic strategies: thiotrophic organisms at hydrothermal vents. Pp. 219–245 in *Symbiosis as a Source of Evolutionary Innovation: Speciation and Morphogenesis*, L. Margulis and R. Fester, eds. MIT Press, Cambridge, Massachusetts.

Vetter, R. D., P. A. Matrai, B. Javor, and J. O'Brien. 1989. Reduced sulfur compounds in the marine environment: analysis by HPLC. Pp. 244–261 in *Biogenic Sulfur in the Environment*, E. S. Saltzman, and W. J. Cooper, ed. American Chemical Society, Washington, DC.

Ward, B. B., R. J. Olson, and M. J. Perry. 1982. Microbial nitrification rates in the primary nitrite maxima off Southern California. *Deep-Sea Res.* **29:** 247–255.

Williams, P. W. 1986. Chemistry of the dissolved and particulate phases in the water column. Pp. 53–83 in *Lecture Notes on Coastal and Estuarine Studies Vol. 15, Plankton Dynamics of the Southern California Bight*, R. W. Eppley, ed. Springer-Verlag, New York.

Wilmot, Jr., D. B., and R. D. Vetter. 1990. The bacterial symbiont from the hydrothermal vent tubeworm *Riftia pachyptila* is a sulfide specialist. *Mar. Biol.* **106:** 273–283.

Zar, J. H. 1984. *Biostatistical Analysis*, second edition. Prentice-Hall, Inc. Englewood Cliffs, New Jersey.

Reference: *Biol. Bull.* **182**: 454–457. (June, 1992)

To Thine Own Self be True? An Addendum to Feldgarden and Yund's Report on Fusion and the Evolution of Allorecognition in Colonial Marine Invertebrates

RICHARD K. GROSBERG[1]

Department of Zoology, Center for Population Biology, University of California, Davis, California 95616

Feldgarden and Yund (1) recently re-examined a question central to understanding the evolution of allorecognition systems in colonial and clonal marine invertebrates: "How does the genetic polymorphism necessary to restrict intergenotypic fusion to kin and clonemates accumulate in natural populations?" They argue that explanations invoking kin selection account fully for neither the extensive allelic polymorphism that characterizes the genetic systems that control allorecognition specificity, nor the apparent phenotypic instability of genetic chimeras. As a more parsimonious explanation than kin selection for these observations, they propose that frequency-dependent selection, acting at the level of the individual, promotes the accumulation of allotypic polymorphism by favoring fusion with self (and preventing fusion with nonself). To place this proposition into a conceptual framework, they cite two of my papers (2, 3) and assert that, "Several authors have noted that kin selection does not provide an obvious explanation for high allotype diversity." As far as it goes, this is an accurate statement, at least with respect to intergenotypic fusion in populations lacking kin structure. In these papers, however, J. F. Quinn and I developed a series of analytical models showing how individual selection could easily maintain allotypic polymorphism through the control of intergenotypic fusion.

So that there can be no misunderstanding about what we said, I quote a summary of our work on allotypic specificity and fusion from a paper published in 1988 (2, pp. 402–403; full references can be found in the original text):

> It appears intuitively that individual selection acting to restrict allogeneic fusion could represent a general and potent selective force favoring the evolution of allorecognition and allotypic specificity (Burnet, 1971, 1973; Buss, 1982). In a theoretical analysis of this problem, Grosberg and Quinn (1988) defined the conditions necessary to favor rare allotypic variants in a single-locus, haploid model. Let c_f be the net per-capita fitness cost of fusion and b_f be the net fitness gain that is due to fusion. The expected fitness of an allorecognition allele, i, upon which fusion is conditioned, is then
>
> $$W_i = 1 + P_i(b_f - c_f) \qquad (12)$$
>
> where P_i is the frequency of allele i. Equation (12) shows that the fitness of an allorecognition allele depends upon both its frequency and the relative costs and benefits of fusion. If b_f is greater than c_f, then W_i will increase as P_i increases and the allele will become fixed in the population. However, if c_f is greater than b_f, then as P_i increases, W_i decreases. Consequently, rare alleles will be favored and allotypic polymorphism will accumulate only when the costs of fusion exceed the benefits. This raises the question of why individuals should ever fuse (Grosberg and Quinn, 1988).
>
> One of the important effects of high levels of allotypic variation is the restriction of fusion to closely related individuals. Although the costs and benefits of genotype fusion should be adjusted according to the relatedness of the fused colonies (Hamilton, 1964; Buss and Green, 1985; Grosberg and Quinn, 1986), the effects of kin selection have not yet been incorporated into mathematical models of allotypic specificity.

I believe this passage leaves little room for misinterpretation, either of our approach to the problem, or of

Received 10 February 1992; accepted 10 March 1992.

the result that frequency-dependent selection, acting at the level of the individual, can favor rare alleles and promote the evolution of polymorphism at allorecognition loci through the restriction of intergenotypic fusion. Nevertheless, a number of biological complexities should temper the conclusion that individual selection is the primary force maintaining allotypic variation. First, as Feldgarden and Yund (1) mention, the theoretical prediction that individual selection can maintain allotypic polymorphism does not preclude the operation of kin selection. In fact, kin selection may be particularly effective in the many taxa of sedentary, clonal invertebrates in which sibling sexual propagules tend to remain spatially associated via restricted dispersal (4–8) or preferential settlement near kin (6, 9). Such a pattern of larval dispersal will, even after only a single generation, lead to kin structure, increased probabilities of fusion, and the opportunity for kin selection. Moreover, there is ample evidence that sexually produced propagules of some sponges, cnidarians, and ascidians can and do fuse soon after settlement (2). Thus, their claim [based on (6)] that, "Larval settlement as a function of future fusibility is the sole observation that we are aware of that is consistent with kin selection but not with the selective pressure of self fusion," could well apply to many clonal marine invertebrates.

Second, if the preservation of clonal integrity is the primary function of allorecognition systems, why should fusion ever be permitted between non-clonemates? In genetic terms, the overriding problem is: why, in many taxa, is only partial, rather than complete, genetic matching among alleles at allorecognition loci required for fusion to occur (2, 10)? After all, allorecognition systems requiring only partial allotypic matching, and based on self-recognition, are far less efficient at prohibiting fusion with nonself than systems requiring complete matching (in which any allelic discrepancy in allotype would lead to rejection and the preservation of genotypic integrity) (11). One answer [the one favored by Feldgarden and Yund (1)] is that intergenotypic fusion is simply a matter of imprecision in the recognition system and may be of little or no selective importance: "Although fusion between kin occurs, such events may simply represent mistakes in recognition due to the limitation of an imperfect system." It could be, as Feldgarden and Yund contend, that the genetics of invertebrate allorecognition are biochemically and phylogenetically constrained, so that partial genetic matching, and the recognition errors that it entails, is an evolutionary necessity, whatever the selective optimum.

I think, however, that this response oversimplifies even the meager amount presently known about the cellular and genetic mechanisms that regulate allorecognition. In so doing, it begs several crucial observations pertinent to the evolution of allorecognition and intergenotypic fusion. In particular, if there were no exceptions to the genetic rule of partial matching in the clades that Feldgarden and Yund cite, then their explanation retains substantial merit. However, in several of the invertebrate phyla that they mention, including some sponges, cnidarians, and ascidians, full allotypic matching appears to be required for fusion to occur (12–16). Similarly, recognition systems based on multiple independent loci are less prone to error than single locus systems with comparable levels of allelic variation (11). Although some well-studied taxa (*e.g.*, the compound ascidian *Botryllus*) have primary allorecognition systems based on a single locus, other taxa appear to have allotypic markers encoded by several loci (17, 18). Finally, in the few systems that have been examined in any sort of detail, individual genotypes appear to distinguish among different classes of nonself (2, 10, 19). I do not know why there is such variation, but taken together, these observations suggest, at least, that more precise allorecognition systems can evolve, but often do not.

There are four other poorly characterized, but nonetheless crucial, aspects of allorecognition that further complicate our understanding of how allotypic specificity evolves. First, although some [but not all, *e.g.*, (20)] genetic chimeras have been found to be **morphologically** unstable (21–23), little is known of the **genetic** stability of these chimeras (24) and thus the true costs and benefits of fusion. Moreover, in the colonial ascidian *Botryllus schlosseri*, the morphological stability of chimeras seems to depend on the relatedness, and perhaps allotypic similarity, of fusion partners (19–23).

Second, in the absence of clone-specific genetic probes, the frequency of chimera formation in natural populations of benthic invertebrates is notoriously difficult to estimate. In general, grafting assays imply that intergenotypic fusion should be rare, provided that there is little kin structure in a population (2). Thus, I am not surprised that taxa such as *Hydractinia symbiologicarpus*, which inhabit mobile substrata, spawn gametes, or have motile, free-swimming larvae, show little evidence of kin structure and consequently little evidence for natural chimeras (25). In contrast, other sessile species that live on fixed surfaces and brood low vagility, sexual offspring, ought to have much higher frequencies of intergenotypic fusion. This might be the case for other hydractiniids, such as *Hydractinia milleri*, and is known to be the case in *Botryllus schlosseri* (7).

Third, as Feldgarden and Yund acknowledge, it is essential to quantify the costs and benefits of fusion, and how these might vary with ontogenetic, genetic, and ecological circumstances. If the situation in a chimera is as simple as one genotype's fitness loss being exactly the other's fitness gain, then, over the long term, it is difficult to see why even the most closely related nonclonemates

should be allowed to fuse (except by recognition error). On the other hand, if costs and benefits depend on ontogenetic, genetic, or ecological factors, or if costs and benefits are not additive, then kin selection may be effective.

Finally, Feldgarden and Yund did not consider contexts other than intergenotypic fusion in which allotypic specificity regulates the nature and outcomes of interactions between conspecifics. For example, in many cnidarians, allotypic disparity leads to aggressive behavior, whereas similarity fails to elicit an aggressive response (2). For this set of alternative behaviors, both Crozier (26) and Grosberg and Quinn (3) showed that individual selection does not provide a straightforward explanation for the maintenance of allotypic variation; with kin structure, however, polymorphism can evolve (27). In still more complex situations, pure fusion or aggression models are unrealistic. For instance, in *Hydractinia symbiolongicarpus*, incompatible colonies usually behave aggressively, whereas compatible genotypes often somatically fuse (28). Theoretical analysis of these behavioral options predicts that allotypic variation can be maintained, but only if fusion is more costly than aggression (3).

The paper by Feldgarden and Yund does focus attention on the idea that the preservation of clonal integrity (which is an extreme form of kin selection) can be an important selective mechanism, an idea first articulated nearly a century ago by Bancroft (29), and echoed over a quarter century ago by Knight-Jones and Moyse (30) and Hamilton (31). The paper further helps to clarify how little we know about the genetics and fitness consequences of allorecognition and intergenotypic fusion. Until more of this sort of information is in hand for a variety of taxa, we should not consider recognition errors and their effects on inclusive fitness as being mere epiphenomena of imperfect allorecognition systems. Consequently, I am reluctant—even in the face of having shown how individual selection can maintain allotypic specificity in the context of fusion—to downplay the potential importance of kin selection.

Acknowledgments

Thanks to D. Brumbaugh, B. Johnson, and C. Pfister for their helpful comments. I am also grateful to A. T. Hun and R. T. Paine for their insightful suggestions. The National Science Foundation has supported this research.

Literature Cited

1. **Feldgarden, M., and P. O. Yund. 1992.** Allorecognition in colonial marine invertebrates: does selection favor fusion with kin, or fusion with self? *Biol. Bull.* **182:** 155–158.
2. **Grosberg, R. K. 1988.** The evolution of allorecognition specificity in clonal invertebrates. *Q. Rev. Biol.* **63:** 377–412.
3. **Grosberg, R. K., and J. F. Quinn. 1988.** The evolution of allorecognition specificity. Pp. 157–167 in *Invertebrate Historecognition*, R. K. Grosberg, D. Hedgecock, and K. Nelson, eds. Plenum Press, New York.
4. **Jackson, J. B. C. 1985.** Distribution and ecology of clonal and aclonal benthic invertebrates. Pp. 297–356 in *Population Biology and Evolution of Clonal Organisms*, J. B. C. Jackson, L. W. Buss, and R. E. Cook, eds. Yale University Press, New Haven.
5. **Jackson, J. B. C. 1986.** Modes of dispersal of clonal benthic invertebrates: consequences for species' distributions and genetic structure of local populations. *Bull. Mar. Sci.* **39:** 588–606.
6. **Grosberg, R. K., and J. F. Quinn. 1986.** The genetic control and consequences of kin recognition by the larvae of a colonial ascidian. *Nature* **322:** 456–459.
7. **Grosberg, R. K. 1987.** Limited dispersal and proximity-dependent mating success in the colonial ascidian *Botryllus schlosseri*. *Evolution* **41:** 372–384.
8. **Keough, M. J., and H. Chernoff. 1987.** Dispersal and population variation in the bryozoan *Bugula neritina*. *Ecology* **68:** 199–210.
9. **Keough, M. J. 1984.** Kin-recognition and the spatial distribution of larvae of the bryozoan *Bugula neritina* (L.). *Evolution* **38:** 142–147.
10. **Neigel, J. E. 1988.** Recognition of self or nonself? Theoretical implications and an empirical test. Pp. 127–142 in *Invertebrate Historecognition*, R. K. Grosberg, D. Hedgecock, and K. Nelson, eds. Plenum Press, New York.
11. **Curtis, A. S. G., J. Kerr, and N. Knowlton. 1982.** Graft rejection in sponges. Genetic structure of accepting and rejecting populations. *Transplantation* 33: 127–133.
12. **Neigel, J. E., and J. C. Avise. 1983.** Histocompatibility bioassays of population structure in marine sponges. *J. Heredity* **74:** 134–140.
13. **Neigel, J. E., and J. C. Avise. 1983.** Clonal diversity and population structure in a reef-building coral, *Acropora cervicornis*: self-recognition analysis and demographic interpretation. *Evolution* **37:** 437–453.
14. **Neigel, J. E., and J. C. Avise. 1985.** The precision of histocompatibility response in clonal recognition in tropical marine sponges. *Evolution* **39:** 724–732.
15. **Wulff, J. L. 1986.** Variation in clone structure of fragmenting coral reef sponges. *Biol. J. Linn. Soc.* **27:** 311–330.
16. **Raftos, D. A., D. A. Briscoe, and N. N. Tait. 1988.** The mode of recognition of allogeneic tissue in the solitary urochordate *Styela plicata*. *Transplantation* **45:** 1123–1126.
17. **Fuke, M. T., and I. Nakamura. 1985.** Pattern of cellular alloreactivity of the solitary ascidian, *Halocynthia roretzi*, in relation to genetic control. *Biol. Bull.* **169:** 631–637.
18. **Hauenschild, C. von. 1956.** Über die Vererbung einer Gewebeverträglichkeits-Eigenschaft bei dem Hydroidpolypen *Hydractinia echinata*. *Z. Naturforsch.* **11b:** 132–138.
19. **Weissman, I. L., V. L. Scofield, Y. Saito, H. Boyd, and B. Rinkevich. 1988.** Speculations on the relationships of two *Botryllus* allorecognition reactions—colony specificity and resorption—to vertebrate histocompatibility. Pp. 67–78 in *Invertebrate Historecognition*, R. K. Grosberg, D. Hedgecock, and K. Nelson, eds. Plenum Press, New York.
20. **Han, M., and Y. Loya. 1990.** Ontogenetic variation in sponge histocompatibility responses. *Biol. Bull.* **179:** 279–286.
21. **Rinkevich, B., and I. L. Weissman. 1987.** A long-term study on fused subclones in the ascidian *Botryllus schlosseri*: the resorption phenomenon (Protochordata: Tunicata). *J. Zool. (Lond.)* **213:** 717–733.
22. **Rinkevich, B., and I. L. Weissman. 1987.** The fate of *Botryllus* larvae cosettled with parental colonies: beneficial or deleterious consequences? *Biol. Bull.* **173:** 474–488.

23. **Rinkevich, B., and I. L. Weissman. 1989.** Variations in the outcomes following chimera formation in the colonial tunicate *Botrylloides schlosseri*. *Bull. Mar. Sci.* **45:** 213–227.
24. **Kingsley, E. A., D. A. Briscoe, and D. A. Raftos. 1989.** Correlation of histocompatibility reactions with fusion between conspecifics in the solitary urochordate *Styela plicata*. *Biol. Bull.* **176:** 282–289.
25. **Yund, P. O., and H. M. Parker. 1989.** Population structure of *Hydractinia* sp. nov. C in the Gulf of Maine. *J. Exp. Mar. Bio. Ecol.* **125:** 63–82.
26. **Crozier, R. H. 1986.** Genetic clonal recognition abilities must be retained by selection for something else. *Evolution* **40:** 1100–1101.
27. **Ratnieks, F. L. W. 1991.** Evolution of discriminatory aggression in marine invertebrates. *J. Theor. Biol.* **152:** 557–565.
28. **Buss, L. W., C. S. McFadden, and D. R. Keene. 1984.** Biology of hydractiniid hydroids. 2. Histocompatibility effector system/competitive mechanisms mediated by nematocyst discharge. *Biol. Bull.* **167:** 139–158.
29. **Bancroft, F. W. 1903.** Variation and fusion of colonies in compound ascidians. *Proc. Calif. Acad. Sci. (Series 3)* **3:** 137–186.
30. **Knight-Jones, E. W., and J. Moyse. 1961.** Intraspecific competition in sedentary marine animals. *Symp. Soc. Exp. Biol.* **15:** 72–95.
31. **Hamilton, W. D. 1964.** The genetical evolution of social behaviour. *J. Theor. Biol.* **7:** 1–52.

Reference: *Biol. Bull.* **182**: 458–459. (June, 1992)

To Thine Own Self be True? Yes! Thou Canst Not Then be False to Any Other. A Reply to Grosberg

PHILIP O. YUND[1] AND MICHAEL FELDGARDEN[2]

[1]*Department of Biological Sciences, University of New Orleans, New Orleans, Louisiana 70148 and*
[2]*Department of Biology, Yale University, New Haven, Connecticut 06511*

Our original paper (1) was motivated by the philosophy that every healthy scientific discipline should have at least two alternative hypotheses (2); our goal was simply to incorporate a consideration of selection favoring self fusion in future work on the selective forces operating on allorecognition systems. We did not intend to resolve this issue, and we do not feel that a resolution is possible given the limitations of current information. Consequently, we welcome Grosberg's commentary (3) on our previous efforts and are thankful for this opportunity to extend the discussion. Grosberg raises a number of interesting points about our argument, three of which merit additional commentary.

First, Grosberg feels that we have misinterpreted a series of models developed with J. F. Quinn (4). We acknowledge that our discussion of their results was too brief to fully justify our interpretation. Nevertheless, we do feel that our interpretation is valid. Grosberg and Quinn did consider the costs and benefits of fusion and aggression at the individual level. However, the costs and benefits were explicitly those associated with fusion with kin. Neither fusion with self, nor any other selective force, was considered as an alternative. Our contribution was an explicit consideration of the selective forces of self fusion, which can be invoked only at the individual level. We did not intend to imply that past work had ignored all forms of selection at the individual level, just the selective pressures of fusion with self.

An additional aspect of our interpretation of Grosberg and Quinn's results involves their predictions from a series of models that consider the consequences of variation in costs and benefits for three cases (4): aggression alone, fusion alone, and fusion as an alternative to aggression. The aggression only model predicts a monomorphic population under all conditions. In both of the remaining cases, polymorphism occurs *only when the costs exceed the benefits* [as cited in Grosberg's quote (3)]. When the benefits are greater than the cost, the initially most frequent allele increases to fixation, and the population becomes monomorphic. We interpret this result as preliminary evidence against fusion with kin generating and maintaining high levels of polymorphism. The scenario of costs exceeding benefits is compatible with neither the basic assumptions behind the evolution of kin fusion, nor the continued existence of allorecognition systems. While Grosberg may now feel that these models show that "individual selection could easily maintain allotypic polymorphism" (3, p. 454), he and Quinn originally reached rather a different conclusion that is in accord with our own interpretation of their work:

> "allotypic polymorphism can be maintained directly by the individual costs and benefits of fusion provided fusion carries a net fitness cost. This raises the question of how fusion conditioned on relatedness can be evolutionarily stable. Our results suggest that selection acting at the level of clonal or kin-aggregations, rather than at the level of the individual, may provide an explanation for the evolution of allotypic specificity through aggression or fusion." (4, p. 157)

> "Because the individual costs and benefits of fusion and aggression cannot readily account for why these behaviors are conditioned on allotypic identity, other explanations must be sought." (4, p. 165)

While Grosberg and Quinn's models do predict polymorphism under some conditions, polymorphism occurs only under a much more restrictive set of circumstances than predicted by selection for fusion with self. A model incorporating both organismal and genotype level effects of kin fusion might lead to a different conclusion, as Grosberg and Quinn suggest (4).

As a second point of discussion, Grosberg mentions evidence of the widespread occurrence of fusion soon after larval settlement as support for the potentially broad impact of kin fusion. We do not dispute that many colonial taxa

Received 23 March 1992; accepted 26 March 1992.

have the capability to fuse soon after metamorphosis. However, the ability of individuals to fuse or reject upon assuming a benthic existence is equally compatible with the selective pressures of both self and kin fusion. Only the occurrence of aggregated larval settlement based on future fusibility is incompatible with the self fusion hypothesis. To the best of our knowledge, evidence of aggregated settlement as a function of shared allorecognition alleles is available only for the ascidian *Botryllus schlosseri*. Although larvae of the bryozoan *Bugula neritina* preferentially settle near relatives (5), subsequent allorecognition interactions between colonies in this species are not known.

Third, Grosberg questions why an error-prone single locus system, based on partial match rules, would evolve in botrylloid ascidians if selection for fusion with self is occurring. He points out that other taxa, including other ascidians, possess multiple locus and full match rule allorecognition systems that would generate fewer errors in recognizing and fusing with self. This is certainly a valid argument. While we feel that phylogenetic constraints are a real possibility that should be seriously considered as an alternative to adaptationist explanations (6), we also recognize the possible validity of Grosberg's interpretation. We have already acknowledged that allorecognition systems in botrylloid ascidians show effects of kin selection due to the existence of aggregated settlement of fusible larvae (1). This does not imply that the same is necessarily true of all other taxa. We chose botrylloids as one of our examples because they are one of the very few taxa for which there is enough information to conduct a preliminary evaluation of both hypotheses, not because we felt that they provided the strongest support for our idea; clearly they do not.

However, there is a second logical conclusion that can be drawn from Grosberg's line of reasoning about genetic mechanisms of allorecognition. Single locus, partial match control of allorecognition in botrylloid ascidians may generate a relatively high frequency of fusion events between kin. By the same logic, multiple locus, full match systems are likely to result in an exceedingly low frequency of fusion among kin in other taxa. For example, a two locus system with full match rules and high levels of polymorphism at both loci (*i.e.*, such that most individuals are heterozygous and parents do not share alleles) will result in all rejection responses between offspring and parents and a fusion frequency among randomly paired full siblings of only 1/16. Multiple paternity of broods will further reduce the fusion frequency among siblings, as half sibs will not fuse. Linkage between allorecognition loci will increase the rate of fusion among sibs, but only to a maximum frequency of 1/4 (in the case of a zero recombination rate, functionally equivalent to a single locus system). These low fusion rates among close relatives will greatly reduce the potential for kin selection to impact allorecognition systems in other taxa. Only if aggregated settlement based on future fusibility is prevalent will kin fusion be common in colonial taxa with multiple locus, full match rules. A reduction in the frequency of fusion with kin is likely to increase the relative frequency of fusion with self (*i.e.*, proportion of fusion events that occur with self *vs.* kin), increasing the potential for selection for self fusion to influence the system.

We feel it very unlikely that either of these two hypotheses can be definitively excluded on the basis of current information on allorecognition systems. More empirical work is clearly required. The task is especially difficult because the two selective forces are not mutually exclusive, and their relative impact is likely to vary among taxa. Although it has traditionally been very difficult to distinguish between self and kin fusion events (7–9), the application of current molecular techniques should render these problems much more tractable. We do not advocate that the possibility of kin selection be abandoned, just that future empirical work consider alternative selective forces as well.

Acknowledgments

We thank John Francis, Steve Gaines, Mike McCartney, and Pam O'Neil for their comments and John Francis for supplying the full text of Polonius' speech to Laertes. Funding was provided by the National Science Foundation and the Louisiana Stimulus for Excellence in Research (NSF/LaSER(1991)-RCD-03).

Literature Cited

1. **Feldgarden, M., and P. O. Yund. 1992.** Allorecognition in colonial marine invertebrates: does selection favor fusion with kin, or fusion with self? *Biol. Bull.* **182:** 155–158.
2. **Platt, J. R. 1964.** Strong inference. *Science* **146:** 347–353.
3. **Grosberg, R. K. 1992.** To thine own self be true? An addendum to Feldgarden and Yund's report on fusion and the evolution of allorecognition in colonial marine invertebrates. *Biol. Bull.* **182:** 454–457.
4. **Grosberg, R. K., and J. F. Quinn. 1988.** The evolution of allorecognition specificity. Pp. 157–167 in *Invertebrate Historecognition*, R. K. Grosberg, D. Hedgecock, and K. Nelson, eds. Plenum Press, New York.
5. **Keough, M. J. 1984.** Kin-recognition and the spatial distribution of larvae of the bryozoan *Bugula neritina* (L.). *Evolution* **38:** 142–147.
6. **Gould, S. J., and R. C. Lewontin. 1979.** The spandrels of San Marco and the Panglossian paradigm: a critique of the adaptationist programme. *Proc. R. Soc. Lond.* **B205:** 581–598.
7. **Curtis, A. S. G., J. Kerr, and N. Knowlton. 1982.** Graft rejection in sponges: genetic structure of accepting and rejecting populations. *Transplantation* **30:** 362–367.
8. **Neigel, J. E., and G. P. Schmahl. 1984.** Phenotypic variation within histocompatibility-defined clones of marine sponges. *Science* **224:** 413–415.
9. **Neigel, J. E., and J. C. Avise. 1985.** The precision of histocompatibility response in clonal recognition in tropical marine sponges. *Evolution* **39:** 724–732.

INDEX

D

E

F

G

H

P

Q

R

S

T

U

V

W

Y

CONTENTS